AVIATION IN THE XXI-ST CENTURY

INTERNATIONAL CIVIL AVIATION ORGANIZATION
NATIONAL ACADEMY OF SCIENCES OF UKRAINE
MINISTRY OF EDUCATION AND SCIENCE,
YOUTH AND SPORT OF UKRAINE
NATIONAL AVIATION UNIVERSITY

PROCEEDINGS

THE FIFTH WORLD CONGRESS "AVIATION IN THE XXI-st CENTURY"

"Safety in Aviation and Space Technologies"

Volume 2

September 25-27, 2012
Kyiv, Ukraine

INTERNATIONAL CIVIL AVIATION ORGANIZATION
NATIONAL ACADEMY OF SCIENCES OF UKRAINE
MINISTRY OF EDUCATION AND SCIENCE,
YOUTH AND SPORT OF UKRAINE
NATIONAL AVIATION UNIVERSITY

PROCEEDINGS

THE FIFTH WORLD CONGRESS "AVIATION IN THE XXI-st CENTURY"

"Safety in Aviation and Space Technologies"

September 25-27, 2012

Volume 2

KYIV 2012

COFOUNDER

- National Aviation Academy State “Azerbaijan Hava Yollari” Closed Join-Stock Company, Azerbaijan
- Georgian Aviation University, Georgia
- JSC “Civil Aviation Academy”, Kazakhstan
- Nanchang Hangkong University, China
- Vilnius Gediminas Technical University, Lithuania
- The State School of Higher Education in Chelm, Poland
- Moscow State Technical University of Civil Aviation, Russia
- The International University of Logistics and Transport in Wroclaw, Poland
- Polish – Ukrainian Research Institute, Poland-Ukraine

** Authors are responsible for the content of the report*

SYMPOSIA

<u>Volume 1</u>

SYMPOSIUM 1. MODERN SPACE AND AVIATION TECHNOLOGIES
1.1 Latest technologies for maintaining aircraft airworthiness
1.2 Fatigue and fracture of aircraft structures
1.3 Aerodynamics and flight safety
1.4 Modern tribotechnologies in aircraft and general purpose mechanical engineering
1.5 Problems of recovery controllability of the aircrafts
1.6 Diagnostic systems in the aerospace complex
1.7 Information security in aviation
1.8 Specialized Computer Systems and CALS – Technology in Aviation
1.9 The intellectual robot-technical measuring complexes and systems
1.10 Advanced information technologies in aviation
1.11 Computer systems
1.12 Mathematical modeling and numerical methods
1.13 Energy installation

<u>Volume 2</u>

SYMPOSIUM 2. UNMANNED AIRCRAFT SYSTEMS (UAS)

SYMPOSIUM 3. AERONAVIGATION AND ATM SYSTEMS
3.1 Air traffic management and service
3.2 Communication, navigation, surveillance
3.3 Avionics
3.4 Aviation English and safety of flight
3.5 Automated process control systems
3.6 Complex systems control
3.7 Radar methods and systems workshop (RMSW-2012)

SYMPOSIUM 4. ENVIRONMENT PROTECTION
4.1 Biotechnology in aviation
4.2 Chemical technology and engineering
4.3 Environmental protection
4.4 Aviation congress school of young scientists ***Aviation and environmental protection from civil aviation impact***

<u>Volume 3</u>

SYMPOSIUM 5. AVIATION CHEMMOTOLOGY

SYMPOSIUM 6. COMMUNICATION FACTOR IN MODERN INTERNATIONAL RELATIONS
6.1 Communication factor in modern international relations
6.2 Modern Ukrainian journalism in the system of international communication

SYMPOSIUM 7. ECONOMY AND MANAGEMENT IN AVIATION

SYMPOSIUM 8. HUMAN FACTOR IN AVIATION
8.1 Language modelling of aviation information systems
8.2 Social, political, moral and psychological components of aviation safety. Psychology of aircraft safe operation and modern ergatic systems

SYMPOSIUM 9. SPATIAL ORGANIZATION OF AIR COMPLEXES

SYMPOSIUM 10. AIR AND SPACE LAW: INTERNATIONAL AND NATIONAL ISSUES OF SECURITY
10.1 Air and space law in international cooperation
10.2. Legal adjusting of safety of flights
10.3. Legal regulation peculiarities of air space use under modern market conditions

SYMPOSIUM 11. CONTINUOUS PROFESSIONAL EDUCATION. UPGRADING AND RECURRENT TRAINING

CONTENTS

3.6 Complex systems control

3.7 RADAR METHODS AND SYSTEMS WORKSHOP (RMSW-2012)

4.4 AVIATION CONGRESS SCHOOL of young scientists "AVIATION AND ENVIRONMENTAL PROTECTION FROM CIVIL AVIATION IMPACT"

UDC 528.7:621.3:629.7

V.P. Kharchenko, Doctor of Science (Engineering), Professor
D.E. Prusov, Cand. of Science (Engineering), Associate Professor
(National Aviation University, Ukraine)

THE COMPLEX WORK ON THE UNMANNED AIRCRAFT SYSTEM PROTOTYPE IN THE NATIONAL AVIATION UNIVERSITY

The integrated approach to the theoretical foundations has been considered for the unmanned aircraft system development, that includes the twin-engine unmanned aircraft, the automation system for optimal control of unmanned aircraft system with self-adaptation elements, the automation system for unmanned aerial vehicles landing, the equipment for secure transmission of radiotelemetering data and video surveillance, the integrated navigation complex of unmanned aircraft .

Safety integration of unmanned aircraft systems (UAS) in uncontrolled airspace is a long work, that involves multi-stakeholder involvement and their expertise in the following areas such as development of airframe, engines, avionics and navigation complex, issuing certificates of crew members and medical examination of UAS-crew, creating systems to detect and prevent the use of spectrum (including the protection against accidental or unlawful interference), providing separation for other aircraft, as well as working out a reliable legal framework, creating the necessary theoretical basis.

In terms of International Civil Aviation Organization (ICAO) objective consideration of the characteristics in addressing unmanned aviation is to provide the fundamental international regulatory framework through Standards and Recommended Practices (SARPs), with supporting Procedures for Air Navigation Services (PANS) and guidance material, to underpin routine operation of UAS throughout the world in a safe, harmonized and seamless manner comparable to that of manned operations.

One of the important factors of industrial-economic complex efficiency is the development of unmanned aircraft systems. Such systems can effectively resolve a wide range of problems from agricultural oriented tasks to environmental monitoring, condition of pipelines, protection of state borders etc. Worldwide experience of UAS using confirms their high efficiency, profitability, and feasibility of increasing their share in the overall structure of both civilian and military aviation.

The theoretical investigation and development the own unmanned aircraft systems, necessary equipment, a comprehensive national regulatory for its application, the development of international cooperation and coordination on UAS regulation is important for Ukraine as a country, which includes the full cycle of development, production, operation of aerial vehicles, training of aviation specialists and has significant potential for development, manufacture and operation of its own unmanned aircraft systems, as well as exporting them overseas.

National priorities for own unmanned aircraft systems application is the operation in various sectors of the economy and in military affairs.

Most aviation works are performed in agriculture, environmental protection, health care, aerial search of mineral resources, study the earth and water surfaces, fighting floods, oil and gas industry, fire protection, participation in disaster mitigation and technogenic disasters, for internal affairs field, and others.

At the same time the economic efficiency of unmanned aircraft systems for these tasks in comparison with classical manned aircraft is much higher, confirming the relevance of creating their own experimental UAS based on the two-engine unmanned aircraft equipped with modern nano-engineering equipment with control based on new information technologies.

Implementation of works in this area provides a comprehensive approach to the UAS creating and using.

Ukraine is one of the few countries that has a powerful air-industrial potential. The development of air-design sectors allows to overcome the lag in the creation, production and operation of competitive unmanned aircraft systems. Existing in Ukraine scientific, technical and technological capacity facilitates the establishment of attractive conditions for public funding and investment in projects on modern UAS creation.

In general, implementation of scientific and technical programs and projects in high-technology air-construction, appearance in the internal market competitive technology, equipment and tools, increasing export potential is one of the priorities of Ukraine's economic development.

The difficult economic situation causes to look for less costly areas of work. One of the ways that allows to realize new ideas and professional experience as a final product is a small size unmanned systems design. Unmanned aviation is used extensively in the civilian sphere to perform the following functions: the border security, the law maintaining, deal with the consequences of natural disasters or technogenic accidents, the environment ecological condition monitoring, etc.

The problems of unmanned aircraft equipment are not connected with the unmanned aircraft, because they are only a part of unmanned aviation complex (UAC), which includes aircraft, modern special on-board equipment and ground control systems, launch and landing. Thus, unmanned aviation complex is a sophisticated aviation technical system which includes one or more unmanned aircraft, control point and communication facilities, equipment startup and rescue service, as well as transportation.

The elaboration of these components in the construction of unmanned aviation complex requires high development of aircraft design, electronics, information and other technologies. Therefore, many countries haven't got a complete cycle of this unique manufacture, beginning with the construction of the aircraft and its equipment and finishing with the target ground control points.

Along with the elaboration, manufacture and application of unmanned aircraft systems regulatory base of common use of airspace by the unmanned aircraft systems and by the manned one is forming in the world.

Lack of systems to prevent collisions between unmanned aircraft with other aircraft, high probability of uncontrolled fall to the ground make the flights of unmanned aircraft impossible in the same space with other aircraft as well as their application in the areas of settlements. As a result the benefits from the use of civil unmanned aircraft systems are lost, and the application of unmanned aircraft systems in the airspace with busy air traffic and in the areas of settlements is completely impossible.

In such civil areas of application as the Earth remote probing, communications and control of borders, relaying signals unmanned aircraft systems reduce the cost of production of services in comparison with traditional space and aeronautical systems.

Concepts of certification, standardization and regulation of unmanned aircraft flights at the level of international governmental and nongovernmental organizations have been creating. (ICAO, 2011).

In Ukraine the field of unmanned aircraft develops very quickly. National Aviation University was one of the first institutions in Ukraine, which drew attention to the problem of development of unmanned aviation complex of civil purposes. Currently in Ukraine there are no such important components as the classification of unmanned aviation complex according to the common terminology, tactical and technical requirements to the complexes from potential customers, regulatory base for creation, testing and operation of the unmanned aviation complex, funding from the concerned central authorities.

The use of unmanned aviation complex in the national economic sector, in the interest of environmental authorities, enterprises of fuel and energy complex and other subjects of the national economy, in the problems of emergency situations, as well as for air surveillance and border security, for the monitoring of the situation on the highways, in the interests of regional bodies of economy, the bodies of land utilization, municipal and regional administrations, etc., which will improve the effectiveness of operational control by means of various departments during the performance of assigned missions in money saving with a help of creation of unified unmanned aviation complex are very important. Ukraine for a short term can receive national advanced unmanned aviation complex of civil purposes with a help of joint efforts of relevant authorities of executive power and their focus on main areas is a topical issue.

According to all listed industry problems Ukraine has a serious technical base, and all the necessary resources to create effective automation unmanned systems. More attention both from the government and business representatives is paid to the projects of unmanned aircraft complexes creation.

The purpose of the complex work is the construction and design principles establishment for the relevance experimental UAS creating based on the two-engine unmanned aircraft equipped with modern engineering equipment with automation control based on new information technologies. The purpose implementation is to obtain new knowledge in the field of unmanned aircraft systems, focused on the UAS use in the economy of Ukraine and other countries. The main use of unmanned aircraft can be defined aerial photography, real-time video surveillance and patrolling of linear and planar objects. The obtained results can allow to Ukrainian developers and manufacturers of unmanned aircraft to get the effective tools for the development of unmanned aircraft systems of national production.

The initial data for the works to create a prototype unmanned aircraft system "Ukraine" on the basis of two-engine unmanned aircraft is following its specifications: Wingspan is 6.0 m; Mass of useful loading is up to 70 kg; Starting weight is up to 200 kg; Max. speed is 250 km / h; Power of engines is 2 x 17 kW; Max. altitude is up to 3,000 m; The method of launch / landing - that of aircraft; Time of deployment in the operating position is up to 0.5 hours.

An integrated approach in the project involves the following objectives:

— the construction principles determination of unmanned aircraft systems on the methodology "The safety management system" according to the international requirements;

— the hybrid composite materials development and production based on the strength criterion;

— the nano-technical complex development and manufacturing for the UAS on-board and ground equipment;

— the control complex development and production for the board and ground UAS systems;

— the scheme-technical solutions development for automation flight trajectory based on new information technologies;

— the methods and algorithms development and implementation for the automation UAV landing on network signals of orbiting satellite systems;

— the information protected data channel "board-to-land, land-to-board" development, the flight control system design, and standardization of protocols recommendations;

— the UAS standard model design, production, and testing with energy efficient avionics equipment;

— the training programs development for UAV operators and UAS ground personnel;

— the normative and technical documentation development for UAS certification.

Purposes and objectives are achieved by performance of works in the following areas:

— development and manufacturing the two-engine unmanned aircraft;

— development the automation system for optimal control of unmanned aircraft system with elements of self-adaptation;

— investigation the hybrid composite materials on strength criteria for use in the unmanned aircraft;

— establishment the automation landing system of unmanned aircraft;

— design and production of the experimental equipment model for secure transmission of radiotelemetering data and video surveillance;

— development and manufacturing the integrated navigating complex for unmanned aircraft;

— development the scientific and methodological support and technical measures for ground personnel training of unmanned aircraft systems;

— development the normative and technical documentation for certification manufacturing of the unmanned aircraft systems.

At the present stage of aviation development the unmanned aircraft systems form a new component of general aviation system, and now the International Civil Aviation Organization ICAO, numerous regional and national organizations such as the European Aviation Safety Agency EASA, the European Organisation for the Safety of Air Navigation EUROCONTROL, the European Defence Agency EDA, the European Space Agency ESA, the European Organization for Civil Aviation Equipment EUROCAE, the North Atlantic Treaty Organization NATO, the U.S. Federal Aviation Administration FAA, the National Aeronautics and Space Administration NASA, the Radio Technical Commission for Aeronautics RTCA, and other organizations are working related to unmanned aircraft systems study, performance and ultimately integration.

These systems are based on the latest developments in the field of aerospace technologies to implement new, more sophisticated uses of aircraft in civil, commercial, or military purposes and to improve flight safety and civil aviation efficiency in general.

However, the pilot removal from the aircraft board defines important technical and operational issues, that requires long study of active and continuous monitoring for the aviation community.

Given the above, National Aviation University in recent years has refined theoretical principles, concepts, technical and technological solutions for the program implementation of unmanned aircraft systems into the practice of Ukraine civil airlines.

For this purpose, were organized a series of works devoted to optimizing the UAV dimension-type, construction, and structure of its air-navigation, telemetry, radiocommunication, and other vital systems, and also personnel training. At the National Aviation University are developed a number of unmanned aircraft systems types to address a wide range of tasks most civilian and military.

In terms of Ukrainian aviation market development is extremely important to develop its own unmanned aircraft systems and national laws - the legal basis of UAS use, that should be based on the modern international norms and standards. In order to combine different groups efforts and research of the National Aviation University scientists and experts according comprehensive implementation of these strategic objectives for the country the performers team has been formed for the research and development the complex work on a unmanned aircraft system prototype generation. This work is a priority direction in the world market regarding the scientific and technical prospects.

UDC 629.735.014-519(043.2)

Samkov O.V., Prof., Dr.Sc. (Eng), Suslova G.A., Professor,
Silkov V.I., Professor, Stepaniuk O.A., post-graduate student
(National Aviation University, Ukraine)

METHODICAL APPROACH TO VALIDATE SOLUTIONS TO FULFILL THE TASKS DEFINED SEARCH OBJECTS ON THE BASIS OF UNMANNED AIRCRAFT SYSTEMS

In this paper, based on a comprehensive measure of "efficiency - cost - agility," the methodical approach to evaluating the effectiveness of the use of unmanned aircraft systems for solving the problem of finding ground targets is suggested. The methodical approach can be used in conducting a comparative evaluation of unmanned aircraft systems, and to justify the decision to perform the tasks specified search objects based on their characteristics.

Introduction

In recent years unmanned aircraft experiencing a revival based on new technologies, materials, computerization and intellectualization of the functional systems of unmanned aircraft systems (UAV).

In this connection, in the first place out tasks associated with the creation of algorithms and software for a wide class of problems for the effective application of UAV. In the general structure of such problems the problem of finding the set of objects occupy an important place, the occurrence of which poses a team task management optimum conditions, the trajectory and flight parameters.

Subject to the requirements of agility and the importance of these tasks the main indicators of their performance evaluation are the time parameters of the specified location, positioning and delivery of information to the consumer.

Obviously, the providing requirements for expediting the search object is an actual problem, whose solution is impossible without modern means of automation (their technical, algorithmic, software and ather software), communications and control, search and detection, and support decision-making, etc . In this case, one of the first to be solved the problem of developing algorithms for determining the optimal trajectories of modes and parameters of the flight.

In this paper a methodological approach to solve the problem of choosing optimum conditions and parameters of the flight trajectory and build on its basis the corresponding algorithms. Such a task selection is based on the optimization of flight parameters for the integrated index of " *efficiency - cost* - agility." The significance of each of these components is determined by the appointment of UAV.

Search of some object (target for military UAV) is often connected with reconnaissance of some area with the help of airborne electrooptical, radar, infrared systems or other means. In this process the system of aerial photography covers a strip of land surface of width B. Considering the speed of flight V to be constant, during time period t the aircraft passes the distance of $L = Vt$ and provides searching of the area

$$S = BL = BVt, \qquad (1)$$

where B is a territory strip width covered by vehicle equipment, L is a length of flight route, V and t are correspondingly the average speed of flight and the time of surveillance duration.

For accurate calculations it is necessary to take into account the coefficient of areas overlapping, which is inevitable during practical scanning.

The flight path depends on the search task. If there is no any information about the object and it is necessary to discover it on some area S, then the flight path can be presented as an ordinary scanning. Such flight can be programmed and accomplished automatically without interference of an operator.

If there is need to discover the object on the basis of preliminary information the flight path can have more complicated profile – horizontal turns, bankings, climb and descent [3]. The operator can interfere into the control, change the flight mode and profile.

Flight altitude is determined by the capabilities of reconnaissance equipment, performances of an aircraft [2]. One of the main requirements to the military purpose UAV altitude is avoidance of being hit by conventional armaments – gunfire, portable air-defense systems.

Strip width of territory cover B is determined by the angle of camera view 2β and flight altitude H (fig. 1)

$$B = 2Htg\beta. \qquad (2)$$

Highlighted peculiarities require use of special indices for assessment of UAV application effectiveness. Let us consider them in details.

Capability of survey (W)

Some authors estimate that the capability of search of reconnaissance unmanned aeronautical systems quantitatively can be assessed by the value of area surveyed in a unit of time [1]. Average value of this index can be obtained from the formula (1), dividing its right and left parts by time

$$W = \frac{S}{t} = \frac{BVt}{t} = BV = 2VHtg\beta, \qquad (3)$$

where V is average speed of flight, B is a width of strip covered by camera view, t is a time of reconnaissance duration. For more accurate assessment it is necessary to consider the probability of reliable target detection, and also the probability of successful passage of the enemy air defense system.

Capability of survey shows how fast the observer can investigate the given area. Capability is a complex index because it takes into account aircraft performances (speed and altitude of flight) and also capacities of surveillance equipment (in particular, the angle of vision area in azimuth).

In case of discrete survey the volume of information is calculated by the number of frames n. It can be determined considering the following assumptions. Provided it is necessary to make a survey of some area S during one flight with the task to search the objects of certain type. For that it is necessary to obtain $n = \kappa_{sq}S/s_1$ frames, where $\kappa_{sq} = ns_1/S$ is a coefficient of surveyed areas overlapping, s_1 is an area of a region on which there can be one or several objects that should be discovered and recognized. To decrease the time spent for survey of the whole area S the value s_1 should be greater. But on a large territory the object can appear to be indistinguishable. Its distinguishability is determined by detail level d (ground resolution). At increasing of altitude the detail level increases and the object of search can appear to be indistinguishable.

Specified objects will be distinguishable, if the detail level of survey does not exceed given value d_{giv}, that is $d \le d_{giv}$. It is evident that optimum altitude of flight will correspond to the condition $d = d_{giv}$. It means that the region of survey s_1 will be maximum, and objects will be distinguishable.

Modern electrooptical systems purposed for surveillance have several angles of vision area: narrow, wide, intermediate. For each of them there will be certain value of s_1. Besides, angles of view area can be different (fig. 1) in azimuth $2\beta_1$ and in angles of location $2\beta_2$. As a result linear dimensions of objects, reproduced by the electrooptical systems, will be also different in directions of B_1 and B_2. Analogically to the formula (2) we will have $B_1 = 2H_1tg\beta_1$, $B_2 = 2H_2tg\beta_2$. As far as usually flight altitude H is significantly greater than linear dimensions of the surveyed region, then it is possible to assume $H_1 \approx H_2 \approx H$. Though at small angles of location instead of altitude H_1 it is necessary to take the distance till the object.

Considering abovementioned, the area of “photographed” region will be equal to

$$s_1 = B_1B_2 = 4H^2tg\beta_1tg\beta_2 \qquad (4)$$

As it is seen from the formula (4), s_1 grows with increase of altitude proportionally to its square, and it depends on angles of view area.

While searching different objects resolution used is not angular but linear one d (level of detail). It allows to determine the type of the object being searched. The less level of detail d is, the clearer picture is on the screen. That is why for the reconnaissance of pinpoint targets linear resolution of electrooptical system should be as less as possible (and therefore better).

Thus, the value d is defined by certain reconnaissance task. Analogically to formula (2) it is connected with the angular resolution via flight altitude (due to smallness of angular resolution it is accepted that tgγ = γ[rad])

$$d = H\gamma \text{ or } H = d/\gamma. \quad (5)$$

From the formula (5) it is seen that at constant angular resolution γ linear resolution d is connected with the altitude by proportional dependence. With increase of altitude it also increases, image on the screen deteriorates and at some altitude the object will appear to be indistinguishable.

Substituting the value of altitude from (5) to the formula (4), we will get the expression for determination of region area

$$s_1 = 4d^2 \frac{tg\beta_1 tg\beta_2}{\gamma^2} = d^2 k_{elp}, \quad (6)$$

where

$$k_{elp} = 4\frac{tg\beta_1 tg\beta_2}{\gamma^2}. \quad (7)$$

k_{elp} is a coefficient of electrooptical system. It combines angles of view and angular resolution of a system, that is comprehensively characterizes electrooptical system. The better resolution (less γ) and the greater angles of system view are, the greater coefficient k_{elp} will be, and, therefore, the greater region area will be surveyed at given level of object detail d.

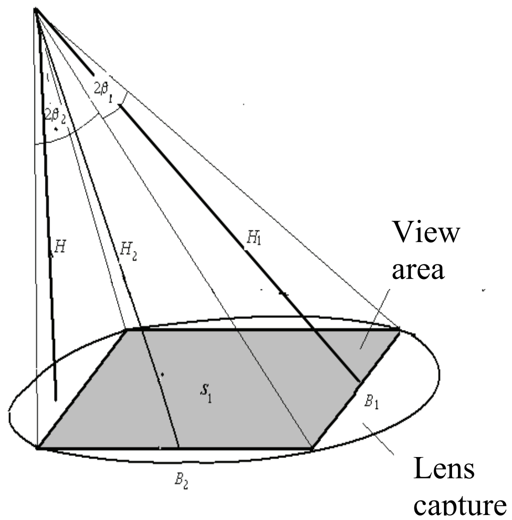

Fig.1. Object identification platform

At constant level of detail d this dependence is linear. The coefficient k_{elp} changes in quite wide limits. The most significant influence on it is caused by angular resolution of a system. Firstly, it can vary from system to system by times, and, secondly, k_{elp} is a quadratic function of angular resolution (of quite small value).

Formula (6) is convenient for practical use. For example, let there be the task to discover airplanes on some area ΔS (if they are present there) with their precise identification. For that the level of detail needed is d = 1 m. Then for certain reconnaissance system according to the formula (7) it is possible to calculate the coefficient k_{elp}, and according to the formula (6) – the value of region area s_1.

Knowing the value of s_1, common area of reconnaissance ΔS and coefficient of its overlapping κ_{ovr}, it is possible to calculate the required volume of information in a form of number of needed frames

$$\Delta n = k_{ovr}\,\Delta S/s_1 = k_{ovr} BV\Delta t/s_1 = k_{ovr} W\Delta t/s_1, \qquad (8)$$

and average rate of their making

$$\dot{n} = \frac{\Delta n}{\Delta t} = k_{ovr}\frac{W}{s_1}\ . \qquad (9)$$

Using value $\dot{n}$ it is possible to calculate the information flow in GBytes/s, which defines the mode of its processing.

Moreover, using formula (5) it is possible to determine the optimum flight altitude, using formula (2) – the width B of covered strip; to set the speed V, to calculate the survey capacity $W = BV$ and calculate the time $t_{ts} = \Delta S/W$ of task accomplishment. The rate of frames transmission will depend on: the sizes of territory region, required for identification of searched target on surveyed region area s_1 and capacity of search W.

The cost of unmanned aeronautical system

It is assumed to estimate it according to several indices:
initial cost of a system C_0; operational costs C_{oper}; flight hour cost C_{fh}; cost of survey of territory region s_1 of given area C_{s1}; cost of reconnaissance flight C_{fl}.

Initial cost consists of the cost of design and manufacture of the aircraft airframe with all the onboard systems, cost of operational load and cost of on-ground systems (C_{gr}), providing aircraft operation

$$C_0 = C^m_{airfr} m_{airfr} + C^m_{opl} m_{opl} + C_{gr}\,, \qquad (10)$$

where C^m_{airfr} is the cost of 1 kg of airframe mass with equipment, but without operational load, C^m_{opl} is the
cost of 1 kg of operational load, m_{airfr} and m_{opl} are masses of correspondingly airframe and operational load.

The cost of operation can be estimated as follows

$$C_{oper} = C^t_{oper} t_{lif}\ , \qquad (11)$$

where C^t_{oper} is the average costs per 1 hour of operation, t_{lif} is the aircraft service life in hours.
If assumed (statistical) number of air missions is equal to N, then the actual service life approximately can be estimated as $t_{lif} = Nt_{max}$, where t_{max} is the maximum flight duration.

Taking into account given assumptions the total cost of unmanned aeronautical system can be estimated as a sum

$$C_{UAS} = C_0 + C_{oper}. \qquad (12)$$

One of the most important indices for comparative assessment of unmanned aeronautical system is the cost of flight hour. It can be assessed by the total of initial cost, maximum flight duration (t_{max}) and use multiplicity – the number of take-offs (N) in the following form:

$$C_{fh} = \frac{C_0}{t_{max} N} + C^t_{oper}\ . \qquad (13)$$

Denominator in this formula determines the aircraft flight time during assumed period of operation.

Now let us determine the cost of unmanned aeronautical system flight. For reconnaissance of some common area $S = BVt$ it is necessary to make $n = S/(k_{ovr} s_1)$ frames. If the probability of the task accomplishment with taking into account all the possible acting factors (operability of equipment, radio visibility, enemy air defense avoidance, possibility of being hit by the antiaircraft defenses or enemy aircraft, etc.) is equal to p_{ts}, then the cost of such flight will be estimated by the value of

$$C_{fl} = C_{s1} * n / p_{ts} . \qquad (14)$$

The value C_{s1} can be determined with the help of flight time and the cost of flight hour. During survey of the region s_1 an aircraft passes the distance of $B_2 = 2H_2 tg\beta_2 = V\Delta t_1$. As a result the flyover time of the given region will be equal to

$$\Delta t_1 = \frac{2H_2 tg\beta_2}{V}. \qquad (15)$$

Then

$$C_{s1} = C_{fh}\Delta t_1 = C_{fh}\frac{2H_2 tg\beta_2}{V} \qquad (16)$$

It is evident, that given index will be one of the most significant. It answers the certain question – what resources are to be spent for discovery of certain object with the level of detail d (for example, a car, an airplane, a ship, etc.), which can be present on the region $s_1 = d^2 k_{elp}$.

Agility

The success of search accomplishment mostly depends on time and quality of information obtaining. The total search time (t_{tst}) can consist of time for fulfillment of separate stages time of: UAV pre-flight maintenance (t_{pfl}); flight to the region of search accomplishment (t_{reg}); search accomplishment (t_{sac}); processing and storage of data (t_{stor}) (if required); data transmission to the control centre (t_{trans}); data processing and transmission to the consumer (t_{proces})

$$t_{tst} = t_{pfl} + t_{reg} + t_{sac} + t_{stor} + t_{trans} + t_{proces} . \qquad (17)$$

The value t characterizes the agility of information obtaining from UAV.

Definition of terms of time of expression (16) is not particularly complex and depends on the characteristics of the equipment.

Conclusions

Thus, methodological approach (Formula 1 ... 17) for the calculation and selection of the optimal trajectory of the UAV and its parameters is proposed, from which developed the corresponding algorithm. Such a task of selection is based on the complex index of "efficiency - cost - agility " and involves two steps: calculation of flight parameters for the different modes of flight drones, and then, the definition of global assessments of performance and selection of optimal flight UAV based on the use of the analytic hierarchy process [6]. The developed algorithm for the calculation and selection of optimal parameters of the UAV flight can be used to support decision-making in the management of the use of UAVs.

References

1. *Rastopchin V.* Elementary principles of the evaluation of ….Ростопчин В.В. Элементарные основы оценки эффективности применения беспилотных авиационных систем для воздушной разведки. – www.avia.ru.

2. Беспилотные летательные аппараты: Методики приближенных расчетов основных параметров и характеристик/ *М.М. Митрахович, А.В. Самков, В.И. Силков* и др.; под об. ред. *В.И. Силкова*. – К.: ЦНИИ ВВТ ВС Украины, 2009. - 302 с.: ил.

4. *Сілков В.І.* Бойове маневрування літальних апаратів. – К.: НАОУ, 2004. – 340 с.

5. *Силков В.И.* Динамика полета летательных аппаратов.– К.: КМУ ГА, 1997. – 425 с.

6. *Saaty Thomas L.* The Hierarchon: A Dictionary of Hierarchies. — Pittsburgh, Pennsylvania: RWS Publications, 1992. — ISBN 0-9620317-5-5 – 496p.

UDC 629.735.014-519:656.7.08 (043.2)

V.P. Kharchenko Doctor of Science (Engineering), Professor
D.O. Bugayko PhD in Economics, Associate Professor
(National Aviation University, Ukraine)

SAFETY AND SECURITY INTEGRATION OF UNMANNED AIRCRAFT SYSTEMS INTO THE WORLD AVIATION SYSTEM: NATIONAL AVIATION UNIVERSITY EXPERIENCE

The principal objective of the aviation regulatory framework is to achieve and maintain the highest possible uniform level of safety and security. In the case of UAS, this means ensuring the safety of any other airspace user as well as the safety of persons and property on the ground.The National Aviation University research experience in the field of safety and security aspects of UAS integration into world aviation system is considered.

1. Introduction

National priorities in unmanned aircraft systems application usage are commercial exploitation and military operation. The most perspective application of the unmanned aircraft systems is in agriculture, construction projects, environmental protection, air ambulance, aerial photography, minerals searching, surface and water investigation, dealing with floods, fire fighting, dealing with the consequences of natural disasters and technological catastrophes, police air patrols and other activities. In comparison with classic manned aviation economic operating benefits of unmanned aircraft systems for the pointed tasks are much more grater. These factors allow to deduce an inference that unmanned aircraft systems development has strategic importance. Identifying the commonalities and differences between manned and unmanned aircraft is the first step toward developing a regulatory framework that will provide, at a minimum, an equivalent level of safety for the integration of UAS into non-segregated airspace [1,2] and at aerodromes. Fundamental and applied complex researches of the safety and security of unmanned aircraft systems application are very important in present situations.

2. UAS Safety Management

The main target of worldwide aviation activity is safety. According to ICAO, safety is the state in which the possibility of harm to persons or of property damage is reduced to, and maintained at or below, an acceptable level through a continuing process of hazard identification and safety risk management [3]. Nowadays unmanned aircraft systems are forming new component of general aviation system and at the present time ICAO, regional and national organizations such as European aviation safety agency (EASA), EUROCONTROL, European Defense Agency (EDA), European Space Agency (ESA), European Organization for Civil Aviation Equipment (EUROCAE), North Atlantic Treaty Organization (NATO), Federal Aviation Administration (FAA), National Aeronautics and Space Administration (NASA), Radio Technical Commission for Aeronautics (RTCA), government and airspace branch are conducting operations connected with their study, determination and finally integration [4]. These systems are based on recent development in the sphere of airspace technology which make possible to realize new types of aviation application in civil / commercial purposes and also to increase flight safety and efficiency of civil aviation application in general. Safety integration of unmanned aircraft systems into uncontrolled air space will be continuous work which includes the participation of many concerned parties with the attraction of their expertise in such spheres as glider elaboration, elaboration of engines, avionics and navigational complex of unmanned aircraft systems, certifications for cockpit crew and medical examination of cockpit crew of unmanned aircraft systems, development of the detection and warning systems, the use of frequency spectrum (including its defense from unlawful interference) and separation maintenance, relatively to other aircraft and the drill of reliable normative base.

From viewpoint of ICAO the purpose of unmanned aviation is to create international normative data base in accordance with Standards and recommended practice of SARPS. It is accompanied with the rules of air navigation service PANS and guidance materials. It is presented like the foundation which provides safe scheduled flight operations of unmanned aircraft systems in all over the world. The term "safety management" includes two key concepts. First is the concept of a State Safety Programme (SSP), which is an integrated set of regulations and activities aimed at improving safety. Second is the concept of a Safety Management System (SMS) which is a systematic approach to managing safety, including the necessary organizational structures, accountabilities, policies and procedures. States are required to establish an SSP to include safety rulemaking, policy development and oversight. Under an SSP, safety rulemaking is based on comprehensive analyses of the State's aviation system. Safety policies are developed based on safety information, including hazard identification and safety risk management, while safety oversight is focused on the effective monitoring of the eight critical elements of the safety oversight function, including areas of significant safety concerns and higher safety risks. As operators introduce UAS into operation, the State's SSP should support analysis of the potential effect on safety of the air navigation system, the safety of the UAS itself and of third parties. It should also determine what role, if any, "equivalent level of safety" and "acceptable means of compliance" will have [5].

3. UAS Security Aspects

Security is a second main target of worldwide aviation activity development. At present, we can identify the following areas of security for UAS:

Physical security - same standards as for manned aircraft: aircraft protection; tampering; access control to remote pilot station.

Cyber security - same standards as for CNS systems: protection of software and data links from hacking; spoofing; interference or malicious hijack.

Airspace security - positive identification of UAVs: UAVs must remain at all time under legitimate control; this implies the control of aircraft must not be delegated to anybody but the authorized owner/operator. Where possible, additional requirements to address the risks shall be imposed on the UAS If necessary, UAVs could be neutralised i.e. sent to a safe area to land or destroyed/crashed in a controlled manner.

The issue UAS security problem includes the following tasks:

- human resource security controls (operators & pilots);
- technical build standards for aircraft (control stations and critical sub-systems);
- roles and responsibilities of ATM authorities and operators (security policy/guidance, incident management, minimum security standards, security oversight)t;
- physical security controls;
- cyber security controls;
- technical controls, general engineering;
- command and control requirements (positive identification);
- acquisition and development controls [6].

4. Fundamental and Applied Complex Researches of the Unmanned Aircraft Systems Safety and Security of at the National Aviation University.

Taking into account the abovementioned, the scientists from National Aviation University (Ukraine) during last decades were working out theoretical principles, concept, technical and process solutions for realization the program of safe implementation of unmanned aircraft systems into the practice of civil aviation. For this purpose a variety of fundamental and applied works which were devoted to the structural optimization, dimension-type of the UAV, the composition of its air navigation, telemetric and other essential systems and personnel training.

The main aim of NAU scientist is to conduct fundamental theoretic research performance in the sphere of safety control and efficiency application of unmanned aircraft systems of next generation during aerial works, acquisition of knowledge concerning safety and integrated aviation efficiency.

At the National Aviation University was developed a line of domestic single engine M – 3 "Border", M-6 "Lark", twin-engine M - 7, M – 7D, M – 7V5 «Sky Patrol» unmanned aerial vehicles (UAVs) and unmanned aircraft with an electric motor «Eye». At the same time ways addressing the problems of integration, search and recognition and processing of satellite systems data, navigation and avionics onboard the UAV.

Fundamental and applied researches of National Aviation University scientists include:

- prototype unmanned aircraft system "Ukraine";
- different types of unmanned aerial vehicles;
- automated system for optimal control of unmanned aerial vehicles with elements of self-adaptation;
- investigation of hybrid composite materials for unmanned aerial vehicles;
- automated landing system for unmanned aerial vehicles;
- automatic control system of unmanned aerial vehicles;
- software modules of unmanned aerial vehicles support and modeling computer system;
- apparatus for secure transmission of radio - telemetry data and video surveillance equipment;
- navigating complex of unmanned aerial vehicles;
- scientific methods of training and ground training equipment for unmanned aircraft systems staff;
- regulatory and technical documentation for certification of unmanned aircraft systems.

The main point of National Aviation University scientific activity is the formation of system approach to all aspects of UAS operation and development.

4. Conclusion

The complex issue of UAS safety and security aspects is the basis for their integration into the global aviation system. National Aviation University considers the development of research in the field of UAS safe and security like one of its main priorities.

References

1. ICAO Global Air Traffic Management Operational Concept (Doc 9854). Montreal: Canada (ICAO), 2005. – 82 p.

2. Global Air Navigation plan (Doc 9750). Montreal: Canada (ICAO), 2005. – 125 p.

3. Safety Management Manual (SMM) (Doc 9859 AN/460). Montreal: Canada (ICAO), 2006. – 290 p.

4. Development of UAS International Regulation and Regulatory Framework / *M.G. Luckiy, V.P. Kharchenko, D.O. Bugayko* // Proceedings of the National Aviation University. – Kyiv, 2011. – № 2 (47). – P. 5–14.

5. Unmanned Aircraft Systems (UAS) (Cir 328 AN/190). Montreal: Canada (ICAO), 2011. – 54 p.

6 *Antonio Nogueras (Head DSS/CM/ATM Security Unit of Eurocontrol)* UAS Security Proceedings of EU UAS Panel Workshop, 13-14th September 2011, Eurocontrol HQ, Brussels: Belgium.

UDC 629.735.33-519:629.735.016.82(045)

Matiychyk M.P., Ph.D., head of SPCUA «Virage» ,
Makarchuk M.V., researcher, SPCUA «Virage»
(National Aviation University, Ukraine)

IMPROVING TAKEOFF PERFORMANCE OF TWIN-ENGINE UAV

Abstract. The results of flight tests of two-engined unmanned aircraft. Considered and investigated the influence of blowing the wings to reduce take-off distance. Calculations fulfilled and received quality indicators to improve takeoff performance of two-engined unmanned aircraft.

The urgency of work. Most well-known unmanned aircraft (UAV) with take-off weight of 300 kg is a native military target loads are applied in the respective unmanned systems. Statistical analysis of data shows that they are mostly single-engine, with a pushing airscrew and having a simplified structure [1]. Simplification of the design touches, means to enhance and lift, as the issue of take-off of military UAV solved due to these methods: the use of accelerators, catapults and etc. In respect of civil aviation, the listed features severely limit the scope of such UAV, resulting in excessive costs to the take-off equipment and its operation.

Resolving the contradiction is to ensure the flight characteristics of the UAV to operating conditions in civil aviation from ground airfields and sites.

During 2010 - 2011 years at NAU conducted work on the development of UAV of normal scheme mounting power plants on well mechanized wing, which allowed to obtain a significant reduction in take-off distance [2]. But it was not established as a distributed gain lift along the wingspan and what are the quality characteristics of specified increment due to the influence of blowing on the propellers on some wings.

The aim is to increase quality characteristics of lift of unmanned aircraft by blowing wing by the power plant (PP).

Solving the problem. The basis for calculation of quality characteristics are the results of flight tests of unmanned aircraft M-7D. It has a cantilever wing with small sweepback angle 7^0, wingspan 5.2 m, an area of 2.85 m^2, elongation 9.2, narrowing 1.47, with a relative thickness 15%, 33% equipped with single slotted flaps and 33% single slotted flapperons with classical arrangement of two-engined PP on the wing (Fig. 1).

Fig. 1. UAV M-7D in the moment of take-off.

During the experiments measured distance of the run was 18 meters, respectively running time was 3 seconds. Measurement was carried from start point till disappearing of traces of the main landing gear wheels on snow. Take-off mass of the aircraft (M_0) was 90 kg.

Known formula for determining the run distance [3]

$$L_{run} = \frac{1}{2g} \frac{V_{take-off}^2}{\frac{N_0}{G} - f}, \qquad (1)$$

where: N_0 - static thrust of PP, kg;

$G = M_0$ – take-off mass of the aircraft, kg;

f - friction coefficient of runway;

$V_{take-off}$ – take-off velocity. According to the experiment, N_0 = 55 kg, G = M_0 = 90 kg,

f = 0.1, - friction coefficient of runway covered with snow.

Take-off velocity determined from by the formula [3]:

$$V_{take-off} = \sqrt{L_{run} \cdot 2g\left(\frac{N_0}{G} - f\right)} = \sqrt{18 \cdot 2 \cdot 9{,}8\left(\frac{55}{90} - 0{,}1\right)} \approx 13{,}5(m/s) = 48{,}6(km/h). \qquad (2)$$

After analyzing the known formula for lift,

$$Y = 0{,}5C_y \cdot \rho \cdot S_w \cdot V^2, \qquad (3)$$

where C_y - lift coefficient;

ρ - air density;

S_w - wing area;

V - velocity of oncoming flow, it is clear that the increase of lift due to blowing wing by airscrews of PP possible only in terms of increasing the flow rate of wing area, which is blown.

To determine the growth speed of oncoming flow by airscrews of PP put a hypothesis about the distribution of lift along the wing into two components. One component is formed by air speed aircraft and the second, by the blowing of the wing by airscrews of PP. To confirm the hypothesis used the following procedure.

First, define the angle of attack of aircraft at the take-off moment and lift coefficient for wing profile. Specific values of these parameters were: $\alpha_{take-off} = 16^0$,

$C_{y.profile.\alpha}$ = 1,3 (for wing profile P-IIIA 15% $\alpha_{take-off} = 16^0$).

During take-off was used following mechanization of wing – single slotted flaps released on 20^0. Accordingly, growth of take-off was [4]:

$$\Delta C_{y.flap.} = к_1 к_2 \Delta C_{y\alpha мах} = 1{,}3 \text{ x } 0{,}7 \text{ x } 1{,}18 = 1{,}07, \qquad (4)$$

where: K_1 = 1,3 - coefficient which takes into account the effect of relative thickness of the wing;

K_2 = 0.7 - factor which takes into account the angle of flaps deflection;

$\Delta C_y \alpha_{max}$ = 1.18 - maximum lift growth rate.

Next, determine that part of lifting force that created by PP:

$$N_Y = N_0 \sin\alpha_{take-off} = 55 \text{ x } 0{,}276 = 15{,}2 \text{ (kg)}; \qquad (5)$$

where $\alpha_{take-off} = 16^0$, take-off angle.

Divided conditionally total lift (Y) on the portion that is formed on part of the wing that is not blown (Y_1) and the part which is formed on the wing area of blowing (Y_2). According to Fig. 2 define specific areas:

$S_{w.1}$ = 1.8 m^2 (wing area that is not blown, shown in white color);

$S_{w.2}$ = 1.05 m^2 (wing area, which is blown, shown in gray color).

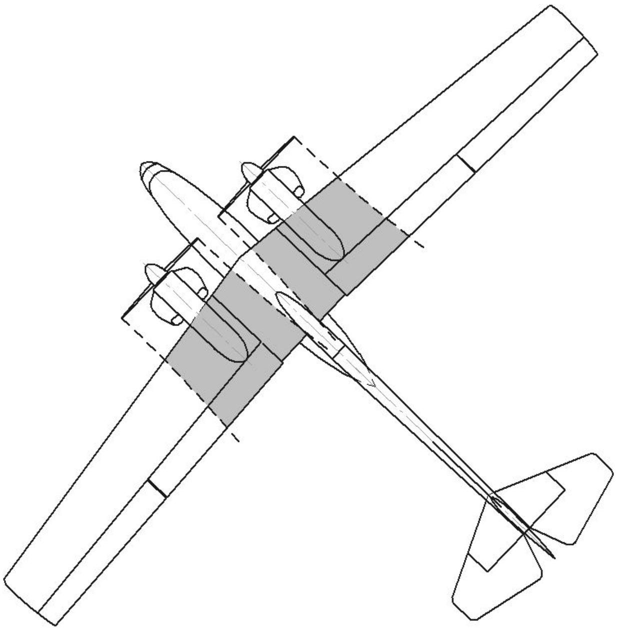

Fig. 2. The projection of M-7D with the hatch area of wing, which is blown

Flaps maintains 39% of the wing that is not blown and 67% of the wing, which is blown. According to the areas mentioned lift coefficients are next:

$$C_{y.1} = C_{y.profile.\alpha} + 0{,}39\Delta C_{y.\ flap} = 1{,}3 + 0{,}39 \times 1{,}07 = 1{,}72; \quad (6)$$

$$C_{y.2} = C_{y.profile.\alpha} + 0{,}67\Delta C_{y.flap} = 1{,}3 + 0{,}67 \times 1{,}07 = 2{,}02. \quad (7)$$

According to formula (3) were:

$$Y_1 = 0{,}5\ C_y.1\ \rho\ S_{w.1}\ V^2_{take\text{-}off} = 0.5 \times 1.72 \times 1.21 \times 1.8 \times 182.25 = 341\ (N) = 34.8\ (kg). \quad (8)$$

In order for the plane began to take-off from the runway, next condition should carry out $Y > M_0$. If providing the total lift force Y = 91kg, power Y_2 will be:

$$Y_2 = Y - Y_1 - N_Y = 91 - 34.8 - 15.2 = 41\ (kg) = 401.8\ (N). \quad (9)$$

Then, turning the formula (3), measured flow rate behind the airscrews of PP:

$$V_{blowtake-off} = \sqrt{\frac{2 \cdot Y_2}{C_{y.2}\rho S_{w.2}}} = \sqrt{\frac{2 \cdot 401{,}8}{2{,}02 \cdot 1{,}21 \cdot 1{,}02}} = 18(m/s) \approx 64{,}8(km/h). \quad (10)$$

Growth of velocity, which is formed by PP determined from the equation [3]:

$$V_{\text{blow}} = \sqrt{V^2{}_{blowtake-off} + V^2_{take-off}} = \sqrt{18^2 - 13{,}5^2} = 11{,}91(m/s) = 42{,}86(km/h). \quad (11)$$

The area which is blown by PP of the total wing area:

$$S_{w.2} / S_w \text{ x } 100\% = 36{,}8\%. \quad (12)$$

The corresponding increase of lift is:

$$\Delta Y_{blow} = 0{,}5\ C_{y.2}\ \rho\ S_{w.2}\ V^2_{blow} = 0{,}5 \text{ x } 2{,}02 \text{ x } 1{,}21 \text{ x } 1{,}05 \text{ x } 11{,}91^2 = 182 \text{ (N)} = 18{,}6 \text{ (kg)}. \quad (13)$$

From the total lift it is:

$$\Delta Y_{blow}/Y \text{ x } 100\% = 18{,}6/91 \text{ x } 100\% = 20\%. \quad (14)$$

Fig. 3 graphically shows the distribution of lift along the wingspan (L) of unmanned aircraft M-7D during take-off, where 1 - the force created by the wing, 2 - flaps, 3 - blowing of wings, 4 - vertical component of thrust PP.

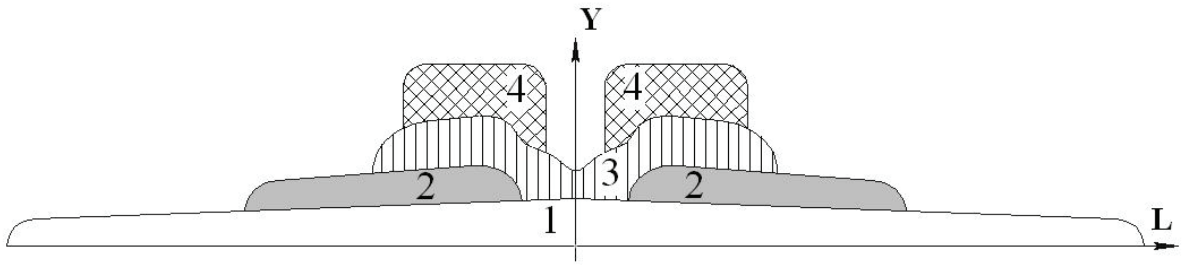

Fig. 3. The distribution of lift on a wingspan UAV M-7D during take-off.

Conclusions

1. When blowing the aircraft M-7D from PP 36.8% of the wing, which is operated by 67% of single slotted flaps, increase of lift by blowing was up to 25%.

2. As seen from the results of the experiment, blowing wings is an essential reserve for the take-off speed reduction and distance of the run of unmanned aircraft with lateral displacement of PP on the wing.

3. As ways of further improving take-off characteristics of two-engined unmanned aircraft we can offer increased area of wing blowing, for example increasing the diameter of propellers, as well as application of more efficient mechanization of wings in the area of blowing, in particular Fowler flaps and slats of maximal possible chords.

Refrences

1. *Marc Deli*. Unmanned Aerial Vehicles // Unmanned Aerial Vehicles and Tarqets. IHS Jan'es. IHS Global Limited 2010. p 28- 380.

2. *Кулик М.С., Харченко В.П., Матійчик М.П, Макарчук М.В.* Багатоцільовий двомоторний безпілотний літальний апарат. Пат. України на корисну модель №62929, Бюл. №18 від 26.09.2011 року - Київ, 2011.

3. *И.В. Остославский,* Аэродинамика самолета. - М.: Государственное издательство оборонной промышленности, 1957г.

4. *А.А. Бадягин, Ф.А. Мухамедов,* Проектирование легких самолетов. - М.: Машиностроение, 1978г.

UDC 629.735.33-519(045)

Smyrnov I.D., researcher, Alekseenko.S.I., researcher, SPCUA "Virage"
(National Aviation University, Ukraine)

HINGE MOMENT CALCULATION OF MOVING AERODYNAMIC SURFACE

Considered variable techniques calculation hinge moment of moving aerodynamic surface. Changes are mode in existing technique. Calculation fulfilled with changes and received torque values of servo.

The urgency of work. At present the problem definition efforts on connecting rods of moving aerodynamic surfaces quite acute, as well as incorrect estimation of these parameters leads to higher economic costs for the use of more powerful servos, or in worst case - amendments to existing structures of aircraft. As shown, the use of wind tunnel to determine the effort on connecting rods of moving aerodynamic surfaces is fairly accurate, but uneconomical for low-cost projects. Currently, for small and unmanned aircraft are widely used indirect methods to study characteristics of the aircraft, which is associated with lower economic and resource costs in comparison with natural methods of investigation. In our view, as an alternative to determine the hinge moments can offer the use of numerical methods. Methods of finding the hinge moment in general similar to the methods described in the works of Lebedev A.A, Chernobrovkyn L.S. "The dynamics of flying unmanned aircraft", but instead of using only the of lifting force coefficient we propose to use the full rate of aerodynamic force coefficient, which we believe is more accurate.

The aim is to calculate hinge moment of moving aerodynamic surface and torque of servo.

Solving the problem. Consider the calculation of hinge moment after the example of elevator UAV M-7V5.The hinge moment of moving aerodynamic surface is calculated by the formula:

$$M_H = P \times l_s . \tag{1}$$

From the formula (1) shows that the hinge moment depends on the aerodynamic forces and the shoulder at the end of which there currently. For the case since elevator formula (1) takes the form:

$$M_H^{EV} = P_{EV} \times l_s^{EV} , \tag{2}$$

where P_{EV} - the total aerodynamic force that creates the elevator, l_s^{EV} – elevator's arm suspension . Full aerodynamic force is calculated by the known lifting force formula, where the rate of total aerodynamic force vector sum of the lifting force coefficient and drag coefficient

$$P = 0{,}5\sqrt{\Delta C_y^2 + \Delta C_x^2}\,\rho V^2 S \tag{3}$$

For a full aerodynamic force that creates elevator formula (3) takes the form:

$$P_{EV} = 0{,}5\sqrt{\Delta C_{yTV}^2 + \Delta C_{xTV}^2}\,\rho V^2 S_{EV} \tag{4}$$

Lifting force coefficient is determined by the formula [2]:

$$\Delta C_y = \Delta C_{\text{ya max}}(K_1, K_2, K_3, K_4, K_5). \tag{5}$$

Since the stabilizer with elevator aerodynamically similar mechanized wing, then the formula (5) takes the form:

$$\Delta C_{yEV} = \Delta C_{\text{ya max}}^{EV}(K_1^{EV}, K_2^{EV}, K_3^{EV}, K_4^{EV}, K_5^{EV}). \tag{6}$$

Coefficient $\Delta C_{\text{ya max}}^{EV}$ is determined from tables of aerodynamic characteristics of mechanized wings [3] for single-slit steering surface. Since the stabilizer with elevator aerodynamically similar mechanized wing, then correction factors K_1^{EV} - K_5^{EV} you can see from the graphs in Fig.1.

$\Delta C_{\text{ya max}}^{EV} = 1{,}18$; $K_1^{EV} = 1{,}15$; $K_2^{EV} = 0{,}8$; $K_3^{EV} = 1{,}1$; $K_4^{EV} = 1{,}2$; $K_5^{EV} = 1$.

At the same time the drag coefficient is determined by the formula [2]:

$$\Delta C_x = \Delta C_{\text{xa min}}(K_{\bar{b}}, K_{\bar{l}}, K_{\phi}, K_{\chi}). \tag{7}$$

Since the stabilizer with elevator aerodynamically similar mechanized wing, then formula (7) takes the form

$$\Delta C_{xEV} = \Delta C^{EV}_{xa\min}(K^{EV}_{\bar{b}}, K^{EV}_{\bar{l}}, K^{EV}_{\phi}, K^{EV}_{\chi}). \tag{8}$$

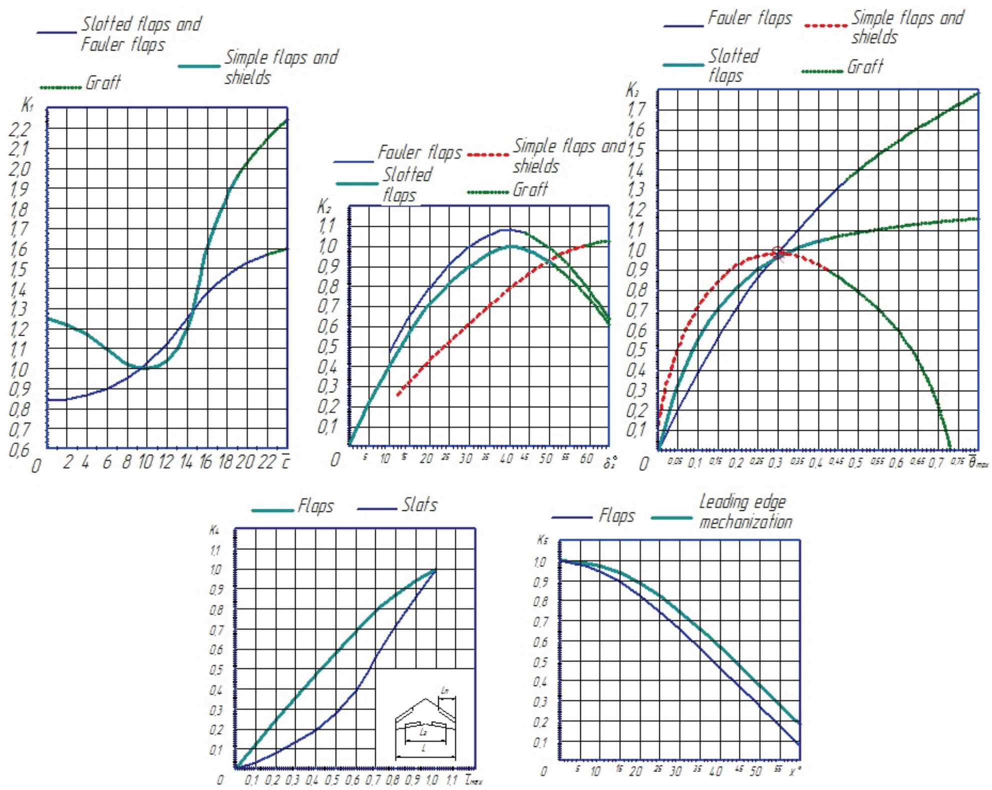

Fig.1 The correction factor K1 ... K5 to determine growth factor lifting force for mechanized wings that take into account the impact:

K_1 - the relative thickness of the wings;
K_2 - the angle of deflection of flaps;
K_3 - relative to the chord flaps;
K_4 - the relative magnitude of flaps;
K_5 - swept to quarter chord wings.

Coefficient $\Delta C^{EV}_{xa\min}$ is determined from tables of aerodynamic characteristics of mechanized wings [3] for single-slit steering surface. Since the stabilizer with elevator aerodynamically similar mechanized wing, then correction factors - you can see from the graphs in Fig.2.

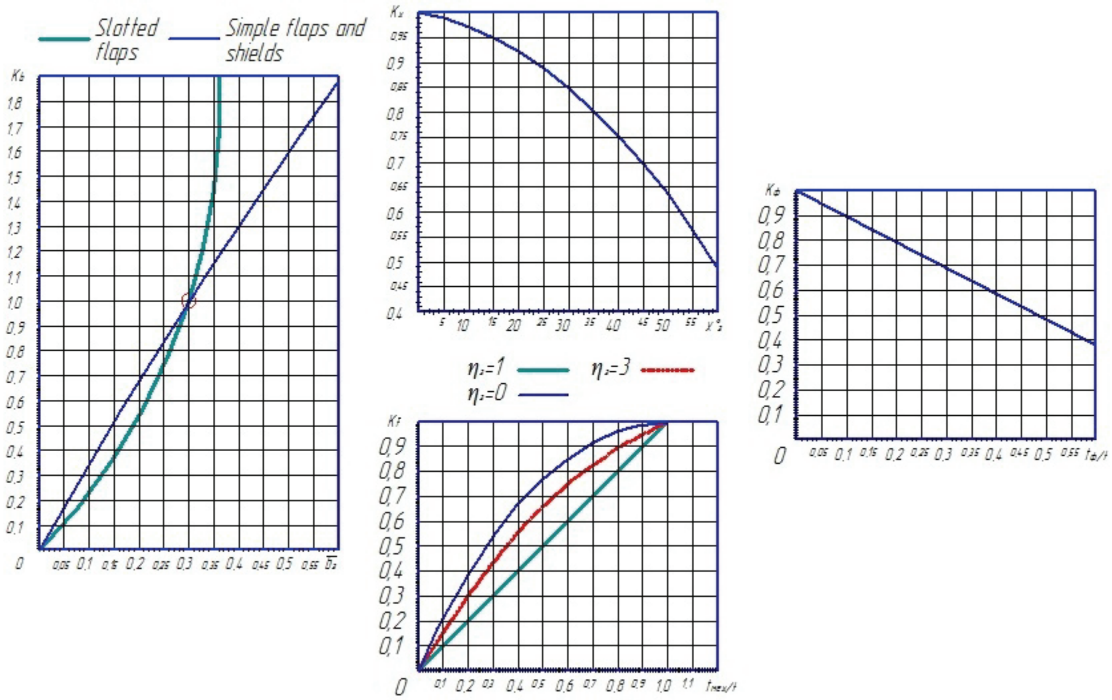

Fig.2 The correction factor to determine the rate coefficient of resistance of mechanization wings that take into account the impact:

$K_{\bar{b}}$ - Relative to the chord flaps;
$K_{\bar{l}}$ - The relative scale of mechanization;
K_{ϕ} - The width of the fuselage;
K_{χ} - The angle swept by the axis hinge flaps.

$$\Delta C_{\text{xa min}}^{EV} = 0{,}13; \qquad K_{\bar{b}}^{EV} = 1{,}5; \qquad K_{\bar{l}}^{EV} = 1; \qquad K_{\phi}^{EV} = 1; \qquad K_{\chi}^{EV} = 1.$$

Using the found coefficients and formulas (5.8) can be calculated ΔC_{yEV} and ΔC_{xEV}:

$$\Delta C_{yEV} = 1{,}18 \times 1{,}15 \times 0{,}8 \times 1{,}1 \times 1{,}2 \times 1 = 1{,}433, \tag{9}$$

$$\Delta C_{xEV} = 0{,}13 \times 1{,}5 \times 1 \times 1 \times 1 = 0{,}195. \tag{10}$$

Full aerodynamic force that creates the elevator by the formula (5.4) is:

$$P_{EV} = 0{,}5\sqrt{1{,}433^2 \times 1{,}195^2} \times 1{,}249 \times 83{,}33^2 \times 0{,}23 = 1442{,}21(\text{N}) = 147{,}01(\text{kg}) \tag{11}$$

Using the values of aerodynamic forces can be calculated shoulder at the end of which there is hinge moment created by rejecting the half height of the maximum steering angle when flying at top speed. To find the length of the shoulder using a technique described in [1] : at the focus point of elevator deposited values of lifting force coefficient and drag coefficient, effective vector the full aerodynamic forces is determined. The next step is to build a line which is this vector and finding the distance between it and the axis of rotation of the elevator and this length is perpendicular going from the axis of rotation to the constructed line.

Find shoulder is 7.5 mm and articulated point that is created on the axis of rotation of the elevator is given by formula (2):

$$M_H^{EV} = 147{,}01 \times 0{,}0075 = 1{,}102(\text{kg} \times \text{m}). \tag{12}$$

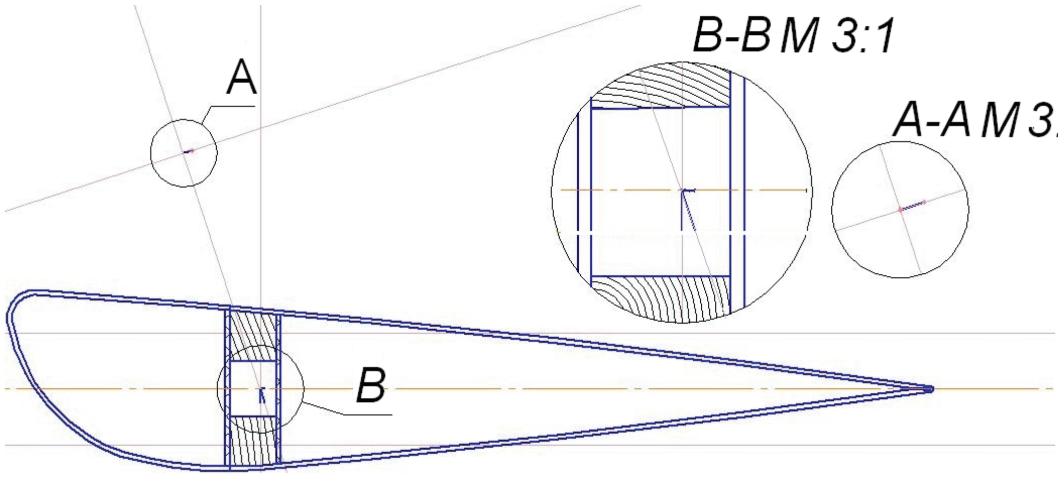

Fig.3 Finding the shoulder joint after the example of elevator of UAV M-7V5.

Necessary servo efforts depends on the length drive rocker of aerodynamic surface and rolling pin length servo, making a further determination of appropriate quite simple. The effort, which occurs at the point of connection drive rocking the elevator servo drives of traction is by dividing the value of the distance between the axis of rotation of the steering wheel height and point of connection of the traction pin (takes very extreme point of the axis of rotation):

$$F_{\kappa EV} = M_H^{EV} / h_{hEV} = 1{,}102 / 0{,}033 = 33{,}394(\mathrm{kg}). \tag{13}$$

Knowing the length of the servo pin can find the time, which should develop servo to cope with existing workloads. Servo arm has a working length of 20 mm, and by this the length of the servo arm torque, that creating by servo (or group of servo drives) must not be less than

$$M_{servo}^{EV} = F_{hEV} \times l_s^{servo} = 33{,}94 \times 0{,}020 = 0{,}6788(\mathrm{kg} \times \mathrm{m}) = 67{,}88(\mathrm{kg} \times \mathrm{cm}) \tag{14}$$

As the elevator of UAV M-7V5 structurally consists of two identical halves, then each half hinge moment is twice less, then servo for steering half height should develop torque 33.94 $\mathrm{kg} \times \mathrm{cm}$.

Conclusions. The proposed method of finding efforts on connecting rods of movable aerodynamic surfaces can be used to develop low-cost projects, where the use of wind tunnel is economically unprofitable.

References

1. *Лебедев А.А., Чернобровкин Л.С.* “Динамика полёта беспилотных летательных аппаратов”, М: Оборонгиз, 1962, – 548 с.

2. Розрахунок міцності основних силових елементів БПС М-7В5 за темою № 1/2010/П “Створення багатоцільового безпілотного літального апарату”, Київ 2011.

3. *Бадягин А А., Мухамедов Ф.А.*,“Проектирование легких самолётов”, М: Машиностроение, 1976, – 208 с.

UDC 004.62: 629.735.33-519 (043.2)

P. Prystavka, dr. of technical sciences, prof. (NAU, Ukraine);
A. Assaul, post-graduate student (NAU, Ukraine);
E. Nichikov, post-graduate student (NAU, Ukraine);
A. Rogatuk, post-graduate student (NAU, Ukraine)

COMPONENTS OF INFORMATION TECHNOLOGY PROCESSING OF DATA OBTAINED FROM UNMANNED AERIAL VEHICLE

The system of automated processing and analysis of digital images and videos obtained from the board of unmanned aerial vehicle offered.

Department of Applied Mathematics, National Aviation University offers the system of automated processing and analysis of digital images and videos obtained from the board of unmanned aerial vehicle. This system is fully developed by the department staff in conjunction with the design office "Virage", which is also a division of the National Aviation University. Next, in Figure 1 is shown the scheme with the basic building blocks of the system.

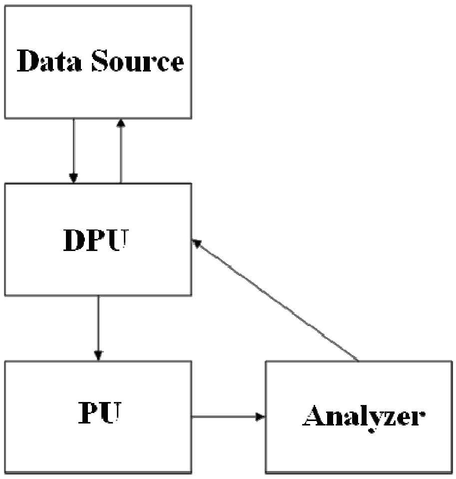

Figure 1. Basic building blocks of the system. Data Source – streaming data, this can be received from unmanned aerial vehicle. DPU – data processing unit. PU – preprocessing unit. Analyzer – data analytics unit

Data Processing Unit Data processing unit allows to solve two major issues: receive and format (or decoding) input data to make it acceptable for analyzer; format (or encoding) the resulting data for transmits it over channels of communication to the sender (UAV, ground stations, etc.). Preprocessing Unit is used for data preparation either for more effective analytics or for visual improvement of digital graphic information which is represented in structured block after DPU's work is finished. Main features are glow (Fig. 2c), digital stabilization (Fig. 2b), edge (Fig. 2c) of images and video. Main features of Analyzer, based on methods [1-3], are presented on Figure 3.

a)  b) 

c)  d) 

Figure 2. PU features. a – image without preprocessing; b – stabilized image;
c – low-pass filtering (glowed image); d – high-pass filtering (edges of image).

PU methods can significantly improve the results of Analyzer. They also can be very helpful for users of the system when processing data is not much legible or has a lot of graphical noise.

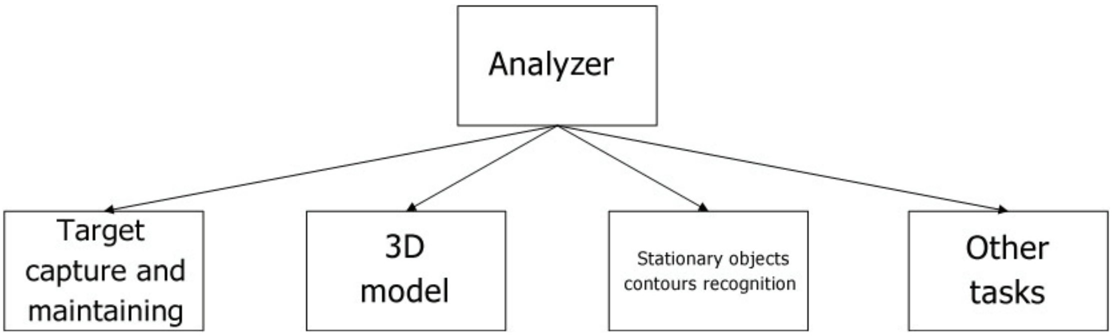

Figure 3. Basic features of Analyzer.

Here are some examples of use Analyzer. On Figure 4 video frame with feature “Target capture and maintaining” is presented. On Figure 5 is presented horizon detection which is a part of “Stationary objects contours recognition” feature.

Figure 4. Target capture and maintaining.

On Figure 4 we can see the system has detected objected and maintaining it. The system can also detect and maintaining multiple objects.

Figure 5. Video frame where horizon line has been detected

Here(Fig. 5) we can see real time detection of horizon line on the video received from design office “Virage”.

One of the important tasks of the system is texture recognition. It can be used to locate hardly noticeable to the human eye objects. As example below (Fig, 6) illustrated searching settlements at image obtained from Landsat [5] satellite.

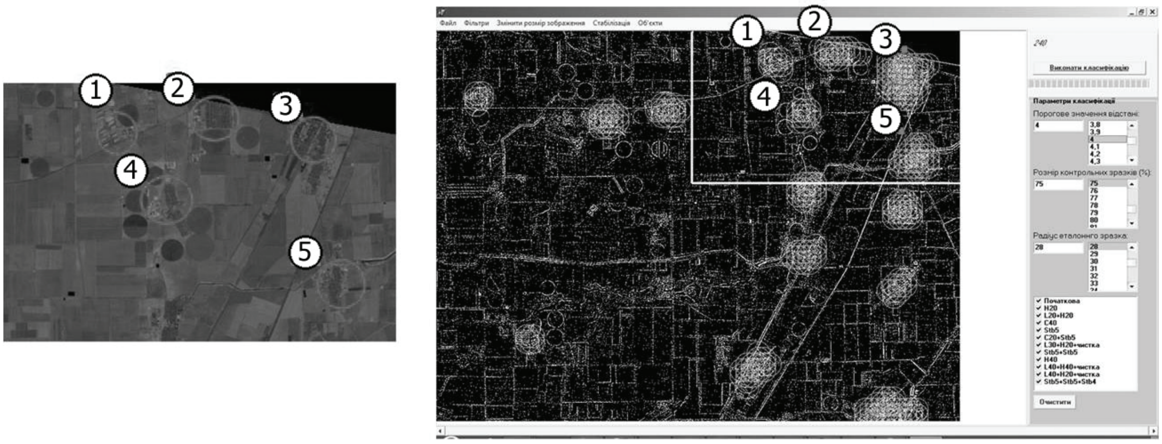

Figure 6. Example of texture recognition.

The system can be used for processing of air photo data, for example image scaling. (Fig. 7).

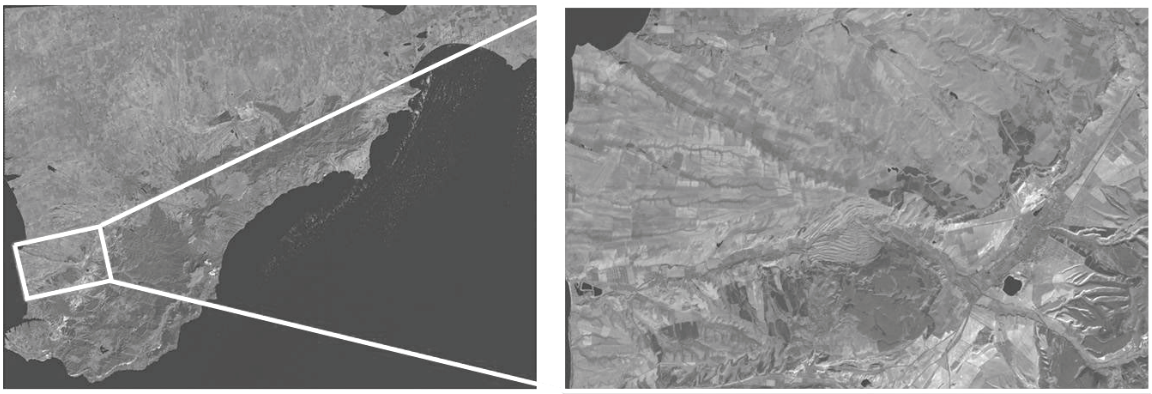

Figure 7. Scaling of a fragment of image obtained from Landsat.

The distortion of the image caused by camera angle can be removed using rectification methods. In the case of perspective rectification we need to know 4 pairs matched points on a map and on a photo. As a result, we get undistorted image, which can be used as a part of a detailed texture of 3D surface. For example, overlay the photo from “M-10 Eye” constructed in with the design office "Virage", at a fragment of a Google Maps [4] (Fig. 8).

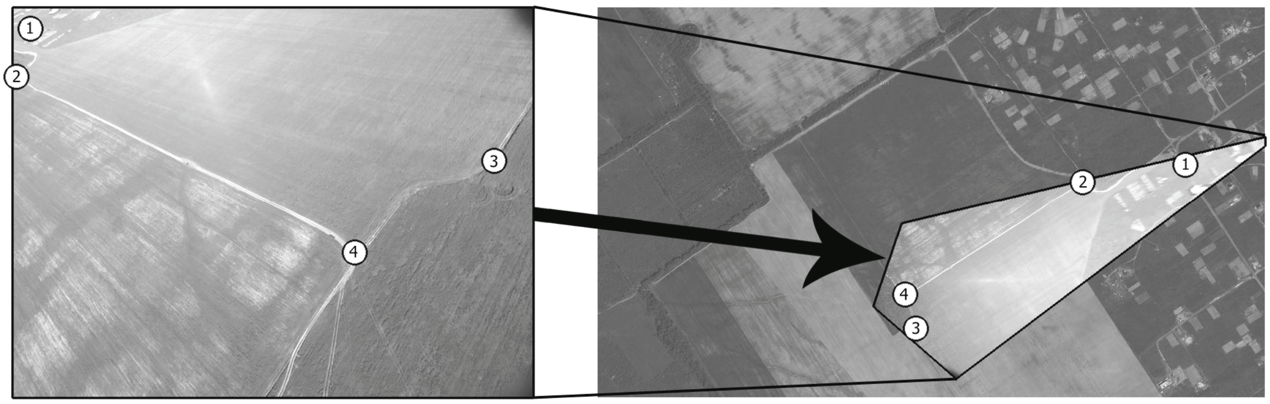

Figure 8. Perspective rectification.

Interactive three-dimensional model of terrain allows conducting flight simulation aircraft, quickly assessing the situation even in the absence of video and more. As an initial data for 3D model can be physical map and rectified photos (Fig. 9).

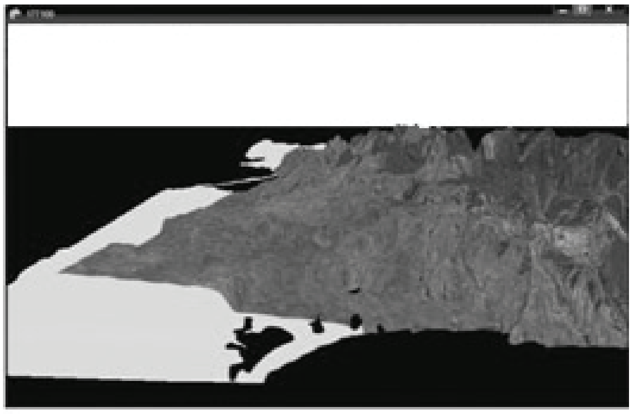

Figure 9. 3D model of Crimea with different textures.

Conclusions

The offered information technology processing of data obtained from UAV include four main components: Data Source, DPU, PU and Analyzer.

Automated system can perform preprocessing of the data, dynamic target capture and maintaining, horizon detection, texture recognition, 3D models of terrain constructing.

The results may have application in developing aircraft simulators for training pilots, navigation systems, three-dimensional catalogs of maps for quick display of remote sensing, monitoring the current status of the airspace and so on. Further research may suggest the improvement of the proposed technology for specific types of aircraft.

References

1. *Приставка П.О.* Поліномаільні сплайни при обробці даних. / *П. О. Приставка*; Д.: Вид-во Дніпропетр. ун-ту, 2004. – 236 с.

2. *Приставка П.О.* Обчислювальні аспекти застосування поліноміальних сплайнів при побудові фільтрів / *П. О. Приставка*; Зб. наук. праць. - Д.: Вид-во Дніпропетр. ун-ту, 2006. - Т.10. - С. 3-14.

3. Приставка П.О. Застосування комбінованих фільтрів на основі поліноміальних сплайнів при обробці растрових зображень / *П. О. Приставка*; Вісн. НАУ.- К.: НАУ.- 2008.- №4. -С. 104-107.

4. Google Maps: https://www.google.com/maps

The Landsat Program: http://landsat.gsfc.nasa.gov/

UDC 528.952

P. Prystavka, dr. of technical sciences, prof. (NAU, Ukraine);
E. Nichikov, post-graduate student (NAU, Ukraine)

THE AUTOMATED SYSTEM "AMAP" FOR CONSTRUCTING 3D MAPS ACCORDING TO AEROSPACE PHOTOGRAPHY

An information technology underlying the automated system "AMap" described. The information technology includes: using physical maps as initial data for 3D surface; using spatial data interpolation methods; using methods of imposing noise and low-pass filtering to model for better user perception, in particular, reducing the "stairs effect"; using digital image stabilization for improving textures quality.

Introduction. At present, a realistic three-dimensional maps can be use to develop navigation systems, three-dimensional catalogs of maps, to control current status of the airspace, in the movies and more. One of promising area is the modeling of 3D maps, where as textures can be used images obtained by unmanned aerial vehicle (UAV). Spatial models of maps based on UAV data can be components of data storage; data can be detailed or aggregated [1] to solve specific problems, such as modeling the current state of airspace, simulation runway of an airport, etc.

Images obtained from UAV, can have great resolution, which does not allow displaying them in full size. In terms of the concept of data storage, it should be noted that images the Earth's surface is a detailed data. Processing and using of such data has some difficulties. At the same time interactive spatial model is a set of aggregated data and enables the user to interact with the map, look at it from different points and angles, view some detailed fragments or the general scene.

The question of building three-dimensional map includes the construction of a model of the terrain based on geodetic measurements and overlay images of Earth's surface binding to fixed points. Also, the process of creating 3D maps can be followed by a need to solve additional problems:

1) increasing counts of relief model data (based on interpolation techniques);
2) changes in the representation of 3D models which contribute to a better perception of the user (the effects of "noise", "smooth", etc.);
3) procedures for handling texture (quality improvement).

The automated system "AMap" implements the methods to solve the issues described above.

Problem. As mentioned, to create three-dimensional maps need to construct a spatial model of the terrain and to bind it to image the Earth's surface. Steps of constructing 3D map are in Fig. 1:

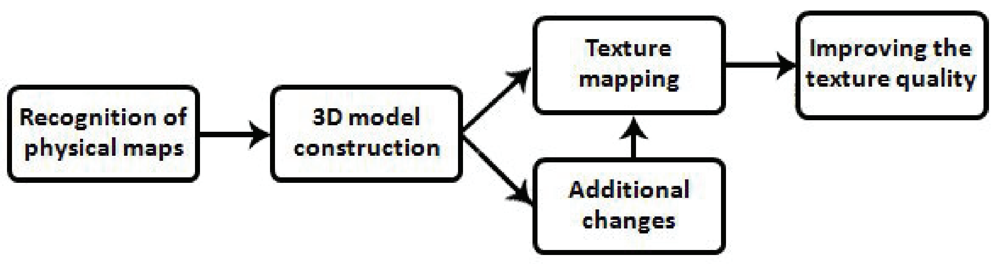

Figure 1. Steps of constructing three-dimensional map.

One of the instruments of the initial data for the model topography is digitizing electronic physical map with the defined heights scale. Physical map is a map that is presented as a schematic diagram of a location and scale heights. In compliance with each color of the heights scale supplied range of heights (Fig. 2).

For definiteness, assume that the physical map presented as bitmap with RGB color model. Denote $p_{i,j}$, $i=\overline{0,W-1}$; $j=\overline{0,L-1}$ - intensity of color pixel component, where W, L - linear dimensions of the image. Let is a digital high resolution image; obtained from remote sensing (e. g.

Landsat) that determines the sample surface of the Earth. Hereinafter we will call this the image texture in terms of texture of 3D model. Denote $p^*_{i,j}$, $i=\overline{0,W^*-1}$; $j=\overline{0,L^*-1}$ - intensity of color pixel component (R, G, or B), where W^*, L^* - linear dimensions of the texture.

Three-dimensional coordinates will be denoted in the Cartesian coordinate system where axes x and z correspond to the width and length of the map and axis y - height above sea level.

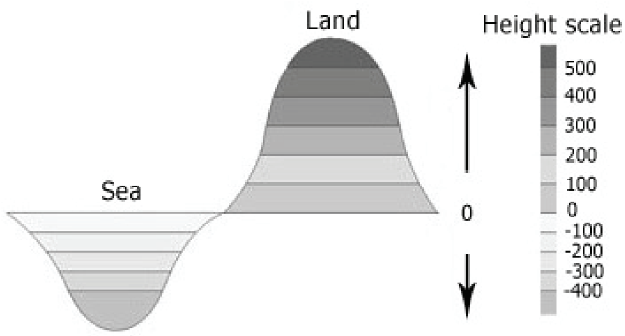

Figure 2. Height scale at a physical map.

There is necessary to develop information technology for construction 3D maps, which allow:

1) recognition of electronic physical map and identification of the heights scale;
2) build a model of spatial locality by using obtained data;
3) binding of realistic textures and the constructed model;
4) improve the quality of overlay texture;
5) changes in the 3D models that contribute to a better perception of the user.

Purpose of article is a description of information that underlies automated system “AMap”.

Basic material. As mentioned the issue of building three-dimensional map includes the construction of a model of the terrain based on survey research and the task of overlay a picture of the Earth's surface by binding fixed point. Next, consider the steps to create 3D maps according to the induced (Fig. 1).

Recognition of physical maps. At this stage there is the task of mapping data in a physical map with spatial coordinates. Put w and l - linear dimensions on axis x and z of fragment spatial models that corresponds to one pixel. Analyzing the height scale, each (i, j) pixel ($i=\overline{0,W-1}$; $j=\overline{0,L-1}$) of physical maps with the intensity of color component $p_{i,j}$ match to the height $h_{i,j}$.

Color of an input image pixel may not coincide with the color from heights scale, for example, if the map has conditional tags, pictures of rivers, city names and other symbols. Then recursively analyzes color values of neighboring pixels, until found necessary value of height.

Build a 3D model. There are many graphics accelerators with hardware to paint 3D objects, removing invisible parts, binding texture etc.

In the previous step was obtained $h_{i,j}$; $i=\overline{0,W-1}$; $j=\overline{0,L-1}$ – the set of points which are formed by a uniform grid. Quite easy to build a triangles network on these points:

$$h_{i,j}h_{i+1,j}h_{i,j+1}, \ldots;\ i=\overline{0,W-2};\ j=\overline{0,L-2}.$$

By using software (DirectX, OpenGL, etc.) these polygonal areas are transferred for further processing accelerator that lets you take advantage of 3D-accelerators [2].

Texture mapping. Rectification may be considered as a transformation process of digital images carried out to obtain distortion of the images. Transformation parameters are obtained by using control points on the uncorrected raw image and their corresponding points on the map. There are three commonly used approaches to perform rectification process. These methods are polynomial, projective, and differential rectifications [3].

Projective transformation is defined by eight parameters, which can be derived from four object points lying in a map and their corresponding texture image coordinates. At the end of the geometric transformation, to obtain the pixel values (gray level values, intensities or color values) of the new image, a radiometric resampling is required. For this purpose, interpolation techniques are used (e.g. interpolation methods based on local polynomial splines, which are close to the average [4]). The rectification of image obtained from Landsat satellite [5] is on Fig. 3.

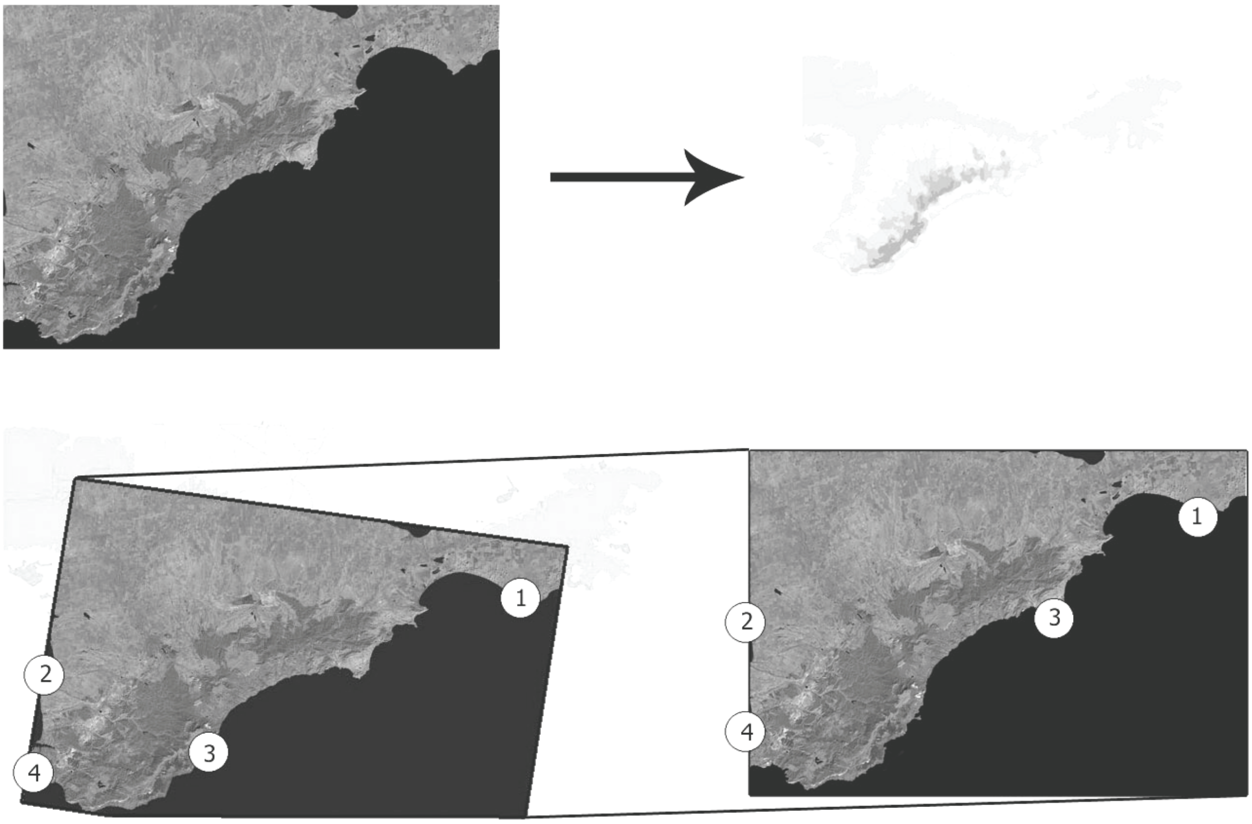

Figure 3. Rectificaton of a texture.

Additional changes. The following changes in the representation of 3D models contribute to a better perception of the user, but not a means of increasing its details. Their use depends on the problem that faces a particular realization of the spatial models.

Imposition of noise. Electronic physical maps contain information about a limited number of sections of height. For visual improvement resulting spatial models, and reduce the "stairs effect" (Fig. 4.a) suggested imposing a random normally distributed noise, which depends on the height of points on which it is imposed, i.e. $\tilde{h}_{i,j} = h_{i,j} + \varepsilon_h$, $i = \overline{0, W-1}$, $j = \overline{0, L-1}$ where $\varepsilon_h = N(0, \sigma_\varepsilon)$ - normalized random variable with mean square deviation $\sigma_\varepsilon = \varphi(h)$ - a function of height, which is chosen so that any values of ε_h didn't go beyond the corresponding section of the heights scale.

Smoothing. After the imposition of noise possible to conduct smoothing of sequence $\tilde{h}_{i,j}$, $i = \overline{0, W-1}$, $j = \overline{0, L-1}$ using of low-frequency filters, to provide "realistic" look of the model. For example [6]:

$$\tilde{h}^*_{i,j} = \sum_{ii=i-r_i}^{i+r_i} \sum_{jj=j-r_j}^{j+r_j} \gamma_{ii-i,jj-j} \tilde{h}_{ii,jj}, \; i = \overline{r_i, W-r_i-1}; \; j = \overline{r_j, L-r_j-1};$$

$(2r_i+1) \times (2r_j+1)$ - size of mask of low-frequency filter; γ - filter mask.

Increasing the number of samples. In general, the number of pixels electronic physical map does not match the number of pixels of a texture: $W \neq W^*$ and $L \neq L^*$. Accordingly, the dimension sequence of h is less than the dimension of texture overlay. To increase the number of periods h is a need for methods of interpolation. To ensure the performance of calculations it is expedient to use a)

b)

c)

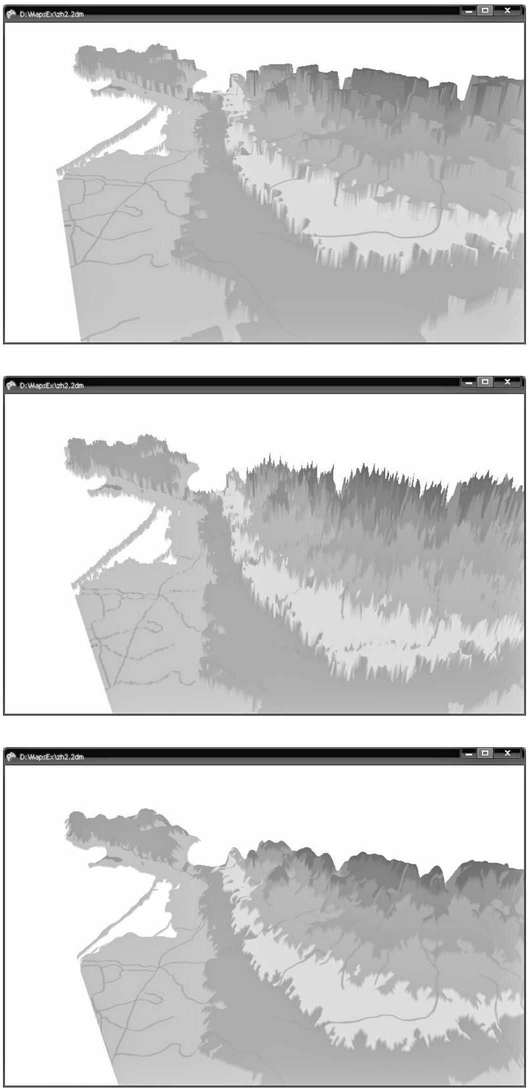

Figure 4. Constructed 3D model with mapped texture: a) intact; b) noisy, c) noisy and smoothed.

the local approximation methods, in particular, to apply local polynomial splines of two variables based on B-splines that, on average, are related to interpolar [4], which can complement the array of vertices of the spatial model to the image size. Algorithms based on these splines have a great performance due to the low number of arithmetic operations and can operate in real time.

Improving the texture quality. The texture obtained by spacecraft may be distorted due to camera movement. This defect is a common on not fixed shooting or shooting from a platform that can be subject to some mechanical effects, such as microvibrations. The result of such defects can be eliminated or at least greatly reduced, not only hardware but also the mathematical processing procedures that operate in real time.

Assume that the distortion caused by the camera movement, i.e. impose a random low-pass filter:

$$p^*_{i,j} = Low(p^0_{i,j})\ ;\ i=\overline{0,W^*-1};\ j=\overline{0,L^*-1},$$

$p^0_{i,j}$ – color components of the ideal undistorted image.

Denote $\left\{\tilde{p}^*_{i,j}\right\}_{i=\overline{0,W^*-1},\, j=\overline{0,L^*-1}}$ – sequence of the color component raster after stabilization. In [7] presented linear operators such that $\tilde{p}^*_{i,j} = C(p^*_{i,j})$, and implemented: $\tilde{p}^*_{i,j} \approx p^0_{i,j}$; $i=\overline{0,W^*-1}$; $j=\overline{0,L^*-1}$, for random mask χ:

$$C(p^*_{i,j}) = \sum_{ii=i-r_i}^{i+r_i} \sum_{jj=j-r_j}^{j+r_j} \chi_{ii-i,jj-j}\, p^0_{ii,jj}\ ;\ i=\overline{r_i, W-r_i-1}\ ;$$

$j=\overline{r_j, L-r_j-1}$.

Software. An automated system “AMap” designed to detect patterns of digital physical maps, identifying the height scale and build three-dimensional models by using obtained data. The system consists of two separate applications, which can operate independently of each other. The first application MapCreator (Fig. 5) implementing electronic identification of physical maps in JPEG or BMP image and save data in file 2dm format.

The second application Map3DBuilder (Fig. 4) allows you to read data from a file 2dm format and implements methods of construction and transformation of the spatial model (blending textures, noisy, smoothing, etc.). System requirements for the second application: CPU: Pentium with a clock speed of at least 1GHz or equivalent processor, RAM: at least 96 MB (256 MB recommended) Operating System: Windows XP Service Pack 3 or higher; screen: resolution 800 x 600, 256 colors, graphics card: DirectX 9.0c with support and support for pixel shader version 1.1. Required Components: Microsoft. NET Framework 3.5 or higher; Microsoft XNA Framework Redistributable 3.0 [8].

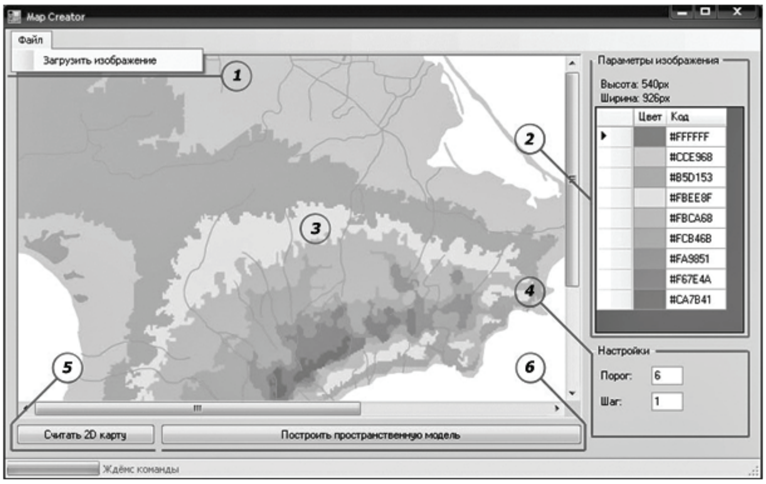

Figure 5. The main window of the first application (1 - home page 2 - picture settings;
3 – workspace; 4 - adjustment; 5 - map reader, 6 - build a 3D model)

Conclusions

An automated system "AMap" implements information technology that includes: using of digitized data of physical maps as maps heights 3D surface; using spatial data interpolation methods based on local polynomial spline interpolation close to the average increase in the number of periods for which there is modeling 3D surface; the methods of imposing noise and low-pass filtering methods to better model the user perception, in particular, reducing the "stairs effect"; using digital image stabilization for improved overlay textures.

The results may have application in developing aircraft simulators for training pilots, navigation systems, three-dimensional catalogs of maps for quick display of remote sensing, monitoring the current status of the airspace and so on. Further research may suggest the development of automated air traffic navigation systems, weather simulation, modeling take-off and landing aircraft, and more.

References

1. Технологии анализа данных: Data Mining, Visual Mining, Text Mining, OLAP / *А. А. Барсегян, М. С. Куприянов, В. В. Степаненко, И. И. Холод*/ - 2-е изд., перераб. и доп. – СПб.: БХВ-Петербург, 2007. – 384 с.

2. *Энджел Э.* Интерактивная компьютерная графика. Вводный курс на базе OpenGL. / Пер. с англ. – 2-е изд. – М.: Вильямс, 2001. – 532 с.

3. *Mahir Serhan Temiz* Rectification of Digital Close Range Images: Sensor Models, Geometric Iimage Transformations and Resampling / *Mahir Serhan Temiz, Sıtkı Külür* - The International Archives of the Photogrammetry, Remote Sensing and Spatial Information Sciences. Vol. XXXVII. Part B5. Beijing 2008.

4. *Приставка П.О.* Полиномаільні сплайни при обробці даних. / *П. О. Приставка*; Д.: Вид-во Дніпропетр. ун-ту, 2004. – 236 с.

5. The Landsat Program: http://landsat.gsfc.nasa.gov/

6. *Приставка П.О.* Обчислювальні аспекти застосування поліноміальних сплайнів при побудові фільтрів / *П. О. Приставка*; Зб. наук. праць. - Д.: Вид-во Дніпропетр. ун-ту, 2006. - Т.10. - С. 3-14.

7. Приставка П.О. Застосування комбінованих фільтрів на основі поліноміальних сплайнів при обробці растрових зображень / *П. О. Приставка*; Вісн. НАУ.- К.: НАУ.- 2008.- №4. -С. 104-107.

8. Microsoft XNA Framework Redistributable 3.0: http://www.microsoft.com/en-us/download/details.aspx?id=22588

UDC 629.735.33-519:004.93'1(045)

O. I. Benesyuk, postgraduate student,
(National Aviation University, Ukraine)

OBJECT RECOGNITION METHODS AND THEIR APPLICATION IN UNMANNED AIRCRAFT SYSTEMS

Object recognition is an important task for enhancement of UAS capabilities and operation safety. The aim of this report is to summarize and compare some of the well-known methods used at different stages of object recognition process and to identify the possibilities of their application in unmanned aircraft systems. Some advantages and disadvantages of these techniques are presented.

Unmanned aircraft systems (UAS) represent the new component of global aviation system. They can provide additional benefits to many industries as well as public sector. UAS are a cheaper alternative to manned aircraft, and are ideally suited for dangerous missions that would be challenging for a human pilot.

Military industry was the pioneer in the use of unmanned aviation, and now the domain of its civil use is expanding rapidly. Today, UAS may be applied for farming, aerial photography, environmental and security monitoring, firefighting and rescue operations, film industry, etc.

However, the use of UAS sets new challenges. Ground collisions and midair collisions present the main UAS operation related hazards with respect to public safety. Both constitute significant hurdles on the way of UAS integration into unsegregated airspace. Effective object recognition system will help to improve both safety of UAV operation and quality of rendered services.

General Process of Object Recognition

The basic components in object recognition are pre-processing, feature extraction and selection, classifier design and optimization. Pre-processing involves noise filtering; smoothing and normalization. Classification problem is the main component of object recognition. The aim of classification process is to extract patterns and to differentiate classes of objects.

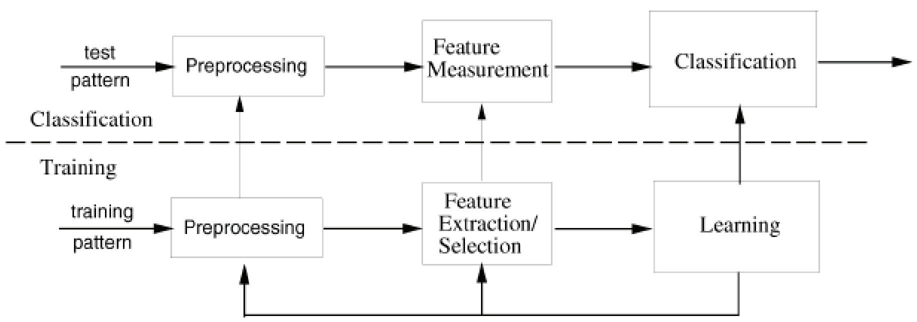

Figure 1. Schematic diagram of statistic pattern recognition process.

Pattern recognition task is often solved by statistic methods, such as template matching, linear and quadratic discriminants, Parzen density estimator, the k-nearest neighbor classifier, and Neural Networks [3].

However these methods are not always convenient, because classification rule has to be designed without knowing the distribution of the measurements in different groups. Recently, Support Vector Machines (SVM) [8] have become very popular in classification processes as they have significant advantages if compared to template matching or even Neural Networks.

Pre-processing

Pre-processing is used for selection of the object of interest from the background. This stage usually includes noise filtering, smoothing and normalization.

Feature selection and extraction

Feature selection is a process that selects a subset of original features. Its final objective is to select the optimal features subset with the help of which the highest accuracy may be obtained.

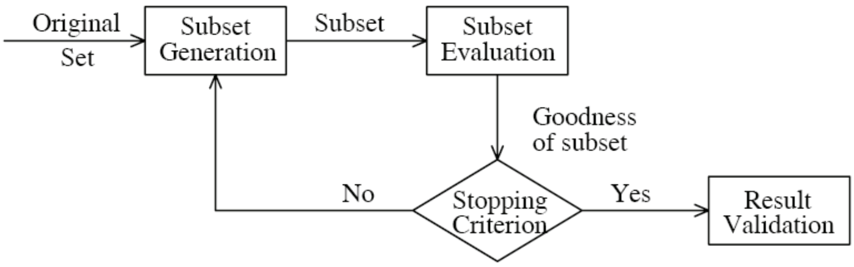

Figure 2. Schematic diagram of feature selection stage.

Filter and wrapper are the two most well known types of feature selection methods [5][8]. Filter methods select the most suitable features according to prior information and their performance is not connected with the classification algorithm.

Feature extraction methods determine an appropriate subspace of dimensionality m in the original feature space of dimensionality d ($m \leq d$). Most of the feature extraction methods are supervised methods. These methods require prior knowledge and training examples with labels. Linear feature extraction method is based on Principal Component Analysis (PCA), Linear Discriminant Analysis, Independent Component Analysis, and project pursuit. Since PCA uses the most expressive features (eigenvectors with the largest eigenvalues), it effectively approximates the data by a linear subspace using the mean squared error criterion [3]. The projection pursuit and independent component analysis (ICA) are more appropriate for non-Gaussian distributions as they do not rely on the second-order property of the data. Among nonlinear feature extraction methods Kernel Principal Component Analysis is used most often. The main idea of kernel PCA is to first map input data into some new feature space F typically via a nonlinear function Φ and then perform a linear PCA in the mapped space. However, the F space often has a very high dimension. To avoid computing the mapping Φ explicitly, kernel PCA employs only Mercer kernels which can be decomposed into a dot product,

$$K(x,y) = \Phi(x) \cdot \Phi(y)$$

As a result, the kernel space has a well-defined metric. Other methods of nonlinear feature extraction include Principal Component Analysis network, nonlinear Principal Component Analysis, nonlinear auto-associative network, Multi-Dimensional Scaling and Self-Organizing Map, etc.

Classification

Many different methods can be used to design a classifier. Let us discuss three most frequently used methods.

The first method is grounded on the similarity principle (template matching). In template matching, a prototype of the pattern to be recognized is available. An object to be recognized is matched against the stored template while taking into account all allowable changes in position and scale.

If all of the class-conditional densities are completely specified, then the optimal Bayes decision rule can be used to design a classifier [3]. However, the class-conditional densities are usually not known in practice and must be learned from the available training patterns. The optimal Bayes decision rule for minimizing the risk of losses can be stated as follows: Assign input pattern x to class ω_i for which the conditional risk

$$R(\omega_i|x) = \sum_{j=1}^{c} L(\omega_i, \omega_j) \cdot P(\omega_j|x)$$

is minimum, where $L(\omega_i, \omega_j)$ is the loss incurred in deciding ω_i, when the true class is ω_j and $P(\omega_j|x)$ is the posterior probability.

The third method involves construction of decision boundaries by optimizing certain error criterion (Fisher’s linear discriminant, multilayer perceptrons, support vector machine).
SVM is one of the most efficient methods as it allows training of generalizable, nonlinear classifiers in high dimensional spaces with the help of a small training set. SVMs generalization error is not related to the dimension of input, but to the boundary with which it separates the data. Thus, SVMs can work well even with a large number of inputs.

In order to reduce the computational load for object recognition many different approaches are used [9][10]. Examples are k-nearest neighbor method, Parzen Window, Clustering, pairwise nearest neighbor (PNN) and Branch-and-bound. K-nearest neighbor method's disadvantage is that the distance must be calculated between an unknown and every prototype each time a sample is recognized. Parzen Window depends on the Kernel function and on the value of the window width. It allows us to obtain complex nonlinear decision boundaries. Clustering method aims at partitioning a given set of N data into M groups so that similar vectors are grouped together.

The main idea of pairwise nearest neighbor method the PNN can be generalized so that we can optimize multi-merging steps. Branch-and bound method employs a search tree for finding the optimal clustering and generates clustering through a series of merging operations.

Optimization

The optimization is performed on each stage of pattern recognition process. In pre-processing, optimization yields best quality of input pattern; optimization techniques are applied during feature selection and extraction stages in order to get optimal feature subsets. During classification stage the task is to minimize classification error.

Application in UAS

Designing of optimal UAS object recognition system is a challenging, but rewarding task. Object recognition system may be applied in navigation and control systems of UAV, allowing autonomous visual guidance and enhanced situation awareness. Since landing is the most critical stage during UAV flight, many studies and publications are focused on runway recognition for autonomous landing [1][6][11]. In [6] a detecting method based on runway area and characteristic points, which makes full use of the runway information and reduce the time of Hough transform is proposed. The combination of Hough transform and least square fitting guarantees the accuracy of the extraction of runway boundaries.

Object recognition from video data allows target detection and tracking [2][4]. In [7] authors proposed to use video data to train a target detection algorithm and measure parameters for an observation model that describes its efficiency. Then a recursive Bayesian estimator to fuse a series of detections over time application was applied, taking into account the observation model and associated with the altitude at which the observations occur.

Conclusion

Intelligent analysis of images provides a lot of mission-specific information and may help to deal with failures of the other sensors onboard the UAV. As safety, cost, and weight are main factors of UAS development it is very important to make use of visual sensors as they provide additional capabilities along with additional safety through situation awareness. Application of object recognition systems will allow more autonomy en-route and during landing, which is a critical stage.

Some of the methods for pattern recognition were discussed and compared. The main idea is that the quality of solution obtained depends on the relevance of patterns and the quality of features subsets obtained. Based on this summary of different methods, a combination of different methods may provide better solutions. Thus, complex object recognition systems that combine several techniques should be developed.

References

1. Andrew Miller and Mubarak Shah and Don Harper. *"Landing a UAV on a Runway Using Image Registration".* Robotics and Automation, 2008. ICRA 2008. IEEE International Conference on Robotics and Automation, p. 182 – 18.

2. Andrew Symington, Sonia Waharte, Simon Julier, Niki Trigoni, "Probabilistic search with agile UAVs*"* 2010 IEEE Conference on Robotics and Automation, Achorage Convention District, Anchorage, Alaska USA, 2010, p. 2840 -2845.

3. Anil K. Jain, Fellow, Robert P.W. Duin, and Jianchang Mao, "Statistical Pattern Recognition: A Review", IEEE Transactions on Pattern Analysis and Machine Intelligence, VOL. 22, No. 1, January 2000, 37 p.

4. *Feng Lin, Ben M. Chen, Tong H. Lee,* Robust "Vision-Based Target Tracking Control System for an Unmanned Helicopter Using Feature Fusion", MVA2009 IAPR Conference on Machine Vision Applications, May 20-22, 2009, Yokohama, JAPAN

5. Huan Liu and Lei Yu, "Toward Integrating Feature Selection Algorithms for Classification and Clustering", Department of Computer Science and Engineering, Arizona State University, 2004, 35 p.

6. Jiajia Shang, Zhongke Shi "Vision-based Runway Recognition for UAV Autonomous Landing", IJCSNS International Journal of Computer Science and Network Security, VOL.7 No.3, March 2007

7. Jiangjian Xiao, Changjiang Yang, Feng Han, and Hui Cheng, "Vehicle and Person Tracking in UAV Videos", Classification of Events, Activities, and Relationships Evaluation and Workshop, Baltimore, 2007.

8. L.Ladha, T.Deepa, "Feature Selection Methods and Algorithms**"** International Journal on Computer Science and Engineering (IJCSE), Vol. 3 No. 5 May 2011, p.1787 -1797.

9. Lihong Zheng and Xiangjian He, "Classification Techniques in Pattern Recognition**",** Conference proceedings ISBN 80-903100-8-7, WSCG'2005, Plzen, Czech Republic. p. 2.

*10. Pasi Fränti, Olli Virmajoki, "*Optimal clustering by merge-based branch-and-bound", Department of Computer Science, University of Joensuu, Finland 2004, p. 18.

11. Srikanth Saripalli, James F. Montgomery, Gaurav S. Sukhatme *"Vision-based Autonomous Landing of an Unmanned Aerial Vehicle"*, Robotic Embedded Systems Laboratory, Robotics Research Laboratory, Department of Computer Science, University of Southern California; Jet Propulsion Laboratory, California Institute of Technology, Los Angeles, CA. 2002

UDC 656. 7.085: 657.71 (045)

M.P. Matijchyk, Ph. D.
V.V. Kabanyachyi, Ph. D.
D.M. Matijchyk
(National Aviation University, Ukraine)

CONCEPTION OF LICENSING OF CIVIL REMOTE PILOTS

A structure of unmanned aircraft system and processing of information by pilot are described. On the grounds of developed structure of unmanned aircraft piloting the conception of licensing of civil remote pilots is developed.

Formulation of the problem. In 1910, inspired by the success of the Brothers Wright young American military engineer from Ohio, Charles Kettering proposed to use an aircraft without a human. Airplane controlled by clockwork at the specified location should drop wings and fall like a bomb on enemy. After gaining support and funding from the U.S. Army he built and tested several models that have received the names of The Kettering Aerial Torpedo, Kettering Bug.

Currently, there is rapid growth in interest in the use of unmanned aircraft systems (UAS) by various organizations that already make their purchase and training of personnel for their operation. As a result of this, the use of unmanned aircrafts (UA) in the civilian sector is currently awaiting the decision of some technical and organizational problems, including licensing of civil remote pilots without which any sustainable use of UA.

Analysis of recent researches and publications. Currently, UA can be divided into two groups: one for flights within visual line of sight and second for flights beyond visual line of sight [1]. Such distribution suggests the use of different control systems. Despite all the dissimilarity of control systems a unity in the methods and techniques of piloting in these cases are kept [2]. This leads to the conclusion about the need to develop a generalized method of both training and licensing of civil remote pilots.

A high and uniform level of both training and licensing should at all times be ensured in civil aviation, by the adoption of common safety rules and by measures ensuring that products, persons and organizations in the Ukraine comply with such rules. This should contribute to facilitating the free movement of goods, persons and organizations in the internal market. The Chicago Convention already provides for minimum standards to ensure the safety of civil aviation. Ukraine essential requirements and rules adopted for their implementation should ensure that Ukraine fulfills the obligations created by the Chicago Convention [3].

Statement of problem. The Ukraine should lay down, in line with standards and recommended practices set by the Chicago Convention, essential requirements applicable to aeronautical products, parts and appliances, to persons and organizations involved in the operation of aircraft, and to persons and products involved in the training and medical examination of pilots.

It would not be appropriate to subject all UA to common rules, in particular UA that are of simple design or operate mainly on a local basis, and those that are home-built or particularly rare or only exist in a small number; such UA should therefore remain under the regulatory control. Consideration should in particular be given to USs with a low maximum take-off mass, which are produced in an industrial manner. UAs involved in commercial air transport, as well as pilots and persons, products and organizations involved in their training and medical examination, should be certified or licensed once they have been found to comply with essential requirements to be laid down by the Ukraine in line with standards and recommended practices set by the Chicago Convention. A person undertaking training to fly an UA must be sufficiently mature educationally, physically and mentally to acquire, retain and demonstrate the relevant theoretical knowledge and practical skill.

Presentation of the main material. An UA defines as one that is operated without the possibility of direct human intervention from within or on the aircraft. ICAO have adopted the term

UAS to designate them as aircraft and to recognize that a UAS includes not only the airframe, but also the associated elements—the control station and communications links – as shown in figure 1.

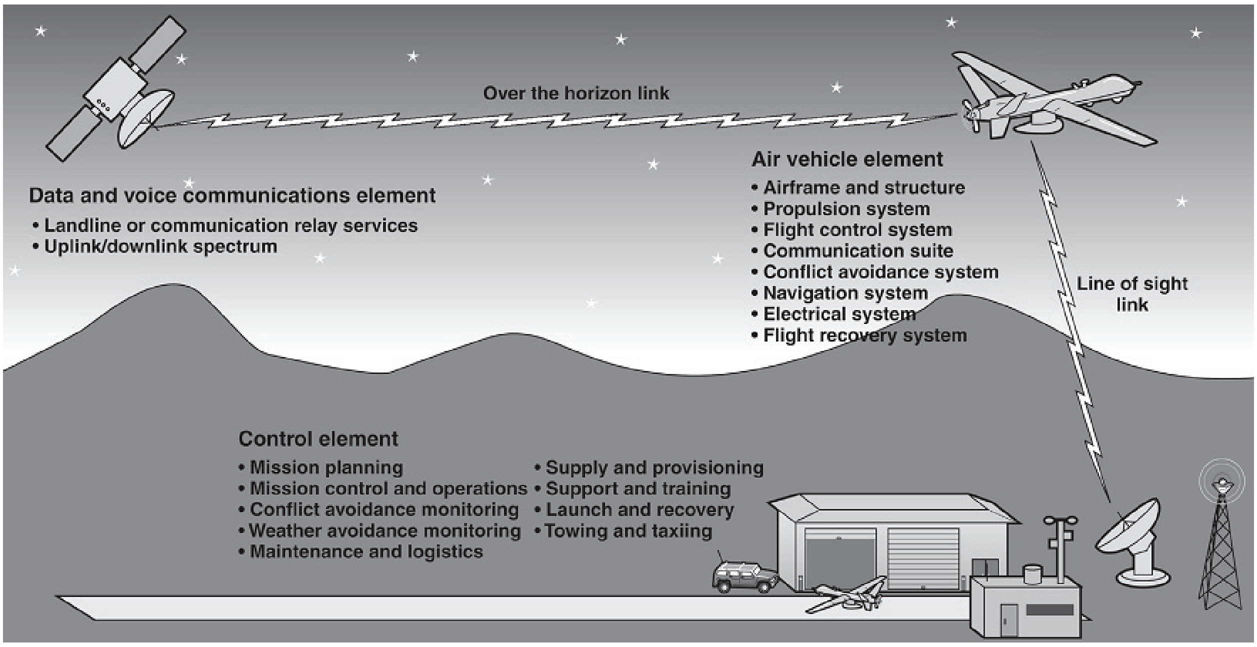

Figure 1. Conceptual Unmanned Aircraft System [4]

In the simplest form a control process is considered (Figure 2) as the processing of information about attitude and movement of UA, operation of its systems. It consists of three main stages [5, 6, 7]:

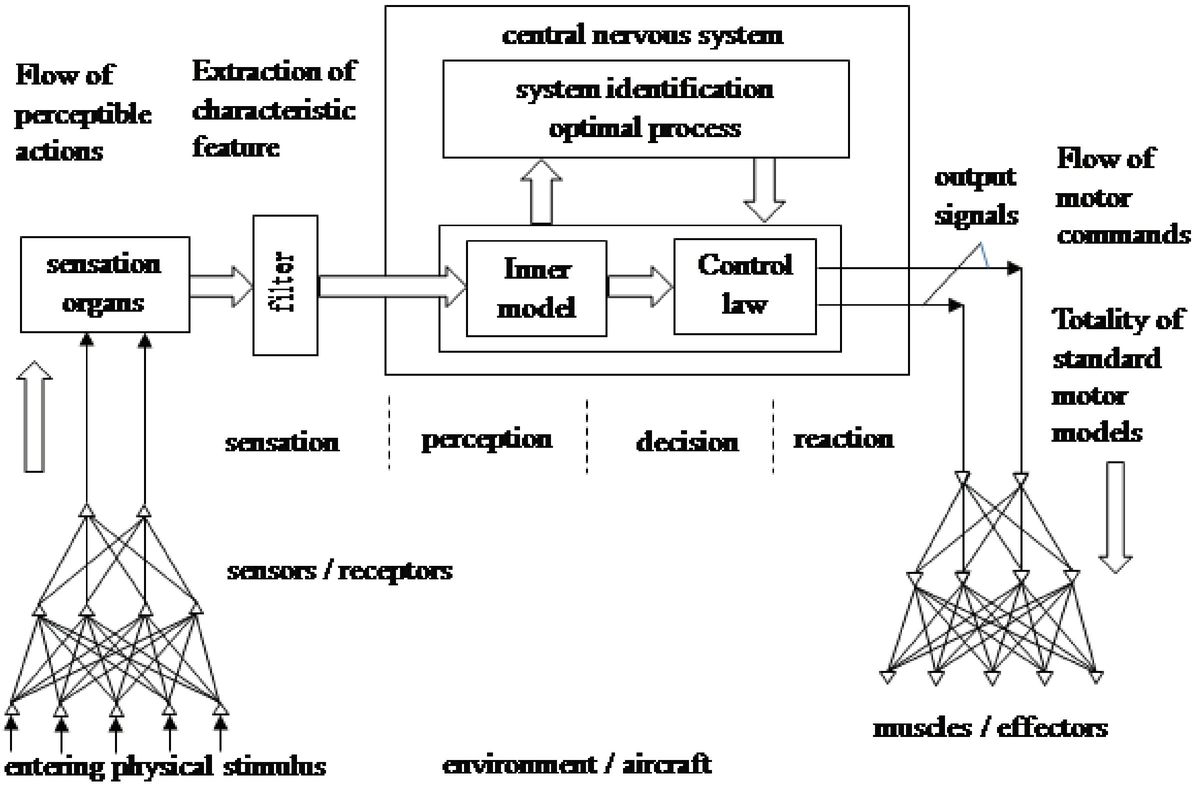

Figure 2. Processing of information by pilot

* Perception of information from environment and instrumentations about attitude and movement of UA, operation of its systems;

* Formation of notion about both state and regime of flight and decision-making on the necessary control action (if the pilot is aware the situation the decision in most cases is simple) based on perception, past experience and comparison of received information with pilot's inner conceptual flight model;

* Implementation of controls that is action on the controls to provide the necessary UA movement, and checkup of its results.

The process structure of UA piloting is shown in Figure 3. The process is a sequence of external pilot actions for detection the UA attitude and subsequent correction of this attitude by remote control system. Deviation signal is the discrepancy between the actual and desired UA attitude. Comparison is conducted by means of both visual and partially hearing analyzers that transfer information to the central nervous system of remote pilot.

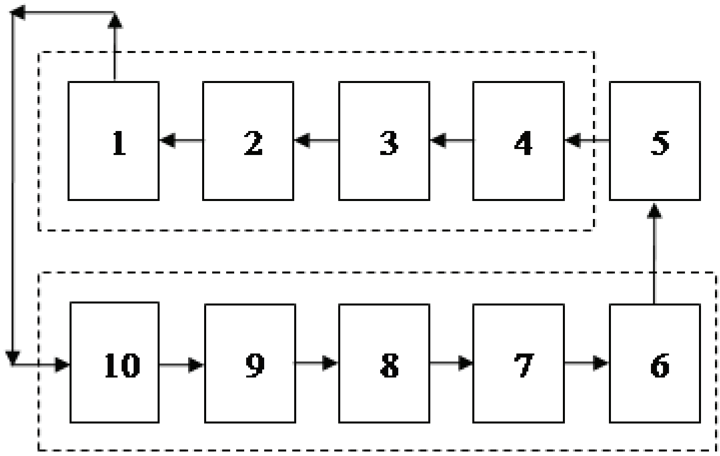

Figure 3. Structure of UA piloting:
1 – UA attitude;
2 – UA control surface deflection;
3 – UA servo mechanism;
4 – UA part of remote control system (receiver);
5 – command and control line;
6 – ground part of remote control system (transmitter);
7 – executive controls (remote pilot hands);
8 – central nervous system of remote pilot;
9 – peripheral nervous system of remote pilot;
10 – analyzers of remote pilot

Actually the remote control system itself is a transmitting-receiving device, transmitting part of which is on the ground control station, and receiving one is on the UA. Command and control line is used to transfer data between the UA and ground control station for UA flight control.

Mobile ground control station are used for flights within visual line of sight. In this case the transmitter of the remote control system equipped with two controls which are deviated by remote pilot hands from a neutral position in two mutually perpendicular directions. The controls allow using simultaneously all three channels of UA control surfaces and control channel of engine control lever. Besides for rapid turn of support functions, important lever or push-button switches may be installed on the tips of the main controls that allow switching them without removing the hand from the main levers. So actually in the process of UA control a pilot use visual and hearing analyzers, and commands executed by the fingers of both hands.

Obviously, as a criterion of the training of UA ground staff may be proposed a set of knowledge required for effective and safe operation of UA that the same criterion for training of manned aircraft.

Conclusions

A remote pilot must acquire and maintain a level of knowledge appropriate to the functions exercised on the UA and proportionate to the risks associated to the type of activity. Such knowledge must include at least the following:

- air law;
- UA general knowledge;
- flight performance and planning;
- human performance and limitations;
- meteorology;

- navigation;
- operational procedures;
- principles of flight;
- communications;
- general flight safety; and
- knowledge of specific UAS.

The acquisition and retention of theoretical knowledge must be demonstrated by continuous assessment during training, and where appropriate, by examinations. An appropriate level of competence in theoretical knowledge must be maintained. Compliance must be demonstrated by regular assessments, examinations, tests or checks.

A remote pilot must acquire and maintain the practical skills as appropriate to exercise his functions on the UA. Such skills must cover the following:

- pre-flight and in-flight activities, including UA performance, mass and balance determination, UA inspection and servicing, fuel planning, weather appreciation, route planning, airspace restrictions and runway availability;
- aerodrome and traffic-pattern operations;
- collision avoidance precautions and procedures;
- control of the UA by external visual reference;
- flight manoeuvres, including in critical situations, and associated 'upset' manoeuvres, as technically achievable;
- normal and cross-wind take-offs and landings;
- flight by reference solely to instruments;
- operational procedures, as appropriate to the type of operation;
- navigation and implementation of rules of the air and related procedures, using as appropriate, visual reference or navigation aids;
- abnormal and emergency operations, including simulated UA equipment malfunctions;
- compliance with air traffic services and communications procedures;
- UA type or class specific aspects;
- additional practical skill training that may be required to mitigate risks associated with specific activities; and
- non-technical skills, including the recognition and management of threats and errors, using an adequate assessment methodology in conjunction with the technical skills assessment.

References

1. Беспилотные авиационные системы (БАС), Циркуляр 328 // Док. ИКАО AN 190, 2011 – 66 с.

2. REGULATION (EC) No 216/2008 OF THE EUROPEAN PARLIAMENT AND OF THE COUNCIL of 20 February 2008 on common rules in the field of civil aviation and establishing a European Aviation Safety Agency, and repealing Council Directive 91/670/EEC, Regulation (EC) No 1592/2002 and Directive 2004/36/EC – 79 p.

3. Конвенция о международной гражданской авиации // Док. ИКАО 7300/8, 2000.

4. Unmanned Aircraft Systems. Accountability Integrity Reliability Federal Actions Needed to Ensure Safety and Expand Their Potential Uses within the National Airspace System (www.gao.gov/fraudnet/fraudnet.htm)// GAO-08-511, May 2008 – 73 p.

5. Ошибка пилота: человеческий фактор / Пер. с англ. А.А. Щеброва. – М.: Транспорт. – 1986. – 262 с.

6. Пономаренко В.А., Лапа В.В. Профессия – летчик: Психологические аспекты. – М.: Воениздат. – 1985. – 136 с.

7. Curry R.E., Hoffman W.C., Young L.R. Pilot Modeling for Manned Simulation// AFTDL TR-76-124. – 1976.

UDC 681.5.015: 378

O.M. Savinov, Ph.D.
T.I. Kharlamova, senior lecturer
(National Aviation University, Ukraine)

THE MODES OF VALIDITY OF REGULATORY REQUIREMENTS IN REGARD TO SPECIALIST TRAINING WHEN UNMANNED AIRCRAFT COMPLEXES OPERATING

Possibility of methods using of the optimization modeling for numerical validity of unmanned aircraft specialists training standards is analyzed.

Problem definition.

Expanding the use of unmanned aircraft complexes recently bring up a problem of their operating that directly depends on specialist job knowledge when unmanned aircraft complexes operating. Unfortunately, at this time there is not any standard in relation to specialists training. Moreover, training of the specialists in the sphere like this does not exist in Ukraine yet. Thus, the task of unmanned aircraft complexes operating specialists training is currently relevant. Besides, with reference to experience of standardization when training of the other aviation specialists, there exist the greatest problem dealing with numerical data validity up to standards and regulatory requirement [1]. Thuswise, validity of regulatory requirement in accordance with specialist training when unmanned aircraft complexes operating is rather relevant.

Analysis of the recent researches and publications. Analogy of aviation specialist training that are fit into different categories is analyzed by the author. We have an opportunity to research the global experience of standardization and rating when pilots training for the furthest extension into the course of specialist training when unmanned aircraft complexes operating.

To create an advance system in connection with aviation specialist training of new generation (NGAP) it was set up target group in May,2009, in compliance with ICAO regulations. NGAP specialists identified the range of aviation professions that demands the developments of qualification criteria (it might be referred to the specialists training when unmanned aircraft complexes operating). NGAP group examined the necessity to work out qualification criteria in compliance with international standards and carry out aviation personal performance review for issue of certificates [1]. American and European requirements are set up [2] based on the basic requirements (minimum standard) according to pilot ability level, experience, preparatory set, issue and recognition of certificates [1], which are brought into requisition by the National Aviation Authorities across the world. In [1] there are equal pilot competences of the multicrew are defined, efficiency criteria to evaluate the standard of knowledge and abilities are proposed to use as well [3]. But requirements of documents are declarative, thus it isn't allowed to accept the valid and optimum decision in relation to training strategy. Moreover, the training process is rather expensive and dynamic.

There is a need to link quality and value of learning in a single non-trivial procedure. Qualification System is the most promising criteria for minimum resources and time. But despite its advantages and development of 22 states of relevant legal documents, qualification training system has not found a mass use yet. Since the implementation of the present time the total number of pilots who trained and prepared according to the program totaled 400, which is 100 times less than the real needs of the global commercial aviation. Reasons:

1) lack of clear quantitative assessments of skill levels;
2) lack of models depending on the level of training versus resources that are used;
3) lack of formal approach to validate the choice of education means;
4) lack of model transition from proper teaching mode to another one;
5) lack of algorithms for optimization cost and training time while providing the required level of flight safety.

All listed issues are completely (or even more, due to less experience) related to the specialist training of the unmanned aircraft complexes.

The aim of the article is to spread the experience of mathematical validity and regulatory requirements for pilots training on the process of specialists training when unmanned aircraft complexes operating.

The main material.

The main components of the qualification approach are the qualifying blocks, qualifying elements, performance criteria, instructional guidelines on the use of objective data and assessment, collection of variables as well. Document [3] considers the following qualification levels:

1) principles of threat and error factors usage, 2) accomplishment of ground-based and pre-flight operations; 3) takeoff operation; 4) making a climb; 5) performance cruising flight, 6) descent operation, 7) landing approach, 8) landing, 9) the execution of post-landing and post-flight operations.

Qualification blocks, qualifying items, performance criteria are determined by analysis of duties and tasks of aviation professionals in relevant to regulations and provide a description of results that can be observed. Basic functions (qualifying blocks) are divided into elements, which set up criteria for evaluating performance of operations and compliance with the duties of crew members.

Program requirements for pilot certification of the multicrew is corresponded to the stages of practical training with a total minimum of 240 hours. The procedure of mastering skills that are necessary for the level of multicrew is integrated with the practice of working knowledge using appropriate means of flight, training and ground training (Table 1).

Table 1

Schematic plan for the pilot training of multicrew

Subjects of training	Preparation stages			
	Advance	Effective operational	Basic	Pilot basic skills
- CRM (Crew Resources Management)	+	+	+	+
- LOFT (Line Oriented Flight Training)	+	-	-	-
- Specific procedures	+	+	-	-
- Standard procedures	+	+	-	-
- Multicrew	-	+	-	-
- All weather procedures	+	+	-	-
- Instrument flying	-	+	+	-
- En-route instrument flight	-	-	+	+
- Nonvisual flight	-	-	+	-
- Solo flight	-	-	-	+
- Landing practice	+	-	-	-
- Annex (a pilot that manages the flight/doesn't manage the flight)	-	-	+	-
- Recovery management of the AC	-	-	+	-
- Flight principles	-	-	-	+
- Cockpit procedures	-	-	-	+

Requirements training plan for multicrew includes four stages of the students training implementation. The students training is progressing to manage a single-engine aircraft, multiengine gas-turbine aircraft, multicrew. Moving on to the next stage of training it is necessary to demonstrate achievement of the objectives of training phase with lower ratings for the S-alike point depending on the level of education y of spent resources [4], is illustrated in Figure 1. For example, the transition to the second stage of the training $y_1(x) \rightarrow y_2(x)$ is done only when the level of training pilots for the first technology $y_1(x)$ will be higher than a given value y_{1zad}. Similarly for the transition $y_2(x) \rightarrow y_3(x)$ is necessity to execute the required facilities $y_2(x) > y_{2zad}$.

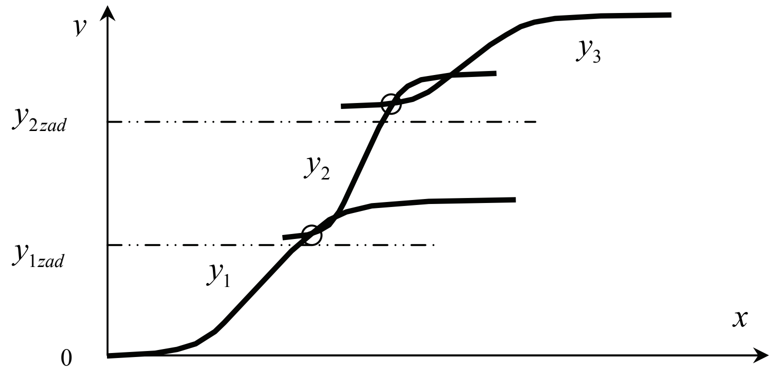

Fig. 1. Quality of training dependence versus lost resources in the process of consistent changes when teaching mode

In fact, the question arises as to both pilots and specialist training on unmanned aircraft complexes operating and the evaluation of the level of training at each stage of education and for the entire curriculum. The level of pilots training is not simply the sum of estimation for the phases. Local evaluation of training in the binary scale of "satisfactory / unsatisfactory" [3] can be transformed only in the same binary assessment for the entire curriculum. In practice, the need for more differentiation of pilots training levels and specialists of unmanned aircraft complexes operating, as for the entire curriculum and when deciding to move to the next phase of training. To solve the present issue let us just imagine the qualifying blocks in a hierarchical structure. The number of individual elements and hierarchical levels can be increased according to degree of detail of qualifying blocks. Proper mathematical training level dependence has the form $y = \underset{i1=\overline{1,n1}}{\aleph}^{1}\left[\beta_{i1}, \underset{i2=\overline{1,n2}}{\aleph}^{1,i1}\left[\beta_{i1,i2}, \underset{i3=\overline{1,n3}}{\aleph}^{1,i1,i2}\left(\beta_{i1,i2,i3}, y_{i1,i2,i3}(x_{i1,i2,i3})\right)\right]\right]$, if $\underset{i3=\overline{1,n3}}{\aleph}^{1,i1,i2}$ is a definite convolution (additive, multiplicative, minimizing, combined, etc.), $1,i1,i2$ - branch code convolution, $i3=\overline{1,n3}$ - the range of indices variation in convolution, β - weight coefficients, $i1,i2,i3$ - index of convolution element. Type of each convolution is chosen depending on the interchangeability degree of related types of training (full interchangeability - additive convolution, full irreplaceability - minimizing, intermediate cases - multiplicative with normalized weight coefficients).

Correlations among different types of training

Besides solving the problem of evaluation training it is necessary to solve the problem of constructing an optimal program of the training course, which determines the sequence of the training types and the best moments of correlation among them. For instance, in the regulations regarding to issue of certification MPL (multicrew) [1-3] it is established the requirement of the total length of pilot training, but it isn’t determined the distribution of the actual flying simulate time. To substantiate the specific numerical indicators of correlation among different types of training it is offered to use the author's method [4], based on forecasting and optimization proficiency models of aviation specialists.

In capacity of model dependence of the pilot proficiency it is selected the logistics one in the form of ordinary differential equations [4] $\frac{dx_L}{dt} = k_L x_L (a_L - x_L)$, if x_L - pilot proficiency level, k_L, a_L - coefficients, t - time. The equation shows the dynamics of proficiency growth due to flight training. Synthetic flight training improves flying skills as well $\frac{dx_T}{dt} = k_T x_T (a_T - x_T)$, if x_T - pilot proficiency level, that is achieved as a result of flight training, k_T, a_T - are coefficients. The quantities a_L and a_T are defined by expert way and show the maximum possible pilot training level that can be achieved through an appropriate type of training. In the example $a_L=1$; $a_T=0{,}45$. Supposing $a_T < a_L$, then the synthetic flight training can be applied only if $x_L < a_T$. It is set up the desired level to be achieved as well.

Besides the positive effect the synthetic flight training could have negative consequences because of the emergence in the absence of real external factors feeling of excessive confidence, undue risk behavior. So, we add to the previous equations $\frac{dx_{Tm}}{dt} = k_{Tm}x_{Tm}(a_{Tm} - x_{Tm})$, if x_{Tm} - the negative impact level of synthetic flight training towards pilot proficiency, k_{Tm}, a_{Tm} - coefficients. This component using only synthetic flight training reduces the overall level of training x_L, but with the continuation of flight training its action on the same law decreases.

Complicated pilot training model has the form:

$$\frac{dx_L}{dt} = k_L x_L (a_L - x_L); \quad \frac{dx_T}{dt} = k_T x_T (a_T - x_T); \quad \frac{dx_{Tm}}{dt} = k_{Tm} x_{Tm} (a_{Tm} - x_{Tm}).$$

The results of numerical simulation in the case of moving from the synthetic flight training to the flight phase of training are demonstrated in Figure 2.. The final correlation is formed by means of synthetic components x_T and flight training; dependence characterizes the negative impact of synthetic training; c - expense to train; moving from the synthetic training towards the flight training takes place at a point with a value of abscissas (15), that is corresponded to a training level as $x_T = 0.4$. Charts (Fig. 2) indicate that increasing training level when flight training in a unit time is much higher than during training on the simulator, but increase of the cost on this type of training per unit time is much higher as well. So, there must be exist a certain point of the optimal moving from one type of training to another one as the criterion of minimum total cost of training to a specified level, and the criterion of minimum time of preparation for a certain proficiency level.

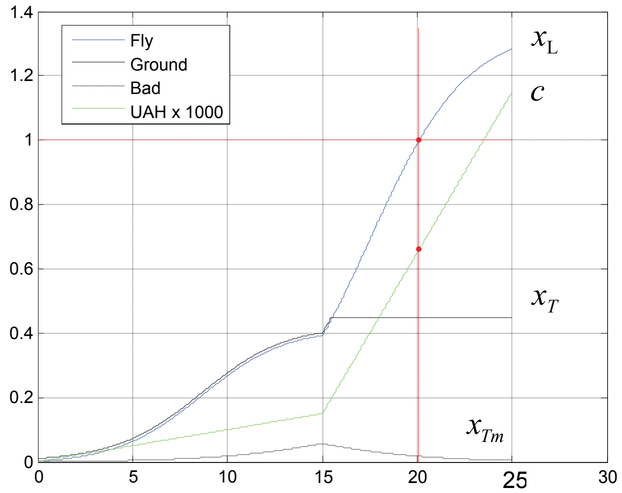

Fig.2. Simulation results of compatible flight and synthetic flight pilot training

To find the optimal point of time moving from the synthetic on to the flight training it was simulated dynamics of learning for all possible values t_2 (with a certain step) within the allowed area. The simulation results demonstrated the dependency of training cost $C(t_2)$, and dependency of training time $T(t_2)$ have certain optimal (minimum) value (Fig. 3). In the first case, it is the optimum criterion for a minimum value $I_C = \min_{t_2}(C(t_2))$,in the second case – a minimum time for training $I_T = \min_{t_2}(T(t_2))$. If it is necessary to satisfy both criteria and solve a multicriterion optimization task, such as coagulation of criteria using the linear convolution with weight coefficient $I_\Sigma = \beta_C \cdot I_C + \beta_T \cdot I_T$ (for n - criterion task) $I_\Sigma = \sum_{i=1}^{n} \beta_i \cdot I_i$. It remains the problem of determining the coefficients β_i which identify the superiority degree of the certain (i-x) criteria. Definition β_i requires consideration of the certain additional facilities that are associated with a specific problem. In particular, for the bicriterion task it is useful to set plurality of Pareto (Fig.4), which provides a good visibility graphics, simplifies incorporation of additional facilities and assessment of the benefit. Two optimal solutions for a minimum cost I_C and time of training I_T are marked in figure. When calculating both decision criteria it is necessary to take into account the additional facilities on the section between points I_C and curve I_T.

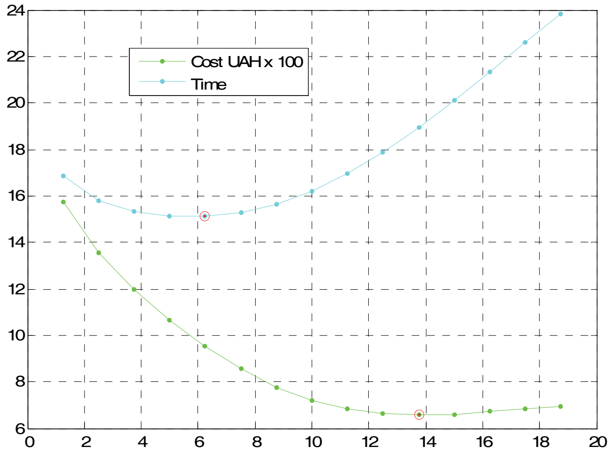

Fig. 3. Dependency of cost $C(t_2)$ and time $T(t_2)$ to achieve a certain proficiency level since the moment t_2 of moving from synthetic on to the flight training

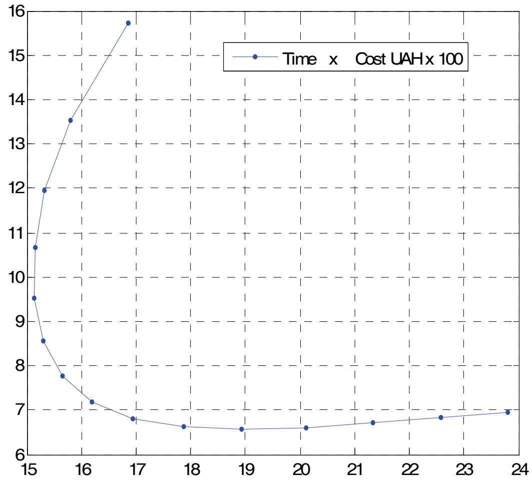

Fig. 4. Plurality of Pareto – the optimal values of time and cost training versus the certain proficiency level

The methods are tested while pilots training, but easily adapted to optimize the specialists training of the unmanned aircraft complexes maintenance. To define the main areas of adaptation for unmanned aircraft complexes maintenance specialists: maintenance specialists training and operators training of the unmanned aircraft complexes. Thus, stage 1 (general aviation omponent) of training can be universal (600-800hours of academic training). On stage 2 specialists of the unmanned aircraft complexes maintenance should take the greatest attention towards the theoretical training on specific subjects, including technical, hardware and advanced types of unmanned aircraft complexes and practical training to improve skills in sphere of unmanned aircraft complexes maintenance. In reference to unmanned aircraft complexes operators training it should be defined the following areas: academic training of the unmanned aircraft complexes operating, acquisition of special skills on unmanned aircraft complex simulator, acquisition of skills to manage a training unmanned remote control aircraft weighed 10-50 kg, acquisition of skills to manage the staff unmanned aircraft.

Conclusions.

1. The problems of validity of the numerical performance standards and regulations of various aviation specialists, including pilots and specialists of unmanned aircraft complexes operating are rather similar.

2. The qualified approach is the most promising in regard to formalization of aviation specialists training.

3. The most appropriate method to validate the regulatory requirements of aviation professionals training, including the unmanned aircraft complexes operating, is the usage of forecasting and optimization models, for instant by the means of author's methods in regard to optimizing the correlations among the different types of training. Future research should be focused on in detail of qualification units and optimization of the proper curriculum for the specialist of unmanned aircraft complexes operating.

References

1. Приложение 1 к Конвенции о международной гражданской авиации «Выдача свидетельств авиационному персоналу». Десятое издание. Международная организация гражданской авиации ICAO, 2006.

2. Вимоги об'єднаної авіаційної влади Європи щодо свідоцтв льотного складу (JAR-FCL1, JAR-FCL2).

3. Подготовка персонала. Правила аэронавигационного обслуживания. Doc 9868. Первое издание. Международная организация гражданской авиации ICAO, 2006.

4. Савінов О.М Моделювання та управління якістю підготовки авіаційних фахівців / Савінов О.М. – К.: Вид-во Нац.авіац. ун-ту «НАУ-друк», 2010. – 172 с.

UDC 629.735.014-519:621:311.243(045)

K.M. Sydorenko, candidate of technical sciences (NAU IACS, Ukraine)
V.I. Budko, candidate of technical sciences (NTUU "KPI", Ukraine)

THE SOLAR ENERGY FOR THE UNMANNED AVIATION

A review of existing solar battery driven pilot less aircrafts was carried out. A balance concerning energy received from the sun that required for aircraft propulsion has been made. Presented also is an evaluation plot of the given index.

Energy efficiency in aviation is a comprehensive problem the solution of which for different aircraft needs individual approach. In some cases costly advanced technologies are resorted to, in other it is conventional mode of energy generation and primary sources of energy (al a rule, it is the airborne gas turbines and jet engines) that are considered more attractive for a specific flying vehicle.

Modern level of technology provides the possibility of gradual change-over to biofuel as the propellant for transport aviation but actual realization of this idea is presently blocked by a multitude of technical and economic factors.

Along most promising types of renewable energy for aviation, specifically for unmanned aerial aviation (UAV) one may readily consider the energy of solar radiation, first such UAV Sunrise I (fig. 1a) performed its maiden flight on 4-th of November 1974 [1].

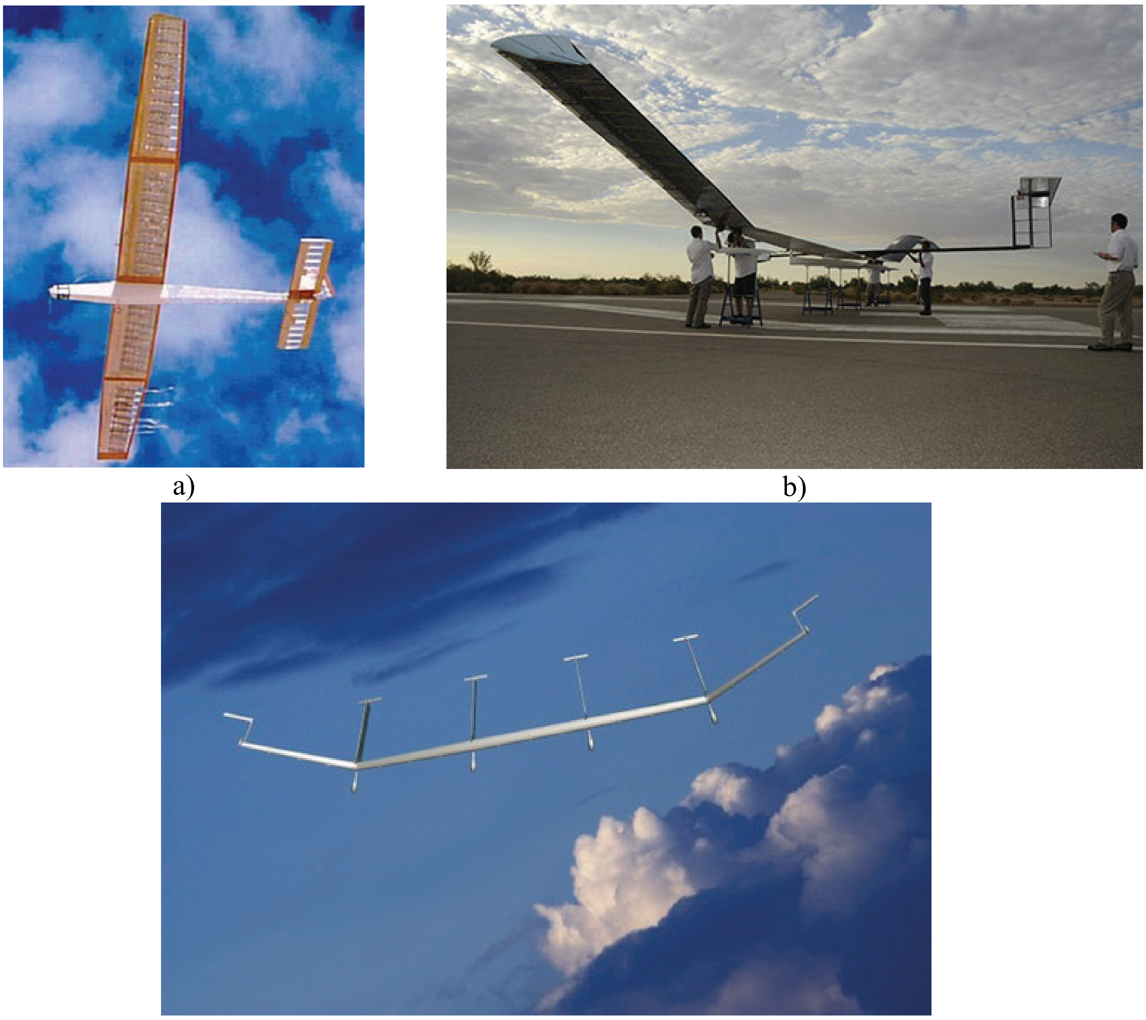

a) b)

c)

Fig. 1. UAV: a) Sunrise I; b) Zephyr; c) Solar Eagle.

One of the latest developments in this field one may consider UAV Zephyr and Solar Eagle (Fig. 1 b, c) [1]. The latter has following characteristics:

- the wing span of 122 m, against 88,4 m for AN 225 “Mria”;
- the net weight 1270 kg;
- the load-carrying capacity over 450 kg;
- the velocity 100-115 km/h;
- the altitude ceiling bigger than 18 km;
- the non-stop flight duration near 5 years.

The most complicated tasks to solve with solar battery driven UAV are zero balance for radiation and required energy consumption.

It is know that the power needed to fly an aircraft is estimated by the following equation (the forces acting on the UAV in flight shown on fig.2) [2]:

$$P_f = F_d v + F_a v \sin(\alpha),$$

where F_d – the drag force;

F_a – the weight;

v – the velocity of the flight of the airplane;

α – the angle of attack of the airplane.

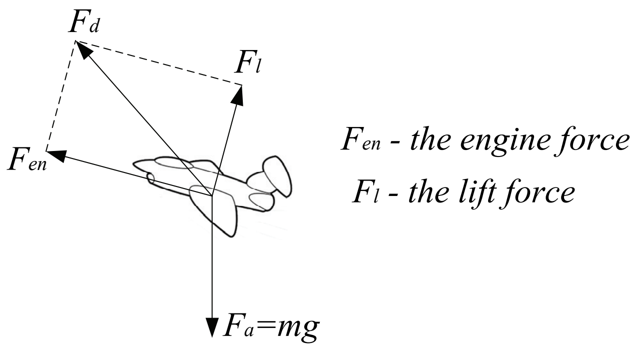

Fig. 2. The forces acting on the UAV in flight.

Energy needed for the realization of flight is equal the integral of power over time [2]:

$$E_f = \int P_f dt .$$

In due time the regime of energy generation by a photovoltaic battery is described by the following equation [3]:

$$E(Q)\begin{cases} 0, \ providing \quad that \quad Q \langle Q_0 \\ E, \ providing \quad that \quad Q_0 \langle Q \langle Q_H \\ E, \ providing \quad that \quad Q_H \le Q \end{cases},$$

where Q_0 – initial total solar radiation in W/m^2 incident on a horizontal plane that is sufficient to start off the generation of electricity by a photovoltaic battery;

Q_H – rated solar radiation in W/m^2 incident on a horizontal plane which is sufficient for a photovoltaic battery to generate enough energy to run airborne equipment;

E – energy that may be generated by a photovoltaic battery at additional solar radiation;

E_H – energy in W/m^2 that is generated by a photovoltaic battery at its rated working conditions [3].

Thus, main indicator of total power self sufficiency of UAV is coefficient k - ratio of the required energy to that received from the sun corrected for the efficiency of its conversion to electricity. Tue value of coefficient k should always be less that 1 at all even most adverse weather conditions. Photovoltaic batteries for UAV should be of the highest conversion efficiency to minimize wings Span and Area.

One more way of decreasing the value of k is pulsing voltage charge mode of airborne equipment batteries that serve as emergency source of energy in case of UAV entering a cloud. Fig. 3 illustrates the dependence of k from E_f and E for UAV in level flight over the capital of Ukraine Kyiv in winter. The initial values of the forces acting on UAV are taken from freely available reference sources.

Insulation data are taken from weather reports and the Atlas of renewable energy sources power potential of Ukraine.

Initial data intervals used from technical characteristic of UAV Zephyr and Solar Eagle.

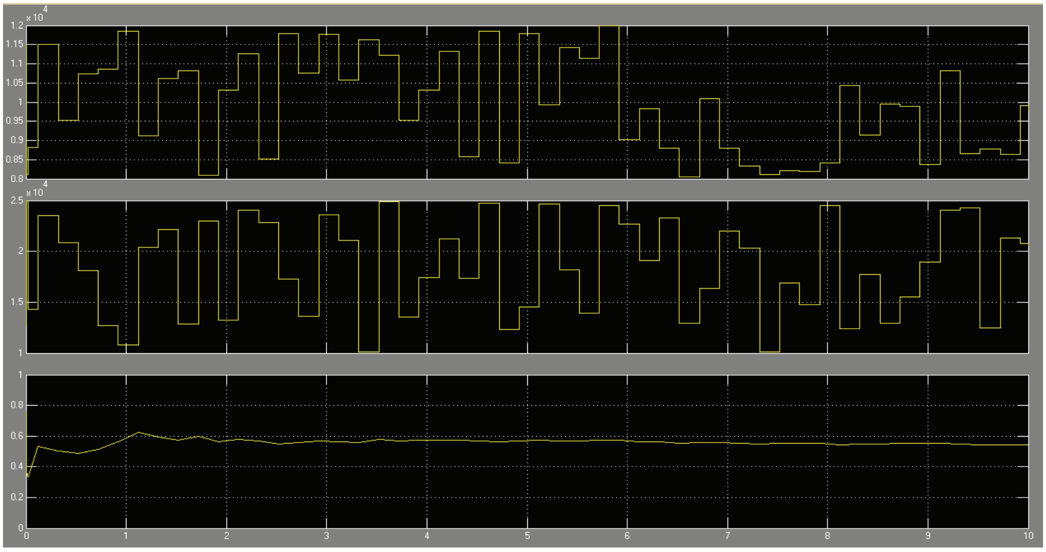

Fig. 3. Dependence of k from E_f and E for UAV.

The analysis of graphic data in fig. 3 shows that respective of solar energy fluctuations coefficient k remains within permitted limits and solar energy is sufficient for the execution of fight.

In first seconds after change-over to solar-battery-powered flight a slight decaying ogullation process of UAV power system is observed. At clear sky conditions this process will be stable with strictly defined k – values in the given interval.

Conclusions: solar energy presents considerable potential as a source of power for UAV. Energy input and consumption can be successfully balanced. Great interest for the promotion of this approach in aircraft industry presents the development of a unified power engineering standard for similar types of UAV for create a unified approach design of power systems. Openness these system technical architecture will pave the way to the dynamic development of UAV powered by solar batteries.

Refferences

1. Sydorenko K. M. – "Use a solar energy for UAV", Actual problems of aircraft: scientific and technical conference, 17-18 octobre 2011p.: abstracts, Kiev, 2011, «VIT» Edelveys», p. 120-124.

2. Vineet Kumar Vashishtha, Ashok Kumar, Rahul Makade, Shasi Lata – "Solar power the future of aviation industry", Int. Journal of Engineering Science and Technology, vol.3, Singapore, 2011, p. 2051-2058.

3. Budko V. I. – "The use of power budget of wind and solar in off-line systems in Ukraine", Renewable energy, Kiev,2010, p. 26-35.

4. K. M. Sydorenko, P. S. Sochenko – "Renewable energy sources: the monograph", Kiev, NAU, 2011, 232 p.

UDC 656.7.05;351.814.2 (043.2)

V.P. Kharchenko, Yu.V. Chynchenko
(National Aviation University, Ukraine)

AIR TRAFFIC CONTROL UNCERTAINTY FACTORS DURING SINGLE PERSON OPERATIONS

The classification of factors that impact staffing in air traffic management during single person operations is considered. The overview of the mitigation strategies highlighted for each of the six topics (degraded system operation, workload extremes, night work, single person operations, position handover and on-the-job training) is considered.

Introduction

The growing traffic, technological changes and commercial pressures makes staffing the air traffic control (ATC) operations complex and challenging [1-4]. To maintain a safe, orderly and expeditious flow of traffic, it is important to staff operational positions safely and to withstand commercial pressure avoiding unnecessary risks. This may require certain safety buffers to cope with expected and unexpected variances (e.g. people, technology, organisation, contextual) [5].

Each controller now responsible for a separate volume of airspace essentially works in isolation of those that may be around him/her. In a fully automated environment, there is not even any opportunity for interaction because the majority of coordination is automatically managed by the 'machine'.

Nevertheless, it is not entirely as bad as one may expect because depending on workload, there are some limited opportunities for interaction with a neighbouring controller.

In a larger centre, and as the workload recedes, volumes of airspace are usually progressively combined until a single controller is ultimately responsible for vast tracts of airspace perhaps stretching halfway across sector of responsibility. At the same time, the next controller (also responsible for a vastly increased expanse of airspace) may be physically located a whole aisle away. Typically, this is the situation at night (with a couple of exceptions).

Classification of factors that impact staffing in air traffic management during single person

operations

Single person operations (SPO) are defined as those periods of time when an operational ATC unit is providing service with only one person present on staff, that being the ATCO.

It is clear that in case of SPO, the redundancy of the human element is missing and therefore procedures need to be in place in the event of a failure of that element whether due to illness, fatigue or overloading [6].

These procedures should limit the levels and duration of traffic to an amount safely handled by alone air traffic controller (ATCO) and should also deal with the possibility of the ATCO becoming unable to perform his/her duties. Procedures should be in place not only for the SPO unit but also for neighbouring units that may be affected. Because traffic may increase unexpectedly or uncontrollably, backup staff should be available on call-in within reasonable time limits to ensure the safe continuation of service. But it should be noted that in the case of an aircraft emergency, it is unlikely that staff could be called in quickly enough to assist in the increased workload.

Another aspect of SPO is the lack of the Four-Eye Principle (4EP). 4EP is defined as the situation where an active controller is accompanied by another appropriately qualified controller whose function includes that of a safety net by monitoring the same working area as the active controller.

Approach environments

In the larger en-route centres that also provide approach services, one such controller may ultimately be responsible for all of the approach airspace around a major capital city airport and be sitting quite remotely from other SPO controllers in the room. Typically, this is the scenario at night. In the smaller terminal control units providing an approach service, it is still a single controller, but now that controller is also the sole person on duty in that terminal control unit.

Tower environments

The reduction in staff in towers – particularly the smaller ones – also created situations where there are now a number of towers around the country which at various times during the day, are manned by a single controller. This scenario may be because the other controller is on a break or, there is simply no other controller needed and therefore none is rostered.

In the larger capital city towers (which are also equipped with a variety of surveillance technologies), the traffic/workload (even on a night shift) still requires at least two controllers. However, in the smaller regional and general aviation towers (usually where there is no radar or other surveillance technology available – yet), there is only a need for a single person – and at night, many of these towers are simply closed.

Single person operations give rise to a number of issues – some of which may give rise to a near-term safety hazard and others which may contribute to a longer-term safety hazard. Clearly, these hazards will need to be mitigated to maintain the safety of the air navigation system in such higher productivity circumstances. As well, there are also issues relating to the welfare of the controller.

Typical (but not necessarily exhaustive) safety hazards needing mitigation are [6]:

1. Controller loss of confidence in decisions in the absence of a ‘sounding board’.
2. Unnoticed or mismanaged errors or threats.
3. Unexpected workload (for example from unscheduled additional traffic; adverse weather impacting on ‘normal’ operations; facility failure leading to additional unfamiliar task load; etc.).
4. Unnoticed reduction in controller’s competence.
5. Reduced opportunity for mentoring (passing on wisdom).
6. Controller does not recognise having reached limit of capacity/competence.
7. Tunnel vision in circumstances where the controller is responsible for a large volume of airspace or a large aerodrome.
8. Loss of standardisation.
9. Emergence of untested or unapproved techniques.
10. Insufficient system knowledge to recognise operational impact of system degradation.

Typical (but not necessarily exhaustive) occupational health and safety hazards which may need mitigation are [7]:

1. Incapacity from a medical event or an accident.
2. Unrecognised or unacknowledged fatigue or medical unfitness (for duty).
3. Psychological stress – ‘it all depends on me’ and perhaps a feeling of inadequacy.
4. Adverse reaction to isolation – particularly in remote locations.
5. Staff security is compromised.
6. Long-term medical fitness.

The overall hazards associated with staffing in air traffic management (ATM) are (figure 1):

- ***Over- and under-staffing:*** Not enough staff to handle properly the traffic, leading to safety occurrences including accidents. Over-staffing may lead to boredom and hence distraction. Also staff may be needed for other tasks;
- ***Traffic variation:*** High-traffic volume may fall into periods when humans are not at their biological peaks. This is influenced by factors such as length of duty and when the peak volume occurs in regard to circadian rhythm;
- ***Competency/recency:*** Competency to open required sectors or to combine certain sectors and recency for controllers, in particular part-time controllers.
- ***Lack of redundancy due to SPO:*** Lack of available redundancy for normal and degraded operations;

- ***Teamwork:*** The quality and efficiency in the different mix of positions, right mix of people and coordination between sectors including the extent of cooperation and assistance available and provided within the team;

- ***Overconfidence:*** Controllers 'can do' mentality i.e. the mentality to do the job whatever the circumstances;

- ***Fit for duty: (fatigue, drugs, alcohol, medical).*** Awareness of fitness for duty state. Balancing personal and professional life and scheduling free time;

- ***Health:*** The impact of working shift overtime and the nature of the job on the individual;

- ***Loss of job satisfaction:*** caused by over- or under-staffing, dropping traffic, rosters or management and social issues.

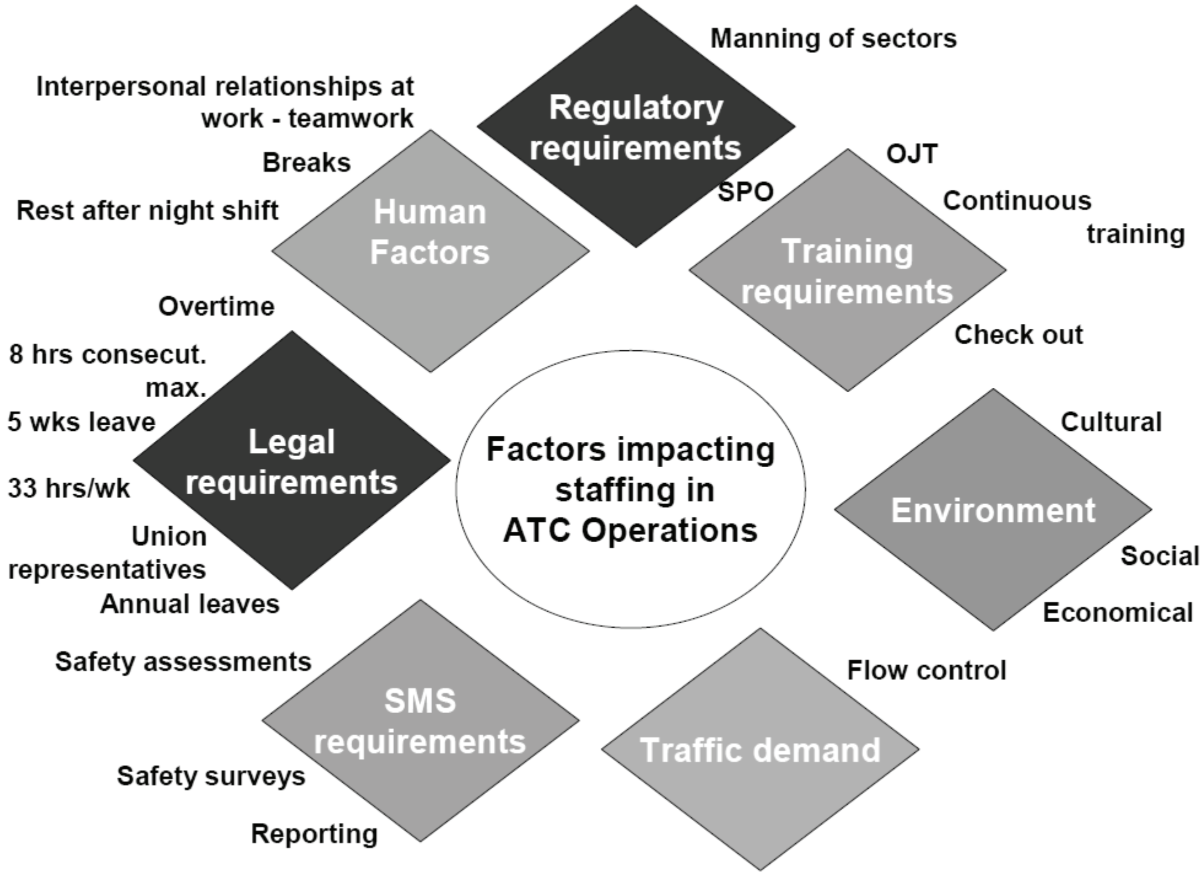

Figure 1. Factors impacting staffing in ATM during SPO

These hazards may vary depending on the different configurations of operational positions (number of working positions required), type of traffic, pattern of traffic, Letter of Agreements and local procedures. The overall outcome could be the same but it is apportioned on different causes depending on en-route, approach, and tower environments.

Mitigation strategies overview

The following paragraphs provide an overview of the mitigation strategies highlighted for each of the six topics (degraded system operation, workload extremes, night work, SPO, position handover and on-the-job training) [6,7].

Degraded system operation

1. Working in planned degraded modes should require an assigned supervisor who is appropriately trained, and procedures designed to support operational staff.

2. A culture of empowerment should be developed to deal with issues not covered in checklists and contingency plans. Clarify roles of all operational staff for these situations. Consider assigning operational command authority to a position/person where appropriate.

3. There should be adequate access to operational and technical support.

4. Training (including simulator training) for operational staff should include understanding the impact of and response required in all types of degraded modes.

Workload extremes

1. Management should review recurring peaks in terms of impact on existing Letter of Agreements, rostering schedules and procedures.

2. Minimum staffing level arising from daily and seasonal traffic variations should be respected. That is only allow staffing to fall below these minimums when a requisite reduction in capacity is implemented or when anticipated traffic levels are below expectations.

3. Supervisors should be trained to monitor staff workload and assess individual and/or team performance limits at a given moment in time taking into account time on position, duration of shift, and workload context.

4. Recognise that low workload has its own hazards; to manage this consider approving extra curricula activity.

5. Consider introducing support tools to improve vigilance during low workload e.g. system alarms.

Night work

1. Strategies should be adopted to mitigate the effects of sleepiness and fatigue. Staff should relieve each other at appropriate times, have frequent breaks (and possibly naps) but with due regard to inherent hazards associated with the handover/takeover process itself, and rotate between positions.

2. Rest facilities should be available and backup staff should be close.

3. Supervisor should collapse and de-collapse sectors in response to unexpected demand (lower or higher). Supervisor should also call in additional staff if required (e.g. in response to negative weather forecast or unscheduled demand). Collapsed sectors should be co-located wherever possible.

SPO

Prior to making a decision to introduce SPO, a risk assessment should be undertaken to validate the decision. Equally, within the unit safety case, contingency plans should be developed for unplanned SPO.

Furthermore, prior to implementing SPO, it is recommended that:

- an operational supervision concept that supports SPO should be developed;
- the system design supporting the SPO concept should be verified;
- operational staff should be specifically trained to transition between two into one and one into two where relevant;
- operational staff should be trained in relevant human factors issues e.g. threat and error management training;
- a legal and corporate framework should be adopted that supports a just culture for incident reporting.

Position handover

1. Operational management should develop checklists for handover and takeover procedures (crosschecks, readouts).

2. Staff should follow a pre-determined checklist and complete the handover form.

3. Staff should be trained to conduct handovers and to be aware of the hazards associated with the handover process.

4. All handover/takeovers should be conducted at a time when doing so will not compromise the information transfer.

5. Operational staff assessment should include handover process on a regular basis.

6. Simultaneous handover of adjacent operational positions should be avoided.

OJT

1. The number of OJT sessions in Ops room at any one time should be restricted to avoid trainees in adjacent positions.

2. OJTI training should include extensive training in 'active monitoring', awareness of distraction issues and in the art of intervention.

3. All trainees should reach a required proficiency level prior to plugging into a 'live' position.

4. Ergonomics of the position should allow the instructor to easily observe all aspects of the position. Appropriate tools should be readily available for the OJTI to enable him/her to intervene rapidly.

5. The OJT trainee should be progressively exposed to training sessions of a duration similar to session lengths that are expected in the live environment.

6. Ad hoc OJT should be avoided i.e. OJT should be formalised, planned, structured, and integrated with employee orientation.

7. Operational roster should be provided, which allow OJT to give adequate briefing and debriefing times to OJTI and student/trainee.

This should also be controlled from the OJTI's viewpoint as it is hard to maintain concentration and situational awareness while observing a trainee, especially for a prolonged amount of time.

Conclusions

SPO eliminate redundancy in the human element of the Aeronautical system. This can lead to a failure of the whole system should the traffic demand on the ATCO exceed his/her abilities or would he/she fall ill. SPO may be detrimental to the well-being of the ATCO by reducing his/her ability to take normal breaks while at the same time increasing the level of stress and fatigue under which he/she is operating. For these reasons, the use of single controller shifts should be strongly discouraged. Where providers choose to use SPO, they - not the ATCO - must bear the responsibility for the resulting risk to the system.

Rostering SPO shall be avoided. In the unlikely event of unavoidable SPO appropriate measurements shall be taken to ensure that the SPO situation will be alleviated as soon as possible. Until such time measures shall be taken to mitigate all impacts of SPO such as: traffic regulation, provide breaks, informing neighbouring ATC units. Procedures shall be in place to implement such measures in an efficient way, not increasing the workload of the ATCO.

The purpose of these theses was to highlight a range of hazards and prevention and mitigation strategies relevant to the selected six topics for staffing an ATC operations. This information can be used, where appropriate, as a checklist for supervisors, and safety managers in Aeronautical service providers, and adapted to the context of the local environment.

References

1. State of global aviation safety 2011. – Montreal: ICAO, 2011. – 80 p.
2. Eurocontrol annual report 2010. – Brussels: Eurocontrol, 2011. – 88 p.
3. Annual safety review 2010. – Cologne: EASA, 2011. – 77 p.
4. Statistical summary of commercial jet airplane accidents, worldwide operations, 1959-2010. – Seattle, Washington: Boeing, 2011. – 27 p.
5. DOC 9859. Safety management manual (SMM). – Montreal: ICAO, 2009. – 284 c.
6. Study report on selected safety issues for staffing ATC operators. – Brussels: Eurocontrol, 2006. – 102 p.
7. Selected safety issues for staffing ATC operators. – Brussels: Eurocontrol, 2007. – 32 p.

UDC: 629.78

V.I. Chepizenko, Phd.Sc.
(National Aviation University, Ukraine)

AIRCRAFTS POLYCONFLICTS RESOLUTION METHOD IN THE FREE FLIGHT MODE

On the basis of use «The natural-scientific system approach» the guaranteed polyconflicts resolution method in the aeronavigation environment has been developed. The method allows to overcome «dimension curse» barrier and provides management realisation by all mobile objects in real time.

Recently attention is given to working out the conflicts resolution methods between aircrafts. Majority developed methods have essential shortcomings which limit possibilities of their use, namely:

- the fragmentariness and the phenomenological approach, subjectivity and use heuristics, that leads to inability to resolve a problem of aircraft plural conflicts on general level;
- inability of many methods to overcome "a dimension damnation" and "domino effects";
- the great time and computing expenses that does not allow to resolve any dimensions conflicts (polyconflicts) in real time.

For elimination of these shortcomings the guaranteed aircrafts polyconflicts resolution method in the free flight mode is offered. The method essence is in formation of the virtual world $\aleph$, the definition of its structural and functional properties, control search by conflict-free movement and carrying over of this control to the real world $\Re$.

The method has several stages.

1. At the first stage borders of the real world $\Re$ (as aeronavigation zone) by means of system of linear inequalities are defined of $\Re$ carry over to the virtual world by means of the mapping operator $\Im^1_{\Re\aleph}$

$$\Re(x_1, x_2) < 0 \overset{\Im^1_{\Re\aleph}}{\Rightarrow} \aleph(z_1, z_2) < 0,$$

here x_1, x_2 - borders co-ordinates $\Re$; z_1, z_2 - borders co-ordinates $\aleph$.

2. Further the positions set of internal prohibited zones and restrictions $\Re$ carry over from $\Re$ in $\aleph$ by means of the mapping operator $\Im^2_{\Re\aleph}$

$$\Re_k(x_{1k}, x_{2k}) < 0 \overset{\Im^2_{\Re\aleph}}{\Rightarrow} \aleph_k(z_{1k}, z_{2k}) < 0,$$
$$k \in \{1, 2, \dots N_{obs}\},\ N_{obs} \in \{N_{\mathrm{h}} \cap N_{\mathrm{f}} \cap N_{din}\},\ \Re_k \in \Re,\ \aleph_k \in \aleph$$

here x_{1k}, x_{2k} – prohibited zones and restrictions co-ordinates in $\Re$; z_{1k}, z_{2k} – prohibited zones and restrictions co-ordinates in $\aleph$; N_{obs} – the general set of internal obstacles and restrictions in $\Re$; N_{h} – hard obstacles and restrictions set in $\Re$; N_{f} – flexible obstacles and restrictions set in $\Re$; N_{din} – dynamic obstacles and restrictions set in $\Re$.

3. The following stage is transferring from $\Re$ in $\aleph$ aircraft positions by means of the mapping operator $\Im^3_{\Re\aleph}$

$$\Re_i(x_{1i}, x_{2i}) \overset{\Im^3_{\Re\aleph}}{\Rightarrow} \aleph_i(z_{1i}, z_{2i}),$$
$$i \in I\{1, 2, \dots N_a\},\ \Re_i \notin \Re_k,\ \aleph_i \notin \aleph_k,$$

here N_a - general aircrafts set in the limited aeronavigation space.

4. Further carrying over from $\Re$ in $\aleph$ goal aircrafts positions by means of the mapping operator $\Im^4_{\Re\aleph}$ is carried out

$$\Re_i(x^*_{1i}, x^*_{2i}) \overset{\Im^4_{\Re\aleph}}{\Rightarrow} \aleph_i(z^*_{1i}, z^*_{2i}),$$
$$i \in I\{1, 2, \dots N_g\}, \quad N_g \geq N_f,$$

here N_g – the general set of goal aircrafts positions in the limited aeronavigation space.

5. The mass and repulsion and attraction potentials are appointed to mapping of everyone aircrafts current positions

$$\forall \aleph_i(z_{1i}(t), z_{2i}(t)) \in \aleph \Rightarrow U_i^+\left(z_{1i}(t), z_{2i}(t), r_i(t), m_i, G\right) +$$
$$+ U_i^-\left(z_{1i}(t), z_{2i}(t), r_i(t), r_{cr\,i}, m_i, G\right),$$
$$i \in I\left\{1, 2, \dots N_f\right\},$$

here U_i^+ and U_i^- – accordingly the attraction and repulsion potentials which "accompany" mobile objects in the virtual world $\aleph$; $r_i(t)$ – distance from *i*-th mobile object; $r_{cr\,i}$ – critical distance from *i*-th mobile object; m_i – mobile objects masses; G – gravitational field constant.

The critical distance $r_i(t)$ in $\aleph$ is set proceeding from standard requirements to protective aircraft zones, separation specifications and other requirements regulated in $\Re$. Necessary condition at appointment of the aircraft protective zones sizes in $\Re$ is

$$r_{cr\,i} \geq \max\left(\Delta x_{1i}, \Delta x_{2\mathrm{i}}\right),$$

here $\Delta x_{1\mathrm{i}}, \Delta x_{2\mathrm{i}}$ – the geometrical sizes *i*-th aircraft in a projection to a horizontal plane (a horizon plane).

6. Repulsion and attraction potentials also appoint to goal (terminal) aircraft positions $\aleph_i(z^*_{1i}, z^*_{2i})$

$$\forall \aleph_i(z^*_{1i}(t), z^*_{2i}(t)) \in \aleph \Rightarrow U_i^+\left(z^*_{1i}(t), z^*_{2i}(t), r_i^*(t), m_i^*, G\right) +$$
$$+ U_i^-\left(z^*_{1i}(t), z^*_{2i}(t), r_i^*, m_i^*, G\right),$$
$$i \in I\left\{1, 2, \dots N_{\mathrm{g}}\right\},$$

here $r_i^*(t)$ - distance from *i*-th goal position of mobile object, m_i^* - goal (terminal) positions masses of mobile objects.

7. Prohibited zones and restrictions of real aeronavigation space are displayed in $\aleph$ geometrical primitive or their combinations. Prohibited zones borders are gravitating points final set, each of which appoint repulsion and attraction potentials

$$\forall \aleph_k(z_{1k}(t), z_{2k}(t)) \in \aleph \Rightarrow U_k^+\left(z_{1k}(t), z_{2k}(t), r_k(t), m_k, G\right) +$$
$$+ U_k^-\left(z_{1k}(t), z_{2k}(t), r_k(t), r_{\kappa p\,k}, m_k, G\right).$$
$$k \in \left\{1, 2, \dots N_{obs}\right\},$$

8. Each point of space $\aleph$ is characterized by the general potential of a virtual gravitational field

$$U_\Sigma(z_1, z_2) = \sum_{i=1}^{N_f} \left(U_i^+\left(z_{1i}(t), z_{2i}(t), r_i(t), m_i, G\right) + U_i^-\left(z_{1i}(t), z_{2i}(t), r_i(t), r_{cr\,i}, m_i, G\right)\right) +$$
$$+ \sum_{i=1}^{N_g}\left(U_i^+\left(z^*_{1i}(t), z^*_{2i}(t), r_i^*(t), m_i^*, G\right) + U_i^-\left(z^*_{1i}(t), z^*_{2i}(t), r_i^*, m_i^*, G\right)\right) +$$
$$+ \sum_{k=1}^{N_{obs}}\left(U_k^+\left(z_{1k}(t), z_{2k}(t), r_k(t), m_k, G\right) + U_k^-\left(z_{1k}(t), z_{2k}(t), r_k(t), r_{cr\,k}, m_k, G\right)\right).$$

Each object entered in $\aleph$ generates indignation of the general virtual force field and is characterized by virtual attraction and repulsion potentials

$$U_i^+ = \frac{Gm_i}{r_{ij}}, \; U_i^- = -\frac{Gm_i}{r_{ij}}.$$

The resultant forces vector in each point $\aleph$ consist of attraction forces F^+ and the repulsion forces F^- generated by all gravitating bodies in $\aleph$

$$F_{ij}^+ = \frac{Gm_i m_j}{r_{ij}^{\alpha}} = U_i^+ \frac{m_j}{r_{ij}^{(\alpha-1)}}, \tag{1}$$

$$F_{ij}^- = \frac{Gm_i m_j r_{cr}}{r_{ij}^{\beta}} = U_i^- \frac{m_j r_{cr}}{r_{ij}^{(\beta-1)}}. \tag{2}$$

Corresponding projections of the attraction and repulsion forces to axes z_1 and z_2 look like

$$F_{ij\,z1}^+ = F_{ij}^+ \frac{|z_{1i} - z_{1j}|}{r_{ij}}, \; F_{ij\,z2}^+ = F_{ij}^+ \frac{|z_{2i} - z_{2j}|}{r_{ij}},$$

$$F_{ij\,z1}^- = F_{ij}^- \frac{|z_{1i} - z_{1j}|}{r_{ij}}, \; F_{ij\,y}^- = F_{ij}^- \frac{|z_i - z_j|}{r_{ij}},$$

$$r_{ij} = \sqrt{(z_{1i} - z_{1j})^2 + (z_{2i} - z_{2j})^2}.$$

The general graphic the forces representation formed by individual gravitating object in the virtual world, is shown on fig. 1.

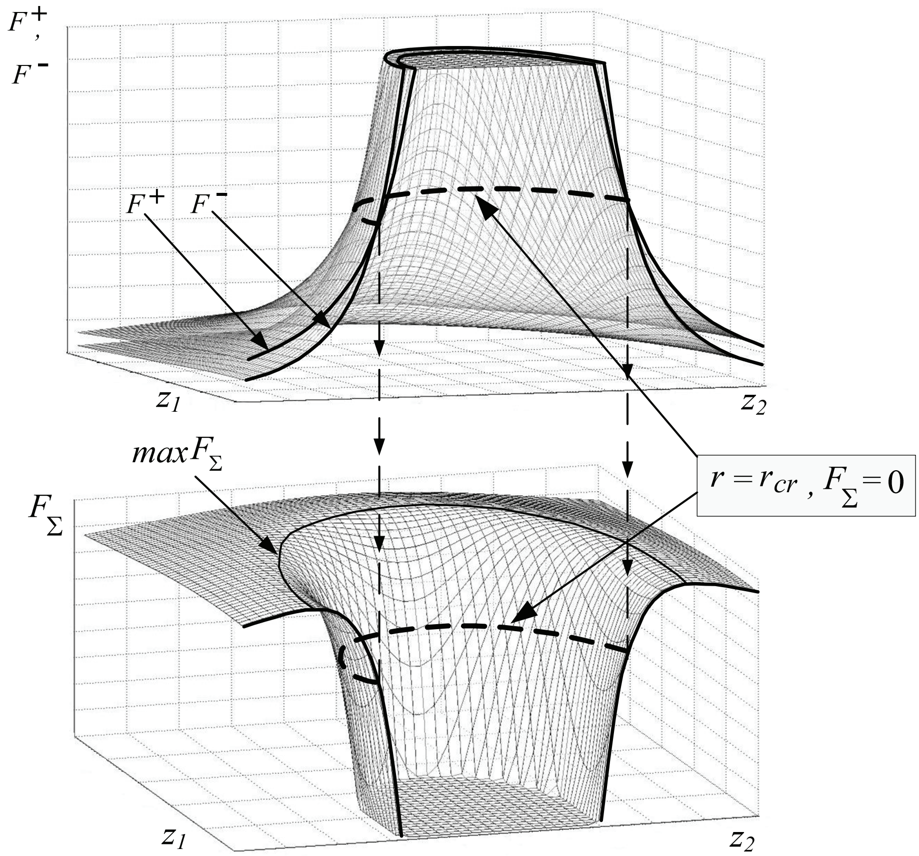

Fig. 1. Surfaces $F(z_1, z_2)$ virtual gravitational field.

In expressions (1) and (2) relation α/β defines a "modular" condition of the environment of the virtual world ("synergetic substance"), that characterises self-organizing degree of polyconflict dynamic system. "Modular" condition of the virtual environment like a modular condition of a matter: gaseous, liquid, crystal etc.

Basic feature and advantage of the virtual world generated thus $\aleph$ is that at rapprochement of material points on critical distance r_{cr} a resultant operating on them force is equaled to zero, i.e. attraction and repulsion forces counterbalance each other. On distance r_{cr} interaction energy of material points E reaches a global minimum which answers the least interaction between bodies. Along with it, the critical distance r_{cr} sets the sizes of aircraft protective zone which is a safety zone. Such zone answers modern separation norms and is defined by necessary navigating characteristics. Absence of the protective zone crossings others aircrafts allows to support the guaranteed safety level of air traffic in a free flight mode and polyconflicts.

Conclusions

The offered method provides:

- the guaranteed polyconflicts resolution of any dimension in 4-D space of any topology;
- realization of safe purposeful free flight for all aircrafts in real time;
- realization of a principle functional homeostasis polyconflict aeronavigation system;
- the account of priority traffic participants.

UDC 629.7.067(045)

S. T. Polishchuk, PhD (National Aviation University, Ukraine)
Y. V. Chynchenko, PhD (National Aviation University, Ukraine)

WORLDWIDE AVIATION OCCURRENCES AND SPACE WEATHER PHENOMENA IN 2011

There are many factors that affect on flight safeties. One of them is space weather. The correlation between space weather parameters and worldwide aviation incidents and accidents is evaluated.

Introduction

At present day a civil aviation is very impotent component of transportation system for many countries. Air travel is one of the safest forms of transportation, but accidents do happen with dramatic and terrifying results. The causes of aviation accidents vary greatly depending on specific circumstances and problems that may develop during the flight process. If entity has been impacted by an aviation accident, it is important to understand the conditions of this event surrounding. Total accidents and fatalities by countries in 2011 is given in Table 1 [1].

State of space weather (SW) is also factor that can lead to aviation occurrences. For instance, a particularly significant SW storm occurred during the October-November 2003 events when the FAA's WAAS system exceeded its vertical protection limit and was deemed unusable for 15 hours and 11 hours on October 29 and 30, 2003 respectively. As satellite-based navigation has a key role in the NextGen and SESAR efforts, the need to monitor and predict SW will grow.

Table 1

World accident statistics in 2011

Country	Accidents	Fatalities
Russia	6	118
Iran	1	77
Ireland	1	6
Indonesia	3	48
Honduras	1	14
Congo	4	120
USA	1	2
Canada	3	15
Argentina	1	22
Afghanistan	1	9
Brazil	1	16
South Korea	1	2
Bolivia	1	8
Haiti	1	3
Nepal	1	19
New Guinea	1	28
Summary	28	507

High-Frequency (HF) communications, the primary and in some cases, sole means of communicating over the poles, is well-known to be affected during SW events. Main SW effects and their impacts to aviation in Table 2 are given [2].

Last years ICAO, FAA and EVROCONTROL devoted much attention to problem of SW parameters integration in air navigation. In 2002 ICAO Divisional Meeting noted that:

1. Space weather recognized as a hazard to aviation.
2. Two operational issues: a) significant increase in polar operations; b) increased use of GNSS for navigation demand the integration of SW in air navigation.

In response to this request the U.S. proposed to develop a manual and training material to educate dispatchers, pilots and controllers on space weather (4-th meeting of Airways Volcano Watch Operations Group (AVWOPSG), 2008).

In 5-th meeting of AVWOPSG the U.S. presented the "Manual on Space Weather Effects in Regard to International Air Navigation" (Peru, March 2010).

Problem statement

From database Aviation Safety Network [1] following that in 2011 there were 2210 aviation incidents and 28 accidents with fatalities 1674 and 507 correspondingly. For this time there were some SW-phenomena and specifically – seven solar proton events (SPE), when the protons flux exceed the average value considerably (Fig. 1) [3].

Table 2

Space Weather Impacts to Aviation

Variety	Effect	Impact to Aviation	Frequency/Mitigations
Electromag-netic radiation of Sun	Ionizes the upper layer of Earth atmosphere	May cause Radio Blackouts. Affecting primarily HF radio on the day side of the Earth	Relatively Frequent. Mitigation is use SATCOM as a backup if available. Affects polar route dispatch
	Produces scintillation of radio signal	May impact SATCOM and GPS reception: > 20 dB signal fading. Primarily in polar and equatorial regions	Frequency depends on latitude and Solar Cycle. Mitigation is redundancy (i.e. multiple satellites) and path diversity
High Energy Particles (protons, electrons)	Damages sensitive electronics	Single Event Upsets – introduces bit errors in high density dynamic RAM.	Frequency depends on Solar Cycle. Design for robustness in the presence of Single Event Upsets
	Creates electric discharges	Can permanently damage satellite electronics	Primarily a concern for spacecraft and sub-orbital flight
	Biological hazard	Increased radiation exposure for crew on high altitude flights – primarily a concern on polar routes	Space Weather forecasting for dispatch support. During storms fly at lower altitudes or avoid polar routes.
Magnetized Plasma	Causes Geomagnetic Storms and disturbances in the ionosphere – increased scintillation in polar and equatorial regions	Can degrade SATCOM availability	Path diversity – multiple SATCOM satellites – use HF or LEO SATCOM as a backup.
		Can degrade GPS position accuracy – primarily a concern for high accuracy precision approach type applications	GNSS augmentation system can monitor for the effects and limit system availability during a storm. Space weather monitoring on dispatch for some operations

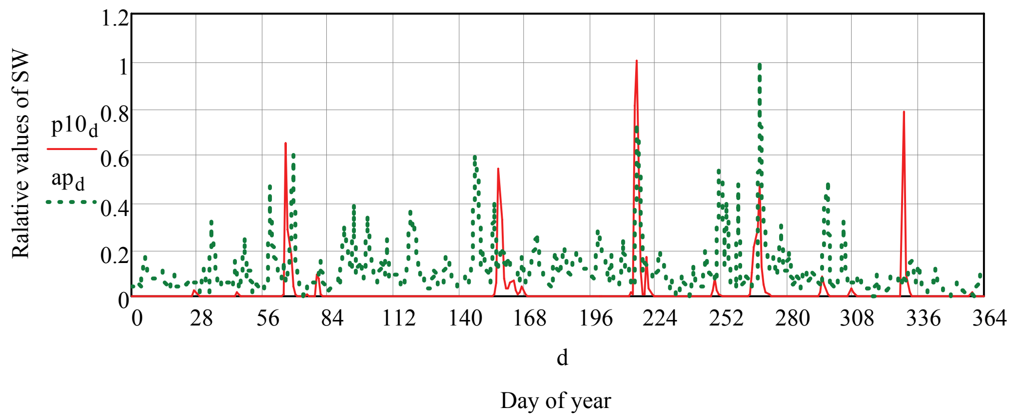

Fig. 1. Time distribution of proton fluence (p10) and planetary index of Earth magnetic field disturbance (ap)

So, the **goal of research** is determination of the correlation between number of worldwide aviation occurrences and parameters of SW-state.

Method of research is correlation analysis.

Result of research. The total accidents and incidents distribution per year is shown in Fig.2 , Fig. 3.

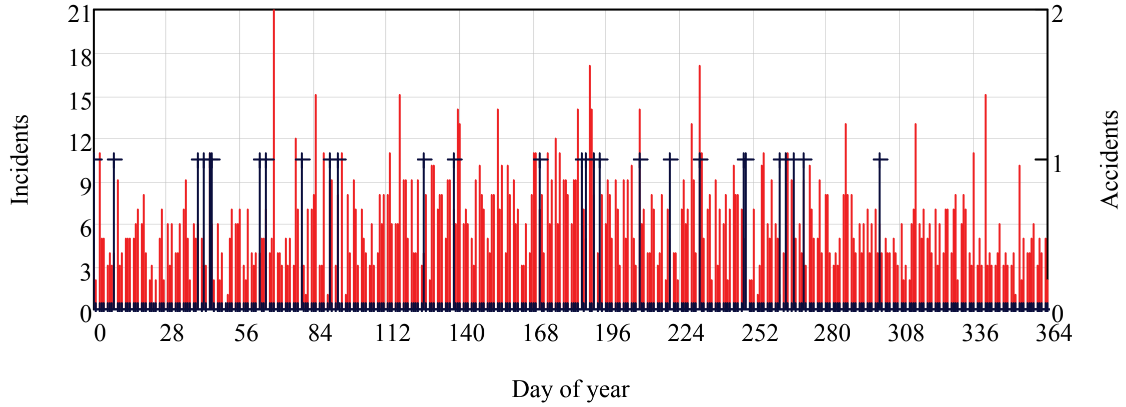

Fig. 2. Time distribution of worldwide occurrences

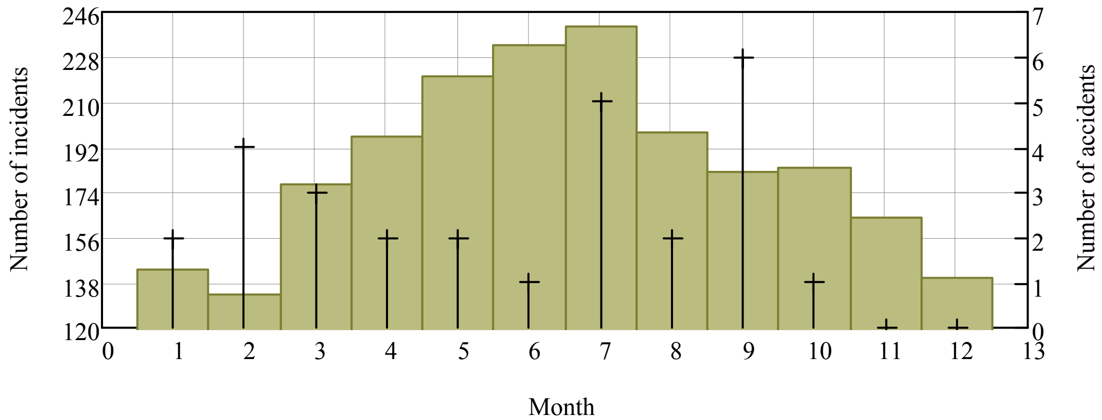

Fig. 3. Sum values of worldwide accidents and incidents per month

Space weather parameters were obtained from data base of National Oceanic and Atmospheric Administration (NOAA) [3]. For SW data analyzing were used the next parameters:

$F10.7$ - sun radio flux with wavelength 10.7 cm, 2800 MHz ($10^{-22}\,\mathrm{W \cdot m^{-2} \cdot Hz^{-1}}$);

SSN - Sun spot number;

$A\mathrm{p}$ - planetary index of Earth magnetic field disturbance;

$P > 1$ - proton fluence with energy greater than 1 MeV ($\mathrm{Proton \cdot s^{-1} \cdot ster^{-1} \cdot cm^{-2}}$);

$P > 10$ - proton fluence with energy greater than 10 MeV;

$P > 100$ - proton fluence with energy greater than 100 MeV;

$E > 0.8$ -electron fluence with energy greater than 0.8 MeV ($\mathrm{Electron \cdot s^{-1} \cdot ster^{-1} \cdot cm^{-2}}$);

$E > 2$ - electron fluence with energy greater than 2 MeV.

First of all, Spearman’s correlation coefficient between total value of occurrences and average value of SW-parameters per day was commutated (Table 3).

Table 3

Correlation between SW-parameters and worldwide occurrences

Occurrences	SW-parameters	Spearman's correlation
Total number of aviation occurrences per day	*F*10.7	-0.107
	SSN	-0.029
	*A*p	0.145
	$P > 1$	0.007
	$P > 10$	-0.127
	$E > 0.8$	0.01
	$E > 2$	0.038

Secondly, the correlation between total value of occurrences and total value of SW-parameters per month was calculated. Maximum value of Spearman's correlation coefficient was obtained between occurrences and *A*p planetary index of Earth magnetic field disturbance, *A*p = 0.678 (Fig. 4).

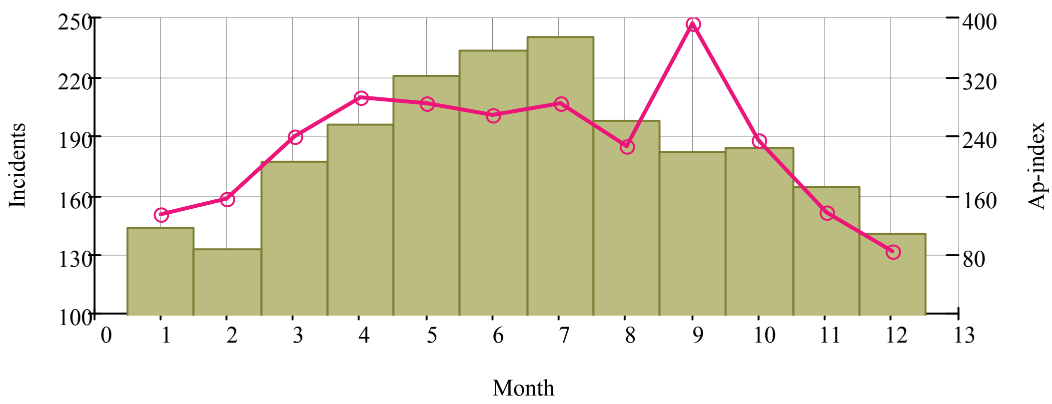

Fig.4. Ratio between total occurrences and *A*p-index per month

The statistical characteristics for occurrences and SW were calculated on next step. In Fig. 5, Fig.6 the probability density function of occurrences and *A*p-index distributions and its approximation are depicted.

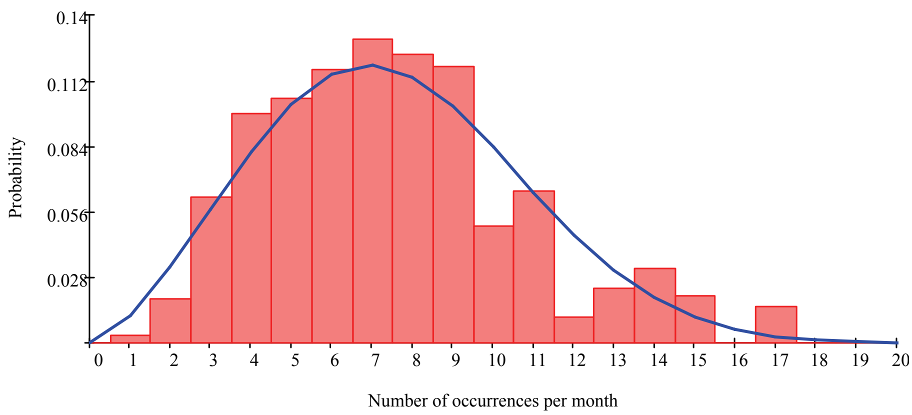

Fig. 5. Probability density function of occurrences

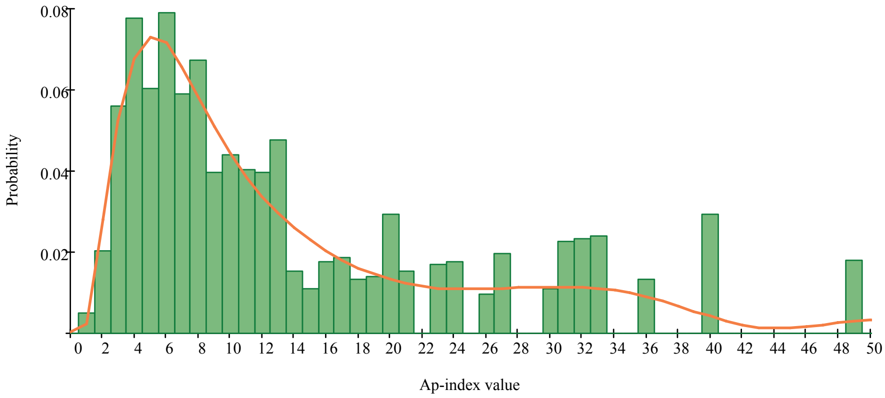

Fig. 6. Probability density function of Ap-index

Finally the cumulative distribution functions for research processes were calculated and their graphical representation in Fig.6 is shown.

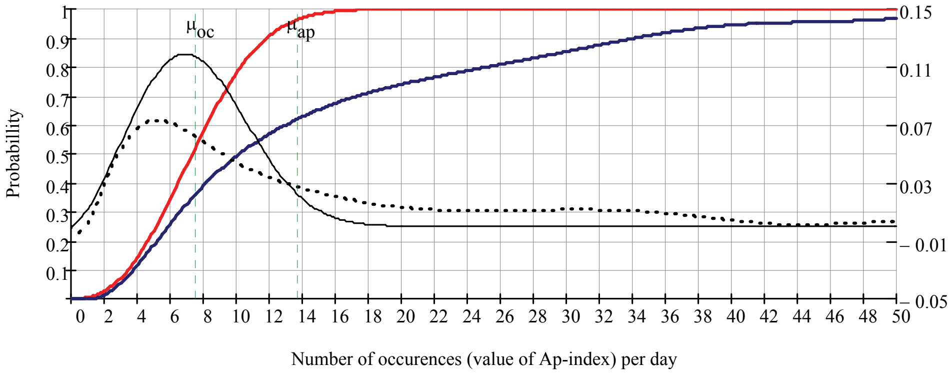

Fig. 6. Cumulative distribution functions for researched processes

Mathematical expectations for probability density functions of occurrences and Ap-index are equal to 7.54 and 13.73 correspondingly, and 3.23 and 11.00 are values for standard deviation.

Conclusion

The most generalizations of investigation consist in:

1. In 2011there were fife pronounced proton events with energy grate than 10 MeV (Solar Radiation Storm) and nine geomagnetic storms with value of Ap-index grate than 40.
2. Correlation analysis of total worldwide occurrences and average values of space weather parameters per day showed the weak correlation between these processes (maximum value is equal to 0.145 between occurrences and Ap-index).
3. Correlation analysis of total worldwide occurrences and average values of Ap-index per month gave Spearman's correlation coefficient value 0.678.
4. The probability density and cumulative distribution functions there were computed for aviation occurrences and Ap-index.
5. In compliance with the computation of statistical characteristics have prognosticated that the probability of aviation occurrences appearance in range from 4 to 10 is equal to 0.67, provided that the probability appearance of Ap-index value in range from 3 to 25 is equal to 0.75.

References

1. *Occurrences in the ASN safety database*.//http://aviation-safety.net/database/ http://aviation-safety.net/database/dblist.php?Year=2011.
2. *Tim Murphy*, Space Weather Effects on Aviation An Overview/ The 2011 SpaceWeather Workshop was held.– April 26-29, 2011.– 42 p.
3. *Space Weather Data and Products*.– http://www.swpc.noaa.gov/Data/index.html.

UDC 656.7.084:519.81(043.2)

D.V. Vasyliev, post-graduate student
(National Aviation University, Ukraine)

MULTIOBJECTIVE OPTIMIZATION OF AIRCRAFT CONFLICTS RESOLUTION

The problem of multiobjective optimization of aircraft conflicts resolution is considered. The optimality criteria, limitations and decision-making model for multiobjective selection of conflict-free trajectory are determined.

Today the important problem is developing of new methods and systems of aircraft conflicts resolution which should ensure the formation of conflict-free trajectories in conditions of high relative dynamics of air traffic according to the selected optimality criteria.

It is necessary to determine the decision variables (alternatives), optimality criteria, set of acceptable decisions and the method of decision choosing for defining the decision-making model for aircraft conflicts resolution.

The decision variables are the trajectories of aircraft flight.

Optimality criteria for aircraft conflicts resolution are: flight safety, regularity and economy of flights, aircraft priorities, maneuvers complexity and passengers comfort.

The main criterion is the flight safety. The problem of aircraft conflict resolution is the problem of determination the flight trajectory which provides maintaining of flight safety at the required level.

Current trends of increasing the intensity of flights causing the need to take into account the criteria of regularity and economy of flights. It is advisable to take into account the individual priorities of aircraft according to their operating conditions, fuel on board, type of flight (lettered, special etc.).

The important criterion for air navigation and air traffic service is the complexity and duration of conflict resolution maneuver. The criterion of comfort receives much attention from airlines because performing of turns with large bank angles, abrupt changes of altitude and speed causes the deterioration of passengers comfort.

It is proposed to perform the optimization by criteria of flight safety C_1, regularity C_2 and economy C_3 for multiobjective aircraft conflicts resolution (fig. 1).

Flight safety level is characterized by the class of air traffic situation which is determined by the metric. Regularity is determined by deviations from the flight plan (deviations from the planned time and deviations from the planned flight level or altitude), economy is determined by fuel consumption.

Aircraft priorities, maneuvers complexity and passengers comfort are transformed into limitations:

- aircraft with engine or equipment failures, aircraft in special flights or aircraft with low fuel on board can’t make maneuvers;
- number of flight profile changes and duration of conflict resolution maneuvers are limited;
- aircraft acceleration and bank angle are limited.

Other limitations are:

- aircraft operational limitations;
- flight rules;
- restricted airspace (prohibited, restricted or dangerous areas);
- areas of dangerous weather phenomena;
- rules of conflicts resolution.

Limitations define the set of acceptable trajectories D from which the optimal trajectory must be selected according to safety, regularity and economy of flights.

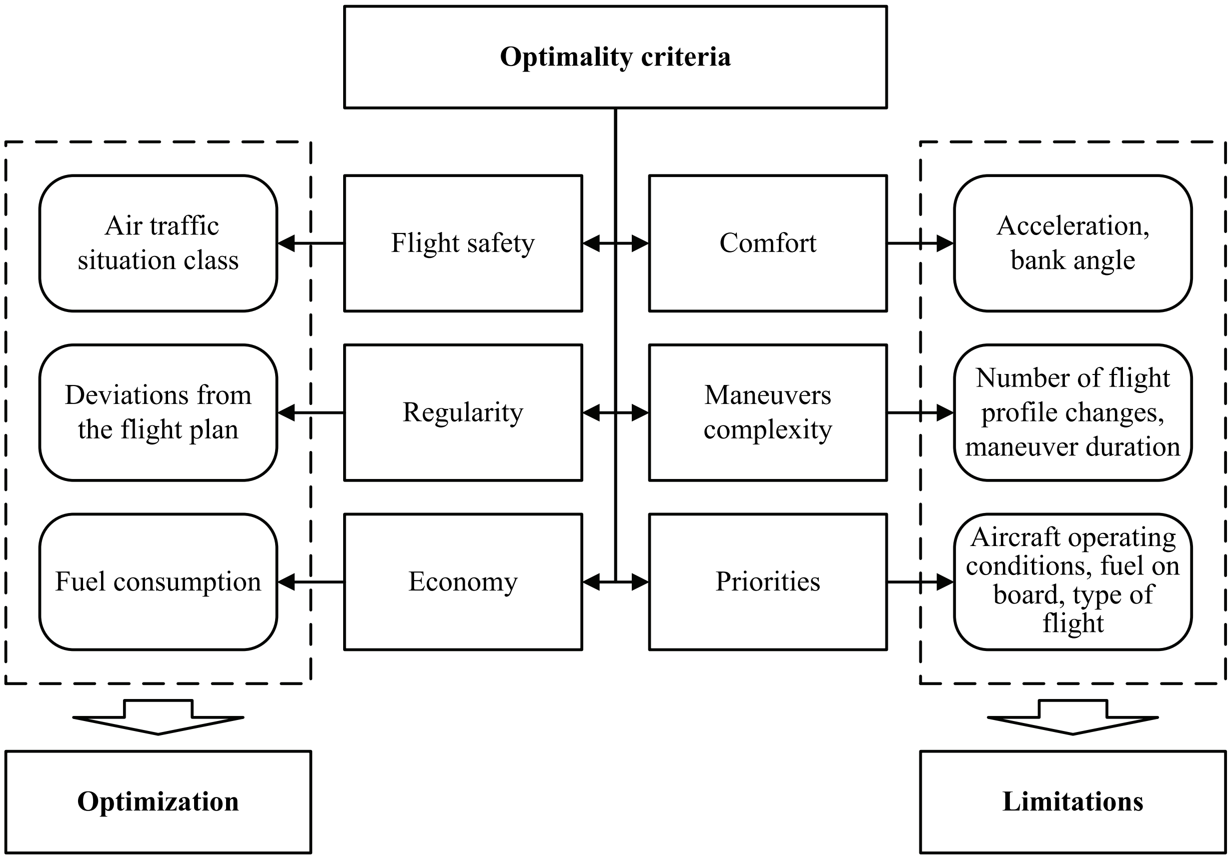

Fig. 1. Optimality criteria for aircraft conflicts resolution

For defined set of trajectories $X \in D$ the problem of optimal trajectory x^* selection is formulated as follows: it is necessary to select the trajectory x^* with minimum of objective (loss) function $F(x)$ from the set of trajectories $X_s \in X$ that provide conflict resolution. Losses are deviations from the flight plan and fuel consumption.

The values of optimality criteria for the trajectory x defined as follows:

$$C_1(x) = f(s(x)),$$
$$C_2(x) = f(\Delta t(x), \Delta h(x)),$$
$$C_3(x) = f(q(x)),$$

where s – value of air traffic situation metric; Δt – deviation from the planned time; Δh – deviation from the planned flight level or altitude; q – fuel consumption; f – normalizing function which provide the membership of criteria values to acceptable set $D_C = \{C \mid C_i \in [0,1], i = \overline{1,3}\}$.

Problem is solved in three stages. The first stage of problem solving is determining the set of trajectories X_s that provide conflict resolution (when $C_1(x) \in S$, where S is the values set for conflict-free situation).

The second stage of solving the problem is the definition of Pareto-optimal alternatives (trajectories) P_x from the set X_s.

The third step is to determine the optimal trajectory x^* from Pareto-optimal set P_x by finding the minimum of objective function:

$$F^* = F(x^*) = \min_{x \in D_x} F(x), \; D_x = P_x.$$

To determine the objective function the linear convolution of regularity criterion C_2 and economy criterion C_3 is used:

$$F(x) = w_2 C_2(x) + w_3 C_3(x),$$

where w – weighting coefficients which define the relative importance of criteria.

Regularity is major factor in comparison with economy. This is due to the fact that significant deviations from planned trajectory may lead the new conflicts, overloads of airspace elements, changes is arrival/departure slots etc.

Optimality criteria are ranked in order of importance decreasing:

$$C_2 \succ C_3 \Leftrightarrow w_2 \geq w_3 .$$

The set of weighting coefficients admissible values is equal to:

$$D_w = \{w \mid w_2 \geq w_3 \geq w_0 \geq 0,\, w_2 + w_3 = 1\}.$$

The values of weighting coefficients w can not be clearly defined. Therefore, the decision-making process should take into account the dependence of the values of weighting coefficients w for each trajectory x from the values of optimality criteria $C(x)$ and minimum value of weighting coefficients w_0.

With known value w_0 determination of weighting coefficients is linear programming problem:

$$w(x) = \arg \max_{w \in D_w} F(x) = \arg \max_{w \in D_w} (w_2 C_2(x) + w_3 C_3(x)).$$

In such case the problem of the optimal trajectory x^* selection is reduced to the following:

$$F^* = F(x^*) = \min_{x \in D_x} \max_{w \in D_w} (w_2 C_2(x) + w_3 C_3(x)).$$

Conclusion

Aircraft conflicts resolution systems should provide the formation of conflict-free trajectories according to optimality criteria of flight safety, regularity and economy with limitations on aircraft priorities, maneuvers complexity and passengers comfort.

The proposed method of optimal trajectory determining from the predefined set of trajectories can be used for developing of modern multiobjective conflict resolution systems.

It is necessary to develop the multiobjective decision-making models and methods for optimal maneuvers selection at sequential multi-step conflict-free trajectories forming.

References

1. *Васильєв Д.В.* Прийняття рішень при багатокритеріальному розв’язанні конфліктних ситуацій між повітряними кораблями / Д.В. Васильєв // Проблеми навігації і управління рухом: всеукр. наук.-практ. конф. студентів та молодих учених, 21-22 листопада 2011 р.: тези доп. – К.: НАУ, 2011. – С. 7.

2. *Bicchi A.* On Optimal Cooperative Conflict Resolution for Air Traffic Management Systems / A. Bicchi, L. Pallottino // IEEE Transactions on Intelligent Transportation Systems, 2000. – Vol. 4, No. 1. – P. 221–232.

3. *Menon P.K.* Optimal Strategies for Free Flight Air Traffic Conflict Resolution / P.K. Menon, G.D. Sweriduk, B. Sridhar // Journal of Guidance, Control and Dynamics, 1999. – No. 22(2). – P.202-211.

4. *Кини Р.Л.* Принятие решений при многих критериях: предпочтения и замещения / Р.Л. Кини, Х. Райфа; пер. с англ. под ред. И.Ф. Шахнова. – М.: Радио и связь, 1981. – 560 с.

5. *Лотов А.В.* Многокритериальные задачи принятия решений: учебное пособие. / А.В. Лотов, И.И. Поспелова. – М.: МАКС Пресс, 2008. – 197 с.

6. *Таха Хэмди А.* Введение в исследование операций, 6-е издание / Хэмди А. Таха; пер. с англ. – М.: Издательский дом «Вильямс», 2001. – 912 с.

UDC 656.7.084(043.2)

S.A. Buinovskyi, junior researcher
(National Aviation University, Ukraine)

CORRECTION OF TRAFFIC COLLISION AVOIDANCE SYSTEM ADVISORIES USING DATA OF GROUND PROXIMITY WARNING SYSTEM

Considered the algorithm for correction of Traffic Collision Avoidance System advisories using data of Ground Proximity Warning System and its verification by computer modeling.

Today the actual task is development of algorithms that should ensure the resolution of conflicts between aircraft with guaranteed safety of obstacle clearance in the direction of flight.

The necessary function is a correction of resolution advisory (RA) issued by Traffic Collision Avoidance System (TCAS) according to the danger of collision with the ground.

The developed algorithm for correction of TCAS advisories using data of Ground Proximity Warning System (GPWS) is presented on fig. 1.

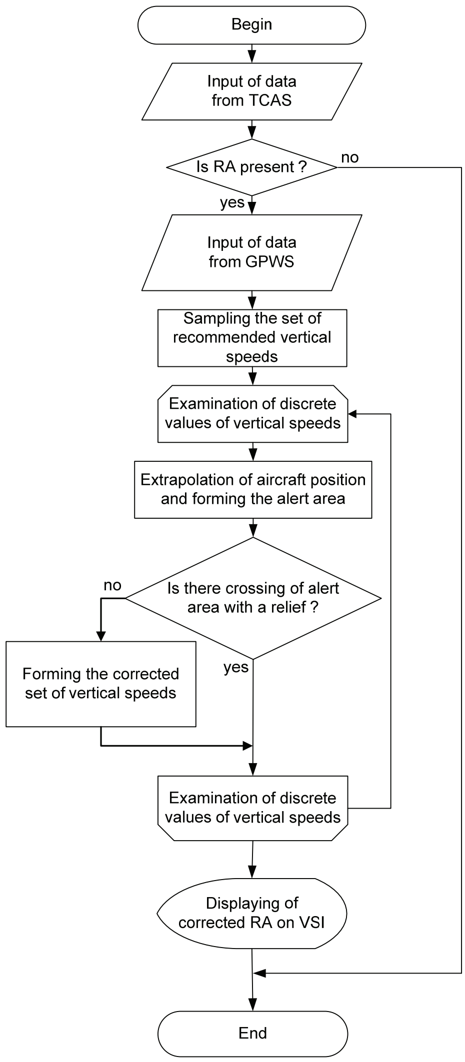

Fig. 1. The algorithm for correction of TCAS advisories using data of GPWS

Principle of work of the offered algorithm consists in the following. The algorithm works when the TCAS gives out RA (set of recommended vertical speeds) for conflict resolution between aircraft.

The information about terrain relief in the direction of aircraft flight is entered from the database of GPWS. Also the altitude, ground and vertical speed is entered.

The set of recommended vertical speeds is sampled with a step ΔV_h.

For every value of recommended vertical speed the alert area of signaling about the insufficient height of flight above an obstacle is built.

If the alert area does not intersect with a terrain, information about which is taken from a GPWS database, such value of the recommended vertical speed is attributed to the set of corrected. It means that flying with such vertical speed during extrapolation time T_e will not cause the danger of collision with terrain. As a result of examination of all discrete values of recommended vertical speed the corrected set will be formed.

Corrected advisories are displaying on the vertical speed indicator (VSI).

For verification the algorithm the special computer program was developed.

The program allows modeling the correction of RA and flight trajectory in discrete moments of time. For modeling the aircraft motion the following system of equations are used:

$$\begin{cases} s(t_i) = s(t_{i-1}) + W(t_{i-1})\Delta t; \\ h(t_i) = h(t_{i-1}) + V_h(t_{i-1})\Delta t; \\ t_i = t_{i-1} + \Delta t, \end{cases}$$

where $s(t_i)$ – distance at moment t_i; $h(t_i)$ – altitude at moment t_i; W – ground speed; V_h – vertical speed; Δt – time discrete.

In this program the algorithms of GPWS «SRPPZ-2000» made by Joint-stock company "Ukrniira" are used to built the alert areas.

It is assumed that the pitch angle changes almost instantly and that crew select the mean value $\overline{V}_h$ from the set of corrected vertical speeds:

$$\overline{V}_h = \frac{V^*_{h\,max} + V^*_{h\,min}}{2},$$

where $V^*_{h\,max}, V^*_{h\,min}$ – maximum and minimum value of the corrected vertical speeds.

For verification the developed algorithm the resolution of conflict situation were modeled: TCAS gives out RA which must be corrected. It was assumed that maximum and minimum values of the recommended vertical speeds are $V_{h\,max} = 0$ m/s, $V_{h\,min} = -10$ m/s, initial aircraft altitude is $h(t_0) = 3000$ feet, obstacle clearance height is 900 feet, extrapolation time for GPWS alert area is $T_e = 30$ s and time discrete is $\Delta t = 5$ s. In direction of flight there is an increasing of terrain elevation from 1500 feet to 1900 feet.

The results of computer modeling are shown on fig. 2 - 4.

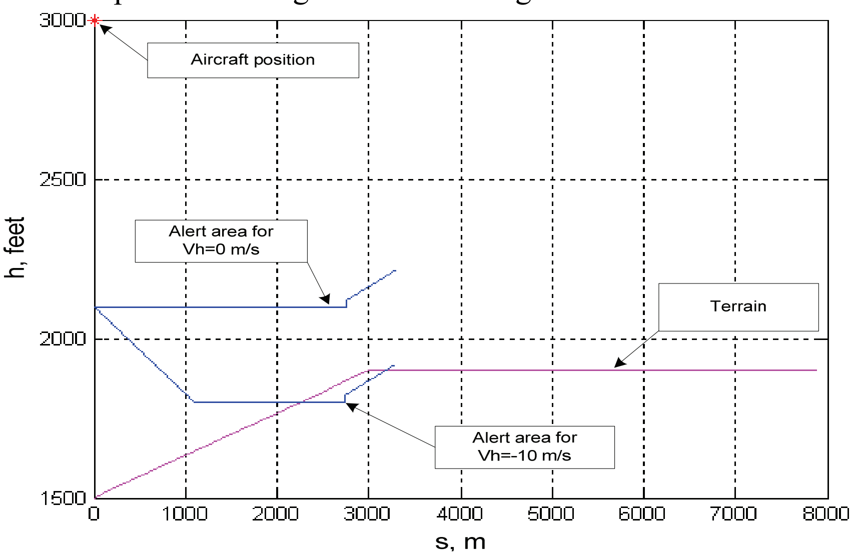

Fig. 2. The GPWS alert areas for initial moment of time

On fig. 3. alert areas are represented for three moments of time: $t = (0;20;45)s$. The algorithm provides the correct calculation of alert areas and finds the intersections with terrain. There are no intersections for the corrected vertical speeds. On fig.4 . the results of TCAS advisories correction are presented.

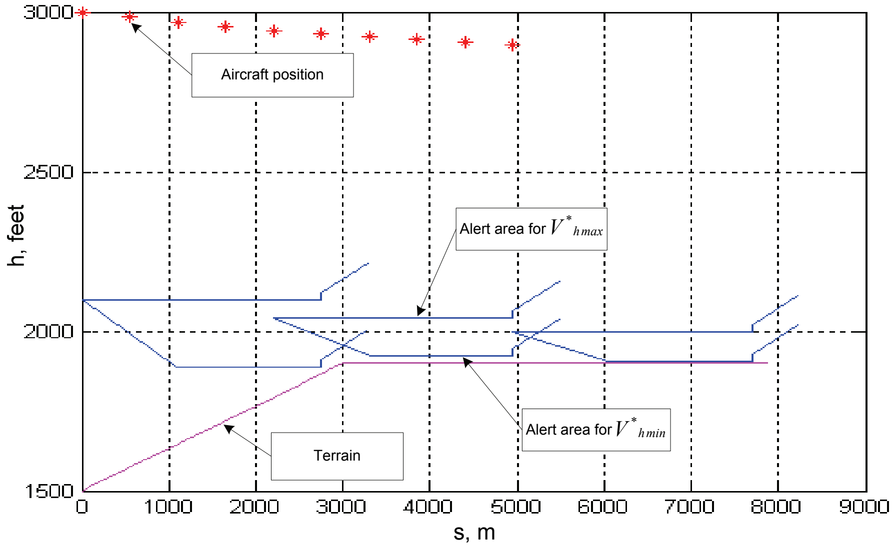

Fig. 3. Aircraft trajectory and GPWS alert areas for corrected vertical speeds

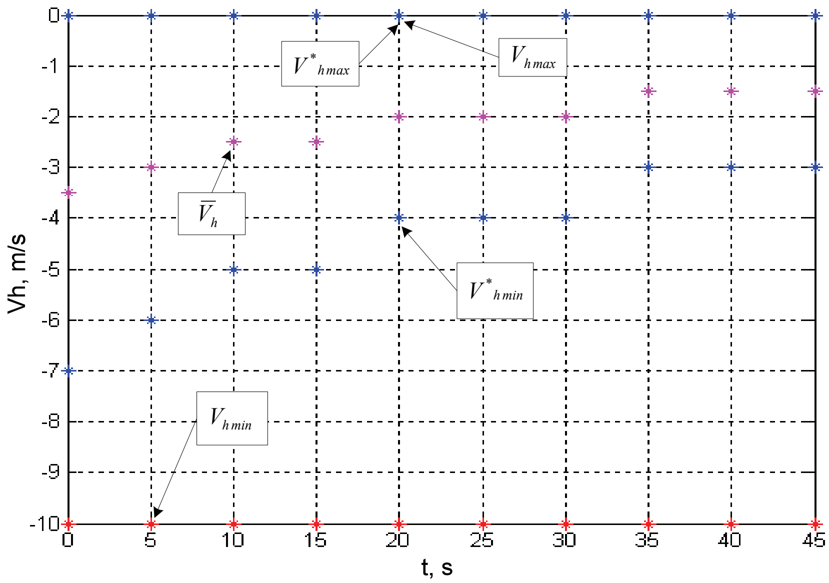

Fig. 4. Recommended by TCAS, corrected and selected vertical speeds

Conclusion

The results of computer modeling confirmed that the developed algorithm provides the correction of TCAS advisories. This algorithm can be used for development of modern systems of conflicts resolution between aircraft with guaranteed safety of obstacle clearance.

References

1. *Харченко В.П.* Аеронавігація: навч. посіб./ В.П. Харченко, Ю.В.Зайцев. – К.: Книжкове вид-во НАУ, 2008. – 272 с.

2. *Система* раннего предупреждения приближения земли СРППЗ-2000. Руководство по технической эксплуатации. ЛИКС.461131.003 РЭ. – УкрНИИРА, 2004. – 114 с.

UDC 656.7.086 (45)

V.P. Kharchenko, Doctor of Engineering, Prof. (National Aviation University)
T.F. Shmelova, Candidate of Engineering, Assoc. Prof. (Kirovograd Flight Academy of the National Aviation University)
Y.V. Sikirda, Candidate of Engineering, Assoc. Prof. (Kirovograd Flight Academy of the National Aviation University)

A METHODOLOGY FOR ANALYSIS OF FLIGHT SITUATION DEVELOPMENT USING GERT'S AND MARKOV'S NETWORKS

The methodology for analysis of flight situation development under influence decision-making by the human-operator of Socio-Technical Air Navigation System in flight emergencies using graphs, stochastic, GERT's, Markov's networks, reflexive theory has been developed. The scenarios of flight situation development using GERT's and Markov's networks have been obtained.

Statement of purpose. Air Navigation System (ANS) in conformity to the principles of functioning may be referred to socio-technical systems within which close co-operation between human and technological components occurs. The more human-operator (H-O) is trying to control a production process being aided by high level technologies, especially in case of distant operation, the more non-transparent becomes the result of the operation of a system, which is accompanied by a high degree risk of causing catastrophic outcomes [1]. Since operations in socio-technical systems generally involve high-risk / high-hazard activities, the consequences of safety breakdowns are often catastrophic in terms of loss of life and property [2]. In the ANS provision of safety is rather actual with the aim of prevention threats on the operational level, for example in flight emergencies.

Statistical data show that human errors account for up 80 % of all causes of aviation accidents [3]. The existing approaches to checking separate aspects (psycho-physiological, behavioural, ergonomic, professional, etc.) do not give the proper consideration to the functional state of H-O in the conditions of the dynamic change of external and internal factors [4]. One of the possible approaches to the solution of these problems is formalization and mathematical presentation of the ANS operators' activities in the form of a complex socio-technical systems on the base of the systemic analysis. Taking into account the influence on decision-making (DM) by H-O of ANS the professional factors (knowledge, habits, skills, experience) as well as the factors of non-professional nature (individual-psychological, psycho-physiological and socio-psychological) [5; 6; 7] enables to predict the H-O's actions and flight situation development with the aid of the informational, analytic and diagnostics Complex for research operator of ANS behaviour in extreme situation.

The purposes of the publication are:

– to develop a methodology for analysis of flight situation development under influence decision-making by H-O of ANS as a complex socio-technical system;

– to calculate the scenarios of the flight situation development under influence socio-factors.

Main part. The environmental conditions determine the reaction of H-O, while the reaction of the latter, in its turn, changes the environmental conditions themselves.

The systemic analysis which has been carried out as well as the formalization of the factors which affect DM by H-O (individual-psychological, psycho-physiological and social-psychological) in the conditions of the progress of a flight situation from normal to catastrophic to obtain [5; 6]:

– the models of preferences by a H-O under the influence of social-psychological factors;

– the models of preferences by a human-operator depending on the significance of individual-psychological factors in the conditions of development flight situations from normal to catastrophic ones;

– the models of diagnostics of psycho-physiological factors at the score of monitoring the emotional state of H-O.

Regarding the Air Navigation System as a complex socio-technical system the research based on methodology of analysis of human-operator's decision-making has been carried out. The impact of individual-psychological and socio-psychological factors on the professional activities of human-operator during the flight situation development from normal to catastrophic has been studied. On the basis of the reflexive theory of bipolar choice the expected risks of DM of the ANS's operator have been studied and the influence of external environment, previous experience and intention of the human-operator has been identified. On the basis of the methods for analysis of decision-making by the H-O of ANS using graphs, stochastic, GERT's, Markov's networks, reflexive theory [5; 6; 8; 9] the methodology for analysis of flight situation development under influence DM by H-O of ANS in flight emergencies (FE) has been developed (table 1).

Table 1

Methodology for analysis of flight situation development under influence DM by H-O of ANS in FE

№	Phase of analysis	Model	Process	Result	Model's para-meters
1	Modelling of DM by H-O in FE under Certainty	Determined models for H-O (controller, pilot) with deterministic run-time procedure	Technology of work of H-O (controller, pilot) in FE Algorithm of work of H-O (controller, pilot) in FE	Structural-hourly table of the actions taken by H-O (controller, pilot) in FE	t_i T_{cr}
		Determined models for a H-O (controller, pilot) with probabilistic run-time procedure	Determination of time t_i (t_i'), required for the performance of *i*-procedure according to the algorithm of work of H-O (controller, pilot) in FE	Network graph of taking the actions by H-O (controller, pilot) in the FE	t_i T_{cr} T_{mid} T_{min} T_{max}
2	Modelling of DM by H-O in FE under Risk	Stochastic models type Decision Trees of DM by H-O (controller, pilot) in FE	The structural analysis of DM by H-O (controller, pilot) in FE	The optimal solution is found by the criterion of an expected value with the principle of risk minimizing	A_{opt}
3	Modelling of DM by H-O in FE under Fuzzy logic	Fuzzy logic to determine quantitative estimates of potential loss	Determination of membership functions in fuzzy logic	Potential loss value in consumption of fuel, incident, breakage, accident, catastrophe	$\{g_r\}$
4	Modelling of DM by H-O in FE in Neural Network	Neural Network Model to determine potential alternative of the flight completion	Determination of weight coefficients of neural network and effectiveness of flight completion	Effectiveness of flight completion at the aerodrome (landing field) Weight coefficients of neural network	Y_G Y_{Gaer} Y_{Glf} W
5	Modelling of DM by H-O in FE under Uncertainty	Matrix of the possible results of the DM by H-O in FE	The analysis of DM by H-O (controller, pilot) in FE using Minimax, Laplace, Savage and Hurwicz criterions	The optimal solution is found by the criterion of Minimax, Laplace, Savage and Hurwicz	A_{opt}
6	Modelling of FE developing	6.1. Stochastic models type GERT's network (Graphical Evaluation and Review Technique) of DM by H-O (controller, pilot) in FE and FE developing	Analysis of the flight situation development from normal to catastrophic and conversely	Mathematical expectation of flight situation development time t_{ij}; variance of flight situation development time t_{ij}; probability of flight situation development p_{ij}	t_{ij} $M[t_{ij}]$ $\delta^2 [t_{ij}]$ p_{ij}. p_{ji} p_{ii}

Continue of table 1

		6.2. Stochastic models type Markov Chains of DM by H-O (controller, pilot) in FE	Analysis of the flight situation development from normal to catastrophic and conversely under choice towards the positive or negative pole	Transmission coefficient of (i, j)-arc in positive choice Transmission coefficient of (i, j)-arc in negative choice Value of risk during transition between flight situations Probabilities of states of flight situation	$W_{ij}(A)$ $W_{ij}(B)$ R_{ij} R_{ji} $p_{lij}(A)$ $p_{lij}(B)$
		6.3. Reflexive models of bipolar choice in FE under the influence of external environment, previous experience and intentional choice by H-O	Modelling of behavioural activity of H-O in FE under the influence of external environment, previous experience and intention in impact of individual-psychological and socio-psychological factors on the professional activities of H-O during the flight situation development	Expected risk of the DM by H-O with taking into account the criterion of the expected value minimization (choice towards the positive pole A) Expected risk of the DM by H-O with taking into account his model of preferences (choice towards the negative pole B) Mixed choice made by H-O Concept of a rational individual's behaviour System of the individual's preferences in a certain situation of the choice	R_A R_B R_{AB} г с
		6.4. Graphical-analytical models of FE development	Graphical-analytical modelling of flight situation development with taking into account individual qualities of H-O	The optimal action of H-O in FE	Y_G
		6.5. Graphical-analytical models of DM by H-O (controller, pilot) in FE	Graphical-analytical modelling of H-O decision-making in FE under influence socio-factors	Scenarios of the flight situation development	S

Scenarios of the flight situation development under influence socio-factors. The value of risk during transition between normal, complicated, difficult, emergency and catastrophic flight situations respectively has determined. The computation of one of the scenarios of the difficult situation development using GERT's network is presented in fig. 1.

Thus according to results of stochastic network analysis of the flight situation development from normal to catastrophic the following values have been obtained:

– mathematical expectation of flight situation development time $t_{ij} – M[t_{ij}]$;

– variance of flight situation development time $t_{ij} – \delta^2 [t_{ij}]$;

– probability of flight situation development $p_{ij} – p_{ij}, p_{ji}, p_{ii}$.

The example of the computation of one of the scenarios of flight situation development using Markov's network in approach performed in bad weather conditions has obtained in [6; 10] and is presented in table 2 and in fig. 2.

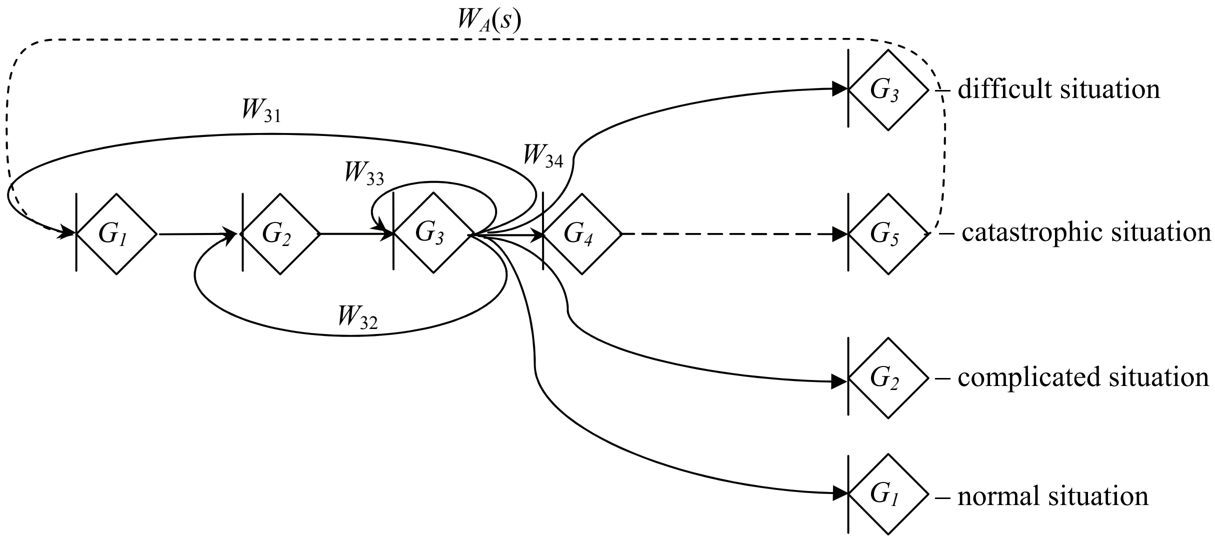

Fig. 1. Stochastic models type GERT's network (Graphical Evaluation and Review Technique) of DM by H-O (controller, pilot) in FE and developing FE: G_1 – normal situation; G_2 – complicated situation; G_3 – difficult situation; G_4 – emergency situation; G_5 – catastrophic situation; W_{ij} – W-function, transmission coefficient of (i, j)-arc

Table 2

The results of computation of the scenarios of flight situations development

Scenarios, *S*	**Probabilities, *p***	**Consequences, *U***	**Expected risks, *R*, c.u.**
S_{4B}	0,7	60	597
	0,3	59	
$S_{3\text{-}4B}$	0,7	28	874
	0,3	27	
$S_{2\text{-}3\text{-}4B}$	0,7	12	991
	0,3	11	
$S_{1\text{-}2\text{-}3\text{-}4B}$	0,7	4	1028
	0,3	3	
S_{1A}	0,7	2	17
	0,3	1	

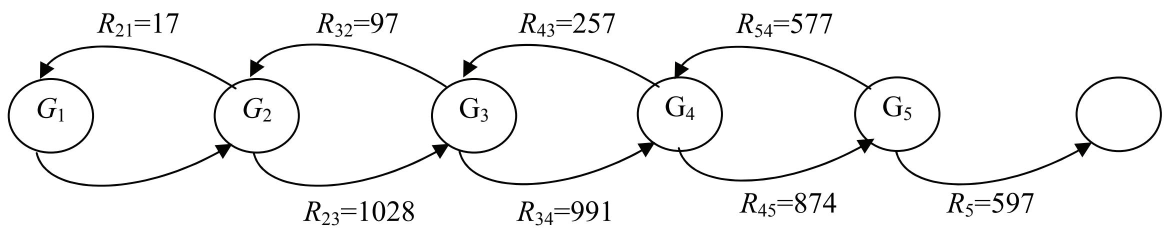

Fig. 2. Markov Chains of the development of flight situations: G_1 ,G_2, G_3, G_4 ,G_5 – normal, complicated, difficult, emergency, catastrophic situations respectively; R_{ij} – value of risk during transition between flight situations

The selection in the direction of the negative pole in compliance with the $S_{1\text{-}2\text{-}3\text{-}4B}$ scenario leads to the maximum expected risk R=1028 conventional units (c.u.). The choice in the direction of the positive pole when the FE occurs at the first stage of DM by H-O of ANS (for example, a flight to a reserve aerodrome in the difficult meteorological conditions) has a risk which is in 60,5 times lesser: R=17 c.u.

Taking into account the influence on DM by H-O of professional factors (knowledge, habits, skills, experience) as well as the factors of non-professional nature (individual-psychological, psycho-physiological and socio-psychological) enables to predict the H-O's actions with the aid of the informational-analytic and diagnostics Complex for research H-O of ANS behaviour in extreme situation. It's including next information, analysis and diagnostics modules: "Prompt" (for information support of the operator when choosing the optimal variant of flight completion in emergency situation), "Diagnosing the emotional state of human operator" (for professional qualities assessment) and "Diagnosing the operator's socionic model" (for defining a socionic type).

Conclusions

On the basis of the methods for analysis of decision-making by the H-O of ANS using graphs, stochastic, GERT's, Markov's networks, reflexive theory the methodology for analysis of flight situation development under influence DM by H-O of ANS in FE has been developed. The computations of the scenarios of flight situation development using GERT's and Markov's networks have been obtained. Models of FE development and of DM by H-O of ANS (controller, pilot) in FE will allow to predict the H-O's actions with the aid of the informational-analytic and diagnostics Complex for research H-O of ANS behaviour in extreme situation.

References

1. Human Factors Guidelines for Safety Audits Manual / Doc. 9806-AN/763. – First Edition. – Canada, Montreal: ICAO, 2002. – 138 p.

2. Cross-Cultural Factors in Aviation: Human Factors Digest №16 // Circ. ICAO 302-AN/175. – Canada, Montreal: ICAO, 2004. – 52 p.

3. *Лейченко С.Д.* Человеческий фактор в авиации: монография в 2-х книгах / С.Д. Лейченко, А.В. Малышевский, Н.Ф. Михайлик. – Кн. 1. – Кировоград: ИМЕКС, 2006. – 512 с.

4. *Keating C.B.* A Methodology for Analysis of Complex Sociotechnical Processes / C.B. Keating, A.A. Fernandez, D.A. Jacobs, P. Kauffmann // Business Process Management Journal. – 2001. – Vol. 7. – Iss. 1. – P. 33–50.

5. *Шмельова Т.Ф.* Аналіз розвитку польотних ситуацій в авіаційній соціотехнічній системі / Т.Ф. Шмельова, Ю.В. Сікірда // Збірник наукових праць Харківського університету Повітряних Сил. – 2011. – Вип. 2 (28). – С. 59–64.

6. *Kharchenko V.P.* Methodology for Analysis of Decision Making in Air Navigation System / V.P. Kharchenko, T.F. Shmelova, Y.V. Sikirda // Proceedings of the National Aviation University. – 2011. – №3. – P. 85–94.

7. *Kharchenko V.P.* Modeling of Behavioral Activity of Air Navigation System's Human-Operator in Flight Emergencies / V.P. Kharchenko, T.F. Shmelova, Y.V. Sikirda // Proceedings of the National Aviation University. – 2012. – №3. – P. 5–17.

8. *Харченко В.П.* Графоаналітичні моделі прийняття рішень людиною-оператором аеронавігаційної системи / В.П. Харченко, Т.Ф. Шмельова, Ю.В. Сікірда // Вісник Національного авіаційного університету. – 2011. – №1. – С. 5–17.

9. *Lefebvre V.A.* Functions of Fast Reflexion in Bipolar Choice / V.A. Lefebvre, J. Adams-Webber // Reflexion processes and operations. – 2001. – №1. – July-December. – T. 1. – P. 34–46.

10. *Харченко В.П.* Стохастичний мережевий аналіз розвитку польотних ситуацій / В.П. Харченко, Т.Ф. Шмельова, Ю.В. Сікірда // АВІА-2011: X міжнар. наук.-техн. конф., Київ, 19-21 квіт. 2011 р.: тези доповідей. – Т. 2. – К.: НАУ, 2011. – С. 7.28–7.31.

UDC 629.735.067:629.735-005.44(043.2)

D.O. Bugayko PhD in Economics, Associate Professor
(National Aviation University, Ukraine)

SAFETY AND EFFECTIVENESS OF CIVIL AVIATION IN CONDITIONS OF AIR TRAFFIC GLOBALIZATION

The principles of civil aviation safety and effectiveness in conditions of air traffic globalization are considered

1. ICAO ATM Global System Safety Approach

Safety will remain the highest priority in aviation, and the safety of air traffic will continue to be the most important consideration in all phases of the life cycle of the ATM system, from concept through to design, development, operation and maintenance. The system safety approach outlined below is holistic, applying across the spectrum of the ATM system, where the system will be considered to include people, procedures and technologies performing specific tasks in a given environment. Maximum effectiveness and efficiency of actions can be obtained by activities undertaken in the early phases of any system's life cycle since correcting problems during requirements definition and design is generally the most effective. Figure 1 depicts this process for the ATM system as a whole. It describes how, starting from the conceptual level and even during operation, different players and disciplines make decisions against different criteria — including safety. These decisions will progressively define the ATM system (i.e. the way in which it is organized and the way in which people, procedures, technologies and information interact to perform a task) [1].

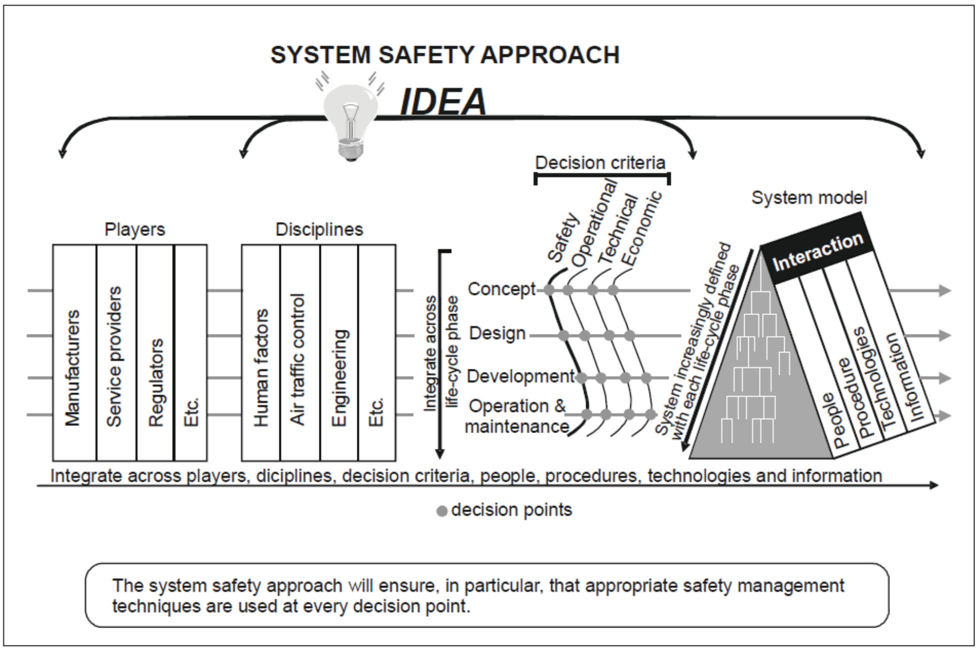

Figure 1. ICAO ATM System Safety Approach

The acceptable or tolerable level of safety will be determined from the perception of safety needs by society and the international community. Acceptable safety will be related to the trust required from the ATM system. The target level of safety will be the minimum level of safety to be achieved in any case. Possibly enforced by regulation, it will be equal to or better than the acceptable level of safety. The target level of safety will be based on risk assessment and acceptance criteria. results in a defined range without compromising acceptable and target levels of safety. These levels of safety could be specified in qualitative and/or quantitative terms, often, but not exclusively, via indicators related to safety occurrences. Examples of the latter include:

- a maximum probability of an undesirable event such as collision, loss of separation or runway incursion;
- a maximum number of accidents per flight hour;
- a maximum number of incidents per aircraft movement;
- a maximum number of valid short-term conflict alerts per aircraft movement.

2. Single European Sky – Regional Globalization of Air Space

Contrary to the United States, Europe does not have a single sky, one in which air navigation is managed at the European level. Furthermore, European airspace is among the busiest in the world with over 33,000 flights on busy days and high airport density. This makes air traffic control even more complex.

The EU Single European Sky is an ambitious initiative launched by the European Commission in 2004 to reform the architecture of European air traffic management. It proposes a legislative approach to meet future capacity and safety needs at a European rather than a local level. The Single European Sky is the only way to provide a uniform and high level of safety and efficiency over Europe's skies.

The key objectives are to

- restructure European airspace as a function of air traffic flows;
- create additional capacity;
- increase the overall efficiency of the air traffic management system.

The major elements of this new institutional and organisational framework for Air Traffic Management in Europe consist of

- separating regulatory activities from service provision, and the possibility of cross-border Air Traffic Management services;
- reorganising European airspace that is no longer constrained by national borders;
- setting common rules and standards, covering a wide range of issues, such as flight data exchanges and telecommunications.

As part of the Single European Sky initiative, SESAR (Single European Sky ATM Research) represents its technological dimension. It will help create a "paradigm shift", supported by state-of-the-art and innovative technology. The SESAR programme will give Europe a high-performance air traffic control infrastructure which will enable the safe and environmentally friendly development of air transport. A partnership programme SESAR aims to eliminate the fragmented approach to European ATM, transform the ATM system, synchronise all stakeholders and federate resources. For the first time, all aviation players are involved in the definition, development and deployment of a pan-European modernisation project. SESAR aims at developing the new generation air traffic management system capable of ensuring the safety and fluidity of air transport worldwide over the next 30 years. It is composed of three phases: The Definition phase (2004-2008) delivered the ATM master plan defining the content, the development and deployment plans of the next generation of ATM systems This definition phase was led by Eurocontrol, and co-funded by the European Commission under the Trans European Network- Transport programme and executed by a large consortium of all air transport stakeholders. The Development phase (2008-2013) will produce the required new generation of technological systems, components and operational procedures as defined in the SESAR ATM Master Plan and Work Programme. The Deployment phase (2014-2020) will see the large scale production and implementation of the new air traffic management infrastructure, composed of fully harmonised and interoperable components guaranteeing high performance air transport activities in Europe [2].

3. Safety and Effectiveness of European Sky

Eurocontrol system research shows the approach phase in total has the highest number of incidents through 2008 to 2010. The highest increase was in 2010 with more than 3.5 reports per 10,000 flights. It means that with this level of reporting, which still is not as high as it should be, during the summer period when across Europe there are more than 30, 000 flights daily there could be at least 20 incidents within the Approach phase and around 5 incidents across en-route phase (see Figure2.) [3].

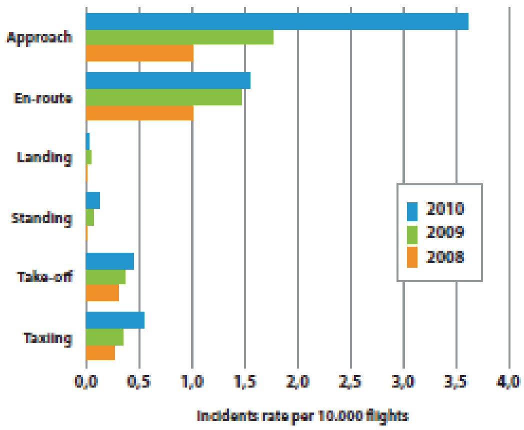

Figure 2: Incident distribution per phases of flight - 2008 - 2010

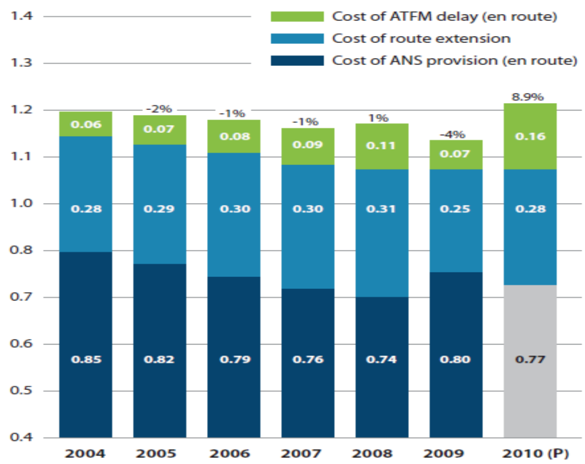

Figure 3: Real unit economic en-route cost [€2009/km]

In response to the dramatic growth in air travel over the past two decades, the fuel crisis and the growing concern about aviation's impact on the environment, the European Commission (EC) passed two Single European Sky (SES) legislative packages – in 2004 and 2009 respectively – to create a framework for the development of the future European aviation network. The total economic en-route unit cost of ANS (charges, delays and flight-inefficiencies) increased significantly in 2010 (9.1%), as shown in Figure 3 [4]. This increase was mainly due to a sharp rise in ATFM delay costs. The cost of longer flights due to avoidance of the ash cloud or congested areas was exacerbated by the significant increase in the cost of aviation fuel. Overall, this was the worst performance since 2004. Containing costs, whilst ensuring sufficient capacity to meet present and future performance objectives, will require a range of substantial changes across the ANS sector. These will not only impact on institutional, organizational and managerial functions, but also on financial, operational and technical issues.

4. Conclusion

Among the key success factors for meeting these future challenges, the following: deserve special focus: driving sustainable long-term change (i.e. short-term cost-effectiveness improvements should not jeopardise the provision of future capacity); maximising the use of existing human and capital resources; engaging in genuine change with the different partners; effective social dialogue to drive sustainable change; explore different degrees of cooperative business opportunities among ANSPs such as FABs; drive cost-effective technological innovation through SESAR; make the most effective use of the network functions; strengthening the medium-term planning process while developing ANSP business flexibility; incentivising the timely delivery of ATC capacity.

References

1. ICAO Global Air Traffic Management Operational Concept (Doc 9854). Montreal: Canada (ICAO), 2005. – 82 p.

2. Principles of Single European Sky Programme Implementation in Ukraine / *V.P. Kharchenko, D.G. Babeichuk, J.V.Chinchenko, D.O. Bugayko* // Proceedings of the National Aviation University. – Kyiv, 2009. – № 4 (47). – P. 9–13.

3. EVAIR Safety Bulletin No 7, EUROCONTROL Voluntary ATM Incident Reporting 2008. Brussels: Belgium, 2011 – 40 p.

4. EUROCONTROL Annual Report 2010 Brussels: Belgium, 2011 – 88 p.

UDC 629.735.05: 53.087.61 (045)

O.V. Solomentsev, Dr., professor
O.V. Zuiev, Ph.D., as. professor
U.M. Khmelko, Ph.D., professor
(National Aviation University, Ukraine)

ANALYSIS OF RADIOELECTRONIC EQUIPMENT DIAGNOSTICS AND RUNNING REPAIR PROGRAMS EFFICIENCY

The diagnostic programs of Radioelectronic Equipment technical state are aimed at searching failed element. A rational variant of the diagnostic programs realization is chosen after the comparative analysis of efficiency with the use of generalized criterion or a set of partial criteria.

Technical diagnostics – is the process of defining the diagnostics object (DO) technical state. The DO technical state changes in case of its elements failures. Therefore technical diagnostics – is actually the process of searching a failed DO element [1; 3; 4; 6; 7; 8].

The methods of Radioelectronic Equipment (REE) technical state diagnostics can be conditionally divided into two groups: statistical and analytical.

Statistical methods are based on application of statistical data of failures and damages in REE units and elements REE, collected and analyzed be forehand.

Analytical methods of REE diagnostics technical state can be conditionally divided into two subgroups. The methods of the first subgroup set the method of checking REE serviceability. The methods of the second subgroup set the sequence of control - measuring operations.

The methods of REE fault- detection differ in the level of material resources consumption (time, cost, necessary control equipment), as well as in qualification of service personnel etc. [1; 2; 3; 4].

A rational variant is chosen after the comparative analysis of efficiency with the use of generalized criterion or a set of partial criteria. In the field of technical diagnostics the following basic efficiency indexes are used:

– D – probability of correct diagnostics. It is complete probability of that diagnostics system determines that technical state, in which DO is indeed;

– $m_1(t_d)$ – mean duration of diagnostics (mathematical expectation of one diagnostics duration);

– $m_1(C_d)$ – average cost of diagnostics (value estimating the mathematical expectation of one diagnostics cost);

– $m_1(Z_d)$ – average labour intensity of diagnostics (value estimating the mathematical expectation of time taken by one diagnostics).

Duration of diagnostics process is a casual value.

To obtaine basic calculation correlations for analyzing diagnostics programs (DP) or running repair programs (RRP) efficiency it is expedient to use the graph-analytic method. For this purpose a graph of technical diagnostics or RRO running process is made, where these operations (graph units) are connected with edges as arrows specifying the sequence of separate operations taking into account the results of decision-making on determining parameters X_i state.

Every edge corresponds to conditional probabilities of transition from the initial state to a neighboring one, as well as other characteristics, for example, duration of technological operation, after which a change in DO technical state, material expenditures on technological operation etc. have taken place.

For drafting graphs it is possible to use corresponding DP or RRP, if they are supplemented with necessary data on resources consumption.

In general case as many graphs are made, as there are elements in RRO. However, if there are no errors during DP control, then it is possible to apply one graph coinciding with DP or RRP image.

The graph of running repair process is built in accordance with the following general rules:

– after decision - making on the RRO functional element failure it is replaced with a serviceable one and the output control of the whole REE is executed;

– if the control testifies the REE up - state, the process of running repair is completed;

– if the RRO output control testifies the device faulty state, then regardless of whether there was replacement of RRO element, or not yet, successive replacement of RRO elements are done and obligatory output control of the whole RRO serviceability is fullfiled until RRO gets serviceable.

On the whole, application of these rules in case of control errors guarantees eventual duration of REE technical diagnostics and running repair process. Diagnostics or running repair graphs include sets of technological operations (STO).

This term determines a TO set, resulting in the search of the failed DM element or RRO serviceability restoration. To this set we refer the operations of DP control, replacement of failed RRO elements, and output control of RRO up - state after its repair. If there are no errors of DP control, the graph of RRO conditions, in the case of *i-th* REE element failure, will include one STO, stipulating restoration of REE serviceability after correct detection and replacement of the failed *i-th* element, by a serviceable one and positive control of the whole REE serviceability. Separate STO make a complete group of events.

Let’s consider DP efficiency analysis. Each STO can be connected with corresponding material resources consumption – average aggregate time of *i-th* STO fulfilment, average aggregate labour intensity of *i-th* STO fulfilment, average aggregate costs of *i-th* STO fulfilment.

Conditional average indexes of a certain DP efficiency during REE diagnostics, if there are no errors in the process of DP control, are determined as

$$m_1(t(S\mathrm{TO}_j / S_j)) = \sum_{i=1}^{l_j} t_{cij} \,,$$

$$m_1(Z(S\mathrm{TO}_j / S_j)) = \sum_{i=1}^{l_j} Z_{cij} \,,$$

$$m_1(C(S\mathrm{TO}_j / S_j)) = \sum_{i=1}^{l_j} C_{cij} \,,$$

where $m_1(t(S\mathrm{TO}_j / S_j))$ – conditional mathematical expectation of total duration of *j-th* STO fulfilment in case of *j-th* DO element failure; $m_1(Z(S\mathrm{TO}_j / S_j))$ – conditional mathematical expectation of *jth* STO set aggregate labour intensity in the case of *j-th* DO element failure; $m_1(C(S\mathrm{TO}_j / S_j))$ – conditional mathematical expectation of *j-th* STO set aggregate costs in the case of *j-th* DO element failure; t_{cij} – mathematical expectation of *i-th* DP control duration in the case of the *j-th* REE DM element failure; Z_{cij} – mathematical expectation of *i-th* DP control labour intensity in the case of *j-th* DM element failure; C_{cij} – mathematical expectation of *i-th* DP control cost in the case of *j-th* DM element failure; *lj* – the quantity of the control operations of detecting *j-th* DO failed element; S_j – DO condition in the case of *j-th* DO element failure.

To determine absolute efficiency indexes it is necessary to fullfil another averaging operation:

$$m_1(t_\mathrm{d}) = \sum_{j=1}^{N} m_1(t(S\mathrm{TO}_j / S_j))Q_j \,;$$

$$m_1(Z_\mathrm{d}) = \sum_{j=1}^{N} m_1(Z(S\mathrm{TO}_j / S_j))Q_j \,; \qquad (1)$$

$$m_1(C_{\text{d}}) = \sum_{j=1}^{N} m_1(C(S\text{TO}_j / S_j))Q_j\,,$$

where $m_1(t_{\text{d}})$ – mathematical expectation of one DO diagnostics duration; $m_1(C_{\text{d}})$ – mathematical expectation of one DO diagnostics cost; $m_1(Z_{\text{d}})$ – mathematical expectation of one DO diagnostics labour intensity; N – total quantity of DO elements; Q_j – probability of *j-th* DO element failure.

Using efficiency indexes $m_1(t_{\text{d}})$, $m_1(C_{\text{d}})$, $m_1(Z_{\text{d}})$, according to formula (1), it is possible to perform a comparative analysis of different DPs efficiency.

If there are no statistical data about DO or RRO elements reliability, probabilities of elements failures *Qi* can be calculated by the known technology [1]. For this purpose the specification to the REE principle electric chart is used, a list and quantity of ERC contained in each DO or RRO element are determined. Assuming, that in terms the reliability theory ERC are connected in series, failures rate of *i-th* DM or RRO element can be calculated according to the formula

$$\text{л}_i = \sum_{j=1}^{K_i} n_{ij}\text{л}_{ij} \tag{2}$$

where K_i – quantity of ERC groups, of which the electric chart of *i-th* element is built (to ERC groups we may refer resistors, capacitors, chips etc.); n_{ij} – quantity of *j-th* group ERC, included in the principle chart of *i-th* element; л_{ij} – average failure rate of *j-th* group ERC, included in the *i-th* DO or RRO element.

Failure rates are taken from reference tables [5], considering operation conditions as normal.

Calculating value of л_i according to formula (2), failure probabilities of DO or RRO elements are determined, assuming, that only one element of the equipment can fail and elements failures are independent of each other:

$$Q_i = \frac{\text{л}_i}{\sum_{j=1}^{N} \text{л}_j}\,.$$

In case errors in DP state classification, both the REE diagnostics and running repair procedures are sharply complicated. There may be the situations of erroneous decisions as to DO or RRO condition, that may result in excessive consumption of resources during REE diagnostics or running repair.

As for the running repair let's note that in case of any element failure RRO state graph will contain as many STOs as there are elements in RRO. In this case only one of all possible STOs will provide faithful detection of the faulty element, others will be characterized with additional consumption of resources due to erroneous replacement of RRO elements as a result errors of DP condition control. Analysing RRP efficiency, it is necessary to make as many RRO state graphs, as there are elements in RRO. These graphs will help to define probabilities of STO performance correctly taking into account which element is faulty, and the probability of the first and second kind errors. According to the probabilities theory certain STO make a complete group of events.

Every STO during RRP can be connected with corresponding conditional consumption of material resources, such as conditional mathematical expectation of *i*-th STO aggregate time during maintenance and in case of the *j*-th RRO element failure $m_1(t(STO_i / S_j))$.

Then conventional average efficiency criteria are calculated as follows:

$$m_1(t_{\text{r}} / S_j) = \sum_{i=1}^{M_j} P(STO_i / S_j) m_1(t(STO_i / S_j))\,,$$

where $m_1(t_r / S_j)$ – conditional mathematical expectation value of time – taking for current repair with RRO *j*-th element faulty; M_j – the number of STO during RRO running repair due to its *j*-th element failure. STO quantity is equal to the quantity of RRO elements; $m_1(t(STO_i / S_j)$ – conditional mathematical expectation of the i-th STO total time during maintenance and in case of the j-th RRO element failure; $P(STO_i / S_j)$ – conditional probability of the i-th STO resulting from RRO j-th element failure.

To determine the RRO efficiency index unconditional value it is necessary to perform one more averaging operation:

$$m_1(t_r) = \sum_{j=1}^{N} m_1(t_r / S_j) P(S_j);$$

$$у(t_r) = (\sum_{j=1}^{N} (m_1(t_r) - m_1(t_r / S_j))^2 P(S_j))^{1/2};$$

$$P(S_j) = Q_j,$$

where N – total RRO elements quantity; Q_j – RRO j-th element failure probability.

The formula for determining correct diagnostics of DO average probability is the following:

$$m_1(D) = \sum_{j=1}^{N} D(S_j) Q_j \quad ,$$

where $D(S_j)$ – is conditional probability of DO correct diagnostics in the case of j-th element failure.

To determine $D(S_j)$ we may consider any of the RRO running repair graphs.

Conclusions

The general approach obtained for the optimal Radioelectronic Equipment diagnostics and running repair programs realization, when solving the problem of that programs efficiency indexes determining. The results can be used for the design and modernization of Radioelectronic Equipment exploitation systems.

References

1. *Семенов А. А., Мелкумян В. Г.* Основи теорії надійності: Навч. посіб. – К.: КМУЦА, 1998. – 84 с.
2. *Новиков В. С.* Техническая эксплуатация авиационного радиоэлектронного оборудования. – М.: Транспорт, 1987. – 261 с.
3. Надежность технических систем: Справочник / Под ред. И. А.Ушакова. – М.: Радио и связь, 1985. – 608 с.
4. *Мелкумян В. Г.* Технологічні системи обслуговуючого типу. Елементи теорії проектування і прикладні задачі експлуатації. – К.: НАУ, 2003. – 171 с.
5. *Пацюра И. В., Корнійчук А.И., Довбыш Л. В.* Надежность электронных систем. – К.: Світ,1997. – 129 с.
6. *ДСТУ–2860.* Надійність техніки. Терміни та визначення. Чинний від 01.01.96. – К.: Держстандарт України, 1995. – 92 с.
7. *ДСТУ 2862–94.* Надійність техніки. Методи розрахунку показників надійності. Загальні вимоги. Чинний від 01.01.97. – К.: Держстандарт України, 1995. – 30 с.
8. *ДСТУ 2470–94.* Надійність техніки. Системи технологічні. Терміни та визначення. – Чинний від 01.01.94. – К.: Держстандарт України, 1995. – 92 с.

UDC 629.735.05: 53.087.61 (045)

O.V. Solomentsev, Dr., professor
I.M. Yashanov, post-graduate student
M.J. Zalisky, Ph.D.
A.O. Musienko, post-graduate student
(National Aviation University, Ukraine)

APPROACH TO OBTAINING MAINTENANCE CHARACTERISTICS OF AVIATION RADIOELECTRONIC EQUIPMENT

Approach to solving the inverse problem in exploitation systems at diagnosing technical state the radio equipment is considered, equations for calculating the maximum numbers of primary exploitation indicators for a given efficiency indicator are listed.

Exploitation's systems of aviation radioelectronic equipment include technological processes and some technological operations for performance of works and provide services in respect technical maintenance and repair of equipment, information processing, decision making, formation of peer reviews, etc [1–3]. To study and modernization of certain technological operations, processes and exploitation's systems characteristics selection as a whole we can distinguish two types of tasks - direct and inverse. When solving the direct problem, usually formed the alternative variants objects design, then calculated numerical values of efficiency indexes of alternative variants and in accordance with set criteria selected the best option [4]. For the solution of the inverse problem for a given level of numerical values of the generalized index of the effectiveness of the whole research object or its individual parts usually determine the numerical values, that are components of the index, using a given criterion of optimality values of these parameters.

In the existing regulatory documents [5] and the scientific and technical literature to estimate the effectiveness of technologic processes, usually calculated parameters of efficiency in the form of mathematical expectation of resources cost and related variances. When solving the direct problem of estimation the effectiveness of systems, there are possible errors, that arise in the evaluation process of conformity complex information parameters specified requirements, and there are possible questions about the timely consideration of parameters of these operations as errors of the first and second kind (using the corresponding conditional probabilities α and β). If the errors of the first and second kind are not taken into account, the overall efficiency of exploitation will be underestimated.

Consider a generalized approach to solving the inverse problem of determining the parameters of the current repair exploitation object, when during estimation under complex information parameters mistakes of the first and second kind are possible. Let have some maintenance object, which consists of n structural elements. For this object is known diagnostic model and diagnostic program. In this case diagnostic model consists of m hierarchical levels of the conformity assessment operations, where $m \le n-1$.

For solving the inverse problem determine the full group of parameters (vector of errors of the first and second kind $\vec{\alpha}$ and $\vec{\beta}$, operations duration vectors of the conformity assessment $\vec{t}_k$, replacement operations of inappropriate items $\vec{t}_{\text{r.i.}}$, etc.), which are a part of one or more efficiency indexes, that characterize the process of current maintenance. One or more parameters defined as optimization. In this case are chosen efficiency criterion (for example, minimum or maximum of some optimization parameter, it does not exceed pre-set level, etc.) to fix other parameters. For convenience and simplification of problem assume, that $\alpha_i = \alpha$; $\beta_i = \beta$; $t_{k_i} = t_k$; $t_{\text{r.i.}_i} = t_{\text{r.i.}}$ for any $i \in (0; m]$.

Performance indicators are: 1) $m_1(t_{\text{cr}})$ – mathematical expectation of current repair duration t_{cr}; 2) $\mu_2(t_{\text{cr}})$ – variance of current repair duration t_{cr}; 3) $m_1(t_{\text{cr}}) + K \cdot \sigma(t_{\text{cr}})$, where K – constant coefficient; $\sigma(t_{\text{cr}})$ – standard deviation of current repair duration t_{cr}.

Consider the case of efficiency index optimization in the form of the mean duration of current repair $m_1(t_{\text{cr}})$. We consider that optimization will be carried out by α, β and t_k. As known diagnostic model and diagnostic program, we can set the dependence

$$m_1(t_{\text{cr}}) = f(\alpha, \beta, t_k).$$

In this case there are seven possible options for solving the inverse problem: optimization for α; optimization for β; optimization for t_k; optimization for α and β; optimization for α and t_k; optimization for β and t_k; optimization for α, β and t_k. Consider each of these options.

In the case of optimization for α it is necessary to find the first derivative function $f(\alpha, \beta, t_k)$ by α. Since diagnosing program has m hierarchical levels of conformity assessment operations, then this function can be represented by a polynomial of m-kind of α with known coefficients (if β and t_k are known), so:

$$f(\alpha, \beta, t_k) = a_m(\beta, t_k)\alpha^m + a_{m-1}(\beta, t_k)\alpha^{m-1} + \ldots + a_1(\beta, t_k)\alpha + a_0(\beta, t_k); \tag{1}$$

$$\begin{cases} \dfrac{\partial f(\alpha, \beta, t_k)}{\partial \alpha} = m a_m(\beta, t_k)\alpha^{m-1} + (m-1)a_{m-1}(\beta, t_k)\alpha^{m-2} + \ldots + a_1(\beta, t_k) = 0; \\ 0 \le \alpha \le 1. \end{cases} \tag{2}$$

By solving equation (2), we can find the optimal value of parameter α.

Optimizing over β is performed similarly: equation (1) is on the parameter β; parameters α and t_k are known.

In case of optimization for t_k function $f(\alpha, \beta, t_k)$ has the form:

$$f(\alpha, \beta, t_k) = a_1(\alpha,\beta)t_k + a_0(\alpha,\beta).$$

Then

$$\frac{\partial f(\alpha,\beta,t_k)}{\partial t_k} = a_1(\alpha,\beta) \ne 0.$$

Therefore, optimization for t_k for the case of finding the minimum $m_1(t_{\text{cr}})$ is impossible. Thus, we conclude, that optimization for (α, t_k), for (β, t_k) and (α, β, t_k) is impossible too. Consider the case of optimization for α and β. It is necessary to solve the system of equations, provided that $0 \le \alpha \le 1$, $0 \le \beta \le 1$:

$$\begin{cases} \dfrac{\partial f(\alpha, \beta, t_k)}{\partial \alpha} = m a_m(\beta, t_k)\alpha^{m-1} + (m-1)a_{m-1}(\beta, t_k)\alpha^{m-2} + \ldots + a_1(\beta, t_k) = 0; \\ \dfrac{\partial f(\alpha, \beta, t_k)}{\partial \beta} = m b_m(\alpha, t_k)\beta^{m-1} + (m-1)b_{m-1}(\alpha, t_k)\beta^{m-2} + \ldots + b_1(\alpha, t_k) = 0. \end{cases} \tag{3}$$

In this case, if $\dfrac{\partial^2 f(\alpha,\beta,t_k)}{\partial \alpha^2} > 0$, then the point (α, β) will have a minimum and otherwise – the maximum.

In view described approach to solving the inverse problem of an example when the object of current repair consists of four elements (E_1, E_2, E_3, E_4), connected in series [2]. For this model, knowing (1) and (2) can be written

$$a_2(\beta, t_k, t_{\text{r.i.}}, t_{\text{c.o.}})\alpha_{\min} = a_1(\beta, t_k, t_{\text{r.i.}}, t_{\text{c.o.}}),$$

$$\alpha_{\min} = \frac{a_1(\beta, t_k, t_{\text{r.i.}}, t_{\text{c.o.}})}{a_2(\beta, t_k, t_{\text{r.i.}}, t_{\text{c.o.}})}, \tag{4}$$

where $t_{\text{c.o.}}$ – time for control of object maintenance characteristics;

$$a_1(\beta,\, t_k, t_{\text{r.i.}}, t_{\text{c.o.}}) = Q_2(1-\beta)(m_1(t(\text{CTO}_1/S_2))) - m_1(t(\text{CTO}_2/S_2)) + Q_3(m_1(t(\text{CTO}_2/S_3))) -$$
$$-(1-\beta)m_1(t(\text{CTO}_3/S_3)) - \beta m_1(t(\text{CTO}_4/S_3)) + Q_4(m_1(t(\text{CTO}_2/S_4))) +$$
$$+m_1(t(\text{CTO}_3/S_4)) + 2m_1(t(\text{CTO}_4/S_4));$$
$$a_2(\beta,\, t_k, t_{\text{r.i.}}, t_{\text{c.o.}}) = 2Q_3(m_1(t(\text{CTO}_1/S_3))) - m_1(t(\text{CTO}_2/S_3)) + 2Q_4(m_1(t(\text{CTO}_1/S_4))) -$$
$$-m_1(t(\text{CTO}_2/S_4)) - m_1(t(\text{CTO}_3/S_4)) + m_1(t(\text{CTO}_4/S_4));$$

$m_1(t(\text{CTO}_1/S_1))$ – mean time of first composition of technological operations with first strategy.

Consider the case of parameter optimization routine maintenance for α and β. First check the possibility of solving the optimization problem by Hessian defining. If Hessian $G>0$, that optimum exists. In this case [2]:

$$\frac{\partial^2 m_1(t_k, t_{\text{r.i.}}, t_{\text{c.o.}}, \alpha, \beta)}{\partial\alpha^2} = 2Q_3(m_1(t(\text{CTO}_1/S_3)) - m_1(t(\text{CTO}_2/S_3)) + m_1(t(\text{CTO}_3/S_1))) +$$
$$+2Q_4(m_1(t(\text{CTO}_1/S_4)) - m_1(t(\text{CTO}_2/S_4)) - m_1(t(\text{CTO}_3/S_4)) + m_1(t(\text{CTO}_4/S_4)));$$
$$\frac{\partial^2 m_1(t_k, t_{\text{r.i.}}, t_{\text{c.o.}}, \alpha, \beta)}{\partial\alpha\partial\beta} = Q_2(m_1(t(\text{CTO}_2/S_2)) - m_1(t(\text{CTO}_1/S_2))) +$$
$$+Q_3(m_1(t(\text{CTO}_3/S_3)) - m_1(t(\text{CTO}_4/S_3)));$$
$$\frac{\partial^2 m_1(t_k, t_{\text{r.i.}}, t_{\text{c.o.}}, \alpha, \beta)}{\partial\beta\partial\alpha} = Q_2(m_1(t(\text{CTO}_2/S_2)) - m_1(t(\text{CTO}_1/S_2))) +$$
$$+Q_3(m_1(t(\text{CTO}_3/S_3)) - m_1(t(\text{CTO}_4/S_3)));$$
$$\frac{\partial^2 m_1(t_k, t_{\text{r.i.}}, t_{\text{c.o.}}, \alpha, \beta)}{\partial\beta^2} = 2Q_1(m_1(t(\text{CTO}_1/S_1)) - m_1(t(\text{CTO}_2/S_1)) + m_1(t(\text{CTO}_4/S_1))) +$$
$$+2Q_2(m_1(t(\text{CTO}_4/S_2)) - m_1(t(\text{CTO}_3/S_2))).$$

Taking into account formula (3) determine the first partial derivatives of efficiency parameter and find the optimal numerical values $(\alpha_{\text{opt}};\beta_{\text{opt}})$, solving the system of equations

$$\begin{cases} a_2(\beta_{\text{opt}},\, t_k, t_{\text{r.i.}}, t_{\text{c.o.}})\alpha_{\text{opt}} = a_1(\beta_{\text{opt}},\, t_k, t_{\text{r.i.}}, t_{\text{c.o.}}), \\ a_2(\alpha_{\text{opt}},\, t_k, t_{\text{r.i.}}, t_{\text{c.o.}})\beta_{\text{opt}} = a_1(\alpha_{\text{opt}},\, t_k, t_{\text{r.i.}}, t_{\text{c.o.}}). \end{cases} \tag{5}$$

Expressing α_{opt} from the first equation of (5) and substituting it into the second equation of this system, we obtain the equation, of which is determined β_{opt}:

$$\beta_{\text{opt}} = \frac{a_1\left(\dfrac{a_1(\beta_{\text{opt}},\, t_k, t_{\text{r.i.}}, t_{\text{c.o.}})}{a_2(\beta_{\text{opt}},\, t_k, t_{\text{r.i.}}, t_{\text{c.o.}})},\, t_k, t_{\text{r.i.}}, t_{\text{c.o.}}\right)}{a_2\left(\dfrac{a_1(\beta_{\text{opt}},\, t_k, t_{\text{r.i.}}, t_{\text{c.o.}})}{a_2(\beta_{\text{opt}},\, t_k, t_{\text{r.i.}}, t_{\text{c.o.}})},\, t_k, t_{\text{r.i.}}, t_{\text{c.o.}}\right)}.$$

Expressing β_{opt} we can find out α_{opt} from (5).

Consider the case of optimization on the efficiency index as a dispersion of the current repair length $\mu_2(t_{\text{cr}})$. As in the case of the mean optimization is carried out with parameters α, β and $t_к$ in general case:

$$\mu_2(t_{\text{cr}}) = f(\alpha, \beta, t_k, m_1(t_{\text{cr}})). \tag{6}$$

For the model given in [2]

$$\mu_2(t_k, t_{\text{r.i.}}, t_{\text{c.o.}}, \alpha, \beta) = \frac{1}{16}\sum_{i=1}^{4}\sum_{j=1}^{4}(m_1(t(\text{CTO}_j/S_i)) - m_1(t_k, t_{\text{r.i.}}, t_{\text{c.o.}}, \alpha, \beta))^2.$$

Consider one-dimensional optimization on the index α. In case, when $t_{ki} = t_k$

$$\mu_2(t_k,t_{\text{r.i.}},t_{\text{c.o.}},\alpha,\beta)=0.25\cdot(2t_k+(t_{\text{r.i.}}+t_{\text{c.o.}})-m_1(t_k,t_{\text{r.i.}},t_{\text{c.o.}},\alpha,\beta))^2+(2t_k+2(t_{\text{r.i.}}+t_{\text{c.o.}})-$$
$$-m_1(t_k,t_{\text{r.i.}},t_{\text{c.o.}},\alpha,\beta))^2+(2t_k+3(t_{\text{r.i.}}+t_{\text{c.o.}})-m_1(t_k,t_{\text{r.i.}},t_{\text{c.o.}},\alpha,\beta))^2+(2t_k+4(t_{\text{r.i.}}+t_{\text{c.o.}})-$$
$$-m_1(t_k,t_{\text{r.i.}},t_{\text{c.o.}},\alpha,\beta))^2.$$

Lets $t_1=2t_k$ and $t_2=t_{\text{r.i.}}+t_{\text{c.o.}}$, then:

$$\mu_2(t_k,t_{\text{r.i.}},t_{\text{c.o.}},\alpha,\beta)=t_1^2+5t_1t_2+7{,}5t_2^2-(2t_1+5t_2)m_1(t_k,t_{\text{r.i.}},t_{\text{c.o.}},\alpha,\beta)+m_1^2(t_k,t_{\text{r.i.}},t_{\text{c.o.}},\alpha,\beta).$$

Lets $t_3=t_1^2+5t_1t_2+7{,}5t_2^2$ та $t_4=2t_1+5t_2$, then:

$$\mu_2(t_k,t_{\text{r.i.}},t_{\text{c.o.}},\alpha,\beta)=t_3-t_4m_1(t_k,t_{\text{r.i.}},t_{\text{c.o.}},\alpha,\beta)+m_1^2(t_k,t_{\text{r.i.}},t_{\text{c.o.}},\alpha,\beta). \tag{7}$$

$$\frac{\partial\mu_2(t_k,t_{\text{r.i.}},t_{\text{c.o.}},\alpha,\beta)}{\partial\alpha}=(2m_1(t_k,t_{\text{r.i.}},t_{\text{c.o.}},\alpha,\beta)-t_4)\frac{\partial m_1(t_k,t_{\text{r.i.}},t_{\text{c.o.}},\alpha,\beta)}{\partial\alpha}=0.$$

As seen from (7) function $\mu_2(t_k,t_{\text{r.i.}},t_{\text{c.o.}},\alpha,\beta)$ will have two extremums. The first extremum is determined using the formula (4). For the second extremum can be written:

$$2(Q_1((1-\beta)^2(t_1+t_2)+\beta(t_1+2t_2))+Q_2(\alpha(1-\beta)(t_1+2t_2)+(1-\beta)(1-\alpha)(t_1+t_2)+$$
$$+\beta(t_1+3t_2))+Q_3(\alpha(t_1+3t_2)+(1-\alpha)(1-\beta)(t_1+t_2)+\beta(1-\alpha)(t_1+4t_2))+$$
$$+Q_4((2\alpha-\alpha^2)(t_1+4t_2)+(1-\alpha)^2(t_1+t_2))-t_4=0.$$

Lets $Q_1((1-\beta)^2(t_1+t_2)+\beta(t_1+2t_2))+Q_2((1-\beta)(t_1+t_2)+\beta(t_1+3t_2)+Q_3(1-\beta)(t_1+t_2)+$ $+\beta(t_1+4t_2))+Q_4(t_1+t_2)-0{,}5t_4=b_0$. Then we have

$$2(b_0+Q_2(\alpha(1-\beta)(t_1+2t_2)-\alpha(1-\beta)(t_1+t_2))+Q_3(\alpha(t_1+3t_2)-\alpha(1-\beta)(t_1+t_2)-$$
$$-\alpha\beta(t_1+4t_2))+Q_4((2\alpha-\alpha^2)(t_1+4t_2)+(\alpha^2-2\alpha)(t_1+t_2))=0.$$

Lets $Q_2(1-\beta)t_2+Q_3(2t_2-3t_2\beta)+Q_4 6t_2=b_1$, $-3Q_4t_2=b_2$. Hence we get, that $b_2\alpha^2+b_1\alpha+b_0=0$. So

$$\alpha^*_{2,3}=-\frac{b_1\pm\sqrt{b_1^2-4b_0b_2}}{2b_2}.$$

Therefore, optimization for dispersion α will have three extremums. Optimization of β is similar. The case of optimization on the index efficiency as a mixture of the mean and standard deviation is considered similar to two previous optimization problem, but an additional can search the optimal parameter K values.

Conclusions

The general approach and the correlation obtained for the optimal values, when solving the inverse problem of determining the parameters of the current maintenance of radioelectronic equipment, when mistakes of the first and second kind are possible in the estimation process under complex information parameters. The results can be used in the design and modernization of radioelectronic equipment exploitation systems.

References

1. *Мелкумян В.Г.* Технологічні системи обслуговуючого типу. Елементи теорії проектування і прикладні задачі експлуатації. – К.: НАУ, 2003. – 171 с.
2. *Заліський М.Ю., Соломенцев О.В., Німич В.В, Яшанов І.М.* Урахування похибок діагностування під час аналізу технологічних операцій // Електроніка та системи управління. – 2007. – №3 (13). – С. 134–140.
3. *Мелкумян В.Г., Семенов А.А.* Основи теорії надійності: Навчальний посібник. – К.: КМУЦА, 1998. – 84 с.
4. *Заліський М.Ю., Німич В.В, Яшанов І.М.* Оцінка відповідності процесів // Проблеми інформатизації та управління. – 2009. – № 2 (26). – С. 52 – 57.
5. *ДСТУ* ISO 9001:2001. Системи управління якістю. Вимоги. – Чинний від 2001–10–01.

UDC 681.5.08: 004.942 (045)

G. Sokolov, Ph.D., associate professor
(National Aviation University, Ukraine)

SIMULATION OF LASER RADAR IN MATLAB

In the present work is carried out simulations at the level of functional scheme by means of MATLAB optoelectronic measurement system of vibration.

Modeling systems at the level functional scheme are widely used in practice of the design [1]. Currently, the literature is proposed to simulate by means of MATLAB using application SIMULINK [2]. This application is particularly useful in the analysis of automation systems. However, when modeling radar systems, in which the complex processing of complex signals occurs, the use of SIMULINK causes unnecessary complication of the model, since it lacks a program library of complex signals. In this case, the use of programming in the core of MATLAB allows more flexible use of the huge potential of this program system to build a more adequate models of radar systems.

In the present work is carried out simulations at the level of functional scheme by means of MATLAB laser optoelectronic measurement system of vibration. Such systems are used in industrial processes, and as a directional microphone. Of course, the proposed approach in modeling can be applied for the analysis of other radar systems.

Laser remote measurement characteristics of low-frequency vibration oscillations used a variety of methods of measurement. In this paper the phase method measurement is considered.
The block diagram of a measuring instrument is shown in Figure 1. In the block diagram used the following notation: GM - generator of the modulating oscillation, L - laser, PD - photodetector, LO – local oscillator, PS - phase shifter at 90 º, Mix1 is the first mixer, Mix 2 - the second mixer, PhD - phase detector, O - optical system , SA - spectrum analyzer.

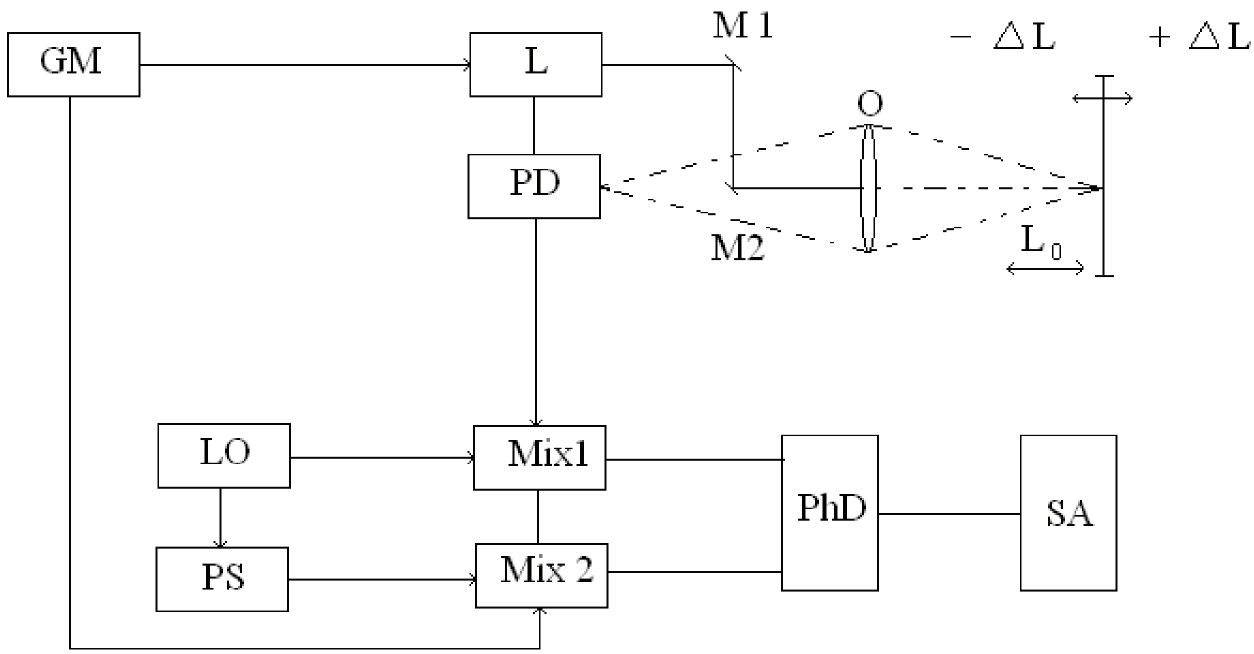

Fig. 1. Block diagram for measuring vibration phase method.

Formation of the measuring signal is as follows.

The radiation of laser L was reflected from the mirrors M1 and M2, is focused on the optical system O and covers the distance L_0 to the glass (L_0 can be up to 100m). The laser beam reflected from the glass, the optical system is focused on the photodetector PD. The output voltage of the photodetector $U^{(0)}_{PhD}$ depends on the laser power P_0, the loss factor in the optical path k_{op} and the sensitivity of the photodetector S_{PD}.

$$U_{PD} = P_0 \cdot k_{op} \cdot S_{PD}. \qquad (1)$$

Power of laser radiation is modulated by the modulating voltage generator GM

$$U_M = U_{M0} \sin(2\pi f_M t) \qquad (2)$$

and has a constant component $P^{(1)}_0$ and variable component

$$P_0^{(2)} = \mathrm{P} \sin(2\pi f_M t) \qquad (3)$$

As a result, the useful output voltage of the photodetector (it's variable component)

$$U_{PD} = P k_{OP} S_{PD} \sin(2\pi f_M t) = U_{PD.O} \sin(2\pi f_M t) \qquad (4)$$

Changing the position of the plane of the reflector on ΔL leads to a phase change of the output signal of the photodetector

$$\Delta\varphi = 4\pi \frac{\Delta L}{\lambda}, \text{ where } \lambda = \frac{c}{f_M} \qquad (5)$$

In the case of vibration of the glass (with frequency f_V)

$$\Delta L = \Delta L_0 \sin(2\pi f_V t) \qquad (6)$$

phase modulation output signal of the photodetector occurs

$$U_{PD} = U_{PD,0} \sin\left[2\pi f_M t + \frac{4\pi \Delta L_0}{\lambda} \sin(2\pi f_V t) \right] \qquad (7)$$

This phase-modulated signal is generally hidden in the interferences as additive and multiplicative. In this paper we proposed the following description of interference:

$$U_{PD}^{(INT)} = U_{PD.0}[1 - k_1 + k_2 U_{U,D}] \sin[2\pi f_M t + \frac{4\pi \Delta L_0}{\lambda} \sin(2\pi f_V t) + k_3 U_{G.D.}], \qquad (8)$$

where k_1 - coefficient determining the overall increase in losses in the optical channel $0 \le k_1 \le 1;$;

k_2 - coefficient determining the amplitude of the fluctuations $k_2 \le k_1$.

k_3 - coefficient increased time dispersion of the additive noise.

$U_{U,D}$ - a random signal with uniform distribution of the probability density in the range [0 ÷ 1].

$U_{G.D,}$ - a random signal with a Gaussian probability density distribution and variance 1;

From this high-frequency complex signal using electronic processing we obtain low-frequency information signal part. Its characteristics are measured by spectrum analyzer.

For this phase-modulated signal is converted down in frequency using a mixer Mix 1 and LO, and then fed to the phase detector PhD. The reference signal of the phase detector of the same intermediate frequency signal generated from the generator of the modulating oscillation GM, and LO with the help of mixer Mix 2. Necessary for PD phase shifter is set at 90 deg. PS. The phase detector produces demodulation of the signal.

The functional diagram of a measuring instrument used for the simulation, is shown in Figure 2.

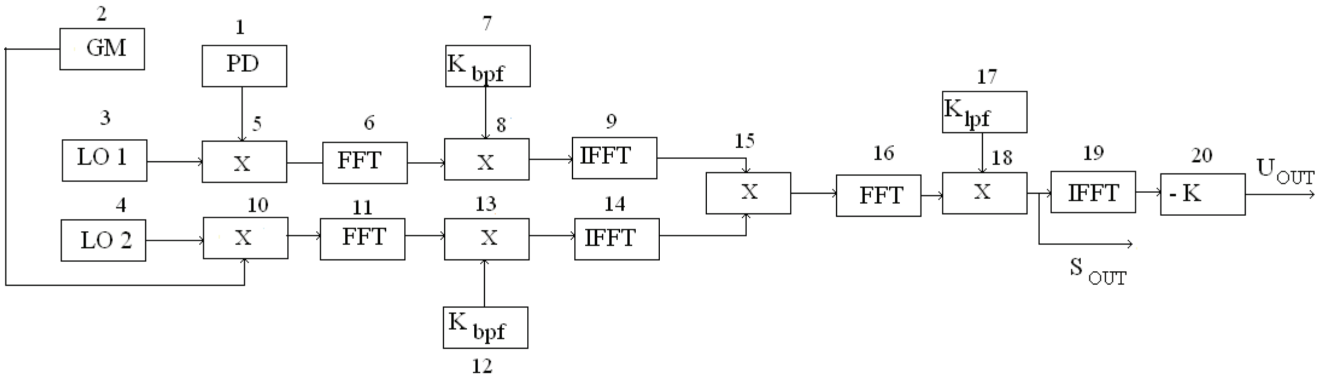

Fig. 2. Functional diagram for measuring vibration phase method.

Features of this model are as follows:
1. The optical part is simulated as generator of the photodetector output signal (Block 1).
2.Phase shifter is modeled by local oscillator 2 (block 4), generating a harmonic signal is shifted by 90 degrees relative to a local oscillator 1 (block 3).
3. The mixer 1 is modeled by a series connection of signal multiplier (block 5) and band-pass filter (blocks 6-9).
4. Blocks 6-9 model filtering the signal by band-pass filter. Filtering performed in the frequency domain, and the spectrum of the filtered signal

$$\dot{S}_{FIL} = \dot{S}_{Inp} \cdot \dot{K}(\omega) \qquad (9)$$

where $\dot{S}_{Inp}$ - the spectrum of the input filter,

$\dot{K}(\omega)$ - frequency factor transmission band-pass filter.

The algorithm applies the filter processing without phase shift:

$$\dot{K}(\omega) = 1 \quad \text{in the pass band ,}$$
$$\qquad (10)$$
$$\dot{K}(\omega) = 0 \quad \text{in the stop band.}$$

The spectrum of the input signal is calculated by algorithm of Fast Fourier transform (FFT). Time function of filter output signal is calculated by algorithm of the Inverse Fast Fourier transform (IFFT). In this case the bandwidth is chosen in the intermediate frequency.
5. The mixer 2 is modeled by a series connection of signal multiplier (block 10) and band-pass filter (blocks 11-14) as well as a mixer 1.
6. The phase detector is modeled by a serial connection signal multiplier (Block 15) and low frequency filter (blocks 16-19).
7. Low-frequency filter is modeled in the same manner as a bandpass filter. Its bandwidth is consistent with the measured vibration frequency of oscillation.
8. Block 20 models the amplifier.
9. To simplify the model spectrum of the phase detector output signal is recorded at the output of signal multiplier PhD (block 18) according to formula (9).

This functional model of a laser optoelectronic measurement system of vibration is implemented in a computer program within the MATLAB and executed in the form of Script-File. It fully describes the signal processing and can be used to evaluate the system operation in a high-power interference.

Below is an example of such evaluation under the following conditions:
1) The frequency of modulation $f_M = 25$ kHz; the intermediate frequency $f_{INT} = 80$ Hz, the frequency of vibration $f_V = 8$ Hz (i.e., adopted scale of frequency 1:1000);
2) The amplitude of oscillations of the generator GM is 1 v, the generators LO 1, LO 2 are 10 v, the amplitude of input signal $U_{PD.O}$ is 1 v, modulation index $\frac{4\pi\Delta L_0}{\lambda} = 0{,}1$.
Figure 3 shows the spectrum of the signal without interferences (curve 1), spectrum the signal with additive interferences, whose level is defined by correlation (11) (curve 2) and the spectrum of the signal with multiplicative interferences, whose level is determined by correlation (12) (curve 3).

$$k_3 = 10\frac{4\pi\Delta L_0}{\lambda}, \quad (11)$$

$$k_1 = k_2 = 0.9, \quad (12)$$

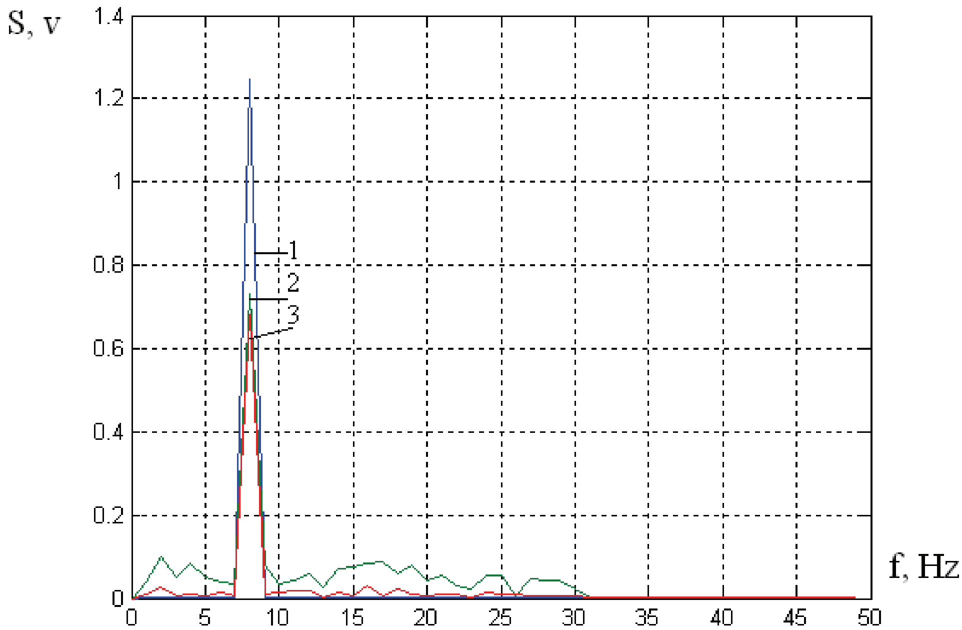

Fig. 3. Spectrum of the radar system output signals at different values of dispersion additive and multiplicative interferences.

Conclusions

Developed a functional model of the laser optoelectronic measurement system of vibration, implemented by means of MATLAB. The mathematical model of additive and multiplicative interferences operation of the laser radar system is proposed. It is shown the possibilities of the program to investigate the influence of the additive and multiplicative interferences on the laser radar system.

References

1. *Борисов Ю.П., Цветнов В.В* Матаматическое моделирование радиотехнических систем и устройств. – М.: Радио и связь, 1985. – 176 с.
2. *Дьяконов В.П.* MATLAB и SIMULINK для радиоинженеров.–М.: ДМК Пресс, 2011. – 976 с.

UDC 629.735.05:621.396.933

E.A. Kovalevskiy, senior staff scientist,
T.L. Malyutenko, assistant,
(National Aviation University, Ukraine)

SATELLITE SIGNALS QUALITY MONITORING IN CASE PERIODIC ANOMALIES

In this article the mathematical simulation of influence of failures on accuracy of navigation determination is considered.

Introduction

The essential increase users of satellite navigation systems (GNSS) causes increase of requirements not only to accuracy parameters, but also to integrity and reliability of navigation information received from them. Integrity control of the GNSS radio navigational field consists of quality control of signals of navigation satellites, quality of information transferred by them for the purpose of maintenance of high reliability of navigation determination and warning of the user of a system status. Different methods of integrity control, including, independent integrity monitoring of (RAIM), onboard autonomous systems (AAIM) are known. A lot of methods of independent integrity monitoring as on the basis of single measurements, and filtrational algorithms of monitoring [1] are developed. However time of informing of users about failures with use of such methods is unsatisfied requirements, for example, to civil aviation. Therefore there is a need for additional methods and monitoring aids of GNSS integrity. One of possible approaches is the organization of ground monitoring services for detections of emergency situations of functioning of GNSS. Today the creation of ground monitoring services is solved, in particular, the Russian monitoring system of the navigation GLONASS/GPS [2] fields. System has to realize two types of monitoring: operational and posteriori. The tasks of operational monitoring are estimation measurement errors of pseudo-ranges on signals of GNSS and inform customers on these errors in real time.

Algorithms of integrity monitoring are based on failure model. Often the failure is represented in the form of the additional random normally distributed error to measured pseudo-range. In the publication [3] the failure model on the basis of Kolmogorov-Fellera equation for discontinuous processes is offered.

The experimental investigations of the navigation receiver operation show that cases of repeating bursts in errors of pseudo-range determination are watched.

In this work the failure is considered in the form of periodic sequence of bursts of errors of measured pseudo-range.

The purpose of this work is to research influence of failures on accuracy of navigation determination by a method of mathematical simulation and also search of ways of monitoring of such anomalies.

Model and exploratory procedure

The exploratory procedure assumes execution of the following operations.

1. By means of the interface of satellite navigation station the data file containing coordinates of selected 4-th satellites in the form of XS, YS, ZS registers.
2. To fix data of topographical binding of station in the form of a vector of coordinates in WGS-84 system – $X_0 = [x_0, y_0, z_0]$.
3. Measured pseudo-ranges are simulated:

$$D_k = \sqrt{(XS_k - x_0)^2 + (YS_k - y_0)^2 + (ZS_k - z_0)^2} + \xi + \theta, \tag{1}$$

where ξ – a standard measurement error of pseudo-range, which on the normal law [M, δ];
θ - the abnormal burst of an error with the period of T and amplitude of I;
k–satellite number.

4. The navigation task is solved in an iterative mode according to expression:

$$\hat{X}_k = \tilde{X}_k + (\tilde{H}^T + \tilde{H})^{-1} \cdot \tilde{H}^T \cdot \Delta y_k, \tag{2}$$

where $\hat{X}$ - an assessment of a coordinates vector on a step of iteration of "k", $X = [XP, YP, ZP]$;

$\tilde{X}_k$ - prior assessment of a coordinates vector;

$\tilde{H}$ - a predicted matrix of direction cosines;

Δy_k - vector of errors of secondary observations.

5. In case of the preset values [M, δ] the spherical error of coordinates determination of station is calculated:

$$\delta_\theta = \sqrt{\Delta x^2 + \Delta y^2 + \Delta z^2}, \tag{3}$$

where Δx, Δy, Δz - errors of coordinates determination XP, YP, ZP respectively.

6. Operations repeat using items 3,4,5 of KR times and the mean square spherical error is calculated when averaging on implementations.

7. For different combinations of parameters of anomalies are built and analyzed histograms of the random functions simulating change of a measurement error of pseudo-range in time.

Results of simulation

Experiment 1

To fix coordinates of the 4-th satellites and set parameters: M=0, δ=4 m. To calculate an error δ_θ using averaging on KR=10000 implementations. In the absence of anomalies it is equal 12 m.

Experiment 2

To change parameters I, T. Anomalies is entered into pseudo-ranges of each satellite in turn. To calculate a root-mean-square error of determination. Results are given in tab. 1.

Table 1

T	I, m	I/T	δ_θ, m			
			Number of satellite			
			1	2	3	4
4	32	8	15	31	22	31
10	80	8	17	33	23	33
20	160	8	17	33	24	34
40	320	8	17	34	24	33
100	800	8	17	34	25	34

To analyze data of tab. 1 we see that the increase in an error of navigation determination depends on multiplication of frequency of bursts on their amplitude. So, errors depend on that in what signal of the satellite there were anomalies.

Experiment 3

To fix the period of repetition T=10 and change values of bursts amplitude. To calculate values of an error δ_θ depending from values $\Delta = I/T$ in case of introduction of anomalies in pseudo-range of each satellite in turn. Let's subtract from it an error received in absence of anomalies. To determine the regression equations using to obtain data $\Delta\delta = a_0 + a_1 \cdot \Delta + a_2 \cdot \Delta^2$.

As a result to receive:

the satellite 1 - $\Delta\delta = -0.235 + 0.059 \cdot \Delta + 0.000006 \cdot \Delta^2$;

the satellite 2 - $\Delta\delta = -1.33 + 2.88 \cdot \Delta$;

the satellite 3 - $\Delta\delta = 0.124 \cdot \Delta + 0.00024 \cdot \Delta^2$;

the satellite 4 - $\Delta\delta = -0.286 + 0.257 \cdot \Delta$.

To analyze the given results we see that the increment of an error of navigation determination as a result of appearance of anomalies in measured pseudo-ranges to any of satellites depends almost linearly on intensity of anomaly Δ. The steepness of this dependence is various for options of introduction of anomalies.

Experiment 4

Let's define the regression equation for values of an error δ_θ (the first line of tab. 1) depending on direction cosines of pseudo-ranges of satellites.

The primary diagram of errors (the upper diagram) and the equation diagram regressions (the lower diagram) are shown on fig. 1

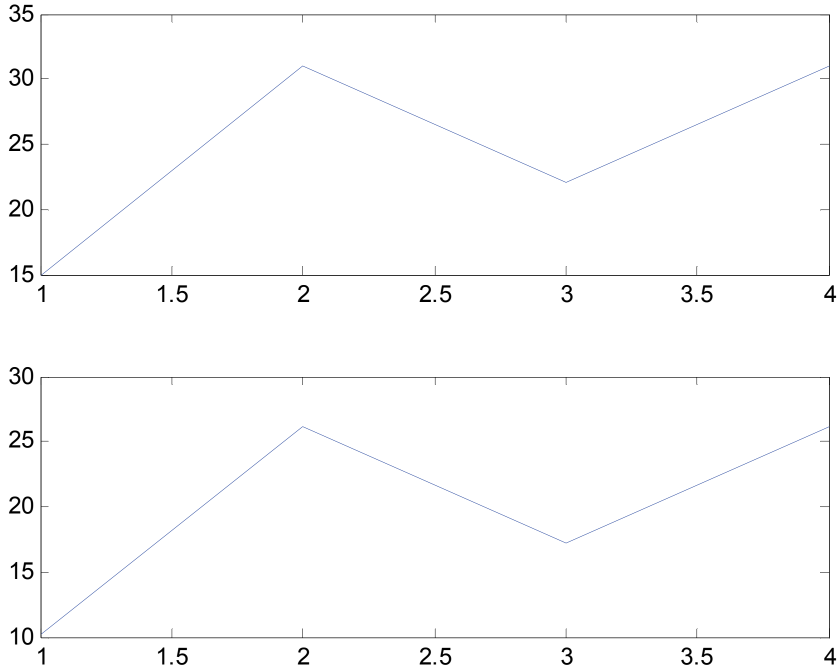

Fig. 1. The primary diagram of errors and the equation diagram regressions

From fig. 1 it is visible that anomaly influence on pseudo-range of the satellite makes a contribution to an error of the navigation determination, depending on direction cosines.

Experiment 5

Let's fix data about constellation from 10 GPS satellites and set parameters of the anomalous errors for each satellite in turn and define δ_θ. To find coefficients of the equation of regression using sampling of 40 values:

$$Y = a + a_1 \cdot \Delta + a_2 \cdot cx + a_3 \cdot cy + a_4 \cdot cz, \tag{4}$$

where cx, cy, cz – direction cosines of pseudo-range projection on the appropriate axes of coordinates.

On fig. 2 the experimental values δ_θ (the upper diagram) and values, receiving from the regression equation (the lower diagram) are given.

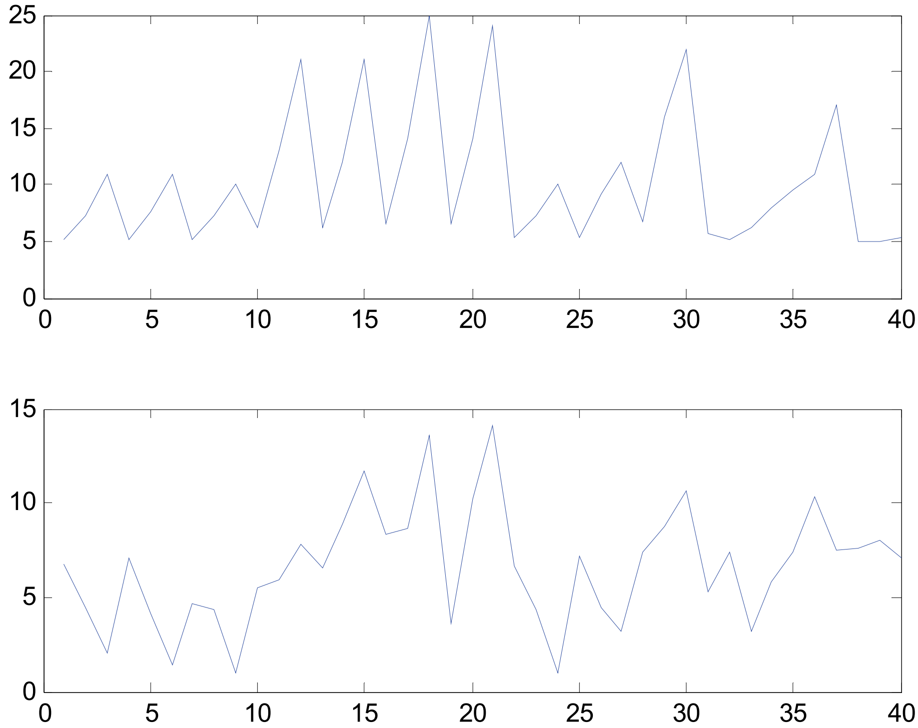

Fig. 2. The experimental values and values, receiving from the regression equation

So from fig. 2, the equation in any approximation reproduces coordinate's errors determination. Reliability of the analysis can be raised by a representativeness of the initial sample.

Experiment 6

Unlike experiment 3 amplitudes of bursts change according to expression

$$I = I_0 + t_p, \quad (5)$$

where t_p - uniformly distributed random variable with parameters [0, t_p].

The results of simulation in case contribution of anomalies in pseudo-range to 1 satellite are given in tab. 2.

Table 2

T	I_0	t_p,m	I_{av}	δ_θ
4	30	4	32	15
4	28	8	32	15
4	26	12	32	15
4	24	16	32	15
4	20	24	32	15

So, from tab. 2 we see, that to increase in an error of coordinates determination of station depends on product repetition frequency on average amplitude of bursts.

Experiment 7

We build the histogram of the accidental process simulating a measurement error of pseudo-range taking into account existence of the abnormal bursts. For T=4, I=0.032 km. Results are given on fig. 3.

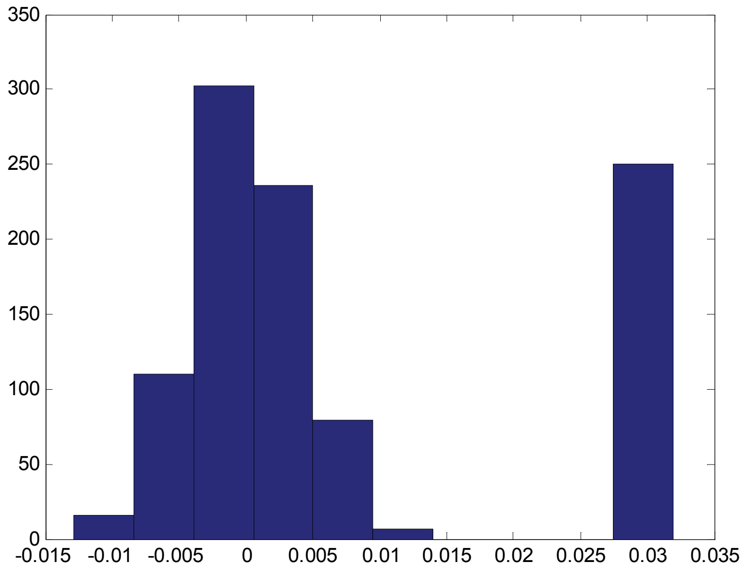

Figure 3

The histogram analysis fig. 3 shows that the periodic sequence of the abnormal bursts is characterized by a column located by the middle in a point of an abscissa axis, equal amplitude, and having height, equal to repetition frequency of burst.

This data allow considering the following scenarios of satellite signals monitoring. By operation of the navigation receiver errors of pseudo-ranges determination to each visible satellite and their angular orientation are fixed. On a sample of the fixed counting the appropriate histograms are built and analyzed. In the presence of anomaly the amplitude and frequency of its repetition is defined.

Two options are possible. In the presence of the equation of regression beforehand received on representative samples (1) the error of coordinates determination is calculated and is compared to threshold value. The second option – a considered error is determined by a simulation way by above given technique.

The offered ways of monitoring can be implemented both in a post-processing mode, and in real time with a certain initial time delay of output of result.

Conclusions

The carried-out researches showed that existence of additional (abnormal) periodically repeating single bursts in pseudo-range counting to one of satellites lead to noticeable errors in the solution of the navigation task. These errors depend on product amplitude of bursts on frequency of their repetition, and also from spatial orientation of the satellite concerning the user. It is shown that the specified dependences can be formalized that allowed to define ways of monitoring of anomalies of this kind.

References

1. ГЛОНАСС. Принципы построения и функционирования. Изд.3 / Под ред. А.И. Перова, В.Н. Харисова. М.: Радиотехника, 2005. – 688 с.

2. ГЛОНАСС. Принципы построения и функционирования. Изд.4 / Под ред. А.И. Перова, В.Н. Харисова. М.: Радиотехника, 2010. – 800 с.

3. *Харисов В.Н., Карпейкин А.В.* Методы нелинейной фильтрации в задаче обнаружения отказов в спутниковых радионавигационных системах // Радиотехника, 1996, №7, с.115-119.

UDC 551.509

N.S. Kuzmenko, student
(National Aviation University, Ukraine)

SOFTWARE FOR STRATEGIC PLANNING AND PERFORMANCE ASSESSMENT IN UKRAINE

The usage of the Strategic Planning & Performance Assessment Tool, built in the framework of the Strategic Planning for Sustainable Performance (SPSP) for Regulator Bodies Method was described.

Introduction

Strategic Planning & Performance Assessment Tool (SPPAT) has been designed to estimate a number of parameters and the evolution of Key Performance Indicators (KPI) in relation to the Plan. The value of the SPPAT is generated by its main function in that it guides and supports the systematic review and update of the subject Strategic Business Plan. This periodic review and update keeps the plan consistent with its strategic objectives, medium level objectives, vision and mission and maintains the planning and implementation process within an envelope of predefined performance in financial efficiency and eventually in safety, capacity and environment protection when adequate respective KPIs become available. Its openness and design adaptivity ensures that when more and different KPIs are adopted they may be easily built in the SPPAT and guide the planning, implementation and monitoring.

Software for strategic planning

SPPAT is a decision making support tool which inter alia has been designed to calculate the Unit Rate for Regulator Bodies, over the planning timeframe, by taking into account the set of recommendations (Basic Objectives, BSO) developed in the Strategic Business Plan.

It is important to note that it does not provide an implementation plan, or a staffing plan.

Among other things, this tool achieves the following:

- assesses Regulator' s costs;
- assesses unit rates for en-route and terminal charges, the unit rate of Regulator and the unit rate of Passengers;
- estimates the evolution of cost per km flown;
- provides reports adapted to the EC Regulations requirements.

Its primary inputs are:

1. the list of planned BSOs, together with their related costs and human effort levels, for both implementation and operations phases;
2. the forecast service units;
3. the forecast Km to be flown;
4. the baseline cost of the service broken down into capital cost, depreciation, operating, staff and other costs, as appropriate.

Functional diagram of the SPPAT is represented on the fig.1 and SPPAT main menu on the fig.2. From this main Menu window all elements of the SPATT functionality can be accessed as follows:

- SPPAT configuration (base tables, SPPAT settings, administrator)
- Business plan information (baseline projec`tions, base year financial data, project (BSO) details, reporting)
- Switch User – Return to the Logon dialog to change the current user;
- Mail Support – create an email to the SPPAT support team;
- Exit – Exit the application.

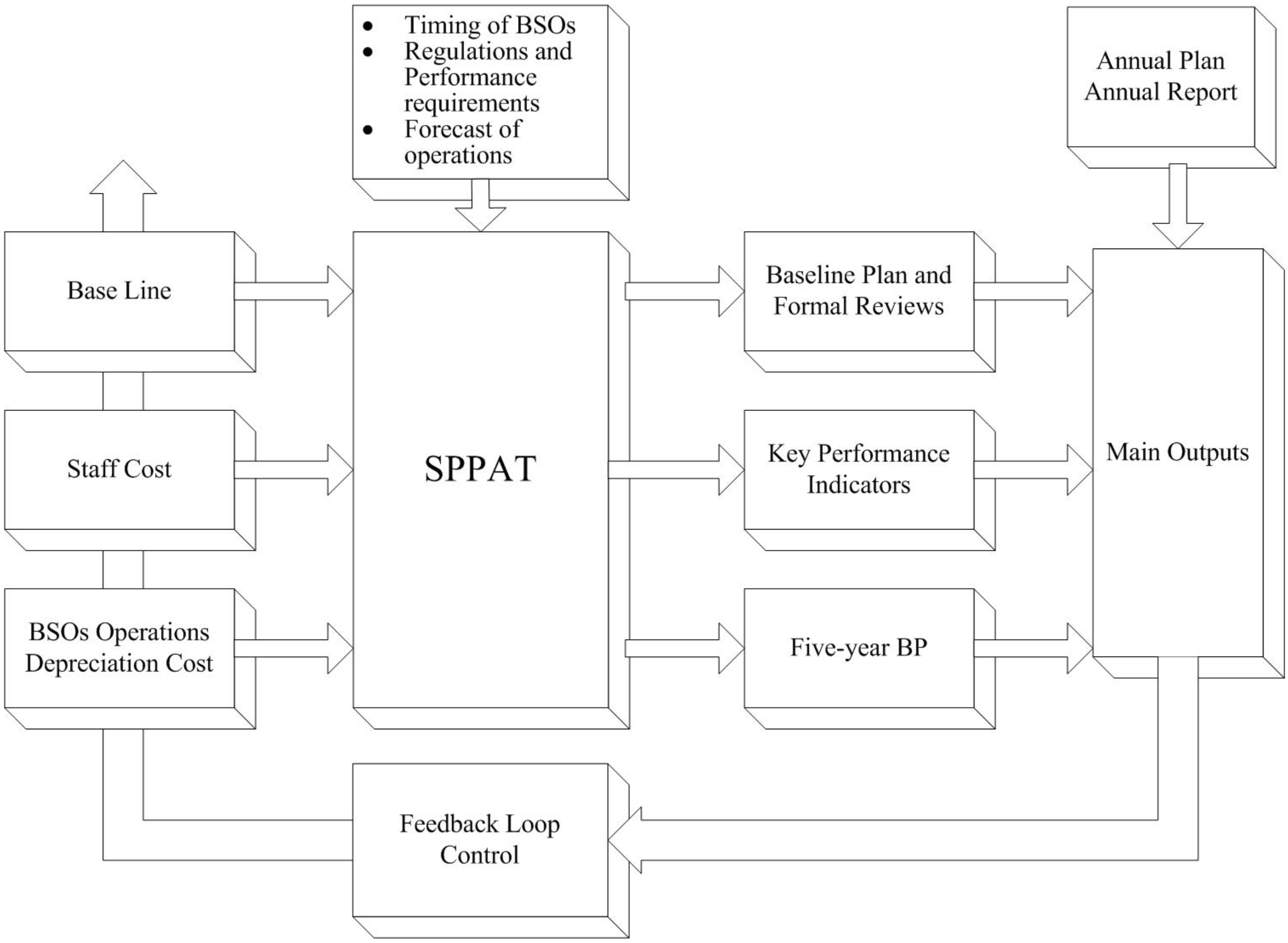

Fig.1. Functional diagram of the SPPAT

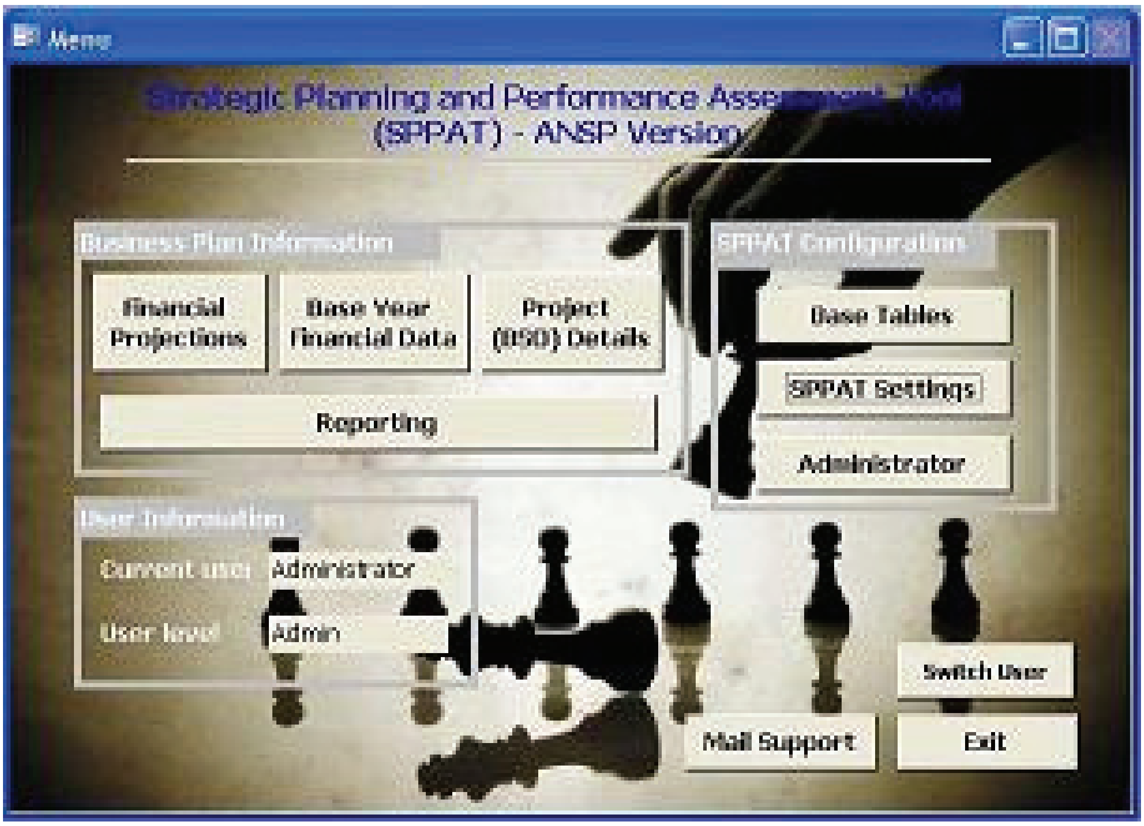

Fig. 2. SPPAT main menu

The SPPAT automatically produces the following 20 reports:

- general overview;
- business plan summary and financial;
- BSO details and financial;
- terminal unit rate;
- en-route unit rate;
- terminal km flown;
- en-route km flown;
- BSO-LSSIP tracking;
- BSO-MLO tracking;
- BSO-STO tracking;
- terminal EC regulation figures and diagram;
- en-route EC regulation figures and diagram;
- tracking actual-estimate;
- crosstab MLO-BSO – abs figures & crosstab MLO-BSO – rel figures;
- SBP annexes;
- summary of annual plan;
- MS projects;
- other EC regulation figures and diagram;
- SESAR OI compliance tracking;
- SES regulation compliance tracking.

For the full functionality of the SPPAT MS access application to be available it is necessary for the following software to also be installed: MS Excel, MS Project and PDF Creator.

The Strategic Planning for Sustainable Performance methodology strongly recommends the annual or even better the six-month review of the SBP in order to keep it up to date, produce organisational learning and apply effective strategic management. The mid-year review aims to check the status of progress and implementation and to trigger remedial action if necessary.

Theoretically everything but at least the Vision/Strategy & Mission pair, STOs, MLOs, and BSOs shall be reviewed and updated through the SPPAT. The manual amendments of various figures and information within the tool will result in corresponding changes of key performance indicators like Unit Rate and Cost per KM and will bring automatic update to various internal SPPAT reports which via the SPPAT internal links will be uploaded and replace the outdated reports included in the previous year SBP word Document.

The amendments will result in automatic update of the MS Project File that could be generated via the report push button “MS Project” as a stand-alone file and then copy and paste in the word document file to replace the old Gant Chart included in the previous year SBP Word Document.

The financial outputs of SPPAT shall be used to update the Financial Chapter of the SBP Document. In the meantime, a number of Financial Figures shall be included manually in the ‘Baseline” sub-view of SPPAT to reflect the financial current situation.

Conclusion

SPPAT is a decision making support tool, which among other things assesses the sustainability and performance of the Strategic Business Plan of Ukrainian ANSP.

References

1. Strategic Planning & Performance Assessment Tool (SPPAT) version for ANSP user manual. EUROCONTROL – EUROCONTROL, Brussels, 2012. – 93p.
2. Official web-site of EUROCONTROL: http://eurocontrol.int

UDC: 629.783:629. 735. 33

V.V. Konin, doctor of technical sciences
E.A. Kovalevskiy, senior staff scientist
T. I. Olevinska, graduate student
(National Aviation University, Ukraine)

GNSS TECHNOLOGY LANDING SYSTEM OPTION FOR FLYING MACHINE

The modeling of final approach path by means of Global navigation satellite system is considered in this article.

Introduction

A global aeronavigation plan in reference to CNS/ATM systems designates GNSS system as a key element of communication, navigation, surveillance systems and systems, which are connected with air traffic organization, as well as a basis the governments can improve the air navigation service. GNSS possesses the potential abilities to maintain all flight phases, providing continues global observation. It allows to exclude the need for plenty of ground-based and on-board systems, which were developed for special requirements at a definite flight stages.

Nowadays precision approach procedures in accordance with first category together with corresponding GNSS equipment are authorized. The 2 and 3 categories requirements are being developing.

GNSS precision approach procedure is marked as GLS procedure approach. The GLS flight path is differently, not like by ILS. Data defining the flight path are transmitted onboard via digital data link as a data block FAS (final approach segment). Onboard equipment GNSS based on geometrical ratios calculates flight path parameters and designates homing characteristics similar to other approach systems, ILS for example.

One should take into account there is no available information in literature how to perform geometrical calculations.

Formulation of the problem and model description

The purpose is to reconstruct the procedure of definition of homing parameters without touching upon the problems of integrity, continuity and operational readiness of maintenance and to investigate precision performance of GLS approach and landing system.

Data block FAS is transmitted aboard in a message type 4 from operational supplement GBAS. In order to define final approach phase path the following elements are transmitted: latitude, longitude and height of threshold pass LTP/FTPL, the difference between delta FPAP latitude and delta FPAP longitude of point FPAP of the runway and corresponding parameters of point LTP/FTP, height of crossing of runway threshold TCH, glide path angle, course width and offset delta -distance from the end of the runway to FPAP. Distance D is known. Onboard equipment GNSS provides airplane center-of-gravity coordinates definition in WGS-84 system with occasional errors.

In order to provide approach and landing aircraft position information relatively the runway is necessary.

As it shown in [2], the parameters of the lateral movement of aircraft on landing are the linear Zb and angular epsilon b separations from equivalent signal zone. Zb equals to perpendicular length put from center-of-gravity of airplane to a vertical flatness crossing the runway. Epsilon b angle is defined as the angle between line with points GARP -LTP/FTP and projection to horizontal flatness which contains the RW, a line from center of gravity of aircraft to GARP point.

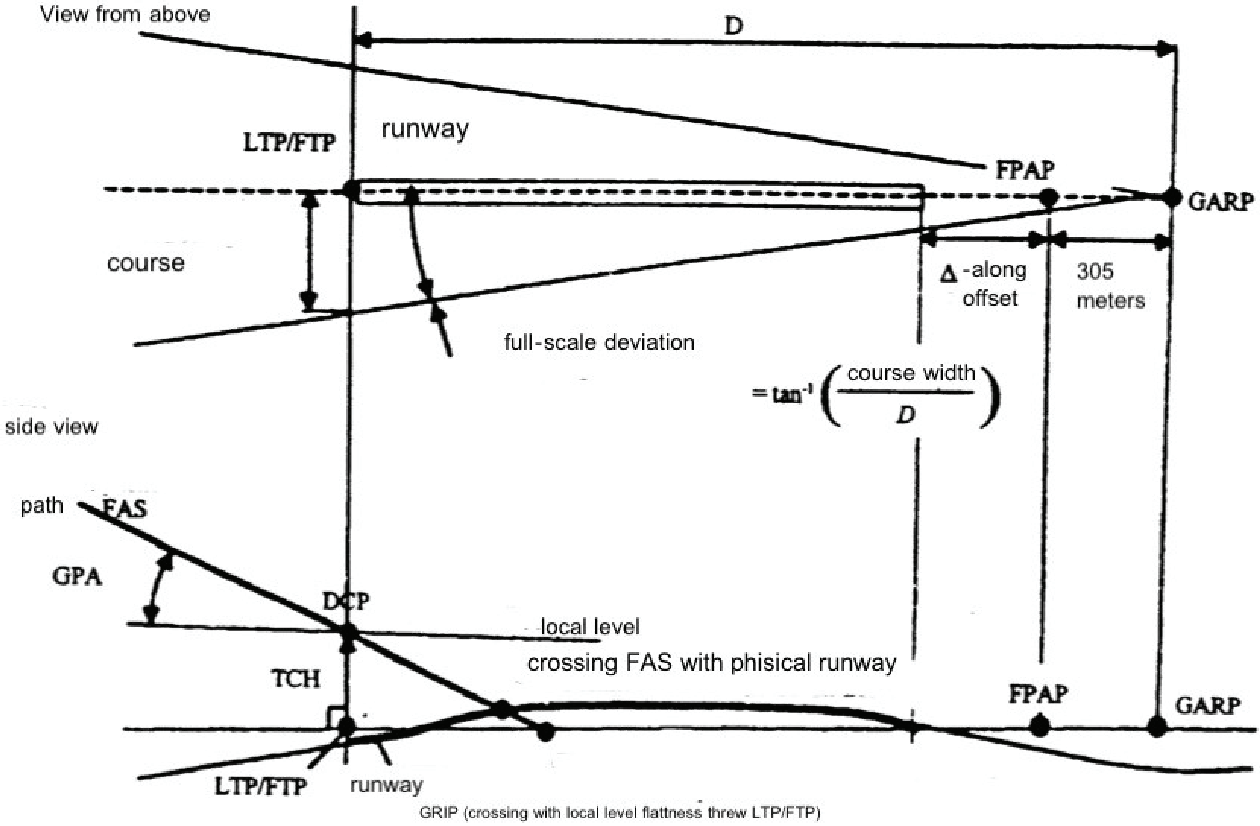

Fig.1. Final approach path

The long across movement parameters of AC on approach are the linear Zp and angular epsilon p separations from equal signal zone of the path

Zh equals to the length of the perpendicular derived from center of gravity of AC to horizontal flatness. Epsilon p angle is defined as the angle between line with points GRIP -DCP and projection the vertical flatness, passing the RW, line with points of center of gravity of AC -GRIP

To perform model investigation the following procedures-functions are developed:

RPM -recounting of spherical coordinates to Decart's;

PLP-calculation of parameters of the common equation of flatness through coordinates of 3points [4];

RTP-calculation of distance from point T to flatness P [4];

PEPP-calculation of coordinates of point of perpendicular crossing from point T to flatness;

RASU -calculation of angle between two vectors in space

Initial data and estimated ratios:

latitude teta L = 50.43 degrees,

longitude -lambda L = 30.43 degrees,

height - hL=200m of point LTP/ FTP,

course width – KS = 140 m,

D = 3000m,

GPA = 3 deg,

TCH = 50m,

FM coordinates: XS = XL – 5000; YS = YL; ZS = ZL + 3000, where XL,YL,ZL are LTP/FTP point coordinates

Latitude – tetaG = tetaL – D/111110;

Longitude – lambdaG = lambdaL;

Height – hG = hL of point GARP.

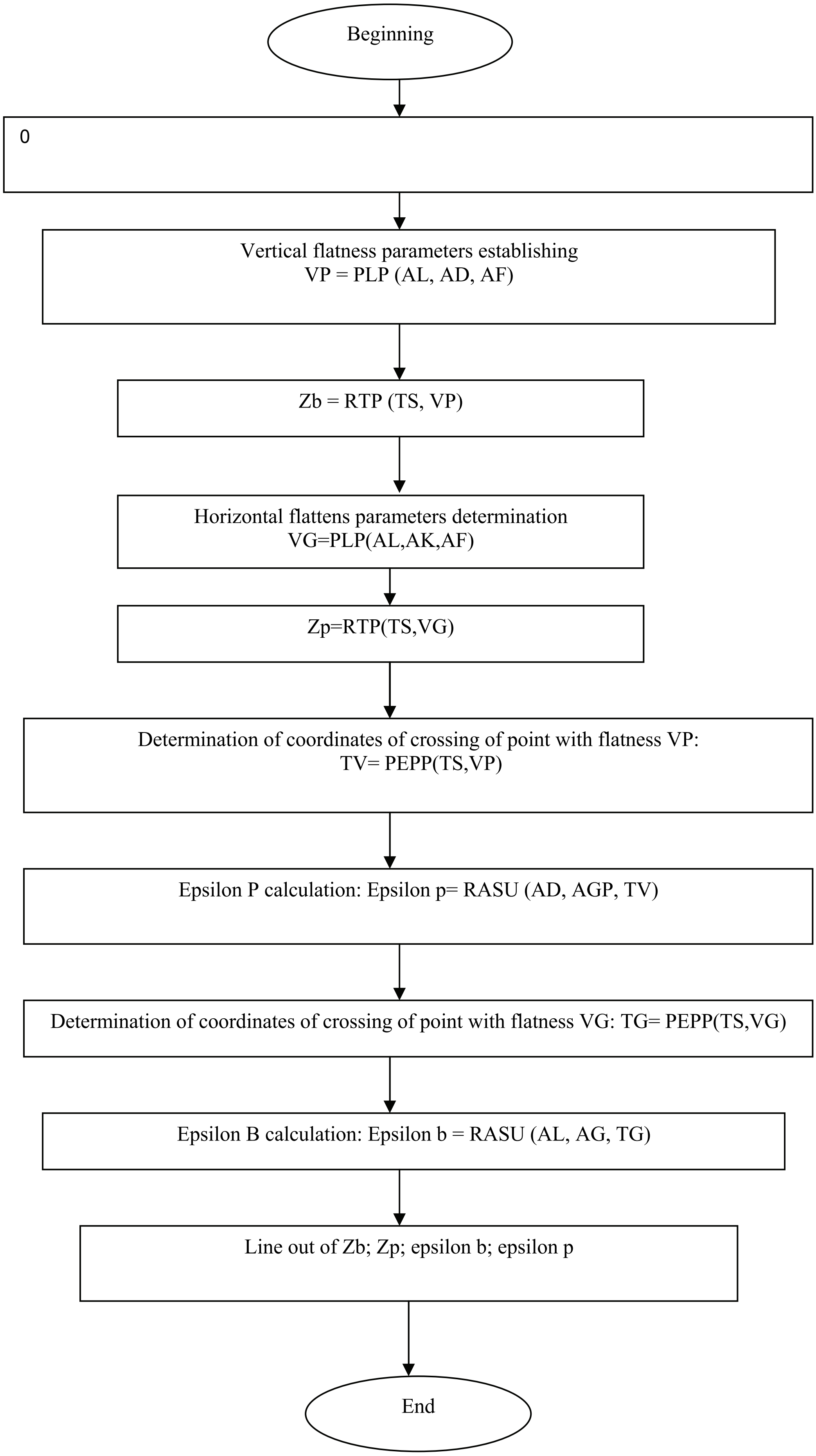

Fig. 2. Block-diagram of program of calculation of homing parameters

Latitude – tetaGP = tetaL – TCH/111110*tg (GPA);
Longitude – lambda GP = lambda L;
Height – hGP = hL of point GRIP.
Latitude – tetaF = tetaL – (D – 305)/111110;
Longitude – lambdaF = lambdaL;
Height – hF = hL of point FPAP.
Latitude – tetaD = tetaL;
Longitude – lambdaD = lambdaL;
Height – hD = hL = TCH of point DCP.

Block-diagram of program of parameters calculation is depicted on figure 2, where AL, AF, AK, AD, AG, AGP -vectors of coordinates of points LTP/FTP, borders KS,DCP, GARP,GRIP accordingly, TS-FM coordinates vector.

Modeling results

The sense of the modeling is the following. For fixed coordinates of FM by means of program (figure 2) the volumes of Zb, Zp, epsilon b, epsilon p are calculated. The occasional mistakes in coordinates calculation by board-based receiver in cycle of realizations added and calculations repeated. The low of mistakes ramification is normal with parameters [0, sD].

The results of declinations of calculated volumes in averaging by 1000 realizations are stated in table, where mZb,mZp,meb, mep are the mathematic expectations, sZb, sZp, seb, sep - mean-square declinations of homing parameters from calculated ones without mistakes introduction. The units of measuring are meters and radians.

Table 1

Results of modeling

sD	10	5	3	1
mZb	- 0.11	- 0.06	- 0.04	0.03
mZp	- 0.06	- 0.09	- 0.05	0.004
meb	$- 1.2*10^{-5}$	$-3.8*10^{-6}$	$3.7*10^{-6}$	$3.8*10^{-6}$
mep	$- 6.3*10^{-8}$	$-9.0*10^{-8}$	$-5.7*10^{-8}$	$3.8*10^{-9}$
sZb	9.99	5.01	2.99	1
sZp	9.94	5	3.01	1
seb	$3.5*10^{-3}$	$5.4*10^{-4}$	$3.2*10^{-4}$	$1.05*10^{-6}$
sep	$1*10^{-5}$	$5.2*10^{-6}$	$3.2*10^{-6}$	$1.0*10^{-6}$

As derives from the obtained results, the mean-square mistakes in linear homing parameters definitions are equal and the angular ones are proportional to mistakes mean-square declinations in FM coordinates calculation.

Conclusions

The performed investigations show that declared model allows to calculate parameters of FM homing in GNSS approach and landing The model also allows to establish dependence of homing calculation errors from mistakes of board-based receiver calculations of coordinates. The results show that for providing of categorized landing differential mode of navigation calculations implementation is necessary.

Literature

1. International standards and Recommended practice (SARPS). ICAO document C – WP/11519 13/2/01
2. Agajanov P.A., Vorobyov V.G., Kuznetsov A.A., Markovich E.D - Automation of air navigation and air traffic control - Moscow, Transport.
3. V.V. Konin, V.P. Kharchenko – Satellite navigation systems – Kyiv, Holteh, 2010. – 520p.
4. Vygodskiy M.Y. – Guide to Higher Mathematics – Moscow, Science, 1977. – 852p.

UDC 621.396

V.P.Kharchenko, PhD, Prof.
Y.M.Barabanov, PhD, Docent
A.M.Grekhov, PhD, Prof.
M.V.Kolchev, Student
(National Aviation University, Ukraine)

MONITORING OF AIR TRAFFIC USING ADS-B SYSTEM

With the purpose of surveillance after air traffic the system was created for ADS-B messages receiving. For this an antenna, ADS-B signals receiver, a decoder were made and software was installed. This system was allocated at the Department of Air Navigation Systems and is used for students training and investigations.

1. Problem

ADS-B is short for Automatic Dependent Surveillance - Broadcast [1]. This is new technology for monitoring air traffic, which is implemented in Europe, USA etc. EUROCONTROL CASCADE program coordinates implementation of ADS-B systems in Europe. That is why it is important for students to study this new technology of surveillance.

2. Analysis of Publications

Equipped with ADS-B transceiver aircraft during all flight transfers in real time their exact position, speed, altitude, course and other information [3]. Access to ADS-B information is free for all. ADS-B signal can be received on earth for the purpose of surveillance (ADS-B-OUT) or other aircraft for information about the surrounding traffic (ADS-B-IN) and avoid collisions [4]. ADS-B-OUT system began operating in 2008, ADS-B-IN - in 2011. System ADS-B-OUT can be used for purposes of self-observation, as well as with radar systems and MLAT (multilateration). For transmition of ADS-B messages transponder Mode S Extended Squitter is used [5]. On-board transponders transmit data at a frequency of 1090 MHz. To receive these messages we must have the receiver signals at that frequency - ADS-B-receiver. The frequency of 1090 MHz belongs to the L-band. Electromagnetic waves with such high frequencies are distributed in the atmosphere straight without being reflected from the ionosphere. Receiving of these signals can only be possible if between aircraft and the receiving antenna is no obstructions. Receiving antenna must be installed as high as possible and have free space in all directions. The greater is the height of the aircraft, the greater is distance that signal may be accepted. For example, the signal from the aircraft, which is at an altitude of 30,000 feet (10 km) may be received up to 350 km. This requires a sensitive antenna and receiver. But if we consider the distance to the aircraft within 100 miles we can receive ADS-B signals even using simple equipment. There are exist some schemes for simple ADS-B systems [6,7].

3. Purpose of Work.

The aim of this work is to build a simple system for receiving ADS-B signals and to use it for monitoring of air traffic.

4. Structural scheme of ADS-B System.

A system that makes ADS-B signals can be used as virtual radar to create real-time picture of air traffic and consists of four components: an antenna, receiver decoder and computer software (Fig.1).

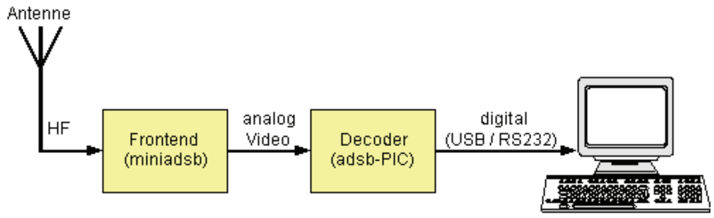

Fig. 1. The system for receiving ADS-B signals

The antenna receives the signal at a frequency of 1090 MHz and converts it into high-frequency electrical signal. The receiver selects, amplifies, demodulates received signals and generates an analog video signal. Decoder converts analog video to digital and detects ADS-B message. ADS-B signals are then transmitted via the USB port on your computer. Using computer software we can decode ADS-B information and generate virtual display radar. In this system miniadsb receiver [6] and adsbPi decoder software adsbScope [7] are implemented.

5. Antenna

Transponder signals are polarized in the vertical plane and they need to be received by an antenna with vertical polarization at a frequency of 1090 MHz. The simplest antenna is a vertical wire with length of 0.13 m [7], which corresponds to half the wavelength of the frequency of 1090 MHz. This is an electric dipole antenna which can receive the signal from all directions.

To increase the sensitivity of the antenna several electric dipoles need to be applied. But if they are placed beside one another then the antenna will cease to be non-directional. Therefore, individual dipoles placed one above the other. In addition, the dipoles must be connected. The top and bottom edges of the dipole oscillate in phase shift of 180 degrees. We have connected dipoles by means of horizontal coils of the length λ / 2 (0.13 m), which serve as devices for the phase shift of 180 degrees (Fig. 2).

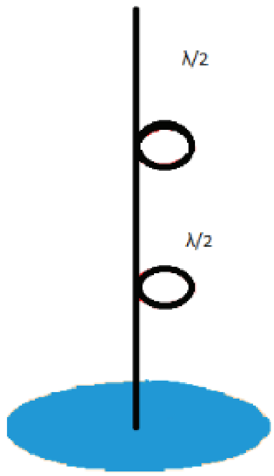

Fig.2. Antenna for receiving ADS-B signals.

Dipoles and coils by itself must be made from one long piece of wire. Wire diameter should provide the necessary rigidity of the antenna. The bottom end of this set of dipoles must be connected to the middle wire of 50 Ohm coaxial cable. For grounding can be used round metal plate with a diameter of λ / 2 (0.13 m) located radially or pieces of wire (at least 4 wires at 90 degrees to each other). Antenna impedance is not consistent with the cable impedance but it can be changed by bending the wires down.

6. ADS-B Receiver.

ADS-B receiver was assembled using the scheme shown in Fig. 3. Antenna us connected via 50 Ohm coaxial cable.

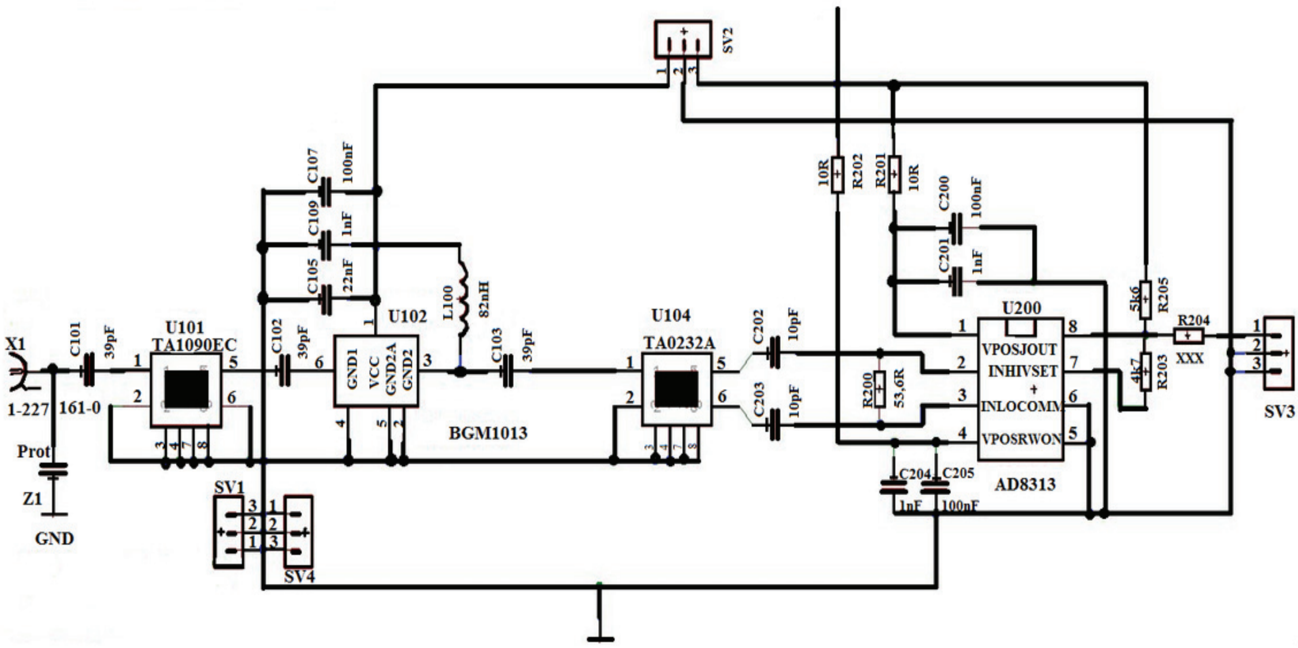

Fig.3. Schematic diagram of the ADS-B receiver

7. ADS-B Decoder

Decoder scheme is given in Fig. 4. The main element is the decoder microcontroller PIC18F2550. It converts analog video to digital using the internal comparator. These ADS-B messages are transferred via the USB port at a PC. The decoder is designed for use with miniadsb receiver and software adsbScope or Planeplotter [7].

8. adsbScope Software

Software adsbScope contains outlines of continents, list of cities, airports list, and a list of aircraft with ICAO numbers of these aircraft information to determine the nationality of aircraft, the location and length of runways, information about air routes, the location and areas of ILS systems, data about ground radar location. When you run the software AdsbScope opens the program, tests subdirectories and loads data files. The program window contains a text field for the decoded data, table for the detected aircraft, decoder control panel and information field (Fig. 5). The data with revealed aircraft are shown in the table between the two text boxes. Figure on the left side of window shows the position, track and additional information about the aircraft. The software counts the number of ADS-B frames (packets) per minute and displays it in the bottom right corner. Also the average number of frames received from an aircraft per a minute is displayed. Besides the software checks the CRC-checksum for each frame.

9. Monitoring of Air Traffic

The user can choose which information must be displayed and what colors are used for different types of objects.

The display is updated at least once per second (usually 4 times a second). The software creates a line (trajectory) from the place where the plane was found for the first time. The first location of the aircraft depicted in the form of a small circle. Next track number is specified, the ID aircraft altitude in feet (FL) and speed in knots. If the plane is unknown (not in the list of aircraft with the numbers of these aircraft ICAO), it only indicates track number. Track number corresponds to the first column of the table in Fig. 5.

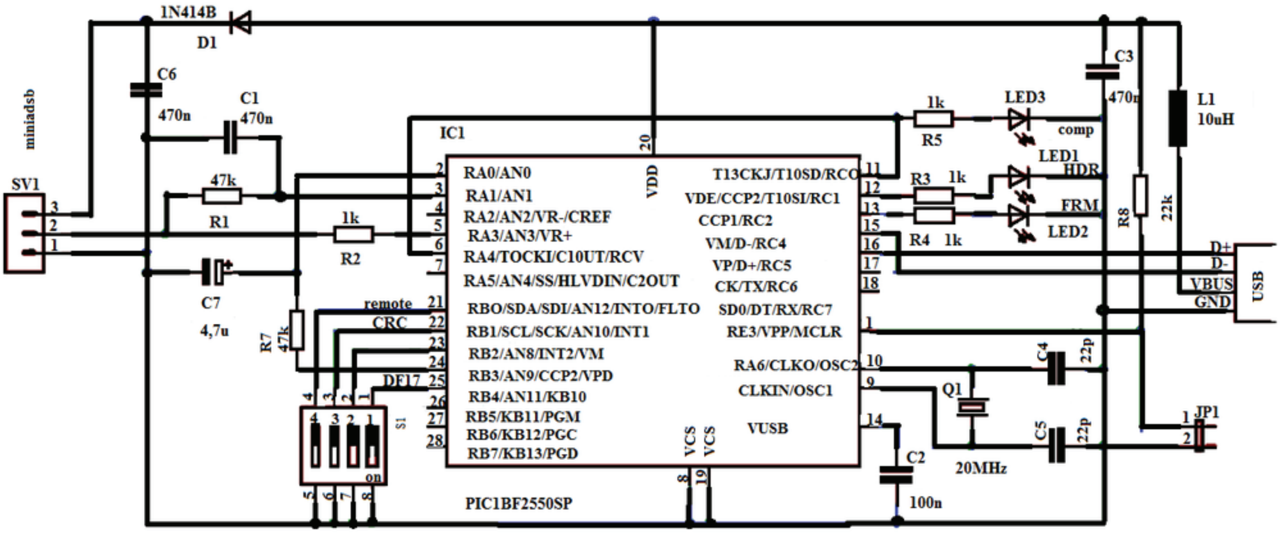

Fig.4. Scheme of a decoder adsbPIC

If at this moment the airplane arrives, its position is based on calculation of the last known location, speed and direction. Flight path from the last known position on a predictable trajectory is shown by dotted line. The user can disable forecasting position. The software selects for each aircraft a random color. The user can select the mode in which the color of the trajectory represents the height of the aircraft. In this mode, 0 is represented feet red, while 20,000 feet - 40,000 feet and green - blue.

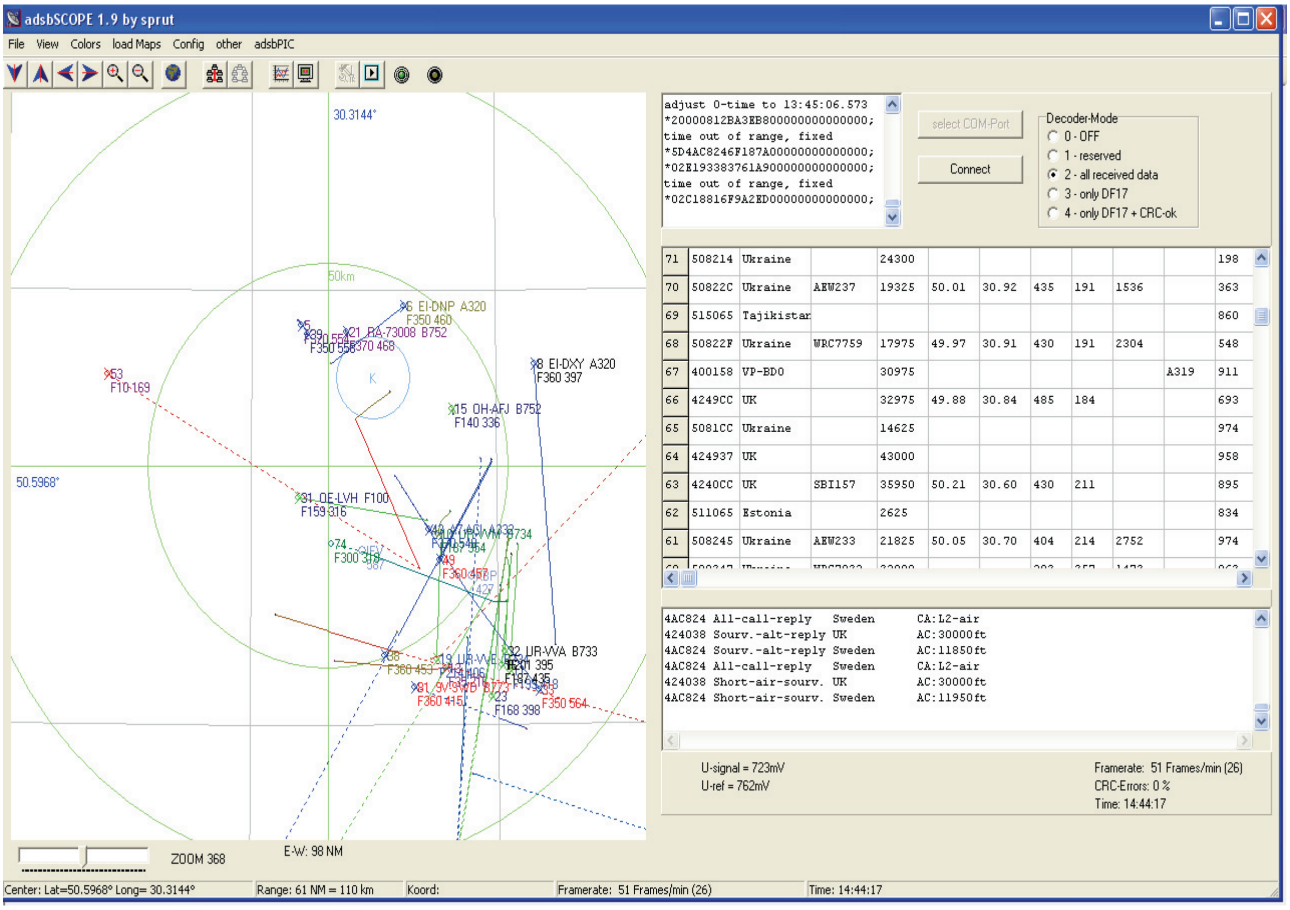

Fig.5. Main window of adsbScope.

10. Results

The following experiments using the system for receiving of ADS-B signals were made:

- Surveillance of air traffic and results (number of aircraft and information about them) were compared with data on the website Flightradar24.com [8];
- The possibility of determining the maximum distance of planes was investigated.

Results of observations are shown in Fig. 6. The distance from the antenna system to the airport "Boryspil" is 47 km and to the airport "Zhulyany" - 23 km. It was possible to watch the planes at a distance of 160 km and altitudes up to 12000 m.

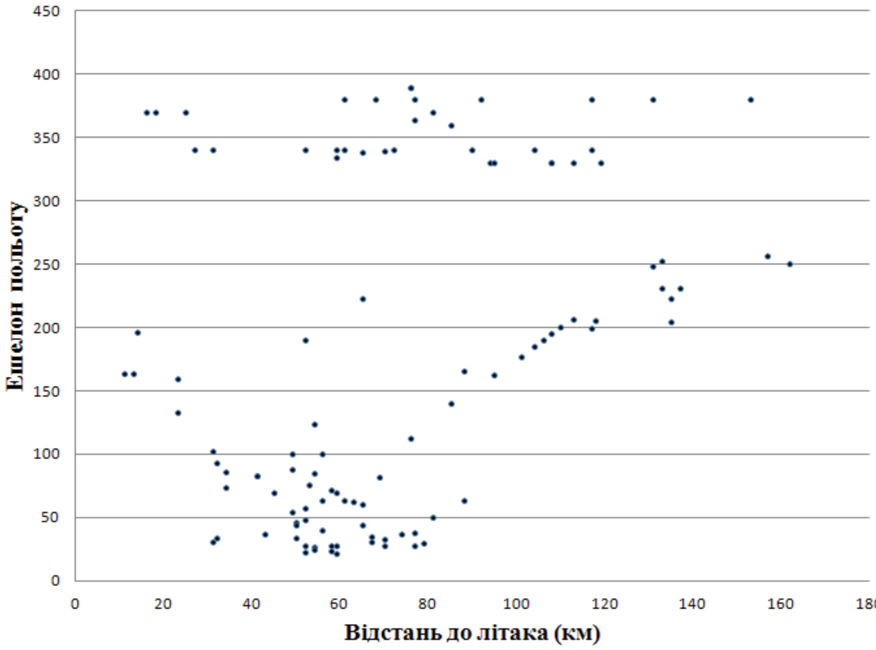

Fig.6. Results of an experiments.

It turned out that the system has a small "blind funnel" and allows you to track planes virtually "above it". The maximum detection range is limited by curvature of the earth's surface and depends on the height of the aircraft.

The antenna for receiving ADS-B signals was mounted on the roof of National Aviation University Building number 11 and can monitor all aircraft in the area of Boryspil airport equipped with the appropriate transceiver. The number of aircraft on Flightradar24 site display coincides with the number of aircraft that "sees" our system.

11.Conclusions

1. The system for receiving of ADS-B signals is created.
2. The system is located at the Department of Air Navigation Systems.
3. The system is used in the process of students training and for student’s research.

List of references

1. EUROCONTROL. ADS-B Sites. //www.eurocontrol.int/ads_b_sites/.
2. The CASCADE Programme. //www.eurocontrol.int/cascade/.
3. Live Flight Tracker. //www.flightradar24.com/.
4. Mode S and ACAS Program. //www.eurocontrol.int/msa/.
5. Guidance for the Operational Introduction of SSR Mode.
//www.eurocontrol.int/eatm/gallery/content/public/library/ssr-mode-s-ops.pdf/.
6. miniADSB – Tutorial. //miniADSB.com/.
7. ADS-B Decoder and Software with PIC18F2550. //www.sprut.de/electronic/pic/projekte/adsb/.
8. Flightradar24. // www.flightradar24.com//

UDC 629.056.6: 629.056.8 (045)

V. Kharchenko, V. Kondratyuk, S. Ilnytska, O. Kutsenko
(National Aviation University, Ukraine)

EXPERIMENTAL VALIDATION OF SMALL INTEGRATED NAVIGATION SYSTEM PROTOTYPE

Description and results of small integrated navigation system prototype experimental validation are provided. One degree-of-freedom rotation table and correspondent measurement equipment have been used for the experiment. For estimation the coordinates' determination accuracy reference trajectory has been calculated using GrafNav/GrafNet package. Results of experiment prove small integrated navigation system functioning efficiency.

Introduction. The integration of GPS (Global Positioning System) and INS (Inertial Navigation System) has been intensively investigated by many researchers along the world for the last decades, but it is still an urgent problem, since the goal is always to improve the integrated navigation solution accuracy, reliability and anti-jamming performance.

With this objective, and the rapid developments in low-cost MEMS Inertial Measurement Unit (IMU) technology, the integration of GPS and INS has taken a new direction. Development of small, low-cost, weight and power consumption integrated navigation system with appropriate quality characteristics that could be applied at small unmanned aerial vehicles is a new branch of research.

Internationally established practice is to use MEMS IMU with 3-axis accelerometers, gyros, magnetometers, barometric altimeter and GNSS (Global Navigation Satellite System) receiver as a basic structure of small integrated navigation system.

Motivation for experiment performing. For efficient functioning of small integrated navigation system (SINS) it's necessary to have two main parts: hardware and software. Software part can be evaluated using different simulations in Matlab or similar software package, but the drawback of such approach is that it doesn't always depicts real situation as when using data from real sensors.

Therefore in this work it is proposed to investigate functioning of SINS prototype created in Aerospace Center in National Aviation University by performing an experiment that is described below.

It is necessary to note that algorithms used for sensors data processing are described in [1-4].

Experiment setup. For small integrated navigation system functioning investigation the following experiment has been performed. Wooden stand (fig.1,3) with the vertical axis of rotation and the arm length 2.35 m (fig. 1) has been placed at the point at National Aviation University territory (fig.4).

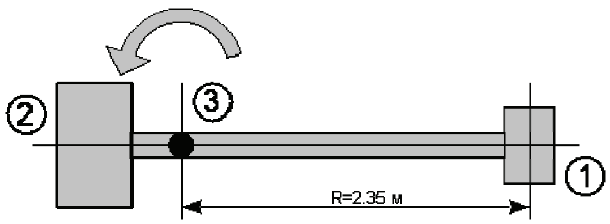

Fig.1 Stand drawing (top view)

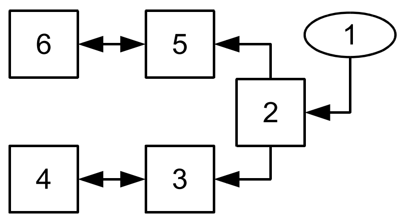

Fig.2 Equipment connection scheme

The point of experiment setup has the following coordinated: 50.438874248 º north latitude, 30.428294371 º east longitude and 195.943 m height relative to ellipsoid WGS-84.

At the fig. 1 the following designations are accepted: 1 – all devices, 2 – notebooks and accumulators (batteries), 3 – stand axis of rotation. Equipment connection scheme is represented at fig. 2, where the following designations are accepted:

1 – the Novatel GPS-703-GGG antenna;

2 – the Antcom 4G12155-XS4-X GNSS signals splitter;

3 – the small integrated navigation system (SINS) prototype, which includes: the Analog Device inertial measurement unit ADIS16362, the Honeywell HMC5843 3-axis magnetometers, the Bosch Sensortec barometric pressure sensor BMP085 and GNSS receiver OEM-V1 by Novatel;

4 – notebook Lenovo IdeaPad S10-3;

5 – miniature AHRS IG-500N by SBG-Systems;

6 - notebook DELL Vostro 3355.

Photo of all connected equipment is represented at fig. 3.

Fig.3 Photo of experimental equipment

Fig.4 Reference trajectory in Google Earth

During the experiment first 5 min static data were gathered, then the stand was rotated clockwise, therefore the direction of rotation about Z axis, pointing downward was positive, which is seen as well from the fig. 2 where the gyros measurements are depicted. The height was constant during experiment.

Signals from navigation satellites received by antenna through the splitter were fed up to the GNSS receiver of SINS prototype and AHRS IG-500N. Sensors data of MINS prototype where recorded at flash card, data from AHRS IG-500N were recorded to the notebook DELL Vostro 3355 with the help of provided by the manufacturer software sbgCenterApplication. The raw measurements of GNSS receiver OEM-V1 were recorded at the notebook Lenovo IdeaPad S10-3 for getting the reference trajectory. After the experiment data were post-processed that is described below.

Now let's consider more detailed sensors of SINS prototype. The ADIS16362 sensor is a complete inertial measurement unit that includes a triaxis gyroscope and triaxis accelerometer. Each sensor in the ADIS16362 combines iMEMS technology with signal conditioning that optimizes dynamic performance. Gyroscopes dynamic range can be tuned (±75, ±150 or ±300 °/s as default), initial sensitivity – 0.05 °/s for 300 °/s dynamic range, output noise – 0.8 °/s rms (no filtering). Accelerometers dynamic range is ±1.7 g, initial sensitivity – 0.33 m/s^2, output noise – 5 mg rms (no filtering). Transferring data to a microcontroller is performed through SPI interface. More detailed ADIS16362 technical specifications are represented at [7].

The Honeywell HMC5843 is a surface mount multi-chip module designed for low field magnetic sensing with a digital interface. The HMC5843 includes 1043 series magneto-resistive sensors plus Honeywell developed ASIC containing amplification, strap drivers, offset cancellation, 12-bit ADC and an I2C serial bus interface. Its field range ± 4 Gauss, resolution – 7 mG. More detailed HMC5843 technical specifications are represented at [8].

The Bosch Sensortec BMP085 is a digital pressure sensor with temperature measurement included. Its pressure range – 300…1100 hPa (+9000 m … -500 m above sea level), resolution - 0.01 hPa, relative accuracy at temperature 25 ºC is ± 0.2 hPa. Connection to a microcontroller is performed via I2C but. The BMP085 delivers the uncompensated value of pressure (16 to 19 bit) and temperature (16 bit), therefore its measurements have to be compensated by the calibration data. More detailed BMP085 technical specifications are represented at [9].

GPS Receiver OEMV-1 is a compact, single frequency receiver that delivers L-band positioning on board [10]. Its performance specification: channel configuration – 14 GPS L1, 2 SBAS; hot start – 35 s, cold start – 60 s; signal reacquisition L1 – 0.5 s typical; measurement and position data rate – up to 20 Hz; horizontal position accuracy (RMS) at single point L1- 1.5 m, velocity accuracy, RMS – 0.03 m/s. Integrated L-band supports OmniSTAR VBS and CDGPS correction services. Receiver provides estimated position and velocity in DOUBLE format. Transferring data to microcontroller is performed through the serial interface UART.

The IG-500N is the GPS enhanced Attitude and Heading Reference System (AHRS) which delivers attitude and position measurements at data rate up to 50 Hz. The IG-500N includes a MEMS based Inertial Measurement Unit (IMU), magnetometers, GPS receiver and a pressure sensor. It provides precise drift-free attitude and position, even in long time turns. Attitude parameters specification: static accuracy - 0.5 °/s for roll and pitch (with stabilized Kalman filter) and 1 °/s for yaw angle (homogenous magnetic field), dynamic accuracy - 1 °/s under good GPS availability and up to 2 °/s at GPS signal loss. Position accuracy at SBAS support is 2 m, after GPS signals loss position accuracy degrades significantly at the next few seconds. Data transferring to a microcontroller can be performed through a serial interface RS-232. More detailed IG-500N technical specifications are represented at [11].

Data processing. Recorded binary data with the C language program are converted in text format for further processing with Matlab software. For each of sensors separate file is created where new parameter is represented by a column and new measurement – by a row.

Internal device timer is synchronized with the global GPS time with the help of GPS receiver signals. Timer resolution is 1 ms.

GNSS data file contains GPS time (week seconds), XYZ coordinates in ECEF (Earth Centered Earth Fixed) coordinate system, estimated coordinate RMS (m), velocities in ECEF, estimated velocities RMS (m/s), solution status and type of navigation task according to [5]. IMU data file contains time (week seconds), angular velocities (rad/s) and specific force (m/s^2) along the measurement axes. Magnetometer data file contains time (week seconds) and measurements of the intensity of the magnetic field (mG) along the measurement axes. In such form data are transferred for the processing in Matlab.

Magnetometer and IMU data rate was 50 Hz (therefore $\Delta t = 2 \cdot 10^{-2}\,c$), GNSS data rate – 1 Hz.

Magnetometer measurements contained errors which are random Gauss distributed values $N_{mag}(M_{mag}, \sigma_{mag})$, where M_{mag} - mathematic expectation, σ_{mag} - RMS of magnetometer measurements in static:

$$M_{mag} = [110.12 \;\; -206.92 \;\;\; 602.05]\,\mathrm{mG}, \; \sigma_{mag} = [\,5.9509 \;\;\; 4.4955 \;\;\; 5.2068]\,\mathrm{mG}.$$

Mathematical expectations of sensor measurements here and further in the present article are calculated by finding the average of static data segment with the help of “mean” command, RMS – by the help of “std” command in Matlab software.

Height measured by the barometric altimeter contained errors which are random variables with Gauss distribution $N_{baro}(M_{baro}, \sigma_{baro})$, with zero mathematical expectation $M_{baro} = 0\,\mathrm{m}$, and $\sigma_{baro} = 0.5\,\mathrm{m}$.

Gyros measurements contained errors which are random variables with Gauss distribution $N_{gyro}(M_{gyro}, \sigma_{gyro})$, where M_{gyro} - mathematical expectation, σ_{gyro} - RMS of gyros measurements in static:

$$M_{gyro} = [\,0.001258 \;\; -0.007280 \;\;\; 0.005174]\,\mathrm{rad/s}, \; \sigma_{gyro} = [\,0.065676 \;\;\; 0.065327 \;\;\; 0.072545]\,\mathrm{rad/s}.$$

Gyros measurements in °/s ($\omega = [\omega_x \;\, \omega_y \;\, \omega_z]$) are represented at fig. 5. Accelerometers measurements in m/s^2 along the body measurement axes ($f = [f_x \;\, f_y \;\, f_z]$) are represented at fig. 6.

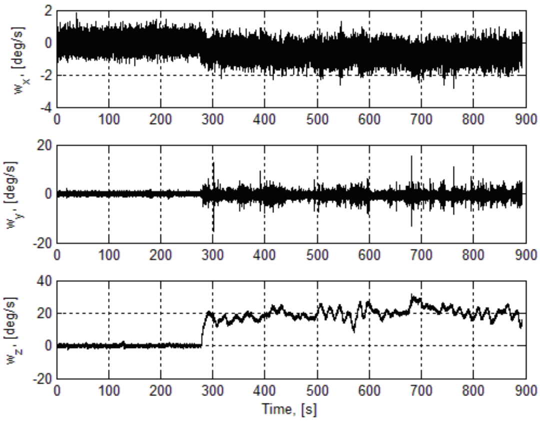

Fig.5 Gyros measurements, deg/s

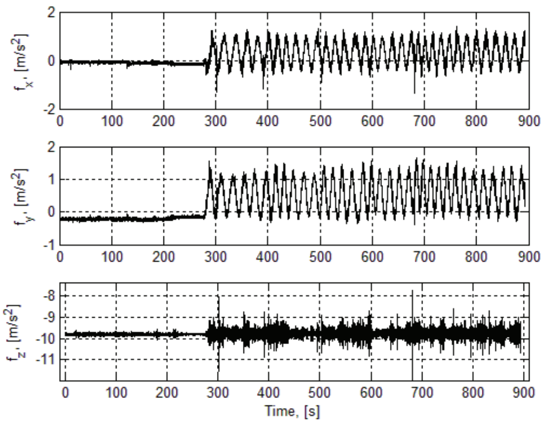

Fig.6 Accelerometers measurements, m/s^2

Accelerometers measurements contained errors which are random variables with Gauss distribution $N_{accel}(M_{accel}, \sigma_{accel})$, where M_{accel} - mathematical expectation, σ_{accel} - RMS of accelerometer measurements in static:

$$M_{accel} = [-0.0728\ \ -0.2174\ \ -9.809]\ \mathrm{m/s^2},\ \sigma_{accel} = [0.23927\ \ 0.18694\ \ 0.25255]\ \mathrm{m/s^2}$$

GPS receiver measurements contained errors which are random variables with Gauss distribution $N_{GPS\_vel}(M_{GPS\_vel}, \sigma_{GPS\_vel})$ and $N_{GPS\_pos}(M_{GPS\_pos}, \sigma_{GPS\_pos})$, where M_{GPS_vel} - mathematical expectation, σ_{GPS_vel} - RMS of velocity estimation, and $M_{GPS\_pos}, \sigma_{GPS\_pos}$ - are mathematical expectation and RMS of position estimation correspondently in static:

$$M_{GPS\_vel} = [-0.0015\ \ 0.0032\ \ 0.0113]\ \mathrm{m/s},\ \sigma_{GPS\_vel} = [0.0240\ \ 0.0181\ \ 0.0243]\ \mathrm{m/s}$$

$$M_{GPS\_pos} = [3509818.82\ \ 2061528.59\ \ 4894172.42]\ \mathrm{m},\ \sigma_{GPS\_pos} = [0.1548\ \ 0.1255\ \ 0.1163]\ \mathrm{m}.$$

As has been told above all calculations have been performed in NED coordinate system with the origin at the following geographic coordinates: 50.438874248 º N latitude, 30.428294371 º E longitude and 195.943 m height relative ellipsoid WGS-84. Therefore before running navigation parameters estimation algorithms all data from GPS file and reference trajectory file were transformed to NED.

Common duration of the experiment was about 900 s where at normal conditions inertial navigation system has been corrected every 1 s from GNSS receiver, magnetometer and barometric altimeter, in case of absence of GNSS signals INS functioned in autonomous mode.

Reference trajectory has been calculated using raw measurements from GNSS receiver OEMV -1 and GrafNav/GrafNet high-precision package by Waypoint. This software is usually used in geodesy for data post-processing from navigation receivers and it allows getting highly accurate coordinates both of stationary and moving points. Reference coordinates estimation is performed using relative navigation method where for the estimated coordinates refinement data from navigation receiver with known coordinates are used. Such receiver is usually called the base station. In our case the receiver from the National Aviation University GNSS monitoring experimental complex has been used. Besides reference coordinates and velocities GrafNav/GrafNet package allows getting their quality characteristics (number of satellites, their visibility, geometric delusion of precision factors, signal-to-noise ratio, etc). Reference trajectory coordinates have been provided in text format for their further processing and comparison in Matlab software package. This data file contains time in GPS week seconds, XYZ coordinates and velocities in ECEF.

Estimated by GrafNav/GrafNet package RMS of calculated reference coordinates is shown at fig. 7. As it can be seen from the figure, it didn't exceed 0.2 m. Values of geometric delusion of precision factors represented at fig. 8 didn't exceed 2.4. It's necessary to note as well that during the experiment setup at least 6 satellites have been used for the navigation solution. Received quality characteristics confirm the good conditions for navigation parameters estimation and reference coordinates calculation.

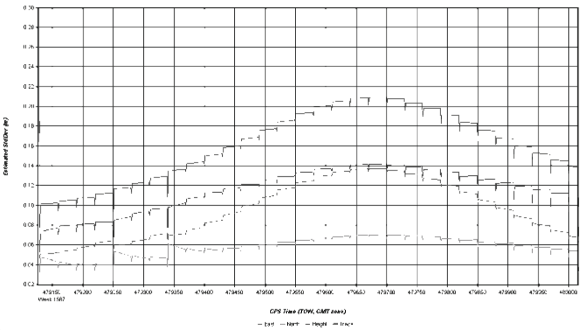

Fig. 7 Estimated RMS of reference coordinates

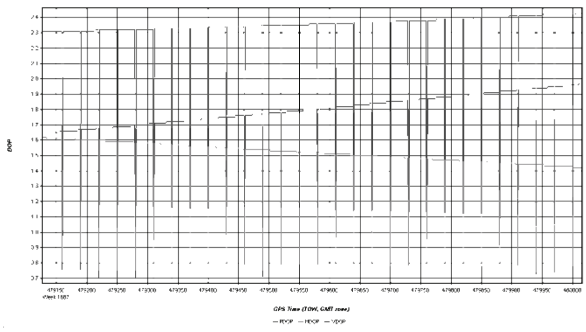

Fig. 8 Geometric delusion of precision factors

Results. Results of data processing in NED are represented at figures 9-12. A part of static measurements and few first turns of SINS of common duration 200 s are represented at figs. 9-11. Fig. 12 depicts results of all experimental data processing of common duration 900 s.

Time dependences of estimated linear velocities in NED are represented at fig. 9. Here black solid line with dots at measurement points depicts measurements from GPS receiver, and grey solid line – linear velocities estimated by SINS. It can be seen that in a normal mode of SINS functioning these velocities practically coincide, and downward component V_down estimated by SINS has even more smooth form. It is necessary to note as well that after GPS signal reacquisition SINS corrected its solution according to the new measurement and continued working in a normal mode.

Time dependences of estimated coordinates in NED are represented at fig. 10. Here black solid line with dots depicts GPS receiver measurements, and grey solid line – SINS estimated linear velocities. It can be seen as well that downward component D estimated by SINS is more accurate than the one received from GPS receiver due to additional correction from barometric altimeter.

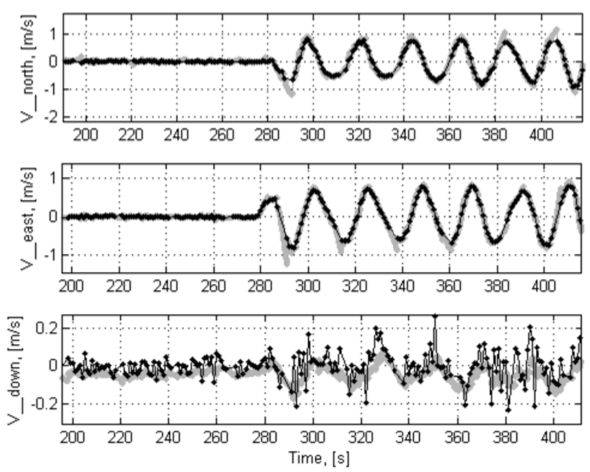

Fig. 9 Velocities in NED

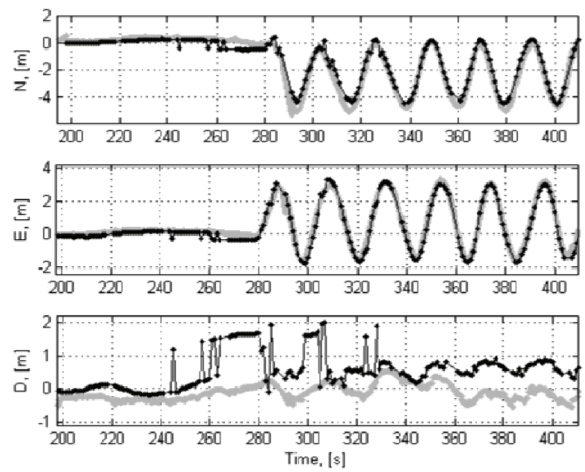

Fig. 10 Coordinates in NED

Time dependences of estimated roll, pitch and yaw angles are represented at fig. 11. Here angles estimated by SINS are depicted by grey color line and angles provided by AHRS IG-500N – by black color line.

Trajectory of equipment motion in a horizontal plane (North, East) is represented at fig. 13. Here the curve of light grey color depicts coordinates from AHRS IG-500N, black line with circles at measurement points – reference coordinates estimated by GrafNav/GrafNet package according the described above method, grey stars – coordinates from GPS receiver, and thin black solid line – SINS estimated coordinates. It can be seen that SINS follows the GPS solution quite accurately. During the experiment there were few gaps of GPS signal with duration up to 5 seconds and SINS functioned in INS autonomous mode. Estimated coordinates during autonomous modes of functioning deviated not more than 2 m, and the direction of rotation had been estimated correctly. After the GPS signal reacquisition SINS corrected its current solution according the received measurements of position and velocity from GPS receiver.

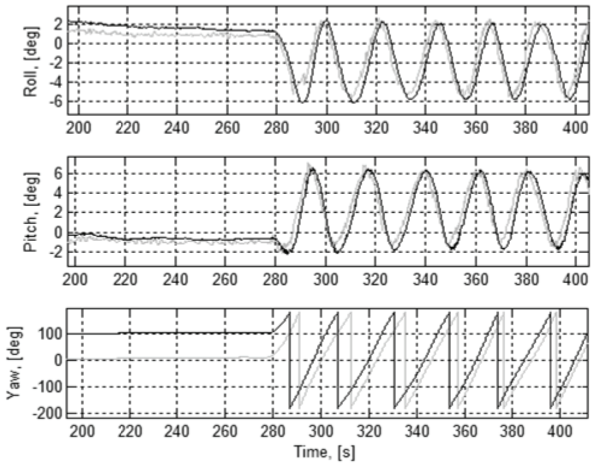

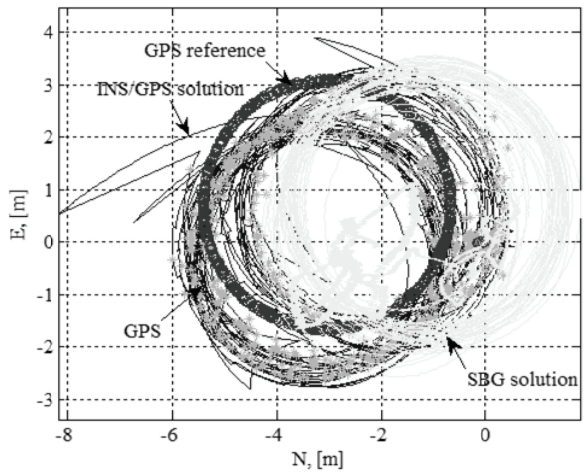

Fig. 11 Roll, pitch, yaw angles

Fig.12 Trajectory of motion in a horizontal plane

As it can be seen from the represented at figs. 9-12 results INS aiding algorithms work efficiently even at the presence of noise and some systematic error components at the measurements of inertial sensors. But this statement is true only at the constant availability of GPS measurement. In other case position and velocity solution will degrade significantly after approximately 10 s of INS autonomous mode of functioning due to the presence of error components in inertial sensors measurements.

Conclusions. At the present work functioning of SINS prototype created in Aerospace Center in National Aviation University had been evaluated through performing an experiment with a circular motion of equipment at a wooden rotational stand. Results received from the data post-processing approve the efficiency of SINS functioning in normal navigation mode.

References

1. *Kharchenko V. P. Analysis of unmanned aerial vehicle kinematic equations integration algorithms / V. P. Kharchenko, S. I. Ilnytska // Proceedings of the NAU – 2010. – №3 (44). – P. 9-17.*

2. *Харченко В.П. Оцінка алгоритму інтегрування рівнянь обертальних рухів безпілотного літального апарату / В.П. Харченко, С.І. Ільницька // Вісник інженерної академії України. - 2010.-№2.- С. 17-21.*

3. *В.П. Харченко, С. І. Ільницька Аналіз ефективності алгоритмів інтегрованої інерціально-супутникової навігаційної системи // Механіка гіроскопічних систем. Науково-технічний збірник "Київський політехнічний інститут" Випуск 22. Київ 2010 - С. 32-43.*

4. *Ларін В.Б., Тунік А.А. О корректировании работы системы инерциальной навигации. // Проблемы управления и информатики. – 2010. – №4. – С. 130-142.*

5. *OEMV® Family . Firmware Reference. Manual. Rev. 3.8., 2010, - 650 p.*

6. *User's manual for GrafNav/GrafNet. Version 8.20. Waypoint Consulting Inc., 2010, - 426p.*

7. *Технічні характеристики інерціального вимірювального блоку ADIS 16362. Електронний ресурс // http://www.analog.com/en/mems-sensors/mems-inertial-measurement-units/adis16362/products/product.html*

8. *Технічні характеристики магнітометра HMC5843. Електронний ресурс // www.honeywell.com/magneticsensors*

9. *Технічні характеристики датчика тиску BMP085. Електронний ресурс // http://www.datasheetarchive.com/BMP085-datasheet.html*

10. *Технічні характеристики ГНСС приймача OEMV-1. Електронний ресурс // novatel.com/Documents/Papers/OEMV-1.pdf*

11. *Технічні характеристики курсовертикалі* IG-500N. *Електронний ресурс // www.sbg-systems.com*

UDC 621.391.254 (045)

R.S. Odarchenko (National Aviation University, Kyiv, Ukraine)

ALGORITHM OF ADAPTIVE CHANGES OF THE OFDM-SYMBOLS CYCLIC PREFIX DURATION IN MODERN WIRELESS COMMUNICATION SYSTEMS

This paper analyzes the phenomenon of interference between a character in wireless communication channels. Analysis of OFDM technology using it to fight the phenomenon of interference between symbolic. Disadvantages of the features of cyclic prefix and an algorithm for adaptive changes in cyclic prefix of OFDM-symbols is shown, which allows you to increase the effective OFDM channels bandwidth.

The specific of many distant communication lines (tropospheric, satellite, etc.) is the multipath nature of radio propagation.

The signal at the point of reception is the sum of a large number of elementary signals with different amplitudes and random time delay [1]. Some rays are delayed relative to each other to a considerable size, causing II (intersymbol interference). Depending on the degree of curvature of the shape of the pulse distinguish large (Fig. 1) and small (Fig. 2) between-symbolic obstacles.

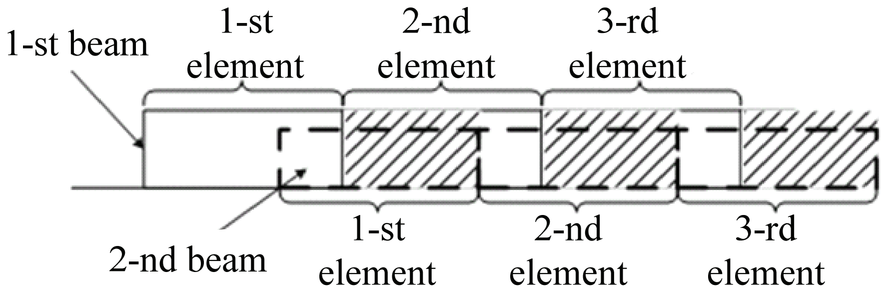

Fig. 1. Large between-symbolic obstacles

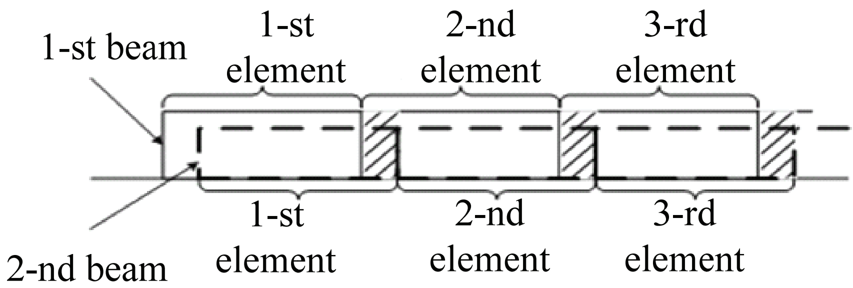

Fig. 2. Small between-symbolic obstacles

The degree of the imposing signals pulse shape curvature depends on the time difference of radio signal propagation in different ways. Usually the distribution time difference across the maximum and IInimum tract called multipath time (t_{mp}). For wireless communication distances distances this value lies in the range of 0.2-0.5 ms. If the pulse duration (τ) less than multipath time, then there are big between-symbolic obstacles. If the pulse duration is much greater than multipath time, the between-symbolic interference causes little influence on the reception, because in this case only a small portion of the element is affected by obstacle.

One of the most effective ways to fight with between-symbolic interference is OFDM technology. The main features of the functioning of this technology are given in [2,3]. The peculiarity of this technology is the using of guard intervals (Fig. 3 [8]).

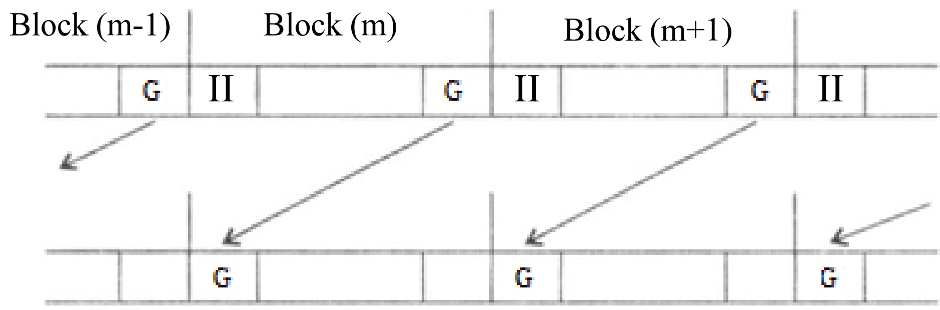

Fig. 3. Using of guard intervals in OFDM symbols

Known methods of OFDM signals forming [4-7] allow for the modulation of signals in modern radio systems: Wi-Fi, Wi-Max, LTE etc.. In these ways to combat the phenomenon of between symbolic interference guard interval of constant duration Tg is used. However, the issue of adaptive changes in the length of the prefix is not considered.

In wireless systems of fourth generation (Wi-Max and LTE) guard interval length can be 1/4, 1/8, 1/16 or 1/32 times of the OFDM symbol length Ts. This duration is determined by the manufacturer and are continuously during the entire period of operation of the system that uses OFDM technology. However, the signal beam can take quite a different way, so much can be late and overlap each other. Multipath time tmp in this case depends on the length of the traversed path of each ray signal separately. Guard interval length Tg must be elected to terms of Tg> tmp, but should be as short as possible to increase the effective OFDM channels bandwidth.

It should be noted that the developed methods will not enable you to adaptively change the length of guard interval. It does not allow full use of OFDM channels bandwidth, thus blurred the impact of between-symbolic interference. Therefore, task adaptive changes in the length of cyclic prefix is a lack of resolve, which makes you to adaptively adjust to environmental conditions by changing the cyclic shift length. This will allow more efficient use of channels bandwidth using OFDM signals.

Choosing the length of cyclic prefix from the condition of Tg> t_{mp} (must be greater than the largest spread signal delay) can avoid the mutual influence of adjacent time symbols of neighboring frequencies. The use of cyclic prefix allows you to remove both the ISS and II (as both a prefix and guard interval).

By preventing the occurrence of II and ISS, cyclic prefix is one way to improve noise immunity of communication through the use of temporal redundancy. "Fee" for the benefit, both in terms of energy costs and in terms of loss in information transfer speed is the same and determined one and the same size.

Since, as noted earlier, such as Wi-Max technology possible following the length of cyclic prefix: Tg = 1/4T, 1/8T, 1/16T, 1/32T (T - OFDM symbol duration without cyclic prefix), which causes Impairment data rate T / (T-Tg): 1,33; 1,142; 1,07; 1,032 for each length of cyclic prefix respectively.

In this situation, to prevent significant reduction of data rates over the network it is necessary to choose the optimal length of cyclic prefix for the provision of broadband subscribers the most access to network resources.

As mentioned earlier, radio rays can pass quite different way, could be late. Multipath time in this case depends on the length of the traversed path of each ray signal separately. Length overcome every track radio signals from the formula can be deterIIned by the following formula:

$$d = \sqrt{\frac{P_T \cdot \lambda^2}{4 \cdot \pi \cdot p(d)}} \tag{1}$$

where:

d – radio track length;

$p(d)$ – power of signal in the length d;

P_T – power of transIItter;

λ - wave length.

Since on receiving side is available information about the power eIItted by the transmitter antenna and the ability to measure the received signal power, you can find some distance from the transmitter to the receiver, which was overcome by each individual beam:

$$d_i = \sqrt{\frac{P_T \cdot \lambda^2}{4 \cdot \pi \cdot p(d_i)}} \qquad (2)$$

After that find the minimum and maximum distances d. Finding their differences can deterIIne the largest difference in length of rays of electromagnetic waves. Knowing this information, you can determine multipath time:

$$t_{mp} = \frac{d_{\max} - d_{\min}}{c}, \qquad (3)$$

where c – speed of light in vacuum.

d_{min}– minimum radio track length;

d_{max} - maximum radio track length;

Thus this simple model to change the of OFDM symbol cyclic prefix length, bringing it closer to the maximum specified in the previous step multipath time.

Based on the developed model can develop an algorithm of adaptive changes of OFDM symbol cyclic prefix, which has the following sequence:

1. Collecting and storing data about the signal power at the input of the receiver;
2. The choice of maximum and minimum signal strength of the input receiving device;
3. Calculation of difference between the largest and smallest facilities rays by the formula (2).
4. Determination of multipath time by the formula (3).
5. Comparison of multipath time with possible values of the length of cyclic prefix and the optimal choice.

For the resulting algorithm may offer the device block diagram for adaptive changes on the OFDM-symbol cyclic prefix length in the formation of OFDM-signals (Fig. 4).

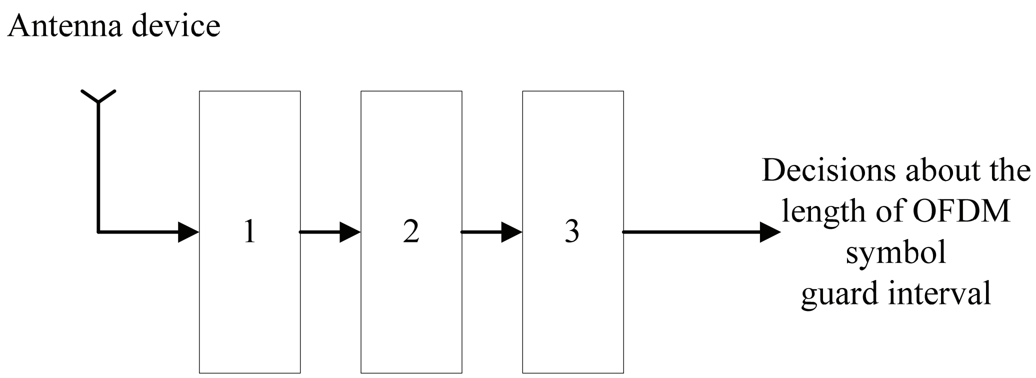

Fig. 4. Device for adaptive changes of the OFDM-symbol cyclic prefix length in the formation of OFDM-signals

Device for adaptive changes of the OFDM-symbol cyclic prefix length in the formation of OFDM-signals contains some kind of antenna device; 1 - received radio signals power meter, and 2 - the storage of received signals power data, 3 - deciding device.

Device for adaptive changes of the OFDM-symbol cyclic prefix length in the formation of OFDM-signals is as follows.

Antenna made useful signal. In adopted radio power meter (1) received signals power is defined. Then information about the measured power delivered to the storage of information about the signal (2) from which data is transmitted in deciding device (3). In deciding the device makes choice of signals with maximum and minimum power calculation time and multipath selection of the optimal length of cyclic prefix. This value is transIItted to the shaper of OFDM-symbols.

Conclusion

In this paper the methods of dealing with interference between a character in the channels of distribution multibeam radio. It describes OFDM technology to combat multipath effects. It has been proposed algorithm, which allows using statistical analysis of data collected on the mobile station power received signals to deterIIne the optimal duration of OFDM symbols cyclic prefix. This allows you to choose the shortest prefix that will provide the maximum effective transmission speed for a given quality. Based on the developed algorithm was proposed block diagram of a device for adaptive changes on the OFDM-symbol cyclic prefix length in the formation of OFDM-signals.

References

1. Мальцев А.А., Пудеев А.В., Рубцов А.Е. Метод адаптивного распределения бит и мощности по поднесущим в OFDM – системах радиосвязи // Известия вузов. Радиофизика. 2001. Т.44, №12. С. 1050 – 1061.
2. Вишневский В., Ляхов А., Портной С, Шахнович И. Широкополосные беспроводные сети передачи информации. М.: Эко-Трендз, 2005, 592 с.
3. Вишневский В., Портной С., Шахнович И. Энцеклопедия WiMAX. Путь к 4G. Москва: Техносфера, 2009. – 472 с.
4. Patent US №2007/0159957, MPC H04J 11/00 (2006.01), 2007
5. Patent US №2009/0304126, MPC H04L 27/06, 2009
6. Patent US № 8000417, MPC H03D 1/04, 2011
7. Patent України № 84411, MPC H04L 27/26, 2003
8. Сюваткин С.В, Есипенко В.И. WiMAX- технология беспроводной связи: теоретические основы, стандарты, применение. БХВ-Петербург, 2005, 368с.

UDC 621.396.6(045)

A.M. Grekhov, PhD, Yu.N. Barabanov, PhD, D.I. Tereshchenko,
(National Aviation University, Ukraine)

MODELING OF THE MESH RADIATING STRUCTURE SIMULATING AIRCRAFT AN-158 AND ONBOARD ANTENNA IRIDIUM USING MMANA-GAL BASIC SOFTWARE

Electromagnetic fields and radiation patterns of the phased array antenna on the AN-158 grid model were calculated using the method of moments and MMANA-GAL software.

An operation of any radio and radar systems is connected with an emission and a reception of electromagnetic waves. As an emission and a reception of electromagnetic waves are carried out by antennas it is obvious that an antenna is a critical element of such systems. Modeling of antenna main characteristics is very important and fundamental stage in the development of antenna systems. At the same time building of antenna radiation pattern needs solving a huge amount of combined equations with large dimensions and hence is impossible without using of computers.

For a calculation of electromagnetic fields and corresponding radiation patterns for directional antennas numerical methods of electrodynamics are used, for example, the method of moments [1]. In this method metallic elements of an antenna are replaced by the equivalent surface with electric currents which create an equivalent model of the object mesh. Then it is necessary to obtain electromagnetic fields created by these currents. For this a metallic surface is divided into elementary segments and electric currents within segments form the distribution of currents on the basis of functions with weights [2-3].

MMANA-GAL basic software [4] was used in this work for simulations. As initial data for a grid model were taken geometric dimensions of the aircraft AN-158. Aircraft mesh model with the antenna image location is shown in Fig.1.

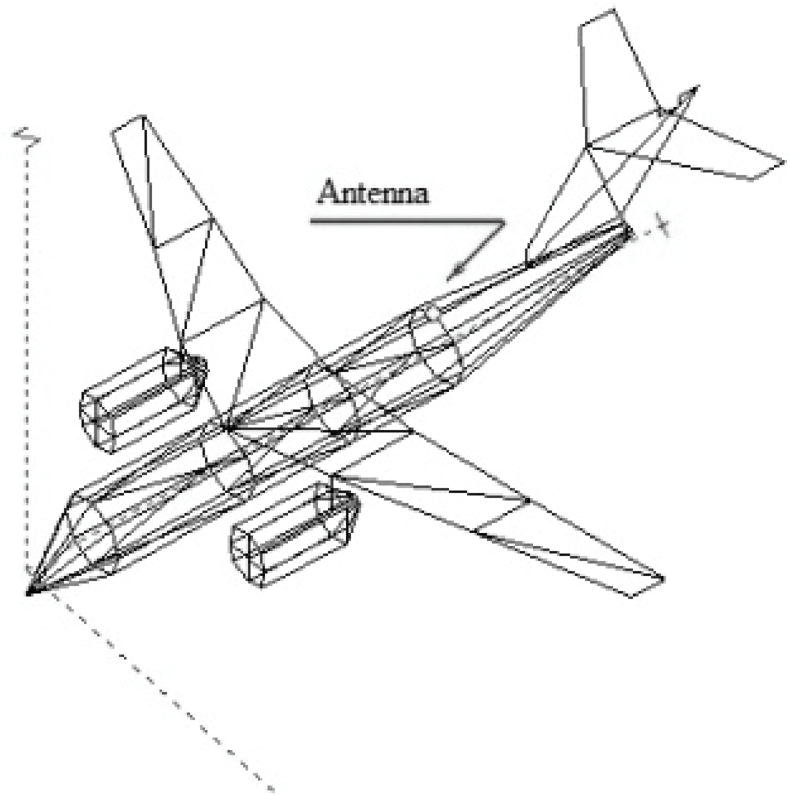

Fig.1. Mesh model of an aircraft with the antenna image location

In this work five variants of antenna arrays was simulated: one emitter, a linear array of three emitters, a linear array of five emitters, a linear array of seven emitters and planar antenna array with nine emitters that are shown in Fig.2. The accuracy of the method of moments is the higher, the smaller a size of elementary segment is. For obtaining an acceptable accuracy the segment size must be taken less than λ/10, where λ – is a wavelength in free space. The number of integral equations equals to the number of elementary segments, and increases with increasing of the object size or with the frequency increasing. Therefore, solving the problem of radio waves scattering on the object using the method of moments requires the solution of integral equations in matrix form of large dimension.

Model calculations were carried out at the frequency of 1600 MHz. This frequency corresponds to the frequency range of low-orbit satellite communication system IRIDIUM. An antenna with the length λ/2 and the horizontal polarization is placed on the fuselage at the distance λ/10 and is oriented along the aircraft axis. MMANA-GAL basic software can provide calculations for 8192 points [4]. In our calculations we took the number of segments 6673 and automatic segmentation of wire grid model into segments of length λ/2. For desktop PC (2-core Pentium 3.0 GHz and 4 GB RAM) a calculation time was 1466.47 seconds.

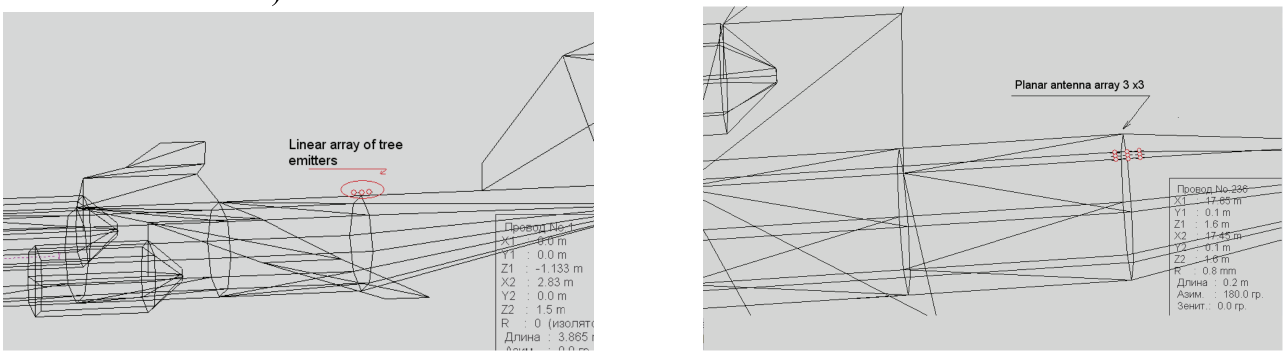

Fig. 2. Aircraft mesh model with the image location of linear array and planar antenna

The program interface for linear array calculation consisting of 3 elements is shown in Fig.3.

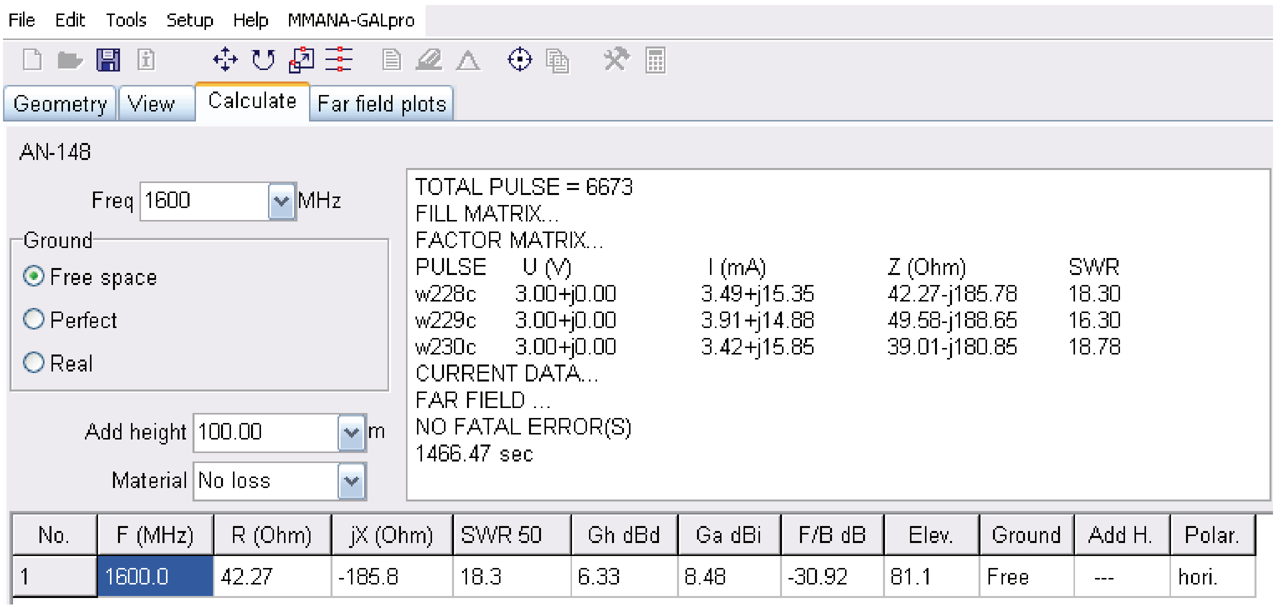

Fig. 3. Program interface for calculation of linear array with three elements

Patterns with horizontal $E_{\varphi\Sigma}(\varphi)|_{\theta=90^0}$ and $E_{\varphi\Sigma}(\theta)|_{\varphi=0^0}$ field components in horizontal XOY and vertical XOZ planes are shown in Table.1.

Table 1

Electric-field intensity vector components	Airplane linear array			
	Single oscillator	Linear lattice from 3 collinear oscillators	Linear lattice from 5 collinear oscillators	Linear lattice from 7 collinear oscillators
1	2	3	4	5
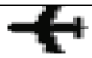 $E_{\varphi\Sigma}(\varphi)\vert_{\theta=90^0}$ XOY plane	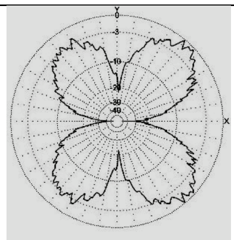	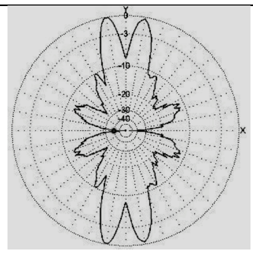	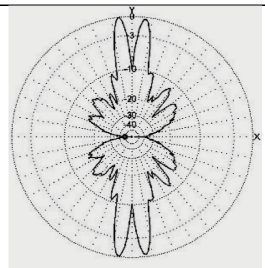	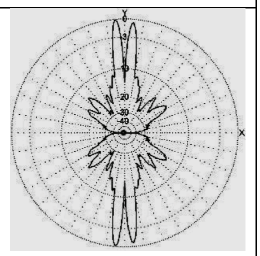
 $E_{\varphi\Sigma}(\theta)\vert_{\varphi=0^0}$ XOZ plane	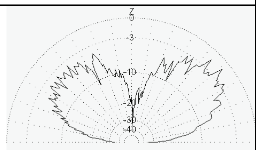	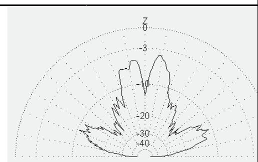	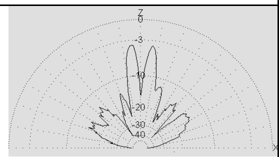	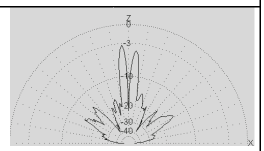

On the Fig.4 3D patterns for the linear lattice from 7 collinear onboard oscillators are shown.

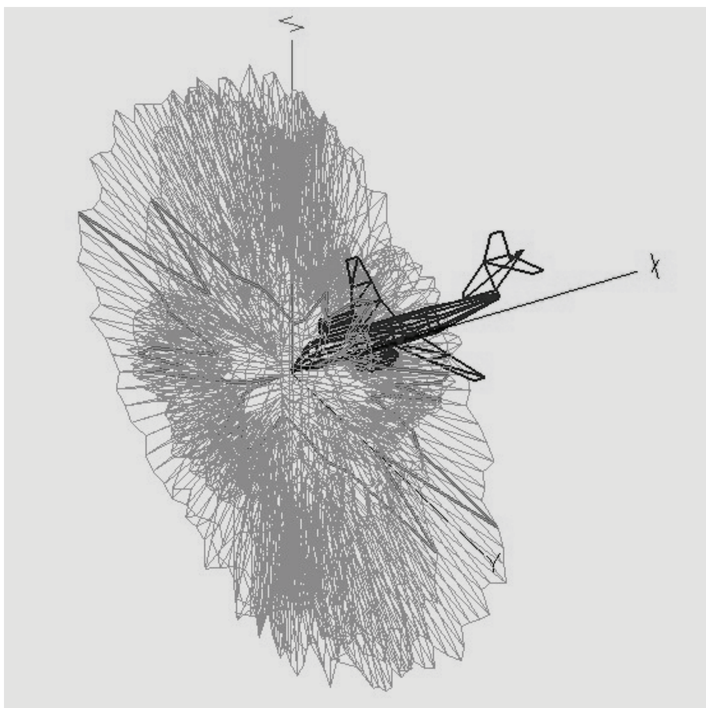

Fig. 4. 3D patterns of onboard linear array from 7 oscillators

A model of a planar equidistant antenna array 3x3 with nine $\lambda/2$ oscillators and the distances between emitters ends along OX axes $\lambda/10$ is shown in Fig. 5 and electric field components are given in Table 2.

Table 2

Electric field intensity components	Planar airplane antenna
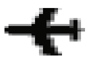 $E_{\varphi\Sigma}(\varphi)\|_{\theta=90^0}$ $E_{\theta\Sigma}(\varphi)\|_{\theta=90^0}$ XOY plane	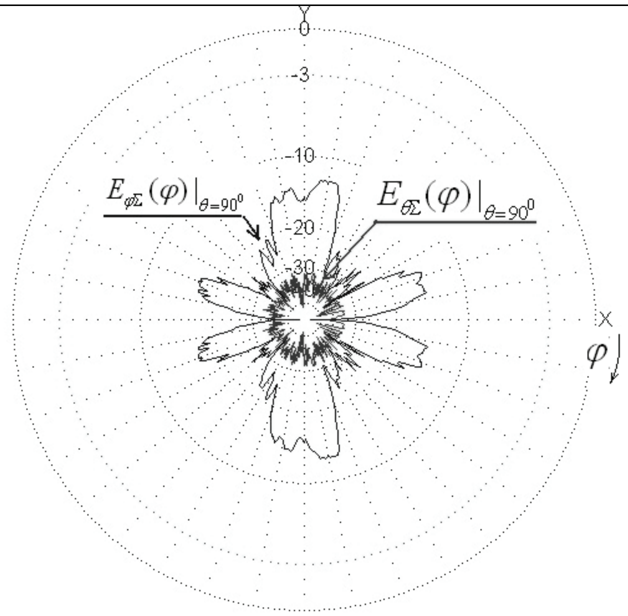
 $E_{\varphi\Sigma}(\theta)\|_{\varphi=0^0}$ $E_{\theta\Sigma}(\theta)\|_{\varphi=0^0}$ XOZ plane	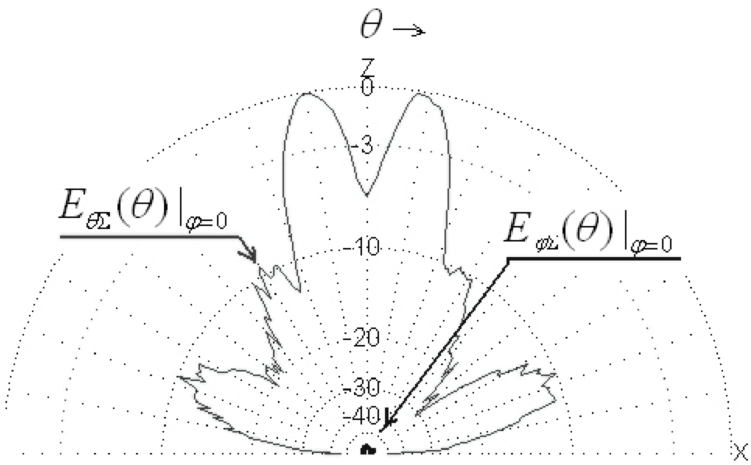

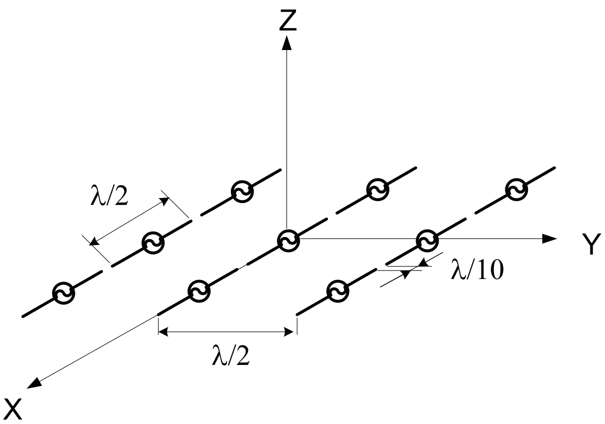

Fig. 5. Model of a planar equidistant antenna array 3x3

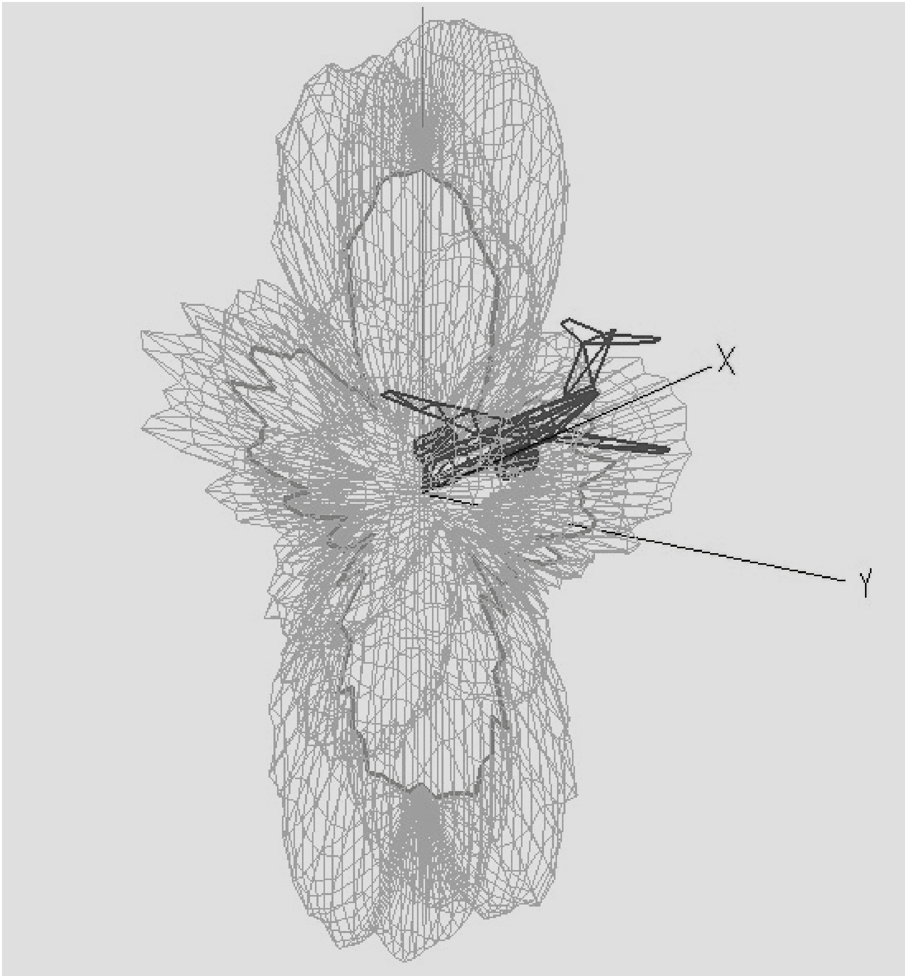

Fig. 6. 3D patterns of the flat equidistant onboard antenna array

Conclusion

Used technique of grid modeling for complex radiating structures with the help MMANA-GAL basic software allows to get the qualitative characteristics of radiation pattern, such as a pattern form, pattern zeros and maxima location. This technique also allows obtaining quantitative characteristics of the radiation field such as input impedance, active and reactive input impedance, standing wave ratio, antenna gain, etc. In general, the grid method for complex emitting structures simulation can be useful at the stage of experimental design work. When creating new communication systems it significantly reduces the cost and time to full-scale tests. This method is also useful for students, postgraduate students and researchers.

References

1. *Mittra R.* Computer techniques for electromagnetics, Volume 7, New York, Pergamon Press, 1973

2. *Барабанов Ю.М., Іванов В.О., Моргун О.А., Чернявський І.І.* Поле штирової антени, встановленої на корпусі літака. Електроніка та системи управління. 2007. – №3(13).–С. 88-95.

3. *Гончаренко И.В.* Антенны КВ и УКВ. Часть IV. Направленные антенны КВ: синфазного и продольного излучения. –М: ИП РадиоСофт. Журнал «Радио», 2007. - 256с.

4. *Гончаренко И.В.* Компьютерное моделирование антенн. Все о программе MMANA. — М.: ИП РадиоСофтЖурнал «Радио». 2002 — 80 с.

UDC 629.783 (043.2)

V.V. Konin, professor of aeronavigation department
F.O. Shyshkov, student
(National Aviation University, Ukraine)

RESEARCH OF EGNOS RELIABILITY IN KIEV

A research of EGNOS work was conducted with a help of a receiver, working in the mode of receiving differential corrections, to find if EGNOS can be used in Ukraine without building a ground station.

Introduction

EGNOS - European Geostationary Navigation Overlay Service is a system of space functional augmentation type SBAS intended to improve performance of GPS, GLONASS and GALILEO on the territory of Europe.

Starting from October 1 2009, EGNOS Open Service provides signal transmission on a satellite navigation receiver with EGNOS option. EGNOS Safety of Life service has become available from March 2nd 2011. Space signals are used for typical safety-critical operation like APV-1, APV-2 and CAT-1 on the territory of Western Europe.

The goal of this work is experimental estimation of EGNOS system performance quality in Ukraine(Kiev particularly) after it has been declared availiable. The processing of the experimental data is performed with PEGASUS software.

Setting the goal of the research

The goal of the research consists in_receiving of the experimental data from GPS and corrections from geostationary satellites AOR-E, IOR-W and Artemis, which are used in EGNOS.

The received messages are processed by PEGASUS software. Using the results conclusions are made if the characteristics of the navigational system fit to the safety requirements of the aviation users.

The coordinates of the receiving station were measured with 5 cm accuracy and considered_as the basic point.

The screen of the receiving station is shown on the Fig. 1.

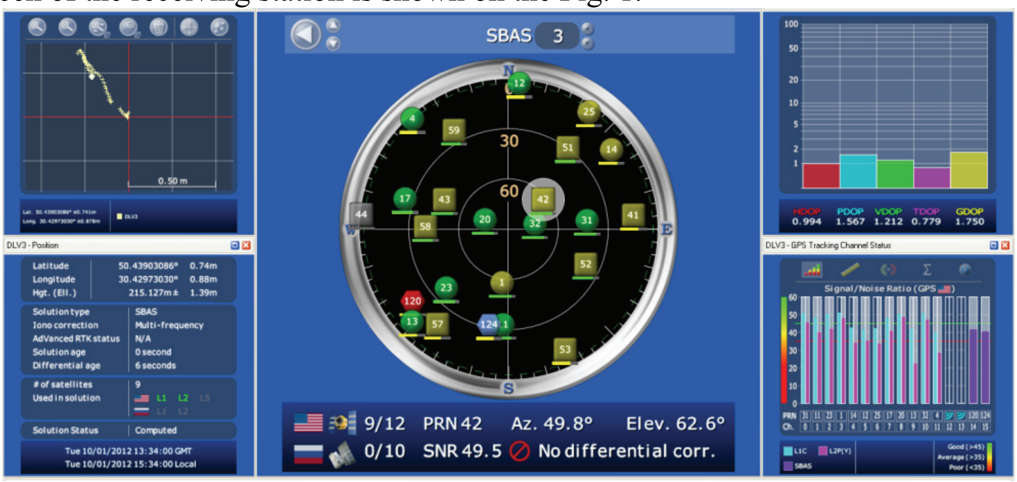

Fig. 1 Station screen.

At the screen GPS satellites and geostationary 120 and 124 satellites, which transmit the messages with corrections, are seen. GLONASS satellites can also be seen on the picture, but they do not use the EGNOS system and therefore are not considered as the part of experiment.

The main characteristics were researched, such as: accuracy (the deviation of coordinates in horizontal and vertical planes from the coordinates of the basic point), the availability of ionospheric corrections(the piercing points of ionosphere), integrity of data and continuity.

Research results

The research of 12th march 2011 is given as an example as typical result.

In order to assess the results general safety requirements for SBAS are presented in table 1.

Table 1

Basic safety requirements for SBAS

Typical Operation	Horizontal Accuracy (95%)	Vertical Accuracy (95%)	Integrity	Time-To-Alert (TTA)	Continuity	Availability
En-route	3.7 km (2.0 NM)	N/A	1 – 1 × 10-7/h	5 min	1 – 1 × 10-4/h to 1 – 1 × 10-8/h	0.99 to 0.99999
En-route Terminal	0.74 km (0.4 NM)	N/A	1 – 1 × 10-7/h	15 s	1 – 1 × 10-4/h to 1 – 1 × 10-8/h	0.99 to 0.99999
Initial approach, Intermediate approach, Non-precision approach (NPA), Departure	220 m (720 ft)	N/A	1 –1x10-7/h	10 s	1 – 1x10-4/h to 1 – 1x10-8/h	0.99 to 0.99999
Approach operations with vertical guidance (APV-I)	16 m (52 ft)	20 m (66 ft)	1 – 2 × 10-7 per approach	10 s	1 – 8 × 10-6 in any 15 s	0.99 to 0.99999
Approach operations with vertical guidance (APV-II)	16 m (52 ft)	8 m (26 ft)	1 – 2 × 10-7 per approach	6 s	1 – 8 × 10-6 in any 15 s	0.99 to 0.99999
Category I precision Approach	16 m (52 ft)	6.0 m to 4.0 m (20 ft to 13 ft)	1 – 2 × 10-7 per approach	6 s	1 – 8 × 10-6 in any 15 s	0.99 to 0.99999

Accuracy in horizontal plane(fig. 2) is displayed as the deviations on North-South and East-West from the basic point.

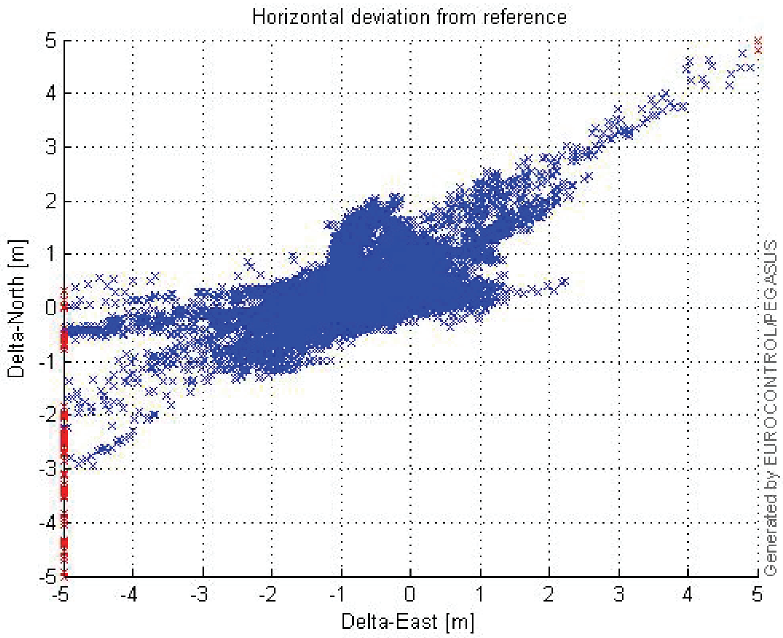

Fig. 2 Accuracy in horizontal plane

The horizontal accuracy of APV-1 category is 1.89 m. Vertical accuracy of APV – 2 is 1.49 m. Both measures were defined from the epochs when APV – 1 was available for normal operation by statistical methods and fit to the requirements for accuracy in table 1.

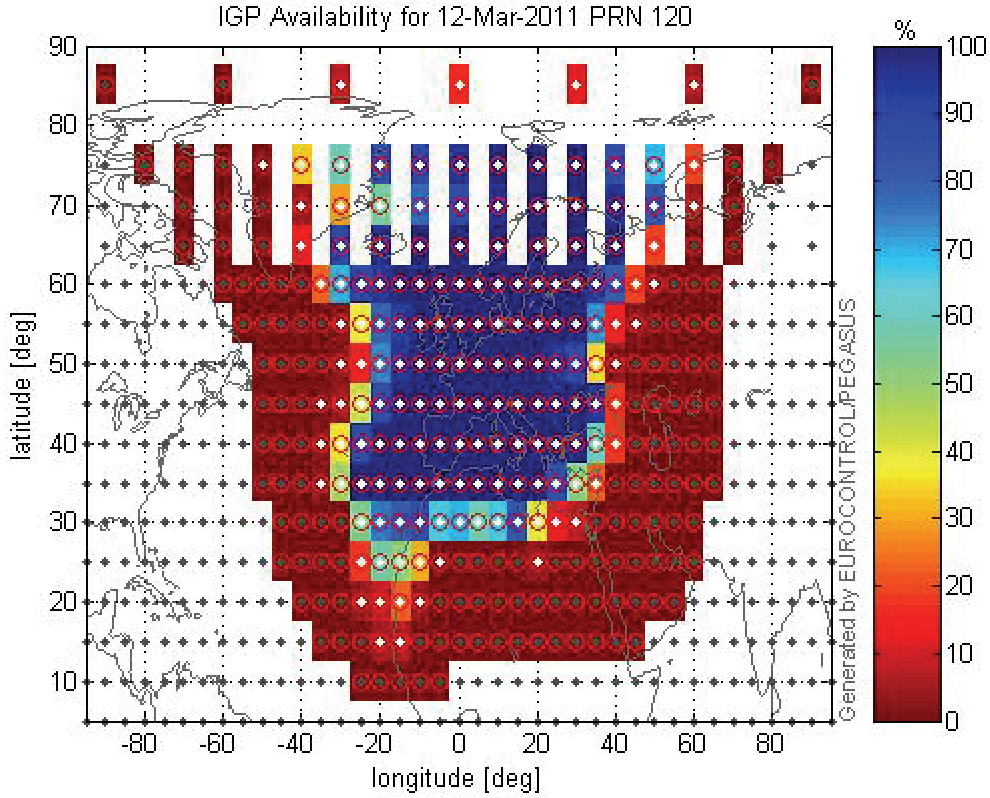

Fig. 3 Availability of piercing points of Ionosphere

The map of availability of the atmosphere piercing points is displayed on fig.3 . Coordinates of Kiev are 30° 30' east 50° 27' north. Availiability for piercing points: 100 % for sattelites to the west, decreasing to the south and north, rapid fall to 30-40 % for satellites to the east.

In order to analyze integrity Stanford plot is used. The measurements which correspond to typical operations of APV-1, APV-2 and CAT-1 for horizontal and vertical planes are shown on fig.4 and fig.5.

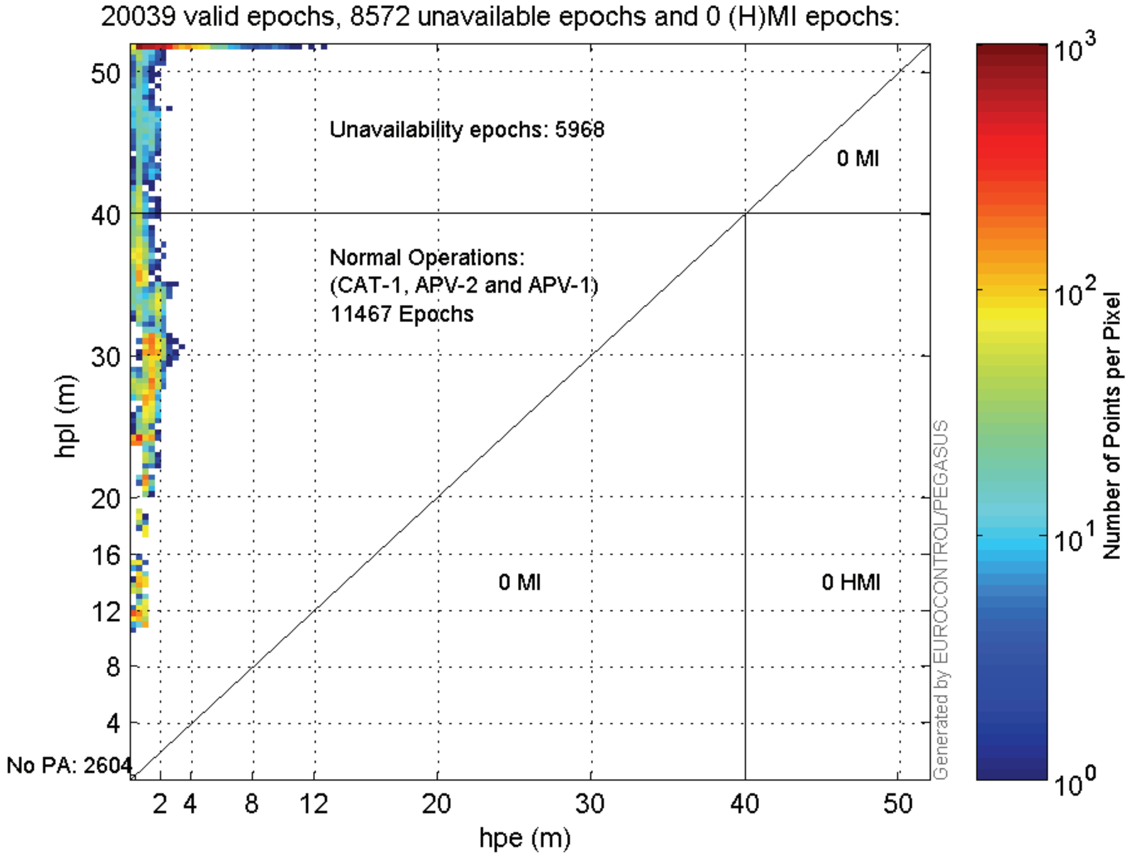

Fig. 4. Horisontal Stanford plot

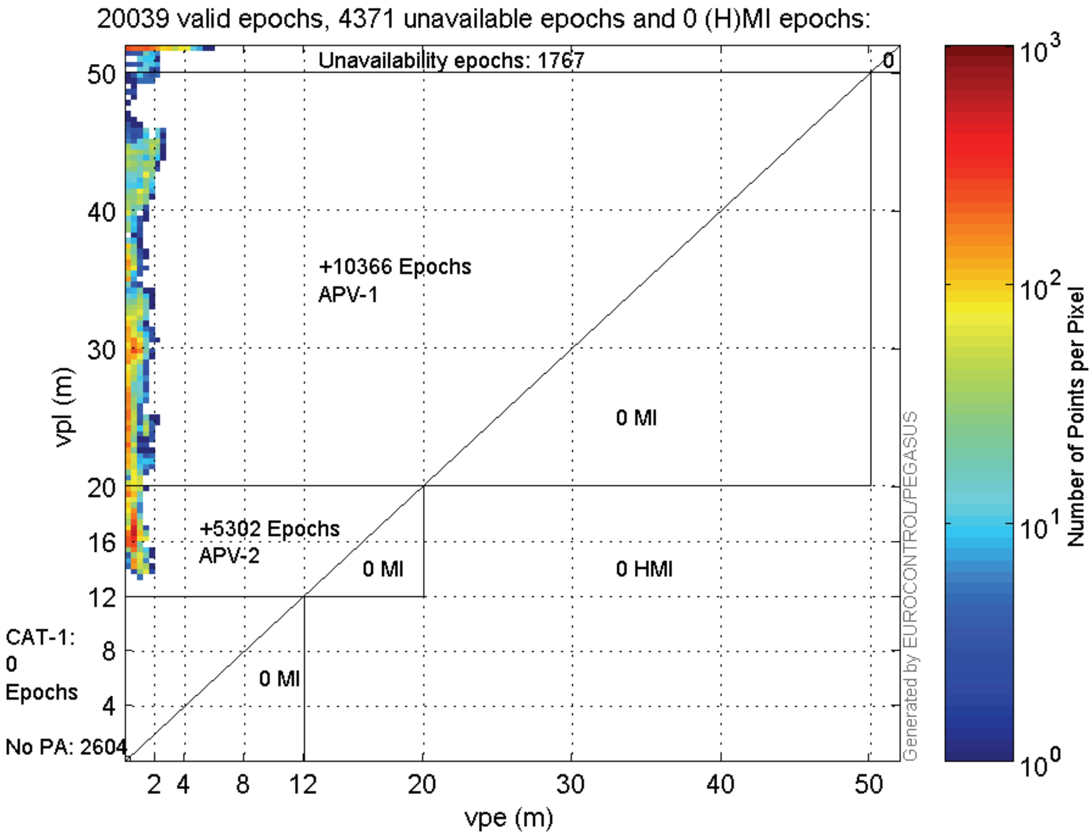

Fig. 5. Vertical Stanford plot

Information about categories is shown in table 2. On the pic 4 and 5 on horizontal axis precision errors are plotted for horizontal (hpe) and vertical (vpe) planes respectfully, on the vertical axes we have alarm limits for horizontal (hpl) and vertical planes (vpl) respectfully. From 20039 valid epochs on pic. 4 11467 epochs are fit for safety critical operations, 5968 epochs exceed the alarm limit of 40 m and 2462 fit only for NPA. From 20039 valid epochs on pic. 5 10366 epochs are fit for APV-1, 5302 for APV-2, no for CAT-1. 1767 epochs exceed the alarm limit of 50 m and 2604 have no precision availiable.

There was no misleading information in the research so according to table 1, integrity requirements are met.

Table 2

ICAO SARPs high level integrity requirements

Typical operation	Time to Alarm	Integrity	Hor. alert limit	Vert. alert limit
NPA	10 s	$1\text{-}10^{-7}$/h	0.3 NM	N/A
APV I	10 s	$1\text{-}2\text{x}10^{-7}$/app	40.0 m	50 m
APV II	6 s	$1\text{-}2\text{x}10^{-7}$/app	40.0 m	20 m
CAT I	6 s	$1\text{-}2\text{x}10^{-7}$/app	40.0 m	15 - 10 m

The most problematic parameter for Ukraine is continuity which is increadibly bad. The discontinuity events for position solution are listed in table 3. Discontinuity events for APV – 1 are listed in table 4.

Duration – time for which discontinuity lasts.

Stable period – time which system run from last discontinuity end to the start of current.

Table 3

Position discontinuity events

Epoch	Duration, s	stable period, s
579503	105	1942
579766	53	158
584309	168	4490
587212	320	2735
591536	1286	4004
595953	1	3131
595955	66	1
596349	160	328

Table 4

Discontinuity events for APV-I

Epoch	Duration, s	stable period, s
579503	105	1942
579766	213	158
581263	800	1284
584309	457	2246
585341	1424	1
587212	320	447
591536	1963	4004
593623	165	3
593793	152	1
594406	12	1
594738	324	320

The low continuity highly influences the overall availability of EGNOS in Ukraine. In the research APV-1 is available only 57.223% and APV-2 – only 26.458% which makes a substantial difference from the standards listed in table 1.

Conclusions

The results state the weak signal quality of EGNOS in Kiev, so that it can not be used for any safety critical operations until a RIMS station is placed.

References

1. USER GUIDE FOR EGNOS APPLICATION DEVELOPERS Ed 1.1, 07/30/2009 103 p
2. PEGASUS Interface Control Document 10/09/2010 286p provided by Euro control
3. GBAS Operational Validation PEGASUS MARS Development 20.03.06 102p
4. SARPS Amendment 77, Annex 10 to the Convention on International Civil Aviation, Aeronautical Telecommunications: International Standards and Recommended Practices, Volume 1, Radio Navigation Aids, November 2002.
5. WADGPS Laboratory (Stanford University). "WAAS Precision Approach Metrics. Accuracy, Integrity, Continuity and Availability," http://waas.stanford.edu/metrics.htm. October 1997.

UDC 629.735.05

I.V. Ostroumov, Ph.D., (National Aviation University, Ukraine)

POSITION DETECTION BY ANGULAR METHOD IN AIR NAVIGATION

The aircraft position detection by angular method has been represented. The VOR/VOR positioning method has been discussed. As a result, errors of angular method in air navigation has been determined.

Introduction

An aircraft position detection is a very important task of navigation. Safety of fly directly depends on it. Nowadays positioning of aircraft is grounded on satellite navigation such as GPS and GLONAS. Satellite navigation is the most accurate method of navigation which is available for airspace operators, but in some cases it will be not suitable to use. In this case some other methods will be suitable to use. Inertial navigation will help here but not so long. Inertial navigation system could not provide good accuracy during the whole time-flight it will be result of multiplied errors. As a result INS will be good during the short time when the primary navigation system (GPS) can't provide position. In this way it is possible to use angular or distances methods of navigation on board of airplane.

Radio navigation aid systems consist of ground radio beacons around the whole ground area and on-board equipment. It is possible to use information from radio navigation aid systems to determine position of aircraft. It is possible to use ground radio beacon such as Non-directional beacon (NDB), VHF omnidirectional range (VOR), Doppler VHF omnidirectional range (DVOR), Tactical Air Navigation (TACAN), Distance Measuring Equipment (DME) with relative on-board equipment for positioning [1,3]. Navigation aids comprise air navigation net which is a big part of air navigation chart.

Position determination

Functional principle of different radio navigation aids is different but all of this systems provide angular information or distances which are possible to mix to have coordinates of aircraft. For example VOR on-board equipment provides the angle (bearing) to the ground VOR station. By bearing from two different VOR ground station with the help of station coordinates will be possible determine position of aircraft.

Each modern airplane has to be equipped with Flight management system(FMS). It is a kind of computer system which can tune on-board radios such as automatic directional finder (ADF), VOR and DME. Inside of FMS memory has been held the latest air navigation data base which contains electronic air navigation chart, airports data, navigation aids data, airways and other navigation information. During the flight FMS is looking on the flight-planed trajectory and tuning ADF and VOR equipment when it will be necessary. As a result pilot always can see bearing to the next navigation aid ground station. By special functionality FMS can determine aircraft location by bearings from two near radio beacons. It is useful in case of very valuable GNSS errors or failures of GNSS equipment. FMS can use bearings to two VOR ground stations or other ADF angular information with ground station location from on-board air navigation data base to determine aircraft location (fig. 1). Then the aircraft position will be used like a primary data for inertial navigation system.

Angular method of navigation is not so suitable, because the position errors are valuable. By value of error it is possible to classify the determination methods in the following way:

1. GNSS;
2. INS;
3. DME/DME;
4. VOR/DME;
5. VOR/VOR.

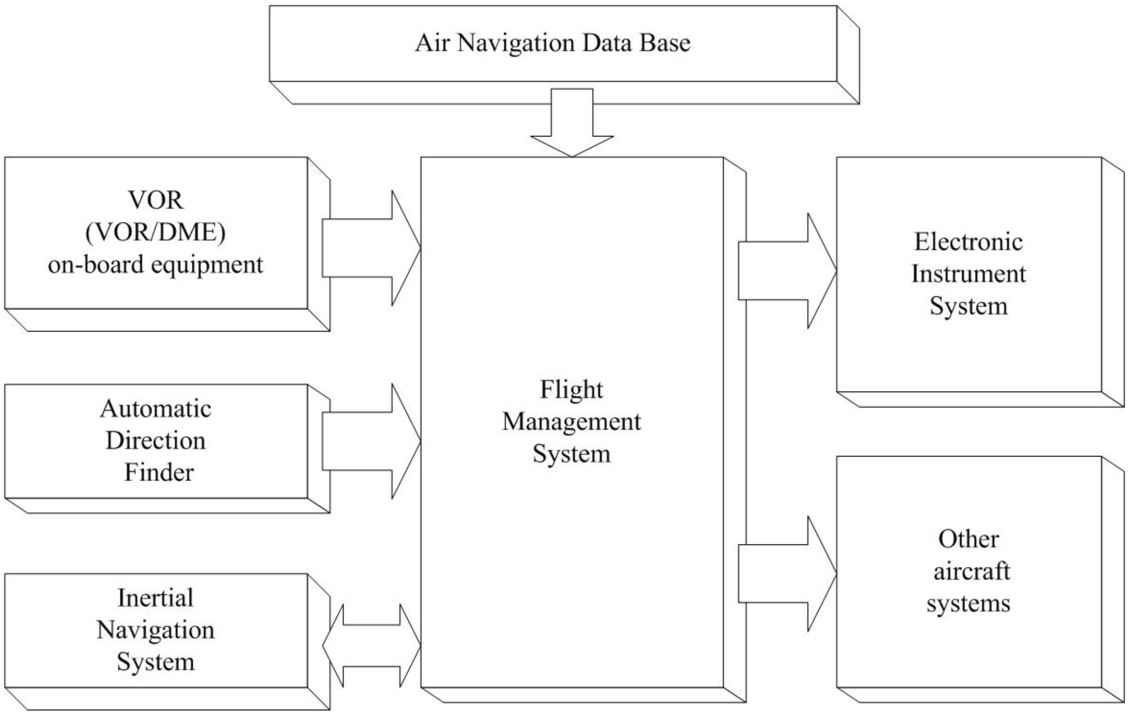

Fig. 1. Structure of on-board equipment

Angular method or Angle of arrival positioning method estimates object position by angles of radio signal arrival. Usually it is the angle between the propagation direction of an incident wave and some reference direction(for example North direction), which is called bearing. Bearing, defined as a fixed direction against which the angle of arrivals are measured, is represented in degrees in a clockwise direction from the North. When the orientation is 0 or pointing to the North, the angle of arrival is absolute, otherwise, relative.

As result it is possible to calculate aircraft position (X and Y) by coordinates of radio signal sources (radio beacons) x_i and y_i and angles A_i. In this case will be discussed multiangular approach. Two angles will be particular case.

To find position it is necessary to solve system of equation[2]:

$$X-x_i=(Y-y_i)\mathrm{tg}(A_i).$$

In matrix form we will have

$$AC^T=B,$$

where

$A_i=[1\ -\mathrm{tg}(A_i)]$,

$C=[X\ Y]$,

$B_i=[x_i\ -y_i\mathrm{tg}(A_i)]$.

The estimated coordinates of the aircraft can be calculated as:

$$C=[(A^TA)^{-1}A^TB]^T.$$

Accuracy of this positioning method depends on angle determination system and geometry of ground stations.

Typical ADF equipment has got errors not more than 10° because influence of electrical interference, twilight/night effect, terrain and coastal effects and attitude effects. Standard VOR systems are more accurate than ADF but are still subject to errors at the ground station, bending distortion of signals caused by terrain effect and avionics errors. The aggregation of all errors is very unlikely to exceed 5°.

Positioning error by angular method will be combined by angles determination error. As a result positioning error represented by area of dash figure on fig.2. The value of error is directly connected with geometry of VOR ground station location.

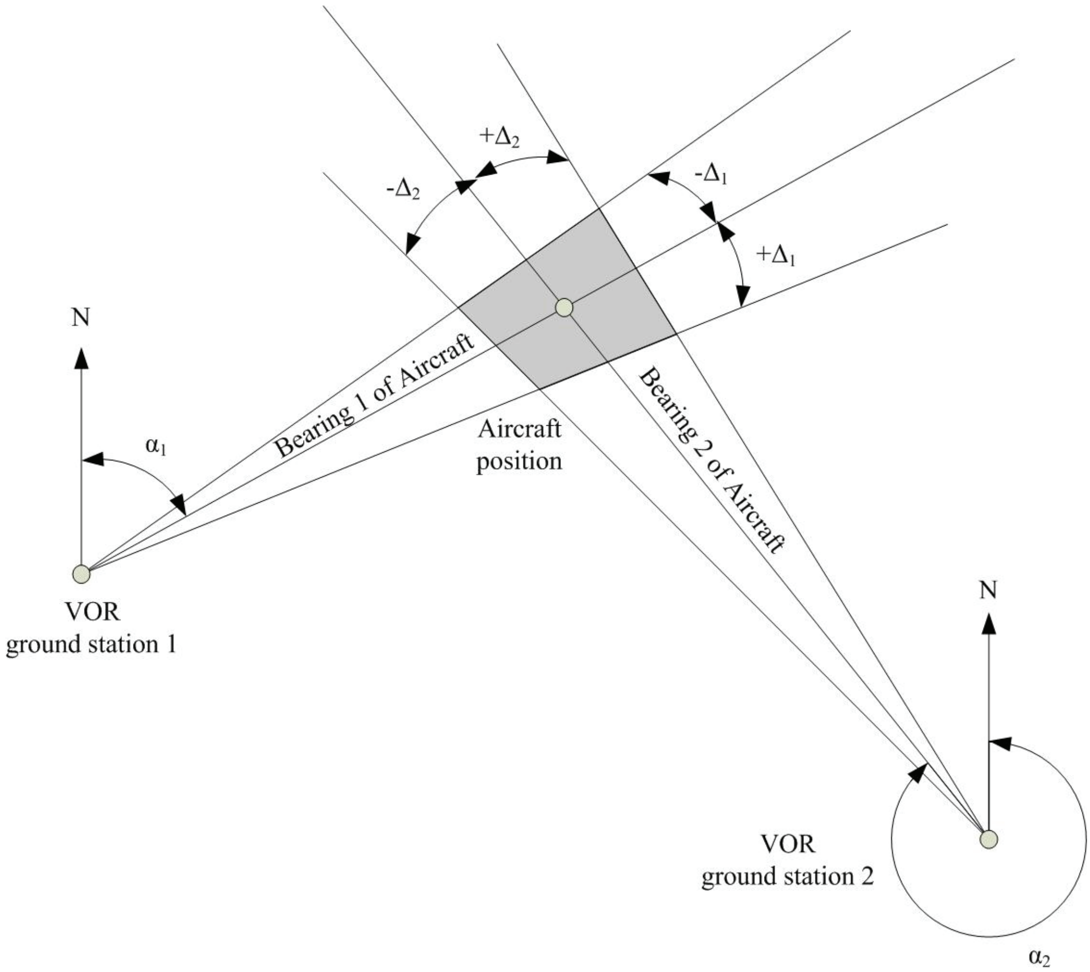

Fig. 2. Error of angular method

Conclusion

Angular method is possible to use in air navigation but in case when we can not use GNSS. As a result VOR bearing is more accurate than ADF, but positioning with angular method mixes errors that increases the resultant errors. Errors depend on geometry of ground station location.

References

1. *Ian Moir*. Civil avionics systems / Ian Moir, Allan Seabridge / AIAA. – 2006. – 396p.

2. *Paweł Kułakowski*. Angle-of-arrival localization based on antenna arrays for wireless sensor networks/ Paweł Kułakowski, Javier Vales-Alonso, Esteban Egea-López, Wiesław Ludwin, Joan García-Haro // Computers and Electrical Engineering. – 2010. – pp.1–6.

3. *Харченко В.П.* Радіомаячні системи ближньої аеронавігації: навч. посіб./ В.П. Харченко, В.Г. Мелкумян, О.П. Сушич. – К.:НАУ, 2011. – 208 с.

G. Büyükaksoy Kaplan Ph.D, A. Lana MSc, F. Ekici BSc
(TUBITAK BILGEM Information Technologies Institute, TURKEY)

GRNNα : A CONTRIBUTION TO GENERAL REGRESSION NEURAL NETWORK FOR ESTIMATING TARGET POSITION

Summary

In this study, we propose an intuitive way for General Regression Neural Network (GRNN) and called it as GRNNα, to estimate the target position in the target tracking problem. In the literature GRNN has only been utilized for estimating the velocity of targets. However, estimation of the target position is also required in many applications. We compare the simulation results of the GRNNα to the well known Kalman Filter.

INTRODUCTION

Target tracking has been performed in a wide variety of applications from military to civilian surveillance systems, especially in Airport Surveillance Radar (ASR) systems. ASR is used to detect and display the position of flying targets at the vicinity of the airport. Estimation of the correct target position and movement from noisy measurement data is one of the most important tasks of the ASR system, which we focused on this work. This task is conducted as a part of the project (KUSRAD) Bird Avoidance Radar in which the vertical and the horizontal radars are integrated. The study represented in this paper employed the simulated track data in compliance with FRUNO Marine Radar FAR that is used for horizontal radar in the project.

The Kalman filter is the most commonly used estimation tool for engineering problems from many disciplines [1]. In the literature, General Regression Neural Network (GRNN) which is proposed for regression [2] is also used for estimating the velocity of the target [3]. In this work, we put forward an intuitive way to estimate the position of the target correctly and compared it with the Standard Kalman Filter by simulating two typical scenarios.

METHODOLOGIES

Kalman Filtering

The Kalman filter uses state vector, the dynamical model and measurement model which are described below. The operations are performed in two steps: prediction and correction, and repeated for each time step recursively. Consider the system dynamics are assumed to be described by the following equations:

$$\boldsymbol{X}_{k+1=}\mathbf{F}\mathbf{X}_k + \mathbf{G}\mathbf{W}_k$$

$$\boldsymbol{Z}_k = \boldsymbol{H}\boldsymbol{X}_k + \boldsymbol{V}_k$$

where X_k denotes state vector in sample k, F and G are state transition and disturbance transition matrices, respectively, and $\mathbf{W}_k$ is the unknown zero-mean Gaussian process noise with assumed known covariance **Q**. In noisy environment, measurements (**Z**) are assumed to be a linear combination of system state variables and they are disturbed by some noise. **H** is the measurement matrix and $\boldsymbol{V}_k$ is zero-mean Gaussian measurement noise with assumed known covariance **R**. The process and measurement noise are assumed to be independent of each other. All these vectors and matrices are given below for only one direction, without the loss of generality.

$$\boldsymbol{X} = [x\ \dot{x}\ \ddot{x}]^T \qquad \boldsymbol{H} = [\ 1\ 0\ 0]$$

$$\boldsymbol{F} = \begin{bmatrix} 1 & dt & dt^2/2 \\ 0 & 1 & dt \\ 0 & 0 & 1 \end{bmatrix} \qquad \boldsymbol{G} = \begin{bmatrix} dt^2/2 & 0\ 0 \\ dt & 0\ 0 \\ 1 & 0\ 0 \end{bmatrix}$$

The prediction phase uses *time update* equation:

$$\boldsymbol{X}_{k+1}^{-} = \mathbf{F}_k \mathbf{X}_k$$

$$\boldsymbol{P}_{k+1}^{-} = \boldsymbol{F}_k \boldsymbol{P}_k \boldsymbol{F}_k^{T} + \boldsymbol{Q}_k$$

Here, $\boldsymbol{X}_{k+1}^{-}$ is the prior estimate, i.e., estimation before correction using measurement update equations. Similarly, $\boldsymbol{P}_{k+1}^{-}$ represents prior error covariance

$$\boldsymbol{P}_{k+1}^{-} = E[(\boldsymbol{X}_{k+1} - \boldsymbol{X}_{k+1}^{-})(\boldsymbol{X}_{k+1} - \boldsymbol{X}_{k+1}^{-})^{T}]$$

The correction phase uses *measurement update* equations:

$$\boldsymbol{K}_{k+1} = \boldsymbol{P}_{k+1}^{-} \boldsymbol{H}^{T} (\boldsymbol{H} \boldsymbol{P}_{k+1}^{-} \boldsymbol{H}^{T} + \boldsymbol{R})^{-1}$$

$$\boldsymbol{X}_{k+1} = \boldsymbol{X}_{k+1}^{-} + \boldsymbol{K}_{k+1} (\mathbf{Z}_k - \mathbf{H}\, \mathbf{X}_{k+1}^{-})$$

$$\mathbf{P}_{k+1} = (\mathrm{I} - \boldsymbol{K}_{k+1} \boldsymbol{H})\, \boldsymbol{P}_{k+1}^{-}$$

Here $\mathbf{K}$ is the Kalman gain matrix and $\boldsymbol{X}_{k+1}$ is the estimated state vector for step k+1. $\mathbf{P}_{k+1}$ and $\boldsymbol{X}_{k+1}$ are stored to be used for the next step.

General Regression Neural Network

The GRNN is a kernel regression methodology [2], contrary to statistical regression methods, just the sampled data are sufficient; i.e. assumptions regarding the relation between dependent and independent variables are not required.

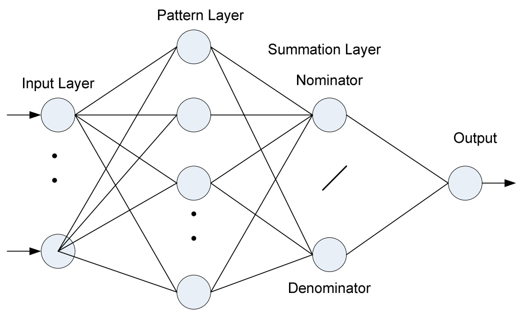

Figure 1 Structure of GRNN

The GRNN is made up of four layers of neurons as shown in Figure 1. Input layer transfers input vector to the pattern layer, where each neuron represents a stored training pattern. The outputs of the pattern layer neurons give Euclidian distance between the input vector and corresponding stored vector. Each neuron in the pattern layer is connected with each of the two neurons in the summation layer: the nominator and the denominator neuron. Whereas the domination neuron calculates the sum of the weighted outputs of the pattern layer, the denomination neuron calculates the non-weighted outputs of the pattern layer. The output layer divides the output of the nominator neuron by the output of the denominator for calculating the prediction value.

The GRNN has been also used for solving target tracking problem in marine radars for almost fifteen years [3]. In these applications, the number of pattern layer neurons is determined by the teaching sequence which is a moving window formed by sequential target velocity components in axis x and y. The estimated velocity components are calculated as in the following. In the rest of the paper, the equations will be given only in axis x for the simplicity's sake.

$$V_{xei} = \frac{\sum_{i=1}^{N} V_{xo_i} \exp\left(-\frac{\|t-t_i\|^2}{2\sigma^2}\right)}{\sum_{i=1}^{N} \exp\left(-\frac{\|t-t_i\|^2}{2\sigma^2}\right)}$$

Here, V_{xe_i} represents ith component of the estimated velocity vector, V_{xo_i} is ith component of the measured velocity vector, σ is smoothing factor of Gaussian kernel functions and t stands for time.

In our project, KUSRAD, estimating the position of the target is required. To the best of our knowledge, GRNN was not exploited for estimating the target position. Before applying the measured position data to the GRNN, we obtained the instantaneous velocity of the target using the following simple equation. $\mathrm{V_{xm}(k) = (X_m(k) - X_m(k-1))/dt}$ (dt is the scan-time of the radar). The velocity values were normalized to 1 and entered to the GRNN filter. After the estimation process completed for one step, the output value was denormalized, in order to compare with ground truth velocity. When the same simple equation is used to calculate the estimated position as, $\mathrm{X_{est}\,(k) = dt \times V_{xest} \;+\; X_{est}\,(k-1)}$, the estimation error of the position positively self feed-backed, especially during maneuver. If the measured position $(\mathrm{X_m(k-1)})$, is used instead of $\mathrm{X_{est}\,(k-1)}$, the effect of noise was always maintained. So we proposed an intuitive way to the problem of estimating the target position in this study. Since there is no knowledge about ground truth and we just have the noisy measurements, we considered a fraction of the difference between measurement and estimation. We defined an additional step, and added a corrective term as follows:

$$\hat{X}_{est}\,(k) = X_{est}(k-1) + V_{est}(k) \times dt$$

$$X_{est}\,(k) = \hat{X}_{est}(k) + \alpha(X_m(k) - \hat{X}_{est}\,(k))$$

We called α as the correction rate, takes a value between 0 and 1. We also called the algorithm as GRNNα.

SIMULATION RESULTS

Simulation Environment

The target trajectory data is generated in two dimensions (x-y plane) using Matlab. Measurement noise is randomly calculated in polar coordinates, converted to the Cartesian coordinated and then added to the ground truth. The standard deviation of the noise is determined using Fruno radar's resolution cell dimensions on range and bearing, adaptively at each scan time rather than using a constant variance during the whole trajectory. Thus the increase in ambiguity of target's position due to the distance of the target from the radar location can be modeled in a more realistic way compared to just adding Gaussian noise with constant variance. Variance of range (σ_r) and variance of bearing (σ_θ) are given as follows where ΔR is the size of range bin, Δθ is the size of bearing bin, SNR is signal to noise ratio. Assuming a uniform distribution in a radar cell, the range and bearing measurement standard deviations are calculated as in [4]:

$$\sigma_r = \frac{\Delta R}{\sqrt{SNR}} + \frac{\Delta R}{2} \qquad \sigma_\theta = \frac{\Delta\theta}{\sqrt{SNR}} + \frac{360}{pulse\ count\ per\ scan}$$

Measurement noise covariance matrix is formed as follows:

$$\boldsymbol{R}_{r\theta} = \begin{bmatrix} \sigma_r^2 & 0 \\ 0 & \sigma_\theta^2 \end{bmatrix}$$

Second term in the standard deviation equation of bearing above is known as encoder accuracy, which defines the ratio of total radar scan angular coverage to the number of pulses transmitted per scan (which is taken as 1440). SNR is 13 dB, ΔR as 15m, Δθ as 1.8°, dt as 1. These values are converted to the Cartesian coordinates using the de-biasing equations as in [5]. For each measurement a different covariance matrix at each radar scan time is calculated. The generated noise is added to the ground truth in order to obtain noisy measurement to be applied to estimation filters.

Scenario – I: In the 1st scenario, at scan 50, it starts to make a maneuver in y axis with an acceleration of 5 m/s^2 for a period of 10 radar scans. Once the maneuver is completed, it moves with constant velocity to the end of the trajectory as shown in Figure 2.

Scenario – II: In the 2nd scenario, after 50 scans, the target makes a coordinated turn with a radius of 500 m for a period of 30 scans. Once the maneuver is completed, it again moves with constant velocity until the start of second maneuver which takes place between scan 124 and scan 167 with a radius of 750 m. After the 2nd maneuver is completed, the target moves with the same velocity to the end of the trajectory as shown in Figure 3.

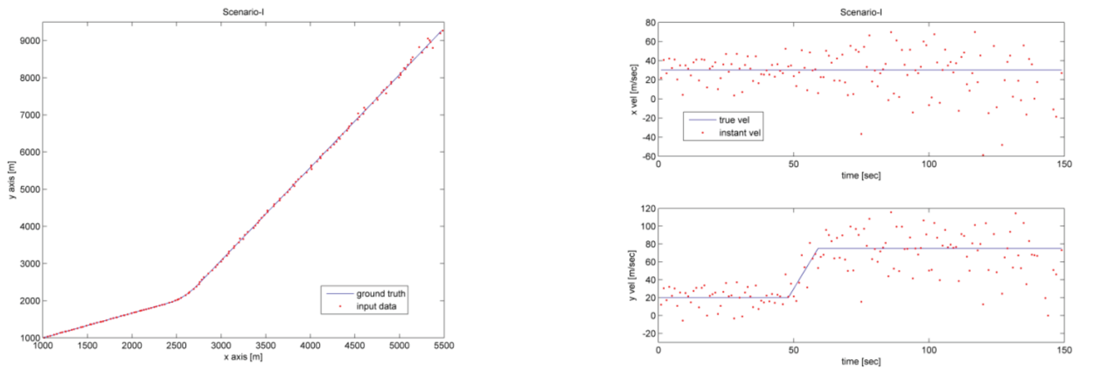

Fig 2 Position and velocity of target trajectory for Scenario –I

Estimation Performance Results

In order to evaluate the performance of the algorithms two criteria were used: Averaged Normalized Position Error (A.N.P.E.) and computational cost. Normalized Position Error defines the ratio of the root mean square of combined position estimation error (P.E.E.) to the root mean square of the combined measurement error (P.M.E.) [6] and $\mathrm{A.N.P.E} = \frac{1}{\mathrm{T}}\sum_{\mathrm{i=1}}^{\mathrm{T}} \mathrm{N.P.E.}$

$$N.P.E.(t) = \frac{P.E.E.(t)}{P.M.E.(t)} = \frac{\sqrt{\sum_{t=1}^{T}(x_{est}(t) - x_{gt}(t))^2 + (y_{est}(t) - y_{gt}(t))^2}}{\sqrt{\sum_{t=1}^{T}(x_m(t) - x_{gt}(t))^2 + (y_m(t) - y_{gt}(t))^2}}$$

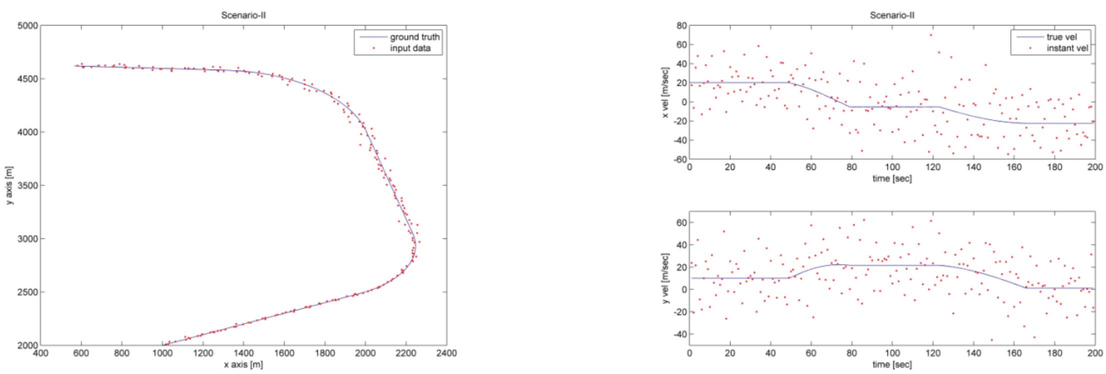

Fig 3 Position and velocity of target trajectory for Scenario -II

The parameter values of the used algorithms empirically determined. Accordingly, the teaching sequence was taken as 8, smoothing factor as 10 and α as 0.3 for GRNN and the process noise for KF as 0.1. The scores are given in Table 1.

Table 1. The results of performance assessment

	KF	GRNN	GRNNα
Scenario -I	0.64	6	0.58
Scenario -II	0.59	3.5	0.54

a) A.N.P.E

	KF	GRNN	GRNNα
Scenario -I	17	4	5
Scenario -II	23	5	6

b) Computational Cost (in msec)

In the Table 1, the scores in the column of GRNN indicate the performance for α as 0, i.e. the contribution of corrective term was excluded. In the column of GRNNα, the scores present the effect of corrective term. The computational cost is also considered as the 2nd evaluation metric. In terms of computational cost, GRNN approaches are found to outperform the Kalman filter.

CONCLUSIONS

In this study, computer simulation is used to compare the estimation filters in terms of average normalized position error and computational cost. As the Table 1 shows, the corrective term makes the result of GRNNα at least as satisfactory as the result of KF in terms of A.N.P.E. Additionally, computational cost of GRNNα is much better than the KF. As a future work, we plan to use different α values through the target course, especially during maneuver.

References

1. *Simon D*, Optimal State Estimation: Kalman, H Infinity and Nonlinear Approaches, 2006, Wiley-Interscience.
2. *Specht D F*, A General Regression Neural Network, IEEE Transactions on Neural Network, Vol. 2, No. 6, 1991.
3. *Kazimierski W, Stateczny A*, Multisensor Tracking of Marine Targets-Decentralized Fusion of Kalman and Neural Filter, Int J. El. and Telecommunications, Vol. 57, No. 1, 2011
4. *Curry G R*, Radar System Performance Modeling, Arctech House, 2005
5. *Lerro D, Bar-Shalom Y*, Tracking with Debiased Consistent Converted Measurements Versus EKF, IEEE Trans Aerospace and Electronic Systems, Vol. 29, No. 3, July 1993.
6. *Efe M.*, Adaptive Approaches to Maneuvering Target Tracking, University of Sussex, PhD Thesis, October 1998

UDC: 629.051:629.3.072:629.7.086

V.V. Konin, doctor of technical sciences, K.O. Mironov, graduate student
(National Aviation University, Kyiv, Ukraine)

MONITORING AND CONTROL TECHNICAL MEANS USED IN AIRPORT INFRASTRUCTURE BASED ON GNSS

This article discusses the principles of construction of a centralized monitoring and control of technical equipment used in airport infrastructure based on GNSS what is responsible for monitoring and controlling the flow of fuel and lubricants by terrestrial means

Introduction

Today, the development of science knowledge in areas such as computer science, radio navigation, electronics, photogrammetry, geodesy, cartography allows you to create a closed system of monitoring and control facilities (hereinafter - SMCF). To create SMCF across the land requires considerable expenditure of money and time resources, but the growth of world economy and the industry can make this system available for use in the scale of individual airports today. The concept of introducing SMCF designated documents ICAO [1]. Introduction SMCF will significantly reduce the risks specified in [2] (chapter 18, paragraph 18.1.4 subparagraphs: a, d, f-q). Consider the fundamental structure and purpose, which are solved by SMCF:

1. Composition of SMCF:
- a navigation equipment [3], mounted on each movable component of system;
- a database describing the objects in the system, a set of constraints, rules, priorities;
- a three-dimensional map of the airport, which includes at least:
  - layer Road with a count;
  - layer of buildings;
  - layer of Wildlife;
  - terrain layer;
- center of automatic decision to create a set of rules and restrictions of movement of objects in real time;
- a system of visual aids and blocking access;
- the server for exchange of information;
- control center;
- a system of self-control and validation;
- reserve system.

2. Objectives of SMCF:
- ensuring safe interaction between objects in the vicinity of the airport in real time;
- construction traffic routing of all objects in general, and each object separately in real time;
- control over the use of technical means (hereinafter - TM) at the airport;
- Monitor the use of the TM to the airport;
- conduction of analytical studies to improve the airport infrastructure, improve safety;
- cost savings due to optimal routing, logistics execution rules;
- reducing the human factor in traffic management in the area of the airport.

SMCF stages of implementation for the purposes of checking the flow lubricants TM

Due to the lack of legislative basis in Ukraine based on the use of SMCF onGNSS. Its implementation requires some preparation, which consists of several stages:

1. Creating a database with a description of the TM system, which must contain at least:

- a unique identifier for each TM (such an identifier can be obtained as follows: if there is a public TM shall be based on numbers it had in his absence - this number ceases unique inventory number to the company (can be changed over time);
- the mark of TM;
- model of TM;
- modification of the TM (can be changed over the time);
- the amount of motor TM (can be changed over the time);
- the type of fuel used;(can be changed over the time);
- securing additional equipment (can be changed over the time);
- the charging person and its data (can be changed over the time).

2. Measurements of rates of consumption of fuels and lubricants (FAL), each individual type of equipment, (it should be understood under the guise of a combination of different combinations of make, model, modification of the motor TM).
3. Creating a unified scheme of calculation consumption rates TM based on individual vehicle [4], [5], [6].
4. Create a single database storing information on the work performed TM (mileage, used motor-hours worked moto-hours of additional equipment, other features of TM).
5. Monitoring daily delivery vehicle traffic logs.
6. Develop mechanisms for comparing the SMCF and information from a single database trip tickets.
7. Installing SMCF all vehicles involved in the system.
8. Daily monitoring of vehicle use on the basis of the mechanism referred to in paragraph 7.
9. The permanent development and improvement of the mechanism referred to in paragraph 7 on the basis of information obtained during the operation.
10. Implementation of logistics software to optimize TM routing involved in the system.
11. Control definition functional responsibilities of all objects with respect to the planned work of analysis differences.
12. A comparison between the planned logistics data and actual TM systems and SMCF (Fig. 1).

The experimental results

The introduction of elements of the SMCF at 35 enterprises of Ukraine for 1405 TM has allowed assess of the effectiveness of such a system:

- an introduction to the work items 1-6 allows you to save up to 10% of the total fuel used by TM;
- introduction to paragraphs 7-10 allows you to save up to 50% on the amount of fuel used by a separate TM and up to 25% of the total FAL used by the TM. For some the size of the TM fuel economy by 100% - was prevented use of a dummy TM.
- an introduction to the work saving of paragraphs points 12-11 to 7% of the total fuel used by TM;
- introduction to paragraph 13 allows the monitoring, evaluation, control of the TM. Using this scheme allows for a total of up to 42% fuel savings and more on the use of the entire fleet.

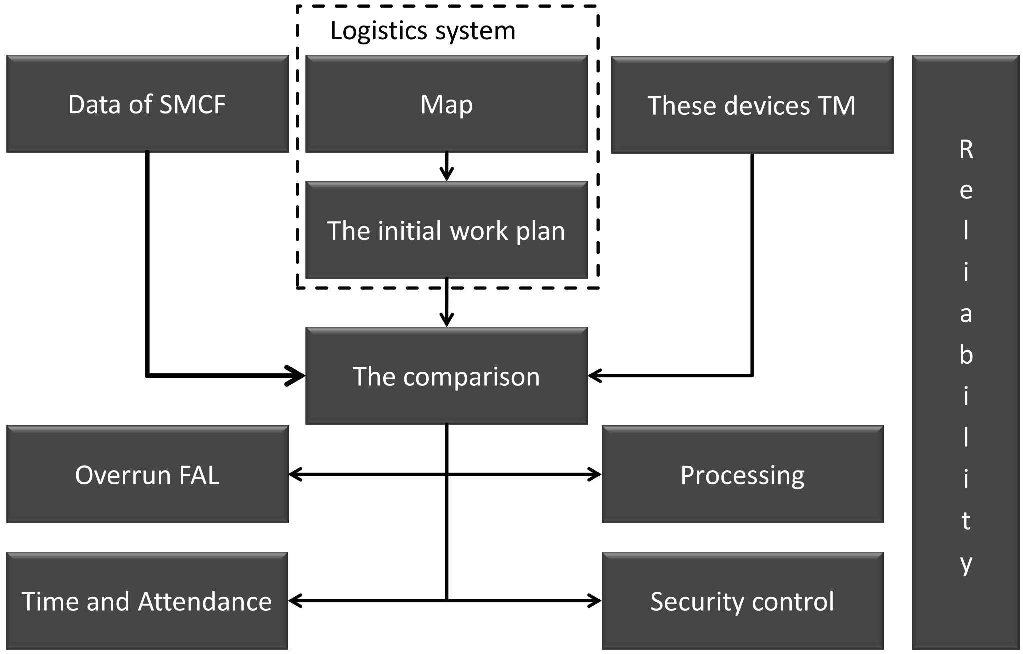

Figure 1 - Scheme of comparing planned and actual performance TM

Analysis of experimental results, conclusions

Introduction of SMCF can take a new level in the management of fleet TM. Among the reasons identified by us as a result of the experiment, the main ones are: dishonesty, irresponsibility of employees responsible for the work of the TM. It is important to note that the experiment was carried out on workers with different levels of wages and different corporate cultures, it was found that the above does not affect the pattern of behavior of employees. Payback system is highly dependent on the total number of operations performed by fleet vehicle, the scheduling algorithm works TM algorithm comparisons, the model revealed damage compensation. In general, the payback period can range from several days to several months.

References

1. International standards and Recommended practice (SARPS). Aeronautical telecommunications annex 10to the convention on international civil aviation, ICAO, 1996.

2. International standards and Recommended practice (SARPS). Safety Management Manual (SMM). Doc.9859 – AN/460. ICAO, 2006.

3. V.V. Konin, V.P. Kharchenko – Satellite navigation systems – Kyiv, Holteh, 2010. – 520p.

4. Наказ міністерства інфраструктури України від 24 січня 2012 року N36 «Про затвердження змін до норм витрат палива і мастильних матеріалів на автомобільному транспорті»

5. Наказ міністерства транспорту України від 10 лютого 1998 року N43 (із змінами)

6. ДБН Д.2.7-2000 «Ресурсні кошторисні норми експлуатації будівельних машин та механізмів» затверджений Наказом Держбуду України від 05.10.2000 № 225

UDC 621.396.98

V. Konin, O. Pogurelskiy
(National Aviation University, Ukraine)

RESULTS OF COMPLEX PROCESSING GPS AND GLONASS DATA IN CASE OF RESTRICTED VISIBILITY OF NAVIGATION SATELLITES

This paper describes result of complex processing navigation data simultaneously received from GPS and GLONASS satellites. The issue of study is accuracy of coordinate calculations in case of limited number of visible satellites both systems. The conclusions about benefits of complex processing GPS and GLONASS navigation data are considered.

Introduction

The diversity and redundancy provided by multiple, independent, compatible and in some respects, interoperable GNSS such as GPS and GLONASS provide a lot of gain. There are scientific and practice interest in the research of positioning accuracy in case of complex processing navigation data received from satellites of both systems. The implementation of complex GNSS data processing is most important in situation of limited visibility of sky due to local obstacles. In some restricted conditions (fig. 1) combinations of visible satellites makes impossible determination of coordinates with the help of data from only one system.

For example, when visible only 3 GPS satellites and 2 GLONASS neither GPS nor GLONASS single-system receiver enable to determine own position. Receivers switch to mode of satellite searching and user cannot obtain renewed instant information about coordinates and velocity. Such situation is very dangerous for aviation and full of troubles for many over clusters of users. The lost of satellites signals in onboard GNSS receiver may take place during aircraft maneuvering in the terminal area. It is possible when own wing overshadows GNSS antenna placed over pilot cockpit. As a result crew may have difficult with correct estimation of flight altitude immediately after the turn.

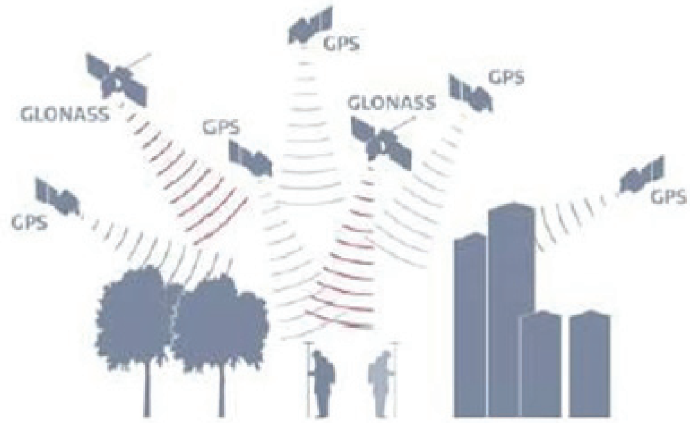

Fig.1 Restricted visibility of satellites due to local obstacles

Car drivers travelling at the mountain roads could lose satellite signal due to natural obstacles such as mountain peaks. Car navigator during some time wouldn’t be able to calculate new coordinates and in its train the driver that uses electronic map would be misinformed about precise location at the road. Also if number of visible satellites from one system is equal or bigger than 4 but less than 6-7 it results in low level of positioning accuracy. Possible solution of this problem is adding data from other navigation system. For example, we can use as additional sources of range data satellites from other satellite navigation system (GPS as additional for GLONASS, or GLONASS as additional for GPS).

Simulation and its results

The aim of research is estimation of positioning accuracy obtained after complex processing GPS and GLONASS data in case of restricted visibility of navigation satellites. It means that total number of satellites should be 5-6. For purposes of simulation such conditions could be achieved with the help of receiver ProPack-V3 software.

There is a built-in command LOCKOUT that allows exclude any satellite from visible constellation.

Fig. 2 shows the general algorithm of research. It combines facility for receiving real navigation data from visible GPS and GLONASS satellites and developed software for complex processing available navigation data and computing position. Obtained results are compared with known coordinates of receiver location for determination of instant accuracy.

Features of complex processing data from two satellite systems impose follow limitations for satellite combinations:

- each system should be provided with minimum 2 satellites;
- minimal total number of both system satellites is equal 5.

So follow combinations of GPS and GLONASS satellites were simulated and researched: 3+2 (fig. 3), 2+3 (fig. 4), 3+3 (fig. 5), 4+2 (fig. 6) and 2+4 (fig. 7).

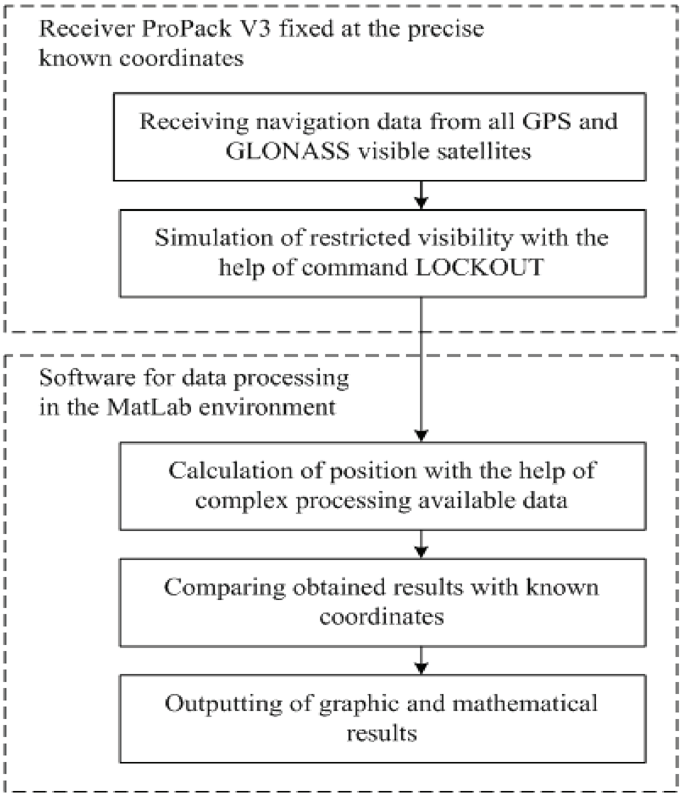

Fig.2 General algorithm of research

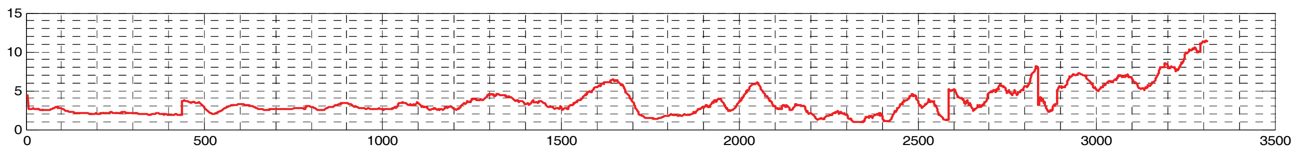

Fig. 3 Instant accuracy for satellites combination 3GPS + 2GLONASS

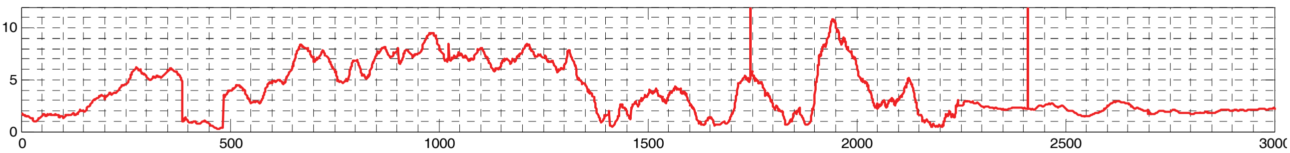

Fig. 4 Instant accuracy for satellites combination 2GPS + 3GLONASS

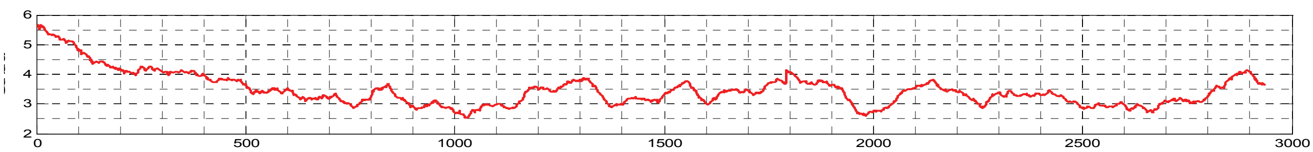

Fig. 5 Instant accuracy for satellites combination 3GPS + 3GLONASS

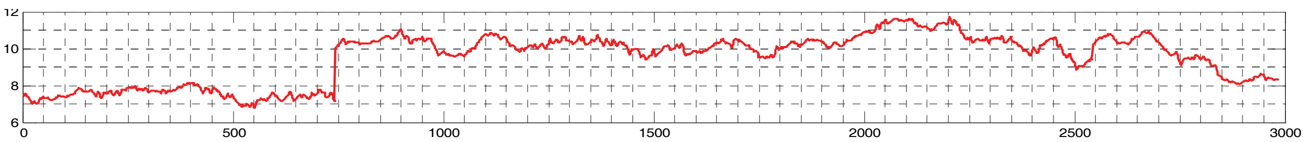

Fig. 6 Instant accuracy for satellites combination 4GPS + 2GLONASS

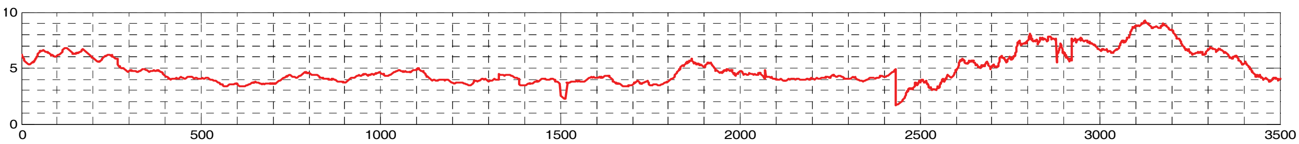

Fig. 6 Instant accuracy for satellites combination 2GPS + 4GLONASS

Table 1 contains results of mathematical processing obtained data.

Table 1.

Parameter	Accuracy of positioning for satellite combinations				
	3+2	2+3	3+3	4+2	2+4
Max error, m	2.767	20.08	5.664	11.694	9.264
Min. error, m	-7.004	0.28	2.527	6.800	1.709
Expected value of error, m	-1.366	3.802	3.460	9.507	4.899
Variance, m^2	2.955	14.309	0.298	1.705	1.920
Standard deviation, м	1.719	4.828	0.546	1.306	1.386

Analysis of the results shows that maximal value of positioning error was 20 m, the expected value of coordinate error in the experiments did not exceed 10. The average value of standard deviation was less than 2 m, which suggests that a 95% deviation in determining the location does not exceed a value of 3 m, and 99% - 3.7 m maximum deviation of 4.8 m occurred configuration 2GPS +3 GLONASS.

Conclusions

Complex processing navigation data from GPS and GLONASS satellites allowed to calculate coordinates of user with medium level of errors. This result was obtained for simulated conditions of restricted visibility of navigation satellites than the maximal number of both system satellites was 6. It proved the advantage of complex processing navigation data – the possibility to calculate coordinates than single-system receiver (GPS or GLONASS) enable to perform this task due to low number of visible satellites.

References

1. Конин В. В. Системы спутниковой радионавигации / В.В. Конин, В.П. Харченко. – К.: Холтех, 2010. 520 с.

2. Глобальная навигационная спутниковая система ГЛОНАСС (Интерфейсный контрольный документ).- редакция 5.1 / Координац. науч.-информ. центр РФ.- М., 2008. - 74с

3. Interface Control Document Global Positioning System (ICD-GPS-200C). – Washington, 1997. – 160 p.

UDC 621.396.933(045)

V.M. Vasyliev, Professor, DSc(Eng.)
(National Aviation University, Ukraine)
K.V. Naumenko (Antonov Company, Ukraine)

COMPARATIVE ASSESSMENT OF ACCURACY OF DISTANCE-MEASURING RADIONAVIGATION SYSTEMS DATA PROCESSING ALGORITHMS

The influence of the different methods of linearization on the accuracy of trajectory estimation at synthesis the algorithms of optimal one-step processing the data of two-positioned distance-measuring radionavigation system is investigated.

Problem statement. Flight safety substantially depends on the true and precise estimation of the aircraft flight trajectory parameters. To determine the coordinates of the moving object the radio navigation surveillance systems are widely used. For processing the data of such surveillance systems, methods and algorithms of optimal trajectory parameters estimation are used with application of the statistical estimation theory. Application of any method requires mathematical description of the process dynamics, which parameters are estimated, and description of relationship between the measured data and the trajectory parameters to be estimated. The principal issue is the choice of the coordinate system for providing solution of the problem with required accuracy, obviousness of represented information about location of aircraft relative to the flight route, derivation the simplest mathematical expressions, minimization of the calculation time, etc.

Primary measurements of the surveillance systems used in the air traffic control systems are functionally connected with the estimated trajectory parameters in a rectangular coordinate system via non-linear expressions. Therefore the mathematical problem statement is in its nature a non-linear one.

As a rule, in real control systems the linear methods of statistical trajectory estimation are used that are both well developed and economic in respect of calculations [1–2]. To use these estimation methods the different methods of linearization are applied [3–5].

In this work, different methods of synthesis of optimal trajectory parameters estimation algorithms are proposed in case of one-step data processing of two-position distance-measuring radio navigation surveillance system, and the effect of different methods of linearization applied for synthesis of these algorithms on the accuracy of trajectory estimation is examined.

Mathematical statement. Conventionally, the mathematical statement of trajectory parameters estimation involves mathematical description of the process to be estimated in general form:

$$\dot{\mathbf{X}}(t) = f\,(\mathbf{X}(t), \mathbf{U}(t), \mathbf{W}(t), t)\,, \tag{1}$$

where $\mathbf{X}$ – state vector; $\mathbf{U}$ – control signals vector; $\mathbf{W}$ – disturbances vector,
and the equation establishing the relationship between the estimated $\mathbf{X}$ and measured $\mathbf{Z}$ parameters

$$\mathbf{Z}(t) = h(\mathbf{X}(t), \mathbf{V}(t), t)\,, \tag{2}$$

where $\mathbf{V}$ – vector of random measurement errors.

For application of linear discrete methods of optimal assessment, the estimated process equation (1) and the measurement equation (2) must be represented in linear form:

$$\mathbf{X}(t_i) = \mathbf{\Phi}\,\mathbf{X}(t_{i-1}) + \mathbf{B}\mathbf{U}(t_{i-1}) + \mathbf{G}\mathbf{W}(t_{i-1})\,, \tag{3}$$

$$\mathbf{Z}(t_i) = \mathbf{H}\mathbf{X}(t_i) + \mathbf{V}(t_i)\,, \tag{4}$$

where $\mathbf{\Phi}$ is the state transition matrix.

For the purposes of aircraft tracking procedure the aircraft movement is described in a rectangular coordinate system. Also it is taking into account the fact that, as a rule, excessive detail of description results in unreasonable complication of the estimation algorithm and problems in its realization. Let us note that in the greater part of their route the aircraft fly in a straight line with constant speed. Taking into account all the above, the model of aircraft movement (3) will take the following form:

$$\mathbf{X}(t_i) = \mathbf{\Phi}\,\mathbf{X}(t_{i-1})\,, \tag{5}$$

where $\mathbf{X} = [x, y, V_x, V_y]^{\mathrm{T}}$; V_x, V_y are the speed components at corresponding coordinates.

The state transition matrix for (5) under assumed conditions is as follows:

$$\mathbf{\Phi} = \begin{bmatrix} 1 & 0 & T & 0 \\ 0 & 1 & 0 & T \\ 0 & 0 & 1 & 0 \\ 0 & 0 & 0 & 1 \end{bmatrix}, \tag{6}$$

where $T = t_i - t_{i-1}$ is the quantization interval assumed to equal the period of data receiving.

This work deals with aircraft trajectory estimation using the data of two-position surveillance system consisting of two distance-measuring radio navigation stations located at the distance of d between them, each of which measures the distances r_1 and r_2 to the aircraft (Fig.1).

The task is to analyze different mathematical description of the relationship between the measurements and the components of the estimated state vector of flight process with subsequent linearization, as well as to examine the effect of linearization on the accuracy of trajectory estimation.

First method of linearization. The first method is used for synthesizing the algorithm of optimal estimation of the parameters of trajectory in a rectangular coordinate system under the condition that preliminarily the measured distances were recalculated to a rectangular system. In such a case the functional relationships between the measured distance r_1, r_2 and the coordinates of the aircraft location in a rectangular x, y coordinate are written in the form of non-linear functions, namely:

$$x = f_1(r_1, r_2) = \frac{r_1^2 - r_2^2 + d^2}{2d}, \tag{7}$$

$$y = f_2(r_1, r_2) = \frac{1}{2d}\left(2r_1^2 d^2 - r_1^4 + 2r_1^2 r_2^2 - r_2^4 + 2r_2^2 d^2 - d^4\right)^{\frac{1}{2}} = \frac{1}{2d}\sqrt{A}\,. \tag{8}$$

Let us find the linearized surveillance equation in the form of (4). Let us represent the measurement recalculated into a rectangular coordinate system in the form of

$$x^*(i) \cong x(i) + v_x(i), \tag{9}$$

$$y^*(i) \cong y(i) + v_y(i), \tag{10}$$

where v_x, v_y are the random errors of evaluation of the corresponding rectangular coordinates.

Let us define $\mathbf{Z} = [x^*, y^*]^{\mathrm{T}}$ – the vector of distance measurement recalculated into a rectangular coordinate system, and $\mathbf{V} = [v_x, v_y]^{\mathrm{T}}$ – the vector of errors of evaluation of the corresponding rectangular coordinates. Then the model of measurements will be written in the state space in a linear form (4), where $\mathbf{H}$ is the observation matrix with the following structure

$$\mathbf{H} = \begin{bmatrix} 1 & 0 & 0 & 0 \\ 0 & 1 & 0 & 0 \end{bmatrix}. \tag{11}$$

Let us find the statistical characteristics of the linearized model of measurements (9), (10). Linearization of the expression (7) yields the expression of the error v_x:

$$v_x = \Delta x = \frac{\partial f_1}{\partial r_1}\Delta r_1 + \frac{\partial f_1}{\partial r_2}\Delta r_2, \tag{12}$$

where $\Delta r_1 = v_{r1}$; $\Delta r_2 = v_{r2}$ are the errors of distance-measuring systems; $\frac{\partial f_1}{\partial r_1} = \frac{r_1}{d}$; $\frac{\partial f_1}{\partial r_2} = -\frac{r_2}{d}$.

Similarly, for the error v_y after linearization of the expression (8) we get:

$$v_y = \Delta y = \frac{\partial f_2}{\partial r_1}\Delta r_1 + \frac{\partial f_2}{\partial r_2}\Delta r_2, \tag{13}$$

where $\frac{\partial f_2}{\partial r_1} = \frac{1}{d\sqrt{A}}\left(d^2 r_1 - r_1^3 + r_1 r_2^2\right)$, $\frac{\partial f_2}{\partial r_2} = \frac{1}{d\sqrt{A}}\left(d^2 r_2 - r_2^3 + r_1^2 r_2\right)$.

On the basis of the obtained expressions (12), (13) the variance of errors of evaluation of rectangular coordinates can be defined. For the x coordinate:

$$\sigma_x^2 = M\{v_x^2\} = \left(\frac{\partial f_1}{\partial r_1}\right)^2 \sigma_{r1}^2 + \left(\frac{\partial f_1}{\partial r_2}\right)^2 \sigma_{r2}^2 = \frac{1}{d^2}\left(r_1^2\sigma_{r1}^2 + r_2^2\sigma_{r2}^2\right). \quad (14)$$

For the y coordinate:

$$\sigma_y^2 = M\{v_y^2\} = \left(\frac{\partial f_2}{\partial r_1}\right)^2 \sigma_{r1}^2 + \left(\frac{\partial f_2}{\partial r_2}\right)^2 \sigma_{r2}^2 = \frac{1}{d^2 A}\left[\left(d^2 r_1 - r_1^3 + r_1 r_2^2\right)^2 \sigma_{r1}^2 + \left(d^2 r_2 - r_2^3 + r_1^2 r_2\right)^2 \sigma_{r2}^2\right]. \quad (15)$$

The mutual correlation of the errors v_x and v_y is:

$$\sigma_{xy}^2 = M\{v_x v_y\} = \frac{\partial f_1}{\partial r_1}\frac{\partial f_2}{\partial r_1}\sigma_{r1}^2 + \frac{\partial f_1}{\partial r_2}\frac{\partial f_2}{\partial r_2}\sigma_{r2}^2 . \quad (16)$$

So, statistical characteristics (14)-(16) of the measurements recalculated into rectangular coordinate are defined by the matrix

$$\mathbf{R} = \begin{bmatrix} r_{11} & r_{12} \\ r_{21} & r_{22} \end{bmatrix}, \quad (17)$$

where $r_{11} = \sigma_x^2$, $r_{22} = \sigma_y^2$, $r_{11} = r_{21} = \sigma_{xy}^2$.

Second method of linearization. Under another method, the mathematical model of distance measurements r_1, r_2 is written as a system of non-linear functions of state vector components in a rectangular coordinate system: $r_1 = h_1(x,y)$, $r_2 = h_2(x,y)$. It is assumed that the errors ν_{r1}, ν_{r2} of distance measurement are additive random values of the "white noise" type

$$r_1^* = h_1(x,y) + \nu_{r1}, \quad r_2^* = h_2(x,y) + \nu_{r2}, \quad (18)$$

with intensities σ_{r1}^2 , σ_{r2}^2 for the first and the second distance-measuring systems correspondingly.

Let us write down the equations defining the relationship between the measurements $\mathbf{Z} = [r_1^*, r_2^*]^{\mathrm{T}}$ (18) and the components x, y of the estimated state vector $\mathbf{X}$:

$$r_1^* = \sqrt{(x+d)^2 + y^2} + \nu_{r1}, \quad (19)$$

$$r_2^* = \sqrt{(d-x)^2 + y^2} + \nu_{r2}. \quad (20)$$

So, the initial mathematical model of measurements is a non-linear function:

$$\mathbf{Z}(t_i) = h(\mathbf{X}(t_i)) + \mathbf{V}(t_i), \quad (21)$$

where $\mathbf{X} = [x, y, V_x, V_y]^{\mathrm{T}}$; $\mathbf{V} = [\nu_{r1}, \nu_{r2}]^{\mathrm{T}}$.

Let us perform linearization of the equations (21) by expansion (19), (20) into the Taylor series in respect of state vector $\hat{\mathbf{X}}$ components. The linearized observation matrix takes the following form:

$$\mathbf{H} = \frac{\partial h}{\partial \vec{X}} = \begin{bmatrix} \dfrac{\partial h_1}{\partial x} & \dfrac{\partial h_1}{\partial y} & 0 & 0 \\ \dfrac{\partial h_2}{\partial x} & \dfrac{\partial h_2}{\partial y} & 0 & 0 \end{bmatrix}, \quad (22)$$

where $\dfrac{\partial h_1}{\partial x} = \dfrac{x}{\sqrt{x^2+y^2}}$, $\dfrac{\partial h_1}{\partial y} = \dfrac{y}{\sqrt{x^2+y^2}}$, $\dfrac{\partial h_2}{\partial x} = -\dfrac{(d-x)}{\sqrt{(d-x)^2+y^2}}$, $\dfrac{\partial h_2}{\partial y} = \dfrac{y}{\sqrt{(d-x)^2+y^2}}$.

As a result we obtain the linearized mathematical model of measurement

$$\mathbf{Z} = \mathbf{H}\Delta\mathbf{X} + \mathbf{V}, \quad (23)$$

where $\Delta\mathbf{X} = \mathbf{X} - \hat{\mathbf{X}}$.

For the measurer's model (21), (23), the measurement errors variance matrix $\mathbf{R}$ is in the form of (17), where $r_{11} = \sigma_{r1}^2$, $r_{22} = \sigma_{r2}^2$, $r_{12} = r_{21} = 0$.

Third method of linearization. By this method the system of two distance-measuring stations is represented as a certain ("virtual") distance and bearing measuring system $r - \alpha$ located in the point of location of one of the stations (for example, let it be the first station (see Fig.1)) that measures the distance to the aircraft r_1^* and the azimuth α_1^*, which is calculated by the measurements r_1^* and r_2^* of both distance-measuring stations using the cosine theorem

$$\alpha_1 = \arccos\left(\frac{r_1^2 - r_2^2 + d^2}{2r_1 d}\right). \tag{24}$$

Let us assume the following mathematical model of the measuring system with additive errors:

$$r_1^* = r_1 + v_{r1}, \tag{25}$$

$$\alpha_1^* = \alpha_1 + v_{\alpha 1}. \tag{26}$$

For providing the correctness of mathematical model of the virtual measuring system (26), let us perform linearization by expansion of the expression (24) into Taylor series in respect of distance values that correspond to the aircraft position, keeping only the first order elements. As a result we will have

$$v_{\alpha 1} = -\frac{1}{r_1 d\sqrt{1-z^2}}\left(\frac{r_1^2 + r_2^2 - d^2}{2r_1} v_{r1} + r_2 v_{r2}\right), \tag{27}$$

where $z = \dfrac{r_1^2 - r_2^2 + d^2}{2r_1 d}$.

Let us determine the variance of the linearized error (27) of the calculated angle α_1

$$\sigma_{\alpha 1}^2 = M\{v_{\alpha 1}^2\} = \frac{1}{r_1^2 d^2 (1-z^2)}\left(\left(\frac{r_1^2 + r_2^2 - d^2}{2r_1}\right)^2 \sigma_{r1}^2 + r_2^2 \sigma_{r2}^2\right). \tag{28}$$

Let us determine mutual correlation of the measured distance r_1 (25) and calculated angle α_1 (26)

$$r_{r1\alpha 1} = M\{v_{r1} v_{\alpha 1}\} = -\frac{1}{\sqrt{1-z^2}}\left(\frac{r_1^2 + r_2^2 - d^2}{2r_1^2 d}\right)\sigma_{r1}^2. \tag{29}$$

Finally, we get the measurement errors variance matrix $\mathbf{R}$ in the form of (17), where $r_{11} = \sigma_{r1}^2$, and $r_{22} = \sigma_{\alpha 1}^2$, $r_{12} = r_{21} = r_{r1\alpha 1}$ are calculated by expressions (28), (29).

For using the linear method of trajectory estimation, we should take the state vector $\mathbf{X} = [r, \alpha, \dot{r}, \dot{\alpha}]^{\mathrm{T}}$ and the same transition matrix $\mathbf{\Phi}$ as (6), and after estimation to recalculate the estimated values r and α into a rectangular x, y coordinate system. With the assumptions indicated above, the observation matrix $\mathbf{H}$ has the same simple structure as in the expression (11).

Computer modeling and comparative assessment. Let us take as the optimal linear trajectory estimation method the recurrent linear Kalman filter, which is widely used in navigation and air traffic control systems. For realization of optimal data processing using the Kalman filter, it is necessary to specify the initial data for the covariance matrix $\mathbf{P}(0)$ of estimating error, the covariance matrix $\mathbf{R}(0)$ of recalculated measurement errors and the state vector $\mathbf{X}(0)$.

The initial values of the elements of the state vector $\mathbf{X}(0)$ were assumed to equal to the initial aircraft position and its modeled flight speed correspondingly. A straight flight of the aircraft was modeled with a constant speed in the direction perpendicular to the base assumed to be $d = 50$ km. The initial position was assumed to be 10 km from the middle of the base.

The root-mean-square errors of the distance measurement were assumed to be $\sigma_{r1} = \sigma_{r2} = \sigma_r = 100$ m. The initial values of the matrix $\mathbf{R}(0)$ were assigned depending on the method.

The initial values for the covariance matrix $\mathbf{P}(0)$ were specified also depending on the linearization method.

The results of computer modeling are presented in Fig.2 showing the value of radial root-mean-square error $\sigma_\rho = \sqrt{p_{11} + p_{22}}$ of aircraft position estimation as a function of removal (coordinate y) aircraft from the base. Curve 1 is the result obtained by modeling the algorithm synthesized by the first method, curve 2 – by the second method, and curve 3 – by the third one.

For comparison, the value of radial root-mean-square error was calculated using the expression $\sigma_\rho = \sqrt{2}\,\sigma_r \operatorname{cosec}\gamma$ [1] (curve 4) for the case when aircraft position is calculated using the measurement data of two distance-measuring stations without any optimal processing.

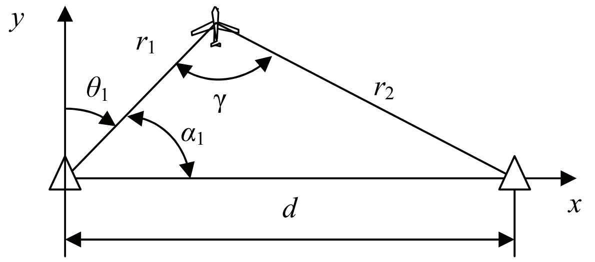

Fig. 1. Relative position of the aircraft and the distance-measuring stations

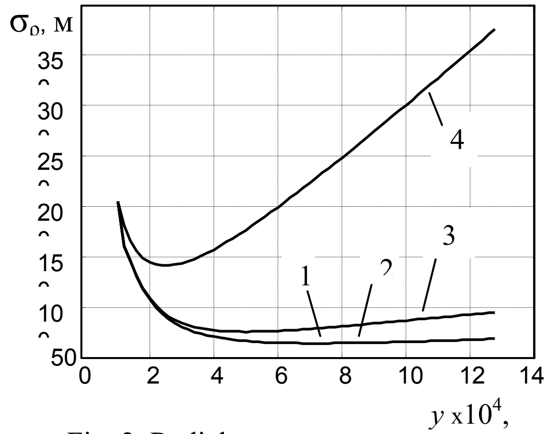

Fig. 2. Radial root-mean-square error of aircraft position estimation

Conclusions

Three methods of synthesis of linearized algorithms of one-step optimal estimation of the aircraft trajectory parameters using the data of two distance-measuring surveillance systems have been shown.

Evaluation of accuracy of the synthesized algorithms via computer modeling shows that in case using the first and second methods the errors of evaluation of aircraft location coordinates practically coincide. The accuracy is somewhat lower in case of use of the third method.

If consider the algorithms from the viewpoint of productivity, then, if we compare the first and the second methods, the first algorithm includes a simple observation matrix $\mathbf{H}$ (11) with constant elements, but at each discretization step the values of the covariance matrix $\mathbf{R}$ (17) of linearized errors should be calculated. The second algorithm, on the contrary, includes a constant matrix $\mathbf{R}$, yet each time the elements of the matrix $\mathbf{H}$ (22) should be calculated. Besides, it should be noted that in this algorithm the difference is estimated and not the vector itself and for estimation of the complete state vector additional computation will be required.

With the third algorithm, just as with the first one, it is required to calculate at each step the elements of the matrix $\mathbf{R}$, yet not all of them and by less complicated equations. However, as evaluation is performed in a polar coordinate system, additional computation will be required for transformation into the rectangular system.

Nevertheless the application of each of the synthesized algorithms considered here considerably increases the accuracy of the trajectory evaluation as compared with the accuracy of the coordinate's calculation without the use of optimal methods.

References

1. *Кондратьев В.С.* Многопозиционные радиотехнические системы /В.С.Кондратьев, А.Ф.Котов, Л.Н.Марков; под. ред. проф. В.В.Цветнова. – М.: Радио и связь, 1986.– 264 с.

2. *Ярлыков М.С.* Статистическая теория радионавигации. – М.: Радио и связь, 1985.– 344 с.

3. *Васильєв В.М., Науменко К.В.* Використання оптимальних методів оцінки траєкторних параметрів за даними радіодалекомірних систем // Вісник НАУ. – 2011. – №4. – С. 20-24.

4. *Васильєв В.М., Науменко К.В.* Оцінка точності оптимального оброблення траєкторних вимірювань багатопозиційних далекомірних систем //Проблеми інформатизації та управління. – 2011. – Вип. 2(30). – С. 31-35.

5. *Васильєв В.М., Науменко К.В.* Підвищення точності траєкторної оцінки в багатопозиційних далекомірних системах спостереження // Зб. наук. праць Військового ін-ту телекомунікацій та інформатизації НТУУ «КПІ». – 2011. – Вип. 2. – С. 6-11.

UDC 528.2: 629.78

A.I. Dokhov, Ph.D., A.M. Lukyanov, A.A. Zhalilo, Ph.D., A.A. Zhelanov, Ph.D.
(Kharkov National University of Radio Electronics, Ukraine)

MILESTONES OF EGNOS TECHNOLOGIES IMPLEMENTATION IN AVIATION OF UKRAINE: INTERNATIONAL PROJECT «EEGS2»

International Project «EGNOS Extension to Eastern Europe: Applications» is currently carried out in the framework of FP7, its orientation for implementation of EGNOS technologies in aviation of Ukraine is considered.

EEGS2 Project objectives

The EEGS2 Project [1] is aimed to demonstrate the benefits of EGNOS, EGNOS Data Access Service (EDAS) and Galileo through applications in the Eastern countries of Europe. The Project has the following three objectives:

– to demonstrate through flight trials the benefits of EGNOS in areas of Eastern Europe where EGNOS is not available;

– to study the impact of the SBAS (Space Based Augmentation System) technology in transport management;

– to promote EDAS, EGNOS and Galileo.

The first objective will be demonstrated through the deployment of avionics on board capable of reading the magicSBAS messages from radio frequency (RF), the definition of flight procedures and the analysis of the performances in real flights in four Eastern European countries. MagicSBAS is a state-of-the-art, multi-constellation, operational SBAS regional differential GNSS augmentation which transmits corrections and non-safety critical integrity information for any interested region.

The EEGS2 Project will be able to understand the performances, benefits and limitations of EGNOS and they will be totally prepared for the extension of ENGOS to the Eastern European countries in the coming future.

EEGS2 Project participants

The EEGS2 Project unites participants from the countries representing EU countries and Eastern European countries:

– GMV Aerospace and Defence SA (Spain, GMV);

– Grupo Mecánica del Vuelo Sistemas S.A. (Spain, GSY);

– Centrum Badan Kosmicznych Polskiej Akademii Nauk (Poland, CBK)

– Romanian Space Agency (Romania, RSA)

– Kharkov National University of Radio Electronics (Ukraine, KhNURE);

– Main Astronomical Observatory of the National Academy of Sciences of Ukraine (Ukraine, MAO);

– Russian Space Systems (Russian Federation, RSS);

– Technical University of Moldova (Moldova, TUM);

– NDConsult Ltd (UK, NDC).

Main tasks of the Project in civil aviation area being solved in Ukraine

The necessary activities needed for the successful development of the SBAS flight trials will be presented here. First, EGNOS flight procedure will be created for use in EGNOS flight trial in Poland. Then, magicSBAS flight procedures will be created for using in magicSBAS flight trials in Moldova, Romania and Ukraine. To carry out flight procedures the target aircrafts must be equipped properly.

In particular, the following tasks will be done.

Procurement of the necessary infrastructure to carry out the demos, such as:

– PCs to host magicSBAS for flight trials;

– user receivers for EGNOS/magicSBAS flight trials;

– RF modems for transmission and reception of magicSBAS corrections;

– laptops for monitoring and visualizing aircraft position during flight trials;
– ADSL/GPRS rent for flight trials;
– other.

GMV will adapt magicSBAS to provide RF broadcast from ground to the aircraft and for monitoring on-board magicSBAS position. The intention is to integrate and validate real-time operation of the processing chain «EDAS+magicSBAS+user receiver+performance monitor».

EDAS output data (ASN1 format) are transformed to magicSBAS (input data - EGNOS RIMS_CG format) to enable demonstrations with the same reference stations data as EGNOS. Note that the conversion is done to feed magicSBAS in real-time.

In order to perform flight trials with the magicSBAS messages the following architecture is foreseen (fig. 1).

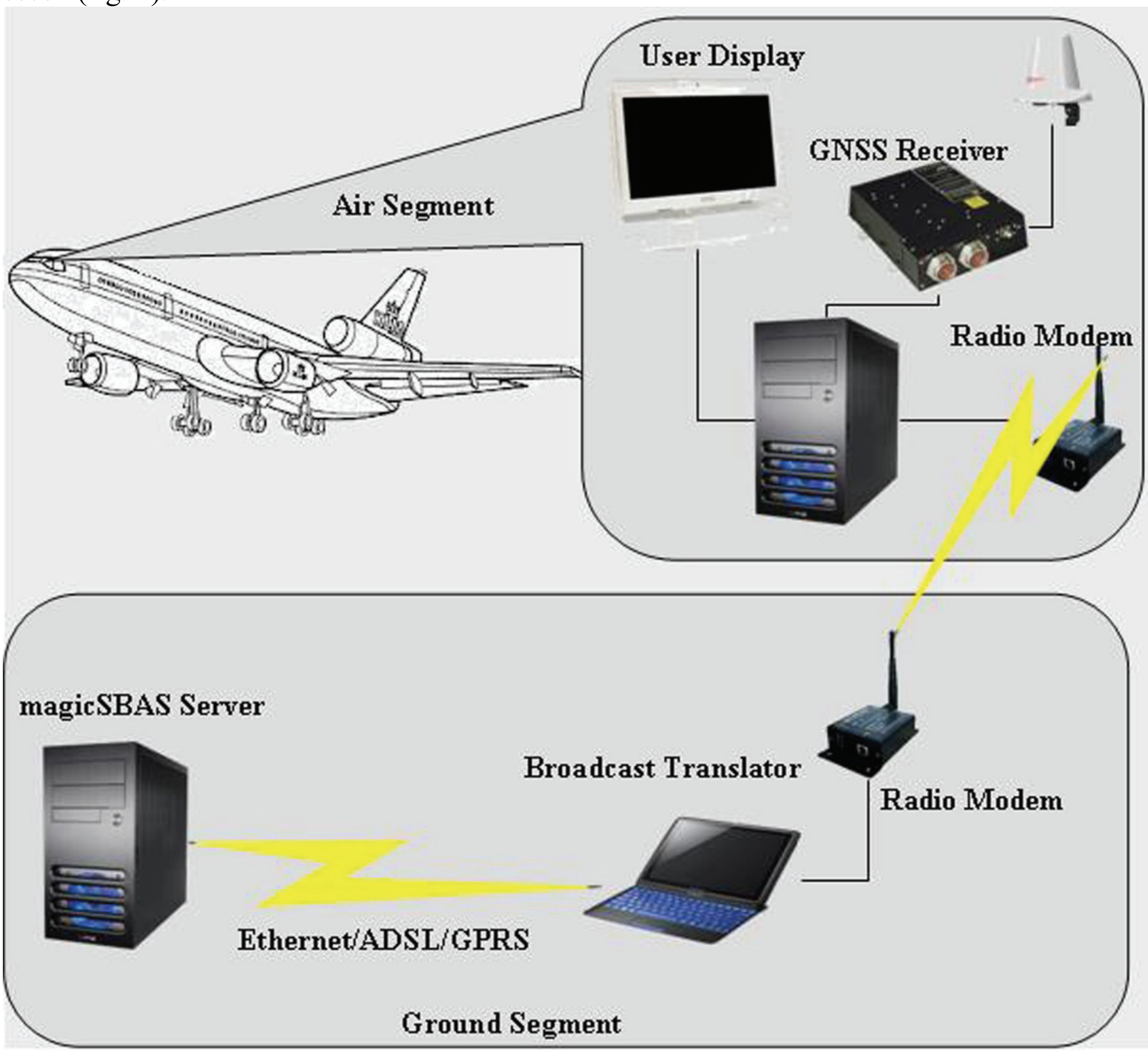

Figure 1 – Architecture of flight trials system

The magicSBAS messages will be generated at GMV (Spain) and sent to the airfield via Ethernet/ADSL/GPRS. These messages will be broadcasted to the aircraft via RF. The pilot in the aircraft will be able to carry out the flight procedure with the console on board.

KhNURE will prepare the flight trials in Ukraine by means of carrying out the necessary preparation activities which will include at least:

– preparing the documentation relevant for the flight trials (objectives, activities, aircraft, airports, date, expected performance, etc) and the necessary documentation allowing the flight trials (certificates as needed);

– providing real-time data transmission from the selected Ukrainian permanent reference stations (using NTRIP format) to form magicSBAS messages for the Ukrainian territory with the APV-I navigation performance at user level;

– planning of participation in flight trials of representatives of the interested organizations;

– monitoring of GPRS/GSM communication for receiving magicSBAS corrections and management of RF communication for the flight trials.

Flight trials using magicSBAS are planned to perform in Ukraine. Therefore, the following activities are foreseen:

– KhNURE will install the necessary elements (RF receiver modem, GPS antenna) on board the aircraft for the correct reception of the RF magicSBAS and GPS signals;

– KhNURE will install the necessary elements (RF transmitter modem and Internet/GPRS/GMS connection) on ground in the flight procedure area for the reception of the magicSBAS corrections in SISNET format and transmission them through RF to the aircraft;

– GMV will install the necessary equipment to be used for the correct realization of the flight procedure and performances monitoring;

– the flight trials will be conducted by KhNURE and the local partners (for the selected airport) and with preliminarily determined duration of flights;

– KhNURE and GMV will analyze the results of magicSBAS navigation performance during flight trials.

The performed flight trials will enable implementing SBAS systems in the countries where EGNOS signal is still not available. The International Civil Aviation Organization (ICAO) during its session of the Assembly (the 36th Assembly, September 18-28, 2007) strongly recommended the use of LPV instrument approach procedure for the whole of the runway infrastructure both as the main or a duplicate one, with step-by-step adoption of it in 2010 (30%), 2014 (70%) and absolute adoption (100%) in 2016.

MagicSBAS/EGNOS navigation technologies will provide the following benefits to the airlines:

– reduction in decision heights;
– reduction in angle of approach;
– better lateral guidance;
– optimized routes, fewer diversions;
– increased safety;
– increased airports capacity;
– allow operation in non ILS-equipped airports.

This project will give a clear idea of efficiency and advantages of EGNOS based technologies which are intensively extended at the present time to pilots and providers who provide supply to satellite differential information.

Technical procurement of the experiments

At the present moment reference GNSS stations SURE (Kharkov), KHAR (Kharkov) and KTVL (Crimea) transmit data in RTCM v.3.0 format for forming magisSBAS corrections for the territory of Ukraine, Moldova and Romania. The data are available via NTRIP caster of MAO NAS of Ukraine (http://194.44.11.4:2101/).

It is planned to carry out the first flight test in the territory of Korotich airfield, near Kharkov. The airfield is a ground runway for light aviation aircrafts.

For carrying out the trials single-engined two-seater XA3-30 aircraft will be used (Fig.2):

– Length ~6,5 m;
– Wingspan ~9,5 m;
– Flight range – up to 400 km;
– Speed – up to 200 km/h.

Figure 2 –XA3-30 Aircraft used for carrying out flight trials

Arrangement/installation of the equipment

It is planned to mount GNSS antenna on the roof of the aircraft cab. Currently possible ways of fixing the antenna which will allow keeping the wing surface undamaged are worked through. The antenna for receiving magicSBAS corrections from the lower hemisphere will be mounted under the bottom of the aircraft. GNSS receiver and a radio modem will be installed on board the aircraft (an area behind the pilot seat). Preliminarily, the set of the equipment will be tested during road tests on a car.

Communication channel «Ground-to-Air»

At the present moment it is considered several ways of realizing the communication with onboard the aircraft with the purpose of correction transmission - GSM channel on the basis of existing communication systems and a separate communication channel.

After coordination of the flight scheme the possibility of using the existing communication channels will be checked up, for instance, GSM, otherwise the necessity of organizing a separate communication channel will arise.

References

1. Collaborative Project, Annex I – "Description of Work", «EGNOS extension to Eastern Europe: applications», Seventh Framework Programme, FP7-Galileo-2011-GSA-1, Galileo.2011.4.3-1 International Activities, **http://www.eegs2-project.eu**

UDC 621.391.82:519.724.2

V. A Shvets, PhD, V.V. Klobukov
(National Aviation University, Ukraine)

ADAPTIVE METHOD OF FORMING WEIGHTS WITHOUT REFERENCE SIGNAL

Describes a method for the control pattern adaptive antenna array to improve the noise immunity of GPS systems in the absence of a reference signal in the user segment.

The above criteria forming weights suggest that the direction of the source is known, or known amplitude and phase distribution of signal channels antenna array, that is to implement these algorithms need a priori knowledge of the signal, or form in the receiving path reference signal. The reference signal can be formed with the adopted mixture signal obstacle.

Mathematically, the reference signal is given by (1.26) [1], [3] and weighting coefficients are determined from the expression (1.27) [1], [3]. From (1.27) [1] to ensure the sustainability of adaptive devices to match a value of 1 / γ (Fig. 1.14) if this is not done growing weights lead to disruption of the system. Also for forming the reference signal [1, 3] proposed transfer service combinations, but in GNSS systems such impossible (GPS and Galileo did not involve the transfer of any additional information). Therefore, to ensure the sustainability of the adaptive antenna system is necessary to eliminate the dependence of weight vector of the reference signal, or remove the signal component from a mixture of signal/interference.

An important requirement for the optimization of weights - the need to eliminate the influence of the signal in the calculation of the inverse matrix interference $\mathbf{R}^{-1}_{\text{сп}}$. Also, to reduce the impact of nonidentity channels AAA (no identity frequency characteristics of receivers, constructive elements no identity AAA, scatter quadrature channels for gain and phase shift and other factors) to calculate weights to exclude signal component in the calculation of the correlation matrix interference. For it is recommended to remove the signal from the mixture signal/interference [2].

Functional scheme for calculating weights without reference signal shown in fig. 1.

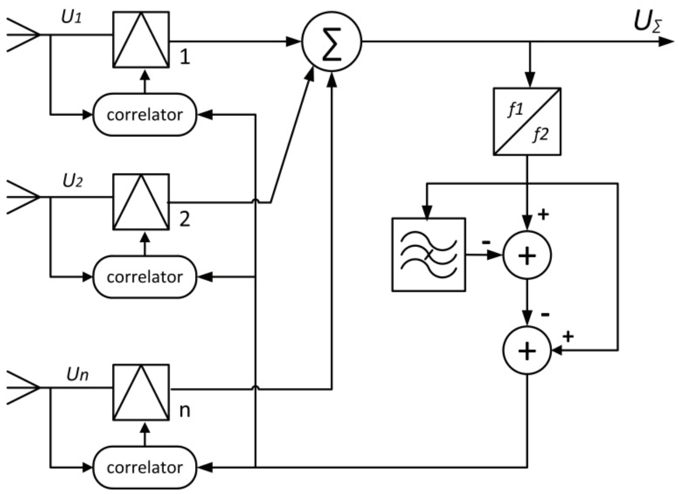

Figure 1

The transducer converts the signal of frequency f_1 in the signal with frequency f_2, which is kept constant. Notch filter cuts out the signal component and takes the stress interference with the opposite sign to the adder, the output of the adder is signal voltage. Voltage noise comes less from a mixture of "signal/interference" voltage signal. Double deduction in order not to alter the correlation matrix of the signal and noise.

The error signal is formed as the difference

$$\varepsilon = \mathbf{w}^{\mathrm{T}}\mathbf{u}_{\text{сп}} - S \tag{1}$$

Squared error

$$\varepsilon^2 = S^2 - 2S\mathbf{w}^{\mathrm{T}} + \mathbf{w}^{\mathrm{T}}\mathbf{u}^*{}_{\text{сп}}\mathbf{u}^{\mathrm{T}}{}_{\text{сп}}\mathbf{w}$$

Finding the expectation of ε^2, we obtain an expression for the mean square error

$$E[\varepsilon^2] = S^2 + \mathbf{w}^{\mathrm{T}}\mathbf{R}_{\text{сп}}\mathbf{w} - 2\mathbf{w}^{\mathrm{T}}\mathbf{r}_{\text{сп,с}}\ , \qquad (2)$$

where $\mathbf{r}_{\text{сп,с}} = \overline{\mathbf{u}^*{}_{\text{сп}}S}$; E – average.

Correlation matrix $\mathbf{R}_{\text{сп}}$ is the sum of the correlation matrix $\mathbf{R}_{\text{п}}$ interference and signal $\mathbf{R}_{\text{c}}$, $\mathbf{R}_{\text{сп}}$= $\mathbf{R}_{\text{п}}$+ $\mathbf{R}_{\text{c}}$. From fig. 1 shows that the formation of the error signal $\mathbf{R}_{\text{сп}}$= $\mathbf{R}_{\text{п}}$+ $\mathbf{R}_{\text{c}}$- $\mathbf{R}_{\text{c}}$= $\mathbf{R}_{\text{п}}$.

Vector $\mathbf{r}_{\text{сп,с}}$ in the expression (2) is a correlation vector voltage $U^*_{\text{сп}i}$ і S (i=1,2, … , N), at S^*_i=0, ie the reference signal is missing

$$\mathbf{r}^{\mathrm{T}}_{\text{сп,с}} = \left[\overline{\mathbf{u}^*{}_{\text{сп}1}}\ \overline{\mathbf{u}^*{}_{\text{сп}2}}\ \ldots\ \overline{\mathbf{u}^*{}_{\text{сп}N}}\ \right],$$

where $U^*_{\text{сп}i}$= $U^*_{\text{п}i}$.

Otherwise

$$\mathbf{r}^{\mathrm{T}}_{\text{сп,с}} = \mathbf{r}^{\mathrm{T}}_{\text{п}}$$

Then the expression (2) takes the form

$$E[\varepsilon^2] = S^2 + \mathbf{w}^{\mathrm{T}}\mathbf{R}_{\text{п}}\mathbf{w} - 2\mathbf{w}^{\mathrm{T}}\mathbf{r}_{\text{п}}\ , \qquad (3)$$

Optimization of the expression (3) in its minimization by selecting weighting coefficients vector w. Since the mean square error (3) quadratic function of the vector **w** it has only minimum which can be found by differentiating (3) and equating to zero the derivative

$$dE[\varepsilon^2\ ]/d\mathbf{w} = 0.\ \text{Так як}\ \ dE[\varepsilon^2\ ]/d\mathbf{w} = 2\mathbf{R}_{\text{п}}\mathbf{w} - 2\mathbf{r}_{\text{п}} \qquad (4)$$

vector weights will be determined by the expression

$$\mathbf{w} = \mathbf{R}_{\text{п}}^{-1}\mathbf{r}_{\text{п}}, \qquad (5)$$

Expression (5) corresponds to the expression Wiener-Hopf for calculating the weights in an adaptive antenna array.

The scheme in fig. 1 to satisfy the minimum mean square error. Here are the results of mathematical modeling. The simulation results (fig. 2, fig. 3) for interference azimuth 241°, elevation 28°, matrix AAA 4×4, dx, dy = 0.25, variance of noise - 1, phase shift interference 0°.

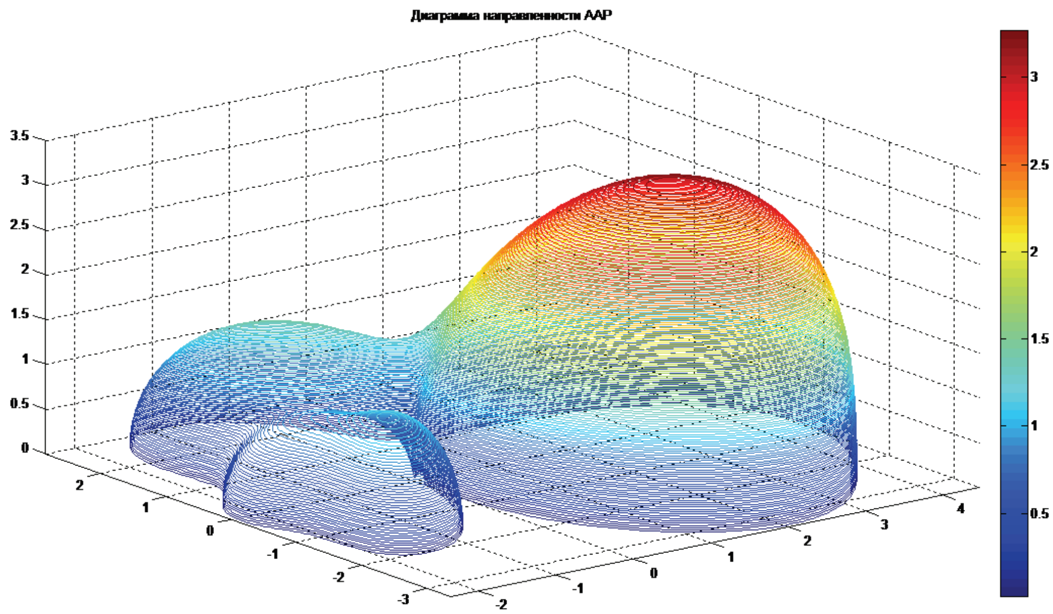

Figure 2

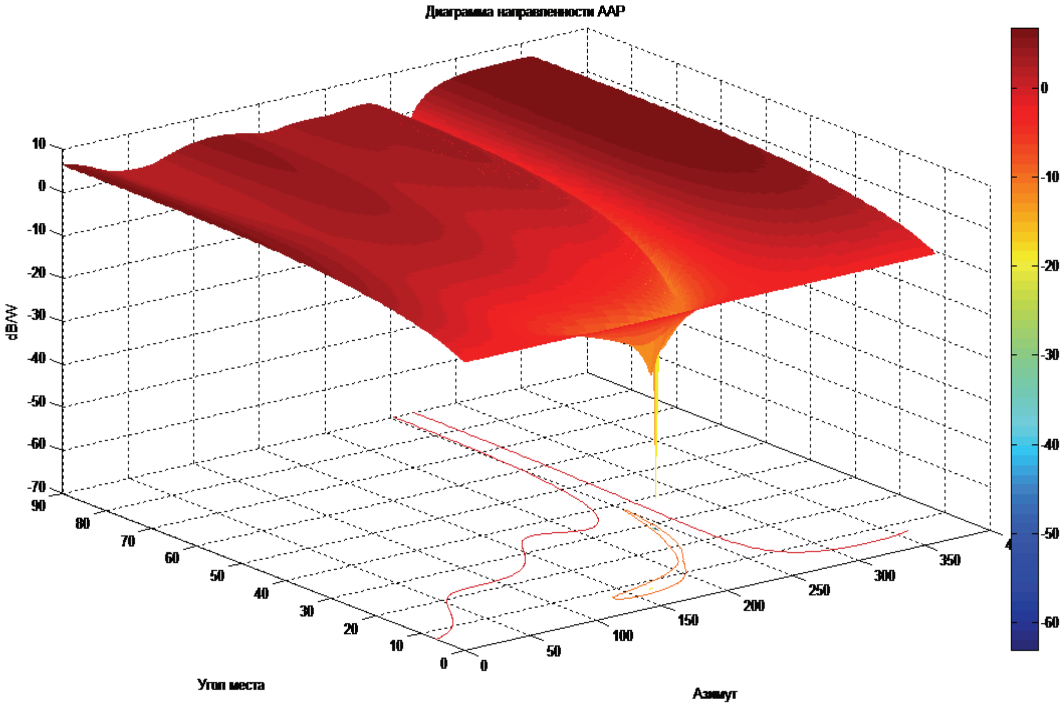

Figure 3

Conclusions

The proposed method allows to calculate the weights to control the pattern AAA GPS systems without knowing the useful signal. These results suggest that the quality of the noise reduction is not worse given in [3].

References

1. Адаптивная компенсация помех в каналах связи / *Ю. В. Лосев, А. Г. Бердников, Э. Ш Гойхман, Б. Д. Сизов* – М.: Радио и связь, 1988. – 208 с.

2. Цифровое формирование диаграммы направленности в фазированных антенних решетках / *Л. Н. Григорьев* – М.: Радиотехника, 2010. – 144 с.

3. Адаптивные антенные решетки: Введение в теорию / *Р. А. Монзинго, Т. У. Миллер* – М.: Радио и связь, 1988. – 448 с.

UDC 681.785.3 (043.2)

M.M. Asanov
O.V. Kozhokhina
A.V. Skrypets, PhD of Tech. Sci.
V.D. Tronko, Dr of Phys. and Math. Sci.
(National Aviation University, Ukraine)

PHOTOPOLARIMETRIC METHOD OF POLARIZATION RADIATION PARAMETERS DETERMINATION

This work is devoted to the development and description of optical radiation Stokes vector components determination method. The method relies on the measurement of ellipticity angle and ellipse azimuth of optical radiation polarization by the photopolarimetric method

Usage of polarization methods for research of different sort of solutions, matters, objects surfaces gives the wide picture of their properties and structure. These methods found application in medicine [1, 2], research of materials surface [3], and also aerospace remote sensing [4 – 6]. There are studies about polarimetric researches of comets [4], asteroids [5], planets moons [5, 6]. During polarimetric researches conclusions about analyzable object properties are done on the basis of the polarization state of its radiation or radiation which interacted with it.

There are a lot of different stokes-polarimeters, which measure all four Stokes vector components *I*, *M*, *C*, *S* [7 – 10]. Some authors think that there are two basic types of diagrams [7, 10]: including polarization transformers with mechanically controlled parameters (polarizers, phase plates and others) and electrically controlled parameters (magnetooptical, electrooptical, acoustooptical cells and others). Work of such stokes-polarimeters is based in forming of equations set which is relative to four Stokes vector components. Radiation intensity, passing through a stokes-polarimeter, at the different azimuths of its component elements is measured for this purpose.

Some authors [8, 9] also sort out the third type of stokes-polarimeters, in which for measuring of Stokes parameters the phase plate rotating with certain frequency is used. During registration of radiation intensity, passed through the rotating phase plate and analyzer motionlessly set before a photodetector, a photoelectric signal is modulated with frequencies, which are multiple of phase plate rotation frequency. This signal carries in itself information about radiation polarization descriptions.

The disadvantages of the first two types of stokes-polarimeters are a necessity of four measurement execution, while changing the azimuths of polarimeter component elements, the optimum values of which calculated for errors minimization. It increases the time of research execution and limits application potentiality of these types of stokes-polarimeters. The disadvantages of multichannel stokes-polarimeters are a presence of large number of component elements, each of which is needed to be orientated with maximal exactness on a certain azimuth, previously calculated for errors minimization.

In the third type of stokes-polarimeters one of the basic errors source is inaccuracy in setting of its component elements on the previously calculated optimum azimuths. In addition, regardless the reducing of measurement duration by these stokes-polarimeters, the received results require considerable time on processing for the calculation of Stokes vector components. Also there are rotating phase plate in the stokes-polarimeter that can decrease reliability of these diagrams during the execution of the prolonged experiments.

But above all, in all types of stokes-polarimeters for Stokes vector components finding intensity is measured, determination exactness of which does not usually exceed 1%.

The photopolarimetric method of Stokes vector components measuring which will allow to raise considerably determination exactness of their relative values is offered in this work.

For polarization radiation parameters determination a photopolarimetric method is offered, basis of which is determination of Stokes vector components relative values through measuring of ellipticity angle ω and ellipse azimuth of optical radiation polarization λ. The offered method of Stokes vector components measuring can be realized, for example, with using of two modulators (see fig. 1) on which by turns control signals are given. As a modulator it is suggested to use the magnetooptical Faraday cell with an yttrium ferrite-garnet crystal. These crystals at the magnetic fields to 80 A/m allow to get the modulation amplitude of polarization plane up to 100^{o}, that enables to work with the low quality optical channels [11].

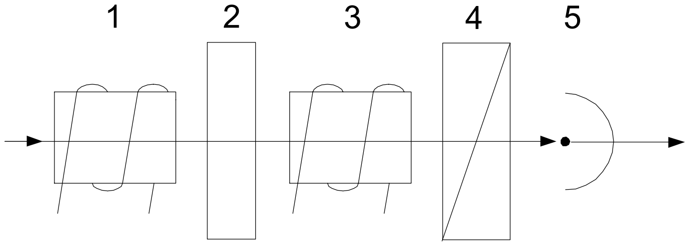

Fig. 1. Block diagram of stokes-polarimeter:
1 – Modulator; 2 – quarter-wave phase plate; 3 – modulator; 4 – analyzer; 5 – photodetector

For λ and ω parameters determination it is necessary to make two measuring. In first case, we orient the most speed plane azimuth of phase plate α in relation to the most transmission plane azimuth of analyzer β on the 90^{o} angle. Control signals will give only on a modulator *1*, a modulator *3* is not connected (see fig. 1). The intensity on analyzer output will be:

$$I_{OUT} = \frac{I}{2}\left[1 - \frac{I'}{I} p' \cos 2\omega \cos 2(\alpha - \lambda + \theta + \theta_{=})\right],$$

where $I = I' + I''$ is the total intensity of incident ray; I', I'' are fully polarized and fully depolarized intensity components of the incident ray respectively; p' is the degree of polarization of modulator; $\theta_{=}$ is the additional polarization plane rotation angle of light, associated to the geometrical defects, retentivity of ferrit; θ is the oscillation angular amplitude of polarization plane vibrations, changing according to the periodic law: $\theta = \theta_0 \Phi(t)$, where $\Phi(t)$ is the arbitrary periodic function, which is vary with time with Ω frequency.

Afterwards adjusting the photopolarimeter on a minimum of the signal on an output, measuring the phase plate azimuth, it is possible to define the λ parameter without knowing the value of ellipticity angle ω:

$$\lambda = \alpha_{\min} + \Delta + \theta_{=},$$

where $\alpha_{\min}$ is the most speed plane azimuth of phase plate, at which the output intensity is minimal; Δ is the measurement error.

The intensity on analyzer output will be:

$$I_{OUT\,\min} = \frac{I}{2}\left[1 - P\cos 2\theta + 2\Delta P \sin 2\theta\right],$$

where $P = pp'p_E = \frac{I'}{I} p' \cos 2\omega$; p is the degree of light polarization in an environment.

For ellipticity angle ω determination we set the most speed plane azimuth of phase plate in the line of major (or minor) axis of polarization ellipse of light. The previous condition is not preserved and control signals are given only on a modulator *3* (see fig. 1). In this case, an expression of the output light intensity will be transformed to the following:

$$I_{OUT} = \frac{I}{2}\left[1 + \frac{I'}{I} p' \cos 2(\omega - \beta + \lambda + \theta + \theta_{=})\right].$$

As well as during determination of the λ parameter, will measure ω, adjusting the photopolarimeter on a minimum of the signal on an output according to the condition:

$$\omega - \beta_{\min} + \lambda + \theta_{=} = \frac{\pi}{2},$$

where $\beta_{\min}$ is the most transmission plane azimuth of the analyzer, at which output intensity is minimal.

The intensity on analyzer output will be following:

$$I_{ВЫХ\ \min} = \frac{I}{2}\left[1 - pp'\cos 2\theta + 2\Delta pp'\sin 2\theta\right].$$

Thereby:

$$\omega = \frac{\pi}{2} + \beta_{\min} - \lambda + \Delta + \theta_{=}.$$

To find all Stokes vector components absolute values it is necessary to define the degree of polarization of the investigated stream p and its intensity I. For this purpose will set a phase plate on a zero azimuth (α=0), and its phase shift on δ=0 (or it is possible to remove the phase plate from the diagram). The intensity on analyzer output will be following in this case:

$$I_{OUT} = \frac{I}{2}\left[1 + \frac{I'}{I}\cos 2\omega \cos 2(\beta - \lambda)\right] = \frac{I}{2}\left[1 + p\cos 2\omega \cos 2(\beta - \lambda)\right].$$

Adjusting the photopolarimeter on a maximum and a minimum of light transmission, will find maximal $I_{OUT\max}$ and minimal $I_{OUT\min}$ intensity on the analyzer output respectively. Expressions for finding of Stokes vector components absolute values are following:

$$I = I_{OUT\max} + I_{OUT\min};$$

$$M = p\cos 2\omega \cos 2\lambda = \frac{I_{OUT\max} - I_{OUT\min}}{I}\cos 2(\alpha_{\min} + \Delta + \theta_{=});$$

$$C = p\cos 2\omega \sin 2\lambda = \frac{I_{OUT\max} - I_{OUT\min}}{I}\sin 2(\alpha_{\min} + \Delta + \theta_{=});$$

$$S = p\sin 2\omega = \frac{I_{OUT\max} - I_{OUT\min}}{I\cos 2\left(\frac{\pi}{2} + \beta_{\min} - \lambda + \Delta\right)}\sin 2\left(\frac{\pi}{2} + \beta_{\min} - \lambda + \Delta + \theta_{=}\right).$$

Conclusions

1. The offered method allows with photopolarimetric exactness, which is up to angular seconds, to determine the relative values of Stokes vector components M, C and S of incident radiation.

2. To find absolute values of all Stokes vector components it is necessary to define fully polarized I' and fully depolarized I'' intensity components of incident ray, that limits measurement exactness to 1%.

3. Usage of the modulator on an yttrium ferrite-garnet will allow to increase exactness of measuring of the ellipticity angle and the ellipse azimuth of polarization, and, consequently, of Stokes vector components M, C and S of incident radiation relative values due to the additional modulation of optical radiation polarization plane.

4. If polarization of incident light ray is circular or near to such, using the offered method is impossible, that is its limitation.

References

1. Застосування оптимізованого класичного поляриметра для визначення вмісту оптично активних речовин в прозорих та темних розчинах / *С. Г. Гарасевич, П. І. Коренюк, Ю. О. Мягченко, С. І. Осипов, О. В. Слободянюк* // Вісник Київського університету, серія: фізико-математичні науки. – 1999. - № 1. – С. 311 – 321.

2. *Рогаткин Д. А.* Об особенности в определении оптических свойств мутных биологических тканей и сред в расчетных задачах медицинской неинвазивной спектрофотометрии / *Д. А. Рогаткин* // Медицинская техника. – 2007. - № 2. – С. 10 – 16.

3. Исследование поляриметрических характеристик оптических дисковых носителей / [*В. В. Петров, А. А. Крючин, С. Н. Савенков* и др.] // Реєстрація, зберігання і обробка даних. – 2009. – Т. 11. – №2. С. 3 – 11.

4. Поляриметрические исследования комет в Крымской астрофизической обсерватории / [*Н. Н. Киселев, В. К. Розенбуш, Н. М. Шаховской* и др.] // Известия Крымской астрофизической обсерватории. – 2007. – Т. 103. – №. 4. – С. 216 – 230.

5. Исследование поляризации излучения избранных высокоальбедных объектов вблизи оппозиции / [*В. К. Розенбуш, Н. Н. Киселев, Н. М. Шаховской* и др.] // Известия Крымской астрофизической обсерватории. – 2007. – Т. 103. – №. 4. – С. 279 – 289.

6. Аврамчук В. В. Фотометрические исследования больших спутников Урана / *В. В. Аврамчук, В. К. Розенбуш, Т. П. Бульба* // Астрономический вестник. – 2007. – Т. 41. – С. 204 – 222.

7. *Шутов А. М.* Оптические схемы устройств измерения параметров поляризованного излучения / *А. М. Шутов* // Оптико-механическая промышленность. – 1985. – № 11. – С. 52 – 56.

8. *Длугунович В. А.* Анализ метода измерения поляризационных характеристик стокс-поляриметром с вращающейся фазовой пластинкой / *В. А. Длугунович, В. Н. Снопко, О. В. Царюк* // Оптический журнал. – 2001. – Т. 68. – № 4. – С. 37 – 42.

9. *Савенков С. Н.* Погрешность определения элементов матрицы Мюллера и ее влияние на решение обратной задачи поляриметрии / *С. Н. Савенков, А. С. Климов, Е. А. Оберемок* // Журнал прикладной спектроскопии. – 2009. – Т. 76. – № 5. – С. 784 – 792.

10. *Савенков С. М.* Стокс-поляриметр на рідкокристалічних комірках: аналіз похибок / *С. М. Савенков, О. С. Клімов, Є. А. Оберемо*к // Вісник Київського університету. Серія: фізико-математичні науки. – 2009. – № 1. – С. 215 – 222.

11. Регистрация угла плоскости колебания линейно поляризованного инфракрасного излучения / *А. И. Ванюрихин, Ю. А. Кузнецов, В. Ф. Майстренко, В. Д. Тронько* // Оптико-механическая промышленность. – 1970. – Вып. 8. – С. 30 – 33.

UDC 621.397.771.537 (043.2)

V.N. Belinsky, Ph.D. lecturer
(National Aviation University, Ukraine)

INFLUENCE SIGNAL/ NOISE IN SEMICONDUCTOR MATRIXES RESOLUTION OF THE DIGITAL REMOTE SENSING SYSTEMS THE EARTH'S SURFACE

We study the method of determining resolution digital remote sensing the Earth's surface to assess the quality digital images

Introduction. Statement of the problem. In [1,2] it was proved that the resolution R of aerophotographic systems (APhS) can be defined as the point of intersection between the through contrast transfer function of the aerial camera $W_s(\nu)$ and the curve of the film threshold contrast $K_c(\nu)$, which is determined by the threshold contrast of a decoder and the filmnoise. The practical implementation of this method has found its development when operating aerial reconnaissance, mapping aerial photography, and aerial surveillance of the Treaty on Open Skies [3]. The resolution of the aviation opto-electronic systems of air surveillance is defined similarly as for the APS (Fig. 1) [4].

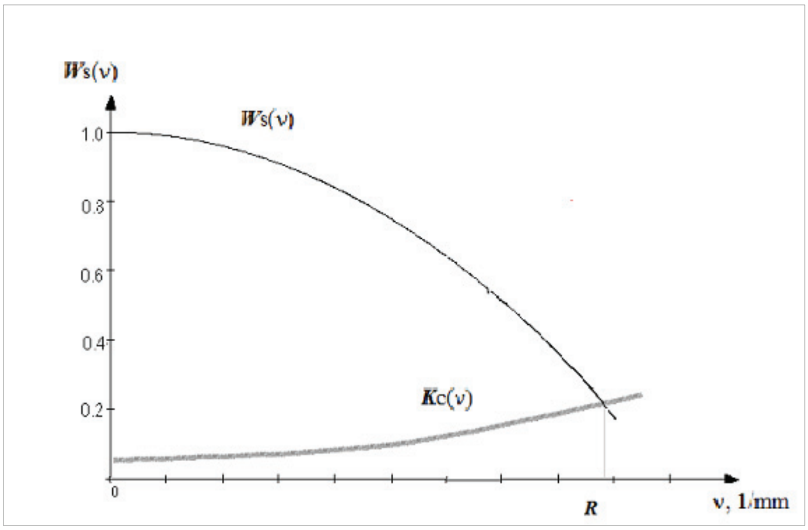

Fig.1. Contrast transfer function of the threshold contrast curve

Analytical interpretation of Fig. 1 has the form shown below :

$$W_s(\nu) = K_c(\nu),$$

$$W_s(\nu) = \sqrt{(0{,}02 \div 0{,}05)^2 + (4 \div 6)^2 D_{\text{ш}}(\nu)/U_{\text{cep}}^2} = \sqrt{(0{,}02 \div 0{,}05)^2 + (4 \div 6)^2 \frac{G_{\text{ш}}(\nu)\nu}{S_{\text{cep}}^2}} \qquad (1)$$

where Dsh and Gsh-variance and power spectral noise; Sser - average signal.

Due to the advent of digital aerial cameras in which the optical image areas are recorded by the semiconductor photomatix, there is a need for scientific justification in applying this method to determine the resolution of digital aerial cameras.

The basic material research,. Semiconductor sensors of video signal are currently being built on the basis of the silicon photodiods matrix or charge-coupled device (CCD). The best parameters and characteristics are possessed by conditioners based on video files - SIP, which turn the light signal (optical image) into electrical signal charges (video). The principle of photo-SIP is based on the properties of the registry, consisting of MOS capacitors that are near located in the line. The transfer of charge packets, the size of which is proportional to the magnitude of exposure is controlled by signal charge transfer by clock pulses [1].

The MOS capacitor (Fig. 1) serves as the basis of photo-CCD.

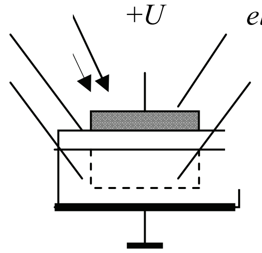

Fig. 2. MOS - capacitor.

The semiconducting silicon substrate, for example p-type, is covered with a layer of silicon oxide dielectric, the thickness of which is $d_0 = 0{,}1 - 0{,}2$ microns, above which the partially transparent metal electrode (gate) is located. Semiconductor substrate and a metal electrode acts as a cover for MOS - capacitor, the specific capacity of which is equal to [4]:

$$C_{\mathrm{SiO_2}} = \frac{\varepsilon_g \varepsilon_0}{d_o} \left[\frac{\mathrm{F}}{\mathrm{m}^2}\right] \quad , \tag{2}$$

where - ε_g relative dielectric constant insulator (silicon oxide). If the shutter apply the benefits of the conservation of charge $+U_{\mathrm{vs}}$ (voltage storage), the minority carriers (electrons) will gather directly under the electrode near the surface of the semiconductor and the major carriers (holes) will move into the interior volume of the semiconductor, because they will be repelled from the electrode. Thus, a free mobile hole depleted region depth ℓ_0 will appear under the electrode on the boundary oxide - semiconductor. In this region, called a pit potential, the charge density is:

$$\rho_{\mathrm{ch}} = -q_{\mathrm{e}} N_{\mathrm{a}} \quad ,$$

where N_{a} - the concentration of acceptor; q_{e} - the electron charge. The distribution of potential within the depleted region along the axis Ox can be obtained by the decision of Poisson equation:

$$\frac{d^2U}{dx^2} = -\frac{\rho_з}{\varepsilon_{Si}\varepsilon_0} = \frac{q_e N_a}{\varepsilon_{Si}\varepsilon_0} \quad , \tag{3}$$

where ε_{Si} - relative dielectric constant of silicon (semiconductor).

Integrating, equation (3) with boundary conditions at, $U_{\ell_0} = 0$, $U_{\ell_0} = 0$, $0 \le x \le \ell_0$ $dU/dx = 0$ (2) we obtain the potential distribution in the form:

$$\varphi(x) = \frac{q_e N_a}{2\varepsilon_{Si}\varepsilon_0}(x - \ell_0)^2 \ ,$$

where ℓ_0 - the so-called deep potential well.

The potential on the boundary of separation $(x = 0)$ is called the surface potential:

$$\varphi_S = \frac{q_e N_a}{2\varepsilon_{Si}\varepsilon_0}\ell_0^{\,2} \ . \tag{4}$$

When the equilibrium conditions according to Kirchhoff law can be written, the potential charge saving package:

$$U_{\mathrm{chp}} = U_{Si} + U_{SiO_2} \tag{5}$$

where U_{Si} and U_{SiO_2} - the voltage drop in silicon and its oxide, respectively.

Given that

$$U_{Si} = \varphi_S + \varphi_{\mathrm{ppc}} \quad \text{and} \tag{6}$$

$$U_{SiO_2} = \frac{q_e n + q_e N_a \ell_0}{C_{SiO_2}} \quad , \tag{7}$$

where φ_{ppc} - the potential of a plane curve of the bottom of the valence band. Combining (4) - (7), we obtain:

$$U_{\text{chp}} - \frac{q_e n}{C_{SiO_2}} = \varphi_S + \varphi_{\text{пчк}} + \frac{\sqrt{2q_e N_a \varepsilon_0 \varepsilon_{Si} \varphi_S}}{C_{SiO_2}} \quad , \tag{8}$$

When completely filled potential well $n = n_{\max}$, and the conductivity of the surface inverted, that is two the potential of the Fermi level:

$$\varphi_S = 2\varphi_F \tag{9}$$

Substituting (8) in (7) and given the fact that in practice the left hand side of (7) is always much more right, the expression for the maximum surface density of carriers in filled potential well will look like:

$$n_{\max} = \frac{C_{SiO_2} U_{\text{chp}}}{q_e} = \frac{\varepsilon_g \varepsilon_0}{q_e} \cdot \frac{U_{\text{chp}}}{d_g}, \tag{10}$$

$$n_{\max} \approx 2 \cdot 10^4 \frac{\text{electrons}}{\text{microns}^2}. \tag{11}$$

For a typical size of the square potential well bottom ($A_{\text{p}} = 10 \times 20$ microns) possible maximum number of electrons in the pit will be:

$$N_{\max} = n_{\max} A_{\text{p}} \approx 4 \cdot 10^6 \quad . \tag{12}$$

If the minimum possible $C_{SiO_2} = 0{,}07\text{pF}$ and $d_o = 100\text{microns}$ the depth of potential well ℓ_0 is located within a few micrometers.

Suppose that a MOS - capacitor from the gate drops optical radiation with a wavelength λ , creating energy light $E_{e,\lambda}$. Then the radiation flux absorbed by the potential pit is equal $\Phi_{e,\lambda} = E_{e,\lambda} A_я$. This flow corresponds to the number of photons absorbed per second

$$N_{\text{ph}} = \frac{\lambda \Phi_{e,\lambda}}{hc} = \frac{E_{e,\lambda} A_{\text{p}} \cdot \lambda}{hc} \quad , \tag{13}$$

where h = 6,62 $*10^{-34}\,\text{J} \cdot \text{c} -$ Planck's constant; *c*-speed of light in the semiconductor, m / s. Multiplying (12) during the accumulation of charges (exposure time $t_{\text{н}}$) and quantum efficiency η_λ, we obtain the number of electrons accumulated in the potential dep well (charuntsi):

$$N_e = \frac{E_{e,\lambda} A_{\text{p}} \lambda t_{\text{н}} \eta_\lambda}{hc} = \frac{E_{e,\lambda} A_{\text{p}} t_{\text{н}} \lambda \eta_\lambda}{hc}. \tag{14}$$

Calculations show that the conditions for the earth's surface of signal electrons in charuntsi 2-3 is hundreds of thousands.

If this minimum number of electrons is limited to the influence of noise ($N_e = N_{\min}$), then dividing $N_{\max}$ by $N_{\min}$, we get the dynamic range $N_{\max} / N_{\min}$ of MOS - capacitor.

The minimum signal package that can be gained charuntsi determined noise level [3].

CCD noise at low light levels measured value of noise equ ivalent signal induced threshold number of photons, which provides the output of signal / noise ratio - $S / N = 1$.

Noise CCD can be determined analytically, given the noise of the following sources: noise Naykvysta address key and reset key of dispersion noise charge $Q_n^2 = k_{\text{B}} TC$ - where C - capacity potential well for noise at the output key, and T - the absolute temperature MOS - capacitor, noise and on the surface intensive traps in the sensitive element and the shift register having a variance $Q_n^2 = k_{\mathrm{B}} T C_t$, where C - effective capacity traps, shot noise detector and register shift is due to dark current -$Q_n^2 = eI_{\mathrm{T}} t_{\mathrm{н}}$, where $t_{\mathrm{н}}$ - time savings, and $I_{\mathrm{т}}$ - current termoheneratsiyi and e - electron charge; noise resulting from the inefficiency of the transfer $\varepsilon_{\text{н.п.}}$, with dispersion $Q_n^2 = \dfrac{1}{(1-\varepsilon_{\text{i.t.}})^{n_{\mathrm{t}}}}$.

In this way noise charge packet

$$N_{\mathrm{ш}} = \mathrm{N}CP_{\mathrm{CCD}} = \frac{\left[k_{\mathrm{B}} T (C + C_t) + eI_T t_H\right]^{1/2}}{(1-\varepsilon_{\text{i.t.}})^{n_{\mathrm{t}}}} \quad , \tag{15}$$

where n_{t} - the number of transfers charge packets. *NEP* not be less noise Naykvysta key reset, the average noise charge is equal to 200 electrons in the original containers $0{,}25 \cdot 10^{-12}\,\mathrm{F}$. To significantly reduce noise reset using a special method of signal processing method called double korrelovanoyi sample the essence of which is that of output voltage noise is subtracted $1/f$. As a result, there is separation of noise from the reset signal charge and simultaneously eliminated the noise type

Thus, one can say that the noise level (rms) in current photo-CCDs, operating at frequencies ΔB = 5-10 MHz (= 1/25-1/30 s), is dozens of electrons. And the noise variance - a few hundred electrons. That is, the value of the minimum video signal ("black” level) N_{bl} =10 - 30 electrons, and the amplitude of the spatial harmonics - $N_s = (N_{wh}-N_{bl}) / 2$, and the level of middle-$N_m = (N_{wh} + N_{bl})/2$.

The inertia of the CCD is determined by the transit time of carriers under the gate, c: a person

$$\tau \approx \frac{b}{2\mu E}, \tag{16}$$

where b - size of the electrode along the direction of charge transfer package, m; μ - mobility of minority carriers; E - the accelerating electric field, V / m Then the bandwidth is, Hz:

$$\Delta B = \frac{1}{2\tau}. \tag{17}$$

Velocity of a charge coupled package is equal to, м/s:

$$\upsilon = \frac{\Delta B}{\Delta \nu}, \tag{18}$$

where $\Delta\nu = 1/2b$ - spatial bandwidth in the CCD matrix plane, мм^{-1} .

Conclusion

Thus, substituting the value $G_{\mathrm{ш}} \Delta \nu = D_{\mathrm{ш}} = N_{\mathrm{ш}}^2$ та $S_{mid}^2 = N_s$ to (1), one can determine the resolution of any digital aerial camera.

References

1. *Jones R.C.*, J. Opt. Soc. Am., 50, 883 (1960**)**

2. *Х.Фризер***.** Фотографическая регистрация информации. – М.:Мир, 1978. - 427с.

3. *T.Orhaug* , *C.Hugo Agren*. F0A Report C , 30666-9.4. September, 1992. - С.22.

4. *Белинский В.Н. Поздеев С.Т.* Авиационная оптико-электроника и светотехника. - К.: КВВАИУ, 1988. - 319 с.

5. *Хромов Л.И., Лебедев Н.В., Цыцулин А.К., Куликов А.Н.* Твёрдотельное телевидение. - М.: Радио и связь, 1986. -185с.

6. Цифровое преобразование изображений: Уч. пособие для вузов/*Быков Р.Е., Фраер Р., Иванов К.В., Манцветов А.А*; под ред. проф. *Р.Е. Быков*а.-М.: Горячая линия - Телеком, 2003. - 228 с.

7. *Бєлінський В.М.* Вплив характеристик напівпровідникових датчиків відеосигналу на якість телевізійного зображення. Зб. Матеріали Міжнародної науково-практичної конференції „Україна в Євроінтеграційних процесах”. – К.: КиМУ. 2007. – С. 26-31.

UDC 331.101:629.735 (043.2)

Y.V. Hryshchenko , PhD of Tech. Sci,
E.M. Hohlov,
V.M. Himin,
Y.Y. Hryshchenko
(National Aviation University, Ukraine)

FLIGHT SAFETY AND HUMAN FACTOR: NEW APPROACH TO PREVENTION OF AVIATION INCIDENTS

This article includes results of new concepts analysis of flight safety

Nowadays ICAO pays more attention to development of new approaches to flight safety and prevention of aviation incidents caused by human factor (faults of the flight crew).

But practice of the latest crashes (Smolensk, Yaroslavl, Indonesia and others) has shown that although there is an attempt to apply new systems of flight safety control on basis of Safety Management Manual, but actually flight practice of crashes investigation is not changed qualitatively.

We represent new approach to prevention of aviation incidents that allows qualitatively change part of incidents caused by human factor and exclude incidents caused by it (fig 1-3).

The approach is analytical, generalizing with new means and new aviation concepts (table 1).

New approach to prevention of aviation incidents caused by human factor (faults of the flight crew) [1]

All nowadays methodologies of flight training and professional training are divided into actions, operations and moves [2].

To the psycho-physiological characteristics of aviation operators the increased requirements on endurance, reaction time, coordination of movements, high noise immunity are demanded. Future specialists must have a strong, balanced and moving nervous system. From a medical point of view they must be able for a work by the health state in their chosen specialty, and from the social – must have a highly developed responsibility for the timeliness and accuracy of their decisions and actions.

During all times the flight processes were the central aviation processes. And also they were preceded by the high negative phenomena and effects. But the main direction in developments in theory of flights safety is explaining of the reasons for the appearance of emergency situations caused by human factor guilt.

I stage

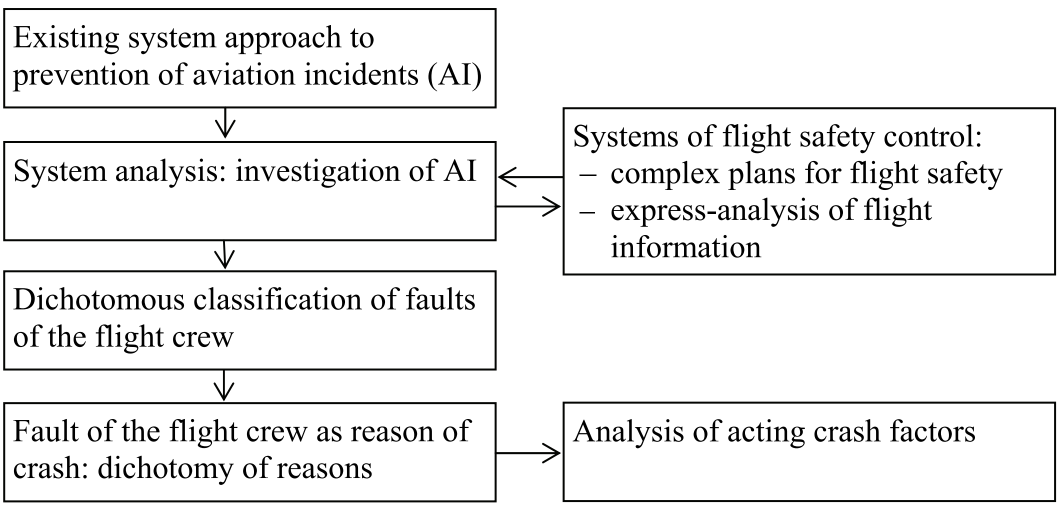

Fig. 1. New approach to prevention of aviation incidents caused by human factor (faults of the flight crew) - I stage.

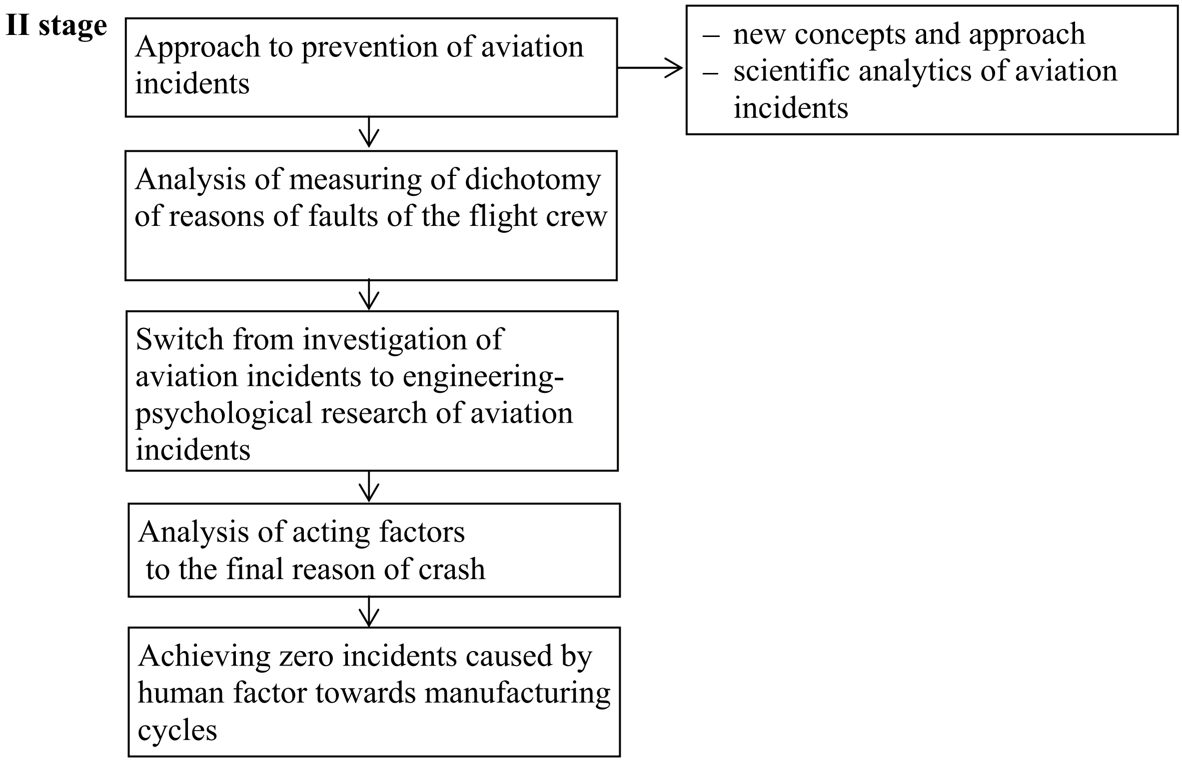

Fig. 2. New approach to prevention of aviation incidents caused by human factor (faults of the flight crew) - II stage.

Considering this question in own researches and publications [1-5], and also relying on statistical data found that about 70% of pilots do not oppose to the factorial loads (FL) (complex failures), which lead to negative consequences such as wrong actions of a pilot in extremely situations; disproportionate and sudden actions by all flight parameters; enter beyond the physiological possibilities. And as a result the pilots unknowledge of way to counteract to factorial loads can lead to flight events, especially at the difficult flight conditions.

At the action of factor loadings there is found a negative phenomenon of a dynamic stereotype amplifying (PDSA) [3-5]. To detection of which is possible by the comparing of the pilot dynamic stereotype (DS) (on the simulator) at the "flight" without failures with its DS under the action of complex failures. That is, if during the process of flight training to achieve the PDSA removal and elimination and to prepare crews to act in extreme situations where they are acted by FL, the human factor in aviation accidents may be decreased.

To increase the general level of safety it’s necessary to review, analyze and systematize the ways to improve the pilots flight training and their indicators and criteria.

One of way to improve the pilots training effectiveness is the selection of operators by the criterion of counteraction to FL through elimination of PDSA.

To detect PDSA of a pilot it’s necessary to compare his flights under the FL action (complex failures on simulators) and at their absence, at following PDSA elimination by showing of this phenomenon presence for its removal during the next flights. That’s why the program for detection of negative PDSA in order to increase flight safety (FS) by HF is necessary.

For the successful operators training to FL counteraction it is necessary to understand the nature of the bilateral process of aircraft.

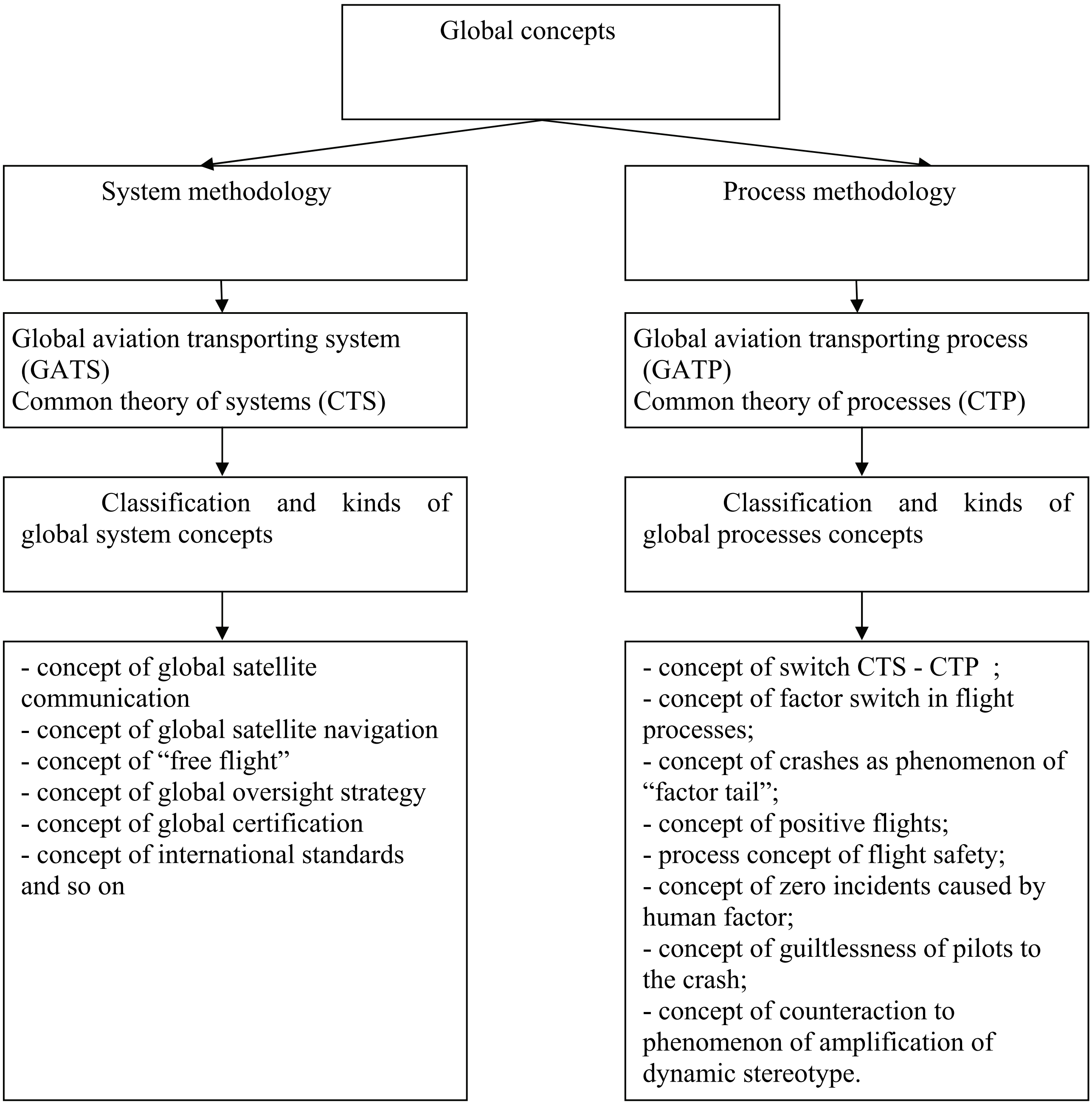

Fig.3. New global aviation concepts that are basis of new approach.

According to curves types, that fix the motor dynamic stereotype (DS) due to the flight parameters changes, under the action of FL and their absence it’s possible to judge about the quality of piloting technology, and do not to identify the deviations from the tolerances. The DS can be divided on to favorable (flight handwriting) and not favorable in the case PDSA occurrence that in any case must be eliminated. However, even during the stage of DS formation, knowing its typical species, it’s should be formed the favorable DS, although it doesn’t in any case exclude the studying for elimination of the negative PDSA.

Counteraction to FL by the way of PDSA elimination does not mean that the operator must simply stop any motion by the control organs. During DS analysis we consider the final result of quality of piloting technique in real and training flights under the influence of environment (at the simulators by own desire the influence of environment can be excluded). The influence force of vertical air flows turbulence and the pilot skill can be defined, for example, by ailerons deflection (δ a) and by parameter of bank angle (γ) on the airplane [2-4].

Table.1

General characteristics of global concepts GATP in the process approach in 1998

№	Type of global concept	General characteristics of area of application
	Concept of switch CTS - CTP	It is necessary for taking into account a cyclic recurrence of scientific progress while switch from 20 to 21 century
	Concept of medius terminas of flights as processes	Centralization to statistics of processes
	Process concept of flight safety	Elimination of negative evaluation of flight safety in the end of 20 century in regions and aviation companies
	Concept of crashes as phenomenon of "factor tail"	Elimination of crashes not as event but as phenomenon by classification of Hohlov
	Concept of classification of positive flights	Taking into account of results (effects) of flights without remarks
	Process concept of flying automatic electronic complex	Representation of processes of new generation aircraft
	Concept of zero incidents by human factors	Eliminating of system reasons of crashes (75-90%) by crew actions to zero level
	Concept of guiltlessness of pilots for the crash	Elimination of fault of flying crew to crash and switch to constructive-technological concept of causality
	Concept of amplifying of dynamic stereotype of pilots	Stress decreasing of flying crew on basis of antistress training

Conclusions

1. On basis of developing Safety System Management Manual, which are old complex plans, with help of which, as 50 years practice showed, it is impossible to change negative results of crashes .
2. For positive qualitative changes in statistics of flight safety, new progressive methods generalizing existing approach of process analysis are needed
3. Applying of suggested approach can let reaching of zero index of incidents caused by human factor while technical cycles.

References

1. *Хохлов Е.М.* Авторский процессный подход. Хохлов Е.М., Аль-Аммори Али. – Киев: "Издательский дом "Компьютерпресс". – 2010, – 176 с.
2. *Олейник В.Г.* Предотвращение авиационных происшествий. Кременчугский лётный колледж. -1995. – 91с.
3. *Грищенко Ю.В.* Подготовка пилотов к полетам в особых ситуациях с учетом явления усиления динамического стереотипа» // Кибернетика и вычислительная техника. К.: НАН Украины. – 2003. – Вып. 139. С. 81-85.
4. *Грищенко Ю.В.* Парные полеты как способ анализа явления усиления динамического стереотипа у пилотов. // Кибернетика и вычислительная техника. К.: НАН Украины. – 2003. – Вып. 140. С. 31-34.
5. *Грищенко Ю.В.* Анализ изменения динамического стереотипа пилотов в процессе лётной подготовки на комплексном тренажёре самолёта. // Кибернетика и вычислительная техника. – К.: НАН Украины, 2004. – Вып. 142. С. 35-40.

UDC 331.101:629.735 (043.2)

V.D. Gulenko,
Y.V. Hryshchenko, PhD of Tech. Sci.,
V.O. Rogozhin, PhD of Tech. Sci.
(National Aviation University, Ukraine)

PROBLEMS OF PILOTS LOSING THEIR SPATIAL ORIENTATION BECAUSE OF AIR TRAFFIC CONTROLLER COMMANDS

The issue of interaction between air traffic controllers and aircraft crews with possible crew errors is discussed. The method of flight model modular transformation is considered required for aircraft large angle banking analysis taking into account the use of factor flight model allowing to drop down the accident rate.

Introduction. Currently, the human factor impacting civil airline flight safety is gradually increasing. Many authors have shown that human errors comprise about 90 % of flight accident causes, and this means the problem is critical. At the same time, aircrafts are among the most reliable and safe transport means, and aircraft accidents are just events of low-probability.

Formulation of the Problem.

The process of air transporting includes various services. One of the most important services is the one controlling air traffic by giving instructions to aircraft crews. Intensive air traffic may force an air traffic controller to instruct an aircraft crew to alter their heading sharply which requires large angle banking.

The banking angle required for horizontal alter heading maneuvering is determined by turn angle (TA) equal, numerically, to the difference between the heading Ψ_s set forth by the air traffic controller and the current aircraft heading Ψ_c (fig.1), that is AT= Ψ_s - Ψ_c .

Successful execution of the traffic controller command is only possible with minimum aircraft turning radius. Execution of the command with no altitude drop is determined by the relation

$$R_p = \frac{V^2}{gtg\gamma_t} \tag{1}$$

Whetre V is flight speed, g is free fall acceleration, γ_t is the turn banking angle when changing the heading as set forth by the traffic controller.

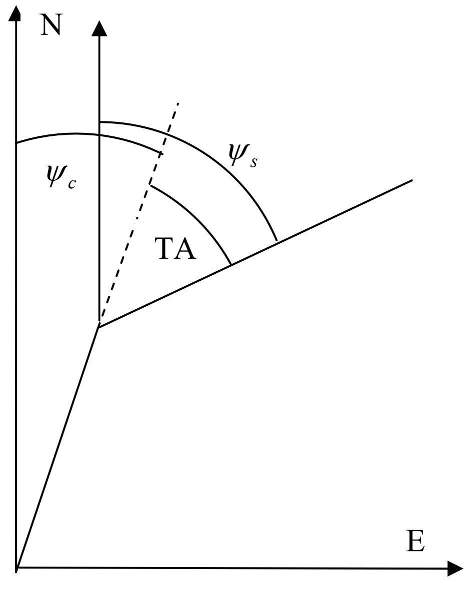

Fig.1 The banking angle required for horizontal alter heading maneuvering

Note that $tg\gamma_t$ is equal, numerically, to the acceleration factor (overloading) impacting the aircraft in horizontal plane.

The expression (1) yields that, for a given flight velocity, ensuring minimum turn radius requires large banking angles, which means large banking angle required to perform such a turn.

In automatic control systems of modern aircrafts, the γ_s, value is generally restricted at low altitudes, for safety, by the value of 15 degrees, while at mid or large altitudes it may reach 30 degrees. When maneuvering in horizontal plane following the traffic controller commands for sharp heading change, the aircraft crew chief shall change to manual control and change the aircraft heading at maximum possible banking.

Let us consider some avionic specificities of such maneuvering. We found that incorrect instrument readout may cause losing spatial orientation (LPO) by the aircraft crew, especially in a new generation aircraft equipped with a direct reading gyrohorizon. Our study has shown that for aircrafts with such reading type, the risk of crossing the LPO threshold is 5.75 times as high as that of aircrafts with reverse reading gyrohorizons. That is, it may be stated that the risk of crossing the LPO threshold for a B-737 aircraft is nearly 6 times as high as that of Il-62M (based on real data used for the comparison).

To prevent such situations, we are proposing a method of modeling the situation of an aircraft crossing the LPO threshold. The method makes it possible, based on analysis of regular flight data, to predict probability of crossing the LPO threshold for a specific crew. If there is such probability, the crew shall be subject to some anti-stress procedure aimed to lower the risk [1].

It is worth to note that currently, much consideration is being given to the LPO issue [2] with sharp publication growth.

Previous researches carried at the Avionics Department have shown that factor errors may cause syllogisms in navigation task solutions [3].

We have shown that it may be possible to use existing mathematical approaches for determining right or left banking risk, but there is no possibility to calculate the risk of losing the banking direction. This is the intrinsic disadvantage of the risk measuring method. We proposed a new method of modeling and assessment of losing the banking angle direction by flight crews with use of modular distributions of flight parameters [1].

Modular Transformation Method.

Modeling with large banking angle (LBA) modular distributions is not only a means of LPO elimination, but also a rather effective prediction method for prevention of flight accidents caused by LPO based on additional analysis (using the procedure included) of data acquired from express analysis of flight data interpretations. It is well known that such primary flight parameter analysis is performed with no functional transformation of the main flight parameters (banking, pitch, heading, altitude, etc.) as random values.

The primary analysis, as has been said already, is based on double-way tolerances in compliance with flight restrictions, with the aircraft control rules not spreading beyond the scope of direct analysis for these parameters or their angular values registered by the aircraft control unit.

However, to solve the problem of light crews losing their LPO, it is necessary not only to use direct flight parameter processing in various coordinate systems but processing with functional transformations of alternating sign parameter moduli or other transformation of random parameter value deviations in flight [4, 5].

Figs. 1 and 2 show distribution types for various aircraft types (B-737 and Il-62 M). It is evident from the figures that these logarithmically normal distributions are qualitatively different in their canonical part widths and “tail” characteristics (“tail” length and area, “tail” effect levels, etc.)

In real flights, modular distributions vs. maximum banking occurred to be logarithmically normal. However, it is worth to note that replacing modular distributions with modular ones and additional transformation of distribution rules are rather complex in their structures and transformation nature. Actually, modular distributions are heterogeneous, in relation to source distribution mean-square deviation (dispersion): the larger dispersion is associated with the modular distribution that is closer to a logarithmically normal one. For an example, let us consider an experimental data array γ_{max} for selection of a theoretical distribution.

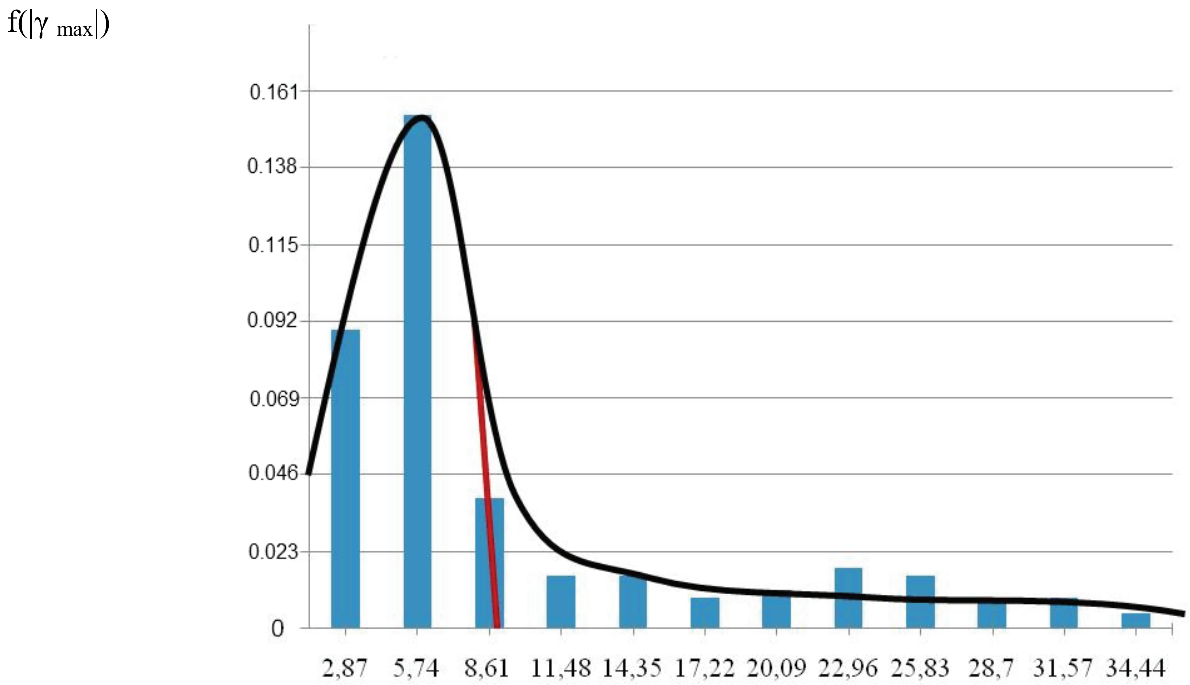

Fig. 1. Distribution density of flights vs. module of maximum banking angle (γmax in degrees) for approaching Boeing-737

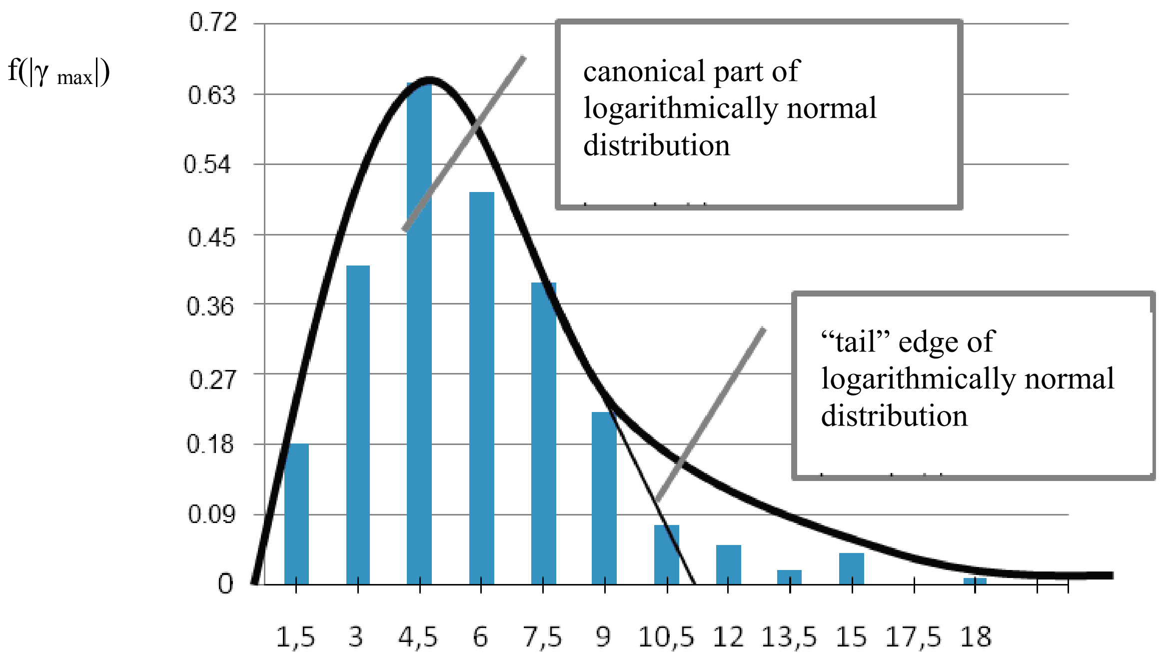

Fig. 2. Distribution density of flights vs. module of maximum banking angle (γmax in degrees) for approaching Il-62 M

Conclusions

1. Taking into account that flight crews lose banking changing direction at large banking angles, modular transformations ought to be used for the mathematical model. Modular values allow to introduce uncertainty in determination of LBA direction.

2. An important aspect of the LPO problem solution is measuring LBA risks using modular distributions to prevent flight accidents.

3. Modular statistical and probabilistic flight distributions, when using aircrafts of various generations, make it necessary to consider two types, alternating sign and index, of warning when flying at large banking angles.

4. With alternating sign warning, determination of LBA direction is an automatic function, while with index warning it is the task of the crew increasing their workloads and the LBA risk.

5. Asymmetry of modular distributions makes it possible to discriminate distribution canonical (normal) parts and “tails”. Taking into consideration that the logarithmical distribution “tail” bears information about large flight parameter deviations and, hence, large banking angles, it becomes possible to measure LBA risks via proportion of canonical and “tail” distribution parts.

6. Modular distribution flight parameters are, in their probabilistic nature, logarithmically normal rules of certain asymmetry having logarithmic distribution “tails”.

7. When analyzing the new model of error causality, it becomes necessary to use generalised variation approaches, the mathematical apparatus used for analyzing maximum deviation parameters over the areas of enforced Sechenov’s reflexes.

References

1. *Гуленко В.Д.* Моделирование и оценка визуальной потери направления угла крена летными экипажами по модульным распределениям параметров полета // . В.Д. Гуленко, Ю.В. Грищенко, В.М. Грибов // Кибернетика и вычислительная техника: Межведомственный сборник научных трудов. – К.: Вид. дім "Академперіодика" НАН України, 2010. – Вып. 160. – С. 43-56.

2. *Овчаров В.Е.* Вечная проблема. ISSN 0235-5000 Проблемы безопасности полетов. - 2009. №. 1. - С. 43-48.

3. *Грищенко Ю.В.* Организация снятия явления усиления динамического стереотипа на комплексном тренажере самолёта в учебно-тренировочном центре // Ю.В. Грищенко, Н.Ф. Дмитриченко, А.Г Ревук // Проблеиы эксплуатации и надежности авиационной техники: Сб. науч. Тр.- К.: КМУГА, 1998. – С. 15-17.

4. *Гуленко В.Д.* Новые подходы к оценке сигнализации больших углов крена на воздушных судах различных поколений. – Материалы IX международной научно-технической конференции «Авиа – 2009». - К.: НАУ, – 2009. – С.12.13 – 12.17.

5. *Пленцов А.П.* . Решение проблемы "потеря пространственной ориентировки лётчиком в полёте"// Мир авионики. Журнал российского авиаприборостротельного альянса. - 2002. - №2. - С.30-32.

UDC 351.814.2 (043.2)

O. V. Kozhokhina,
O. P. Klimenko,
S. I. Rudas
(National Aviation University, Ukraine)

INFORMATION STRESS FACTORS AND DIAGNOSIS TECHNICS FOR AIR TRAFFIC CONTROLLERS

The features of the information stress and the factors that cause them are considered. Biochemical and physiological markers for stress determination are studied.

Stress is often considered as a particular functional state and at the same time as a psycho-physiological reaction of organism to environmental influences that go beyond the boundary of adaptive rules.

The term "stress" was created by Hans Selye in 1929. Originally, Selye used the term "stress" to describe the totality of all non-specific changes (inside the organism), functional or organic. One of his last definitions of stress is that "non-specific reaction of the organism to any demand from the outside" (Selye, 1974) [4].

Thus, in general, stress is a nonspecific component of adaptation, which plays a catalytic role to attract energy and plastic resources for adaptive alteration of the organism.

The stimulus that causes the stress reaction is called a stressor. Due to the features of the stimulus, there are at least two versions of stress: physical (physiological, with one signal) and psycho-emotional (with two signals).

The problem of stability and reliability of the human operator in the conditions of extreme factors and the development of psychological distress has attracted a great attention and gained some shapes as an independent area of research due to the development of technology, automatic control systems, and especially the computerization of all spheres of activity [3].

The operator's profession in the system of air traffic control (ATC) is characterized by high psychological-emotional and intellectual orientation, and is one of the most stressful and emotionally intense types of professional activities. The operator's performance and its ability to carry out the work on time and accurately depends not only on the capacity of the air traffic control system, and the safety in general.

Activities of ATC operator is associated with the periodic, sometimes quite long and intense exposure of (or the expectation of exposure) the extreme values of professional, social, and environmental factors. This exposure is accompanied by negative emotions, overstrain of physical and mental functions and activity degradation. Psychological stress is the most characteristic mental state, developing under the influence of ATC factors.

Development of stress in the extreme conditions of operator's activity can be also connected with the possibility, expectation, the threat of exposure of various stimuli of physico-chemical, psychological (personal), organizational and professional nature on ATC operator. On this basis, this condition can be regarded as a typical form of professional stress. On the other hand, the features of the regulatory mechanisms of this mental state can be referred to the category of psychological stress.

These studies show that in the conditions of influence of the extreme values of information professional factors on the ATC operator the changes in biochemical reactions, a number of physiological functions and some psycho physiological parameters specific for the effects of physical and chemical stressors and which are non-specific adaptive response of the organism were observed.

Non-specific adaptation processes under the extreme exposure of information factors allow us to consider the development of mental state as an information stress of ATC operator.

This kind of stress can be defined as a state of increased mental stress, with symptoms of functional somatic and mental disintegration, negative emotional experiences and performance disturbance resulting from adverse effects of factors of information interoperability of specialist in his professional activity.

Information stress - is a state of ATC operator that is the result of information overload, when he cannot cope with the task, has no time for correct decisions in the required tempo with a high degree of responsibility for the consequences of decisions.

The most common factors causing stress of the information content in the process of professional activity of ATC are:

- Semantic - a) lack of information, b) contradictory information, c) the subjective complexity of the problem, d) low subjective probability of information entry and perception, e) the subjective information risk, f) the redundancy of information, g) the subjective complexity of the problem, h) subjective uncertainty of the presented information, etc.
- Temporal - a) lack of time, b) a high rate of information presentation, c) arrhythmy of the information presentation, d) the uncertainty of the received signal time (unexpectedness), e) increasing information flow, and f) increasing rate of the information presentation, etc.
- Organizational - a) a low probability of an objective presentation of information, b) the objective uncertainty of the moment of information presentation, c) wrong choice of necessary information, d) attention distraction, e) signal omission, f) combined activity, g) the objective complexity of the problem, h) an objective danger of the situation, etc.
- Technical - a) the refusal of the information system, b) interferences in networks, c) signal lock, d) signal shutdown, e) information distortion, f) false information, g) signals interference, h) a contradiction of information signs of the situation, i) insufficient graphic structuring of information, j) mismatch of signal information characteristics etc [2].

How does the information stress express? It is known that the manifestation of the response reactions on the psychological stress can arise depending on the functional system of response and processes that form the behavior of the individual organism during the interaction with the environment.

The difficulty of stress determination has the ambiguity of understanding. Considering the literature definitions of stress, it is assumed that the term stress is not determined by the reaction, but a state of homeostasis, providing the necessary human activity in certain environmental conditions. Stress response is the change of activity level under the influence of various stressors [1].

Biology has progressed in this field greatly, elucidating complex biochemical mechanisms that appear to underlie diverse aspects of stress, shining a necessary light on its clinical relevance and significance.

Despite this, science still runs into the problem of not being able to settle or agree on conceptual and operational definitions of stress. Because stress is ultimately perceived as a subjective experience, it follows that its definition perhaps ought to remain fluid. For a concept so ambiguous and difficult to define, stress nevertheless plays an obvious and predominant role in the everyday lives of humans and nature alike.

There have been many attempts to identify the most sensitive indicators (markers) of psychological stress both biochemical and physiological one. It is noted that the sharp changes occur in the individuals whose level of these constants was higher or lower than the rest. Although the biochemical and physiological indicators of emotional stress reaction are individually very variable, however, we select some of them, with a help of which it will be possible to determine the stress on ATC operator.

The indicators (markers) of heart rate and galvanic skin reflex are the most informative. These two indicators of emotional stress experience the impact of the basic components of emotional reaction (need intensity and prognostic efficiency estimation directed for its satisfaction).

As for the biochemical markers, we can use hemoglobin level of bilirubin and glucose in the blood of ATC operator.

During the stress the hormones (cortisol, epinephrine) come into the blood which rapidly exceeds the level of glucose due to its release from the liver (liver is a place of glucose storage in a modified state - glycogen). This phenomenon is a protective reaction of the organism. As the glucose is the main source of energy, it provides a high level of the body's ability to respond the external stimulus. Consequently, even at the slightest stress a significant hyperglycemia can be observed. When the stress passes, the glucose level returns to normal.

Information stress causes marked reduction of the affinity of hemoglobin for oxygen in the blood, which in turn increases the oxygen tension in hepatocytes and activates free-radical processes in the liver microcosms. Therefore, the hemoglobin level reduces, and at long-term effects of stress level of bilirubin increase.

Laboratory tests of blood, built on invasive techniques are associated with patients traumatizing, the possibility of infection, as well as a fairly lengthy procedure of obtaining a diagnostic result. Therefore, to diagnose the state of air traffic controller it is preferable to use non-invasive methods for determining blood parameters that are superior to laboratory efficiency, effectiveness and economy.

Therefore, a combined non-invasive electro-optical device hemobiliglyukometr (HBG-1) was developed for the diagnosis of adverse effects and stress on the operator’s body. It incorporates new approaches to the processing and correlation of the received information, as well as ergonomic design was developed [6].

Non-invasive measurement of blood parameters such as bilirubin, hemoglobin and glucose in combination with psycho-physiological tests will allow to fully characterize the state of the air traffic controller and depending on the received load improve the efficiency of their operation.

The study of information stress problem in the activity of ATC operators related with the need to clarify the role of various information factors in the formation of the state of stress and mental mechanisms of regulation of this state, the value of personal psychological characteristics in its development, individual susceptibility and the resistance to the stress factors effects, etc.

Identification of psychological patterns of information security activities of the ATC operators, psycho-physiological processes of regulation of labor activity in its interaction with the means of information display and control, and the development of principles and guidelines of reliability support should be the subject of productive researches.

The study of the causes of information stress and mechanisms of their formation will help to reduce their impact on the ATC’s body, thereby enhancing his professional reliability.

References

1. *Бодров В. А.* Информационный стресс: Учебное пособие для вузов. — М.: ПЕР СЭ, 2000. — 352 с.
2. *Калиновская Н.А., Устимов Д.Ю.* Информационно-психологическая безопасность личности как качественная характеристика информационной культуры человека: Монография.– Казань.:2006. –
3. *Дьяченко М.И.* О подходах к изучению эмоциональной устойчивости / М.И. Дьяченко, В.А. Пономаренко // Вопросы психологии. - 1990. -N1 - С.106-116.
4. *Китаев-Смык Л.А.* Психология стресса. - М.: Наука, 1983. - 368с.
5. *Лазарус Р.* Теория стресса и психофизиологические исследования // Эмоциональный стресс / Под ред. Л. Леви. - Л.: Медицина, 1970. - С. 178-208.
6. *Кожохина Е. В.* Неинвазивные методы измерения билирубина, гемоглобина и глюкозы. Прибор гемобилиглюкометр // Научно-технический вестник Санкт-Петербургского государственного университета ИТМО. – 2011. - №2. – С. 157-162.

UDC 351.814.2 (043.2)

O. V. Kozhokhina, Y. V. Hryshchenko, PhD of Tech. Sci.,
(National Aviation University, Ukraine)

METHODS OF AIR TRAFFIC CONTROLLERS ANTI-STRESS TRAINING

Consider work features of air traffic controllers. The main negative factor in their work is stress. Proposed a combined method for determining the stress effect. It's using anti-stress training on the software package "Anti-console" with noninvasive diagnostic blood parameters.

The problem of stability and reliability of the human operator under the action of extreme factors and the development of psychological stress has attracted attention and gained some shape as an independent area of research due to the development of technology, systems of automated production management, and especially the computerization of all spheres of activity.

Air traffic controllers are people trained to expedite and maintain safe and orderly flow of air traffic in the global air traffic control system. The position of air traffic controller is the one that requires highly specialized knowledge, skills, and abilities. Controllers apply separation rules to keep aircraft at a safe distance from each other in their area of responsibility and move all aircraft safely and efficiently through their assigned sector of airspace.

Because controllers have an incredibly large responsibility while on duty (often in aviation, "on position"), the ATC profession is consistently regarded around the world as one of the most challenging careers, and can be notoriously stressful depending on many variables (equipment, configurations, weather, traffic volume, human factors, etc.).

Duty of air traffic controllers is characterized by high psychologically-emotional and intellectual orientation and belongs to the most stressful and emotionally intense types of professional activities. From the efficiency of the controller and their ability to perform their work in time and accurately depends not only the capacity of air traffic management, but also safety in general [3].

Air traffic in modern conditions is a highly complicated problem that is connected with human and organizational factors. It is directed at minimizing the negative basic processes that may occur. These negative processes include various accidents, such as crash, disasters, precedents and other events. In organizing work of air traffic controllers it is necessary to analyze and identify patterns of activity with new approaches to develop new performance indicators, means of improving the work of air traffic controller in normal and extreme conditions.

Statistics on Aviation accidents show that the percentage of accidents, air traffic controllers are responsible for is large enough and it's necessary to optimize their performance. Unfortunately, nowadays, approaches used in the ergonomics, engineering psychology, aviation psychology, aviation medicine and other areas connected to operational factors make it impossible to qualitatively improve the efficiency of air traffic controllers. This is caused by the fact that these approaches are used without a moment analysis of the actual load of air traffic controllers, their degree of fatigue, and loss of workability. That is why the efficiency of air traffic controller can vary in considerable range at normal and stress conditions.

Stress is a term that is commonly used today but has become increasingly difficult to define. It shares, to some extent, common meanings in both the biological and psychologicalsciences. Stress typically describes a negative concept that can have an impact on one's mental and physical well-being, but it is unclear what exactly defines stress and whether or not stress is a cause, an effect, or the process connecting the two. With organisms as complex as humans, stress can take on entirely concrete or abstract meanings with highly subjective qualities, satisfying definitions of both cause and effect in ways that can be both tangible and intangible [1].

Stress is a factor that has the greatest negative effect on professional activities of air traffic controllers, because it affects the quality of their work. Stress has an effect on such psychological parameters as the perseveration of attention, logical thinking, spatial imagination, the mobility of nervous processes, memory and several of physiological processes - heartbeat, blood pressure, etc.

The level of stress and body state of air traffic controllers can be estimated using the following experiments: psychometric test "Внимание" on the Schulte tables, blood pressure, tremor, and the surface temperature of the hands. It's recommended to conduct psychometric test on air traffic controllers on the anti-consoles of the workplaces using a special software package "Anticonsole" testing change of the blood parameters during the load test, as well as before and after them, in addition to these experiments.

Anti-stress training relates to aviation domain such as flight controls, especially to methods for determining the health and preparedness of pilots and air traffic controllers to perform their duties with integrated avionics failures. Anti-stress training is a way to prevent accidents caused by aircraft of the human factor, due to unpreparedness of pilots and air traffic controllers to complex avionics failures in its operation.

Anti console is the technical device. It's operating principle opposite to the principle of common console. The software package "Anti-console" is based on a failure occurs, the software in avionics in the aircraft operator's air traffic control rather than in the usual sequence of keys to change the remote control.

Anti-stress training of pilots and air traffic controllers in case of failures of aviation equipment during its operation using a set of "Anti-console" helps to reduce the number of pill-prepared operators, admitted to the performance of their duties. It will reduce the number of accidents by getting statistical data and analysis of "handwriting" of the operator under normal conditions, a single failure and complete failure of aircraft [2].

To obtain more complete information about the state controller in anti-stress training and checking measurements of some parameters of blood should be performed. This will not only get reliable information about the state of the operator, but also allow estimating the dynamics of changes of their condition during the stress effects and after them.

Laboratory tests of blood based on invasive techniques are associated with injury of patients, the possibility of infection, as well as long procedure of obtaining a diagnostic result. Therefore, for diagnosing the state of air traffic controllers is preferable to use non-invasive method for determining blood parameters that exceed laboratory methods of, effectiveness and efficiency.

When you select blood parameters to estimate the intensity of the negative effects of stress and tiredness on air traffic controllers some requirements should be considered that significantly increase the information content and quality of assessment:

1. The parameter must vary significantly in the period from the beginning of the negative impact until the recovery period.
2. The parameter should be highly correlated with a measure of negative impact.

These requirements correspond to bilirubin, hemoglobin and glucose, which can not only help to identify the air traffic controller's stress, but also their deviation from the norm, may indicate developing diseases associated with stress.

Hemoglobin is the iron-containing oxygen-transport metalloprotein in the red blood cells of all vertebrates as well as the tissues of some invertebrates. Hemoglobin in the blood carries oxygen from the respiratory organs to the rest of the body where it releases the oxygen to burn nutrients to provide energy to power the functions of the organism, and collects the resultant carbon dioxide to bring it back to the respiratory organs to be dispensed from the organism [6].

At increased hemoglobin there are observed fatigue, drowsiness, partial or complete loss of appetite, blurred vision and pale skin. The symptoms of low hemoglobin are: general weakness, dizziness, shortness of breath, palpitations, fainting, drowsiness and headache.

A problem for obtaining accurate data may be the emotional state of the patient, when hemoglobin is measured non-invasively. With excitement initial blood concentration per unit of surface area of skin can increase, the person blushes and this causes an error in the determination of hemoglobin levels noninvasively.

Bilirubin is the yellow breakdown product of normal heme catabolism. Bilirubin is excreted in bile and urine, and elevated levels may indicate certain diseases. It is responsible for the yellow color of bruises, the yellow color of urine, the brown color of faces, and the yellow discoloration in jaundice [6].

Research of recent decades has shown that the low value of bilirubin may indicate coronary heart disease. Elevated levels of bilirubin may indicate a liver disease, intoxication, violation of the right of the digestive enzymes.

Pigmentation of bilirubin appears in the upper layers of the skin. For non-invasive measurement of bilirubin to the patient is required to bleed section of skin tissue by applying pressure of 105 Pa to avoid the error caused by the presence of hemoglobin.

Glucose is a simple sugar (monosaccharide) and an important carbohydrate in biology. Cells use it as the primary source of energy and a metabolic intermediate. Glucose is one of the main products of photosynthesis and fuels for cellular respiration. Glucose exists in several different molecular structures, but all of these structures can be divided into two families of mirror-images (stereoisomers) [6].

During stress into the blood stand out hormones (cortisol, epinephrine) that quickly increase blood glucose due to its release from the liver (liver - a place of storage of glucose in a modified state - glycogen). This phenomenon is a protective reaction of the organism. Since glucose - the main source of energy, it provides a high level of the body's ability to respond to a foreign stimulus. Therefore significant hyperglycemia can be observed even at the slightest stress. The glucose level returns to normal, when the stress is over [4].

Stress causes a pronounced decrease in the affinity of hemoglobin for oxygen in the blood, which in turn increases the oxygen tension in hepatocytes and activates free-radical processes in the liver microsomes. It will therefore be a reduction in the hemoglobin level, and at long-term effects stress increase in the level of bilirubin.

Nowadays non-invasive optical-electronic devices measure, mainly one parameter of blood. They use a broadband pulsed light source with a further analysis of the absorption of light at certain wavelengths due to narrow-band interference filters and separate photodetectors.

Therefore, especially for the diagnosis of negative impacts of stress on the body of the air traffic controller a combined non-invasive electro-optical device hemobiliglucomeasured (HBG-1) was developed. It incorporates new approaches to treatment and correlation of the received information and also ergonomic design was developed [6].

Non-invasive measurement of blood parameters such as bilirubin, hemoglobin and glucose in combination with psycho-physiological tests will allow to fully characterize the state of the air traffic controller and depending on the received load improve the efficiency of their operation.

The goal of this work is at the prevention of accidents associated with the increasing complexity of air traffic controller’s activity and also to identify patterns of activity operators and their teams in the navigation service systems and motion control.

References

1. *Бодров В. А.* Информационный стресс: Учебное пособие для вузов. — *М.: ПЕР СЭ, 2000. — 352 с.*
2. Грищенко Ю. В. Прибор моделирования ошибок операторов на основе антипульта компьютера. / Електроніка та системи управління. *Ю. В. Грищенко, А. П. Слободян, Е. В. Кожохина. – 2007. – №11. – С. 189-193.*
3. *Шевчук Л. М.* Психофізіологічні прояви професійного стресу диспетчерів УПР
4. *Lazarus R.S.* Cognitive and coping processes in emotion // Stress and coping. - N.Y.: Columbia Univ. Press, 1977. - P. 144-157.
5. *Posner M.J.* Components of attention // Psychological Rev. *Posner M.J., Boies S.J.*- 1971. - V. 78. - P. 391-408.
6. *Кожохина Е. В.* Неинвазивные методы измерения билирубина, гемоглобина и глюкозы. Прибор гемобилиглюкометр // Научно-технический вестник Санкт-Петербургского государственного университета ИТМО. – 2011. - №2. – С. 157-162.

UDC 629.735.33.051.01 (043.2)

Prosvirin D.A., post-graduate student
(National Aviation University, Ukraine)

MODEL-BASED DESIGN OF AUTOMATIC FLIGHT CONTROL SYSTEMS

The article deals with the model-based approach to the design of automatic control systems which used for safety critical systems. Advantages of this approach by illustrative example and opportunity of practical use and its manufacturing application are showed.

Design technology of AFCS (automatic control systems) for aircraft is mostly formed so far. There are three major developments in technology design:

1) The creation of mathematical software for modeling the dynamics of controlled movement of aircraft;

2) Software development (on-board programs);

3) Design bench set for semi-natural simulation.

This paper shows the opportunity of using model-based approach for the first development. The model- based design – is an efficient and cost-effective way for control system design. Instead of physical prototypes and text specifications in model- design model is applied. This model is used in all stages of development. This approach to design allows to carry out simulation of whole system entirely as well as its components, in addition to select and justify the structure of the AFCS, to analyze the stability of the system and show compliance of specification requirements for this control system with a given probability. There is a possibility of automatic code generation, testing in continuous mode and verification. Development of mathematical algorithms of synthesis ends in full mathematical model of a closed loop control, including in particular statistical modeling [1].

At the present stage of development of technology product design of aerospace vehicles, including AFCS (automatic flight control systems) for civil aircraft, we can see the trend of carrying the main volume of work on the stage of ground testing, which includes mathematical modeling and semi-natural bench modeling. This is due to primarily economic reasons, since the cost of identifying and eliminating defects at the stages of mathematical modeling, practicing bench and flight tests are in the ratio 1:10:100 [2]. It turns out that the volume of flight tests required for removal of previously unrevealed defects close to zero, and it is only to demonstrate the results achieved, because nearly 80% of all problems that arise when developing appropriate systems shall be decided on the ground. With the development of complex technical systems role of modeling in assessing the parameters of these processes increased considerably. This is explained by characteristics of research objects that are lying in the complexity of functional relationships between system parameters, environmental changing conditions and the estimated parameters.

Model-based approach can be used not only in preparing technical proposals and the formation of technical requirements for new objects but also on the stages of conceptual and technical design, and the debugging samples in closed systems and also on the stage of different kind full-scale tests that determine the characteristics of objects their debugging and possible to move from this stage to further testing or serve as justification for transfer objects to the serial production [3]. Model-based approach provides solving of the next tasks:

justification of tactical technical requirements for AFCS;

implementation of a preliminary analysis of the developed modes and laws of AFCS at the aircraft design stage (see Figure 1, Figure 2);

Maintenance of semi-natural simulation AFCS;

statistical analysis of approach mode with savings of material costs during flight test;

development of recommendations setting paths automatic control during flight test AFCS that reduce time and material costs of full-scale test, certification and more.

As an example, consider the automatic control lateral movement of the main plane which implements through the rudder channel and ailerons. Rudder channel provides short-damping oscillations around the normal axis and eliminates slip angle. Purposive roll and course control provides by ailerons in coordinated turn mode. Testing of the given angle and roll rate providing by simultaneous operation of ailerons and rudder. Development of automatic control laws of lateral movement is based on the principle of decomposition (separation) of ailerons and rudder channel. For this purpose, the original object of the lateral movement divides into two subobjects which are implement flat coordinated turn mode. The following software implementation of the above laws and an example of AFCS research in "Approach mode" with following conditions of research results made in the block simulation system of dynamic systems Simulink / Matlab:

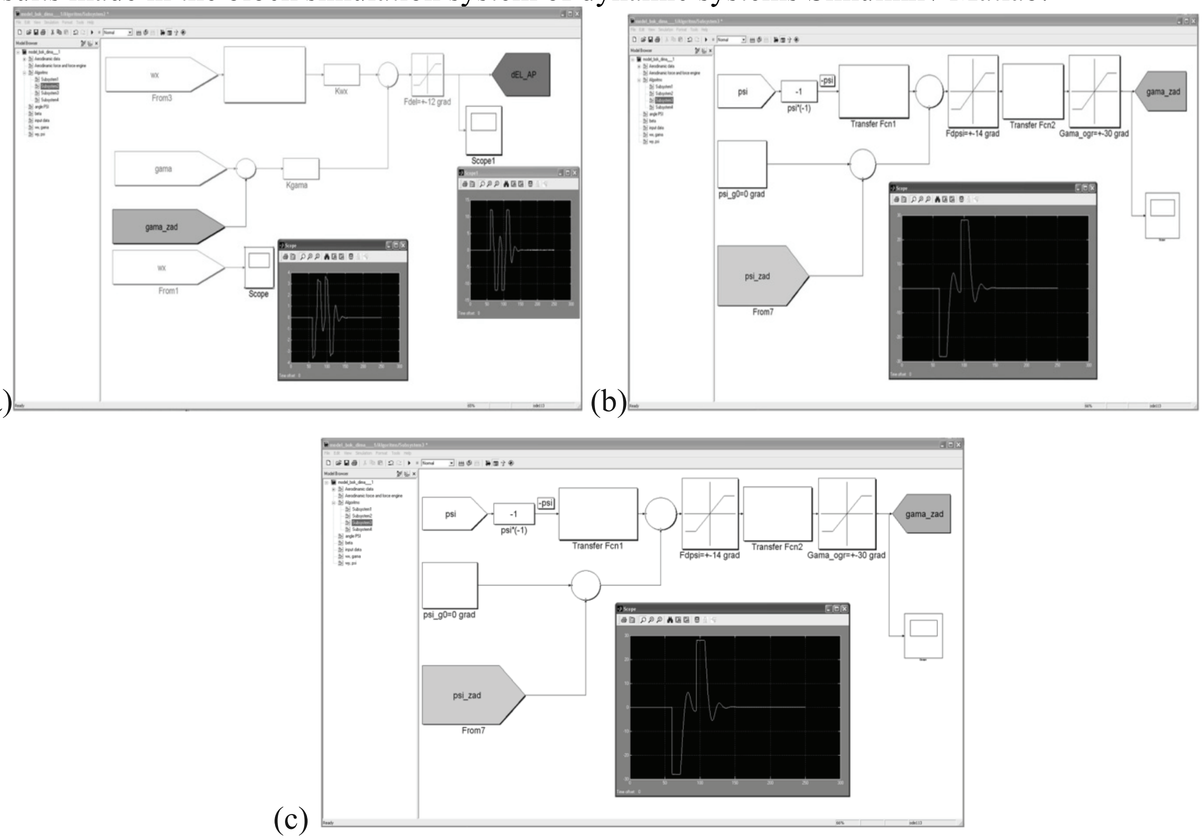

(a) (b) (c)

Fig. 1. Control law in ailerons channel (a) in rudder channel (b), roll angle set.

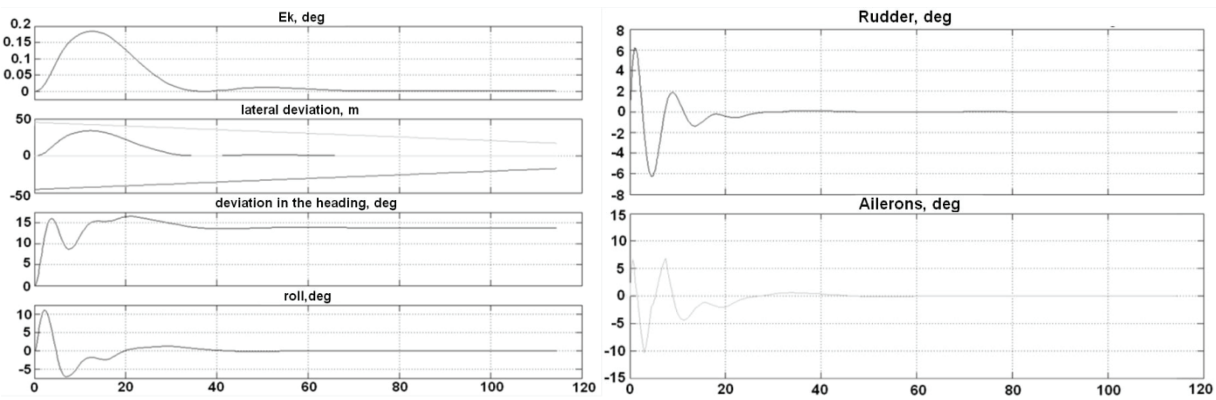

Fig. 2. Research of the AFCS operation in "Approach mode" (with wind disturbance Wz = - 15m / s).

Figure 3-6 presents a brief analysis of the stability of lateral movement. It shows that the aircraft has a itinerary and transversal stability with small value of damping decrement.

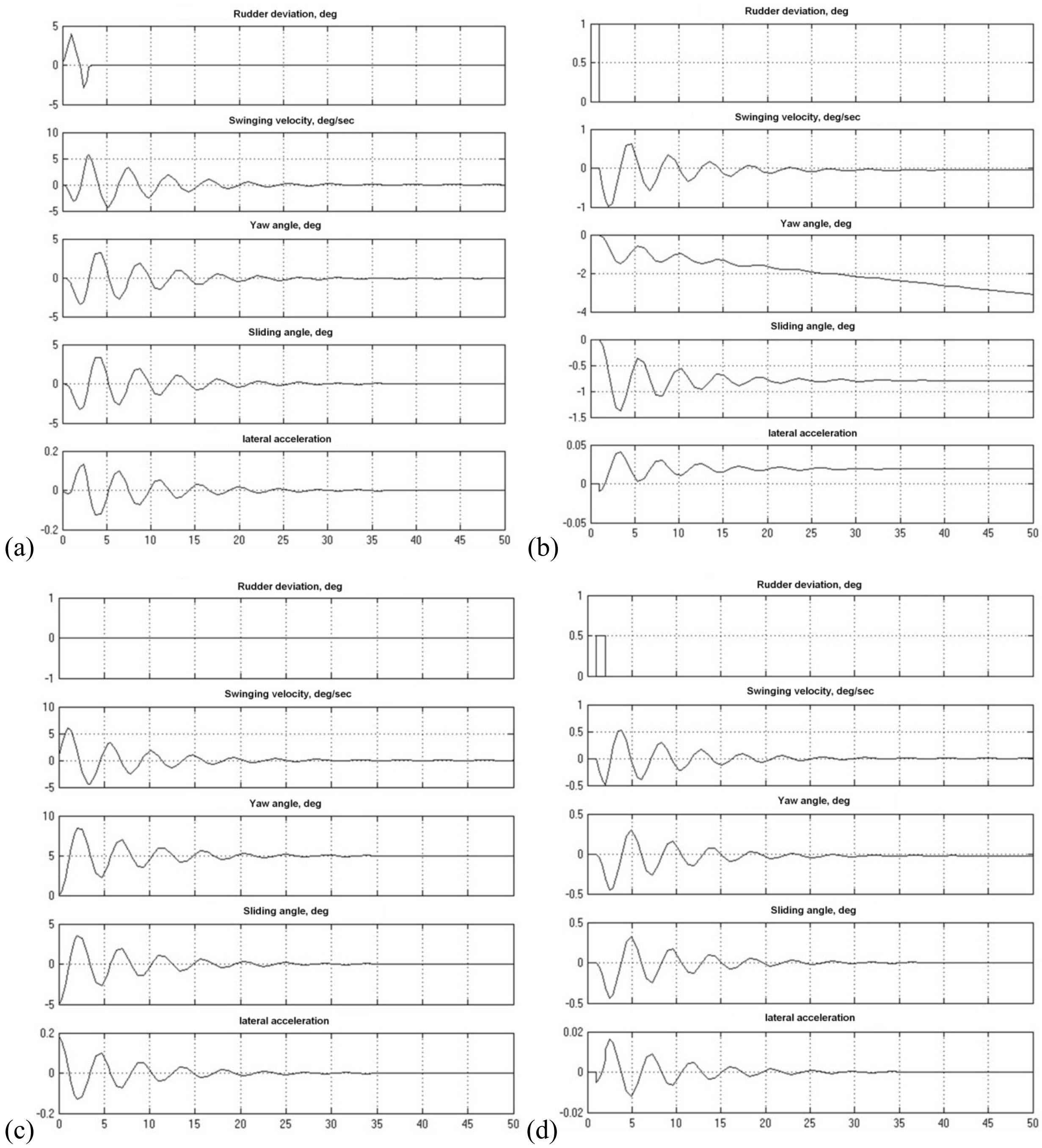

Fig. 3. Step-function gust response PSIwind = 5 deg at Vnp =430km/h, H = 11600m; m = 36000kg; alfao = 5 deg (a), rudder impulse response (b), double rudder impulse response (c), Step-function rudder deviation response

For a visual representation of simulation results FLIGHTGEAR as a tool for visualization is proposed (Fig. 4, 5) [4]. Choice of this flight simulator due to the possibility of free access to its source, and therefore more features unlike its commercial counterparts. In addition Matlab allows to combine Matlab model created in Simulink with virtual reality models of FLIGHTGEAR, created using 3D editors - VRML (Virtual Reality Markup Language) 3ds Max, AC3D, blender and more.

Conclusions

In many cases not possible to assess the qualitative properties of control systems by direct method - full-scale test- through objectively existing limited conditions of their test operation. This and the relative duration, the necessity to spend real resources of funds and engineering tools, significant economic costs of full-scale tests forced to seek more efficient ways of organizational management for the control systems performance assess. A number of quite obvious advantages of model-based approach can promote it to first place among the methods of safety critical systems planning and research. However, it should be given and the main difficulties of this method - the results require a specific reliability qualification and comparison with the results of full-scale tests.

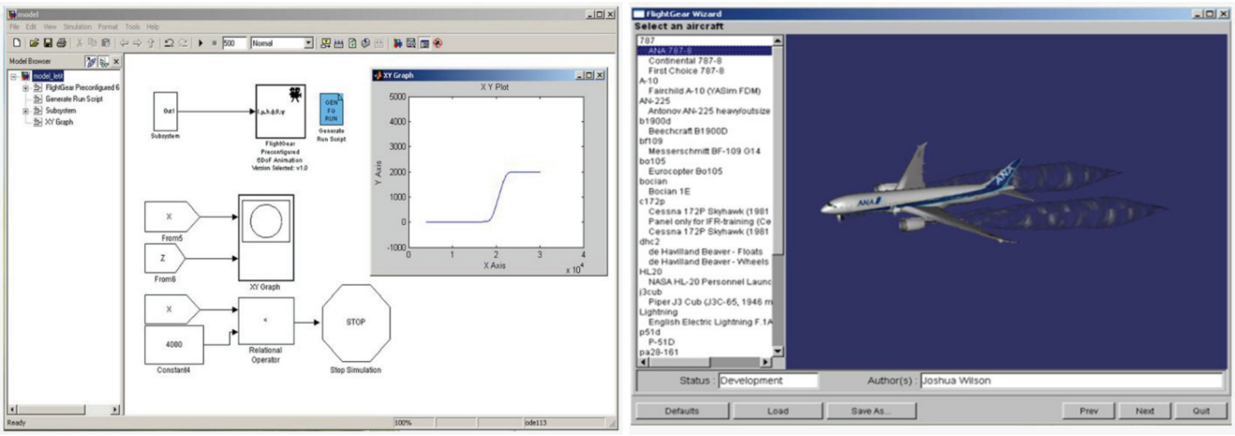

Fig. 4. Aerospace Blockset blocks providing interface to FlightGear.

Fig. 5. FlightGear visualization.

References

1. Навигация и управление летательными аппаратами; [сб. науч. трудов./ науч. ред. А.*Г. Кузнецов* и др.]. – М.: МИЭА, 2010. – 88 с.
2. Теоретические основы испытаний и экспериментальная отработка сложных технических систем / [*Александровская Л.Н., Круглов В.И., Кузнецов А.Г.* и др.]; под ред. *Л.Н. Александровской, В.И. Круглова.* М.: Логос, 2003.-736 с.
3. Методы анализа и оценивания рисков в задачах менеджмента безопасности сложных технических систем / [*Крюков С.П., Бодрунов С.Д., Александровская Л.Н.* и др.]; под ред. *С.П. Крюкова, С.Д. Бодрунова.* – СПб: Корпорация "Аэрокосмическое оборудование", 2007.- 453 с.
4. Model-based Design of a New Lightweight Aircraft", [*Turvesky, A., Gage, S., and Buhr,* C.] AIAA paper 2007-6371, AIAA Modeling and Simulation Technologies Conference and Exhibit, Hilton Head, South Carolina, Aug. 20-23, 2007.-pp.1-15

UDC 629.7.06 (043.2)

K. Sakhno
O. Kozhokhina
(National Aviation University, Ukraine)

APPLICATION OF HEAD-UP DISPLAY TO REDUCE PILOT'S INFORMATION STRESS LEVEL AND IMPROVE FLIGHT EFFICIENCY

Consider head-up display. Investigated the prospects for its use in modern civilian aircraft to decrease stress and increase awareness of the pilots

Recently, Aviation is becoming more widespread and the number of annual freight and passenger traffic increases. Of course, the main and most important task lies with the pilot, in fact, he is responsible not only for the safety of passengers, but also for their lives. Under the influence of various factors (psychological, time of day, weather conditions, etc.), the level of attention, safety, performance can be significantly reduced. For example, in a plane crash in Colombia May 19, according to experts (airliner "Boeing 727" Colombian airline "SAM", which killed 132 people) was caused by the crew, for failing to navigate the difficult weather conditions. In favor of the version of the crew error according to a decryption of the "black box" discovered at the scene. In particular, the tape recording of conversations pilots shortly before the crash showed that they were too late to find that the plane was off course and flying too low. Hardly had the commander to order futures climb as the ship crashed into a mountain slope. Up to this point in the cockpit remained calm.

The main task nowadays is to provide the pilot with the advanced equipment, which will be extremely easy to use, but it will increase the efficiency of the pilot. During the flight, the pilot is constantly replaced by a point of attention up to 80 times per minute, which affects the psychological factors and reduces the pilot's attention. In order to reduce the load on the pilot can use the head-up displays.

The LED on the windshield, head-up display (HUD) - the system of the aircraft, designed to display a character - flight and navigation information on the background of the special circumstances behind the cab.

Use of HUD, would greatly reduce the likelihood of information overload (stress) pilot, who was forced to watch as both of the surrounding space, and for the readings of numerous devices.

Stress in this situation acts as a subjective response and reflects the inner mental state of tension and excitement, this state is interpreted as an emotion, defensive reactions and processes to overcome (coping processes), occurring in man[1, 2, 3]. These processes may contribute to the development and improvement of functional systems, but also cause mental stress [6, 7].

HUD is also used to display not only the symbolic information, but also more complex images - for example, to match the actual image area and the information received from the cameras, working in the infrared. This system allows you to fly at extremely low altitudes in low visibility conditions and at night [8].

How HUD constructed? It's designed as a display on the windshield. A typical HUD contains three primary components: a projector unit, a combiner, and a video generation computer.

The projection unit in a typical HUD is an optical collimator setup: a convex lens or concave mirror with a Cathode ray tube, light emitting diode, or liquid crystal display at its focus. This setup (a design that has been around since the invention of the reflector sight in 1900) produces an image where the light is parallel i.e. perceived to be at infinity.

The combiner is typically an angled flat piece of glass (a beam splitter) located directly in front of the viewer that redirects the projected image from projector in such a way as to see the field of view and the projected infinity image at the same time. Combiners may have special coatings that reflect the monochromatic light projected onto it from the projector unit while allowing all other wavelengths of light to pass through. In some optical layouts combiners may also have a curved surface to refocus the image from the projector.

The computer provides the interface between the HUD (i.e. the projection unit) and the data to be displayed and generates the imagery and symbology to be displayed by the projection unit [8].

In the development of ILS systems require special attention the following factors:

- the surface on which the image should be completely transparent and does not interfere with the review;

- generated image must be collimated (projected at infinity) - otherwise the pilot will have to continually re-focus vision when switching focus from an object in space out of the cockpit on the readings of HUD. Being projected to infinity, the image of the HUD is seen always in focus, regardless of where the pilot is looking, and does not require time-consuming for accommodation.

Existing HUD divided into two types:

- Fixed - consisting of high-brightness electron-beam instrument (EBL), and combined with an optical system projecting an image on the screen in the EBL space out of the cockpit.

- Helmet-mounted - in which the screens are output to the image attached to the helmet pilot. A special system tracks the position of his head, and provides a display on the screens of the relevant information. Determination of the position of the head pilot, and hence the angular coordinates of the line of sight, it allows you to support that goal, which is currently facing his eye. This type of HUD are both monocular (more common), and binocular.

For the entire period of the pilot, from takeoff to landing and finishing exposed psychological various stress. A significant role is played by the attention and concentration, which can increase the pilot using this system (by reducing the number of sensors that will be displayed directly on the windshield) [5,6,7].

Typical aircraft HUDs display airspeed, altitude, a horizon line, heading, turn/bank and slip/skid indicators.

There are other symbols and data available in some HUDs:

▪ boresight or waterline symbol—is fixed on the display and shows where the nose of the aircraft is actually pointing.

▪ flight path vector (FPV) or velocity vector symbol—shows where the aircraft is actually going, the sum of all forces acting on the aircraft. For example, if the aircraft is pitched up but is losing energy, then the FPV symbol will be below the horizon even though the boresight symbol is above the horizon. During approach and landing, a pilot can fly the approach by keeping the FPV symbol at the desired descent angle and touchdown point on the runway.

▪ acceleration indicator or energy cue—typically to the left of the FPV symbol, it is above it if the aircraft is accelerating, and below the FPV symbol if decelerating.

▪ Angle of attack indicator—shows the wing's angle relative to the airflow, often displayed as "α".

▪ navigation data and symbols—for approaches and landings, the flight guidance systems can provide visual cues based on navigation aids such as an Instrument Landing System or augmented Global Positioning System such as the Wide Area Augmentation System. Typically this is a circle which fits inside the flight path vector symbol. Pilots can fly along the correct flight path by "flying to" the guidance cue.

Since being introduced on HUDs, both the FPV and acceleration symbols are becoming standard on head-down displays (HDD). The actual form of the FPV symbol on an HDD is not standardized but is usually a simple aircraft drawing, such as a circle with two short angled lines, (180 ± 30 degrees) and "wings" on the ends of the descending line. Keeping the FPV on the horizon allows the pilot to fly level turns in various angles of bank [8].

In the given situation pilot serves like an operator. It is known that the most characteristic feature of operator activity is mediated by the perception of the outside world and a managed object using the information model. Encoding information on the means of its representation, the use of automation systems deprives a person of a number of significant natural features of control objects, makes it difficult to form an adequate mental image of the object and situation. The transfer of some functions of information training solutions and management of the facility increases the importance of automatic devices for monitoring their performance, resulting in the need to maintain high vigilance and preparedness interventions in the management. Using of control systems of coded information, its representation in a limited space in discrete units, or simultaneous mode are reflected in the processes of forming and maintaining the operational mental images of their interference, mutual induction, or coordination, which ultimately determines the level of sustainability of professionally significant qualities and mental health operator [2].

Any kind of psychological stress (personal, interpersonal, familial, professional, etc.) is basically the information that is the source of its development are external messages, information about the current (actual) or expected, the likely impact of adverse events, or threat of "internal" information in the form of past performances, retrieved from memory information about the psyche of traumatic events, situations and their consequences. These reactions are usually related to the production of negative emotions, the development of anxiety throughout the existence of a conflict situation (real or imagined) until it resolves or subjective overcome this condition. So, in these kinds of psychological stress of unfavorable and dangerous event is the starting point in determining risk of its occurrence, and forming a sense of anxiety, tension on the basis of the functional actualization mental image of the situation of professional activity. In control systems, information processes are the main content of professional work, and arising in the solution of labor problems of problem situations, failures of equipment, the critical modes, erroneous actions, and other disorders that entail adverse effects up to the accidents and disasters, develop on the background of the impact of objective and subjectively very important signal information or misrepresentation, breach of information security management process. In these circumstances, the information is not only a source of information about threatening, difficult, dangerous event, but also a means of regulating the process of countering violations of the emergency exit, and thereby overcome the feeling of anxiety for the poor of its outcome [2].

Steps to resolve the problematic situation in the event of erroneous (delays, inaccuracies) may themselves cause worsening of the problematic, increasing the negative effects of stressful situations. Thus, the operator of the process of information security management system that is associated with signaling the emergence of abnormal modes of operation, the solution of problem tasks, parry, or prevention of violations in the facility, etc., is the main source of information about the threat of adverse effects or consequences . The role of emotions, negative emotions, mental images of actualization of problem situations and their outcomes in these circumstances, certainly large enough, but the dynamism and efficiency of the flow of critical events, the need for intensive (in tempo, volume, variety acts, etc.) activities, availability of information overload, requiring considerable (sometimes excessive) intellectual effort, exhibit the most peculiar features of this type of stress.

The next aspect of the content of the concept of "information stress" is to determine whether the mental state that forms under the influence of extreme values of informational factors, classified as stress. Traditionally, the term "stress" is used to denote non-specific biochemical, physiological and psychological manifestations of activity in the adaptive response to the extreme impact of any significant factors for the organism. Through the deployment of non-specific adaptation processes the body maintains a certain period of time, the integrity and vitality when exposed to stressors. Obviously, non-specific adaptation processes perform stabilizing functions in response to the extreme effects due to consumption of "resources" compensatory functions, resulting in the organism may be possible to meet the challenges before him life problems [2].

Specific areas of study of mental stability of the human operator and psychological stress are largely due to the nature of accidents in transportation, manufacturing, energy, and the urgent tasks of ensuring the effectiveness and safety. Significant influence on the content of these studies have a number of provisions and concepts developed in psychology, namely the systematic organization of operator activity, regulation of mental states, the regulatory role of the mental image of "personal" and "human" factor, the psychological system activity and several others.

The basic psychological features of the operator's activity were the subject of a comprehensive study over the past few decades. In most of these studies the problem of functional stability of the human operator and the stress in a direct statement has not been studied specifically, although a number of issues addressed in it had a connection with this problem. In the category of stress studies often used as a characteristic of the mental state of the human operator or the price of its activities. However, there is no doubt that the study of the causes, mechanisms and consequences of stress and its impact on the quality of a particular management system is necessary to study the factors that characterize the procedural features of operator activity and functional manifestations of human labor activity under these conditions. It is obvious that the value of the functional characteristics of the labor process, laws of manifestation and working to ensure the activity of the human operator, the mechanisms of regulation of his conduct and condition of the extreme conditions make it possible not only to assess the mental state and especially its impact on the reliability of the activity, but also to justify specific recommendations for the maintenance of its at the required level.

The introduction of this system can significantly reduce crashes and accidents by reducing pilot workload information. After the pilot should to have a wide range of information, it checks that must be constantly, switching attention from one sensor to another, thereby reducing the overall level of attention and increases the likelihood of human errors. If the ship "Boeing 727" was fitted with the equipment, the catastrophe could have been prevented, saving the lives of passengers. On most modern aircraft (which are not only available but also have committed traffic) you can install this system. Comfort, and most importantly the life and safety of passengers depend on the pilot, so to ensure its maximum efficiency is a major concern of designers and engineers.

In addition, the use of HUL will greatly reduce the pilot's information stress. They will receive more detailed information on the status of the aircraft in the air.

References

1. *Устимов Д.Ю.* Информационный стресс. Информационно-психологическая безопасность личности как качественная характеристика информационной культуры человека.- Казань,2006.
2. *Бодров В. А.* Информационный стресс: Учебное пособие для вузов. – М.: ПЕР СЭ, 2000. – 352 с.
3. *Лазарус Р.* Теория стресса и психофизиологические исследования // Эмоциональный стресс / Под ред. *Л. Леви. Л.*: Медицина, 1970.
4. *Sharit J., Salvendy G.* Occupational stress: review and reappraisal // Human Factors, 1982. Vol. 24.
5. *Вальдман А. В., Козловская М. М., Медведев О. С.* Фармакологическая регуляция эмоционального стресса. М.: Медицина, 1979, 360 С.
6. *Изард К.* Эмоции человека. М.: Изд-во Моск. ун-та, 1980, 440 с.
7. *Китаев-Смык Л. А.* Психология стресса. М.: Наука, 1983, 368 с.

UDC 681.327.22 (043.2)

O.G. Sitnik, PhD of Tech. Sci, O.O. Chuzha, PhD of Tech Sci
(National Aviation University, Ukraine)

SPATIAL AND FREQUENCY DESCRIPTIONS, POWER SPECTRUMS TO THE ANALYSIS OF PARAMETERS OF IMAGES OF FLIGHT INFORMATION

The present article the authors analyzed the status and relevance of a model close to the real through the use of mathematical tools of game theory and operations research to assess the imaging parameters crewflight information displays for civil aircraft. The authors examined the mechanism of interaction between different components of a single process of testing the readiness of civil aircraft in flight, as factors of influence on the perception of human visual flight information.

Analysis of the last researches, the decision of problem of intercommunication of effects, which are investigated for perception of high-quality flight information a crew on displays in the booth of airplane with application of CALS and their influence on quality of images [1] consists in that which is considered impossible decision of problem of optimum of process of analysis unassisted development of modern positions of theory, is founded in which.

The problem is to study the relationship of various characteristics of the images and their impact on the quality of flight information displays for aircraft cabins [1] using CALS-technologies. In the process of experiments on a designing complex will assume that an image is characterized by a two-dimensional function $\xi(x,y)$, then for the small on sizes area of image areas on the cabin display of kind, in,x,$x+\Delta x$, $y+\Delta y$ it is suggested to find a function

$$F_{xy}(\omega_x,\omega_y)=\frac{1}{2\pi}\int_{x}^{x+\Delta x}\int_{y}^{y+\Delta y}\xi(x,y)e^{-j(\omega_x x+\omega_y y)}dxdy\ , \qquad (1)$$

A function $F_{xy}(\omega_x,\ \omega_y)$ will name a local spatial two-dimensional image, which shows, with which specific gravity to summarize spatial signals in an order to get an initial signal $\xi_{xy}(x,y)$ in the noted area of image. By a local spatial two-dimensional $F_{xy}(\omega_x,\ \omega_y)$ the signal of image is determined by reverse transformation of Fourier

$$\xi_{xy}(x,y)=\frac{1}{2\pi}\int_{-\infty}^{+\infty}\int_{-\infty}^{+\infty}F_{xy}(\omega_x,\omega_y)e^{j(\omega_x x+\omega_y y)}d\omega_x d\omega_y\ , \qquad (2)$$

where ω_x and ω_y - named circular spatial frequencies.

The signals of image are proportional to linear spatial frequencies υ_x and υ_y (taking into account a coefficient 2π). Naturally, that the different areas of image of flight information on displays in the booth of airplane can have different functions $F_{xy}(\omega_x,\ \omega_y)$. Than anymore a size changes$\xi(x,y)$ within the limits of the considered area, the area of spatial frequencies, in which a function $F_{xy}(\omega_x,\ \omega_y)$is substantially different from a zero, becomes wider. An area of existence of local spatial spectrum will be the wider, than any more on this area meets shallow details or than higher level of the signal of image processing. If in the formula (2) of integration to carry out an image within the limits of all plane, that summarizeall values of local spatial spectrums, then will get the so-called two-dimensionalspatial (general or integral) spectrum of all image of flight information on displays in the booth of airplane

$$F(\omega_x,\omega_y)=\frac{1}{2\pi}\int_{-\infty}^{+\infty}\int_{-\infty}^{+\infty}\xi(x,y)e^{-j(\omega_x x+\omega_y y)}dxdy\ , \qquad (3)$$

From expression (3) to reverse transformations of Fourier [6] will pick up thread the function of signal $\xi(x,y)$of all image. Decision of a number of tasks to the analysis of local and general two-dimensionalspatial spectrums of images it appears useful enough. That, at the analysis of images in linear processes, their influence on a signal is simpler determined in spectral presentation, what at research of changes of signal. A linear process can be described spatially frequency by description, that allows by simple correlation to link the frequency spectrums of entrance and initial (in relation to a process) signals of image spatially.

A research purpose is upgrading of perception of images on the displays of airplane taking into account influence of descriptions of displays, equipment of visualization and intercommunication of descriptions of the lighted up flight information on displays in the booth of airplane.

New approach for the decision of problems consists in that in our raising of task by analogy with determination of local two-dimensional spatial spectrum of image will enter the concept of local two-dimensional power spectrum [1]

$$S_{xy}(\omega_x,\omega_y)=\left|F_{xy}(\omega_x,\omega_y)\right|^2 . \tag{4}$$

The proper method from expression (4) is determine the power spectrum of all image (as a sum of local power spectrums of all areas of image). Physical maintenance of power spectrum of image is related to relative energy which carries in itself the signal of image on unit of area of image (therefore more faithful to name his spectrum powers or by the spectral closeness of power) in the interval of frequencies ω_x–$\omega_x+\Delta\omega_x$, ω_y–$\omega_y+\Delta\omega_y$. So, for example, if a function $\xi(x,y)$ is a size, which determines light streams which emanate different parts of image, then functions $S_{xy}(\omega_x, \omega_y)$and $S(\omega_x, \omega_y)$is the frequency distribution of specific values of spatial power of these light streams on the range of spatial frequencies accordingly for a local area and all image.

A scientific result consists in the following: it is experimentally set, if in the process of design to conduct the analysis of information on the power spectrum of primary function $S(\omega_x, \omega_y)$by reverse transformations of Fourier, then by analogy with a formula (4) obsessed quadratic description of signal of image, and by reverse transformation of Fourier get the autocorrelation function of image

$$R(x,y)=\frac{1}{2\pi}\int_{-\infty}^{+\infty}\int_{-\infty}^{+\infty}S(\omega_x,\omega_y)e^{j(\omega_x x+\omega_y y)}d\omega_x d\omega_y . \tag{5}$$

An autocorrelation function can be certain both for the area of image and for all image on the whole. For final functions $\xi(x,y)$ middle statistical descriptions of which do not depend on the order of their adding up, the operation of transformation of autocorrelation function is simplified, because $R(x,y)$ the not co-ordinates of pixel are taken into account in expression, but only their difference. For one-dimensional presentation of signal of image an autocorrelation function can be certain as

$$R(\lambda)=\frac{1}{L}\int_0^L \xi(l)\xi(l+\lambda)dl , \tag{6}$$

where$L$ - is length of involute of all image.

As an autocorrelation function is quadratic description, it is always positive and diminishes on a size with growth λ. At $\lambda\to L$, $R(\lambda)$ aspires the mean value of size to the square ξ. At $\lambda=0$

$$R(0)=\overline{\xi}=\xi^2+\sigma_\xi^2 , \tag{7}$$

where $\xi(l)=\overline{\xi}$. $R(0)-R(\infty)=\sigma_\xi^2$ - characterizes part of power, related to the rejections of size, that is why it it is suggested to name variable component power of signal of image.

Thus, $R(\infty)=\overline{\xi^2}$ answers permanent component power of signal of image. As $R(0)$ equals a sum permanent and variable component powers, it determines complete power of signal of image. In an order to get more universal description which does not depend on concrete values $\overline{\xi}$and σ_ξ^2, it is possible to pass from the function of autocorrelation to the coefficient of autocorrelation

$$r(\lambda)=\frac{R(\lambda)-\overline{\xi^2}}{\sigma_\xi^2} . \tag{8}$$

If a function$R(\lambda)$ changes from complete to permanent component power of signal, then $r(\lambda)$changes from 1 to 0. Transition from the function of autocorrelation to the coefficient of autocorrelation equivalent to replacement of power spectrum$S(\omega)$ the rationed power spectrum $S(\omega)/S(0)$.

Exposition of basic material of research. For description of frequency and power spectrums different numerical parameters are entered, for example maximum frequency of spectrum, coefficient of autocorrelation which is a function from λ. Therefore the autocorrelation function of image $R(\lambda)$can be characterized by an integral to autocorrelation λ_0. An interval of autocorrelation is the parameter of estimation, which determines the local or general for all image sizes of distances, which display elements are highly enough correlated at. For determination of interval of autocorrelation arbitrary suppositions are accepted. More frequent all the interval of autocorrelation is set at minimum values r_{min}, accepted here, that at $r<r_{min}$ intercommunication of display elements is unimportant. Than anymore interval of autocorrelation, the more so interdependent display elements. Sometimes for finding more comfortable to use other assumption, which a width of rectangle (with a height even of unit) the area of which equals an area under a curve is at. In this case an integral λ_0 is determined by the equivalent integral of reliable cross-correlation connection.

The first method of determination λ_0 is any more comfortable for practical realization of tasks on measuring of cross-correlation intercommunications of display elements, and the second method of determination λ_0 - for his theoretical analysis. Under effective maximum frequency of power spectrum ω_n will be to understand the width of such even spectrum in which complete power equals complete power of this concrete spectrum

$$\omega_n = \frac{1}{S(0)}\int_0^{\infty} S(\omega)\,d\omega \quad . \tag{9}$$

Experimental researches rotined in the process of design, that the autocorrelation functions of brightness of flat images were well enough approximated on the average by exponential dependence

$$r(\lambda) = e^{-q\lambda} \quad , \tag{10}$$

where q - is a constant the size of which depends on the type of image.

After numeral mathematical transformations obsessed results of design of process of picture of displays necessary generation for high-quality perception by the crew of flight information. It is set, in the images of flight information on displays in the aircraft cabin is no clear enough orientation in some certain direction and next transformations of images is produced, mainly, in the optical and electron-optical systems with application of izotropic materials of display. Dvomirniy power spectrum of izotropic image in arctic co-ordinates at exponential to the autocorrelation function looks like

$$S(\omega_n) = \frac{q_p}{\sqrt{2\pi}\,(q_p^2 + \omega_p^2)^{3/2}} \, , \tag{11}$$

whereq_p - is a constant the size of which depends on distance between pixels.

For images, which have a coefficient of autocorrelation as експонентної function (11) and the rationed power spectrum (12), interval of autocorrelation $\lambda_0$and effective maximum frequency ω_n, depend only on the co-ordinate q

$$\lambda_0 = \frac{1}{q}\, ; \qquad \omega_n = \frac{\pi}{2} q \tag{12}$$

On (Fig. 1) the graphic arts of coefficients of autocorrelation of four colors of flight information are resulted on displays in the booth of airplane, measured by an optical correlometer. The coefficient of correlation of the objective measurings and subjective estimations appeared observers even *0,98*. Therefore in future we will use a term rizkistna characteristic image, meaning all autocorrelation function (or power spectrum) of image hereunder, including, as one of its important parameters is a value of derivative coefficient of autocorrelation at the beginning of co-ordinates q. The size $q$depends on frequency maintenance of image, in particular from specific gravity in him sharp changes of brightness, shallow details, and also from description of previous processes of transformation of image of flight information on displays in the booth of airplane. It is suggested also to get the function of closeness of distributing of parameter q. Zero values q answer the base-line areas of image, maximal values $q_{loc.max}$ are arrived at in those areas, where the signal of image has maximal changes. On an interval $0 - q_{loc.max}$ the general beds for all image q_{int} (local integral coefficient), which probably, near to the mean value $\overline{q_{loc}}$, but does not equal him, because specific gravity of base-line areas is on images, as a rule, high enough. Thus the coefficient of autocorrelation is obtained by character of function of discrete argument, multiple element of spatial

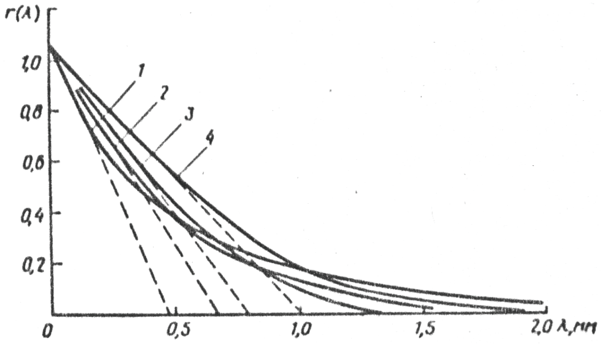

Figure 1. Autocorrelation coefficients of the four primary colors for flight information.

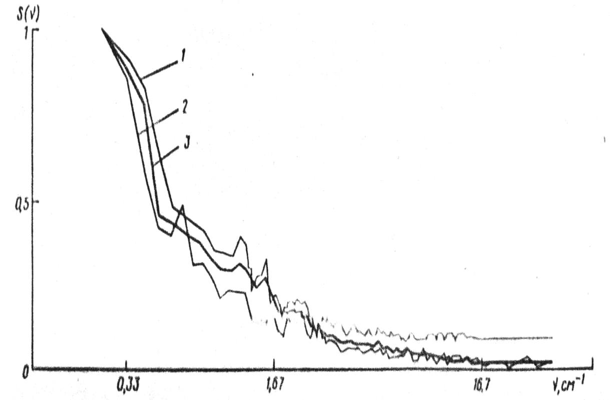

Figure 2. Results of a typical energyspectrum of color flight information.

discretisation of signal ($n\cdot\Delta l$), where n=1,2,3 . At determination of size$r_{инф}(n\cdot\Delta l)$ the informative areas of image must correlate with the signal of n by the base-line areas of the proper level of quantum.

Confirmation of justice of assertions in-process is an analysis of additional parameters of research, which were used for a design. It is set that the values of local coefficient q_{loc} are different from general (integral) for all image q_{int}. At presence of a few (two or three) plans the greatest value q_{loc} as a rule, have areas of image of basic, main plan. If hypothetically to present, that measuring of local coefficient of autocorrelation is carried out on the small enough for areas area of image, then will answer every image weeds local coefficients of autocorrelation restrictedly from above $r(\lambda) = 1$, and from below by a curve $r_{\min}(\lambda)$ (Fig. 2).

Conclusions

Prospects of subsequent researches in scientific subdirection of processing of images consist in that it is first offered untraditional going near the decision of problems of analysis of images of cabin displays. It allows to execute more exact calculations at planning of displays. Practically, more comfortable to figure on by the previous record of discrete and quantized signal with the next including of algorithm of delete of base-line and cropping areas of information. The values of coefficient of autocorrelation are certain by such method will appear considerably less on a size, what got in regular fashion. A priori it is possible to assume that autocorrelation and proper to them power descriptions of signal of image will be more closely associated with the visual estimation of rizkistnyh parameters of image of flight information on displays in the booth of airplane, what generally accepted in the theory of casual processes of function.

References

1. *A.G. Sitnik.* Research and development of the Atlas of optimal configurations, sizes and areas of screen elements and fragments of the underlying managers in the synthesis of color halftone images / / Cybernetics and Systems Analysis. - № 2. - K.: NASU IK, 2000. - S. 134-143.

2. *P.A. Vorobel, OR Datsko.* The image contrast Pidsilennya s vikoristannyam zmini parameters metriv funktsiї nechitkoї nalezhnosti // Visnik OU "Lvivska politehnika." Komp'yuterna inzheneriya that informatsiyni tehnologiї. - № 433.-Lviv: 2001.-S. 233-238.

3. *A.K. Dorosh, V.I. Hamsters.* Sistemotehnika PC `yuterizovanih vidavnichih systems. - K.: IVTS "Vidavnitstvo" Politehnika ", 2002. - 72.

4. *M.F. Kirichenko, M.P. Lepekha.* Zastosuvannya psevdoobernenih i proektsiynih matrix to doslidzhennya keruvannya problems, she sposterezhennya identifikatsiї / Cybernetics and Systems Analysis. - 2002. - № 4. - C. 107-124.

UDC 681.327.22 (043.2)

O.G. Sitnik PhD of Tech. Sci
L.M. Sytianskykh Assist.
(National Aviation University, Ukraine)

ESTIMATES FOR VISUAL FLIGHT INFORMATION CREW UNDER THE INFLUENCE OF PSYCHOLOGICAL FACTORS

Of problem is the study of information criteria for evaluating the error processes tonal transformation and visual perception under the influence of engineering and psychological factors is known that in many famous works of specialists solved the problem of image quality. On the one hand, it is bad, because missed major opportunities of expanding our belief in the doctrine of the imagetheref

Production problems in general and its relationship to important scientific objectives through assessment of performance criteria and process precision tonal transformation and visual study of information criteria for evaluating the error processes tonal transformation and visual perception under the influence of engineering and psychological factors in the study of experimental data process modeling.

Analysis of recent studies in which a solution of the problems is that it seems impossible to solve the problems of existing methods of error evaluation processes tonal transformations, visual perception and information criteria for the study of information criteria for evaluating the error processes tonal transformation and visual perception under the influence of engineering and psychological factors. Methods of estimation accuracy for image analysis showed that incomplete, modern ideas and theories.

The study is to solve important scientific problems - the search for optimal information criterion estimation error process of becoming a tonal (Fig. 1) and visual perception (Fig. 2) has been achieved and done as testing hypotheses. Algorithm research is scientific analysis of the characteristics of interval uncertainty of any quantity that is informative, it is advisable to apply entropy interval $2\Delta\ \xi$,

$$2\Delta\ \xi = e^{H\left(\frac{\xi}{\xi_2}\right)} \tag{1}$$

where $H(\xi 1 / \xi 2)$ — conditional entropy of the distribution criterion of error in determining ξ.

The problems of assessing the quality of documentation (1) and reliability of information found their solution in the systems of image analysis have been resolved and reported as testing of hypotheses. This criterion is often used with reasonable efficiency. The total amount of information defined as J, transmitted by converting image (Fig. 1) with expression

$$J = H(\xi) - H_{cp}\left(\frac{\xi}{\xi_n}\right) \tag{2}$$

where $H(\xi)$ — priori entropy values ξ; $H_{cp}(\xi / \xi_n)$ — average conditional entropy error.

Statement of main results with full justification of scientific findings made in the following way. A definition of conditional entropy of the average error made on the basis of experimental data obtained by simulation of tonal transformations (2) after the intermediate mathematical transformation of expression

$$H_{cp}\left(\frac{\xi}{\xi_n}\right) = \int_{\xi_{\min}}^{\xi_{\max}} \rho(\xi) H\left(\frac{\xi}{\xi_n}\right) d\xi \tag{3}$$

where $\rho(\xi)$ — function of the density distribution of values ξ; $H(\xi /\xi_n)$ — current value of the entropy error.

Process accuracy measurement systems analysis is acceptable (3), while in the information theory of measuring devices are known, it is proposed to consider the value of Q. After comparison, refinement and mathematical transformations deter-mined that it is proportional to the relative entropy pohybtsi

$$Q = \frac{\xi}{2\Delta_\eta} \tag{4}$$

Scientific results that obtained on the basis of the theory and analysis of the methodological apparatus of research presented in is as follows. The difference metrological problems of problem studied in the model analysis process (4) and coupled with the analysis of the accuracy of transformation processes images, is that to improve the signal gradational parameters ξ primary image is converted into secondary nonlinear. In metrology usually measured values and measured on average equal to each other. In our case the function $\eta = f$ (ξ), which characterizes the studied process can be quite arbitrary and more so if the error appears only in the process of transformation, it actually means only error Δ □. This precision signal conversion

$$Q = \frac{\xi\eta'}{2\Delta_\eta} \tag{5}$$

where Δ_η — measurement error.

The transition from formula (4) to (5) occurred due to the fact that the equivalent value of error known pohybtsi Δ η proposes that the only gradient transfer function η'

$$\Delta_\xi \approx \frac{\Delta_\eta}{\eta'} \tag{6}$$

For all real processes, rather than empirical models [2], which have a limited range of conversion, the initial and final parts of the interval η '→ 0. Therefore, changing the accuracy of transformation within the interval for various processes has, in sufficient degree, uniform appearance, namely kolokolopodibnoyi function [4].

Personal contributions of authors is as follows. During the simulation found that the plots for the linear transformation (6), which η '= Const, the accuracy of the process depends on the error Δ η and at Δ $\eta \approx$ Const is constant and the characteristic curve has the form of (Fig. 1) . Then tonal transformation is proposed to estimate the number of gradations allocated to the process in the effective range of (Fig. 2) with the expression

$$G = \int_{\xi_1}^{\xi_2} Q \cdot d(\ln \xi) \tag{7}$$

The value of G (7) is called tonal resolution, which is defined in the process of modeling image analysis, and graphically as the area under the curve value of the logarithmic characteristic precision. Total number of gradations ε, transmitted in the modeling analysis for a particular image is determined

$$\varepsilon = e^J \tag{8}$$

The value of ε (8) offer a resolution to call an information analysis process. It depends, as it follows from above, from the statistical characteristics of the image signal and the effect of errors in the process of tonal image conversion using the developed device that (Fig. 1).

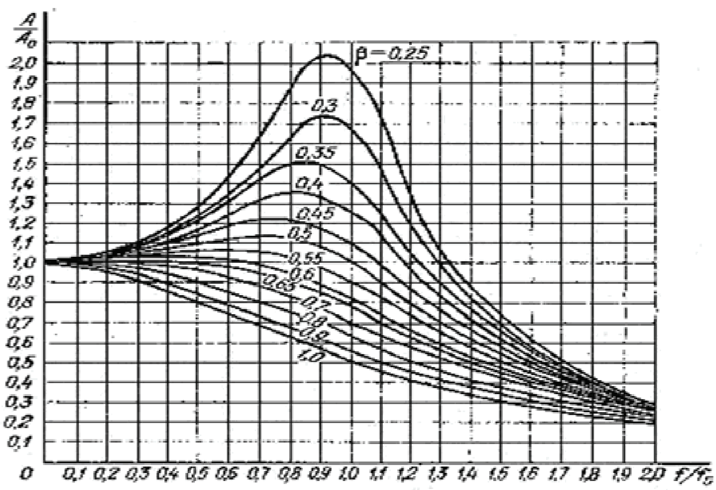

Fig. 1. Information criteria for evaluating the error processes. Information evaluation criteria tonal transformation. Where: A/A0 - the ratio of error processes visual Facilitation of Adaptation

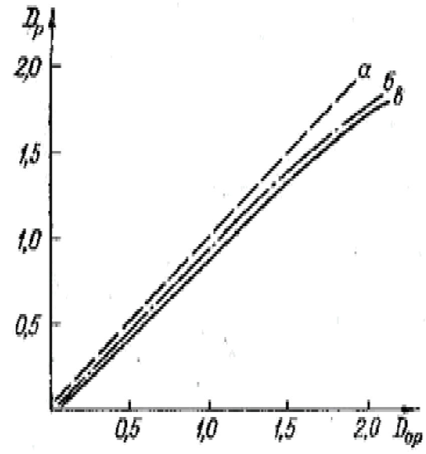

Fig. 2. Information criteria for error; f/f0 - value concept. Where: the process is investigated by frequencies for tonal conversion for different types of analysis using optical-tight media, characterized by coefficients β. Total Dp and Dop to different screens (a, b, c).

Conclusion

The first proposed alternative approach to solving problems of k image analysis on the theory that is based on information criteria, error estimates tonal transformation processes and visual perception, the study of information criteria for evaluating the error processes tonal transformation and visual perception under the influence of engineering and psychological factors. If the initial distribution of the image different from the equal probability, this means that the reserve was to increase the value of e1 to e2, ie G1 (of the eye in the process) <G2 (of the eye after the process) by reducing the interval svitloty secondary image in comparison with primary . However, even in this condition, if G1> G2 it is possible to realize when e2 = G2> e1. Installed on the results of experiments that when G2 <e1, improve secondary flight information in image compared to the original is not possible. Thus, in all considered cases should strive to bring the information capacity of perception of the secondary image to the ability of human eye perception, so that e2 → G2.

References

1. *Avaev AL, Moryn S., Kovalenko PA* Basic concepts of electronic systems and multifunction display controls aircraft / / Aerospace engineering. - 2003. - № 1. - P.43-48.

2. *Boyarsky AN, Lapa VV, AA Oboznov* Psychological study using color coding for multifunctional displays. / / Psychological Journal. - M., 1999. - № 5 - P.75-80.

3. *Ivanov AI, Lapa VV* Features dynamic management object in stereoscopic image / / Psychological Journal. - 2003. - T.24. - № 4. - P.43-46.

4. *Sitnik AG, NI Hodakovskyy* Features DEVELOPMENT Technical Systems of view to Restore zrytelnoy functions of human / / Uusimaa. - № 2. - K.: NASU IR, 2000. - S. 35 – 41..

5. *Ponomarenko VA, Zavalova ND* Aviation Psychology. Moscow: Institute of Aviation and Space Medicine, 1992. - 200 p..

6. *Pon omarenko VA, Lapa VV, AV Chuntul* Ergonomic problems of introducing new display and control the working environment of crew members of aircraft. In the book.: Activities litnyh crew and flight safety. - Moscow: polygraph. - S.146-153.

UDC 629.735.017 (043.2)

O.Tryzna
(National Aviation University, Ukraine)

ENGINEERING-PSYCHOLOGICAL ANALYSIS OF VISUAL INSPECTIONS QUALITY OF OLD AND NEW GENERATION AVIONICS

Represented results of work are connected with analysis of one of technological operations of aircraft maintenance, namely – visual inspection. The analysis of visual inspection technological operations for aircrafts of type AH-24 and AH-148 was performed on the basis of detailed studying and statistical processing of line and base maintenance task cards

Responsibilities connected with aircraft maintenance may be very complicated and may change in conditions, favorable for errors occurrence. Maintenance staff, at least in most developed aviation systems, often works at considerable time deficit. Operators have increased the intensity of aircraft operation in order to avoid economical difficulties of aviation field.

Also, technical specialists should often serve aging aircrafts. Nowadays there are often aircrafts of 20-25 years old in many air transport companies, including the largest ones. Moreover, many operators mean to go on operation of some of them in the near future. The installation of the noise absorbing devices complete sets on the engines of some old aircrafts makes them profitable for operation from economical point of view and from the point of view of environmental protection. However these aircrafts require intensive maintenance. Their airframe need diligent check of fatigue and corrosion prevent general wear. It makes additional load for maintenance staff and creates stress production situations, as additional maintenance is needed. If aging evidences, often intangible, stay undiagnosed, their consequences may be very serious [1].

While maintenance of aging aircrafts, many air transport world companies are filled with aircrafts, corresponding new level of technics development and this increases the volume of works, connected with aircraft maintenance. In the new aircrafts technical achievements are embodied, such as load-bearing element from composite materials, “glass cockpits”, automated systems, built-in-test equipment. The necessity to serve new and old aircrafts requires substantially new knowledge and skills from maintenance staff.

The understanding of the human factor importance during aircraft maintenance at this time increases. Safety and effectiveness of flights on air lines also become more connected with the quality of work of people, checking and serving airlines aircrafts. It makes pay attention to the aspects, connected with the human factor of great importance for aviation safety [2].

In this article there are results of work, connected with analysis of one of technological operations of aircraft maintenance, specifically with visual inspection (VI). This analysis is carried out on the basis of task cards studying as the main document of line maintenance and different checks of base maintenance planning and realization. Two types of aircrafts are considered: AH-24 (as the veteran of ukrainian aviation) and AH-148 – which recently started operation in airlines of Ukraine. The analysis was carried out for visual inspection operations (VIO) of different types of aircrafts.

Analysis of visual inspection technological operations for aircrafts of type AH-24 was realized on the basis of detailed studying and statistical processing of line and base maintenance task cards (issues 18 and 23; issues years – 1984-1986). Task cards were separately considered and correspondingly the data was grouped due to operations for specific type of equipment: navigation, electrical, instrument, fire and conditioning systems. For every technological operation there was counted up the number of visual inspection operation and total number of operations.

In a similar manner the task cards processing for the aircraft AH-148 was performed. As there was an access only for task cards for line maintenance, data is shown only for this type of maintenance.

Generalized data of statistical processing are shown in the tables 1 – 3. In these tables the data is shown in different sections.

So, in the table 1 there is data, characterizing the number of visual inspection operations for different kinds and forms of equipment maintenance of AH-24. In every cell of this table there is data, showing correlation of number of visual inspection technological operations and total number of operations in accordance with task cards for specific type of equipment and also percent correlation of previously shown values of numbers of operations.

Table 1

Number of visual inspection operations for different types and forms of equipment maintenance of AH-24

AH-24							
	Types of equipment	Types of maintenance					
		Line	B a s e (flightf hours)				
			300 ±30	600 ±30	900 ±30	1800 ±30	Total
1	Electrical, %	50/77 65	57/73 78	7/10 70	10/11 91	30/60 50	154/231 67
2	Navigation, %	22/25 88	44/70 63	–	10/13 77	–	76/108 70
3	Instrument, %	43/73 38	74/146 51	1/1 100	17/27	–	135/247 55
4	Fire, %	21/24 88	26/36 72	–	–	5/25 20	52/85 61
5	Oxigen %	13/23 57	54/56 96	–	–	–	67/89 75
Total		149/245 55	255/381 67	8/11 73	37/51 72	35/85 71	484/760 63

In the table 2 there is statistical processing data of task cards in a little bit another section. Here the dependence of equipment inspection operations of specific type for different maintenance types and checks is shown. It is possible to compare the data processing results for both types of aircrafts in this statistical data representation: AH-24 and AH-148.

On the basis of tables 1 and 2 selective data, allowing to compare number of visual inspection operations of different equipment types for aircrafts of type AH-24 and AH-148 was obtained. That data is shown in the table 3.

Statistical data in the table 3 may be represented graphically in the form of bar graph, shown in the figure 1. There are two bar graphs, placed one by one. In every graph on the X-axis there are types of aircraft equipment and on Y-axis – values from the table 3 in columns, characterizing the number of technological operations during maintenance of the given equipment. For every type of equipment there are two columns: left proportional to the general number of operations during line maintenance of the given equipment; right proportional to number of visual inspection operations. Numerical values are marked above every column and it helps to perform qualitative comparison, as well as quantitative.

Statistical task cards processing data, shown in tables 1 – 3 and in the bar graph 1, allow making some previous conclusions about visual inspection operations. First of all it is necessary to mention, that they concern only number of technological operations, connected with maintenance. For more complete statistical picture it would be necessary to obtain expenses on inspection operations execution and general loss of employment in maintenance realization for every group of equipment [3].

General number of visual inspection operations for all types of aircraft equipment of aircraft of type AH-24 is 149, while for AH-148 – only 75, that is twice less, while correlation between visual inspection operations and general number of operations almost match (are correspondingly 149/245 = 55 % and 75/129 = 59 %).

Table 2

Number of visual inspection operations, carried out during line and base maintenance for different equipment types of aircrafts AH-24 and AH-148

Types of maintenance		Number of operations	Electrical	Navigation	Instrument	Fire	Oxygen
AH–24							
Line		Total	77	25	73	24	23
		Visual inspection	50	22	43	21	13
		%	65	88	59	88	57
Base	Check 1 300 ± 30	Total	73	70	146	36	56
		Visual inspection	57	44	74	26	54
		%	78	63	51	72	96
	Check 2 600 ± 30	Total	10	–	1	–	–
		Visual inspection	7	–	1	–	–
		%	70	–	100	–	–
	Check 3 900 ± 30	Total	11	13	27	–	–
		Visual inspection	10	10	17	–	–
		%	91	77	63	–	–
	Check 5 1800 ± 30	Total	60	–	–	25	–
		Visual inspection	30	–	–	5	–
		%	50	–	–	20	–
AH–148							
Line		Total	40	47	31	4	9
		Visual inspection	21	24	25	4	4
		%	47	51	81	100	44

Note: according to check 4 (1200±30 flight hours) there are no visual inspection operations.

Table 3

Correlation of visual inspection operations for aircrafts of type AH-24 and AH-148

Aircraft type	Type of equipment									
	Electrical		Navigation		Instrument		Fire		Oxygen	
AH-24	77	50	25	22	73	43	24	21	23	13
AH-148	40	21	47	24	31	25	4	4	9	4

Five groups were selected from types of aircraft equipment, represented in task cards, as it shown in the tables: 1) electrical; 2) navigation; 3) instrument; 4) fire protection and 5) oxygen equipment. Data comparison shows, that operation distribution by different types of equipment for both aircraft types differs. So, for the aircraft AH-24 electrical and instrument equipment viewing is correspondingly 33 and 29 %, navigation (including communication equipment) and fire protection equipment - approximately about 15 %, and on oxygen equipment – approximately 9 %. For AH-148 relative number of operation due to the equipment types is distributed in following way: instrument -33,5 %, navigation equipment – 32 %, electrical – 25 %, and on fire and oxygen equipment - 11 % from the general number of visual inspection operations. As we can see the main work load of maintenance staff of AH-148 have the instrument and navigation equipment, while for the aircraft of type AH-24 – have instrument and electrical equipment. Operational expenses on fire and air equipment maintenance essentially decreased for AH-148 and have only 11 %, comparing with 23 % for AH-24.

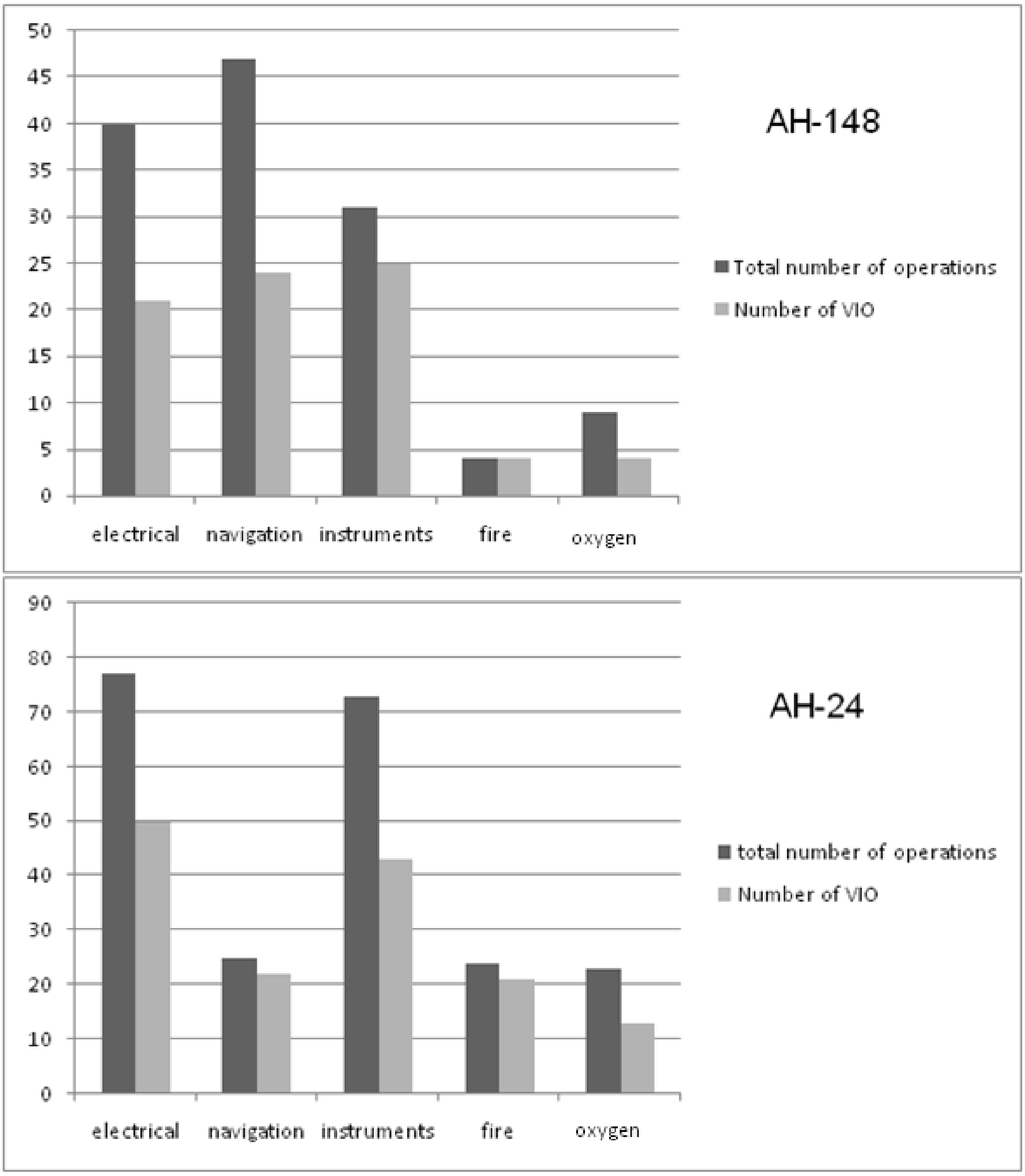

Fig.1. Bar graph of the results of task cards data processing results of the aircrafts AH-148 and AH-24 during line maintenance

Considering base maintenance we can compare data only of aircraft AH-24. As we can see from tables the prevailing number of visual inspection operations has the check 1 maintenance (works, carried out every (300±30) flight hours): 255 operations from 335 – total operations number for all forms of base maintenance.

Analysis shows that number of visual inspection operations is essentially decreased during the transition from lower to higher maintenance check and also depends on type of equipment. For the electrical equipment visual inspection operations are carried out on all checks of base maintenance in every 300, 600, 900 and 1800 flight hours, for navigation and instrument equipment – by checks 1 and 3, for fire – by checks 1 and 5, and for air – only by check 1.

On the bar graphs, showing relation between general number and number of visual inspection operations in test cards of AH-24 and AH-148 (fig.1) general number of operations predominate and it`s obvious, because task cards include not only operations connected with visual inspection, but also include assembly, blocks and systems disassembly, testing with the help of test equipment and some other operations.

Conclusions

1. Maintenance process of AH-24 (beginning from 1962) relatively to the new generation aircraft AH-148 is requiring the expenditure of much labour on general number of technological operations. Labour intensity decrease for AH-148 is reached with the help of new electronic equipment application, new technologies and principally different avionic structure relatively to AH-24.

2. Number of visual inspection operations and their comparison on aircrafts AH-24 and AH-148 shows that these operations take main part of maintenance technological operations of all types, as before. That`s why during the organization of maintenance it`s rather important to organize studying and training of maintenance staff, directed on visual inspection operations accomplishment optimization.

3. During maintenance of AH-148 it is necessary to intensify navigation systems (including communication) maintenance accomplishment control, especially concerning visual inspection checks.

References

1. *Human* Factors Training Manual / DOC 9683 – AN/950. – First edition. – Montreal: ICAO, 1998.

2. *Пилипенко А.А., Скрипец А.В.,ГрищенкоЮ.В* Особенности процесса эксплуатации воздушных судов авиатехниками среднего звена и его информационное обоснование с позиции авиационной инженерной психологи и эргономики // Кибернетика и вычислительная техника. – К.: НАН Украины, 2006. – Вып. 150. – С.38-43.

3. Общая теория статистики./Под ред. *А.А. Спирина, О.Э. Башиной*. – М.: «Финансы и статистика», 1996, - 296с.

UDC 004.5 (043.2)

O.Y. Burov, Dr of Tech. Sci., O.R. Tsarik,
(National Aviation University, Ukraine)

USABILITY OF INTERFACES

The main principles and heuristics of usability, as well as the importance and necessity of user-centered design are considered.

Introduction

In recent years human society evolved from the "industrial society age" and transitioned into the "knowledge society age". This means that knowledge media support migrated from "pen and paper" to computer-based Information Systems.

This evolution introduced some technological, organizational, and methodological changes affecting the demand, workload and stress over the workers, many times in a negative way.

Due to this fact Ergonomics assumed an increasing importance, as a science/technology that deals with the problem of adapting the work to the man, namely in terms of usability.

Usability is a quality or characteristic of a product that denotes how easy this product is to learn and to use [1]; but it is also an ergonomic approach, and a group of principles and techniques aimed at designing usable and accessible products, based on user-centered design.

User-centered design is a structured development methodology that focuses on the needs and characteristics of users, and should be applied from the beginning of the development process in order to make software applications more useful and easy to use [2; 3].

Usability and interfaces – Basic principles and heuristics

In some countries usability is a legal obligation. For instance, in European Union according to the Council Directive, 90/270/EEC, of 29 May, on the minimum safety and health requirements for work with display screen equipment, when designing, selecting, commissioning and modifying software the employer shall take into account the following principles:

- The software must be suitable for the task;
- The software must be easy to use and adaptable to the operator's level of knowledge or experience;
- Systems should provide users with information on its operation;
- Systems must display information in a format and at a pace adapted to users;
- The principles of software ergonomics must be applied, in particular to human data processing.

Therefore to meet these requirements the software development should be accompanied by an evaluation of its usability.

In simple terms, the usability of a system can be seen as the ease with which the system is used by its users, i.e., with the characteristic of being easy to use, or as is often said, to be "user friendly".

Therefore, usability is a feature of interaction between the user and the system. Usability evaluation can be based on a set of attributes, such as, operator performance (completing a task with reduced turnaround times and low error rates), satisfaction or ease of learning.

Usability can also be seen as synonymous of product quality, namely of software quality.

Usability is a critical aspect to consider in the development cycle of applications which requires a user-centered design and carrying out usability testing. Such tests cannot ignore the context of use of the software, which is essential to conduct usability studies. When human-machine interfaces are built taking into account usability criteria, interfaces are capable of allowing an intuitive, efficient, memorable, effective and enjoyable interaction. As Nielsen refers these characteristics influence systems' acceptability by users [4]. Figure 1 schematically represents the relationship of these particular characteristics with others that influence system usability.

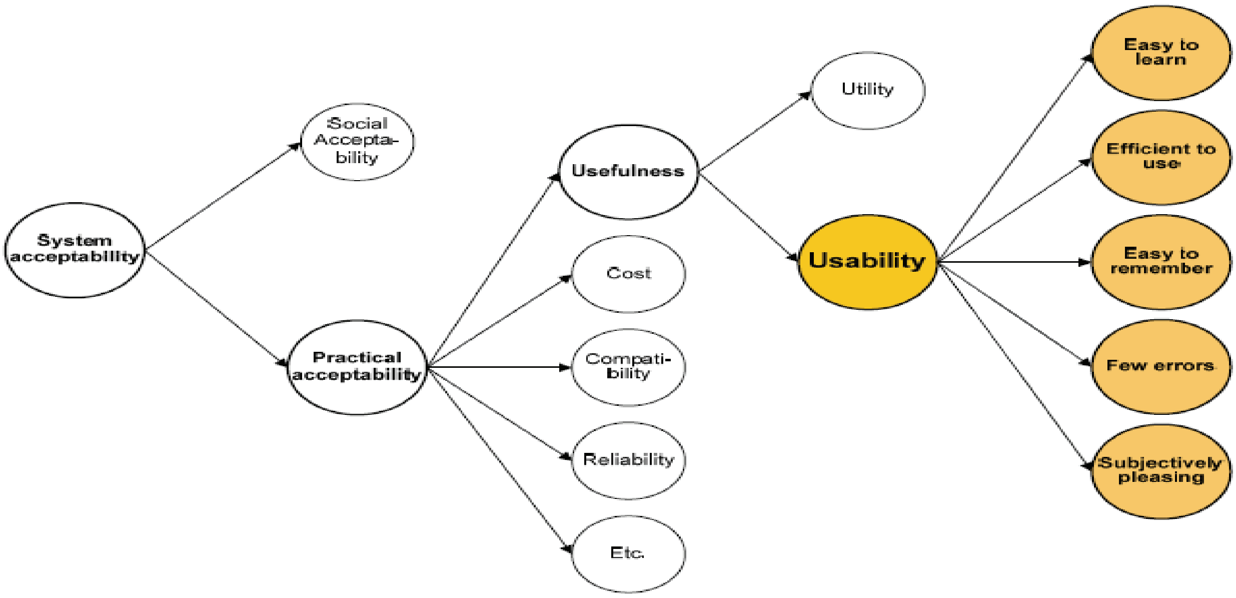

Fig. 1. A Model of the Attributes of System Acceptability (Nielsen, 1993).

Therefore, because of their influence in the usability of a system, it is important to define the concepts inherent to this set of characteristics [4]:

 Ease to learn - the system must be intuitive, i.e. easy to use, allowing even an inexperienced user to be able to work with it satisfactorily;

 Efficiency of use - the system must have an efficient performance, allowing high productivity, i.e., the resources spent to achieve the goals with accuracy and completeness should be minimal;

 Memorability - the use of the system must be easy to remember, even after a period of interregnum;

 Errors frequency - the accuracy and completeness with which users achieve specific objectives. It is a measure of usage, i.e. how well a user can perform his task (e.g. set of actions, physical or cognitive skills necessary to achieve an objective);

 Satisfaction - the attitude of the user towards the system (i.e., desirably a positive attitude and lack of discomfort). Ultimately measures the degree to which each user enjoys interacting with the system.

According to [5], when designing a product to achieve an appropriate usability developers should adopted the following 10 principles:

1. Consistency - similar tasks are performed in the same way;

2. Compatibility - the method of operation is compatible with the expectations of users, based on their knowledge of other types of products and the "outside world";

3. Consideration of user resources - the operation method takes into account the demands imposed to the resources of users during the interaction;

4. Feedback - actions taken by the user are recognized and a meaningful indication of the results of such activities is given;

5. Error Prevention and Recovery - designing a product so that the user likely to err is minimized and that, if errors occur, there may be a quick and easy recovery;

6. User Control - user control over the actions performed by the product and the state in which the product is are maximized;

7. Visual Clarity - the information displayed can be read quickly and easily without causing confusion;

8. Prioritization of Functionality and Information - the most important functionality and information are easily accessible by users;

9. Appropriate Transfer of Technology - appropriate use of technology developed elsewhere in order to improve the usability of the product;

10. Explicitness - offer tips on product functionality and operation method.

The design has also to consider the finite capability of humans to process information, to take decisions, and to act accordingly. These human characteristics have been thoroughly studied in the last decades, considering the Human Computer Interaction. Researchers that became a reference are, for instance, Hick (1952), Fitts (1954), or Miller (1956).

William Hick was a pioneer of experimental psychology and ergonomics. One of his most notorious researches was focused on the time a person takes to make a decision as a result of the possible alternatives, considering the cognitive information capacity, which was expressed as formula known as the Hick's Law [6].

Paul Fitts was a psychologist and a pioneer in human factors, which developed a mathematical model of human motion, known as Fitt's Law, based on rapid aimed movements [7]. This model is used, in the realm of ergonomics and human-computer interaction, to predict the time required to rapidly move to a target area, for instance to point with a hand or a finger, or with a pointing device in a computer interface.

George Miller was a cognitive psychologist that studied the average capacity of the human working memory to hold information. His studies concluded the number of objects an average person can hold is 7 ± 2 [8]. This is known as the Miller's Law or the "magical number 7". One relevant consequence of this finding relates with the ability of humans to evaluate and judge alternatives, which is limited to 4 to 8 alternatives.

Accommodating all these research contributions in a set simple of design principles is problematic; therefore a different approach is the definition of heuristics for the assessment of the interfaces usability. An example of such approach is the work of [9] that developed a set of heuristics to improve performance in the use of computers, which includes the following rules:

- Automate unwanted load:
  - Free cognitive resources for high-level tasks;
  - Eliminate mental calculations, estimations, comparisons, and unnecessary thinking.
- Reduce uncertainty:
  - Display data in a clear and obvious format.
- Condense the data:
  - Reduce the cognitive load, low-level aggregated data turning them into high-level information.
- Present new information with meaningful ways to support their interpretation:
  - Use a familiar framework, making it easier to absorb;
  - Use day-to-day terms, metaphors, etc..
- Use names that are conceptually related to functions:
  - Context-dependent;
  - Trying to improve recall and recognition;
  - Grouping data consistently significantly reduces the search time.
- Limit data-oriented tasks:
  - Reduce time spent in acquiring raw data.
  - Make the appropriate use of colour and graphics.
- Include only information on the screens that the user needs at any given time.
- Provide multiple coding of data, where appropriate.
- Practice a judicious redundancy.

A software program developed taking into account usability principles offers advantages, as decreased time to perform a task; reduced number of errors; reduced learning time, and improved satisfaction of system's users.

User-centered design

One approach to the use of the concept of software usability is the user-centered design. The user-centered design is a structured development methodology that focuses on the needs and characteristics of users, should be applied from the beginning of the development process in order to produce applications software more useful and easier to use [2; 3].

According to ISO 13407 (ISO 13407, 1999), there are four key activities related to user-centered design, which should be planned and implemented in order to incorporate the requirements of usability in the process of software development (see Figure 2). The activities aim to:

- Understand and specify context of use;
- Specify the user and organizational requirements;
- Produce design solutions;
- Evaluate design against requirements.

These activities are performed iteratively, with the cycle being repeated until the usability goals have been achieved.

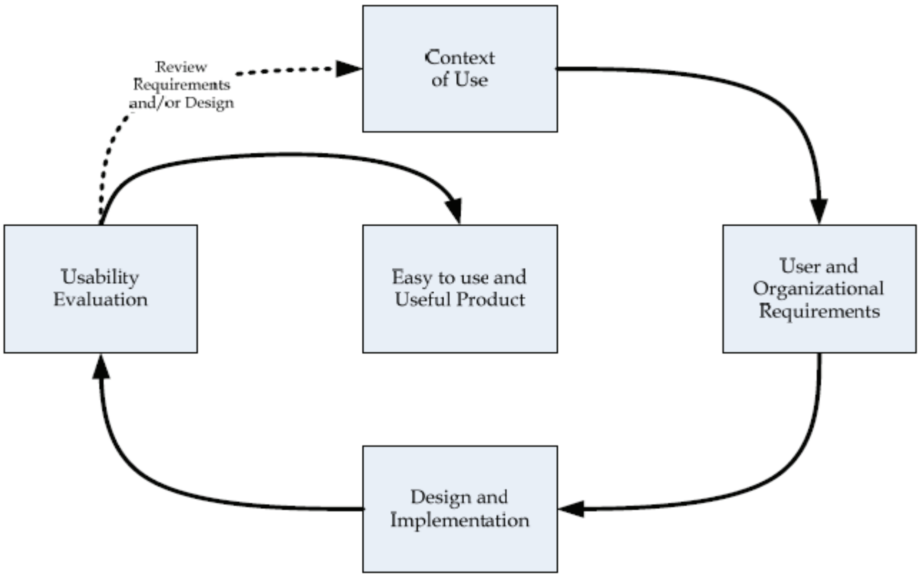

Fig 2. Activities of user-centered design, adapted from ISO 13407 (ISO 13407, 1999).

According to [11], the Usability Engineering process, which aims to implement the activities mentioned above regarding usability evaluation, includes (Figure 3):

- Identify and record critical usability data;
- Data analysis;
- Preparing the report of the evaluation results.

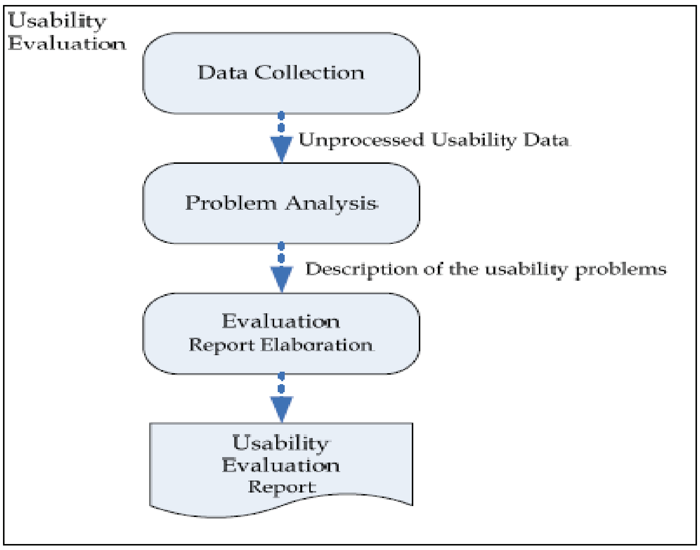

Fig. 3. Usability Evaluation, adapted from [11].

Conclusions

Usability is a critical aspect to consider in the development cycle of software applications, and for this purpose, user-centered design and usability testing must be conducted. The design and testing cannot ignore the context of use of software, whose knowledge is essential.

Usability of a system is characterized by its intuitiveness, efficiency, effectiveness, memorization and satisfaction. Good usability allows decreasing the time to perform tasks, reducing errors, reducing learning time and improving system users' satisfaction.

Usability, process design and development of software have necessarily to be framed by the characteristics of users, tasks to perform and environmental context (social, organizational and physical) for which the product is intended to.

The development of a product must consider the 10 basic usability principles: consistency, compatibility, consideration by the resources of the user, feedback, error prevention and error recovery, user control, clarity of vision, prioritization of functionality and information, appropriate technology transfer, and clarity.

References

1. *Dillon, A.* (2001). Evaluation of Software Usability. In: International Encyclopedia of Ergonomics and Human Factors, W. Karwowski (Ed), pp. 1110-1112, Taylor & Francis

2. *Averboukh, E. A.* (2001). Quality of Life and Usability Engineering. In: International Encyclopedia of Ergonomics and Human Factors, W. Karwowski (Ed.), pp. 1317-1321, Taylor & Francis

3. *Nunes, I. L.* (2006). Ergonomics & Usability - key factors in knowledge society. Enterprise and Work Innovation Studies, Vol. 2, pp. 87-94

4. *Nielsen, J.* (1993). Usability Engineering, Academic Press,

5. *Jordan, P.* (1998). An Introduction to Usability, Taylor & Francis

6. *Hick, W. E.* (1952). On the rate of gain of information. Quarterly Journal of Experimental Psychology, Vol. 4, pp. 11-26

7. *Fitts, P. M.* (1954). The information capacity of the human motor system in controlling the amplitude of movement. Journal of Experimental Psychology, Vol. 47, No 6, pp. 381- 391

8. *Miller, G. A.* (1956). The magic number seven, plus or minus seven. Psychological Review, Vol. 63, No 2, pp. 81-97

9. *Gerhardt-Powals, J.* (1996). Cognitive engineering principles for enhancing human - computer performance. International Journal of Human-Computer Interaction, Vol. 8, No 2, pp. 189–211

10. ISO 13407. (1999). Human-centred design processes for interactive systems. International Organization for Standardization

11. *Howarth, J., Smith-Jackson, T. , Hartson, R.* (2009). Supporting novice usability practitioners with usability engineering tools. Int. J. Human-Computer Studies, Vol. 67, No 6, pp. 533-549

UDC 004.932.721 (043.2)

O.O. Chuzha, PhD of Tech Sci
(National Aviation University, Ukraine)

AUTOMATIC SURVEY-COMPARATIVE NAVIGATIONAL

Today appear one of most perspective survey-comparative methods of navigation. The basic element of such systems is a man which executes an eventual position-fix aircraft. Automatic navigationals on the basis of survey-comparative methods of navigation appear perspective for application in pilotage-navigation complexes of modern air ships

One of the oldest methods of navigation - survey-comparative - has the special value for modern aircrafts. The modern survey-comparative systems provide the integral recreation of complete totality of navigation data, co-operate with side digital calculable machines, correct other sensors of navigation information and appear the major informative link of the system "an aircraft is a crew" [1].

Without regard to the variety of technical realization, essence of survey-comparative methods of navigation consists in determination of location of air ship by comparison of the locality represented on a map or memory of calculable machine, with her actual kind looked after by means of side survey devices (televisional sights, radiolocation systems and other) or by sight. If the images of locality gather on a map and looked after her kind, then the location of object is considered identified, and coordinates of him are defined.

Advantages of survey-comparative methods of navigation are:

- high authenticity and exactness of measuring;
- absence of story errors;
- possibility to conduct measuring in any districts of Earth and circumterrestrial space;
- high level of informative surplus of measuring;
- possibility of the use of the manned(visual orientation) and automated facilities of measuring.

However, there are defects and limitations in the input of survey-comparative methods. Measuring is possible only at visibility of terrene or reference-points. Influence of obstacles - cloudiness, fogs, insufficient luminosity - can substantially bring down efficiency of survey-comparative navigation. In addition, at flights above locality without reference-points (seas, deserts et cetera) this type of navigation needs the presence of the additional brightly-expressed artificial reference-points with a well-known location.

Navigation maintenance of survey-comparative methods of measuring is determined by the type of reference-points and their amount. Comparison of the physical parameters of standard object(area, geometrical forms, spectrum of radiation and other), stopped up in memory of the system, comes in the referencepoint systems true, with the measureable parameters of the real object. A few reference-points are simultaneously used in the reference-point systems. In memory of such systems information is kept not only about the physical parameters of separate reference-points but also coordinates of their mutual position. Advantage of the reference-point systems is a large volume of navigation information, less dependence on the loss of part of information about reference-points and influence of obstacles. However for realization of such systems it is necessary to have the powerful electronic computing engineering.

Realization of survey-comparative methods of navigation is taken to the performance of objective of recognition of reference-points (ground or astronomic) to comparing of them to the standard reference-points the site of that is known, and in relation to these reference-points to set the coordinates of aircraft.

The modern stage of development of scientific and technical progress determines automatic recognition of objects one of priority directions of researches for creation and improvement of automatic survey-comparative navigationals. Much attention in the modern aviation systems the Russian scientists spare the problems of technical sight [2], what examine possibilities of application of the automatic systems of recognition of surface objects for the facilitation of work of crew in the mode of event on landing in difficult terms. In particular the Moscow state scientifically-research institute of the aviation systems and Ryazan state radiotechnical university examine possibilities of application of various types of sensors of a priori information for the systems of technical sight. In particular the Moscow state scientifically-research institute of the aviation systems and Ryazan state radiotechnical university examine possibilities of application of various types of sensors of a priori information for the systems of technical sight.

Depending on physical nature of the perceived signals the sensors of the survey-comparative systems of navigation are divided by: optical (infra-red (thermal imaging), televisional (brightness), laser), radiation and radiotechnical.

Optical sensors (infra-red and televisional) mainly passive type. Televisional (brightness) sensors distinguish signs on the basis of difference of brightness between an object and environment. The lacks of the televisional systems of navigation is technical complication, large sensitiveness to the obstacles and limitation in visibility of reference-points. The televisional system can normally work only at optical visibility of reference-points and at their sufficient illumination.

Infra-red (thermal imaging) sensors distinguish signs on the basis of overfall of thermal (infra-red) contrast between an object and surrounding background. The infrared of energy answers lengths of waves of 700...300000 nm and it is located in part of spectrum, invisible for a human eye. Infra-red devices have a high inertance and limit nature for distances of action. Fog or rain limit their effective application, and the erroneous source of radiations can cause considerable deviation of aircraft from the trajectory of motion.

Radiation sensors have an elaborate design and technical realization, that is why as sensors of the survey-comparative systems not examined.

In radiolocation sensors extraction of features is executed on the basis of treatment of the electromagnetic signals removed from objects. Radiolocation sensors are active or semiactive type. For a radio-location radio waves are used in the range of lengths of waves of order a 1...3 cm. Exactly for such radio waves the atmosphere of Earth is fully transparent. Anymore the shortwave are notedly taken in by the molecules of oxygen and aquatic vapors. The use of long-wave emitters requires a presence onboard of aerials of largenesses.

With the use of laser sensors possible creation of the laser location systems that distinguish signs on the basis of construction of two-dimensional (2D) and three-dimensional (3D) images of objects [3]. Laser sensors can be active or semiactive type.

All enumerated types of sensors differ in information got after their help content that in future can be used for automatic recognition of objects, complication of receipt of information, that depends on the volume of calculations, amount and complication of algorithms, technical account of devices the operationability of the use of the got information. Quality description of sensors is represented on Fig. 1 [4].

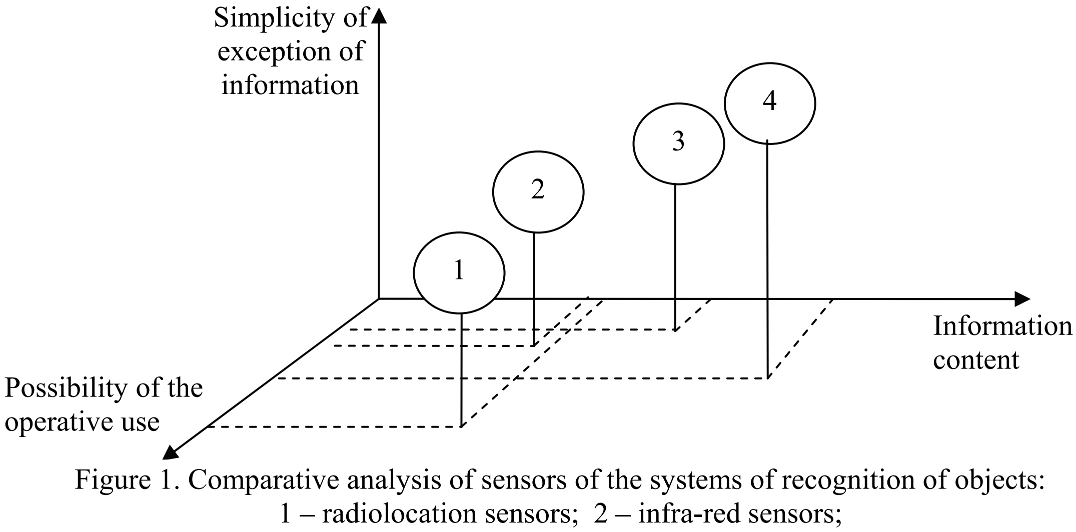

Figure 1. Comparative analysis of sensors of the systems of recognition of objects:
1 – radiolocation sensors; 2 – infra-red sensors;
3 – televisional sensors; 4 – laser three-dimensional (3D) sensors.

The comparative analysis of sensors testifies that maximal information content can be got from televisional and three-dimensional laser sensors, but they have the difficult system of exception of information. Information is most simply withdrawn by infra-red sensors, but taking into account influence of the enumerated factors, this information it can be not enough for correct recognition. Radiolocation sensors have the maximal opportunity of realization, so as allow to find out objects and distinguish their signs on distances in a few ten of kilometres, but the got information it can be not enough for automatic recognition. The analysis of achievements in area of three-dimensional picture generation and creation on their base of automatic identification devices shows that most perspective are the laser systems of three-dimensional picture generation [5].

For registration of three-dimensional (3D) images the active devices of reflection, LADAR behaves to that, - laser device of reflection of three-dimensional space and three-dimensional form of object of supervision apply, as a rule [6]. By basic properties of LADAR, that promote efficiency of the optical systems of reflection, are:

- quality of a 3D image does not depend on the size of contrast that can equal a zero, and from the changes of base-line situation;
- a 3D image contains metrical information about a three-dimensional form and sizes of object of supervision that is basic signs at his recognition;
- possibility of work in the conditions of zero-zero, at subzero transparency of atmosphere and at influence of light obstacles;
- long-range enough of action.

For a three-dimensional picture of objects and their further recognition generation it is necessary to define signs that can be withdrawn on the basis of three-dimensional images and that characterize recognizable objects most full. The analysis of signs of surface objects is conducted on the criterion of utility shows that the most informing signs that does not depend on the type of sensor are geometrical signs (size, area, configuration, volume et cetera). The use is for extraction of geometrical features of laser sensors, that form the three-dimensional images of objects, are most expedient from the point of view of simplicity of receipt of maximal information content for the minimum interval of time.

Principle of three-dimensional picture generation consists in the following (Fig. 2). Measuring of distance (R) in the laser systems (taking into account velocity of light of $c=3\cdot10^8$ m/s) is fixed sometimes (t) passing of radiation from a transmitter to the receiving system of

$$t = 2R / c.$$

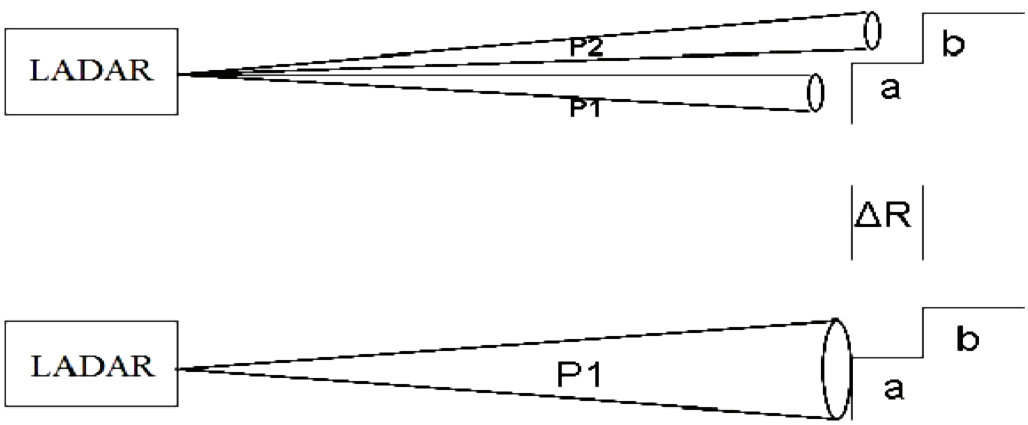

Figure 2. Principle of three-dimensional picture generation by LADAR.

If an object has a spatial form distance to his elements of form (a; b) will be different (R_1 and R_2) and will be fixed by the different elements of matrix transceiver of radiation (P1 and P2 accordingly). Therefore at the irradiation of object by the impulses of nanosecond duration the degree of his spatialness can be characterized the difference of distances to every element of form of

$$\Delta R = (R_1 - R_2).$$

The time-of-flight of radiation for every element of form will consist of time (t) that characterizes minimum distance to the object (R_1) is distance to the object, and sentinel interval (τ) that characterizes distance (ΔR) between the elements of form of object ($a; b$) – id est him spatial constituent:

$$t + \tau = 2(R + \Delta R) / c,$$

where $\tau = 2\Delta R/c$.

Thus fixing every element of transceiver of radiation the sentinel interval of ладар gives an opportunity to get three-dimensional digital representation of earth surface with the reference-points placed on her. In future a survey-comparative navigational will compare the got image to standard and in case of coincidence will allow with probability close 90% to define the coordinates of air ship.

There are some varieties of reference-point navigationals. It the cross-correlation-extreme navigational of robot of that is based on the use of cross-correlation connections between realization of casual functions for determination of navigation parameters of surface objects(coordinates, sizes, orientation) by means of searching for of extremum of cross-correlation function. But integral survey-comparative complex systems of robot of that based on establishment onboard simultaneously a few survey-comparative systems that perceive the pictures of locality and surrounding space sensors with different physical principles of treatment of information. The integral systems of reflection produce to the crew navigation information from the enormous amount of sensors, synthesize on-line, command, control and other data necessary for implementation of tasks to the navigation.

Conclusions

Realization of automatic survey-comparative navigationals is taken to the performance of objective of recognition of surface reference-points, to comparing of them to the standard reference-points the site of that is known, and in relation to these reference-points to set the coordinates of aircraft.

Recognition of surface objects in such systems most expediently can be realized by 3D sensors on the basis of LADAR, that forms digital three-dimensional representation of earth surface. Got a 3D image can be used for the automatic exposure of surface reference-points and determination of them geometrical signs necessary for the job of automatic recognition processing.

Automatic navigationals on the basis of survey-comparative methods of navigation are autonomous and perspective for application on modern air ships. Basic advantages of such systems are high exactness of measuring, absence of story errors, possibility of the use of the automated facilities of measuring.

References

1. *Shivrinskay V.N.* On-board computer systems of navigation and piloting: lecture notes. - Ulyanovsk - 2010. - 148 p.

2. Computer vision in control systems of the mobile objects proceedings of the conference-workshop-2010. No. 4. - M.: DCD, 2011. - 328 p.

3. Flight International, 1989, 22IV, v. 135, № 4166, p. 13.

4. Microprocessing and Microprogramming, 1989, VIII, v. 27, № 1-5, p. 143-146.

5. Aviation Week and Space Technology, 23/XI, 1987, № 21, v. 127, c 24 - 29.

6. *Richmond R.D., Cain S.C.* Direct-Detection LADAR Systems, SPII, Washington. 2010.

UDC 656.7.086 (043.2)

Dr. Olena Petrashchuk, Olgha Volk, research assistant
(National Aviation University, Ukraine)

SAFE SPOKEN INTERACTION IN GROUND-TO-AIR COMMUNICATION

30000 flights per day : the complexity of European airspace demands effective communication between pilot and controller in English. Air Traffic Controllers/Pilots have to take an English Language Test before licence renewal process. The assessment of the Operational level must be done by the testing procedure as prescribed by recommendations in ICAO Doc 9835, Chapter 6 (2010) and Cir 318 (2009).

FUNDAMENTAL AVIATION LANGUAGE ISSUES:
Three critical areas of English competency required for safe *communications* in aviation:

- Air Traffic Control phraseology
- English for specific purposes (emergency)
- English for general purposes (aviation context)

PROFICIENCY EL TEST IN AVIATION : Listening and Speaking components which quality meets requirements to high stake tests, namely face/content validity coefficient should be 0,9, reliability coefficient y – 0,7 (for Speaking test) and 0,9 (for Listening test);

Proved practicality (availability and feasibility of administration);

Verified usefulness/specific needs sensitivity;

Verified job related test setting (simulated work setting).

Various factors might impact Oral Test Quality due to the fact that speaking is a complex phenomenon. It can be characterized in terms of cognitive processes, language knowledge, social interaction, communication strategies, etc. These characteristics are to be taken into account for the test being valid and reliable.

Measurability of an oral speech sample can be considered as a key test quality to obtain reliable test results. Therefore a test setting, contingent, stakes and aims should be taken under consideration. Measurability of an oral speech sample is specifically getting an issue in case of language testing for specificpurposes.'Speaking model': before speaking speakers make choices about the language they use based on:

- what they want to say;
- what medium they are operating in;
- how texts are typically constructed in such situations;
- what grammar they can use
- what words and expressions they can find to express their meanings (Harmer).

Following the L1 vs L2 speaking model the following should be taken into account:

- L2 speakers typically have incomplete knowledge because they don't have the same number of words and rules as L1 speakers;
- L2 speakers speak with more errors and slips and are more hesitant and less automatic then the L1 speaking;
- speech of L2 speakers often reflects traces of L1 which is more developed then L2.

Spoken interaction is provided:

- by producing and negotiating language;
- speaking and listening simultaneously in producing and processing spoken interactions (Schmitt);

- creating speech meaning by both interlocutors 'in joint constructions' (Davidson, Fulcher);through prism of behaviours and strategies;
- at the discourse level, speech behaviour is coordinated by adherence to turn-taking rules.

Speaking is an oral communication and is dependent on others.

The utterances or speech acts are manipulations of language for the purpose of arriving at *'mutual understanding'* between those who communicate. In aviation – between a pilot and a controller. Speech behaviour of these two interactants is based on 'cooperative principle' (Grice) which means that a speaker should:

- make their contribution as informative as required;
- make their contribution true;
- make their contribution relevant;
- avoid obscurity and ambiguity;
- be brief and orderly (Harmer).

Speech behaviour based on the cooperative principle can provide *reciprocity of communication* and, therefore, *mutual understanding.*

Like in real world communication in testing setting a candidate's behaviour can be affected by other participants' behavior, e.g., by an interlocutor during one-to-one interview. In other words, the interlocutor's strategies might impact on a candidate's behaviour.

Matching/mismatching of interviewer and candidate behaviour should be controlled by regarding: level of turn taking, level of rapport, verbal/nonverbal interaction, native/nonnative language participant, interview format and organization.

Therefore the interlocutors' strategies should be within the 'caretaker speech' (Littlewood) format. The 'caretaker speech' is generally spoken more slowly and distinctly, contains shorter utterances, is more grammatical, with fewer broken sentences or false starts, contains fewer complex sentences and less variety of tenses/ vocabulary, is more repetitive and related to the 'here-and-now'. In testing situations it is important for a N/S English examiner/interlocutor to adjust his/her language level to meet or match the level of the L2 candidate.

Communication strategies in real world communication should match interlocution strategies in testing situations of communication:

Communication strategies (Littlewood):

1/ to avoid communicating;
2/ to adjust the message;
3/ to use paraphrase;
4/ to use approximation;
5/ to create new words;
6/ to switch to the native language;
7/ to use non-linguistic resources;
8/ to seek help.

Possibly matched interlocution strategies:

1/ giving a candidate time
2/ seeking 'bottom/top of ELP'
3/ responding to clarification strategy
4/ adapting to L2 candidate
5/ situational/linguistic complication
6/ not accepted
7/ encouraging by gesture, facial expression
8/ unexpected turn of topic

Conclusions:

It is a crucial issue to provide useful testing in aviation. It requires replication of real world spoken language strategies within the testing situation and through interaction between a candidate and an interlocutor. For aviation purpose it is important that an oral interview structure/scenario is to simulate real world spoken strategies based on cooperative principle.

References

1. *Harmer J.*The Practice of English Language Teaching, Fourth Edition.Essex: Pearson Education Limited, 2007. – 87 p.

2. *Schmitt N.*An Introduction to Applied Linguistics.London: Hodder Arnold, 2002. – 204 p.

3. *Davidson F., Fulcher G.* Language Testing and Assessment: an advanced resource book. New York: Routledge, 2007. – 148 p.

4. *Grice H. P.* Logic and Conversation. /Martinich A.P. (ed). Philosophy of Language.New York, NY: OxfordUniversity Press, 1975. – P. 165-175/

5. *Littlewood W.*Foreign and Second Language Learning.Cambridge: CambridgeUniversity Press, 1984. – 79 p.

6. *Stern H.* Fundamental Concepts of Language Teaching. Oxford: OxfordUniversity Press, 1983. – 298 p.

7. Manual on the Implementation of ICAO Language Proficiency Requirements/ ICAO Doc 9835 AN/453: ICAO Second Edition. - Montreal, 2010. – 186 p.

UDC656. 7.086:658.336:811.111:656.7.071.13 (043.2)

K.O. Povoroznyk,senior teacher
(National Aviation University, Ukraine)

EQUAL PARTNERSHIP IN AIRNAVIGATION DIALOGUE AS A CONDITION OF HUMAN FACTOR NEGATIVE IMPACT ELIMINATION DURING R / T COMMUNICATION.

The claims are about a dialogical approach in prospective air traffic controllers aviation English teaching focusing upon the vitality of human factor as a part of successful "air – to– ground" communication.

The primary means of communication between controller and pilots is verbal, through the use of radio telephony (RT). Commands and clearances from the controller allow the pilot to navigate through crowded terminal areas with the required amounts of separation. Controller-pilot communications are also vital for exchanging information about weather, traffic flying under visual flight rules, runway hazards, etc. Communications between controllers are also required for efficient handoffs between sectors, planning, scheduling, and other activities. Consequently, attention has focused on the nature of verbal communications and its role in the overall workload of the controller (Cardosi, 1993; Kanki and Prinzo, 1995; Prinzo and Britton, 1993).

According to the latest research when controllers spend more than half their time communicating with pilots - their traffic awareness becomes disturbed. As a matter of fact , the effect of any task factor or workload driver (such as a visual flight rules or instrument flight rules pop-up) that normally has a small impact on mental workload and performance may substantially increase. Moreover, different aspects of controller-pilot communications (e.g., message length and composition) also have an impact on pilot workload (Morrow, in press; Morrow et al., 1993).

In our research we adhere to the provision that mentioned above aspects referring to human factor should be taken into account while teaching prospective air traffic controllers building the dialogical relationships in radiotelephony communication and, what's really important, represent an interaction between equal partners, despite monologue "relations", that neglect equal partnership.

So, we state that aero navigation communication, from dialogical perspective, is not only lingual equality between interlocutors, but also "no emotional and cultural bias" interaction where neglecting its importance leads to aeronautical communication deformation. It should also be mentioned that there ultimately exists consciousness subjectivity and consequently specificity of mutual understanding in "pilot – controller" communication - therefore, we suggest the basics of psycholinguistics in air traffic controllers education should become an indispensible part.

While Bakhtin M introduces a special concept known as a dialogization of languages, that is vital in our research context for comprehending radiotelephony phraseology and Aviation English correlation, Leontiev A., on his part, stresses the importance of psychophysiological part of lingual organization [5].

According to scholars, sense structure of an operational task creates its own sensory synthesis, which correlates with the quality and contents of self – organizing afferent synthetic merge principles necessary for task resolving.

That is why we accept the idea of the language dialogization that makes a complex unity of interlocutors, for meaning in a language resides not only in my intention but in what I speak at a point between two communicators psychology and linguistically expressed "task – resolving - orientated" intention.

It is also important to mention, Bakhtin's dialogue concept being a vital part of our research intersubject approach theoretical background comprises human factor psychology aspect as well.

Pedagogists and scientists differently applied Bakhtin's dialogue concept provisions. There was developed a theory of the intersubject (dialogical) approach, where the following concepts aimed at the intersubject approach application have been highlighted: personal involvement, textual reincarnation, message and etc; apart with that, three types of messages have been introduced - dialogical, authoritative and conformistic.

According to some scientists, emotional and personal openness of the interlocutors, their psychological empathy, label avoidance are ranged as the key principles of dialogue structure.

It should, also, be mentioned that the relations of communication and activity as a part of multitask operations substantially influence the indexes of the air traffic controllers performance.

In case of non-standard situations two sides of the radiotelephony dialogue may be differently aware of the situational risk factors where the optimal task decision calls for interlocutors capability of rejecting own suggestions and finding adequate argumentation without experiencing linguistic and psychological barriers.

In terms of "pilot – controller" communication we may refer to Lomov's B., definition of the interaction as an organizing component of multitasking; we add here human factor oriented interaction.

On his part, Djakonov G. focuses upon the personal integrity influence upon a dialogue (mainly intra psychic, interpersonal and transpersonal domain) [1].

The core of education is discourse: the dialogue of query and feedback in which both communicators ask and both answer; the dialogue of the joint study by teacher and pupil, the dialogue in which the intervals of silence are no less dialogic than spoken discourse (Cohen)

We may add here that the "intervals of silence" may appear to be in "air - to – ground" communication no less dialogic and helpful in urgencies in case dialogical approach is used in prospective air traffic controllers training.

Buber's dialogue vision reflects communication's "central" role in language which becomes a powerful means during "sense - and - meaning – making" processes.

Exploring Oneself and perceiving the "Other" in its singularity is a two-fold task for every airtraffic controller. Educators must responsibly help prospective airtraffic specialists, developing their psycholinguistic capabilities since that prods an airtraffic controller to'know'pilot's demands better through lingua – psychological cooperation.

Prominenet scholars place much weight on the responsibility of individuals who have to maintain "conscious effort to create the quality of their social space", that is to have an appropriate attitude to being and relationships so that the "I-Thou" could be formed and transformed. In aviation communication such attitude may be ultimately of importance.

The "I-Thou" dialogue has much to do with Buber's community philosophy [2]. As Murphy (1988) points out: "Just as the intimacy of interpersonal relation is rooted in the essential mutuality and reciprocation of the "I-Thou," so the true spirit of community life is traced in his work to the dynamic plurality of the I-We".The plurality of this reciprocation, based on the genuine address of the "I" and the genuine response evoked in the Thou, reflects the quality of the community spirit [7].

According to Buber, education as pure dialogue requires learners to stay open to the reality of the unconditioned and intemporal the unknown and undisclosed [2].

In science, sometimes the focus is shifted upon a special role of personal individual factors affecting the efficiency of dialogical communication. Thus, Karneev R. worked out a conceptual paradigm of pedagogical communication. The given paradigm is based on the understanding of a special role of a dialogue and intersubject approach during communication.

We on our part highly appreciate mentioned - above ideas as far as psycho – physiological characteristics determine the dynamo of reactions and responses during communication, combining efficiency of communication and multitasking, unbiased information perception thus affecting communication safety of air navigation specialists.

So the need for new pedagogical approach is conspicuous and we suggest it is to be based on the intersubject approach during air navigation specialists teaching. We also consider air navigation specialists communication should represent the dialogue of the highest rate that conforms with unique professional features. The analysis of scientific works devoted to the dialogue role in professional communication make us brining forward the conclusion as for the concept of a dialogue of the highest rate, mainly the possibility of the maintenance of the latter on the condition of interpersonal communication, where two personalities, not persons are involved.

Interpersonal communication and interaction phenomena were studied by the following scientists: RodgersC, Jurard C, Lomov B. [4, 7, 6].

Rodgers C. developed theoretical formulations and hypotheses as to the basis of effectiveness in relationships. According to the scholar,individuals sharply different in personality, orientation and procedure can all be effective in a helping relationship, can each be successful in facilitating constructive change or development on the condition they bring to the helping relationship certain attitudinal ingredients. The first of them is congruence. By this Rodgers mean that the feelings the interlocutor is experiencing are available to him, available to his awareness,
Empathy is another ingredient that may excert the effect on communication substantially increasing its performance.

Being the second essential condition in the relationship when he is experiencing an accurate empathic understanding of his communication partner, and is able to communicate some of the significant fragments of that understanding thus providing essential growth-promoting of relationship.

Thus, humanistic psychology representatives (Rodgers K, Jurard C.,) looked into interpersonal communication from position of personal approach representing such main attributes of a personality as sociality, subjectness, morality, transcendicity and uniqueness.

There exist different approaches to interpersonal communication issues study which are brought to a generalized scheme and that is their main drawback. Interpersonal communication (professionally – oriented for our research) may be actualized through interaction, influence, manipulation; it can develop according to the logics of the course of actions or against it, propagate humanistic solutions or demonstrate egotism.

There exist an opinion the interaction merely forms the structure of multitasking at each stage being represented in every component (aim, motives, means of realization)

There was also introduced the fundamental – paradigm concept representing psychological specificity of affect and interaction. (Kovalyov G.)

The scholar asserts the interlocutors subjective characteristics are altered during interaction (the needs, capabilities, relationship, behavior).

The researcher also determines three paradigms of psychological influence strategies. The first paradigm refer to human psyche as a passive object of external influence; another subject paradigm focuses on the personal activity and an optional external influences psyche reflection, where a subject excerts an efficient influence on psychological information.

Subject – subject (dialogue) paradigm represents a special value for our research introducing psyche as an open continuously interacting system with its own means of control. We should mention here, the first two mentioned – above paradigms appeal to monological outlook, intersubject paradigm, on contrary, deals with dialogue perspective.

That is why the psychology of communication influence phenomenon can be both objective and subjective and intersubjective one we refer to interaction phenomenon. So, the main difference between influence and interaction phenomenal reflects different perception perspectives: monologue and dialogue.

We suggest the quality of radiotelephony interaction of air navigation specialist calls for special dialogical readiness formation that shouldn’t be bounded with a communicative dialogue and better resonates with metacommunication (human factor consideration in our research).

Scientists adhere the point that the process of communicative influence presupposes personal outlooks and interlocutor senses being dialogical by its nature that is determined by the intersubject nature of a personality. So, any communicative impulse, despite monological or dialogical elements predominance is a reflection of a personal natural dialogical tendency and appeals to subject – subject innate organization.

According to Dyakonov G. there exist a special form of the intersubject – dialogical methodology type that correlates with such forms and methods of teaching that are centered around multiple co – existences of communicators. Subject – subject, dialogical forms and teaching methods should definitely be realized through personal communication actualization, equal partnership interaction and innate consciousness dialogicity of communicators [1].

The scholar also relates a dialogical (intersubject) approach to the system of active teaching – communication methods is based on understanding of dialogue final importance. Putting into force the issue of education optimization through subject - subject interaction would exert a deep influence on psychic and personal development dimensions of communicators.

Consequently, psycho - personal dialogue dimensions determine educational strategy and prospective professionals communication.

Conclusion

Presently, it is vital to suggest an alternative for organizing professionally - orientated interpersonal dialogue communication from perspective of integral personality concept.

The integral personality concept in our research reflects the specificity of air navigation communication, that features intersubject dialogical communication format. The ATC job environment is unique in the way that a controller experiences a continuous 8 hour state of alert and professional interaction with multiple aircraft crews, where interlocutors (controller - pilot) are out of visual contact, that, in case of unexpected turn of events will definitely aggravate mutual understanding, so seeking for new solutions is a primary goal of us.

References

1. *DyakonovG*Existensial – onthologic dialogue concept.// Communication psychology; Socio – cultural analysis. International Conference recources (Rostov – na-Donu, October, 30- November,1- 2003.). / Editors: Bodalyova A., Ermakov P., Labunska B.- Rostov – na-Donu:Rostov State University, 2003.

2.*Parlmer M., Barnett G.* Progress in communication sciences / Vol. 13: Buber M. State university of New – York, 2005.

3. *Karneev R*Personality specificity research: (Psychology methodology) / Karneev RKarneeva A. // Magazine references "Vestnikobrazovaniya". – 2002. – № 3.

4. *Rojers C. Rogers, Carl.* (1959). A Theory of Therapy, Personality and Interpersonal Relationships as Developed in the Client-centered Framework. In (ed.) S. Koch, Psychology: A Study of a Science. Vol. 3: Formulations of the Person and the Social Context. New York: McGraw Hill.

5. *Bakhtin M.Holquist, M., & C. Emerson* (1981).Glossary. In MM Bakhtin, The Dialogic Imagination: Four Essays by MM Bakhtin.

6. *Lomov B.* Communication and psychic processes // Social psychology methodology issues - M.: Science, – pedagogical research //Mutual cooperation: Methodology, theory, practice- M., Nauka, 1988.

7. *Jurard C.* I andThou // Two symbols of Faith. Vol 2 -M., 1995.

UDC 629.735.067:656.7.071.13(043.2)

Tatiana Kharlamova, lecturer
(National Aviation University, Ukraine)

ENGINEERING COMPETENCY IN AVIATION SAFETY

This paper shows that the roots of the problem lie at a more fundamental level, which is considered as the competency dilemma in engineering education. On the basis of a theoretical analysis, results of research into alternative forms of competency acquisition suggest a more holistic view of competence. As a result of the empirical study, a multi-scale systems model of engineering competence is proposed.

Aviation today faces a series of pressing challenges. These include improving its excellent safety record in the face of projected traffic growth, addressing the need for increased innovation and action to ensure air transport's more sustainable and environmentally-friendly future, and taking advantage of the latest technologies and processes to make aircraft more secure from terrorist threats – even as these same technologies help deliver new levels of convenience to air travellers everywhere.

Compliance with ICAO Standards and Recommended Practices has been a cornerstone of international civil aviation safety. However, a rapidly expanding industry and resource limitations make it increasingly difficult to efficiently and effectively sustain a prescriptive approach to the keeping of safety based upon regulatory compliance exclusively.

Traditional systems for the maintenance of safety are set in motion only after some triggering event, such an accident, incident or reportable event, discloses a safety concern. For this reason, such approaches may be considered outcome-driven and reactive.

Over the past ten years, there has been a 46 percent decrease in the total number of fatal accident, at a time of significant growth in traffic world wide. This is positive but the reality is that the overall accident rate has remained disturbingly stable over the same time frame. Quick and strong action must be undertaken to develop and implement new strategies to bring down the overall accident rate. Zero accidents and zero fatalities are the perfect target for the Aviation industry but very utopian, however the task is to work more efficiently, collaborate more and share information in order to improve upon the Industry's already record [2].

On the other hand, looking to the future, aviation stakeholders are confronted with a pressing human resources challenge: how to ensure there is a strong supply of a strong supply of skilled, competent, personnel to meet the demands of the global air transportation system of the future. Some of the considerations that arise in this regard include:

- in the next 20 years, airlines will need to add 25,000 new aircraft to the current 17,000-strong commercial fleet;
- by 2026, it will be needed 480,000 new technicians to maintain these aircraft and over 350,000 pilots to fly them;
- between 2005 and 2015, 73 percent of the American air traffic controller populations eligible for retirement.

Aviation will also need thousands of airline customer service personnel, air and ground crew and cargo handlers, not to mention many other aviation-related professions – such as travel and cargo agents – to meet the dramatic growth in the aviation industry [5].

Thus, it is equally important to provide a proper training that engages as well as instructs in order to stimulate the minds and retain the attention of the students who will become contributing members of the next generation of aviation professionals. This can be accomplished by increasing awareness in the next generation training graduate of the types of aviation jobs available to them, as well as by better informing potential employers of the available talent pool.

Since the early 1990s, engineering education has met a significant paradigm shift from what was previously an input, content and process orientation towards a system based on educational outcomes. Prominent examples for this development in the context of the drastic social, economic and technological changes is the 1994 American Society for Engineering Education report “Engineering Education for a Changing World”. These report led to the development of Accreditation Board for Engineering and Technology Program Outcomes. The system of educational outcomes brought two fundamental changes in engineering education. Firstly, this development changed the underlying instructional principle of engineering education. More specifically, the aspirational attributes postulated in the respective reports were turned into binding outcomes of the educational process. In the paradigm of outcomes-based education, the teacher selects and delivers specific learning activities which can be mapped to the achievement of defined attributes or competencies [8]. Secondly, the scope of education was extended to encompass the broader aspects of engineering practice, such as cultural and social awareness, and an explicit commitment to the preparation of students for current professional practice [3].

Keeping in the view of the preparation of students for professional competence has always been the ultimate goal of engineering curricula. These are indications that industry requires a more adequate preparation of graduates for the job tasks of real-world engineering. Conversely, “much of the energy in teaching and learning in universities is still focused on developing the observable skills and knowledge dimension” [6], rather than the less easily observable attributes required by industry. This disconnectedness shows that the concept of outcomes-based education in today’s application to engineering education has not been able to fully prepare students for the changing demands of professional practice and also that broader aspects of competence have not found their way into the wider practice of education.

Currently, certain disconnectedness itself exists in a competency gap between university and industry. There are the various dimensions of the competency gap. The apparent gap between university and industry might be illustrated in the following way:

- educates for technical skills versus hires for traits;
- uses academic aptitude tests versus uses behavior-based competence tests;
- uses expert panels approach to determine desired attributes versus uses critical incident methods to determine competency profile;
- tries to achieve a difference in students’ competence versus requires affirmation of a sum of competence;
- scientifically rigorous knowledge versus practical job skills;
- building knowledge versus forming attitudes.

Thus, the goal conflict between university and industry might be performed like this:

- general education versus preparation for specific job tasks;
- ethics versus performance;
- technical breadth versus technical depth;
- different levels of a competency are conflictive versus a certain level of a competency is required;
- generic skills versus specific performance.

Accordingly, companies tend to focus on the person variables when recruiting graduate engineers. This method of behavior-based competency assessment with a predominant focus on the parts of the “competency iceberg below the water line” differs significantly from assessment methods employed in education. At university, students generally experience a range of traditional academic aptitude tests, such as exams, which focus on knowledge and skills. Radcliffe identifies this “Graduate Attribute Paradox” as the reason why the attempt of “developing graduates with those attributes stated by industry may not result in the type of engineer that industry requires” [6].

Industry expects graduates to have the skills and knowledge specified in the learning outcomes. Accordingly, teaching at universities largely focuses on developing skills and knowledge in students. Even the broader social dimensions of the Graduate Attributes are traditionally approached through course content or even isolated in one particular course. This focus on the domain of knowledge and skills does not take into account the competency dimension of traits, motives and self-concept. However, this dimension of the personality is seen as crucial in current competency research. Competence is conceptualized as an iceberg where the skill and knowledge domain form the tip, visible above the waterline, and traits, self-conception and motives make up the base of human competence [6]. More specifically, this means that these person variables were identified as far more reliable predictors of long-term job performance.

Outside the domain of traditional engineering knowledge, the goals of general education and the specific performance requirements of industry can be especially opposing. Many engineering educators advocate the inclusion of elements of liberal education into engineering programs in order to support students' acquisition of the social and ethical awareness specified in the Graduate Attributes. However, it can be questioned if such an inclusion contributes to specific performance in the workplace. At the same time, it might seem to put even more strain on an already overfull curricula and thus further escalate the struggle between the aims of technical breadth or specific education.

Another problem that is commonly overlooked in the application of competence-based education is the requirement of different levels of a competency in different contexts. With a number of competencies, especially on the attitudinal level, it is not the case that the graduate will be more successful in the workplace the more of this competence she acquires. Different job situations require different levels of a competency as a basis for performance. To illustrate this, we might consider a competence such as an engineer's attitude towards risk. Whereas one particular job might require a risk-tolerant person, a risk-seeker, another situation might require a risk-averse attitude to ensure success [4].

On the basis of the existing literature, it is presented a multiscale systems model engineering competence. Simply put, the systems model of engineering competence view in this context means that overall competence is more than the sum of individual competencies.Typically complex systems span several levels of scale from a micro view to a large-scale macro perspective [1]. In the context of engineering, the competence model distinguishes between the entity, individual and context level. These levels are connected through a rich interaction of their respective elements and this interaction determines how competence emerges in a particular context. This model of competence allows a synthesis of aspects of several conceptual views that are employed in different disciplines concerned with competency research.

The multiscale systems model of competence can be used to locate and analyze one example of a holistic learning, and relate this to the requirements of professional practice. Beyond that it needs to be discussed, on a general level, to which extent this understanding of engineering competence can contribute to overcoming some of the aspects of the competency dilemma in engineering education.This proposed conceptual understanding of engineering competence and the holistic view of student learning can be used to derive some initial suggestions to overcome the competency dilemma in engineering education. On the other hand, it is equally apparent that this concept does certainly not offer a complete solution to the issues raised.

Conclusion

The analysis presented brings into question some of the implicit assumptions that underpin the present methods of designing engineering programs based on graduate attributes. The competency dilemma in engineering education, where programs designed to meet the stated needs of industry, still seem to fail to produce graduates with the necessary competencies for successful performance in practice. In order to approach these difficulties, a systems view of competence formation is proposed that acknowledges both intentional and unintentional learning outcomes. The results of an exploratory, empirical investigation into so- called Accidental Competency acquisition are reported. This leads to the proposal of a multiscale systems model of engineering competence to promote a more fundamental and holistic understanding of student competence formation. At a time when accreditation agencies and other authorities are reviewing the operation and success of outcome based education in engineering, the results presented here offer an evidence-based approach to how we might design and evaluate engineering programs in relation to engineering competence in practice. It provides a logical framework for moving beyond a simple process of deriving perceived graduate attributes and mapping these to programs.

What is proposed is more realistic, complex systems perspective for how it is approached the design of engineering education programs, taking into account the formal educational perspective, while also acknowledging the many, subtle ways in which professional competence is developed.

As aviation competes with other industrial sectors for highly skilled professionals, the solutions to attract and retain the best and brightest will be multi-faceted. These solutions will focus on ensuring that all interested candidates have access to quality and affordable aviation education and training. Solutions must also leverage technology to its fullest, utilizing distance learning and e-learning platforms as well as the latest consumer electronics products and telecommunications services.

References

1. *Bar-Yam, Y., Ramalingam*. Making things work: Solving complex problems in a complex world, Cambridge, MA, NECSI, Knowledge Press, 2004.
2. CAAN Souvenir 2010. Civil Aviation Authority of Nepal, 2010, pp.66.
3. Engineers Australia, Changing the culture: Engineering education into the future, Barton, ACT, Engineers Australia, 1996.
4. *Hillson, D. & Murray-Webster, R.*Understanding and managing risk attitude, Aldershot, Hants, England, Burlington, VT, Gower, 2005.
5. ICAO training report. Vol. 1, No. 1, 2011, pp. 44.
6. *Radcliffe, D. F.* “Innovation as a meta graduate attribute for engineers”, International Journal of Engineering Education, Vol. 21, No. 2, IJEE Special Issue: The Entrepreneurial Engineer, 2005, pp. 194-199.
7. *Spencer, L. M. & Spencer, S. M.* Competence at work: models for superior performance, Chichester, UK, Wiley, 1993.
8. *Walther, J. & Radcliffe, D.* “Engineering education: Targeted learning outcomes or Accidental Competencies?”, Proceedings of the Educational Research and Methods Division – 2006 American Society for Engineering Education Annual Conference, Chicago, 2006.

UDC 629.7.07.4:612.881

E.N. Nikolaeva (Aviation Training Center. St. Petersburg, Russia)

METHODOLOGY OF ORGANIZATION OF THE ACADEMIC ACTIVITY OF ENGLISH TEACHING FOR PILOTS

The study analyzes and describes the process of organization of the academic activity of Aviation English teaching for pilots at the Aviation Training Center in St. Petersburg. It states the methodological foundation of the development of didactic materials and test procedure. Further, it summarizes the results of the system use in the academic activity and gives recommendations with respect to its use in the academic activity of pilots.

Introduction

For the last several decades the intensity of flights of aircrafts has dramatically increased in the world, while the issue about mutual understanding between a pilot and flight operations officer during radio communication is particularly pointed. Since English is the international language of radio communication, the inadequate level of proficiency in Aviation English is still the major or concurrent factor in a number of incidents and disasters. The most significant one was the collision of two aircrafts occurred on March 27, 1977 at the Tenerife airfield (the Canary Islands) where 583 people died.

Despite the efforts exerted by most of the countries, the issue of radio communication skills and expertise improvement is still extremely urgent as it needs unceasing attention on the part of airline companies (maintenance of the required level) and control on the part of the state. Nowadays, most of the Russian airline companies has changed their aircraft park and currently operate foreign-manufactured aircrafts, such as Boeing, Airbus, ATR, CRJ, etc., while new aircrafts of Russian make partially incorporate equipment in English. Flight operations manuals and other documents for these types of aircrafts are written in English, and therefore it needs additional knowledge of general and technical English at quite a high level. So, improvement of methods of learning Aviation English remains extremely topical.

Analysis of organization of the academic activity

Till 2007 inRussia, there were the state requirements for learning English for pilots and air traffic controllers, based on the study of radio communication regulations and training of radiotelephone communication skills in standard, non-standart and emergency situations. The drawbacks of such requirements lied in the fact that they didn’t provide for studying the vocabulary for further reading of technical documentation (flight operation manuals, crew operations techniques, etc.) and mastering the ability of holding a conversation on additional topics related to the professional activity (communication with the SAFA procedures inspection, ground-based technical staff, etc.). That’s why the publication of new requirements for learning Aviation English determined the following major tasks and areas of work, i.e. developing training programs, creating the methodic support of academic programs and developing pilot testing systems [1, 2, 3]. In this connection, the issue of determining the area of the English language knowledge to be tested as well as the very methods of English language testing for pilots was mostly discussed. As a result, the following four testing systems were approved for use in the academic activity in Russia ICAO Language Proficiency Test (Association of Russian Aviation Training Centers), RELTA МАИ (training center of the Moscow Aviation Institute), TELLCAP(R) (CompLangTrainingCenter) and the ICAO Aviation English Test (AviationTrainingCenter, St. Petersburg). For the purposes of optimizing and analyzing the use of testing systems the Federal Air Transport Agency (Rosaviatsiya) formed an ongoing task team.

The author met the above mentioned challenges using officially approved study programs, introductory testing systems, comprehension tests at stages provided for by the study program and the ICAO Aviation English Test (Education and Training Center, St. Petersburg), that’s why the results obtained using the said system are given below.

Methodology of meeting the research objective

The methodology of organization of the academic activity of English teaching for pilots was developed on basis of system approaches subject to physiological human abilities to learn didactic materials. The developed system includes the following components:

- organization of preparation and maintaining of knowledge and skills of proficiency in English based on cybernetic principles (feedback system), Table 1;
- the whole set of study programs, methods, textbooks, tests, technical training aids used and completed in compliance with regulated procedures for academic activity organization and performance for achieving a required level of the student's knowledge, abilities and skills in the area under investigation;
- the formed area of the pilot's expertise, based on the requirements provided for in regulatory documents and principles of professional competence [1], Table 2;
- the established scope of material required for learning, based on the analysis of statistics of aviation accidents and the expert survey method, subject to the requirements and recommendations specified in [2,3];
- the realized methods of distance education, based on the recurrence principle (courses are held as often as once in three years); provided that the training course to be divided in two stages: independent preparatory work (distance learning), and day release training in class within the group;
- the process of academic activity organization based on the principle of forming the groups of students having practically the same knowledge level (introductory testing method);
- presentation of the pilot's training in Aviation English as a subsystem of the general system of flight crew members training.

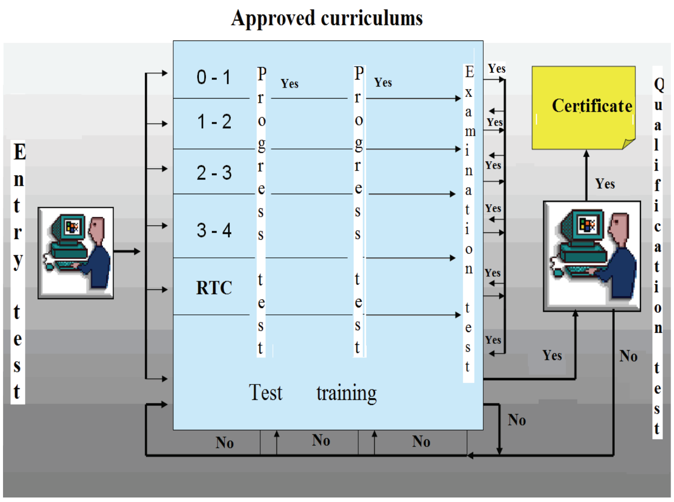

Table 1. Organization of the academic activity.

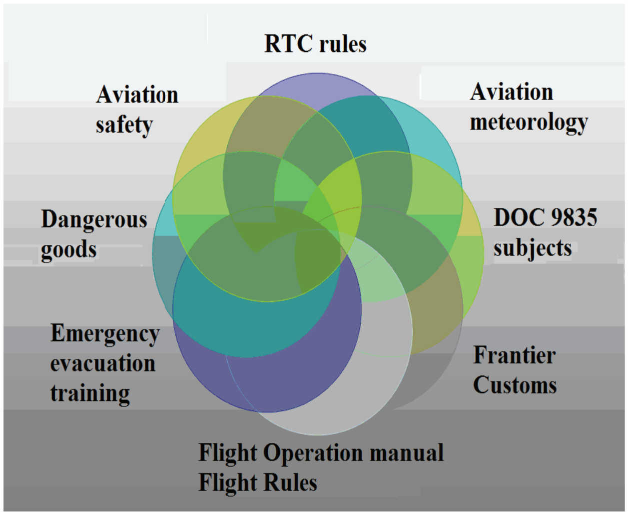

Table 2. Area of the pilot's expertise in Aviation English.

Implementation

The author implemented the above stated methodology of organization of the academic activity of English teaching for pilots at the Aviation Training Center of St. Petersburg. It consists of the training program, intermediate testing system, methods of knowledge evaluation during the training process in order to control the academic activity, the complex of multi-level textbooks recommended for elementary courses, advanced training courses, as well as for individual work, and methods of qualification comprehension testing for determination of the flight crew members' level of proficiency in Aviation English according to the ICAO Language Proficiency Requirements [2]. The process of academic activity organization is based on the principle of forming the groups of students having practically the same knowledge level. The training course is structured so that it allows to develop all types of language activity. Professionally oriented tasks related to actual examples from aviation and radio communication practice enable not only to work with language structures extensively, but also to broad the aviation specialist's professional outlook. Training under the said system can be organized in two variants, i.e. day release training and training with elements of distance learning. The study offers a set of study guides for independent work, methods of distance learning with individual consultations, and substantiates the optimal duration of each training stage.

The obtained results were reported at research and practice conferences and given a favorable expert opinion.

Conclusions

1. The implementation of the developed training system for pilots made it possible:

- to standardize the organization and carrying out of training courses as per the requirements specified in [2,3];

- to develop unified methodological principles and methodic solutions to achieve the state objective, i.e. acquisition of "operational" level of English by pilots as per the ICAO Language Proficiency Requirements [2,3];

- to work out a methodology of maintaining the achieved "operational" level of Aviation English;

- to create conditions to incentify the high-quality task-oriented training of flight crew members who expand into international flights;

- to improve the methods of English training courses for flight crew members through implementation of distance educational technologies and to apply the experience to develop training systems for Aviation English specialists and testing systems for other aviation staff.

2. It's expedient to change (update) the annually developed didactic materials and testing tasks by means of moving the examination tests into the category of training tests.

3. The results of use of the developed training system showed the efficiency of its use by pilots of all age groups, from flight school graduates lacking the experience of flight work to up to 60-year-old pilots with long experience of flight work. The author considers it expedient to use the training and testing system at all stages of the pilot training process, such as initial training at flight schools, assimilation of new (other) types of aircrafts and advanced training courses at aviation training centers.

References

1. Appendix No. 1 to the Convention on International Civil Aviation established by the ICAO "Certificate Issuance to the Aviation Staff" (supplement No. 164 dd. 27/11/03).

2. Doc 9835 AN/453 Manual on the Implementation of ICAO Language Proficiency Requirements. First Edition-2004.

3. Order of the Russian Ministry of Transport No. 90 dd. 09/08/07 On Approval of Federal Aviation Regulations "Requirements for the Flight Crew Members of the Aircrafts of the Civil Aviation of the Russian Federation during the Preparatory Work for International Flights".

UDC 656.7.071.13(045)

L.S. Nemliy, Post-graduate student
(National Aviation University, Ukraine)

THE EFFECT OF PEDAGOGICAL TECHNOLOGY IN FUTURE AIR TRAFFIC CONTROLLER INCTRUCTOR TRAINING

There are a lot of pedagogical technologies.. Interactive methods of teaching are in great importance for air traffic controller instructor training. It makes training at high school effective and more interesting. Future instructors should possess teaching skills during studying at high school and form pedagogical competence. It will give them the ability to organize air traffic controllers training before getting their job position.

Air traffic controller (ATC) instructor is one of the most important person who has much responsibilities in safety of aviation. He organizes the last faze of air traffic controllers' training. Just before the controller gets his position, an instructor should provide him with all necessary information, help to organize a working process in order to control air traffic safety, control, test and provide other necessary details according to the trainee individual abilities to understand and to learn. Good communication skills together with knowledge of current methods and techniques are required due to ATC instructor responsibilities.

To organize teaching process ATC instructor should have pedagogical competence. He deals with ATC trainees, people who are not sure in their knowledge, who always hesitate about the decision to make and they even cannot do any action without the ATC instructor's permission. They are not allowed to act independently till the ATC instructor allows them to do their responsibilities. Provide training, do regular or final tests, control, organize classes, give special classes and some other details of teaching the ATC instructor should possess with.

According to the ATC instructor's responsibilities he has to[1]:

1) develop and maintain high quality common core content classroom (and simulator) training material;
2) provide high quality ATC instruction to trainees in a classroom and simulator environment;
3) initiate quality improvements of training courses;
4) coach trainees and perform assessment duties through verbal and written reports;
5) undertake a programmer of operational refresher and competency checks on an annual basis in accordance with requirements;
6) participate as required in workgroups and task force in the capacity of an ATC exert.

Nowadays ATC instructors are trained at the certificated training center of Uksatse[2]. The specialists of the organization spend much effort to train ATC instructors. Some results of scientific research show us that ATC instructors have got a problem in teaching. The problem they deal every day is a lack of knowledge of teaching methods and techniques. To overcome the problem ATC instructors have got, we propose to start the ATC instructor's training during their studying at high school.

At the university it is possible to organize a special course which can give the future ATC instructors to develop their pedagogical skills. In our scientific research we develop a special course to train students. It will give them opportunity to possess the teaching skills, develop and form pedagogical competence. The aim of this course is to train future ATC instructors to transfer their skills, knowledge and techniques when conducting the on-the-job training to trainee air traffic controllers in an efficient and effective manner to achieve optimum results in a short period of time whilst ensuring safe, orderly and expeditious flow of traffic.

Analyzed a lot of pedagogical and methodical literature we can expect a great result in training ATC as an instructor during his professional training while studying at the university. Class work will give them chance to develop their future professional skills and try themselves in the role of an instructor. New effective pedagogical technology of teaching brings the progress in teacher's skills possession.

Nowadays there are a lot of new methods of teaching which make the work of teachers' easier and pleasant for students. We find the most effective ones interactive methods of teaching. It involves learners to participate, encourage them to study, stimulate discussion and so on. Interactive training is considered to highly effective, because students are afforded the opportunity to learn through active participation. Unlike more traditional, classroom learning environments, where an instructor tells students what they need to know, interactive training challenges students to participate directly in their own learning experience[3].

Interactive teaching is a two way process where in the lecture modifies his or her approach in response to the needs of the learners. The interactive lecture is keenly aware of the learners and their different learning styles. All good lectures are interactive lectures. It is not possible to teach without interaction.

The research shows people listen for only 15-20 attentively without a break. So, an ordinary lecture is not useful. It is necessary to change it into interactive one. A lecturer should make more interactive by involving the group by frequently stopping and asking questions to feedback. For example work groups give opportunity of interactive teaching, interactive games like role play. During classes one can be an instructor another can be a trainee. More practice while studying more skills students possess during training. Students like to be more actively involved, they want to share knowledge and ideas. Teachers who train should keep the students active and involved.

I hear I forget
I see I believe
I do I understand

Confusius

Interactive teaching is important as it is directly based on teamwork. There is a specific way of teaching and studying due to interactive technique. It occurs if all the members of the interaction take part (teachers and students). Interactive technique conduce person-oriented approach to studying. We believe this principle is important for training. In the center of the process there is a student who is active.

To change the attitude to the future profession of the ATC instructor teachers at the university should use interactive technologies. As lots of scientists believe the interactive technologies respond to person-oriented approach to studying, it influences students' interest to future profession.

There are a lot of interactive techniques that can be used during training[4]:

1) Think/Pair/Share
2) Buzz session
3) Case study
4) Incident Process
5) Role Play
6) Brainstorm
7) Discussion
8) Practice session

Get ready for classes a teacher should take into account that changes of teaching methods gives more effect. There are some of them in details.

Think /Pair/ Share

A problem or question should require participant to explain a concept in their own words or to apply, synthesize, or evaluate what they have learned. One minute for individual decision then for pair work comparing the answers. At last sharing the responses with rest of the group is followed.

Case study. Providing an opportunity for learners to apply what they learn in the classroom to real-life experiences has proven to be an effective way of both disseminating and integrating knowledge. The case method is an instructional strategy that engages learners in active discussion about issues and problems inherent in practical application. It can highlight fundamental dilemmas or critical issues and provide a format for role playing ambiguous or controversial scenarios. The case study approach works well in cooperative learning or role playing environments to stimulate critical thinking and awareness of multiple perspectives.

Discussion. There are a variety of ways to stimulate discussion. For example, some faculty begin a lesson with a whole group discussion to refresh students' memories about the assigned reading(s). Other faculty finds it helpful to have students list critical points or emerging issues, or generate a set of questions stemming from the assigned reading(s). These strategies can also be used to help focus large and small group discussions.

Role playing. Some role playing are structured with specific challenges and roles for each participant to play. More true to real life, other role plays exercises are spontaneous, allowing each person involved to act as they desire. To prepare for situations where professionals must be capable of thinking on their feet, the spontaneous role play is particularly helpful.

Brainstorming is an excellent teaching strategy to generate ideas on a given topic. Brainstorming helps promote thinking skills. When students are asked to think of all things related to a concept, they are really being asked to stretch their thinking skills. In usual studying situation student often hesitate about the answer, the technique of brainstorming makes a student to answer quickly, what is in his mind.

Learning by teaching. In this teaching method, students assume the role of teacher and teach their peers. Students who teach others as a group or as individuals must study and understand a topic well enough to teach it to their peers. By having students participate in the teaching process, they gain self-confidence and strengthen their speaking and communication skills.

All interactive methods of teaching give opportunity the students to develop their communicative skills. It will help the future ATC instructors to communicate with their trainees. Also during classes at the university much attention should be paid for each individual. Now they are students at the university and we teach them to teach. In the nearest future they will be instructors themselves. So, using of interactive methods teachers should teach students how to use them in future professional activities. A knowledge of methods is part of a professional base of teaching. Developed and proved skills of using them in a base ground of pedagogical competence. The main aim of our research is to form pedagogical competence of future ATC instructors.

Conclusion

Teachers must engage learners in studying activities that lead to a higher level of understanding and result in the ability to apply what they learned on the job. Interactive teaching is a two-way process of active participant engagement with each other. An interactive technology is a special form of training, which gives each student to feel his success and intellectual abilities. Use of interactive techniques will lead to the formation of pedagogical competence of ATC instructors.

References

1.www.atc-network.com

2. uksatse.ua

3. www.ehow.com

4. http:// math.arizona.edu

UDC 808.2

A.N. Vitryak, master of pedagogy, B.Y. Slipak, master of philology
(Kirovograd Flight Academy of National Aviation University; Ukraine)

ON ACTUAL PROBLEMS OF AVIATION ENGLISH PEDAGOGY

The actual problems of aviation English pedagogy have been dealt with. The prerogative ICAO requirement – availability of natural language competency – requires the decisive upgrading of the existing methodology, approaches, techniques and concrete means, first of all replacement of traditional textbooks and complexes by technologies, usage of algorithmic approaches, development of new-generation dictionaries and accelerated schooling basic English courses.

Two important tendencies which determine development of modern pedagogy of foreign languages are application of basic cybernetic principles and striving for conformity to natural language acquisition in officially established artificial conditions of schooling. In this context we may speak about anthropological pedagogy of foreign languages having at its methodological core the idea: "A student is not only a subject of studies but also a subject of their contents, an active participant of communication, not an active reader, reteller or reanswerer on the basis of a text dealt with".

Introduction of cybernetic ideas presupposes a) implementation of the approaches and techniques dealt with while using modern computers, in particular algorithmic procedures; b) realization of the prerogative pedagogical potential of up-to-date software and hardware ensuring the possibility of reliable control over communicative and cognitive activities of students; c) employment of computer-based and -aided technologies in place of widely-spread nowadays "complexes" designed inherently for extensive teaching (modern academic schedules do not give an opportunity to use them consecutively, one after another because of the scant budget of official classes).

In its turn, usage of technologies requires a) availability of the integrative method (all complexes are devoid of it); b) clear-cut and successive structuring of teaching material (one step principle) without which the efficient through checking and consecutive corrective actions are not achievable; c) specialization of training aids or environment depending on the object of learning: oral speech, reading, writing, auditioning, translation, etc. One of the decisive reasons for poor speakability of most today's schoolleavers lies first of all in the usage of the inadequate training environment – teaching speaking through reading. It is extraordinarily strange but by now there has not been developed yet the efficient technology of teaching audition (fitness for listening with comprehension). The striving to embrace everything in one or few textbooks accounts for the above-mentioned drawbacks.

As one of the adequate technological environments destined for the teaching of basic general and basic aviation English there has been developed ***the system of fully controlled formation of natural spoken language competency***. The practical implementation of the system presupposes the simultaneous involvement of the subgroups of four students. The system provides active spoken practice along with audition on the operational (one new grammatical item → one step) and thereby effectively controllable basis. The discreteness (fragmentation) is being constantly overcome by using the accumulative (aggregative) principle (through successive addition of the former items to a new one in order to create an integral presentation of the whole complex structural phenomenon). The visual demonstration of the inside-subgroup communication based on the application of the ***primary pattern*** used throughout the technology (the pattern allowing to turn the traditional mechanical conjugation into valuable spoken practicing) is presented below.

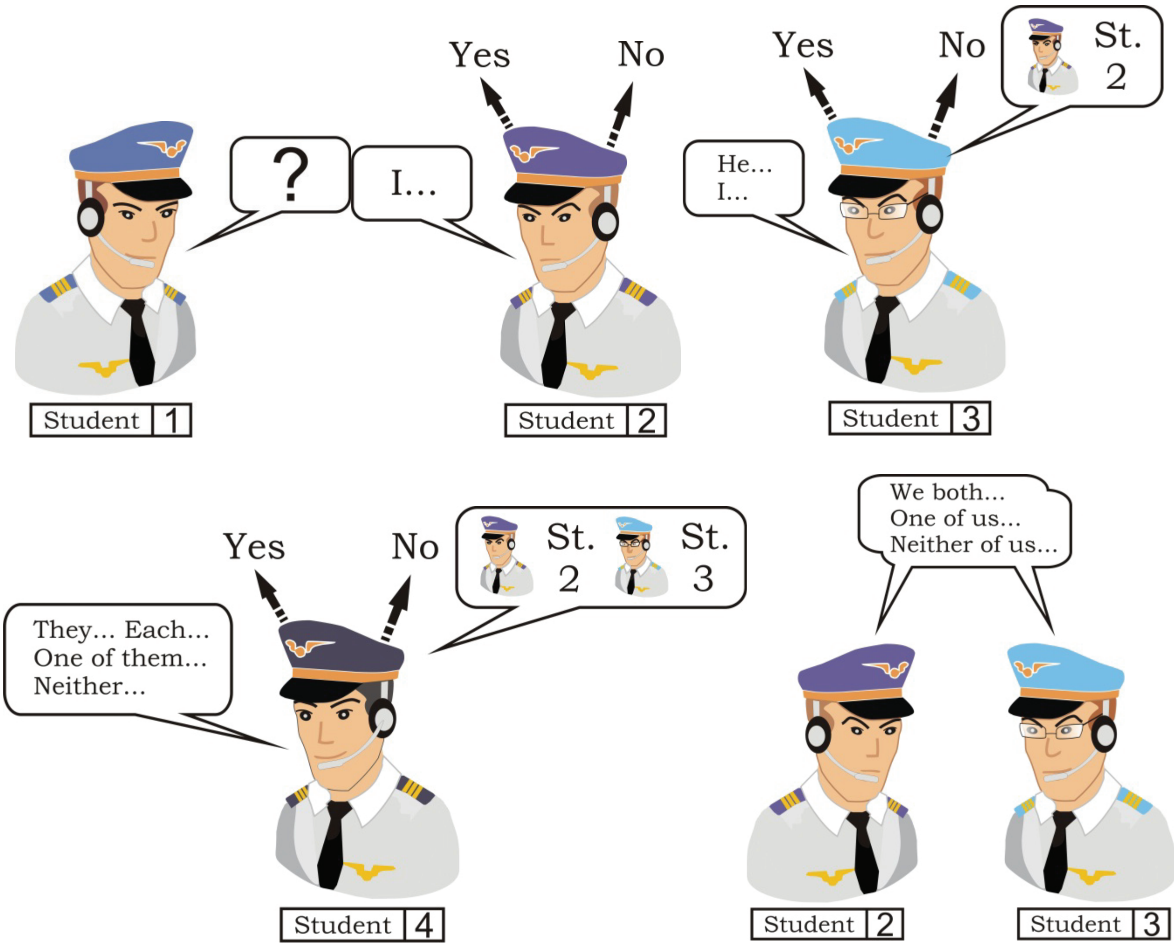

The evident communicative charge of the system is provided by its orientation on formation of the *personified autobiographical memory*, primarily on *professional episodic memory* which enables to avoid the traditional estrangement of students from the contents of a course offered to them. If the technology using the primary pattern is introduced for teaching pilot cadets, not professional pilots, the principle of role games and other procedures may be carried into effect. The technology has already been realized in the form of the textbook "*An **A**viation **B**asic **C**ourse in Structural English through Personified Operations*" (*Part 1* – "*Attitude to actions*"; *Part 2* – "*Actions themselves*") with the special attention to the examples from real air-ground communication and on-board spoken exchange. The development of computer-aided version is now under way.

In connection with usage of computer-based technologies the issue emerges: "Is it possible to develop a completely controllable technology of the English language competency acquisition?" In our opinion and as shown by the practical application, it is possible at the level of the ***basic language***. To achieve mutual understanding let us try to define this notion which presupposes the availability of automatisms of usage of structural operations in the personified (not estranged) communicative environment. Such availability along with lexical freedom provides the good possibilities for performing mental activities in a language being studied. Without such capability it is impossible to shape natural language competency, the latter being the main ICAO requirement, and airmen involved directly in air traffic are doomed to use mechanically the entries of the standard radio telephony phraseology.

The problem of "***basic aviation English***" is known to be in fact "terra incognita" (an unexplored field of the aviation English pedagogy). Up to now practically all textbooks have been devoted to studying or improving the professionally specialized English, to be more exact to air-ground communication, unexpected flight situations having been involved lately. Besides, which is very essential, so far only textbooks have been offered to the "reading men", though, and it is being owned up oftener and oftener, technologies especially computer-assisted or -based ones, are much more effective than textbooks, first of all because they allow to control efficiently the whole process of the language competency acquiring.

We think it worthy of mentioning once more: without the effective basic general and aviation language acquisition use of English in the real conditions of communication will be artificial, mechanistic, “parrot-like”, relying only on the phraseology, not natural.

One more very important, to our thinking methodological notion: formation of the structural automatisms foresees constructive separation of “grammatical” from “lexical” (contents). Practically it may be realized by means of the step by step introducing grammatical structures on the limited high-frequency wording substrate – the principle of one predominant difficulty (in contrast to traditional indiscriminant introduction of either).

Use of ***algorithms*** is a very effective way of intensifying the process of language acquisition and making it natural (people in fact act in customary situations using algorithms being extremely reduced and kept in our subconsciousness.

Exclusively accelerated formation of the phrasal kernel – subject ↔ predicate (eight-ten hours; all grammatical tenses; the active and passive voice patterns) can be achieved due to introducing the specially developed ***5-stepped algorithm***. The psychologically grounded premises of the algorithm are found in the main principle of the *Gestalt psychology* – the integral presentation of a complex object. The algorithm is presented in the form of five graphically represented steps. Some notion of its visual shaping is given below in the picture which presents the first step – choice of the general phrasal scheme applicable in those cases where the possibility to use either the active or the passive voice pattern exists.

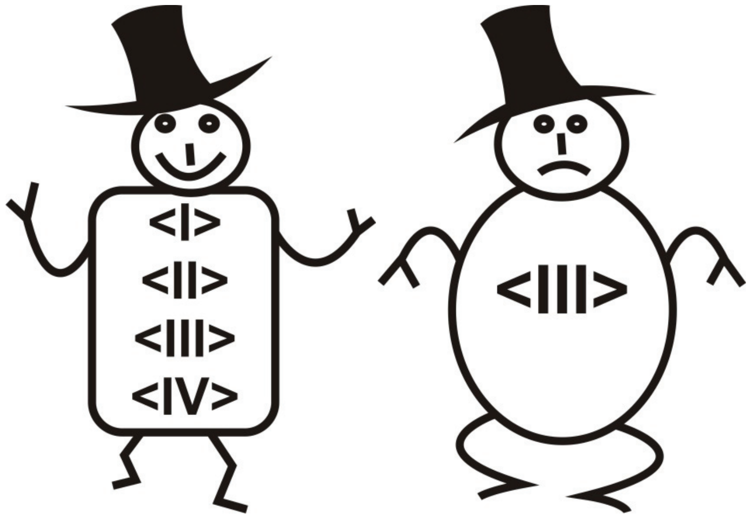

The specially-developed algorithm has been used in the accelerated basic courses in common-use English and aviation English (in contrast to advanced general English and professionally-fixed aviation English). Both accelerated courses may be used simultaneously as two synchronous parallel pedagogical “currents”, which is especially important for initial language acquisition in aviation training establishments.

The substantial innovations (rather additions) are also required in the sphere of the aviation-pertaining vocabulary and materializing it dictionary support.

Two dictionaries of new generation are being developed now in the Flight Academy. They enable to form the autobiographical professional memory, predominantly the professional episodic memory, and the cognitive conceptual memory which in their combination allow to teach English inseparably from development of ability to perform thinking operations by using the language being studied.

Every entry of the “*An* ***A****viation* ***B****asic* ***C****onceptual English Dictionary*” is represented in the form of a tree of logical interdependencies which is ontologically based on interrelations between objects, logical relations between them, operations on objects and on relations between them.

One example from the dictionary is given below.

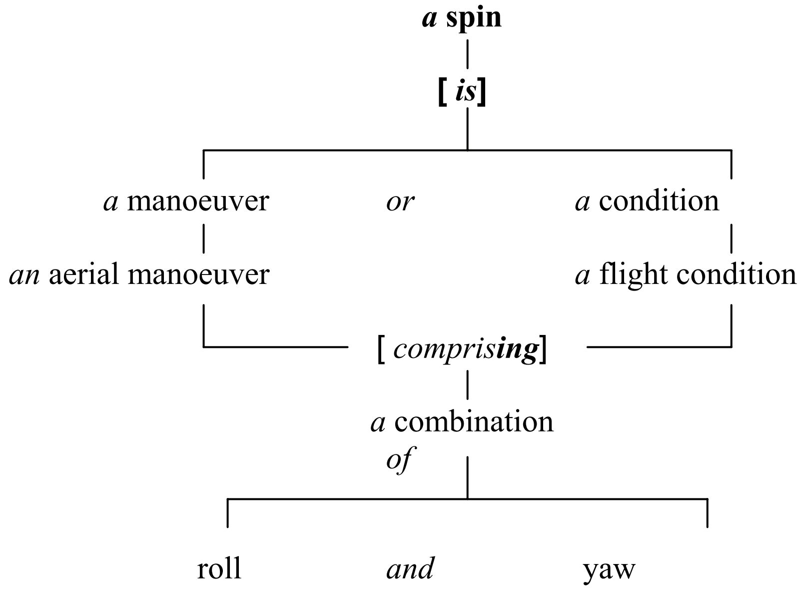

The dictionary “*An* ***A****viation* ***B****asic* ***C****ommunicative English Wording*” is synthetic since it harmonically combines the principal features of widely used traditional dictionaries (glossaries, encyclopedic dictionaries, distributive dictionaries, dictionaries of equivalent means, etc.), which can be illustrated by the example below – a fragment from the episodic field “*Fire on board*”.

heat; to emit [to generate; to produce] {much / tremendous} heat;

fire; fire **warning** (There is a fire warning); {to detect / to prevent / to isolate} fire;

to **catch fire** {on pushback / due to the improper loading of some dangerous goods, their incompatibility / due to electrical problems / because of engine fire / in connection with problems relating to passengers’ baggage, etc.};

fire**danger** [hazard; peril; jeopardy]; fire **threat**;

Some general conclusions

The two main tendencies of modern pedagogy of aviation English have been under consideration – using the adequate cybernetic ideas and approaches as well as striving for conformity to natural language acquisition (in particular, development of adequate training environments). The notion of basic aviation English has been introduced implying the personified acquiring of structural automatisms, freedom of the vocabulary (most frequented situational lexical items) and ability to produce mental operations by using the language being studied. Among the solutions aimed at the natural language competency acquisition there has been proposed usage of technologies, including computer-aided and -based, instead of traditional textbooks and complexes. The technologies provide the reliable control over the schooling process which, due to the proper corrective actions, ensures the efficient formation of spoken capability. The course which has been offered uses the system of fully controlled formation of natural spoken language competency based on the through primary pattern. The accelerated courses of teaching basic general and aviation English which have been approbated make use of the specially developed algorithm of formulating an English phrase. The approbation of the courses as well as of the two new generation dictionaries has proved their efficiency and constantly supported interest of their users, the names of the dictionaries being “*An* ***A****viation* ***B****asic* ***C****onceptual English Dictionary (through the trees of logical interdependencies)*” and “*An* ***A****viation* ***B****asic* ***C****ommunicative English Wording*”. The methodological premises for all teaching materials are found in anthropological psychology, cognitive psychology and Gestalt psychology.

UDC 629.735.067=111(043.2)

Liliya Korol
(National Aviation University, Ukraine)

STANDARTIZATION OF THE ENGLISH LANGUAGE PROFICIENCY REQUIREMENTS FOR AIRCRAFT MAINTENANCE ENGINEERS AS MEANS OF IMPROVEMENT OF AVIATION SAFETY

The article claims that standardization of English proficiency requirements as well as its universal evaluation scale for Aircraft Maintenance Engineers is a vital point in improvement of aviation serviced in general and flights' safety in particular.

An Aircraft Maintenance Engineer (AME) is responsible for the release (certification) of an aircraft after maintenance, inspection, repair or modification. This is a responsible occupation requiring a high degree of responsibility and skill, which specifically are enumerated in MAINTENANCE ORGANISATION APPROVALS – PART 145, PART 66 AND PART 147 by EASA and are standardized by abovementioned organization in order to provide efficiency and safety in the field of aviation. For example, if a person wants to be eligible for the EASA part 66 license, he/she should be knowledgeable in the following 17 Modules:

- Mathematics;
- Physics;
- Electrical fundamentals;
- Electronic fundamentals;
- Digital techniques/Electronic instrument systems;
- Materials & hardware;
- Maintenance practices;
- Basic aerodynamics;
- Human factors;
- Aviation legislation;
- Airframes;
- Helicopters;
- Avionics;
- Engine instruments;
- Jet engines;
- Piston engines;
- Propellers.

Detailed and comprehensive syllabus was developed by the CAA/ EASA for each of the abovementioned Modules describing all topics that are necessary to be covered in order to pass the exam successfully and obtain license of suitable category (A, B1, B2, C).[2] Moreover, there are certain experience and basic knowledge requirements that are obligatory for engineers, who whish to get the desirable qualification. However, we did not manage to find precise and standardized requirements for the English language proficiency of potential examinees despite the fact that all documents and correspondences, as well as examination itself are implied to be held in English, as it was claimed in Foreign Part 145 approvals, User guide for Applicants. [4] In addition to this we should mention the fact that each examination consists of a multi-choice paper for each module and an essay paper for Modules 7, 9 and 10, which are Maintenance practices, Human factors and Aviation legislation. This leads to the fact that the majority of training courses that prepare potential applicants for certificate examination require English Language competency of IELTS 5.5, or equivalent.

We consider the following description of Language knowledge (a working knowledge of the language in which the maintenance data is published + English if required for EU

Airworthiness directives)[4] is not full and it does not give the coherent idea of what language skills should an Applicant posses and what standards of the English language proficiency evaluation or what level classification should be taken into account. Due to this fact employers are likely to have their own internal English assessment, which could be either a specific test which a person needs to pass in order to proceed with his/her application, or alternatively his/her English language proficiency could be even assessed just during HR interviews. This results in ambivalent standards for qualification requirements for aircraft maintenance engineers in different airports. It is widely believed that bigger airline companies tend to pay more attention on level of English proficiency of their ground staff then their smaller counterparts, who deal predominantly with domestic flights, because of financial issues connected with salaries and qualification of workers.

The occupation of Aircraft Maintenance Engineer is nor less important and influential then profession of Air Traffic Controller or pilot when we consider the safety of flights. Nevertheless there is no common detailed evaluation classification of English level proficiency such as scale developed by ICAO for certification of members of cabin crew and Air Traffic Controllers. ICAO amended Annex 1 to add a requirement for all aeroplane and helicopter pilots, flight navigators, flight engineers and air traffic controllers to be assessed in their command of the language used for radio communication. A scale of 1 to 6 has been devised where native speakers would be assessed at Expert Level 6. For those where the language is not the mother tongue ICAO set a minimum of Operational Level 4 for license issue. The abovementioned scale is concentrated mainly on the skills that are involved in radio communication, Speaking and Listening prevailing.

Thus, in order to develop similar scale made specifically for the Aircraft Maintenance Engineers we should investigate what English language skills are dominating in their routine working activity. It is assumed that engineers usually work with documents and maintenance manuals, thus presumably the crucial skills for them would be Reading and Writing, but we suggest further research on this topic.

Both the FAA and EASA (ex-JAA) have had requirements for the English language used by Aircraft Maintenance Technicians in Parts 66-15b, 145-35e and 147 since the 1990s [1,3]. On the other hand, all airlines and MRO organizations are aware of the need for the staff to be proficient in English. However, there is still a missing link which means that many operators struggle to interpret and find appropriate training and assessment solutions to implement these requirements on the flight line, in the hangar and the workshop. The needs vary from one location, activity and skill to another. Unlike the statutory ICAO Language Proficiency Requirements for pilots and controllers, the FAA and EASA requirements contain no rating scale, detailed holistic descriptors or support mechanisms for their implementation. It is not that more regulation is required, but rather practical guidelines to assist with the interpretation of the existing regulations.

Aviation history shows that some incidents or accidents are directly or indirectly due to maintenance errors involving improper use of maintenance documentation. One of the recent analyses of incidents/accident reports and statistics done for EASA defines the following possible meanings of the term "improper use":

- · No use of documentation;
- · Late use of documentation;
- · Partial use of documentation;
- · Misreading of documentation;
- · No respect of documentation content;
- · Use of incorrect documentation. [5]

Misreading of documentations means that documentation is not understood correctly due to lack of language proficiency, content being explicitly misinterpreted. Taking into consideration the fact that the English language is used in the majority of aviation documentation and aircraft technical manuals we are able to claim that engineer's level of English proficiency influences greatly not only on his performance during working activity but on the safety of flights. Furthermore, poor knowledge of English can have disastrous consequences and lead to fatalities.

Accident that happened in 2003, in which twenty-one people were killed when U.S. Airways Express Flight 5481 crashed in Charlotte, North Carolina, can illustrate how insufficient knowledge of the English language of one particular person, who was a mechanic licensed by FAA, can be the reason of deaths and destructions.

One reason for the crash, investigators found, was that low-wage mechanics who can't read English incorrectly connected the cables to some of the plane's control surfaces in the repair shop. The FAA was cited for improper oversight of the repair process.

Repairing airplanes is a complicated process as each aircraft has many manuals. Typically, when mechanics repair a part, they open the manual, consult the book, and make the repair step-by-step. In addition they make a list of every action they take, so the next person to fix the plane (as well as the people who fly it) will know exactly what has been done.

If mechanics don't speak English, the international language of aviation, they can't read the manual and they can't record their activities creating an issue that is putting the whole aircraft and its occupants in danger.

Conclusions

All things considered we should claim that standardization of English language proficiency of aircraft maintenance engineers is a crucial point in aviation safety and the following issues should be investigated thoroughly. First of all we would recommend to define the prevailing language skills that influence the efficiency of AME's performance, whether these are Reading, Listening, Writing or Speaking. Furthermore it would be necessary to develop a comprehensive scale of English language proficiency classification made specifically for aircraft maintenance engineers, which would be as detailed as ICAO Language Proficiency Requirements for pilots and controllers. This is due to the fact that general non-specific requirements of EASA mentioned in Parts 66 and 145 are not enough for standardization of AME's compulsory level of English knowledge. This situation may endanger the safety of flights immensely as the English language is meant to be a prominent tool in AME's working activity.

References

1. http://easa.europa.eu

2. http://easa.europa.eu/agency-measures/acceptable-means-of-compliance-and-guidance-material.php#AMCPart-66

3. *Maintenance organization approvals – Part 145*/ Luxembourg: Publications Office of the European Union, 2010.

4. *Foreign Part 145 approvals. User guide for Applicants.* EASA Doc UG.CAO.00006-001, 2010.

5. *Study on the need of a common worksheet / work card system.* Conducted by BUREAU VERITAS, Specifications N°: EASA/2006/OP/25, 2007.

UDC 528.716(043.2)

M.P.Mukhina, PhD, N.P. Rybak (National Aviation University, Ukraine)

MODEL PREDICTIVE CONTROL WITH ATTRACTOR FOR EXPLORATION TASKS

Novel technique of an attractor together with model predictive control is used to optimize the information gathering during exploration. Information value in the form of number of features and their quality was selected. The area coverage and time consumption are much improved in comparison with Greedy method.

IntroductionNowadays the territory exploration with unmanned aerial vehicles (UAV) finds its application in various areas: mapping of hard-to-reach regions, reconnaissance flights, rescuing and searching flights and others. Finding the best (optimal) trajectory of flight is the urgent problem from the point of view of control and navigation. One of the promising approaches to solution is to use the feature map and its characteristics both in the criteria of optimality of trajectory and in the control.

A feature is the individual measurable properties of the phenomena being observed. For the territory exploration the feature is assumed to be the distinctive area with characteristics which differ from other (e.g., altitude, color, radar image and others). Extracting the features during the flight allows us to compile the feature map and also to test its validity and completeness. Number of features and their quality can be used to formulate the criterion of trajectory selection from the point of view of information value.

The model predictive control(MPC) is used to optimize the forecasts of process behavior. MPC explicitly computes the predicted behavior over some time horizon.

The term MPC, in reality, designates a wide range of control methods that make use of a process model in order to obtain the optimal control value by minimizing a cost function. MPC algorithms differ among themselves mainly due to the model used to represent the process being controlled, the representation of measurement noise and disturbances, and the objective function to be minimized. One disadvantage of such a methodology concerns the computational effort required, as the control actions are obtained by solving a dynamic optimization problem in real time. Regarding high bandwidth applications, such as aeronautics and space, MPC has only recently been studied as a suitable control approach, due to the growth of the processing capability of computational resources, in special with respect to Flight Control Systems (FCS).

Related works Using an attractor for optimal trajectory planning during Simultaneous Localization and Mapping (SLAM) was proposed in work [1]. But the placement of attractor was selected almost randomly, based on state machine with three possible states: improving map, improving localization, and exploration. That's why the selection of the attractor position requiresfurther research.

Paper [2] demonstrated two different strategies for decentralized multi-UAV SLAM trajectory control in order to maximize the accuracy of the resulting map feature estimates. The entropy was selected as a measure of the compactness of a distribution and thusthe completeness of map. It is used as a utility function formulti-UAV trajectory control based on the expected value of thecovariance or information matrix relating to a particular set of vehicleactions.

Paper [3] used a receding time horizon strategy (similar toMPC) for optimal planning and control of UAVs. Thisrequires limited computational resources and offers an explicitmechanism for responding to dynamic environments with obstacles. They perform geolocation incorporating dynamic constraints, though SLAM and coverage were not considered.

Problem statement

Considering the motion model of the UAV we can describe the UAV state vector. The estimated state vector $\hat{\mathbf{x}}(k)$ contains the three-dimensional UAV position $\mathbf{p}^n(k)$, velocity $\mathbf{v}^n(k)$, and Euler angles $\mathbf{\Psi}^n(k)$, and the N three-dimensional feature locations $\mathbf{m}^n{}_i(k)$ in the environment: $\hat{\mathbf{x}}(k) = [\mathbf{p}^n(k), \mathbf{v}^n(k), \mathbf{\Psi}^n(k), \mathbf{m}_1^n(k), \mathbf{m}_2^n(k), ..., \mathbf{m}_N^n(k)]^T$, where i = 1, ..., N and index n indicates the vector that is referenced in a local-level navigation frame (fig. 1).

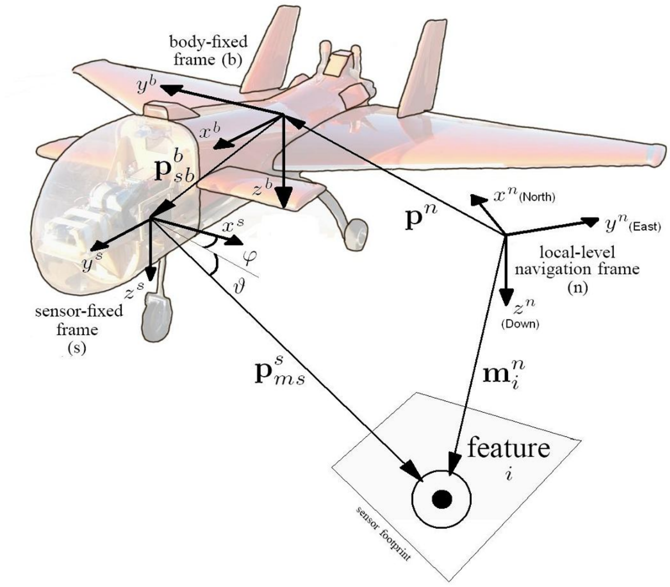

Fig. 1 Relationship between navigation frames

The local-level navigation frame is fixed relative to the surface of the Earth and is placed arbitrarily within the operating area of the UAV, x-axis coincides the north direction, y-axis is directed to east and z-axis point down towards the center of the Earth for creation of right-sided coordinate system.

The state estimate $\hat{\mathbf{x}}(k)$ is predicted forward in time by integrating readings using data of the inertial navigation equations:

$$\begin{bmatrix} \mathbf{p}^n(k) \\ \mathbf{v}^n(k) \\ \mathbf{\Psi}^n(k) \end{bmatrix} = \begin{bmatrix} \mathbf{p}^n(k-1) + \mathbf{v}^n(k)\Delta t \\ \mathbf{v}^n(k-1) + \left[\mathbf{C}_b^n(k-1)\mathbf{f}^b(k) + \mathbf{g}^n\right]\Delta t \\ \mathbf{\Psi}^n(k-1) + \mathbf{E}_b^n(k-1)\mathbf{w}^b(k)\Delta t \end{bmatrix} \tag{1}$$

Where $\mathbf{f}^b$ and $\mathbf{w}^b$ are accelerations and angular rates of body-fixed frame relatively to inertial, $\mathbf{g}^n$ is the acceleration due to gravity, Δt is the integration time step, $\mathbf{C}_b^n$ and $\mathbf{E}_b^n$ are cosine matrix and rotation rate transformation matrix respectively.

Landmark locations are assumed to be stationary and models for landmarks are:

$$\mathbf{m}_i^n(k) = \mathbf{m}_i^n(k-1).$$

We assume that an on-board sensor makes range and azimuth observations of landmark. The ration between position of the feature and attitude of UAV is described by:

$$\mathbf{z}_i(k)=\begin{bmatrix}\rho_i\\ \varphi_i\\ \vartheta_i\end{bmatrix}=\begin{bmatrix}\sqrt{\left(x^s\right)^2+\left(y^s\right)^2+\left(z^s\right)^2}\\ \tan^{-1}\left(\dfrac{y^s}{x^s}\right)\\ \tan^{-1}\left(\dfrac{\left(z^s\right)^2}{\sqrt{\left(x^s\right)^2+\left(y^s\right)^2}}\right)\end{bmatrix} \qquad (2)$$

$$\mathbf{p}_m^s=\mathbf{C}_b^s\mathbf{C}_n^b\left[\mathbf{m}_i^n-\mathbf{p}^n-\mathbf{C}_n^b\mathbf{p}_s^b\right],$$

where $\rho_i, \varphi_i, \vartheta_i$ are the observed range, azimuth and position angle, x^s, y^s andz^s are the Cartesian coordinates, $\mathbf{p}_m^s$ isthe relative position of the landmark with regard tothe sensor, $\mathbf{C}_b^s$ is the transformation matrix from the body frame to the sensor frame, $\mathbf{p}_s^b$ is shift of the body-fixed frame relatively to the sensor –fixed frame. The sensor observation model is general and can be specified to any concrete task.

Let's determine the attractor in the form of point or finite set of points (curve) in order to influence the motion of the UAV to desired locations by influencing the information gain of particular control actions.It is proposed to use the attractor in the form of an artificial feature because the objective function in the MPC strategy is predominately driven by the uncertainty of the features in the map. Through tactical placement of the attractor, the information gain of certain control actions will be increased and thus the motion of the UAV will be directed towards the desired goal. In this approach, the local MPC strategy provides the high level of decisions and goals. The goals are incorporated by the directedness of the incentive provided by the attractor.

Algorithm of MPC with attractor based on information measure At each time step, k, the attractor is placed in the direction of the reference point selected. The attractor needs to be placed in a location visible to the UAV within the planning horizon in order to influence the UAV's decision. It is proposed to place the attractor at a range equivalent to the UAV's sensor range.

The UAV is given an artificial state,$\mathbf{x}_{artificial}$, and artificial covariance,$\mathbf{P}_{artificial}$. The artificial state contains the attractor as a new feature initialized to a position at the UAV'ssensor range in the direction of the exploration point:

$$\mathbf{P}_{artificial}=diag(\mathbf{P}(k)\quad \mathbf{P}_{attractor})$$
$$\mathbf{x}_{artificial}=\left[\hat{\mathbf{x}}(k)^T\quad \mathbf{x}_{attractor}{}^T\right]$$

The UAV sees the attractor asa new feature and is moving to localize it. Once all the exploration points are covered this goal is no longer active.

For the goal of localization improvement, the nearest good feature is selected as the attractor. A good feature is any feature with an uncertainty below a set threshold. If there are no good features then the feature with the lowest uncertaintyis selected, j_s,represents the index of the feature selected.

Only the state vector $\hat{\mathbf{x}}(k)$ is changed. The position of the good feature selected is altered to be at the UAV's sensor range in the direction of the good feature. The covariance $\mathbf{P}(k)$ is left unchanged so the affects of the correlation by observingthe feature is maintained:

$$\mathbf{P}_{artificial}=\mathbf{P}(k)$$
$$\mathbf{x}_{artificial}=\hat{\mathbf{x}}(k)$$
$$\mathbf{x}_{artificial}(j_s)=\mathbf{x}_{attractor}$$

The attractor in this case has a low uncertainty equivalent to the uncertaintyof the good feature selected. The UAV sees the attractor as a good feature and moves towards it to localize.

For the goal of map improvement the nearest poor feature is selected as the attractor. A poor feature is any feature with an uncertainty above a set threshold. If there are no poor features then the feature with the highest uncertainty is selected.

Similarly only the state vector $\hat{\mathbf{x}}(k)$ is changed. The position of the poor feature is set to be at the UAV's sensor range in the direction of the poor feature. The covariance $\mathbf{P}(k)$ is unchanged so that the covariance of the poor feature is maintained.

The UAVsees the attractor as a poor feature and moves towards it to localize it. When all the exploration points have been visited, the UAV may still localize poor features.

The performance of these strategies largely depends onthe density of the features and the sensor range. The larger the sensor range, the higher the amount of features and the smaller the exploration space, the easier the exploration task would be.

Even with the attractor present, there is still no guaranteeof complete coverage. In the case where there are no features for a long distance, the UAV maybecome very uncertain of its pose due to the process noise and will be forced to localizeevery time it attempts to explore in the distance.

The concept that is used forthe estimation of the most optimal attractor position is the information measure. A key measure of information is known as entropy. Entropy quantifies the uncertainty involved in predicting the value of a random variable.The goal of the planning is to minimize the entropy and thus maximize the accuracy of the estimates.

The entropy $H(x)$ of a multivariate Gaussian probability distribution can be calculated from its covariance matrix $\mathbf{P}$ or Fisher information matrix $\mathbf{Y}$ as follows:

$$H(x) = \frac{1}{2}\log\left[(2\pi e)^n |\mathbf{P}|\right] = \frac{1}{2}\log\left[(2\pi e)^n \frac{1}{|\mathbf{Y}|}\right]. \tag{3}$$

At each step k, UAV takes an observation. Range and azimuth of the landmark are measured by the on-board sensor and form the measurement vector (2).

The transformed coordinates of the observed landmarks are recorded on the map. For map updating we also use the empty map and a priori information about potential landmarks. A priori information is the initial information about known landmarks or the information that has already been observed in the past.The map updates after each trial are recorded in the map database.

Taking into account vector $\mathbf{m}$, containing the coordinates of all known landmarks, we form several random points of attractor and then calculate potential trajectories toward them.

At regular intervals the UAV takes its current state estimate relating to the map estimates only, i.e. $\mathbf{x}_m(k)$ and $\mathbf{P}_{mm}(k)$, where:

$$\mathbf{x}_m(k) = \left[m_1^n(k), m_2^n(k), \ldots, m_N^n(k)\right]^T,$$

and $\mathbf{P}_{mm}(k)$ is a $3N \times 3N$ sub-block matrix of the elements of $\mathbf{P}(k)$relating to the map landmark estimates. The UAV then calculates its posterior information:

$$\mathbf{Y}(k) = \mathbf{P}_{mm}^{-1}(k),$$

$$\mathbf{Y}(k) = \mathbf{Y}(k)\mathbf{x}_m(k)$$

The UAV maintains a record of the information update during the last observation (i.e. $\mathbf{Y}(k{-}1)$) which is subtracted from the current information to form the new information that UAV has about the feature map:

$$\mathbf{Y}_{new}(k) = \mathbf{Y}(k) - \mathbf{Y}(k{-}1),$$

$$\mathbf{z}_{new} = \mathbf{z}(k) - \mathbf{z}(k{-}1).$$

When the UAV receives all of the information updates, this information is summed together along with the current UAV information to form the updated estimateof the map landmarks in information form:

$$\mathbf{Y}_{update}(k) = \mathbf{Y}(k) + \mathbf{Y}_{new}(k),$$

$$\mathbf{z}_{update}(k) = \mathbf{z}(k) + \mathbf{z}_{new}(k),$$

A state space estimate of the map landmark locations and covariancecan be calculated:

$$\mathbf{P}_{mm,update}(k) = \mathbf{Y}_{update}^{-1}(k),$$
$$\mathbf{x}_{m,update}(k) = \mathbf{P}_{mm,update}(k)\mathbf{z}_{update}(k) \tag{4}$$

The UAV computes the utility associated with each trajectory by substituting the local posterior information matrix for each potential trajectory into equations (4).The UAV then chooses the trajectory that minimizes the utility (entropy).

After the selection of the most optimal trajectory the control block calculates the required change of calculated parameters in order to reach final point with coordinates x_{final},y_{final}.

During every cycle the recalculation of optimal attractor position is formed. In such way the information is updated and the UAV predictive control is performed.

The developed algorithm was realized in programming language Delphi. The results of simulation are shown in fig. 2.

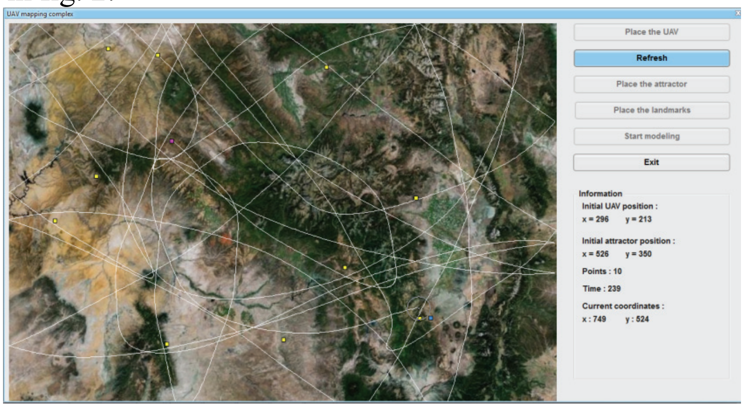

Fig. 2 Interface of realized algorithm

Conclusions

The main drawback of this program is that the UAV can fly only in the limits of map. When the UAV reaches the edges of the map, it will collide with it and the UAV motion will be forced to the opposite direction.

To solve this problem we can allow the UAV to make a turn outside of the map limits. But the time of the flight will increase in several times. So such solution of this problem will not be optimal for mapping task.

References

1. *Cindy Leung, Shoudong Huang, Gamini Dissanayake* "Active SLAM using Model Predictive Control and Attractor based Exploration" //Proceedings of the 2006 IEEE/RSJ International Conference on Intelligent Robots and Systems October 9 - 15, 2006, Beijing, China. – Pp. 5026-5031.

2. *Mitch Bryson and Salah Sukkarieh* "Decentralised trajectory control for multi-UAVSLAM" // Proceeding of the 4th International Symposium on Mechatronics and its Applications (ISM07), Sharjah, U.A.E. March 26-29, 2007. – Pp. 07-1 - 07-6.

3. *E. W. Frew* "Receding Time Horizon Control Using Random Search for UAV Navigation with Passive, Non-cooperative Sensing", AIAA Guidance, Navigation, and Control Conference, CA, August 2005.

UDC 621.317.7.083.92

I. Yu. Sergeyev, Ph.D.,associateprofessor (National Aviation University, Ukraine)

LINEARIZATION OF CHARACTERISTIC OFINTELLIGENTCAPACITANCE SENSOR

An intelligent capacitive sensor which does not require the inclusion of devices such as a microprocessor, microcontroller or programmable logic controller is described. When using the scheme of linearization in a intelligent capacitive sensor, the relative conversion error that is introduced by elements such as resistors, capacitors and op-amp can be as low as one hundredth of a percent.

Introduction In measuring technique as well as in control automation technique, various capacitance sensors are used [1-18].

In a capacitive position sensor, the electrified plate is the sensor surface and the second plate is the target. The electronics continuously change the voltage on the sensor surface. This is the excitation voltage. The amount of current required to change the voltage is detected by the electronics and indicates the amount of capacitance between sensor and target. An AC bridge circuit or other active electronic circuit is typically used to convert the capacity change into a current or voltage signal and output. In ordinary capacitance-based position measurement, the size of the sensor and the target, and the dielectric medium (usually air) remain constant. The only variable is the gap. All changes in capacitance are therefore the result of a change in the position of the target relative to the sensor.

In the general case of capacitive sensor capacitor is the element with electric capacitance, which value depends on sensor input value. And physical principles, on which capacitor structure is based, are different in different sensors though there is wide range of their differences. It includes both ordinary mechanic constructions, in which the capacity of capacitor is assigned by mutual alignment of plates, and unconventional designs, based for example on ferroelectrics or pyroelectrics.

Problem statement. While all these sensors have different principles of operation, developers face the problem, which is common for all sensors. It includes the necessity of acquisition of functional relationship between input and output values of sensor or device, which includes this sensor [1,2,4,6–9,11,14]. There are two aspects of this problem. In the first case, if the sensor has natural nonlinearity, it is necessary to implement its linearization. It means that auxiliary hard or software tools, entered into composition of intelligent sensor, are used to implement linear functional relationship between input and output values. The second case is, when the capacitance sensor has natural linear characteristic and according to certain reasons it is needed to obtain required nonlinearity.

Solution of the problem. Assigned task can be easily solved, when the output value has been already converted into digital code. For this purpose there is need to be, for example, microprocessor, microcontroller, programmable logic controller or even computer in the structure of the device.

Still in the case of intelligent sensor construction this is not desirable to include to its composition hardware components of above-listed devices. In this case designers of intelligent sensor face the necessity to find other solutions, by which assigned task can be achieved with using of hardware, which is more preferable to be included in intelligent sensor. Measuring converters, considered in researches [16-18], and also intelligent capacitance sensor developed by authors, exemplify such devices. The scheme of such sensor is represented infig. 1.

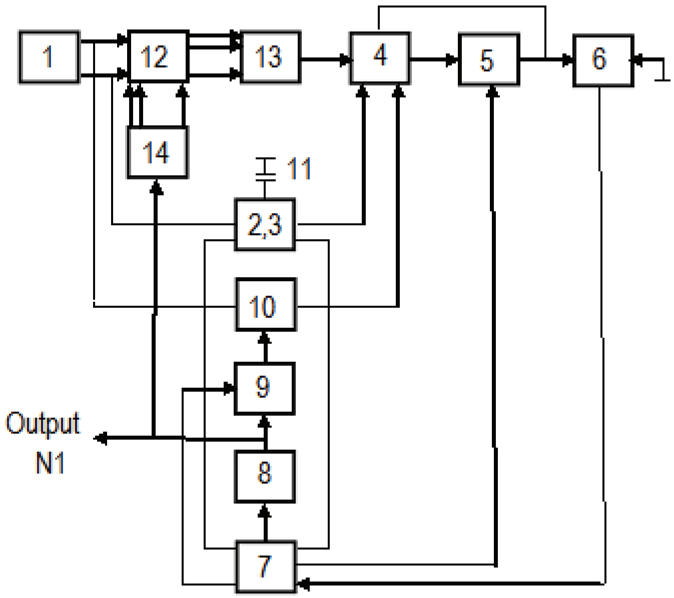

Fig. 1 1 - Source of the reference voltage; 2, 3 – Keys; 4 – Integrator; 5 - Sample-and-hold device; 6 – Comparator; 7 – Synchronization block; 8 - Register of bit-balancing; 9 - Code converter in the time interval; 10 – Key; 11 - Storage capacitor (capacitor of the capacitance sensor); 12 – Switchboard; 13 - Code managed resistive matrix; 14 – Decoder.

The principle of the device Conversion of capacity C_x of capacitance sensor into the code is implemented with the help of iterated-integration transducer. It includes such units as a Source of the reference voltage 1, box of switched capacitor - Keys 2,3 and Storage capacitor (capacitor of the capacitance sensor) 11, Integrator 4 , Sample-and-hold device SH 5, Comparator6, Register of bit-balancing 8, Code converter in the time interval 9, Key 10, controlled bySynchronization block 7.

Required nonlinearity of response of intelligent capacitance sensor is created with the help of Code managed resistive matrix 13, Switchboard 12 and Decoder 14.

Such iterative-integration transducer works cyclically. During every cycle charging of Storage capacitor (capacitor of the capacitance sensor) 11 C_x from Source of the reference voltage 1 is carried out, including subsequent discharging of it at the Integrator 4 input. Also sampling of integrator output voltage is implemented by Sample-and-hold device SH 5. Then follows its storage during time T_c of cycle of continuous integration of Sample-and-hold device SH 5 output voltage by Integrator 4, and its transformation by Register of bit-balancing 8 and Code converter in the time interval 9 into impulse T_x.

Impulse T_x controls the connection of Code managed resistive matrix 13 with Source of the reference voltage 1 by Switchboard 12. Decoder 14 controls Switchboard 12.

To derive equation of conversion of intelligent capacitive sensor let's consider its work in linear mode, i.e. without implementation of linearization. In this case resistors matrix is disconnected with generator input. Let's suppose that voltage at the output of access-storage device is equal to U_0 before the first of concerned cycles. So after the ending of conversion cycle the voltage at the output of access-storage device is equal to:

$$U_1 = U_0 + \frac{E_0 C_x K_{vf}}{C} - \frac{U_H T_c K_{vf}}{R_c} = \frac{E_0 K_{vf}}{C} C_x + U_x \left(1 - \frac{T_c K_{vf}}{R_c}\right),$$

where: E_0 – is output voltage of Source of the reference voltage 1;C_x – capacitor capacitance of Storage capacitor (capacitor of the capacitance sensor)11;C –capacitance of Integrator 4capacitor;i – resistance of Integrator 4 resistor;K_{vf} - Voltage Follower gain.

Similarly, after ending of the *n-th* cycle of transformation we get the formula:

$$U_n = \frac{E_0 K_{vf}}{C} C_x \sum_{j=1}^{n} \left(1 - \frac{T_C K_{vf}}{R_C}\right)^{j-1} + U_0 \left(1 - \frac{T_C K_{vf}}{R_C}\right)^n \quad (1)$$

Expression (1) consists of two parts. One is sum of parts corresponding to geometric progression, which converges at the condition

$$\left|1 - \frac{T_C K_{vf}}{R_C}\right| < 1\,, \qquad (2)$$

Another one is the part $U_0\left(1 - \frac{T_C K_{vf}}{R_C}\right)$ decreasing at the same condition.

If the condition (2) is fulfilled at the steady-state condition ($n\rightarrow\infty$), then the voltage at the output of access-storage device is determined by the expression

$$U_\infty = \lim_{n\rightarrow\infty} U_0 = \frac{E_0 R}{T_C} C_x. \qquad (3)$$

Time of transient process of setting of the voltage is determined by specified accuracy of transformation and actually form a few of cycles.

Code at the output of intelligent capacitance sensor in steady-state condition

$$N_{out} = K_{ADC} U_\infty, \qquad (4)$$

where:K_{ADC} - ADC gain.

Now consider the linearization of the intelligent capacitive sensor, i.e. its work in the nonlinear regime.

Linearization is performed by means of forming of auxiliary component (voltage) in the accordance to the equation (3).

Linearization voltage U_l is formed by the way of integration during impulses T_x of matrix currents are acting. Resistors connect in turn to the outputs $+E_0$ and $-E_0$ of Source of the reference voltage 1. Polarities of reference voltages, which are connected to the corresponded matrix resistors, as well as values of their resistances, are selected against the required curve form of linearization function.

Equation, defining linearization voltage U_l can be represented in the form:

$$U_l = \frac{E_0 K_{vf}}{RC} \sum_{i=1}^{m} \frac{\sin(T_x - t_i) + \sin(t_{i+1} - T_x)}{2R_i} \ \mathrm{sign}\, f'_{lini} \quad , \qquad (5)$$

where:R_i – resistance of i-th resistor of resistor matrix;$i = 1,\dots m$– number of section of piecewise-linear approximation of linearization function f_{lin};f'_{lini} – random linearization function at i-th section of approximation;t_i – the time interval from the beginning of the cycle to the beginning to the i-th interval (connecting of resistorR_i);

$$\text{sign X – signum function: } \mathrm{sign}(X) = \begin{cases} -1, & x > 0 \\ +1, & x \le 0 \end{cases}$$

Convertion equation, taking into account the expressions (3), (4) and (5) can be written as

$$U_{out\,nl} = K_{ADC}\,(U_\infty + U_l).$$

Conclusion

An intelligent capacitive sensor can be constructed according to the considered scheme; it does not require the inclusion of devices such as a microprocessor, microcontroller or programmable logic controller.

In this case, taking into account the errors introduced by such elements as resistors, capacitors and an operational amplifier, an intelligent capacitive sensor can be created according to this circuit, which has relative errors of the conversion at the level of hundredths of a percent.

In this case the formation of a wide range of linearizing functions to obtain the desired conversion function may be possibly.

References

1. *F.N. Toth and G. C. M. Meijer* “A Low-Cost Smart Capacitive Position Sensor”, IEEETransactions on Instrumentation and Measurement, Vol. 41, No. 6, December 1992, pp. 1041-1044.

2. *X. Li, G.C.M. Meijer, G. W. de Jong and J. W. Spronck* “An Accurate Low-Cost Capacitive Absolute Angular-Position Sensor with a Full-Circle Range”, IEEE Transactions onInstrumentation and Measurement, Vol. 45, No. 2, April 1996, pp. 516-520.

3. *X. Li, G.C.M. Meijer and G. W. de Jong* “A Microcontroller-Based Self-Calibration Technique for a Smart Capacitive Angular-Position Sensor”, IEEE Transactions on Instrumentation and Measurement, Vol. 46, No. 4, August 1997, pp. 888-892.

4. *K. Mochizuki, T. Masuda and K. Watanabe* “An Interface Circuit for High-Accuracy Signal Processing of Differential-Capacitance Transducers”, IEEE Transactions on Instrumentation and Measurement, Vol. 47, No. 4, August 1998, pp. 823-827.

5. *W.C. Heerens* “Application of capacitance techniques in sensor design,” J. Phys. E, Sci. Instrum., vol. 19, no. 11, pp. 897–906, Nov. 1986.

6. *R.D. Lee* “The application and principle of an improved capacitive level sensor,” J. Korea Elect. Assoc., vol. 148, no. 4, pp. 37–41, 1989.

7. *F.N. Toth and G. C. M. Meijer* “A low-cost, smart capacitive position sensor,” IEEE Trans. Instrum. Meas., vol. 41, no. 6, pp. 1041–1044, Dec. 1992.

8. *F. Zhu, J. W. Spronck, and W. C. Heerens* “A simple capacitive displacement sensor,” Sens. Actuators A, Phys., vol. 26, no. 1–3, pp. 265–269, Mar. 1991.

9. *L.K. Baxter* Capacitive Sensors. Piscataway, NJ: IEEE Press, 1997.

10. *W.C. Heerens* “Application of capacitance techniques in sensor design,” Phys. E: Sci. Insfrum., vol. 19, pp. 897-906, 1986.

11. *E.C. Heerens* “Basic principles in designing highly reliable multiterminal capacitor sensors and performance of some laboratory test models,” Sens. Actuators, vol. 3, pp. 137–148, 1982/83.

12. *G.W. de Jong, G.C.M. Meijer, K. van der Lingen, J. W. Spronck, A.M. Aalsma, and Th. D. Berteles*“A smart capacitive absolute angularposition sensor,” Sens. Actuators, vol. A41–42, pp. 212–216, 1994.

13. *X. Li* “Low-Cost Smart Capacitive Sensors for Position and Speed Measurement,” Ph.D. dissertation, Electronics Research Lab., Delft Univ. of Technology, Dept. of Electrical Engineering, Delft Univ. Press, Delft, The Netherlands, 1997.

14. *St. Cermak, F.Wandling,W. Zdiarsky, P. Fulmek, and G. Brasseur* “Capacitivesensor for relative angle measurement,” in IEEE Conf. Proc. Instrumentation and Measurement Technology, vol. 2, Baltimore, MD, May 1–4, 2000, pp. 830–833.

15. *Сергеев И.Ю.* Анализ АЦП с динамическим интегратором. // Измерительная техника, 1990. № 6. 38 - 40 с.

16. *Сергеев И.Ю.* Исследование и разработка интегрирующих измерительных преобразователей с итерационной аддитивной коррекцией погрешностей: Дисс. канд. техн. наук.: 05.11.05 – 322 с.

17. *Сергеев И.Ю.* Авт свид СССР № 1016799, кл. G 06 G, 7/26, 07.05.83. Бюл. № 17.

UDC 625.735(043.2)

N.K. Filiashkin, Ph.D, professor,M.V. Novik, graduate student
(National Aviation University, Ukraine)

IMPROVINGTHERELIABILITYOF NAVIGATIONINFORMATIONFORSMALLUAV

This paper presents an analysis of reliability improvement methods of flight control and navigation systems for unmanned aerial vehicle (UAV). Proposed suboptimal algorithms of integration of navigation systems, which employs maximum likelihood methods (MLE) and complementary compensation filter with variable structure. Redundant information about motion parameters from different UAV systems are used in data fusion algorithms. Structure for possible schemes of integration for navigation systems described.

Background and Objective The current approach to navigation data fusion for small and miniature UAV is employ integrated inertial satellite navigation system, as main source of information about flight and navigation parameters. Moreover, sensors of such systems are based on low cost MEMS technology and the Extended Kalman Filter (EKF) as the basic data fusion algorithm. Typically, level of GPS/IMU integration structure is loose or tight.

The main drawback with this approach to system integration is low reliability and precision of sensor's data. The lowreliability ofthe information can lead to loss of the UAV, in particular, the loss of information from the satellite navigation system, for instance caused by satellite radio signal jamming. Rough micromechanical INS unable to provide flight and navigation information with required accuracy, errors degrade exponentially, correction needed even on small autonomous time intervals.

If Kalman filter is based on a complete and perfectly tuned model, the measurements should be zero-mean white noise process otherwise filter is not performing optimally. In practice, it is difficult to know exact values for covariance and from other side with time unmodeled errors will become significant, thus making the filter to diverge. Leading researchers for small UAV platforms solve this problem in most cases using own unique approaches.

In particular in order to overcome divergence large amount Kalman filter modification was developed, for instance: Yasvinsky algorithms, different robust [3] and adaptive extensions [4]. Toreduce the amount ofcomputationused reduced the Kalman filter. Also, other approaches to navigation information filtering were introduced.

Thus, research aimedat improving the reliabilityofflight and navigation systems for smallUAVsare relevant.

StatementofProblemPaperproposes for development of integrate navigation system to focus on improving the reliability and precision of UAV flight navigation algorithms in autonomous mode by maximizing employment of redundancy information, as well as new approaches to problems of data fusion of flight and navigation systems.

SolutionApproachDatafusionofredundantnavigationinformation on board of UAV is proposed to use compensation complementary filter well known from Doppler inertial navigation systems (fig. 1), rather than reduced Kalman filter.

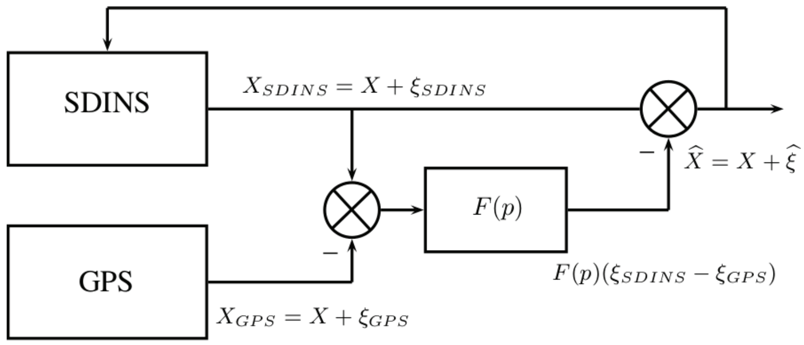

Fig.1

But instead of the classical aperiodic filter $F(p)$ of compensation schemes, authors propose to use a third order filter with variable structure.

$$F(p)=\begin{cases}\dfrac{1}{T_1 p+1} & if \quad t_{\text{up}} \le 3T_1;\\[2mm] \dfrac{3T_2 p+1}{(T_2 p+1)(T_2 p+1)(T_2 p+1)} & if \quad 3T_1 < t_{\text{up}} \le 3T_2;\\[2mm] \dfrac{3T_3 p+1}{(T_3 p+1)(T_3 p+1)(T_3 p+1)} & if \quad 3T_2 < t_{\text{up}},\end{cases}$$

here t_{up} - uptime of compensation complementary filter.

Studies have shown(Fig. 2), such data fusion algorithm givesresults notworse than theKalmanfiltering,without affectingthe stability ofestimation algorithms.

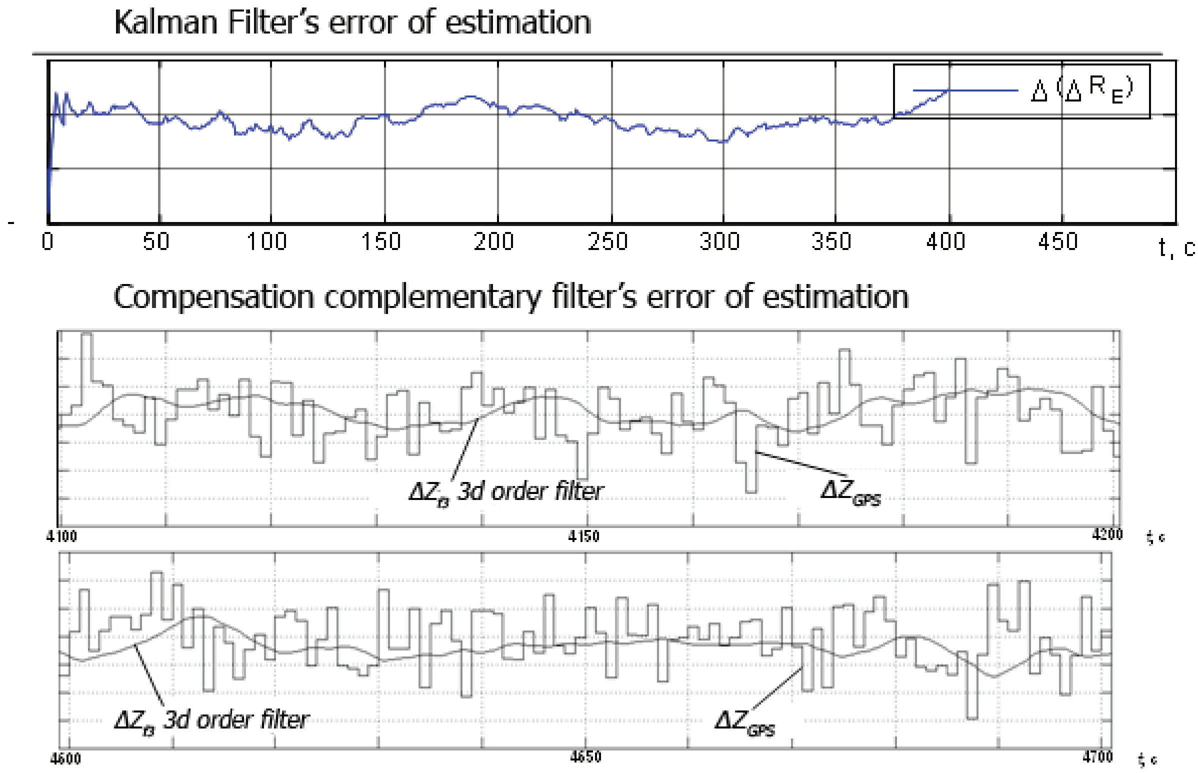

Fig. 2

To improve thereliability of theUAVflight control andnavigation system proposed to complement navigation system with already existing onboard hardware: air-magnetic navigation instruments. To construct such system azimuth corrector (three axis magnetometer) and pressure sensor (bounds errors of vertical channel of inertial system) is used.

Algorithms of additional air-magnectic navigation system are quite simple:

$$\varphi = \varphi_0 + \int \frac{V_{\text{true}}\cos\psi + U\cos\delta}{R_E}dt; \qquad \lambda = \lambda_0 + \int \frac{V_{\text{true}}\sin\psi + U\sin\delta}{R_E}dt;$$

where φ, φ_0, λ, λ_0 – currentandinitialcoordinatesof UAV; $\left(V_{\text{true}}\cos\psi + U\cos\delta\right)$, $\left(V_{\text{true}}\sin\psi + U\sin\delta\right)$ – components ofground speed;R_E – Earth radius; ψ – true magnetic heading.

Barometric altitude H_{B} and true air speed V_{true} computed based on static p and dynamic p_{dyn} pressure.

$$H_{\text{B}} = \frac{T_0}{\tau_{\text{g}}}\left[1-\left(\frac{p}{p_0}\right)^{\frac{\tau_{\text{g}} R_{\text{S}}}{g_0}}\right] \text{for H} \le 11000\text{м}; \; V_{\text{ист}} = \sqrt{2R_{\text{S}}T\left(\frac{k}{k-1}\right)\left[\left(\frac{p_{\text{dyn}}}{p}\right)^{\frac{k-1}{\text{k}}} - 1\right]}$$

whereτ_g– thermalgradient; R_s – specific constant;k – value of adiabat.

The block diagram ofan integratednavigation systemis shown in fig. 3.

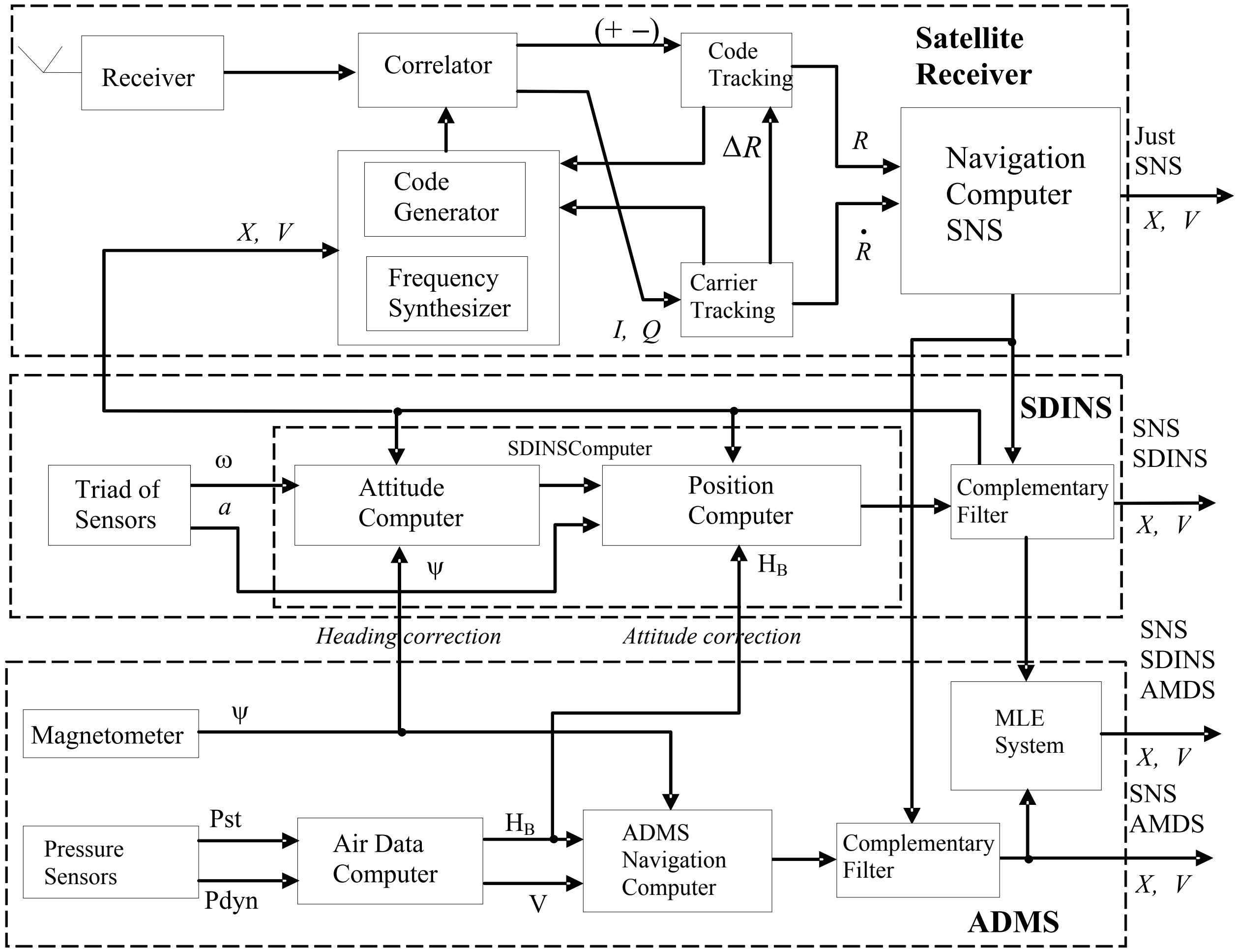

Fig. 3

Inthe normal operation mode, the integratednavigation systemimplementedastwosimilar fusion algorithms: air-magneticand satellitenavigation systems, as well as inertialand satellitenavigation systems.The resulting estimatesof inertial-satellite and satellite-air-magnetic navigation systemsfurtherestimated byMLE method.

Sincethe output of complementary compensation filters current evolution of errors in the first case inertial, in second air-magnetic are observed, there is a possibility of approximating the evolution of these errors, with their further extrapolation. Predicted errors are used in the autonomous operation mode of navigation system, increasing reliability navigation means of UAV (fig. 4).

Naturally, degree of confidence in data of the INS gradually decreases and, eventually, system employs only a purely air-magnetic method of dead reckoning. The accuracy of estimation of flight parameters is reduced with time too, but this approach gives possibility to continue flight and return UAV to home base.

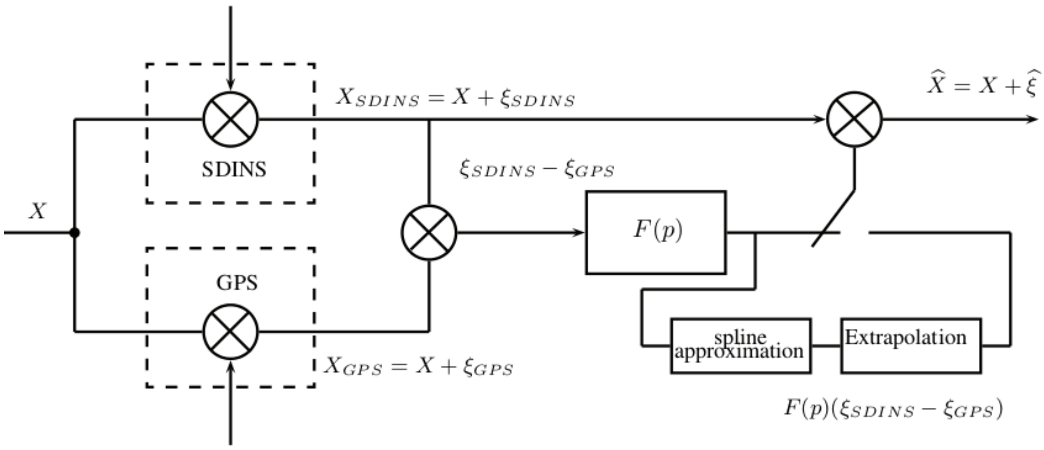

Fig. 4

To improve the reliabilityof attitude parameters,in conjunction withinformationfrom theinertial system, alternative information,received from included functional units.For these purposes,nogyroscopicmeans of orientation measurement is used:magnetic,pyrometric, and aerodynamic. Information fromvarious sourcesis treated asredundantandprocessed to correct theinertialvertical.

Conclusions

The proposedapproach tothe designingof smallUAVnavigation systemssuggeststhe possibility of obtainingadditional informationabout the parameters ofmotionof theobjectfrom included functional units, using it as redundant datain thefusionalgorithms,based onmaximum likelihoodmethodsand complementary compensation filterwith variable structure.This approach introducerobust and stability toestimation algorithms. This approachsignificantly increases thereliability of theinformation supportmissionUAVin autonomousmode ofthe navigation system.

References

1. *Ф.М. Захарін, В.М. Синєглазов, М.К. Філяшкін*. Алгоритмічне забезпечення інерціально-супутникових систем навігації. – К.: Вид-во НАУ, 2011. – 320 с.

2. *В.А. Рогожин, В.М. Синеглазов Н.К. Филяшкин* «Пілотажно-навігаційні комплекси повітряних суден»: К.: НАУ, 2007. – 306 с.

3. *E. A. Wan and R. Van Der Merwe* «The unscented Kalman filter for nonlinear estimation», in Adaptive Systems for Signal Processing, Communications, and Control Symposium 2000. AS-SPCC. The IEEE 2000, 2000, pp. 153–158.

4. *A. H. Mohamed and K. P. Schwarz* «Adaptive Kalman filtering for INS/GPS», Journal of Geodesy, vol. 73, no. 4, pp. 193–203, 1999.

UDC 681.511.4(045)

A.K. Ablesimov, professor,K.A.Polezhay (National Aviation University, Ukraine)

LIMIT CYCLES IN NONLINEAR SYSTEMS OF STABILIZATION

The conditions of appearing of periodic damped oscillations in nonlinear systems of stabilization have been considered.

Introduction and statement of the problem Many systems contains elements, which are described by nonlinear equations and have essentially nonlinear characteristics. Examples are the elements with characteristics such as insensibility zone, saturation (limitation), the ideal relay, the hysteresis loop, the relay with hysteresis, etc. The system, which includes at least one such element is a nonlinear.

Fig. 1 shows a block diagram of a nonlinear system of stabilization.

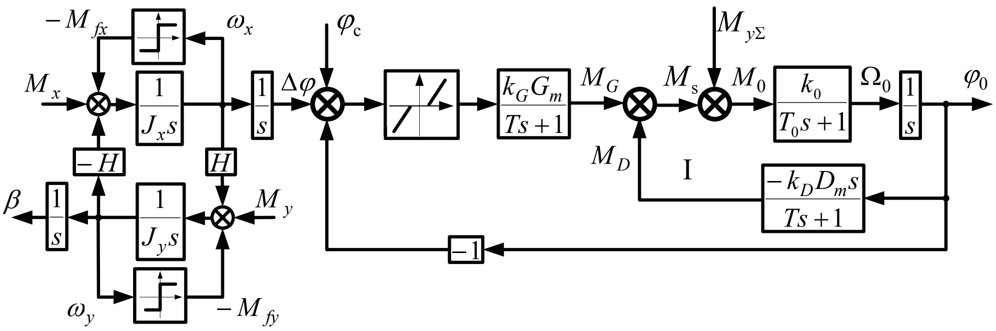

Fig.1 Block diagram of nonlinear system of stabilization

The moment of stabilization is formed through the sensor channel of angular deviation and through the speed sensor of angular deviation of control object

$$\overline{M}_s = \overline{M}_G + \overline{M}_D \equiv k_G G_m + k_D D_m ,$$

where G_m , D_m - structural stiffness and damping of the system, respectively; $0 \le k_G \le 1$ and $0 \le k_D \le 1$ - coefficients of regulating the stiffness and damping.The system regulator has a linear characteristic with insensibility zone. The friction in the frame pillar of gyroscopic angle sensor - a "dry"

$$M_{fx} = -M_{fm}\text{signщ}_x ;$$

$$M_{fy} = -M_{fm}\text{signщ}_y .$$

Thus, the nonlinear system of stabilization consists of both linear and nonlinear elements.

The main feature of nonlinear systems should be consider the appearing possibility of limit cycles in them - periodic undamped oscillations. Thus, amplitude of those undamped oscillations is independent of external influence as well as of initial conditions. In general, the limit cycle may be not sinusoidal.

In this regard in researching of appearing possibility of limit cycles in nonlinear systems of stabilization, determination of their parameters and stability analysis, synthesis of corrective devices, which eliminating the appearance in nonlinear system limit cycle, present considerable interest.

Problem solving Consider the system of stabilization, angle sensor which has not error $\Delta\varphi$, caused by the action of perturbing moments M_x , M_y on the frame of three-stage gyro. If necessary, angle sensor, as a nonlinear element, can be investigated separately for checking the appearance of limit cycles in it.

The principle of superposition does not apply to nonlinear systems, so, we will consider the system that is only under the action of the control signal φ_c. Because of adopted limitations, the block diagram of a nonlinear system of stabilization acquire a typical kind.

After the convolution of contour I and the transition to the frequency domain, we obtain an equivalent of frequency transfer function of the linear part of the stabilization system

$$W(j\text{щ}) = \frac{k_G k_0 G_m}{\left[-\left(T_0 + T\right)\text{щ} + j\left(1 + k_D k_0 D_m - T_0 T \text{щ}^2\right)\right]\text{щ}}. \tag{1}$$

We will apply to the nonlinear element method of harmonic linearization and will find in the handbook on automation the function which describe it [1,2]

$$W_f\left(a_m, \text{щ}\right) = \frac{N_1 + jC_1}{a_m} = k - \frac{2k}{\pi}\left(\arcsin\frac{b}{a_m} + \frac{b}{a_m}\sqrt{1 - \frac{b^2}{a_m^2}}\right), \tag{2}$$

where b - width of the insensibility zone; k - the gain coefficient in the linear regime.

Note that the fundamental difference between harmonic linearization and usual linearization is that if we have harmonic linearization, the nonlinear characteristic we will change to linear, the slope of which depends on the amplitude of the signal at the input of the nonlinear element.

In a closed system can predict the existence of a limit cycle, if for some values of the amplitudes a_{m0} andfrequencies щ_0 of the signal at the input of the nonlinear element the amplitude and phase of the frequency response characteristic (APFRC) of open circuit will be equal to

$$1 + W(j\text{щ}) W_f\left(a_m, \text{щ}\right) = 0. \tag{3}$$

Let's rewrite equation (3) as

$$W(j\text{щ}) = -\frac{1}{W_f\left(a_m, \text{щ}\right)}. \tag{4}$$

The left-hand side of equation (4) is APFRC of linear component of stabilization system. The right-hand side - reverse APFRC of nonlinear element, taken with opposite sign. The parameters $W(j\text{щ})$ are determined only by the frequency of input signal and does not depend on its amplitude. Butparameterslike $\frac{-1}{W_f\left(a_m, \text{щ}\right)}$, areonthecontrary, determined only by the amplitude of the signal at the input of the nonlinear element and does not depend on its frequency.

Therefore, if it build graphical images on complex plane $W(j\text{щ})$and$\frac{-1}{W_f\left(a_m, \text{щ}\right)}$, then the point of its intersection will satisfy the expression (4). The obtained values of the amplitude a_{m0} and frequency щ_0 determine the changing law of the limit cycle.

When plotting the inverse APFRC of nonlinear element, we take into account the particular cases of calculation its describing function

$$W_f\left(a_m = b\right) = k - \frac{2k}{\pi}\left(\arcsin 1 + 1\sqrt{0}\right) = k - \frac{2k}{\pi}\cdot\frac{\pi}{2} = 0;$$

$$W_f\left(a_m \to \infty\right) = k - \frac{2k}{\pi}\left(\arcsin 0 + 0\sqrt{1}\right) = k.$$

Graphical representation of $\frac{-1}{W_f\left(a_m, \text{щ}\right)}$ in the complex plane (fig.2) is a straight line coinciding with the negative direction of the x-axis. The maximum value equal to $\frac{-1}{k}$ the inverse APFRC reaches with $a_m \to \infty$.

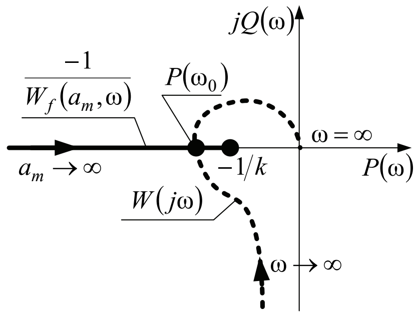

Fig.2 Parameters of the limit cycle

On the basis of the frequency transfer function (1) of the linear component of the system, we find an algorithm calculating its APFRC

$$W(j\text{щ}) = \frac{-k_G k_0 G_m (T_0 + T)}{(T_0 + T)^2 \text{щ}^2 + \left(1 + k_D k_0 D_m - T_0 T \text{щ}^2\right)^2} - j \frac{k_G k_0 G_m \left(1 + k_D k_0 D_m - T_0 T \text{щ}^2\right)}{\left[(T_0 + T)^2 \text{щ}^2 + \left(1 + k_D k_0 D_m - T_0 T \text{щ}^2\right)^2\right]\text{щ}}. \quad (5)$$

APFRC graph $W(j\text{щ})$ on the complex plane, when the frequency щ signal is changes from 0 to ∞ is presented in fig.2 by dotted line.

Let find the coordinate of the point of intersection $W(j\text{щ})$ and $\frac{-1}{W_f(a_m, \text{щ})}$.

First of all we determine from (5) the frequency of possible limit cycle

$$\text{щ}_0 = \sqrt{\frac{1 + k_D k_0 D_m}{T_0 T}}.$$

Substituting the value щ_0 into the real component of equation (5), we find

$$P(\text{щ}_0) = \frac{-k_G k_0 G_m T_0 T}{(T_0 + T)(1 + k_D k_0 D_m)}.$$

A limit cycle will be possible if $\left|\frac{1}{k}\right| < P(\text{щ}_0)$, so $k > \frac{(T_0 + T)(1 + k_D k_0 D_m)}{k_G k_0 G_m T_0 T}$.

The amplitude of a possible limit cycle a_{m0} we find, in accordance with equation (4), after the substitution of values in it for $W(j\text{щ}_0)$ and $W_f(a_m, \text{щ})$

$$\frac{-k_G k_0 G_m T_0 T}{(T_0 + T)(1 + k_D k_0 D_m)} = \frac{-1}{k - \frac{2k}{\pi}\left(\arcsin\frac{b}{a_m} + \frac{b}{a_m}\sqrt{1 - \frac{b^2}{a_m^2}}\right)}. \quad (6)$$

In practice, the amplitude is determined by the tables function $W_f(a_m, \text{щ})$ for found value of left-hand side of equation (6) if there is information about the parameter b of the nonlinear element.

According to the received data we write the variation law of possible limit cycle

$$\varphi_0(t) = -\varphi(t) = -a_{m0} \sin \text{щ}_0 t.$$

In the stable limit cycle the oscillation amplitude returned to its previous value after its change, that is caused by this or any other perturbation. Otherwise, the limit cycle is unstable. If, for example, in a nonlinear system of stabilization an unstable limit cycle is possible, then with amplitude decreasing, due to any factor, these oscillations are damped with time. Conversely, if the oscillation amplitude increases, then it will increase without limit or in system a new limit cycle will arise with another amplitude or with another frequency.

Stability of limit cycle can be estimated, for example, using the criterion of Goldfarb [3]. In accordance with fig.2 we make a conclusion about the unstable limit cycle in the considering nonlinear system.

In any case, it is desirable to avoid the occurrence of limit cycles. This issue can be resolved by introducing into the nonlinear system the correction circuits.

We denote the transfer function of the correctivecircuit $W_{cc}(s)$. Applying to the corrected nonlinear system of stabilization method of describing functions we can be write

$$W_{cc}(j\text{щ})W(j\text{щ}) = -\frac{1}{W_f(a_m, \text{щ})}.$$

Thus, the frequency transfer function of the linear part of the corrected system is determined by the product of the frequency transfer functions of the corrective circuit and of linear component. Therefore, APFRC of the linear part of the corrected system will be a scaled APFRC of its linear component.

Corrective circuit should be chosen with suchfrequency transfer function $W_{cc}(j\text{щ})$, to prevent the crossing in the complex plane of inverse APFRCof nonlinear element and of APFRCof linear part of corrected system.

Let introduce into the nonlinear system of stabilization a corrective circuit with gain coefficient k_{cc}.

Limit cycle will be excluded if the coordinate of the point of intersection of the corrected APFRCof the linear part of the system of stabilization $k_{cc}P(\text{щ}_0)$ will not exceed the maximum value of the inverse APFRCof nonlinear element $\left|\frac{1}{k}\right|$, where $\left|\frac{1}{k}\right| > \frac{k_{cc}k_G k_0 G_m T_0 T}{(T_0 + T)(1 + k_D k_0 D_m)}$.

From the last inequality we find the value of the gain coefficient of the corrective circuit

$$k_{cc} < \frac{(T_0 + T)(1 + k_D k_0 D_m)}{k k_G k_0 G_m T_0 T},$$

which ensures the exclusion of occurrence of the limit cycle.

Conclusions

The presence of nonlinearities in the system of stabilization leads to the possibility of occurrence in the system periodic undamped oscillations - limit cycles.

The existence of a limit cycle and its parameters can be predicted based on the analysis of APFRCof linear component of the system and of inverse APFRCof nonlinear element, taken with the sign "minus". The introduction into the nonlinear system of stabilization corrective circuits will eliminate the possibility of occurrence of limit cycle in the system.

References

1. *Аблесімов О.К., Александров Є.Є., Александрова І.Є.* Автоматичне керування рухомими об'єктами й технологічними процесами. - Харків: НТУ “ХПІ”, 2008. - 443с.

2. *Филлипс Ч., Харбор Р.* Системы управления с обратной связью. – М: Лаборатория Базовых Знаний, 2001. – 616с.

3. *Ким Д.П.* Теория автоматического управления. Т.2. Многомерные, нелинейные, оптимальные и адаптивные системы. –М.: Физматлит, 2004. -464с.

UDC629.735.051-52:004.942(045)

O.V. Melnykov, PhD (National Aviation University, Ukraine)

AIRCRAFT'STRAJECTORY AT THE COMPRESSED TIME SCALE PREDICTION AS THE FLIGHT CONTROL ON-BOARD SYSTEMS INTELLECTUALIZATION

The paper examines approaches to solving the problem of improving the effectiveness and safety of aircraft on the example of the implementation methodology of predictive modeling of the flight path of aircraft in a compressed time scale in the CWU board

Problem statement The past century has brought to humanity not only the rapid development of technology and related amenities in all spheres of life, but also new, not previously known problem - the so-called man-machine, or ergatic, systems. The system of "pilot-aircraft", which soon became regarded as a system of "crew - aircraft - the environment," the first days of operation of aerodynamic aircraft is one of the most heroic and dramatic chapters in the history of human society[1,2,3].

Ensuring the safety of (ES) and the effectiveness of the civil aviation (CA) - material losses caused by an accident (A) are supplemented, as a rule of men Because of this problem (ES) in the CA has an important economic, logistical, moral and ethical value.

The concept of "performance fly" refers to the impact of air transportation of passengers and cargo, providing high levels of regularity and economy. The problem of efficiency, therefore, cost of flight is complex and is located at the junction of several sciences, air operations, flight dynamics, aerodynamics and economy of air transport, and is characterized by safety and efficiency of air traffic.

In the development of the global CA to the fore the problem of preventing or at least significantly reduce the relative amount of AP as a result of improper actions during the flight crews are based on objectively established proper conditions nonoptimal flight crew activity or inactivity. Currently, the most frequent causes of accidents include:collision with the earth's surface or artificial obstacles almost serviceable aircraft (Armed Forces);deterioration or complete loss of control in flight due to Sun exposure is quite determinate internal or external disturbing factors, which could be relatively easy to avoid or overcome.

Task The above reasons are directly related to the activities of the crews to manage the trajectory of the aircraft in the airspace. Consequently, the approach to safety improved performance should be based on scientific research, which is the subject of the flight control by crew the intellectualization of the onboard equipment - automatic on-board intelligent flight control system - as the original draft version of the aircraft type. Consequently, the main task of ensuring aviation safety is a complex system of training and development of flight-training of crew and servise and equipped the aircraft by the highly intelligent and comfortable on-board automated control systems of aircraft on all phases of its flight.

Thus, the purpose of this paper is to introduce a wide range of technical specialists of civil aviation and the main challenges facing the aviation industry of the country, to provide the basic conceptual directions of change, modernization and development of civil aviation from the perspective of the state, as well as to identify appropriate ways of addressing the scientific and technical questions.

Problem solution Analysis of available information and analytical materials allows you to identify the main reasons entailing accidents and disasters, decline in air transport safety and transport.

Considering the educational process and shaped the country's institutions of higher education as the foundation of the cell system efficiency and safety aircraft, it must be noted on the orientation of science teaching and student groups at universities offer specialized techniques and methods for raising issues of safety - designing fault-tolerant, adaptive and robust systems flight control aircraft, equipping them with modern intellectual integrated avionics computer.

Motion control of the aircraft includes a planning problem (installation) of the trajectory, so that one of the promising areas of the problem of prediction and selection of the optimal trajectory of the aircraft in view of its implementation for the given aerodynamic characteristics of aircraft [6,7]. Emphasis is placed on the development and implementation of computational methods in a compressed time scale, realizing the trajectory in real time. It is possible to use software package synthesis paths ("trajectories generator"), which yields physically realizable software ("feed-forward", "predict") and reference ("reference", "desirable") trajectory in the presence of restrictions on the management and environment.

Under consideration is related to the direction of the trajectory simulations of one or more aircraft in the external environment in terms of controlled flights are subject to change (meteo-weather, space sector, the characteristics of aircraft flight).

The generalized structure of the simulation block dynamic model is presented in Fig.1.

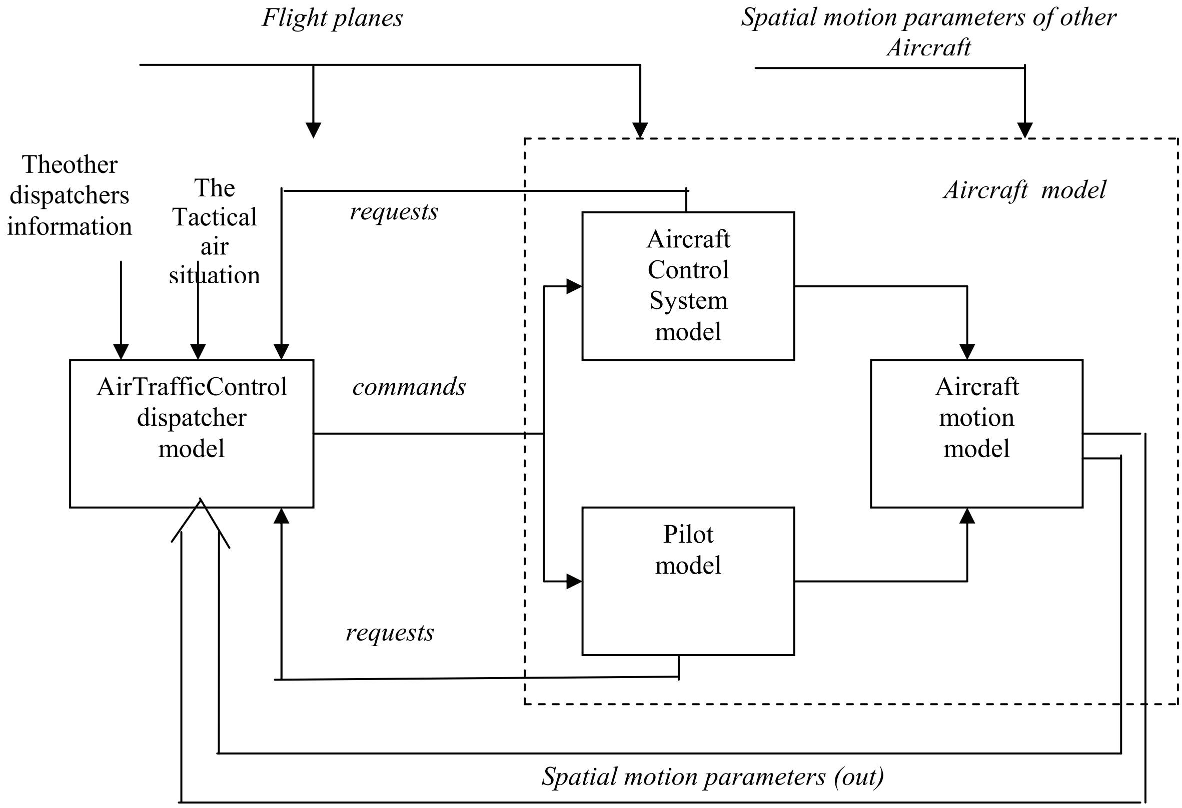

Fig.1 Structure of the dynamic model simulation block

There are two ways of modeling the trajectory:

Option 1 (closer to the scaled-down simulation):

- Controling inputs in the simulation are the values of parameters: latitude φ; geographical longitude λ; drift angle β; roll angle γ, pitching ϑ; gyro- cours ψ; ground (path) speed W_{path}; dash (device) speed V_{mes};
- information from the outputs of navigation sensors comes in a digital computer, and then compute the navigation task; as the actual sensors - inertial system (INS), air data system (ADS), a satellite navigation system (SNS);
- as a result of modeling in the digital computer to control the flight path used by a given value of the roll angle γ_{giv} (for the horizontal plane);
- this information goes to the ACS, and then commands enter to actuators - maneuvering the aircraft;

- as feedback from the ACS in a digital computer - the deviation of the exchange rate (ξ_{cours}), deviation from the glide path (ξ_{glide}).

The structure scheme is shown on fig.2.

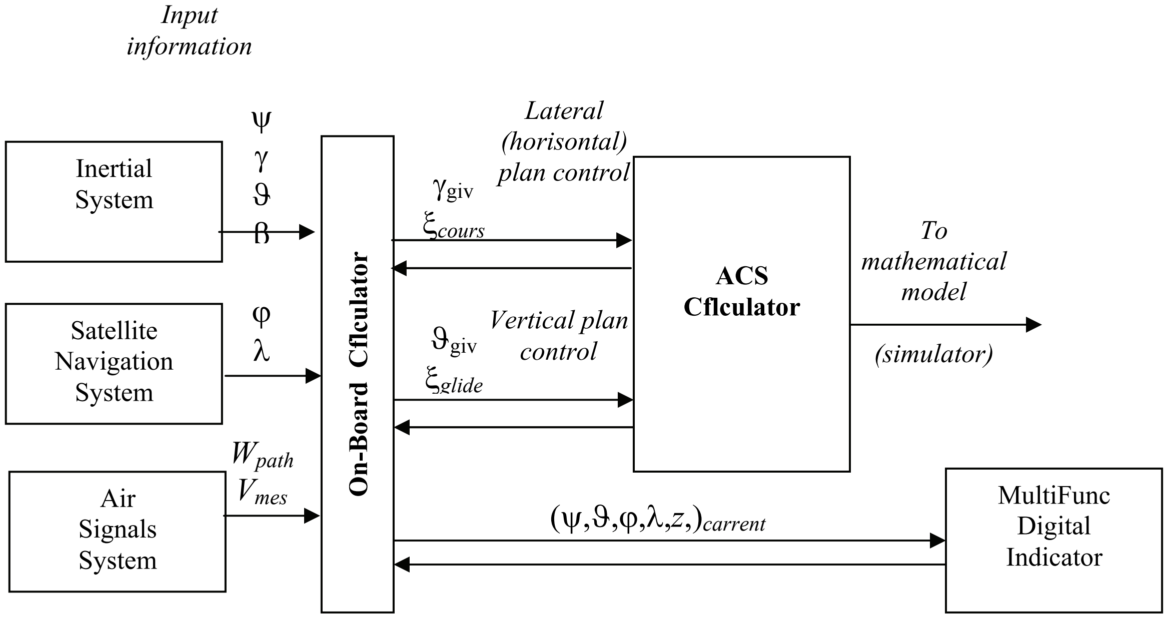

Fig.2 Structure of the 1-st variant simulation block

<u>Option 2 (mathematical modeling and simulation)</u>

- instead of the actual sensor signals using mathematical models (created in the digital computer simulation environment of the sensor and navigation data errors). Block diagram of the system modeling the trajectory shown in Fig.3.

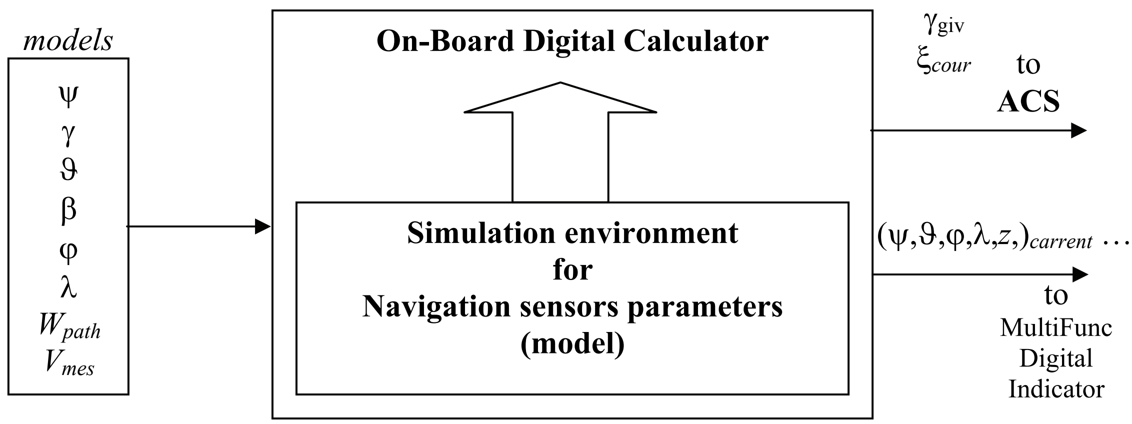

Fig.3 Structure of the 2-d variant simulation block

In general, the simulation process can be shown as the block diagram at Fig. 4 [7,8].

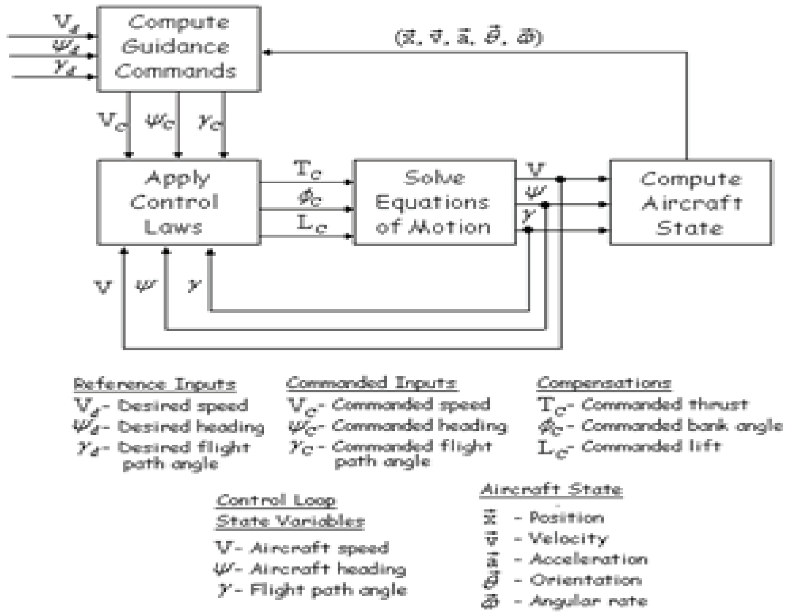

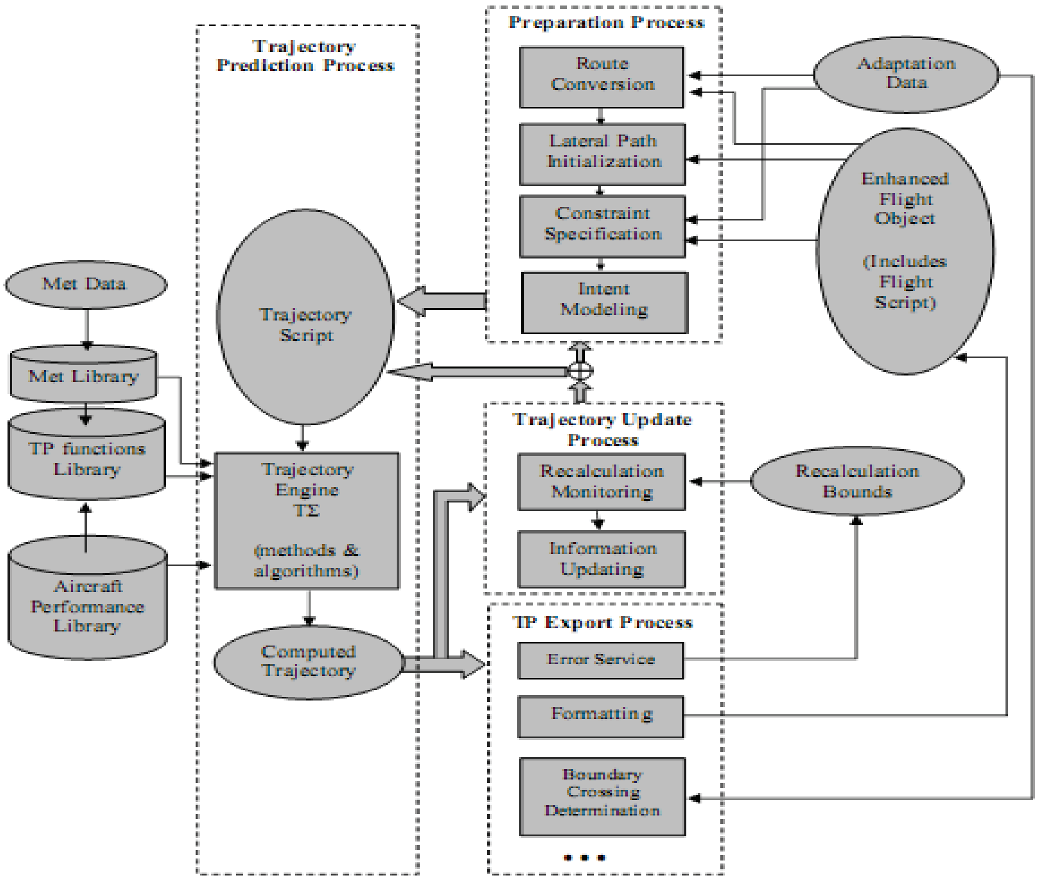

Fig.4. Structure scheme of simulation processes

Trajectories simulation options, consisting (given) of the sample sites (segments) of the trajectory - straight and curved (drop-down, bottom-up), which correspond to the different duration and intensity of maneuvering phases of aircraft flight along the route - are presented in Fig.5 [7,8].

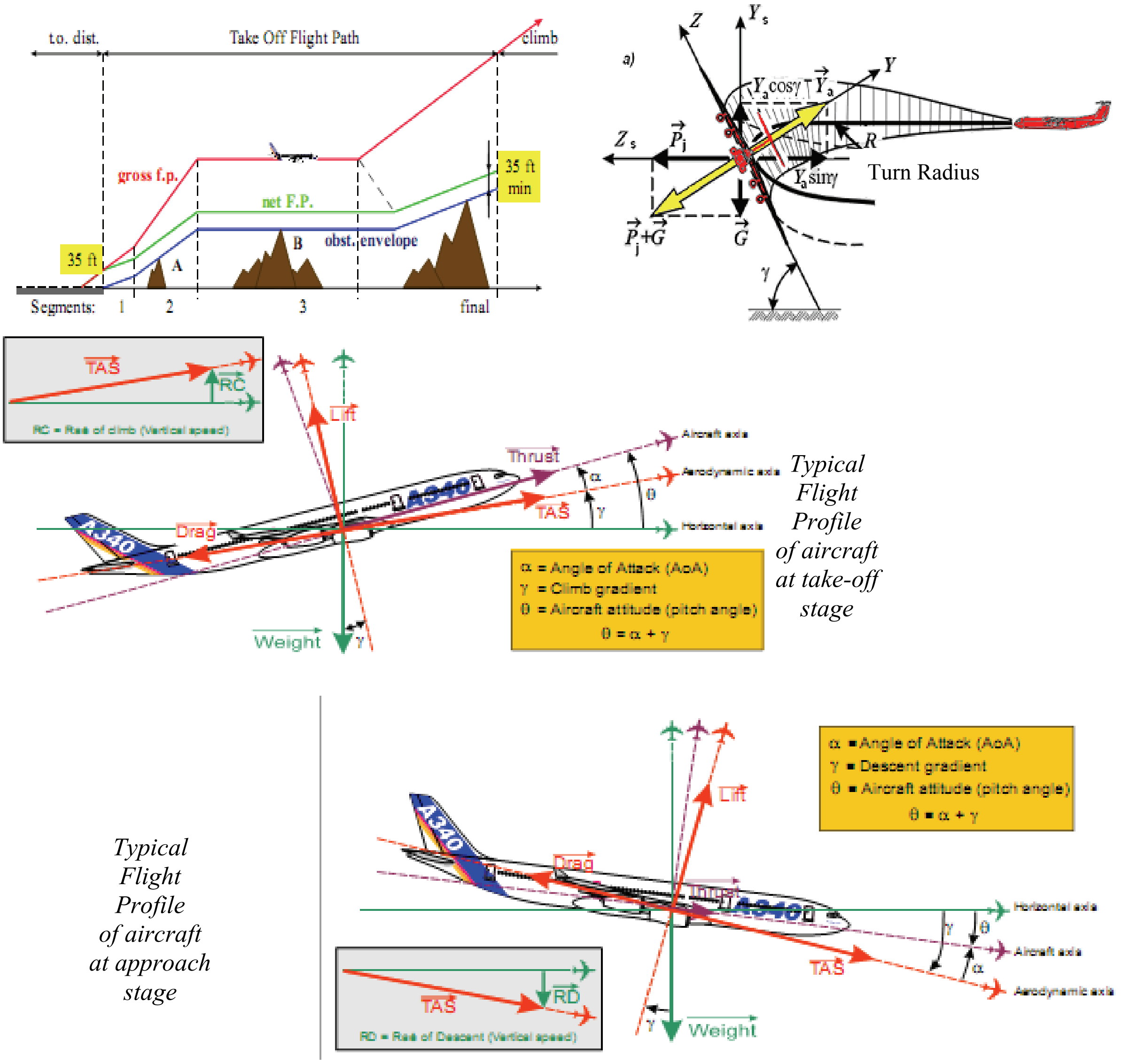

Fig.5. Typical trajectories of aircraft at different flight stages

Fig.6 is shows the simulator programming interface in entered with the results of imaging (visualization) aircraft flight trajectories for several calculated sections (segments).

Conclusions

So, research has shownmore efficient aircraft flight can be carried out in the following areas [2,4,5]:1 - optimization of trajectories and the technology of flight;2- optimization of the aerodynamic configuration ;3- parameter optimization of power plant.

The peculiarity of the flight trajectory optimization mode is the use of economic criteria and accounting requirements for flight safety, Separation and physiology of the passengers. The optimal regimes of flight and the optimal trajectory Sun depend on the technical and economic parameters: the cost of aviation fuel and the equivalent parameter proportional to the value of time, shape the trajectory and time (flight) costs. An increase in the cost of fuel reduces the optimal speed at cruising stage, stages of the climb and descent. Studies show that with increasing ratio of fuel cost to the equivalent parameter tailwind component of wind velocity and a decrease in the coefficient of individual optimal velocity trajectory of civil aircraft. The *optimal flight modes algorithms structure* (*OFMAS*) depends on flight mass index of the cost of fuel, wind direction and speed.

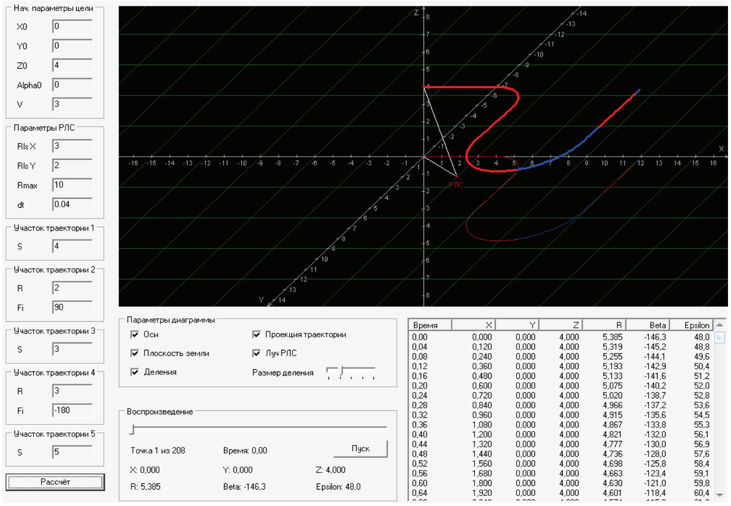

Fig.6. Typical trajectories of aircraft at different flight stages simulator

Algorithms for preemptive model (aircraft trajectory prediction) designed for use such in systems optimization of flight or *on-board flight-navigation complexes* (*BFNC*) as in *ground control (dispatcher) stations*.

Optimization of the aerodynamic design of civilian aircraft is reduced to determining the angles deviation optimal balancing of the stabilizer, elevator, and the alignment deviation on the mechanization of the various phases of flight. Optimal alignment of the aircraft to reduce the loss of aerodynamic balancing quality, extremely close to the rear, the optimal combination of the angles of deflection of the elevator and stabilizer depends on the aerodynamic characteristics of the stabilizer and flight parameters. Algorithms for parameter optimization of aerodynamic configurations are designed for use in the optimal configuration automatic control system (*OC ACS*).

The power plantparameters optimization is reduced to the determination of these parameters to minimize the unit cost of jet fuel for that flight mode. Algorithms for optimization of these parameters are intended for use in the *power plant parameters optimization* (*PPPO*).

References

1. Закон «Модельный закон о безопасности на воздушном транспорте», от 31.10.2007, №997_14. Принят на XXIX пленарном заседании Межпарламентской Ассамблеи государств-участников СНГ, Постановление от 31.10.2007г., №29-10.

2. КОНЦЕПЦИЯ РАЗВИТИЯ ГРАЖДАНСКОЙ АВИАЦИОННОЙ ДЕЯТЕЛЬНОСТИ В УКРАИНЕ. Ідентифікаційний код 25778099, Зареєстровано від 9.12.1999 р. № 0260-99 Г.О.Управлінням юстиції в м.Києві Мінюста України.

3. Global Aviation Safety Roadmap. A strategic action plan for future aviation safety developed jointly by ACI, Airbus, Boeing, CANSO, FSF, IATA and IFALPA for ICAO. December, 2006, -16 p.

4. Глобальный план обеспечения безопасности полетов. ICAO, June, 2007, -25 p.

5. *Андриевский Б.Р., Фрадков А.Л.* Современные направления синтеза систем управления ЛА. –СтП.: Институт проблем машиноведения РАН. 2004, -24 с.

6. *Бахиркин М.В., Орлов В.С.* Распределенная модель динамической воздушной обстановки. Работа вып. при фин. поддержке РФФИ (проект 08-08-00370-а). –М.: РФИИ, 2008, -5 с.

7. *Суслов В.Д., Козис Д.В.* Моделирование траектории полета в навигационных комплексах ЛА в горизонтальной плоскости. –СтП.: Научно-технический вестник Санкт-Петербургского государственного университета информационных технологий, механики и оптики, №3(67). 2010, с. 71-77.

UDC 681.51:629.735.051-514(045)

V.I. Kashmatov, Ph D
(National Aviation University, Ukraine)

RESULTS AND PROSPECTS OF AIRCRAFT MANUAL CONTROL SYSTEMS DEVELOPMENT

The main cause of piloting mistakes due to the overload of pilots vision and attention during the aircraft piloting because of simultaneous solving parallel tasks is stated in this report.
The method of unloading of the pilots vision and attention at the cost of internal kinesthetic contour of human control which is included into the process of aircraft piloting is proposed in this report.

Introduction, analysis of the causes of mistakes piloting. It has passed 100 years since the start of aviation development. During this time, much has changed airframe and its engines appeared and improved automatic control systems and only manual systems and controls have not changed fundamentally. During all this time it has never been questioned the correctness of the original principles of manual controls that have arisen with the advent of the airplane.

However, with increasing of number and complexity of problems solved at the same time by pilot, a problem of rational use of options of the pilot for solving whole complex of tasks. This problem is particularly important for designers of aircraft traffic control systems, as for traffic control for a long time is necessary vision and attention of the pilot, who are diverted to solution of other equally important, performed at the same time, problems.

Test pilots give "good" to manual control systems of aircraft. Designers refer to the pilots, saying, "pilots like the manual control'

However, accidents caused by aircraft crew say otherwise. If the pilots who are controlling the motion of the aircraft die together with passengers, it means that, in fact, they do not like the control system of aircraft.

Accident of aircraft TU-154 in Norilsk shows inconsistency of manual control of angular position and automatic control of the speed of flight [1].

Accident in Irkutsk shows inconsistency of automatic control of angular movement and of manual control of flight speed [2].

Rough landing of IL-86 in Simferopol, TU-154 in Tashkent, Borispol, Sochi shows the difficulty of simultaneous control of the angular position and speed of flight [3].

Death of the commander of plane TU-134 in flight to Vnukovo is evidence of intensive health expenditure of the central nervous system of pilot in the aircraft manual control [4].

The reason for the difficulties of manual control is in reluctance to manual control systems designers to understand the human operator. Due to insufficient knowledge about human operator, he is a "black box".

Medics, with rare exceptions, do not know the equipment and are concentrated in rejection of pilots. Training of pilots is expensive and early removal of the pilots from flight-is an unacceptable luxury.

Ergonomics is trying to solve the "Machine-Man" problem. However, the introduction of the results of this science is prevented by the inertia of thinking of designers, developed over the past hundred years.

Passengers and line pilots are interested in implementing of the results of this science, as they both die in accidents.

However, passengers do not know what can be done to improve flight safety and trust in the designers, naively believing that the designers are doing their best to improve the safety of flight.

Line Pilots rely on the test pilots, that they sort out a plane crash and corrected mistakes of designers.

Designers don't give to test pilots knowledge about achievements in ergonomics, following the line of least cost for the development of control systems and reproduction of the old principles of the new aircraft manual control.

They took vision and attention of the pilot mainly to control of the angular position and speed of flight, and at the same time adding more and more control and monitoring functions in other systems.

Overload of vision and attention of pilot by functions of the simultaneous control and monitoring of multiple systems is a major cause of mistakes of pilot.

Designers do not want to solve the problem of unloading of vision and attention of pilot by improving the design of control systems, allowing more efficient use of the sense organs and central nervous system of pilot, but moving towards increased use of vision and attention, demanding to improve selection, training pilots, and increase the responsibility for piloting mistakes.

However, they can not overcome the natural limitations of man, using unnatural manual control.

The man in the process phylogenesis and ontogenesis (development of humanity and specific individual) has developed a central nervous system, for which the proposed distribution of the control function tools of labor between the sense organs and brain structures is an unnatural and unhealthy.

With unnatural (professional) control skills high quality control in difficult situations can not be achieved.

Presentation of the basic materials of research

Human capabilities depend on the dynamics of the object and method of its inclusion in the control loops of man. Internal and external control loops are distinguished in humans [5]. Internal is used for direct control of objects in his hand, information about them is perceived by kinesthesia, external - for remote control of objects, information about which can be perceived by external senses (vision, hearing ect).

The low level of development of science and technology when aircraft has appeared and ease of inclusion in the outer contour of the aircraft has led to the fact that the issue of inclusion into the inner contour of the aircraft was not placed then and ever since the inclusion of the outer contour of the aircraft was considered the only possible one.

Casual aircraft manual control systems use kinetic control device with visual indication device.

Main disadvantage of visual-kinetic systems is in that the pilot needs vision for all control systems, so he needs to overload and dissipate it.

If the attention of pilot is concentrated on one system, the control in other systems is absent or there is mistake control. Designers try to change pilots with automatics, or to divide its functions between crew due to overload of pilots visual organs. That's why problems of coordination between pilot and automatics and crew arise. These problems are usually more difficult to solve than problems connected with pilots interaction with controls.

The other way of solution of problem of pilots interaction with aircraft is to use invention "Console, system, method of control and stabilization of regulated value of motion of aircraft" [6].

There is not only external visual single-channel, but also internal multi-channel kinesthetic contour, which unloads vision and attention of human during control of objects with different dynamics which are in his hand.

It is needed to create objective model of aircraft's dynamics using the aircraft itself, to take it in hands and to control the objective model, for inclusion of aircraft into internal control contour. In this case the method of external control is called quasiobjective.

Objective model of aircraft dynamics is kinesthetic console in which control element and indicating element of regulated value are combined in a single device.

For this it is necessary to create kinesthetic indicator which can translate information to the hand of operator. This can be done by taking into the hand the pointer of kinesthetic indicator of angular position or speed and to use kinesthetic indicator as the control element in the same time.

Usually external indicators are created as servo systems. Servo system can be used as control element if force will be applied to control column rigidly connected to output shaft of the actuating motor of servo system. Force from servo system must be translated to actuating device of manual system. Deflection of control column under the action of pilot's force can be done negligibly small for eye, but sufficient to cause aircraft motion. Control column must be unmoved until start of motion. Then servo system causes lever to move in the same way as pilot under the action of signal from sensor of regulated value of object and as a result aircraft moves synchronously with pilot.

If disturbances act on the aircraft, than it tends to change its position in space and position of control column.

Pilot in his turn tries to save position of his hand and will counter to control columns deviation and will create signal in servo system of kinesthetic pointer and through actuating device of manual system will counter disturbances.

Simultaneous control of pitch angle and speed of flight was modeled in experiment done in NAU. During simultaneous control aircraft nose-downing causes increase of speed. If pilot moves lever outwards, making aircraft to nose-down, than speed control column tries to move forward showing increase of speed. Pilot holding control column of kinesthetic speed indicator through actuating mechanism of thrust automaton remotely moves engine control column to the side of speed decrease. As a result of pilots interaction with two control columns control and stabilization of pitch angle is done. Pilot uses his vision mainly for discrete control of correctness of change of pitch angle and absence of change of speed. Continuous pitch angle control and stabilization of speed is performed by internal kinesthetic contour without vision of pilot, using only objective control skills.

All people have skills to control objects with dynamics similar to dynamics of aircraft so process of control of speed and pitch angle don't need special training.

Initial training needed for both types of control lies in prescribing direction of applied forces and corresponding to them motion of pointers. In manual mode it is needed to make additional control law: needed deviation of lever in dependence on needed deviation of pointer.

In quasiobjective method the control law pilot makes himself commanding to deviate pitch lever from initial position to needed one and speed control column to hold in its position.

Conclusions

1. Unload of vision and attention of pilot with the help of kinesthesia allow to increase quality of control of parallel tasks solved by pilot, to improve pilots physical state, and to increase flying age of pilot.

2. Usage of pilot's objective skills for control of aircraft will decrease training time of pilots and will assist in aircrafts transformation into a personal vehicle.

3. Quasiobjective aircraft motion control system opens new direction of automatization. It is suggested to include internal contour of human with the help of kinesthetic console instead of change of human operator by machine. Main task of machine is not in replacement of human but in full-scale modeling of aircrafts dynamics.

Prospects of further research of quasiobjective aircraft motion control.

Perspectives of further researches in this case depend on cooperation of Secretariat of ICAO and usage of quasiobjective control in practice of designers of aircraft motion control systems.

Author of report expects for cooperation of ICAO Secretariat to this usage of quasiobjective control mentioning ICAO official documentation which descripts dependence of flight safety from human factor and the ways of safety increase. In foreword to ICAO document №217-AN/132 in statement 1 is told:"nearly three fourth of accidents are caused by non optimal human actions and this shows that every achievement in this sphere will help to increase the level of flight safety";

In statement 6 of this document it is told “ICAO Secretariat will tend to help countries by requesting additional information about present materials from different sources about researches made in countries and help from different organizations and private persons.”

In document ICAO № 277-AN/163 during quoting of speech of president of ICAO dr. Assas Kotayt on opening of fourth international ICAO symposium about flight safety and human factor the main way for improving of safety is shown.

1. “Remember human can not do more than system in which he works can allow; ways for understanding of human factors in sphere of flight safety will depend in large measure on you.”

2.”My proposition is rather easy: human abilities must be taken into a count on the stage of designing of our systems, before they will be used.”

Reference

1. *Кашматов В. И.* Эргономический анализ катастрофы самолета Ту-154 Б-2 в аэропорту «Норильск». Сб. обзорной информации «Проблемы безопасности полетов». М.: ВИНИТИ. 1999. – Вып. 6 – С. 3 – 8.
2. *Кашматов В. И.* Эргономический анализ причин ошибок техники пилотирования экипажа самолета Ту-154 М при катастрофе в районе аэропорта «Иркутск» 3.07.2001 г. Сб. материалов IV Международной научно-технической конференции «Авиа-2002» 23-25 апреля Т.II – 2002 г. – С. 59 – 61.
3. *Кашматов В. И.* Эргономический анализ ошибочных действий пилота при грубой посадке / Промежуточный отчет о НИР № 536-В86. Определение и специфика общих факторных нагрузок и анализ ошибочных действий с целью проведения антистрессовой подготовки летного и диспетчерского состава в свете директив министерства ГА №11, 12 – 1986. – 10 с.
4. *Кашматов В. И.* Эргономический анализ инцидента с самолетом Ту-134А UR 65135 ОАО авиакомпании «Авиалинии Украины». Материалы I научно-методической конференции «Безопасность жизни и деятельности человека – образование, наука, практика». К., НАУ. 2002. – С. 137–139.
5. *Чхаидзе Л. В.* Координация произвольных движений человека в условиях космического полета. Изд-во «Наука». М.: – 1965. – 134 с.
6. *Кашматов В. И.* Описание к патенту на изобретение № 2128600 РФ МКИ В 64С «Пульт, система способ управления и стабилизации регулируемой величины движения летательного аппарата». заявитель и патентообладатель В. И. Кашматов заявл. 15.08.95; опубл. 10.04.99. Бюл. 10 Москва. №10.

UDC 629. 735.05: 621.38 (045)

Kozlov A.P., PhD
(National Aviation University, Ukraine.)

ONBOARD DENSITY METER OF JET FUEL

Necessity of measuring the density of jet fuel is considered. A brief review of current density meters is given. It is proposed a device for measuring the density of jet fuel, built on the hydrostatic principle. Differentional manometer with capacitive sensor of micromovings is proposed for apply. That device takes ability to design a equipment with placement on the outside of the fuel tank

Today state of avionic, the introduction of computer technology in the aviation equipment, as well as increased demands on the efficiency of aviation equipment require improvement the quality of the most important parameters of the aircraft systems. This, in turn, refers to the fuel gauging system (TGS).

A brief analysis of operating experience TGS shows, that the level of reliability, measurement errors, maintenance costs need to be further improved. At the present time to measure the amount of fuel on board the aircraft are generally used technical means, based on measuring the level of fuel in the tanks. To determine the amount of mass (stock) fuel is necessary to have information about the density of the fuel tank, as the massive amount of fuel calculated in terms of fuel, measured in each tank, and fuel density. On the majority of aircraft fuel density is not measured, the assumed value of the known density of a particular type of fuel (T-1, TS-1, T-6, etc.) is entered manually on the remote control flight engineer [1].

The dependence of the volume of fuel from its level in the tank is nonlinear. This is due to variable cross-section area of the tank. Removal of non-linearity in capacitive fuel level profiling is achieved by capacitive level sensors. With the introduction of digital technology in the equipment of modern aircraft is the use of digital processing of initial information

The firm "Honeywell" has developed a modern digital system measuring the amount of fuel (FQIS), which is currently used on the Boeing 767. Measuring the amount of fuel is performed capacitive fuel level, which uses vertically oriented cylindrical capacitive sensors. One of the significant advantages of the system is FQIS introduction to the device measuring the density of jet fuel. This allows the system to be tolerant to changes in fuel composition without compromising accuracy. FQIS system also has the ability to withstand high levels of accuracy for fuel contamination. Massive amount of fuel in the system FQIS calculated in terms of fuel, measured in each tank, and the density of the fuel in the tank is measured by the densitometer. Designed system based on digital data processing techniques. The system has a dual-channel digital data processing in the CPU, digital display (indicator) of fuel on the dashboard, the continuous measurement of the density of fuel in each tank, both in flight and on ground.

Operating the system FQIS shows a significant advantage of the digital system of measuring the amount of fuel, which has in its onboard aircraft fuel density meter. Obviously, there is need for the development and implementation of such systems in new types of domestic aircraft and the upgrading of existing measuring systems of jet fuel.

The use of densitometers in the TGS will provide information about the mass amount of jet fuel on the board of aircraft. On the recommendations of ICAO new equipment must have a minimum investment of time and funds for its maintenance during operation. As one of the ways to achieve this requirement, a recommendation is to develop equipment with placement on the outside of the fuel tank

Thus, it is necessary to choose the principle of the action densitometer and to develop design densitometer for placement on the outside of the fuel tank

Analysis of the existing meters of liquid density shows the following. By the method of measuring the density of liquid density meters are divided into the following groups: float, weight, hydrostatic, radioisotope, vibration and ultrasound.

Float and weight densitometers can be used only on inanimate objects

Radioisotope densitometer (Boeing-767) uses the principle of attenuation of gamma particles emitted by a source of low-intensive (an isotope of Americium 241), the weakening of the radiation intensity is a function of the density of the material during the passage of particles through it. The number of gamma particles that reach each of the two detector tube densitometer, the processor is calculated (Fig. 1).. Passage of particles through a range of different distances in the fuel to each tube detector, allows us to calculate the density of the relative numbers of particles that reach each tube. This radiometric approach using a dual detector simplifies design and improves the accuracy of the densitometer measurement of density by excluding such factors as: the initial intensity of the radiation source, the fall of the intensity of the radiation source, the voltage supply tube detector, the effect of temperature on the tube detector and electronics

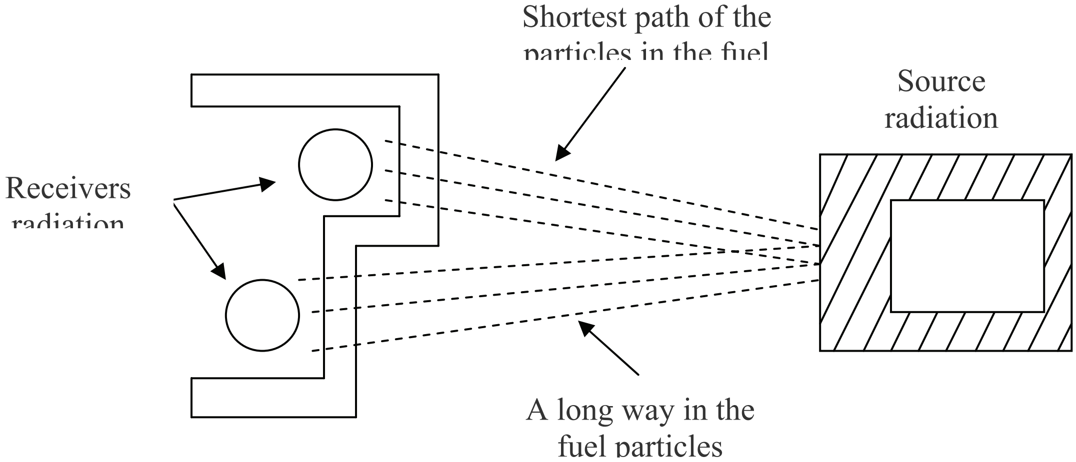

Fig. 1. The principle of the radiometric density meter

Density depends on the type and temperature of the fuel. Temperature dependence of the density of the fuel is defined as

$$\rho = \rho_0 (1 - \beta T),$$

where ρ_0 - the fuel density at 20°C, β - temperature coefficient of the fuel, T - temperature of the fuel °C. To eliminate the methodical error, which associated from the change of fuel and the ambient temperature, the measurement of fuel supply in terms of mass, is necessary to apply different methods that take into account these factors. Radiometric density meter can not be applied to solve that problem. Its application requires placement on the inside of the fuel tank (innertank placement).

The operating principle of an ultrasonic densitometer based on the dependence of sound speed ***c*** in a medium from a density of its: $c = \frac{1}{\sqrt{\beta\rho}}$

where β - coefficient of adiabatic compressibility

However, ultrasound densitometer also applies to the innertank equipment

Vibration densitometer of fluid. Vibration densitometer is a hollow cylinder, which is located between the electromagnetic induction coil and sensor of the cylinder deformation. The signal of the inductive sensor to the input of the amplifier. The output of the amplifier is fed to the electromagnetic coil. The chain of "coil - cylinder - sensor" is a positive-feedback amplifier, which are excited by own (resonant) oscillations of the cylinder. The resonant frequency of vibration of the cylinder in a substance depends on the density of matter, is less than the frequency, the greater the density of a controlled substance.

Vibration measuring the density of liquids ВИП 2МР - budget alternative to the densitometer foreign manufacturers. His work is also based on the measurement of the oscillation period of the original configuration of a hollow tube filled with test liquid, and then calculating the value of its density using the results of the preliminary calibration of the two substances of known density, such as air and water. In the apparatus is automatic conversion of the results obtained in the density associated with the performance. The vibrating densitometer can be placed outside the tank.

The *hydrostatic densitometer* is proposed to apply. Linear dependence of the pressure of the liquid column a fixed size from the density of the controlled fluid is used in the hydrostatic densitometer. The pressure of the liquid column is measured directly, such as a membrane manometer, or indirectly - by blowing air through the fluid whose pressure is proportional to the column of liquid. For elimination the effect of variations in temperature and level of the liquid is often used a differential method: measure the differential pressure by the differential manometer.

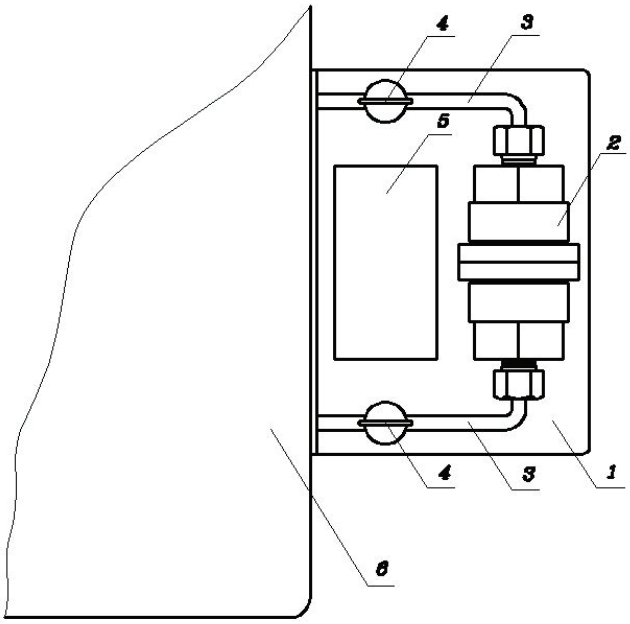

Fig. 2. The densitometer with outside the tank placement.
1 base, 2-difmanometer, 3-pipes, 4-crains, 5 electronic block, 6-tank

Review and analysis of patents and technical literature, and also other documentation, shows that the most suitable manometer is discussed in [2]. This design is used in the development of onboard density meter of jet fuel placed outside the tank (Fig. 2). Body of differential manometer 2 is placed on the base 1, which is located on the bottom of the tank 6. The hydrostatic pressure of the upper and lower levels enters into the upper and lower difmanometer units across pipes 3 with cranes 4. On the ground plane is placed electronic block

The operating principle of the difmanometer is based on a combination of the two manometric assemblies with a common mobile node. His movement is converted into an electrical signal by means of a differential capacitive sensor; the capacitance is measured by a transformer bridge

Significant features of the device:

- sensing element (SE) is a membrane unit, made an all-metal with the body, which eliminates errors and operational difficulties associated with the clamped (fixed) membrane, as well as increase the temperature stability of the device;
- desktop SE provides the deflection of not more than 0.1mm, which allows to obtain a sufficiently high linearity:

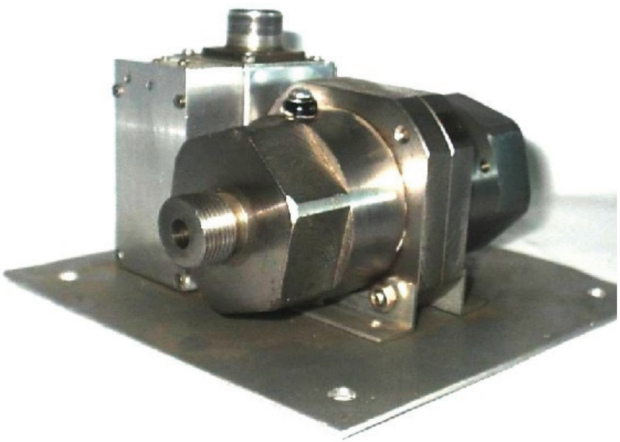
Fig. 3. The pilot device of difmanometer/

- the device used electrical power capacity differential converter with one-sided readout of useful information, thus avoiding the complexities of providing meaningful contact with the movable part of the sensor;
- use of a transformer bridge can dramatically reduce the measurement error

For the execution experimental researches was make a pilot device (Fig. 3)

As shown by experimental studies, the amount of information capacity differential pressure transducer is small enough and equal $10^{-3}...10^{-4}$*pF*. To obtain sufficient accuracy of such measurements need to apply a measuring device with a sensitivity of better than 6^{-10} *pF*.

Review and analysis of measurement devices [3, 4, 5] shows, that transformer measuring bridges are most appropriated.

The main features of such bridge measuring circuits are high stability, good resistance to the influence of external electromagnetic interference and internal stray electric and magnetic connections, a wide frequency range, and exceptional flexibility, providing a variety of measurement modes and opportunities in addressing the diverse functional tasks.

Experimental studies have shown the very real attainability of such results. In order to improve the accuracy of that method of measuring the multi-filyar windings with close electromagnetic coupling are applied. That to ensure the error is not more than 0.001%. One of the main advantages of transforming the shoulder elements with close ties is exceptional stability of the shoulder under the influence of the parasitic conductance, which shunt these elements. A significant advantage of inductively coupled elements of the shoulder is also a high thermal and temporal stability of the relationship apart.

The densitometer circuit of jet fuel is designed, it is constructed on the basis of a transformer bridge the digital trim (Fig. 4). The scheme works as follows

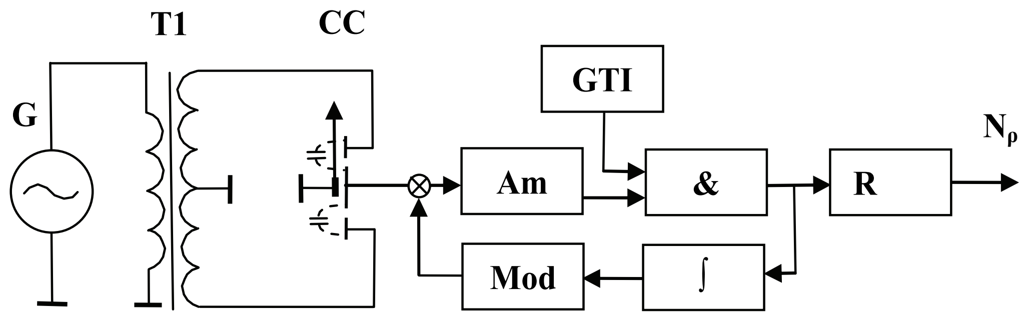

Fig. 4. Measuring circuit of densitometer with a digital balancing.

Supply voltage of the shoulder transformer T1 served with generator G. The shoulder antiphase voltage supplied to the high-potential electrodes of the capacitive converter CC. As discussed above, is used densitometer with capacity differential converter which have one-sided readout of information. Grounded movable part of the sensor is moved, when the difference of pressures is appeared, after it the capacitance between the electrodes of low-grade and high-potential CC is changing. The signal from the low-potential electrode go to the input of the preamplifier with a high impedance input Am. Generator of time impulses GTI sends a signal to one input of logical element AND-NO(**&**). The signal from the amplifier output of Am gives permission for the passage of impulses GTI to the counter R. The value of the digital code N_ρ gradually increases. The impulse signal go to the input of the integrator ∫, with the increasing output of the integrator signal is fed to the modulator Mod. The reference voltage to the modulator is fed to the generator G with separate windings (in the Fig.4 is not shown). The signal of the modulator is fed to the input of the amplifier out of phase with the signal of unbalance of the bridge. Upon reaching the equality signal output will be equal to zero. The logical element AND-NO close pulsing with the GTI. The resulting value $N\rho$ code carries information about the measured value of density.

Conclusions

The construction of the proposed densitometer with placement on the outside of the fuel tank will significantly reduce maintenance costs. The construction of the difmanometer, which is part of the hydrostatic densitometer, provides the required accuracy. The efficiency of the device is tested experimentally. The developed measuring circuit is easy to implement existing components that will lead to the production process of manufacturing of densitometers. The accuracy of measurements that can be achieved by measuring the proposed scheme makes it possible to carry out continuous quality control of aviation fuel during refueling and during the flight. The measured values of the density of jet fuel are given an electric signal in digital form (binary code) that allows the software to process the information on the digital computer

References

1. Справочник авиационного инженера. М., Транспорт. 1978. – 400 с.

2. Козлов А. П., *Хаданович В. О.* Об'ємометрична паливовимірювальна система повітряного корабля. Електроніка та системи управління. – 2010. – Вип. 4.

3. *Трансформаторные* измерительные мосты. Под общ. ред. чл. - корр. АН СССР К. Б. Карандеева. – М.: Энергия, 1970. – 280 с. *Гриневич Ф.Б., Новик А.И.* Измерительные компенсационно-мостовые устройства с ёмкостными датчиками. – К.: Наукова думка, 1987. – 112 с.

4. *Бугров А.В.* Высокочастотные емкостные преобразователи и приборы контроля качества. М.,Машиностроение. 1982, 96 с.

UDC 629.735.33-519(045)

N.F. Tupitsin, Ph.D, O.S. Yurchenko, Ph.D (National Aviation University, Ukraine)

PECULIARITIES OF GAS-DYNAMIC METHOD OF TAKEOFF AND LANDING UAV

The peculiarities of gas-dynamic method take-off and landing an aircraft by using an artificial air flow were considered. The transient characteristics speed of horizontal and vertical air flows, which realized in gas-dynamic device takeoff and landing were obtained.

Introduction The One of the major tasks, which arise at the development of new aircraft, decrease of runway length.

The takeoff aircraft are defined as process of its transition from a stationary state relative to the earth in a state of flight. The landing aircraft (or UAV) can be defined as a process inverse for takeoff.

Most of the currently used methods of takeoff and landing have been proposed and investigated in the first decades of the XX century to the early days of development aviation [1-2].

From the large list of ways takeoff and landing with a truncated runway in this paper we consider two only: 1) inhibition of the aircraft by propeller engine [1], 2) takeoff (landing) by the wind [2] or counter artificial air flow (CAAF) [3].

First method is most commonly used for heavy transport aircrafts. In the case braking during landing with help by propeller of engine are two possible ways to solve the problem: changing the direction of rotation of the screw on the inverse, a permutation of the propeller blades on a negative angle of attack.

It should be noted that, for example, the engine D-18 (JSC "Motor Sich"), which is installed on transport aircrafts An-124 "Ruslan" and AN-225 "Mriya", is equipped a device with effective back draft. This device is established in the circuit the fan.

For the light aircrafts the reverse thrust (or braking by propeller engine aircraft), as a rule does not apply. A more rational way of deceleration of these aircraft is to create CAAF.

The essence of this method of takeoff and landing aircraft's is that with the help of two - the main and additional installations of gas-dynamic (IGD)create perpendicular to each other a two artificial air flow [5]. With help these air flows it's possible to decelerate UAV and then to land it. at the takeoff, one of the air flows lift UAV from the beginning , and then the second one keep it while it's accelerating. At the same time direction of horizontal air flow varies in dependence on mode of flight: landing or takeoff.

Statement task Calculations show that a headwind (or CAAF) is an effective and universal means of braking the aircraft [3,4]. The disadvantages of this method are the need for a brake the entire profile UAV with CAAF, which causes great difficulties for the aircraft with the wings of high aspect ratio. For the practical implementation of the method takeoff and landing with the CAAF must solve several issues, namely: 1) Choose the type of UAV; 2. Choose the type of gas-dynamic system (fan system); 3) calculate the required parameters of the selected system for takeoff and landing UAV; 4) develop an automatic control system of gas-dynamic installation.

Ways of task solving. For effective use of the IGD (of fan) and for creating a CAAF in the front of UAV with the greater speed than the speed near IGD, it is advisable to apply the confuser, which converts a circular shape of CAAF 1, for example, into an elliptical 2 (Fig. 1). If using UAVs with wings of high aspect ratio it is required to use a diffuser (Fig. 2), but the speed of CAAF in the front of UAV will be less than the speed near IGD. The form of the vertical stabilizer and the wing of UAV significantly affect the efficiency of application of considered gas-dynamic method. For example, this method is more efficient for the aircraft type biplane.

И-153 (front view (see Fig. 1)) with the wings of small aspect ratio 3, it is due to the effect of increasing the speed of CAAF past confuser in comparison with the aircraft Аккорд-201 (front view (see Fig. 2)) with the wings of high aspect ratio.

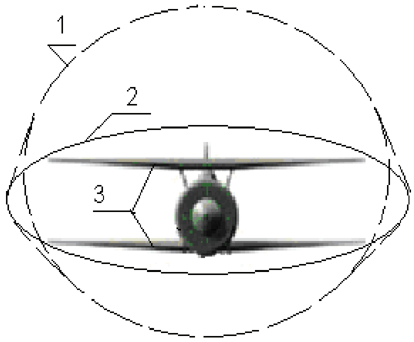

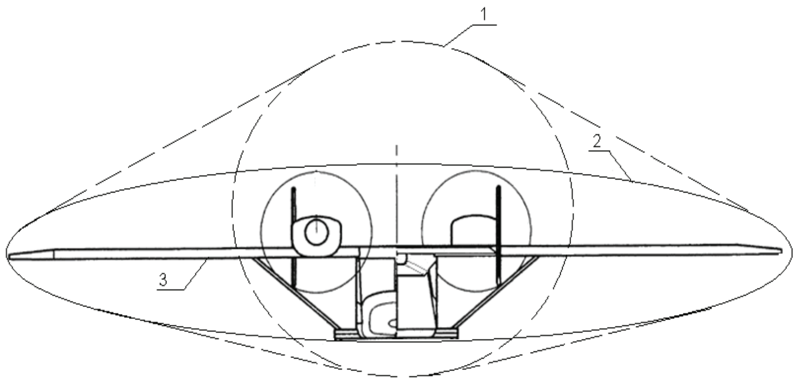

Fig.1 Fig.2

Not hard to compute that the speed of CAAF in the front of UAV will be approximately two times higher than it near IGD.

As noted earlier, the main functional elements of the device that implements theconsidered method are two IGD. Due to the ease of maintenance and the ability to create a uniform CAAF as a IGD are chosen the ventilators. From analyze different types of IGD and from comparison their sizes with the size of the UAV as the primary and additional IGD were selected the fans B0-6-300-8.

Block diagram of the automatic control system IGD is shown on fig. 3.

This scheme operates in the following way: in the control unit of IGD are set the parameters given UAV and height of lifting, also this unit receives information about the current height of UAV from position sensor. This unit forms the control signal on IGD 1 and IGD 2.

Iinstallation of gas-dynamic 2createsartificialair flowwhichraises theUAVat defined height.In the control unit IGD receives information on the height and compares with given height. Iinstallation of gas-dynamic 1runsparallel to the IGD 2.Intime,when theUAVreaches thedefinedheight ($H = H_d$), the speed of horizontalair flow$V_{hf}$is equal to speed of takeoff ofUAV $V_{takeoff}$.

Example for calculating the characteristics ofACS IGD Simulation ofautomaticcontrol systemof gas-dynamicunit for verticalchannel was implementedinMatLabenvironmentandis shown onFig. 4.

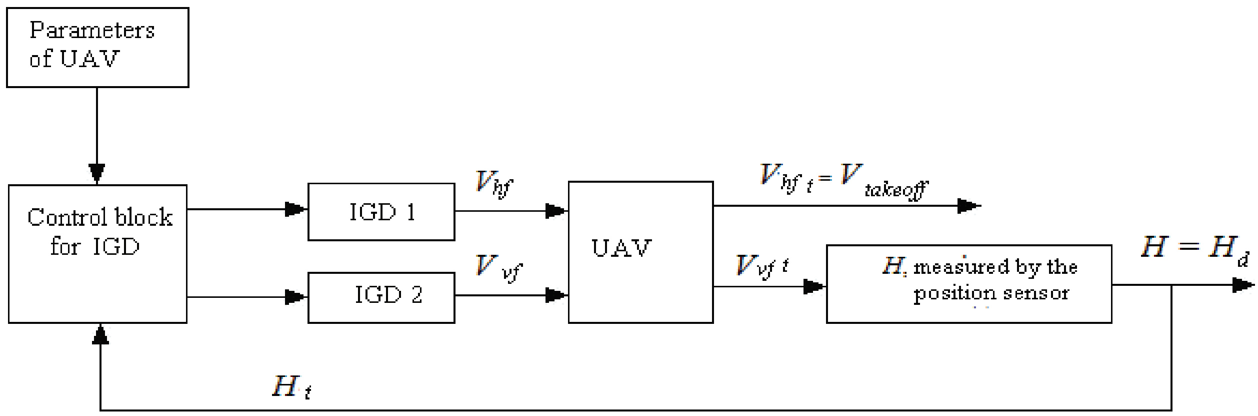

Fig. 3

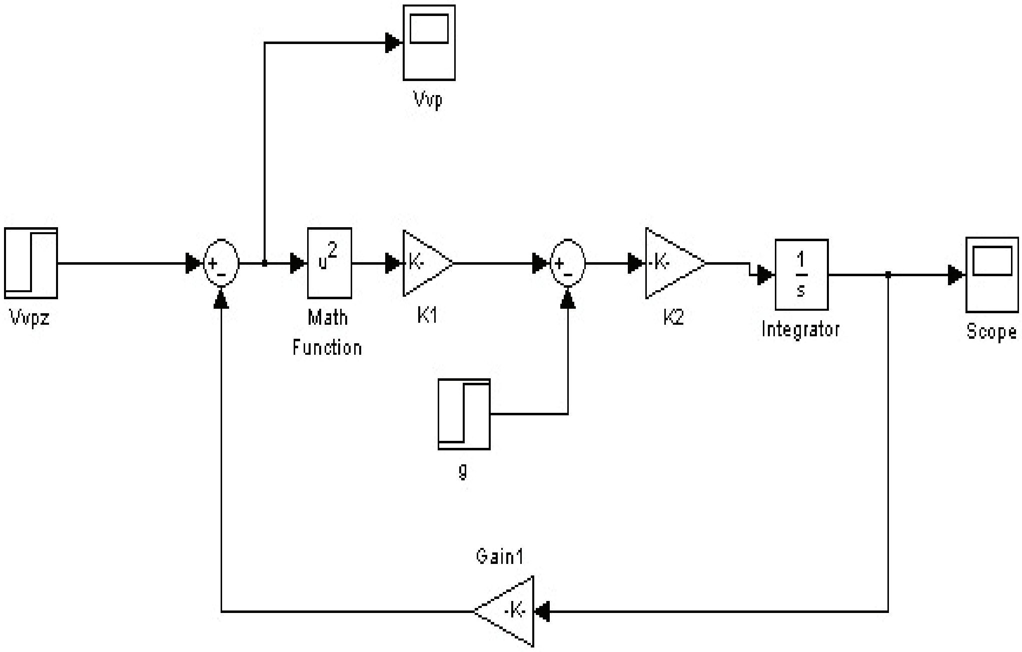

Fig.4

As a result of simulation were obtained the following transient response: 1) the speed of vertical air flow (fig. 5), 2) graph of transient characteristic of height lifting UAV's (fig. 6).

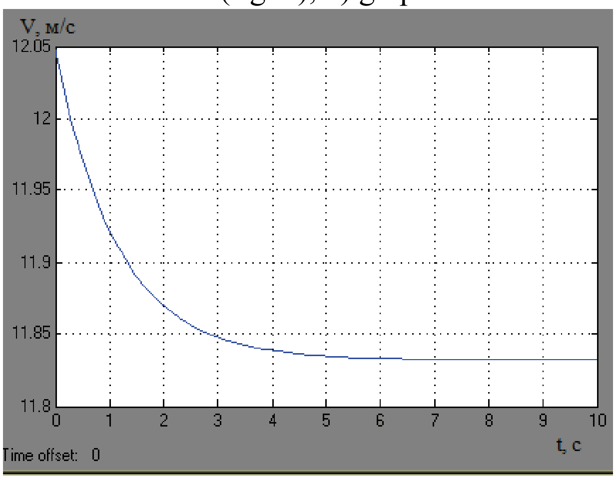

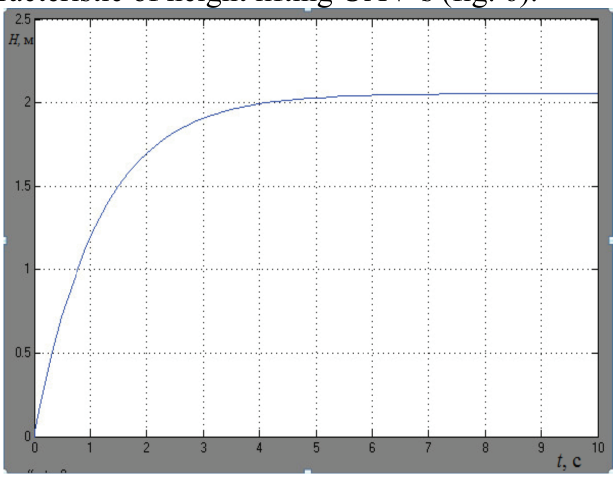

Fig.5

Fig.6

Simulation of automatic control system of gas-dynamic unit for horizontal channel was implemented in MatLab environment and is shown on Fig.7

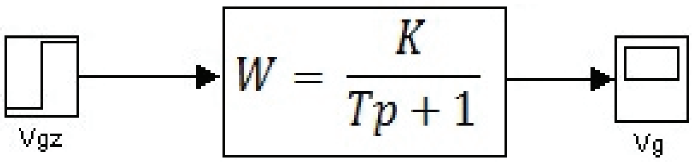

Fig.7

As a result, it was obtained graph of modeling of the transient characteristic of speed of the horizontal air flow (fig. 8).

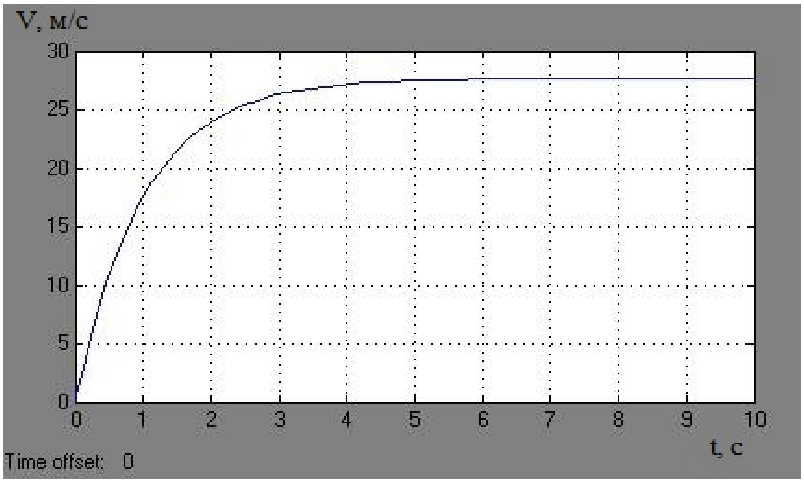

Fig.8

Conclusion

It was simulated automatic control system for IGD during takeoff of UAV from ground landing gear, which implements the gas-dynamic method of takeoff and landing . It was obtained the transient characteristics of speeds of horizontal and vertical air flows.

A calculation of the lifting height of UAV was made also.

References

1. *А. фон дер Мюль* Торможение винтом при посадке/ Взлет и посадка. Сборник переводов под общей ред. В.Л. Александрова. М.: Изд. БНТ, 1946. С. 92-96.

2. *Г. Винтер, В. Мейер*Длина пробега самолета с торможением и без торможения при встречном ветре/ Взлет и посадка. Сборник переводов под общей ред. В.Л. Александрова. М.: Изд. БНТ, 1946. С. 69-75.

3. *Тупицин Н. Ф., Тупіцина Н.М.* Спосіб посадки літального апарата патент Пат. №52597 Україна, МКИ B64C 25/00. – № и201005783; Заявл. 12.05.2010;Опубл. 25.08.2010, Бюл. №16. – 10 с.

4. *Тупицин Н. Ф., Тупіцина Н.М.* Пристрій посадки літального апарата. Патент №52596 Україна, МКИ B64C 25/00. – № и201005781; Заявл. 12.05.2010; Опубл. 25.08.2010, Бюл. №16. – 8 с.

5. *Тупицин Н. Ф., Дмитриенко Б.І., Степаненко І.О.* Етапи функціонування газодинамічного злітно-посадкового пристрою та літального апарата// Електроніка та системи управління. – 2012. – №1(31). – С. 10–14.

UDC 689.3.19/16

V.M. Sineglasov, Ph.D., Professor, O.S. Yurchenko, Ph.D., N.F.Tupitsin, Ph.D.
(National Aviation University, Ukraine)

EVALUATION OF SYSTEMCOSTFORDYNAMICSEGMENT ALLOCATION OFMEMORY

The estimates of system overhead are given for the dynamic allocation of segment memory.

Statement of problem In Denning's works [1-2] the general estimation and classification of the fragmentation arising at realization of virtual memory are given. The concept "fragmentation" means a presence of unused portions in memory which cannot be used. According to [1-2] there are an external, internal and tabulated fragmentation. If not used spaces arise between blocks of memory, the external fragmentation takes place. Formation of "holes" inside of blocks testifies to an internal fragmentation. At page virtual memory (i.e. the fixed length of blocks) the external fragmentation does not happen, as each removed page is replaced another, the same size, and backlashes between them are not formed.

However the internal fragmentation can take place: there is it because the size of demanded memory is approximated in greater party to an integer of pages.

In computing systems with virtual memory and segment distribution all free memory is allocated in the form of set of the free segments scattered between occupied segments as their employment and clearing occurs in the casual manner(fig1). D.Knut [3] has proved a rule « fifty percent » which establishes a parity between number occupied and number of free segments. According to this rule if the system of memory aspires to a condition of balance at which in system is available on the average N the occupied segments the average quantity of free segments equally approximately.

The degree of an external fragmentation at segment distribution is defined as the total size of free segments. The external fragmentation takes place in case

$$S \rangle \max\{x_i\},$$

$$\sum_{i=1}^{m} x_i \rangle S,$$

where S - the needed size of memory, and $\{x_i\}$ ($i = 1, 2, \ldots, m \approx \frac{N}{2}$) – sequence of the sizes of free segments.

The table fragmentation is generated by that the part of physical cells of memory are allocated for the service information of system of dynamic allocation of memory (DAM) - tables of correspondence. Thus, these cells cannot be used for memory allocation.

The internal fragmentation according to [1-2] takes place only at page virtual memory. Actually this fragmentation is inherent also in virtual memory with segment system of DAM, in particular, because of difficulties accounting and allocation of segments of too small sizes.

Let's consider this case.

Let σ - a segment due to which occurs memory allocation for the next demand. The size of this segment should be equal specified in the demand or more it. Let a difference between the size σ and by size, specified in the requirement, it is equal Δl words anda relativelyhigh. Then a necessary part of a segment σ is allocated to the requirement, and the rest is made out as a new free segment in the size in Δl words. If youdo the samewhen Δl words is not enough words, there will be too small free segment. Such segment only "litters" system as, as a rule, cannot satisfy to any requirement.

System DAM would become more productive, having allocated the requirement all free segment. "Having offered" Δl words of memory, the system can not consider too fine free segments, that in turn, leads to reduction of time of search of a suitable segment in the list of free segments. This methodof neglectingthe smallfreesegmentsis observedalmosteverywhere in thesegmentDAMsystemsand serves as asource of internalfragmentation.

For differentiation of free segments on greater and small it is enteredthe boundaryvalue $\Delta l_{\min}$. Free segment of size $\Delta l \geq \Delta l_{\min}$ words It is made out as a new free segment, and at $\Delta l \langle \Delta l_{\min}$ system DAM allocates to the requirement whole free segment, not forming new**.** Thus, in system DAM maximal admissible internal fragmentation on each occupied segment and minimal size a free segment will be equal $\Delta l_{\min}$ words.

Estimating fragmentation with segment DAM, Denning gives only a rough estimate of the lower relative number of "lost" memory that is available for use by data or programs to the entire memory. The specified relation designated here through f_1, In Denning's estimation considers losses only on an external fragmentation.

Below estimation Denning is specified and also is given expressions for relative losses on internal and external fragmentations, influence of each of a component on operating ratio of memory and a parity intermeal is specified by them.

Conclusion of estimations of the fragmentation of memory If to designate through $K_{\min}$ the ration between the average size of the occupied segment S_0 (the law of distribution values the occupied segment and a rule of definition S_0 is assumed to be the same as in the3]) and the minimal size of a free segment, and through $K_{\max}$is the relation between S_0 and the maximal size of a free segment it is not difficult according to [1-2] to receive

$$\frac{K_{\max}}{2+K_{\max}} \geq f_1 \geq \frac{K_{\min}}{2+K_{\min}} \qquad (1)$$

In this inequality an estimation from below values f_1 is Denning's estimation.

If to neglect by value of table fragmentation in view of its insignificant share in total amount «lost» memories (unit of percent), relative losses on a full fragmentation $f_1 = f_e + f_i$, where $f_e = \frac{NK_{cp}S_0}{2M_0}$ – relative losses on an external fragmentation [1], $f_i = \frac{N\Delta l_{\min}}{2M_0}$ – relative losses on an internal fragmentation. Here$N$ – Number occupied segments, M_0 – size of distributed memory in words, and K_{cp} It is defined on the basis of a rule « fifty percent»:

$$M_0 = NS_0(1+\frac{K_{cp}}{2}) \qquad (2)$$

If to assume, that relative losses on internal a fragmentation should be less $f_2 \leq \gamma$ (γ< 1), and taking into account the expressions for f_e and f_i we have following formulas (fig. 2):

$$\begin{cases} f_e = \frac{NK_{cp}S_0}{2M_0}, \\ f_i = \frac{\Delta l_{\min} N}{2M_0}, \\ \Delta l_{\min} \langle \gamma \frac{2M_0}{N}, \end{cases} \qquad (3$$

where $N_{опт}$– some average of the occupied segments in memory, but $N_{\max}$ – number of the occupied segments if is not present free segments in memory.

Formulas (3) allow to estimate costs on internal a fragmentation depending on a degree of using of memory and more reasonably to approach to an estimation of quality memory allocation. From (3) it is visible, that at an overload of system (if N>N_{opt} – typical operating mode), internal fragmentation plays a significant role. Balanced systems DAM and planning multiprogram mix demand a choice of some optimum values $\Delta l_{\min}$ and$N$.

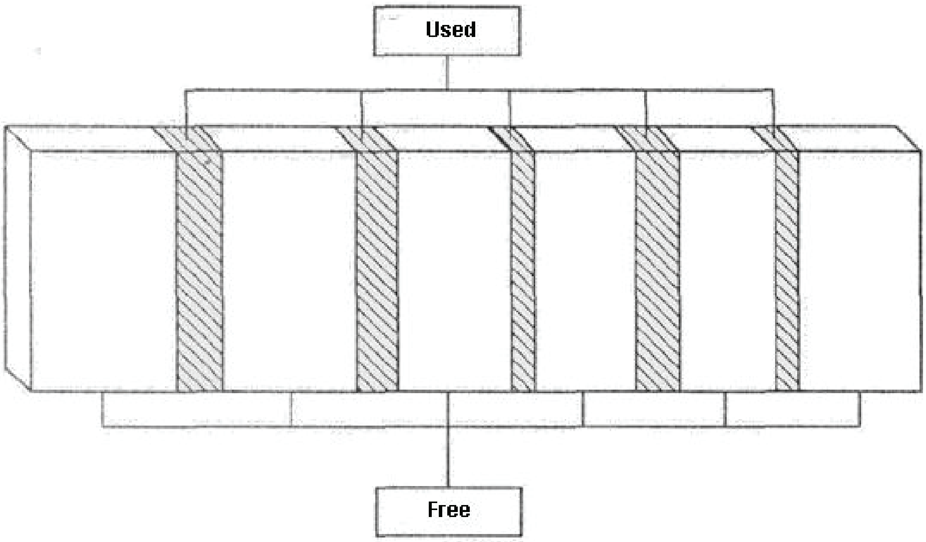

Fig. 1

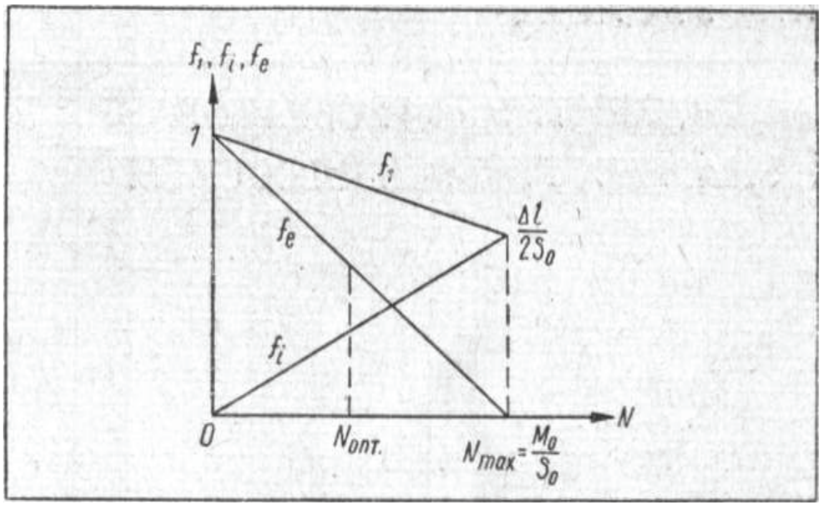

Fig. 2

References

1. *Denning P. J.* Origin of Virtual Machines and Other Virtualities // AHC, Vol. 23, № 3, 2001. P. 73.

2. *Denning P. J.* Virtual Memory. – Computing Serveys, 1970, v. 2. № 3

3. *Кнут Д.Е.* Искусство программирования. Том 1. Основные алгоритмы – М.: Вильмс, 2010 – 720с.

UDC 629.735.072.8.08:004.383.5(043.2)

Apenko N.V. teacher (KITZ NAU, Ukraine, Kyiv)

CLASSIFICATION SYSTEM MODELING IN VISUALIZATION OF CREATION AIRCRAFT SIMULATORS

In today's world of high technology is creating important visualization. Methods and ways of creating images in aircraft simulators, developing countries every year. Creating images that reflect most of the world - is key to realistic training pilots in emergency situations and skills with real equipment.

At present, a realistic simulator is an important milestone in the training of future pilots. Mathematical modeling allows you to create and implement clear and quality images including light and shadow elements. But in creating such elements important to consider and atmospheric phenomena such as rain, snow, fog, etc. In mathematical modeling should be considered such values as: volume, texture surfaces, which are modeled, light and shadow effects, etc.

Realization of these requirements will create a quality and reliable images and allow for future modeling exercise scene in real time with high image quality.

This line of research is an urgent task to develop mathematical models in visualization systems training complexes.

Mathematical modeling of the system visualization refers to the main chain in the creation of the simulator. The way will be calculated movement of the object in the scene depends on realistic images. In simplified form, process modeling pictures of objects divided into stages: signs of visible objects, modeling, texture surfaces, mathematical modeling of light effects on the falling objects, mathematical modeling of shadow effects for objects. We know many definitions of visible objects. Such as: a method of tracing, the method of direct routing - z-buffer algorithm, sorting by depth, methods of scanning range, etc.

Widespread nowadays software interfaces to the graphics hardware such as OpenGL and DirectX, the image used for the synthesis of a variety of direct tracing method using z-buffer. Existing graphical 3D-accelerators also working on direct tracing method and are designed to accelerate the operations mentioned APIs.

The advantages of z-buffer algorithm over other algorithms direct tracing - linear dependence of the number of comparisons in the z-buffer on the degree of detail of objects (ie the number of GP in the object).

Disadvantages:

- Calculation of proportional screening stage of GP. In practice, the only type of CP that can be displayed by this algorithm are polygons, leading to low feasibility (the lack of direct methods for tracing).
- Limited precision z-buffer leads to improper display of objects;
- Inaccuracy calculate the coordinates of z leads to poor connections polygons that share a common edge;
- A large burden on the GPU-channel memory due to repeated overwriting buffer frame and heavy use of Z-buffer;
- Distortion of the shape surface defined analytically, resulting triangulation;
- To reduce the effect of triangulation, ie to smooth the edges and very realistic synthesis of light within the triangle to perform interpolation, for example, Gouraud or Phong;
- Inability to calculate physically accurate shadows, reflection and refraction;
- Great difficulties arise in the synthesis of specific objects, such as fog, clouds, smoke, processing particles (dust, snow, rain, etc..), Especially change dynamically;
- Even more difficult is an interactive visualization of the bill.

Improving the quality of image that is synthesized, conducted by increasing the number of triangles. As a result of volume calculations for complex scenes increases considerably. This leads to the need to improve performance GPU in the synthesis of images of the same scene.

- These flaws deprived tracing method with an expanded set of graphic primitives.

It has the following features:

- Synthesis of potential surfaces, which are described analytically without prior their triangulation, which significantly reduces the requirements for the memory needed to store data;
- Comprehensive list of graphics primitives helps to construct objects of complex shape (earth and water terrain, clouds, etc.). As graphical primitives for reverse method can be used as a plane (polygons) and the surface of the second and higher orders;
- Simplifies the calculation and application of light texture, which reduces the requirement for performance evaluator at this stage;
- Removed one of the main problems of processing graphic information via direct routing. This lack of capacity bandwidth between memory and GPU, because when you turn off triangulation sharply reduced the volume of information transmitted is usually necessary to describe the large number of triangles.

Tracing gives much greater degree of realism. In contrast to the z-buffer algorithm, where the only type of GP is a polygon, in tracing algorithms can be used polygons [1], and curved surfaces [2], so approximate curved objects ranges (as is done by direct tracing) does not need. So, to tasks scenes of the same detail fewer data (for example, to store only the coordinates of the center of the sphere and its radius instead of storing the coordinates of all vertices of approximating polygon).

Other advantages of the method of tracing refers to the requirement for automatic angular resolution [3], paralleling opportunities in operations, the ability to accurately determine the direct lighting and shading of objects, specular reflection, refraction through a transparent medium, and others.

Disadvantages: Unlike algorithms that operate on the method of direct routing, the existing implementation of ray-tracing algorithms have low productivity, undeveloped mathematical models, algorithms and structures for GPU implementation of the method of tracing in real time. To reduce the memory required to raster and vector textures, apply algorithm packing, and unpacking at eliminating sanded. It allows physically reliably visualize the phenomena associated with scattering of light by particles, such as, for example, fog, atmospheric haze, dynamically changing clouds, smoke, different weather conditions. The same approach underlies bills visualization. Thus, all objects are synthesized uniform, computer works with all objects equally, whether the cloud, aircraft, surface, and so forth.

It should be noted that this approach can be applied to existing 3D polygonal data as triangles is also a special case of the enlarged set of graphic primitives.

Problem areas requiring further research are:

- synthesis scenes big spaces;
- account refraction of light in dynamically changing environments;
- visualization of gas-dynamic environments;
- interactive model of full illumination.

Classification methods for modeling image visualization system simulators can divided into the following categories [4]:

– without geometry
– with implicit geometry;
– with discrete geometry;
– with polygonal geometry.

These methods (Figure 3.1) should be considered rather as a continuous spectrum, the discrete set of methods.

On the right is the spectrum of traditional screen version with support for textured geometry. Indeed, texturing refers to methods of screen-based images. This approach is based on the exact geometry and a small number of images used to create textures.

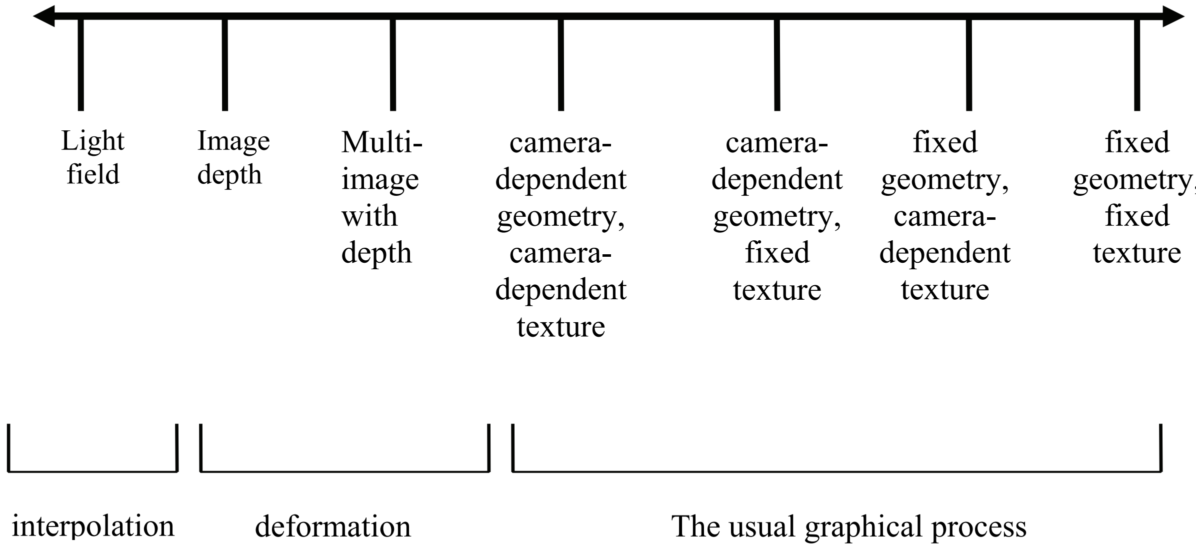

Then the spectrum located the methods used in discrete geometry notion: depth maps (maps of range) [5], multi-layered depth maps [6], multi-tree depth maps [7]. These methods use the principle of back projection for the synthesis of new images. Three-dimensional coordinates of each point of the original image is restored by the well-known depth (distance) and then projected to a new species plane.

Thus methods following categories do not require explicit geometric models. Instead, most require matching features (such as dots or lines) on the initial set of images. To generate such correspondences using computer vision technology.

1. *Бояковский Ю.М., Галактионов В.А.* Графические протоколы (обзор). - Автометрия.- 1978.- № 5.- С. 3-11.

2. *Белецкий А.Я., Павлов А.Б., Фомичев В.С, Ярмоленко А.М.* Принципы построения панорамной телевизионно-компьютерной системы визуализации внекабинной обстановки // Проблемы авионики: Сб. науч. тр. – К.: КМУГА, 1997. – С.3-7.

3. *Бобков В.А., Кислюк О.С., Хамидулин А.В.* Формирование растровых графических изображений пространственных объектов, построенных методом конструктивной геометрии // Программирование. – 1989. – № 3. – С.88-92.

4. *Бойко Е.И.* Время реакции человека. – М.: Изд-во "Медицина", 1964. – 440 с.

5. *Вавилова Н.И.* Модели и алгоритмы автоматизированного проектирования макетов сцен мультимедиа тренажеров. Диссертация на соиск. уч. ст. к.т.н. Тверь. 2002

6. *Винер Н.* Кибернетика, или управление и связь в животном и машине. – М., 1983.

7. *Власов С.В., Маслобоев Ю.В., Савенко К.В., Чижик С.Е.* Векторный геометрический процессор систем визуализации реального времени // Автометрия. – 1994. – № 6. – С. 43-49.

UDC 004.032.26

V.M.Sineglazov, Ph.D. (*National Aviation University, Ukraine)*
E.I. Chumachenko, Ph.D., O.Yu. Levitsky
(National Technical University of Ukraine "KPI", Ukraine)

TRAININGRADIAL-BASIS NEURAL NETWORKS FOR THE PROBLEMS OF DIAGNOSIS SOLUTION

The task of diagnosis has taken a central place in modern society's everyday life and various spheres of its activity. It isof particular importance in medicine, due to the necessity of prompt recognition of disease type and purpose of timely treatment. Due to the variety of different symptoms and the presence of a large number of similar in the form of manifestation, but different in essence anomalies, the solution of this problem requires the use of elements of artificial intelligence such as neural networks.The task of diagnosis is as a matter of fact related to the tasks of classification, the mathematical formulation which can be summarized as follows.

Problem Statement of Classification Let X− the set of descriptions of objects, Y− the set of numbers (or names) of classes. There is unknown target dependence is a mapping$y$ *: $X \to Y$, whose values are known only to the objects of a finite training population:

$$X^m = \{(x_1, y_1),...,(x_m, y_m)\}\,. \tag{1}$$

It's required to construct an algorithm capable of classifying an arbitrary object $x \in X$ to set Y [1]. We'll consider methods for solving this problem.

Review of Methods for Solving the Classification Problem Sufficiently large number of papers [2-7] is devoted to solving classification problems. The main methods for the solution of which are as follows:

- Bayesian (naive) classification [2];
- Classification by support vectors [3, 4];
- Classification using the nearest neighbor method [5];
- Classification using decision trees [6];
- Classification using artificial neural networks [7].

The main drawback of most of the above mentioned approaches is the difficulty (impossibility) of solving the problem of classification in case of proximity of featured items which are subject to classification, belonging to different classes, as well as the presence of non-empty intersection of sets of attributes of objects belonging to different classes. Neural networks [8] have learning abilities that can overcome these drawbacks; however, the use of artificial neural networks (ANN) isthe preferred approach for solving this problem. ANN is determined by such characteristics as topology (a type of network), network structure (number of hidden layers, inputs, outputs).

In the works of authors [10] proved the reasonability of using radial basis ANN for solving the problem of diagnosis.

The efficiency of the network to solve the problem of diagnostics is determined by the quality of the solution of structural and parametric synthesis task, the complexity of the solution of which depends on the type of input variables to the ANN, which can be numeric, binary, linguistic, unclearly specified, images (data arrays). These features define the approaches to solving the problem of structural and parametric synthesis task.

In the works of authors [10, 11] it was shown that the input data in the form of images could be reduced to a numerical input data through the use of image processing algorithms and depicting the essential features.

The functioning of the network involves preset by solving the problem of parametric (structural-parametric synthesis). The effectiveness of this task depends on learning algorithms, the result of which is the type of activation function (a function that computes the output of an artificial neuron), the value of the thresholds (the activation function in which the neuron receives dragging and non-zero value) and weights (numerical coefficient reflecting the importance of the input connections when entering into the adder).There is a sufficiently large number of papers [8, 11]devoted to solving the problem of structural and parametric synthesis. The quality of the learning process is determined by the length of training sample and the rate of convergence of the configuration process (learning). Let's consider the learning of radial basis ANN structure, which is shown in Figure 1. In the networks with radial basis function, neurons implement the function, radially varying around the selected center and taking nonzero values only in the vicinity of the center, we introduce a concept such as the coordinates of the center of the neuron.

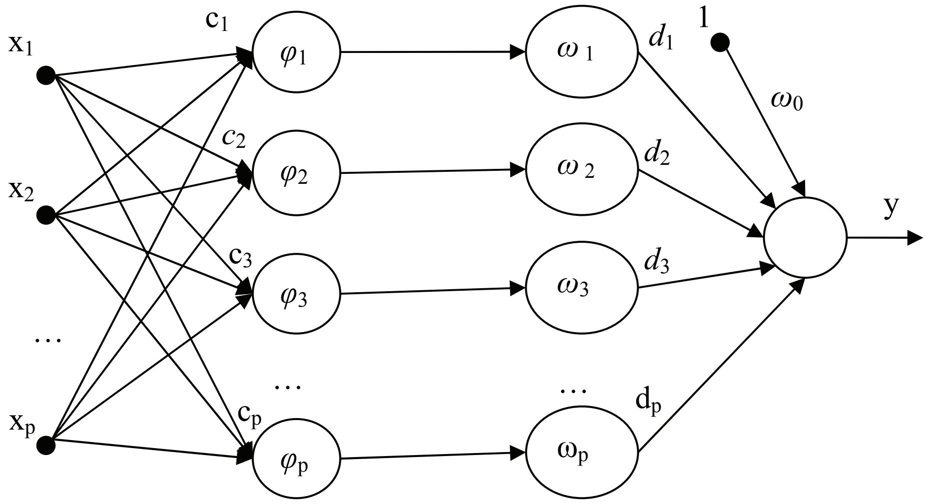

Fig. 1. The structure of the radial basis network.

In Fig. 1 the following notation designate: x_1,x_2, ..., x_p– the input signals; p– the number of neurons in the first (input) layer; φ_1,φ_2, ..., φ_p–multidimensional activation function, which can be expressed as $\vec{\varphi}(\vec{x}) = (\vec{x} - \vec{c}_i)$; $\vec{c}_i$ – coordinates of the *i-th* neuron; d_i– value of the function mapping *the i-th* neuron; ω_i– weighting factor of *i-th*neuron connection; y– the output of radial basis ANN.

Problem Statement of Learning The relationship between the input and output data of radial basis networks can be defined by a system of equations

$$\begin{bmatrix} \varphi_{11} & \varphi_{12} & \cdots & \varphi_{1p} \\ \varphi_{21} & \varphi_{22} & \cdots & \varphi_{2p} \\ \vdots & \vdots & & \vdots \\ \varphi_{p1} & \varphi_{p2} & \cdots & \varphi_{pp} \end{bmatrix} \begin{bmatrix} \omega_1 \\ \omega_2 \\ \vdots \\ \omega_p \end{bmatrix} = \begin{bmatrix} d_1 \\ d_2 \\ \vdots \\ d_p \end{bmatrix} \tag{2}$$

whereφ_{ij}($i \in \overline{1, p}$, $j \in \overline{1, p}$) – the value of the activation function for the *i-th* input neuron *j;* ω_i($i \in \overline{1, p}$)– The value of the weight factor for the *i-th* neuron; d_i– display the value of *the i-th* neuron; p– the number of neurons in the hidden layer.

Display function is such a function whose value is equal to the product of the value of the function activating the neuron to the corresponding weighting factor.

It's required to determine the type of activation functions φ_{ij} and the weights at the output of the hidden layer ω_i($i \in \overline{1, p}$) on the basis of minimizing the quality criterion defined as

$$E_p = \frac{1}{2}(d_p - O(\varphi_p, \omega_p))^2, \tag{3}$$

whereE_p– value of the criterion for the *p-th* training pair (a pair consists of the values of the activation function φ_p and the corresponding values at the output obtained from the training set d_p);$O(\varphi_p, \omega_p)$– value of the display function, obtained as the result of network work.

The task of learning is toset up so the weightsω_i, so that they for any training pair (φ_p, d_p) give the minimum value of the $E_p$criterion.

The output of radial basis ANN is calculated as a weighted sum of the signal elements

$$y_i = \sum_{p=1}^{\infty}(\omega_p \varphi_i). \tag{4}$$

In the radial basis network,activation function for each item is determined by a Gaussian function

$$\varphi_i = \exp\left(-\frac{\sum_{j=1}^{n}(x_j - c_{ij})^2}{2\sigma_i^2}\right) \tag{5}$$

Whereσ_i– the width of the Gaussian function of *i-th* neuron;c_{i1}, c_{i2}, ..., c_{in} - coordinates of the *i-th* neuron.

As a result, learning is reduced to:

- selection of centers $c_i$and parameters σ_i;
- selection of the weights $\omega_i$of the hidden layer neurons.

As a result, the criterion (3) takes the form

$$E_p = \frac{1}{2}(d_p - \omega_p \exp(-\frac{\sum_{j=1}^{n}(x_j - c_{ij})^2}{2\sigma_i^2}))^2. \tag{6}$$

Synthesis of Learning Algorithm Since ω_i can be determined on the basis of solutions of type(2)equations, the main problem is the choice of learning c_i and $\sigma_{i.}$

To solve this problem use of particle swarm algorithm is proposed [12]. In the classical form the algorithm is used for optimization of continuous nonlinear functions. Particle swarm algorithm is widely used, among others, in the problems of machine learning, parametric and structural optimization (shapes, sizes and topologies) in the design, in the fields of biochemistry and biomechanics [12]. The particle swarm model is based on control of distances between the particles. The current state of the particle is characterized by the coordinates in the solution space (that is, in fact, related with it decision), as well as by the velocity vector of displacement. Both of these parameters are chosen randomly at the initial stage of the assignment of values. In addition, each particle stores the coordinates of the found bestposition, and best of all the passed by the particles locations - this simulates the instantaneous exchange of information between the particles. At each step of the algorithm length and the direction of the velocity vector of each particle are changed in accordance with the information about the found optima

$$v_i(t+1) = v_i(t) + a_1 Rnd(P_i^{best}(t) - x_i(t)) + a_2 Rnd(G_i^{best}(t) - x_i(t)) \tag{7}$$

where$v$– particle velocity vector *(*v_i–it`s*i-th* component);a_1,a_2– constant acceleration with positive values;P^{best}– the best point found by the particle;G^{best}– the best point of all passed (all swarm) particles in the system;x– current position of the particle;*Rnd*– random number between 0 and 1 inclusive.

After calculating the direction vector v, the particle moves to a point

$$x(t + 1) = x(t) + v(t + 1). \tag{8}$$

If necessary, the values of the best points for each particle and all particles as a wholeare updated. After this cycle is repeated.

In this paper, we propose to use a modified particle swarm algorithm, called the "canonical". Its advantage over the classical algorithm is that it eliminates the need to "guess" the appropriate values of adjustable parameters of the algorithm (and the direction of the acceleration), controlling the convergence of the particles [13]

$$v_i(t+1) = \lambda\left(v_i(t) + a_1 Rnd(P_i^{best}(t) - x_i(t)) + a_2 Rnd(G_i^{best}(t) - x_i(t))\right) \tag{9}$$

whereλ − the compression ratio.

$$\lambda = \frac{2k}{\left|2 - a - \sqrt{a^2 - 4a}\right|}; \tag{10}$$

$a = a_1 + a_2 > 4$;

k − limiting factor for speed control.

With respect to the radial basis ANN (9) takes the form

$$v_i(t+1) = \lambda\left(v_i(t) + a_1 Rnd(P_i^{best}(t) - c_i(t)) + a_2 Rnd(G_i^{best}(t) - c_i(t))\right) \tag{11}$$

where c_i–coordinates of the *i-th* neuron.

We introduce concepts such as quality criterion centers, the adjustment speed, the best position for the center of each neuron.

The criterion of quality centers. Let R_{ij} be the Euclidean distance between the centers of the *i-th* and *j-th* neuron. Then the change in distance between the centers of the neurons

$$\Delta_{ij}(t) = (R_{ij}(t) - R_{ij}(t-1)), \qquad (12)$$

where t–number of iterations.

Quality criterion is the maximum change Δ_{ij} (12) which are defined as

$$\Delta_{i\max}(t) = \max_{j=1..p}(R_{ij}(t) - R_{ij}(t-1)). \qquad (13)$$

Then, the center is considered acceptable if the change $\Delta_{i\max}(t)$ is lower than the limit of ε, which is determined experimentally. As a result, we obtain the criterion of quality centers

$$\max_{j=1..p}(R_{ij}(t) - R_{ij}(t-1)) < \varepsilon. \qquad (14)$$

Adjustment of acceleration a_1. Acceleration is directly proportional to the maximum $\Delta_{i\max}(t)$ for all neurons. That is:

$$\Delta_{ij\max}(t) = \max_{\substack{j=1..p \\ i=1..p}}(R_{ij}(t) - R_{ij}(t-1)). \qquad (15)$$

Adjustment of acceleration a_2. Acceleration directly proportional to the $\Delta_{i\max}(t)$.

The best position for the center of each neuron P^{best} will be those coordinates in the ε neighborhood of which the coordinates of the centers find themselvesmost often.

The overall position of the best G^{best} will be the coordinates in a neighborhood of ε,where every neuron is found most often.

Now the algorithm for finding the best centers of neurons is as follows.

1. Determination of the initial values of the centers of neurons randomly.
2. Score centers by quality (14).
3. Determination of the initial values of the accelerations a_1, a_2.
4. Adjustment of acceleration in accordance with formulas (15) and (13).
5. Calculate the next position of the centers c_i using formula (11).
6. Saving the best position for each particle P^{best} and overall a better position G^{best}.
7. Score points by quality (14) and return to Step 4.
8. Defining σ by formula

$$\sigma_i = \frac{\max_{j=1..p} R_{ij}}{\sqrt{2p}}. \qquad (15)$$

9. Determination of the weight coefficients using the formula (6).

ExampleHere is an example of finding the minimum value of the error criterion (6). Schedule an error criterion is a surface in three-dimensional space. In the figures high values are indicated by a lighter color and smaller- by darker. The particles of the swarm are marked with yellow dots. Big red dot denotes the best minimum value at each iteration.

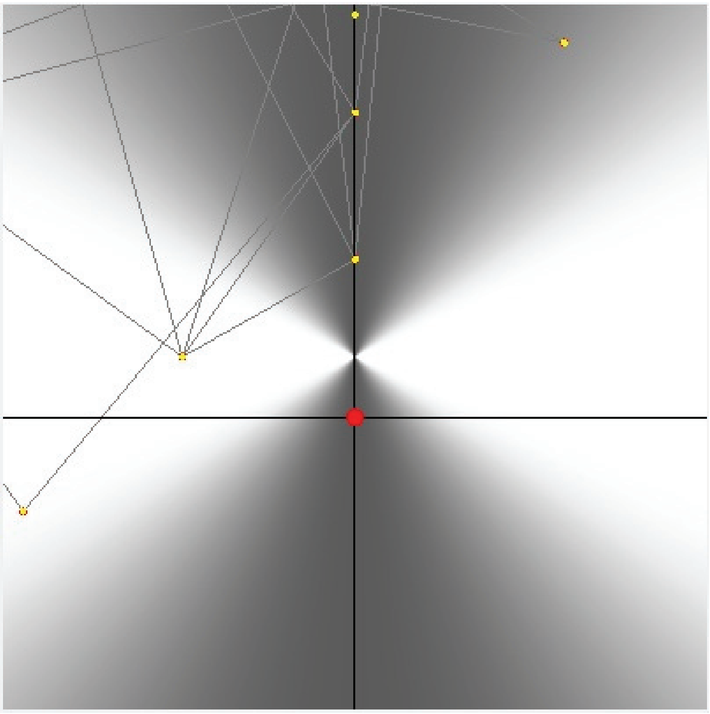

Fig. 2. Determination of the initial values of the particles randomly.

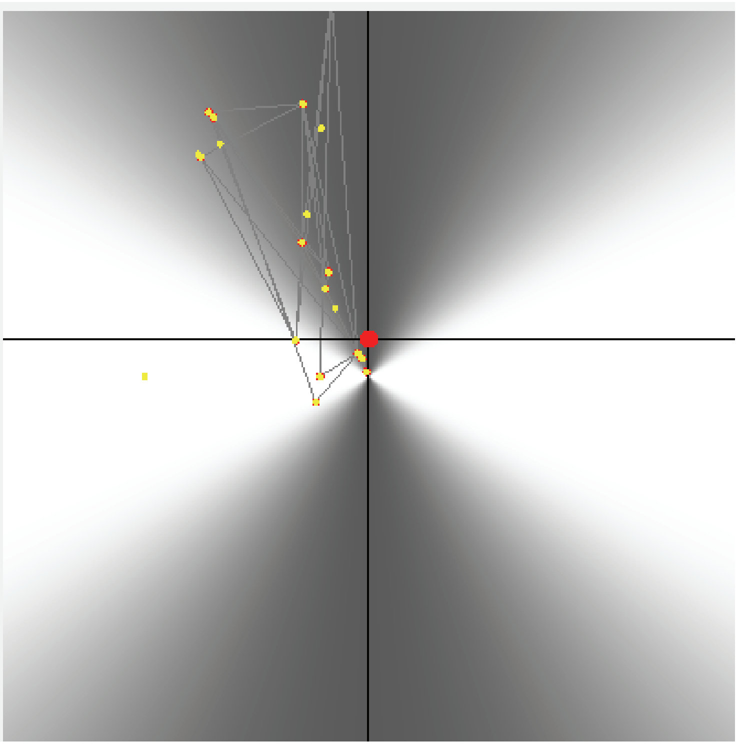

Fig. 3 .The position of the particles after 20 iterations.

Conclusions

As a result of the work done to solve the problem of training a radial-basis method based on particle swarm algorithmhas been developed. This method can reduce the load on the computer system, which executes learning, accelerating it.

References

1. *Воронцов К.В.* «Комбинаторная теория надежности обучения по прецедентам», Дис. док. физ.-мат. наук: 05-13-17. — Москва: Вычислительный центр РАН, 2010. — 271 с. 1-42с.

2. *Субботин С. В., Большаков Д. Ю.* «Применение байесовского классификатора для распознавания классов целей», журнал радиоэлектроники РАН №4, 2006, электронный журнал, ISSN 1684-1719

3. *Воронцов К.В.* «Лекции по статистическим (байесовским) алгоритмам классификации», MachineLearning.ru, 2008. — 39c.

4. *Воронцов К.В.* «Лекции по методу опорных векторов», MachineLearning.ru, 2007. — 18c.

5. *Воронцов К.В.* «Лекции по метрическим алгоритмам классификации» MachineLearning.ru 2008. — 15c.

6. *Круглов В. В., Борисов В. В.* «Искусственные нейронные сети. Теория и практика», 2-е издание, Москва: Гарячая линия – Телеком, 2002. — 377c., 8-140c.

7. *Демиденко Е. З.* «Оптимизация и регрессия». Москва: Наука. 1989. —296c.

8. *Чумаченко Е. И., Левицкий О. Ю.* Разработка алгоритмов обработки изображений для задач диагностики.- Електроніка та системи управління. – Киев 2011. — 167c. 57- 66

9. *Бодянский Е.В., Руденко О.Г.* Искусственные нейронные сети: архитектуры, обучение, применения. — Харьков.: Телетех. — 2004. — 167c.

10. *R. Mendes, J. Kennedy, J. Neves*, "The fully informed particle swarm: Simpler, maybe better" // IEEE Transactions on Evolutionary Computation, №8 (3), 2004. — 204–210p.

11. *Yann LeCun, J. S. Denker, S. Solla, R. E. Howard and L. D. Jackel*: Optimal Brain Damage, in Touretzky, David (Eds), Advances in Neural Information Processing Systems 2 (NIPS 1989), Morgan Kaufman, Denver, CO, 1990 — 9p.

12. *Y. LeCun and Y. Bengio*: Convolutional Networks for Images, Speech, and Time-Series, in Arbib, M. A. (Eds), The Handbook of Brain Theory and Neural Networks, MIT Press, 1995 — 14p.

13. *Y. LeCun, L. Bottou, G. Orr and K. Muller: Efficient BackProp, in Orr, G. and Muller K. (Eds),* Neural Networks: Tricks of the trade, Springer, 1998 — 44p.

14. *Ranzato Marc'Aurelio, Christopher Poultney, Sumit Chopra and Yann LeCun:* Efficient Learning of Sparse Representations with an Energy-Based Model, in J. Platt et al. (Eds), Advances in Neural Information Processing Systems (NIPS 2006), MIT Press, 2006 — 8p.

15. *Levenberg, K. A* Method for the Solution of Certain Problems in Last Squares. Quart. Appl. Math. 1944. — Vol. 2. P. 164 —168.

16. *J. Kennedy, R. C. Eberhart* "Particle swarm optimization" // In Proceedings of IEEE International Conference on Neural Networks, 1995. . —vol.4 1942–1948pp.

17. *M. Clerc, J. Kennedy* "The particle swarm – explosion, stability, and convergence in a multidimensional complex space" // IEEE Transactions on Evolutionary Computation, №6 (1), 2002. — 58–73pp.

UDC 004.032.26

V.M. Sineglazov, PhD, (National Aviation University, Ukraine)
E.I.Chumachenko, PhD, V.S.Gorbatiuk
(National Technical University of Ukraine "KPI", Ukraine)

ONE APPROACH FOR THE FORECASTING TASK SOLUTION

The article describes the main methods of forecasting and offers a new algorithm based on the group method of data handling and artificial neural networks. Algorithm was tested on real data and showed better results than neural networks.Also experimental dependence of the mean square prediction error obtained with this algorithm and neural networks, from the number of points in the training set was found.

IntroductionForecasting has always been and will be one of the most interesting to mankind themes, because knowledge of the future is perhaps one of its most cherished desires. However, people using the results of the forecast, should understand the risk of choosing inappropriate methods of forecasting, since incorrect predictions can lead to making the wrong decisions.

A large part of the apparatus of forecasting used today was developed in the nineteenth century. An example is the procedure of regression analysis. But with the advent and development of computer technology forecasting unit began to evolve and became more complex.More and more complex methods that require ever-increasing computing power began to appear. They were group method of data handling, artificial neural networks.

The purpose of this paper is to develop a new forecasting method that takes into account and uses the increased power of modern computing.

The mathematical formulation of the problem of forecasting Let us have n discrete samples $\{x_1, x_2,...,x_n\}$ at successive time points $t_1,t_2,...,t_n$. Then the problem of prediction (Fig. 1) consists of prediction of the value x_{n+k} at some future point of time t_{n+k} where k is the duration of the forecast: $x_{n+k} = F(x_1, x_2,..., x_n)$,where F is some unknown function.

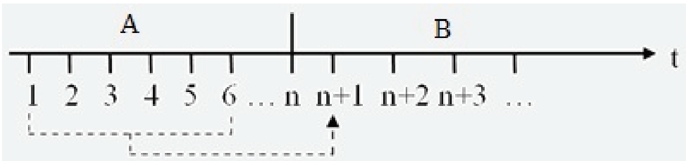

Fig. 1 Graphical illustration of the problem statement forecasting:
A - known values, B - the forecast period

An algorithm for solving the problem of forecasting In this issue a forecasting algorithmbased on two common methods –artificial neural networks (ANN) and group method of data handling (GMDH) is offered.

The proposed algorithm combines the advantages of both ANN and GMDH: a gradual increase in the complexity of the model (GMDH) and the ability of ANN to train. It consists of the following steps:

1. Preprocessingof source data, including getting rid of outliers&data normalization, etc. (See [1], [2], [3], [4]). This stage is often more important than stage of modeling. Also you should take into account the specific characteristics of the forecasted process, such as seasonality of values in the case of predicting the various atmospheric parameters, the trend component in the majority of financial processes, etc.

The study [3] shows the importance of getting rid of unwanted outliers in the source data when using artificial neural networks. It is important to determine whether specific value is accidental and therefore unwantedoutlier, or is this outlier informative. To do this, you should consider the process you are forecasting, for example, if you want to build a model of energy consumption of some region depending on the day of the week, then it should be noted that energy consumption on weekends will be dramatically different from the consumption on weekdays and, consequently, the value of consumption over the weekend will not constitute unwantedoutliers. In this case, during the training of the network, it would be reasonable to include a binary value, showing whether this day is a weekend or not, as an additional input.

If it is known that the process does not include informative outliers, there are several basic algorithms of getting rid of accidental outliers:

• The simplest algorithm based on the characteristics of a stochastic variable, according to which an outlier is a value, which deviates from the average value by an amount greater than 2 ... 3 mean square deviation σ^2.

• The Tukey 53Halgorithm [4] that uses the principle that the median is a robust estimator of the mean to generate a smooth time sequence that can be subtracted from the original signal:

2. Usingthe data windowing, two matrices are formed from the sourcedata $X = \{x_n, n = 1 \ldots N\}$, where N is a number of samples, obtained from the previous stage of processing:

$$X^{(0)} = \begin{bmatrix} x_1 & x_2 & \cdots & x_k \\ x_{k+2} & x_{k+3} & \cdots & x_{2*k+1} \\ \cdots & \cdots & \cdots & \cdots \\ x_{N-k-1} & x_{N-k} & \cdots & x_{N-1} \end{bmatrix}, \; y = \begin{bmatrix} x_{k+1} \\ x_{2*k+2} \\ \cdots \\ x_N \end{bmatrix},$$

where***k*** is the size of the window. Attention should be paid to the selection of ***k***: it would be reasonable to start with some small number $k = 1..5$ (depending on the training set size), and if after the end of the algorithm the MSE is unsatisfactory, start to increment ***k*** slowly. With the help of these matrices networks will be trained - each row vector $\overline{x}_n = \{x_{n1}, x_{n2}, \ldots, x_{nk}\}, n = 1 \ldots m$ (where m is a number of rows) of the matrix $X^{(0)}$ and the corresponding value y_n are anindependent sample, and a column vector $\vec{x}_z = \{x_{z1}, x_{z2}, \ldots, x_{zm}\}, z = 1 \ldots k$ - a separate variable.

3. The resulting samples are divided according tosome ratio (usually $0.7m : 0.3m$) into the training and testing sets.

4. The type of base functions is determined, namely, on what variables do they depend, for example $f_l = f(x_i, x_j)$, or $f_l = f(x_i, x_j, x_i * x_j, x_i^2, x_j^2)$ where $l = 1 \ldots C_k^2$ is the number of possibilities to choose two variables from the k possible (in the general case $l = 1 \ldots C_k^O$, where O is the number of variables, taken as arguments of support functions). In contrast to the GMDH, where the concrete form of functions is also determined (for example $f_l = a_0 + a_1 * x_i + a_2 * x_j$) in this algorithm only variables onwhichthe base functions will depend are selected (powers of the variables and their covariance can be represented as additional variables), whilethe determination of the function values dependence from variables will be performed by the neural network.

5. The topology of the neural networks to be usedis selected (i.e. multilayer perceptron (MP), radial-basis neural network etc.) and also an activation function of neurons is chosen.

5. C_k^O neural networks are constructed (O - number of variables taken into account in support functions, for the above example o = 2) with one output, one hidden layer with a small amount of neurons (about 3) in it, and the right amount of inputs (forsupport functions of form $f_l = f(x_i, x_j)$ a network must have two inputs, for $f_l = f(x_i, x_j, x_i * x_j, x_i^2, x_j^2)$ - 5 inputs, etc.).

Also, amount of neurons in the hidden layer can be varied in the case of unsatisfactory MSE after the end of the algorithm. But usually, since the algorithm complicates the forecasting model from iteration to iteration by itself, there is no need in too complex neural networks (with amount of neurons in hidden layer $\geq$ 10).

6. Each neural network is matched with a specific base function, namely the variables to be fed to the inputs of the network are selected (for example, for support functions of form $f_l = f(x_i, x_j, x_i * x_j, x_i^2, x_j^2)$one network will work with the variables $x_1, x_2, x_1 * x_2, x_1^2, x_2^2$and the

training set.

7. In this step the initial data for the next iteration of the algorithm should be composed. For this,you should determine the mean square error (MSE) of each network on the test set and select bestnetworks(also you can select a smaller amount, but add to them original variables which were the inputs to networks with a small MSE), and then create a new matrix:

$$X^{(1)} = \begin{bmatrix} h_{11} & h_{12} & \dots & h_{1k} \\ h_{21} & h_{22} & \dots & h_{2k} \\ \dots & \dots & \dots & \dots \\ h_{m1} & h_{m2} & \dots & h_{mk} \end{bmatrix},$$

where h_{ij} is the output value of the j-th neural network when it is given the inputs of the i-th sample, $i = 1 \dots m, j = 1 \dots k$ (or the original variable).

8. Next iteration is performed, but as the source data a matrix $X^{(1)}$ is taken. Iterations are performed until the MSE value of networks on the test setdecreases, or until we reach the desired MSE.

9.During each iteration of the algorithm the weights and the structures of networks (and / or the original variables) that were selected to make the source matrix for the next iteration should be remembered. After reaching the required MSE (or reaching the iteration, after which MSE starts increasing) we should stop performing the iterations, and select the only network that will forecast the further values. For further forecasting of some value x_c using the obtained results weshould:

• Create sourcesample $inp = \{x_{c-k-1}, x_{c-k}, \dots, x_{c-1}\}$;

• Use this sample as the inputs for thenetworks that were used to obtain the source matrix of the second iteration, and using the obtained output values(and / or the original variables) make a new input sample for the second iteration;

• Repeat theprevious step until the input sample for the iteration, at which the algorithmwas stopped, is created, and then use it as the input for the selected network, whoseoutput will be a forecast of the value x_c.

Application results of the proposed algorithm For the testing of the proposed algorithm a public set of the annual copper prices from 1800 to 1997 was used.

For comparison of the algorithm's application results, the multilayer perceptron with single output neuron, 2 hidden layers, 8 neurons in the first, 5 – in the second layer, and 5 inputs was also built. MP, as well as the proposed algorithm, was trained only on the training set. Since it's known that ANN are proneto"getting stuck" in local minimums of the network's cost function, about ten MPs were trained, and the perceptron with the minimal MSE was chosen.

Comparison of the results got with the usage of ANN and proposed algorithm without and with data preprocessing is shown on the Figure 2 and 3 respectively.

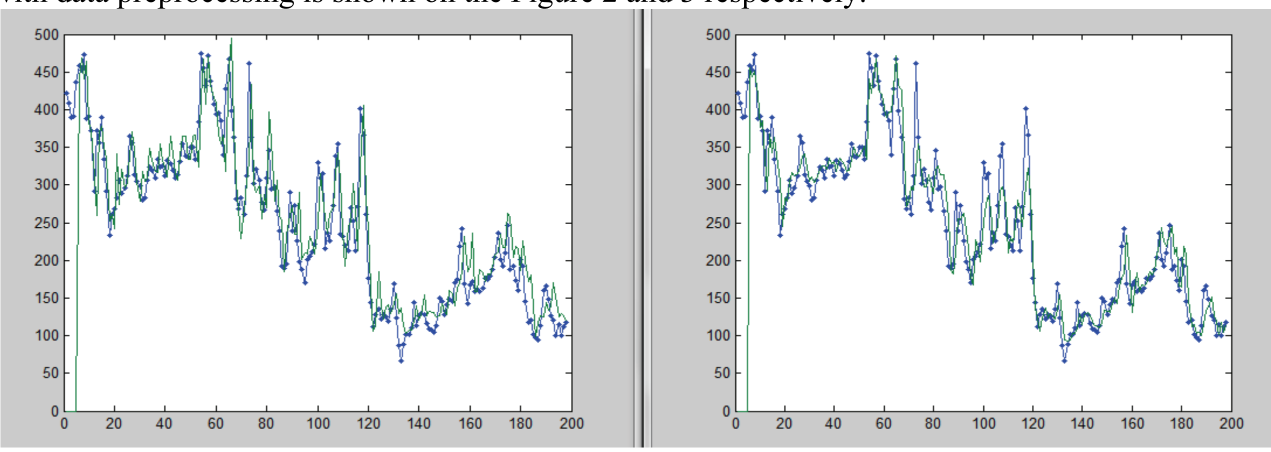

Fig. 2 – Comparison of the prediction results of ANN (on the left) and the proposed algorithm (on the right) (without data preprocessing). - prediction, - actual

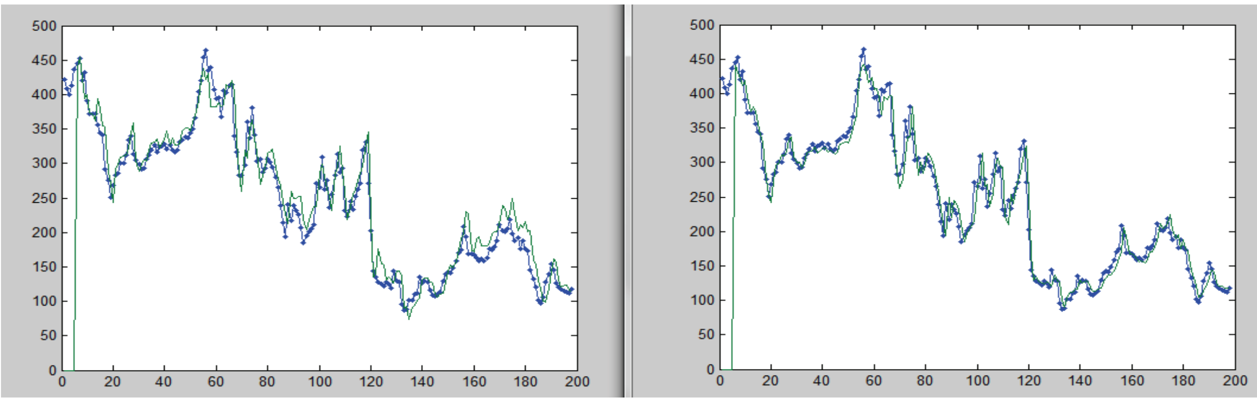

Fig. 3 – Comparison of the prediction results of ANN (on the left) and the proposed algorithm (on the right) (with data preprocessing). - prediction, - actual

As the algorithm of data preprocessing the previously described Tukey 53Halgorithm was used.

The MSE value without data preprocessing: ANN – 1256.5, algorithm – 920.0306; with data preprocessing: ANN – 507.0927, algorithm – 355.4813.

From the both Figures is noticeable, that trained perceptron predicts the values of the testing set worse (the very last values), while proposed algorithm forecasts values of the both training and testing setsequally well, what indicates the more accurate model of the process. Also, an algorithm showed a goodMSEwhile predicting without data preprocessing, what gives the possibility of its application for forecasting noisy data.

For the comparison of the proposed algorithm and ANN with the different number of samples in a training set, the MSE of the algorithm and ANN were calculated on the entire set, got after their training on the training set with varying number of samples in it. Results are represented graphically on the Figure 4:

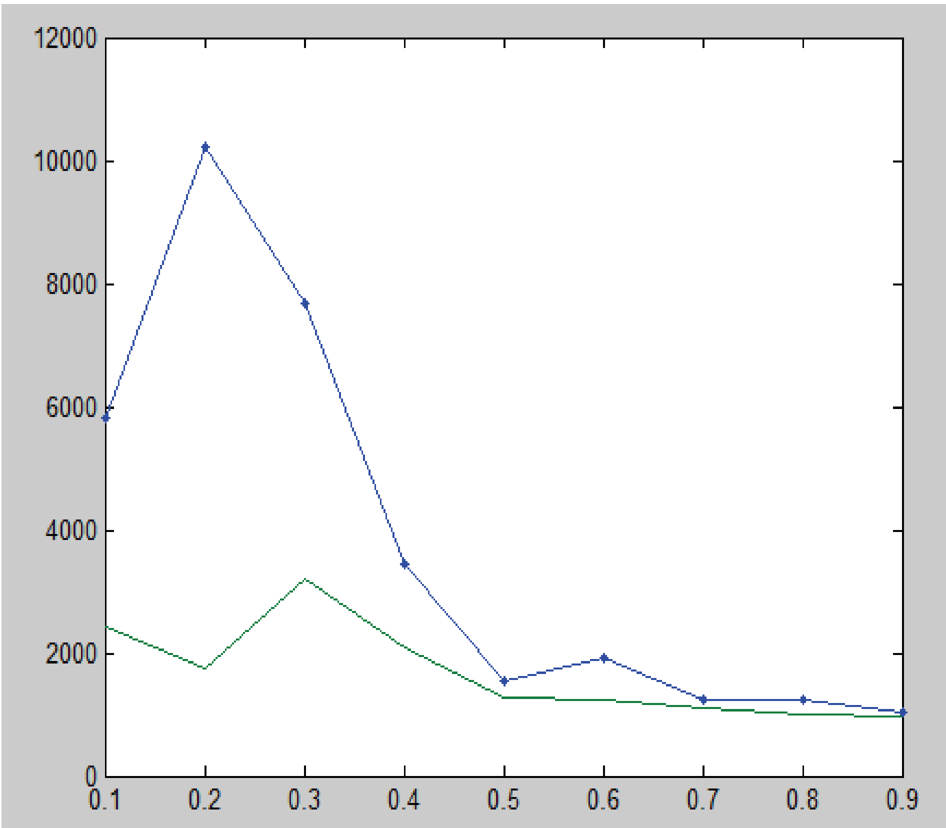

Fig. 4 – Graphical representation of MSE of the algorithm and ANN depending on the number of samples in a training set: - MSE of the algorithm, - ANN's mean square error

The first K*m exampleswere selected into the training set, where $K = 0.1 \ldots 0.9$, m – general number of source examples (193 for this case). As seen from Figure 1, algorithm gives way less MSE with the little number of samplesin training set, indicating more adequate model of the process.

Also it can be mentioned, that starting from particular K valueMSE of both network and algorithm sharply increases, indicating insufficient informational capability of the training set, and as the result, incomplete model.

Conclusions

Proposed algorithm has shown better results in comparison with the artificial neural networks, bothin the conditions of noisy data, and with the small size of the training set, which means its suitabilityfor further usage inforecasting tasks.

References

1. *Amir F. A., Samir I. S.* A comparison between neural-network forecasting techniques – case study: river flow forecasting. // IEEE Transactions on neural networks, vol. 10, no. 2, march 1999. — p. 402–409.

2. *Mohsen H., Yazdan S.* Artificial neural network approach for short term load forecasting for Illam region. // World Academy of Science, Engineering and Technology 28 2007. — p. 280-284.

3. *Jerome T. C., Douglas R. M., Atlas L. E.* Recurrent neural networks and robust time series prediction. // IEEE transactions on neural networks, vol. 5, no. 2, march 1994. — p. 240-254.

4. *Irina Klevecka, Janis Lelis*Pre-Processing of Input Data of Neural Networks: The Case of Forecasting Telecommunication Network Traffic. // Telektronikk 3/4.2008. – p. 168-178.

UDC: 681.526.4

A.O. Nazarenko, graduate student
(Institute of engineering thermophysics NAS of Ukraine)

AUTOMATEDSYSTEM FOR REGULATION HEAT CONSUMPTION

In the report there is a speech about the automated system of regulation heat consumption with use weather-depend regulator, the resulted short technical characteristics, a principle and algorithm of work.

Presently, when power resources indefatigably rise in price, the question of economy of heat costs sharply as there is no time. In municipal power system of the dress with use of different methods of warming of buildings, more an effective utilization of energy carriers, use of alternative production technologies of heat, considerable economy are given by modern intellectual thermal points. Using individual heating schedules, it is possible to reach about 30 percent of economy of heat. And if the building is equipped by the thermal counter, the same economy of means. Heart of each thermal point is theautomatedsystem for regulationheat consumption with weather-depend regulator (Fig. 1) which supervises over giving of heat to consumers.

This system intended for work as individual thermal point in inhabited, administrative and industrial buildings.
It provides optimization of process of heat exchange, weather-depend regulation of temperature of the heat-carrier in heating systems according to the heating schedule, correction of the schedule depending on time of a time, day of week, etc.

The basic technical characteristics:

- thermal capacity 0,3-1,0 Gkal;
- a range of regulation of temperature of the heat-carrier 30-90℃;
- automatic maintenance of comfortable temperature indoors.

Regulation of temperature of the heat-carrier in a heating contour on temperature of external air

Regulation of temperature of the heat-carrier in a heating contour is spent on calculated by a regulator value t_{set}^{0} (the temperature is set). Value t_{set}^{0} is size replaceable and is calculated by a regulator proceeding from temperature of external air under the temperature schedule

Schedule parameters (Fig. 2) are set by the serviceman at regulator adjustment, proceeding from operational characteristics of heating system, a thermal design of a building and requirements to a temperature mode indoors. In drawing it is resulted the typical heating schedule which is set by manufacture.

Schedule parameters (as well as all other working parameters set at adjustment of a regulator) behave haughtily in the built in non-volatile memory and remain in it throughout all term of operation, including at adeenergized regulator.

This function allows to avoid "overheat" a premise owing to change of weather conditions and not enough operative reaction to it district heatingorganizations which often takes place. If the manufacturer of heat and the consumer one the economy of energy carriers takes place.

Correction of temperature of the heat-carrier in a heating contour on time of days, workers and the days off.

The temperature t_{set}^{0} can be corrected on factor K for different time of days and pays off under the formula(2)

The factor K is set from the menu for the different periods of days (a maximum eight). The factor K can change from-50 % to +50 % with step-type behaviour of 5 %.
The variant of the hourly graph is resulted in a Fig. 3

Where $T_1 - T_8$ time points of change of the graph of heating, at time passage through point T the factor K accepts new value and keeps it to passage of the following point.

Time-temperature graph consists of eight points of transition, if desirable quantity of points of transition less than eight on "superfluous" points of transition of value of factor K does not change. Points T_4, T_5, T_6 and T_8 on the graph.

For days off and the working days time-temperature graph'sare set . At the enterprise are established by days off all Saturdays and Sundays, and also the state holidays of Ukraine. If necessary by means of the menu probably to make any day the day off or workers.

Using the given function it is possible to reduce temperature in heated premises, when there are no people (for example at night for office buildings), thus to reach considerable economy of power resources.

Experimental data heat consumptionfor buildings of 4409 sq.m. with the automated control system are resulted by the area in a Fig. 4 and 5.

Economy on the case the area of 4,4 thousand in sq. m - 34,8 %, or 25,8 thousand grn.

Formula:

$$(t_{sw}^0) = f(t_a^0) \tag{1}$$

where(t_{sw}^0)- heat-carrier temperature in a submitting pipe,

(t_a^0)- temperature of external air.

$$t_{set}^0 = t_{set}^0 + (t_{set}^0 \times K)/100 \tag{2}$$

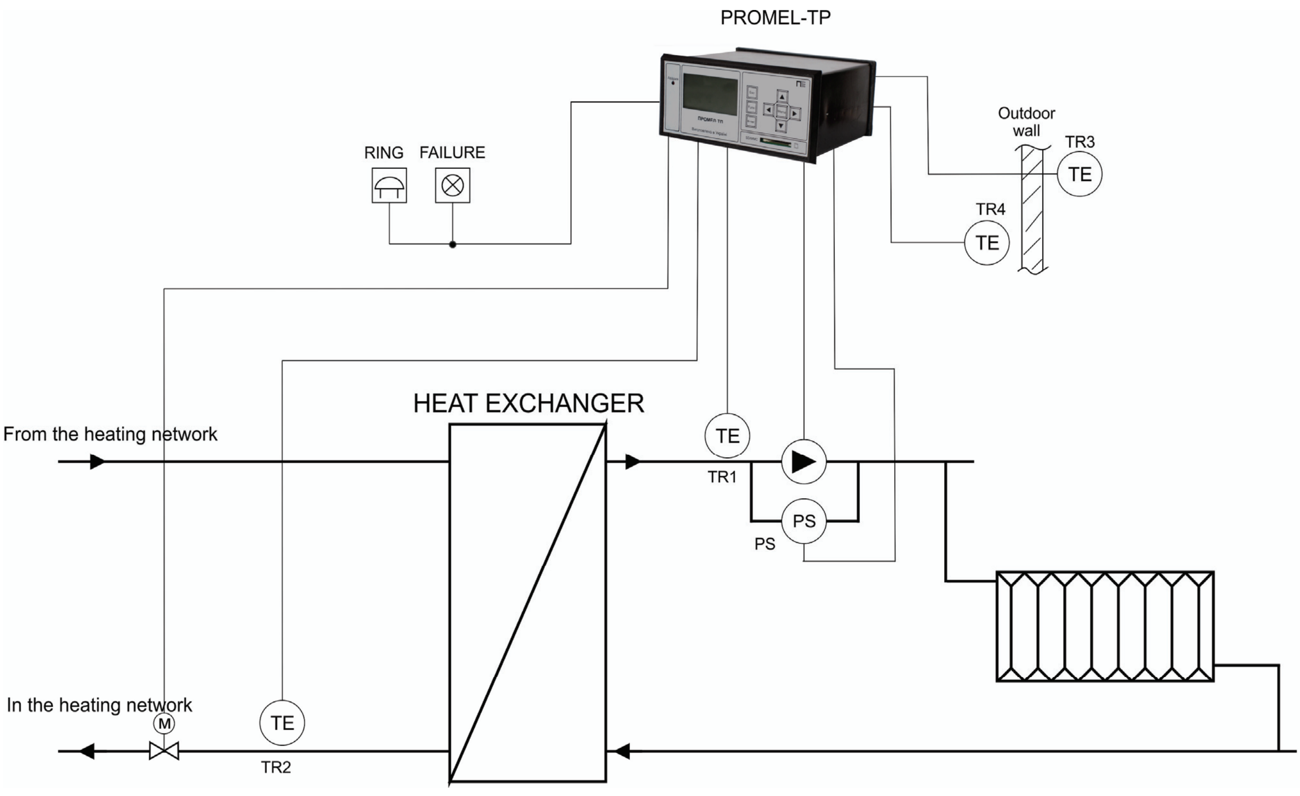

Fig.1. A simplified diagram of the automated control system of heat consumption.

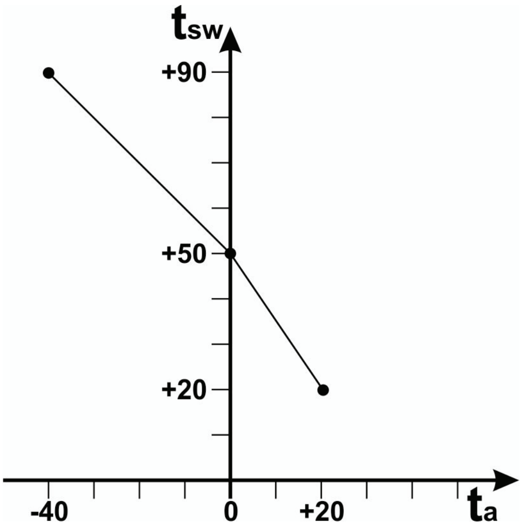

Fig.2. Graph of the temperature of coolant in the heating circuit of outdoor temperature

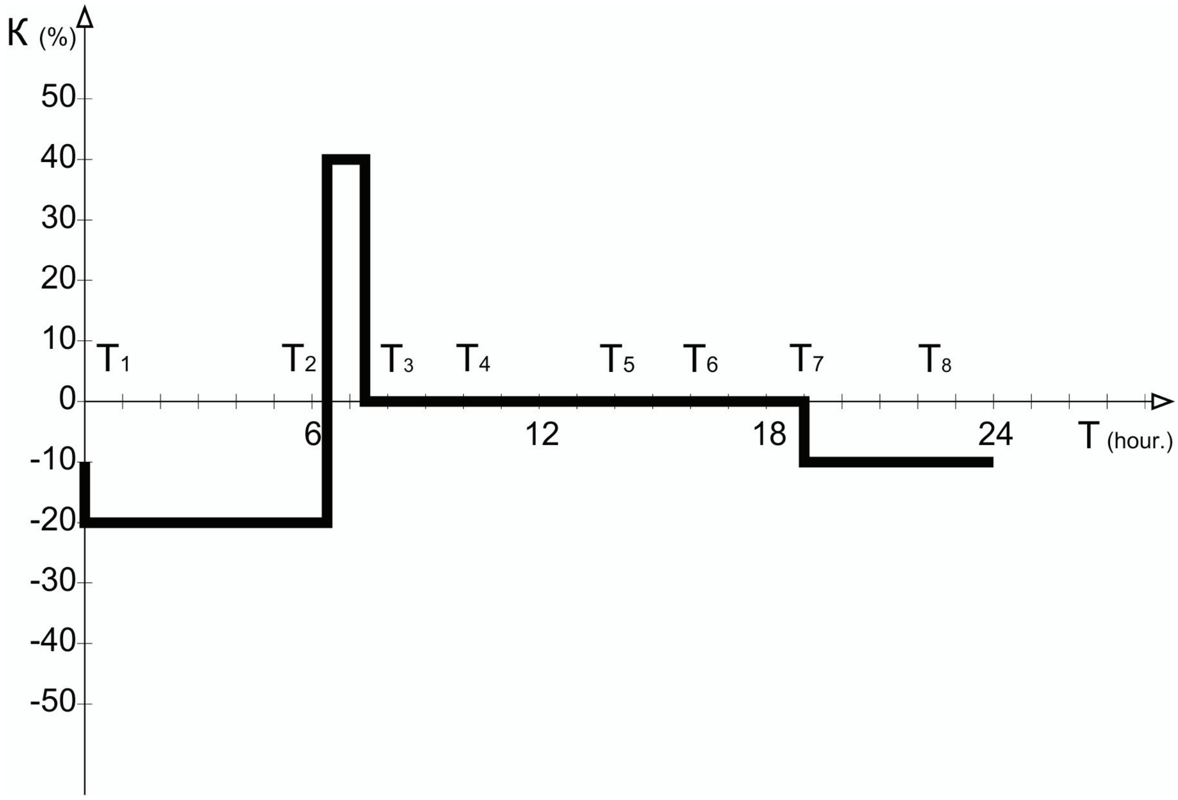

Fig.3 Time-temperature graph.

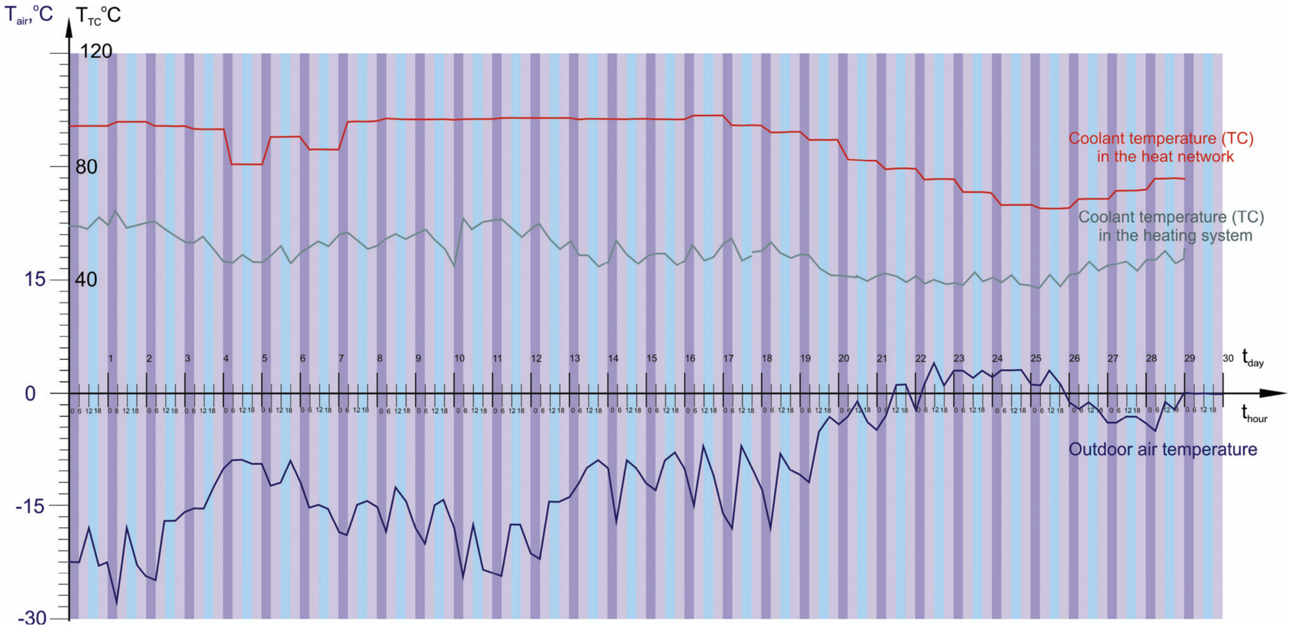

Fig. 4 Temperature graphs for February 2012

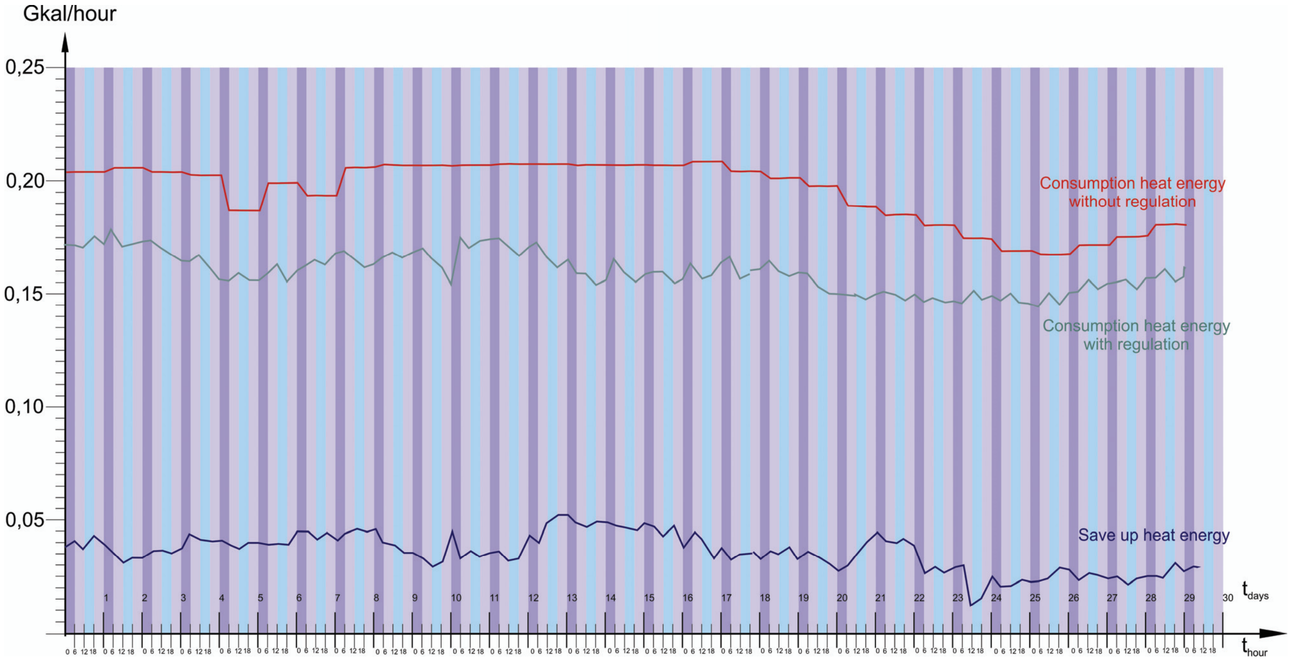

Fig. 5 Graphs heat consumption for February 2012

Conclusions

The introduction of automated control system for heat consumption allows consumers not only save energy while maintaining optimum temperature in the rooms, but in situations with limited funding to maintain a minimum flow of heat necessary to prevent destruction of the building.

Investigated the potential for introduction of automated control system for heat consumption, saving energy by reducing the temperature in the room during the absence of men. Weather-dependentregulationgave return money ofASKTonbuilding №1ITTFNational Academy of Sciencesof Ukraine forone heatingseason.

References

1. Automation of heat supply systems by regulators company "Danfoss".CatalogueofCompany "Danfoss".(UK.00..5O,5/97)

2. *VytalevV.P., NikolayevV.B., SeldynN.N.* Operation of heating units and systems of heat consumption. Manual. – M.: Stroyyzdat. 1988. – 326 p.

3. *GrebenshchikovV.*About regulation in heat and cooling – K.: Akva-Term.- 2004.- № 4(7).- 78p.

4. SBC B.2.2-15-2005. Houses. The main provisions.- K.: Ukrarhbud-Inform, 2005.- 36 p.

5. *ZhukA.Z., KozlovB.M.* Optimizationofheatingsystemsand water supply - Problems of energy saving- 2002.- № 1.- 13 p.

6. NazarenkoO.O., GovnorukY.G. Weather-dependregulation of heating systems – Nova tema. – 2010. - №3. – 54p.

7. *Pyrkov V.V.*Modern heating units. Automation and regulation. – K.: II SE «Taki Spravy», 2008. - 252 p.

8. Recommendationsontheapplicationoffundsautomaticallyregulationsystems ofheatingandhot water supply operated residentialbuildings. - Moscow: ONTYAKHname. K. D. Pamfylova, 1988.

9. SNiP 2.04.05-91. Heating, ventilation and conditioning. - Moscow: APP TSYTP, 1992.

UDC 681.513(045)

V. N. Azarskov, Doct. of Sci. (Eng.)(National Aviation University, Ukraine)
L. S. Zhiteckii, PhD in Control Systems (National Aviation University, Ukraine)
S. A. Nikolaienko (National Aviation University, Ukraine)

SOME ASYMPTOTIC RESULTS FOR ONLINE LEARNING IN NEURAL NETWORKS USED AS MODELS OF COMPLEX SYSTEMS

Asymptotic properties of online gradient algorithms with a constant step size employed for learning in neural networks having hidden layer are studied. The sufficient conditions guaranteeing the convergence of these algorithms in the random environment are established.

Neural networks containing at least one hidden layer play a role of universal approximations for any reasonable complex nonlinear mapping. This fact motivates the theoretical studies of learning algorithms for the neural networks. Significant breakthrough in this research area has been achieved in recent works [1, 2]. Namely, the convergence results have been derived in [1] provided that input signals have a probabilistic nature. In their stochastic approach, the learning rate goes to zero as the learning process tends to infinity. Unfortunately, this gives that the learning goes faster in the beginning and slows down in the late stage. The convergence analysis of learning algorithms with deterministic (non-stochastic) nature has been given in [2] by assuming that the learning set is finite. The difficulties in establishing the convergence results are that the neural networks contain the parameters which appear nonlinearly in their equations. To the best of author's knowledge, there are no results in literature concerning the convergence properties of training procedures with a fixed step size applicable to the case of infinite learning set.

This paper generalizes some results obtained by the authors in [3]. The main effort is focused on establishing sufficient conditions under which the online gradient algorithms applied for sequential learning neural networks with a constant step size will converge in the case of infinite learning set. The key idea in studying their asymptotic properties is based on exploiting the stochastic counterpart of the Lyapunov function method, which is known in the probability theory as the supermartingale.

Let

$$y = F(x) \tag{1}$$

be some nonlinear unknown function describing a complex system. In this equation, $y \in \mathrm{IR}$ and $x \in \mathrm{IR}^N$ are the output scalar and input vector variables, respectively, available for the measurement at each *n*th time instant $(n = 1, 2, \ldots)$. This implies that

$$y(n) = F(x(n-1)) \tag{2}$$

with an unknown mapping $F:\ \mathrm{IR}^N \to \mathrm{IR}$.

To approximate (1), the two-layer neural network containing M $(M \geq 1)$ neurons in its hidden layer is employed. The inputs to the each *j*th neuron of this layer at the time instant n are the components of $x(n-1)$. Its output signal at the *n*th time instant is given by

$$y_j^{(1)}(n) = \sigma\left(b_j^{(1)} + \sum_{i=1}^{N} w_{ij}^{(1)} x_i(n-1)\right), \quad j = 1, \ldots, M, \tag{3}$$

where $x_i(n-1)$ denotes the *i*th component of $x(n-1)$, and $w_{ij}^{(1)}$ and $b_j^{(1)}$ are the weight coefficients and the bias of this *j*th neuron, respectively. $\sigma(\cdot)$ represents the so-called activation function. There is only one neuron in the output (second) layer, whose inputs are the outputs of the hidden layer's neurons. The output signal of second layer, $y^{(2)}(n)$, at the time instant n is determined by

$$y^{(2)}(n) = \sum_{j=1}^{M} w_j^{(2)} y_j^{(1)}(n) + b^{(2)}, \tag{4}$$

where $w_1^{(2)},\dots,w_M^{(2)}$ are the weights of this neuron and $b^{(2)}$ is its bias.

Since $\sigma(\cdot)$ is assumed to be nonlinear, it follows from (3), (4) together with (2) that $y^{(2)}(n)$ is a nonlinear function depending on $x(n-1)$ and also on the $(M(N+2)+1)$-dimensional parameter vector

$$w=[w_{11}^{(1)},\dots,w_{N1}^{(1)},b_1^{(1)},\dots,w_{1M}^{(1)},\dots,w_{NM}^{(1)},b_M^{(1)} \vdots w_1^{(2)},\dots,w_M^{(2)},b^{(2)}]^T.$$

To emphasize this fact, define the output signal of the neural network in the form

$$y^{(2)}(n)=\mathrm{NN}(x(n-1),\,w) \tag{5}$$

with $\mathrm{NN}:\ \mathrm{IR}^N\times\mathrm{IR}^{M(N+2)+1}\to\mathrm{IR}.$

The following basic assumption is made. There exists at least an unique $w=w^*\in\mathrm{IR}^{M(N+2)+1}$ such that $F(x)$ can explicitly be approximated by $\mathrm{NN}(x,\,w^*)$ in the sense of

$$F(x)\equiv\mathrm{NN}(x,\,w^*) \tag{6}$$

for all x from a given compact set $X\subset\mathrm{IR}^N$.

Define the training sequence $\{(x(n-1),\,y(n))\}_{n=1}^{\infty}$ of the measurable pairs in which $x(n-1)$s are taken randomly from X. Then, the online learning algorithm for updating the parameter estimate $w(n)$ is formulated as the following standard recursive gradient procedure:

$$w(n)=w(n-1)+\eta\,\tilde{e}(n,w(n-1))\ \mathrm{grad}_w\mathrm{NN}(x(n-1),w(n-1)). \tag{7}$$

In this algorithm,

$$\tilde{e}(n,w(n-1))=y(n)-\mathrm{NN}(x(n-1),\,w(n-1)) \tag{8}$$

is the current estimation error and $\mathrm{grad}_w\mathrm{NN}(x(n-1),w(n-1))$ denotes the gradient of $\mathrm{NN}(x,\,w)$ at the point $w=w(n-1)$, and $\eta\equiv\mathrm{const}>0$ is its step size (the learning rate) .

The problem is to study the properties of sequence $\{w(n)\}$ caused by (7), (8) as n tends to ∞.

To study the asymptotic behavior of (7), (8), the scalar non-negative function $V(w)$ given by

$$V(w)=0\ \text{ for } w=w^*,\qquad V(w)>0\ \text{ for } w\neq w^* \tag{9}$$

is exploited.

The variable $V_n:=V(w(n))$ becomes immediately the Lyapunov function of the algorithm (7), (8) if only

$$V_n\le V_{n-1}\quad\forall n. \tag{10}$$

Since $V_n\ge 0,$ the condition (10) under which V_n does not increase is sufficient for existing a limit

$$\lim_{n\to\infty} V_n=V_\infty, \tag{11}$$

where V_∞ is a random number depending on $w(0)$ and $\{x(n)\}$.

In the presence of the one-point $W^*=\{w^*\},$ the function $V(w)$ satisfying (9) is usually chosen as

$$V(w)=\left\|w^*-w\right\|^2, \tag{12}$$

where $\|\cdot\|$ denotes the Euclidean vector norm. It turned out that if the neural network contains the hidden layer, then W^* consists of several isolated w^*s. In particular, in the simplest case, when there is one neuron in the hidden layer $(N=1,\ M=1)$ and $\sigma(\cdot)$ is described by

$$\sigma(s)=\frac{1}{1+\exp(-s)}, \tag{13}$$

the set W^* contains two points: $\mathbf{w}_1^*=[w_1^*,w_2^*,w_3^*,w_4^*]^T$ and $\mathbf{w}_2^*=[-w_1^*,-w_2^*,-w_3^*,w_3^*+w_4^*]^T$.

In the case when W^* is not one-point, $V(w)$ is designed as

$$V(w) = \inf_{\mathbf{w}^* \in W^*} \left\| w^* - w \right\|^2 \qquad (14)$$

but not as defined in (12).

We first observed in simulation examples that $\{w(n)\}$ may not converge even in the presence of bounded $\{x(n)\}$ if there are no additional restrictions on this input sequence. Such an ultimate feature of (7), (8) implies that

$$\lim_{n\to\infty} w(n) = w_\infty \qquad (15)$$

may not exist. Nevertheless, if (15) is achieved, then the following asymptotic properties of $\{w(n)\}$ can be established:

a) $\{w(n)\}$ converges to some w_∞ in sense of (15) with

$$w_\infty \in \lim\inf W_n,$$

where

$$\lim\inf W_n := \bigcup_{n=1}^{\infty} \bigcap_{k=n}^{\infty} W_k$$

denotes the limit set in which $W_n := \{w: \ y(n) - \mathrm{NN}(x(n-1), w) = 0\}$;

b) the identification error given by (8) satisfies

$$\lim_{n\to\infty} \tilde{e}(n, w(n-1)) = 0. \qquad (16)$$

Note that $\lim\inf W_n$ represents a nonlinear manifold on $\mathrm{IR}^{M(N+2)+1}$ whose dimension satisfies

$$0 \le \dim \lim\inf W_n \le M(N+2).$$

To demonstrate these asymptotic properties, three simulation experiments with

$$y = \frac{3.75 + 0.05\exp(-7.15x)}{1 + 0.19\exp(-7.15x)}$$

was performed. This nonlinear function can explicitly be approximated by the two-layer neural network described by (5), (6), (8) and (13) with $w_{11}^{(1)*} = 7.15$, $b_1^{(1)*} = 1.65$, $w_1^{(2)*} = 3.45$, $b^{(2)*} = 0.3$. In all of these experiments, η was taken as $\eta = 0.02$.

The simulation results are depicted in Figures 1-3.

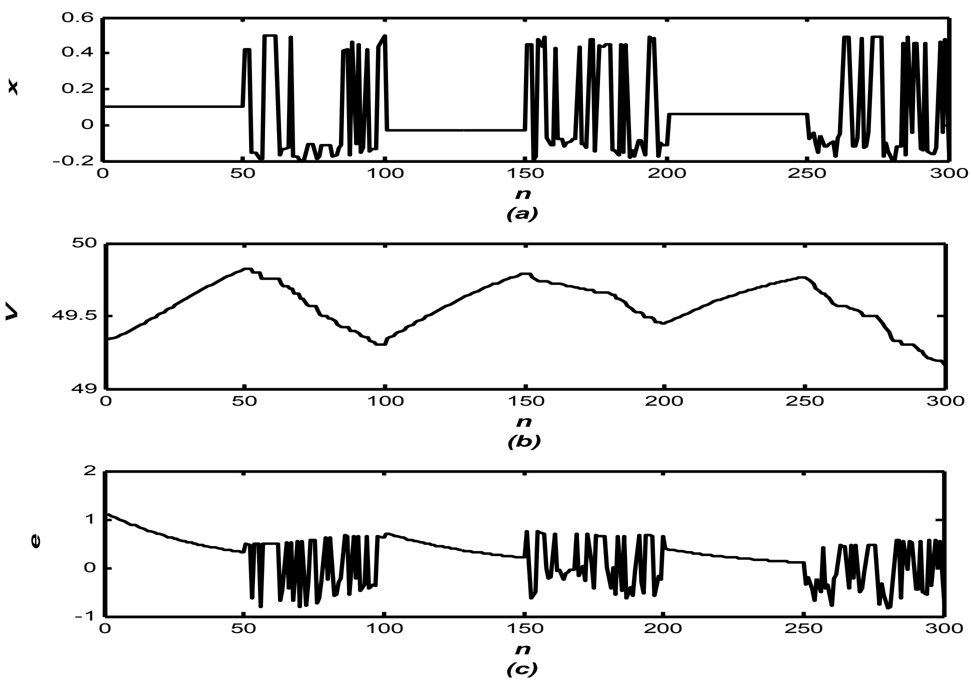

Fig. 1. Learning processes in simulation experiment 1:

(a) the input signal; (b) the function V_n given by (14); (c) the current model error

Fig. 1 shows that $\{V_n\}$ has no limit if the input sequence $\{x(n)\}$ is non-stochastic. (The definition of the non-stochastic sequence can be found in the paper [3].) In this case, the model error $\widetilde{e}(n, w(n-1))$ does not go to zero, i. e., (16) is not satisfied.

In second experiment, $x(n)$s were sequentially chosen from the finite set containing three points: $x^{(1)}$ =-0.4442; $x^{(2)} = 0.5158$; $x^{(3)}$ =0.8761. Fig. 2 illustrates the result of this experiment with initial $w_{11}^{(1)}(0) = 0.529$, $b_1^{(1)}(0)$ =-0.5012, $w_1^{(2)}(0)$ =-0.9168, $b^{(2)}(0) = 1.0409$.

We can observe that $\{V_n\}$ is convergent, however its convergence is not monotonic as in (10). It turned out that in this case, $\{w(n)\}$ converges to $w_\infty =$[5.4120, 1.3172, 3.8233, -0.0475]^T which lies on $\liminf W_n$ but not to one of two points $w_1^* =$[7.15, 1.65, 3.45, 0.3]^T or to $w_1^* =$[-7.15, -1.65, -3.45, 3.75]^T.

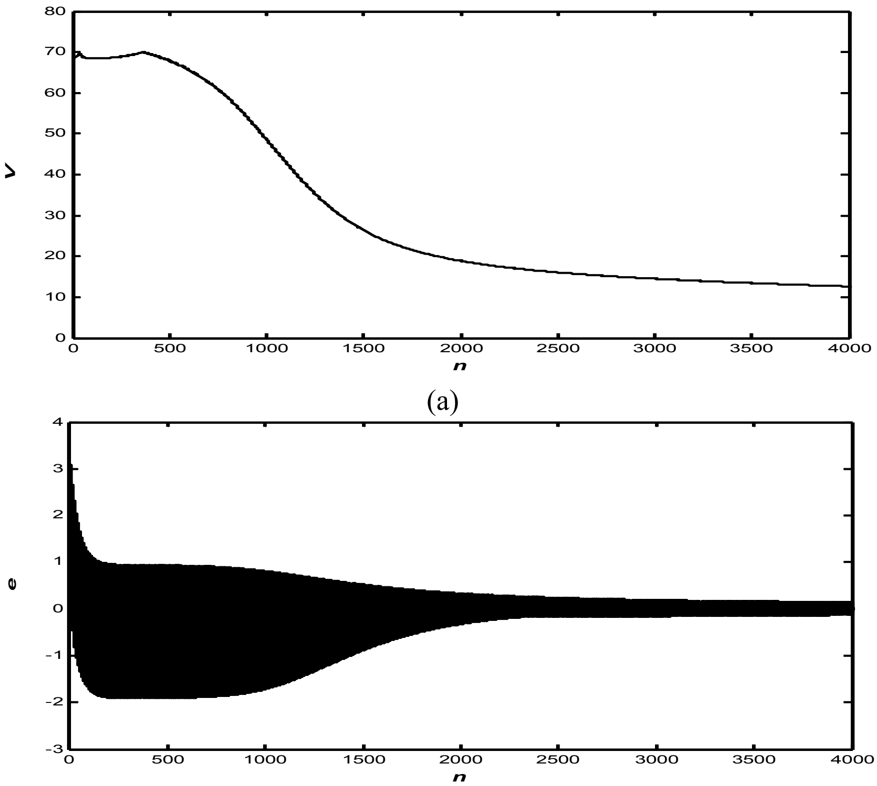

(a)

(b)

Fig. 2. Learning processes in simulation experiment 2:
(a) the function V_n given by (14); (b) the current model error

The case where $\{V_n\}$ converges monotonically is demonstrated in Fig. 3. In this case, the initial estimates were chosen as: $w_{11}^{(1)}(0) = 1.4$, $b_1^{(1)}(0)$ =-0.1, $w_1^{(2)}(0)$ =-0.56, $b^{(2)}(0) = 0.46$.

It turned out that $\{w(n)\}$ tends to the limit point $w_1^* =$[7.15, 1.65, 3.45, 0.3]^T as $n \to \infty$.

Our main theoretical result concerning the asymptotical behavior of (7), (8) is based on following additional assumptions:

$\{x_i(n)\}$ are the stochastic sequences of independent random variables having the probability density function

$$p(x(n) \mid x(n-1), \ldots, x(0)) \equiv p(x(n)) := p(x) \qquad (17)$$

with the properties that

$$P\{x(n) \in X'\} = \int_{x \in X'} p(x)\, dx > 0, \tag{18}$$

for any subset $X' \subset X$, and

$$P\{x(n) \in X''\} = 0 \tag{19}$$

if $\dim X'' = 0$, where $P\{\cdot\}$ denotes the probability of corresponding event.

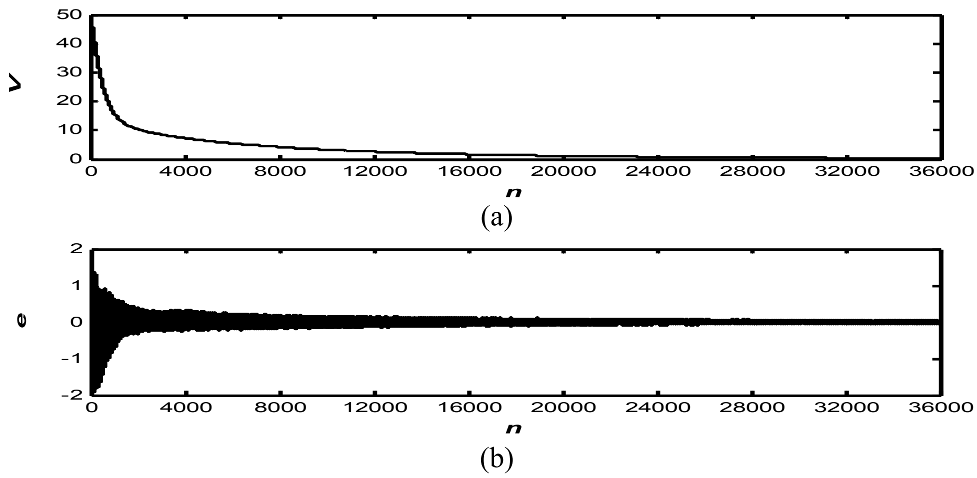

Fig. 3. Learning processes in simulation experiment 3:
(a) the function V_n given by (14); (b) the current model error

Let $W(w^*)$ denote a neighborhood of some $w^* \in W^*$ which does not contain another points of W^*. With this $W(w^*)$, we have established that if the assumptions (6), (17) – (19) are satisfied and the conditions

$$0 < \eta < 2,$$

$$\int_{x \in X} [\mathrm{NN}(x, w^*) - \mathrm{NN}(x, w)] \mathrm{grad}_w^T \mathrm{NN}(x, w)(w^* - w) p(x)\, dx \geq$$

$$\geq \int_{x \in X} [\mathrm{NN}(x, w^*) - \mathrm{NN}(x, w)]^2 \|\mathrm{grad}_w \mathrm{NN}(x, w)\|^2 p(x)\, dx$$

hold for any $x \in X$ and for arbitrary w from $W(w^*)$, then the limit (11) is valid with probability 1. Again, $\lim_{n\to\infty} w(n) = w^*$ almost sure (a. s.).

The proof of this result essentially utilizes the Borel – Cantelli lemma and Doob's martingale convergence theorem (see [3]).

Conclusions

In general case, the standard online gradient algorithms applied to sequential learning in neural networks with hidden layer may not converge. To guarantee their convergence, certain conditions need to be satisfied.

References

1. *Zhang H., Wu W., Liu F., Yao M.* Boundedness and convergence of online gradient method with penalty for feedforward neural networks // IEEE Trans. Neural Networks. – 2009. – 20, N 6. – P. 1050–1054.

2. *Xu Z., Zhang R., Jing W.* When does online BP training converge? // IEEE Trans. Neural Networks. – 2009. – 20, N 9. – P. 1529–1539.

3. *Azarskov V. N., Zhiteckii L. S., Nikolaienko S. A.* Convergence of learning algorithms in neural networks for adaptive identification of nonlinearly parameterized systems // Proc. 16th IFAC Symposium on System Identification (Brussels, Belgium, July 10 – 13, 2012). – 2012. – P. 323 – 328.

UDC 681.511.42.037.5(045)

A.A. Tunik, Prof, Doct. of Sci.(Eng.) (National Aviation University, Ukraine)
O.P. Basanets, PhD in Control Systems (National Aviation University, Ukraine)
M.M. Komnatska, PhD in Control Systems (National Aviation University, Ukraine)

LMI-BASED DESIGN OF SPINNING RIGID BODY ROBUST FLIGT CONTROL

This paper considers the problem of static output feedback (SOF) controller design with guaranteed cost and disturbance attenuation for robust flight control system (FCS) of spinning rigid body. The proposed design approach is based on the iterative linear matrix inequalities algorithm. The developed procedure of SOF controller synthesis is applied for synthesis of PID-controller, which is usually applied for spinning rigid body flight control. The simulation results prove the efficiency of the proposed approach.

Introduction

Automatic flight control of the spinning rockets and missiles is the basic mean for increasing their accuracy. Design procedures of such systems encounter with some essential difficulties connected with uncertainties of the controlled plant parameters and uncertainties of the mathematical models of the exogenous disturbances acting during control process. As far as the lifespan of these objects is very short additional problems occur that connected with law cost design and power consumption in order to be implemented onboard computer with restricted abilities. In turn, it leads to the limited number of navigation sensors, their size and weight. These circumstances lead to the application of the robust control theory for solving the problem of a static output feedback (SOF) controller design. The main advantage of SOF design is that it requires only available signals from the plant to be controlled. The SOF problem concerns finding a static or feedback gain to achieve certain desired closed-loop characteristics. A survey devoted to this problem is presented in [1]. Following this line of research, we consider the problem of robust static output controller synthesis for rotating solid body with guaranteed cost and disturbance attenuation at a predetermined level γ via LMI technique [2–7].

In the existing practice of flight control of such plants the application of the PID-controllers is very common approach. So far as PID-controllers belong to the dynamic output feedback, one of the main features of this paper implies reducing of the PID control law synthesis to the synthesis of the SOF. To illustrate the efficiency of the proposed approach a longitudinal channel of spinning rigid body is used as a case study.

Problem statement and preliminaries

A mathematical model of rotating solid body is derived as an envelope of amplitude modulated signal [3–4]. A state space vector of the longitudinal channel is $\mathbf{x}=[y,\dot{y},\ddot{y}]$, where y is the beam axis deflection, $\dot{y},\ddot{y}$ is the first and the second derivative of beam axis deflection, respectively. The control input vector $\mathbf{u}=\left[\ \delta_r\ \right]^T$ is represented by rudder deflection [3–4]. The control law is designed taking into account only variables that are available for measurement.

Let us consider the mathematical model of the controlled plant described by a difference equation

$$\begin{aligned}\mathbf{x}(k+1)&=\mathbf{A}_i\mathbf{x}(k)+\mathbf{B}_i\mathbf{u}(k)+\mathbf{B}_{g_i}g(k)\\ \mathbf{y}(k)&=\mathbf{C}\mathbf{x}(k)+\mathbf{F}r(k)\end{aligned}\tag{1}$$

where matrices $\mathbf{A}_i,\mathbf{B}_i$ are the elements of some polytope that satisfy the following condition $[\mathbf{A}\quad \mathbf{B}]\in Co\left\{[\mathbf{A}_1\quad \mathbf{B}_1],...,[\mathbf{A}_N\quad \mathbf{B}_N]\right\}$, i=1,...,N; $\mathbf{x}(k)$ is the state space vector, $\mathbf{u}(k)$ is the control vector, $\mathbf{y}(k)$ is the output vector of the system used for output feedback design and $g(k)$ is a disturbance vector. $\mathbf{A}\in\mathbf{R}^{n\times n},\mathbf{B}\in\mathbf{R}^{m\times n},\mathbf{C}\in\mathbf{R}^{p\times n}$ are known matrices of appropriate dimensions.

The functional diagram of closed loop system with PID – controller in a loop has the following structure (see Fig. 1)

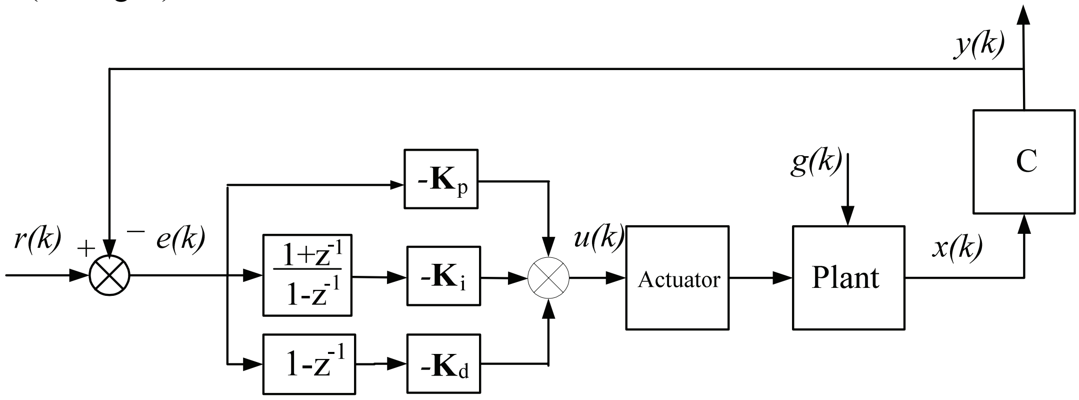

Figure 1 Control system

To facilitate procedure of dynamic feedback control design let us incorporate PID controller dynamics into plant dynamics. Furthermore, the controller dynamics is represented as a collection of static and dynamic parts. Thus, the dynamic part of the controller is described by the difference equations as follows

$$\begin{aligned} w(\mathrm{k+1}) &= \mathbf{F}w(\mathrm{k}) + \mathbf{G}\mathrm{e}(\mathrm{k}), \\ v(\mathrm{k}) &= \mathbf{M}w(\mathrm{k}) + \mathbf{J}\mathrm{e}(\mathrm{k}) \end{aligned} , \tag{2}$$

where $w(\mathrm{k})$ is the state space vector of PID – controller; $v(\mathrm{k})$ is the output vector of PID – controller; $\mathrm{e}(\mathrm{k}) = \mathrm{r}(\mathrm{k}) - \mathrm{y}(\mathrm{k})$ is a stabilization error. $\mathbf{F}$, $\mathbf{G}$, $\mathbf{M}$, $\mathbf{J}$ are known matrices chosen to include the desired structure in the controller. The static part of the PID – controller is given as a column matrix in the following way

$$\mathbf{K} = \begin{bmatrix} \mathbf{K}_{\mathrm{p}} & \mathbf{K}_{\mathrm{i}} & \mathbf{K}_{\mathrm{d}} \end{bmatrix}^{\mathrm{T}}. \tag{3}$$

Thus, the structure of closed –loop system with PID – controller in the loop is possible to represent in the following way (Fig.2)

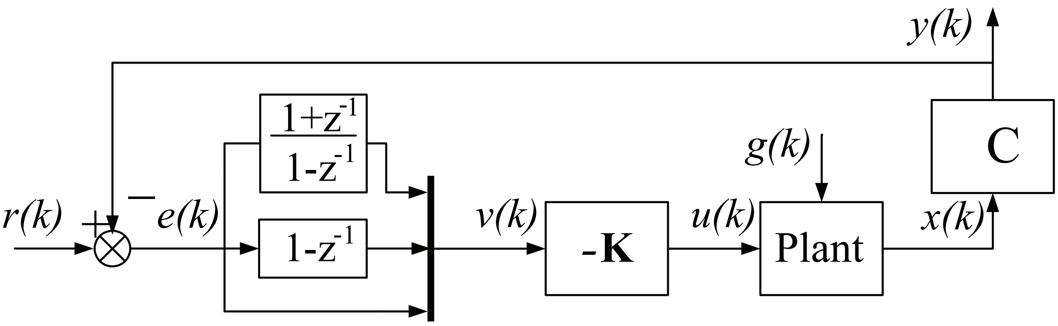

Figure 2 Structural block – scheme of closed-loop system

In order to solve the problem PID – controller design let us reduce it to the problem of static output feedback design. Further, it is possible to solve our problem in LMI (linear matrix inequality) form. The PID – controller dynamics and output equations may be rewritten in augmented form as [3]:

$$\begin{bmatrix} \mathbf{x}(\mathrm{k+1}) \\ w(\mathrm{k+1}) \end{bmatrix} = \begin{bmatrix} \mathbf{A}_{\mathrm{i}} & 0 \\ -\mathbf{GH} & \mathbf{F} \end{bmatrix} \begin{bmatrix} \mathbf{x}(\mathrm{k}) \\ w(\mathrm{k}) \end{bmatrix} + \begin{bmatrix} \mathbf{B}_{\mathrm{i}} \\ 0 \end{bmatrix} \mathbf{u}(\mathbf{k}) + \begin{bmatrix} 0 \\ \mathbf{G} \end{bmatrix} \mathbf{r}(\mathrm{k}) + \begin{bmatrix} \mathbf{B}_{g_{\mathrm{i}}} \\ 0 \end{bmatrix} g(\mathrm{k}),$$

$$\begin{bmatrix} \mathbf{y}(\mathrm{k}) \\ v(\mathrm{k}) \end{bmatrix} = \begin{bmatrix} \mathbf{C} & 0 \\ -\mathbf{JH} & \mathbf{M} \end{bmatrix} \begin{bmatrix} \mathbf{x}(\mathrm{k}) \\ w(\mathrm{k}) \end{bmatrix} + \begin{bmatrix} 0 \\ \mathbf{J} \end{bmatrix} \mathbf{r}(\mathrm{k}),$$

The control law is given by

$$\mathbf{u}(k) = -\mathbf{K}\mathbf{y}(k) = -\mathbf{K}\,\mathbf{C}\,\mathbf{x}(k) = -\mathbf{K}\nu(k) \tag{4}$$

where $\mathbf{y} = [v]$, $\mathbf{x} = [x \quad w]^{T}$ and $\mathbf{K}$ is a constant output feedback gain, that minimizes performance index

$$\mathbf{J} = \sum_{k} \left\|\mathbf{z}(k)\right\|^{2} = \sum_{k} \left(\mathbf{x}^{T}(k)\mathbf{Q}\mathbf{x}(k) + \mathbf{u}^{T}(k)\mathbf{R}\mathbf{u}(k)\right),$$

where $\mathbf{Q} \geq 0$ and $\mathbf{R} > 0$ are diagonal matrices, weighting each state and control variables, respectively.Output signal $\mathbf{z}(k)$ used for performance evaluation is defined as follows:

$$\mathbf{z} = \begin{bmatrix} \sqrt{\mathbf{Q}} & 0 \\ 0 & \sqrt{\mathbf{R}} \end{bmatrix} \begin{bmatrix} \mathbf{x} \\ \mathbf{u} \end{bmatrix}.$$

Bounded L_2 Gain Design Problem

The system L_2 gain is said to be bounded or attenuated by γ if [3, 7 –8]:

$$\frac{\sum_{k} \left\|\mathbf{z}(k)\right\|^{2}}{\sum_{k} \left\|g(k)\right\|^{2}} = \frac{\sum_{k} \left(\mathbf{x}^{T}(k)\mathbf{Q}\,\mathbf{x}(k) + \mathbf{u}^{T}(k)\mathbf{R}\mathbf{u}(k)\right)}{\sum_{k} \left(g^{T}(k)g(k)\right)} \leq \gamma^{2}.$$

Therefore, it is necessary to find constant output feedback gain matrix $\mathbf{K}$ that stabilizes the control plant such that the infinity norm of the transfer function referring exogenous input to performance output $\mathbf{z}(k)$ approaches minimum. The minimum gain is denoted by γ^{*}.

According to the proposed approach, in this paper it is necessary to find SOF controller that simultaneously stabilizes the set of autonomous systems (1). The output feedback gain matrix $\mathbf{K}$ could be found by solving the following iterative LMI:

$$\begin{bmatrix}
\mathbf{Y}_n & \mathbf{Y}_n(\mathbf{A}_i - \mathbf{M}\mathbf{Y}_n^{-1} - \mathbf{F})^{T} & \mathbf{Y}_n & \mathbf{B}_{g_i}^{T} & \mathbf{F}\mathbf{Y}_n + \mathbf{Y}_n F^{T} & \mathbf{B}_i^{T} & \mathbf{Y}_n\mathbf{L}_n^{T} \\
(\mathbf{A}_i - \mathbf{M}\mathbf{Y}_n^{-1} - \mathbf{F})\mathbf{Y}_n & -\mathbf{Y}_n & 0 & 0 & 0 & 0 & 0 \\
\mathbf{Y}_n & 0 & -\mathbf{Q}^{-1} & 0 & 0 & 0 & 0 \\
\mathbf{B}_{g_i} & 0 & 0 & -\gamma^{2}\mathbf{I} & 0 & 0 & 0 \\
0 & 0 & 0 & 0 & \mathbf{I} & 0 & 0 \\
\mathbf{B}_i & 0 & 0 & 0 & 0 & -\mathbf{R} & 0 \\
\mathbf{L}_n\mathbf{Y}_n & 0 & 0 & 0 & 0 & 0 & -\mathbf{R}
\end{bmatrix} < 0, \tag{5}$$

where $i = 1, \ldots, N$ in (5) denotes the set of models associated with certain operating conditions within the flight envelope. The matrices $\mathbf{K}$ and $\mathbf{L}$ for each n-th iteration are updated as follows:

$$\mathbf{K}_{n+1} = \mathbf{R}^{-1}\left(\mathbf{B}^{T}\mathbf{P}_n + \mathbf{L}_n\right)\mathbf{C}^{T}\left(\mathbf{C}\mathbf{C}^{T}\right)^{-1}$$

$$\mathbf{L}_{n+1} = \mathbf{R}\,\mathbf{K}_{n+1}\mathbf{C} - \mathbf{B}^{T}\mathbf{P}_n$$

On the last stage a convergence is checked, namely if $\left\|\mathbf{K}_n - \mathbf{K}_{n+1}\right\| \leq \varepsilon$ (if $\mathbf{K}_{n+1}$ and $\mathbf{K}_n$ are close enough to each other) than terminate and set $\mathbf{K} = \mathbf{K}_{n+1}$, otherwise set $n = n+1$ and solve the inequality (5).

Case Study

To illustrate the efficiency of the proposed approach a longitudinal channel of spinning rigid body flight control system as a part of the laser beam guidance system is used as a case study [3]. The extended state space vector of longitudinal channel with PID – controller in a feedback has the following form $\mathbf{x}_{ex}^{PID} = [y, \dot{y}, \ddot{y}, \int y]^{T}$, where y is the beam axis deflection, $\dot{y}, \ddot{y}$ is the first and the second derivative of beam axis deflection, respectively. The control input vector is as defined above. The extended state space and control matrices for nominal and parametrically perturbed models have the following form

$$\mathbf{A}_{n_{ex}}^{PID} = \begin{bmatrix} 1 & -0.0006 & 7.48\cdot10^{-6} & 0 \\ 0 & -0.8 & -0.0068 & 0 \\ 0 & 164.4 & -0.7944 & 0 \\ 0.02 & 8.7\cdot10^{-6} & 8.53\cdot10^{-8} & 1 \end{bmatrix}, \quad \mathbf{B}_{n_{ex}}^{PID} = \begin{bmatrix} 9.7\cdot10^{-3} \\ 0.8511 \\ -77.74 \\ 9.03\cdot10^{-5} \end{bmatrix}, \quad \mathbf{C}_{n_{ex}}^{PID} = \begin{bmatrix} 1 & 0 & 0 & 0 \\ 0 & 1 & 0 & 0 \\ 0 & 0 & 0 & 1 \end{bmatrix},$$

$$\mathbf{A}_{p_{ex}}^{PID} = \begin{bmatrix} 1 & -6.59\cdot10^{-4} & 9.89\cdot10^{-7} & 0 \\ 0 & -0.909 & -0.0066 & 0 \\ 0 & 61.3 & 0.9136 & 0 \\ 0.02 & 2.53\cdot10^{-6} & 2.24\cdot10^{-7} & 1 \end{bmatrix}, \quad \mathbf{B}_{p_{ex}}^{PID} = \begin{bmatrix} 0.0639 \\ 0.2814 \\ -189.6 \\ 6.1\cdot10^{-4} \end{bmatrix}, \quad \mathbf{C}_{p_{ex}}^{PID} = \begin{bmatrix} 1 & 0 & 0 & 0 \\ 0 & 1 & 0 & 0 \\ 0 & 0 & 0 & 1 \end{bmatrix}.$$

The resulting coefficients of PID – controller are given below

$$\mathbf{K}_p = 2.75\,,\ \mathbf{K}_d = 1.7087\,,\ \mathbf{K}_i = 0.0099\,.$$

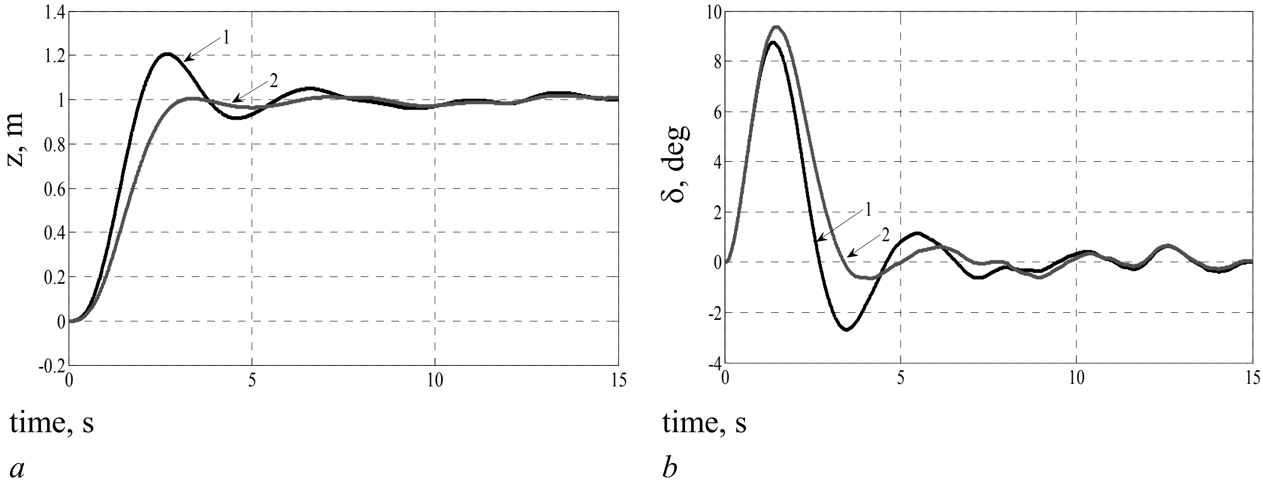

Figure 3. Simulation results of closed – loop system with PID – controller in a loop for nominal (1) and parametrically perturbed (2) models:
a – deflection from beam axis in m; *b* – rudder deflection in deg.

The H_2-norms of the closed loop system sensitivity functions for the nominal and perturbed models are: $H_{2n} = 0.0501$ and $H_{2p} = 0.0208$. The H_∞-norms for a set of nominal and perturbed closed loop complementary sensitivity functions are found to be equal to $H_{\infty n} = 1.3521$ and $H_{\infty p} = 1.7430$. As it is known from the robust control theory [8] small values of these norms show that desirable compromise between performance and robustness of the control system is achieved.

Conclusions

The simulation results of spinning rigid body motion prove the effectiveness of the proposed control approach. The required flight performances are respected as well as the robustness of the closed loop system. Thus, the SOF design algorithm based on LMI provides easy and efficient control.

References

1. *Syrmos V.L.* Static Output Feedback: a survey / *V.L. Syrmos, C. Abdallah and P. Dorato* // Proceedings of 33rd IEEE Conference on Decision and Control, Orlando, FL. – pp. 837 – 842.
2. *Boyd S.* Linear Matrix Inequalities in System and Control Theory / *S. Boyd, L. El Ghaoui, E. Feron, V. Balakrishnan*.– Philadelphia, PA SIAM, 1994.–416 p.
3. *Басанец О.П.* Моделирование процесса наведения по лучу вращающегося твердого тела / *О.П. Басанец, А.А. Туник* // Електроніка та системи управління. – 2010. – №4. – С. 148–155.
4. *О.П. Басанец* Синтез следящей системы наведения вращающегося БПЛА с помощью линейных матричных неравенств / *О.П. Басанец, А.А. Туник* // Кибернетика и вычислительная техника. – 2011. – Выпуск 164. – С.17–28.
5. . *Gadewadikar J.* Necessary and Sufficient Conditions for H-infinity Static Output Feedback Control / *J. Gadewadikar, F. Lewis, M. Abu-Khalaf //* Journal of Guidance, Control and Dynamics.– 2006.– Vol. 29.– pp. 915 – 921.
6. *Gadewadikar J.* Aircraft Flight Controller Tracking Design Using H-Infinity Static Output-Feedback / *J. Gadewadikar, F. Lewis //* Transactions of the Institute of Measurement and Control.– 2006.–Vol. 28.– No.8.– pp. 429 – 440.
7. *Tunik A*.A. An ILMI Design of Flight Control System with Fuzzy Controllers / *A.A. Tunik, M.M. Komnatska* // Інформаційні системи, механіка, керування. – 2010. Випуск 5. – С. 119–129.
8. *Kwakernaak H*. Robust Control and H_∞ - Optimization / *H. Kwakernaak* // Automatica. – 1993. – Vol.29. – №.2. – P. 255–273.

UDC 621.396.933; 629.783 (045)

Larin V.B., Tunik A.A., Valdenmayer G.G.
(National Aviation University, Ukraine)

ACCELERATED INITIAL ALIGNMENT PROCEDURE OF STRAP-DOWN INERTIAL NAVIGATION SYSTEM BASED ON EXTENDED KALMAN FILTERING AND STOCHASTIC APPROXIMATION

The initial alignment procedure of the strap-down inertial navigation system (SINS) consisting of two stages is proposed. The 1st stage is the coarse alignment procedure using accelerometers and magnetometers data. The 2nd stage is the improving fine alignment procedure due to the combined application of the Kalman filter and the stochastic approximation algorithm. Developed initial alignment algorithm allows to accelerate execution and to increase accuracy of the entire procedure.

The sensor unit of the modern SINS consists of 3-axis rate gyros and 3-axis accelerometers based on MEMS technology. These systems don't measure absolute attitude. They obtain the angle of orientation due to integrating data from 3-axis rate gyros. But any integration procedure needs to possess the information about initial attitude. Concerning this to obtain the correct information about current orientation it is necessary to carry out an essential pre-flight procedure – initial alignment.

The main essence of initial alignment procedure is to determine the angles of the UAV's orientation in the selected navigation frame. Experience of using SINS in UAV navigation shows the accuracy of initial alignment procedure is very crucial, because accuracy of determining attitude of UAV in flight depends on accuracy of this procedure. Therefore nowadays the efforts of many researchers from around the world are aimed at developing such a procedure of initial alignment, which satisfies two basic requirements. On the one hand this procedure has to require minimal computation time and complexity of implementation in the on-board computers, and on the other hand it has to ensure maximum accuracy of determining UAV's attitude [1].

The main advantage of most SINS based on MEMS-sensors is small size and price. However these sensors have several disadvantages, the main ones are low accuracy and measurement errors that accumulate over time. Despite the low accuracy of the sensors, requirements to accuracy and speed of measuring main navigation parameters (position, velocity, attitude) is quite high because UAVs are very manoeuvrable. Therefore, this condition demands to integrate various sensors and use advanced mathematical algorithms for data processing.

In the article some mathematical algorithms to accelerate this procedure and improve its accuracy will be considered. Initial alignment procedure consists of two phases:

- coarse alignment – preliminary estimation of initial attitude;
- fine alignment – precise determination of angles of orientation.

Coarse alignment is quite easy for implementation. It is a preliminary determination of the attitude of SINS using simple analytical calculation and data from sensors (accelerometers, gyros, magnetometers). Results of coarse alignment are applied as initial values for fine alignment.

The procedure of fine alignment is more complicated and requires more time for conducting because of using advanced mathematical methods of stochastic estimation. The most popular mathematical algorithm used in SINS fine alignment is Extended Kalman Filter (EKF).

The most commonly applied way of the UAV initial attitude determination is an autonomous alignment, which uses the data of only sensors of SINS (accelerometers and gyros), without information from external sensors (magnetometer, altimeter, etc.).

However it is known that gyros based on MEMS technologies don't have high precision and resolution, as a result, they can't measure the components of angular rate of the Earth rotation. Therefore, the use of data from only accelerometers and gyros during the initial alignment of the navigation system will lead to mistaken determination of the initial attitude of SINS. To avoid this problem it has been proposed to use magnetometers and accelerometers data for initial alignment of SINS based on MEMS-sensors.

For coarse alignment the method proposed in the article [1] is applied. This method employs data of magnetometers, accelerometers and determines the initial quaternion of SINS orientation.

Having calculated the vectors of the components of the magnetic field of the Earth **M** and gravitational acceleration **G** in the navigation frame and received the vectors of sensor readings – vector of magnetometer readings **m** and accelerometer readings **g** in the inertial frame, the quaternion that describes the rotation to the coincide frames is determined.

Firstly the vector $\mathbf{k_0}$ in the navigation frame is calculated:

$$k_0 = [M \times G].$$

Secondly the vector $\mathbf{k_1}$ in the inertial frame is calculated.

$$k_1 = [m \times g].$$

Then the angle $\boldsymbol{f}$ between vectors $\mathbf{k_0}$ and $\mathbf{k_1}$ is determined

$$s = k_0 \times k_1; \qquad c = k_0 \circ k_1; \qquad f = arctg\frac{norm(s)}{c}, \tag{1}$$

where $\boldsymbol{s}$ – cross product of $\mathbf{k_0}$ and $\mathbf{k_1}$, $\boldsymbol{c}$ – scalar product of $\mathbf{k_0}$ and $\mathbf{k_1}$.

Having calculated the angle $\boldsymbol{f}$ it is possible to introduce the quaternion of rotation $\mathbf{q_0}$ [1]:

$$q_0 = \left[cos\left(\frac{f}{2}\right) \quad s_x\, sin\left(\frac{f}{2}\right) \quad s_y\, sin\left(\frac{f}{2}\right) \quad s_z\, sin\left(\frac{f}{2}\right) \right], \tag{2}$$

where $\mathbf{s_x}$, $\mathbf{s_y}$, $\mathbf{s_z}$ – elements of vector $\boldsymbol{s}$ from expression (1).

In the same way the angle of rotation of vector $\mathbf{k_1}$ around axis Oy (East) of navigation frame is determined

$$s = [p_0 \times p]; \qquad c = p_0 \circ p, \qquad j = arctg\frac{norm(s)}{c}. \tag{3}$$

where

$$p_0 = \frac{M+G}{norm(M+G)}; \; p_1 = \frac{m+g}{norm(m+g)}; \;\; p = A^T p_1, \tag{4}$$

A – Direction Cosine Matrix (DCM) calculated from quaternion $\mathbf{q_0}$.

Having calculated the angle $\boldsymbol{j}$ it is possible to introduce the quaternion of rotation $\mathbf{q_1}$ according to expression (2):

$$q_1 = \left[cos\left(\frac{j}{2}\right) \quad s_x\, sin\left(\frac{j}{2}\right) \quad s_y\, sin\left(\frac{j}{2}\right) \quad s_z\, sin\left(\frac{j}{2}\right) \right]. \tag{5}$$

Finally quaternions $\mathbf{q_1}$ and $\mathbf{q_0}$ are multiplied to acquire the quaternion of rotation **q**, that describes the initial attitude of SINS in navigation frame:

$$q = q_0 \times q_1. \tag{6}$$

Using proposed algorithm of coarse alignment it is impossible to obtain precise information about initial orientation, because the result will include all measuring errors of sensors.

In order to receive more accurate initial attitude it is necessary to perform procedure of fine alignment. As it has previously been said the fine initial alignment algorithm (IAA) is based on applying Extended Kalman Filter [3].

Transition matrix **C** (or Direction Cosine Matrix DCM) transforms the orientation of SINS from inertial to navigation frame and it has to be determined as a result of IAA performing. The initial estimation of matrix **C** is calculated from mean value of quaternion **q** received as a result of coarse alignment. Then this value of matrix **C** is estimated and calculated more precisely. If at some i-step of this procedure matrix **C** could be estimated as C_i^*, then it would contain some misalignment described by some matrix **A** and so:

$$C = A_i \cdot C_i^* \tag{7}$$

The main assumption is based on the small values of misalignment angles ϕ_x, ϕ_y, ϕ_z. This assumption makes possible to present matrix $\mathbf{A_i}$ as follows:

$$A_i \cong I + \Phi_i \qquad \Phi_i = \begin{bmatrix} 0 & -\phi_z(i) & \phi_y(i) \\ \phi_z(i) & 0 & -\phi_x(i) \\ -\phi_y(i) & \phi_x(i) & 0 \end{bmatrix} \tag{8}$$

and I is the unit 3×3 matrix. The vector of the misalignment angles $\phi = [\phi_x, \phi_y, \phi_z]'$ is the state vector of the Kalman filter (KF). Since these angles are constant during alignment procedure, its derivatives are equal to zero: $d\phi / dt = 0$, the state-space matrix in discrete form is equal to I and the state-space noise is absent. This fact eliminates procedures of state-space and covariance matrix propagation, only updating after measurement's vector $\phi = [\phi_x, \phi_y, \phi_z]'$ and covariance matrix P remains. It essentially simplifies the KF procedure. If $\vec{a}$ and $\vec{m}$ are the vectors of total (gravity and centripetal) acceleration and the Earth magnetic field respectively, then the measurement could be represented as

$$m_a = \vec{a}_N - C^* \cdot \vec{a}_S, \qquad m_m = \vec{m}_N - C^* \cdot \vec{m}_S, \tag{9}$$

where $\vec{a}_N, \vec{m}_N$ are aforementioned vectors in the navigation frame and $\vec{a}_S, \vec{m}_S$ are the same vectors in the inertial frame. The pair $\vec{a}_N, \vec{m}_N$ could be easily determined for given local latitude of this frame's common origin, while the pair $\vec{a}_S, \vec{m}_S$ is determined by the real measurements.

Vector $M = [m_a, m_\omega]'$ could be considered as the measured estimation of misalignment. After introducing the following vectors:

$$\alpha = C^* \cdot \vec{a}_S, \qquad \beta = C^* \cdot \vec{m}_S, \ , \tag{10}$$

it is possible to introduce the following matrices:

$$H_a = \begin{bmatrix} 0 & \alpha_z & -\alpha_y \\ -\alpha_z & 0 & \alpha_x \\ \alpha_y & -\alpha_x & 0 \end{bmatrix}, \qquad H_\omega = \begin{bmatrix} 0 & \beta_z & -\beta_y \\ -\beta_z & 0 & \beta_x \\ \beta_y & -\beta_x & 0 \end{bmatrix}. \tag{11}$$

These matrices could be incorporated into one matrix of measurement H:

$$H = [H_{a,} H_\omega]'. \tag{12}$$

Using this matrix it is possible to calculate theoretical estimation M_{th} of the measured vector M:

$$M_{th} = H \cdot \phi + C_\eta \cdot \eta, \tag{13}$$

where vector $\eta = [\vec{\tilde{a}}, \vec{\tilde{m}}]'$ is the vector of measurements' noises and matrix C_η is equal:

$$C\eta = \begin{bmatrix} C^* & 0_3 \\ 0_3 & C^* \end{bmatrix}, \tag{14}$$

matrix 0_3 being 3×3 zero matrix. Covariance matrices of accelerometers and magnetometers noises are denoted as C_{oa}, C_{om}, then covariance matrix of measurements R would be equal:

$$R = \begin{bmatrix} C^* C_{oa} C^{*T} & 0_3 \\ 0_3 & C^* C_{om} C^{*T} \end{bmatrix} \tag{15}$$

So the innovation vector In necessary for updating the state vector ϕ and covariance matrix P of state variables could be expressed as

$$In = M - M_{th}. \tag{16}$$

Now it is possible to represent the whole algorithm at each i-step as following procedure:
1. Calculation of the Kalman gain matrix:

$$K_i = P_{i-1} \cdot H_i^T \cdot (H_i \cdot P_{i-1} \cdot H_i^T + R_i)^{-1} \tag{17}$$

2. State vector updating

$$\phi_i = \phi_{i-1} + K_i \cdot (M_i - H_i \cdot \phi_{i-1}) \tag{18}$$

3. Covariance matrix updating

$$P_i = (I - K_i \cdot H_i) \cdot P_{i-1} \tag{19}$$

4. Calculation of the matrix Φ_i and updating the matrix C_i^* :

$$C_i^* = (I + \Phi_i) \cdot C_{i-1}^* \ . \tag{20}$$

Final result of procedure is the estimated values of misalignment angles via elements of matrix Ci*: $c_{23}^*(N) = \phi_x, c_{13}^*(N) = -\phi_y, c_{12}^*(N) = \phi_z$. N number of last step of alignment procedure.

This algorithm was applied to the initial alignment procedure of the motionless body with a good result but some convergence-related problems remained. They could be explained by the following reasons. From equation (20) it follows that to produce final result from KF variables it is necessary to produce their additional integration. So if KF converges, but convergence is slow, then after KF state variables integration large values of error may occur. Further improvement of algorithm was made on the basis of combination KF and accelerated stochastic approximation approach [4]. As it was shown in [4] SA could enhance the estimation of weakly observable variables. We denote the state vector updating increment in (18) as:

$$in(i) = K_i \cdot (M_i - H_i \cdot \phi_{i-1}) \tag{21}$$

and so: $$\phi_i = \phi_{i-1} + in(i)\ . \tag{22}$$

Due to the [4] application of combined (KF+SA)-procedure gives

$$\phi_i = \phi_{i-1} + in(i) + S_a(i) \cdot in(i) \tag{23}$$,

and so due to the (22) state vector, updated after SA-procedure, could be expressed as:

$$\phi_i = \phi_i + S_a(i) \cdot (\phi_i - \phi_{i-1}), \tag{24}$$

where $S_a(i)$ is the matrix coefficient of the stochastic approximation. In the simplest Robbins-Monroe SA-procedure it is equal to the simplest value $S_a(i) = 1/i$. In the more sophisticated but more effective accelerated Kesten method of SA-procedure its value depends on the actual behaviour of smoothed sequence [5]. The scalar stochastic approximation gains $S_a(i)$ (i=1,…, N) for each j-th estimated variable is calculated due to the following expressions:

for i=1,2 : $S_a(i) = 1/i$,

for i>2 : $S_j(i) = 1/t_j(i)$,

where : $$t_j(i) = 2 + \sum_{i=3}^{\infty}\{-0.5 \cdot sign[(in_j(i) - in_j(i-1)) \cdot (in_j(i-1) - in_j(i-2))] - 1\}. \tag{25}$$

The main idea of this SA-procedure is based on the fact that SA-gain is decreasing only, when sign of the expression inside the square brackets of (25) is negative, and so innovations are changing their signs in the vicinity of steady- state point. In other case the increment of $t_j(i)$ is zero and the value $S_j(i)$ is the same as at the previous step, thus accelerating the convergence and accuracy of this procedure in comparison with the simplest Robbins-Monroe SA- procedure. Experimentally it was proved that for accelerating of the convergence of this procedure it is much better to use the accumulated first differences of innovations.

In order to check the efficiency of proposed algorithms their simulation in Matlab was conducted. For mathematical simulation the following values of the RMS of accelerometers and magnetometers measurement noises were accepted accordingly: $\sigma_a = 0.02\, m/s^2$, $\sigma_m = 3\,°/s$. The simulation of the initial alignment algorithm has lasted for 220 s. Two different combinations of mathematical methods have been applied:

- IAA without stochastic approximation and coarse alignment;
- IAA with stochastic approximation and coarse alignment.

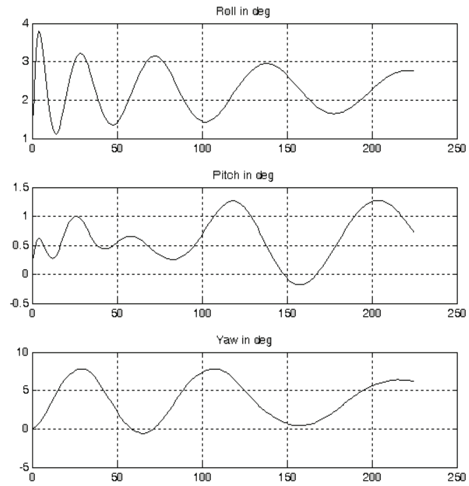

Fig 1 – Angles of initial attitude (IAA without stochastic approximation and coarse alignment)

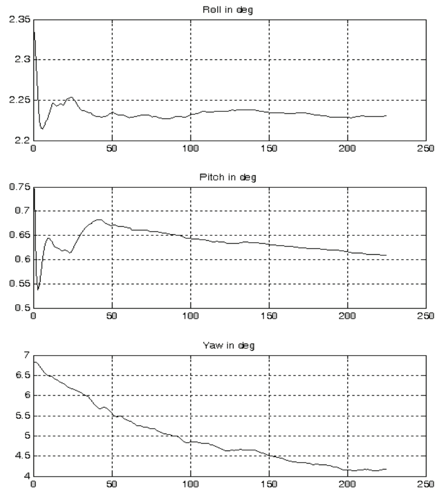

Fig 2 – Angles of initial attitude (IAA with stochastic approximation and coarse alignment)

As it can be seen from Fig. 1, the IAA based on EKF without coarse alignment and stochastic approximation algorithms is unstable and does not provide sufficient conditions for convergence of procedure KF, and therefore the algorithm does not provide sufficient accuracy.

As it is shown in Figure 2, the IAA with stochastic approximation methods of Robbins-Monroe and Kesten significantly improves the accuracy of determination of the initial attitude and significantly accelerates the procedure.

As shown in Figure 1-2, the best accuracy of the initial attitude is provided to pitch and roll, because these angles are determined by data of the accelerometers that provide quite precise measurements in the static mode without significant noise and errors. The accuracy of yaw is worse, since it is based on data of magnetometer, which possesses a number of errors and noise in both dynamic and static modes. However, applying the developed IAA allows to obtain much higher accuracy of the initial attitude in comparison with classical methods (EKF). Thus, measurement accuracy of initial angles are estimated as follows: pitch and roll - 0,02 °, yaw - 0,2 °

Conclusion

In the article combined apply of EKF and SA algorithms for initial alignment procedure is proposed. The apply of two SA algorithms – Robbins-Monroe and Kesten, significantly accelerated initial alignment procedure and improved the accuracy of determination of initial attitude despite using MEMS sensors with low precision as a source of information.

References

1. *В.Б. Ларін, А.А. Тунік, Г.Г. Вальденмайєр.* Процедура початкової виставки безплатформової інерціальної навігаційної статті (БІНС) для малого безпілотного літального апарату (МБПЛА) // Системи управління, навігації та зв'язку. – 2012. - №1(21). - С.1-11

2. *J.J.Deist Jr., A.A.Sutherland Jr.* Strapdown Inertial System Alignment Using Statistical Filters: A Simplified Formulation. AIAA Journal, vol.11,1973, No.4, pp.452-456.

3. *Grewal M.S., Andrews A.P.* Kalman Filtering.– Englewood Cliffs, N.J.: Prentice Hall, 1993.– 381 p.

4. *J.C.Kim, S.J.Lee, A.A.Tunik.* The Nonlinear State Estimation of the Aircraft using the Adaptive Extended Kalman Filter. Journal of Control, Automation and Systems Engineering, ICASE, Korea, Vol.5, No.2, 1999, pp. 158-165.

5. *H.Kesten.* Accelerated Stochastic Approximation. Ann.Math.Stat.,29 (1958), pp. 41-59

UDC 629.3.025.2

O.A. Sushchenko, Cand. of Sci. (Eng.), (National Aviation University, Ukraine)

ROBUST OPTIMIZATION OF THE PRECISION NAVIGATION MARINE SYSTEMS

The problems of optimal precision navigation marine systems design taking into consideration uncertainty of their mathematical description and the external disturbances are considered. The basic modes of operation of the systems to be studied are listed. The modern methods of the parametrical and structural robust optimization suitable for both modernization and creation of the new systems are studied.

The instrument making industry of the Ukraine has significant achievements in the area of the precision navigation systems attended for exploitation at the marine vehicles.

Such systems allow solving the following specific tasks such as:

1) the coarse stabilization of navigation sensors (the accelerometers) in the mode of the previous leveling;

2) the precise stabilization of navigation sensors (the gyros and accelerometers) in the mode of the precision leveling;

3) the initial alignment (setting to the meridian);

4) the combined stabilization and precision heading determination in the mode of the gyrocompass;

5) the combined stabilization and precision direction determination in the mode of the gyroazimuth;

6) the calibration of navigation sensors during the process on functioning and berthing.

The structural scheme of the precision navigation marine system is represented in fig. 1.

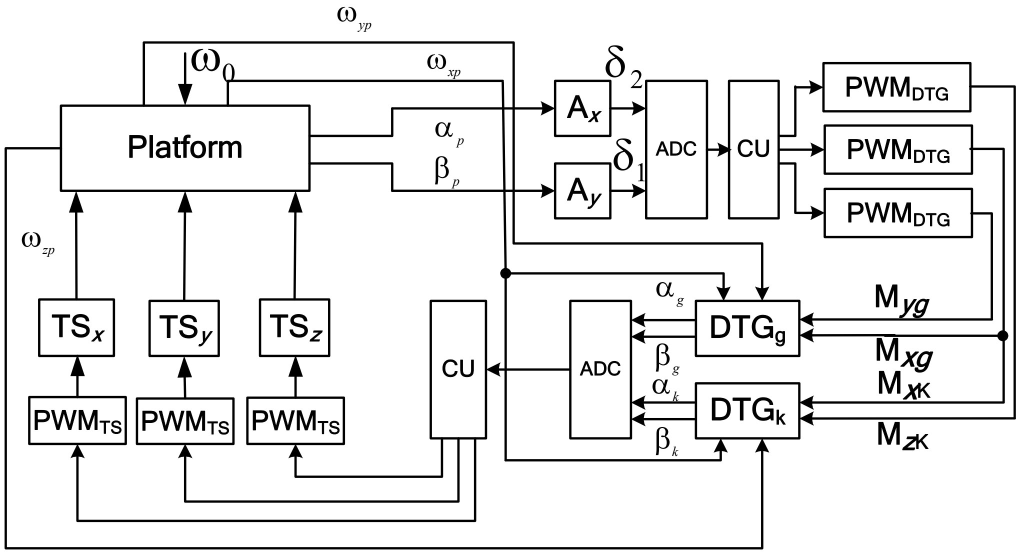

Fig. 1. The structural scheme of the precision navigation marine system: A is the accelerometer; CU is the calculating unit; PWM is the pulse width modulator; ADC – analog-to-digital converter; DTG_g is the dynamically tuned gyro (the vertical gyro); DTG_h is the dynamically tuned gyro (the heading measuring instrument); TS – is the torque sensor

Design of the precision navigation system for solution of the above stated tasks is implemented in conditions of uncertainties caused both inaccuracies of the mathematical descriptions of the real systems and influence of the internal and external disturbances. Mainly, the navigation systems designed for exploitation at the marine vehicles are subjected to influence of disturbances caused by the sea irregular waves. The modern approach to solution of this problem is connected with synthesis of the robust systems able to operate in conditions of the parametrical structured and the external coordinate disturbances.

Improvement of the control systems may be implemented in two directions including operational system development and creation of the new systems. The operational system development in conditions of uncertainties it is convenient to realize by means of the robust parametrical optimization. In the presence of sufficient a priori information contents about the analogous systems creation of the new systems may be based on the parametric optimization too. But the modern approach to design of the new systems foresees using of the H_∞-synthesis that is the robust structural optimization providing design of a system in the conditions of uncertainties.

One of the modern approaches to definition of the robust optimization quality criterions is using of the H_∞-norm of the matrix function of the closed loop system complementary sensitivity function [2, 6]. In this case the quality criterion and the formalized statement of the problem may be represented in the form

$$J_{H_\infty p}(K) = \| \mathbf{Ц}(K) \|_\infty , \tag{1}$$

$$K^* = \arg \inf_{K \in D} J_{H_\infty}(K) \tag{2}$$

if the following condition

$$K(s) \in D\,,\; D : \mathrm{Re}\,|\,\mathrm{eig}(I + L(s))\,| < 0 \tag{3}$$

is satisfied, where $J_{H_\infty p}(K)$ is the optimization quality criterion. In the general case this criterion represents the H_∞-norm of the matrix function of the closed loop system complementary sensitivity function $Ц(K,s)$; $K(s)$ is the matrix of transfer functions of the controller; $\|\cdot\|_\infty$ is the notation of the H_∞-norm; $W(s)$ is the matrix of transfer functions of the control object; $L(s) = K(s)W(s)$.

To increase efficiency of the robust parametric optimization is possible using the mixed H_2/H_∞ approach. In this case, the complex quality criterion may be described by the following expression

$$J_{H_2/H_\infty} = \lambda_2^{\mathrm{nom\,d}} \| Ц(K) \|_2^{\mathrm{nom\,d}} + \lambda_2^{\mathrm{nom\,s}} \| Ц(K) \|_2^{\mathrm{nom\,s}} + \sum_{i=1}^{n} \lambda_{2_i}^{\mathrm{dis\,s}} \| Ц(K) \|_{2_i}^{\mathrm{dis\,s}} + \sum_{i=1}^{n} \lambda_{2_i}^{\mathrm{dis\,d}} \| Ц(K) \|_{2_i}^{\mathrm{dis\,d}} +$$

$$+ \lambda_\infty^{\mathrm{nom}} \| Ц(K) \|_\infty^{\mathrm{nom}} + \sum_{i=1}^{n} \lambda_\infty^{\mathrm{dis\,i}} \| Ц(K) \|_\infty^{\mathrm{dis\,i}} + PF ,$$

where $\|\cdot\|_2^{\mathrm{nom\,d}}$, $\|\cdot\|_2^{\mathrm{nom\,s}}$, $\|\cdot\|_{2_i}^{\mathrm{dis\,s}}$, $\|\cdot\|_{2_i}^{\mathrm{dis\,d}}$ are H_2-norms of the transfer functions of a nominal system and a system disturbed by the parametrical structured disturbances for the deterministic and stochastic cases; $\|\cdot\|_\infty^{\mathrm{nom}}$, $\|\cdot\|_\infty^{\mathrm{dis\,i}}$ are the H_∞-norms of the transfer functions of a nominal system and a system disturbed by the parametrical structured disturbances; $\lambda_2^{\mathrm{nom\,d}}, \lambda_2^{\mathrm{nom\,s}}, \lambda_\infty^{\mathrm{nom}}, \lambda_{2_i}^{\mathrm{dis\,d}}, \lambda_{2_i}^{\mathrm{dis\,s}}, \lambda_\infty^{\mathrm{dis\,i}}$ are the weighting coefficients of the appropriate norms; n is a number of a system's models disturbed by the parametrical structured disturbances; PF is the penalty function satisfying the stability conditions during a process of the optimization.

Then the statement of the H_2/H_∞-optimization problem (1), (2) under condition that the condition (3) is satisfied becomes:

$$K^* = \arg \inf_{K \in D} J_{H_2/H_\infty}(K) .$$

Such approach to the optimization is called the multi-purpose as it allows to find a compromise between a system's accuracy and robustness indexes which represent the different conflicting purposes [2].

The methodical provision of the parametrical H_2/H_∞-optimization includes creation of the mathematical descriptions of the control system in the space of states, and taking into consideration all the non-linearities peculiar to a real system; determination of the minimal and balanced realizations of the linearized models and application of the optimization method based on the genetic algorithms. During the cyclic execution of this method at every its step the following operations are carried out such as calculation of the H_2, H_∞-norms of the synthesized system, analysis of the poles location at the plane of the complex variable and correspondingly indirect indexes of the transient quality, forming of the penalty function by this analysis results and determination of a system's optimization complex criterion. Checking of the synthesis results is implemented by means of the nonlinear model as much as possible close to the real system. In the case of the unacceptable results the parametrical optimization procedure must be repeated after change of the initial conditions or the weighting coefficients.

Results of the parametrical H_2 / H_∞-optimization for the precision navigation marine system in the mode of the previous leveling are represented in [4]. As for other modes of a system operation, it is convenient study the navigation and stabilization contours separately taking into consideration their complexity. The main purpose of the navigation contours optimization is determination of the control laws coefficients, as the form of the control laws for the studied systems is defined by the many years experience of such systems design. Therefore use of the H_2 / H_∞-optimization is the most convenient in the given case. The results of the parametric optimization of the system navigation contours in the mode of precise leveling[5] are presented in fig. 2.

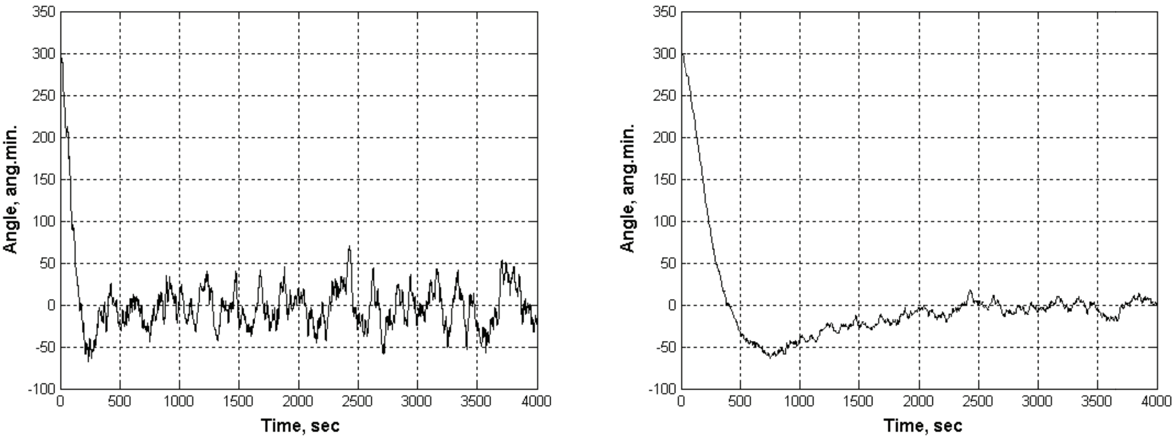

a *b*

Fig. 2. The angle of platform deviation from the plane of horizon (an angle of the pitch) in the mode of the precise leveling: *a* – for non-optimized system; *b* – for optimized system

The results of the parametrical optimization of a system's navigation contours in the mode of the initial alignment or setting to the meridian [5] are represented in fig. 3.

The robust structural optimization is based on solution of two Riccati equations, checking of some conditions [6] and minimization of the H_∞-norm of a system's mixed sensitivity function which includes the plant G, the controller K and is defined by the vector of outputs z, which characterises the system quality, the vector of inputs r and also the control u and observation y vectors [6]. The modern approach to solution of the robust structural H_∞-optimization is based on forming of the desirable frequency characteristics of a system. Such approach is implemented by means of forming of the augmented plant due to connection of the weighting transfer functions. The H_∞-norm of the mixed sensitivity function of the augmented system is used as the optimization criterion

$$J_{H_\infty s} = \left\| \begin{bmatrix} W_1 S \\ W_2 R \\ W_3 T \end{bmatrix} \right\|_\infty ,$$

where W_1, W_2, W_3 are the weighting transfer functions, S, R, T are the sensitivity functions by the given signal, control and the complementary sensitivity function

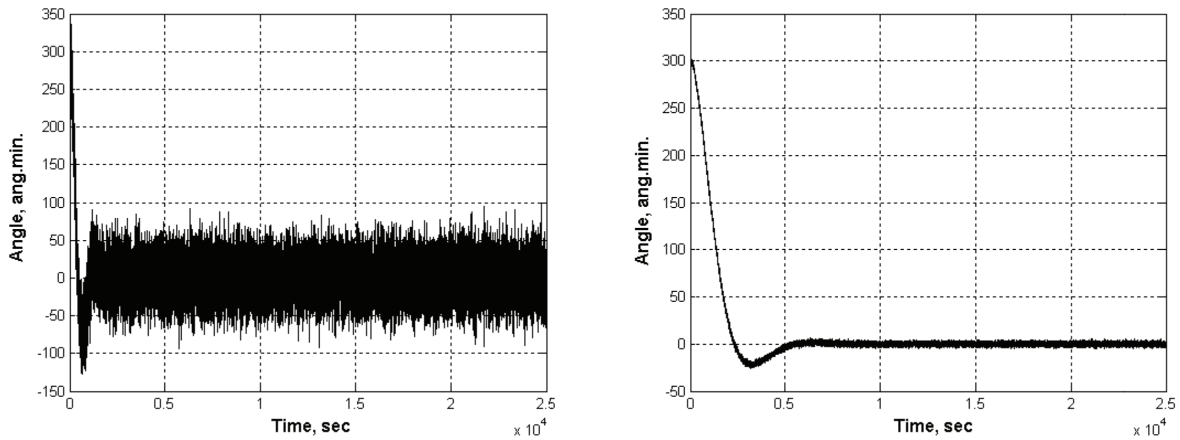

a *b*

Fig. 3. An angle of the azimuth in the mode of the initial alignment: *a* – for the non-optimized system; *b* – for the optimized system

The statement of the structural H_∞-optimization by the method of the mixed sensitivity is represented in fig. 4.

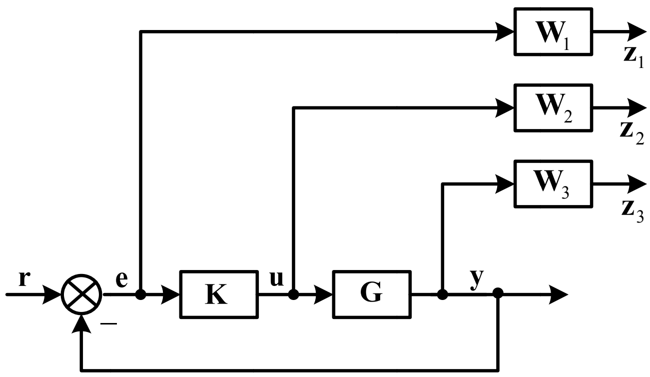

Fig. 4. H_∞-optimization by the method of the mixed sensitivity

In the system of the computer-aided design Robust Control Toolbox the structural synthesis of the H_∞-controller by the method of the mixed sensitivity is implemented by means of functions *augtf*, *hinfopt*, which provide creation of a system's model in the space of states and execution of the H_∞-synthesis procedure. The results of the structural optimization of the precision navigation system by the method of the mixed sensitivity are represented in fig. 5.

The successes of the H_∞-synthesis by the method of the mixed sensitivity essentially depends on the choice of the weighting transfer functions. In many cases the choice of these coefficients is carried out by the empiric methods taking unto account experience of the studied systems design.

As a rule, the controller synthesized by the structural method represents a system of sufficiently high order. There are some approaches [3] to reduction of the synthesized controllers such as reduction of a system's model before the H_∞-synthesis procedure, reduction of a system's model after the H_∞-synthesis procedure and use of the special methods which provide creation of a system with the reduced order.

The comparative analysis has been shown that in this case the reduction of the synthesized controller is convenient to carry out after H_∞-synthesis procedure termination. The reduction of the controller of the studied system may be carried out by means of the function *balmr*, which provides reduction of the controller to the fifth order.

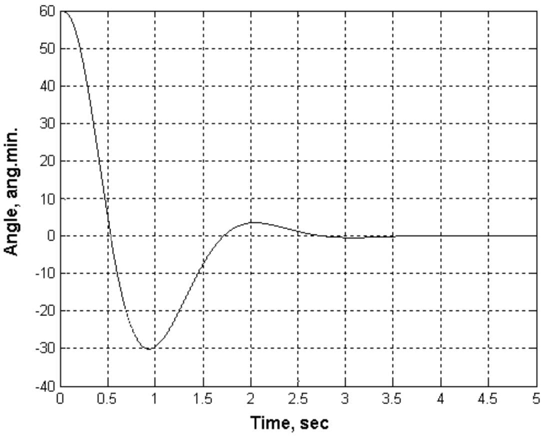

a

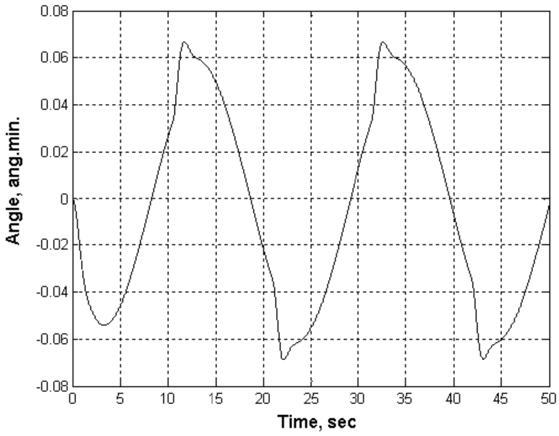

b

Fig. 5. Results of the structural optimization: the transient (*a*), the dynamical error (*б*)

Conclusions

The approaches to development of the operational systems and design of the new systems of the wide class based on the methods of the parametrical and structural robust optimization are analyzed in the paper. The simulation results for synthesized precision navigation marine systems are represented.

References

1. Hilkert J.M. Inertially stabilized platform technology / J.M. Hilkert // IEEE Control Systems Magazine. –2008. – No 1. – P. 47-64.

2. Tunik A. A. Parametric optimization procedure for robust flight control system design / A.A. Tunik, H. Rye, H.C. Lee // KSAS International Journal. – 2001. – Vol. 2. – No 2. – P. 95 – 107.

3. Сущенко О.А. Робастна параметрична оптимізація систем стабілізації наземних рухомих об'єктів / О.А. Сущенко // Вісник Національного авіаційного університету. – 2008. – № 4.– С. 26 – 32.

4. Сущенко О.А. Робастна параметрична оптимізація системи стабілізації та визначення курсу / О.А. Сущенко // Електроніка та системи управління. –2009. – №1(19). – С. 111–118.

5. Сущенко О.А. Параметрична оптимізація навігаційних контурів багаторежимної системи стабілізації та визначення курсу / О.А. Сущенко //Вісник Національного авіаційного університету.– 2009.– №3. – С. 67 – 75.

6. Skogestad S. Multivariable Feedback Control / S. Skogestad, I. Postlethwaite. – New York: Jonh Wiley, 1997. – 559 p.

7. Сущенко О.А. Особливості проектування робастної системи стабілізації для навігаційних комплексів морського призначення / О.А. Сущенко // Електроніка та системи керування. – 2010. – № 3(25). – С. 95–101.

8. Gu D. Robust Control Design with MATLAB / D. Gu, P. Petkov, M. Konstantinov – London: Springer-Verlag, 2005.– 389p.

UDC 53.088:62 – 754.2 (045)

V. Apostolyuk, Ph.D
(National Aviation University, Ukraine)

MODELLING TRAJECTORY ROTATION IN CORIOLIS VIBRATORY GYROSCOPES

In this paper transfer functions were developed and corresponding transient processes for the sensitive element motion trajectory angle of rotation are studied. Simple approximations are suggested and its accuracy is demonstrated using numerical simulations.

In view of constantly growing market for micromechanical angular rate sensors Coriolis vibratory gyroscopes (CVGs) have received significant amount of attention from the MEMS sensors design specialists due to the promising possibility to fabricate sensitive elements of such gyroscopes in miniature form by using modern microelectronic mass-production technologies. While conventional angular rate measurement is based on detection of the rotation induced oscillations amplitude (secondary amplitude) [1], trajectory analysis approaches are utilised as well [2, 3]. The latter also allows designing rate integrating sensors, which are more suitable for attitude and navigation applications [3, 4]. This paper addresses problems related to modelling angle of the sensitive element motion trajectory rotation due to the presence of the external angular rate.

One could consider the CVG sensitive element as a two-dimensional pendulum, whose steady state trajectory forms a rotated ellipse, as shown in Figure 1.

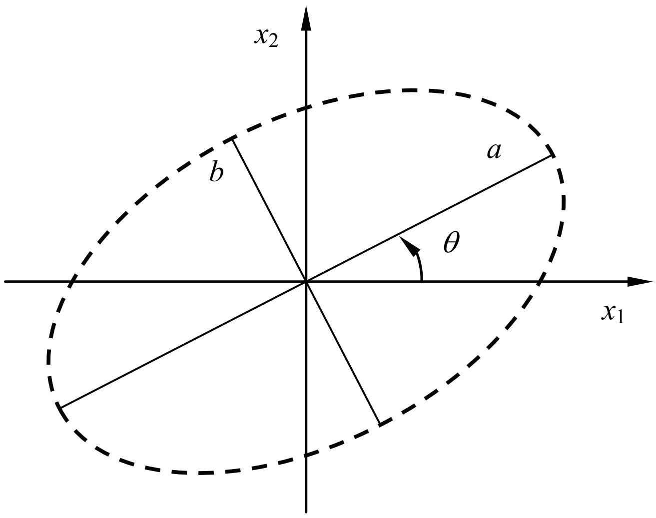

Fig. 1. Sensitive element motion trajectory

In this figure, a and b are the big and small half-axes of the ellipse, θ is the angle of the ellipse rotation relatively to the axes of primary x_1 and secondary x_2 oscillations. It is well-known, that these parameters (namely half-axes and angle of rotation) depend on amplitudes and phases of primary and secondary oscillations, which in turn depend on parameters of the sensitive element design and unknown angular rate. The problem, which is to be addressed in this paper, is to develop and analyse mathematical model of the θ angle transient processes due to the angular rate.

In general case, angle of the trajectory rotation is given by the following expression [2]:

$$\theta = \frac{1}{2}\tan^{-1}\left[\frac{2A_1A_2\cos\varphi}{A_1^2 - A_2^2}\right]. \quad (1)$$

Here A_1 and A_2 are the primary and secondary amplitudes of the sensitive element oscillations, φ is the phase shift between the primary and secondary oscillations.

In the most generalized form, motion equations of the CVG sensitive element both with translational and rotational motion could be represented in the following form [1]:

$$\begin{cases} \ddot{x}_1 + 2\zeta_1 k_1 \dot{x}_1 + (k_1^2 - d_1\Omega^2)x_1 + g_1\Omega\dot{x}_2 + d_3\dot{\Omega}x_2 = q_1(t), \\ \ddot{x}_2 + 2\zeta_2 k_2 \dot{x}_2 + (k_2^2 - d_2\Omega^2)x_2 - g_2\Omega\dot{x}_1 - \dot{\Omega}x_1 = q_2(t). \end{cases} \tag{2}$$

Here x_1 and x_2 are the generalized coordinates that describe primary (excited) and secondary (sensed) motions of the sensitive element respectively, k_1 and k_2 are the corresponding natural frequencies, ζ_1 and ζ_2 are the dimensionless relative damping coefficients, Ω is the measured angular rate, which is orthogonal to the axes of primary and secondary motions, q_1 and q_2 are the generalized accelerations due to the external forces acting on the sensitive element. The remaining dimensionless coefficients are different for the sensitive elements exploiting either translational or rotational motion. For the translational sensitive element they are $d_1 = d_2 = 1$, $d_3 = m_2/(m_1 + m_2)$, $g_1 = 2m_2/(m_1 + m_2)$, $g_2 = 2$, where were m_1 and m_2 are the masses of the outer frame and the internal massive element.

Steady state solution of the equations (2) in terms of amplitudes and phases of primary and secondary oscillations can be represented as follows:

$$\begin{gathered} A_1 = \frac{q_{10}}{k^2\sqrt{(1-\delta\omega^2)^2 + 4\zeta_1^2\delta\omega^2}}, \\ A_2 = \frac{A_1 g_2 \delta\omega}{\sqrt{\delta k^4 + \delta\omega^2 - 2\delta k^2\delta\omega^2(1-2\zeta_2^2)}}\delta\Omega, \\ \varphi_1 = -\arctan\frac{2\delta\omega\zeta_1}{1-\delta\omega}, \\ \varphi_2 = -\arctan\frac{\delta k^2 - (1 + 4\zeta_1\zeta_2\delta k + \delta k^2)\delta\omega^2 + \delta\omega^4}{2\delta k\delta\omega(\zeta_2 + \zeta_1\delta k) - 2\delta\omega^3(\zeta_1 + \zeta_2\delta k)}. \end{gathered} \tag{3}$$

Here q_{10} is the amplitude of accelerations created by the primary excitation system, k is the primary natural frequency, $\delta\omega = \omega / k$ is the relative excitation frequency, $\delta k = k_2 / k_1$ is the ratio of the secondary and primary natural frequencies, $\delta\Omega = \Omega / k$ is the relative angular rate. Angular rate is assumed to be negligible in comparison to the natural frequencies.

One should note that the sensitive element trajectory parameters depend on the phase shift $\varphi = \varphi_2 - \varphi_1$ between primary and secondary phases. Most importantly, based upon (3), phases of do not depend on angular rate. In case of the primary resonance ($\delta\omega = 1$), cosine of this phase shift can be calculated as

$$\cos\varphi = \frac{2\zeta_2\delta k}{\sqrt{\delta k^4 - 2(1-2\zeta_2^2)\delta k^2 + 1}}. \tag{4}$$

Expressions (3) along with the phase shift representations (4) can now be used to analyse parameters of the actual trajectory of the CVG sensitive element. However, dependencies (3) and (4) are the steady state solutions, which do not allow studying transient processes when external angular rate is applied.

As has been demonstrated in [5], Laplace transformation of the secondary amplitude is

$$A_2(s) = \frac{q_{10}g_2}{4k_1^2\zeta_1(s + k_2\zeta_2)}\Omega(s). \tag{5}$$

Using expressions (3-5) we can modify expression (1) to the following form

$$\theta(s) = \frac{1}{2}\tan^{-1}\left[\frac{8g_2k\zeta_2\delta k(s + k\zeta_2\delta k)}{[4(s + k\zeta_2\delta k)^2 - g_2^2k^2\delta\Omega^2(s)]\sqrt{\delta k^4 - 2(1-2\zeta_2^2)\delta k^2 + 1}}\delta\Omega(s)\right]. \tag{6}$$

Apparently expression (6) is non-linear in terms of the input angular rate. However, taking into account that relative angular rate is small ($\delta\Omega << 1$), expression (6) can be linearised with respect to the small $\delta\Omega$ as follows:

$$\theta(s) \approx \frac{g_2 k\zeta_2 \delta k}{(s + k\zeta_2\delta k)\sqrt{\delta k^4 - 2(1-2\zeta_2^2)\delta k^2 + 1}}\delta\Omega(s)\,. \tag{7}$$

Finally, assuming matching natural frequencies of primary and secondary oscillations ($\delta k = 1$), expression (7) can be further simplified as

$$\theta(s) \approx \frac{g_2 k}{2(s + k\zeta_2)}\delta\Omega(s)\,. \tag{8}$$

Steady state of the obtained expression (8) is in perfect agreement with the previously published steady state expressions for the motion trajectory angle of rotation [2].

Numerical simulation of the sensitive element motion trajectory based on the equations (2) is shown in Figure 2.

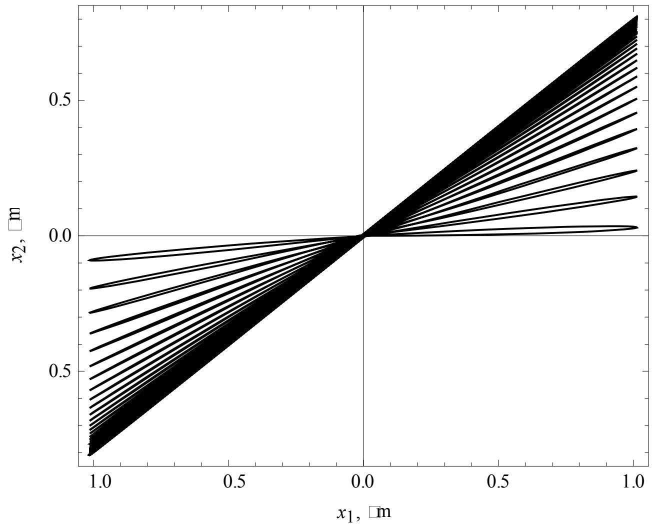

Fig. 2. CVG sensitive element motion trajectory

Primary oscillations are assumed to be already settled and constant angular rate is applied. Corresponding simulations for the angle of trajectory rotation are shown in Figure 3.

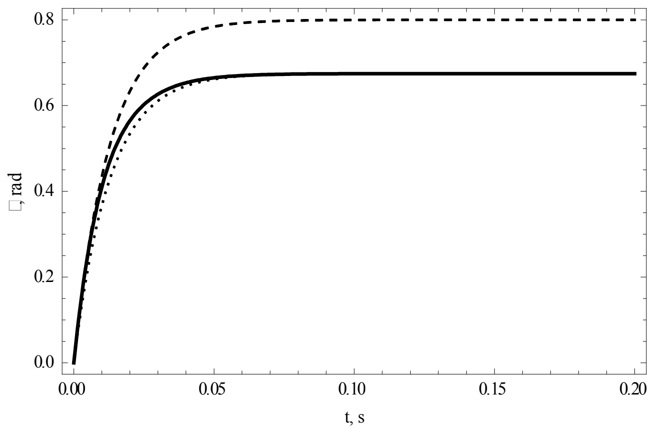

Fig. 3. Transient process simulations
(solid – accurately simulated, dashed – simplified approximation,
dotted – improved approximation)

Here dashed line corresponds to the simplified approximation (8). One can see that significant steady state error is present. In order to remove this error, expression (6) can be used to produce improved approximation in the following form:

$$\theta(s) = \frac{1}{2}\tan^{-1}\left[\frac{4g_2\zeta_2\delta k}{\sqrt{\delta k^4 - 2(1-2\zeta_2^2)\delta k^2 + 1}}\right]\frac{\zeta_2 k\delta k}{s + \zeta_2 k\delta k}\delta\Omega(s)\,. \tag{6}$$

Numerical simulations of the improved approximation (6) are represented by the dotted line in Figure 3. One can see, that improved approximation (6) is accurate in representation of the angle of trajectory rotation transient processes for most of the practical applications.

Conclusions

Developed model for the angle of trajectory rotation of a CVG sensitive element allow designing miniature angular rate sensors based on the trajectory analysis contrary to the conventional secondary amplitude detection. Derived transfer functions can be used to develop filtering and control systems that will improve its measurement performances. The latter is suggested as a topic for the future research.

References

1. *Apostolyuk V.* Theory and Design of Micromechanical Vibratory Gyroscopes // MEMS/NEMS Handbook (Ed: Cornelius T. Leondes), Springer, 2006, Vol.1, Chapter 6, pp. 173-195.

2. *Apostolyuk V., Gorbunovich I.* Mathematical Model of Coriolis Vibratory Gyroscopes Motion Trajectory // Mechanics of Gyroscopic Systems.– 2010.– №21.– C.5-12.

3. *Shkel A., Horowitz R., Seshia A., Park S., Howe R.* Dynamics and control of micromachined gyroscopes // Proceeding of the American Control Conference, 1999, vol. 3, pp. 2119–2124.

4. *Prikhodko I., Zotov S., Trusov A., Shkel A.* Foucault Pendulum on a Chip: Rate Integrating Silicon MEMS Gyroscope // Sensors and Actuators A: Physical, Vol. 177, April 2012, pp. 67–78.

5. *Apostolyuk V.* Dynamics of Coriolis Vibratory Gyroscopes in Control Systems // Systems of Control, Navigation, and Communication. – 2010. – No. 1 (13) . – P. 62-66.

UDC 629.735:656.71.06:621.31 (045)

S.S. Devyatkina, candidate of technical sciences (National Aviation University, Ukraine)

THE CONCEPTION OF FLIGHT SAFETY MANAGEMENT FOR CIVIL AVIATION AIRPORTS

The conception of flight safety management for civil aviation airports based on risk modeling is suggested. Main advantages of the implementation of this conception for civil aviation airports are considered and analyzed.

Nowadays flight safety in civil aviation is the most important task of government aviation branch worldwide. In spite of all efforts spent on achieving zero accidents and incidents level, they are happening with different types of aircraft in different countries. That is why the aviation experts of world famous organizations such as ICAO, IATA, FSF, FAA made the conclusion that the existing approach to flight safety providing became not effective and does not satisfy modern demands to aviation transportation. According to last ICAO standards and recommended practice [1, 2] the new concept of flight safety must be implemented in aviation practice of whole world.

The main sense of this new concept is that only flight safety providing approach is not enough and it must be changed by safety management approach. Safety management approach has to be implemented on two levels – government policy level and in all civil aviation organizations such as airlines, aerodromes, aviation service and factories, aviation educational institutions. Practically the new safety management approach is realized as Safety Management System.

The Safety Management System is a systematic approach to managing safety, including the necessary organizational structures, accountabilities, policies and procedures. There are three main aspects of Safety Management System:

- Systematic of activity – safety management activities is based on pre-determined plan, which takes into account the individual features of organization.
- Pro-active approach – an approach that emphasizes hazard identification and risks control before negative events that affect safety occur.
- Transparency of activity – all safety management activities are documented and visible.

In order to understand safety management, it is necessary to consider what is meant by safety. The previous definition of flight safety was the follow. Flight safety is a ability of aviation transport system that provides passengers and cargo transportation without hazards for human life's and health. While the elimination of accidents and serious incidents would be desirable, a one hundred per cent safety rate is an unachievable goal. Unfortunately it is impossible to create human-machine system free from technical failures and human errors, hence free from any risk.

The new definition of flight safety recommended by ICAO standards [2] is the next. Safety is the state in which the risk of harm to persons or of property damage is reduced to, and maintained at or below, an acceptable level through a continuing process of hazard identification and risk management.

Safety management system is based on risk control conception. However it is impossible to control something having no possibility to measure it. That is why the risk control process consists of the next steps:

- risks definition – at all stages of technological process, which creates risk;
- risks normalizing – having normalized values of risk for risk assessment procedure;
- risk assessment – to make a conclusion about risk acceptability;
- risk prognostication – to make the forecast about risk's level in the future.

This report is devoted to Safety Management System implementation in civil aviation airports.

There are special requirements in the last edition of ICAO standards and recommended practice [1] concerning the necessity of creating an effective Safety Management Systems in every civil aviation airport.

These demands form the normative basis and powerful aid for creating an effective system for controlling risk on every civil aviation airport. It is necessary implement Safety Management System in aerodromes because these organizations provide very important flight safety stages – taxiing, take-off, final approach and landing. The activity of every airport should provide the minimum risk during every stage of flight and create maximum comfortable conditions for the aircraft's crew.

Statistics data show that most accidents and incidents occur during take-off, approach and landing. All these parts of flight are fulfilled in the aerodrome zone (Pict. 1). This picture demonstrates that about 55% of accidents/incidents are happened during the flight which takes 6% of the whole flight time. These statistics proves the importance and necessity of risk controlling by implementation of modern Safety Management System.

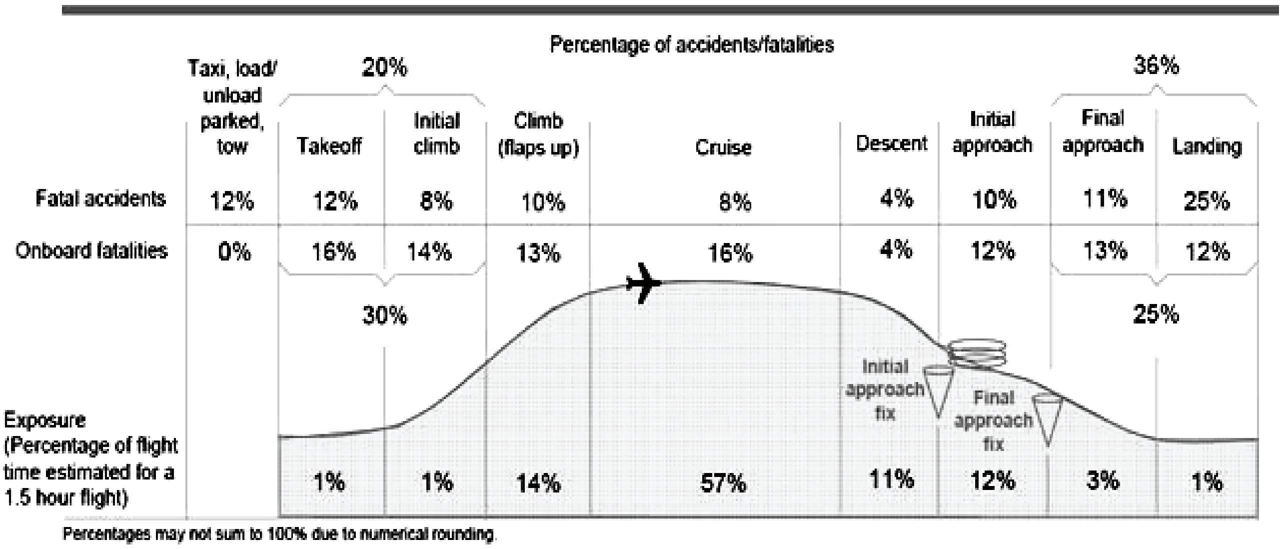

Source: Statistical Summary of Commercial Jet Airplane Accidents, 1959 - 2008, Boeing

Picture 1. Accidents and Fatalities by Phase of Flight

Civil aviation airport or even aerodrome is a branchy organization which contains aviation personal, different equipment, normative documents and rules, areas of responsibilities, special bureaucratic structure. Safety Management System must become a significant part of airport's structure and take all responsibilities connecting with risk control function.

The main idea of risk concept is that the safety is considered as a condition under which the risk of harm or damage is not equal to zero but limited to an acceptable level. The safety hazards creating risk may become evident after an obvious breach of safety, which may be classified as an accident or incident. This approach is retroactive and archaic and it may not be used anymore. In modern approach risk must be proactively identified through formal safety management programs before an actual safety event occurs.

After the identification of safety hazard, the associated risks must be assessed and made the conclusion about its acceptability. If the risk level is not acceptable, i.e. its value is more than normalized value, it is necessary to develop some effective actions to reduce risk's value and make it in compliance with standard values.

Picture 2 demonstrates the triangle of risk's acceptability. This triangle shows the correlation between acceptable, not acceptable and minimally achieved risk.

One of the main tasks of Safety Management System of civil aviation airport is by analyzing costs and profits connecting with flight safety providing make all risk levels acceptable or minimally achieved.

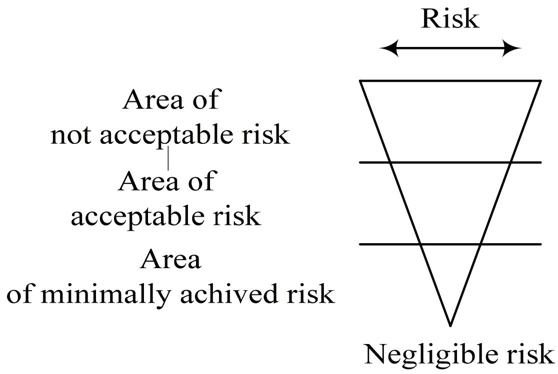

Picture 2. Triangle of risk

The Conception of flight safety management for civil aviation airports suggested in this report provides the risks identification method based on the mathematical approach as an alternative approach to the method of expert estimation and risk matrix.

Conclusions

The advantages of mathematical approach are: the higher accuracy, clearness and the possibility to reduce risk level at every stage of its creation. This mathematical approach requires the creation of mathematic models of risks for take-off, taxiing, final approach and landing.

These models consider all potential safety hazards may be created by each aerodrome departments. The transparency of these risks models provides the possibility of development the defense at every necessary stage of flight providing process hence reducing risks values.

References

1. Annex 14 to the Convention of International Civil Aviation Organization. Aerodromes. Vol. 1. Aerodrome Design and Operations, in 2 vol. / edit. 5, july 2009.

2. Doc 9859. Safety Management Manual (SMM). - 2nd edit. – 2009., AN/474. International Civil Aviation Organization.

UDC 629.52.7

O. A. Mashkov, professor, doctor of technical science
(National Aviation University, Ukraine)

METHODS OF MAINTENANCE OF FUNCTIONAL STABILITY OF ONBOARD INFORMATION AND CONTROL COMPLEXES OF AIRCRAFT

Introduction. *The transition to creation and application of reusable space systems represents a regular stage in development of missile-space and aerospace engineering in common process of development and use of the space. Intensive development of the near space with the purposes of its peaceful use results in the necessity of fading ways of reducing the cost of payloads launching into orbit. For this purpose, as is known, various reusable systems are being developed, which should basically lower the cost of launching payloads reasonably big number of restarts. However, on the way of aerospace systems development, there appear new problems, connected with providing high reliability, fault tolerance, with fulfillment of semi-natural and natural of experiments, etc.*

1. Problems of the schematic decisions.

Application of aviation means of start permits to realize multiline at launching, descent and landing. However, demands additional costs of starting weight as compared to mass of vertical start by means of rocket - carriers (RC). Consequently, the use of such means becomes profitable only with big number or starts.

The advantage of aerospace systems (ASS) consists also in absence of zones of alienation, opportunity of launching at big range of orbit angle deviation, including minor mobility of launching.

Of late the technical decisions of ASS are studied in many countries, by many firms and in many research institutes. First consist of a heavy plane – carrier (PC), capable of bearing booster stage and launched orbital plane (OP) on its outside suspender. The second scheme is – one-stage, orbital, for example a “Hotol” type with engines and fuel, enabling to accelerator launching into orbit.

However, the optimum tire-stage scheme, is the one accelerator is hypersonic plane, capable of launching orbital stage at a speed, corresponding to number M=3 ...5. In this case, as researcher show, total weight of a system can be the in order of 350-450 tn at a payload 2…7tn.

Certainly, the most perspective reusable orbital airplane is one-stage plane. However, its creation except for the solution of the whole complex of aerothermodynamics problems, problems of development of constructive materials for high temperatures, poses the problem of creation rather a complex combined engine, capable of creating effective thrust at the entire range of speeds. There should be a combination of modes THE (turbojet engine), DFAJE (direct flow air-jet engine), liquid jet engine. I thus, it is proposed to reduce considerably fuel consumption by means of gradual transition from one type of engine to the other (by way of increased the number M of flights). Use of a liquid jet engine only on modes of flight with number M 10…15 considerably reduces the consumption fuel and, hence, starting weight. At the same time is necessary to take into account extreme temperature loads – up to 3000 K.

If it becomes possible to solve the problems of creation of a combined impellent installation of acceptable weight, this will enable to reduce considerably the starting weight at transition to a one-stage aero-space plane, by means of replacing multistage of the airplane effect for multistage regime of engine operation.

Development of ASS also requires great costs and can be a subject of international cooperation for distribution of the possible contributions from each contributing country.

In the near future, the most acceptable is the development of ASS on the basis of near-sound of a plane – carrier as a main means o launching. Analysis of the statistics about dimensions and weights of satellites indicate to such way. It is necessary to develop means of launching for loads up to 10 tons. The degree of pay loads by such made of launching will be more than 80%.

In view of these requirements the project multitarget ASS (MASS) was developed in the former USSR. The project has in 1st basis a 2-stage launching system. The base plane AN-225 “Mriya” is used, as the first stage, and the second stage consist of a orbital reusable plane and expendable external fuel tank.

In the former USSR valuable experience on creation of a reusable orbital plane “Buran” was received. The systems of the orbital ship, design and heat-shielding are designed for 100 trips on a route Earth – Orbit – Earth.

While developing OP "Buran" problems of aerodynamics, heat-shielding, stability and controllability were successfully resolved. Problematic is the process of division of units of ASS in atmosphere. The outline of flight at division ASS consists of several parts: thrust in horizontal flight, maneuver of a type "hill", executed with the purpose achieving maximum values of height of flight altitude flight speed, angle of trajectory deviation. During system transfer to normal overboard reasonably close to zero division of units of ASS is executed. On the process of division are imposed the rigid safety requirements such, as excluding of cob-lows of dividing parts, when they are in direct affinity; not getting of a plane - carrier (PC) in a gas; jet of a rocket engine of the second stage (OP + fuel tank).

2. Problems of security functional stability.

One of serious problems when developing reusable aerospace system is the problem of security of reliability, solvability, safety of all system as a whole and in particular its information control complex. Here it is necessary to take into account that increasing reliability of elements, introducing structural and temporary redundancy, applying interchangeability and regeneration ability it, appears possible to guarantee fault tolerance of the system, i.e. Its ability normal to function with a number of elements failure.

However, for a complex system, such as the onboard information-control complex of a reusable aerospace system, characteristic is the opportunity of such combinations of events, whole separate probability is small, and as a sum, such “improbable” combinations too many. Even specially created monitoring protection systems and oriented to simple review of possible dangerous situations, cannot guarantee protection against any random combinations of failures and other adverse effects. And in remains completely defenseless.

In this connection, there arises the task to develop such algorithm of control, which could ensure the opportunity to control the object or image under any condition or failure to keep in order it at optimum "distance" from borders of danger at the minimum time to start object. The realization of the program of control onboard of multitarget aerospace system (MASS) should ensure the successful solution of one of the following problems:

The fulfillment of abnormal launching into orbit, when with sufficient level of probability rescue of the whole vehicle together with the crew and payload is provided at the same time preserving of opportunities of repeated use of MASS and payload;

The emergency rescue of MASS or crew, when safety of the crew is guaranteed, but at rescue MASS infringements of conditions or regular operation are possible, owing to which for repeated use MASS significant repair jobs are not necessary. In their turn each of these problems can be presented as a problem of functional diagnostics of random phenomena in the form of abnormal situations and control the object on parity or abnormal situations with the purpose or of it development.

As experience of flights of planes of Space Shuttle type “Buran” has shown, the occurrence of various abnormal situations is connected in the failures of information, computing and power subsystems of onboard information-control complex (OICC). There was necessity to take a decision on restoration of lost functions. Let’s assume that if the restoration of function occurs at the final moment of a time without participation of a person – operator it is considered. That OICC has functional stability.

The functional stability is provided by redistribution of resources inside information, computing, power subsystems; changes of the program of functioning of the OICC. The main reason for minor functional stability to abnormal situations is insufficient readiness of OIMC computing system to identification and actions in unforeseen conditions. In general the position of problem on neutralization of abnormal situation looks as follows.

Let there be the vector $Z = [Z_1, Z_2, \dots Z_n]$ of the characteristics of abnormal situation, as a set of ambiguities $W=\{W_1, W_2, \dots W_m\}$, reflecting the existence of qualitative unformulated factors, conditions connections of subsystems OICC and of it elements.

Let's introduce an integrated parameter of efficiency of $J(Z,W)$ functioning. To the vector of perturbation $\Phi = [Z^T W^T]^T$ it is possible to pose in conformity with a set of control influences $U=\{U_1,U_2,\dots U_p\}$, here T - is symbol of transpose.

Then there is algorithm A, such, that A: $\Phi \rightarrow 0$.

In its turn, any elementary control effects V_j will transform the output characteristic of process of functioning OICC J. Algorithms of such transformations will be $B: U \rightarrow J$. Since the vector of perturbation Φ is considered as random, so value of J is random.

The problem of neutralization consequences of abnormal situation consists in search of control effect U, stabilizing process of functioning of OICC, i.e. the one giving a minimum dispersion of value J for a interval of a time τ, not exceeding given significance at appropriate density of distribution f(J, t).

$$D(J) = \iint_{-\infty}^{\infty} J^2 f(J,t)\,dJ\,dt \rightarrow \min .$$

All possible abnormal situations can conventionally be divided into three groups:

The situations, when disturbances during functioning of OICC come from the outside (for example, in case of unpredicted external disturbances directive instruction about urgent change of function program of OICC);

Infringements, caused by internal factors OICC, such as failure and failures of subsystems;

Latent infringements of work of OICC, expressed in a systematic deviation of values of parameters of reliability and efficiency of functioning, which can be detected only by analysis of OICC work for a long period of a time.

Algorithm of failures identification of is as followings. On the basis of mathematical modeling images – standards of situations, correspond to specific failure in ASS flight are formed in memory of an onboard computing system. At recognition the first of abnormal signal in OICC computing

System the image – standard of failure, the most probable just for a given signal is restored in memory. Active recognition of basic attributes of failure in their space-temporary development is further performed. If the assembled information corresponds to the considered image - standard, abnormal situation is identified in OICC. If by any attribute the image - the standard does not develop, the computing system OICC continues search - comparison, until identifies the special situation.

The specific character of such OICC structure is that the identification of abnormal situation is executed in a real or accelerated time on the background of ASS flight. If the situation is not obvious, the problem of recognition consists not only in locating situation of accepted classification, but also in its identification. The output of solution in this case takes place in two stages: the possible reasons of abnormal situation are first established, and then rational plan for liquidation of these reasons is formed.

For OICC synthesis steady to failures, as well as for the analysis of their functioning at abnormal situations it is necessary to establish mathematical model, adequately describing these failures.

For the OICC description, where it is necessary to consider possibility of failures, let's introduce a random unknown vector of parameters Г (t), that determines, for moment, the structure and parameters of OICC. Abnormal situations result in sudden changes of elements of this vector. The equation of a condition and supervision over OICC appear, in this case, dependent on of vector F (t) (changing at a random moment) and in general case can be presented as follows:

$$\dot{X} = F\left[X(t), \Gamma(t), U(t), W(t)\right]$$

$$Y = H\left[X(t), \Gamma(t), V(t)\right],\ \Gamma(t) \in Ш$$

where F and H -unknown functions; Ω - space of possible significances F(t); X(t) - vector of condition; Y(t) – vector measurements; U(t) - vector of control; W(t) - vector of protuberance ; V(t) - vector of errors of measurements.

However, without going into detail of the statistics of random vector of parameters Г(t), it is difficult to receive theoretical results. Therefore, first of all it is necessary to introduce the space of possible significances of a vector Г(t). If this space is continuous, the vector Г(t) can accept infinite set of values in the given area, if is discrete - the number of values is finite. In the latter case all values of vector F(t) can be numbered voluntarily - $\Gamma^i(t)$ i=1, N, and index N can be considered as number of the structure. In which OIMC is at the moment.

Let's divide the problem of identification of OIMC abnormal situations in two stages.

1. Identification of failure. When solving this problem place of a source of failure (in information-measuring, computing or power part of OIMC) is determined.

2. Identification of a degree of damage of components of OIMC and determination of a possibility for their further use, with possibly worsened characteristics. As research shows, these estimations can be used for the introduction of the compensating amendments in OIMC.

The simplest solution of the problem of failures direction is the use of failure-safe filters. If for such filter we use Calman filter, corresponding to the model of a normally functioning system, then gradually the filter will lose its sensitivity to newly input data, owing to the decrease of the matrix transmission factor. Therefore, when in dynamics of a system sharp changes occur, the Calman filter will react to them enough slowly, and in order to detect these changes it is necessary to save sensitivity to new data.

It can be achieved by one of the following ways:

- use of filters with final memory;
- input of restriction from below on values of filter amplification factor.

Simple restriction of a factor of filter amplification from below results in an increase of sensitivity of a filter to current data. As a result, it becomes possible to detect sharp changes in dynamics of OIMC. It should, however, notice, that the detection of these changes is made indirectly by means of supervision over the character of behavior of evaluation of a vector of a condition X on the output of the filter. In this case the characteristics of noise stability in conditions of normal functioning of OIMC are certainly worsened.

More effective appears the use of the so called exponent Calman filters. In these filters an increase of correlation matrix of filtration errors P(t) in S time is made compulsory, where S>1 is under duress executed.

The physical sense of such approach is reduced to that the influence of the previous measurements to current evaluation is exponentionally damping, and filter becomes more sensitive to new data.

However, in common case there is no regular procedure for choosing size S, which entails the necessity to execute large volume of preliminary mathematical modeling.

Use of the above filters for detecting faults is connected with necessity to satisfy inconsistent requirements. On the one hand, it is necessary for ensure filter sensitivity, on the other - high noise stability in normal system functioning mode. It can partly be achieved, if two filters systems are simultaneously used - one main, with parameters of a normally functioning system, the other auxiliary - a filter, sensitive to failures and used only for detection of failures.

Other approach to synthesis of filters, sensitive to specific kinds of failures is based on the use of two confidence areas – one built along nominal trajectory dynamic system in which there are no failures, the other built along values Calman filter received in measurements processing. When these two confident area deviate, fact of occurrence of failure is fixed.

On the basis of the above principles functionally stably onboard information-control complexes of a multitarget aerospace system can be developed.

3. Problems of automated designing of control system.

The analysis of approaches to designing of a aerospace engineering permits to note a number of essential defects. First, there is back of a uniform methodological concept and adequate mathematical apparatus of designing. Secondly, software of designing are not enough advanced. Thirdly, the necessity for realization of large volume of seminatural and natural experiments essentially prolongs the process of designing and makes it more expensive.

Thus at present the designing of a aerospace engineering requires customer and designers large investments and huge intellectual costs. The most important is the stage of early designing of vehicle, when faulty accepted decision can essentially lower efficiency of their use.

The author developed mathematical methods, models and programs for automated research of process of management of aerospace systems at various stages of flight.

The developed techniques permit to execute:

- Analysis of the characteristics of immunity and controllability of vehicles;
- Synthesis of optimum algorithms of management and navigation;
- Development of kinds of Information provision of crew;
- Development of algorithms of hand-operated management at various levels of information provision of crew;
- Research into problems of interaction between automatic, direct and hand-operated control modes, as well as conditions of transition from one mode to another.

Underlying the developed software of the simulating complex are:

- methods or optimization of trajectories movement;
- modeling of real onboard algorithms of control with the use of models of platformless inertial navigating system and models of gauges of the primary information;
- modeling of dynamics of flight with the account of atmosphere turbulence, gravitation field and liquid oscillation;
- algorithms of adaptive hand-operated management with use of a procedure of flexible distribution of functions between a crew and automatics of a control system;
- algorithms of quality image formation of the pilot-navigating information to the crew on the basis of formation of three dimensional space images.

Conclusion. The perspective projects of aerospace systems are characterized by the greater integration of aero and space-rocket engineering. Use of aerodynamic bearing properties for launching in to space will become a prevailing principle in ASS of 21st century. In these systems the newest constructional materials and onboard equipment installations will be applied.

However, from the entire variety of the perspective projects the greater are chances for realization with those ones, which take into account the requirements of reliability, reusability, economic efficiency and ecological safety, low cost of development and possessing technological and element base, that will give opportunity to ensure minimum terms prior to the beginning of operation and fast recoupment.

References

1. *Sivov N.S., Mashkov O.A.* Control Problems of Two-Stage Aerospace System on Atmosphere Flight Way / First International Aerospace conference: Perspectives of mastering outer space, Moscow, 1992, p.73.
2. *Gostev V.I., Mashkov V.A., Mashkov O.A*. Intermodular exchange of diagnostic information in self-diagnostic of complex system / Cybernetics and computing Tehnology, Discrete Control Systems, 1995, pp. 95-103.
3. *Gostev V.I., Mashkov V.A., Mashkov O.A*. Self-diagnostic of modular systems in random perfomance of elementary tests / Cybernetics and computing Tehnology, Discrete Control Systems, 1995, №105, pp. 104-112.
4. *Mashkov O.A.* Method of control algorithm synthesis for multi-dimensional automatic systems on the basis of dynamic back tasks solution / Науково-методичний збірник: доповіді Аерокосмічної Академії України. – К.: КІВПС, 1997, С. 75-86/
5. *Gostev V.I., Mashkov V.A., Mashkov O.A.* Methods for providing fault tolerance of airborne computer system through their self-control / Cybernetics and computing Tehnology, Discrete Control Systems, Allerton press, inc, 150 Fifth Avenue, New York, NY10011, №109, 1999, p. 33-44.
6. *Gostev V.I., Mashkov V.A., Mashkov O.A.* Self-diagnosis of modular system in random perfomance of elementary tests / Cybernetics and computing Tehnology, Discrete Control Systems, Allerton press, inc, 150 Fifth Avenue, New York, NY10011, №105, 1999, pp. 104-112.
7. *Gostev V.I., Mashkov V.A., Mashkov O.A.* Intermodular exchange of diagnosis information in Self-diagnosis of complex systems / Cybernetics and computing Tehnology, Discrete Control Systems, 1999, №105, pp. 95-103.
8. *Mashkov O.A., Mashkov V.A.* Fault-Tolerant of Computing Systems based on the Self-diagnosis by the traveling kerling Principle / ALLERTON PRESS INC., Cybernetics and Computing Technology (Argatic control system), 1999, pp. 89-94.

UDC 681.518.5

V.M. Azarskov, Dr. Techn. Sciences (National Aviation University, Ukraine)
V.I. Bogomya, Dr. of Philosophy (National Aviation University, Ukraine)

JUSTIFICATION OF REQUIREMENTS FOR A LONG-TERM GROUND AUTOMATED COMPLEX OF SPACECRAFT CONTROL IN GEOSTATIONARY ORBIT

In this article we present requirements for a long-term ground automated complex of spacecraft control in geostationary orbit, as a part of the methodology of enhancement of the functioning effectiveness of spacecraft control long-term systems.

Existing approaches to construction of a long-term ground automated complex of spacecraft control in geostationary orbit are normally based on the use of landing procedures under which parameters and management are optimized, provided the display is essentially characterized by one task (goal). Herewith the ideology of parametric synthesis with using of all traditional search methods of optimization is used. For example, under the existing approaches and the availability of favorable financing terms, the duration of the process of creating modern samples of space systems from concept to the first flight is at least 3-4 years, and under the development of fundamentally new concepts – is up to 7-10 years. In these circumstances, the price of possible research errors is naturally growing, which are practically impossible to fend off at the stage of systems application [1-2].

Current trends and features of the development of ground automated complexes of spacecraft control in geostationary orbit, as complex technical systems, are arising the requirements for quality and terms of their creation in terms of economy and resources. These requirements determine the urgency of developing the methodology of enhancement of the functioning effectiveness of spacecraft control long-term systems in geostationary orbit, under which to reach the required level of performance the best resources are used. Under the methodology, the authors mean set of principles, approaches, theoretical methods and techniques of research process improvement, implemented as a tested sequence of actions or operations (methods and techniques) to ensure the performance of conceptual synthesis [3] (see Fig. 1) .

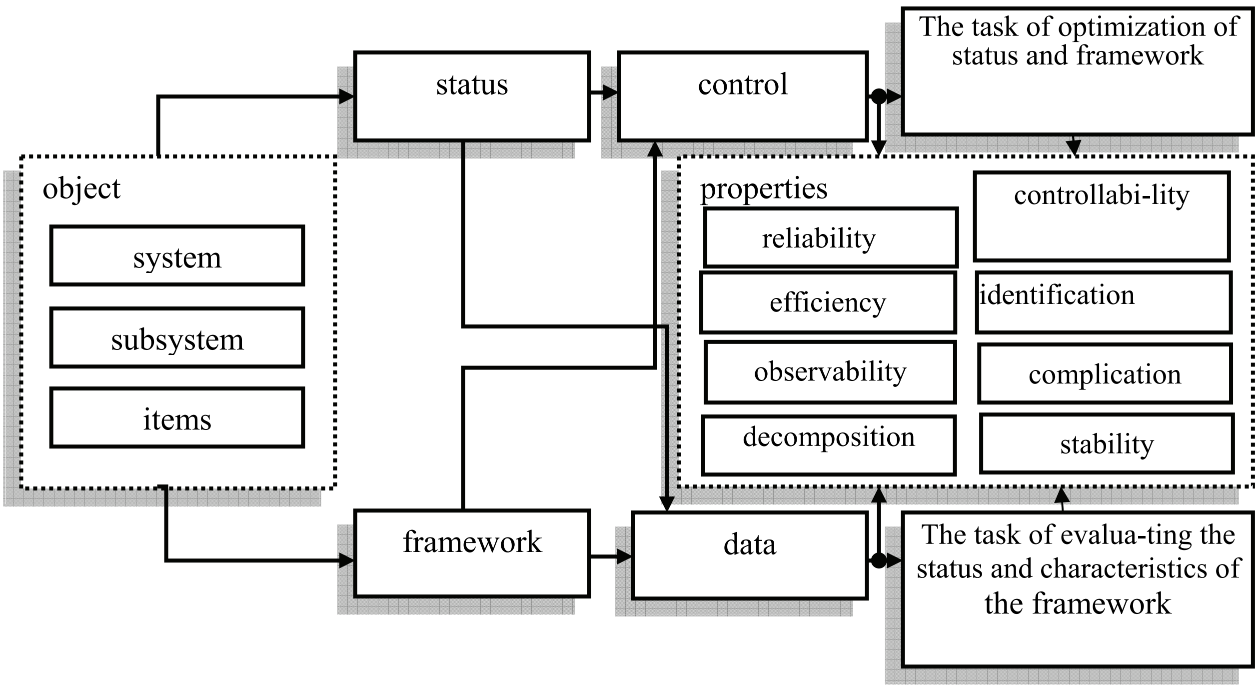

Fig. 2. Logic circuit interconnection properties of scientific validity

Formation and justification of the technical look of long-term ground automated complex of spacecraft control in geostationary orbit is the task of multicriteria parametric synthesis [2-4].

At the first stage of creating the adaptive ground automated complex of spacecraft control in geostationary orbit the designed object is described by a limited set of common parameters.

The system will be definitely determined by the set of parameters $y = \{y_j\}_{j=1}^{\alpha}$ which are optimized.

The analysis of projected conditions of creation and use of the system show the system of parametric restrictions on the numerical value of each characteristic in their entirety as:

$$в_{j_{\min}} \le y_j \le в_{j_{\max}}, j = \overline{1,б}, \tag{1}$$

where $\beta_{j\min}$, $\beta_{j\max}$ – respectively permissible lower and upper limits of numerical values change , and y_j - characteristics. The quality system is evaluated by the set of partial conflicting criteria, which represent the functions of parameters and form a m-dimensional vector:

$$\varphi = \{\varphi_i(y)\}_{i=1}^{m}. \tag{2}$$

It is necessary to define such values of parameters $y^* = \{y^*{}_j\}_{j=1}^{б}$ under which the vector of criteria is optimized (1) at known constraints (2).

Considering the process of spacecraft control in geostationary orbit as a sequence of two stages - making a decision and its implementation - in accordance with the following it is necessary to define following modification levels of administrative decision: theoretically found and practically implemented. In relation to the first the concept of "quality" should be applied and to the other – “efficiency”. Thus, the quality of administrative decision - is the degree to which the parameters of the selected decision alternative meet a particular system of characteristics that satisfies an operator and allows the efficient implementation of the decision. Therefore, the general requirements should include: scientific validity; unity; timeliness; reality; adaptability.

The scientific validity of spacecraft control in geostationary orbit is primarily determined by the degree of consideration of space technology functioning and development, trends in the economy development and society as a whole. Therefore, the scientific validity of management depends on the competence of an expert who makes a decision at every level of management. An expert may be competent and make high-quality decisions and effectively implement it if only he has special knowledge. The decision will be competent if it adequately reflects the purpose and objectives of management based on knowledge of the real situation, with clear organization of the work of authorities, and also organization of the rapid restoration of broken administration.

The most common properties of scientific validity are: stability, manageability, observation, identification, complexity, decomposition.

Stability. The stability of the system refers to the ability to maintain its behavior at the output within certain limits at any time under small perturbations in the initial state and structure.

Manageability. The ability of system to pass from any initial state to the final state for limited time with acceptable impacts. Using the notion of manageability under the system analysis the question of scope will be pointed out, and under the synthesis - the question of the fundamental structure and possible management restrictions.

Observation. System observation refers to the possibility of unambiguous determination of the condition and structure characteristics for a known signal at the output.

Identification. Identification refers to the opportunity to define the system structure for known signals at its input and output. If the system is identified, it is called closed, otherwise it is known as an open system [2,4].

Complexity. The concept of complexity is associated with many different conditions of the system and the indivisibility of its structure. If the system consists of *n* elements, we can consider the $n \times (n\text{-}1)$ connections between them.

Decomposition. The ability of the system to split into independent parts (subsystems). Decomposition property of some systems (assessment tasks) is closely related to the property of observation.

Besides, it should be noted that for ground automated complex of spacecraft control in geostationary orbit, as a technical system, apart from these properties there are such important performance properties as *reliability* and *efficiency*.

Analysis of processes that operate in the ground automated complex of spacecraft control in geostationary orbit shows two interconnected flows of signals: control signals flow and information flow. Control Flow is used to provide the desired purpose of system functioning. The information flow is used to develop the necessary control signals. Control Flow is related to optimization problem of system structure and condition of the system. Information flow is related to the problem of evaluation of the system condition and structure characteristics (with known structure). The interrelation of above entered concepts should be provided in a logical diagram (Fig. 2).

Unity. Unity of spacecraft control in geostationary orbit can not be achieved except through a sequence of complementary, consistent partial solutions which have organizationally purposeful, motivating, controlling and regulating nature.

Timeliness. The quality of the decision made on spacecraft in geostationary orbit in terms of real time is determined by its timeliness.

Reality. Decisions should be made and accepted considering the objective possibilities of space and ground segment.

Thus, spacecraft control in geostationary orbit can be considered high-qualified if it meets all the requirements listed above. Herewith we are talking about the conditions of the system since the failure of at least one of them leads to defects in quality and therefore the loss of efficiency, or even impossibility of its implementation.

Adaptability. Factor of changing impacts on the process of spacecraft control in geostationary orbit, dictates the necessity to perform another condition - adaptability.

As it is known, the process of synthesis of system control always provides for, firstly, precisely articulated management goals, and secondly, the availability of a priori information about the management object and the nature of perturbation acting on it. The volume of a priori information may be different. However, in this case the principal one is the question of sufficiency or insufficiency of a priori information about the object for achievement of the articulated management goals.

Management systems, built by using a priori information, sufficient to achieve the goal of management, are related to non-adaptive, regardless of the implemented management principle, the presence of feedback, randomness or determination of perturbations, used computational tools, etc. If the volume of a priori information about object properties can not achieve the articulated control goals, then the focus should be on adaptive control system. Thus, the adaptive control systems should include only such systems, which are designed for operation under a priori uncertainty and which in the operation process automatically adapt to random changes in the properties of the object and the environment.

According to the level of formalization of a priori uncertainty known approaches to building adaptive systems are divided into: parametric adaptation under which a priori uncertainty is the lack of knowledge of the parameters of the managing object, non-parametric adaptation, under which a priori uncertainty is not directly related to any parameters.

In both cases, uncertainty is reduced on the basis of successive observations of input and output signals in the management process. The objectives of spacecraft in geostationary orbit in terms of setting are closer related to the objectives of parametric adaptation.

According to the organization of process adaptation the used methods are divided into: searching, which are characterized by an iterative process of movement to achieve the required quality control; non-searching, based on the use of some necessary (sufficient) conditions of the required quality control.

According to the purposes of organization adaptations can be distinguished as: systems with special properties, operation of which makes the management process take some required properties, which may include stability, sensitivity to any perturbation or a priori information errors, etc.; optimal systems which ensure minimization of some functionals, reflecting the quality of controlled movement.

The use of non-searching systems with parametric adaptation seems to be more perspective for the flight control of spacecraft in geostationary orbit. These systems allow the maximum use of a priori information about the structure and parameters of the spacecraft.

The most developed type of adaptive control systems are obviously adaptive optimal control systems that combine high adaptation to the operation conditions with the movement control optimization and energy consumption for management with the chosen criterion of quality.

Implementation of adaptive optimal control of spacecraft flight will provide an opportunity to successfully solve the problem of creating a new generation of ground automated control system spacecraft due to: a significant expansion of the range of conditions in the use of different types of spacecraft; provision of comprehensive optimization of system functions performance; increase of safety of the spacecraft flight, including boundary modes (near border areas of operational modes); decrease in time and resource spending for development and operation of certain elements of the system due to the high level of unification.

Among the current approaches to building adaptive spacecraft control systems in geostationary orbit, there are various theoretical premises and techniques. The analysis of publications [1,2,4,5] allows to draw conclusions about the current state and the construction of adaptive spacecraft flight control systems.

Conclusions. Firstly, the concept of building adaptive spacecraft flight control systems in geostationary orbit based on combination of identification process parameters, evaluation of the state and optimization of a control signal are dominant. Secondly, the most common at this time is the identification of the selected model parameters of spacecraft movement with the help of algorithms that implement the method of least squares. Thirdly, the creation of spacecraft control laws one can observe using analytical relations of the real process and its reference models, analytical use of regulators that allows to determine linear feedback for the line facilities, optimal in the sense of quadratic criteria.

Noteworthy is the idea of combination of different principles of automatic configuration management systems. Thus, the unification of a setting by the parameters of the environment parameter adaptation [4-7] allows to take advantage of these approaches without the defects inherent to each of them separately. Software configuration by environment settings will provide a high speed device control system until the changes in the state and compensate emerging issues of sustainability.

Thus, nowadays the use of adaptive spacecraft control systems in geostationary orbit seems to be quite perspective. Research in this area, being developed in different countries, include sufficiently large number of approaches to the construction of such adaptive systems. However, in general, the problem of adaptive spacecraft control in geostationary orbit is far from comprehensive solution and that determines the relevance of research in this area.

References

1. *Molotov E.P.* Nazemnye radiotehnicheskie sistemy upravlenija kosmicheskimi apparatami.–M.:FIZMATLIT, 2004.–256 p.

2. *Solov'jov V. A. Upravlenie kosmicheskimi poletami : ucheb. posobie: v 2 ch. / V. A. Solov'jov, L. N. Lysenko, V. E. Ljubinskij* ; pod obw. red. L. N. Lysenko. M. : Izd-vo MGTU im. N. Je. Baumana, 2009.–chast' 1.–476 p.

3. *V. Azarskov, V.Bogomya, D. Bloha, V. Davydov.* Povyshenie effektivnosti sistemy upravlenija kosmicheskimi apparatami putem ispol'zovanija morskogo punkta./ Elektronika ta sistemi upravlinnja.–K.:NAU, 2012.–№1(31).–P.76–83.

4. *Degtjarev K.L., Sirazetdinov T.K.* Teoreticheskie osnovy optimal'nogo upravlenija uprugimi kosmicheskimi apparatami.–M.:Mashinostroenie,1986.–216 p.

5. Statisticheskaja dinamika i optimizacija upravlenija letatel'nyh apparatov: Uch.posobie dlja aviacionnyh special'nostej vuzov/*A.A.Lebedev, V.T.Bobronnikov, M.N. Krasil'wikov, V.V.Malyshev*.–M.:Mashinostroenie, 1985.–280 p.

6. Kosmicheskie sistemy svjazi: Ucheb. posobie / *V. F. Mihajlov, V. I. Moshkin, I. V. Bragin;* GUAP. SPb., 2006.– 174 p.

7. *Kravec V.G.* Avtomatizirovannye sistemy upravlenija kosmicheskim poletami.–M.:Mashinostroenie, 1995.–250 p.

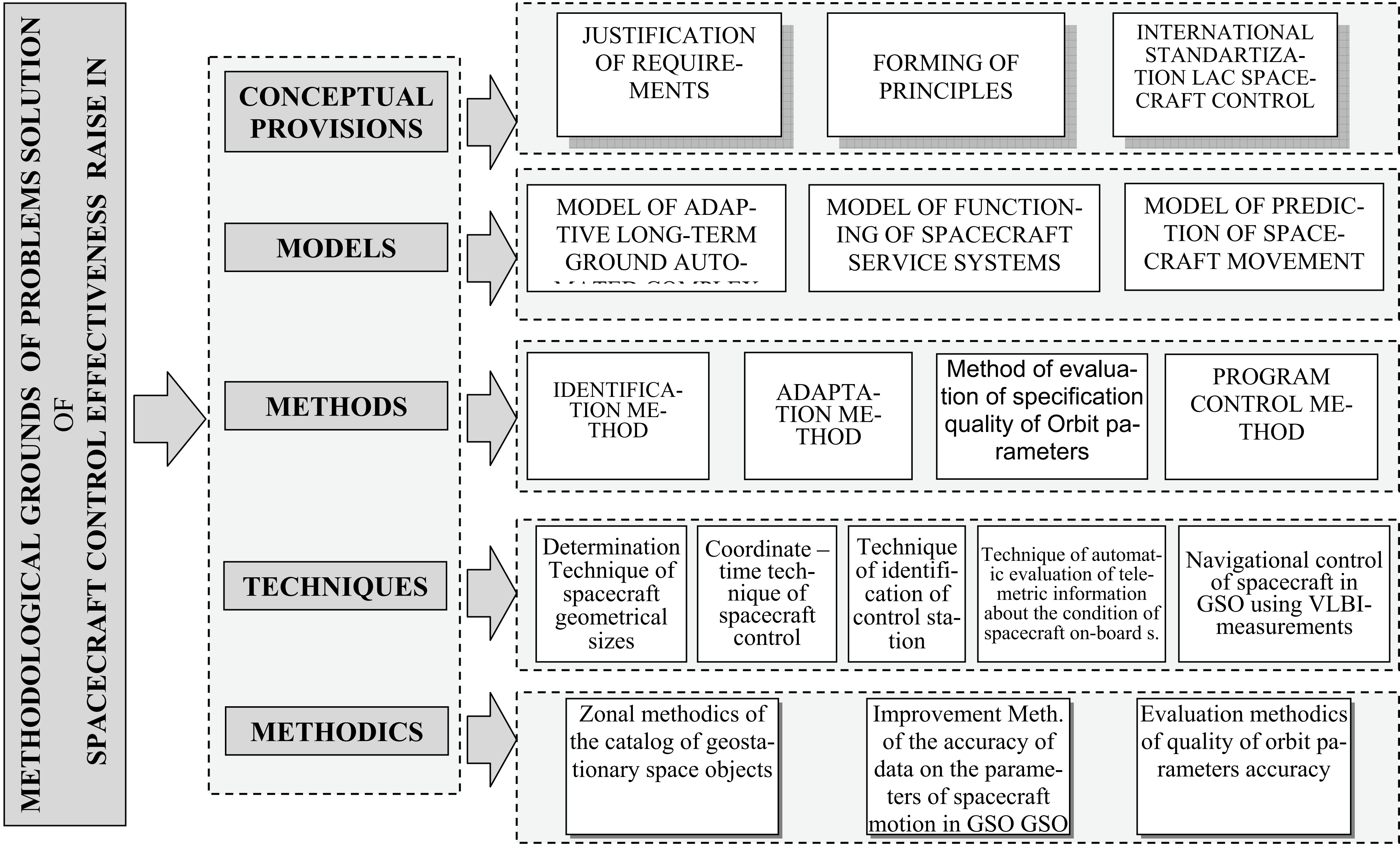

Fig. 1. Methodological grounds of solution of the problem of raise of spacecraft control effectiveness in geostationary orbit

UDC 681.13

V.V. Pavlov, doctor of technical science (NAU, Ukraine)
K.A. Kopytova, post graduate student (IRTCofITandS NANU)

COMPLEX AIRCRAFT CONTROL SYSTEM WITH DISTRIBUTED AERODYNAMICS

The article is dedicated to design method of computational model of composite traffic control of aircraft with command flight path. A method of reducing wind gust loads acting on the wing of an aircraft involves adjusting the aerodynamic configuration of the wing so as to alter the distribution of lift generated by wing. The required adjustment of the lift distribution is preferably achieved by deflecting some part of wing mechanization during climb and descent.

Our investigation aims at improving the quality of preselected altitude hold and compensate wind gust loads.

The task is development of automatic control system of flight altitude, which controls directly lift generation of wing.

Our aim is achieved by using invariance theory and active automatic control system. Simulation is performed at MATLAB with SimuLink. Aerodynamic Clark Y wing design is applied [1]. The method of mean-square deviation of output signal from specified value is used for the quality evaluation of results.

Now more and more attention it is given to keeping quality of flight altitude in the perturbed atmosphere. For compensation of wind gust loads on itinerant aircraft in flight level active and passive methods of decrease in loadings from vertical wind gust are used. It is possible to refer change of aerodynamic and geometrical characteristics of a wing to a passive method. It is possible to carry the automatic systems operating directly carrying power of a wing, for example the flap to active methods, a quencher of carrying power and other types of wing mechanization, the autopilot with the signal of an overload influencing an elevator [2].

The theory of invariance found wide application in practice at creation of high-quality systems of automatic control. Its application allows to define structure of dynamic system and size of its parameters such that the mistake caused by action on system of indignations, was disappearing small or equal to zero [3].

Applying the theory of invariance and having added in a contour of flight altitude control (picture 1) an additional contour of direct control of lift, using control of rotary surfaces of a wing in a mode of control surfaces, allows to parry action of wind indignations on a trajectory of flight (picture 2). Such system of creation of aerodynamic forces with application it for a multicomponent altitude control of the aircraft will allow to increase quality of working off of maneuver of evasion in a conflict situation from an traffic collision avoidance system (TCAS II) and to reduce time for aircraft divergence, without creating thus new conflict situations.

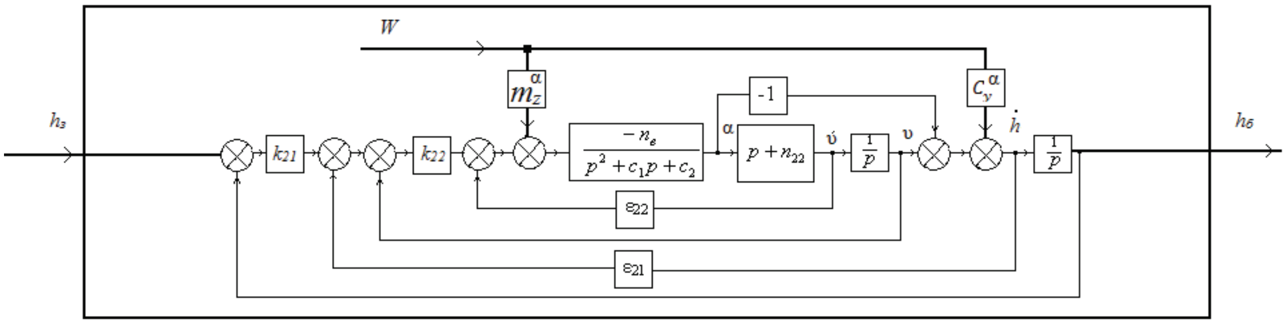

Picture 1. The contour of flight altitude control

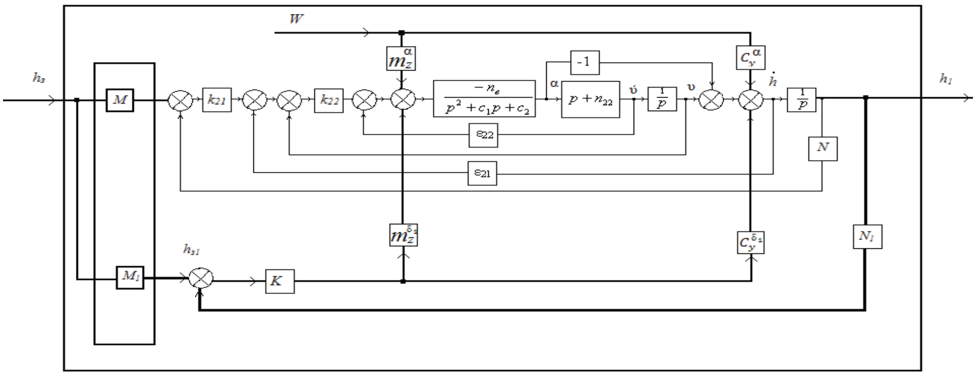

Picture 2. The contour of flight altitude control with additional contour of direct control of lift

Turn of additional managing directors of surfaces, such as the flap, demands considerable efforts and energy expenses therefore instead of fast creation of carrying power by a deviation of the flap compensations of action of flaws by means of slow working off of the set signal of change of height of flight by means of an elevator deviation prefer. Besides, energetically capacious deviation of the flap not only increases a gradient of carrying power, but also increases a gradient of front resistance and causes the diving moment of aircraft. For preservation of speed of flight because of increase in value of front resistance it is necessary to change speed of flight, having changed draft of the engine that isn't desirable in a conflict situation.

Fast reaction of system to a flaw is the effective solution of a task. Use of individual elements of mechanization of a wing or their combination depending on height of flight, number of the Move, an available profile of a wing, it is possible to calculate energetically favorable combination of change of a wing configuration for parrying of atmospheric indignations with the most favorable combination of change of gradients of carrying power, front resistance and the pitch moment [4].

The multicomponent altitude control of aircraft at performance of maneuver of evasion in a conflict situation will allow to synchronize work of an elevator and wing mechanization for timely working off of the set signal of evasion from TCAS II and parrying of wind gusts (picture 3).

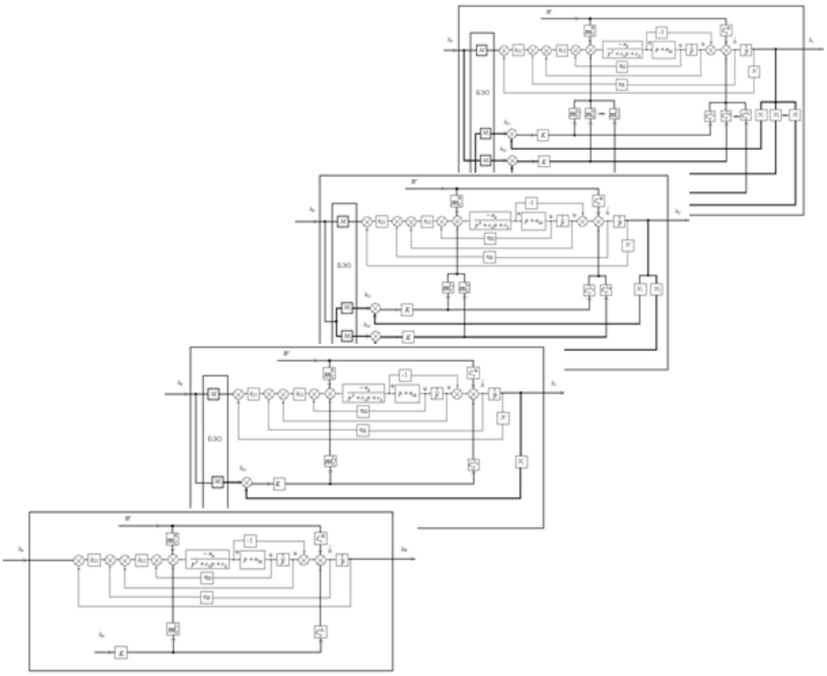
Picture 3. The multicomponent altitude control of aircraft

Having entered weight factors into system of a multicomponent altitude control, we will receive an expert assessment as will correctly dispose of change of mechanization of a wing in a conflict situation and to unload with its help the main control path in height of flight. Distribution of aerodynamic forces and the moments leads to loading reduction from action of flaws. The distributed multicomponent architecture of such control system allows to exercise adaptive administration of dynamic system [5].

To use high-speed (active) mechanization of a wing, for change of a gradient of carrying power, move apart cracks, control with which not only are energetically favorable, but also change a gradient of carrying power without essential change of a gradient of front resistance and the pitch moment. Energy losses on change of a wing configuration are opposed to quality of performance of maneuver of evasion in the indignant atmosphere.

On safety of flight of aircraft in an flight level, carrying out evasion maneuver in a conflict situation, quality of dynamics of working off influences as actions of a vertical wind gusts and the set signal on change of flight altitude by a contour of automatic control in flight altitude which can be raised having applied system of creation of aerodynamic forces and its use to a multicomponent altitude control.

A computational model of aircraft movement in altitude control loop of flight is designed with the use of composite control technology. Composite technology of flight altitude control allows improving the quality of preselected altitude hold and compensating turbulence. Deviation area between input signal and output signal developed by elevation rudder in altitude control loop of flight is 8,9 times more than the same developed by wing mechanization (picture 4).

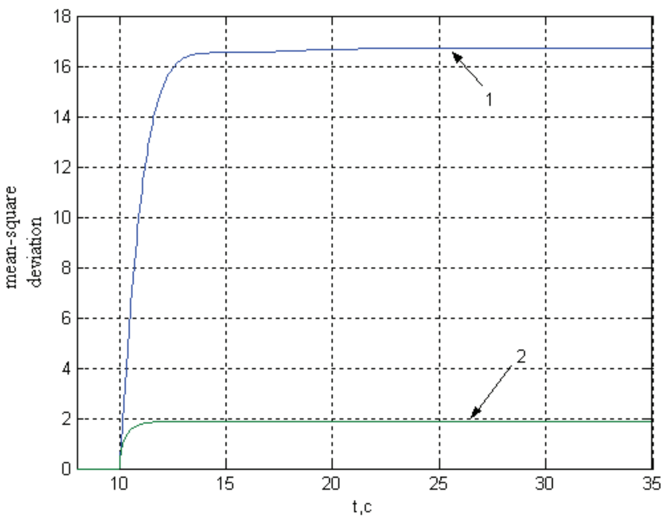

Picture 4. The mean-square deviation from a preset value in flight control path in height by means: 1–elevator; 2–mechanization covered.

Conclusion

An advantage of developed composite control technology is the use of aerodynamic scheme of changing wing profile as additional control surface. Improving the quality of preselected altitude hold allows to decrease the time for compensating turbulence and increase flight safety level.

References

1. *Weick F.E., Shortal J.A.* The Effect of Multiple Fixed Slots and Traiking-Edge Flap on the Lift and Drag of a Clark Y Airfoil. – N.A.C.A., Report №427, 1930 – pp.531-536.

2. *Мхитарян А.М.* Динамика полёта. – М.: Машиностроение, 1978. – 424с.

3. *Шевелёв А.Г.* Исследование систем стабилизации самолёта. Диссертация на соискание учёной степени кандидата технических наук. – К.: КИИГА, 1961. – 206с.

4. *Павлов В.В.* Интеллектуализация авионики для решения конфликтных задач безопасности движения воздушных судов/ В.В. Павлов, Е.А. Копытова // Кибернетика и вычислительная техника. – 2010. - №161. – С. 35.-.41.

5. *Павлов В.В.* Технические эргатические системы // В.В. Павлов, А.Н. Воронин, В.Н. Голего, А.М. Мелешев, О.С. Яковлев– К.: «Вища школа», 1977. – 344с.

UDC 519.6: 621.396.96

N.M. Glazunov, D.Sc. (*phys.-math.*)
F.J. Yanovsky, D.Sc. (*eng.*)
(*National Aviation University, Ukraine*)

MATHEMATICAL MODELS AND METHODS TO RADAR

We review mathematical models and methods to radarand investigate some new problem which connects with anisotropy of media, where the radar is operating. Most considerations relate to the theory of radar from group theoretic perspective.

Introduction

The invention of radar, and its steady improvement over the years are based on insights and experiments by H. Hertz, A. Popov, C. Hulsmeyer and many otherresearchers and engineers as well as on mathematical models and methods of electrodynamics and other branches of science[1–4].One of the mathematical bases of the radar is the set of Maxwell equations and some other equations, together with the solutions of these equations in various spaces and media. For theoretical and applied research,the symmetry is important, more exactly the symmetry of space, medium, and the symmetry of the corresponding differential equations. In mathematics, symmetriesare represented by groups.

Recently the anisotropy ofthe cosmic microwave backgroundwas discovered [5,6], in particular, using radars and radio telescopes. The anisotropy is also manifested in some other media where radar operates. Apparently, the best-known example of an anisotropic medium is a crystal; the crystal lattice shows different properties in different directions. Mathematical models of crystal lattices are geometric lattices and lattice automorphisms. They usually are represented by groups.

There is a special class of groups, named anisotropic groups. An important class of anisotropic spaces is class of spaces with a metric function, or Finsler metric, called Finsler spaces. In this consideration we restrict ourselves to spaces with anisotropy similar to the anisotropy of the crystal lattice.

In this paper, we provide an overview of mathematical models and methods for radar, and in this regard, we study some problems of anisotropic groups. In accordance with this, majority of our considerations apply to the theory of the radar in terms of group theory.

The content of the paper is following. First, we recall and reformulate some mathematical foundations of radar. This includes the equations that describe the radiation energy density, as well as the energy density backscattered by the target that is returned to the radar; check of statistical hypothesesto determine target presence (hypothesisH_1) or target absence(hypothesis H_0); radar waveform parameters and their selection, ambiguity function.

In this extended summary we present the ambiguity function in the context of the group theory and the theory of anisotropic groups. The material is presented concisely.

Ambiguity function and group theory

Radar ambiguity function [10] describes the properties of the sounding waveform. Normally it is a two-dimensional function of time delay and Doppler frequency. The ambiguity function is determined by the properties of the radar, and does not depend on any particular target scenario. There are different definitions of ambiguity function. Initially it was restricted to narrowband signals. Later it was expanded to describe the propagation delay and Doppler relationship of wideband signals [11].A new approach to the definition of the ambiguity function using the notion of the copula and nonparametric extension of the wideband ambiguity function for random radar signals was suggestedin [12, 13]. Generalization for the case of MIMO radar is done in [14]. Here we consider the ambiguity function in conjunction with the group theory [4].

Let $w(t)$ be the radar waveform. The ambiguity function $A_W(t,f)$is the two dimensional function which measures the ability of that particular waveform $w(t)$ to allow the radar system to estimate accurately the location and velocity of the target. In the framework of “range-Doppler” (t,v)plane the scene of the radar can be regards as a linear combination

$$scene(t) = \sum_k c_k \delta(t - r_k, v - v_k)$$

wherer_k are distances of scatterers which moving with velocities v_k relative to radar[4].In the case when the transmitter and receiver are collocated the signal returned to the receiver has the form

$$ret(t) = \sum_k c_k w(t - 2r_k) e^{4\pi i v_k f_c t}$$

wheref_c is the carrier frequency. The expression

$$\int w(\tau - 2r)\, e^{4\pi i v_k f_c t} \overline{v(\tau - t)} d\tau$$

describes the behavior of radar. After some transformations the radar ambiguity function has the form

$$A_{w,v}(t,f) = \int w(\tau) e^{2\pi i f \tau} \overline{v(\tau - t)} d\tau.$$

The connection of the radar ambiguity function with the multiplier representation of $\mathbb{R}^2$ is given in [4].$\mathbb{R}^2$is an example of linear algebraic group. Below we recall the framework of linear algebraic groups and partially the framework of anisotropic groups.

Linear algebraic groups

Roughlyspeaking an algebraic group is the structure of variety plus the group structure on the variety [7]. Present shortly here a framework of linear algebraic groups and anisotropic groups. We follow to [7,8].

Let k be a field, $\bar{k}$ beits algebraic closure, $M(n,k)$ - the ring of all $n \times n$ matrices over k.

$$X(k) = M(n,k) = k^{n^2}$$

In Zarisski topology the closed sets in $X(k)$ are algebraic sets, i.e. sets of zeros in k^{n^2} the polynomials $p(x_{11}, x_{12}, \cdots, x_{nn}) = 0$.

$GL(n,k)$ - the group of all invertible $n \times n$ matrices over k.

$GL(n,k)$is the affine variety in k^{n^2+1} under identification

$$g = (g_{ij}) \mapsto (g_{11}, g_{12}, \cdots, g_{nn}, (\det g)^{-1}).$$

A subgroup G in $GL(n,k)$ is called the *algebraic group of matrices*, if G is the closed set in $GL(n,k)$, i.e. there exists the set of polynomials $p_\alpha = p_\alpha(x_{11}, x_{12}, \cdots, x_{nn}) \in k[x_{11}, x_{12}, \cdots, x_{nn}] (\alpha \in J)$, such that

$$G = \{g = (g_{ij}) \in GL(n,k) | p_\alpha(g_{ij}) = 0, (\alpha \in J)\}.$$

The ring $k[G] = k[g_{11}, g_{12}, \cdots, g_{nn}, (\det g)^{-1}] = k[x_{11}, x_{12}, \cdots, x_{nn}, z]/I$,where I is the ideal of polynomials from variables $x_{11}, x_{12}, \cdots, x_{nn}, z$, which vanished on G. Here G is considered as the subset of the set k^{n^2+1} under the inclusion of $GL(n,k)$in k^{n^2+1}.

An element x of the algebraic group G is called *nilpotent* if there exists natural $r \geq 1$ such that $x^r = 0$. This condition is equivalent to the condition that all eigenvalues of x are zero.

An element x of the algebraic group G is called unipotent if $x - 1$ is nilpotent. This condition is equivalent to the condition that all eigenvalues of x are 1.

An element x of the algebraic group G is called *semisimple* if x can be reduced to the diagonal form.

Representations

Rational representation of G is the morphism $\rho: G \to GL(m,k)$. Let consider G as the group of matrices, so $k[G] = k[g_{11}, g_{12}, \cdots, g_{nn}, (\det g)^{-1}]$.

Then each element of the matrix $\rho(g)$ is the polynomial from $g_{11}, g_{12}, \cdots, g_{nn}, (\det g)^{-1}$.

Characters

The one dimensional character of G is the rational representation of degree 1: $\chi: G \to GL_1$. Below we will consider the one dimensional characters only and will call their characters.

For G we denote by $\hat{G}$ the group of characters of G.

Algebraic tori

Algebraic group G is the algebraic torus, if it is isomorphic to the product of d copies of GL_1 (where $d = \dim G$).

Let T be the torus of dimension d. Then each element of T can be represented as the set $(x_1, \cdots, x_d)$, $x_i \in k$.

The character χ of the torus T can be represented as

$$\chi(x) = x_1^{n_1}, x_2^{n_2} \cdots x_d^{n_d},$$

where $n_i \in \mathbb{Z}$, so $\hat{T} \simeq \mathbb{Z}^d$.

Theorem[7]. Let T be the torus over k. Then the next conditions are equivalent:

a) All characters of$T$ are defined over k: $\hat{T} = \hat{T}_k$.
b) $T$is reducible to the diagonal form over k.
c) For every representation $\rho: T \to GL(m,k)$ over k the group $\rho(T)$ is diagonalizable over k.

The torus that satisfies the equivalent conditions a) – c) is called the *splitted$k$ $-$torus* and that it is splittedover k.

Definition. A torus is called anisotropic over k, if $\hat{T}_k = \{1\}$.

Let k be the field of real numbers or the field of p $-$adic numbers.

Then the 1-dimensional torus T_k will anisotropic if and only if it is isomorphic to $SO(2,k)$ (the circle).

The torus T_k is compact if and only if it is anisotropic, i.e. is the product of circles.

Anisotropic reductive groups

Connected reductive group G over k*is called anisotropic*, if it has no k-splitted tori $S \neq \{e\}$.

Example. Let F be the nondegenatate quadratic form in the $k-$vector space V with coefficients in k. Let $G = O(F)$ be the orthogonal group relatively F. Then G is anisotropic over k if and only if F does not represent 0over k.

Lattice representations and theta functions

Lattice representation of the lattice subgroup $\mathbb{Z}^2$ of $\mathbb{R}^2$ and other lattice representations involve theta functions. Some algebraic and number-theoretic resultsin the field are presented in chapters 3 and 6 in the book[9]. We will specify the results to the radar theory framework.

Conclusions

We have given a short review and the results of our investigations in the field of mathematical models and methods in radar. Most considerations relate to the theory of radar from group theoretic perspective. Simulation of the presented algebraic approach has shown the improvement over the conventional procedures.

In the talk, more details of the general framework of group-theoretic models and methods in radar and signal processing, present lattice models and methods of anisotropic media will be presented. Algorithms for group theory to radar and estimation of the complexity of these algorithms will be presented.

These results relate to the computer algebra of radar as well as to the efficiency of radar models and methods.

References

1. *Moran W.*The mathematics of radar // Twentieth Century Harmonic Analysis. Boston: Kluwer, 2001. – P. 93-120.
2. Proceedings 2011 Microwaves, Radar and Remote Sensing Symposium // Eds. F. Yanovsky. – Kiev. – 2011. – 394 p.
3. *Wicks M., Himet B.*Four problems in radar // Computational noncommutative algebra and applications. Boston: Kluwer, 2003. – P. 57-73.
4. *Morgan W., MantonJ.*Group theory in radar and signal processing// Ibid. – P. 339-362.
5. *SmootIII,G.F.* The anisotropy of the cosmic background radiation: the discovery and scientific importance // Uspehifizicheskihnauk (Advances of Physic Science), Vol. 177, No 12. – 2006. – P.1295 – 1317 (In Russian).
6. *SazhinM. V. Anisotropy and polarization of cosmic background radiation. The last data //* Uspehifizicheskihnauk (Advances of Physic Science), Vol. 174, No 2. – 2004. – P.197 – 205. (In Russian).
7. *Borel, Armand, Linear algebraic groups, Graduate Texts in Mathematics*, Berlin, New York: Springer-Verlag, 1969, (2nd ed 1991); Translation into Russian: Moscow, Mir, 1972. – 269 pp.
8. *GlazunovN. M.OnFinslergeometrieswithsymmetric functions and anisotropic groups//* VIIIInternational Conference “Finsler ”конференция «Finsler Extensions of Relativity Theory », Moscow, Bauman Moscow State Technical University. – 2012. – P. 63– 64 (in Russian).
9. *GlazunovN. M., SkobelevV. V., SkobelevVG.Manifolds over rings*. *Theory and Applications*. Institute of Applied Mathematics and Mechanicsof NAS of Ukraine, Donetsk, 2011. – 323 pp.
10. *Woodward P.M. Probability and Information Theory with Applications to Radar, Norwood, MA: Artech House, 1980.*
11. *L. Sibul, L. Ziomek, ”Generalised wideband crossambiguityfunctiom”*, IEEE International Conference on Acoustics, Speech, and Signal Processing, ICASSP '81.01/05/198105/1981; 6:1239–1242.
12. *R.B. Sinitsyn and F.J. Yanovsky, Copula Ambiguity Function for Wideband Random Radar Signals*, The International IEEE Conference on Microwaves, Communications Antennas and Electronic Systems, Tel-Aviv, Israel, November 7-9, 2011, 5 pp.
13. *Bokal, Z.M., Sinitsyn, R.B., and Yanovsky,* F.J. *Generalized copula ambiguity function application for radar signal processing*, Proceedings Microwaves, Radar and Remote Sensing Symposium (MRRS), 2011, 25-27 Aug. 2011, 313 – 316.
14. *R.B. Sinitsyn and F.J. Yanovsky, MIMO Radar Copula Ambiguity Function*, European Radar Conference EuRAD-2012, Amsterdam, The Netherlands, Oct 31-Nov 2, 2012, 1-4.

S. F. Kolomiets,
Dep. of Mathematical Problems of Wave Propagation Processes. Moscow Institute of Physics and Technology, Dolgoprydniy, Russia.

TECHNIQUE OF SPACE DISCRETISATION FOR CW-RADARS

This report is devoted to a discussion of the approaches to measuring distance by means of CW radars. Corresponding techniques of space discretisation would be especially in demand for probing within an atmospheric boundary layer which is unsearchable by means of high power pulsed radars.

Introduction

In any science there are fundamental problems, the solution of which requires a substantial period of time. It would not be a great mistake to say that for atmospheric measurements in general and for radar measurements in particular the main problem of this kind is reliability and accuracy of such measurements. It is obvious that more reliable and accurate measurements in the atmosphere could provide us with unique facilities for further insights into its nature. Our civilization has finally recognized that far from being robust, atmospheric system is better described as a touchy balance among a number of natural forces that we barely understand. So we need to make our measurements with higher accuracy to make new models of the atmospheric processes more adequate.

Despite the fact that a present-day situation calls persistently for measurements, weather radars are still a tool for observations, but not for measurements. One can conclude, even after a very brief analysis, that most techniques which have been developed to date for measurements by means of weather radars are only hopes on measurements *per se*. The problem is that almost all of such techniques use *a priori* information about the microstructure of the object of interest. Indeed, the microstructure of any meteorological targets changes significantly with time and space. Therefore, true measurement techniques must take into account not only a great variety of models of a radar echo but also a well-developed set of clear-cut criteria of applicability as well as means of accuracy assurance [1].

Despite the fact that there are some resources for some improvements of radar return interpretations based on conventional models of distributed point targets for pulsed radars [2, 3], it is the very question about acceptability of pulsed radar for fine measurements in the atmosphere that is still open. As aptly remarked in [4] entire history of radar development in general, but especially its first stage, is a history of the competition between pulsed and continuous-wave radars.

In Russia one of the first works devoted to radars were made in 1932-1933 by academicans L. I. Mandelshtam, N. D. Papaleksi and their collaborators. They were concentrated on the development of an interferometric range finder and provided foundation for distance measurement techniques using CW. Yet later the situation had changed dramatically. In a very short period of time after the work by Y. B. Kobzarev in 1937 pulsed radars received such rapid development, that they replaced CW radars almost everywhere. Nevertheless specific weaknesses of pulsed mode began to play a role after the World War II as the range of radar application grew significantly.

Specific Limitations of Pulsed Weather Radars

Modern studies of specific limitations of pulsed weather radars showed that – apart from well-known near field problems, difficulties with generation of high power pulses and contradiction between the distance, spatial discretisation and feasible pulse power – additional constraints on the accuracy of radar measurements arise from imperfections in the envelope of the probing pulse of the weather radar caused by the technical limitations of the thyratron modulator and magnetron oscillator in a radar transmitter [4]. As follows from [5], for instance, the typical deviations of the actual probing pulse envelope from perfectly rectangular are approximately 2–3% in rise time and 18–20% in fall time as measured from the pulse width corresponding to the half magnitude level. The top of the pulse is rounded mainly at the leading edge, in the range of 12–13% of the maximum magnitude, and distorted by small-scale (in comparison with the pulse width) random fluctuations within a range of 7–10% from the maximum magnitude.

Pulse parameters, including the maximum radiated power and the duration, are generally not stable and vary in a range of 5–10% from their base values. In addition, hydrometeors extending along the radar volume are illuminated irregularly because of the random variation of the envelope along its length and from pulse to pulse.

Space Disctretisation Techniques of CW-Radars

In the light of limitations of pulsed weather radars it is rather interesting to estimate measuring capabilities of CW radars. This interest is deepened when we consider great success of passive facilities in the way of atmospheric measurements. Unfortunately, in the realm of CW-radars the ideas of L. I. Mandelshtam, N. D. Papaleksi are still almost the only foundation for distance measuring while they are practically not applicable to distributed scatterers. Hence, before one can start estimating measuring capabilities of CW radars in meteorology and geophysics it is necessary to find something new for space disctretisation which, at the same time, would be applicable for the specific of the atmospheric measurements.

The rapid development of pulse radars in the 1960-th result in the fact that most part of radar theory was expressed in corresponding terms. In particular, the main radar equation for distributed point targets which was developed in the days of giddy success of pulsed radar was expressed in the form applicable for pulse radars only:

$$P_r = \Pi_M \cdot \frac{Z}{L^2}$$

where: Z is a reflectivity factor of meteorological target; L is a distance to the radar volume; Π_m is an energy potential for distributed points target and pulsed mode $\Pi_M = \Pi_1 \cdot K_M$, where $\Pi_1 = \frac{P_t \cdot G \cdot A}{16\pi^2}$ is a conventional energy potential (applicable for a point target). It implies that a point target is being illuminated by radar with antenna's input power P_t, transmitting antenna's gain G and the area of the receiving antenna A. Factor K_M is, in turn, a product of multiplication of two other factors K_D and K_V: $K_D = \frac{\pi^5}{\lambda^4} \cdot |K|$ - accounts for diffractions on scatterers, $K_V = \frac{\pi c \tau \theta^2}{8}$ accounts for a pulse volume (θ is a width of the main lobe, τ is a pulse length). One can arrive at the following expression (where $|K| \approx 1$ being neglected) by combining together all the logically separated factors from above:

$$P_r = P_t \left(\frac{G \cdot A \cdot \pi^4 \theta^2}{16\lambda^4} \right) \left(\frac{c\tau}{4L^2} \right) Z$$

Assuming $\tau = dT$, $L = cT/2$ and taking S/N = 1 as a measure of minimum level of useful signal, one can write the following quantitative estimation of the effective probing distance L for CW radar with receiver noise P_n:

$$L = \frac{P_t}{P_n} \left(\frac{G \cdot A \cdot \pi^4 \theta^2}{16c\lambda^4} \right) Z$$

Conclusions

All the expressions of this report are to illustrate the possibility to discretize the distance by means of CW radars just by changing antenna's input power P_t. For getting more precise expressions it is necessary to solve corresponding radiative transfer equations.

It has to be noted that the problem stated in this report is very similar to that of passive probing in the atmosphere, but taking into account a possibility of the variation of transmitter output power. Based on the ideas presented, one can conclude that in CW radar probing it is not necessary to change frequency – as it holds true in passive probing – in order to change a weighting function and so the distance. There is a simpler way of space disctretisation based right on the variation of transmitter power and further comparison of two successive samples.

On the other hand, it is important that this approach is oriented on distributed targets only and not applicable in the case of point target. Basically, it seems to be complementary to the idea of L. I. Mandelshtam, N. D. Papaleksi which is not applicable right in the case of distributed targets.

Finally, great success of passive measuring techniques suggest that active CW probing with space discretization can find its way to real radars oriented on measurements. Such equipment would be especially in demand for probing within an atmospheric boundary layer which is unsearchable by means of high power pulsed radars.

References

1. *A. G. Gorelik, S. F. Kolomiets*, "Radio Waves Scattering on Distributed Scatterers and Stochastic Approaches in Radar Meteorology" (in Russian), Scientific miscellany of Moscow State University of Civil Aviation, 117, (2006). http://www.mstuca.ru/scientific_work/research_herald/
2. *A.G. Gorelik and S. F. Kolomiets*, "New Approach To Smoke Detection By Means Of Doppler Radar", Proceedings of MRRS 2011 (Microwave, Radars and Remote Sensing) , August 25-27, Kyiv, Ukraine.
3. *Kolomiets S. F.* "Generalized Multiplicative Coefficient of Z-R Relationship Deduced Under the Assumption of Modified Gamma DSD and Its Use Within a Wide Range of Wavelength and Time Intervals", Proceedings of the fourth world congress "Aviation in the XXI-st century", V.2 "Safety in Aviation and Space technologies", p. 22-7-22-10, September 21-23, 2010 Kyiv, Ukraine.
4. M. I. Skolnik, Radar Handbook, 2nd edition (McGraw-Hill, New York, 1990).
5. *B. S. Yurchak*, "Effective Droplet Number and Droplet Spectra Parameters That Determine the Radar Backscatter from Clouds and Rain", J. Russian Meteorology and Hydrology, 34, 1 (2009).

UDC 629.7.058.54 (045)

I. Prokopenko, Doctor of Science, Professor (National Aviation University, Ukraine)
V. Vovk, postgraduate student (National Aviation University, Ukraine)

ONE-SURVEY-DETECTION AND ESTIMATION OF TRAJECTORY PARAMETERS OF RAPID RADAR TARGETS

In this paper problems of one-survey-detection of rapid radar targets and estimation of parameters of their trajectories are considered. The method of estimation of trajectory parameters is based on ordinary least squares method. A statistical modeling was performed and detection characteristics were obtained

The tasks of detecting of moving radar targets and estimation of parameters of their trajectories are the tasks of secondary stage of radar signals processing. Classically, solutions of such tasks are based on multi-survey integration [1]: the values of samples obtained at each of m surveys are integrated and such integral value is compared with a detection threshold.

In case of rapid targets detection tasks, it is necessary to reduce the number of surveys before decision of presence of a target will be made. Such rapid targets produce the number of samples instead of one. In this case energy reflected from the target is distributed along the entire trajectory, forming a track. This "blurring" effect causes decreasing of detection threshold in the initial radar signal processing stage until the complete elimination of such detection procedure. The group of algorithms that use such "raw" data is called Track-Before-Detect (TBD) algorithms [2], [3]. However, to obtain reasonable probability of correct detection for low signal-to-noise ratio, these algorithms use the information obtained consequently in several radar surveys. To increase the probability of correct detection for constant false alarm probability in the case of one-survey-detection of rapid targets there is need to integrate the values of samples along the track, which was produced by the target during one survey cycle.

One of the tasks that appear in such one-survey integration is choosing of samples to determine the parameters of the track, since threshold processing on the stage of initial processing of the radar signal is absent.

The second task is the task of estimation of parameters of the trajectory along which integration will be made. One of the known techniques of estimation of parameters of parametric curves is the Hough transform [4]. In this paper we proposed to make such estimation based on the ordinary least squares (OLS) method. As will be shown below, the use of OLS provides a smaller estimation of parameters of the trajectory error in case of low signal-to-noise ratio and a higher probability of correct detection with the same probability of false alarm.

Target and sensor models

The signal at the input of the detector – a sequence of radio pulses with constant carrier frequency, random phase and constant amplitude v_S.

The noise is an additive Gaussian random process.

Then, the signal-noise model is:

$$s = \begin{cases} v_S \cos(\omega t + \varphi) + w, & \text{along trajectory,} \\ w, & \text{outside the trajectory,} \end{cases}$$

where $w \sim \mathrm{N}(0, \sigma_N)$, σ_N – standard deviation of noise; $\mathrm{N}(m, \sigma)$ denotes Gaussian distribution with mean m and standard deviation σ^2.

Since curvilinear motion can be approximated by straight line segments in the small intervals, straight line model was chosen as target trajectory model.

Image for analysis is formed from the output of the amplitude detector. Values of image samples are distributed with Rayleigh-Rice distribution, if they belong to the trajectory of target, and with Rayleigh distribution if they do not:

$$
z_{x,y} \sim \begin{cases} \dfrac{w_{x,y}}{\sigma_N} \exp\left(\dfrac{-\left(w_{x,y}^2 + v_S\right)}{2\sigma_N^2} \right) I_0\left(\dfrac{w_{x,y} v_S}{\sigma_N^2} \right), & \text{if samples belong to the trajectory of the target,} \\ \dfrac{w_{x,y}}{\sigma_N} \exp\left(\dfrac{-\left(w_{x,y}^2\right)}{2\sigma_N^2} \right), & \text{otherwise,} \end{cases} \tag{1}
$$

where $I_0(\cdot)$ is a Modified Bessel function of zero order, (x, y) – sample coordinates.

Sample images with tracks that corresponds to the model described by (1) for different signal-to-noise ratios are presented in Fig.1.

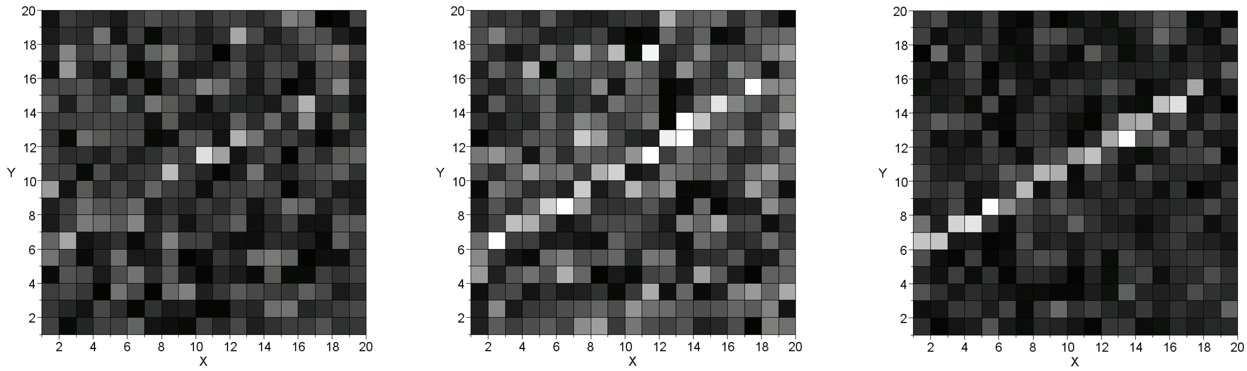

a) b) cac)

Figure1 – Image with track of radar target with signal-to-noise ratio 7 dB (a), 10 dB (b) and 15 dB (c)

Target detection and trajectory parameters estimation algorithm

For estimation of trajectory parameters we propose to select the maxima for each of the columns or rows of analyzed images. These samples we will call "basic samples".

Mean square deviation of these basic samples from the potential stripe line, which the trajectory belongs to, is defined as:

$$
e = \frac{1}{n} \sum_{i=1}^{n} \left(x_i \sin\varphi + y_i \cos\varphi - \rho \right)^2 , \tag{2}
$$

where ρ –"distance" to the straight from the origin; φ – angle between the straight and the Ox axis (Fig. 2), (x_i, y_i) – coordinates of i-th basic sample; n – number of basic samples.

Since we propose to use as a method of estimation of trajectory parameters the OLS method, then trajectory parameters are determined as the solution of the following equations, relatively to ρ and φ:

$$
\begin{cases} \dfrac{\partial e}{\partial \rho} = -\dfrac{2}{n} \sum_{i=1}^{n} \left(x_i \sin\varphi + y_i \cos\varphi - \rho \right) = 0, \\ \dfrac{\partial e}{\partial \varphi} = \dfrac{2}{n} \sum_{i=1}^{n} \left(x_i \sin\varphi + y_i \cos\varphi - \rho \right)\left(x_i \cos\varphi - y_i \sin\varphi \right) = 0. \end{cases} \tag{3}
$$

After mathematical transformation, the system of equations (3) transforms to:

$$
\begin{cases} \rho = \sin\varphi \cdot E[x] + \cos\varphi \cdot E[y], \\ \left(\cos^2\varphi - \sin^2\varphi\right)\left(E[x] - E[x]E[y]\right) + \cos\varphi \sin\varphi \left(E\left[x^2\right] - E^2[x] - E\left[y^2\right] + E^2[y]\right) = 0, \end{cases} \tag{4}
$$

whence we obtain:

$$
\begin{cases} \rho = \sin\varphi \cdot E[x] + \cos\varphi \cdot E[y], \\ \left(4A^2 + B^2\right)p^2 - \left(4A^2 + B^2\right)p + A^2 = 0, \end{cases} \tag{5}
$$

where $E[\cdot]$ – mean of the expression in brackets; $p = \cos^2\varphi$;

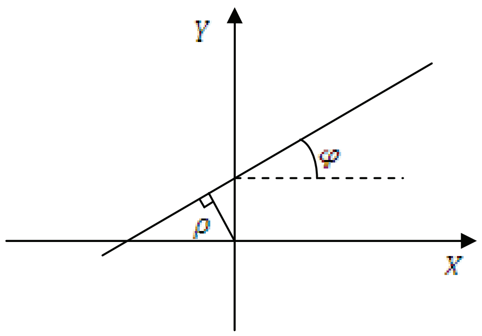

Figure 2 – Geometric parameters of a straight line

$A = E[x] - E[x]E[y]$;
$B = E[y^2] - E^2[y] - E[x^2] + E^2[x]$.

The roots of quadratic equation (5) meet the minima and maxima of expression (2). We can identify which of the root minimizes (2), as follows. Let (ρ_1, φ_1) and (ρ_2, φ_2) is the roots of the system (3) that correspond to the roots of the quadratic equation in (5), and $\Delta\varphi$ is the some small value. Then we should choose such values (ρ, φ), for which addition of $\Delta\varphi$ to φ will cause increase of value, calculated by (2).

The sign of $\cos\varphi$ can be obtained as follows. Let $\sin\varphi = \sqrt{1-p} \geq 0$. Then, as it can be seen from (4):

$$\begin{cases} \cos\varphi = \sqrt{p}, & \text{if } \left(\sqrt{p} \geq \sin\varphi \wedge A \geq 0 \wedge B \geq 0\right) \vee \\ & \vee \left(\sqrt{p} \geq \sin\varphi \wedge A < 0 \wedge B < 0\right) \vee \\ & \vee \left(\sqrt{p} < \sin\varphi \wedge A \geq 0 \wedge B < 0\right) \vee \\ & \vee \left(\sqrt{p} < \sin\varphi \wedge A < 0 \wedge B \geq 0\right), \\ \cos\varphi = \sqrt{p}, & \text{otherwise}, \end{cases}$$

while ρ can be either positive and negative values.

To make a decision about target availability integration of values of basic samples along obtained trajectory is performing. Since the probability that the basic samples lie on a certain straight is very low, the accumulation is carried out in a certain band around the line. Thus, statistics, calculated for each image is:

$$S = \frac{1}{Q}\sum_i w_i a_i,$$

where a_i – value of i-th base sample; $w_i = 1$, if i-th base sample lies within integration strip, and $w_i = 0$, otherwise; Q – sum of all samples within integration strip.

Another option is to build a statistics by integration maximal values in each row (or column) of image within the integration strip along obtained trajectory. The advantage of this approach is the consideration, in case of correct estimation of trajectory parameters, more values that correspond to the actual track, even if in the corresponding column (or row) of analyzed image maxima does not correspond to it.

Statistical modeling and simulation results

Detection characteristics for the proposed methods derived from statistical modeling are shown in Fig. 3.

These characteristics were obtained as a result of 10,000 simulations for each value of signal-to-noise ratio at probability of false alarm0.01. Image dimensions are 16×16 pixels. Integration strip width is 2. Detection characteristics in case when Hough transform instead of OLS is used to obtain trajectory parameters are shown for comparison. The ideal detection characteristics, in case when integration is making along actual track are also shown.

To analyze the performance of the estimation the parameters of the trajectory of target the following characteristic was used:

$$E = \sqrt{\frac{1}{n}\sum_i \left(y_i - y_i^*\right)^2}, \tag{6}$$

where y_i – ordinate of the actual track point in a coordinate system where that track is parallel to the

Ox axis; y_i^* – corresponding ordinate (in the same coordinate system) of the track point, which lies on a line with parameters obtained as a result of the proposed method.

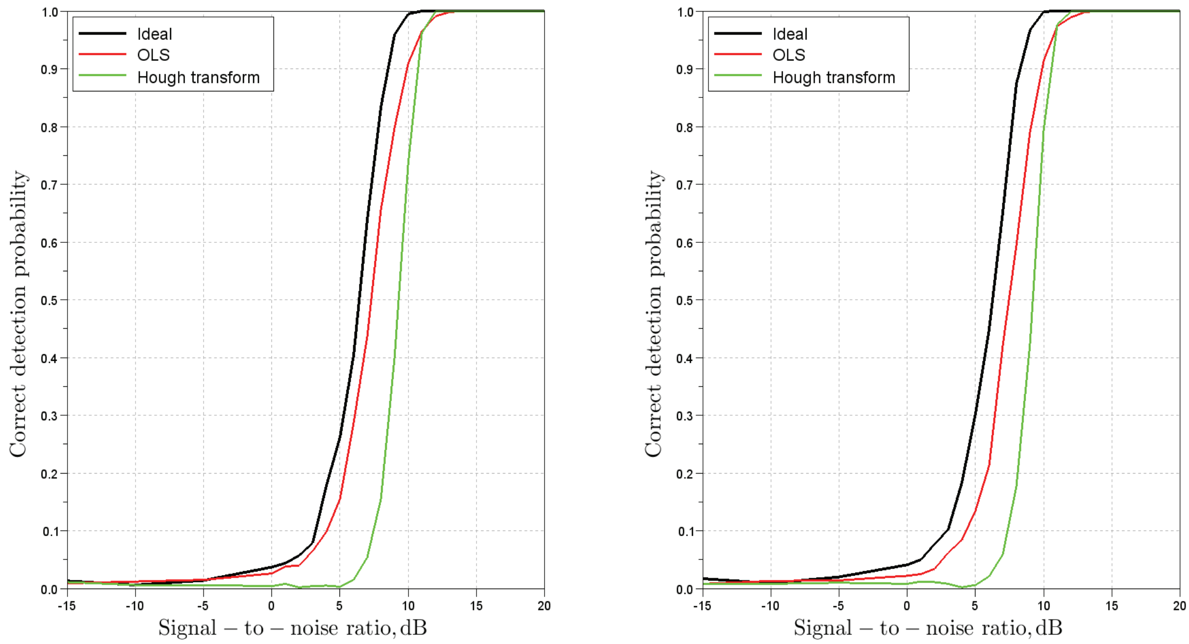

a) b)

Figure 3 – Detection characteristics obtained by the integration of values of basic references in an integration strip (a) and by the integration of maximum values along the track within an integration strip (b)

The obtained performance of the proposed algorithm for different signal-to-noise ratios and the same characteristics in case of use the Hough transform is shown in Fig. 4. Mean of the absolute errors of trajectory parameters estimation is also shown.

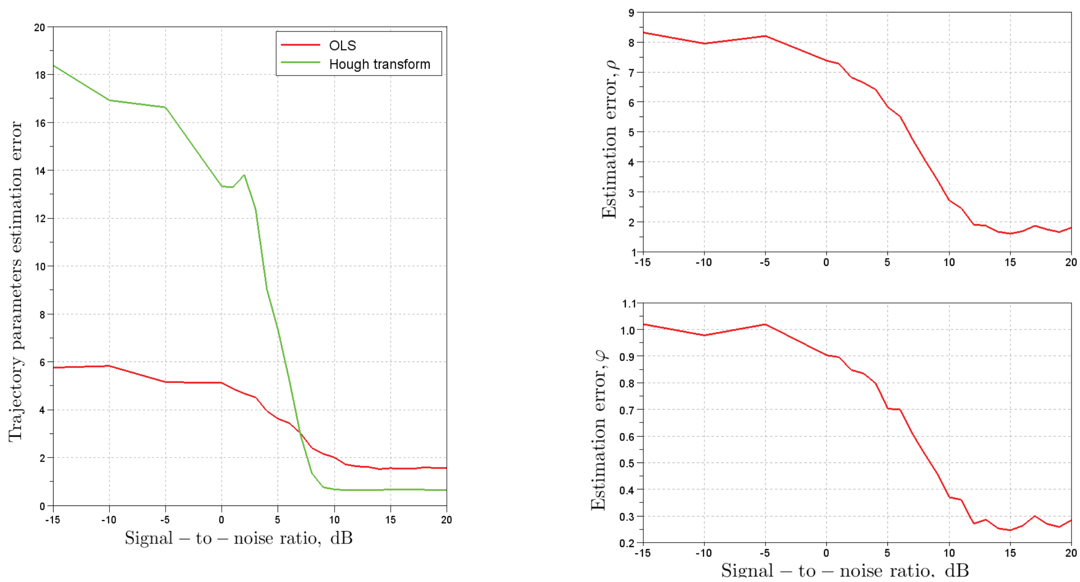

a) b)

Figure 4 – Trajectory parameters estimation errors:
a) complex estimation errors according to (6);
b) mean of trajectory parameters absolute estimation errors

Although the Hough transform gives a smaller trajectory parameters estimation error, but the characteristics of detection in case of using this method is shifted towards higher values of signal-to-noise ratio compared with the characteristics corresponding to OLS. This is conditioned by the peculiarities of the Hough transform technique, the need to establish a higher threshold of detection for the same probability of false alarm.

Conclusions

In this paper an algorithm for detection of rapid radar targets and estimation their trajectory parameters (in case of linear trajectory model), based on OLS method was purposed. A statistical modeling showed that the proposed algorithm gives better results in case of detection weak targets and estimation of their trajectory parameters, than usage of a common method of Hough transform.

Comparative analysis of two algorithms – parametric integration in case of known target trajectory and adaptive estimation of parameters of the trajectory with subsequent integration along the reconstructed path showed that the proposed algorithm provides very high efficiency. It concedes an optimal algorithm for detection of targets with known trajectory at 4.5 dB in a threshold signal with the probability of correct detection $D = 0.9$ and probability of false alarm $F = 0.01$. Analyzed images had dimensions of 16×16 pixels.

References

1. *Kuzmin S. Z.* Fundamentals of digital radar data processing. Moscow: Soviet radio, 1974 – 432 p.
2. *Y. Boers, H. Driessen,* “Particle filter based track before detect algorithms”, Signal and Data Processing of Small Targets, pp. 20-30, 2003.
3. *S. Buzzi, M. Lops, L. Venturino,* and *M. Ferri*, “Track-before-detect procedures in a multi-target environment”, IEEE Trans. on Aerospace and Electronic Systems, vol.44, pp. 1135-1150, 2008.
4. *D. H. Ballard*, “Generalizing the Hough Transform to Detect Arbitrary Shapes”, Pattern Recognition, Vol.13, No.2, p.111-122, 1981.

A.G. Gorelik, S.F. Kolomiets,
Dep. of mathematical problems of wave propagation processes.
Moscow institute of physics and technology, Dolgoprydniy, Russia.

RAYLEIGH SCATTERING REVISED

This article is devoted to a discussion of limits and a range of application of Rayleigh scattering model which is widely used in the radar meteorology. The mathematical ideas and the model of a scattered signal formation that are outlined in the article may be seen as a qualitative foundation for a technique of two-wavelength synchronous radar measurements in the coincident radar volume when both wavelengths correspond to Rayleigh's diffraction on hydrometeors. Such a technique could open the door for the retrieval of new (or additional) information about the microstructure of meteorological objects.

Introduction. The Earth's atmosphere is a puzzle and a great concern. Its unpredictable weather has always been a force to be reckoned with, but until recent times our trust was implicit in the robustness of the atmospheric system as the foundation of our biosphere. Far from being robust, this system is better described as a balance among a number of natural forces that we barely understand. Our concern is deepened when we consider the threat to this balance from our fast-growing civilization and its effluents. It is obvious that more reliable and accurate measurements in the atmosphere could provide us with unique facilities for further insights into the nature of its natural forces. Despite the fact that a present-day situation calls persistently for measurements, weather radars are still a tool for observations, but not for measurements.

It is sobering to realize that most techniques which have been developed to date for measurements by means of weather radars are only hopes on measurements *per se*. The problem is that almost all of such techniques use *a priori* information about the microstructure of the object of interest. Indeed, the microstructure of any meteorological targets changes significantly with time and space. Therefore, true measurement techniques must take into account not only a great variety of models of a radar echo but also a well-developed set of clear-cut criteria of applicability as well as means of accuracy assurance [1].

Despite the fact that there are some resources for some improvements of radar return interpretations based on classic models [2, 3], it is only a multiwavelength approach that seems to provide us with an adequate set of the arguments measured right in the radar volume and required for true measurement techniques [4].

Generally, there are two independent approaches to an interpretation of radar returns nowadays. One of them is based on fluctuations of the dielectric constant, while the other one is concentrated on spatial packaging and dynamics of individual particles no matter how small they are. Unfortunately, there is no brilliant idea to date on how to apply such powerful means of signal processing as Doppler or polarimetric techniques within the first one. At the same time, the second one is just what we need for the efficient application of them.

The most disappointing is that each of the approaches is applicable within certain non-overlapping ranges of wavelengths and there is no bridge between them which could be practically useful. Therefore, even if one makes a two-wavelength measurement within the ranges of applicability of the approaches discussed, there will be no grounds for synergy of interpretations anyway.

Synergy can be achieved, to a certain extent, by a synchronous use of Rayleigh's and Mie's waves for sounding within coincident volumes, nevertheless an overcoming of impediments preventing an efficient use of several Rayleigh's waves could assure a dramatic expansion of weather radars' capabilities.

Rayleigh's and Einstein's Formuli

Fundamentally, rayleigh scattering refers to the selective scattering of light by molecules much smaller than the wavelength of light. In a classic article [5], rayleigh showed that the scattering for a single molecule increases as the fourth power of the frequency and hence explained why the sky is blue. Further there were many researchers who did contribute to the theory of light scattering of but did not add the lucidity to the problem.

Historically, Einstein was the first who went over from scatterers to their fluctuations (more precise to the fluctuations of dielectric constant value) and expanded dramatically a range of applicability of Rayleigh's formula *ipso facto*. Unfortunately, he gave us no idea as to limits of that range. Using an implicit assumption about the exponential-type of distributions of dielectric constant fluctuations and taking into account that this distributions could be related to fluctuations of the number of scatterers, Einstein concluded that Rayleigh's formula was wrong but it gave the right quantitative result. Unfortunately, relations between the distributions of dielectric constant fluctuations and the fluctuations of the number of scatterers can be explained by making a connection with specific and profound thermodynamic ideas which were discussed in the optic literature very rarely to say nothing of radar publications.

Basically, a mean value of any exponential-type distribution must be equal to a variance. The fluctuations of scatterers can be parameterized by the variance calculated on a certain period of time through all unit volumes which constitute a scattering volume. The number of scatterers in the scattering volume can be described by their mean number calculated on a certain period of time. Therefore one can use – for asymptotically long periods of time – either fluctuations of the number of scatterers among all unit volumes (Einstein's formula) or the average number of scatterers in the whole scattering volume (Rayleigh's formula). Both approaches lead us to the same value of the intensity of scattered field.

As it emphasized in [6], despite the outstanding role of Einstein's work in the semi-quantitative explanation of the 'origin of the blue of the sky', the implicit assumptions used by him played a malicious trick with further generations of physicists. Even though Rayleigh scattering has been analyzed extensively, fundamental ambiguities in introductory texts are not eliminated completely. Moreover, these ambiguities have already caused an error to be foreseen [7], published [8], amplified [9], and cited with approval [10], before being corrected [11]. Everything indicated that in the light of all the lesions learned and based on modern experimental data, it is time to address these issues again [11, 12, 13].

Relative Fluctuations and Spatial Correlations

In this report we should address several ambiguities associated with Rayleigh scattering as it is widely used in radar meteorology. Not 'before more harm is done' – as it holds true in optics – but in attempt to find theoretical foundation for a new type of multiwavelength techniques of radar measurements.

The most important concern for us in this work will be the clear-cut physical reasons for a reduction of Rayleigh scattering corresponding to a growth of scatterers' concentration. This phenomenon is well established experimentally in the optics [14, 15, 16]. Why did it not take place in case of more sparse scatterers? The main question is to what extent this phenomenon can impact on radar signals and if this impact is different at different wavelengths?

For the purpose of radar meteorology we should consider a backscattering and pulsed incident radiation instead of a classic lateral scattering and continuous incident radiation. Taking into account that we are going to use the experimental data obtained in controlled laboratory experiments with x-rays or visible light and therefore being described only with multiple scattering concepts; all the findings in the report will be qualitative only. Another difference between the models which we are going to consider and those applicable in radar meteorology lies in the important role played in the latter by particle size distribution (PSD). For the sake of simplicity PSD will be left without consideration, as opposite to a clasterisation of particles which is of interest in the optics as well as in the radars.

It is interesting that atomic and condensed matter physicists, for example, approach the reduction of Rayleigh scattering in dense systems from different directions. From the atomic physics side, it is the correlations between the atoms that occur with increasing density that reduces the scattering. From the condensed matter point of view, a uniform density results in no lateral Rayleigh scattering. It is the fluctuations in the atomic density on the wavelength scale that is responsible for such scattering. Such fluctuations are inevitable for gases, where the equality between the mean and the variance of fluctuations holds true. In condensed phases at low temperatures, these fluctuations are reduced, with a corresponding decrease in Rayleigh scattering.

In other words, different physicists attribute a reduction of Rayleigh scattering to different processes today. As one can see, both approaches attribute the reduction to the 'external factors' which are not accounted initially in the classic model of Rayleigh scattering: low external temperatures or correlations between atoms.

The important role played by correlations was emphasized by Rayleigh in his days [5]. He conjectured as to whether or not the theory would be applicable to dense gases, liquids, and solids and concluded that "it is more than doubtful whether the calculations are applicable to such a case" because correlations begin to play a role. Further he supposed that "when the volume occupied by the molecules is no longer very small compared with the whole volume, the fact that two molecules cannot occupy the same space detracts from the random character of the distribution. And when, as in liquids and solids, there is some approach to a regular spacing, the scattered light must be much less than upon a theory of random distribution."

As one can see, Rayleigh attributed 'some approach to a regular spacing' as an intrinsic feature of the behavior of the random distribution when the volume occupied by the scatterers is no longer very small. Despite emphasizing of the outstanding role of correlations, classic works give us no idea on how to calculate them and how large the volume occupied by the scatterers can be seen as large enough for the appearance of correlations. Most modern approaches simply admit uncorrelated fluctuations as though these fluctuations are in continuous medium with no dependence on the particle nature of matter. In the authors of [6] opinion, this line of reasoning follows from a misinterpretation of the seminal works of Smoluchowski and Einstein, who calculated the scattering using thermodynamic arguments without explicit reference to the atomic nature of matter. These thermodynamic arguments do not rule out the possibility that the microscopic origin of Rayleigh scattering can be traced to the scattering on individual particles.

Being armed and motivated by Rayleigh's observation we are ready to revisit these issues. But before we go any further we should give some consideration to a wide-spread superstition about the importance of the ratio of the wavelength of incident radiation to the mean interparticle distance. The common wisdom is that the ratio of the interparticle distance to the wavelength determines the strength of the scattering [17, 18]. Therefore it could be seen as a parameterization of the task. This conclusion must be wrong and the correct view is to go back to Rayleigh's comment: As long as the particles are uncorrelated as in an ideal gas the scattering increases with the number of particles regardless of the ratio of their mean separation to the wavelength.

Transition Processes

There are several long standing problems that need to be solved first. The main one of them is how we can detect transitional processes between sparse and dense scatterers in the experiment? The second one is can we basically model them by the introduction of spatial correlations between the particles and how accurate can we do it? All these questions have recently been answered in the atomic physics. We hope that these results will serve as a food for thought in radar remote sensing.

Fundamentally, there is more than one way to a simulation of correlations. One of the possible approaches lies in the introduction – by any means – of some 'regularity' into a pure random sample. For instance, correlations can be simulated if we place rN particles at random in the interval (r is an integer greater than or equal to 1) and then remove $(r-1)$ nearest neighbors keeping particles 1, $r+1$, $2r+1$, $3r+1$,... It is not difficult to understand how this model introduces correlations between the particles. As it is illustrated on Fig. 1, by removing a nearest neighbor, it is less likely to find two closely spaced particles.

This type of an introduction of correlations allows us to tune easily a degree of inserted correlations and evaluate it correspondingly. What is more, it is turned to be a good model of the real observations made by x-rays in dense gaseous and liquid phase of rubidium (see Fig. 2). It is assumed, that a scattered signal is proportional to a structure factor G defined as $G = \overline{|S|^2}$, where $S = \sum_{j=1}^{N} e^{ikx_j}$ (a vector sum of the field scattered on distributed particles), x_j is an abscissa of j-th scatterer and the averaging is made over all possible configurations of the particles.

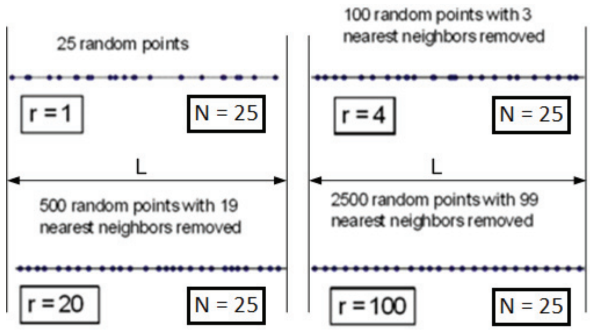

Fig. 1. Particles placed on a line at random with nearest neighbors removed. N – the number of particles, L – the sampling length, r - the number of the neighbors removed. It is clear from the figure that removal of nearest neighbors builds in correlation between particle positions [9].

Factor G is equal to N (number of particles) for a scattering on randomly distributed scatterers and equal to N^2 for Bragg scattering by a grating. Therefore the ratio of G to N can indicate to what extent our model resembles the classic Rayleigh model.

At first glance, this brilliant result has nothing to do with any scattering suppression. Instead, looking at the pike of the curve at Fig. 2 (c) one could deduce that correlations cause an increase of scattering at the long wavelengths end of the x-ray spectrum used. Most likely, we shall attribute this ‘suspicious behaviour’ to clasterisation. If this conjecture holds true, then G/N ratio can be accepted as a measure of the medium clasterisation. Undoubtedly, this amplification of scattering is

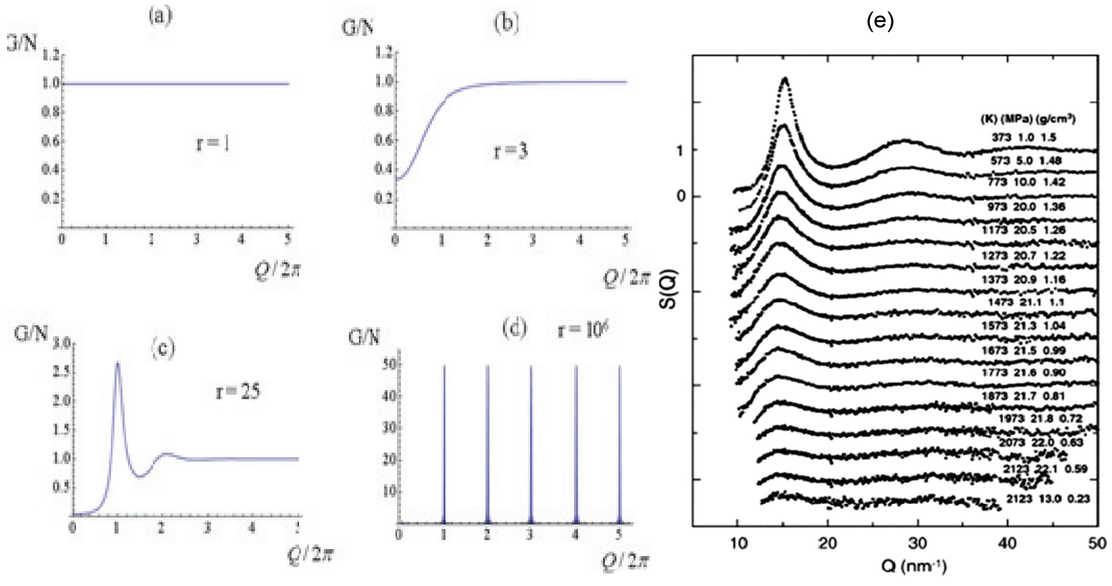

Fig. 2. Graphs of the structure function $\tilde{G}N$ as a function of $\tilde{Q}2\pi$, (where $Q = \frac{kL}{N}$, k – is a wave number, L and N – see Fig.1.) Calculations for several values of r: (a) *r*=1, (b) *r*=3, (c) *r*=25, (d) *r*=1,000,000 [9]. (e) - experimental curves of the structure factor S(Q) for x-ray diffraction from rubidium (S(Q) corresponds to G/N in Fig. 1.]. The lowest curve corresponds to a dense gas and the other curves to the liquid phase [10].

also very important. Of course, this result cannot be directly applicable to radars and there is still a lot of work here, but the idea about new arguments for the task parameterization is worth it.

One can get the idea about how far it is still from the radar reality and, at the same time, how important the question discussed by looking at Fig. 3 reprinted from [19]. Experiment discussed in [19] was devoted to the measurement of the period of time between the moment when cloud has initially been formed and when it begins producing big droplets falling into the Earth's surface.

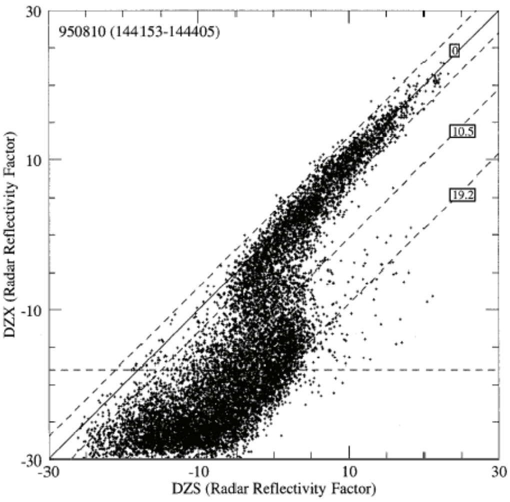

Fig. 3. Scatter diagram of DZX (dBZ at X-band) versus DZS (dBZ at S-band) from []. Data was collected at the same date and time from the whole volume scan of a few shall cumulus clouds that include some precipitation

An ideal Bragg scattering signal, leads to a wavelength dependence such that a pure Bragg echo at X-band is about 19 dB weaker than at S-band. In ideal Rayleigh scattering from clouds, all of the radar return comes from spherical, liquid water drops that are small enough that the Rayleigh approximation applies. If both the Rayleigh and the Bragg scattering components are ideal, then it is only possible for dBZ at X-band to range from 19 dB less than that at S-band to equal to it. Figure 3 is showing that 19 dB is in fact a reasonably good upper bound at the lower values of reflectivity factor where Bragg scattering is important. The trend of DZS-DZX values toward 0 dB at higher reflectivities is expected from Rayleigh scattering on big droplets at both bands. In the region where the points fill the space between the 0- and 19-dB lines, one does not know the extent to which these are due to mixtures of Bragg and Rayleigh scattering or to nonideal Bragg and Mie scattering. It appears reasonable that most of this is due to mixtures.

However, there are too many cases of DZS-DZX about 10 dB. These pose a problem because with a difference that great, DZS must be dominated by Bragg scattering, but at the same time DZX must be dominated by scattering from the hydrometeors. There appears to be a strong correlation between the Bragg and Rayleigh scattering that is unexplained at present. Therefore deciphering the dual-wavelength data – even if they have been collected synchronously from coincident radar volumes – turns out not to be entirely straightforward.

Getting back to the subject of the report, we must conclude that either correlation has nothing to do with Rayleigh scattering suppression or there is more than one type of correlations.

Bragg Scattering and Bragg Suppression

A first idea coming to mind is about the scale of correlations. As one can see the pike of the curve at Fig. 2 (c) corresponds to the argument Q/2π equal to unity, while the trough of the curve is right over one and a half. There is another hump located directly above the number two on the abscissa. Then oscillations have been dumped completely.

By the look of things, the best explanation of such a behavior is the following. Distributed scatterers with a mean length of space-correlations $\overline{\ell}$ exhibit either quasi-Bragg scattering while $\overline{\ell} = n\lambda$, where $n \in R$ and λ is the wavelength of incident radiation or the suppression of scattering while $\overline{\ell} = ((n+1)/2)\lambda$. The latter is also an explainable fact taking into account that in this case the number of the scatterers located in all positive half-waves will correlate with those of negative half-waves. Therefore, oscillations of the field scattered on all particles will partly eliminate each other during a vector summation in space.

As a matter of fact, following this line of reasoning one can arrive at the following consequence. Bragg scattering and Rayleigh scattering suppression is just different sides of the same coin. One cannot exist without the other. Therefore, Bragg suppression might be seen as a quite appropriate term for this phenomenon as well.

To put the problem in perspective and make the consequence more general, let us look at other works [15, 16, 20]. The former presents the results obtained in the controlled laboratory experiments with He-Ne laser and the uniform latex microspheres (with mean diameter of 0.091μm) suspended in water. Experimental result was interpreted in terms of the dense medium radiative transfer (DMRT) theory. The observed phenomena could not be explained by the conventional radiative transfer theory, and DMRT theory developed by the authors was in agreement with the experimental features.

It was shown in [16] that with an increasing fractional volume of scatterers greater than 5-10 percent, the measured bistatic intensities at an observation angle of 4º begin decreasing monotonically, almost linearly. This decrease continues up to 45-50 percent where the line changes the angle and becomes steeper. From 0.001 to 5-10 percent the intensity nonlinearly grows up to three times. Conventional radiative transfer theory predicts only a monotonic increase with the concentration.

Unfortunately, there was not a second laser and we cannot check the conjecture made above and related to Bragg suppression. Anyway the suppression of scattering was detected although interpreted in terms of the radiation transfer theory and multiple scattering.

As far as multiple scattering is concerned, it was B. Yurchak who predicted qualitatively a similar behavior of intensity corresponding to the growth of concentration of scatterers without utilization of multiple scattering concepts. In developing the slice model, he arrived at the following expression for the intensity:

$$\langle P\rangle = \frac{1}{2}N\left[Var(a) + \langle a\rangle^2\chi\right]$$

where <*a*> and *Var(a)* are the mean and variance, respectively, of the magnitudes of the elementary signals scattered on particles of a certain slice; <*n*> and *Var(n)* are the mean and variance of the number of particles in the slice, respectively; *N* is the mean number of particles in the while volume and $\chi = Var(n)/\langle n\rangle$ is a relative variance of the number of particles in the whole volume.

Argument χ, known also as Poisson index, represents the assumption which was mentioned above as the assumption made by Einstein regarding to the equality between the mean and the variance that is required for Rayleigh's formula to be correct. Fundamentally, if this equality holds true, then one can evaluate *N* based on the mean intensity of a scattered signal $\langle P\rangle$ in spite the fact that the scattering takes place on fluctuations of the dielectric constant. Yurchak's equation transforms into the known weather radar equation when the fluctuations obey the Poisson law (i.e. $\chi = 1$) and the expression in brackets is proportional to the sixth moment of a droplet spectrum.

Given a finite volume of the slice, it is obvious that there must be a maximum of particles in the slice. The argument χ is equal to unity until there is enough room in the slice. In this case any Poisson's deviation of the number of particles can take place. Otherwise, the mean of the number of particles in the slice $\langle n\rangle$ becomes greater than its variation $Var(n)$, therefore χ becomes less than unity. The latter, in turn, cases a suppression of the backscattering. In [20] the maximum of particles is written as $n_{\max} = (1-\beta)V_s/V_p$, where V_p is a volume of individual particle, $\beta < 1$ is a packaging factor for spheres in the slice and V_s is a volume of slice.

As far as we can say, it is a very general explanation. The slice approach implies utilization of a plane wave and, as a consequence, one dimensional task of wave propagation. Hence, if we define a slice as a set of points in space with equal phases calculated from an idealized origin, then we have to admit that the field scattered on the particles of the slice will be added coherently. Therefore, while there is more than one scatterer in the slice, the magnitude of the field scattered on them will fluctuate much wider than an incoherent sum of elementary scattered fields.

Even if we assume a set of such slices, we will never arrive – without special corrections – at the equality between the mean number of scatterers in the volume and the variance of the field scattered on them. In different words there must be a threshold of scatterers filling in the volume above which elementary scattered fields begin to interact coherently. In order to account for this process, at least qualitatively, it is necessary to redress the concept of χ as follows:

$$\chi = \frac{Var(n)}{\langle n \rangle} \cdot \frac{Var(P)}{\langle na^2 \rangle}$$

When coherent summation takes place, the second ratio on the right side is greater that unity. The more elementary fields added coherently in the signal, the more χ. Finally, when the first ratio on the right side begin to decrease following the process described above, argument χ is already far greater than unity.

The threshold of a coherent summation is much less than slice's maximum of particles $n_{\max}$. Its estimation varies depending on required accuracy and signal purity but always less than a total number of slices in the whole volume, that is *(Q - <n>) = k·Stdev(n)*, where *Q* is a total number of slices in the radar volume, *k = 1, 2, 3… 6* is a factor of signal purity expressing to what extent a received signal is free from the elementary fields added coherently.

Based on the concepts and experimental data discussed above, one can make a diagram as in Fig. 4. The key question is whether slices can be seen as a part of physical reality and one can detect by any means an impact of their size on the signal received or they just a 'trick' of theorist which can be used merely to direct a thought during a qualitative analysis. In case of slices is the part of the reality their thickness will be one of the most arguments of task parameterization. Specifically, it defines the limits of areas with different type of scattering showed in the Fig. 4. What is more it could be used for a transition to wavelength from fractional volume units on the abscissa.

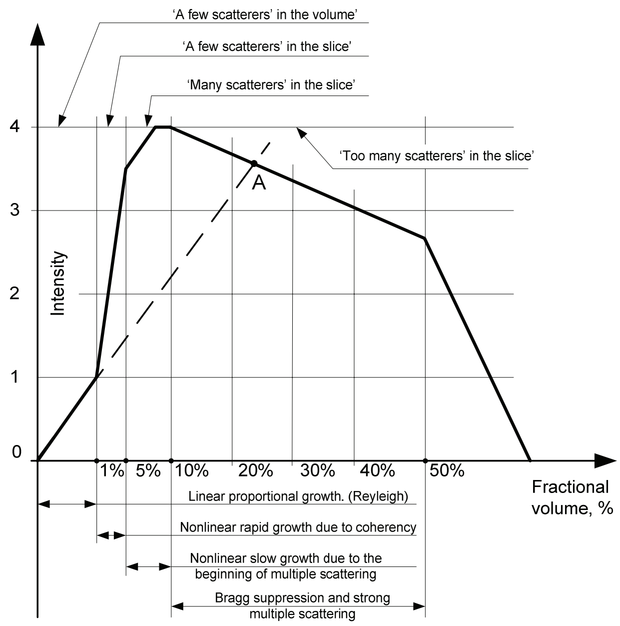

Fig. 4. The diagram of scattering compiled based on the concepts and experimental data discussed in the report. Fractional volume of scatterers would be replaced with wavelengths if the slices of finite thickness are turn out to be a part of physical reality. In this case, it would define the limits of the areas of different types of scattering pointed out in the figure by arrows.

Conclusions

It is quite obvious that getting reliable estimations of the number of particles in the radar volume is not generally possible in a field experiment to say nothing about having a controlled variation of one parameter of interest. In hopes of getting new findings that should help to eliminate fundamental ambiguities in the model of Rayleigh scattering and provide a solid foundation of further development, the main focus of researchers is put on colloidal, atomic and molecular physics.

We discussed few works to illustrate some basic ideas. First of all, it is a suppression of scattering observed while fractional volume of scatterers is growing and when it has overcome a certain threshold. All the experimental data discussed was obtained in dense medium and other conditions that are corresponding to multiple scattering.

In doing this one can use the idea of correlations that could be introduced into the model of spatially distributed particles by several means. Two of them have been discussed in the report: the nearest neighbor removal and the slices. We conjectured that – from the point of view of the multiwavelength approach to the scattering of light in partly correlated medium – it would be better to look at Bragg scattering and suppression as at an indivisible process and unique feature of multiwavelength scattering.

Hence, the ratio of the mean correlation length $\bar{\ell}$ to the wavelength λ of incident radiation can be seen as a good candidate for the main arguments of multiwavelength scattering parameterization. Moreover, it is advisable to use two specially selected wavelengths for a reliable determination of the correlation distance, such that one of which will show an increase of the scattering, while the other - the suppression. However, the question about real grounds for the use of such models and interpretation of models' arguments in terms of clear-cut physical concepts is still open.

The use of the slice approach seems to be more appropriate in case of sparse scatterers and if the thickness of the slice is a finite value one can find all the necessary evidences that $\langle P \rangle$ will decrease while the thickness of slice will grow (see Fig. 5). Fundamentally, it means that, even in case of sparse scatterers, there are also two concurrent and rival processes: a growth of backscattering intensity which is proportional to N and an intensity suppression which is proportional to the slice size.

Assuming that the thickness of the slice is corresponding to the wavelength of incident radiation, one can arrive at different $\langle P \rangle$ for different wavelengths, even if these waves are Rayleigh's. If such a thickness can be changed artificially, then different $\langle P \rangle$ would correspond to different slice thicknesses at the same wavelength. Both cases – if they find required experimental evidences – lead us to the conclusion that there may be a new way of two-wavelength synchronous radar measurements in the coincident radar volume using the wavelengths that are corresponding to Rayleigh's diffraction on hydrometeors. Such a technique could provide a solid foundation for the retrieval of new (or additional) information about the microstructure of meteorological objects even in the case of sparse scatterers.

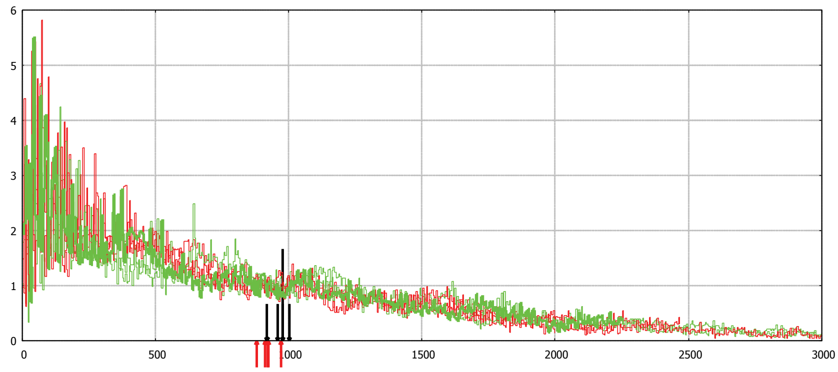

Fig.5. Calculations of the mean intensity of the pure incoherent signal scattered on 1000 (in average) simulated particles of equal size with averaging (down-top red arrows) within a slice and without it (top-down black arrows).

Several vertical arrows standing for mean values illustrate their variation. Interparticle distances had Poison's distribution and the size of the scattering volume was equal to 100 half-wavelengths, while slice thickness was equal to λ/10. In case of slice averaging the mean value is fluctuating closer to the origin. Given the slice thickness it is impossible to achieve a value of mean intensity of averaged scatterers less than 92% of the true mean value of a fully incoherent signal.

Given a finite size of the report, we intentionally do not touch upon a question about the size of slices as it is a very important subject and at the same time a long standing problem deserving a special discussion. In radar meteorology it was considered at great length as long ago as in the first editions of [21, 22]. One can refer to [23] for some additional clarification.

Apart from slice approach we have also shown that the backscattering should include a partially coherent component if concentration overcomes a certain threshold. Despite the fact that we illustrated it by means of slice approach, this may have nothing to do with slices and occurs due to the fact that the three dimensional distribution of scatterers collapses to one-dimensional in the case of using an abstraction of a plane wave and so one must take into account non-ordinary Poisson processes. Partly coherent scattering means that multiple scattering will start to play a role from a higher level of intensity in comparison with pure Rayleigh's intensity calculated based on information about the number of scatterers in the volume.

References

1. *A. G. Gorelik, S. F. Kolomiets*, “Radio Waves Scattering on Distributed Scatterers and Stochastic Approaches in Radar Meteorology” (in Russian), Scientific miscellany of Moscow State University of Civil Aviation, 117, (2006). http://www.mstuca.ru/scientific_work/research_herald/
2. *A.G. Gorelik and S. F. Kolomiets*, “New Approach To Smoke Detection By Means Of Doppler Radar”, Proceedings of MRRS 2011 (Microwave, Radars and Remote Sensing) , August 25-27, Kyiv, Ukraine.
3. *Kolomiets S. F.* “Generalized Multiplicative Coefficient of Z-R Relationship Deduced Under the Assumption of Modified Gamma DSD and Its Use Within a Wide Range of Wavelength and Time Intervals”, Proceedings of the fourth world congress "Aviation in the XXI-st century", V.2 "Safety in Aviation and Space technologies", p. 22-7-22-10, September 21-23, 2010 Kyiv, Ukraine.
4. *Gorelik A. G., Kolomiets S. F.,* “The Study of Dynamic Processes in Clouds and Rain by Means of Multiwavelength Doppler Radar”, Proceedings of the fourth world congress "Aviation in the XXI-st century", V.2 "Safety in Aviation and Space technologies", p. 22-11 - 22-15. September 21-23, 2010 Kyiv, Ukraine.
5. *Lord Rayleigh,* “On the transmission of light through an atmosphere containing small particles in suspension, and on the origin of the blue of the sky,” Philos. Mag. 47, 375–384 (1899).
6. *C. F. Bohren and E. E. Clothiaux*, Fundamentals of Atmospheric Radiation, 3rd ed. Wiley, Weinheim, 2006, p. 153.
7. *H. A. Stuart*, Molekülstruktur, Verlag Julius Springer, Berlin (1934).
8. *D. V. Hoyt*, J. Appl. Meteorol. 16, 432 , (1977).
9. *C. Fröhlich and G. E. Shaw*, Appl. Opt. 19, 1773 (1980).
10. *E. P. Shettle, F. X. Kneizys, and W. O. Gallery*, Appl. Opt. 19, 2873, (1980).
11. *A. T. Young*, Appl. Opt. 19, 3427 (1980).
12. *A. T. Young*, Appl. Opt. 20, 4, (1981).
13. *A. G. Rojo, P. R. Berman*, Am. J. Phys. 78 (1), 2010.
14. *K. Matsuda, M. Inui, M. Kusakari, and K. Tamura*, J. Non-Cryst. Solids 353, 3380–3383 (2007).
15. *Y. Kuga and A. Ishimaru,* J. Optical Soc. of America, No. 8, 1 (1984).
16. *B. Wen, L. Tsang, D. P. Winebrenner, and A. Ishimaru*, “Dense Medium Radiative Transfer Theory: Comparison with Experiment and Application to Microwave Remote Sensing and Polarimetry,” IEEE Transactions on Geosciences and Remote Sensing, No. 1, 28 (1990).
17. *E. Hecht*, Optics, 4th ed. Addison-Wesley, New York, 2001, p. 90.
18. *K. S. Shifrin*, Scattering of Light in a Turbid Medium (Gostekhteoretizdat, Moscow-Leningrad, 1951), Chap. 2, p. 25; NASA tech. transl. F-477 (NASA,Washington, D.C., 1968).
19. *C. A. Knight, L. J. Miller*, J. Atmos. Sci., 55, 2974–2992 (1998)
20. *B. S. Yurchak*, “Effective Droplet Number and Droplet Spectra Parameters That Determine the Radar Backscatter from Clouds and Rain”, J. Russian Meteorology and Hydrology, 34, 1 (2009).
21. Threshold Signals, ed. by J. L. Lawson and G. E. Uhlenbeck, McGraw-Hill, (1950).
22. Propagation of Short Radio Waves, ed. by D. E. Kerr, McGraw-Hill, (1951).
23. *B. S. Yurchak*, “Assessment of the Contribution of Small-scale Correlated Fluctuations of Water Content to Radar Backscatter from Clouds and Rain,” in Problems of Cloud Physics, Collected Papers, Memorial Issue Dedicated to Prof. S.M. Shmeter (GU “NITs Planeta,” Moscow, 2008).

Mariusz Zych
[1st: Bumar Elektronika S.A. Warsaw, Poland
2nd: Institute of Electronic Systems, Warsaw University of Technology, Warsaw, Poland]

GROUND PENETRATION RADAR SIMULATIONS OF NON-HOMOGENEOUS SOIL WITH CST STUDIO SUITE

The paper describes the simulation results for a ground penetrating radar with CST Studio Suite. Non homogeneous soil composed of four different materials has been investigated by pulse GPR. The aim of the experiment is to obtain fully focused image of the tested soil structure. The raw GPR data collected with CST Studio Suite has been processed using Matlab. Simulation results presented in the paper show good possibility of focused SAR method for underground targets imaging.

I. INTRODUCTION

CST Studio Suite is the powerful simulation platform for electromagnetic field problems. The transient solver gives appropriate results of non-homogeneous soil imaging. In order to obtain raw GPR data, wideband horn antenna, transmitting and receiving signal, has been applied. Decisive parameter during selection of appropriate antenna is S11. S11 refers to the ratio of signal that reflects from the port for a signal incident on that port. The main aim of ground penetrating radar is to obtain good resolution of underground targets. Before one can perform real data measurement it is recommended to simulate radar scene with professional electromagnetic simulator. In that way many measurement problems can be avoided, what is more, the best radar parameters (such as type of antenna, type and bandwidth of transmitted signal) can be selected.

The CST transient solver calculates the development of fields through time at discrete locations and at discrete time samples. Program provides possibility of various propagating signal properties and tested soil structure definition. Moreover CST performs irregular time sampling of simulated data. If radar transmit signal with linear frequency modulation, CST Studio sample rate for that part of the signal with higher frequencies will be much greater than for lower frequencies part. This gives good accuracy of computed date, however collected data need to be resampled before performing pulse compression.

Presented simulation with CST Studio Suite has been prepared in Bumar Elektronika S.A.

II. SIMULATED RADAR SCENE

The simulated soil structure is composed of four materials of different electric permittivity values. The analyzed ground has 2 meters length in GPR movement direction, 0.7 m width and its thickness is 0.6 m. The main component of the model is dry sand which covers loamy soil, bones and forty years old concrete. Selected horn antenna is positioned 10 cm above the ground. GPR antenna has been placed in 145 points, the movement step is 1 cm which gives 1,45 m of simulated raw data. Investigated non-homogeneous soil structure is presented in Fig. 2.1. Each of the layers of the ground, made of loamy soil, bones and forty years old concrete and located inside dry soil, have shapes of prism. Analyzing the plane intersecting the soil in movement and depth direction, these layers have shapes of triangles. Loamy soil has the following coordinates of vertices [cm]: (0,-15), (0,-45), (170,-10). Medium made of bones has coordinates of vertices [cm]: (200,-10), (200,-30), (80,-40). The third layer made of forty years old concrete has coordinates of vertices [cm]: (0,-60), (140,-60), (140,-40). At the border of two medium with different permittivity values electromagnetic wave is reflected [1][3]. GPR performance is based on

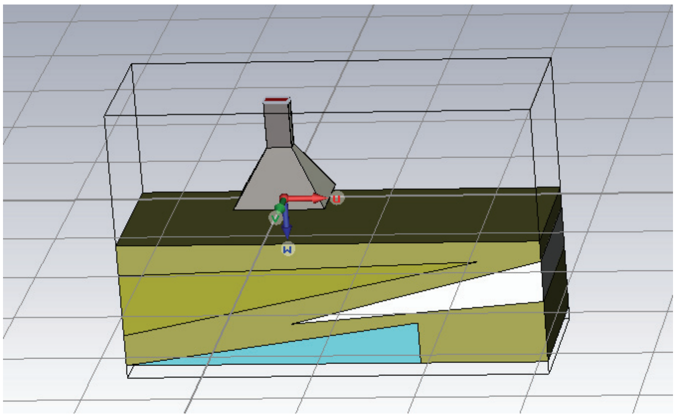

Fig. ***Fig. 2.1 Tested soil structure*** reflection phenomenon. Unfortunately, image of buried objects generated by ground penetrating radar does not correspond to its geometrical representation. The image collected from single point target has hyperbolical shape [3][4]. The radius of this curve is strongly connected with target depth and electrical parameters of the soil surrounding the object. Increase in depth of an object or decrease in permittivity causes increase in the radius of curve [5]. Direction of propagated wave is dependent on soil properties. What is more, each layer of the ground attenuates electromagnetic wave, which causes the maximum range equal to several meters [1]. Ground is heterogeneous medium, for these reason, the GPR signal processing is much more sophisticated than in other types of radars. The aim of the experiment is to obtain fully focused image of each soil component. Improvement of pulse GPR resolution in depth direction can be obtained using signal with linear frequency modulation LFM [6]. Depth resolution for LFM pulse is inversely related to signal bandwidth. The matched filter output for pulse radar with linear frequency modulation can be approximated as sinc(x) function. LFM has significant sidelobes at the level of about -13 dB which can mask weak echoes from deeper located objects [5][6]. Commonly know method of LFM sidelobes suppression is based on window function application [5]. This operation can suppress sidelobes to the required level. Time domain weighting are used to suppress Gibbs oscillations caused by the truncation of a Fourier series. However, matched filter amplitude weighting causes mismatches, which reduces signal to noise ratio. As a consequence, maximum radar range is decreased [5]. Presented simulation results has been achieved for LFM signal with bandwidth $\boldsymbol{B}$ = 2 GHz, time duration $\boldsymbol{\tau}$ = 5ns, carrier frequency $\boldsymbol{f_C}$ is equal to 2 GHz.

III. RAW GPR DATA PROCESSING

Raw GPR data calculated with CST Studio Suite need to be processed in order to obtain radar image. As it has been mentioned, CST performs irregular time sampling. Before pulse compression can be done, collected data need to be resampled. It can be done using Matlab interpolation method called interp1. Resampled raw data is given in Fig. 3.1 and contains signal reflected from antenna port. Undesired S11 signal has been removed using lattice filter based on Burg's algorithm [2] (Fig. 3.2). For that purpose, S11 data without soil has been calculated and used as reference signal $\boldsymbol{x_{ref}}$. Signal labeled as $\boldsymbol{x_{rec}}$ is signal reflected from soil structure. Lattice filter is described by following equations [2]:

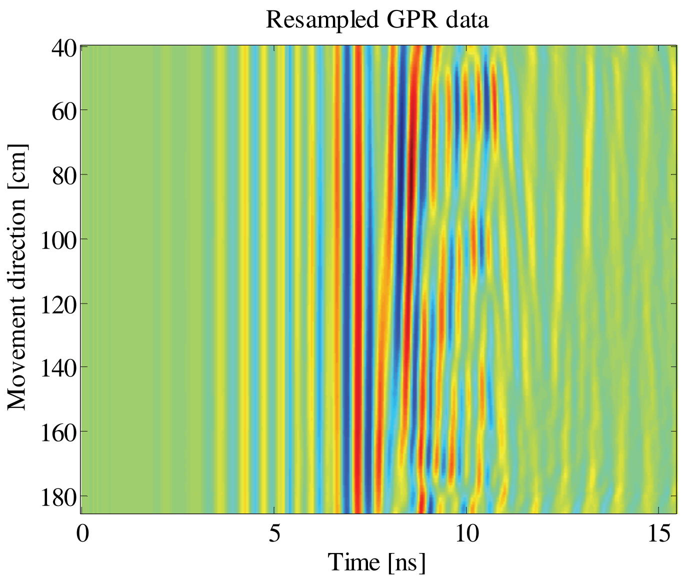

Fig. 3.1 Raw data

$$h_i = \frac{\sum_{n=0}^{N-1} x_{rec}(i)\, x^*_{b(i-1)}(n)}{\sum_{n=0}^{N-1} \left| x_{b(i-1)}(n) \right|^2} \qquad \textbf{(3.1)}$$

$$K_i = \frac{\sum_{n=i+1}^{N} x_{b(i-1)}(n-1)\, x^*_{f(i-1)}(n)}{\sum_{n=i+1}^{N} \left(\left| x_{b(i-1)}(n-1) \right|^2 + \left| x^*_{f(i-1)}(n) \right|^2 \right)} \qquad \textbf{(3.2)}$$

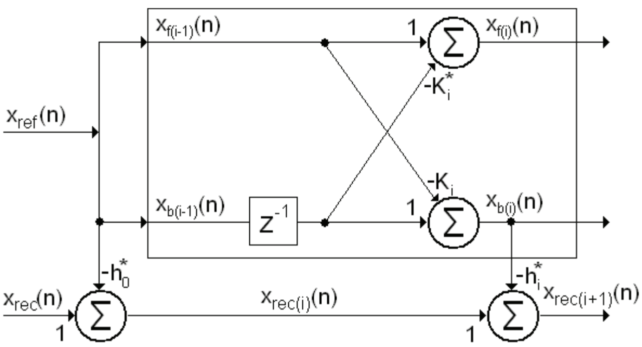

Fig. 3.2 Lattice filter

After removing S11 spectrum of raw data is still located around carrier frequency and need to be demodulated. LFM signal is given at the first input of mixer, at the second input coherent heterodyne signal is given. At the mixer output demodulated signal is obtained.

The next step of the computation is low-pass filtering. That process removes undesired signal spectrum components. The spectrum of demodulated GPR data after low-pass filtering is visible in Fig. 3.3. Low-pass signal representation in time domain is presented in Fig. 3.4. Calculated data does not give enough information about soil structure, the depth of an layer cannot be reliable determined. However, processed in described way echo GPR signal can be subjected to pulse compression [6]. Depth compressed GPR data is visible in Fig. 3.5. In order to suppress sidelobes level, the matched filter is weighted by Hamming window. Theoretically [6], level of Hamming window sidelobes is -41 dB. Matched filter output of signal with linear frequency modulation is characterized by good depth resolution on condition that time duration and pulse bandwidth product is large enough. Analyzing Fig. 3.5 one can see, that the first reflection from the antenna port (S11), which has been suppressed by lattice filter, is visible in fourth ns. Due to lattice filtration, undesired S11 does not mask remaining reflections. The echo signal reflected from the border between air and sand return to the GPR after 7 ns. The strongest amplitude of echo signal is obtained from the border between dry sand and loamy soil and is located from 8th to 9th ns. Echo signal reflected from the rest of soil layers are barely seen. CST Studio Suite introduces noise associated with carried out computations, it is good seen in reflected signal from second to 4th nanosecond, where there should not be any echo signal. Unfortunately, presented results does not meet requirements, not every layers can be detected from Fig. 3.5. The general objective of digital signal processing as applied to surface penetrating radar is either to present processed image that can be readily interpreted by operator. For that purpose cross range resolution must be increased. These requirements may be satisfied by performing focused SAR filtering in movement direction [3][7]. Nevertheless, majority of know ground penetrating radar devices use non-

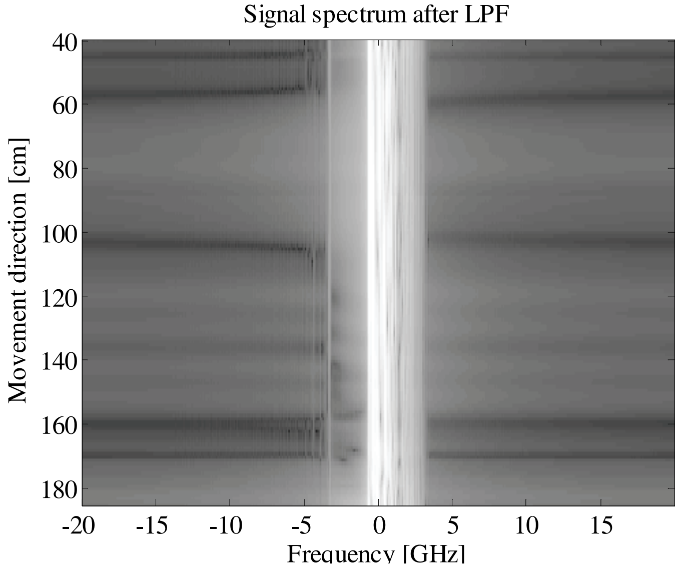

Fig. 3.3 Signal spectrum after LPF

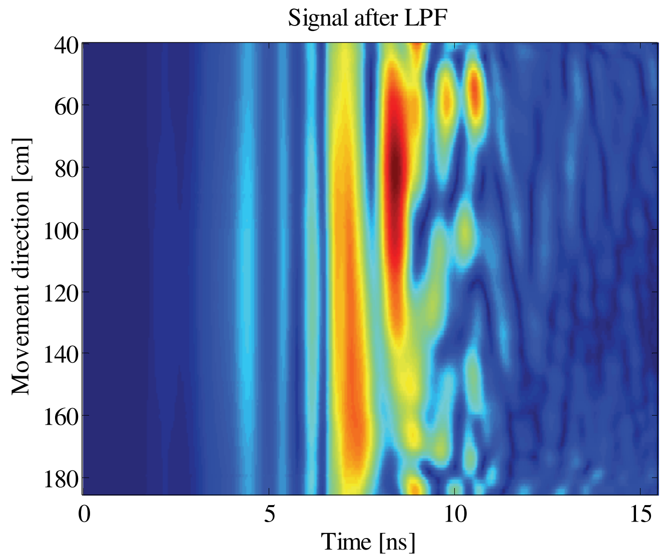

Fig. 3.4 Signal after low-pass filtering

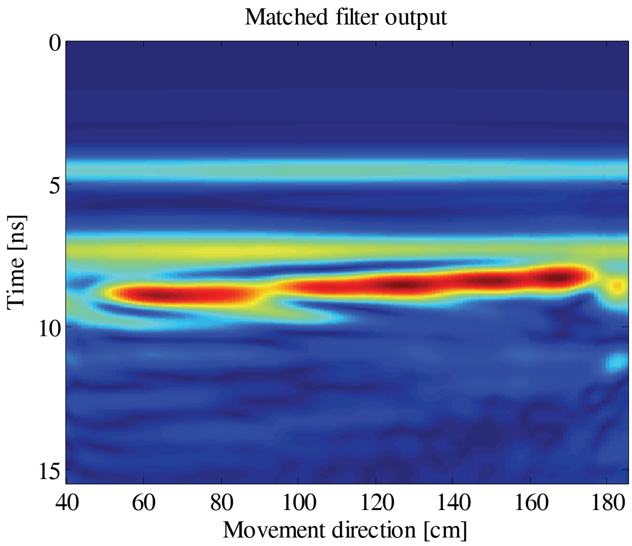

Fig. 3.5 Matched filter output

coherent Hough Transform in order to increase image resolution in movement direction [1][8]. That technique is based on detection of specific, hyperbolical shapes in depth compressed image. Hough Transform provides good results on condition that analyzed image has good quality and curve shapes are easily distinguish [4]. When obtained image is contaminated by high level noise, non-coherent algorithm will not give expected results [8]. For that reason SAR technique is much effective and allows to achieve optimal cross range resolution.

IV. FOCUSED SAR FILTERING

Two dimensional SAR filtering, presented in the article, has been performed in few steps. Depth compressed data initially is divided into blocks [4][5]. For each block, 2D matched filter is prepared. SAR filter properties are strong connected with the depth of an target and permittivity value of surrounding medium. Calculated matched filter is convolved with selected block and the nearest neighborhood. Filtered three blocks are then multiplied by Hamming window to smooth the final image. After calculating the convolution for all blocks, overlapping blocks are summed. GRP image after applying focused SAR algorithm is presented in Fig. 4.1. During the SAR filtration a constant value of electric permittivity, equal to permittivity of dry soil, has been assumed. What is more, the image has been shifted in such a way that the first reflection from the dry sand is now located at 0 m depth. As a consequence of digital signal processing, reflections from each of layers constituting soil structure has been observed.

The signal parameters such as bandwidth and time duration does not give the theoretical range resolution. In order to improve image resolution longer signal or FMCW GPR should be used.

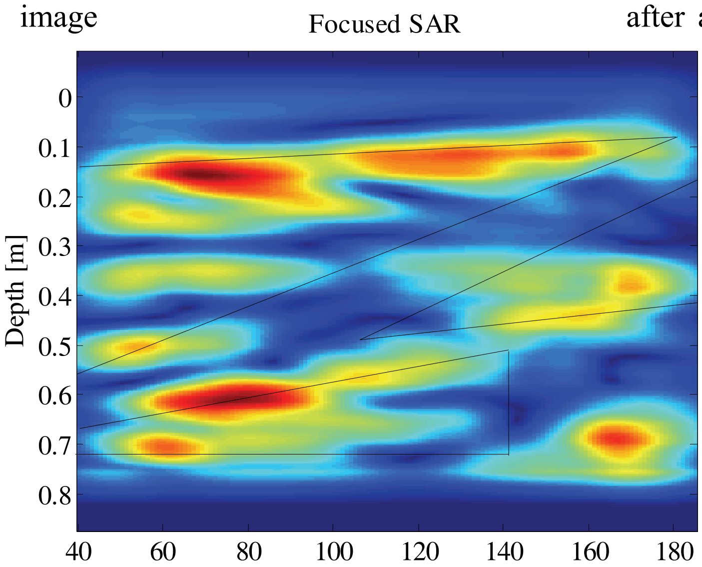

Fig. 4.1 Focused SAR image

V. CONCLUSIONS

- CST Studio Suite can be used to simulate different kind of GPR, allows to design complicated soil structures and antenna.
- Calculated by CST data need to be resampled before performing digital signal processing
- Focused image obtained with CST data gives good results.
- Presented ground penetrating radar could be used to investigate the soil structure, unless the permittivity coefficients is correctly determined

REFERENCES

[1] D. J. Daniels, *Ground penetrating radar 2nd edition,* The Institution of Engineering and Technology, London 2007.

[2] S. Haykin, *Adaptive Filter Theory, Fourth edition,* Pearson Education Inc., 2007, India

[3] M. Zych, *AutoESP – An Iterative Algorithm of Soil Permittivity Estimation for GPR*, w: Proceedings of the European Radar Conference, 2011, ss. 49-52

[4] M. Zych, *Comparison of using SAR processing and Hough transform as a methods for GPR radar image creation*, w: Proc. The Fourth World Congress "Aviation in the XXI-st Century – Safety in Aviation and Space Technologies, 2010, 22.106-22.112

[5] M. Zych, *Suppression of GPR range sidelobes based on NLFM signal*, International Radar Symposium 2012, Proceedings, 23-25.05.2012, Warsaw, Poland

[6] M. I. Skolnik, *Introduction to radar systems 2nd edition,* McGraw-Hill, Inc. 1981

[7] J. C. Curlander, R. N. McDonough, *Synthetic aperture radar, Systems and Signal Processing,* John Wiley & Sons Inc., Canada 1991.

[8] [8] A. Simi, S. Bracciali, G. Manacorda, *Hough transform based automatic pipe detection for array GPR: algorithm development and on-site tests*

UDC 629.735.05

V.V. Ulansky, D.Sc., V.G. Antoshkin, D.S. Draga, N.E. Kornitsky, B.V. Pauk, O.S. Ponomarev
(National Aviation University, Ukraine)

THE DESIGN AND OPTIMIZATION OF VOLTAGE CONTROLLED OSCILLATORS IN 0.13μm CMOS TECHNOLOGY FOR 3G AND BLUETOOTH TRANSCEIVERS

This paper describes the design and optimization of LC voltage-controlled oscillators (VCOs) for 3G and Bluetooth transceivers in 0.13-μm, 1.2V CMOS technology. The proposed technique is illustrated by optimizing seven different MOS LC VCOs. The best optimized VCOs exhibit a phase noise of -134.6dBc/Hz and -139.16dBc/Hz at 3MHz offset from the carrier, 0.52mW and 0.36mW power consumption, 4.9% and 3.4% total harmonic distortion, respectively, for 3G and Bluetooth transceivers.

Introduction. Modern mobile cell phones have 3G network coverage and use Bluetooth transceivers for data transmission. Ukrainian 3G mobile network operators have deployed UMTS-FDD technology in 2100MHz frequency band. Future developments in 3G technology in Europe are expected in 2600MHz frequency band, which is divided by uplink band (2500 - 2570MHz) and downlink band (2620 -2690MHz). With a channel spacing of 5 MHz, the total bandwidth allocated for future 3G mobile services is 140 MHz, which will result in having a total number of 28 channels. Bluetooth is a low-power wireless technology deployed with radio equipment operating on the widely used 2.4 GHz spread-spectrum band. The Bluetooth standard was designed for targeting short-range wireless communications with data rates of 1Mb/s at 10m distance. The phase-locked loop (PLL) of a Bluetooth transceiver has to be able to provide frequencies from 2402MHz to 2480MHz with channel spacing of 1MHz. A crucial PLL component for both 3G and Bluetooth transceivers is the VCO. The main concern for VCO design is low phase noise, low power consumption and low output harmonic level, which is a measure of the VCO energy at harmonics of the fundamental frequency. In published papers, for example [1-2], the VCOs were designed and optimized without taking into account the amount of distortion in the generated sinusoidal signals. Besides that, the performance of the designed VCOs was not compared with the performance of VCOs having other topologies in the same CMOS technology. In this paper, seven different MOS cross-coupled VCO topologies are optimized for perspective 3G and Bluetooth applications using new figure of merit (FOM).

VCO topologies. Seven different VCO topologies were designed and optimized. The NMOS differential cross-coupled VCO without and with a tail current source is shown, respectively, in Fig. 1 (a) and (b).

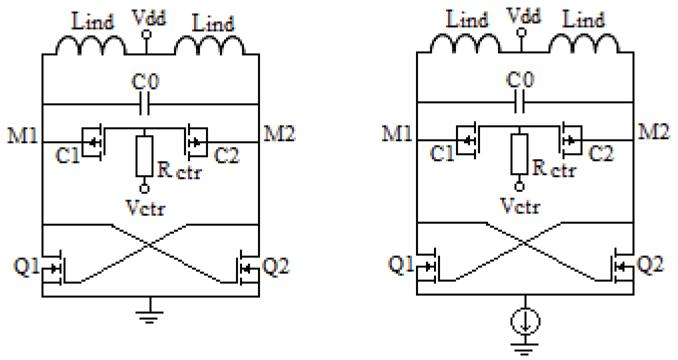

(a) (b)

Fig. 1. NMOS differential cross-coupled VCOs: (a) without a tail current source, (b) with a tail current source

The PMOS differential cross-coupled VCOs are shown in Fig. 2.

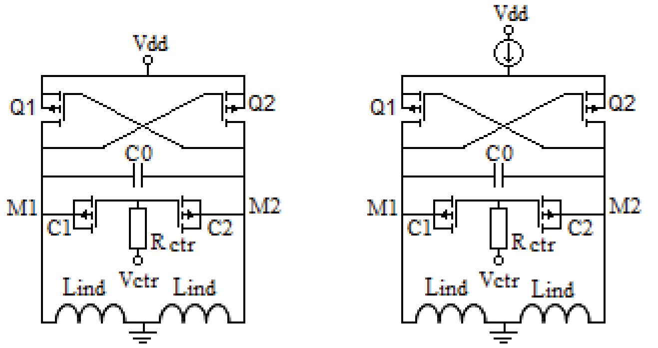

(a) (b)

Fig. 2. PMOS differential cross-coupled VCOs: (a) without a tail current source, (b) with a tail current source

The PMOS transistors M1 and M2 in the circuits of Fig. 1 and 2 represent the contrary connected varactors controlled by a variable dc voltage V_{ctr} applied through resistor R_{ctr}.

In Fig. 3 the CMOS cross-coupled VCOs are shown. Fig. 4 shows the schematic of a PMOS differential Colpitts VCO [3]. Only the PMOS transistors are used in the circuit of Fig. 4.

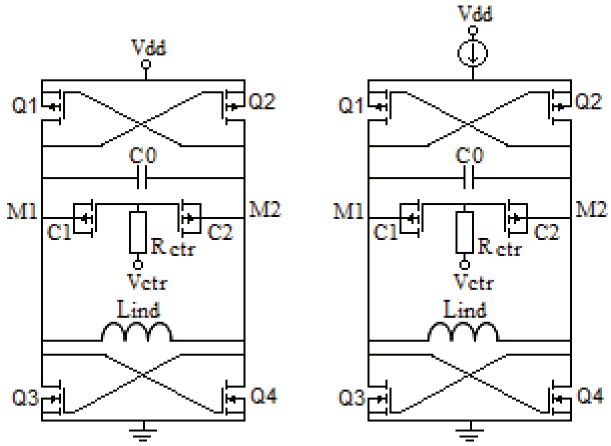

(a) (b)

Fig. 3. CMOS differential cross-coupled VCOs; (a) without a current-source, (b) with a PMOS current source

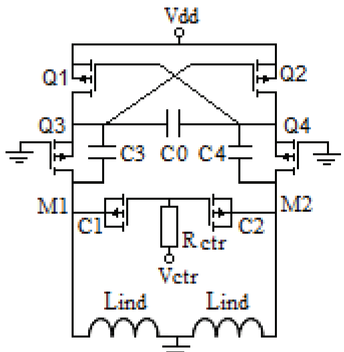

Fig. 4. PMOS differential Colpitts VCO

Figure of merit. A common FOM for performance comparison of different VCOs is given by [1]

$$FOM_1 = L(\Delta f) - 20\log(f_0/\Delta f) + 10\log(P_{diss}/1\mathrm{mW}),$$

where $L(\Delta f)$ is the phase noise at a frequency offset Δf, f_0 is the central oscillation frequency in the VCO tuning band, and P_{diss} is the VCO power dissipation. Lower (more negative) values of FOM represent better VCO performance. The main drawback of FOM_1 is that it does not take into account the amount of distortion in the generated sinusoidal signals. The proposed FOM is expressed as

$$FOM_2 = L(\Delta f) - 20\log(f_0/\Delta f) + 10\log(P_{diss}/1\text{mW}) + 20\log(THD\%/1\%), \tag{1}$$

where $THD\%$ is the total harmonic distortion (THD) of the generated signal expressed in %. The last term in equation (1) is positive if $THD\%>1\%$ and negative if $THD\%<1\%$. Thus, FOM_2 is sensitive to the amount of distortion in the VCO signal. The VCOs with larger THD will have less performance than those having smaller distortions.

Design variables and optimization criterion. For given CMOS technology with fixed transistor channel length, which is 0.13μm in our case, the VCO phase noise, power consumption and THD depend on the transistor channel width (W), inductor and varactor performance, tuning source resistor (R_{ctr}) and capacitor C_0. The standard way to design an on-chip spiral inductor is to lay out square spiral metal trace on the silicon substrate with one or more standard metal interconnection layers. A spiral inductor layout and its commonly used equivalent circuit model are, respectively, shown in Fig. 5 (a) and (b). The design parameters of an inductor are usually given by the number of turns (n), metal width (w), metal-to-metal spacing (s), and outer radios (h). The inductor dimensions w, s, and h can be optimized by using computer aided tools such as ASITIC, MICROWIND, SONET, ADS Momentum, and so on. If dimensions w, s, and h have been chosen, then the coil inductance L_{ind} is a function of n.

Frequency dependent series resistance $R_0(f)$ has the biggest impact on the inductor quality factor Q_{ind}, which in turn seriously affects the VCO performance. The use of multilayer spiral inductors can significantly reduce $R_0(f)$ and increase Q_{ind}.

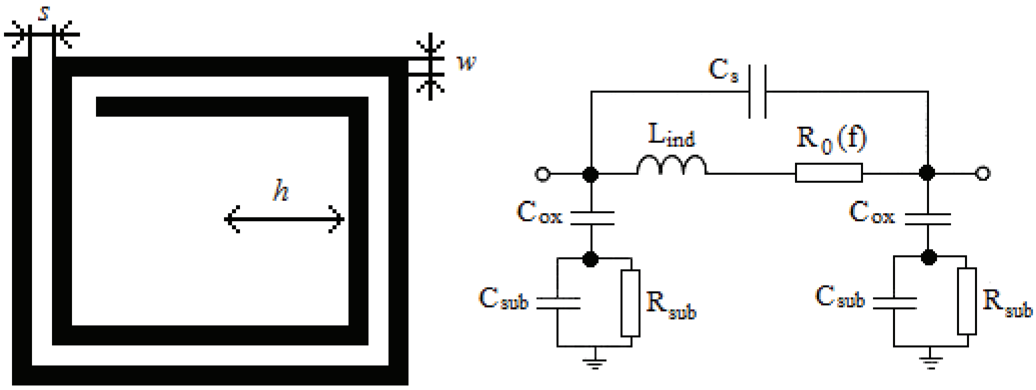

Fig. 5. Spiral inductor: (a) - layout, (b) - equivalent circuit

An analytical equation for frequency dependence of the resistance of a multi-turn spiral inductor with taking into account the skin and proximity effects was derived from fundamental electromagnetic principles [4]

$$R_0(f) = R_{0dc}\left(1 + 0.1\,\omega^2/\omega_{crit}^2\right), \tag{2}$$

$$\omega_{crit} = 3.1\frac{P \cdot R_{sheet}}{\mu_0 \cdot w^2},$$

where R_{0dc} is the dc resistance of the coil, w is the metal width, $P = w + s$ is the metal pitch, R_{sheet} is the metal sheet resistance, $\mu_0 \approx 1.257\times10^{-6}$ H/m is the magnetic permeability of the free space.

The dc resistance R_{0dc} of the multilayer inductors in different CMOS technologies can easily be simulated by CAD tools, for example, MICROWIND.

As well known, a MOS transistor with drain, source and bulk connected together realizes a MOS capacitor with capacitance dependent on the voltage applied between source and gate. For both inversion mode and accumulation mode MOS varactors, one of the most critical parameter is the tuning ratio $C_{v\max}/C_{v\min}$, which is usually a little higher than 2 [5]. For 3G and Bluetooth transceivers, this tuning ratio is more than sufficient because the required tuning range is, respectively, 140 and 80 MHz. Moreover, the capacitor C_0 is used to reduce the tuning band in the VCO circuits of Fig. 1 – 4. If the MOS transistor channel length is fixed, the varactor capacitance is proportional to the channel width W_{var} . The channel width of a MOS varactor can reach many hundreds of micrometers significantly increasing the parasitic resistance along the gate, which in turn reduces the varactor quality factor. Such transistors are usually designed with big number of fingers (N_v), so that $W_{\text{var}} = N_v W_v$, where W_v is the channel width of a split varactor transistor. Thus, we introduce two new variables W_v and N_v .

It should be pointed out that the core VCO transistors, labeled as Q_i (i=1, …, 4) in Fig. 1 - 4, must also be decomposed into multi-finger MOS transistors with gates of minimum size such that $W = N_{tr} W_{tr}$ for the same reason as varactors, where N_{tr} and W_{tr} are, respectively, number of fingers and channel width of a split core VCO transistor.

The value of resistor R_{ctr} has certain influence on both VCO phase noise and THD. In general, when R_{ctr} increases the VCO THD decreases, but the VCO phase noise increases due to the resistance thermal noise induced to the VCO through the tuning port. Thus, in terms of equation (1) there should be a value of R_{ctr} which minimizes FOM_2.

The proposed VCO optimization criterion is presented as follows:

$$\min FOM_2(W_{tr}, N_{tr}, W_v, N_v, R_{ctr}, C_0, L_{ind}) \tag{3}$$
$$V_m \geq V_m^*, f_{osc,\min} \leq f_{\min}^*, f_{osc,\max} \geq f_{\max}^*,$$

where V_m is the voltage amplitude across the tank, V_m^* is the minimum required output voltage amplitude, $f_{\min}^*$ and $f_{\max}^*$ represent the required frequency band of the VCO operation including additional bands, which must be used due to unavoidable process variations during the integrated circuit fabrication. The additional bands should be about 10-15% of the VCO frequency tuning band. In the case of Bluetooth transceiver, we can choose $f_{\min}^* = 2388\,\text{MHz}$ and $f_{\max}^* = 2492\,\text{MHz}$. Analogically, frequencies $f_{\min}^*$ and $f_{\max}^*$ can be chosen for 3G transceiver. The first constraint ($V_m \geq V_m^*$) indicates that the oscillator must have an excess of the loop gain required to compensate all losses at resonance providing sufficient voltage amplitude across the tank. A VCO with small amount of excess gain results in $V_m < V_m^*$. The VCO with large amount of excess gain satisfies the first condition, $V_m > V_m^*$, but it generates a greater harmonic content in the output waveform. The VCO designer should balance the need for enough excess gain providing $V_m \geq V_m^*$ and the need to keep THD low. This feature is taken into account in the criterion (3), because FOM_2 is dependent on THD.

Optimization results. The VCOs shown in Fig. 1 – 4 were designed and optimized according to criterion (3). The value of V_m^* was chosen to be 80% of the supply voltage. All MOS transistors were simulated using SPICE BSIM3v3.1 parameters of SCN013 0.13µm CMOS technology [6]. The VCO optimization results are given in Tables 1 and 2. The designed six metal layer spiral inductor has the following geometric parameters: w=25µm, s=2µm and h=65µm. As seen from Tables 1 and 2, the best performance has the PMOS Colpitts VCO. The capacitors C_3 and C_4 in the circuit of Fig 4 have values 1pF and 1.7pF, respectively, for 3G and Bluetooth VCOs.

Optimization results for the VCO of 3G transceiver

Table 1

VCO 3G transceiver	L_{ind} (nH)	R_{ctr} (Ω)	C_0 (pF)	Transistors			Varactors		$L(3\,\text{MHz})$ (dBc/Hz)	P_{diss} (mW)	THD %	FOM (dBc/Hz)	
				W_{tr} (μm)	NF_{tr}		W_v (μm)	NF_v				FOM_1	FOM_2
					Core	Current source							
NMOS	5	250	0.15	0.5	4	-	5	53	-133.4	2.50	8.6	-188.2	-169.5
NMOS+CS	5	220	0.15	1	3	3	5	53	-134.7	1.48	7.94	-191.7	-173.7
PMOS	5	210	0.15	1	3	-	5	53	-134.5	1.14	3.93	-192.7	-180.8
PMOS+CS	5	230	0.15	1	4	10	5	52	-134.0	0.93	3.86	-193.1	-181.3
CMOS	9	170	0.16	1	18, 7	-	5	50	-131.1	5.29	9.0	-182.6	-163.5
CMOS+CS	9	30	0.16	1	18,7	18	5	51	-132.7	3.64	12.3	-185.8	-164.0
PMOS Colpitts	5	150	0.2	1	11	-	5	52	-134.6	0.36	4.90	-197.8	-184.0

Optimization results for the VCO of Bluetooth transceiver

Table 2

VCO Bluetooth transceiver	L_{ind} (nH)	R_{ctr} (Ω)	C_0 (pF)	Transistors			Varactors		$L(3\,\text{MHz})$ (dBc/Hz)	P_{diss} (mW)	THD %	FOM (dBc/Hz)	
				W_{tr} (μm)	NF_{tr}		W_v (μm)	NF_v				FOM_1	FOM_2
					Core	Current source							
NMOS	5	250	0.3	1	2	-	1	147	137.2	2.59	7.69	-191.3	-173.6
NMOS+CS	5	210	0.3	1	3	3	5	29	-137.8	1.48	6.88	-194.3	-177.6
PMOS	5	200	0.3	1	3	-	5	29	-138.6	1.14	2.83	-196.2	-187.2
PMOS+CS	5	220	0.3	1	4	14	1	143	-138.5	1.05	2.92	-196.5	-187.2
CMOS	9	170	0.3	1	18, 7	-	2	73	-132.8	5.27	8.10	-183.8	-165.6
CMOS+CS	9	30	0.3	1	18,7	18	5	30	-134.1	3.64	11.87	-186.7	-165.2
PMOS Colpitts	5	130	0.4	1	16	-	5	31	-139.1	0.52	3.44	-200.1	-189.4

It should be noted that the PMOS VCOs have also a very good performance in terms of FOM_2 which is only $2 \div 3$ dB lower than that of PMOS Colpitts VCO. The NMOS and CMOS VCOs have much less performance and cannot be proposed for realization in 3G and Bluetooth transceivers.

Conclusion. New criterion has been proposed for optimizing cross–coupled MOS VCOs. It is sensitive not only to the VCO phase noise and power consumption but also to the total harmonic distortion of generated signals. The design variables have been selected and analyzed. It has been shown that the PMOS Colpitts VCO has the best performance among seven examined topologies.

References

[1] *D. Ham, A. Hajimiri,* “Concepts and methods in optimization of integrated *LC* VCOs”, IEEE J. of Solid-State Circuits, vol. 36, no. 6, pp. 896–909, June 2001.

[2] *S. Ryu,* “Design issues of CMOS VCO for RF transceivers”, J. of the Korean institute of electromagnetic engineering and science”, vol. 9, no. 1, pp. 25–31, Mar. 2009.

[3] *M. Tsai, Y. Cho, H. Wang,* “A 5-GHz low phase noise differential Colpitts CMOS VCO”, IEEE microwave and wireless components letters, vol. 15, no. 5, pp. 327–329, May 2005.

[4] *W. B. Kuhn and N. M. Ibrahim,* “Analysis of current crowding effects in multiturn spiral inductors,” IEEE Trans. Microwave Theory Tech., vol. 49, pp. 31–38, Jan. 2001.

[5] *P. Andreani, S. Mattison,* “On the use of MOS varactors in RF VCOs”, Phase locking in high performance systems, edited by B. Razavi, pp. 157–162, Willey–Interscience, 2003.

[6] ftp://ftp.isi.edu/pub/mosis/vendors/ibm–013/t97l_1_8rf_8lm_dm–params.txt.

Hemlata Soni, Electronics & communication,
(Techno India NJR Institute of Technology, India)
Pushtivardhan Soni, Electronics & communication
(Techno India NJR Institute of Technology, India)
Bhoopendra Sharma, Electronics & communication
(Techno India NJR Institute of Technology, India)
Pradeep Chhawcharia, Electronics & communication
(Techno India NJR Institute of Technology, India)

A NEW DESIGN OF BAND NOTCHED MICROSTRIP ANTENNA FOR UWB APPLICATIONS

In this paper a new ultra wideband (UWB) antenna is proposed with band notch characteristics to avoid interference with WLAN//HIPERLAN in 5.15 GHz – 5.85 GHz band. In proposed antenna a wide impedance bandwidth is achieved (3.4 GHz – 12 GHz) to fulfill requirements of UWB for future applications. The proposed antenna is investigated with partial ground plane. It has a simple geometry and by introducing three slots band rejection characteristics of proposed antenna are achieved. The measured S_{11} is well below -10 dB & measured radiation patterns are near omnidirectional.

1. Introduction

Ultra Wideband is a carrier less short range communications technology which transmits the information in the form of very short pulses. This former military technology has gained a lot of popularity among researchers and the wireless industry after the FCC [1] permitted the marketing and operation of UWB. UWB has promised to offer high data rates at short distances with low power, primarily due to wide resolution bandwidth. The FCC in the USA has allocated a frequency band 3.1 GHz to 10.6 GHz for UWB transmission and released a mask which indicates the power levels to keep the narrow band incumbents spectrum free from interference.

Compact and cheap ultra wideband antennas are needed for numerous UWB applications like wireless communications, indoor positioning and medical imaging. Several single-feed planar microstrip antennas such as Elliptically-shaped antenna with slots [2], curved rectangle with slot antenna [3], Variable slot type antennas [4], Cicular shape with variable slot [5], rectangle with steps & slot [6]. In all these structures a partial ground has been proposed, providing attractive solutions that can be readily incorporated under an UWB system. Similarly in [7] a band notched UWB antenna proposed by changing partial ground geometry rather than main patch as in cases of [2-6]. But tuning of back patch is difficult task.

In this paper, a new UWB antenna is proposed with a very simple structure by cutting three slots
& corner notched rectangle patch with partial ground of rectangle shape & compact size of 30*X*24.5 mm^2. Here notches & slots are made in such a way that current distribution is not effected & antenna is perfectly matched for an impedance bandwidth of 3.4 GHz – 12 GHz.

2. Antenna structure

Proposed antenna is designed in three phases. In first phase a rectangle patch with partial ground is designed as shown in figure 1.In next phase a single step is created at lower edges of patch of figure 1 to match antenna for UWB bandwidth as given in figure 2 & in last phase a slot line of hat type shape is etched at centre of modified patch antenna of figure 2 and design is given in figure 3 to make it a band rejected UWB antenna.

In next phase an experiment is done by inverting the shape of slot line and an inverted hat shape slot is etched on the centre of the patch as shown in figure 4. Dimensions of antennas are listed in table 1.

The antenna is fabricated on FR4 (roger) substrate having thickness 1.6 mm & relative dielectric constant of 4.65. The area covered by antenna geometry is 30 *X* 24.5 mm^2. The antenna is simulated on Commercial software FEKO suite 6.1, based on Method of Moment (MOM).

Table-1

Dimensions of Antennas

W_p	l_p	W_s	l_s	W_t	W_f	l_f	W_n	l_n	S_1	S_2	S_3	S_4	W_w
16.0 mm	12.5 mm	30.0 mm	11.5 mm	6.5 mm	3.0 mm	12.0 mm	3.0 mm	3.0 mm	3.5 mm	3.0 mm	3.0 mm	4.0 mm	0.5 mm

3. Results

The prototypes of proposed antennas are shown in figure 3 and figure 4. Figure 5 and figure 6 shows the simulated S11 (in dB) parameters of antennas. It is observed that for 3.4 GHz to 12 GHz, the return loss is much below than -10 dB. As given in fig.5 there is a smooth transition from conventional patch to band rejected printed UWB antenna, the proposed band rejected antenna shows best S11 results in simulation environment as compare to other models & it is well below -10 dB except range of 5.15 to 5.85 GHz. As shown in figure 5, the measured results of S11 is well below -10dB mark for entire range of 3.4 – 5 GHz & then it start increasing in between 5 – 6 GHz with a maximum value of 0 dB. After 5.85 GHz it starts decreasing steadily & at 6 GHz it touches to -17.5 dB. After word it maintains its level of S11 consistently in between -15 to -25 dB in between 6 – 12 GHz. The minimum value of S11 is achieved of -23.83 dB at 4.2 GHz. The figure 6 shows the simulated results S11 (in dB) of antenna shown in figure 4, which is also well below -10dB for entire range of frequency band from 3.4 – 12 GHz except band 5.1 – 5.85 GHz, as shown in figure 6. The minimum value of S11 is achieved of -36.58 dB at 11.39 GHz. As shown in figure 3 and figure 4, the design has three slots in patch geometry. By changing the area of these slots one can tune band rejection characteristics of UWB antenna. Here these dimensions are designated as s_1 & s_4. By changing these dimensions one can achieve above mentioned objective. The current distribution for proposed antennas for band rejected rectangular patch antennas is shown in Figure 7. Based on the current distribution of proposed antennas calculated by FEKO suite 6.1, we can find that the currents are concentrated near the slits at the notched frequency, while they are distributed mostly near the edges of the arms at the other frequencies. Therefore, we can expect that inserted slits have a function to notch the particular frequency band, here slot line work as stub that plays a short circuit. Therefore, it prevents the antenna from impedance matching at the notched frequency. As shown in figure 8, all the antennas exhibit omnidirectional pattern for H-plane at 3 GHz, 7 GHz and 11 GHz for each type of antenna where it is a characteristic of monopole antenna. All antennas exhibit eight shape lobe pattern for E-plane at lower frequencies as we increase frequency the lo**b**e start tilting from 0^o towards positive side as shown in figure 8. In figure 9 simulated gain of proposed band rejected antenna (fig. 3 and fig 4) has been shown, the gain of antenna is very low & reduced at notch frequencies drastically.

4. Conclusion

A novel compact band notched ultra wideband rectangle printed antenna has been designed. The impedance bandwidth is much higher than required UWB band which can be used by future application of UWB systems. Moreover by visualizing radiation pattern, the proposed antenna can be effectively used for UWB applications.

5. References

1. *Yi-cheng lin and kuan-jung hung,* “Compact Ultra wideband Rectangular Aperture Antenna and Band-Notched Designs”, IEEE Transactions Antennas and Propagation Vol. 54, No. 11, November 2006

2. *Tao Yuan, Cheng Wei Qiu, Le Wei Li,1Mook Seng Leong and Qun Zhang,* “Elliptically Shaped Ultra Wide Band Patch Antenna with Band – Notch Features”, Microwave & Optical Technology Letters Vol. 50, No. 3, March 2008

3. *Wen-jun Lui, Chong-hu Cheng, and Hong-bo Zhu,* “Improved Frequency Notched Ultra wideband Slot Antenna Using Square Ring Resonator”. IEEE Transactions Antennas and Propagation Vol. 55, No. 9, September 2007

4. *Qing Qi Pei, Cheng-Wei Qiu, Tao Yuan, and Said Zouhdi,* “Hybrid Shaped Ultra Wide Band Antenna”, Microwave and Optical Technology Letters, Vol. 49, No. 10, October 2007

5. *X.C.Yin, C.L.Ruan, S.G.Mo, C.Y.Ding, and J.H.Chu,* “A Compact Ultra Wide Band Microstrip Antenna with multiple Notches”, PIER 84, 321–332, 2008

6. *S.H. Choi, J.K. Park, S.K. Kim and J.Y. Park,* “A new ultra-wideband antenna for UWB applications”, Microwave Opt. Technol. Lett., Vol. 40, No. 5, pp. 399-401, Mar. 2004

7. *Jia Yi Sze and Jen Yi Shiu,* “Design of Band-Notched Ultra wideband Square aperture Antenna With a Hat-Shaped Back-Patch”, IEEE Transactions Antennas and Propagation Vol. 56, No.10, October 2008

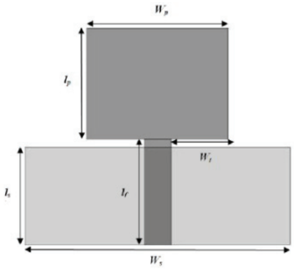

Figure 1

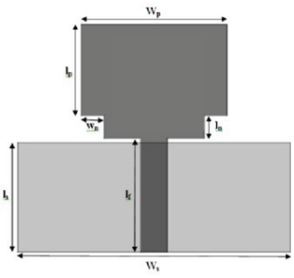

Figure 1

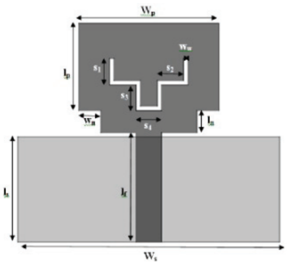

Figure 2

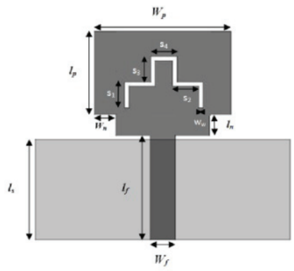

Figure 3

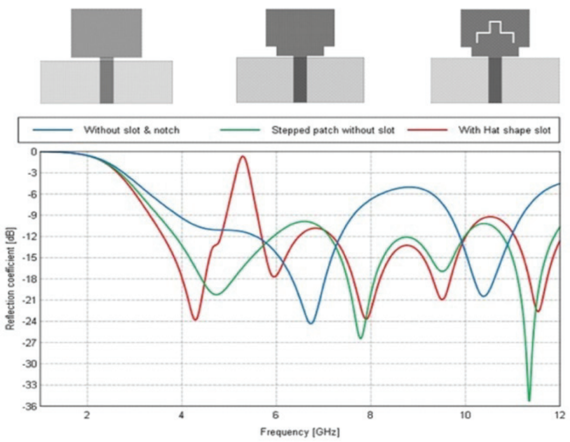

Figure 4: Simulated return loss comparison of proposed antennas (Figure 1,2,3)

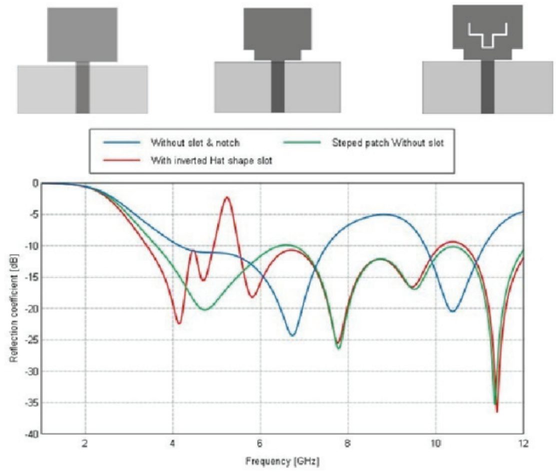

Figure 5: Simulated return loss comparison of proposed antennas (figure 1,2,4)

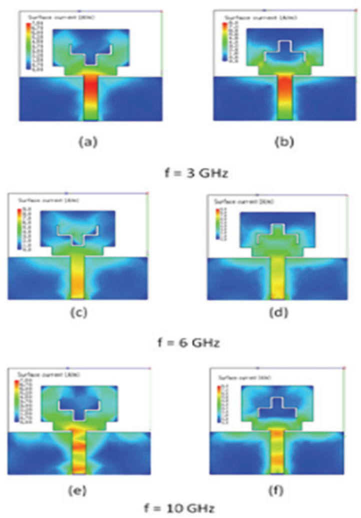

Figure 6: Current distribution on the surface of patch and ground plane for different frequencies of band rejected UWB antennas

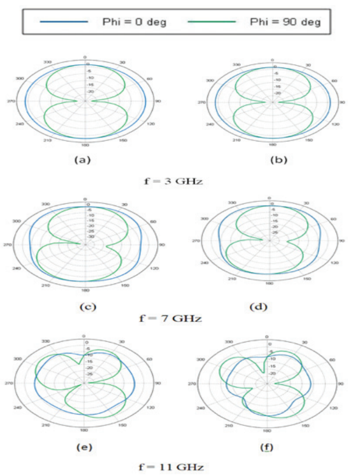

Figure 7: Simulated radiation patterns in azimuth & elevation plane of proposed band rejected UWB antennas (Figure 3, 4) (in figure (a), (c), (e) for figure 3, and (b), (d) (f) for figure 4)

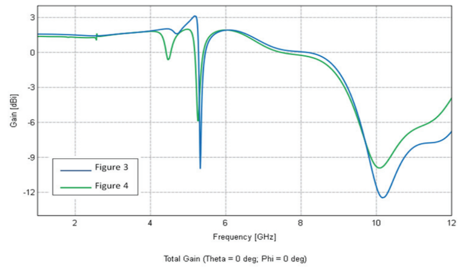

Figure 8: Simulated Gain (dBi) of proposed band rejected UWB antennas (Figure 3, 4)

Hemlata Soni, Electronics & communication
(Techno India NJR Institute of Technology, India)
Pushtivardhan Soni, Electronics & communication
(Techno India NJR Institute of Technology, India)
Bhoopendra Sharma, Electronics & communication
(Techno India NJR Institute of Technology, India)
Pradeep Chhawcharia, Electronics & communication
(Techno India NJR Institute of Technology, India)

DOUBLE SIDE MICROSTRIP ANTENNAS WITH THREE SLOTS FOR UWB APPLICATIONS WITH BAND REJECTION CHARACTERISTICS

In this paper, we propose two new ultra-wideband (UWB) antennas for UWB applications. The proposed antenna is designed to operate from 3.2 to 12 GHz. Both consist of a rectangular patch with two steps on primary radiator. To obtain band notch characteristics, In first design the three slots are orientated in hat shape where as in other design it is in form of inverted hat shape. Details of the proposed antenna designs and results are presented and discussed.

INTRODUCTION

In 2001 FCC announces the UWB band for commercial application with strong history in defense for many communication applications with broadband and spread-spectrum features in radar systems [1]. Since then researchers are doing great job to device antennas for UWB band (1.3–20 GHz) with respect to 10-dB impedance [2, 3, 4, and 5].

In this paper, we are proposing two ultra wide band antennas for UWB applications with very simplified structure. As it is evident that IEEE 802.11 WLAN occupied band between 5.15 to 5.85 GHz so to avoid the interference in case both are coexist in same scenario a band rejection characteristic has be implemented within UWB band in above mention range of frequencies. To implement such constrain we have implanted three slots in antenna geometry. The orientation of slots in one case is hat shape and in other design it is inverted. The proposed antenna consists of a rectangular patch with two steps, three slots on the patch, and a partial ground plane. Investigations based on experiments and simulations are conducted. The simulation is performed using the commercially available simulation software FEKO. The proposed antenna is successfully implemented and the simulated results show reasonable agreement within 3.2–12-GHz frequency range for return loss below -10 dB along with good band notch characteristics in between 5.15 to 5.85 GHz. Radiation patterns and gains are also examined.

ANTENNA STRUCTURE

The antenna structure consists of a stepped patch with hat shape slot at the centre of the patch. The ground plane of the antenna is partially fabricated to provide wider bandwidth. Later on the configuration of Hat shape slot is inverted which also provide approximately same performance as Hat shape slot.

Proposed antenna is designed in three phases. In first phase a rectangle patch with partial ground is designed as shown in figure 1.In next phase a single step is created at lower edges of patch of figure 1 to match antenna for UWB bandwidth as given in figure 2 & in last phase a slot line of inverted hat type is etched at centre of modified patch antenna of figure 2 and design is given in figure 3 to make it a band rejected UWB antenna. Dimensions of antennas are listed in table 1.

The antenna is fabricated on FR4 (roger) substrate having thickness 1.65 mm & relative dielectric constant of 4.65. The area covered by antenna geometry is 30 X 24.5 mm^2. The antenna is simulated on Commercial software FEKO suite 6.1, based on Method of Moment (MOM).

Table-2

Dimensions of Antennas

W_p	l_p	W_s	l_s	W_t	W_f	l_f	W_n	l_n	S_1	S_2	S_3	S_4
16.0 mm	12.5 mm	30.0 mm	11.5 mm	6.5 mm	3.0 mm	12.0 mm	3.0 mm	3.0 mm	3.5 mm	3.0 mm	3.0 mm	4.0 mm

RESULTS

The prototypes of proposed antennas are shown in figure 2 and figure 4. Figure 5 and figure 6 shows the simulated S11 (in dB) parameters of antennas. It is observed that for 3.4 GHz to 12 GHz, the return loss is much below than -10 dB. As given in fig.2 and figure 4, there is a smooth transition from conventional patch to band rejected printed UWB antenna, the proposed band rejected antenna shows best S11 results in simulation environment as compare to other models & it is well below -10 dB except range of 5.15 to 5.85 GHz. As shown in figure 5, the measured results of S11 is well below -10dB mark for entire range of 3.4 – 5 GHz & then it start increasing in between 5 – 6 GHz with a maximum value of 0 dB. After 5.85 GHz it starts decreasing steadily. After word it maintains its level of S11 consistently in between -15 to -45 dB in between 6 – 12 GHz. The minimum value of S11 is achieved of -48 dB at 11.5 GHz. The figure 6 shows the simulated results S11 (in dB) of antenna shown in figure 3 and figure 4, which is also well below -10dB for entire range of frequency band from 3.4 – 12 GHz except band, as shown in figure 6. The minimum value of S11 is achieved of -36.58 dB at 4.3 GHz.

As shown in figure 2 and figure 4, the design has three slots in patch geometry. By changing the area of these slots one can tune band rejection characteristics of UWB antenna. Here these dimensions are designated as s_1 & s_4. By changing these dimensions one can achieve above mentioned objective.

The current distribution for proposed antennas for band rejected rectangular patch antennas is shown in Figure 8. Based on the current distribution of proposed antennas calculated by FEKO suite 6.1, we can find that the currents are concentrated near the slots at the notched frequency, while they are distributed mostly near the edges of the arms at the other frequencies. Therefore, we can expect that inserted slots have a function to notch the particular frequency band, here slot line work as stub that plays a short circuit. Therefore, it prevents the antenna from impedance matching at the notched frequency. All the antennas exhibit omnidirectional pattern for H-plane at 3 GHz, 7 GHz and 11 GHz for each type of antenna where it is a characteristic of monopole antenna. All antennas exhibit eight shape lobe patterns for E-plane at lower frequencies as we increase frequency the lo**b**e start tilting from 0^{o} towards positive side as shown in figure 8. In figure 9 simulated gain of proposed band rejected antenna (fig.2 and fig 4) has been shown, the gain of antenna is very low & reduced at notch frequencies drastically.

CONCLUSIONS

A novel compact band notched ultra wideband rectangle printed antenna has been designed. The impedance bandwidth is much higher than required UWB band which can be used by future application of UWB systems. Moreover by visualizing radiation pattern, the proposed antenna can be effectively used for UWB applications.

REFERENCES

1. *Yi-Cheng Lin and Kuan-Jung Hung,* "Compact Ultra wideband Rectangular Aperture Antenna and Band-Notched Designs", IEEE Transactions Antennas and Propagation Vol. 54, No. 11, November 2006

2. *Tao Yuan, Cheng Wei Qiu, Le Wei Li,1Mook Seng Leong and Qun Zhang,* "Elliptically Shaped Ultra Wide Band Patch Antenna with Band – Notch Features", Microwave & Optical Technology Letters Vol. 50, No. 3, March 2008

3. *Wen-jun Lui, Chong-hu Cheng, and Hong-bo Zhu,* "Improved Frequency Notched Ultra wideband Slot Antenna Using Square Ring Resonator". IEEE Transactions Antennas and Propagation Vol. 55, No. 9, September 2007

4. *Qing Qi Pei, Cheng-Wei Qiu, Tao Yuan, and Said Zouhdi,* "Hybrid Shaped Ultra Wide Band Antenna", Microwave and Optical Technology Letters, Vol. 49, No. 10, October 2007

5. *X.C.Yin, C.L.Ruan, S.G.Mo, C.Y.Ding, and J.H.Chu,* "A Compact Ultra Wide Band Microstrip Antenna with multiple Notches", PIER 84, 321–332, 2008

6. *S.H. Choi, J.K. Park, S.K. Kim and J.Y. Park,* "A new ultra-wideband antenna for UWB applications", Microwave Opt. Technol. Lett., Vol. 40, No. 5, pp. 399-401, Mar. 2004

7. *Jia Yi Sze and Jen Yi Shiu,* "Design of Band-Notched Ultra wideband Square aperture Antenna With a Hat-Shaped Back-Patch", IEEE Transactions Antennas and Propagation Vol. 56, No.10, October 2008

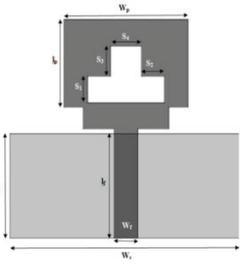

Figure 9

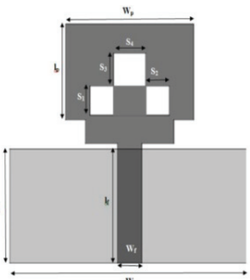

Figure 10

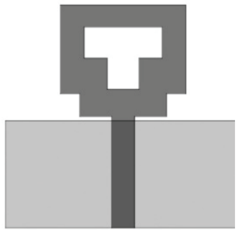

Figure 11

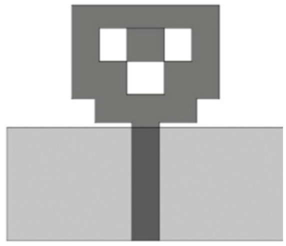

Figure 12

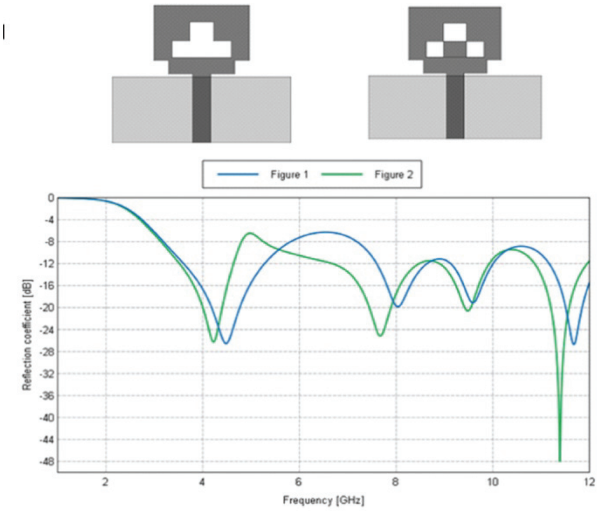

Figure 13: Simulated return loss comparison of proposed antennas (Figure 1,2,3)

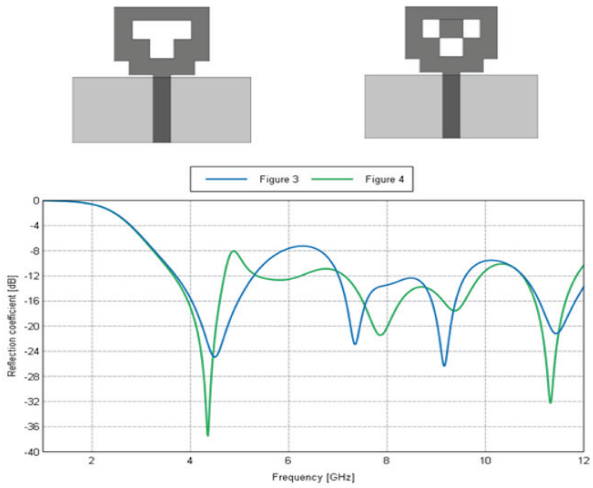

Figure 14: Simulated return loss comparison of proposed antennas (figure 1,2,4)

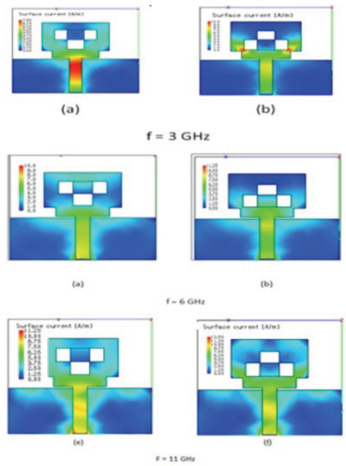

Figure 15: Current distribution on the surface of patch and ground plane for different frequencies of band rejected UWB antennas

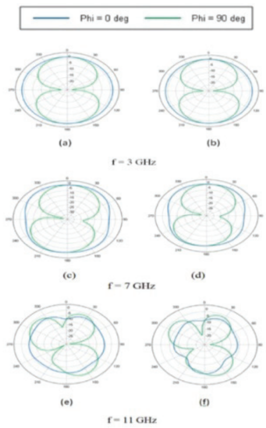

Figure 16: Simulated radiation patterns in azimuth & elevation plane of proposed band rejected UWB antennas (Figure 3, 4) (in figure (a), (c), (e) for figure 3, and (b), (d) (f) for figure 4)

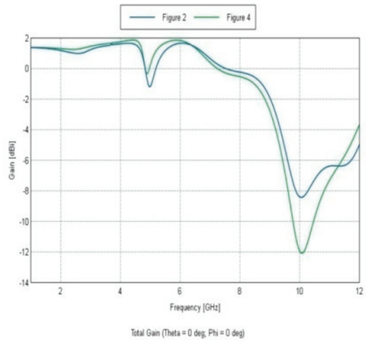

Figure 17: Simulated Gain (dBi) of proposed band rejected UWB antennas (Figure 3, 4)

MSc. B.Pompeo, MSc. L.Pralon, MSc. M.Pralon, MSc. H.Cioquetta, MSc. G.Beltrão and Dr. R.Mendes
B. Pompeo, L.Pralon and M. Pralon are with the Brazilian Army Technological Center, Rio de Janeiro, RJ – Brazil;
H. Cioquetta and G. Beltrão are with Orbisat da Amazônia - Campinas, SP - Brazil
R. Mendes is with State University of Campinas - Campinas, SP - Brazil

RADIATION PATTERN GENERATION USING A MODIFIED LEAST SQUARES METHOD

Current excitation of each active antenna element in a phased array antenna allow to generate a specific beam shape. This paper proposes the use in radar systems of an optimization method for generating a radiation pattern based on the least squares methods, besides compare this method to two distinct algorithms well spread in the literature.

INTRODUCTION

Nowadays, many systems employ phased array antennas, e.g, radio stations, space probes, meteorological radars and modern military radar systems [1]. Therefore, it has been verified an increase in researches related to this area. Since each application requires an adequate design, the appropriate geometry and the optimum current distribution of each active antenna element in a phased array antenna should be carefully studied in order to achieve maximum performance. The present work addresses only the optimization of the current distribution, because, generally, geometry characteristics have to comply with budget and hardware availability.

Phased array systems employ a set of radiating elements geometrically configured and strategically excited in order to obtain a specific radiation pattern. Each element is feed with a different amplitude and phase, conforming the resultant radiation pattern of the array. The existence of multiple elements allows to control and model the antenna pattern, more precisely, achieving lower sidelobes levels, electronic steer of the radiation pattern main lobe and nulls generation in specified directions.

For mathematical analysis purpose, each elements excitation is considered as complex variables. Thus, it is possible to derive the phase and amplitude distributions using optimization methods. Nevertheless, since each application may require a unique beam shape, there is not a single method that guarantees optimum performance for all radiation pattern generations.

Several methods have been proposed to design radiation pattern, such as analytical approaches [2], genetic algorithms [3,4] and convex optimization [5]. This paper focuses on providing the excitation vector for a linear uniform array in the horizontal plane so that the total radiation pattern results in a shape that is closest to the desired pattern as possible. In order to achieve this goal, an optimization method, primarily employed in acoustics [6], is proposed based on a modified least squares approach.

This work is divided in four sections. In Section II, a brief overview on phased array antennas is performed. In Section III, the conventional least squares method along with the proposed method, based on the former, are presented. In Section IV, simulation results are taken into consideration, performing a comparison of the proposed algorithm with the well known Woodward-Lawson method and a simple Genetic Algorithm approach. Finally, a conclusion on the performance of the proposed method is made.

LINEAR PHASED ARRAY ANTENNA

A linear uniform phased array antenna consists of active elements placed in a line and equally spaced by a distance *dx*. Once *dx* and the kind of antenna for each element is defined, the resulting pattern generated by the array follows (1).

$$f(\theta,\phi) = \sum_{i=1}^{n} U_i w_i e^{\frac{-j2\pi R_i \cos(\theta)\sin(\phi)}{\lambda}} \tag{1}$$

where U_i is the radiation pattern for each element i, w_i is the complex excitation of each element i, R_i is the distance from a fixed point to each element i, ϕ is the elevation of a fixed point from the horizontal plane that crosses the normal line to the antenna, θ is the azimuth of a fixed point from the normal angle in respect to the antenna and λ is the transmitted/received signal wavelength.

In the present work, the phase component related to ϕ can be suppressed since, for horizontal plane arrays, this component is the same to all the array elements. It is also considered that the wave is traveling from a far point ($R_i >> \lambda$) and so, can be referred as planar.

Based on the above concerns and using matrix notation, so that it can better be applied in optimization techniques, (1) can be rewritten as (2).

$$\mathbf{D = Aw} \tag{2}$$

where **D** is the radiation pattern generated by the antenna, **w** is the weight vector applied to each the array element and **A** is the isotropic element directivity pattern matrix, where the columns are the elements, from 1 to n, and the lines, the elevation angles, from -90º to 90º, given by:

$$A = \begin{bmatrix} a_{-90^\circ,1} & a_{-90^\circ,2} & \cdots & a_{-90^\circ,n} \\ \vdots & \vdots & \ddots & \vdots \\ a_{90^\circ,1} & a_{90^\circ,2} & \cdots & a_{90^\circ,n} \end{bmatrix} \tag{3}$$

Assuming $w_i = \|w_i\| e^{j\alpha_i}$, it is necessary to find the values for $\|w_i\|$ and α_i that results in the desired pattern, given the matrix **A**, which represents the physics model. In the present work, a modified least squares method applied to find the vector w is analyzed in order to generate a beam shape that is closest to the desired pattern **D** as possible.

LEAST SQUARES ANALYSIS

The least squares method is a linear method specially applicable when there is the need to estimate a set of variables in order to achieve a desired curve, minimizing the mean square error between the resultant curve and the desired one. Such algorithm is very popular, fast, easy to implement and widespread in the literature. Therefore, considering the element excitations as complex variables, it's verified that it is possible to derive the phase and amplitude distributions using this method.

This method minimizes the mean square difference between the calculated data and desired data, and so, the cost function can be written by

$$J(\beta) = \sum_{n=0}^{N-1} (x[n] - s[n])^2 \tag{4}$$

Let D be a desired radiation pattern, A the element directivity pattern matrix shown in (3) and w the excitation current vector, then (4) can be given by

$$J(w) = \sum_{n=0}^{N-1} (\mathbf{D}_n - \boldsymbol{A}w)^2 \equiv (\mathbf{D} - \boldsymbol{A}w)^T(\mathbf{D} - \boldsymbol{A}w) \tag{5}$$

The estimated vector $\widehat{w}$, that minimizes equation (5) is given by [7]

$$\widehat{w} = (A^T A)^{-1} A^T D \tag{6}$$

This method guarantees to minimize the squared difference between the desired radiation pattern and the calculated data. However, since the beam shaping **D** is a complex vector, the method calculates the least squared error considering both the phase and amplitude this vector. Nevertheless, in radar applications, the designer is only interested in the radiation pattern magnitude. Therefore, our focus is to determine a good estimator that syntheses only the magnitude of the directivity pattern, followed by minimization approaches, if possible, in this nonlinear problem.

Magnitude least squares problem

In the previous discussion, both magnitude and phase of the desired directivity pattern were taken into account in the cost function. In this approach, phase error and magnitude error are treated equally. Thus, a better synthesize to antennas radiation pattern excludes the phase of the desired pattern from the cost function (7).

$$\min_{x \in C} \| |\boldsymbol{Aw}| - |\boldsymbol{D}| \|_2^2 \equiv \min_{w \in C} \sum_{i=1}^{n} (|A_i w| - |D_i|)^2 \tag{7}$$

This analyses is a modification of the least squares method and is called magnitude least-squares. Unlike the traditional method, it is a non-convex formulation. Therefore, it is possible that local minima exist, which can jeopardize the performance of the algorithm.

Equation (7) can be reformulated and developed as a conventional least square problem, subject to certain adjustments. Therefore, the optimization method is written as

$$\min_{w \in C} \sum_{i=1}^{n} (A_i w - D_i z_i)^2 \tag{8}$$

where z_i is a complex number on the unit circle whose phase equals $A_i w$ phase.

Equation (8) can be solved through an iterative variable exchange method. This algorithm is ruled by the following steps [6]:

1. Choose a tolerance $\varepsilon > 0$ and a maximum number of iterations.
2. Choose any initial vector w.
3. Set $z_i = \frac{D_i}{|D_i|}$ for all i
4. Hold z fixed and find a new w as the solution to the equation (6)
5. Repeat steps 3 and 4 until the error decreases more than ε or the number of iteration exceed the maximum iterations

It's important to observe that this method is only capable of finding local solutions, which can be optimal or not.

Simulations were carried out in order to verify to proposed algorithm performance. In the present analyses a cosecant squared pattern was taken as a desired radiation pattern. This is a well known shape in air surveillance radar that guarantees maximum antenna power gain associated to the horizon (ϕ approximately zero degrees) and decays as cosec^2 ϕ until a maximum elevation angle [8]. In this work, it was considered a maximum gain to elevation angles between 0^o and 10^o, following a cosec^2 ϕ from 10^o until 35^o and minimum levels for the others.

Two distinct algorithms were implemented, using *Matlab*, in order to evaluate the performance of the proposed modified least squares method. A simple genetic algorithm approach, where the individuals are double vectors that represent the amplitude and phase excitation of each antenna active element was taken into consideration. Crossover and mutation were performed on a population consisting of two hundreds individuals and evolved for one thousands generation. The other approach considered in the analysis was the well known Woodward-Lawson method [2]. The results are showed in figure 1.

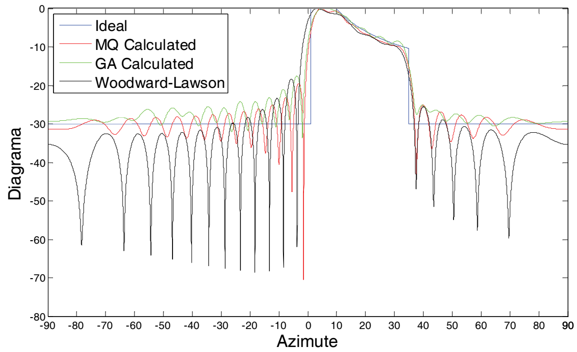

Figure 18 - Radiation pattern generation methods comparison

It is verified that all methods introduce ripples in the main lobe of the generated radiation pattern. For a better view, Figure 2 highlights the resultant pattern main lobes.

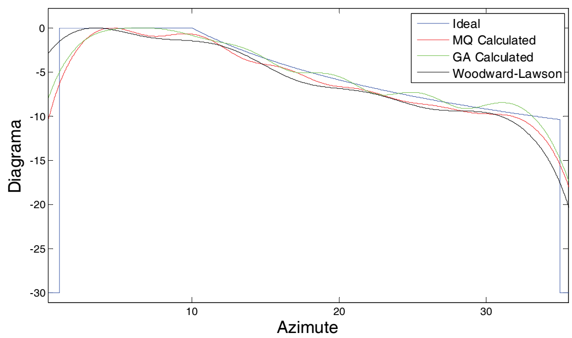

Figure 2

CONCLUSIONS

In this paper, we have presented a modified least squares method for generation of phased array antennas radiation pattern for radar application. The proposed method is used to determine the phase and amplitude excitations of each radiation elements on the array in order to achieve a desired radiation pattern.

Mathematical analysis showed that the modified least squares method focuses on minimizing the error between the absolute value of the radiation pattern achieved during the iterations and the absolute value of the desired radiation pattern. Such approach was firstly proposed to solve acoustic related problems and adapted, in present work, to phased array application. It is important to highlight that, unlike the traditional least squares methods, it is a non-convex algorithm, and result in local minima, not necessarily the optimal solution.

Simulations were carried out in order to compare the performance between the proposed method and two wide spread distinct methods employed for the same purpose: Genetic Algorithm and Woodward-Lawson approaches. Results showed that the proposed method provides the better ***cost effective between the three methods used.***

When compared to Woodward-Lawson method, the proposed method provides a less mean square error, reducing both the ripple on the main lobe and the sidelobes levels. Furthermore, since the Woodward-Lawson method is based on a sum of sinc(x) functions, it´s performance is dependent on the sincs shapes and positions on the elevation space.

When compared to a simple genetic algorithm approach, it could be observed that genetic algorithm approach is more flexible in determining the cost function, which can be very useful if specifics constraints have to be met. On the other hand, the performance of the latter is extremely dependent on the parameters chosen for the evolution process. Thus, much more caution has to be employed during the design of a genetic algorithm approach, which can decrease significantly the algorithm performance, increasing either the execution time or the mean square error of the output.

Nevertheless, the results obtained when the proposed method is employed shows similar mean square error when compared to genetic algorithm, but an execution time far lesser, making them more attractive for radar applications that have little constraint to comply with.

REFERENCES

1. *M. A.Richards, J. A. Scheer and W. A. Holm*, Principles of Modern Radar - Basic Principles, Raleigh, 2010.
2. *C. Balanis*, Antenna Theory—Analysis and Design. New York: Wiley, 1982.
3. *R. L. Haupt*, An Introduction to Genetic Algorithm for Electromagnetics, IEEE AP Magazine, April 1995 vol. 37, No. 2, pp 7-15.
4. *Soltankarimi, J. Nourinia and Ch. Ghobadi,* Side Lobe Level Optimization in Phased Array Antennas Using Genetic Algorithm, ISSTA2004, Sydney, Australia, 30 August 2004.
5. *S. A. Vorobyov, A. B. Gershman, and Z.-Q. Luo*, “Robust adaptive beamforming using worst-case performance optimization: A solution to the signal mismatch problem,” *IEEE Trans. Signal Processing*, Vol. 51, No. 2, 313–324, February 2003.
6. *P. W. Kassakian*, Convex approximation and optimization with applications in magnitude filter design and radiation pattern synthesis, PhD thesis, University of California, Berkeley, 2006.
7. *S. M. Kay*, Fundamentals of Statistical Signal Processing - Estimation Theory, Prentice Hall PTR, Upper Saddle River, New Jersey, 1993
8. *H. Meikle*, Modern Radar Systems, Artech House, Norwood, 2001.

Yahya S. H. Khraisat
Electrical and Electronics Department
Al-Balqa' Applied University/ Al-Huson university College, Jordan

WEARABLE ANTENNA FOR GPS APPLICATIONS

In this paper a single element rectangular patch antenna suitable for GPS applications has been developed and simulated. This antenna operates at 2.4 GHz. The antenna is simulated using IE3D simulator. The results for return loss, gain and radiation patterns are obtained. A comparison between inset feed and coaxial probe feed is demonstrated.

1. Introduction:

An antenna is a device for converting electromagnetic radiation in space into electrical currents in conductors or vice-versa, depending on whether it is being used for receiving or for transmitting, respectively.

One of the most widely used types of antenna is microstrip patch antenna. Microstrip antenna has been widely used in radio equipments from 100MHz to 100GHz, especially for the devices in the aircraft and ground portable devices. Microstrip antennas are often given priority for the application when low profile radiators are required, even if some performances are not as good as the general antennas [1].

Portable electronic devices have become part and parcel of everyday human life. Modern mobile phones are quite often carried throughout the day and they allow not just telephone calls alone but also provide internet access, multimedia, personal digital assistant and GPS functionality. This form of `always on' and constantly connected status is a step towards the pervasive computing paradigm [2]. In future, a person is likely to carry a range of devices and sensors, including medical sensors which constantly communicate with each other and the outside world. It is of paramount importance to provide this functionality as unobtrusively as possible [2]. A key technology to achieve this goal is wearable electronics and antennas. For the convenience of the user, wearable antennas need to be hidden and of low profile. This requires a possible integration of these antenna elements within everyday clothing. Microstrip patch is a representative candidate for any wearable application, as it can be made conformal for integration into clothing. [3-9]

In this paper, we designed a single rectangular patch antenna. There are several software programs that can be used in design and simulated the performance of the patch antenna such as HFSS, antenna magus and IE3D which we used.

1.2 Aim and objectives:

The aim of this paper is to design wearable rectangular microstrip patch antenna, studying antenna features (i.e. directivity, gain, efficiency), at 2.45 GHz, and study the effect of antenna dimensions Length (L), Width (W) and substrate parameters relative dielectric constant (εr), substrate thickness (h) on the Radiation parameters of Bandwidth and Beam-width.

2. Antenna Design Procedure:

The geometry of a GPS antenna developed for wearable applications is shown in figure 1. In order to design this type of antenna, it is necessary to know the exact value of dielectric constant of the substrate material chosen. The permittivity of the fabric is easily extracted from the measured resonant frequency of a patch radiator designed using an assumed approximate value of the substrate dielectric constant. The permittivity of the polyester fabric is determined as 1.44, from the knowledge of shift in measured frequency from design frequency.

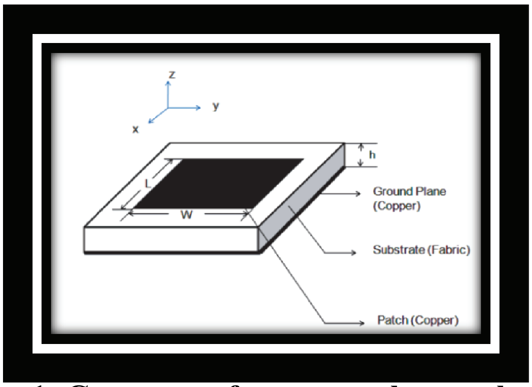

Figure 1: Geometry of a rectangular patch antenna for wearable application .

Initially we designed a single rectangular Microstrip patch antenna to understand the effect of its parameters.

Dielectric Constant of the Substrate ε_r :

The dielectric material that used here in my design of this Microstrip Patch Antenna is Polyester with ε_r=1.4 . The permittivity variation is ±0.020.

- **The frequency of the operation (f_0):**

The operational frequency for the Patch antenna has been selected as 2.45 GHz which is the frequency of the WLAN.

- **Height of the dielectric substrate (h):**

The height of the antenna has been found as 2. 85mm.

The parameters of our antenna are shown below in table 1:

*Table 1: **The initial parameters***

ε_r	1.4
H	2. 85 mm
f_0	2.45 GHz

In this design, we used two feeding techniques namely (coaxial feed probe and Inset feed). We started our simulation and design with coaxial feed probe, and then we simulated the inset feed.

2.1 Design procedure steps:

1- determination of the inset feed depth (yo) :

The feed point must be located at that point on the patch, where the input impedance is 50 Ω for the resonant frequency.

In my study, I used trial and error methods to obtain the optimum feed depth, where the return loss is most negative.

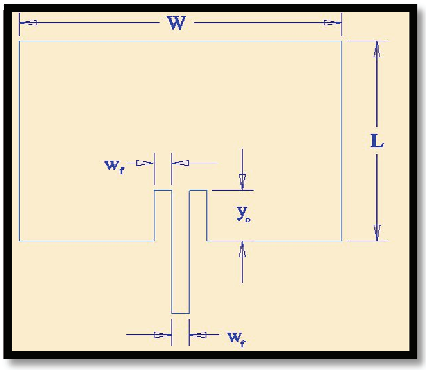

Figure 2: single patch antenna

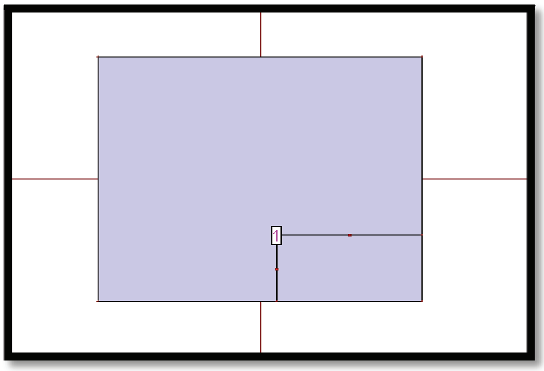

Figure 3: Microstrip patch antenna with coaxial probe feed.

2- Calculation for the inset feed:

- We found the value of the W_{f1} =0.5 mm and W_{f2} =2.2 mm.
- The value of the y_0 is 4 mm. As shown in the figure 2.

For probe feed:

From figure 3, we found the point that had the maximum return loss and gain is the point that has the coordinates: (2.975,-11.15)

A. 2.3 Modeling and Fabrication of antennas

The modeling of antennas is performed using Method of Moments (MoM) based IE3D simulator [11]. The parameters of the patch antenna are shown below in table 2

Table 2. **Designed values of dimensions of various antennas developed at resonant frequency.**

Name of the antenna	Length (*L*) in mm	Width (*W*) in mm	ΔL in mm	ε_r eff
Polyester for Inset	47.9	55.43	1.73	1
Polyester for probe	48	55.43	1.73	1

3. Simulation results:

3.1 Return Loss Characteristics

The inset feed is designed to have an inset depth of 4 mm, feed line width of 2.2 mm, and feed path length of 12mm. Frequency range of (1-3) GHz is selected and 201 frequency points are selected over this range to obtain accurate results.

By using inset depth of 4mm, we got return loss of -31.25 dB which considered being good result.

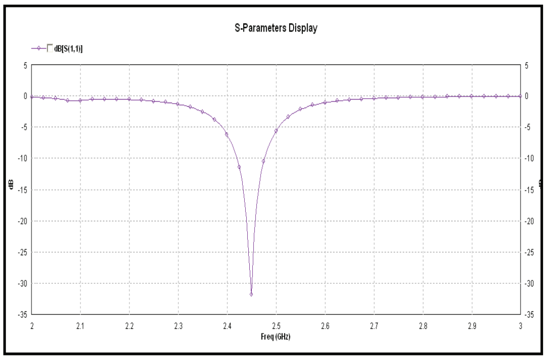

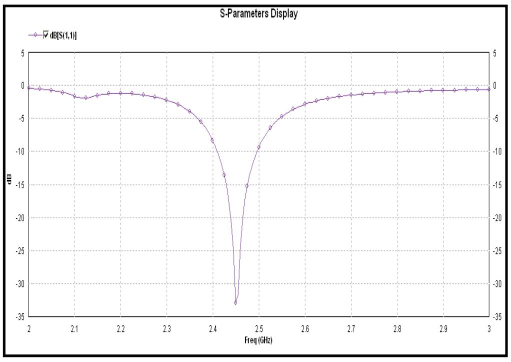

Figure 4: S11 parameter of Single patch antenna with Inset feed.

Figure 5: S11 parameter of Single patch antenna with coaxial probe.

The probe feeding is designed to have coordinates (2.975, -11.15), frequency range of (1-3) GHz. 201 frequency points are selected over this range to obtain accurate results.

I got return loss of -32.82 dBi which considered being good result.

Table 3: **Comparing between two feeding techniques**.

Feeding Technique	Resonant frequency (GHz)	S11 parameter (dB)
Coaxial probe	2.45	32.82
Inset feed	2.45	31.25

3.2 Far-field Radiation Pattern Characteristics

Since a microstrip patch antenna radiates normal to its patch surface, the elevation pattern for φ =0 and φ =90 degrees would be important.

Figure 6 shows the radiation pattern of inset feed and the antenna gain around 2.45 GHz.

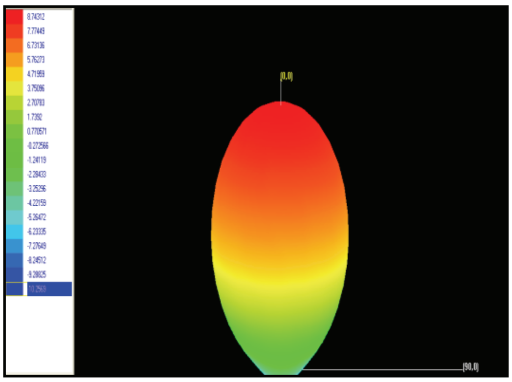

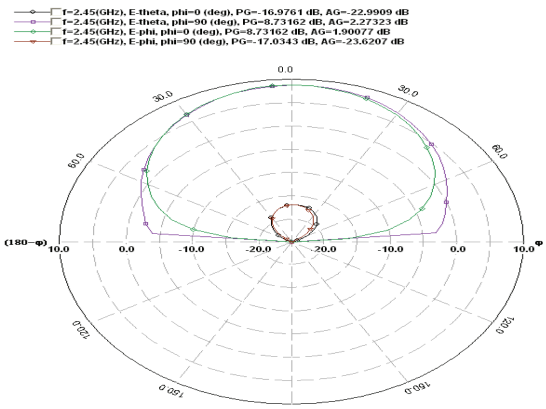

Figure 6: Antenna 3D radiation pattern for inset

Figure 7: 2D feed radiation power with Inset feed.

The maximum gain is obtained in the broadside and this measured to be 8.732 dBi.

Since a microstrip patch antenna radiates normal to its patch surface, the elevation pattern for φ =0 and φ =90 degrees would be important.

Figure 8 shows the radiation pattern of coaxial probe feed and the antenna gain around 2.45GHz .

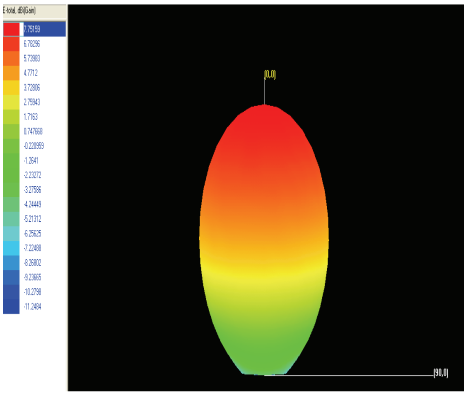

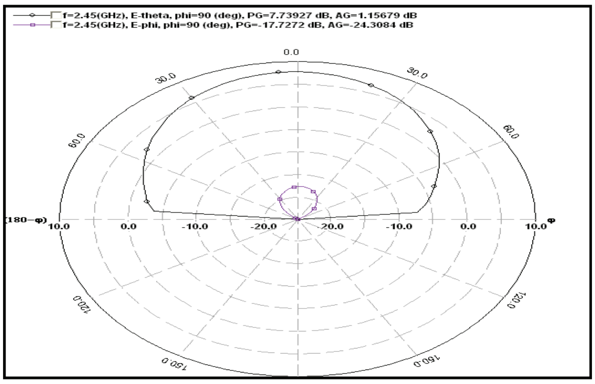

Figure 8: 3D radiation pattern **Figure 9: 2D radiation power with coaxial with probe feed probe feed**

The maximum gain is obtained in the broadside which measured to be 7.752 dBi.

Feeding Technique	Gain (dBi)	3 dB beam-width
Coaxial probe	7.752	88.54
Inset feed	8.732	82.762

Table 4: Gain and 3dB beam width for coaxial probe and inset feed

4. Conclusions

In this paper a single element rectangular patch antenna has been designed and simulated. Two feeding techniques namely inset and probe were investigated. The inset feed demonstrates better results for return loss, antenna radiation pattern and gain. From this work we can say that microstrip patch antenna is suitable for wearable applications.

References

1. "Ubiquitous computing," http://en.wikipedia.org/wiki/Ubiquitous_ computing.
2. S. Sankaralingam and B. Gupta, "Development of Textile Antennas for Body Wearable Applications and Investigations on Their Performance Under Bent Conditions", PIERS B, Vol. 22, 53-71, 2010.
3. Salomen, P. and H. Hurme, "Modeling of a fabric GPS antenna for wearable applications," Proceedings of IASTED International Conference Modeling and Simulation, Vol. 1, 18–23, 2003.
4. Salomen, P. and H. Hurme, "A novel fabric WLAN antenna for wearable applications," Proceedings of IEEE APS International Symposium, Vol. 2, 700–703, June 2003.
5. Tanaka, M. and J. H. Jang, "Wearable microstrip antenna," *Proceedings of IEEE APS International Symposium and URSI North American Radio Science Meeting, Columbus, OH, USA,June 2003.*
6. Wong, K. L. and C. I. Lin, "Characteristics of a 2.4 GHz compact shorted patch antenna in close proximity to a lossy medium," *Microwave Optical Technology Letters, Vol. 45, No. 6, 480–483, 2005.*
7. Antenna theory and design reversed edition, Robert S.Elliott University of California Los Angeles, California IEEE .4ntennas & Propagation Society, Sponsor.
8. Wearable applications," Proceedings of IASTED International Conference Modeling and Simulation, Vol. 1, 18–23, 2003.
9. F. I. Tseng and D. K. Cheng, "Optimum Scannable Planar Arrays with an Invariant Side. Lobe Level," Proc. IEEE, 56 (1968), 1771-78.
10. en.wikipedia.org
11. www.wipl-d.com

Gaspare Galati, Gabriele Pavan – Tor Vergata University
E.E Dept. and Centro "Vito Volterra" – Via del Politecnico, Rome, ITALY

PHASE-NOISE SIGNALS DESIGN FOR MODERN RADAR APPLICATIONS

This work presents the main characteristics of the phase noise signals through a statistical characterization, including an analysis of the autocorrelation and cross-correlation properties.

1. Orthogonal Waveform Design

The waveform design and optimization is one of the main focus of the research in multistatic and multifunction radar [1], [7]. For example, in MIMO radar applications typically *M* codes are required in the set, where *M* is the number of transmit elements. The main requirements of a pair of signals with complex envelope $s_i(t)$ and $s_j(t)$ for $i, j = 1, \dots, M$, pulsewidth *T* and same power, are defined by:

- Peak Side Lobe Ratio (desired $< -30\ dB$):

$$PSLR = 20log_{10}\left\{\frac{\max_i(s_i)}{\max_k(m_k)}\right\} \tag{1}$$

where $s_i = sidelobe\ samples, m_k = mainlobe\ samples.$

- Mean Envelope to Peak Power Ratio:

$$MEPPR = \frac{\frac{1}{T}\int_0^T |s(t)|^2 dt}{max(|s(t)|^2)} \tag{2}$$

- Normalized cross-correlation (it measures the orthogonality):

$$r_{ij}(t) = 20log_{10}\left\{\frac{|R_{ij}(t)|}{|R_{i(j)}(0)|}\right\} \tag{3}$$

where $R_{ij}(t) = \int s_i^*(\theta)s_j(t+\theta)d\theta$; desired $r_{ij}(t) < -30\ dB$.

- Spectral band occupancy. Sometimes this item is overlooked, especially when noise-like waveforms are concerned, but it is of paramount importance in most real-world radars.

Othogonality may be easily imposed in the time and frequency domain, but these approaches can suffer from performance degradation and the orthogonality in the signal space is the preferred design option.

A good candidates to design deterministic signals that satisfy the orthogonal requirements are the well-known *"up"* and *"down" chirp* (Linear-FM and Non-LFM) [2], but in this case only one pair of signals can be defined. To obtain *M* pairs of signals the Costas codes represents a possible solution [3]. In addition more recent research on orthogonal signals proposed the use of normal or *interleaved* OFDM techniques [4]. The main limitation of the OFDM approach is due to the non-constant envelope of the signals, i.e. the transmitter does not work to the maximum power. Another class of waveforms, i.e. the Phase Noise signals, has two main advantages as compared to the signals introduced before. The former is the possibility to generate a large number of orthogonal signals, that is of great importance, for example, in MIMO radar systems. The latter is about the detectability, in fact they are random signal so they place limitation on the detection, the identification and the eventual spoofing of the signal, an element of great importance in many military applications which require low detectability of the active system. Finally the *MEPPR* can reach the unity.

For a phase noise signal the complex envelope can be written as:

$$s(t) = A \cdot exp\ \{j[2\pi f_0 t + \varphi(t)]\} \cdot rect_T(t) \tag{4}$$

where A is the constant amplitude, $rect_T(t)$ is a function that is 0 outside the interval $[-T/2, +T/2]$ and 1 inside it (with T the pulse length), f_0 is the carrier frequency and $\varphi(t)$ is the phase process modulating the noise signal $s(t)$.

In the following we present three methods to generate the phase noise signals highlighting strengths and weaknesses.

2. Phase Noise Signals [5]

In [5] Axelsson supposed for $\varphi(t)$ a zero-mean Gaussian process with root mean square (*rms*) σ and a given power with a density spectrum within the band b. He showed that the normalized autocorrelation function of the signal $s(t)$ can be written in a close-form expression as:

$$R(\tau) = exp\{-\sigma^2[1-\rho(\tau)]\} \tag{5}$$

where $\rho(\tau)$ is the correlation coefficient of $\varphi(t)$. For example $\rho(\tau) = \frac{sin(\pi b\tau)}{(\pi b\tau)}$ for a constant spectrum within the band b. The autocorrelation $R(\tau)$ depends on the bandwidth b, on the pulse length *T* and on the *rms* σ. An increase of *T*, and consequently of the compression ratio (the time-bandwidth product), causes a reduction of the range sidelobe level, whereas the mainlobe width remains fixed being independent of *T* and dependent on *b* only. Finally the *rms* σ has two different effects. The former is on the sidelobe level: an increase of σ brings to a decrease of the sidelobe level and so to an improvement of PSLR.

The latter concerns the resolution. The *rms* value in fact establishes a connection between the bandwidth of the modulated signal and the bandwidth of the modulating signal *b*. In detail, when σ increases the final bandwidth increases too. As a consequence a high *rms* value gives an improved resolution (Figure 19).

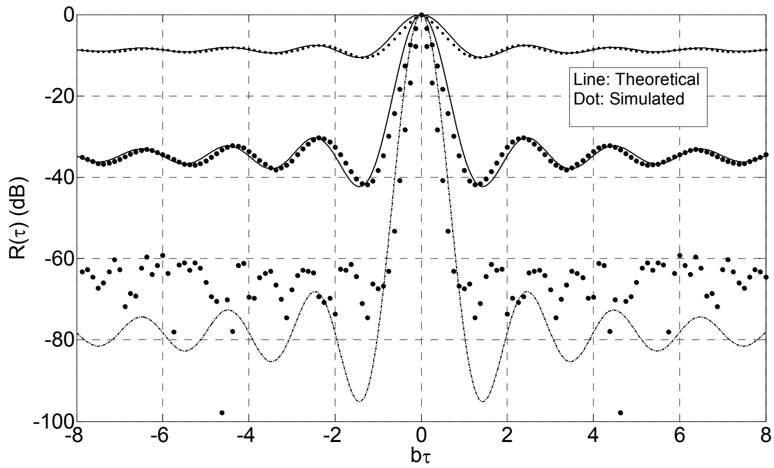

Figure 19 – Normalized autocorrelation for Phase Noise (compression ratio= 1000).

In [5] a simple relation between the *rms bandwidth* of the phase modulated signal (B_{rms}) and the *rms bandwidth* of the phase modulating noise (b_{rms}) has been found:

$$B_{rms} = \sigma \cdot b_{rms} \tag{6}$$

On the other hand, as regard the sidelobe suppression, the expression of the autocorrelation function introduced in [5] would show a progressive improvement of the sidelobe suppression as σ increases. However the periodic nature of $\varphi(t)$ with a folding in the [-π, +π] interval has been neglected in [5], and in reality, the introduced model can be used only for values of σ significantly smaller than π.

The Gaussian noise, used to modulate the signal phase, is usually defined as an uniform distribution in the range [-π, +π] with a standard deviation of $\pi/\sqrt{3} \cong 1.8$ *rad*. Therefore, if σ is too large ($\sigma > \pi/\sqrt{3}$), the resultant phase doesn't have a Gaussian distribution, the mathematical formulation introduced in [5] cannot be used. This is evidentiated, inter alia, in Figure 19 where the difference between Axelsson's theory and experiments (by simulation) is clear for $\sigma = 3$.

On the other hand, in relation with real application, it would be better to generate the signal through a white Gaussian process with its *in phase* and *in quadrature* components (I, Q) that are *band-limited* as desired. This is shown in the ensuing section.

3. An Iterative Algorithm to Generate Phase Noise Signals

To control the spectrum-width and to reduce the PSLR of the generated phase noise signals, we propose an iterative algorithm as shown in Figure 20. It is based on alternative projections in frequency and in time domain. The filtering is implemented in frequency domain while the amplitude limitation (ZMNL = Zero-Memory-Non-Linearity) in time domain. The input to the algorithm is a zero-mean white complex Gaussian process $(I + jQ)$ with power $2\sigma^2$.

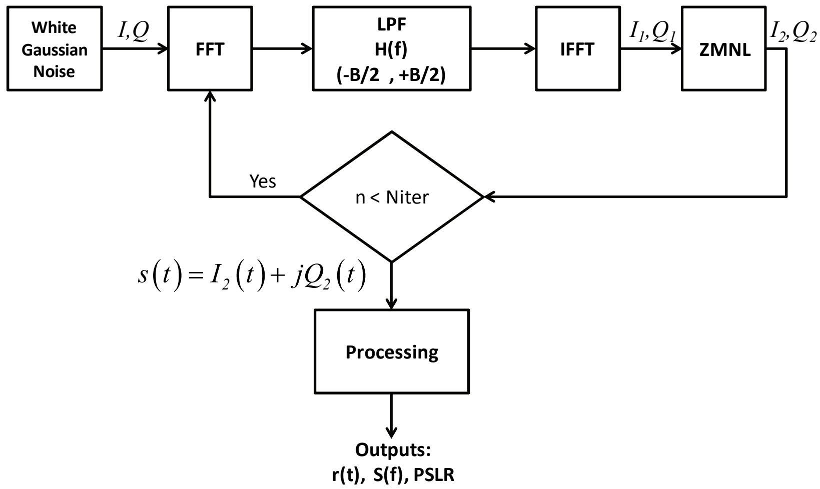

Figure 20 – Block diagram of the iterative algorithm to generate phase noise signals. Legenda: LPF = Low Pass Filter, ZMNL = Zero-Memory-Non-Linearity, Niter = number of iterations.

First we consider for ZMNL a *hard limiter*, i.e.:

$$I_2 = \frac{I_1}{\sqrt{I_1^2+Q_1^2}} \quad , \quad Q_2 = \frac{Q_1}{\sqrt{I_1^2+Q_1^2}} \tag{7}$$

Figure 21 shows the PSLR with respect to the number of iterations considering three different initial sequences for the white Gaussian noise. The PSLR converges after some tens of iterations to -31 dB in the best case. The PSLR varies from –25 dB to –31 dB.

Figure 22 reports an example of density spectrum in comparison with them of Linear and Non-Linear up and down chirp. The spectrum remains strictly band-limited as desired.
With respect to the orthogonality property, in Figure 23 the cross-correlation is compared with a pair of generated phase noise signals. In comparison with the up and down chirp (LFM and NLFM), it results a loss of 8-10 dB.

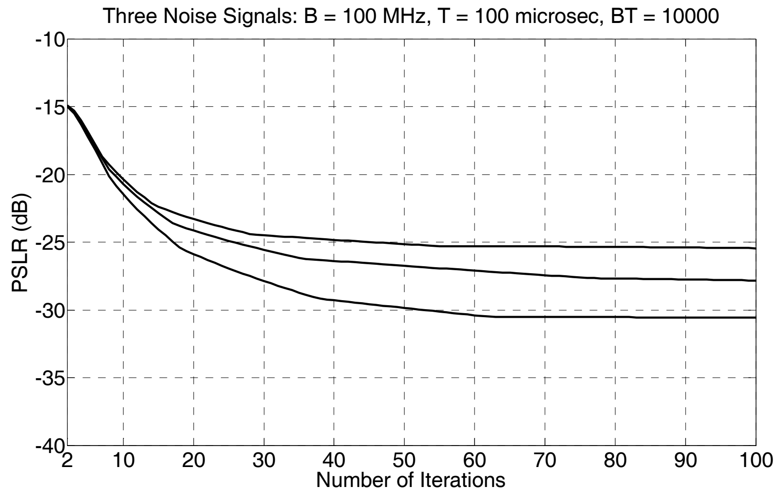

Figure 21 – PSLR versus the number of iterations:. three examples of convergence.

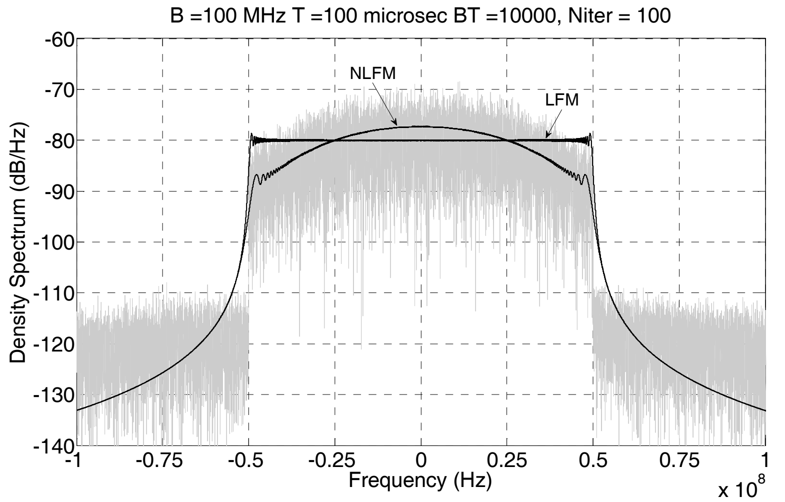

Figure 22 – Density spectrum of a phase noise signal with a band of 100 MHz.

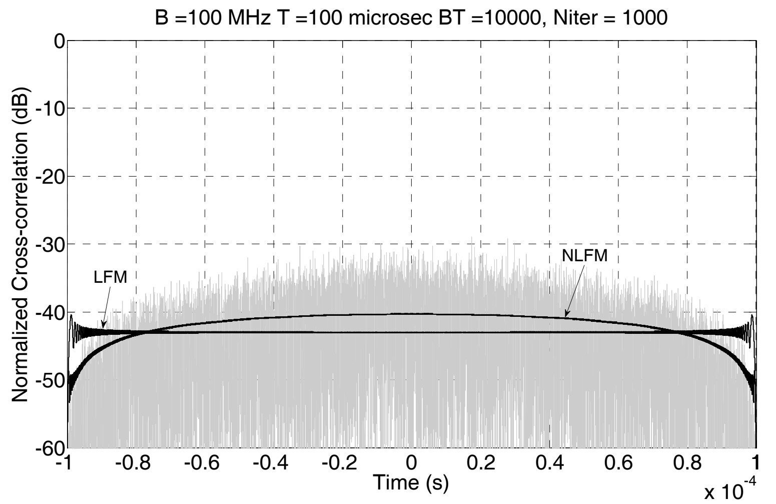

Figure 23 – Normalized cross-correlation of a pair of phase noise signal with a band of 100 MHz and a compression ratio of 10000, and of a pair up and down chirp LFM and NLFM.

Considering now an amplitude *soft limiter* for the ZMNL (see *Figure 24* for the I/O characteristic):

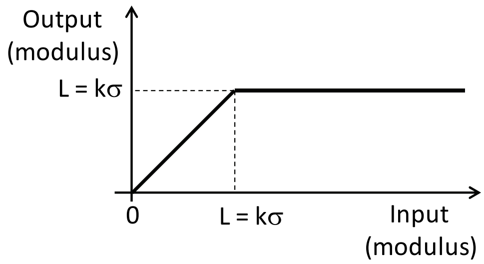

Figure 24 – Soft limiter I/O characteristic.

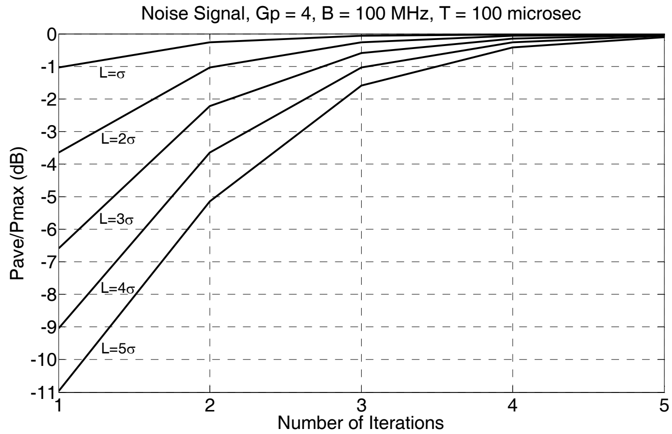

Figure 25 – MEPPR vs the number of iterations.

and indicating with G_p the power gain of the Low Pass Filter of Figure 20, the Mean Envelope to Peak Power Ratio has been evaluated and it depends on the number of iterations m, and on the ratio $k = \frac{L}{\sigma}$ being L the threshold of the soft limiter. It results [8]:

$$MEPPR = \frac{2(G_p)^{m-1}}{k^2}\left[1 - exp\left(-\frac{k^2}{2(G_p)^{m-1}}\right)\right] \; ; \quad m = 1,2,\ldots \tag{8}$$

Figure 7 shows that only four iterations (in the worst case when $L = 5\sigma$ and the effect of the limiter is negligible) are needed to obtain a MEPPR between $-1\ dB$ and $0\ dB$.

By increasing the number of iterations, as shown in the case of *hard limiter*, the PSLR decreases up to $-30\ dB$ circa as shown in Figure 26 for two different values of the threshold L.

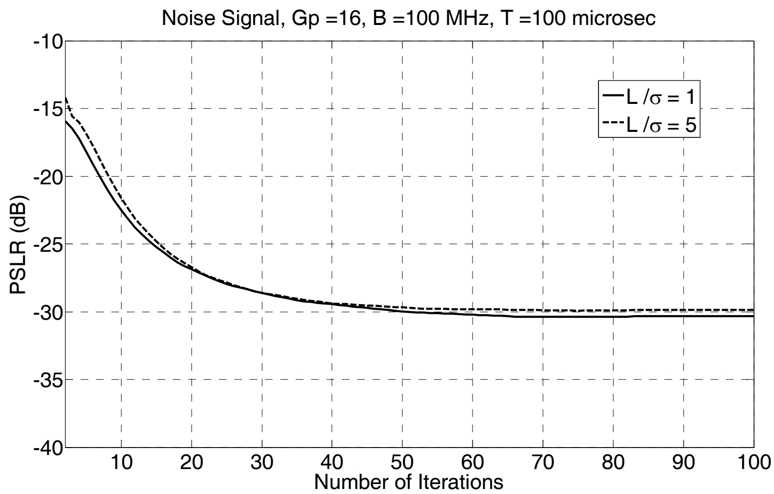

Figure 26 – PSLR versus the number of iterations considering a soft limiter. Two examples of convergence for $L = \sigma$ and $L = 5\sigma$.

4. Closed-form Algorithm to Generate Phase Noise Signals

This mathematical approach is based on the following considerations. For a real Gaussian process Van Vleck and Middleton [6] showed that the autocorrelation (R_t with $t = t_2 - t_1$) of the output from a *hard limiter* is related with the input autocorrelation (r) by the well known *arcsin-law*:

$$R_t = \frac{2}{\pi} arcsin(r) \tag{9}$$

Considering a complex Gaussian process, the correlation R_t after the hard limiter will be between $\frac{z_1^*}{|z_1|} = \frac{x_1 - jy_1}{\sqrt{x_1^2+y_1^2}}$ and $\frac{z_2}{|z_2|} = \frac{x_2+jy_2}{\sqrt{x_2^2+y_2^2}}$:

$$R_t = E\left\{\frac{z_1^* z_2}{|z_1||z_2|}\right\} = E\left\{\frac{x_1x_2+y_1y_2+j(x_1y_2-x_2y_1)}{\sqrt{x_1^2+y_1^2}\sqrt{x_2^2+y_2^2}}\right\} = u + jv \tag{10}$$

where E{·} is the statistical mean operator. Supposing a symmetrical power density spectrum with respect to the origin, the correlation is real and $v = 0$. Equation (10) has been evaluated in [8] , and it results:

$$R_t = b_0 r + \sum_{n=1}^{\infty} b_n \cdot r^{2n+1} \tag{11}$$

being $b_0 = \frac{\pi}{4}$ and for $n \geq 1$, $b_n = c_n - c_{n-1}$, where the expression of c_n is given in [8]. Figure 27 shows R_t versus the input correlation r for real and complex Gaussian process.

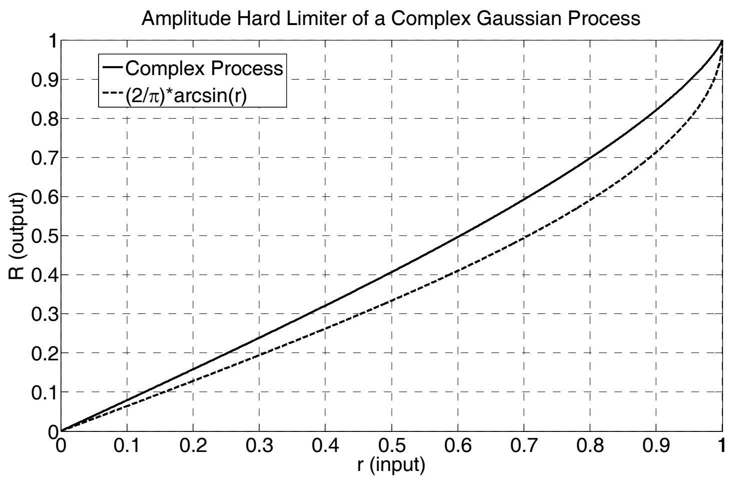

Figure 27 – Output autocorrelation from a hard limiter versus the input autocorrelation.

Inverting eq. (11) it is possible to pre-distort the input autocorrelation to the hard limiter to obtain a desired R_t.

In a such way the requirements listed at the beginning of section I can be met with no need for iterations. In fact, (a) the output autocorrelation is chosen in order to satisfy the PSLR requirement and the spectral band requirement, (b) the MEPPR requirement is satisfied by a suitable choice of the parameter k (ref. Figure 6) of the limiter (the hard limiter being the situation $k \to 0$) and (c) the orthogonality is obtained by the randomness of the white Gaussian input sequence, and may be enhanced by proper choices of the generated output sequences.

5. Conclusions

Multistatic and multifunction radar call for the design of sets of orthogonal waveforms with large enough Peak-to-Side-Lobe-Ratio of the autocorrelation function, fairly good mean power to peak power ratio and assigned spectral occupancy. Having shown that there are conceptual drawbacks in the Axelsson's method [5], we have started investigations on two new methods, i.e. a recursive and non-recursive one. Preliminar results have been presented.

References

[1] G. Galati, G. Pavan, *"Orthogonal and Complementary Radar Signals for Multichannel Applications"*, Proc. EuRad 2011. Manchester (UK), 12-14 October 2011, pp. 178-181, 2011.

[2] G. Galati, G. Pavan, *"Waveform Radar Design using Orthogonal and Complementary Codes"*, Prace PIT vol. 145, 2010, pp. 28-44.

http://www.pit.edu.pl/biblioteka/publikacje-instytutu/sekcja/prace-pit.

[3] N. Levanon, E. Mozeson, *"Radar Signals"*, IEEE Press, Wiley-Interscience, Jhon Wiley & Sons, 2004.

[4] O. A. Krasnov, Z. Wang, R.F. Tigrek, P. van Genderen, *"OFDM waveforms for a fully polarimetric weather radar"*, Proc. of ESAV'11, Capri 12-14 september 2011, pp. 69-75. ISBN 978890348235.

[5] R. J. Axelsson, *"Noise Radar Using Random Phase and Frequency Modulation"*, IEEE Transactions on Geoscience and Remote Sensing, vol. 42, n. 11, November 2004, pp. 2370-2384.

[6] J. H. Van Vleck, D. Middleton *"The Spectrum of Clipped Noise"* Proceeding of the IEEE, vol. 54 n. 1, January 1966, pp. 2-19.

[7] Lei Xu, Qilian Liang *"Zero Correlation Zone Sequence Pair Sets for MIMO Radar"* IEEE Trans. on AEROSPACE AND ELECTRONIC SYSTEMS Vol. 48, N. 3 July 2012.

[8] G. Galati, G. Pavan *"Signal processing and waveforms design for Low-Probability-of-Intercept (LPI) noise radar" Submitted paper*.

UDC 621.3:681.34

V.V. Abramova, PhD Student, S.K. Abramov, Candidate of Technical Science, V.V. Lukin, Doctor of Technical Science (National Aerospace University, Ukraine)
B. Vozel, PhD, K. Chehdi, Professor (University of Rennes I, France)

SCATTER-PLOT BASED BLIND ESTIMATION OF MIXED NOISE PARAMETERS FOR REMOTE SENSING IMAGE PROCESSING

Mixed noise parameters are often to be estimated blindly for images acquired by multichannel remote sensing sensors. Two approaches to carry out such an automatic estimation in spatial and spectral domains are considered for spatially uncorrelated noise. They are analyzed for a set of test images. It is demonstrated that the latter approach based on robust curve fitting into scatter-plot provides more accurate estimation.

A tendency in modern remote sensing (RS) is to apply multichannel systems (sensors) placed on-board of airborne and spaceborne carriers [1]. Examples of such RS systems are multi- and hyperspectral sensors, dual and multi-polarization radars. Although modern RS systems have more perfect apparatus, acquired images are in more or less degree noisy. The presence of noise affects final results of RS data interpretation. Thus, noise type and characteristics are to be taken into account at practically all stages of multichannel RS data processing including compression, filtering, and classification or object detection.

A problem is that noise type and/or characteristics can be unknown or partly known in advance. They can vary from one imaging session to another and be considerably different for channels (components, sub-bands) of multichannel images [2]. This makes necessary estimation of noise characteristics (and, sometimes, type) for RS data at hand.

If the number of channels is large and/or if processing is to be carried out on-board, it is impossible to perform such estimation in interactive manner. Thus, blind (automatic) estimation is required and it should be fast and accurate enough [2, 3]. There are quite many blind estimation methods able to perform well enough for the case of pure additive noise (see [4] and references therein). There are also rather efficient methods for estimating variance (or efficient number of looks) for pure multiplicative noise [5]. However, recent thorough studies of noise characteristics in images formed by modern sensors clearly show that noise is signal dependent (not pure additive or multiplicative) [1, 6, 7]. Then, one has to estimate dependence of local variance on local mean or parameters of a model that describes this dependence under assumption that this noise model is valid for analyzed images.

Most of existing methods for the latter case (i.e., known and/or accepted noise model) exploit scatter-plots of local variance estimates (depending upon local mean) obtained in scanning windows or blocks that tessellate an entire image or its parts (detected quasi-homogeneous fragments) [5-9]. To understand the essence of these methods, it is worth stressing that local estimates of noise variance can be normal (i.e., close to a true value for a given block) and abnormal (i.e., differing considerably from a true value). The first type of estimates is basically obtained in image blocks located in homogeneous regions whilst the second type of local estimates relate to blocks positioned on heterogeneities as edges, textures, small-sized details and their neighborhoods.

Then, different operations and image/noise properties are exploited to separate normal and abnormal local estimates or to minimize the negative influence of the latter ones on final estimates of signal-dependent noise parameters. In particular, curve robust fitting into scatter-plots is used to diminish the influence of abnormal local estimates [5-8]. Another approach is to somehow determine (detect) quasi-homogeneous blocks and to form a scatter-plot using only the local estimates for these blocks [8, 9]. Combined approaches are also possible [8]. Probably, the most accurate estimation is provided by the method [9] that is based on fractal Brownian model and Fisher information analysis. This allows finding scanning window positions that provide accurate information on noise statistics. However, this technique is not fast enough.

Another approach is proposed and studied in [3, 8]. Abnormal local estimates are partly removed due to image pre-segmentation and quasi-homogeneous regions' determination. Then, robust curve fitting into the obtained scatter-plot or determined cluster centers is carried out to reduce the influence of remainder abnormal local estimates. Double weighted fitting is recommended to improve performance. This method is fast since all the operations including pre-segmentation, discrimination map forming, local estimate obtaining, cluster center determination, and robust fitting itself are easy and fast.

However, accuracy of this approach is worth improving. The main reason of biased estimation of signal dependent noise parameters is a limited accuracy and biasedness of initial local estimates considered normal. These local estimates are obtained in spatial domain and they are essentially affected by image content (image heterogeneity in blocks). This effect appears itself most pronouncedly for highly textural images and/or if noise is not intensive.

An idea of current research is that local estimates in spatial domain can be replaced within the scatter-plot based approach by local estimates in spectral domain. Recall that blind estimation in spectral domain has been demonstrated to be less sensitive to image heterogeneity (texture) for the case of pure additive noise [3, 10] under assumption that noise is spatially uncorrelated. Note that the method [10] has not been extended to signal dependent noise case yet. Moreover, it has been shown recently that Gaussianity tests can serve for selecting orthogonal transform (for example, discrete cosine transform – DCT) coefficients that are affected by image content in the least degree [11, 12]. Then, their statistics is in the first order determined by noise statistics. This allows estimating noise variance by processing proper DCT coefficients. The goal of this paper is to check this idea and to study the performance of the corresponding estimators.

Without losing generality, let us assume that signal-dependent noise variance fits the model $\sigma^2_{loc} = \sigma^2_a + k\bar{I}_{loc}$ where σ^2_a denotes variance of signal-independent component and k is a parameter of signal dependent (quasi-Poissonian) component. This model fits noise statistics for new generation of hyperspectral sensors [6, 9] where the signal-dependent component is prevailing.

Component images of multichannel RS data are processed separately (this can be done in parallel). The main steps of processing are the following:

1) Carry out pre-segmentation of a given image; the method [13] that does not require a priori information on noise type and statistics can be applied for this purpose; its outcome is a pre-segmented images that usually has from five to fifteen levels;

2) Obtain a discrimination map for the segmented image; a way to do this is described in [14]; this map discriminates blocks that can be considered quasi-homogeneous from other ones that relate to edges and textures with high probability;

3) Obtain local estimates for the detected quasi-homogeneous blocks of each level, form a scatter-plot and determine cluster-centers characterized by coordinate $(\hat{\sigma}^2_{cl\,m};\hat{I}_{cl\,m})$ for each m-th level, $m = 1,...,N_{cl}$, where $\hat{\sigma}^2_{cl\,m}$ and $\hat{I}_{cl\,m}$ are estimates of variance and mean for the m-th cluster, N_{cl} is the number of clusters;

4) Carry out robust fitting the line $Y = a + bX$ into a set of cluster centers and accept the determined parameters a and b as the estimates of $\hat{\sigma}^2_a$ and $\hat{k}$ for the considered model, respectively; double weighted fitting [8] has been used for this purpose; moreover, a restriction on non-negativity of both estimates has been imposed.

The difference between the earlier method [8] and the proposed approach is at stage 3. For the novel approach, the operations are the following. Suppose that one has N_q quasi-homogeneous blocks of size 8x8 pixels for an l-th level of the pre-segmented image discrimination map. Then:

1) For each q-th block ($q = 1,...,N_q$), apply 2D DCT with getting a set of DCT coefficients $D_q(r,s), r = 0,...,7, s = 0,...,7$ where $D_q(0,0)$ defines mean for a q-th block and is not used in further analysis.

2) For each pair of r and s, form a set $\{D_q(r,s)\}, q=1,...,N_q$ and calculate the estimate $\sigma^2_{rs}=(1.483\text{med}\left|D_q(r,s)\right|, q=1,...,N_q)^2$ for this pair of r and s; find the minimal estimate σ^2_{min} among all pairs of r and s;

3) Analyze Gaussianity of $\{D_q(r,s)\}, q=1,...,N_q$ for each pair of r and s; if the Gaussianity test is passed, remain the estimate $\hat{\sigma}^2_{rs}=(1.483\text{med}\left|D_q(r,s)\right|, q=1,...,N_q)^2$ for further analysis;

4) Jointly process the remained estimates $\hat{\sigma}^2_{rs}$ (this can be done by their averaging or median finding, the latter variant has been used) and, in this manner, get the estimate $\hat{\sigma}^2_m$; if there are no remained estimates, then $\hat{\sigma}^2_m=\sigma^2_{min}$;

5) The estimate $\hat{I}_{cl\,m}$ is obtained as mean of the corresponding cluster elements after pre-segmentation.

Let us give an example of the cluster centers for the test image Airfield corrupted by mixed noise with $\sigma^2_a=30$ and $k=1$. Fig 1 presents the scatter-plot of local estimates obtained in spatial domain for all possible blocks positions and the true curve $Y=\sigma^2_a+kX$. It is seen that there are many local estimates that are placed far from this curve, i.e. these local estimates are abnormal. The cluster centers for the method [8] are marked by red squares and the cluster centers for the proposed method based on DCT coefficient analysis are marked by green triangles. It is seen that cluster centers for the latter approach are placed, on the average, more close to the true line. This allows expecting more accurate estimation of the parameters σ^2_a and k.

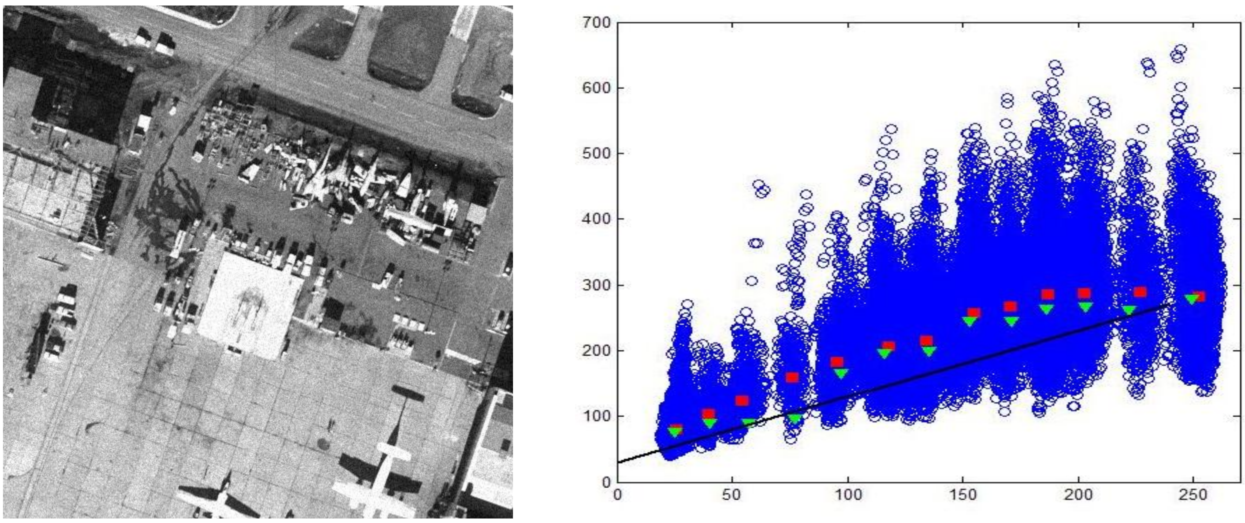

a b

Fig. 1. Test image Airfield corrupted by mixed (signal dependent) noise with $\sigma^2_a=30$ and $k=1$ (a) and its local variance scatter-plot with marked cluster centers (b)

There are different ways to characterize performance of blind methods for mixed noise parameter estimation. One of them has been used in [8]. For each test image and used set of σ^2_a and k, a large number of noise realization have been simulated. The estimates $\hat{\sigma}^2_a$ and $\hat{k}$ have been obtained and processed with getting estimation bias $\delta_{var\,add}$ and δ_k, estimation variances σ^2_{var} and demonstrated that in most situations $\delta^2_{\text{var add}} >> \sigma^2_{\text{var}}$ and $\delta^2_k >> \sigma^2_k$. Thus, it is possible to pay main attention to considering estimation bias for only one realization of the mixed noise.

Since blind methods should perform well for any image under processing irrespectively to its properties (complexity), it is worth analyzing many (tens) of different test images. Such opportunity is provided by the database TID2008 [15] that contains noise-free color images to which simulated noise with desired statistical characteristics can be artificially added. Thus, the mixed noise with $\sigma^2_a = 30$ and $k = 1$ has been simulated to model hyperspectral images. The estimates $\hat{\sigma}^2_a$ and $\hat{k}$ have been obtained by separate processing of each color component of each color image in the database (totally 25 color images). The obtained estimates $\hat{\sigma}^2_a$ are shown in Fig. 2,a-c (the corresponding color for R, G, and B components), solid black lines with round markers are used for the method [8], dashed lines with square markers for the proposed method. Horizontal axis index corresponds to the test image index in TID2008. The estimates $\hat{k}$ are shown in the similar manner in Fig. 2,d-f. Horizontal lines show the true values of the corresponding parameters of the mixed noise.

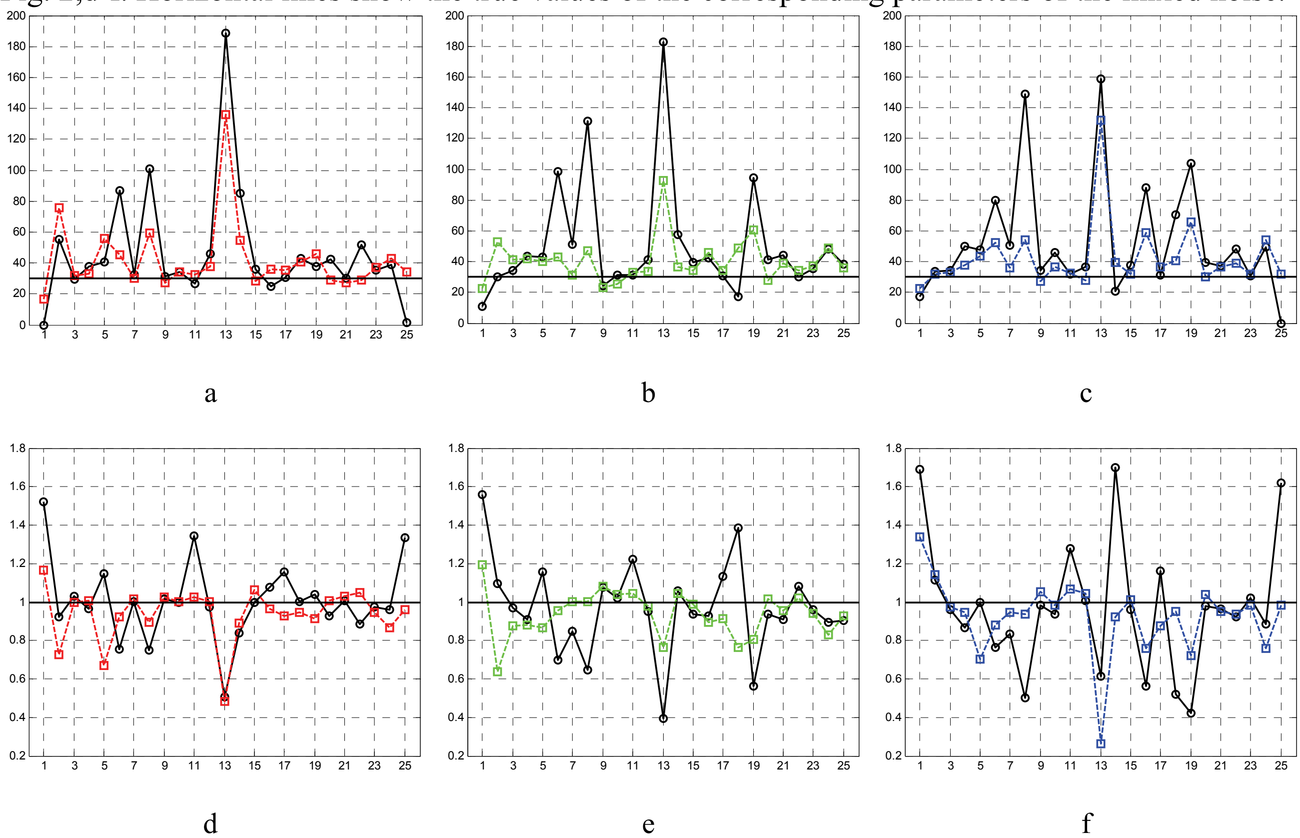

Fig. 2. Estimates of $\hat{\sigma}^2_a$ (a - c) and $\hat{k}$ (d - f) for the proposed method and method [8] obtained for test images from TID2008 database

Before starting analyzing the obtained data, it is worth mentioning that the images ## 1, 5, 13, 14, and 18 are the most textural in the database TID2008.

Analysis shows the following. First, for the method [8], there are several cases when the estimates $\hat{\sigma}^2_a$ are equal to zero, i.e. imposed limitations act. This happens twice for the red component (Fig. 2,a) and once for the blue component (Fig. 2,c).

There are also considerably biased estimates for several images where the largest is the error for the test images # 8 and 13. Although the estimates $\hat{\sigma}^2_a$ for the proposed method are considerably biased for these images as well, the estimation errors are smaller. For other test images which are less complex (textural), both methods produce the estimates of comparable accuracy.

The estimates $\hat{k}$ also have several “outliers” and they mostly happen for the most textural test images. Meanwhile, the estimates $\hat{k}$ for the proposed method are, on the average, more accurate than for the method [8].

One more interesting tendency can be observed. If an estimate $\hat{\sigma}_a^2$ is larger than the true value, then the corresponding estimate $\hat{k}$ is, most probably, less than the true value of k. This shows that the estimates $\hat{\sigma}_a^2$ and $\hat{k}$ are mutually dependent where correlation coefficient for them is less than unity. More detailed analysis is worth performing in future.

Therefore, the proposed method allows obtaining more accurate estimation of cluster centers. In turn, this leads to higher accuracy of estimating the mixed noise parameters especially for highly textural images. One drawback of blind estimation methods operating in spectral domain is that they produce considerably biased local estimates if noise is spatially correlated. Thus, our future research will be focused on finding ways to avoid this drawback.

References

1. *A. Barducci, D. Guzzi, P. Marcoionni,* and *I. Pippi*, "CHRIS-Proba performance evaluation: signal-to-noise ratio, instrument efficiency and data quality from acquisitions over San Rossore (Italy) test site", *Proc. 3-rd ESA CHRIS/Proba Workshop*, Italy, 2005.
2. *P.J. Curran* and *J.L. Dungan*, "Estimation of signal-to-noise; a new procedure applied to AVIRIS data", *IEEE Transactions on Geoscience and Remote Sensing*, 1989, Vol. 27, pp. 620-628.
3. *S. Abramov, V. Zabrodina, V. Lukin, B. Vozel, K. Chehdi*, and *J. Astola*, "Methods for Blind Estimation of the Variance of Mixed Noise and Their Performance Analysis", In: *Numerical Analysis – Theory and Application*, Ed. Jan Awrejcewicz, InTech, 2011. ISBN: 978-953-307-389-7.
4. *B. Vozel, S. Abramov, K. Chehdi, V. Lukin, N. Ponomarenko, M. Uss,* and *J. Astola*, Blind methods for noise evaluation in multi-component images, In: *Multivariate Image Processing,* pp. 263-295, 2009, France.
5. *G. Ramponi* and *R. D'Alvise*, "Automatic Estimation of the Noise Variance in SAR Images for Use in Speckle Filtering", *Proc. of EEE-EURASIP Workshop on Nonlinear Signal and Image Processing*, Antalya, Turkey, Vol. 2, pp. 835-838, 1999.
6. *B. Aiazzi, L. Alparone, A. Barducci, S. Baronti, P. Marcoinni, I. Pippi,* and *M. Selva*, "Noise modelling and estimation of hyperspectral data from airborne imaging spectrometers", *Annals of Geophysics*, Vol. 49, No. 1, February 2006.
7. *C. Liu, R. Szeliski, S.B. Kang, C.L. Zitnick,* and *W.T. Freeman*, "Automatic estimation and removal of noise from a single image", *IEEE Transactions on Pattern Analysis and Machine Intelligence*, Vol. 30, No 2, pp. 299-314.
8. *V. Zabrodina, S. Abramov, V. Lukin, J. Astola, B Vozel,* and *K. Chehdi*, "Blind Estimation of mixed noise parameters in images using robust regression curve fitting", *Proceedings* of the *19th EUSIPCO Conference*, Barselona, Spain, 2011, pp.1135 - 1139. ISSN 2076-1465.
9. *M. Uss, B. Vozel, V. Lukin,* and *K. Chehdi*, "Local Signal-Dependent Noise Variance Estimation from Hyperspectral Textural Images" *IEEE Journal of Selected Topics in Signal Processing,* Vol. 5, No. 2, 2011, DOI: 10.1109/JSTSP.2010.2104312.
10. *N.N. Ponomarenko, V.V. Lukin, S.K. Abramov, K.O. Egiazarian,* and *J. Astola*, "Blind evaluation of additive noise variance in textured images by nonlinear processing of block DCT coefficients," *Image Processing: Algorithms and Systems II: Proc. of Internat. Conf.,* SPIE Vol. 5014, pp. 178-189, 2003.
11. *A. Roenko, D. Kurkin, V. Lukin,* and *I. Djurovic*, "New Estimators for Tail Heaviness Parameter of Generalized Gaussian Distribution", *Proceedings of MECO*, Bar, Montenegro, June 19-21, 2012, 4 p.
12. *D. Zoran* and *Y. Weiss*, "Scale Invariance and Noise in Natural Images", *ICCV*, pp. 2209-2216, 2009.
13. *L. Klaine, B. Vozel,* and *K. Chehdi*, "Unsupervised Variational Classification Through Image Multi-Thresholding", *Proceedings of the 13th EUSIPCO Conference*, Antalya, Turkey, 2005.
14. *V. Lukin, S. Abramov, B. Vozel, K. Chehdi,* and *J. Astola*, "Segmentation-based method for blind evaluation of noise variance in images," *SPIE Journal on Applied Remote Sensing*, Vol. 2, Aug. 2008, open access paper.
15. Tampere Image Database 2008 TID2008, v. 1.0, Available from: http://ponomarenko.info/tid2008.htm

UDC 621.3:681.34

A.V. Naumenko, Student, V.V. Lukin, Doctor of Technical Science
(National Aerospace University, Ukraine)
K. Egiazarian, Professor (Tampere University of Technology, Finland)

NEURAL NETWORK BASED EDGE DETECTION IN PREFILTERED SAR IMAGES

A task of edge detection in one-look SAR images is considered. It is proposed to apply the local statistic Lee filter first and then to use a neural network (NN) trained beforehand for test images. Three local parameters defined in 5x5 scanning windows are exploited as NN inputs. ROC curves are presented demonstrating advantages of the proposed approach. Real-life image examples illustrating the obtained results are presented.

SAR imaging from airborne and spaceborne platforms has gained popularity due to its ability to provide remote sensing (RS) data in all-weather conditions during day and night [1]. Another advantage of SAR systems is high spatial resolution reaching 2m x 2m and even better. Such limit resolution is reached if an SAR operates in one-look mode. However, in this case, acquired images are corrupted by fully developed speckle that considerably deteriorates their quality and makes problematic solving further tasks of image processing and interpreting.

Edge detection is a basic operation in SAR image processing applied directly or indirectly for image filtering and segmentation. Reliable detection of edges and other heterogeneities [1-4] is not an easy task (especially if edge contrasts are low) due to several factors. The first factor is intensive multiplicative noise present in SAR images. The second factor is non-Gaussianity of speckle probability density function (PDF). The third factor is spatial correlation of speckle often present in real-life data [1, 4]. Recall that most edge and heterogeneity detectors are designed under assumption of pure additive, Gaussian and spatially uncorrelated noise [5, 6].

A considerably smaller number of edge detectors can be applied for the considered case of real-life speckle. One way is to apply variance stabilizing transform (of logarithmic type) to convert an image corrupted by pure multiplicative noise to the corresponding image corrupted by additive noise [9]. However, although noise becomes additive, it is not Gaussian [1] and still spatially correlated. Another way is to modify edge detectors to account for multiplicative nature of speckle. This can be done by normalizing local statistics by local mean, squared local mean or some other parameters [4, 7]. Meanwhile, for all modified edge detectors, there are certain advantages and drawbacks. The main problem is in detection of edges and small details with low contrast.

One possible solution is to apply few elementary edge detectors (EEDs) and to aggregate their outcomes by preliminarily learnt neural network [8]. The NN-based detector [8] has demonstrated itself to provide improved detection of low contrast edges and fine details under condition that used elementary detectors are efficient enough. Three EEDs selected after several trials [8] are relative variance [3, 5], Harris edge detector [9], and an edge detector based on comparison of discrete cosine transform (DCT) coefficient amplitudes to certain thresholds. All elementary detectors operate in 5x5 scanning windows (SW).

In spite of the provided benefits, better detection is still desirable. Our idea is that further improved performance of a NN-based detector can be achieved if an SAR image is pre-filtered properly. Thus, this paper deals with studying this opportunity.

Image model and training set forming

For performance analysis of different edge detectors and training set forming, we have created several test images with different edge contrasts where speckle is modeled as Rayleigh-distributed i.i.d. random values. Speckle is modeled as pure multiplicative noise with $\langle \mu_{ij} \rangle = 1$ (i and j denote pixel indices) and speckle variance $\sigma_\mu^2 = 0.273$ that corresponds to one-look amplitude SAR data.

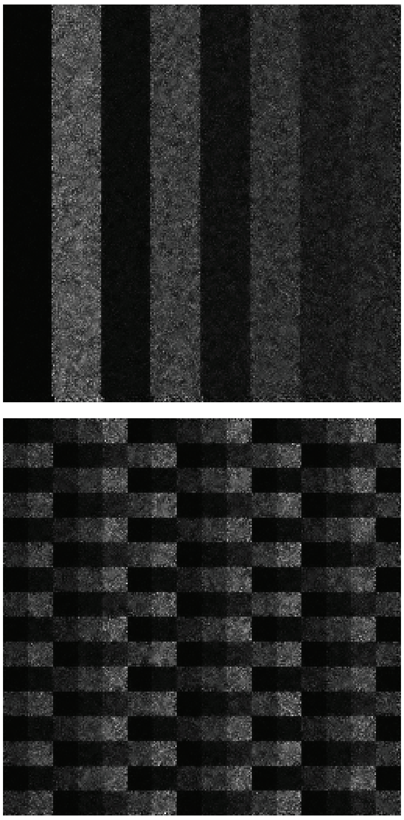
Fig.1 Test images

Most existing edge detectors possess high computational efficiency. Thus, for an NN detector to be designed it is desirable to provide high computational efficiency as well. This could be achieved if the following requirements are satisfied:

- pre-filtering is fast;
- elementary edge detectors are simple enough and are able to operate in parallel;
- pre-filtering process and edge detection can be carried out in a pipeline manner;
- a NN has a simple structure and it is able to work fast after training.

Among filters that meet the above requirements, mean and median filters could be recalled. Both of them are capable to suppress multiplicative noise. However, these methods have a significant drawback: edges and fine details of a processed image are smoothed (for the mean filter) or even removed (for the median filter) after such pre-processing. This means that useful information of the image can be lost and it is undesirable in edge detection task.

Thus, another filtering method which should preserve edges and, at the same time, perform efficient noise suppression is needed. For this purpose, one can apply some locally adaptive algorithm. In particular, this can be local statistic Lee or Frost filters [1]. We prefer to exploit the former one because it is faster. This filtering algorithm uses the relative local variance (RLV) as a local activity parameter. RLV is quite sensitive to low-contrast edges.

Efficiency analysis of several EEDs applied to original images has been carried out in [8]. However, image pre-filtering alters noise properties. Therefore, additional analysis of EED properties should be performed for this case. All EED outputs are calculated in 5x5 SW. For experiments, we have chosen the following four EEDs [8]:

RLV: $\delta_{ij} = \sigma_{ij}^2 / (\sigma_\mu^2 \bar{I}_{ij}^2)$ where σ_{ij}^2 is the local variance in a given SW; $\bar{I}_{ij}$ is the local mean;

Quasirange (QR) [2]: $QR_{ij} = \left(I_{ij}^{(q)} - I_{ij}^{(p)} \right) / \left(I_{ij}^{(q)} + I_{ij}^{(p)} \right),\ q = 20, p = 6$ where $I_{ij}^{(q)}$ and $I_{ij}^{(p)}$ are q-th and p-th order statistics, respectively;

Ratio-based Harris edge detector [9]: the ratios of the means in four directions in 5x5 SW are calculated; these values are used for calculation of the final output: $R_{ij} = \min(R_1, R_2)$, where $R_1 = \mathrm{Det}(M_1) - k \cdot \mathrm{Tr}^2(M_1)$, $R_2 = \mathrm{Det}(M_2) - k \cdot \mathrm{Tr}^2(M_2)$, k is empirical constant (k=0.04 in our experiments); M_1 and M_2 are calculated as: $M_1 = \begin{bmatrix} I_h^2 & I_h I_v \\ I_h I_v & I_v^2 \end{bmatrix}, M_2 = \begin{bmatrix} I_{md}^2 & I_{md} I_{ad} \\ I_{md} I_{ad} & I_{ad}^2 \end{bmatrix}$, where I_h, I_v, I_{md}, I_{ad} are the ratios of means in different SW parts (left and right, top and bottom, under the main diagonal and upper the main diagonal, under the side diagonal and upper the side diagonal, respectively);

DCT-based edge detector: edge detection principle consists in the following - DCT-spectrum in a given SW is calculated; if the window is located on an edge, there is a larger number of DCT-coefficients that exceed a certain threshold than mean number of such DCT coefficients for SWs in homogeneous regions; in our experiments, the threshold for this type of noise is set as $0.8\bar{I}_{ij} \approx 1.6\bar{I}_{ij}\sigma_\mu$.

As a basic criteria of any edge detector efficiency, the dependence of correct detection probability P_{cd} on false alarm rate P_{fa} [1] (the so-called ROC) is used. For ROC curve obtaining, the number of correct outputs in edge neighborhoods with all possible contrasts of a test image used (just for one pixel left and right from the edge in our case) is to be calculated first. This number is then normalized by the total number of edge neighborhood pixels. The estimation of false alarm rate P_{fa} is carried out in homogeneous regions of the test image by calculating the total number of alarms and dividing it by the total number of pixels in these regions. For the EEDs described above, these dependences are presented in Fig. 2. Their analysis shows that all parameters have approximately the same efficiency for the considered type of noise.

In addition, edge detector efficiency can be characterized by dependences of correct detection probability on contrast. P_{cd} is calculated the same way as described above. The contrast value is obtained for clear test images as ratio of intensity value from one side of the edge to intensity from another. Contrast is always positive which means that a larger intensity is divided by smaller. For the same detectors, these curves are shown in Fig. 3.

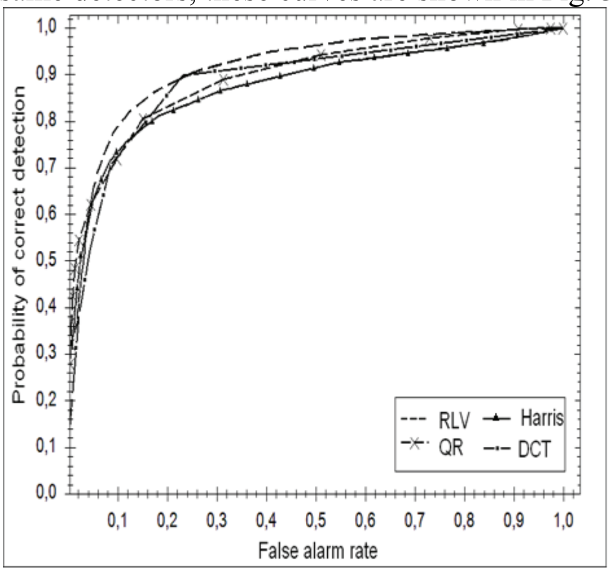

Fig. 2 The ROC curves for described detectors

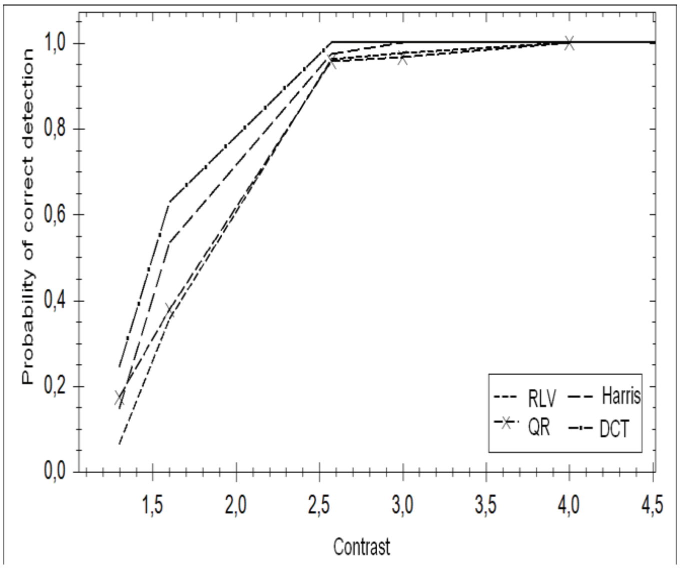

Fig.3 The probability of correct detection on contrast dependences

The presented dependences show that for all detectors the contrast about 4.5..5 is enough for reliable edge detection (with $P_{cd} \rightarrow 1$). The exception is the DCT-based EED that needs the smaller contrast (about 2.5..3) to produce the same results.

All the considered parameters have better results for filtered images than being applied to original data. Thus, it can be expected that their output joint processing by a trained NN will be able to produce better results than the similar edge detector [8] designed for non-filtered images.

Neural network features

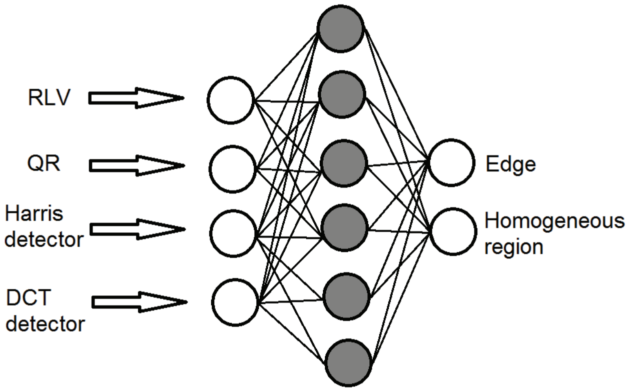

Fig. 4 The NN structure

For our experiments, a feed-forward NN similar to that one used in [8] has been designed. There is also description of structure features and training procedure in [8]. Here, we just notice specific features of this NN.

The NN is designed to recognize two classes: “edge” and “homogeneous region” and consists of 3 layers. There are 4 neurons in the input layer that correspond to input local parameters’ number, 5 neurons in the hidden layer (defined by empirical rules), and 2 neurons in the output layer (appropriate to defining classes). The NN structure is presented in Fig. 4.

We have used supervised learning for test images to train the NN (specifically the back propagation algorithm). The training set is formed of vectors of four EED outputs for 5x5 fragments of the test images. Also, it should be noticed that input parameters are based on different image features: the RLV and QR use spatial statistics, the Harris edge detector employs geometrical features and the DCT-based detector takes into account spectral statistics. This makes our NN detector able to combine all of these features and also to be invariant to the edge direction.

Obtained results

The obtained edge maps for neural detector are presented in Fig. 5. It is seen that low-contrast edges are more distinguishable than for the edge maps for the NN detector designed without pre-filtering. The practically significant values of false alarm rate and the corresponding values of probability of correct detection are shown in Table 1. The results for the neural detector without preliminary filtering are presented as well. The ROC curves are given in Fig. 6. Their analysis shows that with preliminary filtering a significant increase of probability of correct detection is provided (about 0.2…0.4 for the most important false alarm rate values of 0.1…0.2). The curve for the proposed method is now higher than the other ones, especially in regions that correspond to the contrasts of 1.2..2.5 which are the most important for solving practical problems.

The edge detectors work results *Table 1*

	P_c for different edge detectors					
P_f	RLV	QR	Harris detector	DCT-based detector	Neural detector (with pre-filtering)	Neural detector (without prefiltering)
0.1	0.79	0.72	0.73	0.71	0.87	0.49
0.2	0.87	0.83	0.82	0.85	0.93	0.73
0.4	0.94	0.91	0.89	0.91	0.97	0.88

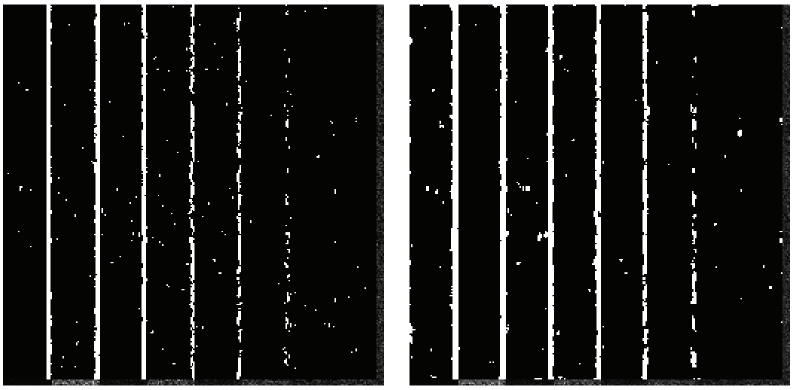

a b

Fig. 5 Edge maps for neural detector without (a) and with (b) preliminary filtration also it better detects low-contrast edges.

The efficiency of our approach can also be proved visually. In Fig. 7, there are edge maps for real SAR-images after filtering for the proposed method and for the RLV for comparison. The speckle in these images has spatial correlation and the NN has been trained for images without it. Therefore, we have carried out preliminary decimation by two times for both coordinates. The obtained results demonstrate that the NN detector can localize edges and fine details with better accuracy and

Conclusions

The modified method of joint analysis of several local parameters using neural network is proposed. It is shown that preliminary filtering of images corrupted by intensive noise could improve the detection performance not only for all considered local parameters but, substantially, for the neural network edge detector. The most important achievement is that detection of low-contrast edges and fine details is significantly improved. This allows expecting better edge/detail preservation at further stages of image processing (filtering, pattern recognition).

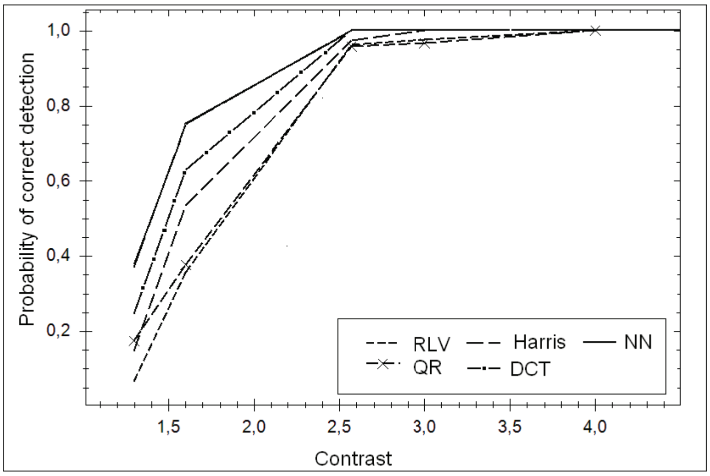

Fig. 6 The ROC curves

a b c

Fig. 7 A real SAR-image (a), RLV edge map(b), edge map for proposed neural detector (c)

References

1.*C. Oliver, S. Quegan.* Understanding Synthetic Aperture Radar Images – SciTech Publishing, 2004. – 486 p.

2.*A.C.Bovik*,1988. On detecting edges in speckle imagery. IEEE Trans ASSP.36(10),pp.1618-1627.

3.*L. Perlovsky, W.H. Schoendorf, B.J. Burdick, D.M. Tye*, Model-based neural network for target detection in SAR images, IEEE Transactions on image processing, Vol. 6, No. 1. - January 1997. – pp. 203 – 216.

4.*V.P. Melnik, V.V. Lukin, A.A. Zelensky, J.T. Astola, P Kuosmanen*, Local activity indicators: analysis and application to hard-switching adaptive filtering of images, Optical Engineering Journal. - 2001. - Vol. 40, No 8. - pp. 1441-1445.

5.*V.V. Lukin, V.P. Melnik, A.B. Pogrebniak, A.A. Zelensky, J.T. Astola, K.P. Saarinen*, Digital adaptive robust algorithms for radar image filtering, Journal of Electronic Imaging. - Vol. 5, No.3. - July 1996. - pp. 410-421.

6.*I. Pitas, A.N. Venetsanopoulos*, Nonlinear Digital Filters: Principles and Applications - Boston (USA): Kluwer Academic Publisher, 1990. – 321 p.

7.S. Solbo. T. Eltoft, A wavelet domain filter for correlated speckle, Proceedings of EUSIPCO, 2006, 5p.

8.*А.В. Науменко, В.В. Лукин*, Детектирование границ на изображениях с помощью искусственной нейронной сети, Авиационно-космическая техника и технология – 2012. – Вып. 2. – С. 101-110.

9.*X. Kang, C. Han, Y. Yang, T. Tao*, SAR image edge detection by ratio-based Harris Method, Proceedings of ICASSP 2006 Proceedings. - Vol. 2. - May 2006. - PP. 837 -840.

UDC 519.22 (045)

Prokopenko I.G., Dr.Sci.Tech., prof.
Martynchuk I.A., engineer
(National Aviation University, Ukraine)

MODELLING AND REGRESSION APPROXIMATION OF DEPENDENCE OF AN OPTIMAL SMOOTHING PARAMETER ON THE SAMPLE SIZE FOR KERNEL PROBABILITY DENSITY ESTIMATION

The substantiation of a choice of the smoothing parameter for kernel approximation of probability density is brought in this work. The optimising problem of search of the smoothing parameter by the set criterion is formulated. The software allows to model random variables with any truncated probability density function.

Kernel probability density function (PDF) estimation on experimental data $\eta_0,\dots,\eta_{N-1}$ are widely used in the assumption of its continuity and smoothness [1]. This estimation looks like

$$f_h^*(x) = \frac{1}{N\cdot h}\cdot\sum_{n=0}^{N-1} K\left(\frac{x-\eta_n}{h}\right), \tag{1}$$

where $K(x)$ – is the kernel function, possessing property

$$\int_{-\infty}^{\infty} K(x)dx = 1, \tag{2}$$

N – is the sample size, h – is the smoothing parameter or scale parameter, η – is the sample of a random variable.

Rectangular and Gaussian kernels

$$K(x) = \begin{cases} 0.5 & if \quad -1 \le x \le 1, \\ 0 & otherwise; \end{cases}, \tag{3}$$

$$K(x) = \frac{1}{\sqrt{2\pi}}\cdot\exp\left(-\frac{x^2}{2}\right) \tag{4}$$

find a wide application at construction of kernel estimations.

Quality of the estimation (1) depends on value of smoothing parameter h. Criterion of quality in this work is an intersection of areas under theoretical PDF $f(x)$ and its estimation $f_h^*(x)$. The criterion essence is clear from fig. 1.

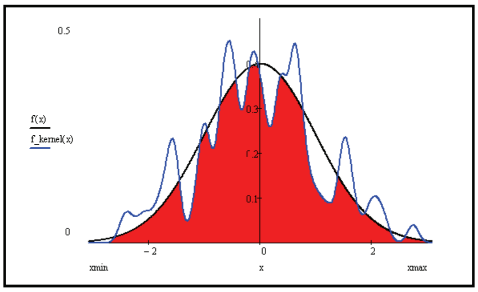

Fig. 1. An intersection of areas under theoretical PDF and its kernel estimation

We define a problem of search of optimum smoothing parameter for the specified sample size at kernel probability density estimation by a method of statistical modelling.

Let there is an one-dimensional theoretical probability density with the given necessary parameters $f(x,a_0,a_1,\dots,a_{K-1})$. This function is truncated at the left and on the right to borders $x_{\min} = F^{-1}(\alpha_L)$ and $x_{\max} = F^{-1}(\alpha_R)$ accordingly, where $F^{-1}(\alpha)$ – inverse function to probability distribution function (quantile function). Borders are chosen so that the probability density normalizing condition with the chosen accuracy was satisfied. On Neumann's method (a principle of Monte-Carlo) the sample of random numbers of size N is generated, which distributed under the given theoretical distribution law. It also will be an initial material for modelling.

On the obtained sample the kernel estimation of PDF is constructed at the given smoothing parameter *h* and the value of quality criterion is calculated

$$R(h) = \int_{x_{\min}}^{x_{\max}} \min\left\{f_h^{\,*}(x), f(x)\right\} dx \,. \tag{5}$$

Further the such value h_{opt} is found at which the maximum of criterion (5) is achieved.

On the obtained dependence of optimum smoothing parameter on sample size the regression model is constructed by the method of least squares.

Let's bring results of modelling (fig. 2) for normal probability density with mean $\mu = 0$, and standard deviation $\sigma = 1$ at following parameters:

1) a minimum and maximum value of *x* variable of theoretical probability density *f(x)* – $x_{\min} = F^{-1}(0.001)$, $x_{\max} = F^{-1}(0.999)$;

2) a number of discretization intervals of the kernel and theoretical probability density (for numerical integration) – *100*;

3) a method of numerical integration (at calculation of intersection of areas) – middle rectangles;

4) a kernel – $K(x) = \dfrac{1}{\sqrt{2\pi}} \cdot \exp\left(-\dfrac{x^2}{2}\right)$;

5) a quantity of samples – *10*;

6) a maximum sample size – *10 000*;

7) a search method of maximum in functional dependence (5) – a golden section.

The search accuracy of maximum in function *R(h)* on the segment *[h_{min}; h_{max}]* is $\varepsilon = 1 \cdot 10^{-3}$. The segment *[$h_{min}$; h_{max}]* is selected thus that quantity of intervals of discretization of kernel probability density was enough for correct execution of numerical integration.

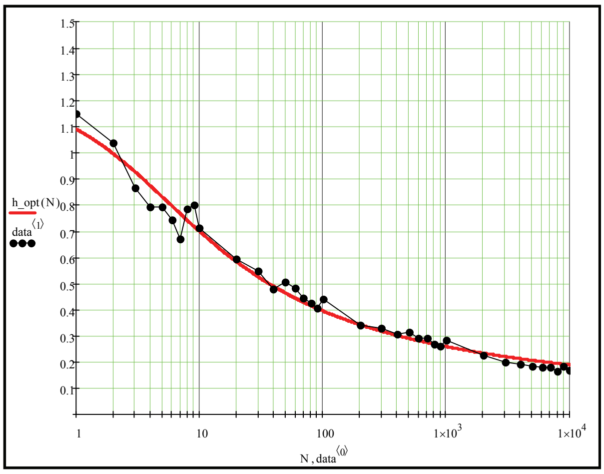

Fig. 2a. Dependence of the optimum value of the scale parameter on the sample size (pointwise line) and its regression approximation (solid line)

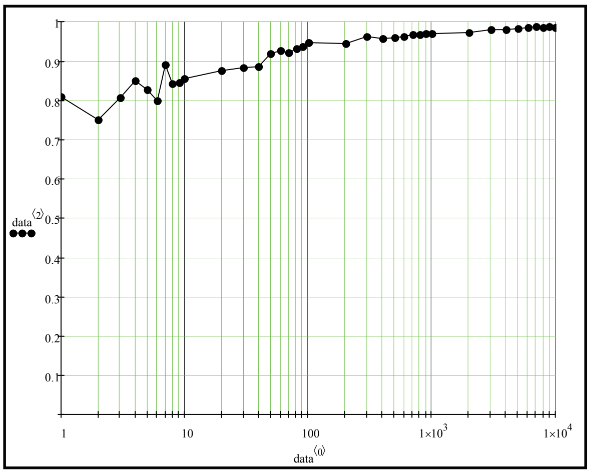

Fig. 2b. Dependence of the quality criterion value (with optimum scale parameter) on the sample size

In the given work the regression model [2] has been fitted, which enough precisely approximates dependence of optimum value of scale parameter on sample size

$$h_{opt}(N) = \frac{a}{\log_{10}(N+c)} + b \,. \tag{6}$$

Such probability densities have been involved in modelling: Beta, Cauchy, Chi-squared, Exponential, F, Gamma, Logistic, Log-Normal, Normal, Rayleigh, Student's T, Uniform, Weibull.

Let's bring the table with various distributions and formulas for $h_{opt}(N)$

Table 1

№	Probability density name	Probability density function *f(x)*	Probability density parameters	Probability density domain	Regression approximation of dependence $h_{opt}(N)$
1	Beta	$f(x) := \frac{\Gamma(s1+s2)}{\Gamma(s1)\cdot\Gamma(s2)} x^{s1-1}\cdot(1-x)^{s2-1}$	$s1 := 2$ $s2 := 2$	$x_{min} := F^{-1}(0.001)$ $x_{max} := F^{-1}(0.999)$	$h\_opt(N) := \frac{0.196\ln(10)}{\ln(N+3.796)} - 8.079\times10^{-3}$
2	Cauchy	$f(x) := \left[\pi\cdot s\cdot\left[1+\left(\frac{x-l}{s}\right)^2\right]\right]^{-1}$	$l := 0$ $s := 1$	$x_{min} := F^{-1}(0.1)$ $x_{max} := F^{-1}(0.9)$	$h\_opt(N) := \frac{0.516\ln(10)}{\ln(N+1.832)} + 0.402$
3	Chi-squared	$f(x) := \frac{\exp\left(-\frac{x}{2}\right)}{2\cdot\Gamma\left(\frac{d}{2}\right)}\cdot\left(\frac{x}{2}\right)^{\frac{d}{2}-1}$	$d := 100$	$x_{min} := F^{-1}(0.001)$ $x_{max} := F^{-1}(0.999)$	$h\_opt(N) := \frac{8.834\ln(10)}{\ln(N+1.769)} + 0.838$
4	Exponential	$f(x) := r\cdot\exp(-r\cdot x)$	$r := 1$	$x_{min} := F^{-1}(0.001)$ $x_{max} := F^{-1}(0.999)$	$h\_opt(N) := \frac{0.559\ln(10)}{\ln(N+3.616)} - 0.12$
5	F	$f(x) := \frac{d1^{0.5\cdot d1}\cdot d2^{0.5\cdot d2}\cdot\Gamma\left(\frac{d1+d2}{2}\right)}{\Gamma(0.5\cdot d1)\cdot\Gamma(0.5\cdot d2)}\cdot\frac{x^{0.5\cdot(d1-2)}}{(d2+d1\cdot x)^{0.5\cdot(d1+d2)}}$	$d1 := 10$ $d2 := 100$	$x_{min} := F^{-1}(0.001)$ $x_{max} := F^{-1}(0.999)$	$h\_opt(N) := \frac{0.306\ln(10)}{\ln(N+2.436)} + 1.92\times10^{-3}$
6	Gamma	$f(x) := \frac{x^{s-1}\exp(-x)}{\Gamma(s)}$	$s := 2$	$x_{min} := F^{-1}(0.001)$ $x_{max} := F^{-1}(0.999)$	$h\_opt(N) := \frac{0.919\ln(10)}{\ln(N+4.01)} - 0.086$
7	Logistic	$f(x) := \frac{\exp\left(-\frac{x-l}{s}\right)}{s\cdot\left(1+\exp\left(-\frac{x-l}{s}\right)\right)^2}$	$l := 1$ $s := 1$	$x_{min} := F^{-1}(0.001)$ $x_{max} := F^{-1}(0.999)$	$h\_opt(N) := \frac{1.364\ln(10)}{\ln(N+3.887)} - 0.041$
8	Log-Normal	$f(x) := \frac{1}{\sqrt{2\pi}\cdot\sigma\cdot x}\cdot\exp\left[-\frac{1}{2\cdot\sigma^2}\cdot(\ln(x)-\mu)^2\right]$	$\mu := 0$ $\sigma := 1$	$x_{min} := F^{-1}(0.001)$ $x_{max} := F^{-1}(0.9)$	$h\_opt(N) := \frac{0.498\ln(10)}{\ln(N+2.48)} - 0.063$
9	Normal	$f(x) := \frac{1}{\sqrt{2\pi}\cdot\sigma}\cdot\exp\left[-\frac{(x-\mu)^2}{2\sigma^2}\right]$	$\mu := 0$ $\sigma := 1$	$x_{min} := F^{-1}(0.001)$ $x_{max} := F^{-1}(0.999)$	$h\_opt(N) := \frac{0.841\cdot\ln(10)}{\ln(N+4.719)} - 0.021$
10	Rayleigh	$f(x) := \frac{x}{\sigma^2}\cdot\exp\left(-\frac{x^2}{2\sigma^2}\right)$	$\sigma := 1$	$x_{min} := F^{-1}(0.001)$ $x_{max} := F^{-1}(0.999)$	$h\_opt(N) := \frac{0.534\ln(10)}{\ln(N+4.498)} - 0.019$
11	Student's T	$f(x) := \frac{\Gamma\left(\frac{d+1}{2}\right)}{\Gamma\left(\frac{d}{2}\right)\cdot\sqrt{\pi\cdot d}}\cdot\left(1+\frac{x^2}{d}\right)^{-[0.5\cdot(d+1)]}$	$d := 100$	$x_{min} := F^{-1}(0.001)$ $x_{max} := F^{-1}(0.999)$	$h\_opt(N) := \frac{0.782\cdot\ln(10)}{\ln(N+3.6)} - 2.83\times10^{-3}$
12	Uniform	$f(x) := \frac{1}{bu-au}$	$au := -0.5$	$x_{min} := F^{-1}(0.001)$	$h\_opt(N) := \frac{0.23\cdot\ln(10)}{\ln(N+2.853)} - 0.045$

			bu := 0.5	$x_{max} := F^{-1}(0.999)$	
13	Weibull	$f(x) := s \cdot x^{s-1} \cdot \exp\left(-x^{s}\right)$	s := 10	$x_{min} := F^{-1}(0.001)$ $x_{max} := F^{-1}(0.999)$	$h\_opt(N) := \frac{0.077 \cdot \ln(10)}{\ln(N + 2.703)} + 2.28 \times 10^{-3}$

For an example with normal density ($\mu = 0$, $\sigma = 1$) the parameters of regression model will be the following: $a = 0.841$, $b = -0.021$, $c = 4.719$.

Conclusions

For each kind of probability density function there is a dependence of optimum smoothing parameter of a kernel estimation of this density on the sample size of experimental data.

At construction of kernel estimation the choice of optimum smoothing parameter of probability density function should be made proceeding from a priori information on a kind of this density.

References

1. *Devroye L., Gyorfi L.* – Nonparametric Density Estimation: The L1 View. John Wiley & Sons, New York, 1985. Translated under the title Neparametricheskoe ocenivanie plotnosti. L1 podhod, Moscow: Mir, 1988, 408 p.

2. *E. Z. Demidenko* – Linejnaja i nelinejnaja regressii (Linear and nonlinear regression), Moscow: Finansy i statistika, 1981, 302 p.

3. *Panteleev A. V.* – Metody optimizacii v primerah i zadachah (Optimization methods in examples and problems), Moscow: Visshaja shkola, 2005, 544 p.

UDC 621.382.681

M.K.Baizhumanov, Doctor of technical science (Academy of the Civil Aviation, Almaty, Republic Kazakhstan),
A.A.Tuyakbayev, Doctor of technical science (Academy of the Civil Aviation, Almaty, Republic Kazakhstan),
V.K.Bishimbaev, Doctor of technical science, professor (Member of Parliament),
D.A.Tuyakbaev, Master Student ("GAZI" University, Ankara, Turkey)

COMPENSATION OF RADIATION DAMAGE IN THE INTEGRATED CIRCUITS ON MOS TRANSISTORS

Major changes when radiation damage of MOS transistors is found in threshold voltages. These changes can be used to their mutual compensation.

This approach allowed to develop the inverter on the MOS transistors [1,2], characterized by the high radiation resistance (Fig.1).As you can see, this converter excluding the active load transistors, has an additional MOS transistor and three resistors that are insensitive to radiation. Theone terminal of theresistorR1is connected toa commonpower busand the other terminalto the common substrateof theactiveloadtransistors andthe source ofthe additionalMOStransistor. Drain of an additionaltransistor is connected to the othercommonpower bus. The gate of the additionalgattransistoris connected toa common pointbetween the other tworesistorsforminga voltage dividerbetween thepower buses. It should benoted that all thetransistorsare identical; they are producedin the same technological cyclethat causesthe samechange in theirthreshold voltages. Therefore, in theproposed scheme thesimilarchanges inthe thresholdvoltage of MOStransistor and of an additionalMOStransistorinverter(activeand loadtransistors)willcompensate each other. Thisis the reason forthe increaseof MS of the proposed inverterasshown by experimentalresults.

The compensation of the threshold voltage of MOS transistors is limited by the value of the inverters power supply voltage. For correct operation of the inverter it is necessary to choose the voltage divider resistors R2 and R3 so that the voltage on the gate of the transistor T3 provides the beginning stage of the transistor opening. Resistor R1 must provide the voltage drop changes on the transistor that are proportional to the positive charge changes in the gate dielectric device, i.e. the threshold voltage of MOS transistors.

It should be noted that the circuit shown in Figure 1 is valid for n-channel transistors. For p-channel transistors, the connection to external power supply is necessary (Fig. 2). Resistor valuesof the voltage divider R2 and R3 in this scheme must satisfy the condition of the maximum opening of an additional transistor T3. At the same time the positive power supply is connected to the resistor R1. Under the influence of the penetrating radiation, the accumulation of positive charge in the dielectric leads to the threshold voltage increase of the p-channel transistors and to the decreasing current flowing through the transistor T3. This, in turn, leads to the increase in the voltage drop across the transistor T3, i.e. to the increase in the positive potential at its source and to the decreasing the voltage drop across the resistor R1. The resistor R1 should be chosen so that the decreasing of voltage drop across the R1 would be inversely proportional to the increase of positive charge in the dielectric.

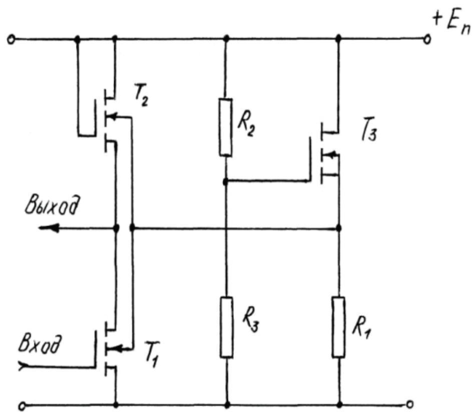

Figure 1.Inverter on the n-channel MOS transistors that characterized with increased radiation resistance.

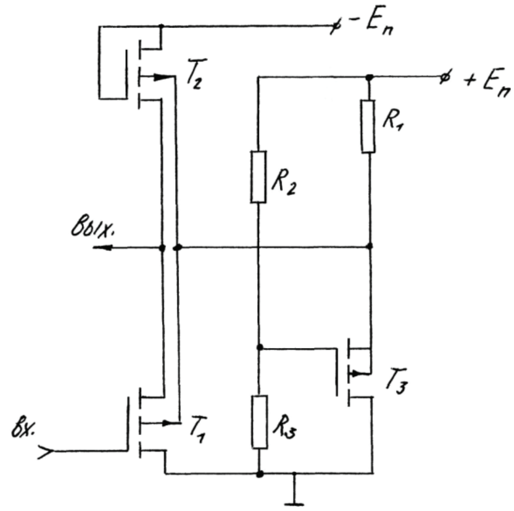

Figure 2.The inverter on the p-channel MOS transistors that characterized with increased radiation resistance.

The proposed scheme of the MOS transistors threshold voltage changes compensation during irradiation, implemented for the inverter can be used for any integrated circuit on MOS transistors [3]. It is enough to produce the main integrated circuits (IC) crystal, additional MOS transistor and three resistors on the same substrate and in the same technological cycle [3]when realization of IS on the MOS transistors taking into account the proposed method of mutual compensation of the changes in threshold voltages during irradiation. The resistors should be isolated from each other and from the main crystal. During metallization the one terminal of the first resistor should be connected to the common (negative) power bus. Another terminal of the first transistor should be connected to the main crystal substrate and to the source of additional MOS transistor. The additional MOS transistor drain should be connected to another common power contact. The additional MOS transistor gate should be connected to the common point between the other two resistors forming a voltage divider between the power buses. This realization of IS on the n-channel MOS transistors must lead to the mutual compensation of the additional changes in the threshold voltages of the additional transistor and the transistors of the basic crystal circuit. In case of the IS on the p-channel MOS transistors, the elements connection during metallization is shown in Figure 2.

In is more difficult to realize the mutual compensation of the threshold voltage changes during irradiation in a CMOS IC. However, in this case the implementation of the proposed method is possible as well. For this purpose it is necessary to provide the connection of all substrates of MOS transistors located in the pockets when metallization. The two additional transistors of different conductivity should be used instead of one additional transistor and connect them as it was discussed above. For example, it is possible to use the connection shown in Fig. 3 [4] for the inverter on CMOS transistors.

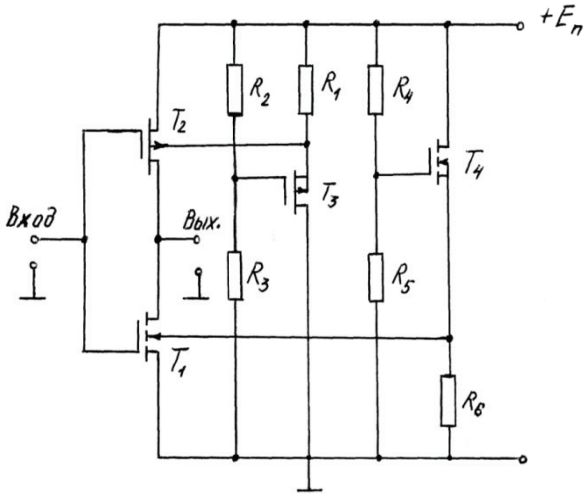

Figure 3. Inverter on CMOS transistors characterized with increased radiation resistance.

Thus, the mutual compensation of the threshold voltage changes of MOS transistors during irradiation can be realized with proposed methods for both MOS IC, and CMOS IC.

The efficiency of the proposed inverter in the fields of radiation emission has been investigated with various settings that simulate effects of impulsive type, and continuous emissions. The experimental dependences of the threshold voltage changes of MOS transistors, obtained under the action of γ -rays, fast electrons and neutrons are shown in Fig. 4, 5 and 6 respectively. From the analysis of the dependencies it can be concluded that the threshold voltage of the MIS transistors are the most sensitive to the effects of γ -rays and fast electrons. From the Figure 4 it can be concluded that the initial values of the threshold voltages u_o can be used for the transistors rejection, i.e., the smaller the initial value of u_o, the higher the radiation resistance of MIS transistors p-channel are.

Experimental studies of this stage were appointed to determine the dependences of the threshold voltages changes of MOS transistors on integrated fluxes of different radiation types.

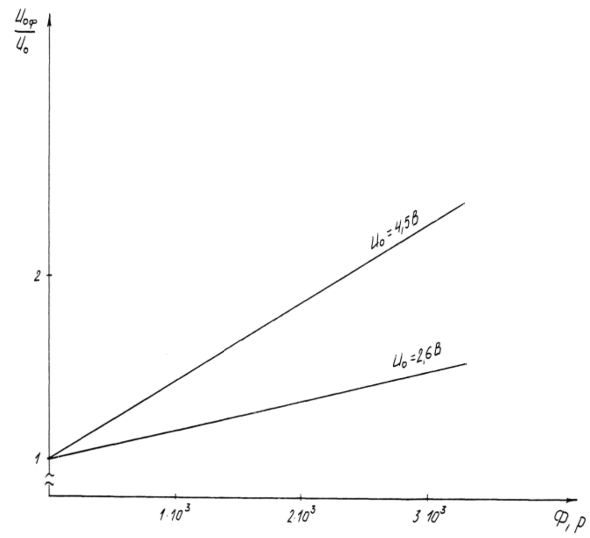

Figure 4. Experimental dependences of the threshold voltages changes of MOS transistors on integrated flux of γ - rays.

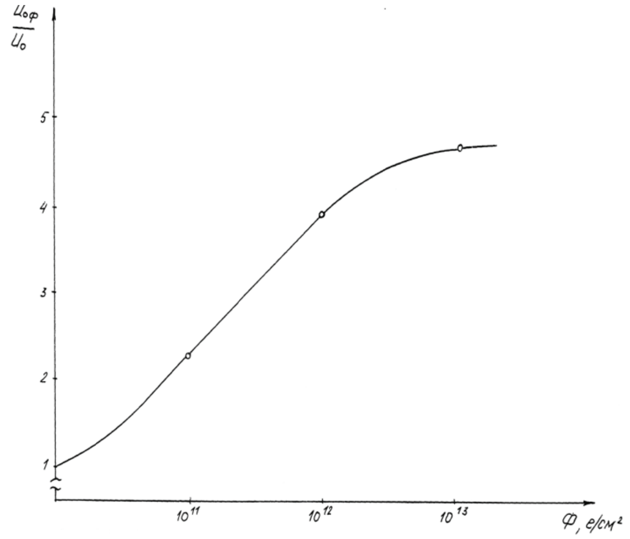

Figure 5. Experimental dependence of the threshold voltage changes of the MOS transistor on the integrated flux of fast electrons.

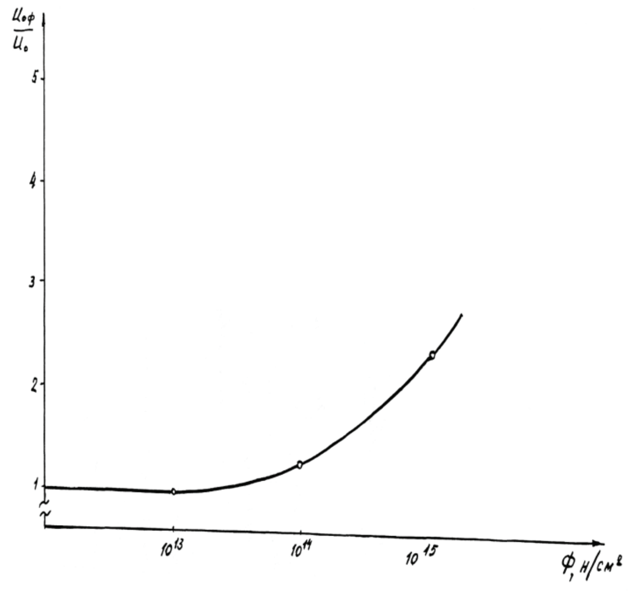

Figure 6.Experimental dependence of the threshold voltage changes of the MOS transistor on the integrated flux of fast neutrons.

The study of the operability of the proposed inverters (Fig. 1), performed on three MOS transistors shows that their quality in comparison with the conventional is higher: sharper fronts of the pulses. The electron irradiation reveals that the parametric compensation from the substrate provides a gain in the threshold voltage of the main transistor operating in active mode. This is explained by the fact that the growth of voltage from the substrate pulls on a charge carriers. This leads to the decreasing effect of the positive charge accumulated in the oxide of silicon (in the gate dielectric). It is possible to say that effect of the positive charge accumulated in the oxide of silicon is compensated. In general, this effect leads to the increase in radiation resistance of integrated circuits on MOS transistors.

Studies aimed at the growing increase in radiation resistance of semiconductor electronic circuits resulted in patents [5, 6]. The first is "Method of manufacturing CMOS integrated circuits", which proposes to produce p-channel over the n-channel transistors using the common gate between them. These achieved by technological operations of films deposition of amorphous silicon, silicon oxide and metal. The second is "Complementary Transistors". The second proposes to use the p-channel and n-channel transistors in the single crystal on the basis of silicon, gallium arsenide, gallium phosphide, silicon carbide or other wide-gap material. The one of the transistors is close and another is open if any signal on the common gate. Usually when zero signal influence the n-channel transistor is closed and p-channel is open. When positive pulse signal influence the n-channel transistor is open, and p-channel is closed. It should be noted that the gate of n-channel transistor must not be open. It should be noted that the field-effect transistors with controlled p-n junction have high radiation resistance. It is about 1 ÷ 2 orders higher than bipolar transistors magnitude and 3 ÷ 4 orders higher than that of MIS transistors. The proposed "complementary transistors" allows to create energy-efficient integrated circuits, such as CMOS integrated circuits, but without the silicon oxide film. The silicon oxide film reduces the radiation resistance sufficiently.

Regarding "Method of manufacturing CMOS integrated circuits" we can say that they cannot show latch-up effect, as the p-channel and n-channel transistors in these structures are sufficiently insulated with a thick layer of silicon oxide. The high radiation resistance is proved by the fact that these transistors are produced using the films of hydrogenated and fluorinated amorphous silicon.

Conclusions

1. Radiation resistance of the IC on MOS transistors can be greatly enhanced with the help of the circuit design, in which the same changes in threshold voltage of MOS transistors compensate each other.

2. We propose the construction based on the controlled p-and n-channel transistors of complementary structure that increase the radiation resistance and energy efficiency of the IS.

3. Method of manufacturing CMOS integrated circuits that help to reduce the probability of thyristor effect was proposed.

References

1. Ladygin E.A., Goryunov N.N., Tuyakbayev A.A. and others. Inverter. Author's Certificate. № 1505359, priority of 07.07.1987, registered in the State Register of Inventions of the Soviet Union 01.05.1989.(in Russian).

2. LadyginE.A., Goryunov N.N., Panichkin A.V., Tuyakbayev A.A. Inverter TIR transistors.Author'sCertificate. № 1223822, priority of 20.07.1984, registered in the State Register of Inventions of the Soviet Union 08.12.1985.(in Russian).

3. Ladygin E.A., Goryunov N.N., TuyakbayevA.A. TIR and other integrated circuit. Author's Certificate. № 1475421, priority of 23.04.1987, registered in the State Register of Inventions of the Soviet Union 22.12.1988.(in Russian).

[4. Tuyakbayev A.A., Baekenov M.A., Iskakov B.M. CMOS integrated circuit. Predpatent RK № 4791, priority of 22.06.1995, published 16.06.1997 in the bulletin Number 2.(in Russian).

5. Aldamzharov K.B., TuyakbayevA.A. Method of manufacturing CMOS integrated circuits. Patent number 11,243, publ. 15.02.2007, Bull. № 2.(in Russian).

6. Aldamzharov K.B., Tuyakbayev A.A. Complementary transistor. Patent number 14587, publ.15.02.2007 in the bulletin Number 2.(in Russian).

UDC 621.382.681

A.A.Tuyakbayev, Doctor of technical science
(Academy of the Civil Aviation,
Almaty, Republic Kazakhstan,. Baizhumanov, Doctor of technical science
(Academy of the Civil Aviation, Almaty, Republic Kazakhstan),
D.A.Tuyakbaev, Master student ("GAZI" University, Ankara, Turkey, t.dak@mail.ru)

SINGLE-LEVEL MODEL FORSIMULATION OFTHE EFFECT OF ELECTRONIRRADIATION ONTRANSISTORS

In this work the single-level model for determination of the constant of radiating change of lifetime of minority carriers in the base of n-p-n transistors is developed. DLTS spectra in the base area of n-p-n transistors are modeled, and results of calculations are obtained and discussed.

I. INTRODUCTION

Radiating effect in semiconductor devices leads to degradation of almost all parameters of bipolar transistors. Among these parameters the base current transmission static coefficient is changed most significantly. These changes are caused by the fact that irradiation leads to change of lifetime, concentration and mobility of charge carriers at various areas of a semiconductor devices. In this work the single-level model for determination of the constant of radiating change of a lifetime of minority carriers in the base of n-p-n transistors is developed, DLTS spectra in the base area of n-p-n transistors are modeled, and results of calculations are obtained and discussed.

II. MODELING

Thus in silicon at the levels of an alloying corresponding to the base areas of transistors, the lifetime of non-basic charge carriers changes quite strongly. For this it is possible to use the expression

$$\frac{1}{\tau_{\phi}} = \frac{1}{\tau_0} + K_{\tau} * \Phi, \qquad (1)$$

where$K_{\tau}$is the proportionality factor defining the rate of changes of lifetime of non-basic charge carriers irradiation (a constant of radiating change of lifetime of charge carriers); Φ is an integrated stream of radiation; τ_0 is an initial value of lifetime of charge carriers in different structure areas.

In the given expression it is difficult to define the value of a constant of radiating change of charge carries lifetime. For this purpose it is possible to use two-level model of the Messenger that is true for a neutron irradiation [1].

Single-level model is possible to use for simulation of influence of an electronic irradiation:

$$K_{\tau} = \frac{1}{\frac{1}{CR_P}\left(\frac{n_0 + n_e + \Delta n}{n_0 + p_0 + \Delta n}\right) + \frac{1}{CR_n}\left(\frac{p_0 + p_e + \Delta n}{n_0 + p_0 + \Delta n}\right)}, \qquad (2)$$

where

$$n_e = N_c * exp\left(-\frac{\varphi_c - \varphi_e}{\varphi_T}\right), \qquad (3)$$

$$p_e = N_V * exp\left(-\frac{\varphi_e - \varphi_V}{\varphi_T}\right), \qquad (4)$$

$$R_P = \sigma_P * \sqrt{3 * K * T/m_P} \quad , \tag{5}$$

$$R_n = \sigma_n * \sqrt{3 * K * T/m_n} \quad , \tag{6}$$

N_c, N_v are densities of quantum conditions;
φ_c is a width of the forbidden zone of a semiconductor material;
m_n, m_p are effective weights of the electron and holes;
K is Boltzmann constant;
σ_n ,σ_p are effective sections of capture of the electron and holes;
C is the rateintroductionof recombination centers.

Parameter φ_e in the expressions (3) and (4) in our case corresponds to the level H(0,45), i.e. φ_e = 0.45 eV. The last mentioned is related with experimental researches by Deep Level Transient Spectroscopy (DLTS) of n-p-n transistors. It have been shown that at relaxation spectroscopy of deep levels, center H(0,45) (vacancy-boron) is closer to the middle of the forbidden zone, and consequently, the concentration increasing this center leads to the reduction of lifetime of non-basic carriers in the base.

In expression (2), it is difficult to model the dependence of speed of introduction of the radiating center C from the degree of an alloying of a material as well as from the electrons energy, and also to consider the frequency of an irradiation.

As a result of estimations of experimental data the specified parameter for p-type silicon is offered to be counted, using following formulas:

$$C = K1C_0 \lg(NA/NAo) \ , \tag{7}$$

$$C_o = K2 \ln(Ee - 1) \ , \tag{8}$$

where $N_{Ao}$is reference concentration of the boron impurity in silicon, for example 10^{14} cm^{-3};
K1, K2 are the factors of proportionality defined from experimental data; for p-Si, K1 = 3,
K2 = $3.4 \cdot 10^{-3}$; N_A is concentration of boron impurity in silicon, in investigated area of the device.

It is necessary to notice that the resulted formulas are correct at devices irradiation with fast electrons under normal conditions, i.e. at room temperature. In Fig. 1 the families of the curves received with given formulas, dependences of speed of introduction of radiating center H(0,45) on energy of electrons, and concentration of boronN_A are shown. From Fig.1 it is possible to see that theoretical results are in quite good agreement with experimental data.

Using expression (2) the values of constants of radiation change of lifetime of carriers depending on electrons energy and concentration of boron N_A have been calculated as wellthese data are resulted in Fig. 2.

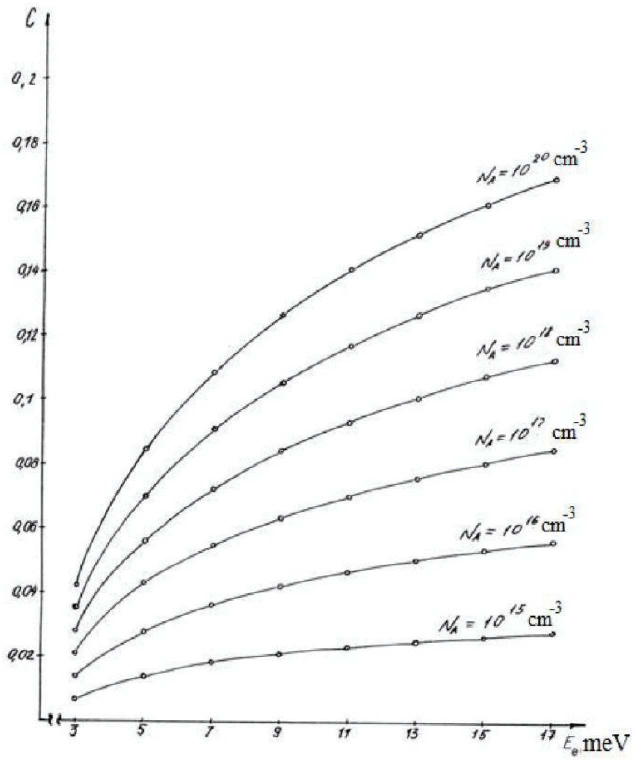

Figure 1. Calculated dependences of speed of introduction of radiation centers H (0,45) from electrons energy and degrees of an alloying of a material.

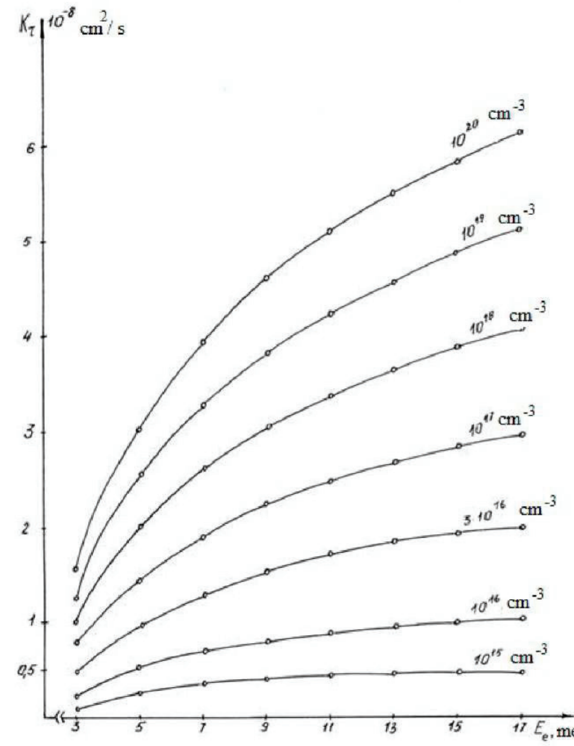

Figure 2. Calculated dependences of a constant of radiation change of carriers lifetime from electrons energy and degrees of an alloying of a material.

The values of amplification factor of a current of the base current transistors h_{21ef} have been calculated and resulted in Fig. 3. It is in good correspondence with experimental data.

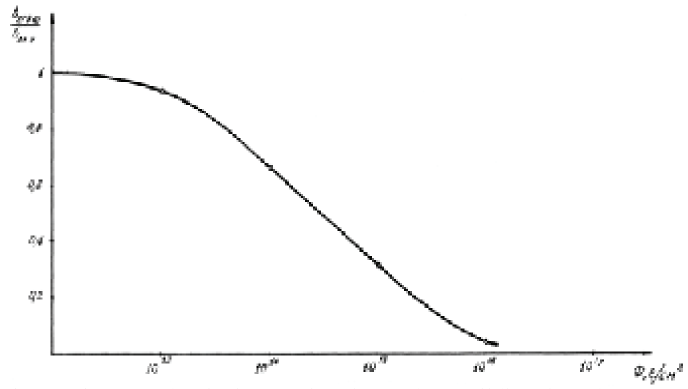

Figure 3. Calculated dependence of relative reduction of amplification factor of silicon bipolar transistors KT 315 at electronic irradiation (Ee = 5 meV).

Values of constants K_T were substituted in the formula

$$h_{21Э} = \frac{1}{\frac{1}{h_{21Э}} + \frac{1}{2\pi f_T} K_\tau \Phi},$$

in calculating the radiation resistance of the transistors fabricated using the radiation-thermal processes must be received by the speed the introduction of center H(0.45) reduce to three times, as is evident from the data of DLTS [2] (fig. 4), but otherwise method of calculation remains the same. The results of calculation of the radiation resistance transistors are shown in Figure 5, and they are in good agreement with experimental data.

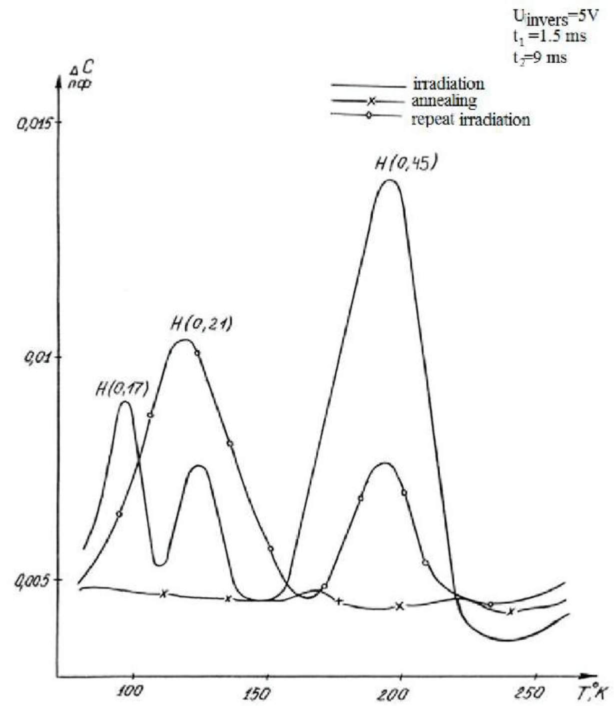

Figure 4. DLTS - spectra in basic area of the transistors irradiated with electrons with energy.
5 meV and flow of 5•10^{15} e/cm^2.

Center H (0,45) - is a complex vacancy + atom of boron
Center H (0,21) - is a complex divacancy + atom of boron

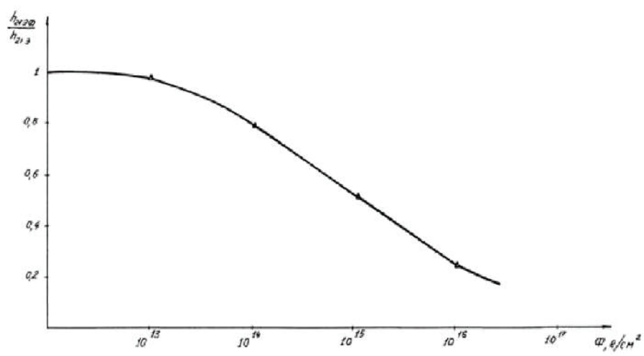

Figure 5.Calculated dependence of the relative decrease in the gain of silicon bipolar transistors made with the use of radiation-thermal processes under electron irradiation (Ee = 5 meV).

Thus, the proposedsingle-levelmodel allows us toaccurately determinethe constantchangesthe radiativelifetime ofminority carriersin the base ofn-p-ntransistorsunder electron irradiationand thusallows tosimulate theelectron irradiation influence on thesemiconductortransistor circuits.

III. CONCLUSIONS

Thesingle-levelmodel to determinethe constantchanges inthe radiativelifetime ofminority carriersin the base ofn-p-ntransistorsunder electronirradiation is shown. TheDLTSspectra of thebase ofn-p-ntransistors under therepeated irradiationwith fast electronsand annealing are given.

References

1. V.S.Vavilov, N.A.Ukhin, "Radiation effects in semiconductors and semi-conductor instruments." Atomizdat, Moscow, 1969. (in Russian).
2. N.N.Gorjunov, E.A.Ladygin, and A.A.Tuyakbayev. Research of kinetics of accumulation and annealing of radiation defects in bipolar transistor structures." News of ANKazSSR. A series physical and mathematical, Alma-Ata, 1987, N°2 (in Russian).

UDC 546.26:539.52:544.623

D.E. Aznakayeva, N.M. Nischenko, E.G.Aznakayev
National Aviation University, Ukraine

INFLUENCE OF ELECTROMAGNETIC WAVES ON CARBON NANOTUBES COMPOSITES

Abstract. Reflected properties of different objects such as plane, space apparatus, solar cells, and so on depend from physical and chemical characteristics of the surface of its materials. The dielectric constant is such characteristic which depends from composite construction of surface material. This paper researches dielectric properties of different composites which are dependent from carbon nanotubes as effective surface materials. In particular, the influence of infrared (IR) irradiation on thermal resistance of carbon nanotubes (CNTs) composites was studied as well as the interaction of non-monochromatic infrared irradiation with composites carbon nanotubes and the influence of irradiation on physical properties of composite carbon nanotubes (CNTs) - polytetrafluorethylene (F4) depending on the concentration of CNTs was investigated. Also, the 5% CNT composite of F4 change of monochromatic infrared irradiation intensity from the sample's thickness was investigated. It is found that under decreasing of thickness of the composite F4-CNT, the rapid drop of passing monochromatic irradiation intensity (λ = 1.06 μm) was observed. The sample thickness range varies from 0.1 mm to 0.6 mm. This phenomenon is explained due to a change in orientation of the CNTs from chaotic orientation to orientation along the direction of the F4-CNT sample's surface. It leads to the increased efficiency of monochromatic infrared irradiation absorption.

INTRODUCTION

Contemporary materials for aerospace vehicles and aerospace electronics must be lightweight and have a strong thermal resistance to overheating. The strong IR radiation acts on the surface of the aerospace stations. So, investigation of the properties of such new type of materials as carbon nanotubes composites is very actual for aerospace technology.

Much attention has been paid to problems related to the study of interaction of electromagnetic radiation with an array of small particles of various shapes and dispersed systems based on them. The urgency of such studies is caused by nontrivial physical properties of arrays of small particles and disperse systems, as well as the possibility of their use in the new set of absorbing and scattering materials with new optical properties for the purposes of such promising areas as nanophysics, optoelectronics, plasmonics [1]. The interaction of light with nanostructured substance is the essence of nanooptics. Unusual is the fact that the size of nanoparticles (~ 10 nm) is much smaller than the wavelength of light (400-700 nm), that is 1-2 orders smaller than the diffraction limit. The wave of light would have to avoiding such small objects and interact with them, but previous studies have shown that it is not true.

Often it is assumed that the electromagnetic wave is not sensitive to details of the structure of small particles compared to the wavelength of incident radiation. But one of the most interesting features of nanoparticles is that they can reveal optical properties which are almost entirely determined by their shape and are similar to the properties of solid materials.

Nonlinear optical properties of nanoclusters in transparent medium is a separate field of research. The most detailed studies of the nanocluster's optical properties of noble metals - Ag, Au, Pt, and metals with high conductivity - Cu and Al are needed. The absorption maximums-also have been found in the spectra of nanoparticles Li, In, K, Na, Ca [2]. The peculiarity of the metal nanoparticles optical properties is a plasmon resonance absorption and scattering associated with the interaction of electromagnetic radiation from the plasma of free electrons in the metal. The spectral position of these features (400-700 nm) depends on the material, its size, shape and energy of free electrons in the nanoparticles.

An important characteristic of plasmon resonance is a local increase of the electromagnetic wave fields' amplitude inside and around nanoparticles in ten times as compared with an average amplitude of the field in the array. Moreover, the plasmon nanostructure in certain conditions behaves almost like an absolute black body; it absorbs up to 99% of incident electromagnetic irradiation. The most interesting optical properties of metal nanoparticles are associated with the excitations of localized plasmons. This is primarily manifested in increasing of the effective cross section of light resonant absorption by metal nanoparticles, which can repeatedly exceed its geometrical dimensions. That is why multilayer carbon nanotubes, placed in the matrix of polytetrafluorethylene, have been chosen as an object of investigation. Generally, carbon nanotubes (CNT) have good electro- and thermal conductivity and mechanical stability and are considered as one of the most perspective objects of nanoelectronics. They are elements of such electronic systems, as cold field emitters [3-5], super condensers [6], solar elements [7], nano-electromechanical systems [8], sensors [9], etc.

The coating of cells material in solar batteries by metal nanoparticles makes possible to essentially improve the light transformation into electricity. It allows improving the red waves of light usage in ten times; and efficiency of solar batteries can be improved on 30 % as a whole.

Developed are devices which reacts to the total spectrum of an optical range of electromagnetic waves based on carbon nanotubes. Application of such detectors is extremely wide: cells of solar batteries with high efficiency, digital cameras working at very low light exposure, an artificial retina, and etc. Detectors based on carbon nanotubes can be formed on the flexible polymeric support, that makes them cheaper in manufacturing and absolute harmless for human.

METHODS OF MEASUREMRNT

We used two sources of generation of infrared irradiation: a light source of non-monochromatic filament bulb - a laser unit which generated a monochromatic beam of wavelength λ = 1,06 μm with generation time τ = 1-2 ms, and the energy source of the beam with E = 100 mJ.

Installation of F4-CNT for measurement of infrared non-monochromatic irradiation of composites with different percentage of CNTs consisted of a metal sample - a standard Al, and a metal sample – an Al sensor on which a thin layer (or as a flattened tablets of investigated samples F4-CNT) with different concentration of CNTs were layered. Both metal samples (Al - standard and sensor) have been connected to a multimeter using differential thermocouple. The flow of electromagnetic irradiation which was generated and emitted by filament bulb interacted with Al-standard and composited F4-CNT. The result values of this interaction in substances generated by the flow of free charge carriers, which led to thermoelectric force have been recorded using a multimeter. The received values of voltage of standard and investigated composite F4-CNT are transferred in values of temperature, using graduated table for thermocouple chromel-alumel.

The experimental equipment for the measurement scheme of monochromatic infrared irradiation of composite F4-5% CNT with different thickness consisted of a metal structure, the reception element, a recording unit and the laser sources. By means of F4-5% CNT mechanical compression model, the different thickness was received. Then, a sample of specific thickness layered on the glass was settled between two metal discs, which were further connected by screws. This metal structure attached to the measuring head, which fixed the value of energy of laser irradiation, passed through the sample. The laser irradiation power (or energy) was measured with device and converted into an equivalent value of thermoelectric power for recording.

The purpose of this experiment was to study the nature of change in the intensity of absorbed infrared radiation, depending on the thickness of the investigated sample.

RESULTS AND DISCUSSIONS

The received graphs depend on heating temperature of samples F4, F4-0.5% CNT, F4-0.1% CNT, F4-1% CNT, F4-2% CNT, F4-3% CNT, F4-5% CNT, F4-10% CNT, F4-15% CNT, F4-25% CNT from concentration of CNTs in sample and absorbed electromagnetic irradiation by F4-5% CNT with different thickness.

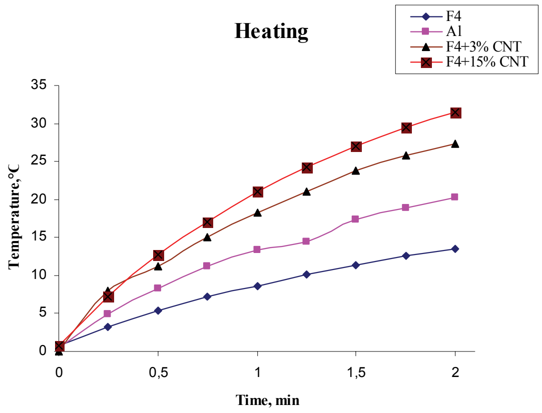

Figure 1. Dependence of heating temperature T, °C of standard Al sample, F4 and composites F4-3% CNT, F4-15% CNT from heating time t, min.

The rate of composite heating F4-CNT (Fig.1) corresponds to the content of 15% of CNTs.

The more slowly heated composite with a lower percentage of CNTs in the structure of F4-3% CNT, even more slowly is heated the sample F4. Analyzing the obtained dependences, we can conclude that increasing the percentage of carbon nanotubes in the sample F4-CNT leads to an increase in heat transfer processes and processes of thermo conductivity in the composite.

It was investigated the heating speed of composite F4 with different percentage of CNTs relate to standard Al sample (Fig. 2). In the Figure 2 ΔT, °C is the temperature difference between heating temperature of standard Al sample and heating temperature of composites F4-CNT; k, % is the percentage of CNTs in composites F4-CNT.

The resulting graph has non-monotonic behavior of the temperature ΔT,°C of k, %. The first stage of adding a small amount of CNTs to F4 leads to an increase of values ΔT, but interesting behavior is observed for 2% of CNTs in F4. There is the sharp decline of curve for ΔT (k) values from 6.42, °C to 5.47, °C. However, with greater addition of CNTs into the F4 the function ΔT (k) grows; it achieves satiation and after that the curve monotonously declines ΔT (k).

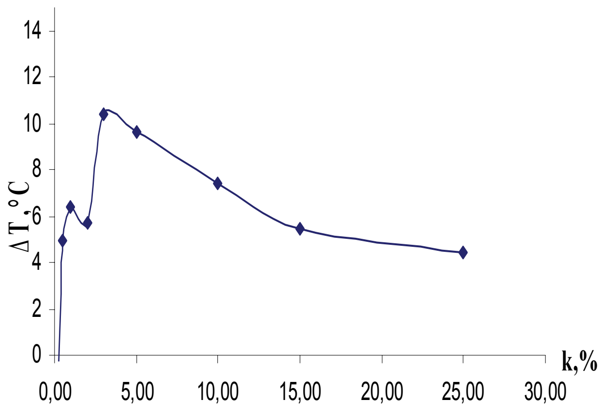

Figure 2. Dependence of ΔT, °C between heating temperature of standard Al sample and heating temperature of composites F4, F4-0.5% CNT, F4-0.1% CNT, F4-1% CNT, F4-2% CNT, F4-3% CNT, F4-5% CNT, F4-10% CNT, F4-15% CNT, F4-25% CNT from percentage of CNTs k, % in composite

This non-monotonic behavior of heating temperature rate of the sample relative to the standard can be explained using the following Figure 3.

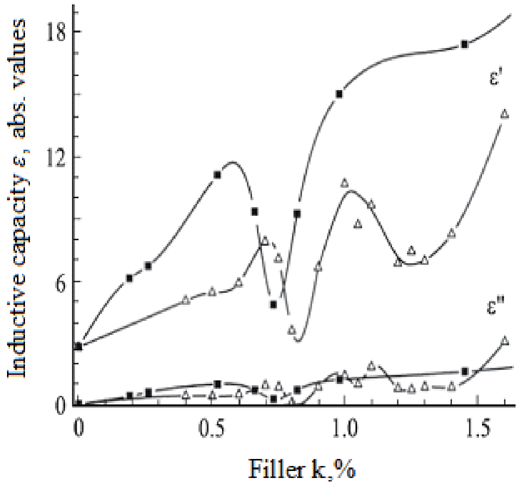

Figure 3. Dependence of inductive capacity (dielectric constant) of composite ε, abs. values, from the filler concentration k, % [10]

The comparison of Fig. 2 and Fig. 3 shows the tendency of heating temperature change behavior of the sample and changes in inductive capacity (dielectric constant) ε of medium from the concentration of filler in it.

Causes of the detected anomalies have not yet been determined. However, we can make the following assumptions. In the investigated system, insulator-conductor inductive capacity (dielectric constant) ε behavior determined by the Maxwell-Wagner polarization [11], surface energy as a conductor [12] and insulator, and conductivity of the whole system and its proximity to the percolation threshold [13]. At low concentrations of filler in the composite are formed meshwork, and ε value increases due to the Maxwell-Wagner polarization. However, with increasing concentration and with the presence of a large difference in surface energy of F4 and carbon nanotubes, the composite structure becomes unstable and the nanotubes begin to form conglomerates, which surface is less than the total surface of their constituent nanotubes.

As a result, Maxwell-Wagner polarization decreases. Additionally, changes in the nanostructure, which is a result of mechanical mixing and compression in the polymer, changes its shape from elongated to globular, leads to the displacement threshold percolation in the direction of large concentrations and reduces the dielectric constant ε of composite.

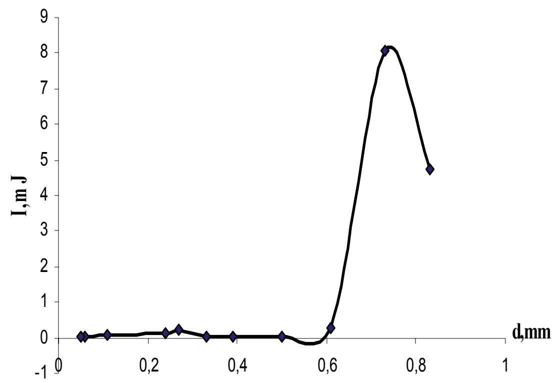

Figure 4. Dependence of the intensity of absorbed irradiation I, mJ from thickness d, mm composite F4-5% CNT

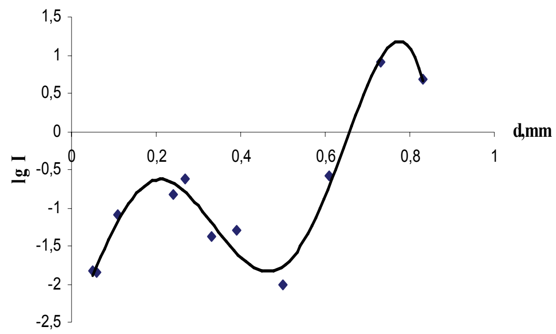

Fig. 5. Dependence of the logarithm of absorbed irradiation intensity lg I, from thickness d, mm of composite F4-5% CNT

The result of all these mechanisms reduce the value of the dielectric constant ε. Further the dielectric constant ε value increasing with filler concentration increasing in the composite leads to increase of the number of agglomerates and bundles of nanotubes, which reduces the dielectric layer between the major structures and leads to increases of electrical capacity. Due to the random variation of sizes and forms of nanotubes agglomerates decreases the value of dielectric constant ε. Below the changes in the intensity of absorbed irradiation after passing a laser (monochromatic) radiation through the sample F4-5% CNT of different thickness are presented (Fig. 4, 5). During a mechanical receipt of the sample F4-5% CNT with different thickness, orientation of carbon nanotubes changed from vertical to, mostly, horizontal, CNT oriented along the sample surface. As a result of F4-CNT sample anisotropy the intensity of irradiation which absorbed and passed through sample started to change and began to depend on the size and orientation of particles in composite F4-5% CNT. So, the dielectric and reflected properties of composites change also.

CONCLUSIONS

With decreasing thickness of the composite with carbon nanotubes F4-CNT, observed is a rapid drop of intensity of passing monochromatic infrared irradiation (λ = 1,06 μm) in the range of sample thickness 0,1 - 0,6 mm~~,~~ due to reorientation of CNTs from chaotic to the direction along the sample surface F4-CNT. This increases the efficiency of monochromatic infrared irradiation absorption by composites. The dielectric and reflected properties of composites change also.

REFERENCES

1. *W.L. Barnes, A.N. Dereux, and T.W. Ebbesen*, Nature, vol. 424, № 6950, p. 824, 2003.
2. *D.I. Rizenkov, Nanomaterials*: Science Laboratory, Moscow, 2008.
3. *M.I. Shakir et al., Nanotechnology*, vol. 17: p. 41, 2006.
4. *A.N. De Jonge, J.N. Bonard*, Proc. Roy. Soc. London, vol. A 362, p. 2239, 2004.
5. *Y. Cheng, O. Zhou, C.R*. Phys., vol. 4: p. 1021, 2003.
6. *D.N. Futaba et al*., Nature Mater., vol. 5, p. 987, 2006.
7. *P.V. Kamat,* Nanotoday, vol. 1 (4), p. 20, 2006.
8. *J.E. Jang et al*., Appl. Phys. Lett., vol. 87, p. 163114.
9. Metal., Sensors Actuators, Bill 111, p. 181, 2005.
10. *V.E. Muradyan*, Journal of Technical Physics, Moscow, vol. 80, № 2, p. 83, 2010.
11. *A.R. Chippel*, Dielectrics and Waves, Moscow: I.L., 1960, p. 351.
12. *A. Mdarhri*, *F. Carmona*, Appl. Phys., vol. 103, № 5, p. 054 303-1.
13. *Sockov V.A., Borisov A.V*., Journal of Technical Physics, Moscow, vol. 77, № 11, p.103, 2007.

UDC 537.87; 537.86

C. Castrejon-M., V. Grimalsky, S. Koshevaya
(CIICAp, Autonomous University of State Morelos (UAEM), Mexico
Yu. Rapoport (Physical Faculty, T. Shevchenko National University, Kiev 03022, Ukraine)

SUPERHETERODYNE AMPLIFICATION OF OPTICAL AND TERAHERTZ BEAMS IN NITRIDE FILMS

Superheterodyne amplification of electromagnetic pulses of finite widths in optical and terahertz ranges is investigated under three-wave interaction with a space charge wave in n-GaN or n-InN films. Space charge waves at the frequencies $f \le 500$ GHz are amplified due to the negative differential conductivity, their finite widths lead to decrease of the amplification. It is considered the three-wave interaction of two counterpropagating electromagnetic waves with the space charge wave in dielectric waveguides based on nitride films placed on a dielectric substrate. This superheterodyne amplification of the electromagnetic pulses is ~30 dB at the distances ≤100 μm.

1. INTRODUCTION

The radiation of the terahertz range f = 100 GHz...30 THz is widely used in spectroscopy, medicine, scanning, and environmental science [1]. Now the sources of the THz radiation are both electron tubes (gyrotrons, backward wave tubes), and lasers. These sources are not well compatible with the traditional millimeter wave devices. An alternative way can be the superheterodyne amplification of electromagnetic waves (EMW) under three-wave resonant interaction in semiconductor films where the negative differential conductivity (NDC) occurs. This method is based on the transfer of amplification of space charge wave (SCW) to the electromagnetic wave at higher frequency.

The amplification of SCW of microwave range in *n*-GaAs films due to NDC was investigated for long time [2]. It was investigated also the transfer of amplification from SCW to EMW at higher frequencies under three-wave interaction [3], i.e. superheterodyne amplification [4]. But the frequency range of amplified SCW in GaAs films is $f \le 50$ GHz. The efficiency of superheterodyne amplification can be improved with using the new semiconductor materials like nitrides GaN and InN [5-6]. These materials possess the following useful properties: the critical fields for observing NDC are high $E_c \sim 100$ kV/cm; an extended frequency range for NDC $f \le 500$ GHz; high temperature stability up till 500 K, NDC under high doping levels $n_0 \le 10^{18}$ cm^{-3}.

In this report the amplification of SCW beams due to NDC is investigated in nitride (GaN, InN) films at the frequencies $f \le 400$ GHz. The finite width of SCW leads to decrease of increments of amplification. For amplification of EM waves in optical and higher part of THz range the superheterodyne amplification is investigated. The superheterodyne amplification of EM waves in waveguides based on nitride films is effective, namely, the values of 20…40 dB can reach at the lengths of 10…50 μm. An influence of the finite widths of EM waves has been taken into account.

2. AMPLIFICATION OF SCW IN NITRIDE FILMS

It is considered *n*-GaN or *n*-InN film of submicron thickness placed on a dielectric substrate, Fig. 1. The nitride film is at $0 < x < 2l$, a dielectric substrate is at $x < 0$. Above at $x > 2l$ there is either vacuum or dielectric. The bias constant electric field is aligned along *OZ* axis, SCW propagate along *OZ* too. The dynamics of SCW is described by the equations of motion of the electron fluid jointly with the Poisson equation for the electric field. At the frequency range $f \le 400$ GHz the simplest diffusion-drift equation can be applied:

$$\frac{\partial n}{\partial t} + div(\vec{v}(E)n - D\nabla n) = 0, \quad \vec{v} = \mu(|E|)\vec{E}; \quad div(\varepsilon_0 \varepsilon(x)\nabla\tilde{\varphi}) = -e(n - n_0), \quad \vec{E} = -\nabla\tilde{\varphi} + E_0 \; (1)$$

Here n is the electron concentration, $\tilde{\varphi}$ is the potential of variable electric field, $\boldsymbol{v}$ is the electron drift velocity, n_0 is an equilibrium electron concentration, which is equal to the donor one; D is the diffusion coefficient, $\mu(E)$ is the electron mobility, E_0 is a bias constant electric field. The data for nitrides GaN, InN are taken from [5,6]. The coordinate frame is aligned along the crystalline axes. The lower indices 1,2,3 are related to the substrate, film, and the region over the film. The corresponding dielectric permittivities in the microwave range are $\varepsilon_1, \varepsilon_2, \varepsilon_3$.

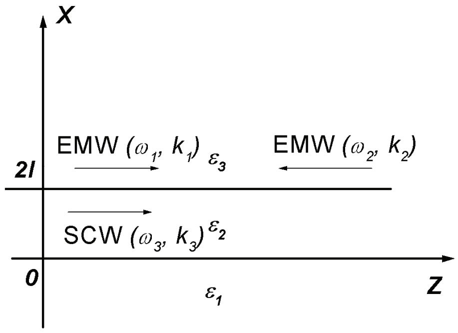

Fig. 1. Geometry of the problem. The region $0 < x < 2l$ is a nitride film, $x < 0$ is a dielectric substrate, $x > 2l$ is either vacuum or dielectric. The interacting waves are two EM waves (ω_1, k_1), (ω_2, k_2), and a space charge wave (ω_3, k_3). The waves are nonuniform along OY axis.

Here the linear amplification of SCW due to NDC is considered. At the surfaces of the film the following boundary conditions are used for the density of the current $\boldsymbol{j}$ [2]:

$$j_x(x=0)=0, \quad j_x(x=2l)=0; \quad \vec{j}=e(\vec{v}(E)n-D\nabla n) \tag{2}$$

Eqs. (1) and (2) have been linearized, and the solutions for the perturbation of electron concentration $\tilde{n}$ and for the variable part of the electric potential $\tilde{\varphi}$ are searched as the travelling wave $\sim exp(i(\omega t-k_z z-k_y y))$. Now an attention is paid to the nonuniform case $k_y \neq 0$. The dispersion equation for SCW $k_z = k(\omega,k_y)$ has been got from the substitution of the partial solutions within each partial region to the boundary conditions (2) and standard electric boundary conditions. In the case of spatial amplification of SCW, when a frequency ω and a transverse wave number k_y are real ($\omega > 0$), the longitudinal wave number is complex. $k_z = k_z' + ik_z''$ ($k_z' > 0$), within a certain frequency range there exists $k_z'' > 0$. The case of NDC is under consideration: $dv/dE < 0$.

The spatial increment k_z'' depends essentially on the value of k_y. It is possible to write down:

$$k_z''(\omega,k_y) \approx k''(\omega,0) - gk_y^2; \quad g \approx 2l\frac{\omega_M}{\omega}\frac{\varepsilon_2}{\varepsilon_1+\varepsilon_3} \tag{3}$$

Here $v_0 = \mu(E_0)E_0$ is the constant part of the drift velocity, $\mu = \mu(E_0) = v_0/E_0$; $\omega_M = en_0\mu/\varepsilon_0\varepsilon_2$ is the Maxwellian relaxation frequency. Therefore, a relatively small transverse nonuniformity of the beam of SCW ≤5 μm results in decrease of amplification, because the value of $\omega_M \sim 10^{13}$ s^{-1} is high.

The parameters of the zinc blende n-GaN have been used: the electron concentration is $n_0 = 2\times10^{17}$ cm^{-3}, the bias electric field is $E_0 \approx 150$ kV/cm, the drift velocity is $v_0 \approx 2.4\times10^7$ cm/s; the thickness of the film is $2l = 0.5$ μm; the permittivity of GaN in the microwave range is $\varepsilon_2 = 9.7$; the permittivities of contacting regions are $\varepsilon_1 = \varepsilon_3 = 3{,}9$ (SiO_2). The amplification of transversely uniform SCW occurs in the frequency range $f \leq 400$ GHz and the maximum value of the spatial increment is $k_z'' \approx 2\times10^4$ cm^{-1} at the frequency $f \approx 150$ GHz. When compared with n-GaAs films, in n-GaN films it is possible to obtain the amplification of SCW at essentially higher frequencies $f \geq 200$ GHz. For n-InN films the results are similar to n-GaN ones, but the bias electric field can be lower, $E_0 \sim 100$ kV/cm, and the concentrations can be even higher than in GaN, $n_0 \leq 2\times10^{18}$ cm^{-3}.

3. SUPERHETERODYNE AMPLIFICATION OF EM WAVE BEAMS

The nitride film is the waveguide for EM waves when the condition is satisfied: $\varepsilon_{2EM} > \varepsilon_{1EM}, \varepsilon_{3EM}$. Here $\varepsilon_{1,2,3\,EM}$ are corresponding permittivities in optical or THz ranges, which differ from their values in the microwave range due to frequency dispersion [5-8]. In such a dielectric waveguide it is possible to realize the resonant three-wave interaction of the following waves localized along *OX* axis: forward EMW at the frequency ω_1 and the longitudinal wave number k_1, backward EMW ω_2, $-|k_2|$, and SCW ω_3, k_3. The resonant conditions are, see Fig. 1:

$$\omega_3 = \omega_1 - \omega_2, \quad k_3 = k_1 + |k_2| \qquad (4)$$

The frequencies of EMW and SCW are of about: $\omega_{1,2} \sim 10^{14}...10^{15}$ s^{-1}, $\omega_3 \approx 2\omega_1 \times (v_0 \varepsilon_{2EM}^{1/2}/c) \sim 4\times10^{11}...4\times10^{12}$ s^{-1} ($f_3 = \omega_3/2\pi \sim 70…700$ GHz) in the case of *n*-GaN film. Here $v_0 \approx 2.4\times10^7$ cm/s is the velocity of SCW [5,6].

The nonlinear interaction is due to the modulation of the permittivity in the optical range (at higher frequencies) by SCW and due to the ponderomotive action of EMW to SCW in the microwave range (at lower frequencies). In the case of moderate nonlinearity it is possible to describe this resonant interaction by means of slowly varying wave amplitudes [3,4,7,8].

For EMW the Maxwell equations are:

$$\nabla \times \vec{H} = \varepsilon_0 \varepsilon(x) \frac{\partial \vec{E}}{\partial t} + \vec{j}, \quad \vec{j} = e(n_0 + \tilde{n})\vec{v}; \quad \nabla \times \vec{E} = -(1/\varepsilon_0 c^2)\frac{\partial \vec{H}}{\partial t}, \quad m^* \frac{\partial \vec{v}}{\partial t} \approx e\vec{E} \qquad (5)$$

Here m^* is the effective electron mass, $\tilde{n}$ is the variable electron concentration of SCW; $\vec{v}$ is high frequency electron velocity. It is investigated the interaction of transverse electric (TE) EM modes: $E = E_y$, the magnetic field is $\boldsymbol{H} = (H_x, 0, H_z)$.

The solutions of Eqs. (5) and Eqs. (1) are searched in the form:

$$E(x,y,z,t) = \frac{1}{2}(A_1(y,z,t)\exp(i(\omega_1 t - k_1 z)) + A_2(y,z,t)\exp(i(\omega_2 t - k_2 z)))F_1(x) + c.c.$$
$$\tilde{n} = -\frac{i}{2}U(y,z,t)F_3(x)\exp(i(\omega_3 t - k_3 z)) + c.c. \qquad (6)$$

Here $A_{1,2}(y,z,t)$, $U(y,z,t)$ are slowly varying amplitudes for EMW and SCW, $F_1(x)$, $F_3(x)$ are linear transverse profiles of the waves. When using the orthogonality of waveguide modes [8], it is possible to get the coupled equations for slowly varying amplitudes:

$$\frac{\partial A_1}{\partial z} + \frac{1}{v_1}\frac{\partial A_1}{\partial t} + \frac{i}{2k_1}\frac{\partial^2 A_1}{\partial y^2} + \Gamma_1 A_1 = \alpha_1 A_2 U; \quad \frac{\partial A_2}{\partial z} - \frac{1}{v_2}\frac{\partial A_2}{\partial t} - \frac{i}{2|k_2|}\frac{\partial^2 A_2}{\partial y^2} - \Gamma_1 A_2 = \alpha_1 A_1 U^*;$$
$$\frac{\partial U}{\partial z} + \frac{1}{v_0}\frac{\partial U}{\partial t} - g\frac{\partial^2 U}{\partial y^2} - \Gamma_3 U = \alpha_3 A_1 A_2^*; \quad g \approx 2l\frac{\omega_M}{\omega}\frac{\varepsilon_2}{\varepsilon_1 + \varepsilon_3} \qquad (7)$$

Here the dissipation coefficients for EM modes have been introduced $\Gamma_1 = \Gamma_2$; $\Gamma_3 > 0$ is the increment of spatial amplification of SCW that has been considered in Sec. 2 (at $k_y = 0$). One can see that the transverse nonuniformity of EMW leads to diffraction [8], whereas the nonuniformity of SCW appears like the diffusion.

The expressions for the coefficients α_1, α_3 are:

$$\alpha_1 = \frac{\omega_p^2}{4c^2 k_1}\frac{S}{\int_{-\infty}^{+\infty} F_1^2(x)dx}; \quad \alpha_3 = \frac{ie\mu_d k_1 k_3}{m^* \omega_1^2}\frac{S}{\int_0^{2l} F_3^2(x)dx}; \quad S = \int_0^{2l} F_3(x)F_1^2(x)dx \qquad (8)$$

Here S is the overlap integral of transverse profiles of EM modes with SCW along *OX* axis. Note that the coefficient α_3 is complex. Our calculations have shown that the value of the overlap integral is maximum $S \approx 1$ in the symmetrical dielectric waveguides for the fundamental EM modes. The transverse profiles are normalized as $\int_{-\infty}^{+\infty} F_1^2(x)dx = \int_0^{2l} F_3^2(x)dx = 1$ μm. It is possible to use the following structures of dielectric waveguides: the substrate SiO_2 – *n*-GaN (or *n*-InN) film– SiO_2; AlN – *n*-GaN film – AlN. The electron concentration is $n_0 = 2\times10^{17}$ cm^{-3}, the thickness of the film is $2l = 0.5$ μm, the permittivities in the optical range are $\varepsilon_{1\,EM} = \varepsilon_{3\,EM} = 2$ (SiO_2); $\varepsilon_{2\,EM} = 5.8$. The frequencies of the EMW are $\omega_1 \approx 6.5\times10^{14}$ s^{-1}, the corresponding resonant frequency of SCW is ω_3

$\approx 2.2\times10^{12}$ s^{-1} ($f_3 \approx 350$ GHz); the permittivities in the millimeter wave range of the media are $\varepsilon_1 = \varepsilon_3 = 3.9$, $\varepsilon_2 = 9.7$.

It is investigated the superheterodyne amplification of a weak input pulse of EMW at the carrier frequency ω_1, i.e. the transfer of amplification of SCW due to NDC to EMW at higher frequency in the presence of the pump EMW at the frequency ω_2. For this case the Eqs. (7) are added by the boundary conditions:

$$A_1(z=0, y, t) = A_{10}\Phi(t)\cdot\Psi(y); \quad A_2(z=L_z, t) = A_{20}; \quad U(z=0,t)=0 \quad (|A_{20}| >> |A_{10}|), \quad (9)$$

where A_{10} is a maximum amplitude of the weak input pulse at the frequency ω_1, $\Phi(t)$ is the temporal shape of the pulse, $\Psi(y)$ is its transverse shape; A_{20} is the constant amplitude of the EM pump wave.

The mechanism of the superheterodyne amplification is as follows [3,4]. Because of the three-wave interaction, the mixing of two EMW results in the generation of SCW at lower frequency. Then SCW is amplified in a medium with NDC. In that turn, in the output of the system the amplified EM wave appears at the frequency ω_1.

Direct numerical simulations of Eqs. (7), (9) have shown the amplification of EM pulses of 0.1...20 ns durations. The amplified EM pulse preserves its shape. The numerical estimations for the *n*-GaN or *n*-InN film with the electron concentration $n_0 = 2\times10^{17}$ cm^{-3} of the thickness $2l = 0.5$ μm have demonstrated that it is possible to get the amplification of EMW 20...40 dB at the waveguide length ≤ 100 μm; the intensity of EM pump wave is ≈100 kW/cm^2. The frequency of SCW is $\omega_3 \approx 1.5...4\times10^{12}$ s^{-1}, the frequencies of EMW are $\omega_{1,2} \approx 3\times10^{14}...10^{15}$ s^{-1}. Transverse bell-like nonuniformity $\Psi(y)$ is not important, when the width of the input EM pulse is greater than 5 μm.

4. CONCLUSIONS

Amplification of space charge waves at the frequencies $f \le 400$ GHz in the dielectric waveguides based on *n*-GaN or *n*-InN films can reach the values of 20 dB at the distances of 20 μm. The transverse nonuniformity of SCW beams leads to decrease of increments of amplification.

The transfer of amplification under three-wave resonant interaction from the space charge wave to the electromagnetic wave at higher frequencies $\omega_1 \sim 10^{14}...10^{15}$ s^{-1} can be realized in dielectric waveguides based on nitride films of 0.5 μm thicknesses with electron concentrations ~2×10^{17} cm^{-3}. This superheterodyne amplification can reach 20...40 dB at the lengths 10...100 μm.

The work is supported by SEP-CONACyT, Mexico.

REFERENCES

1. *P.H. Siegel*, Terahertz Technology. ***IEEE Trans. MTT,*** Vol. 50, No 3, pp. 910-919, **2002.**
2. *A.A. Barybin*, Waves in Thin Film Semiconductor Structures with Hot Electrons. Moscow, Nauka, 1986, 288 pp. (in Russ.).
3. *S. Koshevaya, V. Grimalsky, J. Escobedo-Alatorre, and M. Tecpoyotl-Torres,* Superheterodyne amplification of sub-millimeter electromagnetic waves in an *n*-GaAs film. Microelectronics Journal, Vol. 34, No 4, pp. 231-235, 2003.
4. *A.L. Kalapusha, N.Ya. Kotsarenko,* Acoustoelectronic parametric amplification of EM waves of infrared and optical ranges in planar optical waveguides. Radioelectronics and Communications Systems (Izv. VUZ, Radioelektron.), Vol. 26, No. 5, pp. 71-72, 1983.
5. *M.E. Levinshtein, S.L. Rumyantsev, and M.S. Shur,* Properties of advanced semiconductor materials: GaN, AlN, InN. N.Y., Wiley-Interscience, 2001, 280 pp. (www.ioffe.ru/SVA/NSM/Semicond/GaN/)
6. *S.C. Jain, M. Willander, J. Narayan, and R. Van Overstraeten,* III-nitrides: growth, characterization, and properties. Journ. Appl. Phys., Vol. 87, No 3, pp. 965-1006, 2000.
7. *G.E. Chaika, V.N. Malnev, M.I. Panfilov,* Interaction of light with space charge waves. Proc. SPIE, Vol. 2795, pp. 279-285, 1996.
8. *D. Marcuse,* Theory of Dielectric Optical Waveguides. N.Y., Academic Press, 1991, 470 pp.

UDC 621.396.96

Yu. A.Averyanova, Candidate of Technical Science, (National Aviation University, Ukraine)

MODERN AND PROSPECTIVE METHODS FOR DANGEROUS METEOROLOGICAL PHENOMENA OBSERVATION

In this paper the modern and prospective polarimetric methods and approaches for obtaining information about dangerous weather phenomena are considered and analyzed. The advantages that indicate the novel possibilities of the modern and prospective onboard systems are shown. The consideration is made from the position of creating global network for data obtaining, transmission and exchange.

Introduction. Operative and reliable meteorological information is one of the main components required to keep and enhance the safety level of aviation under the modern tendencies of aviation development [1]. The modern tendencies including the prospective global air traffic control (ATC) as well as CNS/ATM and Free Flight concepts implementation demand:

- developing the distributed ATC system that allow to adopt operatively the aircraft flight trajectory to the constantly changed flight conditions and
- reducing the human factor influence.

The realization of mentioned demands requires the development and uses of the high-tech systems for information obtaining, exchange and distribution. The key moment in the system is possibility for the aircraft crew to make operative access to the necessary information.

Different concepts were proposed recently and used partly to advance the aviation to the modern tendencies and requirements. In [2] the overview and requirements to the AMDAR (Aircraft Meteorological Data Relay) system are presented. The AMDAR system implies the commercial aircrafts equipment with apparatus for automatic atmospheric parameters measurements and further transferring the information to the corresponding services. The similar concepts for combined operation of fixed and dynamic networks to obtain and disseminate meteorological information were proposed in [3, 4]. In these works the aircrafts are considered as dynamic platforms for measuring devices to obtain meteorological information at any stages of the flight. In [5,6] the similar system is proposed for use with ADS-B system as well as A Next Generation Aviation Safety Strategic Goal proposes in [7]. The ADS-B IN/OUT system [8] gives possibility to make operative data exchange between aircrafts, aircraft and ground services. The system allows to select the optional information from those dynamic sensor (aircraft) the position of which is the most interesting for aircraft crew. This is important ability of the system helps aircraft crew to take a decision under the conditions of air traffic growth.

Modern level of technological achievements allows aircrafts not to be only a platform for the set of devices for measuring standard atmospheric parameters but to be an integral unit for quite operative obtaining, processing and indicating complex weather phenomena information. Therefore it is reasonable to develop and use the multifunctional systems that can make operative alert about dangerous phenomena presence along the flight rout. In this paper the overview of the novel technologies and methods for remote sensing of atmosphere is made. All of the presented methods and techniques are possible to use for operative detecting dangerous weather phenomena during the aircraft flight.

Novel and prospective abilities of onboard systems to obtain operative meteorological information. In [9] the overview of the modern radars possibilities is made. The work [9]

- proposes to use the new Doppler-Polarimetric radars to obtain information about wide range of meteorological phenomena,
- shows the possibilities of Doppler-Polarimetric approach,

- proposes algorithms for obtaining diagnostic and prognostic information about microstructure, dynamics, behavior of meteorological formation, including algorithms for estimating level of hazard.

Nowadays, the aircraft crew uses synoptic information mostly for familiarizing with icing-in-flight and even thunderstorm location and trajectory. The real situation about icing intensity, ice shape and type usually gets clear due to performances change when flying or even after landing. However the operative information about cloud microstructure would be useful for flight trajectory correction when avoiding getting into hazardous region.

In [9, 10, 11] the standard Doppler –Polarimetric characteristics of reflected from weather object radar signals are used to detect dangerous icing-in-flight regions and regions of hail activity. These characteristics are Differential Reflectivity $Z_{DR} = 10\log\frac{|S_{hh}|^2}{|S_{vv}|^2}$ and Linear Depolarization Ratio $L_{DR} = 10\log\frac{|S_{hv}|^2}{|S_{vv}|^2}$. The Differential reflectivity Z_{DR} operates with so called co-polarized Doppler spectra S_{hh} and S_{vv}, the Linear Depolarization Ratio L_{DR} considers also cross-polarized component of Doppler spectrum S_{hv}. The cross-polarized component is obtained when Doppler –polarimetric radar transmits signal of horizontal polarization and receives reflected from weather object signal of vertical polarization or vice versa. The comparison of these parameters allows to make a conclusion about shape of clouds or precipitation constituents.

In [12] the possibility to use polarimetry for dynamic atmospheric phenomena detection is considered. The approach is based on the fact that that the influence of wind phenomena including atmospheric turbulence on liquid hydrometeors leads to changing their shape and spatial orientation. As a result, the electromagnetic wave changes their polarization with respect to the sounding wave polarization when reflection from the hydrometeors assemble. Therefore the value and character of changing polarization angle of reflected electromagnetic wave are the informative parameters that characterize the degree of phenomena influence on the hydrometeors. In [13] the weather objects like collection of water droplets are considered as vibrating objects with unstable shape. The polarimetry is proposed for use in this work to evaluate the drops vibration impact into the reflected radar signal to improve the estimate of dropsize distribution, rain intensity and dynamic phenomena influence.

In [14, 15] the polarimetric radar that is possible to realize with the set of receiving antennas or phase array antenna for onboard realization is presented. The approach presented in [14, 15] relates polarimetric radar parameters with turbulence and other wind phenomena. The approach is based on the notion of polarization spectrum, that is, the reflected energy distribution over polarization components. The approach and device presented in [14, 15] allow to evaluate the wind related phenomena intensity with the change of polarization spectrum components avoiding bulky calculations and processing operations. This fact is important for operative detection of the phenomena that influence aviation and flight operation.

In [16] the approach that allows to estimate signal depolarization caused by dynamic atmospheric processes using a single transmitter-receiver antenna with definite polarization properties is proposed. The proposed approach allows to make a selection of reflected signal low frequency component change due to depolarization caused by turbulence or other wind phenomena from changes caused by other factors. The profit of unipolarized antenna use is that the amplitude fluctuations of reflected signal in the receiving antenna have higher energetic level than signals received with cross-polarized antenna. This fact can simplify separating the net components of reflected signal from noises. The given approach can be realized on the base of modern weather radars including Doppler weather radars. This fact is promising for enlarging Doppler weather radars possibility for wind related phenomena determination.

To classify turbulence by its intensity taking into account polarization characteristics of reflected from weather object signals is proposed in [17]. In work [17] the simulation of turbulence detection is based on the approach presented in [16], and then turbulence classification by its intensity is made using the statistical data about variance of random process of low frequency (LF) component change as information parameter. The classification of turbulence by its intensity according accepted ICAO criterion into light, moderate and strong is shown in Fig.1. The level of integrated probability of errors for turbulence of different intensity lies along ordinate axis. Solid line corresponds to the integrated probability of error as a threshold function when detecting strong turbulence. Dotted line corresponds to the integrated probability of error as a threshold function when detecting moderate turbulence. Dashed line shows the integrated probability of error as a threshold function when detecting severe turbulence. The value of variance of random process of LF component change due to change of polarization angle of reflected from weather object wave (informative parameter) lies along abscises axis.

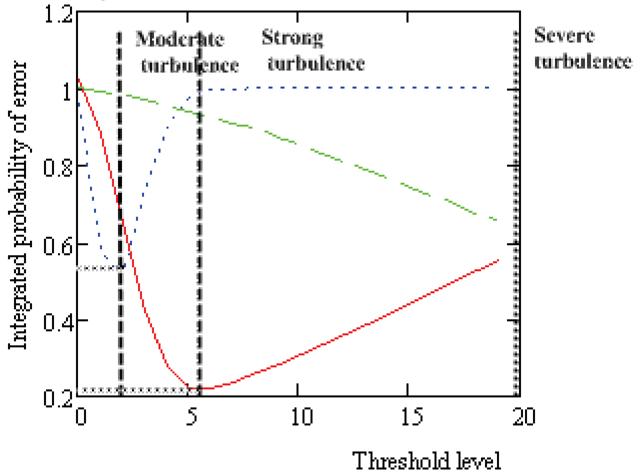

Fig.1 Turbulence intensity classification

The vertical dotted lines separate the regions for informative parameter values that correspond to different intensity of turbulence taking into consideration the minimum values of integrated probability of error for relevant turbulence intensity. The separation of strong turbulence from moderate is possible to make at higher level of probability than separation of moderate from light. The minimum integrated probability of error is achieved when detection of strong turbulence. It has the order of about 0.1. It is important to note that this level corresponds to the results obtained with some other methods for turbulence detection and classification, for example when Doppler spectrum width is used for turbulence intensity estimate [18].

One more hazard to aircraft flights that need operative estimate is volcano ash clouds. The necessity for operative detection of volcano ash clouds during the aircraft flight is provided by some peculiarities of volcano ash behavior. The peculiarities are:

- volcano ash clouds can be present at different layers of atmosphere during quite long period dependently synoptic situation;
- volcano ash clouds can be distributed over large areas with dangerous concentration of abrasive particles;
- volcano ash clouds can travel with wind far away from the source of origin;
- the possible harm to the aircraft depends on the micro particles nature of volcano ash clouds;
- the harmful sequences of ash particles ingress can be revealed far off the volcano ash cloud.

As it was mentioned, the volcano ash clouds distribution depends on wind conditions at different atmospheric layers significantly. The wind conditions of the atmosphere are the subject to change; therefore it is very important to have operative information about volcano ash areas and abrasive particles concentration in them. In [19, 20] the different approach to detect volcano ash clouds with onboard systems is proposed. The work [21] mentions the possibility to distribute the operative information amongst the concerned customers with novel systems of data exchange (ADS-B, Mode-S, AMDAR).

Conclusions. In this paper the novel possibilities for onboard radar systems were analyzed. The special emphasis was paid on the systems enable to make polarization analysis of reflected from weather objects radar signals. The common advantages of the presented methods and approaches for aviation related tasks are:

1. The use of polarimetry in the conventional radar systems and Doppler radar systems for traditional tasks (microstructure identification) as well as for quite untraditional solutions (wind related phenomena detection and estimate) enhances onboard equipment possibilities significantly.
2. The combined use of Doppler and polarimetric technique allows to obtain many-sided information about dangerous atmospheric phenomena. As a result, the evaluation of the possible influence on flight operation can be more correct.
3. Some of the presented polarimetric approaches [14,15] do not require complicated signal processing and can be profitable when temporal restrictions for dangerous phenomena detection, for example when onboard detection of severe weather connected with wind.
4. The other benefit of the polarimery is that the presented approaches are possible to realize on the base of modern equipment avoiding expensive developing of separate devices.

The mentioned advantages indicate the novel possibilities for the modern and prospective onboard systems. It allows us to consider the aircrafts not only as customers of information but as an dynamic element for comprehensive meteorological information obtaining in the global aviation transport network. The use of aircraft as dynamic element for complex meteorological information obtaining and dissemination will help to develop the distributed ATC system that allow to adopt operatively the aircraft flight trajectory to the constantly changed flight conditions as well as to reduce the human factor influence on the aviation transport network operation.

References

1. *World* Wide CNS/ATM Systems Implementer// ICAO, RIO Conference 1998.
2. Global Observing System, www.wmo.ch/web/www/OSY.GOS.html
3. *Яновский Ф.И., Фишман Б.Е.* Анализ возможностей повышения информативности наблюдений за атмосферным электричеством. "4 Всесоюзный симпозиум по атмосферному электричеству": Тезисы докладов, Нальчик, 1990, С. 23-24
4. *Яновский Ф.И.* Концепция единой сети наблюдений атмосферного электричества и опасных метеоявлений. "Пассивная радиолокация гроз". Доклад на Научном совете АН СССР по проблеме "Статистическая радиофизика", Препринт. - Рига, 1990, С. 1-10.
5. *Yanovsky F.J.*, Weather Data Obtaining and Dissemination Using ADS-B
6. Аверьянова Ю.А., Яновський Ф.Й., Динамічна складова глобальної інтерактивної мережі одержання та обміну метеорологічними даними, Вісник -К.: НАУ, 2011. Том 4- стор. 36-41
7. *Darr S., Ricks W., Lemos K.A.,* Safer Systems: A NextGen Aviation Safety Strategic Goal// IEEE Aerospace and Electronic SYSTEMS Magazine. – June 2010, ISSN 0885-8985 - Volume 25, #6 - p.9-14
8. Major Contractfor ADS-B Weather System, Safety and Technology Trends, Monday, March, 31, 2008, http//: www.aviationtoday.com/asw/categoris/military/20657.html
9. *Yanovsky F., Averyanova Yu.***,** New Concept of Multifunctional Weather Radar/ Proceedings of International Radar Symposium (IRS 2009), 09-11 September, 2009, Hamburg, Germany, pp.449-455.
10. Braun I.M. Development and investigation of hail detection algorithms. Second World Congress "Safety in Aviation" // MRRS 2005, September 19-21, 2005, National Aviation University, Kiev, Ukraine, pp.155-158. *PitercevA.A. and Yanovsky F.J,* Polarimetric Method of

Remote Predicting a Zone of Icing-in-Flight in Clouds and Precipitation, Microwaves, Radar and Remote Sensing Symposium (MRRS 2011). Kiev. – 220-223.

11. Averyanova Yu. 2004, 'Use of Doppler-Polarimetric parameters for wind phenomena localization', Proceedings of the 34th European microwave Week (EuRAD 2004,), 11-15 October, Amsterdam, The Netherlands - pp. 29-32.

12. Yuliya Averyanova, Echo-Signal from Hydrometeors. Spatial and Temporal Estimation of Polarization Spectrum Components // Proceedings of International Radar Symposium (IRS 2011), 7-9 September, 2011, Leipzig, Germany , pp. 263-266. ПАТЕНТ на корисну модель Поляриметричний радіолокатор/ *Авер'янова Ю. А., Аверьянов А. О., Яновський Ф. Й.* - № u200804248; заявл. 04.04.2008; опубл. 26.08.2008, Бюл. № 16.

13. *Averyanova Yu., Averyanov A., Yanovsky F.J.* Polarization signal components estimate in weather radar: Proc. of 12th Intern. Conf. on Mathematical methods in electromagnetic theory. – Odessa, 2008. - P. 360-362.

14. *Averyanova Yu., Averyanov A., Yanovsky F.J.* Influence of turbulence onto Depolarization of Signals Rflected from Hydrometeor,- Proc. Of International Radar Symposium (IRS 2010), Vilnus. – 501-504.

15. *Averyanova Yu., Yanovsky F.J., Averyanov A.,* Turbulence intensity classification based on estimating statistical polarimetric parameters of radar reflections from rain, - Proc. of Statistical Methods and Signal and Data Processing (SMSDP 2010), Kiev.- 95-98.

16. F.J. Yanovsky, *Meteorological-navigation Radar systems of Air Vehicle,* - Kiev, Publishing House of NAU, 2003, - 304p. (In Ukrainian).

17. *F.S.Marzano, G. Vulpiani, and W.I.Rose,* Meteorological Characterization of Microwave Radar Reflectivity Due to Volcanic Ash Clouds, IEEE Transactions on Geoscience and Remote Sensing, Vol.44, No.2, February 2006, pp.313-327.

18. ESA Earth Observation Mission Science Division, University of Munich, Meteorological Institute, 2010, Website: http://www.esa.int/esaLP/SEMJTTF098G_index_0.html

19. *F.Yanovsky.* Specified for Air Safaty, Monitoring Atmospheric Phenomena Including the Volcano Dust, Proceedings of Interational Radar Symposium (IRS 2010), 16-18 June, 2010, Vilnius, Lithuania.

UDC: 517.518.45

N. A. Mironov, Candidate of Science (Eng)
(National Aviation University, Ukraine)

TRANSIENT PROCESSES AND THE FOURIER TRANSFORM

The Fourier transform is widely used for analysis of linear electric systems. However, in case of transient analysis leading to distortion of information in electronic information systems, the Fourier transform is not widely applied due to the constraints that are traditional for this method. The main restrictions are:

a) requirement of absolute integrability of the processes in the system;

b) assertion about the applicability of the Fourier method at zero initial conditions only.

Therefore, the analysis of transient processes refers traditionally to Laplace transform method, which is considered free of these shortcomings of the Fourier method. Moreover, to date numerous tables of direct and inverse Laplace transform are prepared.

In view of the foregoing, the analysis of the systems and transients in them is normally conducted by different methods. This causes some technical disadvantages. In addition, the Laplace transform does not satisfy the needs of practice in full [1]. The purpose of this paper is to modify the Fourier transform method to cover the problems of transient process analysis in electrical systems by overcoming the conventional restrictions on the use of this method.

In the following discussion we take into account that in Laplace transform, the requirement of absolute integrability can be eliminated by multiplying of the investigated processes by the decaying exponential multiplier. Because of this, however, the processes must be only "one-sided". One-sided process is identically equal to zero for negative moments. This is not significant in most cases for the calculation of transients in electric power systems or systems of power electronics. However, in some cases, a two-sided process should be considered as an adequate model.

In the recent publication [1] a different modification of the Fourier transform was proposed: Fourier transform on the complex plane (FTCP), where processes may be one-sided or two-sided, and not necessarily integrable completely. In work [1] it was also shown that for the calculation of FTCP, the existing tables of direct Laplace transform can used. So, by using PFKP the requirement of absolute integrability of the studied processes eliminated.

Regarding the initial conditions, in the paper we show that they are necessary in case of applying the Laplace transform. In case of the Fourier transform method applied, the initial conditions are taken into account automatically, if free processes, which appear at the time of commutation, are modeled by two-sided processes.

Conclusions. Based on the results of the analysis and the examples illustrating these results, it is reasonable to conclude the following:

- when the Fourier transform method is used for transient process analysis, the requirement of absolute integrability of the processes can be easily removed if we apply (if necessary) the Fourier transform on the complex plane;
- when calculating the transient processes using Fourier transform, non-zero initial conditions are taken into account automatically in case of application of two-sided free process models;
- implementation of the above-mentioned conditions does not increase the complexity of calculations.

Thus, it has shown that the method of the Fourier transform can be used as a single analysis method for linear systems and transient processes in these systems.

References

1. Mironov N. A. Fourier transform on the complex plane // Radiotekhnika. – 2004. –No 6. –P. 71–77.

UDC: 621.396.96

A. N. Mikolushko, Ph.D. Student, Engineer
(National Aviation University, Ukraine)

RADAR DETECTION OF VOLCANIC ASH CLOUD: MAXIMUM RANGE

This work is devoted to properties of a volcanic ash and methods of its monitoring with use of polarimetric radar. Maximum range of volcanic ash zones radar detection in the atmosphere is estimated.

Introduction

The termination of air traffic over Europe, caused by ashes cloud after a volcanic eruption, forced the world community to start to develop more effective strategy connected with emission of volcanic ash influence on safety of flights. Such strategy should be based on exact information on real extent of presence of a volcanic ash in air space and about its possible influence on the aircrafts which have appeared in such overcast. For this reason in addition to detection and monitoring of dangerous zones in the troposphere, connected with meteorological formations, zones of a volcanic ash should be considered also as objects of surveillance in connection with safety of flights, ecological and economic safety.

Characteristic of particles of a volcanic ash

Volcanoes are powerful sources of a dust matter, releasing into atmosphere the enormous quantity of a smoke and a volcanic ash [1]. In effect, the volcanic ash represents extremely small particles of the sprayed rock which structure reflects composition of the magma which is in a volcano. Therefore the structure of clouds of a volcanic ash is differed depending on a concrete volcano. However as a whole it consists mainly of silica (> 50 %) and in smaller quantities of oxides of aluminum, iron, calcium and sodium. Silica is present at ashes in the form of glass silicates and under an electronic microscope reminds small splinters of glass with keen edges. This glass silicate material possesses big hardness and possesses extremely high abrasive properties.

Besides of the abrasive character of a volcanic ash, its other important property is the temperature of melting. As the volcanic ash consists mainly of the glass silicates which temperature of melting (~1100°C) is lower than temperature in the jet engines working at the mode of normal draft (1400 °C), it can be melted and be postponed in the heated part of the main contour of the engine that conducts to its serious damages.

The firm mass which is thrown out at volcanic eruptions is highly various and includes components of the size from extremely small particles (< 5 mm) to large pieces of rock. The average size of particles in a cloud of volcanic ash decreases over time in process of subsidence of larger and heavier particles from this cloud. Concentration of ashes depends on height of lifting of initial ash column and weather conditions, such as wind speed and wind shift at different heights, and also on drop temperature. As a whole the term "volcanic ash" belongs to the description of particles < 2 mm in diameter. Clouds of volcanic ash, with which aircraft are faced more often, consist of the smallest particles (< 0,1 mm in diameter) [2].

As a rule, clouds of ash are formed above the flight level 6100 m (FL200), but the bottom border of an initial cloud depends on height of the volcanic crater and speed of the eruption of volcanic material. First of all, visible signs of volcano eruption are huge white clouds of steam if the crater is located below the ice cover. Clouds of steam rise continuously and often mask by itself the ash ejections which almost always occur in chaotic sequence [1].

Assessment of possibility of detection

Taking into account that an ash cloud can be compared with a cloud of hydrometeors of the various sizes, shapes and microphysical parameters, the methods developed for detection of meteoformations, their identification and recognition, can be possibly, adapted and used for the purpose of monitoring of a volcanic dust [3-5, 15].

One of widely used models of particle size distribution is gamma distribution in the following shape:

$$N(D) = N_0 D^{\mu} e^{-\Lambda D^{\mu}} \quad . \tag{1}$$

Graphic representation of this distribution is presented in Fig. 1 at Λ=4 and three values of parameter μ =1; 1,5; 2. Axis x is equivalent diameter of scatterers, and y axis is number of particles of this diameter in the unit of volume [14].

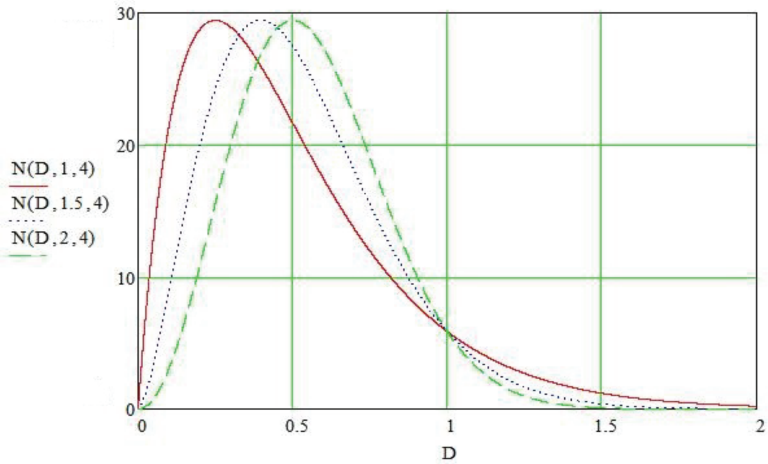

Figure 1. Model of distribution of particles of a volcanic ash in the sizes

Similarly to the case of radar detection of precipitation, we will use a parameter of reflecting object of a volcanic origin - radar reflectivity factor Z [$\mathrm{mm}^6/\mathrm{m}^3$] which is the zero moment of function of particles distribution in the sizes

$$Z = \int_{D\min}^{D\max} N(D) D^6 dD, \tag{2}$$

where $D_{\min}$ an $D_{\max}$ - the minimum and maximum sizes of scatterers in the reflecting volume respectively. The value Z is the characteristic of the most reflecting object.

Let's make a quantitative assessment of radar reflectivity factor of volcanic ash. Let N_0=320, Λ=4; μ=1 that provides a good consent of model (1) with data of real measurements [6], and limits of integration $D_{\min}$=0, $D_{\max}$=2 (according to Fig. 1).

As follows from equation (2) radar reflectivity factor is equal $Z = 13{,}462\mathrm{mm}^6/\mathrm{m}^3$. Let's estimate the power of the reflected signal P_r at the input of radar receiver, proceeding from the equation of a radar-location of the meteorological volume distributed targets [7].

$$P_r = \frac{0{,}75 P_t G_a \tau c Z 10^{-18} K_{\varepsilon}}{\lambda (R \cdot 10^3)^2}, \tag{3}$$

where P_t - power of sounding pulse; G_a - antenna gain; τ - duration of a sounding pulse; c - velocity of light; K_{ε} - the factor depended on complex dielectric permittivity of a particle substance; λ - wavelength; R - range the reflecting volume under study.

Let us parameters of a radar system are: $P_t = 10\mathrm{kW}$, $G_a = 1000$, $\lambda = 3{,}2\,\mathrm{cm}$, $\tau = 2$ μs; and the parameters of the object under study are: $Z = 13$ and $K_{\varepsilon} = 0{,}4$ that is a typical value for volcanic ash [14]. In Fig. 2 the result of power calculation of capacity of the reflected signal from range is given at the specified parameters.

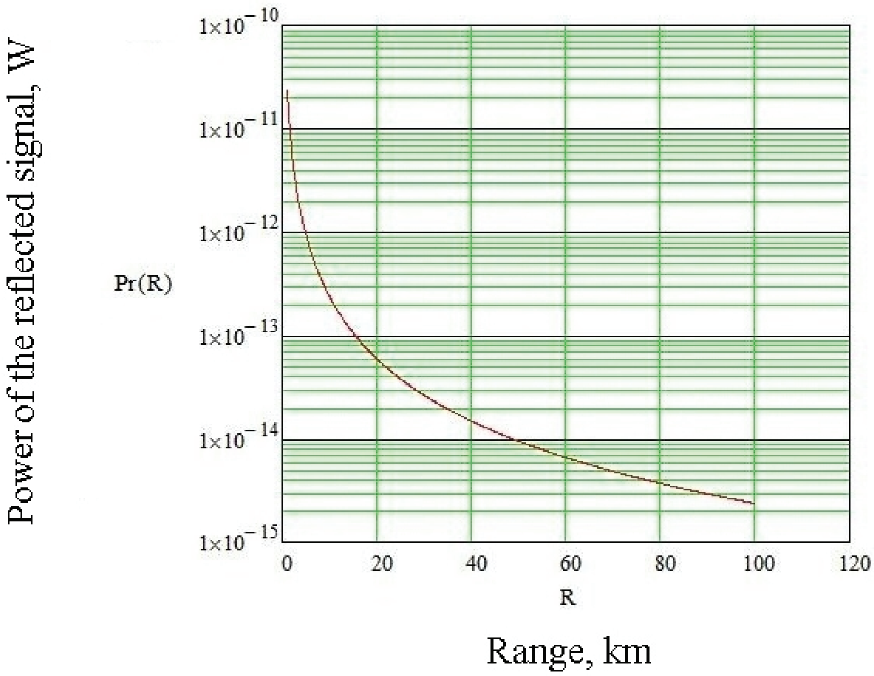

Fig. 2. An assessment of power of the reflected signal

Thus, calculation shows that airborne X-band radar is able to detect a signal reflected from a cloud of volcanic ash at range, sufficient for pilot's decision-making. From the plot it is seen that sensitivity of 10^{-14} W corresponds to the maximum detection range of around 50 km.

For application of methods of recognizing hydrometeors [3-5] and selecting zones of volcanic ash detected, it is necessary to provide polarimetric properties to the radar. This is quite real technical task [10].

Taking into account that volcanic ash is considered as a kind of atmospheric aerosol, it can be advisable to use millimeter radar [8] for monitoring volcanic ash zones.

The assumption about scatterers noncoherence allows to consider that the total radar cross section (RCS) of a set of scatterers will be equal to the sum of RCSs separate particles which simultaneously take part in formation of the reflected signal [10]:

$$\sigma_s = \sum_{\Delta V} \sigma_i \,, \tag{4}$$

where σ_i - the RCS of separately taken i-particle.

Let's introduce a value of the specific RCS, which characterizes reflecting properties of a volume unit.

$$\sigma_0 = \sum_i N_i \sigma_i (D_i, \lambda) \,, \tag{5}$$

where N_i is the number of particles of size D_i in a volume unit, $\sigma_i(D_i,\lambda)$ is RCS of an i-th particle at wavelength λ.

Consider that

$$\sigma_s = \sum_{\Delta V} \sigma_i = \sigma_0 \Delta V = \frac{1}{8} \pi R^2 \theta_{0,5}^2 \tau c \sigma_0 \,, \tag{6}$$

where $\theta_{0,5}$ is the width of the sector-shaped antenna pattern (at a half power level).

The cloud can consist of particles of different sizes, but as a part of reflectors there can be one prevailing reflector which gives the stable reflected signal that corresponds to a picture with effect of a bright point. Then, if the radius of a particle is known, say, $r_i = 0.05$ mm, and if we consider a prevailing reflector as a dielectric sphere, then [8, 12]:

$$\sigma_i = \left(\frac{\sqrt{\varepsilon}-1}{\sqrt{\varepsilon}+1}\right)\pi r_i^2, \tag{7}$$

where ε is dielectric permittivity. As volcanic ash consists mainly of silica, i.e. silicon dioxide SiO_2 ($\varepsilon = 3.9$), and clouds of a volcanic ash which are faced aircrafts generally consist of particles less than 0,1 mm in diameter, then having accepted $r_i = 0.05$mm, and for example $\theta_{0.5} = 3$, we receive $\sigma_i = 2.5 \cdot 10^{-3}$. Then, if for example, $N_i = 1000$ having substituted (7) in (5) we receive, $\sigma_0 = 2.5$ and $\sigma_S = 5 \cdot 10^{14}$:

Let's try to calculate the maximum range at which the cloud of particles [11] can be revealed:

$$R_{\max} = \sqrt[4]{\frac{P_t}{P_r} \cdot \frac{G_a \cdot S_a \cdot \sigma_s}{(4\pi)^2}}, \tag{8}$$

where S_a is the effective antenna aperture, and P_r is the power of the accepted signal defined by sensitivity of the receiver [11], which

$$P_r = \frac{P_t \cdot G_a \cdot S_a \cdot \sigma_s}{(4\pi)^2 R^4}, \tag{9}$$

where $R = 150$ km.

The effective antenna aperture S_a is connected with an antenna gain G_a [13]:

$$S_a = \frac{G_a \lambda^2}{2\pi}, \tag{10}$$

Having substituted (10) in (9), and (9) in (8), we receive value $R_{\max} = 1.5 \cdot 10^5 m$.

Conclusions

In this paper the properties of volcanic ash as the object of radar surveillance has been considered. The method of volcanic ash zones monitoring with use of polarimetric radar has been grounded.

The carried-out calculations have allowed to make the conclusion that radar systems of centimeter and millimeter wave band can be useful for monitoring clouds of volcanic ash, especially when using polarizing methods of sounding and signal processing for the purpose of recognition of reflecting particles types.

Active sounding in a millimeter range of wavelengths [9] is perspective for monitoring clouds of volcanic ash.

The complex use of methods of the remote sensing intended for monitoring of dangerous weather conditions has especially high potential for wide application at safety of flights in the conditions of atmosphere pollution by a volcanic ash.

References

[1] L.S. Ivlev, "Microstructural features of aerosols of volcanic origin", Optics of Atmosphere and Ocean, v.9, No 8, pp. 1039-1057, 1996 (In Russian).

[2] "Manual on clouds of volcanic ash, radioactive materials and toxic chemicals", ICAO, 178 pp., 2007 (In Russian).

[3] F.J. Yanovsky, "Doppler-polarimetric approach to microwave remote sensing of precipitation", Proceedings 6th International Kharkov Symposium on Physics and Engineering of Microwaves, Millimeter and Submillimeter Waves, 1, pp. 436-438, 2007.

[4] F.J. Yanovsky and L.P. Ligthart, "Microwave scattering on atmospheric particles", 6th International Conference on Antenna Theory and Techniques, pp. 26-31, 2007.

[5] F.J. Yanovsky, "Inferring microstructure and turbulence properties in rain through observations and simulations of signal spectra measured with Doppler–polarimetric radars", In: Polarimetric Detection, Characterization, and Remote Sensing, Springer, 545 pp., 2011.

[6] F.S. Marzano, G.V., and W.I. Rose, "Microphysical Characterization of Microwave Radar Reflectivity Due to Volcanic Ash Clouds", IEEE Transactions on Geoscience and Remote Sensing, Vol. 44, No. 2, February 2006, pp. 313-327, 2006.

[7] F.J. Yanovsky, "Airborne meteorological-navigation radars. Physical bases, main parameters and design principles", Kiev: Institute of Civil Aviation Engineers Press, – 82 pp., 1982 (In Russian).

[8] O.A.Voitovich, A.M. Linkova, G.I. Hlopov, "Study of a two-frequency method of remote sensing firm aerosols", Radiophysics and Electronics, vol. 14, No 2, pp. 169-176, 2009 (In Russian).

[9] Yu.Yu. Kulikov, V.G. Ryskin, "About transparency of the polar atmosphere for millimeter radio astronomy", Izvestiya vuzov. Radiophysics. V. XL, No 12. – pp. 1479-1488, 1997 (In Russian).

[10] F.J. Yanovsky, "Meteorological-navigation radar systems of air vehicles", Kiev, NAU Publishing House, 304 pp., 2003 (In Ukrainian).

[11] P.V. Makovetsky, V.G. Vasilyev, "Reflection of radar signals", Lectures, Leningrad Institute of Aviation Instrument-Making. – 50 pp., 1975 (In Russian).

[12] P.A. Bakulev, "Radar systems", Textbook, Moscow: Radiotekhnika. – 320 pp., 2004 (In Russian).

[13] V.A. Gulshin, A.S. Sadomovsky, "Problem book on radar" (for students of Radio Engineering Specialty), Ulyanovsk: Ulyanovsk State Technical University, 60 pp., 2006 (In Russian).

[14] A. N. Mykolushko, F. J. Yanovsky, "Possibilities of Detection and Monitoring of Volcanic Ash", Proceedings 4th International Radio Electronics Forum "Applied Radio Electronics. The State and Perspective of Development" IRF–2011, V. 1, Chapter 1. – pp. 94–97, 2011 (In Russian).

[15] F. J. Yanovsky. "Specified for Air Safety, Monitoring Atmospheric Phenomena Including the Volcano Dust" (Invited Paper). Proceedings 11th International Radar Symposium IRS-2010, Vol.1, pp. 2-6, 2010.

UDC 654.9

K.V. Kolesnik, Candidat of Science., A.V. Kipensky,
Doctor of Science., E.I. Sokol, Doctor of Science, NTU "KhPI",

THE USE OF RADIOLOCATION CONTROL METHODS TO PROTECT THE PERIMETERS OF LARGE OBJECTS

To detect an intruder for the perimeter security of a large object it is proposed to use radiolocation sensors. The sensors are chosen with taking into account the use conditions, which are inhomogeneous along the object perimeter. The way to simplify a synthesis of the security system is to use a space imaging data.

In today's conditions, when terrorism becomes a planetary problem, the issue of ensuring security of various objects has become one of the most topical both for organizations and enterprises and in general for the state. Need to settle security problems caused rapid development of technology in this area, the development of an extensive range of products and systems for security purposes, the establishment and modernization of methods of providing security for objects perimeter [1-3]. However, the security of ***large objects*** (airports, oil depots, power electrical installations, etc.) with limited access requires solving a number of additional challenges determined by the great length of the perimeters with the various terms of use for methods and systems to ensure security.

The purpose of this paper is to show the effectiveness of using different radiolocation methods and tools for perimeter security of large objects, where characteristics of these tools may compensate various environmental influences on each particular part of secured perimeter.

The large object is some organizational and industrial structure located over a large area (with a different topography, vegetation, level of electromagnetic fields, etc.) and composed of buildings and structures with common perimeter (Fig. 1). To prevent unauthorized access to the object the monitoring tools are placed along the inner side of its perimeter composed into a united security system.

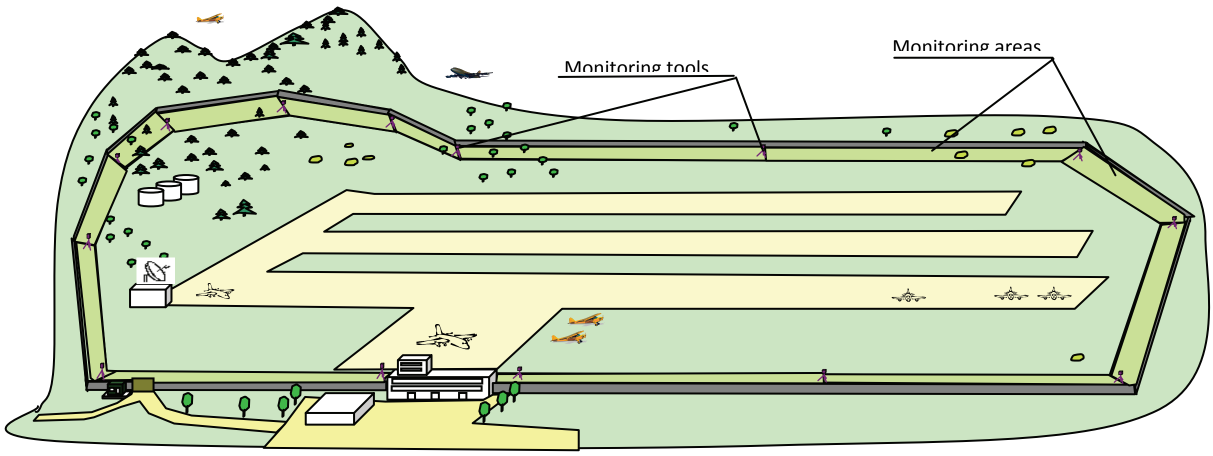

Fig. 1. Example of location of perimeter security system of a large object

To localize the region of violation as well as compensate the influence of environment on the effectiveness of the monitoring system, the entire secured perimeter is divided into a number of control zones. Within each of these zones one or more tools are set to monitor the presence of an intruder. From a technical point of view a security system of the perimeter of a large object can be considered as telemetry system, with functions of collecting, processing and presentation of information about the state of the object [4-6]. In general case the block diagram of a security system of the perimeter of large objects can have the structure shown in Fig. 2.

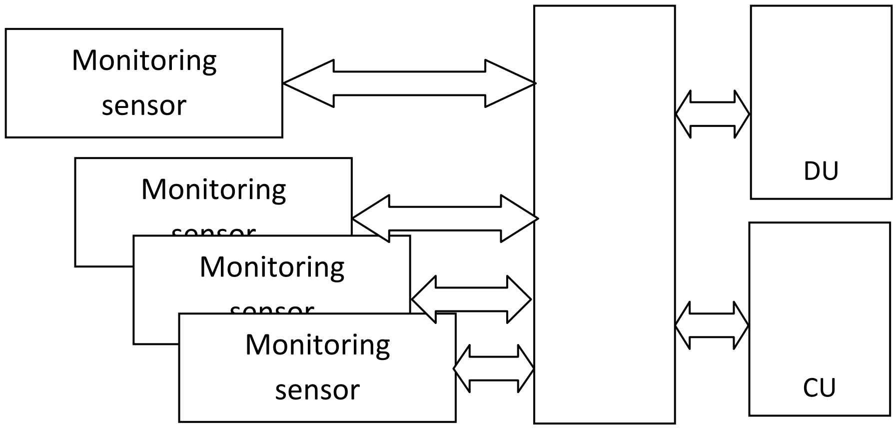

Fig. 2. The block diagram of a security system of the perimeter of a large object:

CCS – central control system for perimeter security;
DU – display unit of the system state;

To identify a person or group of people trying to make unauthorized entry to the object the sensors of various types are used. Type of sensors is determined by the physical phenomena underlying the principles of their actions:

- the infrared radiation of biological object;
- reflection of electromagnetic waves with optical and radio-frequency spectrum;
- scattering of acoustic and electromagnetic waves;
- the change of magnetic or electrostatic fields, etc.

According to the principles of use, radar facilities are classified as: radio ray, radio wave, infrared, optical, acoustic, ultrasonic, etc. [1-3].

The efficiency of various radiolocation controls will be different under different conditions of their use. That is why the solution to the problem of identification of an intruder into the perimeter of a large secured object has a number of features [4].

First of all, this is work in the near zone (from several to hundreds meters) allowing to localize the place of intrusion. In addition, it is necessary to build a narrow radiation pattern without side lobes, thereby reducing the likelihood of misoperations, and thus improve the efficiency of security system.

Furthermore, it is important not to have dead space near the receiving and transmitting antennas, due to the necessity to provide a continuous field along the secured perimeter throughout the entire volume.

Moreover, there are some limitations on the power and frequency characteristics of the radiolocation tools, which are defined by their noise immunity, stability to electronic resistance, as well as the possibility of impact on staff, ensuring the security of the object.

The lower bound of radio receiving route sensitivity of security systems is usually defined such as to ensure the separation of noise from animals, birds and underlying vegetation. Also for this purpose an adaptive processing of received information is often used

Let us consider the use of radiolocation monitoring methods of an intruder presence by the example of two-position radio ray tool (Fig. 3).

a)

b)

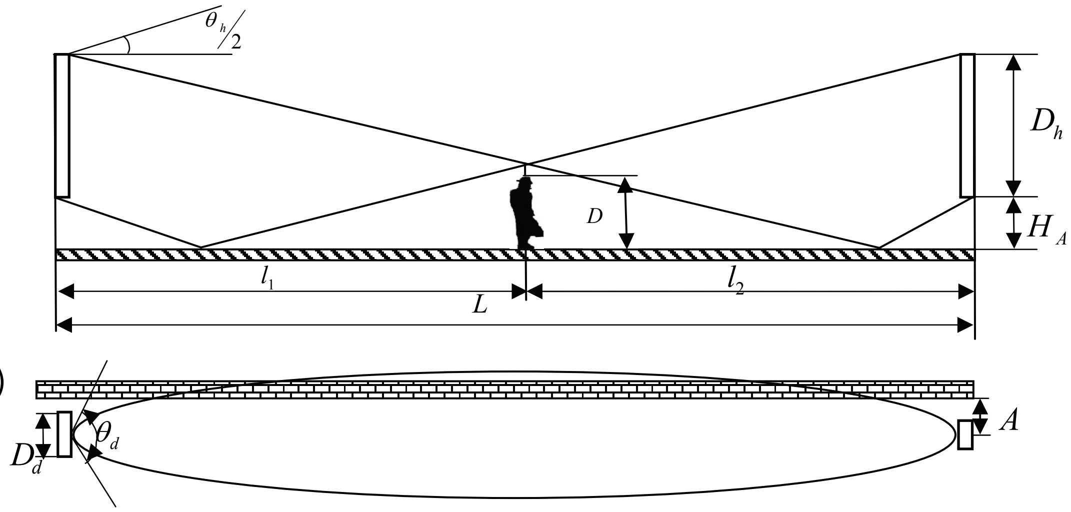

Fig. 3 Two-position radio ray tool

In the figure we use the following notation:

L – the distance between the receiving and transmitting antennas;

l_1, l_2 – the distance from the intruder to the transmitting and receiving antennas respectively;

D – the height of the intruder;

$D_d, \theta_d, D_h, \theta_h$ – the geometric parameters of antennas;

H_A – the distance between the antennas and the ground;

A – the distance between the antennas and a vertical barrier.

Two-position radio ray tool is a set of receiving and transmitting devices that create an electromagnetic field of a given configuration, defined by the parameters of the antennas and the control area of the object, and

$$P_{REC} = P_{TR}\left(\frac{G_\lambda \lambda}{4\pi L}\right)^2 |F|, \tag{1}$$

where:

P_{REC}, P_{TR} – power at the input of the receiving antenna and at the output of the transmitting antenna respectively;

G_λ – antenna gain;

λ – the wavelength of electromagnetic radiation.

Influence of surface roughness (terrain, buildings, vegetation, etc.) of control zones to the work of the radiolocation tool is considered in an attenuation index

$$|F| = \sqrt{1 + n^2 - 2n\mathrm{Cos}\Omega}\,, \tag{2}$$

where:

n – the reflection coefficient of the surface;

Ω – phase of the reflected wave.

It is known that the propagation of radio waves from the transmitting antenna to the receiver forms a complex interference pattern. When $D >> \lambda$ RF-scattering region is determined by the ratio of the typical height D of the intruder to the radius R_1 of the first Fresnel zone. For the most of radiolocation control tools the condition of Fresnel diffraction $D/R_1 \sim 1$ is true. When an intruder moves across the secured region, he consecutively closes the Fresnel zones. It causes the receiver input signal to get a particular form. This form allows identifying the presence of the intruder in the monitoring area [1].

Therefore the quality of the radiolocation control tool functioning significantly depends not only on the geometrical parameters of the antennas ($D_d, \theta_d, D_h, \theta_h$) and the conditions of their placement, but also on the surface roughness of control zones.

Also, the performance of the radiolocation tools strongly depends on climatic conditions and other conditions of use:

- geological (topography, type and chemical composition of soil, water space, seismic activity);
- biological (plants, animals, birds, insects);
- climatic (wind, dust, sand, atmospheric precipitates, fog, solar radiation, temperature, thunderstorms, seasonal behaviour, etc.);
- electromagnetic fields and radiation;
- acoustic vibrations;
- level of radioactivity;
- level of illumination, etc.

Considering aforesaid, to create effective systems for perimeter security of large objects it is advisable and promising to use the technology capabilities and methods of geographic information systems (GIS) [9, 10].

GIS-technology is based on processing of space mapping information about the state of a secured object with its subsequent refinement for each control zone of the perimeter (Fig. 4).

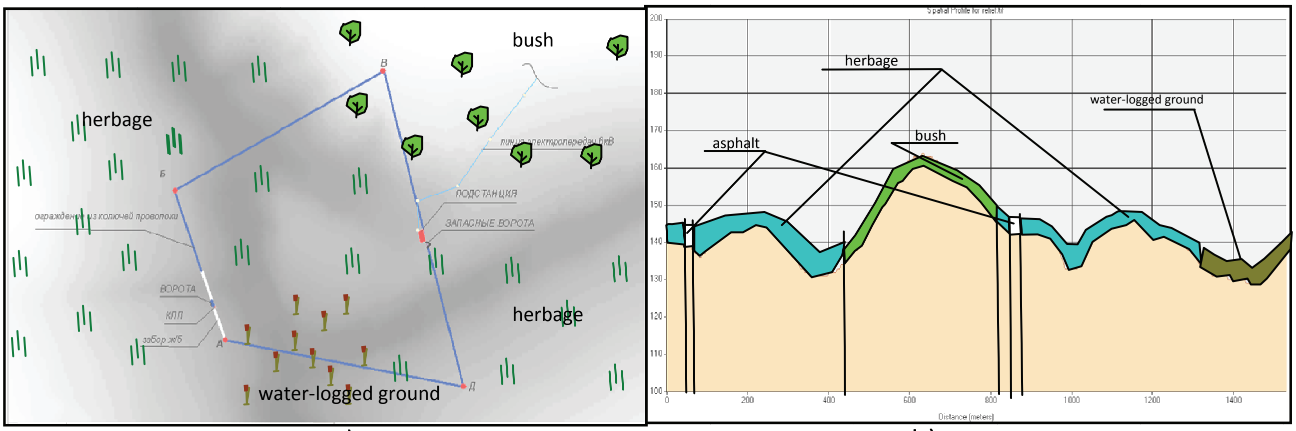

a) b)

Fig. 4. Example of using GIS-technology for the construction of the object perimeter by coordinates (a) and its profile (b) on a digital terrain map

Knowing the secured object coordinates and using digital maps you can get information about the profile of the perimeter of the object and the characteristics of each control zone. Then, having geo-information model of a specific object and information about the capabilities of existing radiolocation tools, it is easy enough to solve the optimization problem (discrete choice of radiolocation control tools with regard to the conditions of their use) for each control zone of the secured perimeter [11, 12].

Conclusions

To effectively protect the perimeters of large objects it is advisable to use radiolocation control methods. Due to the large extent of the secured perimeter of such objects one should consider the possibility of various conditions of use for the radiolocation tools in the different zones. In addition, for each specific zone of the perimeter one should choose such kind of control tool which is most effective for the respective conditions of use. It is possible to simplify the choice of control tools through the use of data obtained by space mapping.

References

1. *Ivanov I.V.*. Security of perimeters. – Moscow: Radio I svyaz, 1997. – 98c. (In Russian)
2. *Magauenov R.G.* Alarm systems: basic theory and principles of construction. – M.: Goryachaya linia-Telekom, 2008. – 496 p. (In Russian)
3. *Kolesnik K.V., Smaglyuk V.V., Churyumov G.I.* The concept of building radioengineering systems for the perimeters security of large objects // Tekhnologia i konstruirovanie v elektronnoy apparature. – Odessa: Politekhperiodika. – 2008. – № 4 (76). – P. 19-22. (In Russian)
4. *Kolesnik K.V., Polyakov G.E., Churyumov G.I.* Analysis of the principles of design and evaluation of state-of-the-art of radioengineering systems for the perimeters security of the object // Tekhnichna elektrodynamika. Tematychnyy vyp. «Power electronics and energy efficiency». – Kiev: IED NANU. – Part 2. – 2009. – P. 104-108. (In Russian)
5. *Kolesnik K.V., Smaglyuk V.V., Vinogradob G.M.* Features of construction of electronic systems for the perimeters security of large objects // Materialy VIII MNPK «Modern information and electronic technology». – Odessa: 2007. – P. 303. (In Russian)
6. *Kolesnik K.V., Smaglyuk V.V., Churyumov G.I.* A generalized block diagram of radioengineering systems for the perimeters security of large objects // Materialy IX MNPK «Modern information and electronic technology». – Odessa, 2008. – P. 223. (In Russian)
7. *Kolesnik K.V., Churyumov G.I.* Analytical review of the technical means of perimeters security of large objects // Технічна електродінаміка. Tekhnichna elektrodynamika. Tematychnyy vyp. «Power electronics and energy efficiency». – Kiev: IED NANU. – Part 5. – 2008. – P. 127-132. (In Russian)
8. *Kolesnik K.V., Churyumov G.I., Smaglyuk V.V.* Monitoring methods of human presence in the security systems of objects // Tekhnichna elektrodynamika. Tematychnyy vyp. «Power electronics and energy efficiency». – Kiev: IED NANU. – Part 5. – 2007. – P. 121-124. (In Russian)
9. ERDAS IMAGINE. Tour Guides. December 05 2005. Geospatial Imaging, LLC. Norcross. Georgia. Leica Geosystems.
10. *Kolesnik K.V., Machehin Yu.P., Churyumov G.I.* Methods for static modeling of radioengineering monitoring systems for the perimeters security of objects // Zbirnyk naukovyh prats KhUPS MO Ukrayiny «Information processing systems». – Kharkiv: KhUPS. – 2010. – № 1(82). – P. 61-65. (In Russian)
11. *Kolesnik K.V., Kipensky A.V., Kolesnik K.V.,* Методика оценки качества радиотехнических систем охраны периметров территориально-распределенных объектов Methods of quality assurance of radioengineering systems for the perimeter security of geographically distributed objects // Materialy IX MNPK «Modern information and electronic technology». – Odessa, 2012. – P. 175. (In Russian)
12. *Kolesnik K.V., Kipensky A.V., Machehin Yu.P., Churyumov G.I.* The use of formalized indicators to assess the quality in the design of radioengineering systems for the perimeter security of geographically distributed objects // Technology and design of electronic equipment. – Odessa: Politekhperiodika. – 2012. – № 4 (94).– P. 31-35. (In Russian)

UDC 621.37

G.Sokolovska, Postgraduate Student (NAU, Kiev)
L. Scherbak, Doctor of Technical Sciences (NAU, Kiev)

RADIOTECHNICAL SYSTEMS OF DETECTION RADIO SIGNALS AND EVALUATION OF THEIR CHARACTERISTICS UNDER THE INFLUENCE OF NOISE

The models of radio signals and radio detection of radio signals, proposed methods for evaluating their characteristics depending on the signal bandwidth.

Introduction. Scientific and technical problems of detection of radio signals and evaluation of their characteristics under the influence of noise were researched in the second half of the twentieth century and still relevant at this stage of development of radio systems. It should be noted that a considerable number of publications, radio detection tasks and tasks evaluation of their characteristics are the research on separate areas. Each of these areas devoted a significant amount of scientific publications. In most cases, consider the following sequence: first, consider the problems of detection, and then - task of evaluating the characteristics of radio signals the detected by the action of interference. The development of radio systems, the widespread use of computers and modern information technology has considerably expanded the potential of radio systems and, in spite of the number of results for the detection of radio signals and evaluation of their characteristics, such scientific and technical problem continues to be relevant and important today.

In this paper we will focus on models of radio signals, will be described in broadband and narrowband signals. It also describes the main methods used to detect radio signals and evaluation of characteristics of the data signals. These include the correlation method for broadband radio signals and method for processing radio signals using the discrete Hilbert transformation for narrowband radio signals.

Models of radio signals. The physical nature of the formation of radio signals as a combination of information signals and noise in most cases subjected to the action of random factors and, according to the classification of Kolmogorov, the modeling radio signals available with three different formations:

- the signal can be described by deterministic models, which are uniquely determined by initial conditions, but the initial conditions are random;
- signal as a function of time is random, ie described by a random process or random field;
- describes the temporal dynamics of the signal in different combinations, in most cases, additive or multiplicative mixture of signal and noise as random process.

Broadband signals. By broadband or a noise signal (noise) understands the realization of a stationary random process for which following condition is satisfied:

$$B = \Delta FT >> 1,$$

where ΔF means the bandwidth of the spectral density of the random process in Hz, T - a time interval of observation the implementation of studied process, and the value of B is called base of such a signal in seconds.

From this definition it follows that in its essence the definition is arbitrary, but in terms of classification of the signals is physically reasonable. If you specify this definition, it should be satisfy the following conditions

$$\Delta F >> 1 \text{ (Hz)}$$

that is, the value of the band of power spectral density a stationary random process should take a broad band of frequencies in Hz.

The properties of these signals makes them promising as well in solving some problems in communacation systems, primarily for the operation of the system. Noise signals can be used in the construction of continuous (eg, FM), pulse (eg, time-pulse modulation) and discrete (eg, pulse code modulation) communication systems.

Narrowband signals. In some cases, the input radio signals are narrowband stationary signals - that is, those for which the spectral density (energy spectrum) is concentrated in a small band of frequencies Δf around a certain center frequency $f_0 >> \Delta f$.

The investigated narrowband radio signal is defined as

$$u(t) = A(t)\cos\Phi(t),\ t \in T \tag{1}$$

Where the function $A(t)$ called bypass, and $\Phi(t)$ the phase of signal $u(\omega, t)$ for deterministic signals and

$$u(\omega,t) = A(\omega,t)\cos\Phi(\omega,t), t \in T \tag{2}$$

for random radio signals, where $\omega \in \Omega$ - elementary event in the space of elementary events.

On the basis of models can be described a significant amount of information signals. But the structure of this model requires some justification. If defined the right side of equation (1) or (2), there is $A(t)$ and $\Phi(t)$, then the model is uniquely defined. But if you defined the left side of (1) or (2), in general, two functions $A(t)$ and $\Phi(t)$ can not determine.

It is known that the most significant influence on the results of detection in radar systems has a number of external and internal interference: to industrial, from lightning, space, internal (thermal, shot, flicker noise). Therefore, in formulation of problems for detection of radio signals interference action is necessary to consider the action of various factors, including the conditions of radio wave propagation in real time, the characteristics of radar detection systems, signal detection and interference.

Methods of processing of radio signals. In this paper we consider two statistical methods of processing of broadband and narrowband radar signals. Classification of the investigated signal is in some sense conditional and is defined as the formulation and the specific tasks.

The proposed statistical methods for processing these signals differ from each other and include the following.

Correlation method. It is assumed that a given model of the radar signal is represented as an additive mix

$$\xi(\omega,t) = \zeta(\omega,t) + \eta(\omega,t), t \in (-\infty,\infty), \tag{3}$$

where $\zeta(\omega,t)$ is useful signal (usually limited in time and frequency), $\eta(\omega,t)$ is stationary random noise with zero mean and variance σ^2.

The statistical formulation of the problem of radar analysis of the additive mix (1) is the set of realizations

$$x_j(t) = s_j(t) + n_j(t), j \in N. \tag{4}$$

Features of the proposed statistical method for processing broadband radar signals consist of the following:

- method refers to the correlation method of signal processing;
- method is based on a preliminary orthogonal filtering the input radar signal of the form (1), followed by the traditional correlation signal processing.

Implementation of the proposed method of statistical analysis of radar signal interference effects shown in Fig. 1.

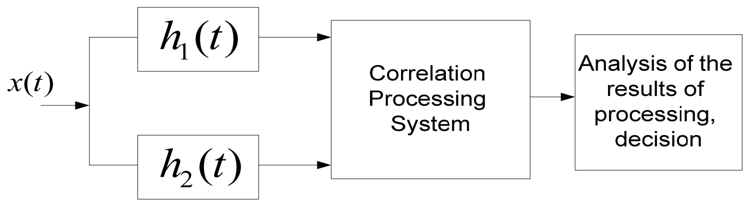

Figure 1. Structure of the correlation processing system with orthogonal linear pre-filtering of the input signals

The diagram in Fig. 1 shows the correlation structure of the system, in contrast to the traditional, made a preliminary filtering of signals orthogonal linear filter impulse response functions $\{h_j(t), j = 1,2\}$ which satisfy the orthogonal condition

$$\int_0^\infty h_1(t)h_2(t)dt = 0. \tag{5}$$

Under the influence of "white noise" on a linear filter with the impulse response function $h_j(t), j = 1,2$. The impulse response function of such filter is described by a random process of "colored noise", more precisely a linear stationary process in the form

$$\eta_j(\omega, t) = \int_0^\infty h_j(t-\tau)\eta(\omega,\tau)d\tau \cdot \tag{6}$$

where $\eta(\omega, t)$ is white noise process.

If the input correlation system with pre-filtering of the orthogonal input signals (Fig. 1) receives a random signal such as "white noise" $\gamma(\omega, t)$ as centered ergodic process with uncorrelated (independent) values, the response of such system is

$$R_{12}(\tau) = M\{\eta_1(\omega,t), \eta_2(\omega,t+\tau)\} = \sigma^2 \int_0^\infty h_1(t)h_2(t+\tau)d\tau, \tag{7}$$

where σ^2 is power spectral density of "white noise ".

From the expression (4) and taking into account (3) with equal $\tau = 0$ we obtain

$$R_{12}(0) \equiv 0. \tag{8}$$

Let us examine this result in more details.

Under the influence of a random process such as "white noise" responses of orthogonal linear filters, like linear stationary processes in general, in the absence of their mutual time shift are uncorrelated.

The result of obtained form (6), i.e. in the absence of mutual shift between the responses $\eta_1(\omega,t)$ and $\eta_2(\omega,t)$ can be obtained using other methods of statistical signal processing. Depending on the mechanism of formation of shot noise the two Poisson random process are used But by selecting the appropriate orthogonal filter result (6) mutual shift response filters can be obtained in the time interval, which has significant practical value [12, 13].

[13] justifies the choice of orthogonal linear filters, impulse response functions that describe the orthonormal Laguerre functions form

$$h_j(t) = \alpha L_{j-1}(2\alpha t)\exp(-\alpha t)U(t),\ j \in N, \tag{9}$$

where α is filter setting (when used on a LC-elements $\alpha = 1/\sqrt{LC}$, for RC-elements $\alpha = 1/RC$) $L_n(t)$ - Laguerre polynomial n-th order, $U(t)$ is Heaviside function.

When the input signal (1), where the additive noise $\eta(\omega,t)$ is a centered white noise and useful signal $\zeta(\omega,t)$ is any signal that is different from white noise, the response of the correlation of the input orthogonal Laguerre filters (Fig. 1) is represented as

$$R(\tau) = R_s(\tau) + R_n(\tau), \tag{10}$$

where the mutual correlation function of the Laguerre filter $R_n(\tau)$ responses when exposed to noise $\eta(\omega,t)$ of the form (1) with impulse response functions

$$\begin{aligned} &h_i(t) = \alpha L_{i-1}(2\alpha t)\exp(-\alpha t)U(t) \\ &h_j(t) = \alpha L_{j-1}(2\alpha t)\exp(-\alpha t)U(t), \\ &j > i; i, j \in N \end{aligned} \tag{11}$$

described by

$$R_n(\tau) = \frac{(-1)^{i+j-1}}{(j-1)}\sigma^2\alpha^2 L^1_{j-i-1}(2\alpha\tau)\times\exp(-\alpha\tau)U(\tau), j > i, \tag{12}$$

from the last expression we obtain the following result

$$R_n(\tau) \equiv 0 \text{ при } \tau \in (-\infty, 0], \tag{13}$$

where $L^1_n(t)$ is generalized Laguerre polynomial of n-th order, and σ^2 is power spectral density of white noise.

Based on the foregoing, as well as the results of publications [12, 13] on the application of statistical correlation method with pre-filtering the input signals orthogonal linear Laguerre filters in the problems of detection of radar signals in the presence of additive noise can draw the following conclusions:

• under the influence of additive white noise the responses of orthogonal Laguerre filters are uncorrelated to the axis of their mutual time shift, which makes it possible to detect any arbitrary signal, different from white noise;

• the theoretical studies of this makes it possible to get asymptotically singular case detection signal in additive white noise;

• the proposed statistical method makes it possible to solve a wide range of tasks of detection of broadband radar signals in the presence of additive noise, the latter of which can be described by a white noise process, as well as linear random process (colored noise) to improve signal to noise ratio at the output of the correlation system.

A method of processing of radio signals based on the discrete Hilbert transform. It is assumed that the model of the radar signal is also described as (1) and represents a narrowband random process [6, 14].

Application of computer equipment, as well as statistical phase meter [14] makes it possible to fully utilize the capabilities and ensure the effectiveness of the known method of envelope and phase (the method of complex amplitudes) for statistical analysis of narrowband radar signals. By its very nature this method is an implementation of a more general method of forming the quadrature components of the type cos and sin of the signal on the basis of the Hilbert transform. Realization of discrete, and in some cases moving the discrete Hilbert transform [14], signal processing system provides an opportunity to propose a system of statistical processing of narrowband radar signals, shown in Fig.2.

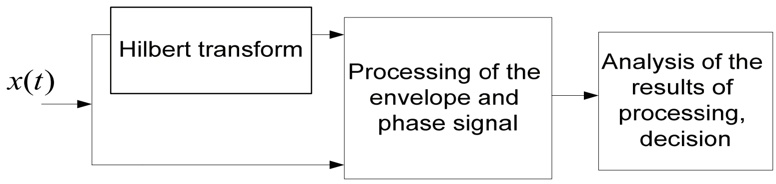

Figure 2. The structure of narrowband radar signal processing

Consider the basic operations of signal processing with such a system [14]:

• under the influence of the input signal $\xi(\omega,t)$ type (1) at the converter output Hilbert formed by the conjugate Hilbert signal $\xi_H(\omega,t)$;

• formed signals are given by

$$\xi(\omega,t) = A(\omega,t)\cos\Phi(\omega,t); \tag{14}$$

$$\xi_H(\omega,t) = A(\omega,t)\sin\Phi(\omega,t); \tag{15}$$

• random processes $A(\omega,t)$ and $\Phi(\omega,t)$ are called the amplitude and phase characteristics of the quadrature components, which are given by

$$A(\omega,t) = \sqrt{\xi^2(\omega,t) + \xi_H^2(\omega,t)}; \tag{16}$$

$$\begin{aligned}\Phi(\omega,t) = arctg\frac{\xi_H(\omega,t)}{\xi x(\omega,t)} + \frac{\pi}{2}\{2 - sign\xi_H(\omega,t)[1 + sign\xi(\omega,t)]\} + \\ + K[\xi(\omega,t),\xi_H(\omega,t)] = L[\xi(\omega,t),\xi_H(\omega,t)] + K[\xi(\omega,t),\xi_H(\omega,t)],\end{aligned} \tag{17}$$

where $L[\xi(\omega,t),\xi_H(\omega,t)]$ is the operator of a clear definition of the phase characteristic in the range $[0,2\pi)$, $K[\cdot]$ is operator of sweep phase characteristics of signals;

• statistical processing characteristics $A(\omega, t)$ and $\Phi(\omega, t)$ is the main task of the statistical processing of narrowband radar signals;

• one new information phase characteristic of narrowband radar signals is a phase difference characteristic of the emitted and received signals as the difference of the characteristics of the random signals.

Thus, as a statistical method of processing narrowband radar signal processing method was proposed using mainly discrete (moving discrete) Hilbert transform [6].

Conclusion. This paper provides an analysis of radiotechnical systems to detect of radio signals and to evaluate their characteristics under the influence of noise. The models of broadband and narrowband radio signals, which are used in radar systems. For these models, signal processing methods are presented: the correlation method of processing of broadband signals with orthogonal pre-filtered using filters Laguerre and narrowband radio signal processing method using moving discrete Hilbert transform.

References

[1]*P.M. Woodward*. Probability and Information Theory, with Applications to Radar. – London: Pergamon, 1953.

[2] *Carl W. Helstrom*. Statistical theory of signal detection. – NY: Pergamon Press, 1960. – 364 p.

[3] *Charles E. Cook, Marvin Bernfeld*. Radar signals; an introduction to theory and application. – NY.: Academic Press, 1967. – 531 p.

[4] *H. Van Trees*, Detection, Estimation and Modulation Theory—Part III. – NY: Wiley, 1968.

[5] *R. Price*. Detectors for Radar Astronomy. In: Radar Astronomy. J.V. Evans and T. Hagfors Eds. New York, McGraw-Hill, 1968.

[6] *Y. Sosulin*. Theoretical Foundations of Radar and radio navigation: Textbook. manual for high schools. – Moscow.: Radio & Communications, 1992. – 304 p.

[7] *Hamish Meikle*. Modern Radar Systems. – Boston: Artech House, 2001. – 563 p.

[8] *N. Wiener*. Nonlinear Problems in Random Theory. – NY: John Wiley& Sons, 1958.

[9] *J.W. Lee*. Synthesis of Electronic Network by Means of the Fouries Transforms of Laguerre's Functions. – J.: Math.Phys., 1932. – P. 84 – 113.

[10] *R. Arens*. Complex Envelopes for . – Envelopes of Normal Noise. Trans.: IRE, 1957.

[11] *J. Dugundji*. Envelopes and Pre-Envelopes of Real Waveforms. Trans. IRE, 1962.

[12] *B. Marchenko*. The method of stochastic integral representations and its applications in electronics. - Kiev: Naukova Dumka, 1973. – 192p.

[13] *B. Marchenko, L. Scherbak*. Linear stochastic processes and their applications. - Kiev: Naukova Dumka, 1975. – 144p.

[14] *Y. Kuts, L. Scherbak*. Statistical fazometriya. - Ternopil: Publishing TSTU. "Ivan Pulyui", 2009. – 384 c.

A. A. Vertiy[1] Prof. Dr., A. V. Pavlyuchenko[1,2] Dr., A.G. Denisov[2] Dr., F. Hacizade[3] Prof. Dr., D. Riza[3], A. Kholmatov[3] Dr.
([1]International Laboratory for High Technology (ILHT), TUBITAK-MRC, MI, Dr. Zeki Acar Street, 41470, Gebze-Kocaeli, Turkey)
([2]State Research Center "Iceberg", Ukraine
([3]National Research Institute of Electronics and Cryptology (UEKAE), TUBITAK-MRC, MI, Gebze-Kocaeli, Turkey)

MILLIMETER AND SUB-MILLIMETER WAVE RADIOMETRIC IMAGING SYSTEMS

In this work, we demonstrate working prototypes of radiometric scanning systems that operate in 8-mm and 3-mm frequency range. Main technical characteristics of scanning systems are discussed. Besides, we elaborate on the ways to decrease the overall scanning time and improvement in the sensitivity of corresponding systems. Different methods of receiving radiometric data and processing techniques are compared.

INTRODUCTION

It is widely known [1, 2] that increase in the operating frequency range causes increase of the sky brightness temperature, which is a power of the illuminate radiation and contribute to the sharper radiometric contrast of different objects. The main advantage of utilizing the electromagnetic waves in mm and sub-mm band is their robust and almost lossless propagation through bad weather mediums such as rain, smoke, snow, fog and sand storms, where optic systems are not effective. Another advantage of such band is its ability to propagate through different materials and clothes [3-5]. These characteristic properties of the band make the basis of working principles of the large amount of radiometric security systems [4-11]. For instance, passive millimeter-wave imaging systems are very promising for detection of dangerous and outlaw objects (weapons, explosives, drugs, etc.), which are generally tediously concealed under persons' clothing and are not detectable using conventional systems. Because of the terroristic acts that take place in the last decade, the high-resolution radiometric systems for fast imaging at short distances are essential for personal weapon control in public places. Besides, due to the ability of penetration through poor weather conditions, the radiometric imaging possesses a great promise as a means to aid aviation in low visibility conditions [4, 6, 7, 9].

In this work, we show different prototypes of passive radiometric systems, which work in 8-mm (33-38 GHz) and 3-mm (90-104 GHz) frequency range. We provide technical characteristics of utilized antenna setups, receivers and mechanical scanning modules, as well as discuss different radiometric data processing and visualization techniques. We also demonstrate scanning results of different objects obtained from 10 m to 2.5 km distance and acquired in 3 to 600 seconds scan time.

IMAGING SYSTEM DESCRIPTION

A.8th-mm multichannel imaging system setup

The focal plane array is formed on base of radiometric sensors [6], which are direct detection receivers with input low-noise amplifiers. The sensors operate in frequency band $33-38GHz$ and have temperature sensitivity not worse than $10mK/\sqrt{Hz}$ in total power mode. Small sizes of the sensors and stretched configuration provide its efficient packing into array. The array contains 32 sensors located in a shape of two venial rows and presented in Fig.1.a. A multibeam quasioptical antenna consists of the main antenna and feeds located in a focal plane of the main antenna. The prime-focus-fed parabolic reflector is used as a main antenna. The reflector has diameter $D = 900mm$ providing the beam width near 0.6° at $3dB$ level. The dielectric rods antennas are used as feeds. Each teed is connected with its sensor and directed to the center of the main antenna. The reflector with feeds in total plane forms 32 beams. The angle between adjacent beams in vertical plane is 0.46° and total angle of view in vertical plane is 16 degrees.

a) b) c)

Figure 1. a) Photo of multichannel radiometric imaging system; b) Image and c) photo of the same scene.

The antenna with array is attached to the scanning mechanism, which provides the antenna scanning in horizontal plane by angle ± 60 degrees. The scanning mechanism includes the optical sensor of the angle, which gives information about the antenna position in any time during system operation. The signals reading is carried out through each 0.17 degree (1 pixel) in full angle of view in horizontal plane equal to 90 degrees. In order to form an image on monitor screen the software – hardware complex has been developed. Computer sets the operating modes for scanning mechanism, carries out processing of the received signals, and forms the image on a monitor. The computer with a monitor is placed separately from scanning receiver unit at convenient distance and is connected to the unit by means of special cable. The investigations of the system in natural conditions were carried out. In Fig.1.b the image of SPE «Saturn» yard territory obtained with help of the developed system is shown. For comparison in Fig.1.c the photo of the same scene is shown. Sufficiently good quality of the image in 8 mm wave's band is demonstrated. The time of scan was 3seconds.

B. A prototype sub-THz imaging scaning system

The 2-D sub-THz imaging system is presented in Fig.2.a and was used as a tool for conducting radiometric experiments and receiving images of different objects. The scanning system consists of a focusing lens manufactured from polyethylene, radiometric receiver with a horn antenna, two-coordinate device for mechanical moving of the receiver [5-11], ADC and PC for data storage, visualization of the information received and system managing.

The superheterodyne radiometric receiver for extremely high frequency range (3-mm band) was developed and created in ILHT. The radiometric receiver is created as a waveguide superheterodyne scheme with a low-noise amplifier at the input. The front-end part of radiometric receiver is presented in Fig.2.b. The receiver heterodyne consists of a master oscillator based on Gann diode and on low-noise buffer amplifier. A mixer is made by balance scheme using *AsGa* Schottky diodes. Conversion losses of the mixer did not exceed $6.5dB$ in working frequency band. Intermediate frequency section consists of three low-noise amplifiers and a band filter. Amplification factor of the intermediate frequency section was more than $50dB$ and noise factor was $1.1dB$. The detector was done by voltage doubling scheme on Schottky diodes. Working frequency range of the receiver was from 97 to $104GHz$. The receiver sensitivity measured and adjusted to one second was $\Delta T = 0.0031K$. Temperature inside the receiver is supported at the level of $45^\circ C$ with accuracy no less than $\pm 0.1^\circ C$.

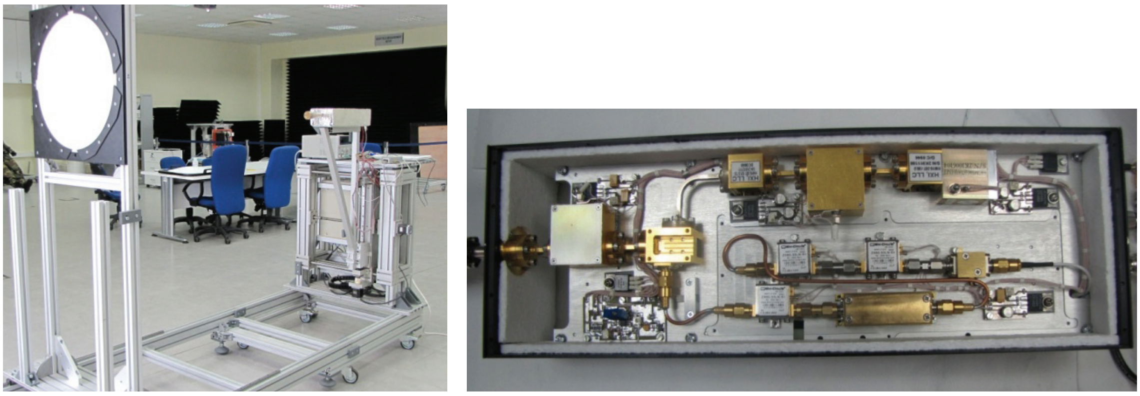

a) *b)*

Figure 2. a) Photo of 2D passive scanning radiometric system; b) front-end part of the radiometric receiver.

Value of radiometric gain [1-3] obtaining as the following formula $q = \sqrt{\Delta f \cdot \tau}$, shows a signal which q times smaller than intrinsic noises of the receiver and it may be registered by radiometer. For achieving different values of the radiometric gain when conducting experiments, different filters with $\tau = 1ms$, $\tau = 10ms$ и $\tau = 100ms$ were manufactured. The output of receiver signals for filters with different integration time is presented in Fig.3.

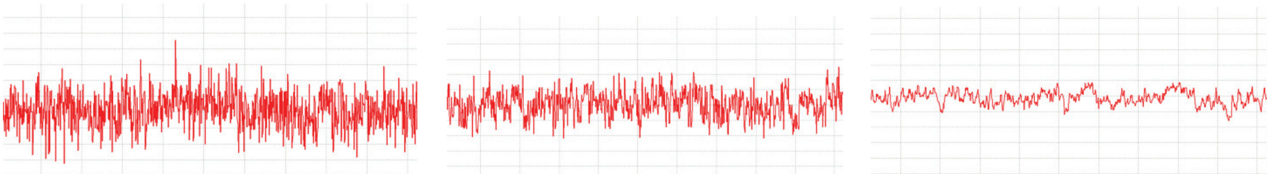

a) *в)* *c)*

Figure 3. Output of receiver signals: a) $\tau = 1ms$; b) $\tau = 10ms$; c) $\tau = 100ms$. The vertical scale is 10mV/div, horisontal scale is 10s/div.

It is known [1, 2], that when energy with power of P incidents on an arbitrary material than part of this power P_ρ is reflected, the other part of the power P_α is absorbed, and the third part of the incident power P_τ passes through the material. Reflection factor, absorption factor and transmission coefficient are connected with each other by the following equation:

$$\rho + \alpha + \tau = {P_\rho}/{P} + {P_\alpha}/{P} + {P_\tau}/{P} = 1,$$

and usually $\tau \approx 0$, so $\rho + \alpha \cong 1$. In literature you may find that $\tau \approx 0$, but practically $\tau \neq 0$, thus, part of the power passes through the material and this part may be registered. In his work [4] the author gives only results of investigations of the reflection factor of some materials at frequencies of $94GHz$. In our work investigations of reflection factor for different construction materials were carried out in the first series of experiments. This irradiation from the cold sky was employed as non-coherent illuminating radiation. The materials under investigation were located at the distance of $2m$ from the lens and they totally overlapped its aperture. The results of the experimental investigations of the transmission factors of different construction materials for the frequency range of $97 - 104GHz$ are given in Tab.1.

TABLE 1. Transmission factor for different construction materials.

Type of material	**Transmission**	**Type of**	**Transmission**
concrete	0.000174	fiberglass	0.003
brick	0.000133	cellular plastic	0.00458
marble	0.000522	beech galley	0.000893
gypsum	0.00148	window pane	0.08125
pine (dry)	0.000601	plywood	0.0458
plasterboard	0.0365	paper board	0.151
fiberglass	0.003	board-on-edge	0.0032
polyethylene (film)	0.1717		

In the next series of experiments a pattern of letter "A" made from absorbing material was fixed on the metal reflector retranslating irradiation of the cold sky. Scanning of the object, letter "A", was conducted in two regimes: the first regime with using of different construction materials placed on the way of radiometric signal propagation and the other regime - without such materials. Photo and the radiometric image obtained for letter "A" when scanning without obstacles and through plasterboard are presented in Fig.4, correspondingly.

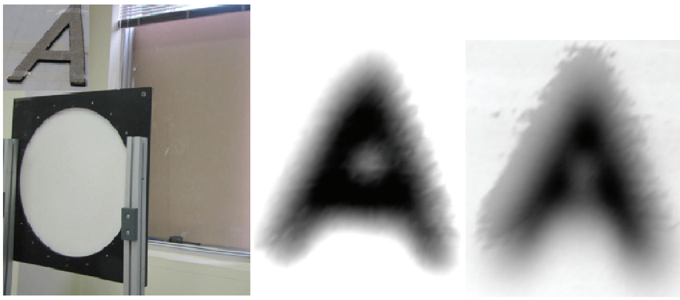

a) *в)* *c)*

Figure 4. Radiometric scanning at distance of 10m: a) photo of the scanning system and photo of letter «A»; в) radiometric image of an object without wall; c) radiometric image of the object behind the wall made from plasterboard.

The experiments carried out showed us possibility of obtaining radiometric images of objects located behind obstacles if transmission coefficient of materials no less than 0.005. One should notice good quality of the obtained radiometric images for contrast objects located at distances from $10m$ to $150m$. In paper [11] showed a possibility of detection of weapon and other different dangerous objects concealed under person's clothing with reflection factor less than 0.2. In our experiments we investigated possibilities of detection of weapons and other objects concealed under the winter clothing (clothing with high reflection factor $\rho \leq 0.4$), and the person was behind the wall ($\tau \geq 0.005$) at distance of $10m$. One of the results obtained is presented in Fig.5. Radiometric image of dangerous objects (weapons) with reflection factor of $\rho \approx 1$ has sufficient dependence on the angle of view. Results of the experiments are given in Fig.5. At the foreground of the radiometric image one can see a gun concealed under winter clothing at distance of $10m$, at the right behind there is a building at distance of $150m$, and at the background at the top there are floating clouds.

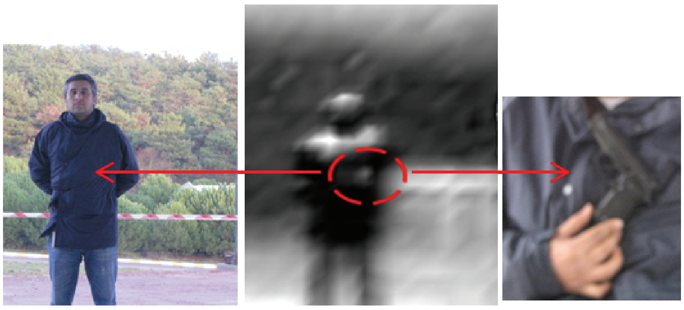

Figure 5. Photo and radiometric image when scanning weapon concealed under clothing at distance of $10m$, building at distance of $150m$ and clouds at the background. The outline of the gun is marked by the dotted line.

Landscape where the experiments were carried out allowed to scan objects at the sea surface and to estimate maximum operational range of the system. Its photo and radiometric image are represented in Fig.6. In the images one can see low-contrast sea targets – ships located at distance of $1000m$ (Fig. 6.a and 6.b), at distance of $2500m$ (Fig.6.c and 6.d) and also an opposite side of a bay located at distance of $10km$. Difference in radiometric images in Fig.6.b and Fig.6.d is image inversion. It may be explained by different elevation angles for scanning. In the first case, Fig. 6.b, the scanning system was fixed at the level of $10m$ above the sea level, and in the second case, Fig. 6.d, the level was approximately $300m$ above the sea level. The time of 2D scanning was 600 sec for resoluthion 32x32 pixels.

a) *b)* *c)* *d)*

Figure 6. Radiometric measurements at sea: a) photo and b) ship image at distance of 1000m; c) photo and d) ship image at distance of 2500 m. The outline of the ship is marked by the dotted line.

C. A prototype sub-THz multichannel imaging scaning system

This radiometric system is designed as a multichannel sub-THz system. The scanning system consists of quasioptical antenna system, receiver array, and mechanical scanner with the control system of its movement, ADC array and personal computer with developed software.

The quasioptical antenna system consists of parabolic mirror with diameter of $1.2m$ and feed system which is situated in the image plane. The focal distance of antenna system is $1.32m$. The design of the feed system is analogous to the feed systems in 8-mm frequency range, which has small geometry, which allows to form a compact array of the receiver with feed system. Wideband low-noise receiver was designed and manufacture in State Research Center “Iceberg” for 3-mm band passive radiometric measurements and presented in Fig. 7.a, 7.b. Receiver is based on total power scheme and involves the active AsGa elements. The receiver has waveguide input that allows using the different types of horn or dielectric-rod antennas and makes possible the measurements of receiver parameters by standard equipments.

Radiometric signal from waveguide-to-microstrip transmission comes to the four cascaded amplifier of radiofrequency. This gain distribution amplifier is based on balanced three-stage low noise monolithic HEMT amplifiers. Amplifier output signal is detected. The detector operates in the quadratic regime with zero bias. The detector load is a low frequency filter of the seven units. Useful signal after detector is amplified. This amplifier provides detector output isolation, matching between analog and digital circuits. The measured quantity of the operation frequency range of the receiver made up $90-100GHz$. The gain factor of linear part of the receiver in operation frequency range is no less than $52dB$. The temperature sensitivity of the receiver is $0.67mV/K$. The installable gap of the integration time is $1ms-1s$. The second wideband low-noise receiver, which is presented in Fig.7.c, 7.d, was initially developed as a component of receiver array (designed by A. Pavlyuchenko). The receiver is notable for lower bandpass flatness in operation frequency range, higher gain factor and lower dimension and weight. Both of the receivers have similar other parameters.

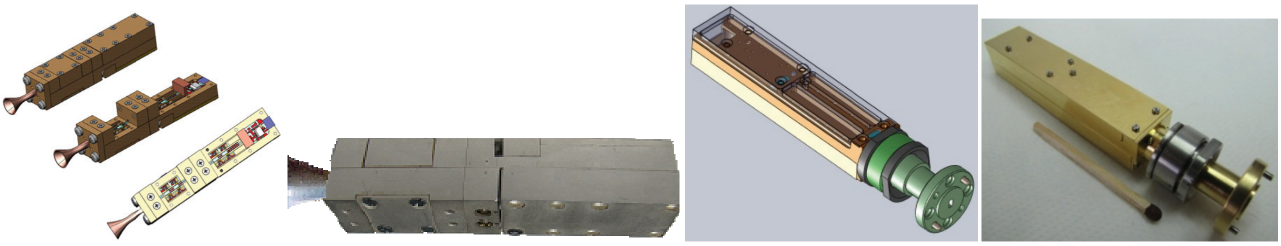

a) *b)* *c)* *d)*

Figure 7. Radiometric Radiometric wideband low-noise total power receiver: a, c) model and photo of receiver designed and created in State Research Center "Iceberg"; b), d) model and photo of the new receiver designed and created by A. Pavlyuchenko.

The 3D model of the system and its realization are depicted on the Fig. 8, left and right, respectively. The system is built on top of the moving circular platform. The platform can rotate about its axis and tilt. The rotation and tilting are accomplished by two servomotors. The sensor is mounted onto the stake in front of the reflector and is propelled by a small DC motor. All of the motors are computer controlled. Positions of the reflector and the sensor stake can be adjusted and have 2 degrees of freedom relative to each other.

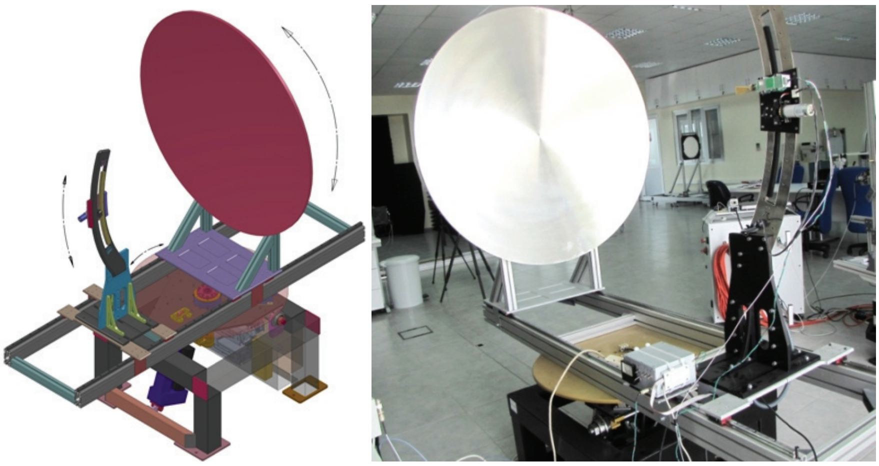

Figure 8. This figure depicts a 3D model (left) and the setup of the developed scanner (right). Arrows on the 3D model indicate pathways along which movement is controlled by their corresponding motors.

D. *Image acquisition*

Particularly, the system can operate in two different image scanning modes, which we name moving platform and moving sensor, respectively. The results of these experiments are represented in Fig.9. Both of the modes aim at sampling the scan area with a single point sensor, however differ in the

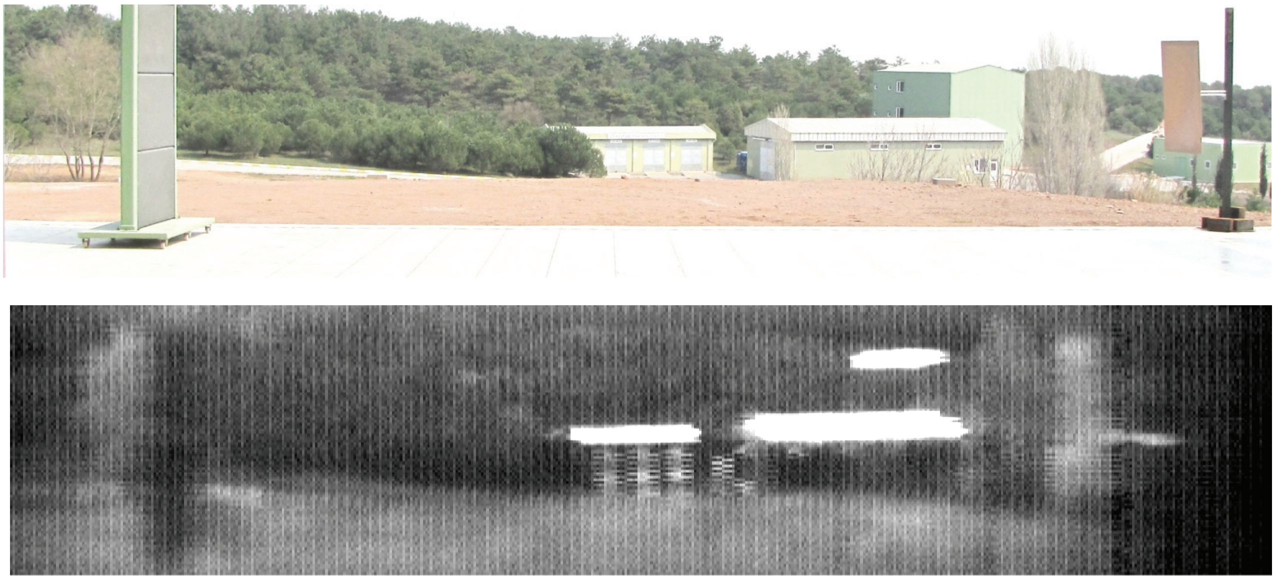

Figure 9. This figure depicts an ordinary photograph of a scaned area (up) and its corrsponding radiometric scan (down) obtained our system at an approximate distance of 150m.

approach the area is being covered. In the moving platform mode, the position of the sensor is fixed before the scan is started. Then, the system's platform performs alternating horizontal and vertical (tilt) moves to scan the area. In contrary, in the moving sensor mode the platform inclination is fixed and the scan is performed by alternating horizontal movement of the platform and sensor head movement along its stake.

E. Image processing and visualization

In this section, we shortly describe image processing and visualization techniques we are performing to process radiometric data acquired by the scanner. All of the implemented techniques are made available to the operator as well as can be flexibly assembled into the integrated image processing pipeline to attain better results. First of all, to prepare the radiometric data for display it is mapped to a gray scale palette. We perform this mapping using contrast stretching technique, which linearly maps raw radiometric values to a range of [0-255]. For instance, the Fig.10.b demonstrates the result of mapping the radiometric data (depicted on the Fig.10.a to a gray scale, where 1% of pixel values at each end are saturated. Histogram equalization is another method to enhance image contrast, however was not very efficient in our case. Instead, we use contrast-limited adaptive histogram equalization (CLAHE) [12], which divides image into a grid and then operates on each cell separately rather than processing entire image as ordinary histogram equalization does. CLAHE uses bilinear interpolation to

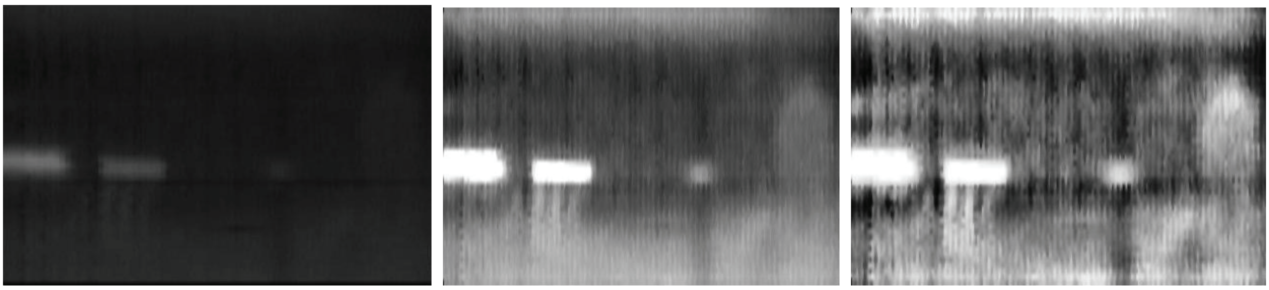

a) *b)* *c)*

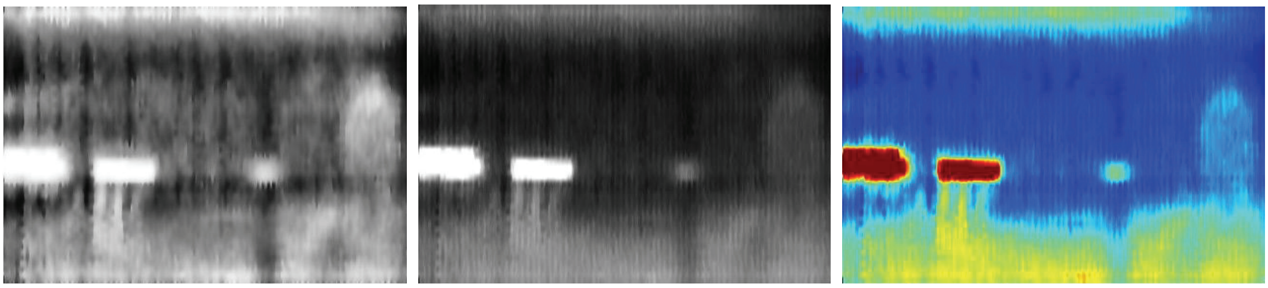

d) *e)* *f)*

Figure 10. This figure depicts results of applying various image processing techniques to the radiometric data: a) unprocessed data b) contrast stretching, c) CLAHE applied to b, d) Wiener filter applied to c, e) gamma correction applied to b, f) false coloring using user adjustable color palette.

smooth artificially induced boundaries and stitch processed cells into a final result. The Fig.10.c depicts result of applying CLAHE to the image on the Fig.10.b. Besides, we provide gamma correction functionality to maximize the visual quality of the result image and let the user adjust its parameter as appropriate. The Fig.10.e demonstrate application of the gamma correction. Radiometric data is rather noisy and the noise is gradually amplified when subsequent contrast enhancement methods are applied. In order to suppress noise and enhance visual quality of the image, we use Wiener filter [13] that adaptively smoothes image according to its local variation and at the same time preserves edges and other high frequency content. Fig.10.d result of applying Wiener filter.

It is well known that humans can differentiate between 20-30 grayscale tones at the same time, while on the other hand the color is comprehended much better [14]. We provide an option of mapping grayscale images to a number of different color palettes as well as let the user to edit the color palette according to his/her needs. For instance, the Fig.10.f demonstrates such false color mapping.

Conclusions

The paper shows the possibility of creation of radiometric scaning systems in 8 and 3 millimeter frequency range. The prinsiples which were taken as basis for 32-channel radiometric scaning system experimentally proved that chosen desing was right. This principles were used while designing radiometric system in sub-THz frequency range. 32-channel radiometric system which works in $33-38GHz$ frequency range is build with usage of low-noise total power receivers which provides obtaining of the radiometric image during 3 seconds.

While increasing operating frequency of radiometric systems up to $90-100GHz$ (sub-THz band), radiometric image contrast increase too, which allows to increase usage area of such systems. With the usage of total power receivers which work in frequency range of $90-100GHz$ the sensetivity of $0.67mV/K$ is received. The developing up to the receivers which are based on superheterodyne scheme and are working in frequency range of $97-104GHz$ allowed to reach the sensetivity of $\Delta T = 0.0031K$ $(\tau = 1s)$. Weight and gross geometry coefficients of the receiver in waveguide performance are creating technical problems while realisation of the multichannel radiometric system.

The high sensetivity of superheterodyne receiver allowed to hold the experiments to determinate and fixate dangerous objects and weapon which was hidden under winter clothes and through walls made from different materials from the distance of 10 meters. The experiments to determine transmission coeficient for different building materials were held. The maximum quantity of transmission coeficient for buildeng materials which allowed radiometric scanning was experimentally determined. The losses in polyethylene dielectric lens which was used in this radiometric system, did not stop the experiments with low luminance contrast targets at the distance up till the $2500m$.

References

1. N. Skou. Microwave radiometer systems: design and analysis. US: *Artech House*, pp.222, 1986.
2. D. V. Korolkov. Radioteleskopy and radiometry. *Nauka,* Moscow, 1973.
3. N. Skou, and S. S. Kristersen. Comparison of Imagery from a Scanning and a Pushbroom Microwave Radiometer. *IEEE Proc. Of IGARSS-91*, pp. 2107-2110, 1991.
4. R. Appleby and N. Anderton. Millimeter-Wave and Submillimeter-Wave Imaging for Security and Surveillance. *Proc. of the IEEE*, vol.95, No.8, pp. 1683-1690, Aug.2007.
5. A. S. Turk, A. K. Hocaogly, A. A. Vertiy. *Subsurface sensing.* J. Wiley & Sons Inc., pp.890, 2011.
6. V. N. Radzikhovsky, V. P. Gorishniak, S. E. Kuzmin, B. M. Shevchuk. 16-channels millimeter-waves radiometric imaging system. *MSMW2001 Symposium Proceedings*. Kharkov. Ukraine, June 4-9, pp. 466-4613, 2001.
7. A. Pergande. New steps for Passive Millimeter Imaging. *Proceedings of SPIE in Passive Millimeter-Wave Imaging Technology X*, Orlando, FL, USA, vol. 6548, pp. 654802-1-654802-4, April 2007.
8. A. Vertiy, M. Tekbas, A. Kizilhan, S. Panin and S. Ozbek. Sub-terahertz Radiometric Imaging System for Concealed Weapon Detection. *PIERS-2010*, Cambridge, US, 2010.
9. A. Vertiy, S. Ozbek, A. Pavlyuchenko, S. Panin, M. Tekbas, A. Kizilhan, H. Cetinkaya and A. Unal. Short- and Long-Range Passive Imaging in Millimeter-Wave-Band. *URSI GASS-2011,* Istambul, 2011.
10. A. Vertiy, S. Ozbek, A. Pavlyuchenko, S. Panin, M. Tekbas, A. Kizilhan, H. Cetinkaya and A. Unal. Passive radiometric imaging systems in millimeter wavelength range. *2011 IEEE AP-S/URSI*, Washington, US, 2011.
11. I.Prudyus, O. Denysov, L. Lazko. Image processing in the complex monitoring system radiometric channel. *TCSET-2006*, February 28 – March 4, pp. 271-272, Lviv – Slavsko, Ukraine, 2006.
12. Zuiderveld, K. Contrast Limited Adaptive Histograph Equalization. Graphic Gems IV. San Diego. *Academic Press Professional*, pp. 474–485. 1994.
13. Lim, Jae S. Two-Dimensional Signal and Image Processing. Englewood Cliffs. NJ. *Prentice Hall*, pp. 548. 1990.
14. G. Buchsbaum, A. Gottschalk. Trichromacy, opponent colors coding and optimum color information transmission in the retina. *Proc. R. Soc. Lond. B*, vol. 220, pp. 89–113, 1983.

UDC: 551.508

E.A.Miller (Central Aerological Observatory, Russia)
E.N.Kadygrov, Doctor of Science Degree (Central Aerological Observatory, Russia)
A.V.Troitsky, Doctor of Science Degree (Radiophysical Research Institute, Russia)
A.N.Shaposhnikov (Central Aerological Observatory, Russia)

AUTOMATIC MEASURING SYSTEM FOR REMOTE SENSING FOR MONITORING ADVERSE WEATHER CONDITIONS

Abstract.

In Central Aerological Observatory jointly with the specialists from the Radiophysical Research Institute in the end of '90th years of the last century designed the remote method of measuring temperature profiles of ABL based on measurements of self-emitting heat radiation of atmosphere on frequency near 60 GHz. The evolution of the equipment based on experiences and results of temperature profiles measurements are presented in the report.

II. INTRODUCTION

The lower atmospheric layer as opposed to the rest of the atmosphere is characterized by significant intra-diurnal variability of all meteorological characteristics. Monitoring its state using conventional technology, i.e. radio sounding, is incompatible with the space and time scale of this variability. To ensure the representativeness of the analysis of the results of actual measurements of models need to have tools that provide long time series of data available for the maximum heights of the atmospheric boundary layer (ABL). Microwave temperature profiler (MTP-5) has been developed as an instrument for continuous measurements of the temperature stratification in boundary layer. [1] The study of atmospheric boundary layer thermal structure is of huge interest for multiple applications, particularly it concerns works in Polar Regions. The first application for monitoring in Polar Region was for diamond quarry in Russian Yakutia region since 1992. The specific of this measurements was not only in wide range of the operating temperature (-60÷ -70°C), but also in the scanning of the depth of quarry.

a) b) c)

Figure 1. a) MTP-5 (one of the first versions) on Alaska (USA) 1996, b) North part of Sakhalin Island (Russia) 1999-2000 and c) MTP-5P Antarctica station Dome C 2002-2003 and 2004-2005.

Experience of creation and usage of this device allowed making a version of MTP-5 for unattended work in extreme weather events. These devices also were utilized in Polar Regions:

Kola Peninsula, north of Sakhalin island, Barrow station (Alaska), on ice-breaker in North Pole district during SHEBA (Surface Heat Budget of the Arctic Ocean) (Fig.1). The experience in use of these devices showed that it was necessary to have maximum height vertical resolution in lower layers of ABL for the investigations. All these requirements led to the creation of the new profiler MTP-5P – special version of the MTP-5 device (Fig. 1c).

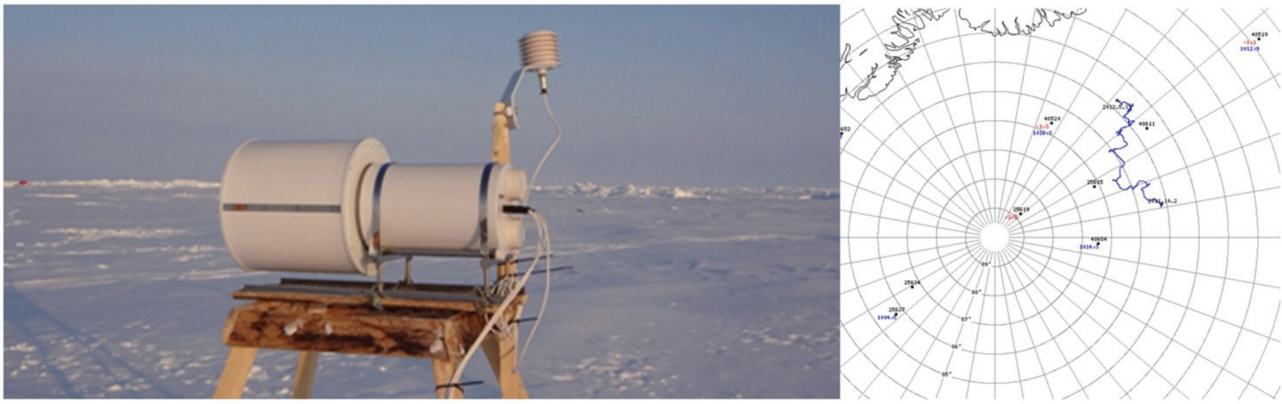

Figure 2. MTP-5PE on Russian drifting station North Pole – 39: April 2012. 83.7N 111.9W.

Evolution of the antenna's system and of other parts of the device has been based on the previous experiences of creation and usage and gave us a new upgraded version of MTP-5PE (Fig.2). MTP-5PE also has good vertical resolution in first 100 meters (10 m) due to the antenna system with a narrow beam (about 1 degree) and can operate in an ambient temperature range from -80 to +45 degrees.

III. Evolution of the technical parameters

From November 2002 to March 2003 profiler MTP-5P successfully had passed tests on Antarctic French-Italian continental station Dome-C (75006'S and 123023'E, height above sea level 3233 m, distance from coast 1100 m) [2,3]. Successful tests of MTP-5P during Antarctic summer allowed testing MTP-5P in more severe conditions. It was realized on all-the-year-round French-Italian station "Concordia" (near Dome-C where expeditions made only in Antarctic summer).

Polar profiler has vertical resolution 10-25 m on first 100 meters above Earth surface and keeps full capacity for work at very low temperatures (down to -80C). Main parts of device are high sensitive microwave radiometer tuned on frequency 60 GHz (5 mm wave length), antenna system which provides width of directional diagram 0,50, scanner made in the Netherlands company Kipp&Zonen, microprocessor device and meteo protection system. Applying of large antenna mirror which was necessary for thin beam caused problems with meteo shield. In contrast to MTP-5 the MTP-5P fixed radio transparent covering of antenna, with the result that the device needed maintenance in conditions of liquid precipitation.

For solving this problem a new modification of device which kept advantages of polar version and high-altitude modification MTP-5HE was created (Fig 2). Active meteo shield makes device unattended for any weather conditions, the newest antenna system provides high accuracy of temperature profiles measurements in a layer of 100-200 m, and using of receiver with frequency 56,6 GHz provides availability to install temperature profiles up to 1000 meters. The theoretical distribution of the errors in temperature profiles measurements and retrieval as inverse task were confirmed as result the statistical comparison with the operational radiosonde observations (RAOBs). The root-mean-square (RMS) error is in range from 0.2 up to 1.2 degree for the heights range from 0 up to 1000m with the error of height determination about 25%.

In Moscow the MTP-5PE has been calibrated by the use of special microwave target with different temperatures. The procedures of the self calibration also have been tested. The procedures of self calibration have made the correction by the use of the algorithm in software by use signal from horizon and sensors data. This technology is well known and applicable for MTP-5 because it work in range near 60 GHz [4, 5].

IV. Results of measurements

In Antarctica, long-lived stable ABLs are in direct contact with the free atmosphere. Then the standard theory of the nocturnal stable ABL is not applicable. Instead of the ABL as such, we need to consider a two-layer system consisted of the ABL and the capping inversion developing in the course of time due to the persisting radiative cooling of the ice/snow surface. [3]

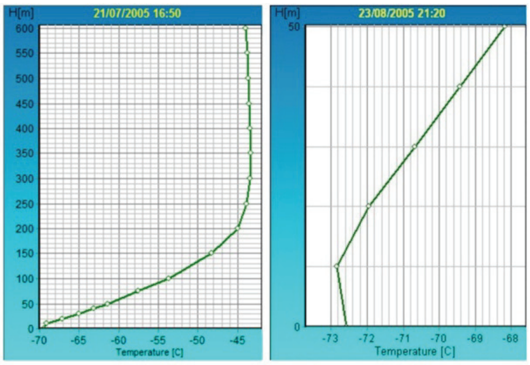

a) b)

Figure 3. The example of the temperature profiles typical for winter season (a) and with elevated inversion in first 50 m (b) have been measured on station Dome-C in July-August 2005.

Here, ABLs - the layers with large turbulent kinetic energy - are generally shallow (about 30 m), while the capping inversions, with rather low turbulent kinetic energy but strong temperature fluctuations and hence pronounced turbulent potential energy, could be quite deep. From the mean temperature profiles it is impossible to distinguish between the ABL and the capping inversion. [3]

The example on Fig.3 (a) illustrates the typical temperature profiles for winter season for stable boundary layer and good resolution of the first 50 m temperature stratification.

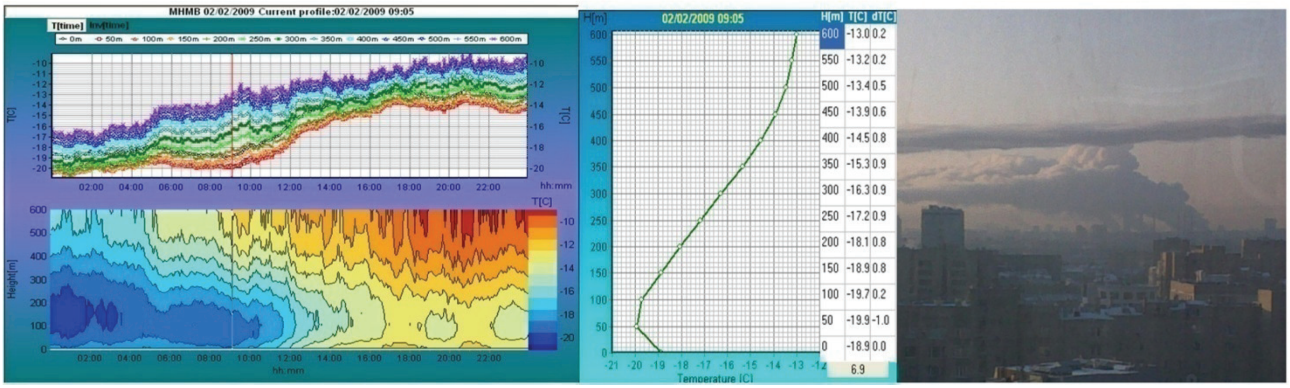

Figure 4. The example of the temperature profiles typical for winter season during strong temperature inversion in Moscow on 02/02/2009 and pictures from centre of the city are shown.

The preferences of the continuously measurement is allow to have results of monitoring ABL not only for scientific tasks, but for ecological services also. On Fig. 4 has been shown the results of measurement in Moscow during strong inversions in winter time. MTP-5 data has been successfully used continually for ecological by Moscow ecology service last 6 years.

Since 2009 the measuring system developed on base of MTP-5 and 4000 series SoDARs have been installed in Rome Fiumincino airport for monitoring of the fog. The SoDAR 4000 offers the highest resolution data available allowing for data recovery in 5 meter increments. This SoDAR measures wind starting at the 30m level up to the 200m level (Fig.5).

Figure 5. The installation of the fog monitoring system in Fiumicino airport (Rome, Italy) in 2009.

Hoefler Consulting Group (HCG), Anchorage, Alaska, has installed a meteorological monitoring station located on Endeavor Island, adjacent to Endicott Island, 28 kilometres northeast of Prudhoe Bay, Alaska. The Endeavor Island (Alaska) meteorological monitoring station, which began operation on May 15, 2010, is instrumented with MTP-5PE, for the purpose of obtaining atmospheric temperatures at multiple levels up to 1,000 meters above ground level. The intent is to use the resulting temperature profiles to support atmospheric modelling necessary for permitting petroleum development in the area. Besides, high resolution capabilities of antenna system and installation algorithm quality allowed observe double inversion in polar region in a 300 meters layer and retrieval high elevated inversion. The example of the double inversion and result of comparison with radiosounding data are shown on Fig.6.

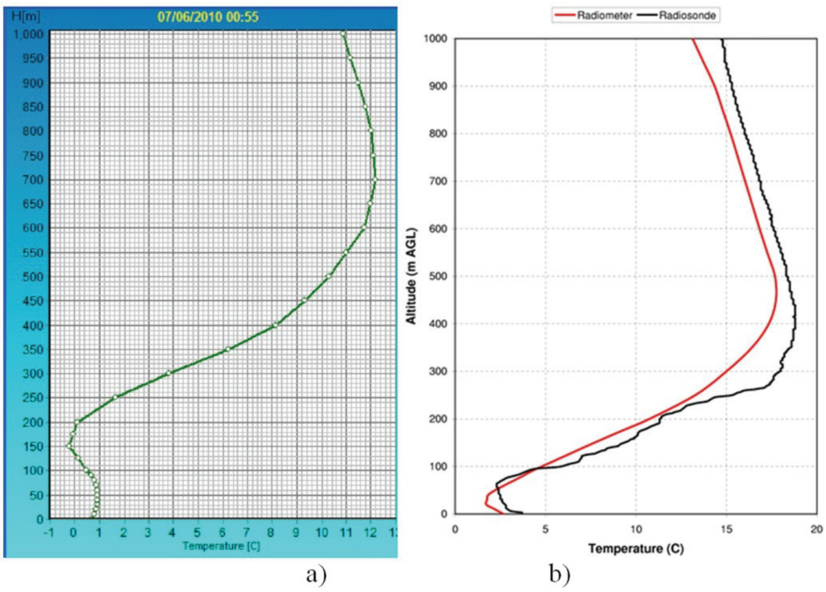

Figure 6. Temperature profiles typical for Endeavor Island summer (a) and example of comparison with radiosounding data(b) on Alaska is shown 2010.

The profiler MTP-5PE provides continuous (every 5 min.) measurements of the temperature profiles of ABL on Russian polar drifting station-39 (Arctic and Antarctic Research Institute - AARI of the Russian Federal Service on hydrometeorology and environmental protection) since April 2012 (Fig.7). Device was installed on station and had operated in automatic mode. There was unusual dynamic of the inversion in boundary layer during this period (Fig.7).

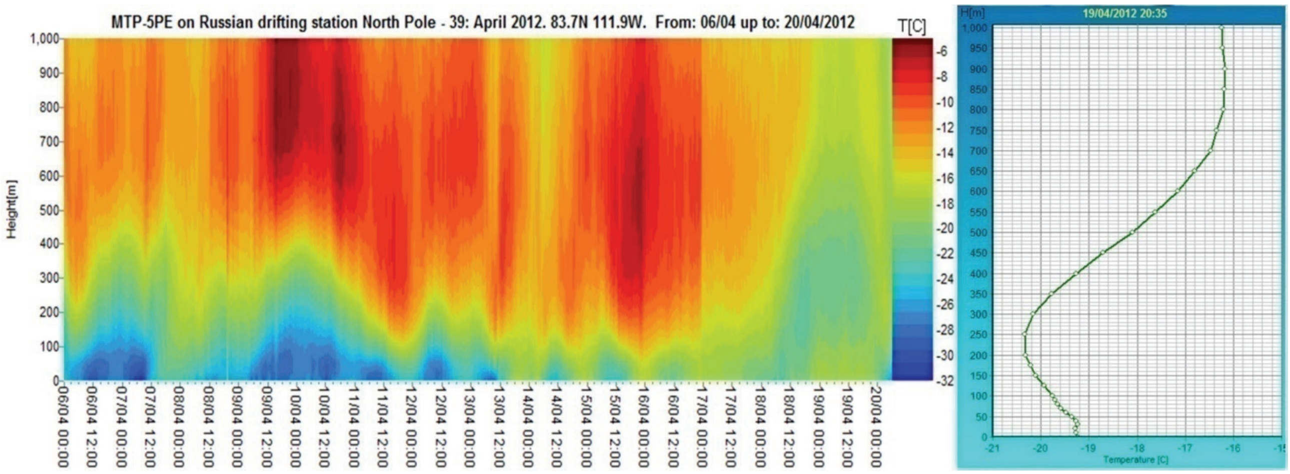

Figure 7. The time series for polar region were measured by use MTP-5PE version (April 2012).

V. Conclusions

New automatic measurement system based on MTP-5 allowed to measuring temperature profiles up to heights 1000 meters practically in all weather conditions (with outside temperature up to minus 80C). Besides, high resolution capabilities of antenna system and installation algorithm quality allowed observing double inversion in polar region in a 300 meters layer. Such systems are allowed to have results of monitoring ABL not only for scientific tasks, but for ecological services also.

VI. References

1. *Troitsky A. V., Gajkovich K. P., Gromov V. D., Kadygrov E. N., and Kosov A. S.* (1993) Thermal sounding of the atmospheric boundary layer in the oxygen absorption band center at 60 GHz. IEEE Trans. Geosci. Remote Sens. 31:116–120

2. *Argentini S, Conidi A, Viola A, Mastrantonio G, Ferrara N, Petenko I, Kadygrov E N, Koldaev A V, Viazankin A. S* 2005 Temperature measurements at Dome C using a new microwave temperature profiler. X Workshop sull'atmosfera antartica, Roma (22-24 ottobre, 2003)

3. *Argentini, S., Pietroni, I., Mastrantonio, G., Viola, A., Zilitinchevich, S.,* 2007, “Characteristics of the night and day time atmospheric boundary layer at Dome C, Antarctica”, EAS Publ. Series 22, 49

4. *Troitsky A. V.* (1986) Remote definition of the atmosphere temperature from spectral radiometric measurements in the line λ = 5 mm. Izv. Vuzov Radiophysics XXIX:878–886

5. *Kadygrov E.N., and D.R. Pick.* The potential for temperature retrieval from an angular-scanning single-channel microwave radiometer and some comparison with in situ observation. Meteorol. Appl., 1998, 5, 393-404.

A. A. Vertiy Prof. Dr., A. V. Pavlyuchenko Dr.
(International Laboratory for High Technology, TUBITAK-MRC, MI, Dr. Zeki Acar Street, 41470, Gebze-Kocaeli, Turkey)

EXTREMELY HIGH FREQUENCY RADIOMETRIC IMAGING SYSTEM

A prototype of a multipurpose scanning radiometric imaging system of extremely high frequency range $97-104GHz$ *with sensitivity of* $\Delta T = 0.0031K(\tau = 1s)$ *for* $1ms \le \tau \le 100ms$ *is presented in the work. Investigations of transmission factors of different materials are carried out for through-wall detection of different objects as well as for detection of weapons concealed under the clothing. Results of radiometric measurements of objects located on the sea surface at distances in between 10m to 2.5km are also given.*

INTRODUCTION

Passive millimeter-wave imaging systems are very promising for detection of dangerous objects (weapons, explosives, drugs, etc.) concealed under persons' clothing, without revealing itself. Because of the terroristic threats in the last decade, the high-resolution radiometric systems for fast imaging at short distances are essential for personal weapon control in public places. Owing to ability to penetrate poor weather for surveillance in the long-range regime, the radiometric imaging holds great promise as a means to aid aviation in low visibility conditions.

Millimeter-wave imaging systems have shortages of low speed of operation and small spatial resolution in comparison with optical systems [1, 2]. It is usual to solve this problem by using multi channel scheme of the imaging sensor module. Such array of sensors is capable of 2-D scenes in real time. Unfortunately this high cost design has disadvantages of the channel identity and stability. Spatial resolution constrained by the Rayleigh criterion is determined first of all by the receiver sensitivity and image reproduction quality of antenna. Low-noise amplifiers and low aberration antenna systems are intended for improving the spatial resolution.

In this work a prototype of a passive scanning radiometric system operating in frequency range of *97-104 GHz* and employing high sensitive receiver created on super-heterodyne scheme is presented. Polyethylene lens antenna with the aperture size *500 mm* was used for carrying out radiometric experiments for distances to objects from *10 m* to *2.5 km*. Investigations of reflection factors of different construction materials are carried out for through-wall detection of different objects as well as for detection of weapons concealed under person’s clothing. The receiver sensitivity achieved allowed us to conduct radiometric scanning of low contrast objects such as ships at different elevation angles for distances from *1 km* to *2.5 km*. The aim of the work was investigation of potential possibilities of the system and areas of applications of this high sensitive radiometric system.

IMAGING SYSTEM DESCRIPTION

A. Owerview

A modified 2-D scanning system presented on Fig.1 was used as a tool for conducting radiometric experiments and receiving images of different objects. The scanning system consists of focusing lens [3, 4] manufactured from polyethylene, radiometric receiver with a horn antenna, two-coordinate device for mechanical moving of the receiver [3, 5], analog-to-digital converter and PC for data storage, visualization of the information received and system managing.

Figure 1. Photo of 2D passive scanning radiometric system.

B. *Superheterodyne receiver*

The superheterodyne radiometric receiver for extremely high frequency range (3-mm band) was developed and created in ILHT. The radiometric receiver is created as a waveguide superheterodyne scheme with a low-noise amplifier at the input. The front-end part of radiometric receiver is presented on Fig.2. Employment of the low-noise amplifier at the receiver input allows to decrease noise factor and to increase its sensitivity [6-8]. The receiver heterodyne consists of a master oscillator based on Gann diode and on low-noise buffer amplifier. A mixer is made by balance scheme using AsGa Schottky diodes. Conversion losses of the mixer did not exceed $6.5dB$ in working frequency band. Intermediate frequency section consists of three low-noise amplifiers and a band filter. Amplification factor of the intermediate frequency section was more than $50dB$ and noise factor was $1.1dB$. The detector was done by voltage doubling scheme on Schottky diodes.

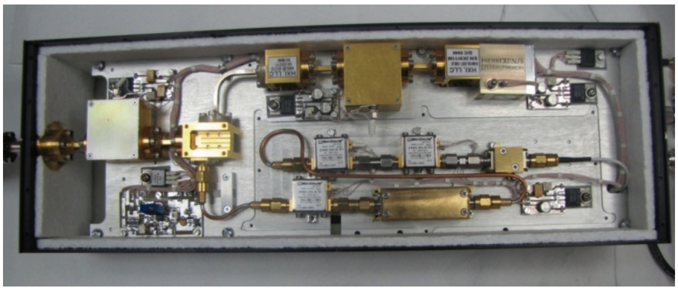

Figure 2.Front-end part of radiometric receiver.

Working frequency range of the receiver was from $97GHz$ to $104GHz$. The receiver sensitivity measured and adjusted to one second was $\Delta T = 0.0031K$. The radiometric receivers are characterized by the amplifier factor between $60dB$ to $120dB$, thus obtaining minimum fluctuations of the amplifier factor is a very complicated problem and is an actual problem in the radiometry [7, 8]. In this case this problem is solved by using double supply voltage stabilization of all the units in combination with temperature stabilization of the whole receiver. Temperature inside the receiver is supported at the level of $45^{\circ}C$ with accuracy no less than $\pm 0.05^{\circ}C$. As a result the given temperature regime of the receiver was achieved, deviations of the output fluctuations do not exceed $10mV$ (for integration constant value of $100ms$).

Value of radiometric gain [7, 8] is obtained as the following formula $q = \sqrt{\Delta f \cdot \tau}$, shows a signal which q times smaller than intrinsic noises of the receiver and it may be registered by radiometer. For achieving different values of the radiometric gain when conducting experiments, different filters with $\tau = 1ms$, $\tau = 10ms$ и $\tau = 100ms$ were manufactured. The output of receiver signals for filters with different integration time is presented on Fig.3.

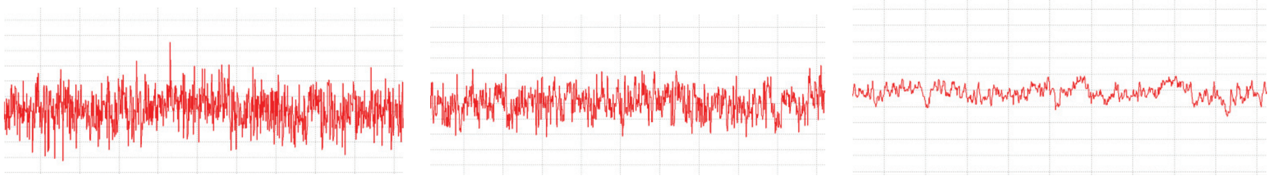

a) *в)* *c)*

Figure 3. Output of receiver signals: a) $\tau = 1ms$;b) $\tau = 10ms$;c) $\tau = 100ms$. The vertical scale is 10mV/div, the horisontal scale is 10s/div.

Coaxial input and output of the filters gave the opportunity to change the value of the radiometric gain of the receiver q when carrying out the experiments during very short time.

EXPERIMENTAL RESULTS

It is known [7, 9], that when energy with power of P incidents on an arbitrary material than part of this power P_ρ is reflected, the other part of the power P_α is absorbed, and the third part of the incident power P_τ passes through the material. Reflection factor, absorption factor and transmission coefficient are connected with each other by the following equation:

$$\rho + \alpha + \tau = {P_\rho}/{P} + {P_\alpha}/{P} + {P_\tau}/{P} = 1,$$

and usually $\tau \approx 0$, so $\rho + \alpha \cong 1$. In literature you may find that $\tau \approx 0$, but practically $\tau \neq 0$, thus, part of the power passes through the material and this part may be registered. In his work [10] the author gives only results of investigations of the reflection factor of some materials at frequencies of $94 GHz$.

In this work investigations of reflection factor for different construction materials were carried out in the first series of experiments. For these experiments the high sensitive radiometric scanning system was used, and irradiation of the cold sky which was supplied by a metal plate located at the distance of $10m$ from the receiving lens at the angle of 45°. This irradiation from the cold sky was employed as non-coherent illuminating radiation. The materials under investigation were located at the distance of $2m$ from the lens and they totally overlapped its aperture. The results of the experimental investigations of the transmission factors of different construction materials for the frequency range of $97 - 104 GHz$ are given in Tab.1.

TABLE 1. Transmission factor for different construction materials.

Type of material	Transmission factor, τ	Type of material	Transmission factor, τ
concrete	0.000174	fiberglass	0.003
brick	0.000133	cellular plastic	0.00458
marble	0.000522	beech galley	0.000893
gypsum	0.00148	window pane	0.08125
pine (dry)	0.000601	plywood	0.0458
plasterboard	0.0365	paper board	0.151
polyethylene (film)	0.1717	board-on-edge floor	0.0032

In the next series of experiments a pattern of letter “A” made from absorbing material was fixed on the metal reflector retranslating irradiation of the cold sky. Scanning of the object, letter “A”, was conducted in two regimes: the first regime with using of different construction materials placed on the way of radiometric signal propagation and the other regime - without such materials. Photo and the radiometric image obtained for letter “A” when scanning without obstacles and through plasterboard are presented on Fig.4, correspondingly.

The experiments carried out showed the possibility of obtaining radiometric images of objects located behind obstacles if transmission coefficient of materials no less than 0.005 0. One should notice good quality of the obtained radiometric images for contrast objects located at distances from $10m$ to $150m$.

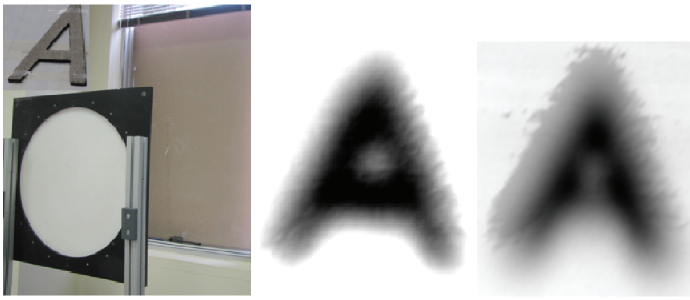

a) *в)* *c)*

Figure 4. Radiometric scanning at distance of 10m: a) photo of the scanning system and photo of letter «A»; в) radiometric image of an object without wall; c) radiometric image of the object behind the wall made from plasterboard.

In paper [11] a possibility of detection of weapon and other different dangerous objects concealed under person's clothing is shown. However, it should be noticed that in the most of the experiments described light summer clothing with reflection factor less than 0.2 was used. In our experiments we investigated possibilities of detection of weapons and other objects concealed under the winter clothing (clothing with high reflection factor $\rho \le 0.4$), and the person was behind the wall ($\tau \ge 0.005$) at distance of $10m$. One of the results obtained is presented on Fig.3. Radiometric image of dangerous objects (weapons) with reflection factor of $\rho \approx 1$ has sufficient dependence on the angle of view.

For one-to-one detection of objects concealed under the clothing, it is necessary to obtain scanned images at different angles. It may be illustrated by Fig.5. On Fig.5c a gun concealed at chest of a person has a smaller radiometric contrast than when scanning it at angle of 45 degrees (Fig.5d).

a) *в)* *c)* *d)*

Figure 5.Photo, radiometric image: a), c) frontal position; b), d) position at random angle. The outline of the gun is marked by the dotted line.

During the experiments, the value of radiometric gain was changed and such its value was found so that concealed weapon and other objects may be detected at distances of $10m$ and also objects located at distances of $150m$ at the same scene and clouds in the sky.

As it was mentioned above, the lens antenna system was used in the scanning system that did not allow obtaining in-focus image of objects located at different distances. Results of the experiments are given on Fig.6. At the foreground of the radiometric image one can see a gun concealed under winter clothing at distance of $10m$, at the right behind there is a building at distance of $150m$, and at the background at the top there are floating clouds.

Figure 6. Photo and radiometric image when scanning weapon concealed under clothing at distance of $10m$, building at distance of $150m$ and clouds at the background. The outline of the gun is marked by the dotted line.

Landscape where the experiments were carried out allowed to scan objects at the sea surface and to estimate maximum operational range of the system. The photo and radiometric image are represented on Fig.7. In the images one can see low-contrast sea targets – ships located at distance of $1000m$ (Fig. 7a and b), at distance of $2500m$ (Fig.7c and d) and also an opposite side of a bay located at distance of $10km$.

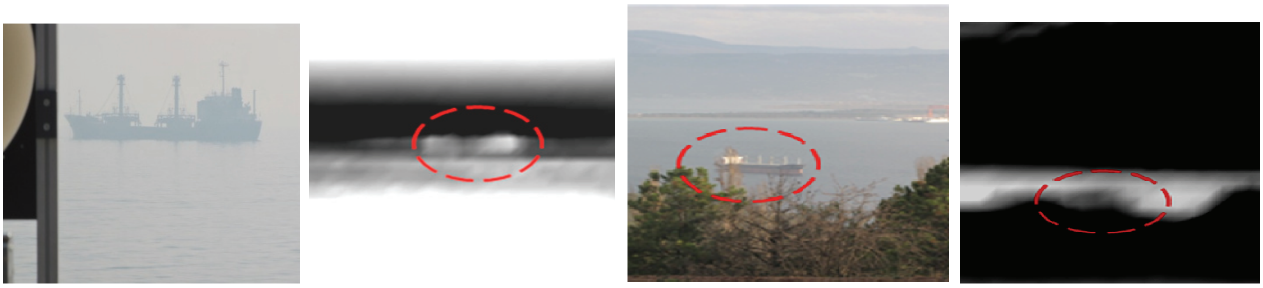

a) *b)* *c)* *d)*

Figure 7. Radiometric measurements at sea: a) photo and b) ship image at distance of 1000m; c) photo and d) ship image at distance of 2500 m. The outline of the ship is marked by the dotted line.

Difference in radiometric images on Fig.7b and Fig.7d are image inversion. It may be explained by different elevation angles for scanning. In the first case, Fig. 7b, the scanning system was fixed at the level of $10m$ above the sea level, and in the second case, Fig. 7d, the level was approximately $300m$ above the sea level.

CONCLUSIONS

In the work possibility of creating of multipurpose scanning radiometric system operating in frequency range of $97-104GHz$ with sensitivity of $\Delta T = 0.0031K$ $(\tau = 1s)$ for $1ms \le \tau \le 100ms$ was demonstrated. The system provides obtaining of radiometric images as for weapon concealed under person's clothing at distance of $10m$ as well as low-contrast sea targets at distance of $2500m$. Investigations of reflection factors of different construction materials were conducted, the possibility of detecting of objects and people behind walls as well as weapon concealed under person's clothing behind walls at distance of $10m$ were shown.

References

1. A. Pergande. New steps for Passive Millimeter Imaging. *Proceedings of SPIE in Passive Millimeter-Wave Imaging Technology X*, Orlando, FL, USA, vol. 6548, pp. 654802-1-654802-4, April 2007.

2. M. Born and E. Wolf. *Principles of optics.* Cambridge: Cambridge University Press,1999.

3. A. Vertiy, M. Tekbas, A. Kizilhan, S. Panin and S. Ozbek. Sub-terahertz Radiometric Imaging System for Concealed Weapon Detection. *PIERS-2010*, Cambridge, US, 2010.

4. A. Vertiy, S. Ozbek, A. Pavlyuchenko, S. Panin, M. Tekbas, A. Kizilhan, H. Cetinkaya and A. Unal. Short- and Long-Range Passive Imaging in Millimeter-Wave-Band. *URSI GASS-2011,* Istambul, 2011.

5. A. Vertiy, S. Ozbek, A. Pavlyuchenko, S. Panin, M. Tekbas, A. Kizilhan, H. Cetinkaya and A. Unal. Passive radiometric imaging systems in millimeter wavelength range. *2011 IEEE AP-S/URSI*, Washington, US, 2011.

6. A. S. Turk, A. K. Hocaogly, A. A. Vertiy. *Subsurface sensing.* J. Wiley & Sons Inc., pp.890, 2011.

7. N. Skou. *Microwave radiometer systems: design and analysis*. US: Artech House, pp.222, 1986.

8. D. V. Korolkov. *Radioteleskopy and radiometry.* Nauka, Moscow, 1973.

9. M. I. Finckelshtein. *Theory of radiolocation.* Sov. Radio, Moscow, 1973.

10. R. Appleby. Mechanically scanned real time passive millimeter wave imaging at 94 GHz. *Proc.SPIE*, vol.5077, pp.1-6, 2003.

11. R. Appleby and N. Anderton. Millimeter-Wave and Submillimeter-Wave Imaging for Security and Surveillance. *Proc. of the IEEE*, vol.95, No.8, pp. 1683-1690, Aug.2007.

UDC. 319.61.126.

A. B. Veselovskaya, A. M. Linkova, G.I. Khlopov, Doctor of Science
(Institute of RadioPhysics and Electronics J. Usikov by name of National Academy of Science of Ukraine, Ukraine)

DOUBLE FREQUENCY SOUNDING OF ELLIPSOIDAL WATER DROPS

The peculiarities of nonspherical water drops double frequency sounding are studied. The study is performed in the framework of the Pruppacher`s model for ellipsoidal drops using theory of dipole moments for calculation of drops backscattering. It was shown that differential radar cross-section of ellipsoidal drops practically does not differ from spherical drops with equal root-mean-cube diameter. The comparison with the experimental data confirms the validity of the assumptions used

Traditionally used single frequency sounding on the base of so called Z-I- relation [1] does not permit to obtain single-valued restoration of the precipitation parameters (intensity, water content etc.) and the methods of double frequency sounding are developed intensively [2, 3] for example in the framework of Tropical Rainfall Measuring Mission (TRMM) [4] and Global Precipitation Measurement (GPM) [5]. The main advantage of such methods is ability of precipitation microstructure parameters measuring that permits to study practically all others characteristics. Besides of this the use of double frequency sounding can provide single valued solution of inverse problem [6] using combined method of microstructure parameters profile measurements with subject to signal attenuation due to precipitation.

In general, the double-frequency method is based on measuring of differential radar cross section (RCS) of the precipitation as a ratio of their specific RCS at two frequencies $\sigma_d = \frac{\sigma_0(\lambda_1)}{\sigma_0(\lambda_2)}$, where $\sigma_0 = \int_0^\infty dr\sigma(r,\lambda)N(r)$, $\sigma(r,\lambda)$ - RCS of a single drop, $N(r)$ - particles distribution on size [2-4]. At that the assumption about spherical drop shape is traditionally used that permits to use rigorous solution of the electromagnetic scattering problem on dielectric sphere (Mie theory) [7] for calculation of the value $\sigma(r,\lambda) = \sigma_s(r,\lambda)$. But shape of the drops, especially of large drops, notably differs from spherical form and the applicability of this assumption must be examined additionally. That is why the goal of the present paper is to estimate the influence of the water drops nonsphericity on results of double frequency sounding.

Shape of the drops in steady fall. The distortion of the drop spherical shape – fig. 1a can be described in the framework of the Pruppacher's model [8] which is valid when wind impact is absent and in the steady-state fall. In this case the drop has shape of biaxial ellipsoid with horizontal axis 2b and vertical axis 2a – fig. 1b. The root-mean-cubic radius (RMCR) of such drop $r_3 = \sqrt[3]{ab^2}$ is widely used and defines the eccentricity (ratio of ellipsoid semiaxes) [8]

$$e = \frac{a}{b} = \begin{cases} \left(1 - \frac{9}{16} r_3 \rho_m \frac{V_\infty^2}{\gamma}\right)^{\frac{1}{2}} & \text{for } 0 \le r_3 \le 0{,}45 \text{ mm} \\ 1{,}03 - 0{,}124\, r_3 & \text{for } 0{,}45 \le r_3 \le 4{,}5 \text{ mm} \end{cases} \tag{1}$$

where $\rho_m = 1{,}1937 \cdot 10^{-6}$ - density of saturated water streams (g·mm^{-3}), V_∞ - velocity of steady drops fall (mm.p.s), $\gamma = 72{,}75$ - water surface tension (g·s^{-2}) at the temperature $T = 20°$ C.

The dependence of steady-state velocity of drop fall (m.p.s) on their RMCR (mm) may be approximated as follows [2] $V(r_3) = 9{,}65 - 10{,}3e^{-1{,}2r_3}$ which asymptotically tends to the value 10 m.p.s. This permits to calculate the drop eccentricity on RMCR – fig.2a and the calculated dependence is shown in fig. 2b where the horizontal axis rises more rapidly than vertical which is important for electromagnetic scattering.

Electromagnetic scattering of ellipsoidal drops. To calculate the scattering from ellipsoidal drop we use the approximate method based on calculation of dipole moments [9]. Omitting the calculation details it is possible to show that RCS of ellipsoidal drop along small and large axes equals to $\sigma_{x,y} = I_{x,y} \cdot \sigma_s$, where $I_{x,y}$ - components of the scattering intensity

$$I_x = \frac{\left[\left(g-g'\right)\alpha_1\left(\alpha_2 \sin\alpha + \alpha_1 \cos\alpha\right) + g' \cos\alpha\right]^2}{g_s^2}; \qquad I_y = \frac{\left[\left(g-g'\right)\alpha_2\left(\alpha_2 \sin\alpha + \alpha_1 \cos\alpha\right) + g' \sin\alpha\right]^2}{g_s^2}; \qquad (3)$$

where $g = \frac{ab^2}{3} \cdot \frac{\varepsilon' - 1}{1 + (\varepsilon' - 1)q}$, and $g' = \frac{ab^2}{3} \cdot \frac{\varepsilon' - 1}{1 + (\varepsilon' - 1)q'}$, ε' - real part of drop dielectric constant,. $q = \frac{1}{l^2}\left(1 - \sqrt{\frac{1-l^2}{l^2}} \arcsin l\right)$, $q' = \frac{1}{2} - \frac{1}{2}q$, $l = \sqrt{1-e^2}$, σ_s - RCS of spherical drop, for which $g = g' = g_s = r_3^3 \frac{\varepsilon' - 1}{\varepsilon' + 2}$, $\{\alpha_1, \ \alpha_2, \ \alpha_3\}$ - direction cosines for transformation coordinates system of the drop to system of radar antenna [9]. For Ver polarization $\alpha = 90^\circ$, $\alpha_1 = 0$, $\alpha_2 = 1$, $\alpha_3 = 0$, scattered energy equals $I_x = 0$, $I_y = \frac{g^2}{g_s^2}$, for Hor polarization $\alpha = 0^\circ$, $\alpha_1 = 1$, $\alpha_2 = 0$, $\alpha_3 = 0$ and scattered energy $I_x = \frac{g'^2}{g_s^2}$, $I_y = 0$.

To calculate RCS of a spherical drop we used rigorous theory Mie [7, 11] in the form

$$\sigma_s(r_3) = \frac{1}{\rho^2}\left|\sum_{n=1}^{\infty}(-1)^n(2n+1)(a_n - b_n)\right|^2 \qquad (4)$$

where $\rho = \frac{2\pi}{\lambda} r_3$, a_n and b_n Mie coefficient, expressions of which are given in [7].

To calculate complex dielectric constant $\dot{\varepsilon} = \varepsilon' - j\varepsilon''$ we used generalized formulas of Debay [10] that provide good accuracy in microwaves. So in the fig. 3 the dependences of normalized RCS on RMCR are shown for wavebands λ = 8,6 mm –a) and λ = 3,2 см – b) (curves *1* correspond to Hor polarization and curves 2 – to Ver polarization). For comparison the curves *3* are presented for spherical drops that confirms the evident relation – RCS of ellipsoidal drop at Hor polarization is always larger than RCS of spherical drop and does not exceed the RCS of ellipsoidal drop on Ver polarization. It is necessary to note that curves *1* and *2* have practically the same divergence for orthogonal polarizations when RMCR increases in different wavebands which leads to important result: the differential RCS of ellipsoidal an spherical drops of equal volume practically does not differ in wide range of RMCR and for different combinations of wavebands – fig.4 (fig.4a – Hor polarization, fig. 4b – Ver polarization, curves *1* correspond to λ_1= 0,86 cm and λ_2= 3,2 cm, curves *2* - λ_1= 0,86 cm and λ_2= 10 cm). So in the framework of the present consideration the data of double frequency sounding practically does not depend on shape of the drops and the assumption concerning their sphericity is quite true.

From the other side, the approximate character of the calculations performed it is necessary to estimate the validity of the assumptions used. For this to do we compare the data obtained with the results of more rigorous calculations of electromagnetic scattering on ellipsoidal drop on the base of Pruppacher model in 8 mm waveband. The results of comparison are shown in fig. 5, where curves 1 correspond to the present data and curves *2* – to the data of [11], fig. 5a presents data for Ver polarization and fig.5b – for Hor polarization of incident waves. As one can see the approximate solution practically does not differ from more rigorous calculations [11] when RMCR does not exceed $2r_3 \leq 3$ mm (diffraction parameter $\rho_d = \frac{2\pi r_3}{\lambda}\sqrt{\varepsilon'} \leq 10$).

In spite of disagreement of the data presented for large drops it is necessary to note that diameter of the main number of drops at European area does not exceed $2r_3$=0,8÷0,9 mm [9] and maximal diameter $2r_3$=3 mm occurs in heavy shower with intensity more than $I \geq 50\div60$ mm.p.h, the probability of which ≤ 0,1 % [12]. That is why it is reasonable to assume that the error due to the approximate calculations of RCS for large drops $2r_3 \geq 3$ mm in total RCS of polydisperse medium in general case will be negligible quantity.

The conclusion regarding small impact of nonsphericity of rain drops on double frequency sounding does not conflicted with the data of experimental study in wavelengths λ= 8,2 mm and λ=3,2 cm [13]. In the paper citied the electromagnetic scattering studied using drops, the shape of which notably differs from spherical – fig. 6. But in this case the drop stretched in vertical direction (not became flat) due to peculiarities of the drops forming and short distance of free fall. But in the case under consideration the direction of elongation does not matter and the data of obtained by double frequency sounding r_{2f} well correspond to contact measurements on the base of RMCR r_v and photographing r_f, at that the data discrepancy does not exceed 4 % (see table).

So the experimental data presented in [13] indirectly confirm the possibility of double frequency sounding use for measurement of dimensions of nonspherical water drops with accuracy that is quite enough for practical needs.

Reference

1. *Doviak R.J.* Doppler radar and meteorological observations: Translation from English / *R. Doviak, D.S. Zrnic*. – L.: Gidrometeoizdat, 1988. – 509 p.

2. *Menenghini R.* On the equivalence of dual-wavelength and dual-polarization equations for estimations of the raindrop size distribution / *R. Menenghini, L. Liao* // J. Atmos. and oceanic technology. – 2007. – V. 24. – P. 806-820.

3. *Khlopov G.* Profiling of rain parameters by double frequency radar / *G. Khlopov, A. Linkova, O. Voitovych* // Proc. Microwaves, Radar and Remote Sensing Symposium MRRS'2011, Kiev, August 25-27 2011. – Kiev, 2011. – P. 213-216.

4. Tropical Rainfall Measuring Mission: description [Electronic resource] / Goddard space flight center, NASA. – http://www.trmm.gsfc.nasa.gov. – 20.04.2011.

5. Global Precipitation Measurement: description [Electronic resource] / Goddard space flight center, NASA. – http://pmm.nasa.gov/GPM. – 20.04.2011.

6. *Linkova A.* Double frequency sounding of liquid precipitation by weather radar MRL-1 / *Ye. N. Belov, O. A. Voitovich, A. M. Linkova, G.A. Rudnev, G. I. Khlopov, S.I. Khomenko* // RadioPhysics and Electronics. – 2012. – Vol. 3 (17), № 1. – P. 49-59.

7. *Van-der-Hulst G.* Light scattering by small particles: Translation from English. / *Van-der-Hulst G*. – M.: Izdatelstvo inostrannoj literatury, 1961. – 536 p.

8. *H. R. Pruppacher and K. V. Beard*, «A wind tunnel investigation of the internal circulation and shape of water drops falling at terminal velocity in air», Quart. J. Met. Soc., vol. 96, pp. 247-256, Apr. 1970.

9. *Shupatskij A. B.* Radar measurement of intensity and some others characteristics of precipitation. – M.: Gidrometeoizdat, 1960. – 119 P.

10. *Ayvazyan G. M.* Radio propagation of millimeter and submillimeter waves in clouds. Edited by prof. *G.G. Shukin*. L.: Gidrometeoizdat, 1991.

11. *Oguchi T.* Propagation and scattering of electromagnetic waves in rain and others hydrometeors*,* TIIER, Vol. 71, №9, 1983.

12. *Kulemin G.P.* Millimeter-Wave Radar Targets and Clutter. Edited by D. Barton. Artech House, Boston-London, 2003, 327 P.

13. *Voitovich O. A., Linkova A.M., Khlopov G.I., Khomenko S.I.* Remote measurement of water drops sizes by double frequency sounding // RadioPhysics and Electronics. 2010. Vol 1(15), N 4, P.78-84.

UDC:621.396.95

V.K.Ivanov, DSc, A.Ya.Matveev, PhD, V.N.Tsymbal, PhD,
S.Ye.Yatsevich, PhD, (IRE of NAS of Ukraine, Ukraine)

AIRBORNE RADAR – THERMAL INFRARED DIAGNOSING OF OVERWATERING SOILS

In the paper are analyzed results of overwatering soils combined monitoring by airborne remote sensing complex ARSC-30 Ka-band SLAR and thermal IR scanner, realized sequentially during day- and night-time of dry autumn season. It is shown a good mutual supplement thermal infrared and microwave data to the underflooding manifestations identification.

Effects of aviation monitoring of the subsurface overwatered soil zones, in particular of the underflooded areas as result of subsurface water rise, are analyzed. Full-scale experiments were conducted in the conditions of different seasons - in the winter, in the summer and in the autumn by means of the Ka-band side looking airborne radar SLAR, thermal IR scanner "Malahit-1" and aerial monochrome photo camera AFA-41/7,5.

Effects of autumnal surveying [*Konyukhov*, 2010] have appeared the most informative. The visual analysis thermal IR (consecutive, day-time and night-), radar and optical images of test range has allowed to identify (except zones of vegetation well observed on the optical images, typical for boggy areas) manifesting effect of thermal inverse of a zones in a various degree is subsurface the moist and remoistened soil as on agriculture fields, and in immediate proximity from the railway. These zones are distinctly observed in the form of darknesses on night-time IR images, (for example on fields №2 and №3, fig. 1b). Precipitations around test range during aviation monitoring and within previous two weeks it was not observed.

On fig. 1 presents images of test range around settlement the Horoshee Ozero, obtained by airborne remote sensing complex ARSC-30 in a day-time and night-time in the beginning of October (a - IR day-time, b- IR night-time and c - SLAR) are given.

The numbers marks the fields that were investigated. By arrows the explored sections (columns) transiting through the same sites of fields on various images are shown. Images of these columns are presented on fig.2.

On fig.1d it is presented zoomed IR the day-time image of a field №3 with tracks of a haul of straw, by a horizontal arrow are scored a straw stack, and vertical arrows of a solar blind zones behind forest belts. On fig.1e - the optical image of a field №3 obtained by an aerial survey (winter). And on fig.1f the strip image of a column «e» in the field 3 (fig.1d), transiting through a stack of straw and a blind zone is shown.

Comparison IR (day-time and night-) and SLAR images, and also columns of these images transiting through the same sites of fields, allows coming to conclusion that:

- Day-time thermal IR images (fig.1a) are substantially formed under the influence of the solar radiation scattered by a ground surface and caused by distinctions in albedo of fields and objects;
- Night-time IR images (fig.1b) demonstrate the significant residual effect of day-time action of a solar radiation on their thermal state - for example, an average thermal radiation of a field №1 (fig.2b,) (which during daylight hours most intensively scattered a solar radiation) much more low than at a field №3 (fig.2h) on which tracks of a haul of straw (as colder) also are well stand out;
-The dry autumnal season is a favorable time for radar - thermal IR monitoring of underflooding manifestations, since they (fig.1b, 2f) are distinctly manifested on night-time IR images (are marked by flag indicators, in the main on not used fields, for example in the field №2). Thus SLAR image (fig. 1c) testifies that weed vegetation coating not used fields, for example a field №2, has practically growth stopped. SLAR here it practically "does not see".

And canopy variations where vegetation growth has not stopped yet (on kitchen gardens with various late crops of a field №4, and field №5 with winter wheat young growth) are observed SLAR well enough (fig.2h,). Judging by night-time IR to the image of kitchen gardens in the field №4 and from the settlement opposite side Horoshee Ozero the vegetation, which vegetation growth is prolonged, could mask of underflooding manifestations essentially.

Full-scale aviation experiments was accompanied by land contact measuring of soil humidity (confirmed presence of underfloodings in remotely found out sites [*Rodzock*, 2005]), weather data on temperature of soil, water and air in night and day time were thus gained also.

Considering that fact that the most stable reference value is water temperature in ponds (+9^{0}C in the afternoon and +8^{0}C at night), and the ground surface temperature changed from +13^{0}C in the afternoon to +3^{0}C at night, and guessing that the soil of a field №1 (having the greatest albedo) has least saved up heat in day-time at the expense of a solar radiation and consequently the temperature of its surface is closest to measured on a meteorological station at night, estimates of temperature contrasts (concerning averages on matching field on night IR images) zones of underflooding manifestations - (3,5^0 - 4^0) and zones of different albedo, for example, tracks of a haul of straw - (2^0 - 3^0) have been conducted.

Comparison of these effects allows to conclude that the negative temperature contrasts on intensity night-time IR radiation in itself cannot be a trusty sign of definition of underfloodings manifestations since they may be caused by various factors. Trusty definition is possible only on the basis of system of the attributes considering of accumulation of heat in a soil at the expense of a solar radiation, heat flow variations in depth of a soil (called by changes of the subsurface humidity) and a vegetation stratum over a ground. Analyzing so-called multivariate «spaces of attributes» is necessary.

On fig. 3 the image three-dimensional «spaces of attributes» on which axes are put aside intensity measured in computer levels of samples of columns (fig. 2) day-time IR ($I_{IR,\ d.t.,\ comp.lev}$), night-time IR ($I_{IR,\ n.t.,\ comp.lev.}$) and SLAR images ($I_{SLAR,\ comp.lev}$). The white round scores the attributes matching to zones of underflooding manifestations. It is visible that for requirements of conducting of full-scale experiment (dry autumn) attributes of underflooding zones can be reliably identified in three-dimensional «space of attributes», built by results of consecutive day-time – night-time radar - thermal IR sensing.

Conclusions

The analysis of effects of full-scale experiments on aviation radar – thermal infrared monitoring of the underflooded areas as result of subsurface water rise, has shown that in the conditions of dry autumn sharing of data of consecutive day-time and night-time sensing allows in three-dimensional space of attributes (IR -day, IR -night and SLAR) it is quite reliably identify the zone of soil overwatering manifestation, as without vegetation, and coated with vegetation.

References

1. Radar Techniques and Facilities for On-Line Remote Sensing of the Earth from Aerospace Carriers / *A. G. Boyev, V. B. Yefimov, V. N. Tsymbal and others // edited by S.N. Konyukhov, V. I. Dranovsky, V. N. Tsymbal.* – Kharkov (Ukraine): Publishing house Sheynina O. V. – 2010. -428 p. ; *http://www.studmed.ru/priborostroenie-radio-i-svyaz/radiolokaciya/?page=2&sort=type*

2.*Rodzok G. P, Gunchenko V. O, Tsymbal V. N.* Definition of underflooding of territories with use humidity-level gauge of radio waves band //Materials of 3rd Scient.Pract.Conf. «UNEDFLOODINGS-2005»: Pressing problems of the forestalling and struggle against a regional underflooding of lands. 2005. Lazurnoe, the Kherson region NPTS «ECOLOGY, the SCIENCE, ENGINEERING». 2005. P. 26-27 (on ukr.).

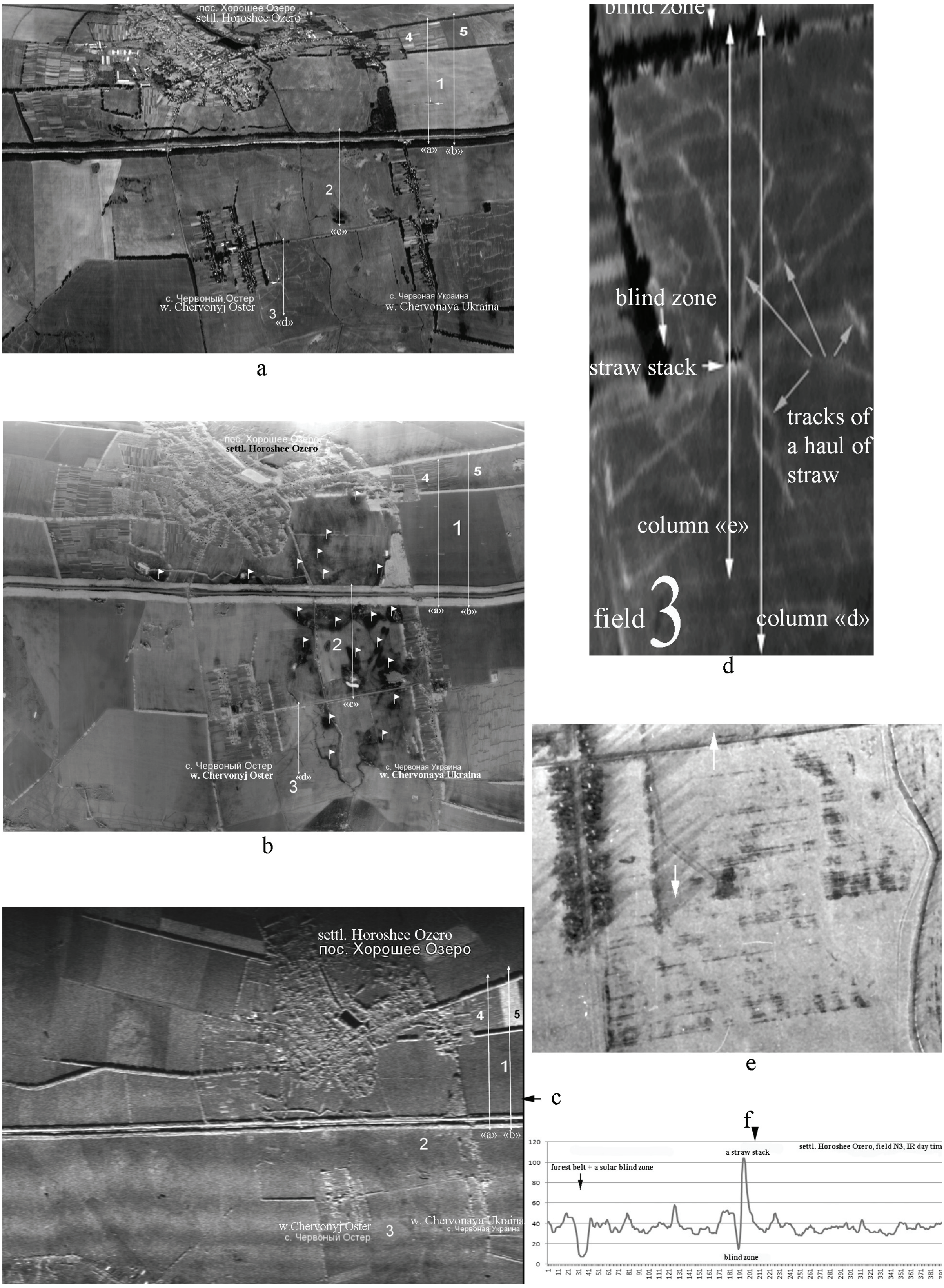

Fig. 1. The images of test range obtained in a day-time and night-time in an autumnal continuance of 2004 (a - IR day-time, b- IR night-time and c - SLAR), d - zoomed IR the day-time image of a field №3 with tracks of a haul of straw (the horizontal arrow marks the image of a stack of straw, and vertical arrows of a solar blind zones behind forest belts), d - the optical image of a field №3 obtained by an aerial survey (winter), e - the strip image of a column in the field 3 (fig. 1d), transiting through a stack of straw and a blind zone.

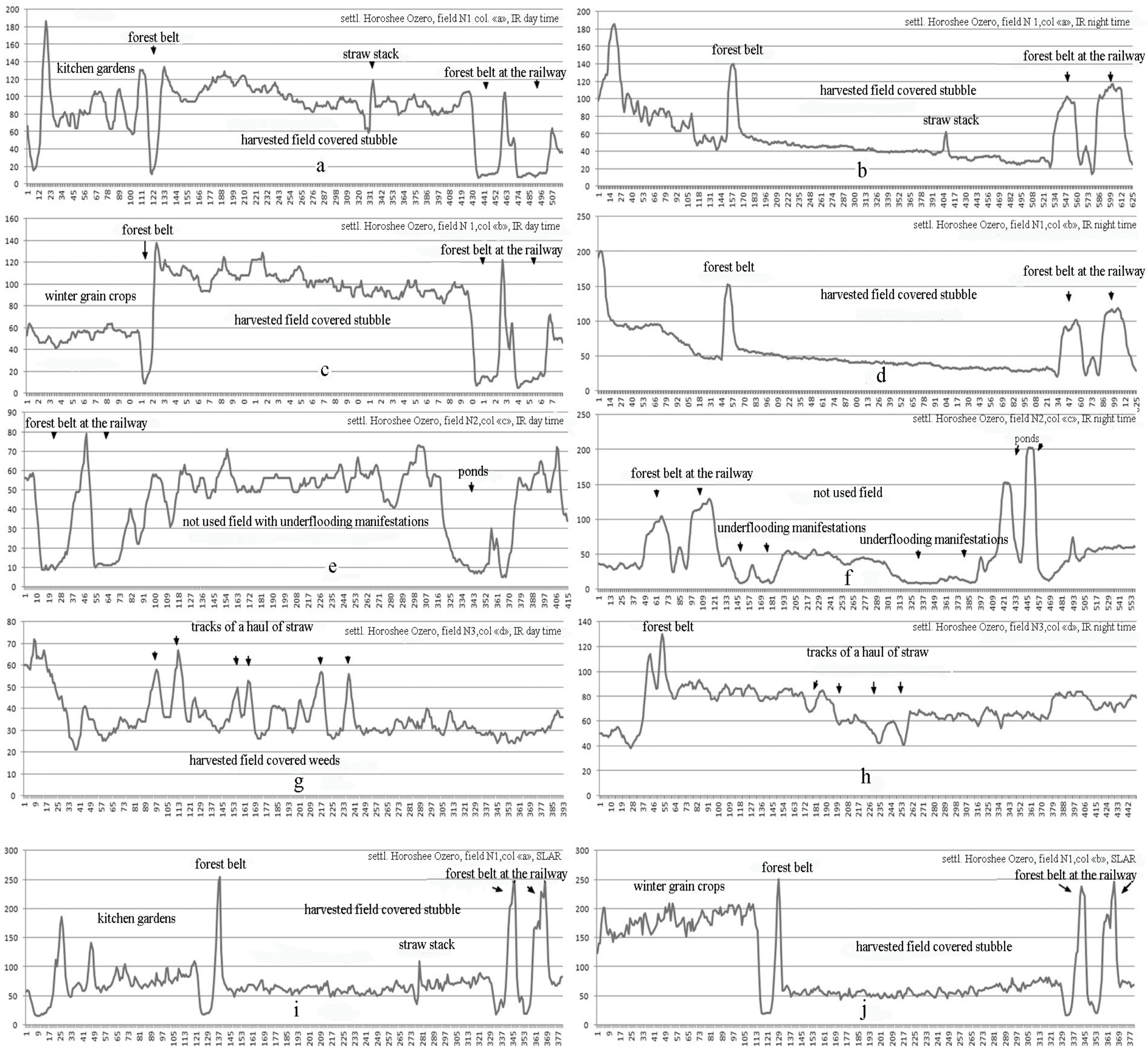

Fig. 2. Strip images of columns IR and SLAR images marked on fig. 1:

- column "a" (IR day-time -a, night-time -b) transiting from below upwards through forest belt at the railway, the harvested field covered stubble, forest belt, kitchen gardens with various crops;

- column “b” (IR day-time - c, night-time -d) transiting through forest belt at the railway, a field covered stubble, forest belt, a field of shoots of winter wheat;

- column "c" (IR day-time -e, night-time -f) transiting through an open pond, the boggy patch, the thrown field with underflooding manifestations and forest belt at the railway;

- column “d” (IR day-time –g, night-time -h) transiting through the harvested field with tracks of transportation (haul) of straw, partially overgrown a tall weeds;

- columns “e” (SLAR -i) and –“f” (SLAR -j).

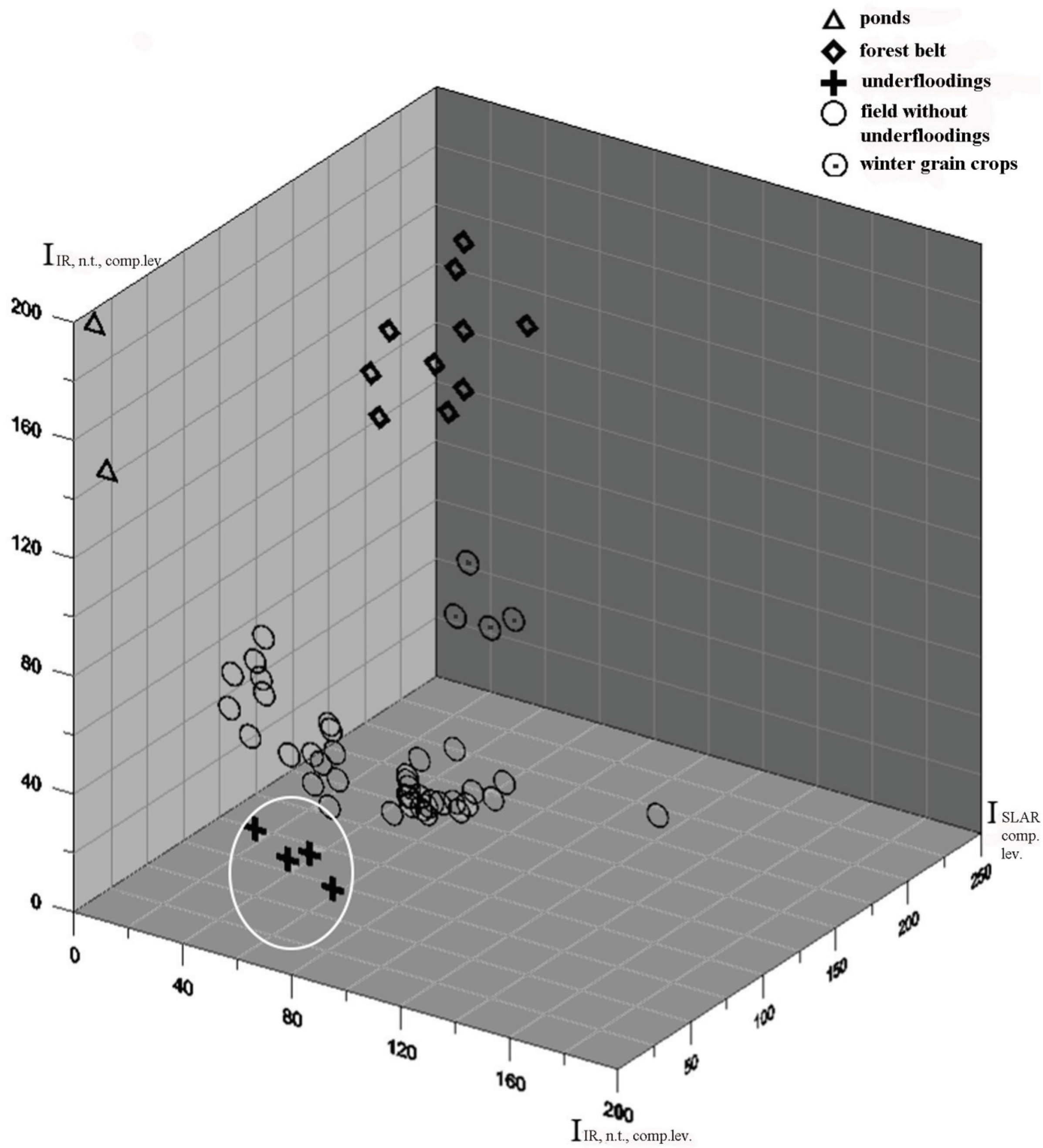

Fig. 3. Three-dimensional «space of attributes», built by results of consecutive day-time – night-time radar - thermal IR and SLAR sensing. On image axes: intensity measured in computer levels of samples of columns day-time IR ($I_{IR,\ d.t.,\ comp.lev}$), night-time IR ($I_{IR,\ n.t.,\ comp.lev.}$) and SLAR images ($I_{SLAR,\ comp.lev}$). The white circle marks values corresponding to underflooding manifestations zones.

UDC 681.7: 534.4: 621.396.96

F. J. Yanovsky, Ph.D., D.Sc.(Eng)
(National Aviation University, Ukraine)

SPECTRAL-POLARIMETRIC METHOD OF OBJECTS AND PHENOMENA OBSERVATION

This paper introduces a new method of remote sensing that combines spectral and polarimetric features of signals received from distant objects, providing spectral analysis of polarimetric variables. The detailed theory is developed for the case rain observation, however generalization for other objects is made, and some examples of spectral polarimetric approach application in different fields are presented.

Introduction

Remote sensing as the process of obtaining information on distant objects without direct physical contact with them has received wide development. It includes the study of the earth's surface from flying vehicle, obtaining information about the atmosphere and the objects in the atmosphere, astronomical and astrophysical observations, and more. Radiation, as a rule of electromagnetic nature, including light, is used as an information carrier in remote sensing. Sometimes radioactive radiation or acoustic oscillations (for example, in the atmosphere or in water) can be used. In this paper, we restrict ourselves to electromagnetic radiation.

Active and passive remote sensing techniques have been developed and applied in a wide range of operating frequencies of electromagnetic oscillations. Various characteristics of radiation are used as informative parameters. Spectral analysis of signals is probably one of the most popular signal processing procedures to obtain information about the object under study. In active radar, polarization remote sensing techniques are widely used. Numerous polarimetric parameters are known that carry various information about the characteristics of objects. Doppler-polarimetric approach that was developed for remote sensing of clouds and precipitation [1 - 7] allows us to obtain information about velocities and shape of the scatterers in the resolution volume.

In this paper we attempt to generalize this approach to a broad class of problems in remote sensing of natural phenomena and objects. A new spectral-polarimetric method is useful to explore of remote objects and natural phenomena. The essence of the method is explained below.

Statement of Problem

Suppose that there are real world, some aspects of which we would like to explore. That part of the real world (system), which represents those system aspects, which are interesting for us, is the object of study. Let us define what means to explore? By this we mean, roughly speaking, to construct some mathematical models that improve our understanding of the research object, allows to make predictions about its future state or behavior, and may provide information about how to control that part of the real world (system), which is the object of our study. The exploration (as a process) can be implemented by collecting data, the introducing these data into the mathematical model, analysis of the model to adjust the data collection procedures, including conducting experiments on the system, if possible. The problem becomes much more complicated, if the object is remote, inaccessible to direct physical contact, as well as for the controlled change of its state. However, for specific objects and situations, it is possible to construct a phenomenological model to calculate the informative parameters that can be assessed with some accuracy using the results of experimental observations.

We focus onto the polarimetric informative parameters that are known to carry information about the nature of the formation of an electromagnetic signal, such as the shape and spatial orientation of the object, or a scatterer the case of active radar. On the other hand, if the received signal is not monochromatic that is satisfied almost always, we can analyze density of the polarimetric parameter on its frequency components, ie the spectral density of a polarimetric parameter. Thus, we arrive at the notion of spectral polarimetric characteristics. While a conventional polarimetric parameter characterizes the integral properties of the resolution volume of the object under study, a spectral-polarimetric characteristic, which is a function of frequency, gives an idea of the fine structure of the scatterers within the resolution volume. Thus, this approach provides a kind of the super-resolution, when it is possible to distinguish between scatterers within a resolution volume, though without specifying the exact location of them inside this resolution volume.

The physical interpretation of the results of spectral-polarimetric analysis should depend on the nature of the object and essence of the problem being solved. Special case when the resolution volume is filled with non-spherical (in general case) scatterers that can move with different velocities, leads to Doppler polarimetry. In this case, the physical meaning of the argument of the spectral density of a Doppler-polarimetric parameter is the frequency associated with the radial velocity of the scatterers corresponding to the their shape and orientation.

Doppler Polarimetry in Case of Rain Observation

Doppler approach. Doppler radar is able to measure important parameters of target speed, however radial velocity depends on the number of factors and moreover, there are a number of scatterers in a resolution volume. In reality we deal with Doppler spectrum $S(*)$ which is power spectrum of complex signal that is expressed as function of Doppler frequency f or velocity v.

In case of the velocity as the argument, $S(v)$ is interpreted as reflectivity weighted distribution of radial velocities of scatterers in resolution volume. Thus, $S(v)dv$ means received power in the velocity interval dv. In case of such definition $S(v)$ is normalized as

$$\int_{-\infty}^{\infty} S(v)dv = \overline{P}_{Rx} \qquad (1)$$

where $\overline{P}_{Rx}$ is mean received power.

Doppler spectrum definition given above yields the following Doppler spectrum model of rain with $N(D)$ as drop size distribution, $p_p(v/D)$ as probability density of radial velocity of a droplet of given size (equivalent diameter) D, and $\sigma(D)$ as RCS of the droplet:

$$S_v(v) \sim \int_{D_{\min}}^{D_{\max}} p_p(v/D)\sigma(D)N(D)dD. \qquad (2)$$

This model is useful for interpretation of measured estimates $S_v(v)$ based on Fourier transform over the received signal.

In meteorological practice, only three Doppler spectrum parameters are normally used: zero moment (mean power or reflectivity factor), first ordinary moment (mean Doppler velocity) and second central moment (Doppler velocity variance) [8] though there are plenty research works, for example, [9 - 11] describing more complete application of Doppler spectrum.

Nevertheless, the main problems of Doppler approach are: influence of carrier velocity of the radar and antenna beam scanning; widening spectrum width due to limited (non-infinitely narrow) breadth of the antenna beam; influence of the sounding waveform and antenna pattern; influence of wind; ambiguity of velocity measurement because of sounding waveform modulation; inertia of scatterers when evaluating turbulence parameters.

Polarimetric approach. Complete description of a radar target can be done with the help of eight numbers, which constitute the scattering matrix:

$$[S] = \begin{bmatrix} s_{HH} & s_{HV} \\ s_{VH} & s_{VV} \end{bmatrix} \tag{3}$$

where quantities s_{xy} , $x = H;V$, $y = H;V$ are in general complex with modulus S_{xy} and argument ψ_{xy}. In expression (3) indexes mean polarization of receive component of scattered signal (first one) and sounding wave (second one), say, H = horizontal and V = vertical. In general case any orthogonal polarization basis can be use.

Scattering matrix is individual for each object or a class of objects and provides a target signature. Perfect reflectors reflect waves in such a fashion that an incident wave with H polarization remains H, and an incident wave with V polarization remains V but is phase shifted 180^{o}.

In reality it is difficult to measure absolute values of amplitudes and phases. That is why relative measurables are often used, for example, such values as S_{HH} / S_{VV}, S_{HY} / S_{VV}, $\psi_{HH} - \psi_{VV}$. For example, a typical polarimetric variable is differential reflectivity that is defined as

$$Z_{DR} = 10\log\frac{|s_{hh}|^2}{|s_{vv}|^2} \tag{4}$$

and related with shape and orientation of a scatterer. For spherical scatterer Z_{DR}=0.

A number of other important polarimetric variables are known and used [12]. Polarimetric approach is attractive because it is associated with relative measurements and multi-parametric systems; it is very sensitive to the shape and orientation of scatterers and is able to provide the signature of a target. However, it does not give any information about target speed. Polarimetric approach can be implemented with conventional (non-coherent) radar. However, nowadays application of coherent radar with polarization diversity is not a rarity. The question is how to use the advantages of such radar by the best way.

Doppler-polarimetric approach. Operational Doppler radars with polarization diversity, more often, just dual-polarization Doppler radars, are normally able to provide users with standard Doppler and polarimetric information in different modes. In contrast to that, Doppler (spectral) polarimetry tries to answer a new interesting question about the behavior of polarimetric parameters in case of reflection from scatterers that are within the resolution volume but are moving with different velocities.

For example, in the radar system with linear orthogonal polarization, instead of differential reflectivity (4) in works [2, 4] the following function is used

$$sZ_{DR}(f) = 10\log\frac{S_{hh}(f)}{S_{vv}(f)}, \tag{5}$$

that first was named ‘specific differential reflectivity’ [1] (in terms of frequency per unit), but later – spectral differential reflectivity [4]; it also can be named as spectral density of differential reflectivity [13].

A major improvement for understanding the microstructure of precipitation can be achieved by combining simultaneous Doppler and polarimetric information. Two power Doppler spectra, *hh* and *vv* must be measured simultaneously in order to obtain the Doppler velocity spectrum of Z_{DR}, that is, $sZ_{DR}(v)$. Thus, the spectral differential reflectivity is defined for each Doppler velocity.

A lot of other Doppler-polarimetric functions and parameters were proposed and studied, for example, spectral differential phase (or spectral density of differential phase) [2, 10, 14], spectral linear depolarization ratio [1, 15], spectral covariance matrix [16], spectral density of the copolar correlation coefficient [10], differential Doppler velocity [5, 17], etc.

It was shown that spectral polarimetric approach can be used for detailed measures of the microstructure of precipitation and melting layer zone [2], turbulence intensity estimation [4], microstructure of rain determination [5, 17, 18], for retrieving winds and determination of scatterer types, separating birds and insects [13], recognition of hydrometeor type [19]. Основные работы выполненные в этой области основаны на применении микроволновой радиолокационной техники (S-band, C-band, X-band, and sometimes even mm-wave band).

Detailed theory was developed relatively Doppler-polarimetric sounding of rain [7]. However, successful experimental works are known for different tasks of atmosphere remote sensing.

Generalization of the Spectral Polarimetric Approach

In this section we try to show that the spectral polarimetric approach is more general than the application of microwave Doppler-polarimetric radar remote sensing of the atmosphere considered above. It is reasonable to discuss the generality of the spectral-polarimetric approach, basing on the following characteristics:

- objects of study;
- methods of remote sensing;
- operational frequency-bands;
- physical meaning of the frequency in the spectrum;
- application areas.

First of all, note that it is logically to extend this approach not only to other meteorological objects, but also to any objects of research. Strictly speaking, the above problem of recognition between insects and birds in the atmosphere (that are not really meteorological objects) confirm that such an approach is effective for the detection of any objects having a complex shape and moving with different velocities.

Doppler polarimetric meteorological radar uses active methods of sounding. However the spectral polarimetry is suitable not only for active, but also for semi-active and possibly passive systems of remote sensing. Semi-active we mean a system that receives the signal scattered by the observation object that is illuminated by outside source of artificial radiation, which is initially designed and used for other purpose. Passive systems are taking the natural radiation of the object of observation.

For the spectral polarimetry is essential that the information carrier is characterized by a polarization capability. Therefore, it is clear that this approach is suitable for electromagnetic waves of any frequency-bands, including light.

Especially interesting to note that the spectral frequencies can characterize not only velocities of the scatterers (that is characteristic for Doppler polarimetry), but very different properties of the object of study, for example, the chemical composition of substances, through which the radiation. Therefore, the interpretation of analysis results and their physical meaning can be completely different, unconnected with velocities of the scatterers.

Application areas of spectral-polarimetric approach to remote sensing are extremely diverse. Even if you only rely on the results of Doppler-polarimetric radar, it can be argued that these results are important for aviation, meteorology, climatology, hydrology and agriculture. They are useful for communications, radar and navigation, as they allow to diagnose the state of the atmosphere especially the conditions of propagation, as well as for radar target detection in clouds and precipitation. Astronomy and astrophysics [20] is a separate interesting area of spectral-polarimetric method application.

The phenomenon known as planetshine occurs when reflected sunlight from a planet illuminates the night side of one of its moons. Typically, this results in the moon's night side being bathed in a soft, faint lightThe best known example of planetshine is earthshine, which can be seen from Earth when the Moon is a thin crescent [21] because the Moon is illuminated not only by the

Sun light directly but also by the light reflected from the Earth that illuminates slightly the shadowy side of the Moon. Related with this phenomenon, a very illustrative example of the use of spectral polarimetry in astrophysics to search for life in the universe was recently published in ”Nature” journal [22]. In that article, the results of the Moon observation over ESO’s Paranal Observatory in Chile, 27 October 2011 are presented. After reflection from the Earth the colors in the light are significantly changed. By observing earthshine astronomers can study the properties of light reflected from the Earth as if it were an exoplanet and search for signs of life. The reflected light is also strongly polarized in contrast with Sun light. Studying the polarization as well as the spectrum, that is, the intensity at different colors allows for much more sensitive tests for the presence of life.

In the atmosphere of a planet, the main biologically produced gases are oxygen, ozone, methane and carbon dioxide. But these can all occur naturally in a planet’s atmosphere without the presence of life. What constitutes a biosignature is the simultaneous presence of these gases in quantities that are only compatible with the presence of life [22]. If life were suddenly to disappear and no longer continuously replenish these gases they would react and recombine. Some would quickly disappear and the characteristic biosignatures would disappear with them.

This example provides the highest generalization level of spectral polarimetry.

Conclusion

A new generalized method of remote sensing that combines spectral and polarimetric features of signals received from distant objects and phenomena has been described. It has been shown that producing spectral analysis of polarimetric variables it is possible to derive various information about properties of distant objects and phenomena. The detailed theory was developed for the case of rain observation, however generalization for other objects has been done, and some examples of spectral polarimetric approach application in very different fields has been presented.

References

[7] F. J. Yanovsky, “Model of the relationship between Doppler and polarization parameters of the radar signal from precipitation”. Report No IRCTR-S-002-98. TU-Delft, The Netherlands, 108 pp., 1998.

[8] C. M. H. Unal, D. N. Moiseev, F. J. Yanovsky, H. W. J. Russchenberg, “Radar Doppler polarimetry applied to precipitation measurements: Introduction of the spectral differential reflectivity”, 30-th Conf. Radar Meteorol. AMS, Boston, 316-318, 2001.

[9] F.J. Yanovsky, “Phenomenological Models of Doppler-Polarimetric Microwave Remote Sensing of Clouds and Precipitation”, IEEE International Geoscience and Remote Sensing Symposium, IGARSS '02, Toronto, Canada, 2002, Vol. 3, pp. 1905 -1907, 2002.

[10] F.J. Yanovsky, H.W.J. Russchenberg, and C.M.H. Unal, “Retrieval of Information about Turbulence in Rain by Using Doppler-Polarimetric Radar”, IEEE Transactions on Microwave Theory and Techniques, Feb., Vol. 53, No 2, pp. 444 – 450, 2005.

[11] D. N. Glushko, F. J. Yanovsky, “Analysis of differential Doppler velocity for remote sensing of clouds and precipitation with dual-polarization S-band radar”, International Journal of Microwave and Wireless Technologies (Cambridge University Press), Vol. 2, issue 3-4, pp. 391-398, 2010.

[12] F. J. Yanovsky, Yu. A. Averyanova, “Meteorological Applications of Multiparameter Polarimetric Radar”, European Radar Conference (EuRAD-2011), Manchester, UK, pp.1-4, 2011.

[13] F. Yanovsky, “Inferring microstructure and turbulence properties in rain through observations and simulations of signal spectra measured with Doppler–polarimetric radars”, Book Chapter in: Polarimetric Detection, Characterization, and Remote Sensing // M.I. Mishchenko et al. (eds.), Springer, pp. 501-545, 2011.

[14] R. Doviak and D. Zrnic, Doppler radar and weather observations, Academic Press, 2nd edition, San Diego, CA, 562 pp., 1993.

[15] D. S. Zrnic and R. J. Doviak, “Velocity spectra of vortices scanned with a pulsed-Doppler radar”. J. Appl. Meteorol., 14, pp. 1531–1539, 1975.

[16] S. Bachmann, D. Zrnic, “Spectral Density of Polarimetric Variables Separating Biological Scatterers in the VAD Display”, J. Atmos. Oceanic Technol., 24, 1186–1198, 2007.

[17] F. Yanovsky, Y. Ostrovsky, V. Marchuk, "Algorithms for Object Recognition by Weather Radar", Proceedings International Radar Symposium IRS-2008, Wroclaw, Poland, pp. 241-244, 2008.

[18] Bringi V.N. and V. Chandrasekar, Polarimetric Doppler Weather Radar, Principles and Applications, Cambridge University Press, 636 pp., 2001.

[19] S. Bachmann, D. Zrnic, "Spectral polarimetric VAD separates bird from insect (wind) velocities", Proceedings of ERAD 2006, Fourth European Conference on Radar in Meteorology and Hydrology, Barcelona, Spain, P2.3, p. 96 (4 pp.), 2006.

[20] V. Kezys, E. Torlaschi, and S. Haykin, "Potential capabilities of coherent dual polarization X-band radar", Proc. 26th Int. Conf. on Radar Meteorology, Norman, OK, 106–108, 1993.

[21] Christine Unal, "Spectral Polarimetric Radar Clutter Suppression to Enhance Atmospheric Echoes", Journal of Atmospheric and Oceanic Technology Vol. 26, pp. 1781-1797, 2009.

[22] C. M. H. and D. N. Moisseev, "Combined Doppler and polarimetric radar measurements: Correction for spectrum aliasing and non simultaneous polarimetric measurements", J. Atmos. Oceanic Technol., 21, pp. 443–456, 2004.

[23] R. Wilson, A.J. Illingworth, and T.M. Blackman, "Differential Doppler velocity: a radar parameter for characterizing hydrometeor size distributions", J. Appl. Meteorology, 36, 649–663, 1997.

[24] H. W. J. Russchenberg, "Doppler Polarimetric Radar Measurements of the Gamma Drop Size Distribution of Rain", Journal of Applied Meteorology, Vol. 32, pp. 1815-1825, 1993.

[25] Y. P. Ostrovsky, F. J. Yanovsky, H. Rohling, "Turbulence and precipitation classification based on Doppler-polarimetric radar data", Proceedings of the European Microwave Association, Vol. 3, Issue 1, pp. 57-61, 2007.

[26] M. I. Mishchenko, Y. S. Yatskiv, V. K. Rosenbush, G. Videen (eds.), Polarimetric Detection, Characterization, and Remote Sensing, Springer, 545 p., 2011.

[27] Wikipedia, http://en.wikipedia.org/wiki/Planetshine

[28] M. F. Sterzik, S. Bagnulo, E. Palle et al, "Biosignatures as revealed by spectropolarimetry of Earthshine", Nature, 483,64–66, March 2012.

UDC: 621.396.6

L.V. Sibruk, Doctor of Science (NAU, Ukraine)
D.P. Bondarenko, postgraduate (NAU, Ukraine)
D.L. Sibruk, postgraduate (NAU, Ukraine)

THE DEVELOPMENT OF PROGRAM MODEL FOR ELECTROMAGNETIC COMPATIBILITY ESTIMATION

The paper addresses the problem of electromagnetic compatibility of television transmitters (standard dvb-t2) with existing radio relay and troposphere stations. The simulation program is based on Rec. and comparison of results by models ITU-R P.452 and ITU-R P.1546. Examples of computations and experimental investigations are given.

On November 26th 2008 the State program of digital broadcasting in Ukraine was approved. The aims of program are to implement the decisions adopted by Ukraine at the Regional Radiocommunication Conference of ITU-R in Geneva in 2006, which envisages the transition from analog to digital broadcasting by 2015.

The country must build an infrastructure for digital broadcasting with guaranteed coverage throughout the territory in the band 470-862 MHz (fourth and fifth television band).

An obligatory step in obtaining permission for broadcasting is positive decision about electromagnetic compatibility of digital broadcasting with other radio electronic equipment (REE), including radio relay and troposphere stations (RRS and TRRS).

Standards DVB-T2 are based on the algorithm coding audio and video MPEG-4 [1-3]. Implementation of standards DVB-T2 stipulates construction single-frequency synchronous network SFN. In single-frequency network synchronization of operation should be provided with satellite transmitters or terrestrial channels. Radiated symbols have to be identical.

In the DVB standard modulation COFDM (OFDM with previous coding) is used. TV signal of 8, 7, 6 MHz bandwidth is formed using orthogonal carrier, the frequencies of which are defined as:

$$f_n(t) = \cos\left[2\pi\left(f_0 + n/\tau\right)t\right],$$

where: f_0 - the lower frequency of range; n - the number of sub-currier 1 до N ; τ - time interval of transmission of one symbol.

During modulation packet data stream is divided by N parts, which modulate carriers with less speed. Carrier frequency offset

$$\Delta f_n = \frac{1}{\tau}.$$

To preserve orthogonality and prevent intersymbol interference that may arise as a result of multipath propagation, each symbol interval obtain protective value of $0{,}25\,\tau$.

In the 8 MHz bandwidth, used in Europe, the maximum carrier number $8 \times 1024 = 8192$ or $8K$. Each carrier is modulated by 4-position quadrature phase shift keying (QPSK) or 16-, 64-, or 256-position quadrature amplitude modulation (QAM). Accordingly, one modulation symbol on carrier transfers from two to eight bits.

Also according to the number of quadrature modulation levels the data stream is divided into: 2 sub-streams for QPSK, 4 sub-streams for 16- position QAM. So during demultiplexing the first bit appears in the first sub-stream etc. Sense of internal interleaving is permutation by definite individual rule in each sub-stream of bits by block with length 126 bits. In parallel outputs of the internal interleaving block the modulation symbol is formed with two, four or six digits. One carrier transfers one symbol. Therefore, using $8K$ mode simultaneously is radiated 48 groups of 126 symbols, that corresponds to 6048 carriers with useful information, or 12×126=1512 carriers using $2K$ mode. QAM-symbols are divided into different sub-channel of OFDM interleaving, which allows to restore the information at a loss OFDM-symbol. Complex signal of OFDM-symbol [3] is written

$$S_n = \sum_{k=0}^{N-1} C_k (nT) e^{i2\pi knT/n} , \qquad (1)$$

where: T - discrete time interval; n - reference number.

Expression (1) identical to the Fourier inversion at sampling interval equals to the ratio of duration of one transmission symbol to the carrier number.

Radiated DVB signal looks like noise-type with Gauss distribution. Spectrum of signal consists of a large number of partial spectral modulated carriers. Due to this spectrum is practically continuous.

Radio frequency mask of DVB-T2 radiation signal is presented at Fig. 1 [4].

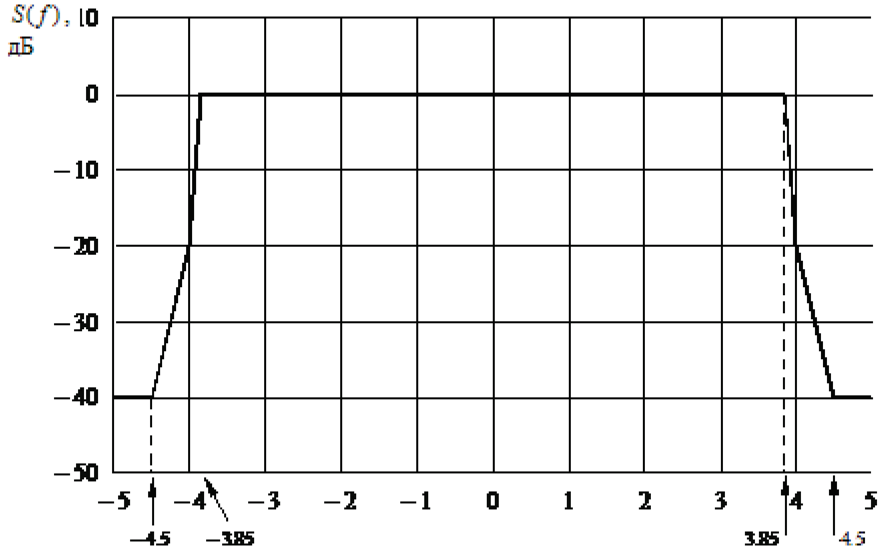

Fig. 1 Radio frequency mask of digital television with bandwidth of 8 MHz

Typical antenna system can be built on the basis of firm ELTI sectored antennas TVA 31/50 or TVA 24/50, which have a similar structure and different number of radiators (respectively 4 and 2). TVA 24/50 can radiate waves with horizontal or vertical polarization (depending on the spatial position) in a working range of 470-862 MHz, directivity factor 6.8 ... 9 dB (with respect to the dipole), bandwidth in E and H planes $2\theta_{0,5}^{E} = 56^o$, $2\theta_{0,5}^{H} = 49^o$.

Many types and combinations of interference path may exist between stations on the surface of the Earth, and between these stations and stations in space, and prediction methods are required for each situation. This paper addresses one of the more important sets of interference problems, i.e. those situations where there is a potential for interference between microwave radio stations located on the surface of the Earth. The method [5] includes a complementary set of propagation models which ensure that the predictions embrace all the significant interference propagation mechanisms that can arise. Methods for analyzing the radio-meteorological and topographical features of the path are provided so that predictions can be prepared for any practical interference path falling within the scope of the procedure up to a distance limit of 10 000 km.

Microwave interference may arise through a range of propagation mechanisms whose individual dominance depends on climate, radio frequency, time percentage of interest, distance and path topography. At any one time a single mechanism or more than one may be present. The principal interference propagation mechanisms are as follows:

– *Line-of-sight* (Fig. 2): The most straightforward interference propagation situation is when a line-of-sight transmission path exists under normal (i.e. well-mixed) atmospheric conditions. However, an additional complexity can come into play when subpath diffraction causes a slight increase in signal level above that normally expected. Also, on all but the shortest paths (i.e. paths longer than about 5 km) signal levels can often be significantly enhanced for short periods of time by multipath and focusing effects resulting from atmospheric stratification (see Fig. 2).

– *Diffraction* (Fig. 2): Beyond line-of-sight (LoS) and under normal conditions, diffraction effects generally dominate wherever significant signal levels are to be found. For services where anomalous short-term problems are not important, the accuracy to which diffraction can be modelled generally determines the density of systems that can be achieved. The diffraction prediction capability must have sufficient utility to cover smooth-earth, discrete obstacle and irregular (unstructured) terrain situations.
– *Tropospheric scatter* (Fig. 2): This mechanism defines the "background" interference level for longer paths (e.g. more than 100-150 km) where the diffraction field becomes very weak. However, except for a few special cases involving sensitive earth stations or very high power interferers (e.g. radar systems), interference via troposcatter will be at too low a level to be significant.

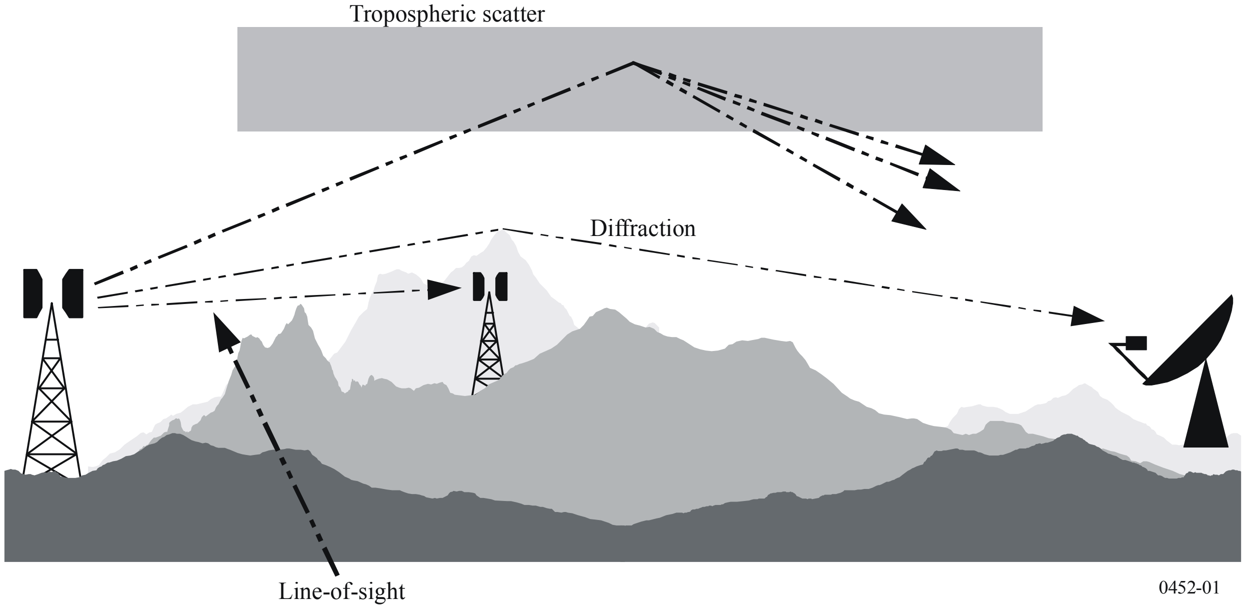

Fig. 2 Long-term interference propagation mechanisms

Computer program is used for thin-route RRS and TRRS [6-10]. Detail description of EMC evaluation procedures is considered in paper [11]. Parameters and placement location of RRS transmitters are placed in database MS-SQL. Computation results for definite examples are presented in Table 1, terrain for consider examples – on Fig. 3 and Fig. 4.

The raw data for computations:

- distance – 20 km;
- two pairs coordinates of RRS (coordinates of TV transmitters are chosen from database), RRS parameters and characteristics;
- frequency 475 MHz.

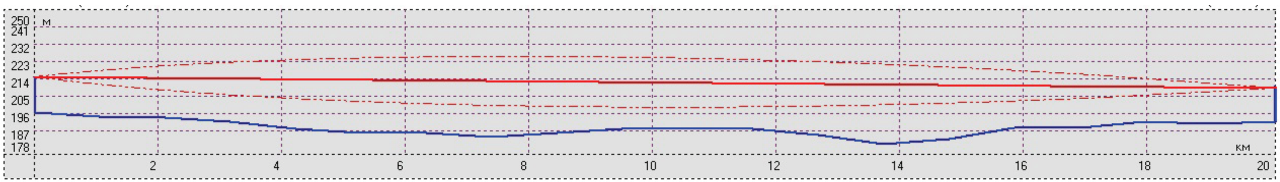

Fig. 3 Propagation path with simple terrain

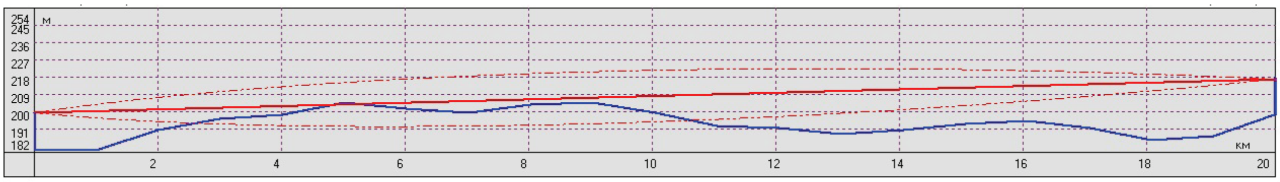

Fig. 4 Propagation path with interference

Table 1

Computation experimental investigations results

Model	Signal level for Radioline on Fig. 3	Signal level for Radioline on Fig. 4
ITU-1546	-109.6 dBW	-109.6 dBW
ITU-452	-84.5 dBW	-101.8 dBW
Experimental investigations	-87 dBW	-102 dBW

Results in Table 1 indicate that designed computer program can be used for frequency planning during digital TV implementation.

References

1. *Довідник* з радіомоніторингу / Під аг. Ред.. П.В. Слободянюка. – Ніжин: ТОВ «Видавництво Аспект-Поліграф», 2008. -588 с.
2. *ETSI TR101 190:* 2004 Digital Video Broadcasting (DVB); Implementation guidelines for DVB terrestrial services; Transmission aspects.
3. *Вишневский В.М., Ляхов А.И., Портной С.Л., Шахнович И.В.* Широкополосные беспроводные сети передачи информации. – М.: Техносфера, 2005. – 592 с.
4. *Recommendation* ITU-R BT.1206. Spectrum shaping limits for Digital Television Broadcasting.
5. *Recommendation* ITU-R P.452-14. Prediction procedure for the evaluation of microwave interference between stations on the surface of the Earth.
6. *www*.interpolitex.rasu.ru/index.php.
7. *www*.radioscanner.ru/photo/antennas/relay.php
8. *vkmtuci*.edu.mhost.ru/texcba/rrlspravka.htm
9. *www*.omskindustry.ru/firm.asp?skl=7579
10. *www*.techtorg.ru/firm.asp?skl=7579
11. *Іванов В.О., Решетнік М.В., Бондаренко Д.П.* Алгоритм розрахунку норм частотно-територіального рознесення радіоелектронних засобів. – К.: Вісник ДУІКТ. – 2007. – Том5(3). – С.262 – 270.

UDC 621.396.962.25

K.A. Lukin, V.P. Palamarchuk, P.L. Vyplavin, and V.V. Kudriashov
(Laboratory for Nonlinear Dynamics of Electronic Systems,
Usikov Institute for Radiophysics and Electronics NAS of Ukraine, Ukraine)

RANGE-AZIMUTH RADIOMETRIC IMAGING USING KA-BAND NOISE WAVEFORM SYNTHETIC APERTURE RADAR

Radiometric monitoring allows obtaining unique information about emissivity of the objects. It doesn't require generation and radiation of sounding signals. In the work, a principle for radiometric range - cross range imaging for short distances is considered. This principle comprises interferometric radiometer and antennas with synthesized beam. The work describes the proposed imaging principle and experimental results obtained. Radiometric imaging was performed using the proposed algorithm implemented in ground based Ka-band noise waveform synthetic aperture radar. The possibility of detection of thermal radiation using the investigated equipment has been confirmed. The obtained results can be applied in homeland security for detection of concealed objects.

1. Introduction. Imaging of distant targets using their thermal radiation is may be realized using interferometric systems based upon measurement of difference in paths of the registered radiation towards two or more receiving antennas [1, 2]. This approach has been developed in long wave radar astronomy for improvement of angular resolution of radio telescopes [3]. Imaging in millimeter waveband is often done using multichannel reception using linear antenna array and mechanical or frequency scanning along axis perpendicular to the array [4]. Further development of this approach consists in realization of 2D aperture synthesis which enables radiometric coherent imaging in plane perpendicular to the antenna beam. Such images contain not only amplitude information but also information concerning relative phase [3, 5]. Radiometric imaging in azimuth-range plane has been investigated in work [2]. The author described possibility of generation of radiometric images by combination of information about interferometer response and angular position of narrow beam of antenna at one of the receivers of radio interferometer. Each pixel of such image is obtained as crossing of area of equal difference of paths of the received signal and antenna pattern of antenna. Nevertheless, factors limiting usage of this approach and possibility of obtaining of 2D resolution using combination of radiometric data and principles of synthetic aperture radar have not been investigated in this book. Current work is devoted to investigation of radiometric imaging and proving the concept of 2D imaging by passive SAR. Experimental investigations have been carried out using a ground based Ka-band radiometer based upon Ground Based noise waveform SAR [6]. This SAR uses novel antennas with synthetic aperture [7].

2. Imaging using passive regime of ground based SAR. The main idea of the proposed approach to imaging consists in using interferometric radiometer with moving of one of the antennas for realizing synthetic aperture. This scheme enables obtaining two dimensional images of objects at short range. This is possible due to the fact that shifting of one antenna of interferometric radiometer with respect to stable target changes phase relations between signals obtained in channels of the radiometer. For different positions of the target these phase relations will depend on antenna positions in different way. This fact can be used for building a reference function (a function of antenna position) and performing co-variation of radiometer returns with it. This gives a chance to improve the azimuth resolution and to some limit to generate 2D images. The paper is devoted to investigation of possibility and constraints of generation of 2D images using this approach at short ranges.

For realization of spatial scanning we use synthetic aperture antennas [7]. This is a special type of antennas phase center of which is moved along a real aperture. Phase centers of antennas are moved in stepped like manner and signals are being recorded only when the antennas are stationary. This enables using common in SAR principle of splitting of the processing into two parts. The first step in passive SAR is to perform cross-correlation between signals received in two channels. This will give information concerning path difference between signals. The second stage consists in co-variation of those signals obtained in different antenna positions with corresponding reference function.

Relative delay of the signals $\Delta\tau(x,y)$ is equal to $\Delta l(x,y)/c$, where $\Delta l(x,y) = l_1(x,y) - l_2(x,y)$ is range difference between the target with coordinates (x,y) to the antennas of the radiometer [2]. Difference of paths lengths $\Delta l(x,y)$ can't be higher than the distance between antennas l_B. At each of antenna positions a value of delay difference $\Delta\tau_a(x,y)$ is equal to:

$$\Delta\tau_a(x,y) = \frac{\Delta l_a(x,\ y)}{c} \tag{1}$$

Cross correlation function between signals received by reference channel of interferometric system $S_{1,a}(t+\tau)$ and the second receiver $S^*_{2,a}(t+\tau_a)$ can be estimated as[8]:

$$R_a(\tau,T) = \frac{1}{T}\cdot\int_0^T S_{1,a}(t+\tau)\cdot S^*_{2,a}(t+\tau_a)d\tau, \tag{2}$$

where: T is an integration time;

$\tau \in [-\frac{l_B}{c};\frac{l_B}{c}]$ is the mutual delay of the signals introduced for compensation of $\Delta\tau_a(x,y)$;

symbol * denotes complex conjunction.

Compression of the signals by path length difference consists in estimation of cross-correlation $R_a(\tau,T)$ for the required mutual delay values and for all antenna positions.

Movement of phase center of antenna with synthetic aperture causes change in path of the radiowaves in waveguide. This change has to be taken into account during processing. Estimation of phase shift is easier to perform in frequency domain by adding corresponding phase shifts to all of the frequency components of the signals. Using known [9] relation for the main wave of rectangular waveguide this phase shift can be estimated using the following relation:

$$\varphi_a(\lambda_i) = 2\pi l_a\sqrt{\frac{\varepsilon\mu}{\lambda_i^2} - \frac{1}{(2p)^2}}, \tag{3}$$

where: $\lambda_i = c/f_i$ is wavelength of the given frequency in free space;

l_a is waveguide length corresponding to antenna position a;

ε, μ are relative electric and magnet permittivity;

p is the width of wide wall of the waveguide.

For effectiveness correlation processing (2) has been performed in frequency domain using fast Fourier transform. Taking into account (3) the cross-correlation (2) of the received signals is:

$$R_a(\tau) = \sum_{\omega_{min}}^{\omega_{max}} S_{1,a}{}^*(\omega_i)\cdot\frac{S_{2,a}(\omega_i)}{e^{j\varphi_a(\omega_i)}}\cdot e^{j\omega_i\tau} \tag{4}$$

The second step of the processing uses the results of correlation processing. It consists in estimation on the basis of theoretical response from current point of space an expected variation of radar returns as a function of antenna position. Then the received signals are compared with this reference function via co-variation. Relation for generation of coherent radar image $I(x,y)$ in time domain and with common simplification consisting in neglecting of amplitude term of reference function has the following form:

$$I(x,y) = \sum_{a=1}^{N_a} R_a\left[\Delta\tau_a(x,y)\right] \cdot e^{j\omega_c \Delta\tau_a(x,y)}, \tag{5}$$

where: ω_c is the central circular frequency of radio spectrum,

N_a is the number of antenna positions in the performed scan.

Thus, image formation consists in matched filtration of the radar returns and their summing up with taking into account phase difference between the signals from a target received by two antennas of radiometer (5).

4. Experimental setup. The aim of the experiment was to form coherent radar images using noise waveform ground based SAR [6] in passive regime. In order to check operation of the equipment in passive regime first we used two stable horn antennas and regime of interferometric radiometer without spatial scanning with SAR antenna [2].

In this case lines of possible targets positions can be depicted on a plane using the following relation:

$$I(x,y) = R\left[\Delta\tau(x,y)\right]. \tag{6}$$

Experimental investigations have been carried out in a laboratory. Base of interferometric radiometer was l_B=*6 m*. A noise generator was used as a target with controlled output power. It was placed on the distance of 4 m from the plane of receiving antennas. Relative delay of the signals from this target to the antennas of radiometer was nearly –2.7 τ. Correlation between input signals is shown in fig. 4. Maximum at -2.7 corresponds to position of the target. Maximum at $\Delta\tau=0$ is caused by signal leakage between channels of ADC.

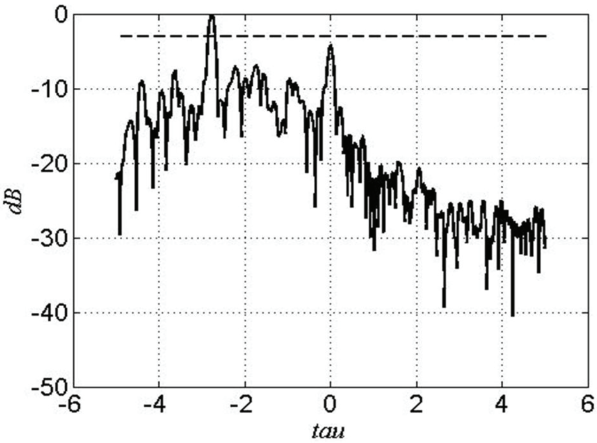

Fig. 4 Signal from passive SAR operating in regime of interferometric radiometer – correlation between input signals of channels

These results were plotted to figure 5 using relation (6). Such plot shows all possible positions of the target. In this regime coordinates of the target are measured ambiguously which is seen as a hyperbola of possible target's positions going through the real target coordinates (shown as a white circle in the figure). Resolving of targets in range is possible at short ranges by scanning of the space by moving antenna and performing SAR imaging procedures to the obtained data. Such experiment has been carried out using one static antenna and one antenna with synthetic aperture. The same noise generator was used as a target. It was placed at distance 2.5 m from the antennas. Figure 6 shows example of image obtained via SAR processing of the radiometric data gathered from all antenna positions. The target position is marked by a circle in the figure. Second response in the figure corresponds to leakage in ADC.

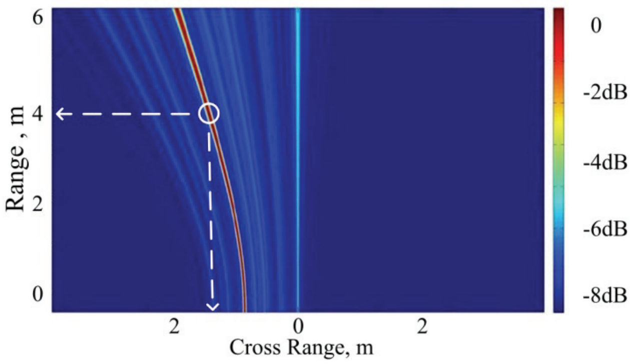

Fig. 5 Radiometric image obtained using interferometric regime of radiometer without spatial scanning by moving antenna

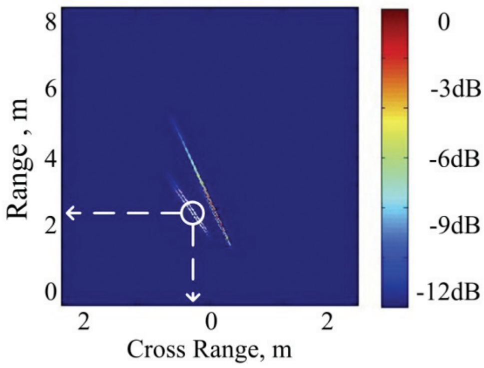

Fig. 6 Radiometric image obtained in passive SAR regime

Besides, we have carried out estimation of dynamic range of ADC. Lack of dynamic range of ADC would lead to inability to achieve theoretical processing gain at high values of integration time. This would limit ability of the system to extract useful signal from noise, cross-talk and leakage. We have investigated dependence of output SNR on integration time in the limits of processing gain of 18 to 69 dB. This has been done using two schemes shown in fig. 7. The first scheme enabled to evaluate processing gain for the case of correlated signals in channels of the receiver. The second one enabled to measure increase of the output power of the radiometer for the case of uncorrelated signals at the inputs receiver channels. The output SNR showed good agreement with the expected processing gain which proved that the ADC has enough dynamic range and low enough leakage for our radiometric experiments.

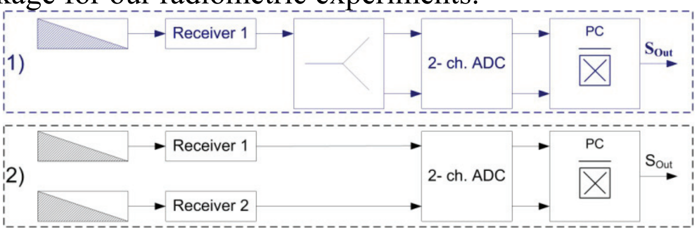

Fig. 7 Scheme of experiment for estimation of interferometer output SNR on the processing gain

In order to validate ability of the radiometer to detect objects on the background of self noise of the receivers and to detect difference in thermal radiation of objects it is necessary to measure the minimal increase of the signal amplitude which can be registered by the equipment. In order to do that we compared responses of the radiometer from ceiling (fig. 8.a), sky (fig. 8.a) and two different loads on two channels of the receiver (fig. 7). The experiment was repeated several times in order to compare different realizations of these signals. The output levels of the radiometer (fig.8.b) show that the system is able to detect contrast between sky, ceiling and self noise, but changing in time parameters of the equipment lead to some variations in the output levels for each of the targets.

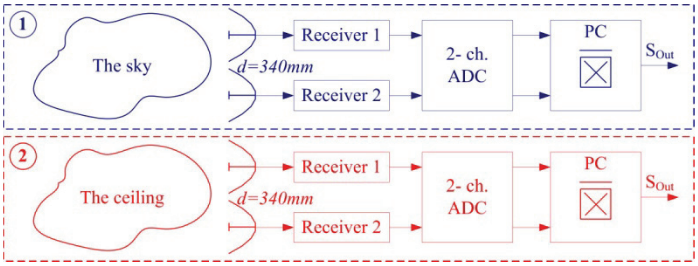

a

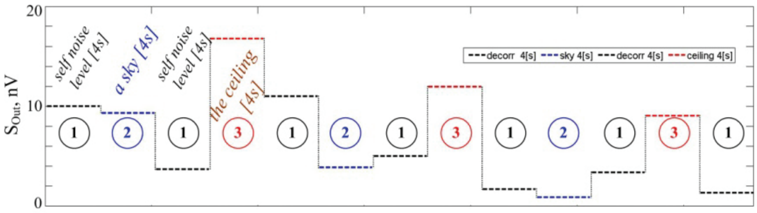

b

Fig. 8 Interferometer output signal level: self noise, sky and room ceiling:
a – the experiment scheme;
b – interferometer output signal levels.

Conclusions. In the work, a principle for SAR imaging using radiometer with scanning antennas with synthetic aperture has been proposed. Unlike others, this approach enables generation of two dimensional images in plane range-azimuth at short ranges. This approach has been tested using Ka-band ground based noise waveform SAR operating in passive regime [6]. It has been shown in the experiments that this equipment has power sensitivity of $8{\cdot}10^{-17}$ W. Minimal detected power is $1{,}3{\cdot}10^{-12}$ W. It has been shown that the system can have processing gain of up to 69 dB without saturation by ADC dynamic range. The proposed approach has been tested experimentally. Coherent radar images of noise signals source have been generated in regimes of interferometric radiometer and radiometric SAR. Operation in both regimes has shown good agreement with theoretical expectations.

References

1. *Almazov V.B.* Methods for passive radar. – Kh.: «VIRTA», 1974.- 85 pp.
2. *Edelsohn* at al. Interferometric radiometer. US patent No. 4.990.925, 1991, 14 pp
3. *Thompson A.R., Moran J.M., Swenson G.W.* Interferometry and synthesis in radio astronomy. – M.: «Mir», 1989, 568 pp.
4. *Shilo et. al.* Microwave radiometric system «ZIR» for the customs service // Technology and design in the electric equipment, 2003, №3, стр. 11-13.
5. *Jian Dong, Ronghua Shi, Ke Chen, Quingxia Li, Wentai Lei.* An external calibration method for compensating for the mutual coupling effect in large aperture synthesis radiometers. // International Journal of Antennas and Propagation, 2011, vol. 2011, 8 pp.
6. *Lukin K. A. et. al.* Ka–Band Bistatic Ground-Based Noise Waveform SAR for Short-Range Applications // IET Radar, Sonar & Navigation 2008, vol. 2, no. 4, pp. 233–243.
7. *Lukin K.A.* Scanning Synthetic Radiation Pattern Antennas // Radioelectronics and communications systems. Vol. 53 No. 4 2010, pp.219-224
8. *Lukin K.A.* Millimeter-Wave Band Noise Radar // Telecommunications and radio engineering. Vol. 68 No. 14 2009, pp.1229-1255
9. *Nikolskiy V.V., Nikolskaya T.I.* Electrodynamics and propagation. – M.: «Nauka», 1989, 544 pp.

UDC 602:4(045)

O.A. Vasylchenko, PhD of Medical Sciences,
O.R. Aliieva, Master of Biotechnology,
O.L. Matvyeyeva, PhD of Technical Sciences,
M.M. Baranovsky, Doctor of Agricultural Sciences
(National Aviation University, Institute of Ecological Safety, Ukraine)

MICROORGANISMS PARTICIPATION IN OIL HYDROCARBONS BIODEGRADATION

One of the actual problems today is oil and petroleum pollution of environment. Some of microorganisms may destroy hydrocarbons, that's why may be used for bioremediation of these pollutions or may course fuels microbiological damage. Microorganisms involved in hydrocarbons biodegradation adapt their metabolism to the changed environmental conditions.

Oil and petroleum products environmental pollution is very serious problem today. Soils and water in Ukraine are contaminated greatly, mostly near the airfields, fuel depots, oil storage depots, refineries, oil wells, parking lots, gas stations, etc. This impurity has not only toxic, but fire hazard, and physical coating of the environment. On the one hand, microorganisms may destroy oil and petroleum pollutions, so they may be used for remediation of environment; on the other hand microbiological damage of air transport fuels is also an actual problem [1].

Oil or petroleum is natural disperse system of liquid organic compounds, the main parts of which are hydrocarbons of various molecular weights. It is a mixture of about 1000 individual substances [2]. Oil in common usage includes all liquid, gaseous, and solid (e.g., paraffin) hydrocarbons. Lighter hydrocarbons as methane, ethane, propane and butane occur as gases, while pentane and heavier ones are in the form of liquids or solids [3].

Hydrocarbons in the environment can be decomposed mainly by bacteria, algae, yeast and fungi [4, 5]. Surfactants usage increases hydrocarbons solubility and promotes their further biodegradation [6]. The petroleum pollutants bioremediation is depends on microbial biosurfactant synthesis from hydrocarbons. Since the hydrocarbons are not soluble in water, one of the important properties of strains capable to utilize hydrophobic substrates is their ability to synthesize bioemulsifiers [7]. Biosurfactants production depends on the following conditions:

– carbon source nature in medium, its hydrophilicity degree;
– nitrogen source nature, carbon/nitrogen ratio in medium;
– culture growth phase.

Temperature, pH, medium aeration, cultivation method, metal cations and antibiotics presence in medium also have effect.

Carbon source in medium, especially its hydrophilic or hydrophobic nature, has a crucial role for the surfactants synthesis. It can induce or repress the synthesis of biological surface active substances. Some microorganisms' ability to reduce surface tension and emulsifying activity occur only during their growth on hydrocarbon substrates [8].

Various classes' hydrocarbons decomposition mechanisms are essentially different. This fact results in individual spectrum of hydrocarbons consumption for different microorganisms. Aliphatic hydrocarbons are demonstrative example of organic substances that are biodegradable. Alkanes are the easiest to be ruined; alkenes and alkynes are following [9]. The components consisting of straight chains degrade easier than those with branched chains [10]. Aromatic hydrocarbons can be degraded during aerobic and anaerobic biological processes [9, 11].

N-Alkanes, isoalkanes, naphthenes, polycyclic aromatic hydrocarbons and adjacent heteroaromatic hydrocarbons have specific metabolic pathways. Biodegradation of straight chain alkanes occurs through β-oxidation. Natural isoalkanes with saturated isoprenoid structure are oxidized through citronellol pathway. An increase of cytochromes group, as well as the high content of ATP, increased cellular respiration, increased number of flavins is characteristic for microorganisms growing on media with n-alkanes. The number of mitochondria increases and endoplasmic reticulum development is enhanced in eukaryotes [12].

Many strains of bacteria are capable of heteroaromatic hydrocarbon compounds degradation (mainly sulfur compounds) [13]. Aromatic hydrocarbons with heteroatoms biodegradation is often accompanied by denitrification, sulfate reduction or methane production in anaerobic conditions. Benzene and toluene anaerobic transformation is accompanied with methane production. This process can be characterized as enzymatic one. There are partial oxidation and partial reduction of the substrate with methane and carbon dioxide formation as end products. In addition, trivalent ferrum and manganese oxides may be alternative electron acceptors in appropriate anoxic conditions [14].

Light oil fractions partially inhibit heterotrophic microorganisms but act also as a substrate for hydrocarbon degrading microorganisms. Heavier fractions are less toxic to microorganisms, but they are not actively metabolized [15].

Possibility of microbial growth on hydrocarbon medium is provided by combination of two factors: biochemical complementarity of organism and resistance to hydrocarbon toxic action. Considering polycomponent character of petroleum pollution, microorganism (association of microorganisms) should be able to grow on most components of pollutant and be resistant to their toxic action for complete mineralization of oil products. Hydrocarbons degrading bacteria have developed special mechanisms of resistance to hydrocarbons in evolution process that are expressed in the metabolism peculiarities and cell structure. These features include ultrastructural cell displacement (inclusions of different density formation, cytoplasm fragmentation, membrane unit enhanced development, an overgrowth of the cell wall), capsules formation, metabolic activity changing. The special changes in cell structure organization are increased content of fatty acids in the cell wall, synthesis of specific lipids, intracellular inclusions of various purposes formation [12].

Bacteria that utilize hydrocarbons are of the genera *Corynebacterium*, *Mycobacterium*, *Nocardia*, *Rhodococcus; of Achromobacter*, *Acinetobacter*, *Alcaligenes*, *Arthrobacter*, *Bacillus*, *Beijerenckia, Brevibacterium*, *Flavobacterium*, *Mycobacterium, Pseudomonas, Rhodococcus* spp. Fungi are of *Aureobasidium*, *Candida*, *Mortierella Penicillium, Polisporum, Rhodotorula*, *Sporobolomyces Trichoderma* spp. [16].

Oil at low concentrations has a stimulating effect for soil biota because it is an energy substrate for a large group of microorganisms. Significant petroleum soil pollution, which occurs at emergency spills, is accompanied by acute toxic oil effects on organisms [17].

Petroleum hydrocarbons are characterized by strong antibacterial effect and can cause cell lysis. However, some bacteria show a high resistance to these substances. That’s why these microorganisms may contaminate hydrocarbon fuels, namely bacteria of *Pseudomonas, Micrococcus, Micobacterium* genera, fungi *Cladosporium, Aspergillus, Penicillum, Altemaria* etc. *Ps. Aerugenosa* is the bacteria of great importance, fungi *Cladosporium resinae* are named “kerosene fungi” due to their prevalence as fuel biodamage microorganisms [18]. For these microorganisms a single organic compound can be as a source of carbon, energy and reducing power; they are chemo-organotrophic heterotrophs. One of the key mechanisms for the suppression of the hydrocarbons toxic effect is hydrocarbons oxidizing enzymes synthesis. The same mechanism provides the cell with carbon and energy for biosynthetic processes [12].

Conclusions

1. Microorganisms’ metabolism and growth may be inhibited by even low oil or petroleum products concentrations.
2. Petroleum hydrocarbons have strong antibacterial effect, but some microorganisms can adapt to their high concentrations.
3. The most important in hydrocarbons biodegradation is their interaction with the surface of the microbial cell.
4. Synthesis of hydrocarbons oxidizing enzymes is one of the key mechanisms in

microorganisms' adaptation to high hydrocarbons concentration.

5. Surface active substances' synthesis is important in hydrocarbons' biodegradation.

References

1. *Matvyeyeva E., Vasylchenko O., Demyanko D. Problem of hydrocarbon fuels microbiological damage //* Инженерия транспорта и организация перевозок: XV конф. молодых ученых Литвы «Наука – будущее Литвы», 4 мая 2012 г.: сб. статей. – Вильнюс, 2012. –С.42-45.
2. *Speight J. G.* Handbook of Petroleum Analysis. – New Jersey: John Wiley & Sons, 2002. – 455 p.
3. *Hyne N. J.* Nontechnical guide to petroleum geology, exploration, drilling, and production. – Oklahoma: Penn Well Corporation, 2001. – 598 p.
4. *Elshafie A.,* AlKindi A.Y., Al-Busaidi S. et al. Biodegradation of crude oil and n-alkanes by fungi isolated from Oman // Mar. Pollut. Bull. – 2007. – V.54. – P. 1692–1096.
5. Fallgren P. *H., Jin S.* Biodegradation of petroleum compounds in soil by a solid-phase circulating bioreactor with poultry manure amendments // J. Environ. Sci. Health A Tox Hazard Subst Environ. Eng. – 2008. – V.43, N2. – P. 125–131.
6. *Cerniglia C. E.* Biodegradation of polycyclic aromatic hydrocarbons // Biodegradation. – 1992. – V.3. – P. 351–368.
7. *Kitamoto D., Ikegami T., Suzuki G. T.* Microbial conversion of n-alkanes into glycolipid biosurfactants, mannosylerythritol lipids, by *Pseudozyma* (*Candida antarctica*) // Biotechnology Letters. – 2001. – V.23. – P. 1709–1714.
8. *Batista S.B., Mounteer A.H., Amorim F.R.* et. al. Isolation and characterization of biosurfactant/bioemulsifier-producing bacteria from petroleum contaminated sites // Bioresource Technology. – 2006. – N 97. – P. 868–875.
9. *Osuji L. C., Ozioma A.* Environmental degradation of polluting aromatic and aliphatic hydrocarbons: a case study // Chem. Biodivers. – 2007. – V.4. – P. 424–430.
10. *Матвеева Е.Л., Васильченко О.А., Демянко Д.А.* Микробиологическое поражение авиационных топлив // Системи озброєння і військова техніка. – 2011. – № 2(26). – С. 152–156.
11. *Haggblom M. M., Youngster L. K., Somsamak P., Richnow H. H.* Anaerobic biodegradation of methyl tertbutyl ether (MTBE) and related fuel oxygenates // Adv. Appl. Microbiol. – 2007. – Vol. 62. – P. 1–20.
12. *Мельников Д.А.* Распределение признаков биодеградации углеводородов и оценка технологически важных свойств нефтеокисляющих бактерий: дис. … канд. биол. наук: 03.00.23 / Мельников Дмитрий Александрович. – Краснодар, 2005. – 131 с.
13. *Oldfield C., Wood N.T., Gilbert S.* Desulphurisation of benzotiphene nad dibenzotiophene by actinomycete organisms belonging to the genus *Rhodococci,* and related Taxa // Antonie van Leeuwenhoek. – 1998. – V.4. – P. 119–132.
14. *Burland S., Edwards E.* Anaerobic benzene biodegradation linked to nitrate reduction // Appl. Environ. Microbiol. – 1999. – V.65. – P. 529–533.
15. *Головченко А.В., Полянская Л.М.* Влияние нефти на численность, биомассу и жизнеспособность грибов в верховых торфяниках // Микробиология. – 2001. – Т.70, №1.– С. 111–117.
16. *Vasylchenko O.A., Aliieva O. R., Matvyeyeva O. L., Salata A. M.* Biotechnological aspects of hydrocarbons biodegradation // Біотехнологія. – 2012. – Т.5. – №2. – С.41-50.
17. *Гузев В.С.* Влияние масляной кислоты на физиологическую активность углеводородокисляющих родококков / В.С. Гузев, М.И. Волде, И.С. Куличевская, Л.В. Лысак // Микробиология – 2001. – Т.70, №3. – С. 313 – 320.
18. *Robbins J.A., Levy R.* A rewiew of the microbiological degradation of fuel // Directory Microbiocides for the protection of Materials. [ed. By W. Paulus]. Netherlands: Kluwer Academic Publishers/ - 2004, p.177-201.

UDC 502.174. 3; 628.336.6

V.V. Gorupa senior lector,
L.S. Iastremska, PhD Agricultural Sciences.
(National Aviation University, Ukraine)

INSTALLATION FOR BIOGAS FROM SLUDGE NATURAL RESERVOIRS

Considered device for producing biogas from sludge natural water reservoirs as alternative sources of energy, which is characterized by a low metal content and high rates of productivity.

Nontraditional & renewable energy resources has recently become one of the promising areas of developed countries in the world, an important component of the new post-industrial technological development. Ukraine imports 75% of natural gas, 85% of crude oil and petroleum products, so the transition to alternative sources of energy for energy security is the most important and necessary.

The problem of transition to new fuels will be feasible, and in the civil and military aviation where it is possible to predict a steady increase in the intensity of flights and fuel. Now in aviation, one of the promising renewable energy sources, is to obtain biogas (methane) - a very clean and much cheaper fossil fuels. Then methane liquefies. Liquefied natural gas (LNG) is significantly less air pollution, its heating value 15 per cent higher than jet fuel, storage of LNG in liquid form simpler (temperature of about minus 160 ° C, which is almost 100 degrees higher than the storage of liquid hydrogen that was used previously) [1].

For biogas to search for new areas and raw materials. These raw materials include natural water reservoirs.

Fresh water - common ground ecosystems are lakes, ponds, rivers, canals, etc. [2]. They are characterized by two econiches: water phase (thickness), and sediment. The process of methanogenesis takes place almost entirely in the sediment. In this regard, the highest concentrations of methane detected in the interstitial water of precipitation (water, part of the sludge; pore water). The concentration of methane depends mainly on the intensity of methane formation. If the intensity of methane formation is higher than the rate of its removal, there is a glut of sludge gas. Depending on the structure of the precipitate formed accumulation of gas, the so-called gas traps, of which, under certain conditions, the gas can go into the water and the atmosphere in the form of gas bubbles. At a certain concentration of CH_4 is a glut of water at a depth of methane, is determined by the hydrostatic pressure, barometric pressure, temperature and total salt content. In the pore water sediments of deep lakes of methane concentration is very high - 13 mmol CH_4 /l.

With the accumulation of a sufficiently large number of gas bubbles as they rise from the sludge as a result of violations of the structure of the precipitate, it indicates an intensive of methane formation in the water. The composition of these gases is different depending on the reservoir and is presented in table. 1.

Table 1

Qualitative and quantitative composition of the gas reservoirs of natural sediments [3]

Substance	Contents,% (volume concentration)
CH_4	40 – 95
N_2	2 – 55
CO_2	0 – 5

Oxygen and hydrogen may be contained in the gas bubbles in small quantities. During the lifting gas bubbles through the water layer is exchanged gases. Emission of methane into the atmosphere is carbon loss for a given ecosystem. Because there are differences in the composition of gases selected directly above the sediment surface or near water. Gases from the littoral sediments of lakes tend to contain less nitrogen and more CH4 than gases from profundal sediment [3]. In addition, the rise of gas bubbles from the sediment leads to the mixing water (convection CH4), resulting minerals present in sediment in the area of anaerobic decomposition of organic matter, which is also a product of anaerobic decomposition (phosphate, ammonium), distributed by water, that is introduction of "fertilizer" in the water.

Distribution of methane in the sediment depends on the content of oxygen in the water column. Thus, if the water over sediment no oxygen, the concentration of methane in the sediment increases sharply at the border dividing phase sediment/water. If the oxygen in the water distributed in a way that reaches the surface sediment, the sediment formed in aerobic surface layer, in which the intense oxidation of methane. In these conditions the concentration of methane increases only in the deeper anoxic sediment layers. The accumulation of methane in water is only possible if the water contains no oxygen. Once methane enters the zone containing oxygen, it is oxidized to CO_2 through life metanotrophic bacteria. Therefore, the concentration of CH_4 in water and some oligotrophic lakes mesotrophic and most flowing waters (rivers) are very low and rarely exceed 1 mmol CH_4 /l [3]. For epilimniona evtotrophic stratified reservoirs is also characterized by low concentrations of dissolved methane. After mixing the water column of lake methane content, as a result of its oxidation, is reduced.

Contents cells methanogenic bacteria in fresh waters varies (within 2 - 3 orders of magnitude) depending on the season. The maximum occur in late summer (august), that at the end of the period of stagnation and minimum falls in november - january. These fluctuations in the number of methanogenic due to changes in temperature, change of stagnation and circulation (changes in anaerobic and aerobic condition of the surface layer of sediment in the reservoir area profundalniy) and differences in sedimentation of organic matter [3]. In very deep lakes with small seasonal variations in temperature hipolimnion and in the deeper layers of sediment in general there is no clear temporal changes in the number of cells methanogenic.

For biogas from sludge natural reservoirs proposed installation, which floats on the surface of the pond [4]. It contains a collection of case-made without bottom, bottom screw, pontoons, independent energy source, gearbox, drive bottom and screw device for adjusting the depth of diving screw (Fig. 1).

Wake up river silt with methane in the sediment, perform bottom screw. The capture of biogas from water collection is carried out without a bottom, that distinguishes the unit from the previous designs biogas units (BU) [5, 6]. Consequently, no typical elements BU: bioreactor, conveyor for sludge, heating of the biomass, its mixing, adding bacterial cultures and methane fermentation.

Installation is set on a water surface of the pond. Bottom screw *(1)* driven by an autonomous energy sources *(7)*, gear *(8)* and about *(9)*. Screw begins to rotate. Using the device control diving *(6)* ground screw immersed to the desired depth of the process. When rotating the screw elements of his work shift silt layer and its thickness is allocated biogas. Marked gases of lower density than water. Because of this they move up and get into the body-collection *(4)*. With body-collection *(4)*. through the nozzle *(5)* selected gases are removed to clean the unit and digests. Rate speed gear set. Rate set based on the minimum number of conditions that ensured progress sludge. Float installation using third-party funds floating in the water, or by tension cables, which are mounted on the banks of the river. Plant capacity to 10 m^3 / h, weight - 190 kg [5].

The use of such facilities in our country is very promising, because it is branched network of rivers and reservoirs. Ukraine has a water surface area of about 2 • 1010 m2. There are 14 major rivers with a length of 5000 km, 123 of river length of 101-500 km, 968 rivers with a length of 25-100 km, the 3020 river length of 10-25km, 68790 small rivers with a length of 10 km [7]. The presence of these rivers, especially small and medium makes it possible to obtain from them a significant amount of biogas through the use of organic matter who they are.

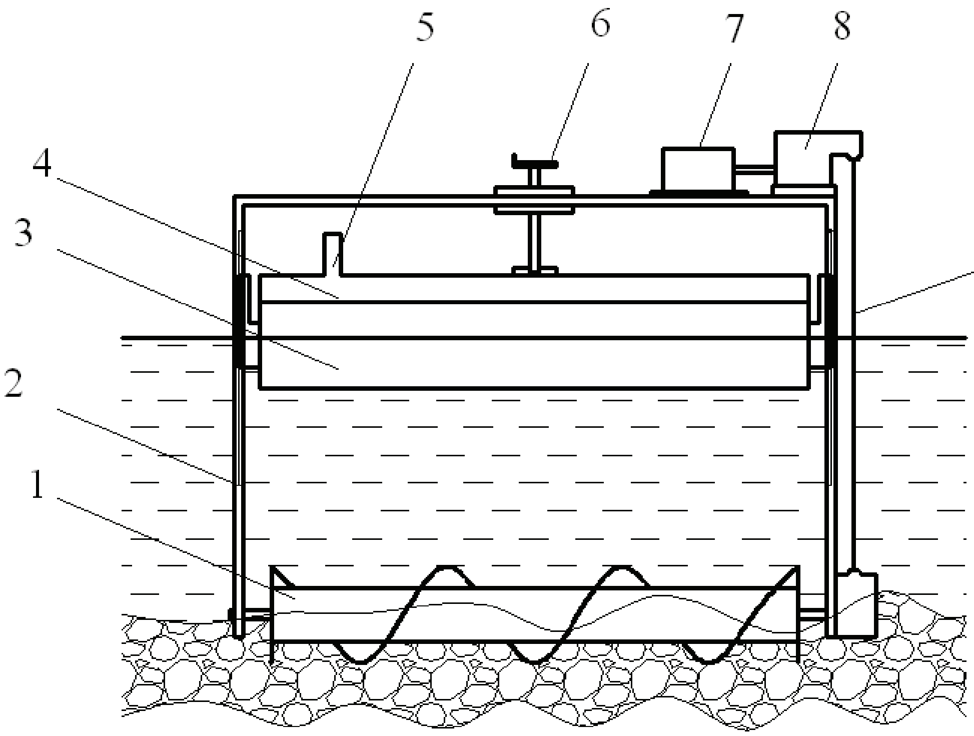

Fig. 1. Installation for biogas production from natural water bodies
1 - bottom screw; 2 - frame; 3 - pantone; 4 - corpus-collector; 5 - tube to drain the gas mixture; 6 - a device for regulating the depth of immersion; 7 - an independent source of energy;
8 – gear; 9 - wire bottom the screw

Conclusions

Thus, the presence of a large number of reservoirs in Ukraine makes it possible to obtain from them a significant amount of biogas proposed a new device from the mud of natural bodies of water, which is characterized by a low metal content, and install high performance of productivity.

References

1. *Zaderiyenko S.* Global trends in the use of alternative fuels in aviation / Systems weapons and military equipment. – H: HUPS, 2008. – № 2 (14). – P.33-35. [in Ukrainian]
2. *Khimki R.V., Merezhko A.I., Babko R.V.* Small rivers – the research, preservation, restoration. – K: Institute of Ecology. – 2003. – 380 p.
3. *Malashenko Y.R., Hayer Yu., Berger U. etc*. Biology and methane-forming and methane-oxidizing microorganisms / K: "Naukova Dumka", 1993. – 255 p. [in Russian]
4. *Gorupa V. V., Pavlyuh L.I., Zozulja L.A.* Installation for biogas. Patent UA 51083, MPK (2009) C12 P 5/00 Bull. – №12. – 2010. [in Ukrainian]
5. Types of biogas plants. - [Electronic resource]. – Mode of access: http://bio-energy.com.ua/
6. *Adamenko I.O., Adamenko I.O.* Fermentator of biogas. Patent UA 78110, MPK (2007) S12P 5/00 S12M 1/107 C02F 11/04, Bull. –№2. –2007. [in Ukrainian]
7. *Bogachev N.Y., Hranovich I.L., Chen Qi.* Rationale for the strategy of water resources at risk // Engineering Ecology. – 2000. – № 6. – P.2-21.

UDC 579.83+579.851.1

L.A. Khrokalo PhD, A.I. Doloman.
(National Technical University of Ukraine "Kyiv Poitecnic Institute")
L.S. Iastremska, PhD
(National Aviation University, Ukraine)

SELECTION OF METHANOGENIC BACTERIA FOR IMPROVING THE BIOGAS PRODUCTION

Overview of methane digestion and characteristic bacteria is provided. Selection of methane-producing bacteria pure cultures conducted on Zhilina's grows media with methanol and sodium acetate from storage cultures on a base of fermented residue from pig manure and wood, pig manure, poultry excrements, sewage sludge. Emissions of gases were analyzed on gas chromatograph. Pure cultures of the family Methanosarcinaceae were obtained on agar medium by the method of Hungate.

Biogas, the perspective renewable fuel has obtained from different wastes and biomass sources used in heat and electricity power engineering and transport (aviation) as well. The components of biogas are CH_4 (55-80 %), CO_2 (15-45 %), H_2 (1-4%), H_2S and mercaptans (about 3 %), NH_3 and N_2 (less than 1 %). Biogas is obtained by anaerobic digestion of organic compounds due to enzyme activity of specific bacteria community. The heat capacity of biogas is strongly depend on methane content and determine by substrate (feedstock) and parameters of fermentations such as temperature, pH, ammonium content *etc*. Other important aspect of fermentation activity is composition of bacteria community. Common anaerobic digestion consists of a series of bacterial events that convert organic compounds to methane, carbon dioxide, other primary compounds and new bacterial cells. These events are commonly considered as a three-stage process. The first stage of the process involves the hydrolysis of solids (particulate and colloidal wastes). The hydrolysis of these wastes results in the production of simplistic, soluble organic compounds (volatile acids and alcohols).The second stage of the process, acetogenesis, involves the conversion of the volatile acids and alcohols to substrates such as acetic acid (CH_3COOH), carbon dioxide and hydrogen gases. The third and final stage of the process, methanogenesis, is provided by methane-forming bacteria and lead to methane production.

Methane-forming bacteria (other name methanogenic) are singular group of organisms which can produce methane (no other organism produces methane!). Methanogenic bacteria are morphologically various groups that have diameter sizes of individual cells $0.1–15 \times 10^{-6}$ m of different shapes and growth patterns. There can be found as individual rods, curved rods, spirals, cocci or grouped as irregular clusters of cells, chains of cells or filaments, and sarcina or cuboid arrangements. Methanogenic bacteria are some of the oldest bacteria and are grouped in the domain *Archaea.* This domain is also included extremely halophilic bacteria, thermoacidophilic bacteria, and extremely thermophilic bacteria. However, the methane-forming bacteria are different from all other bacteria. They are oxygen-sensitive strict anaerobes, tolerate high concentrations of salt and could be found in habitats that are rich in destructive organic compounds in which oxygen is rapidly removed through microbial activity. Many ones occur as symbionts in animal digestive tracts. The rumen is a special organ in the digestive tract of cows, goats, sheep and some other herbivores, in which the destruction of cellulose and complex polysaccharides occurs. Ruminants cannot survive without such bacteria. The bacteria inhabit digestive tract obtain compounds and energy and ruminant animals get simply assimilated nutrients. Methane-forming bacteria also have unusually high sulfur content: approximately 2.5% of the total dry weight of the cell is sulfur. Some ones are capable of fixing molecular nitrogen. Methane-forming bacteria are classified according to their structure, substrate utilization, types of enzymes produced and temperature range of growth. Recently more than 60 species of methane-forming bacteria are identified. In microbial consortia methanogenic bacteria grow on limited number of substrates. *Methanobacterium formicium* (most abundant bacteria in nature) grows on hydrogen and carbon dioxide and formate. But the majority of methane is produced by two genera of acetotrophic methanogens, *Methanosarcina* and *Methanothrix*. All methane-forming bacteria grow best in an environment with an ORP (oxidation-reduction potential) less than – 300 mV [1] .

The samples for cultivation of methanogenic bacteria involved in original experiment were such: fermented residue from pig manure and wood wastes; fermented residue from pig manure; pig manure; poultry excrements; sludge from station of waste water treatment. Storage bacteria culture have been cultivated in strict anaerobic conditions and temperature + 30 ^{0}C on Zhilina's liquid grows media with pH 6,0-8,0 (KH_2PO_4 – 1,5 g and NH_4Cl – 1,5 g dissolved in 500 ml of distilled water; $MgCl_2 \cdot 6H_2O$ – 0,15 g and $CaCl_2 \cdot 2H_2O$ – 0,3 g – in 500 ml; $NaHCO_3$ – 1,5 g and $Na_2S \cdot 9H_2O$ – 0,75 g – in 350 ml; yeast solution – 0,15 g in 150 ml of distilled water) sterilized in the autoclave. Storage cultures grew in 250 ml glass bottle filled in half-null by liquid nutrient media and blow out by argon gas using copper needle. Resazurin solution 0,1 % have been used as indicator of anaerobic conditions. Bottles were hermetic closed up by rubber plug kipped by wire yarn. Antibiotic amoxicillin is used for keeping the pure cultures of methane-forming bacteria 0,12 g/l. Selection of methanogenic bacteria have been made by grow of storage culture patterns on Zhilina's liquid media with add-on source of carbon feed. Methanol or sodium acetate was the carbon sources for growing of pure culture of methanogenic bacteria. Finally, the reinoculation of methanogenic bacteria has been made on solid agar medium a modified method by Hungate [2].

The purity of selection was controlled by microscopy and gas emissions. Gas compounds have been analyzed by gas chromatograph LHM-8MD. Microslides were colored by Gram method and viewed under light microscopy in lens magnification × 1875 and bacteria identification was provided by keys [3, 4].

Cultures that were isolated from different samples were grown for 9 days of the three models each replication according to standard procedure. Since accumulation of anaerobic microbial community biomass the patterns with high emission of carbon dioxide and low content of nitrogen were selected for pure culture of methane-producing bacteria growing. Pure cultures grew on liquid nutrient medium with additions of methanol (first experimental series) and sodium acetate (second series). Cultivation of pure cultures conducted in 9 days, gas emission was estimated on the 3th, 6th, 9th days of experiment (fig. 1).

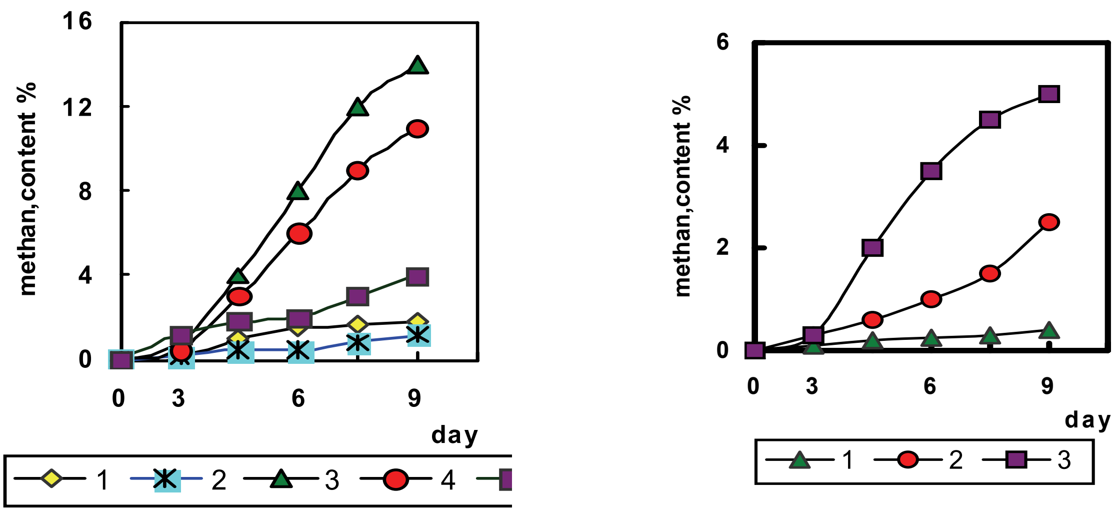

a)
1 - fermented pig manure & wood,
2- fermented pig manure, 3 - pig manure,
4 - poultry excrements, 5 - sludge)

b)
1 - pig manure, 2- poultry excrements,
3-sludge)

Fig. 1. Rates of methane emission of pure bacteria cultures on mediums:
with methanol (a), sodium acetate (b)

High yields of methane were observed in 9-day cultivation in the samples isolated from poultry excreta and sewage sludge on substrates - acetate and methanol, respectively. Obviously, these ecological niches are of great variety and population density of methane-producing bacteria.

Microscopy of cells of pure cultures showed a high number of coccus cells (a) and collected in bags irregular clusters (b), isolated from all samples growing on methanol and sodium acetate. Identification determined, that the isolated cultures may belong to the family *Methanosarcinaceae.*

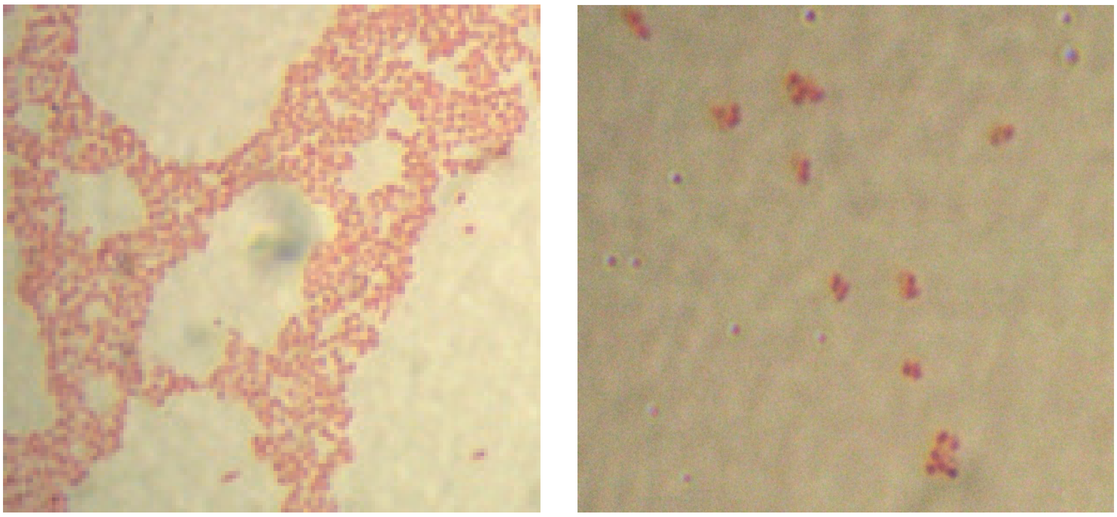

(a) (b)

Fig. 2. Light microscopy of Gram-negative coccus cells (a), irregular clusters (b), increase × 1875

Conclusions

Selection of methane-producing bacteria pure cultures conducted on Zhilina's grows media with methanol and sodium acetate from storage cultures on a base of fermented residue from pig manure and wood, pig manure, poultry excrements, sewage sludge. Experiment results also demonstrated that activity of anaerobic digestion and methane emission is larger in patterns with bacteria communities than pure culture of methane-producing bacteria. The possibilities of further bacteria selection and construction the preparation of specific bacteria community for industrial application needs to be further investigated.

References

1. *Gerardi M.* The Microbiology of Anaerobic Digesters / M. Gerardi. – USA : Wiley-Interscience, 2003. – 177 p.

2. *Tashirev A.B., Danko Y.N., Chernyshenko D.V.* Technique selection of isolated colonies of anaerobic bacteria in bottles // Microbiological Journal – 1988. – vol.50, –N 4. – P. 89-90. [in Russian]

3. *Bergey's* Manual of determinatie bacteriology. In two vol. (ninth edition) / Ed.: John G. Holt and others [in Russinan transl.]. – Moscow : Mir, 1997, vol. 2. – 368 p.

4. *Iastremska L. S.* Identification of thermophilic anaerobic microorganisms detached from methane-tank // Microbiological Journal. – 1993. – vol. 55, N 6. – P. 8-17. [in Russian]

UDC 577.152.34:577.151.5

N.A. Nidialkova, O.V. Matselyukh, PhD,
L.D. Varbanets, Prof.
(Institute of microbiology and viorology, National Academyof Sciences of Ukraine)
E.G. Garkavaya, Prof.
(National Aviation University, Ukraine)

THE PEPTIDASES OF *BACILLUS THURINGIENSIS* IMV B-7324 AS BASIS OF CARDIOVASCULAR MEANS FOR PILOTS TREATMENT

Peptidases with fibrinolytic and elastolytic activities were isolated and purified from culture liquid of Bacillus thuringiensis IMV B-7324. It was shown that molecular weights of tested enzymes were 24-26 kDa. On the basis on the substrate specificity we may suggest its possible application in medicine for treatment of various cardiovascular diseases by removing of blood clots.

Cardiovascular diseases are serious problem currently both for the people and for members of certain professions especially those in which the human and environmental factors play an important role. Pilot profession belongs to this category. Navigating by airplane pilot makes decisions about the actions of the crew in extraordinary situations. Therefore, he must possess such qualities as good health, ability to concentrate attention and stability to stress. It's known that among the occupational diseases of pilots are cardiovascular diseases, heart attacks, varicose veins, break of blood pressure. In addition, among the pilots myocardiosclerosis disease dominates (29%). It causes by the formation of scar tissue in the heart muscle that replaces myocardium and can deform the heart valves. The formation of clots is one of the reasons of cardiovascular diseases in blood vessels. In clinical practice the fibrinolytic agents are most effective and can break down blood clots. Fibrinolytic enzymes are these agents and can be isolated from microorganisms including bacteria, actinomycetes and fungi. Bacteria of the *Bacillus* genus are the most widely used for obtaining of such enzymes. Therefore isolation of microbial fibrinolytic enzymes is important for the use and range of drug and nutritional supplements whose action is directed at the prevention of thrombosis and other related diseases. Thus the main aim of this research was isolation of *Bacillus thuringiensis* IMV B-7324 peptidases and study of their substrate specificity which determine practical application.

The object of investigation was strain *B. thuringiensis* IMV B-7324 grown during two days, incubating on a gyratory shaker at 200 rpm at 42 °C in the 750 ml Erlenmeyer flasks with 200 ml of the nutritious medium (g/l): maltose – 19,0, $(NH_4)_2SO_4$ – 12,0, KH_2PO_4 – 1,6, $ZnSO_4 \cdot 7H_2O$ – 0,25, $MgSO_4 \cdot 7H_2O$ – 0,75, pH 7,5.

The fibrinolytic activity was measured by Masada method [1] using fibrin as a substrate. The reaction mixture contained 1 mg of fibrin, 1,8 ml of 0,01 M Tris-HCl buffer (pH 7,5) and 0,2 ml of tested enzyme solution, incubated during 30 min at 37 °C. After incubation 2 ml of 10 % trichlorocetic acid was added to stop the reaction. The solution was centrifuged and the supernatant was assayed for absorbance 275 nm. A unit of fibrinolytic activity was calculated as enzyme quantity that increased absorbance on 0,01 per min.

It was found two peaks during purification of the enzyme preparation by gel-filtration chromatography on TSK Toyopearl HW-55 (fig. 1). First peak (I) corresponds to an enzyme with elastolytic and fibrinolytic action, and second peak (II) – another enzyme that also can degrade insoluble fibrin. These peaks differ from each other only quantitative parameters of activities and protein.

The received peptidase preparations with fibrinolytic and elastolytic activity was further purified by ion-exchange chromatography with a step gradient from 0 to 1 M of NaCl on column with TSK DEAE 650 (M) (Toyosoda, Japan) (fig. 2). It was shown that using 0.01 M of Tris-HCl buffer (pH 7,5) enzymes go out before start of salt gradient. It associated with a total positive charge of the enzyme molecules under these conditions. As a result of the second stage a part of protein impurities was removed. The fibrinolytic and elastolytic activity of the purified peptidase (I) and fibrinolytic activity of the purified peptidase (II) were respectively in 15.4 and 15.5, 19.9 times higher in compare with the culture supernatant.

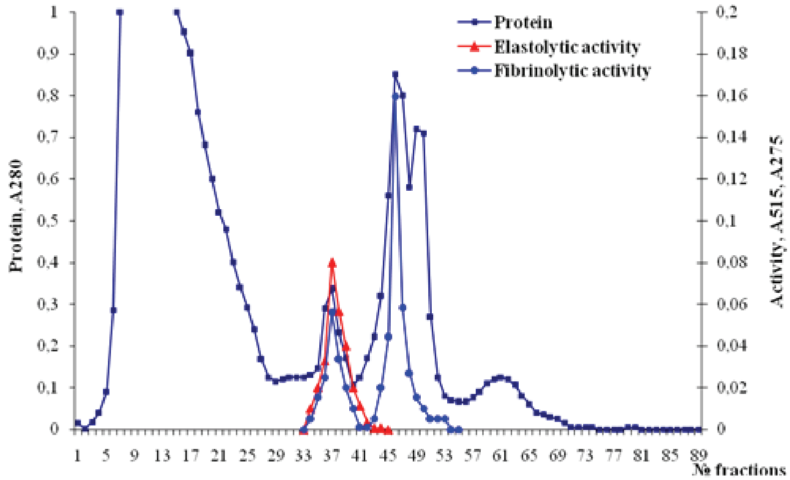

Fig. 1. Elution profile of complex enzyme preparation on TSK Toyopearl HW-55

a

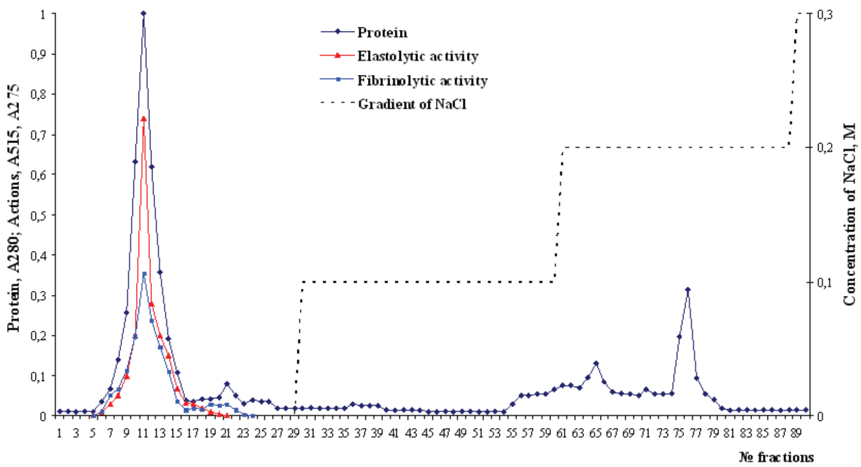

b

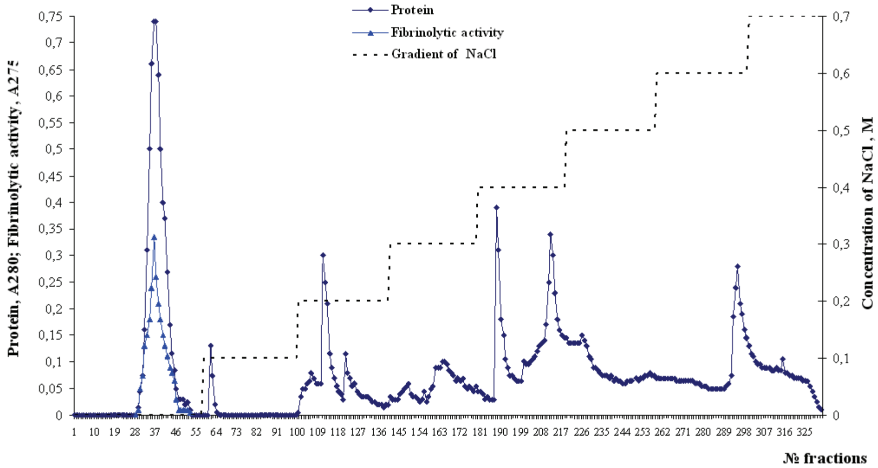

Fig. 2. Elution profile of peptidase preparations on TSK Toyopearl DEAE 650(M) with a gradient of NaCl from 0 to 1 M

A – peptidase (I) with elastolytic and fibrinolytic activity, B – peptidase (II) with fibrinolytic activity

The results of gel-electrophoresis in SDS-polyacrylamide gel system (fig. 3B) indicated on homogeneity of the isolated enzymes. It was shown that a molecular weight of peptidase (I) and (II) are about 26 and 24 kDa, respectively. The results of gel-filtration on Sepharose 6B (fig. 3A) confirmed those obtained by gel-electrophoresis in SDS-polyacrylamide gel. These data suggest that the isolated enzymes are monomeric proteins.

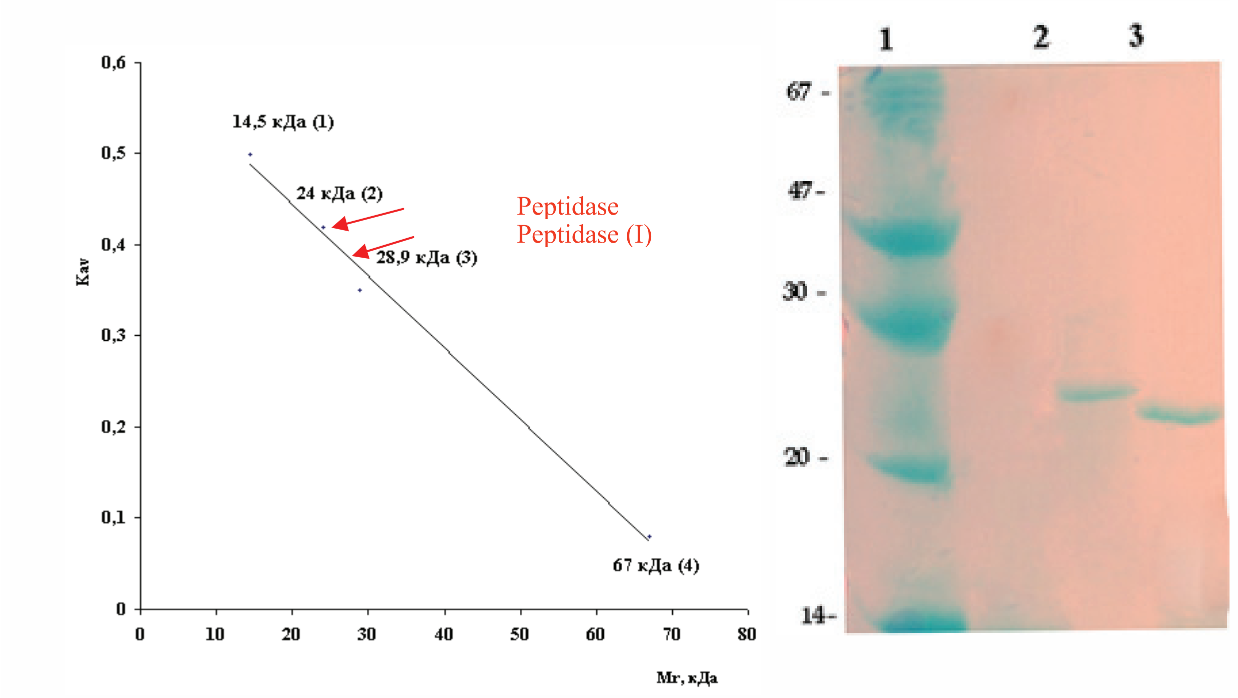

Fig. 3. Molecular weight of purified enzyme preparations on Sepharose 6B (A), SDS-polyacrylamide gel electrophoresis (B): 1 – proteins-markers, 2 – peptidase (I), 3 – peptidase (II)

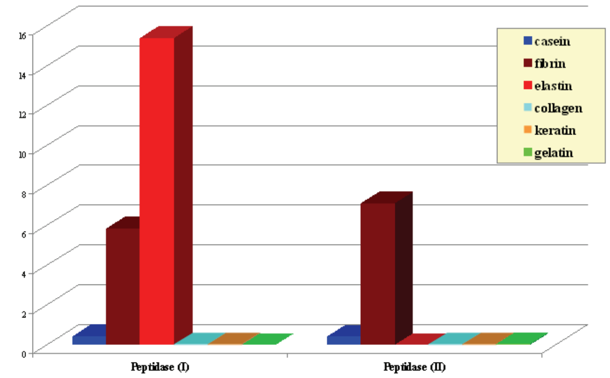

Fig. 4. The substrate specificity of peptidase (I) and (II)

Hydrolysis of natural substrates (fig. 4) by purified peptidases demonstrated that the peptidase (I) shown the specificity to the fibrin and elastin, and the peptidase (II) – fibrin. Besides both enzymes completely degraded the fibrinogen during half hour. The data on substrate specificity give a possibility to suggest that tested *B. thuringiensis* IMV B-7324 peptidases can be applied for treatment of various cardiovascular diseases and removing the fibrin clots.

Summary

From *B. thuringiensis* IMV B-7324 have been isolated and purified peptidases with fibrinolytic and elastolytic activities which molecular weights were 24-26 kDa. On the basis on the substrate specificity we may suggest its possible application in medicine for treatment of various cardiovascular diseases by removing of blood clots.

Reference

1. *Masada M.* Determination of the thrombolytic activity of Natto extract // Food style. – 2004. – V. 8, N 1. – P. 92-95.

UDC 615+57-022.532

I.S. Chekman, corr. member of NAS and NAMS of Ukraine, prof.,
N.O. Gorchakova, prof., P.V. Simonov, postgraduate
(Bogomolets National Medical University, Ukraine.)
K.G. Garkava, prof. (National Aviation University, Ukraine.)

NANOSCIENCE, NANOPHARMACOLOGY, NANOBIOTECHNOLOGY: POSSIBLE ADOPTION INTO AVIATION

Research in nanoscience may be considered as one of the most prominent achievements of humanity in the previous century. Nanoscience gave rise to studies of properties of nanoscale biological and synthetic materials and their use in different fields, particularly, in aviation. Also scientists are greatly interested in biosensors' design, which may be used in search of explosives during flights and to monitor an influence of different pollutants on the environment.

The second half of the twentieth century has been marked by significant achievements in various fields: physics, chemistry, medicine, biology, military technology, and aviation. Research in nanoscience may be considered as one of the most prominent achievements of humanity in the previous century. The progress that is expected after an implementation of nanoscience into life is associated with following features.

First of all, studies on pharmacological, biochemical, physicochemical, colloidochemical mechanisms of interaction of nanoparticles with biological objects (cells of macro- and microorganisms) will not only determine their positive or negative impact on biostructures and environment, but contribute into the search of effective and safe protectors of functional activity of cells and organs, and into their wide application in engineering, aviation, agriculture, and medicine as effective drugs, as well as carriers for drug and physiologically active substances delivery to a pathological process.

The second feature of nanoscience. Due to the challenges of science and practical needs of mankind the field of research at the intersection of various biological and technical disciplines emerged. Scientists of different specialties began to study the properties of nanoscaled materials, discover laws of their interaction with other nanoparticles. Obtained results are being implemented in life, and that is a convincing example of an integration process in development of mankind and an acquirement of some practical achievements in a short term. Thus, the Silix (nanodispersed silica sorbent), nanosilver ointment, nanoiron capsules and other preparations are already implemented in medicinal practice.

The third feature of nanoscience is the great interest of scientists and manufacturers in this area, which contributed to the implementation of results in industry, medicine, agriculture, electronics, biology, pharmacology, pharmacy, etc. According to the Internet the number of publications in nanoscience, nanotechnology, nanomedicine exceeds the number of scientific articles in other disciplines. Small size, chemical composition, structure, large surface area and shape – these are the basic properties that provide nanoparticles advantage over other materials, while simultaneously providing their possible toxic effects on biological systems and the environment.

The fourth feature is that the received scientific facts and practical results show that mankind has discovered fundamentally new properties of natural and synthetic matter. It is already established that nanomaterials have increased number of surface atoms, moreover, surface tension and surface energy of nanoparticles, interatomic distances, heat capacity, thermodynamic and optical properties are changed, which leads to a peculiar effect of nanostructures on the human body and the environment.

The fifth feature is that many biological objects and physiologically active substances are nano in size. Thus, most cell organelles (nucleus, lysosomes, mitochondria, ribosomes, DNA, RNA, etc), biological agents (albumin, antibodies), drugs (acetylsalicylic acid, quercetin, retinol), neurotransmitters (adrenaline, acetylcholine), physiologically active substances of plant (atropine, digoxin, chlorophyll) and animal origin (insulin, hemoglobin) are at the nanoscale [13].

While analyzing studies of domestic and foreign scientists in nanotechnology, one can summarize – intensive research on development of new methods of synthesis of nanoparticles with different structure and origin is conducted in the world.

Present nanoscience deals with such types of synthetic nanomaterials [4, 5]: liposomes, nanorods, nanotubes, nanofilms, fullerenes, nanospheres, quantum dots, dendrimeres, nanowires, nanocomposites, nanofibers, and nanocapsules.

Pharmacological and pharmaceutical basics of nanopreparations' development read that nanoparticles of organic and inorganic compounds may serve as substances for a synthesis of fundamentally new drugs as products of nanotechnology. These substances include fullerenes, dendrimeres, liposomes, nanometals (silver, copper, iron, etc). Basic requirements for nanopreparations are:

1) much more pronounced therapeutic effect compared with a similar drug that is used in medical practice;

2) fewer side effects than a similar drug causes;

3) stability and retaining of chemical structure over time;

4) an absence of influence on clinicopharmacological properties of drugs used in medical practice;

5) positive pharmacoeconomic parameters;

6) convenient dosage form;

7) affordable and environmentally friendly manufacturing [16].

A new direction in a development of nanopreparations is a formation of complexes between known medicines and nanoparticles, nanocapsules, nanotubes, dendrimeres, and fullerenes, which will contribute to a deeper entry of such complexes to pathological process, causing an effective pharmacotherapy of a disease [16].

In terms of air and space flights a structure and properties of common drugs may change. In contrast, nanoparticulate drugs have several unique advantages: medicines are protected from degradation during their transport to a destination. Moreover, nanoparticles can actively or passively accumulate in target organs and release desired dose at the right time. An increase in specific surface area of nanodrugs with simultaneous size reduction will in turn increase their therapeutic activity. That enables a wide range of new therapeutic techniques and reduces the toxic effects of new drugs on the human body [12, 20, 26]. For example, not only ZnO nanoparticles have pronounced antibacterial properties, but also are able to absorb a wide spectrum of electromagnetic radiation (ultraviolet, microwave, infrared, and radio) and therefore may protect pilots from radiation [13].

Ukrainian scientists have been conducting intensive research in nanoscience and nanotechnology. The National Academy of Sciences of Ukraine in the context of the special program "Nanostructured Systems, Nanomaterials, and Nanotechnology" continues a research in physics of metals and alloys, surface chemistry, powder technology, microelectronics, colloid nanosolutions, sorbents, medicines, which are based on nanotechnology. The Ministry of Education and Science of Ukraine jointly with the Ministry of Industrial Policy of Ukraine has created the Ukrainian-Russian inter-agency scientific and technical program "Nanophysics and Nanoelectronics". The use of nanomaterials in clinical practice is studied in institutes of the National Academy of Medical Sciences of Ukraine, Ukrainian national and medical universities.

The results of studies, carried out by domestic scientists, are introduced into practice. The A.A. Chuiko Institute of Surface Chemistry of National Academy of Sciences of Ukraine (dir. – the member of NAS of Ukraine, M.T. Kartel) jointly with domestic scientific and medical institutions for the first time in the world has developed, researched and introduced into medical practice the new drug with sorption and detoxication properties based on nanodispersed silica, called "Silix"

[17]. The Department of Pharmacology and Clinical Pharmacology of the Bogomolets National Medical University has developed a new dosage form – the suspension based on nanodispersed silica. It minimizes the toxicity and adverse effects on a liver function of such compounds as sodium fluoride and sodium nitrite, and antituberculous drugs: isoniazid, pyrazinamide, ethambutol, which differ in mechanisms of negative effect on the body and in chemical structure. The pharmacological activity of nanodispersed silica suspension exceeds that of conventional silica preparations [7]. This drug can be used for detoxification during air and space flights.

The R.E. Kavetsky Institute of Experimental Pathology, Oncology and Radiobiology (dir. – the member of NAS of Ukraine, V.F. Chekhun) jointly with the E.O. Paton Electric Welding Institute of NAS of Ukraine develops new types of colloidal systems with Fe_3O_4 magnetic nanoparticles with the aim to design new anticancer drugs [8]. The L.V. Gromashevsky Institute of Epidemiology and Infectious Diseases of NAMS of Ukraine (dir. – prof. V.F. Mariyevskyy) together with the laboratory of electron-beam technology of inorganic materials for medicine of E.O. Paton Electric Welding Institute and the Bogomolets National Medical University has found out that silver and copper nanoparticles showed a pronounced antimicrobial action against Staphylococcus aureus, than conventional medications of these metals [6].

One of the first domestic liposome-based drugs is Lipin – joint development of the Institute of Pharmacology and Toxicology of NAMS of Ukraine (dir. – prof. T.A. Buhtiyarova) and Kharkov pharmaceutical company “Biolik”. The main component of the drug is the phosphatidylcholine nanocapsules. Phosphatidylcholine is a natural component of biological membranes. The preparation shows antihypoxic action, inhibits processes of lipid peroxidation, increases non-specific immunity [1]. The study on nanoscience, nanotechnology and nanomedicine is also held in other Ukrainian research groups. In a joint research laboratory “Electron-beam nanotechnology of inorganic materials for medicine" of E.O. Paton Electric Welding Institute and the Bogomolets National Medical University the technology of copper and silver nanoparticles’ synthesis has been developed, the study of their pharmacological activity has been carried out, and methods for determining the size of nanoparticles have been proposed. Further research with the aim to develop new highly efficient drugs based on nanotechnology of molecular beams for the treatment of various diseases will have theoretical and practical importance for the development of medical science and technology.

An attention must be drawn to the need of in-depth study of physiological, biochemical and physico-chemical mechanisms of action of new nanopreparations and development of appropriate dosage forms’ technology for successful application in medical practice.

A large series of nanochemistry studies has been conducted at the F.D. Ovcharenko Institute of Biocolloidal Chemistry of NAS of Ukraine (dir. – prof. Z.R. Ulberg). According to Z.R. Ulberg et al. the molecular structure of complexes “nanometal-biomolecules” has been determined. Basic mechanisms that determine the sorption and heterocoagulation processes, as well as an adhesion of particles on a surface of cells have been found out. Among them, there is the colloidal chemistry process – the formation of electrical bilayer of a cell and a charge on its surface. In this case changes in electrokinetic phenomena take place, including diffusion-phoresis transport of nanoparticles, transmembrane potential and function of electrical channels. Marked changes are determined by a magnitude and sign of a charge of nanoparticles. The authors developed a model of bio-targeting bilayer in which the main parameters are the equilibrium electrical potential that occurs during dissociation of functional groups on the surface of cells, and nonequilibrium potential that results from active transport of protons [9, 11].

Cell biomembrane is the main structure responsible for the processes of interaction with nanoparticles. Biochemical factors, responsible for accumulation of ultrafine colloidal particles such as gold particles 10–20 nm in size on the cell surface, are the membrane ATP-ase activity and respiratory chain enzymes function. As performed by Z.R. Ulberg et al., Mg-ATP-ase activity of a biological membrane consists of two components: azide-sensitive (63%) and azide-resistant (37%). Azide-sensitive ATP-ase causes the functioning of respiratory chain of a plasma membrane of bacteria, and azide-resistant – transmembrane transport of gold nanoparticles into cells [2, 3, 10].

When human organism is exposed to extreme factors during flights, metal nanoparticles can contribute into protection of the organism in hypoxia (magnesium nanoparticles) and anemia (iron nanoparticles) due to regulation of enzyme systems.

Further development of new highly efficient nanotechnology-based drugs has great theoretical and practical importance for the development of medical science and practice.

Thanks to new studies in nanobiotechnology, a new class of biochips has been developed. Lab-on-a-chip has built-in nanooptical, mechanical and electronic processors that are capable of detecting and separating objects on one platform [23, 24, 25], which can be used in aerial and space flights.

According to foreign nanotechnology experts' point of view, the attention should be paid to the implantation of biosensors and individualization of therapeutic methods. This means further technological improvement of existing biochips, increase in their biocompatibility, reliability and accuracy. In addition to in-depth knowledge of complex intracellular processes, individual genetic testing is important for prevention of genetic tendency to certain diseases. One chip with the size of a postage stamp will replace a range of equipment needed for the DNA/RNA analysis, an identification of genetic modification of organisms, early diagnosis of cancer, a study of cell transfection efficiency, a determination of gene expression, a quantitative determination of proteins, etc [15, 19, 22].

Nowadays, special attention is paid to a creation of miniature devices that can be placed in human body for diagnostic and therapeutic purposes. Existing devices allow diagnostics of only individual systems and organs [30].

In recent years, researchers from different scientific fields (physicists, chemists, biologists, pharmacists, physicians) and production workers, especially of the electronics industry and biotechnology, have concentrated on studying the properties of sensors and biosensors [18, 29].

An interest to sensors occurred with the necessity to find explosives, particularly during aircraft flight [28]. Biosensors are special systems of highly sensitive elements that have the ability to determine the amount of substances formed during the reaction due to their high selectivity [27].

During a production of pharmaceuticals and medical products (drugs, enzymes, antibodies, medical devices), industrial products (extremely pure substances, metals, organic compounds) a large variety of processes is used. This requires the monitoring of their technology at industrial enterprises using sensors and biosensors. Scientists have concluded that temperature, pressure and other parameters in production must be constantly monitored. Biosensor systems have already begun being used to control production processes and carry out environmental monitoring [14, 21].

Conclusions Scientific research on design and study of properties of nanoparticles and new biosensors, which may be used in medicinal practice during flights, continues. The analysis of carried out study shows an intensification of such research activity. A study on nanomaterials and biosensors toxicology, their possible negative influence on an organism and the environment is of great importance.

References

1. *Григор'єва Г. С.* Реальна нанофармакологія: становлення, міфи та успіх ліпосомофармакології // Фармакологія та лікарська токсикологія. – 2007. – Т. 4, №5. – С. 83–88.

2. *Данилович Г. В., Грузіна Т. Г., Ульберг З. Р. та спів.* Ідентіфікація та каталітичні властивості Mg^{2+} – залежної АТР-гідролази плазматичних мембран Bacillus sp B 4253, здатних до накопичення золота // Укр. біохім. журн. – 2004. – Т. 76, №5. – С. 45–51.

3. *Данилович Г. В., Грузіна Т. Г., Ульберг З. Р. та спів.* Вплив іонного та колоїдного золота на АТР-гідролазні ферментні системи в мембрані мікроорганізмів Bacillus sp B4253 та Bacillus sp B4851 // Укр. біохім. журн. – 2007. – Т. 79, №4. – С. 46–51.

4. *Елецкий А. В.* Углеродные нанотрубки и их эмиссионные свойства // Успехи физических наук. – 2002. – Т. 172, №4. – С. 401–438.

5. *Кац Е. А.* Фуллерены, углеродные нанотрубки и нанокластеры: Родословная форм и

идей. – М.: Изд-во ЛКИ, 2008. – 296 с.
6. *Москаленко В. Ф., Лісовий В. М., Чекман І. С. та спів.* Наукові основи наномедицини, нанофармакології та нанофармації // Вісник Національного медичного університету ім. О.О. Богомольця. – 2009. – №2. – С. 17–31.
7. *Ніцак О. В., Казак Л. І., Чекман І. С.* Ефективність суспензії нанодисперсного кремнезему при гепатиті, викликаному ізоніазидом // Фармакологія та лікарська токсикологія. – 2008. – №1/2/3. – С. 66–69.
8. *Патон Б. Є., Москаленко В. Ф., Чекман І. С. та спів.* Нанонаука і нанотехнології: технічний, медичний та соціальний аспекти // Вісн. НАН України. – 2009. – №6. – С. 18–26.
9. *Ульберг З. Р., Грузина Т. Г., Перцев Н. В.* Коллоидно-химические свойства биологических наносистем. Биомембраны // Коллоидно-химические основы нанонауки. – К.: Академпериодика, 2005. – С. 199–237.
10. *Ульберг З. Р., Карамушка В. И., Грузина Т. Г. и соавт.* Влияние протонофоров на гетерокоагуляцию бактериальных клеток и минеральных частиц // Коллоидн. журн. – 1990. – Т. 52, №1. – С. 172–175.
11. *Ульберг З. Р., Полищук Т. А., Марочко Л. Г. и соавт.* Коллоидно-химический механизм связывания металлов микроорганизмами // Коллоидный журнал. – 1994. – Т. 58, №4. – С. 554–558.
12. *Хромов О. С., Соловйов А. І.* Експериментальне обґрунтування застосування фосфатидилхолінових ліпосом у медицині // Фармакологія та лікарська токсикологія. – 2008. – №4(5). – С. 88–98.
13. *Чекман І. С.* Нанофармакологія. – К.: Задруга, 2011. – 424 с.
14. *Чекман І. С., Горчакова Н. О.* Біосенсори: стан та перспективи наукових досліджень // Наука та інновації. – 2008. – Т. 4, № 3. – С. 75–79.
15. *Чекман І. С., Рибачук А. В.* Нанобіотехнології: клініко-фармакологічний аспект // Ліки України. – 2010. – №1. – С. 88–92.
16. *Чекман І. С., Ульберг З. Р., Маланчук В. О. та спів.* Нанонаука, нанобіологія, нанофармація. – К.: Поліграф плюс, 2012. – 328 с.
17. *Чуйко А. А., Погорелый В. К., Пентюк А. А. и соавт.* Медицинская химия и клиническое применение диоксида кремния. – К.: Наукова думка, 2003. – 415 с.
18. *Becker Th., Hitzmann B., Maffer K et al.* Future aspects of bioprocess monitoring // Adv. Biochem. Engin – 2007. – Vol. 105. – P. 249–293.
19. *Blick R. J., Revel A. T., Hansen E. J.* Find GDPs: identification of primers for labeling microbial transcriptomes for DNA microarray analysis // Bioinformatics. – 2003. – Vol. 19. – P. 1718–1719.
20. *Cui D., Gao H.* Advance and prospect of bionanomaterials // Biotechnol. Prog. – 2003. – Vol. 19. – P. 683–692.
21. *Haes A. J., Van Duyne R. P.* Nanosensors enable portable detectors for environment and medical applications // Laser Focus World. – 2003. – Vol. 39, №5. – P.153–156.
22. *Huang W., Marth G.* EagleView: A genome assembly viewer for next generation sequencing technologies // Genome Res. – 2008. – Vol. 18. – P. 1538–1543.
23. *Ji H., Jiang H., Ma W. et al.* An integrated software system for analyzing ChIP-chip and ChIP-seq data // National Biotechnology. – 2008. – Vol. 26. – P. 1293–1300.
24. *Lemoine S., Combes F., Le Crom S.* An evaluation of custom microarray applications: the oligonucleotide design challenge // Nucleic Acids Research. – 2009. – Vol. 37, №6. – P. 1726–1739.
25. *Ma H., Horiuchi K. Y.* Chemical microarray: a new tool for drug screening and discovery // Drug discovery today. – 2006. – Vol. 11, №13/14. – P. 661–668.
26. *Medina C., Santos-Martinez M. J., Radomski A. et al.* Nanoparticles: pharmacological and toxicological significance // Br. J. Pharmacol. – 2007. – Vol. 150. – P. 552–558.
27. *Mehrvar M., Aldi M.* Recent developments, characteristics and potential applications of electrochemical biosensors // Anal. Sci. – 2004. – Vol. 20. – P. 1113–1126.
28. *Singh S.* Sensors – an effective approach for the detection of explosives // J. of Hazardous materials. – 2007. – Vol. 144, №1–2 – P. 15–28.
29. *Wolfbeis O. S.* Fiber-optic chemical sensors and biosensors // Anal. Chem. – 2004. – Vol. 76, №12. – P. 3269–3283.
30. *Yakutseni P., Kozyrev S.* Present and prospect of nanobiotechnology // 1st Saint-Petersburg International Workshop on NanoBioTechnologies, SPb, Russia. – 2006. – P. 14.

UDC 631.46.631.445.41:631.84

I.M. Malinovska, Doctor of Agricultural Science.,
N.A . Zinovieva, assistant.
(National Aviation University, Ukraine.)

THE INFLUENCE OF LONG – TERM SOIL CONTAMINATION BY AVIATION FUEL ON MICROBIOLOGICAL PROCESSES

Soil pollution with oil products during 7 months leads to substantial changes in the number, physiological activities of microorganisms and directivity of soil microbiological processes. In comparison with short-term contamination, the number of polysaccharide bacteria by 4.12 times at pollutant concentration of 5%; by 2.29 times at 20%. The number of nitrifying agents reduces by 4.86 times at the concentration of oil products at 1%; 7.62 at 5%; 4.62 at 10%, and 14.1 times at 20%.

The xenobiotics containing aromatic hydrocarbons are one of the most spread anthropogenic pollutants. Penetration of oil products into the environment leads to ecologically dangerous alterations of soil biological properties, disorder of the subsurface microbiocenosis [1]. It is known that subsurface microbial communities take active part in the processes of the natural hydrocarbon destruction [2]. The destruction identity depends on the number of hydrocarbon oxidizing microorganisms and total quantity of the heterotrophic microorganisms in the polluted soil. Researches of the directivity and microbiological processes in the polluted with the oil products soils are an important background for developing efficient techniques of treatment the areas contaminated with the oil products.

A simulation study was performed with use of gray wood light clayey soil of a monitoring landfill of intensive technology corn and grain crop laboratory of the NSC "Institute of Agronomy of the NAAS". It was contained in the 20-cm layer of soil: earth humus 2.74%, alkali-hydrolyzable nitrogen 9.33 mg, movable phosphorus 3.8 mg, and exchange potassium of 15.3 mg for 100 g of dry soil, $pH_{(KCl)}$ – 5.6. Phytocoenosis of the fallow areas formed as a result of extemporaneous weediness during 22 years and is mainly represented with grasses. The soil was selected in autumn and restored its biological activity by means of hydrating and thermostat control at 25°C during 21 days before the research. Aviation fuel of TS-1 brand was entered in the concentrations from 0 till 20% as an aqueous emulsion. Seeds of grass mix were sown in a part of the vessels 8 days before introducing the oil products, and a sterile glucose solution (1%) was added in a day. Control was soil without oil. The state of microbiocenosis was studied in 1, 23 days and 7 months after introducing the oil products by conventional methods [3].

Incubating of the soil contaminated with the aviation fuel during 6 months leads to significant changes in the number and physiological activities of the soil microorganisms in comparison with the original state and the contamination term of 23 days (tab. 1) [4]. Thus, the number of ammonifying microbes increased by 1.18 at the concentration of the petroleum products of 1%; 5.46 – at 5%; 7.15 – at 10%; 5.11 – at 20% during 7 months in comparison with the 23rd day that proves activation of aviation fuel destruction with soil microorganisms. Similar regularities are observed in regard of other microorganism groups also: number of mineral nitrogen immobilizing bacteria increases by 2.64 times at the concentration of oil products of 5%; 4.82 – at 10%; 2.40 – at 20% for 6 months of incubating. The ammonifying number increases in parallel to increase of oil product content and their maximal number is observed at the concentration of oil products of 10% (tab. 1). Introducing oil products in the concentration of 20% leads to reduction of ammonifying microorganisms quantity by 2.05 in comparison with the 10%-concentration that was observed in previous studies [4, 5].

Quantity of microorganisms in the soil contaminated with the aviation fuel exceeds their number in control group significantly (tab. 1). Thus, quantity of ammonifying microbes exceed the number of the control group by 2.33 times; mineral nitrogen immobilizing bacteria by 2.01;

oligotrophic by 1.34, denitrifying bacteria by 1.26; cellulolytic bacteria by 3.52, polysaccharide synthesizing bacteria by 1.78 times at the oil product concentration of 1%. The difference with other pollution dosages is even more dramatic that is related to including oil products in metabolic fates of soil microorganisms. The regularities obtained differ from those established by A.N. Dulgerov which stated continued reduce of microorganism total quantity, nitrifying and cellulolytic agents after introducing petroleum products during 3 months [6].

Nitrifying bacteria are impaired with the toxic affect of the pollutant both in 23 days, and 7 months: their quantity decreases in comparison with the non-polluted soil by 4.9-14.7 times (tab. 1). Besides, the nitrifying bacteria number decreases in comparison with their quantity on the 23rd day of incubating: by 4.86 at the oil product concentration of 1%; 7.62 at 5%; 4.62 at 10%; 14.1 at 20% (tab. 1). Therefore, the negative effect of the oil products for the nitrifying bacteria aggravates with the course of time and increases in parallel with the growth of contamination level. The inhibiting effect of the oil products is connected, on the one part, with creation of anaerobic conditions in the soil, and with their high sensitivity to the water soluble organic substances which concentration in the soil solution increases significantly as a result of microbial degradation of aviation kerosene molecules, on another one.

It is very important to study the regularities of change quantity of polysaccharide synthesizing bacteria in the polluted soils because the polysaccharides form surfactant complexes with the bacterial proteins possessing the properties of emulsifiers for hydrophobous oil molecules [7-8]. It was demonstrated that introduction of petroleum products during a day leads to decrease of polysaccharide synthesizing microorganisms both in the unplanted soil and root zone in the previous researches [4]. The quantity of polysaccharide synthesizing microorganisms in the variants with the aviation fuel drew after the following incubating of the polluted soil, and it exceeded the indices for the unpolluted soil by 9.0–34.3 times in 23 days [5]. After 7 months of incubating the polluted soil the number of polysaccharide synthesizing microorganisms increased by 4.12 times at the aviation fuel concentration of 5%; 1.48 – at 10%, 2.29 – at 20% in comparison with the 23rd day. Thus, the continued hatching of the soil contaminated with the aviation fuel leads to significant increase of the quantity of polysaccharide synthesizing bacteria that take direct part in petroleum products destruction making them more available for consuming by microorganisms.

During 7 months of hatching the soil polluted with the petroleum products, directivity and intensity of microbiological processes is changed. While intensity of mineralization processes increased in parallel with the growth of aviation fuel content in a day after their introducing, it decreased with the increase of pollution level in 23 days [4, 5]. Intensity of mineralization processes in the polluted soil losses dependence on the pollutant concentration in 7 months. Thus, index of pedotrophicity fluctuates within the borders 0.049-0.56, index of oligotrophicity – 0.31-0.41, index of nitrogen mineralization – within the borders 0.78-0.97 (tab. 2).

Introducing aviation fuel into the soil leads to decrease of humus decomposition activity in comparison with the control variant: by 10.5 times at the concentration of aviation fuel 5%; 16.8 times at 10%; 7.5 times – at 20%. Possibly, the oil product molecules play the part of the most available substrate for autochthonic and heterotrophic microorganisms than humus substances that decreases activity of decomposition of the latter. Hatching of the contaminated soil during 7 months leaded to phytotoxicity reduction by 4.45 times in comparison with the term of hatching of 23 days at the concentration of aviation fuel 5% (tab. 2). Growth of test plants appears at the concentration of aviation fuel of 10 and 20% while seeds of fall wheat did not sprout in 23 days after introducing the fuel into these variants [5]. At the same time phytotoxicity of the soil at maximum pollution is still exceeding the phytotoxicity of the control variant by 2.38 times, and by 25.4% at 10% of pollution. The soil phytotoxicity remains at the indice level of 23-day hatching at the fuel concentration of 1%, and exceeds the rate of the control variant by 10%.

Adding glucose into the soil as a possible co-metabolite of aviation fuel allowed forming microbiocenosis differing from microbial community of the soil without glucose with somewhat increased quantity of the microorganisms of the carbon cycle and reduced quantity of the nitrogen cycle and mineral phosphate mobilizing bacteria on the 23rd day of hatching (tab.1). In this case it was decomposed by 3.0% of aviation fuel more in this variant that evidences for more intensive course of the processes including those being destructive in regard of fuel (tab.2). Glucose adding intensifies developing the organic soil substance by 2.84 times, nitrogen mineralization by 3.59, increases index of oligotrophicity by 3.94 times (tab. 2). Adding glucose during the first periods of observance reduces activity of humus mineralization and polluted soil phytotoxicity, and does not influence on these indices in comparison with the variant without applying glucose in 7 months.

Conclusion

Changes in the quantity and physiological activity of the subsurface microorganisms in comparison with the 23-day term of contamination. In particular, the quantity of ammonifying and polysaccharide synthesizing microorganisms taking direct part in aviation fuel decomposition is significantly increasing, and the number of nitrifying bacteria decreases in length of time and increase of pollution level.

Introducing easily available substrates into the soils polluted with the aviation fuel create conditions to form powerful and stable microbiocenosis providing more active destruction of pollutants in comparison with microbiocenoses of the soils without adding ectogenous substrates.

References

1. *Alvarez P.J.J.* Substrate interactions of benzene, toluene, and para-xylene during microbial degradation by pure cultures and mixed culture aquifer slurries / P. J. J. Alvarez, T. M. Vogel // Applied and Environmental Microbiology. – 1991. - Vol. 57, N. 10. - P. 2981–2985.

2. *Bachoon D.S.* Microbial community dynamics and evaluation of bioremediation strategies in oil-impacted salt marsh sediment microcosms / D. S. Bachoon, R. Araujo, M. Molina, R. E. Hodson // Journal of Industrial Microbiology & Biotechnology. – 2001. – Vol. 27. – P. 72–79.

3. *Малиновська І.М.* Мікробіологічні процеси в ризосфері рослин у забрудненому нафтопродуктами грунті /І. М. Малиновська, Н. А. Зінов'єва // Мікробіологія і біотехнологія. – 2011. – №2. – С.83-91.

4. *Малиновська І. М.* Вплив забруднення сірого лісового ґрунту нафтопродуктами на його фітотоксичні властивості та стан мікробіоценозу / І. М. Малиновська, Н. А. Зінов'єва // Збірник наукових праць Інституту землеробства . – К.:Ексмо. – 2010. – Вип.1–2. – С.61–69.

5. *Малиновська І. М.* Деградація нафтопродуктів аборигенними мікробними угрупуваннями сірого лісового грунту / І. М. Малиновська, Н. А. Зінов'єва // Вісник Харківського нац. аграр. унів. Сер «Біологія». – 2011. – Вип. 2– С.105-112.

6. *Дульгеров А. Н.* Углеаммонийные соли и бактериальный препарат «Десна» – важнейжие факторы рекультивации поч, загрезненных углеводородами нефти / А. Н. Дульгеров, А. Ю. Нудьга // Елементи регуляції в рослинництві / Збірник наукових праць. – К. : ВВП „Компас", 1998. – С. 256–259.

7. *Noordman W. H.* Rhamnolipid stimulates uptake of hydrophobic compounds by *Pseudomonas aeruginosa* / W. H. Noordman, D. B. Janssen. // Appl. Environ. Microbiol. Rev. – 2002. – Vol. 68, N 9. –P. 4502–4508.

8. *Walzer G.* The Acinetobacter outer membrane protein A (OmpA) is a secreted emulsifier / G. Walzer, M. Rosenberg, E. Z. Ron // Environ. Microbiol. – 2006. – 8, N 6. –P. 1026–1032.

Table 1.

Quantity of microorganisms in gray wood soil in 7 months after introducing aviation fuel in increasing concentration

Variants	Microorganisms, million CFU/g soil													
	ammonifying	mineral nitrogen immobilizing	oligotrophic	Azotobacter, % fouling of soil lumps	denitrifying	nitrifying	pedotrophic	cellulolytic	polysaccharide synthesizing	autochtonic	streptomycetes	micromycetes	mineral phosphate mobilizing	K_r
Control	90,2	101,3	65,2	0,00	124,2	1,03	112,3	30,6	5,62	44,0	30,1	0,19	30,2	1,15
1% AF	210,3	204,1	87,1	0,00	156,1	0,14	116,6	107,7	10,0	41,5	12,9	0,18	19,9	0,97
5% AF	1480,1	1304,3	463,0	0,67	173,3	0,13	825,1	280,7	187,1	30,8	39,9	0,15	122,9	1,55
10% AF	2184,1	2092,2	421,1	0,67	168,4	0,21	1073,4	295,9	342,2	25,1	38,5	0,09	109,9	1,39
20% AF	1067,0	828,2	364,4	0,00	179,7	0,07	539,1	337,4	173,0	28,2	26,6	0,19	117,3	1,25
5% AF + 1% Glucose	244,0	770,6	297,6	0,00	166,7	0,24	388,1	252,4	103,2	17,4	14,9	0,15	104,0	1,08
HIP_{05}	15,5	12,3	7,14	0,04	5,02	0,03	4,00	9,51	3,86	2,14	3,78	0,03	4,85	

Note: AF - aviation fuel, CFU –colony-forming units.

Table 2.

Performance intensity of mineralization processes and phytotoxic properties gray wood soil in 7 months after introducing aviation fuel in increasing concentration

Variants	Index of pedotrophicity	Index of oligotrophicity	Index of nitrogen mineralization	Humus mineralization activity, %	Number of degraded AF, mg/g soil		Mass of 100 plant test crops - wheat, g		
					23 days	7 months	stem	roots	total mass
Control	1,25	0,72	1,12	39,2	0	0	8,33	5,97	14,3
1% AF	0,55	0,41	0,97	35,6	4,20	0,82	7,35	5,67	13,0
5% AF	0,56	0,31	0,88	3,73	21,1	3,00	7,29	7,18	14,5
10% AF	0,49	0,19	0,96	2,34	42,4	1,60	6,06	5,29	11,4
20% AF	0,51	0,34	0,78	5,23	84,8		2,25	3,75	6,00
5% AF + 1% Glucose	1,59	1,22	3,16	4,48	21,3	4,00	6,92	7,50	14,4

Note: AF - aviation fuel.

UDC 658.336:159.944 (045)

O.M.Kovalev, PhD,
A.O. Pavlov, student.
(National Aviation University, Ukraine)
O.O. Lynnyk, assistant.
(Bogomolets National Medical University, Ukraine)

INCREASE PSYCHOPHYSICAL HEALTH OPERATORS IN AVIATION

The main indicators of mental and physical health of operators and flight crews that could adversely affect safety. We describe the indications and the positive results of "Jodis-concentrate" in 83 adults and 576 children aged 7 to 17 years. Proposed to be used in conjunction with modern methods of mind-body workout biologically active iodine concentration of 20 mg/dm^3.

The World Health Organization in 1946 adopted the following definition of health: "Health - a state of complete physical, mental and social well-being and not merely absence of disease or infirmity". Of course, this definition is too broad and likely reflects the state to which to aspire. Health - is primarily a condition of the body, which indicates compliance with the structure and function, as well as the ability of regulatory systems to maintain constant internal environment (homeostasis). Health is reflected in the fact that in response to everyday stimuli appear adequate reaction to the character and strength, time and duration are characteristic for most people this population. Conclusions about the health or normal state of the organism on the basis of anthropometric do, physiological, and biochemical studies. In assessing the human health are not only anatomical and physiological criteria, but also social, particularly the degree of participation in work and social activities [1].

The main criteria for mental and physical health are the following indicators: somatic and psychic.

"To fly reliably it's very important to know how to control an aircraft but it's more important to know how to control yourself. My successes in aviation are often conditioned by high knowledge of equipment. That's right..., but for 1%, but for 99% - by skill to recognize, to learn and to improve myself. It's necessary to begin with study of basis of psychology" - said M.M. Gromov, the test-pilot [2].

General expediency of investigations and developments in the field of aviation medicine consists of provision of complex registration of a human factor during construction and operation of equipment with the purpose of increase of efficiency of aviation, flight safety, working capability of aviation specialists, their health care and continuation of professional length of service.

Would be appropriate to give an answer to the question - what is the essence of mind-body workout? Psychophysical training - a method of self on the body with a change in muscle tone, controlled breathing, pictorial representation of the normal functioning of organs, verbal reinforcement to improve the mental and physical capacity, training of active attention, will, memory development, the formation of self-control and adequate response to stimuli [3].

Scientists of the whole world are conducting active search for efficient protection against negative impact of industrial and ecological factors and fatique of operators in aviation. Some researchers suggest computerization of training of pilots (Yu.A. Tutushkin, 2002), but such manner of acquiring knowledges is a considerable loading on a human being. Some researchers suggest special simulators (M.V. Dvornikov, V.K. Stepanov, 1999) which are, as a rule, too cumbersome and expensive.

In our opinion, improve mental and physical health of the operators in the aviation industry can achieve in a complex modern methods of mind-body training [4] with pharmacological methods. This product - a biologically active iodine at a concentration of 20 mg/dm^3.

Iodine deficiency in the body has a 1.5 billion inhabitants of the planet. Ukraine, which experienced the horror of Chernobyl, in the present ranks first in the world of thyroid disease in children and adults, cancer, hepatitis, tuberculosis, AIDS and others. UN puts the problem iodine deficiency one level the problem of AIDS. Only 10 years (1993 - 2003) to 25.7% increase in the number of cancer patients. Near three thousand children are diagnosed with "thyroid cancer" were operated. There is degeneration of humanity, and lack of iodine removes future generations to mental deterioration. Women of childbearing age are considered one of the most vulnerable groups, so worry about the health of the child to his birth. Pregnancy can trigger thyroid disease, and to pregnant women escape this pathology, it is necessary to carry out prevention iodine deficiency. 80% of women in Europe suffer mastopathy. The scientists proved that the breast is a direct consequence of iodine deficiency.

Biological effects of iodine-containing substances is that hitting the body, iodine is actively involved in the synthesis of thyroxine and thus provides a normalization of thyroid function, which is often suppressed, such as those that are long in the exclusion zone. Normalization of the level of thyroxine in the body reduces atherogenic factors arising in the body against hormonal imbalance caused by ionizing radiation.

Many of iodine contained in sea fish, seaweed, food additive "Elamin." A number of nutrients also in dairy products, potatoes, millet, buckwheat, chokeberry.

Average daily demand for the mineral iodine (ICG) is different for the following categories: infants 0-5 months. - 40, 6-11 months. - 50, children 1-3 years - 70, 4-8 years - 90 men 11-14 years - 120, 15-51 year and older - 150, women 11-51 years of age - 150, pregnant women - 175, feeding mothers - 200.

But for the average daily accumulation needs minerals iodine person should eat plenty of vegetable or animal products that virtually impossible. Today found a solution of iodine deficiency. This «Iodis-concentrate - Jodis-concentrate" mineral water, saturated by a special technology with iodine ions, the product resulting from the long, rigorous efforts of the Ukrainian scientist, professor, academician of Ukrainian Technological Academy Vasil Melnichenko. Analogues of "iodine-concentrate" in the world no.

The concentration of iodine in the product is 20 mg/dm^3. The total mineralization, g/dm^3: 0,4-0,8. Chemical composition, mg / dm^3: sodium + potassium 10-100, 50-150 calcium, magnesium 10-100, chloride <50, sulphates <50, hydrocarbons 300-600. The content of organic matter <30 (or the composition of drinking water per GOST 2874.82).

Professional research proven to water "iodine" on indicators of iodine deficiency in school-age children in school number 9 Obolon district of Kyiv. It was studied 576 schoolchildren aged 7 to 17 months naprotyazi12 and received the following positive results: 4.8 times increase in the number of children with high levels of physical health, 30% increased performance of their intellectual tests, rose 2.2 times the quality of understanding, 2 times reduced the incidence of thyroid cancer in children.

Approved methods of the established procedure for using "iodine-concentrate" in the physiotherapy treatment, which at present practically introduced in Ukrainian spa hospitals. The effectiveness of "iodine-concentrate" as proven by clinical trials: Institute of Toxicology and Ecohygiene them. L. Medvedya, Institute of Radiology and Radiation Medicine, the Ukrainian Research Institute of medical rehabilitation and balneology.

Full security (failure overdose) established the Department of Food Hygiene of the O. Bogomoltsa National Medical University. Cytology and safety confirmed by numerous personal observations of people taking "iodine - concentrate" in different cities of Ukraine. Use products enriched "Jodis-concentrate" which is a source of iodine, helps prevent diseases associated with lack of iodine in the body. The product has radioprotective properties.

Thus, the further introduction of iodine-containing substances nutrition is a prerequisite for the effectiveness of biological effects of diets that may improve human health, strengthen the defenses of the body, to increase efficiency.

Characteristics of "Jodis-concentrate."

Product: "Raw materials for the production of iodized products" Jodis - concentrate "TU U 14326060.003-98 or TU U 15.9-30631018-007:2005.

Ingredients: High quality water is enriched with a special technology polyatomic ions of iodine (Technology patent number RSSHA.99/00020, Geneva, Switzerland, 22.08.2001).

Form release: An aqueous solution with a concentration of biologically active iodine (BAI) 20 mg/dm^3. Allowed an easy and natural taste of iodine residue of mineral salts.

Purpose: Prevention of diseases caused by iodine deficiency, normalization of iodine status, radioprotector.

Indications for use: When the manifestation of symptoms of iodine deficiency: Endocrine: thyroid dysfunction, goiter, impaired metabolic processes and heat transfer, diabetes mellitus;

immunodeficient: frequent colds and infections, weakened immune system;

cardiology: atherosclerosis (resistant to treatment with diet and medications), arrhythmia, in which the use of special drugs does not give a tangible and lasting effect, increasing the diastolic (lower) pressure due to swelling of the vascular walls;

anemic: decrease in hemoglobin in the blood, where iron therapy provides only modest results;

osteochondrosis: weakness and muscle pain in arms, chest and lumbar sciatica, in which conventional treatment is not effective;

edema: swelling around the eye or general, in which the receiving diuretics aggravates the condition, creating dependence on them;

bronchopulmonary: swelling of the airways leading to chronic bronchitis and acute respiratory diseases;

dermatological: hair loss, change in appearance and properties of hair and skin, prolonged healing of damaged skin;

gynecological: menstrual disorders, irregular periods, sometimes the lack thereof, infertility, breast, irritation and cracked nipples;

Somatic: fatigue, intolerance to heat and cold, diarrhea or constipation, weight changes, tremors, drowsiness, lethargy, frequent occurrence of headaches;

Psychic: mental irritability, depressed mood, forgetfulness, inexplicable bouts of depression, lower IQ, depression, inner restlessness, mental instability, impaired memory and attention.

Deceleration of the physical and intellectual development in children.

The most dangerous diseases caused by iodine deficiency in the body: male and female infertility, miscarriages, birth of dead children, premature birth, deaf-mutism, mental retardation (iodine deficiency reduces mental capacity, even in adulthood), acute mental disorders, cretinism.

The product is recommended for the Ministry of Health use school-age children for the prevention of iodine deficiency (Appendix to Conclution of sanitary-epiodemialogical expertise. № 05.03.02-06/49526 b u) 01/11/2005).

How to use: "Jodis - concentrate" (JC), taken orally, by adding to the first meal, milk porridge, milk, yogurt, water, juices, tea, coffee, etc... Add just before use in individual dishes. Do not depend on the meal. Thermal stability.

Water used for the enrichment of IR must meet the standard for drinking water (absolutely can not use chlorinated water).

Crimean Scientific-Research Institute of Physical Methods of Treatment and Medical Climatology them. Sechenov recommends the use of infrared externally in the form of rinses, baths, applications, and other physical therapy.

The recommended daily intake of iodine standards (Guidelines for Drinking-water Quality. Volume 1. ELO, Geneva, 1994) provide for the maximum allowable rate of no more than 1000 micrograms per day.

Interaction with drugs: Due to their properties interact with any medication without rejection, has the versatility of a good natural stabilizer, increases the effectiveness of drugs by 30%.

Side effects: None identified. An overdose of biologically active iodine is not possible. It does not cause hyperthyroidism.

Shelf life: 12 months.

Storage: Optimal storage of the product at a temperature of 5° - 20° C. According to studies, JC - resistant to heat treatment and sunlight.

Packaging: Plastic packaging capacity of 0.5 liters.

Producer: LLC "NPK" Jodis "IPC" Yark-Kiev ".

Here are some partial results of people taking “Jodis-concentrate”.

Anna Pavlenko, Dnepropetrovsk, agree, "JC" in the spring of 2005 and immediately became easier when I deliver varied from headaches to normal pressure. I went from a state of severe depression, we can say thanks to the "JC" I survived, believed in the best in the salvation of themselves and families - because when the family heal one person, it gets saved the whole family. Three winters have not had the flu. If you are working 12-14 hours on my feet all the joints are aching feet, lifting the region - above the foot. The pains were very strong. But, thank God, for "JC"! I began to make lotion at night. The results of miraculous: in such cases I can not sleep, relax, and get up in the morning alive and well, wear shoes, which was yesterday, "would not fit," because "JC" relieves pain, swelling, inflammation, normalize salt metabolism. Cloth, which I put for the night, damping the "JC", even after washing is tough, impregnated with salt. I drink, "JC" constantly, morning and evening for 1 tsp. He inspires me, makes a save.

Conclusions

Thus, the data on the biological action of iodine-containing compounds, 72 positive personal feedback from patients, 11 people - own observations after receiving "Jodis-concentrate" allow us to conclude the need for further observation and ability to use the product "Jodis-concentrate" to improve the mental and physical health operators and flight crews.

References

1.Patologicheskaya physiology: Uchebn.dlya students med.vuzov / *N.N.Zayko, Yu.V.Byts, A.V.Ataman* et al: ed. *N.N.Zayko, Yu.V.Bytsya*.-3rd ed.-Moscow: MEDpress-Inform, 2002.-644 pp. (In Russian).

2.*Korotkov B.*, *Dzhurinska T.* History of Development and Modern Problems of Aviation Psychology / / Wings of Ukraine. In 2003. 20-25 January. P.6. (In Russian).

3.*Kovalev A.*, *Nichiporuk V.* Operator's Psychophysical Training in Aviation / / Aviation in the XXI-st Century: The World Congress. - Kyiv, NAU, 2003. - P.7.20-7.24.

4.*Dineyka K.* 10 lessons psychophysical training. - Moscow, Physical Education and Sport, 1987.-62, pp. (In Russian).

UDC 621:891, 601.2

V.F. Labunets Ph.D., professor,V.G. Lazariev assistant,
(National Aviation University, Ukraine)
R. J. Belevtsev, (Doctor, professor, correspond.member of NASU,
(IEG, Ukraine)
I. P. Kozlova, Doctor bio.sciences
(Zabolotny Institute of Microbiology and Virology NASU, Ukraine)

BIOTECHNOLOGY PERSPECTIVES IN SURFACE ENGINEERING. REVIEW

In this review the prospects of biotech production, beneficial properties and imperfections are considered in terms of materials and tribology. Attention is focused on the dissemination of general trends in industrial growth the role of bioprocessing on the field of technologies of surface treatment materials

Biological technologies are employed in all new fields of of industrial production. On obtaining of enzymatic products, medicines, and to the bioleaching of ores and the production of polymers [1-3], production volumes continue to grow. This is resulting in the transfer of accumulated technological experience to adjacent areas of science and industry.

Here we will consider possible ways for the development of industrial biological technology, which the surface engineering and, in particular, tribological materials provide. Summing up the experience of biogeochemistry and microbiology, and taking into account the experience and the scientific approach of existing technologies, we note that the effect of surface modification is widely studied in hydrometallurgy [4-6]. In microbiology and microbial ecology studies over many decades of microbial corrosion has accumulated a great experience [7].

Therefore, armed with knowledge of of several scientific fields we must now pay attention to the state of the art in tribology and to where among the surface treatment technologies application of biological methods and approaches look more promising and profitable

At a manufacturing of machines a great influence on the quality, reliability and durability of the details have a variety of factors. The reliability and durability of the most loaded conjugate parts of the machines depends largely on the correctness of the choice of manufacturing method, destination an appropriate metal reinforcing and quality of assembly. A promising direction in improving the design of the machine is to create a self-regulating and self-healing units and a power supply. The essence of these design decisions is that a system or device will be adjusted or regulated automatically and the observed constancy of the basic geometric parameters of the dual unit in operation [8].

Methods of machine parts durability increasing can be divided into three main groups:

- Design;
- Technology;
- Operational.

Technological methods to improve the durability of machines include measures to improve the properties of materials used in the design. Properties of the details begin to emerge in the process of casting, welding, forming and machining

A further increase of machine parts durability is carried out through the use of various methods of surface hardening and coating - thermal, chemical and thermal electropulse, electromagnetic, laser and other treatments, surfacing, sputtering, implantation, self-propagating high temperature synthesis and other [9].

Progressive way to improve the performance of parts of friction units operating without lubrication under extreme conditions, is to apply for one of the contacting surfaces solid lubrication coverage. Tribological characteristics of friction units depend strongly on the stress-strain state solid lubrication coverage during its interaction with the solid surface. Depending on the contact conditions, coating thickness, the load parameters of the microgeometry and the physical and mechanical properties of solid lubrication coverage, there will be elastic, plastic or elastic-plastic deformation [10].

Determining influence on the processes of friction and wear have the load, type of stress state, the scheme of interaction. As for the stress, it should be noted: the stresses acting in the direction perpendicular to the vector of load application, increasing tightness of deformation, preventing the transition to plasticity. The tangential stresses caused by the friction force, contribute to the plastic state of material offensive and reduce the carrying capacity of friction units. The presence of sulfur on the working surface of the moving parts reduces the shear stresses due to the formation of sulfides and low-melting eutectics.

One of the conditions to reduce friction [11] in some areas of the mechanical contact of metals, is a relatively rapid decrease in contact stress. At presence of soft surface layers, it is easily carried out due to plastic flow. Accompanied by an increase in contact area.

The process of deformation of some of the most loaded sites should take place only in the surface layers, without involving the deformation of the layers located below, when implemented generally positive gradient of the shear resistance, formulated by Kragelsky [12].

It should be noted that, based on the minimization of friction is a universal phenomenon of structural adaptability described by Kostetskiy [13]. This phenomenon is realized in friction of any material within a certain range of external factors, which confirms its universality, and is characterized by self-regulation processes of activation, passivation, and formation of shielding secondary structures.

When activated, the surface layers of the material moving to the anomalous non-equilibrium, an unstable state. From the viewpoint of thermodynamics such a material tends to move toward equilibrium. Therefore, the activation processes at friction conditions are always followed with passivation processes.

In the process of passivation of the surface of solids in friction are three main groups of reactions:

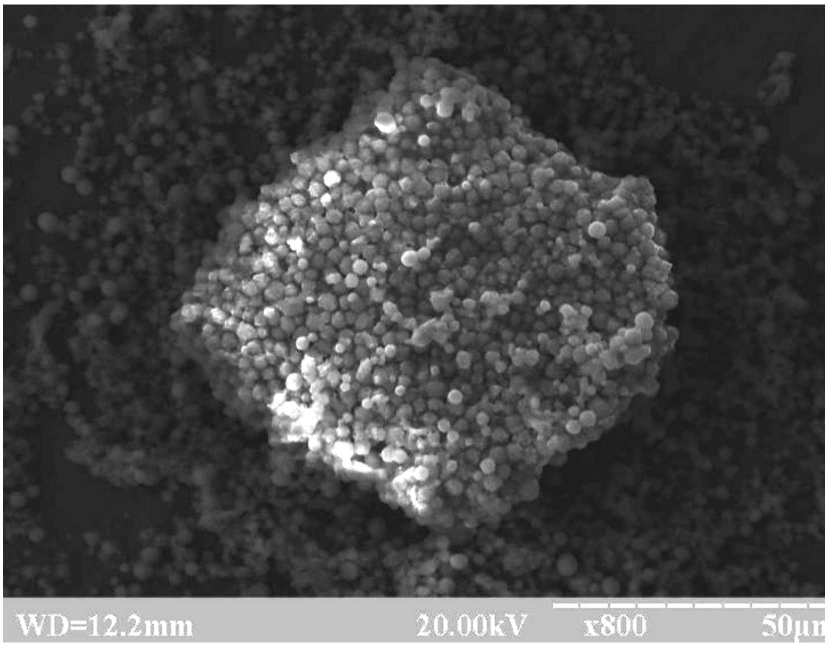

Fig. 1 *Thiobacillus thioparus* colony

- Interaction with the active components of the environment;
- Interaction with the counterface material;

- An internal restructuring of the surface layers.

Control of passivation process is carried out by adding special chemical additives to lubricant. To reduce friction and wear S, P, O, Cl, N, B – additives are widely used [14]. And it is necessary to remark that S, P, O, Cl, N are biogenic elements that are present in every living cell.

Increasing of antifrictional properties and wear resistance of friction parts of machines, including sliding bearings through the thermodiffusion process is possible with diffusion processes and chemical reactions that occur in the surface layers details of machines and the formation of sulfides, selenides, phosphides, and chlorides. As a result, above all, seizure resistance increases, and the the running-in processes are accelerated [15].

Most of presently used technological of surface hardening, coating and modification of the working surfaces can be characterized by power consumption, the duration of the process and environmental issues. Therefore, to meet rapidly growing demands for performance properties of materials tribosystems need to find new and better materials and methods to improve the durability, reliability and durability of the friction units of modern technology. Very promising in this regard is the creation of protective layers (secondary structures) using biotechnology [16, 1].

At the spot of our research work – microorganisms *Thiobacillus thioparus* which are well known as a factor of microbial corrosion. Their high activity in microbial-metal interaction is beyond controversy. On fig.1 a colony of *T.thio*. shown and spheric particles of sulfur selectively extracted from agarous media (agarous Bejerink media) and mineralized with bacterial cells are well seen. Spectrum on fig.2 shows that in chemical composition of that colony of all analytical diapason (Energy dispersive spectrometer, from C to U) only sulfur is present in significant (99,9 %) concentration.

It is reasonable to assume that some modifications in media components are allowing wide range of substances and compounds to be immobilised via biomineralisation. Research methods and practical approach in the field of microbial biomineralised nanoparticles are observed in [17].

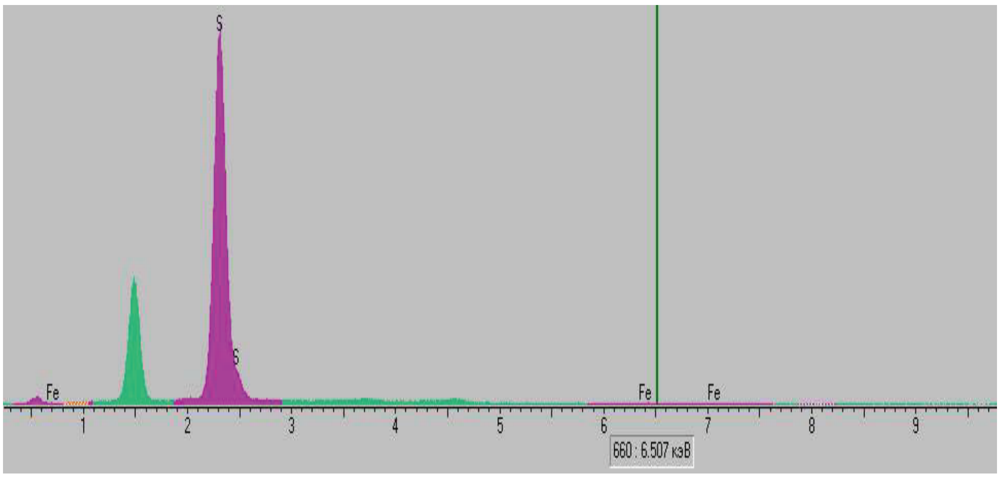

Fig. 2 EDS Spectrum of colony shown on fig.1. (Green marked peak near 1,5keV is Al K-series - sampleholder underlight)

This review devoted to the search of promising ways to improve technological and service properties of materials, expanding the limits of their functional purpose showed that at this time, this problem is solved by the use of traditional engineering methods. However, their high energy, the need to combine several technological milestones and compliance with current environmental regulations lead to new ways to ensure the required physical-chemical and mechanical properties [16].

Analysis of literature sources on materials and tribology, thermodynamics, biogeochemical processes, geochemical activity of microorganisms and biotechnology allowed to develop approaches to study the effect of certain groups of sulfur, iron, nitrogen and carbon cycles bacteria on friction properties of materials. Such an interaction where both ways biogeochemical and tribochemical are present, can be modeled and, after a comprehensive study could became part of technologies of surface treatment materials. However, more time is required for the formation of concepts of really profitable, ready to replace the well-established technology.

References

1. *Hiroshi Shimizu*' Metabolic Engineering – Integrating Methodologies of Molecular Breeding and Bioprocess Systems Engineering / Journal of Bioscience and Bioengineering. 2002. Vol. 94, No. 6, P. 563-573.

2. *M. Gavrilescu, Y. Chisti*. Biotechnology – a sustainable alternative for chemical industry / Biotechnology Advances 23 (2005) P. 471–499

3. *Rao, K.H.,* et al., Minerals bioprocessing: R & D needs in mineral biobeneficiation, Hydrometallurgy (2010), 104(3-4): P.465-470.

4. *Y. Rodriguez , A. Ballester , M.L. Blázquez, F. González, J.A. Miňoz* . New information on the pyrite bioleaching mechanism at low and high temperature Hydrometallurgy 71 (2003) P. 37–46.

5. *E. Mielczarski, J.A. Mielczarski* / Surface modification at the molecular level in mineral beneficiation. / Int. J. Miner. Process. 72 (2003) P. 129–140.

6. *L.A. Warren, E.A. Haackr* Biogeochemical controls on metal behaviour in freshwater environments / Earth-Science Reviews 54 (2001) P. 261–320.

7. *Андреюк Е. И., Билай В. И., Коваль Э. З., Козлова И. А.* Микробная коррозия и её возбудители // К.: Наукова думка, 1980. – 288с.

8. Методы повышения долговечности деталей машин // *В.Н.Ткачёв, Б.М. Фиштейн, В.Д.Власенко, В.А.Уланов.* – М.: Машиностроение, 1971. – 272с.

9. *Лабунец В.Ф. , Али Ризк*. Триботехнические характеристики покрытий с аморфно-кристаллической структурой // Нові матеріали і технології в металургії та машинобудуванні. – Запоріжжя: ЗДТУ, 1999. - №2. – С. 67 – 69.

10. *Дёмкин Н.Б., Алексеев В.М., Сутягин О.В.* Исследование деформирования твердосмазочного покрытия // Трение и Износ. 1988. Т.9. - №3. – С.389 – 396.

11. *Буше Н.А., Копытько В.В*. Совместимость трущихся поверхностей. – М.: Наука. 1981. – 127с.

12. *Крагельский И.В*. Трение и знос. – М.: Машиностроение, 1968. – 480с.

13. Поверхностная прочность материалов при трении / *Б.И.Костецкий, И.Г.Носовский* и др. – К.: Техніка , 1976. – 296 с.

14. *Виноградов Ю.М*. Трение и износ модифицированных материалов. – М.: Наука, 1972. – 150 с.

15. Надежность и долговечность машин / *Б.И.Костецкий, И.Г.Носовский, Л.И.Бершадский, А.К.Караулов*. – К.: Техніка, 1975. – 408 с.

16. Микробная модификация поверхности материалов. / *А.П.Кудрин, В.Ф.Лабунец, В.Г.Лазарев* и др. // Восточно-Европейский журнал передових технологий, 2005. - № 5 (17). – С. 68 – 75.

17. Metal Nanoparticles in Microbiology / Ed. By *Mahendra Rai, Nelson Duran*. – Berlin: Springer-Verlag Heidelberg, 2011. – 303 p

UDC 57.083.3:615.322:504.054(045)

K.A. Dovgopola post-graduate student, T.V. Shevtsova post-graduate student,
(National Aviation University, Ukraine)

USING OF *PLANTAGO MAJOR* L. AND *TRIFOLIUM PRATENSE* L. FOR PURIFICATION SOIL AIRFIELDS FROM HEAVY METALS

The content of heavy metals in soils and medicinal plants which were collected in the territory, adjacent to airfield «Zhulyany» in Kyiv region, airfield in Nizhyn, Chernihiv region and in Phytopreparation Plantago major L., Trifolium pratense L. The immunological studies were held using water-salt extracts made from medicinal plants to determine the effects of heavy metals on the pharmaceutical properties of plants.

Currently, the importance given to find medicinal plants as sources of new biologically active compounds for herbal remedies.

There is a need to take into account the environmental condition of the territory where the planned collection of plants. For quantitative and qualitative composition of active substances in plants depends on the conditions in which they develop, especially from soil and groundwater, but the anthropogenic impact on the biosphere is so varied that often leads to degradation of the environment of human life.

The study of adaptation of certain species of medicinal plants that grow in the near airfields allows you to determine the level of flow through the soil to plants of heavy metals, the level of biological plant resistance to contamination and for cleaning the soil by these plants.

Found that the use of medicinal plants collected in areas with a high content of heavy metals, can endanger human health, adversely affecting physiological processes. Because of medicinal raw materials, heavy metals pass into dosage forms, and then enter the human body [1].

Therefore the problem of environmental clean soil and herbs, as well as analysis of the impact of heavy metals on the quality of plant material is particularly relevant.

The aim of our work was to study the level of accumulation of heavy metals in soil and their influence on the pharmacological action of red clover (*Trifolium pratense* L.) and plantain (*Plantago major* L.).

To achieve this goal have been identified following tasks:

- determine the level of maximum permissible concentrations of heavy metals to soil and plants;
- determine soil purification by red clover and plantain;
- to develop research methodology content of heavy metals in soil and plant material and immunological methods;
- establish links between the concentration of metals and pharmacological properties of plants.

Medicinal plants and soil samples were collected in the territory adjacent to airfields Kyiv «Zhulyany» in Kyiv region and Nijinsky airport in Chernihiv region. For the control plants were taken, sold in pharmacies in dried form without impurities, pharmaceutical companies LikFarma «Adonis» and Viola.

Plants were collected in the period from early July to late August research areas in compliance with the collection and preparation of plant material installed in pharmacognosy, as well as compliance methods of sampling soil and plants GOST 27262-87 and GOST 17.4.3.01-83.

The survey was used inflorescences and grass clover, plantain leaves, these parts of plants used in official medicine.

Chemical composition of plants characterized by variability – the ability under the influence of different factors to acquire new chemical signs of previous or lose. Therefore, the formation and accumulation in medicinal plants of biologically active substances is a dynamic process that is associated with the phases of development and environmental factors [2].

Established that the effect of metals on plants depends on soil composition, the nature of the chemical elements, and of ionic or other form of combination, which can be removed from the soil plant [3].

Also be aware that plants differently learn some metals such as lead, even at high concentrations in the soil it is in poorly soluble compounds and therefore its level in the plant will be smaller.

So much zinc accumulates in plants and kept them; copper and cadmium accumulated weakly and strongly maintained in plants; lead accumulates weakly and poorly maintained in plants.

Therefore, to establish the level of accumulation of metals plant from the soil was found heavy metals in soil samples collected, which are taken according to GOST 3118-77 1N HCl solution.

The study was conducted in three times repeated to correct errors.

Then it was found accumulation of metals in plant raw materials by research guidelines «for field and laboratory studies in controlling pollution metals» [4].

To establish relationships between the concentration of metals and pharmacological properties of the studied plants were used immunological methods.

Method of determining the phagocytic activity of blood cells by NBT-test allows to find out the status of local immunity in the human impact of water-salt extracts from medicinal plants [5].

Methods of determination of phagocytic activity of neutrophils, based on the ability of phagocytes to capture particles of latex, which are colored by Romanovsky-Himza in blue-blue color [6].

The data research analysis of heavy metals in soil samples collected near the airport «Zhulyany» Nijinsky and airport are presented in table 1.

Table 1

Analysis of heavy metal content in soil samples

Metal	airport «Zhulyany», mg / kg	Nijinsky airfield, mg / kg	MPC, GOST 3034-84, 3210-85, 42-128-4433-87, mg / kg
Zn	12.77	11.28	23.0
Cu	4.59	4.56	3.00
Pb	5.88	9.93	20.0
Cd	0.15	0.17	1.00

Thus the content of Zn, Pb and Cd in soil samples does not exceed the norms for Cu, this figure exceeds the norm by 1.5 times.

Tables 2 and 3 represent data on heavy metals in samples of medicinal plants collected in the territory adjacent to airfields and pharmaceutical drugs from pharmacies.

Table 2

The content of copper and zinc in samples of medicinal plants

Place of collection materials	Copper (mg / kg)		Zinc (mg / kg)	
	Plantain	Clover	Plantain	Clover
airport «Zhulyany»	10.26	10.95	56.70	51.60
Nijinsky airfield	9.65	9.14	23.80	60.10
Phytomedication	7.05	6.39	47.70	31.10
MPC	5.00	5.00	10.00	10.00

Table 3

The content of lead and cadmium in samples of medicinal plants

Place of collection materials	Lead (mg / kg)		Cadmium (mg / kg)	
	Plantain	Clover	Plantain	Clover
airport «Zhulyany»	6.39	4.86	0.20	0.75
Nijinsky airfield	3.83	3.31	0.30	0.25
Phytomedication	4.49	2.28	0.43	0.19
MPC	0.50	0.50	0.03	0.03

Results of the data suggest that the most contaminated samples are near airports, including airport «Zhulyany» relatively clean from all three samples can be considered a plant raw material is sold in pharmacies. The content of heavy metals in samples of medicinal plants compared with the soil exceeds by 2-3 times, this property of plants to accumulate heavy metals can be used as one method of cleaning soil.

These immunological research as a result of spontaneous NBT-test using water-salt extracts of grass and clover leaves of plantain are presented in table 4.

Table 4

Results of determination of phagocytic activity of blood cells by NBT-test

Plants	Airport «Zhulyany»		Nijinsky airfield		Phytomedication plants	
	NBT - positive cells, %	CMC, s.u.	NBT - positive cells, %	CMC, s.u.	NBT - positive cells, %	CMC, s.u.
Plantain	48.28±2.2*	0.34±0.02*	48.89±2.2*	0.33±0.02*	49.62±2.3*	0.35±0.02*
Clover	49.72±2.3*	0.37±0.02*	49.00±2.3*	0.37±0.02*	51.62±2.3	0.39±0.02
Control	51.55±2.3	0.41±0.02	51.55±2.3	0.41±0.02	51.55±2.3	0.41±0.02

Where* – probable difference from control

The study of the phagocytic activity of neutrophils by the influence of water-salt extraction of grass clover and plantain leaves are presented in table 5.

Table 5

Results of determination of phagocytic activity of neutrophils

Plants	airport «Zhulyany»		Nijinsky airfield		Phytomedication plants	
	Pi, %	Pn, %	Pi, %	Pn, %	Pi, %	Pn, %
Plantain	85.00±2.18	5.44±0.15	86.00±2.18*	5.57±0.15*	82.00±2.18*	5.40±0.15*
Clover	80.00±2.18*	5.18±0.15*	82.00±2.18*	5.27±0.15*	84.00±2.18	5.50±0.15
Control	89.00±2.3	5.18±0.02	89.00±2.3	5.18±0.02	89.00±2.3	5.18±0.02

Where * – probable difference from control.

Conclusions

All components of the biosphere actively collect discarded hazardous substances (liquid and dispersed chemical elements and their compounds) in amounts that greatly exceed their natural content. A significant source of pollution is heavy metals. They have the ability to accumulate in significant amounts in soils, which can lead to deterioration of their quality and reduce productivity.

Soil contaminated with heavy metals is a secondary source of contamination of plants. The content of heavy metals in plant raw materials is 2-3 times higher than their content in the soil. Whereas it is planned to continue research to determine changes in the level of heavy metals in soils using plants.

The most contaminated samples are near the airports, including airport «Zhulyany» relatively clean from all three samples can be considered plant raw materials, goods in pharmacies.

But according to the NBT-test and the level of phagocytic activity of neutrophils biologically active compounds from grass and clover leaf plantain compared with the data control positively influence the activity of phagocytes. We can make the assumption that these plants have certain defense mechanisms that block the negative effects of heavy metals on the biochemical processes in the experimental plants.

Thus, the study of protective mechanisms of herbs can be used to increase the resistance of the human body under the influence of negative environmental factors.

References

1. Государственная фармакопея Российской Федерации XII, ч. 1. 2008. – 700 с.

2. Ковальов В. М., Фармакогнозія з основами біохімії рослин / [В. М. Ковальов, О. І. Павлій, Т. І. Ісакова]. Підруч для студ. вищ. фар мац. навч. закл. та фар мац. ф-тів вищих мед. навч. закл. ІІІ-ІV рівнів акрид. (2-е вид.) – Х. : Вид-во НФаУ, МТК-книга. 2004. – 704 с.

3. Перепелиця О.П. Екохімія та ендоекологія елементів / [О.П. Перепелиця] Довід. з екол. Захисту. – К. : Екохім, 2004. – 735 с.

4. Методические рекомендации по проведению полевых и лабораторних исследований почв и растений при контроле загрязнения окружающей среды металлами / ГОСТ 17.4.3.01. – М. : Гидрометеоиздат. – 1981. – 9-33 с.

5. Нагоев Б.С. Модификация цитохимического метода восстановления нитросинего тетразолия // Лаб. дело. – 1986. – №8. – С. 7-11.

6. Комаров Ф.И. Биохимические исследования в клинике / [Ф.И. Комаров, Б.Ф. Коровкин, В.В. Меньшиков]. – Л. : Медицина, 1981. – 408 с.

UDC 631.461:504.054(045)

I.M. Malinovskaya, Doctor of Agricultural Sciences, Y.I. Litvin
(National Aviation University, Ukraine)

MICROBIAL COMMUNITIES OF GREY FOREST SOIL POLLUTED INCREASING DOSES OF HEAVY METALS

The state of microbial populations of grey forest soil contaminated with heavy metals in doses of 5, 10, 100 MAC was studied in the presence and absence of vegetating phytocenosis. The magnitude and direction of changes in microbial processes are shown depending on the level of soil contamination with heavy metals and the presence of vegetation.

Heavy metals are widespread pollutants of the biosphere [1, 2]. For today they take second place in the degree of danger, giving way only to pesticides and far ahead of such well-known pollutants like carbon dioxide and sulfur. Environmental contamination with heavy metals conditioned to their wide use in industrial production and deficiencies in the treatment systems, causing pollutants are coming to the environment with gas and dust industrial emissions, motor vehicles, additives of fertilizers, pesticides, etc. [1].

The model experiment was conducted using the grey forest soil type large dusty and light loam from the monitoring-proving ground of department of adaptive intensive technology of cereals and maize SRI "Institute of Agriculture NAAS" (experimental farm "Chabany", Kievo-Svyatoshinskiy district of Kyiv region). In the 0-20 cm soil layer contained: 2,74% of humus, 9,33 mg of alkaline hydrolyzed nitrogen, 36,8 mg of mobile phosphorus and 15,3 mg of exchangeable potassium per 100 gr dry soil pH (KCl) – 5,6. Phytocenosis of fallow land plots formed as a result of spontaneous overgrowth for 23 years and represented mainly cereal grasses. Soil was taken in autumn before the experiment and its biological activity was restored with moisture and temperature control from 25°C during 21 days. It was studied variants of the artificially created backgrounds of zinc and lead: 3, 4 – exceeding MPC in 5 times, 5, 6 – exceeding MPC in 10 times; 7, 8 – exceeding MPC in 100 times. As a control sample it was taken soil with natural concentrations of heavy metals. Soluble fraction of metals in acid was taken into consideration when creating backgrounds pollution, since it is the main man-made component of the stock of heavy metals in soil.

In 8 days before the introduction of heavy metals in vessels were sowed the seed of maize. In the control vessels for equalization of nitrogen level brought solution of KNO3 in an appropriate concentration.

Condition of microbial communities was studied in 32 days after brought heavy metals. Number, physiological and biochemical activity of major ecological and trophic groups of microorganisms and orientation microbiological processes were determined by methods described previously in our publications [3].

As seen from Table 1, the number of ammonification microorganisms as a result of contamination with heavy metals increased in 2,09-2,19 times compared with control in soil without plants; in soil with phytocenosis it increased at 26,4-31,4%. The number of ammonification microorganisms is growing at least in the studied doses of heavy metals and in the future it does not depend on the dose of pollutants. At short-term pollution (1 day) entry of heavy metals resulted in a significant decrease of ammonification microorganisms in variants without plants as well with phytocenosis [4]. Thus, the influence mechanism of heavy metals on the number of ammonification organism is changing over time of staying of soil in contaminated condition.

The number of autochthonous microorganisms at short-term pollution of soil with heavy metals also significantly decreased [4]. Over the 32 days of the incubation, this regularity is preserved, except option with a dose of heavy metal in 5 MPC without phytocenosis, where the increase of the autochthonous microorganisms in comparison with unpolluted soil (Table 1). In soil without plants reduced the number of autochthonous microorganisms in direct proportion to the level of contamination, and in the rhizosphere phytocenosis reduced compared with the control at 19,4-65,2% and almost independent of the level of contamination. Thus, mechanisms of action of heavy metals on microorganisms of various ecological, trophic and functional groups differ, but relatively a few of them are changing over time.

Plants with their root secretions act as protectors of azotobacter, its number of plants in rhizosphere higher than in soil without plants: in the control – in 5,97 times, with 5 MPC – in 9,7 times, with 10 MPC – in 14,9 times (Table 1). At the maximum level of contamination with heavy metals (100 MAC) the number of azotobacter in soil without plant exceeds its number in the rhizosphere plants. Perhaps, plants cannot perform the protective function of azotobacter through biochemical stress at high levels of soil contamination with heavy metals. The results of the study of physiological and biochemical activity of microorganisms show at the protective function of plant to azotobacter. Thus, soil contamination with heavy metals suppresses the physiological and biochemical activity azotobacter and this figure can be considered indicator of grey forest soil contamination at levels of contamination in 5-100 MPC in the absence of vegetation, as well at the contamination levels of 10-100 MPC – in soils with phytocenosis.

At short-term soil contamination with heavy metals the number of denitrificators in soil without plants is reduced in direct proportion to increasing doses of contamination [4]. Over the 32-day contamination the number of denitrificators in soil without plants is also reduced in proportion to the level of contamination: with 5 MAC - in 5,47 times, with 10 MPC - in 7,32 times, with 100 MPC - in 16.9 times. In the presence of plants the number of denitrificators reduced to a certain size, at which almost no effect of pollutant dose.

Number, physiological and biochemical activities of polysaccharide-synthesizing microorganisms in soil polluted with heavy metals is an important indicator, because bacterial polysaccharides are the protectors against nonspecific toxic effects of heavy metals [6]. At short-term pollution synthesis of polysaccharides is not yet becoming an advantage for producers in the competitive struggle for survival, so the number of polysaccharide-synthesizing microorganisms decreases in soil without plants and in the rhizosphere phytocenosis [4]. Over the 32-day incubation of contaminated soil the number of polysaccharide-synthesizing microorganisms is increased, especially in the rhizosphere plants, with 5 MPC - in 2,24 times, with 10 MPC - in 6,89, with 100 MPC - in 1,67 times (Table 1). Maximum number of polysaccharide-synthesizing microorganisms observed in variant with contamination in 10 MPC, further increasing the dose of pollution does not increase the number of microorganisms of the group, possibly due to general toxic effects of heavy metals. Thus, it was confirmed the results of model studies [6] about the protective action of bacterial polysaccharides relatively heavy metals in grey forest soil.

According to literature data, heavy metals inhibit the mineralization of organic compounds in soil [7, 8]. Our results are consistent with literature data: in soil without plants pedotrophic index decreases in variant with 5 MPC – at 76,6%, with 10 MPC – at 43,2%, with 100 MAC – at 133,6%, in the rhizosphere phytocenosis consumption of organic matter significantly reduces only at the maximum contamination (Table 2). The intensity of mineralization of nitrogen compounds decreases in soil without plants with 5 MPC in 3,20 times, with 10 MPC - in 2,27 times, with 100 MAC - in 1,57 times, in rhizosphere plants, especially for medium and maximum levels of pollution, mineralization of nitrogen compounds is intensifies at 73,4%. Thus, the orientation of mineralization processes in soil contaminated with heavy metals depends on the level of contamination and the presence of vegetation.

In the example with wheat and soybean plants previously it was shown that the activity of mineralization of humus compounds in rhizosphere plants is lower than in soil without phytocenosis [9,10]. The obtained data confirm this pattern: activity of humus mineralization in the root zone of maize is below than in soil without plants: in variant with no pollution - at 66,2%, with 5 MAC - at 90,2%, with 10 MPC - at 77,0%, with 100 MAC - at 18,4% (Table 2). Thus, degradation of humus compounds proceeds more intensively in soil without plants where no constant flow of substances that easily utilized in the root secretions. With the increasing of level of soil contamination with heavy metals plants less affect to mineralization of humus compounds.

Contamination with heavy metals resulted in a significant phytotoxicity increase in soil without plant: with 5 MPC - at 8,40%, with 10 MPC - at 16,2%, in soil with phytocenosis the increasing of phytotoxicity was observed only in variant with 10 MPC - at 15,7% (Table 2). The dose of heavy metals in 100 MPC was so toxic that the seeds of test plants not sprouted.

Conclusions

At medium-term contamination of grey forest soil with heavy metals observed significant changes in the state of microbial groups, slowed down most of the studies mineralization processes, increases the accumulation of toxic substances. The scope and direction of these changes depend on the level of soil contamination and the presence of vegetation.

Azotobacter can be attributed to an important group of microorganisms that are indicators of ecological purity of soil; its number is reduced with entry of heavy metals and some other pollutants, including petroleum products [3, 5].

Denitrifying microorganisms also be considered as diagnostic group of contamination with heavy metals in short-term and medium-term contamination of soils without vegetating phytocenosis.

References

1. *Водяницкий Ю.Н.* Изучение тяжелых металлов в почвах. – М.: ГНУ Почвенный институт им. В.В. Докучаева РАСХН, 2005. – 110 с.
2. *АндреюкК.І., Іутинська Г.О., Антипчук А.Ф. та ін.* Функціонування мікробних ценозів ґрунту в умовах антропогенного навантаження / К.:Обереги, 2001. – 240с.
3. *Малиновська І.М., Зінов'єва Н.А.* Мікробіологічні процеси в ризосфері рослин у забрудненому нафтопродуктами ґрунті // Мікробіологія і біотехнологія. – 2011. – №2. – С.83-91.
4. *Малиновська І.М., Літвін Ю.І.,* Перебіг мікробіологічних процесів у сірому лісовому ґрунті за короткострокого забруднення важкими металами // Мікробіологія і біотехнологія. – 2012. – In print
5. *Малиновська І.М., Зінов'єва Н.А.* Спрямованість та інтенсивність мікробіологічних процесів у забрудненому нафтопродуктами темно-сірому опідзоленому ґрунті // Вісник Полтавської державної аграрної академії. – 2010. – № 4. – С. 17–23.
6. *Dudman W.F.* The role of surface polysaccharides in natural environments // Surface carbohydrates of the procariotic cell / Ed. I.W. Suthrland. – New York: Acad.Press, 1977. – P. 357–414.
7. *El-Shinnawi M.M, Omran M.S.* Effect of different levels of a trace element nutritional mixture on organic matter decomposition and the number of certain heterotrophs in soil // Rostl. Vyroba. – 1976. – vol. 22, N 1. – P. 11–17.
8. *Landa E.R., Frank S.C.* Effect of mercuric chloride on carbon mineralization in soils // Plant and Soil. – 1978. – vol. 49, N 1. – P. 179–183.
9. *Малиновська І.М., Черниш О.О., Романчук О.П.* Особливості мікробних комплексів сірого лісового ґрунту перелогів та агроценозів // Збірник наукових праць Інституту землеробства. – К.: ЕКМО, 2007. – Вип.2. – С. 29–34.
10. *Малиновська І.М.* Стан мікробіоценозу ризосфери сої за комплексного оброблення насіння фосфатмобілізуючими мікроорганізмами і *Bradyrhizobium japonicum 71T* // Агроекологічний журн. – 2007. – №3. – С. 79–83.

Table 1

Influence of heavy metals on the number of microorganisms in the grey forest soil polluted with heavy metals during 32 days, million CFU*/g of absolutely dry soil

№	Variant	Ammonificators	Immobilizators of mineral nitrogen	Oligonitrophilic microorganisms	Azotobacter, % of soil lumps fouling	Denitrificators	Nitrificators	Pedotrophic microorganisms	Cellulose-digesting bacterias	Polysaccharide-synthesizing microorganisms	Autochthonous microorganisms	Streptomycetes	Micromicetes	Mobilizators of mineral phosphates	K_r	Acid-forming microorganisms
1	Control without plants	240,6	93,9	75,3	0,670	128,1	0,248	83,8	153,3	5,82	21,9	44,2	0,023	23,3	0,611	0,390
2	Control + phytocenosis	730,9	68,7	21,4	4,00	121,8	0,484	117,4	65,0	5,54	18,5	28,8	0,173	10,0	0,313	2,58
3	5 MAC without plants	502,5	61,2	25,7	0,010	23,4	0,725	98,9	90,8	1,56	32,7	30,0	0,058	10,1	0,698	0,010
4	5 MPC + phytocenosis	368,9	30,0	22,4	90,7	48,7	0,974	64,2	76,1	12,3	11,2	20,6	0,144	6,12	0,543	0,010
5	10 MPC without plants	526,3	90,4	30,4	0,670	17,5	1,08	127,9	101,4	7,02	19,6	56,5	0,031	11,3	0,170	0,390
6	10 MPC + phytocenosis	923,9	150,7	78,4	10,0	59,0	0,496	150,7	83,7	37,9	13,1	39,0	0,246	19,9	0,406	9,09
7	100 MPC without plants	516,7	128,2	20,6	20,0	7,58	0,390	76,9	71,1	4,27	13,4	45,9	0,128	12,8	0,353	15,2
8	100 MPC + phytocenosis	960,9	156,5	53,7	4,67	26,6	1,16	105,1	95,1	9,21	15,5	54,9	0,391	13,8	1,16	1,53
	LSD05	15,3	6,11	3,16	1,82	4,45	0,160	5,68	2,00	0,54	2,97	1,99	0,009	0,94		0,005

Note: CFU* – colony form unit

Table 2

Indicators of intensity of mineralization processes and phytotoxic properties of grey forest soil contaminated with heavy metals during 32 days

№	Variant	Pedotrophic index	Oligotrophic coefficient	Coefficient of nitrogen mineralization	Activity of humus mineralization, %	Intensity of soil respiration mg CO2 /kg soil	Weight of 100 plant test crops - winter wheat, g		
							stem	roots	total weight
1	Control without plants	0,348	0,313	0,390	26,1	204,9	7,71	5,19	12,9
2	Control + phytocenosis	0,161	0,029	0,094	15,7	194,9	6,85	6,45	13,3
3	5 MAC without plants	0,197	0,051	0,122	33,1	192,8	6,51	5,39	11,9
4	5 MPC + phytocenosis	0,174	0,060	0,081	17,4	285,8	7,15	5,85	13,0
5	10 MPC without plants	0,243	0,058	0,172	15,4	128,7	6,28	4,82	11,1
6	10 MPC + phytocenosis	0,163	0,085	0,163	8,70	187,4	6,61	4,89	11,5
7	100 MPC without plants	0,149	0,040	0,248	17,4	115,4	Due to high toxicity of the soil seed test culture not sprouted		
8	100 MPC + phytocenosis	0,109	0,056	0,163	14,7	278,5			
	LSD_{05}						0,12	0,08	0,11

UDC 661.183.7

O.I. Kosenko, Kand.of Chem.Scien, A.D. Kustovska, Kand.of Chem.Scien.
(National Aviation University, Ukraine)

STRUCTURE AND PHASE TRANSFORMATIONS IN THE SYSTEM $Fe_2O_3 : SiO_2$ IN THE HYDROTHERMAL CONDITIONS

Laws of hydrothermal modification of porous structure and phase composition of jointly precipitated iron-silica gels with various proportion of $Fe_2O_3 : SiO_2$ were investigated. The results were explained by combined action of mass transport and phase transformations and mutual influence of components on these processes.

In the modern petroleum-refining industry, in the manufacture of aviation and automobile fuels the spectrum of catalytic processes is permanently extended. This is connected, at first, with attraction in the manufacture of petroleum with high content of heavy metals, sulphur compounds and other undesirable admixtures, and at second, with permanently increasing demands to the quality of fuel. Elaboration of a new catalytic processes demands also of creation of catalysts and blank substrates for catalytic active substances with various porous structure and the surface nature [1]. Among of blank substrates for catalytic active substances the binary oxide-hydroxide systems on the base of silica gel attract more and more attention of researchers because in these systems due to mutual influence of components the mobility of not only regulation of porous structure, but also acid-base properties exists.

Considerable number of researches devoted to the synthesis of the binary siliceous porous materials, in that the systems are observed that composition include together with silicium oxide oxides of aluminium, iron, titanium, zirconium, tin, magnesium, chromium and other metals [2-5], but the main attention of these researches is spared to finding synthesis conditions, influence of composition on the porous structure, changing of the structure over influence of certain factors.

It is known that the porous structure of sorbents can be changed both on the synthesis stages and by means of various methods of processing of hydrogel or xerogel, and the second approach gives the wider possibility to structure modification. The most effective method of modification is hydrothermal [6]. Lows of hydrothermal modification of the structure were better studied for silica gel [7]. The main peculiarity of metal oxides, that is distinguished they from silica, is possibility of passing of crystallization processes at hydrothermal conditions that cause to the specific character of porous structure changing. This fact explains interest to the complex investigations of modification influence not only on the porosity but also on the phase composition and dispersity of binary jointly precipitated systems that opens the ways to understanding mechanism of processes of porous materials skeleton rebuilding and synthesis blank substrates with needed structure and crystallinity.

The purpose of the given work was the investigation of lows of hydrothermal modification of jointly precipitated iron-silica gels with various proportion of $Fe_2O_3 : SiO_2$ to creation of algorithm of synthesis these systems with in advance given parameters of porous structure, phase and chemical composition and degree of phase crystallinity.

The initial samples of jointly precipitated iron-silica gels were obtained by addition of 1M solution of Na_2SiO_3 to the 1M solution of $FeCl_3$ at intensive stirring to achieve pH=9. Choosing of pH was determined accounting of fullness of metal precipitation (as hydroxide) and conditions of precipitation of silica (SiO_2) as a dense precipitate. To achieve needed pH the solution of HCl was added to the solution of $FeCl_3$ and the solution of NH_4OH was added to the solution of Na_2SiO_3. The obtained precipitates were washed by distilled water till absence of qualitative reactions of the ammonium ion and chloride ion. The precipitate was squeezed on the filter and moist paste (hydrogel) was obtained, after drying of it at the room temperature xerogel was received.

According to this technique the samples of iron-silica gels with content of Fe_2O_3 8, 40, 60, 80 % mass was synthesized.

Hydrothermal modification (HTM) of the samples was carried out in steel autoclaves with teflon bushing at the temperatures 373, 473, 573 and 673 K during 6 hours. In the autoclave distilled water was added in quantity that was needed to achieve saturate vapour pressure at the given temperature (373 K – 1 atm, 473 K – 15 atm, 573 K – 85 atm, 673 K ~ 200 atm).

The porous structure parameters of samples – a specific surface area (S), limiting sorption volume of pores (V_S) and diameters of pores (d) – were calculated on the base of isotherms of methanol adsorption by the equations of the BET theory, a total volume of pores (V_Σ) was determined by the method of percolation [8,9].

The results of influence on porosity of hydrogels and xerogels with different relation of Fe_2O_3 : SiO_2 are presented in table 1.

Table 1

Influence of HTM conditions on the iron-silica gel porous structure

Fe_2O_3, % mass	T, K	HTM (xerogel)				HTM (hydrogel)			
		S, m^2/g	V_S, sm^3/g	V_Σ, sm^3/g	d, Å	S, m^2/г	V_S, sm^3/g	V_Σ, sm^3/g	d, Å
8	Initial	582	1,01	1,25	86	582	1,01	1,25	86
	373	456	0,82	1,33	117	469	1,08	1,46	125
	473	226	0,45	1,24	219	156	0,51	1,62	415
	573	70	0,14	0,36	206	89	0,40	1,38	620
	673	19	0,07	0,30	630	17	0,18	2,49	5860
40	Initial	366	0,34	0,72	79	366	0,34	0,72	79
	373	455	0,44	0,85	75	481	0,45	0,71	58
	473	358	0,42	0,90	101	428	0,44	0,65	61
	573	231	0,42	0,83	144	185	0,37	0,52	112
	673	102	0,41	0,82	322	78	0,21	2,12	1080
60	Initial	392	0,22	0,37	38	392	0,22	0,37	38
	373	433	0,29	0,45	42	427	0,45	0,49	46
	473	301	0,32	0,32	43	247	0,31	0,32	52
	573	177	0,33	0,32	72	119	0,40	1,82	612
	673	73	0,32	0,36	197	41	0,23	0,97	946
80	Initial	396	0,31	0,32	32	396	0,31	0,32	32
	373	393	0,31	0,34	35	390	0,35	0,36	37
	473	208	0,32	0,35	67	107	0,64	0,83	310
	573	77	0,37	0,33	171	68	0,33	1,25	736
	673	49	0,35	0,38	310	42	0,31	1,08	1020
100	Initial	290	0,22	0,22	30	290	0,22	0,22	30
	373	270	0,27	0,26	39	277	0,25	0,25	36
	473	23	0,17	0,18	313	64	0,19	0.19	119
	573	17	0,23	0,24	564	29	0,14	-	-
	673	24	0,22	0,22	364	44	0,11	-	-

The analysis of data of the table shows that a biggest specific surface area, limiting sorption volume of pores and total volume of pores has initial iron-silica gel with 8 % Fe_2O_3. For initial samples another compositions a specific surface area is approximately identical and lies in the ranges 360 – 390 m^2/g, but limiting sorption volume of pores, total volume of pores and diameters of pores are essential smaller.

In result of HTM both of hydrogels and xerogels at increasing of temperature of processing the general tendency decreasing of a specific surface area, increasing of diameters of pores and insignificant change of limiting sorption volume of pores is observed, and different character of changing of total volume of pores: if for xerogels the change of V_{Σ} varies in a small limits, at processing of hydrogels a total volume of pores grows in 2-3 times and diameter of pores grows more essential. For the sample with the small contain of iron (8 % Fe_2O_3) the biggest changes of parameters of porous structure are showed at HTM both of xerogel and hydrogel.

To explain changes that take place at HTM of iron-silica gels not enough to take into account only processes of solution-precipitation of colloid particles and surface diffusion, because at hydrothermal conditions can proceed phase transformations both of a pure components and a new compounds, that are formed at HTM. Therefore investigation of phase composition of iron-silica gels with different relation of components by method of X-ray analyses was carried out. Diffractograms of samples were recorded with help of diffractometer ДРОН-3М using copper Kα radiation and Ni filter. The results are presented in the table 2.

Table 2

Influence of HTM conditions on the phase composition of iron-silica gels

T, K	Fe_2O_3 8 % mass	Fe_2O_3, 40 % mass	Fe_2O_3, 60 % mass	Fe_2O_3, 80 % mass
HTM (xerogel)				
Initial	amorphous	amorphous	amorphous	amorphous
373	amorphous	amorphous	amorphous	amorphous
473	amorphous	amorphous	amorphous	hematite
573	amorphous	amorphous	hematite	hematite
673	acmite + α-cristobalite	hematite	hematite	hematite
HTM (hydrogel)				
Initial	amorphous	amorphous	amorphous	amorphous
373	amorphous	amorphous	amorphous	amorphous
473	amorphous	amorphous	hematite	hematite
573	amorphous	hematite	hematite	hematite
673	acmite + α-cristobalite	hematite + α-cristobalite	hematite	hematite

The data of X-ray analyses show that all initial samples are amorphous whereas HTM both of xerogels and hydrogels causes to appearance of crystalline phases in it and at the simulated conditions degree of crystallization of hydrogels with 40–80 % mass Fe_2O_3 is higher than degree of crystallization of corresponding xerogels, thereto phase composition of a products of HTM of iron-silica gels depend on the relation of components in the system: the sample with 8% Fe_2O_3 crystallizes in α- cristobalite (SiO_2) and acmite ($NaFeSi_2O_6$), but at increasing of iron content in samples only hematite (Fe_2O_3) is identified on the diffractograms.

The X-ray analyses data are well coordinated with results of adsorption-structure investigation and indicate that phase transformations are one of main factors that determine ways of hydrothermal modification of iron-silica gels. On the base of conducted investigations the obtained results can be explained both by mass transfer processes that proceed in colloid systems at HTM and phase transformation processes.

At precipitation of silica gel with negative charged colloid particles and iron hydroxide with positive charge mutual coagulation of particles of silica gel and iron hydroxide, that precipitate simultaneously, occurs and silica shows protective effect by the way of adsorption on the surface of iron hydroxide particles, screening the particles one from another and prevention of crystals growth [3]. This explains formation of more developed porous structure of iron-silica gels in comparison with pure iron gel and their bigger stability at HTM (table 1).

Effect of growing of iron-silica gels specific surface area at the low HTM temperatures can be explained by the fact that at HTM conditions water vapour reduces the free surface energy of solid due to that the rate of formation of new phase nucleuses increases that causes growth of dispersity of a system. Further decreasing of specific surface area at increasing HTM temperature is connected with crystals growth and processes of solution-precipitation that are repeatedly accelerated at HTM due to not only high temperatures but also presence of moisture. In result of these processes initial particles growth and, corresponding, specific surface area decreases.

Conclusion

The lows of structure and phase transformations of jointly precipitated iron-silica gels with various proportion of Fe_2O_3 : SiO_2 at hydrothermal conditions were investigated that promote to better understand mechanisms of mutual influence of components in the binary systems.

The general tendencies at increasing HTM temperature both of xerogels and hydrogels are decreasing of a specific surface area and increasing of diameters of pores and structure changing is more expressed for hydrogel then xerogel. The biggest changes of porous structure parameters are observed for sample with small content of iron (8 % Fe_2O_3), in which the main processes are connected with screened action of silica and its transfer, while the biggest changes of crystalline structure - for samples with content of Fe_2O_3 > 40 %, where essential role begin to play the processes of crystallization of iron compounds.

It was shown that by variation of conditions of hydrothermal modification iron-silica gels with various iron content can be obtained that have in advance given values of specific surface area (20-600 m^2/g), sorption volume of pores (0,1-1 sm^3/g), total volume of pores (0,3-2,5 sm^3/g), diameters of pores (30-5000 Å).

The discovered lows allow to choosing conditions of synthesis of iron-silica gels with necessary porosity and phase composition that in considerable degree define possibilities their application in catalytic processes.

References

1. *Нефедов Б.К., Радченко Е.Д., Алиев Р.Р.* Катализаторы процессов углубленной переработки нефти. – М. : Химия, 1992. – 266 с.

2. *Неймарк И.Е.* Синтетические минеральные адсорбенты и носители катализаторов. – Киев : Наукова думка, 1982. – 104 с.

3. *Ермоленко Н.Ф., Эфрос М.Д.* Регулирование пористой структуры окисных адсорбентов и катализаторов. – Минск : Наука и техника, 1981. – 288 с.

4. *Лисичкин Г.В.* Модифицированные кремнеземы в сорбции, катализе и хроматографии. М. : Химия, 1986. – 248 с.

5. *Сидорчук В.В., Кагановский В.А., Чертов В.М.* Влияние гидротермальной обработки на структуру бинарных адсорбентов $ZrO_2 \cdot SiO_2$, $SnO_2 \cdot SiO_2$ // Докл. АН УССР. Сер. Б. – 1984. – С. 58 – 60.

6. *Комаров В.С., Дубницкая И.Б.* Физико-химические основы регулирования пористой структуры адсорбентов и катализаторов. – Минск : Наука и техника, 1981. – 336 с.

7. *Косенко О.І., Кустовська А.Д.* Гідротермальне модифікування структури силікагелю // Вісник НАУ. – 2009. –№ 3 (40). – С. 283– 286.

8. *Кельцев Н.В.* Основы адсорбционной техники. – М.: Химия, 1984. – 592 с.

9. *Грег С., Синг К.* Адсорбция, удельная поверхность, пористость: пер. с англ. – М. : Мир, 1970. – 407 с.

UDC 544.475 (045)

V. Ledovskih, Dr. Professor.; S. Levchenko, Assistant;
S. Tulainov, student (National Aviation University, Ukraine)

SYNERGIC MIXTURES PROTECTIVE ACTION AS THE FUNCTION OF WATER-SALINE MEDIUM COMPONENTS NATURE AND RATIO OF ITS CONCENTRATIONS AT CORROSION OF STEEL

The relation between the ratio of concentrations of components in binary mixtures of adsorption and passivation effects inhibitors; its influence on the corrosion-electrochemical behavior in aqueous salt mediums (method of isomolar series) was studied. It was shown that this effect has an extremum character, where the most corrosion inhibition of anodic reaction is achieved at synergistic maximum where also achieved almost complete corrosion protection.

Modern industry is characterized by the use of large capacity equipment and technological installations of high corrosivity. These include circulating water systems, lubricating fluids, oil production, refining systems and others. To protect metal from electrochemical corrosion propagation were used combined inhibitors - a mixture of substances that is able to demonstrate an increased efficiency compared with those for individual components. The phenomena of synergism were found at inhibition of metal corrosion in acidic, neutral media and in atmosphere [1-15].

One could assume that the efficiency of the combined compositions at protection of metals against corrosion in neutral aqueous salt mediums depends on the nature of components and their relative concentrations in the aggressive medium.

The purpose of this paper is to investigate the influence of the concentrations ratio of adsorption surfactants components on inorganic passivators and to determine the existence of synergy maxima, which is important matter for effective steel protection in aqueous salt solutions.

Method

Electrochemical and corrosion behavior of steels 08кп and Ст.20 was studied in aqueous salt solution (0.3 g / l NaCl, Na_2SO_4, $NaHCO_3$) in presence of surfactants of adsorption (mono-and triethanolamine) and passivation (sodium nitrite) actions by isomolar series method.

Potentiostatic polarization measurement were made using a potentiostat П5827М using chlorin-silver standard reference electrode with recalculation of potentials onto standard SHE scale.

Corrosion rate of steel in the background and inhibited solutions were determined by mass metry during 260 hours at room temperature ($20^{\circ}C$) and recalculated to the corresponding values of corrosion current density

The surface activity of surfactant was determined by measuring the surface tension of its aqueous solutions at the interface with air (Rehbinder instrument) [16].

Results and Discussion

The steels investigated in aqueous salt solution at absence of inhibitors additives undergo anodic corrosion oxidation in the active region, while reduction of oxygen-depolarizor is limited by slowed down stage diffusion, as it is evidenced by the presence of region of boundary current on the cathodic curves (Fig. 1).

Individual adsorption effect additives - triethanolamine (TEA) and monoethanolamine (MEA) are also able to inhibit the anodic reaction of ionization of steel to some extent. Corrosion potential and metal active dissolution region naturally is shifted into positive direction. At the same time the presence of amines in solution practically does not affect the kinetics of cathodic oxygen reduction. According to mass-metrical measurements amines at low concentrations slightly slow down the corrosion process, such as at triethanolamine concentration of 3×10^{-2} mol / l the ratio of corrosion of 08кп steel inhibition is $\gamma = 1{,}3$.

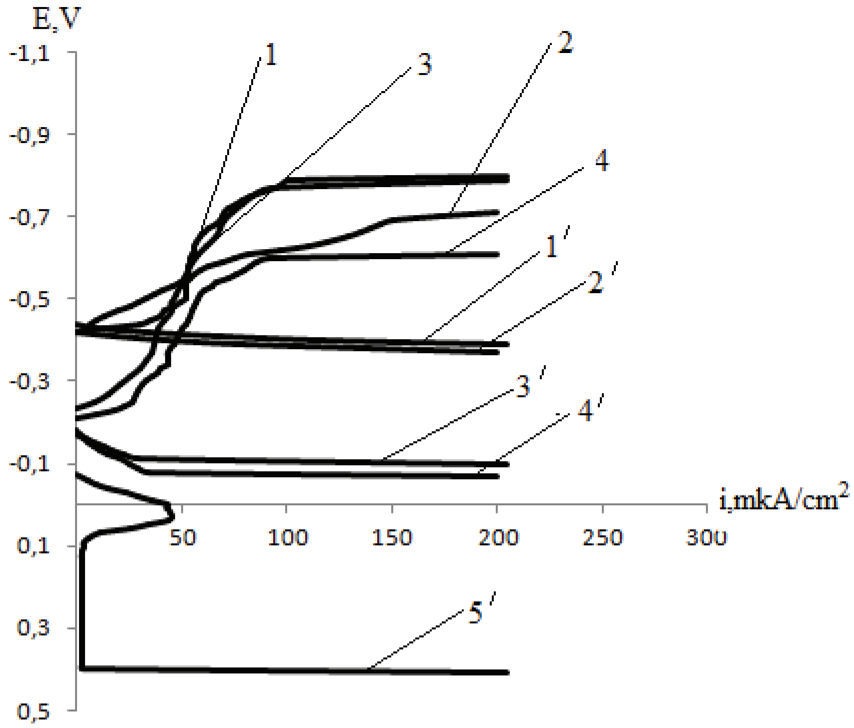

Figure. 1. Potentiostatic cathodic and anodic (with bar) polarization curves of steel 08кп and Steel 20: respectively

1.1 and 2.2 - in tape water model saline solution (0.3 g / l NaCl, $NaHCO_3$, Na_2SO_4); and steel 08кп in solution with additives (30 mmol / L): 3.3 - triethanolamine, 4,4 - monoethanolamine 5 - sodium nitrite.

Compared to triethanolamine, monoetanolamine at the same molar concentration in the aqueous salt solution creates a stronger influence on electrochemical and corrosion behavior of steel (Fig. 1). This can be attributed to its higher basicity and surface activity. Measurement of surface tension of solutions of certain additives on the interface liquid-air has shown its diminishing at the transition from triethanolamine (pKa = 7.77) to monoethanolamine (pKa = 9.5) (Fig. 2).

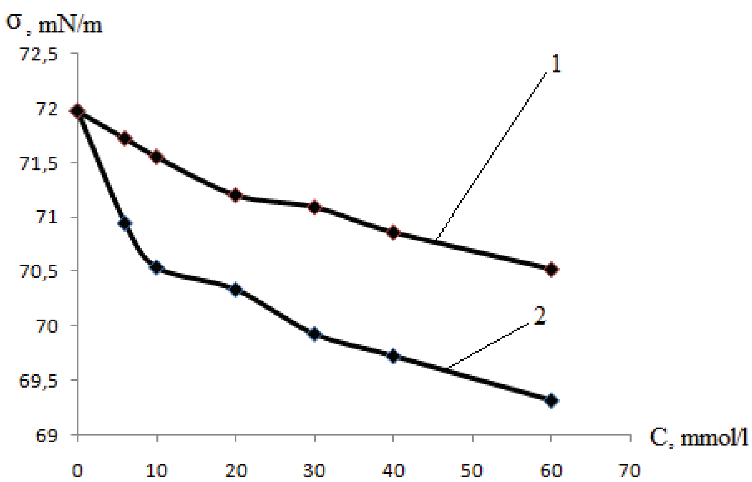

Figure 2. The influence of additions of amines on the surface tension of water-salt solution:
1 - triethanolamine 2 - monoetanolamine.

Sodium nitrite at low concentrations can strongly inhibit the anodic reaction of corrosion process and some potential to contribute to transformation of the metal in passive state (Fig. 1). In agreement with this, mass metrical measurements have shown its higher protective property, which, for example, at concentration 3×10^{-2} mol / L were equal $\gamma = 45,3$.

Much more effectively works the mixture of amines with nitrite. In its presence corrosion potential is strongly shifted towards positive values, followed by surface passivation in the wide range of potentials and pitting formation potential shifts far from the stationary. Very small also are full passivation current densities, which determine the final rate of corrosion process in a whole (Fig. 3).

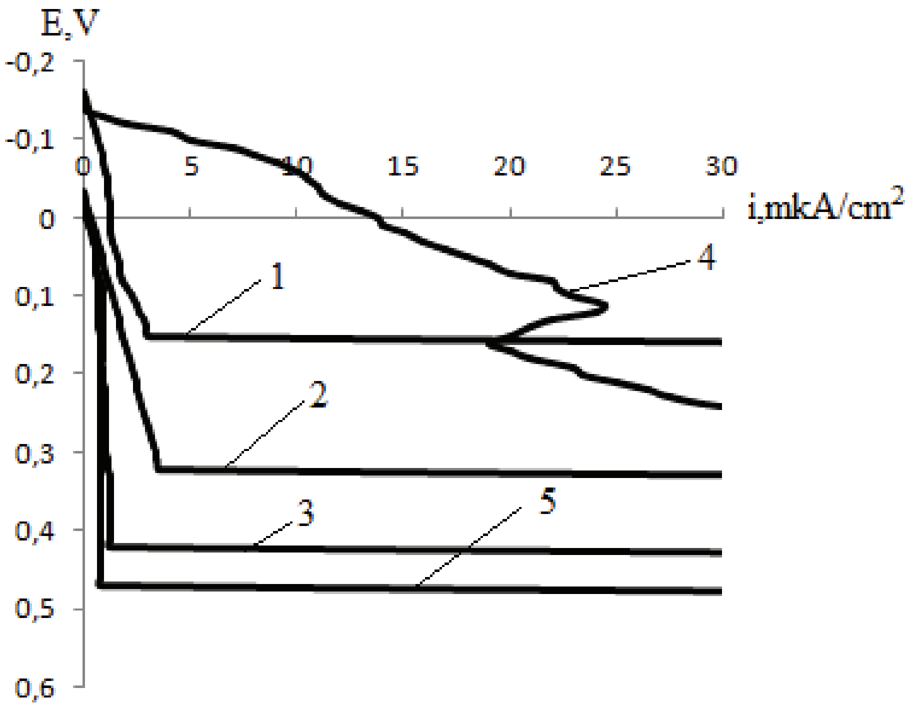

Figure. 3. Anode potentiostatic curves of 08кп steel in aqueous salt solution in presence of combined compositions with different ratios of components:
1 - TEA (5 mmol / l) + $NaNO_2$ (25 mmol / l) 2 - TEA (20 mmol / l) + $NaNO_2$ (10 mmol / L), 3 - TEA (15 mmol / l) + $NaNO_2$ (15 mmol / L), 4 - TEA (25 mmol / l) + $NaNO_2$ (5 mmol / L), 5 - MEA (15 mmol / l) + $NaNO_2$ (15 mmol / l).

Our studies have shown that influence of mixtures of additives on the parameters of the passivated state of metals in water-salt mediums and also its corrosion inhibition effect depends not only on the nature of components, but also is the function of adsorption and passivation component concentrations ratio. On figure 3 it is seen a significant dependence from the last factor of such electrochemical characteristics of steel as its potential of corrosion, zone of passivation potentials, the full passivation current density and also the pitting forming potential. This parameters determine the protective properties of inhibition mixtures.

For systematic clarification of this issue we have used the method of isomolar series, where we have explored the influence of these characteristics of steel in aqueous salt solution with amine-nitrite mixtures at various molar ratio of components within their constant total molar concentration range (Fig. 4).

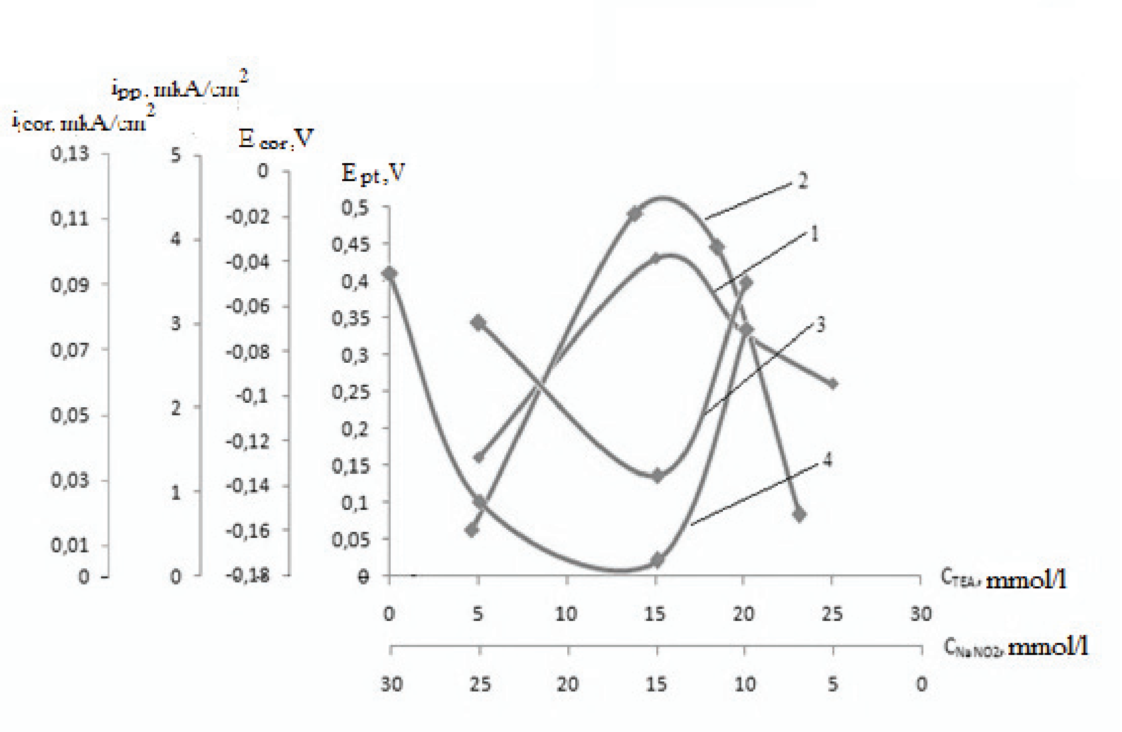

Figure. 4. Electrochemical parameters of anodic behavior of steel in aqueous salt solution as a function of components concentrations ratio in mixtures of TEA-$NaNO_2$ at constant total concentration of 30 mmol / l (isomolar series):

1 – pitting forming potential (E_{pt}) 2 - corrosion potential (E_{cor}) 3 - full passivation current density (i_{PP}), 4 – current flow indicator of corrosion rate (and $_{corresponding}$ calculated on base of massmetric measurements)

From the curves presented in Figure 4, we can see that the dependence of the parameters of anodic behavior of steel from the molar ratio of amine-nitrite is extreme in its nature. The largest magnitudes of compositions efficiency is observed at synergic maximums, which are achieved at close values of molar concentration ratios of adsorption and passivation components and meet the conditions of its optimal combined action. Thus there is achieved almost complete protection of metal from corrosion.

Conclusions

1. Inhibiting properties of synergic mixtures of adsorption surfactants with passivating components at corrosion of steel in neutral aqueous salt mediums depend on the nature of the components and on the ratio of their concentrations.
2. Increase of the surface activity of surfactant is accompanied with increase of its efficiency at application, it is observed both as an individual as well as in the synergic compositions, emphasizing the absorption mechanism of action.
3. Dependence of efficiency of mixtures on the molar concentrations ratio is characterized by occurrence of maximum synergy, there is reached a maximum level of influence of additives on the electrochemical behavior of steel and its corrosion protection. That phenomena should be considered at creating and at using of efficient corrosion inhibitory methods.

References

1. *Алцибеева А.И., Левин С.З.* Ингибиторы коррозии металлов. Л.: Химия. 1968. 264с.

2. *Лосев В.В.* Влияние галоидных ионов и органических катионов на электрохимическое поведение железа в кислых растворах. – Докл. АН СССР, 1953, т. 38, №3, с. 499-502.

3. *Иофа З.А.* Эффекты синергизма и антогонизма при адсорбции и действии поверхностно-активных веществ на электрохимические реакции и коррозию железа. – Защита металлов,1972, т.8, №2, с. 139-145.

4. Миндюк А.К., Свист Е.Н., Гопаненко А.Н.Эффективность совместной защиты стали в серной кислоте ингибиторами и поверхностно-активными анионами. – Коррозия и защита в нефтегазовой промышленности, 1975, №2, с.6-9.

5. *Федоров Ю.В.* К вопросу о действии смесей ингибиторов, В кН.: Тр. III Международного конгресса по коррозии металлов. М.: МИР, 1968,т. 2, с. 150-162.

6. *Подобаев Н.И., Либенский А.П.* Влияние анионного состава и pH коррозионной среды на адсорбцию и защитное действие солей алкилбензилпиридиния. – Уч. зап. Моск. гос. пед. ин-та. 1971, №340, с.131-141.

7. *Антропов Л.И., Погребеева И.С., Дремова Г.И.* О совместном влиянии галоидных ионов и четвертичных солей пиридиновых оснований на кислотную коррозию металлов. – Электрохимия, 1972, т.8, с.108-112.

8. *Антропов Л.И., Погребова И.С.* Связь между адсорбцией органических соединений и их влиянием на коррозию металлов в кислых средах. В кн. Итоги науки и техники. Коррозия и защита от коррозии. М.: ВИНИТИ, 1973, т. 2, с. 27-112.

9. *Антропов Л.И., Макушкин Е.М., Панасенко В.Ф.* Ингибиторы коррозии металлов. К.: Техника, 1981, 184с.

10. *Розенфельд И.Л.* Ингибиторы коррозии. М.: Химия, 1977,351с.

11. *Ледовских В.М.* Синергическое ингибирование кислотной коррозии стали. – Защита металлов,1984, т. XX, №1, с. 54-61.

12. *Иванов Е.С., Гликина Ф.В.* Исследование пассивирующих свойств растворов ПАВ с добавками нитрита натрия. – Защита металлов, 1972, вып. 4,с. 484-486.

13. *Ледовских В.М.* Синергическое ингибирование коррозии стали в нейтральных средах композициями азотистых органических оснований с нитритом натрия. – Защита металлов, 1983, т. XIX, с. 84-91.

14. *Розенфельд И.Л., Фролова Л.В., Тавадзе Н.Н.* Синергический эффект при защите стали от коррозии неорганическими ингибиторами в нейтральных электролитах. – Защита металлов,1980, т. XVI, №2, с. 133-136.

15. *Донченко М., Фроленкова С., Білоусова Н., Срібна О.* Пасивуюча обробка заліза та маловуглецевої сталі для тимчасового захисту від атмосферної корозії // Фізико-хімічна механіка матеріалів. Електрохімічний захист і корозійний контроль. -2007. – Спец. вип.. №6. – С. 124-129.

16. *Жигач К.Д., Ребиндер П.А.* Поверхностная активность гидрофильных коллоидов. Журнал физической химии, 1939, т.13, с. 94-105.

UDC 621.899(045)

V.M. Ledovskih, Dr.Chem.Sci.; O.M. Davydenko, student;
E.O. Rogova, student (National Aviation University, Ukraine)

CATHODE REDUCTION OF ALIPHATIC ALDEHYDES ON CADMIUM ELECTRODE FOR REGENERATION OF WASTE MOTOR OILS

T*he results of studies of aliphatic aldehydes reduction as products of oxidation of motor oils on cadmium cathode in sulfuric acid-water-alcohol medium are presented. With potentiostatic polarization measurements was determined the diffusion mechanism of the cathodic process and conditions of its proceeding. Electrolysis of aldehyde solution at controlled potential threshold current has shown that the cathodic reduction process occurs rapidly with almost quantitative conversion of the starting substance. Chromatographic analysis has revealed the major products of aldehyde electroreduction – the corresponding alcohols and hydrocarbons. There put forward assumptions about the formation mechanism ofsuch chemical compounds as pinacone and pinacoline.*

World volume of lubricants, which are produced on the basis of major mineral oils and, partially, synthetic ones reach 0.8% from the total of crude petroleum application[1].

During application of oils they undergo physical and chemical transformations which are induced by: oxidation of hydrocarbons, the additives decompositions, engine parts wear products accumulation, mechanical impurities and water pesence. These changes impair the performance properties of oils and lead to the impossibility of their application.

The main reason for the negative transformation of oils is an effect of oxygen action on the hydrocarbon components at elevated temperatures. Consequently, there form carbonyl compounds, end products of oxidation of which are a carboxylic acids. The last belong to the most dangerous impurities in oils, as they increase the acid number, corrosivity of construction materials, viscosity of the medium, change the thermal conductivity. [2, 3].

However, waste oils is a valuable raw material for recycling. Yield of oil from recycled raw materials is 80%, while from petroleum only 10-15% [2-6].

Therefore, the development and improvement of the waste oils regeneration process is an important scientific and engineering task.

The processes of oxidation of oils

Hydrocarbons that compose the bulk of major oils, are greatly differing in molecular structure (paraffin, naphtenic, aromatic and naphtenic-aromatic compounds), of which 60-70% are naphteno-paraffin hydrocarbons [7].

Oxidation of oils at its application proceeds by a chain mechanism. The primary products are organic hydroperoxides (C – O – OH), which are formed at addition of oxygen to the C-H bond of hydrocarbon. Later they undergo decomposition into groups of compounds, the first of which are aldehydes, ketones, acids, hydroxy acids, asphaltenic acid, and the second – are neutral products - phenols, resins, pyrobitumens, carbenes [7.8].

Hydroperoxide may also undergo oxidation by oxygen at C-H bond to form diatomic hydroperoxide groups at two adjacent carbon atoms which promotes decomposition of substances at the C-C bonds into ketones and acids [8].

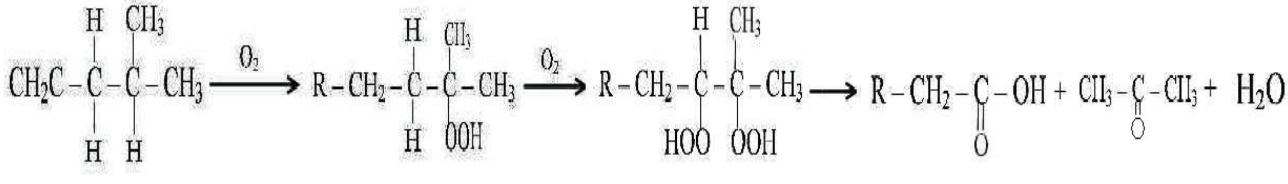

Oxidation of alkylaromatic hydrocarbons with short chains also proceeds via the stage of hydro peroxides and gives phenols and ketones:

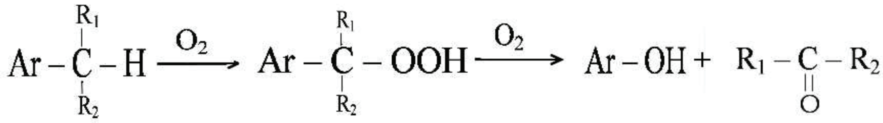

Aldehydes, in its turn, can undergo oxidation to carboxylic acids with the same number of carbon atoms and these processes also occur through the stage of formation and decomposition of peroxide compounds - peroxo-acids [9].

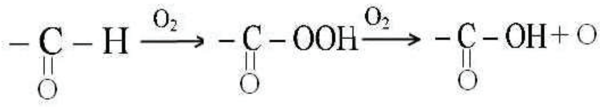

Electroreduction of carbonyl compounds

Organic carbonyl substances, which include aldehydes and ketones, can undergo reduction at their solutions electrolysis cathodic process. Carbonyl group in the molecules of these compounds are polar group, due to displacement of valence electrons to the most electronegative oxygen: the atoms gain partial effective charges - positive on carbon and negative at oxygen. The presence of positively polarized carbon atom determines the possibility of its adsorption on the negatively charged cathode surface during electrolysis [10].

For electroreduction of carbonyl compounds were used metals with high hydrogen overvoltage, in this case the electron transfer onto reducing substance in acidic mediums is previously subjected to protonation, which makes the course of electrochemical reactions easier [10, 11]. So on cadmium cathode propionic aldehyde was reduced to propanate, while methylpropylketone and diethylketon to pentane. For reduction of carbonyl compounds to secondary alcohols the most suitable electrode materials were mercury and lead, for the products of hydrodimeryzation like pinakone it was zinc, mercury and lead. Elevation of such values as cathode potential, solution pH, temperature and conducting of electrolysis at high cathode current density leads to the reduction of carbonyl compounds into hydrocarbons while lowering of these values - to alcohols and hydrodimers.

Purpose of work - a study the electrochemical reduction of aliphatic aldehydes in sulfuric acid-water-alcohol solution on cadmium electrode and analysis of the formed products by gas-liquid chromatography.

Experimental

Research of electroreduction of aliphatic aldehydes was performed for a case of isovaleric aldehyde $CH_3CH(CH_3)CH_2CHO$, M = 86,13 g/mol, m.p. = -51˚C, b.p. = 92,5˚C..

Polarization measurements were performed using potentiostat П-5727 M in potentiostatic mode.

We used termostatic 3x-electrode cell with a porous glass divided partition cathode and anode volumes.

Auxiliary electrode was Pt, potentials of the working electrode (Cd), were measured against comparision chlorine-silver electrode and recalculated onto the standard hydrogen scale. Cathode polarization curves for cadmium were measured after installation of stationary potential. Background solution composition was: 920 cm^3 isopropyl alcohol, 19.8 cm^3 sulfuric acid, 22.4 cm^3 of distilled water.

Preparative electroreduction process for aldehyde was performed by electrolysis at controlled potential which corresponded to limiting current of substance electroreduction.

Products of electrochemical conversion of substances were studied by chromatographic method [12] using gas-liquid chromatograph ЛХМ-8МД.

Results and discussion

Figure 1 shows the potentiostatic polarization curve of cadmium cathodic polarization in the background solution. The curve has one wave of electroreduction, which corresponds to the limiting diffusion current of dissolved oxygen reduction at electrode reaction:

$$O_2 + 4H^+ + 4e = 2H_2O$$

The polarization curve for Cd electrode in the solution of aliphatic aldehyde had two waves of reduction and is characterized by two areas corresponding to limiting current of oxygen and organic matter diffusion (Fig. 1).

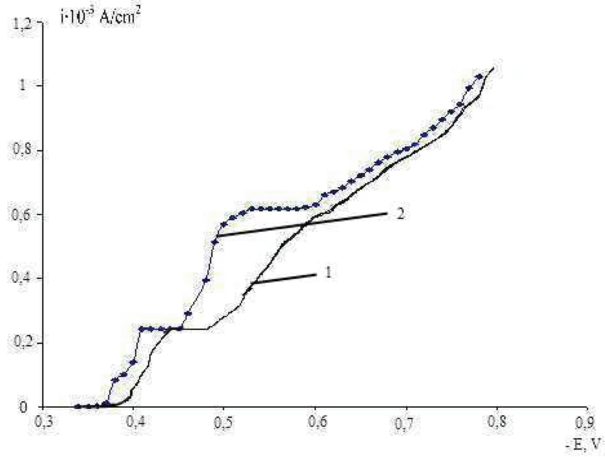

Fig. 1. Polarization curves of cadmium: 1 - in background solution; 2 - in presence of 0.5 mol/l of isovaleric aldehyde

These our observations are consistent with literature data concerning the possibility of cathodic reduction of carbonyl compounds in dilute acid solutions [12-14]. The equation for the density limit diffusion current for a flat electrode has form [12]:

$$i = nFc\sqrt{\frac{D}{\pi \cdot \tau}}$$

where n is number of electrons participating in potential forming reaction stage; F - Faraday number c - molar concentration of depolarizer, mol / l, D - diffusion coefficient of the substance; τ - time of electrolysis.

From equation it is seen that the diffusion current density should vary inversely proportional to the electrolysis time square root. We have been used this dependence to control the process of electroreduction of carbonyl compounds.

In Fig. 2 we can see that the curve of threshold current declines at controlled potential of aldehyde electroreduction quite rapidly, it is evidenced by reduction of the diffusion limiting current, which is determined by the fall of aldehyde concentration in solution. In indisturbed solution the process is completed in about 20-25 minutes.

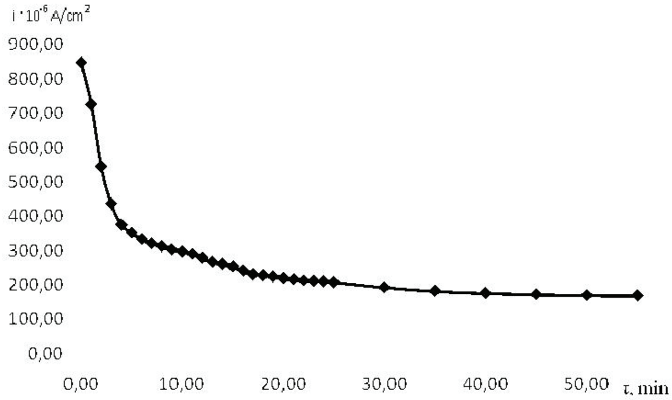

Fig. 2. Isovaleric aldehyde reduction in sulfuric acid- water-alcohol solution threshold current density

To determine the products of electrochemical reduction of aldehyde reaction solution was transferred into a flask for the distillation with deflegmator. At beginning some 3-4 cm^3 of distillate was sampled for chromatographic analysis in view of possible formation of saturated hydrocarbon isopentane, boiling point of which is lower than that of solvent - isopropyl alcohol which at chromatography has to come out before the solvent.

At the subsequent distillation of the reaction mass an azeotrop isopropanol-water was removed. It contains 83% ethanol and 17% water and boils at temperature 81˚C. Consequently water is removed together with isopropyl alcohol.

A small residual solution was subjected to chromatographic analysis. For identification ofchromatographic peaks were used reference samples of possible products of aldehyde electroreduction in order to determine its retention times under the same conditions.

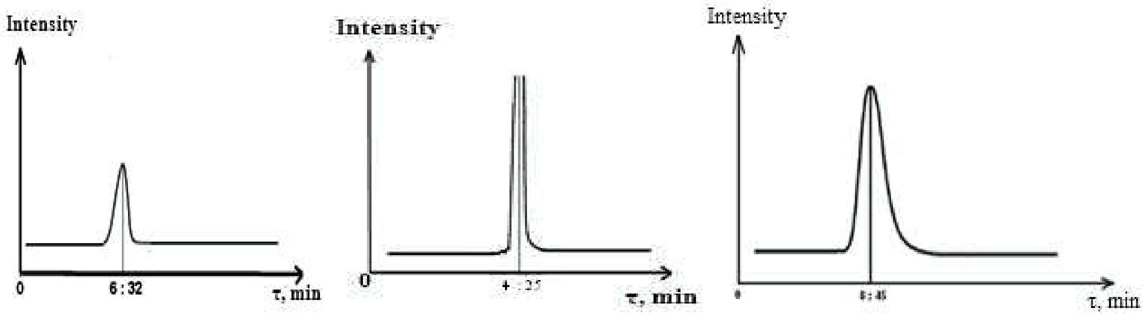

Fig.3. Chromatogramm of reference substances and - isopentane (injecton temperature 150 ˚C, column thermostat 30˚C), b - isopropanol (evaporator temperature 150 ˚ C, column thermostat 30 ˚ C).

Chromatogramm of isovaleric aldehyde electroreduction products is shown in Fig. 4.

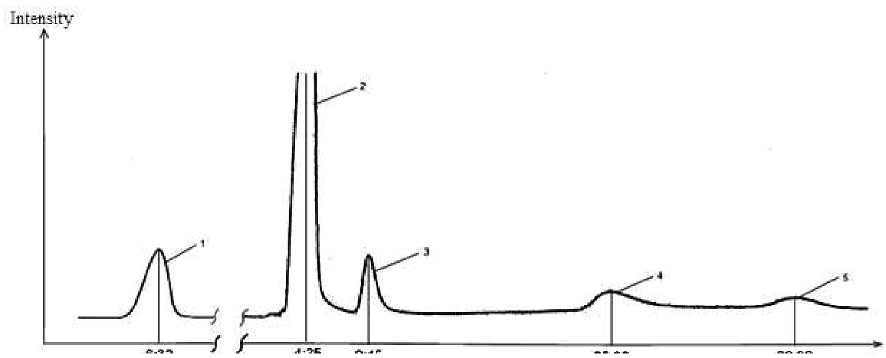

Fig. 4. Chromatographic analysis of isovaleric aldehyde electroreduction products on Cd - electrode in sulfuric acid-, water-alcohol solution: 1 - isopentane, 2 - isopropanol (solvent) 3 - isopenthanol 4 - product of pinacon-pinacoline rearrangement of substituted glycols into 2-isobutyl-4-metylpenthanal 5 - substituted glycol - diisobutyl -1.2 - ethylene glycol.

The formation of the substances listed in Figure 4, can be explained with the following considerations:

It can be assumed that the chromatographic peak 4 is the product of further transformation of the electrochemically resulted glycol derivative (type pinacone) in pinacolinic rearrangement: This our opinion is consistent with the known ability of pinaconic type substances to rearrange onto pinakone type compounds in acidic mediums [12].

Conclusions

1. Electroreduction of aliphatic aldehydes on Cd-electrode with high overvoltage of hydrogen in acidic media proceeds with a significant rate and leads to the formation of hydrocarbons, alcohols, to thew type pinacone substituted glycols, and to the products of pinacon-pinacolin rearrangement of the last in the medium of sulfuric acid.

2. It is shown that the electrochemical reduction of oxygen-containing compounds into safe and corrosion-inactive substances may be appropriate for the use in the process of used motor oils regeneration .

References

1. *Чайка О. Г., Ковальчук О. З., Чайка Ю. А.* Моніторинг утворення відпрацьованих олив// Зб. Наук. пр. – Львів: «Львівська політехніка», 2009. – С. 221-224.
2. *Гуреев А. А., Фукс И. Г., Лашхи В. Л.* Хіммотологія. – М.: Химия, 1986. – 368 с.
3. Регенерация отработанных масел и их повторное использование. Обзорная информация/Сост.: *К. В. Рыбаков, В. П. Коваленко.* – М.: АгроНИИТЭИИТО, 1989. 86 с.
4. *Школьников В. М.,* Гордукалов *А. А., Юзефович В. И., Петросова М. Р.* Анализ зарубежных подходов к проблеме утилизации отработанных нефтепродуктов. – 2004. - № 1. С. 36-39.
5. *Чайка О. Г. Чайка Ю. А.* Порівняльний аналіз методів очищення відпрацьованих олив на Україні та за її межами// Зб. Нак. пр. – Львів: «Львівська політехніка», 2009, С. 224 – 228.
6. *Шашкин П. И., Брай И. В.* Регенерация отработанных нефтяных масел. – М.: Химия, 1970. – 303 с.
7. *Венцель С. В.* Применение смазочных масел в двигателях внутренього згорания. М.: Химия, 1979. – 240 с.
8. *Иванов К. И.* промежуточные продукты и промежуточные реакции автоокисления углеводородов. – М.: Гостоптехиздат, 1949. – 246 с.
9. *Ракин Я. Ф., Самуйлов А. В.* Изменение характеристик моторного масла в процессе эксплуатации, автотракторных двигателей.// Учен. Зб. Института СХПР НовГУ, т. 1 в. 3-х т, 2006.
10. *Томилов А. П., Майрановский С.Г., Фиошин М.Я., Смирнов В.А.* Электрохимия органических соединений. Л.: Химия, 1968 г. 592 с.
11. *Антропов Л. І.* Теоретична електрохімія. – К.: Либідь, 1993. – 542 с.
12. *Ногаре С. Д., Джувет Р. С.* Газо-жидкостная хроматография. Теория и практика. Л.: Недра, 1966. – 472 с.

UDC 541.678.5

F.G. Fabulyak, D.Sc., D.V. Karandiei, student.
(National Aviation University, Ukraine)

MODIFICATION OF POLYETHYLENE MATERIALS BY PROPANETRIOL-1,2,3

Studied influence of propanetriol-1,2,3 at the relaxing behavior of high pressure polyethylene. Addition propantriol-1,2,3 resulting in displacement processes dipole-segmental relaxation towards higher frequencies.

Achievement of polimeric industry in recent years - the development of new food brands polyethylene, hygienic certification packages for chemical stability and development of various additives in polyethylene materials - deprived most consumers of stereotypes of former days. An important feature of these materials is that they have a whole set of properties (strength, elasticity, wide temperature range, hardness, high electrical insulating properties, inertness to many chemicals and chemical resistance, physiologically harmless, non-toxic), which makes it the products indispensable in everyday life and industry. But along with all the valuable properties of polyethylene has several drawbacks, including the ability to cracking, brittleness during large and long-term loads.

And as to polyethylene materials in process of their prevalence the demand of improvement of a complex of properties and elimination of lacks according to concrete service conditions it puts difficult enough and interesting problems which first of all consist in increase adaptability to manufacture at application of products of polyethylene before researchers is constantly made.

Therefore for polyethylene materials special value has increase of indicators of firmness. Therefore introduction in structure of polyethylene of substances of small molecular weight, the functional and structural organisation can lead to effects of plasticization which together with preservation of available properties will improve elasticity, hardness, wear resistance of materials and so on. Therefore propanetriol-1,2,3 is rather actual at updating of polyethylene materials Low density polyethylene (LDPE) - a soft elastic material obtained by polymerization of ethylene in an autoclave or tubular reactor ..

The main features of the molecular structure of LDPE: highly developed branching and a large polydispersity in molecular weight, which determine the supramolecular structure and physical properties of polyethylene.

In LDPE macromolecules found vinylidene unsaturation (Table 1). The explanation of the origin of the transmission chain of the polymer revealed the main termination reaction of growing macroradicals, i.e. the reaction responsible for the value a number average molecular weight HDPE.

These features of molecular structure of LDPE and now distinguish it from all known synthetic polymers. Let us consider the results of the study of molecular structure and fundamental properties of this polymer.

Table 1

Indicators characterizing the structure of the polymer chain polyethylene of high pressure

Index	
The total number of CH_3 groups per 1000 carbon atoms	21,6
The number of end groups CH_3 per 1000 carbon atoms	4,5
Ethylene offshoot	14,4
The total number of double bonds per 1000 carbon atoms	0,4-0,6
including	
Vinyl double bonds (R–CH=CH_2),%	17
Vinylidene double bonds ($\genfrac{}{}{0pt}{}{R}{R'}\!\!>C=CH_2$),%	71

Trans-vinylene double bonds (R–CH=CH–R'),%	12
Oxygen-containing group, %	10^{-3}–10^{-4}
The degree of crystallization, %	50-65
Density, g/cm3	0,91-0,93

Experimental part

Polyethylene compositions in the form of films were reception by a moulding method. Propanetriol-1, 2.3 was added to microfine high-pressure polyethylene LDPE-158 in the ratio of 2% of the total mass, evenly distributed throughout the volume of the polymer. Further samples were melted under pressure, cooled and aged for some time and research at the bridge AC. For detection of dipole relaxation in polyethylene containing 2% propanetriol-1, 2,3 were carried out dielectric studies in the frequency range 1-100 kHz on a bridge AC P-5083. Were analyzed tangent of dielectric loss angle (tgδ), permittivity (ε'), dielectric loss factor (ε''), resistivity (ρ) and conductivity (γ). On the basis of data were constructed graphs of dependence of frequency (f) from of the dielectric loss angle (tgδ) (Fig. 1), the frequency from of the dielectric permittivity (ε ') (Fig. 2), the frequency from of dielectric loss factor (ε'') (Fig. 3), the frequency from of resistivity (ρ_v) (Fig. 4) and frequency from of electrical (γ) (Fig. 5) for the original model and modified by propanetriol-1, 2,3 samples of polyethylene.

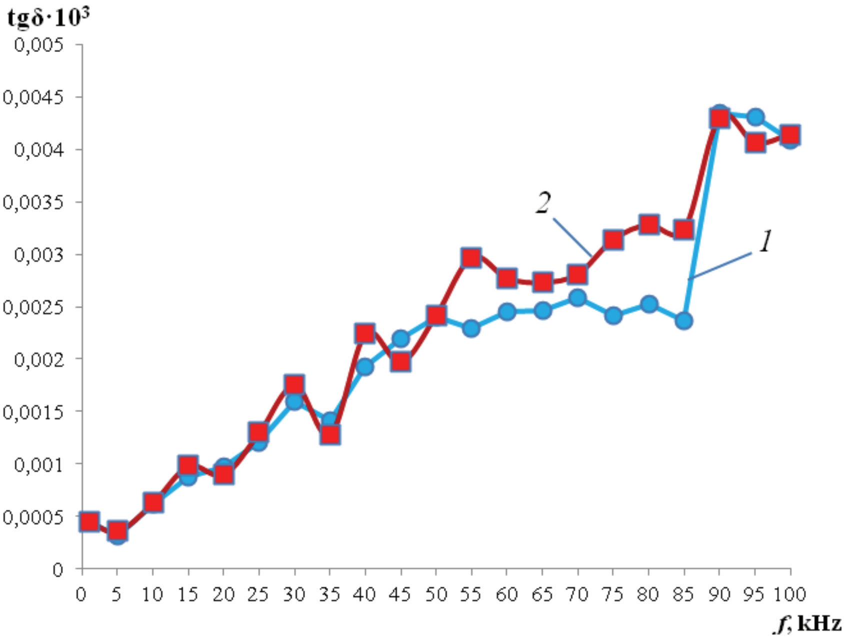

Figure 1. Dependence tgδ from change the frequency *f* for the original (1) and modified by propanetriol-1,2,3 (2) samples of polyethylene

For the original and the modified sample at a frequency of 90 kHz observed dipole-group relaxation of polyethylene, which is created largely by polar groups C=O groups and double bonds (vinyl,trans-vinylene, vinylidene). The dipole-segmental relaxation processes for the original sample occur at frequencies of 30, 50 and 70 kHz. In the modified sample is necessary to note a broad line of dipole-segmental relaxation from 15 to 55 kHz, which shows four distinct dipole-segmental relaxation processes at 15, 30, 40 and 55 kHz. This means improving the mobility of not only large segments, but less than the segmental mobility of kinetic units is higher than the group. This is because the molecules of propanetriol-1,2,3 through physical interaction of individual members, placed in the intermolecular space and thus help to increase the flexibility of macromolecules of polyethylene.

Graph of dependence of dielectric constant on frequency for the original and modified samples of polyethylene are shown in Fig. 2:

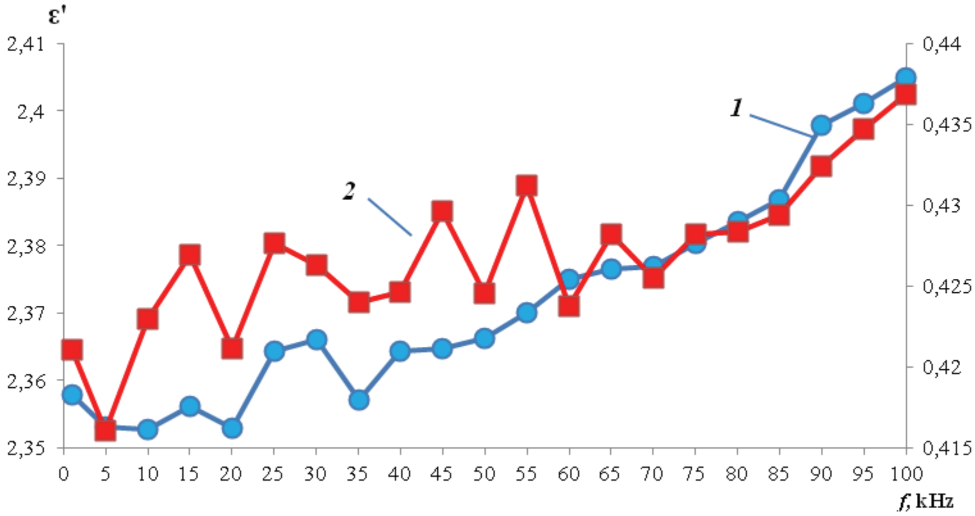

Figure 2. The dependence of the dielectric constant ε' from frequency *f* for the original (1) and modified by propanetriol-1, 2,3 (2) samples of polyethylene

Graph of dependence of the coefficient of dielectric loss on frequency for the original and modified polyethylene samples are shown in Fig. 3:

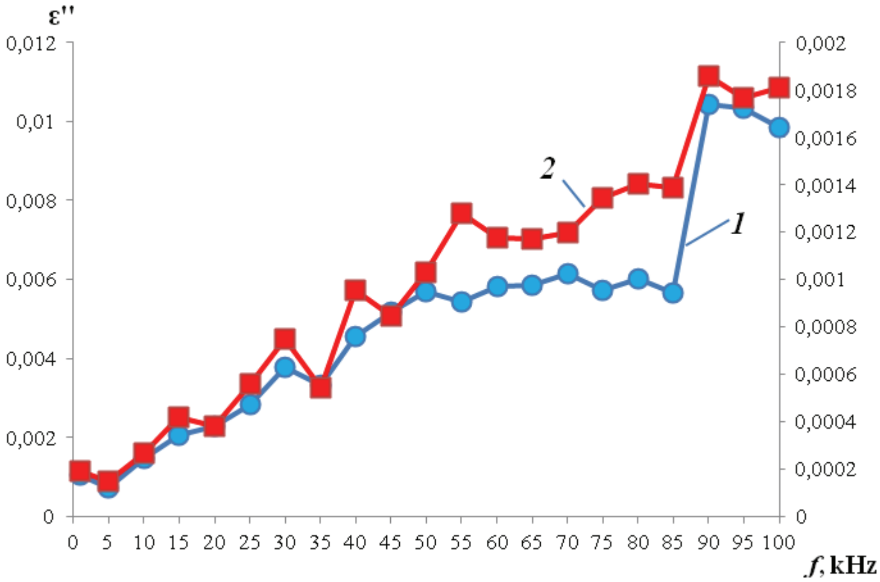

Figure 3. Dependence of dielectric loss from frequency *f* for the original (1) and modified by propanetriol-1,2,3 (2) samples of polyethylene

The analysis carried dependencies should be noted that adding propanetriol-1,2,3 to polyethylene of high pressure leads to an increase segmental mobility of the modified polymer and on the basis of the received characteristics of the method dielectric definitions can be predict that polyethylene products from obtained modified polymer will have along with initial hardness, reduced brittleness and increased impact strength.

Graph of dependence of resistivity from the frequency shown in fig. 4:

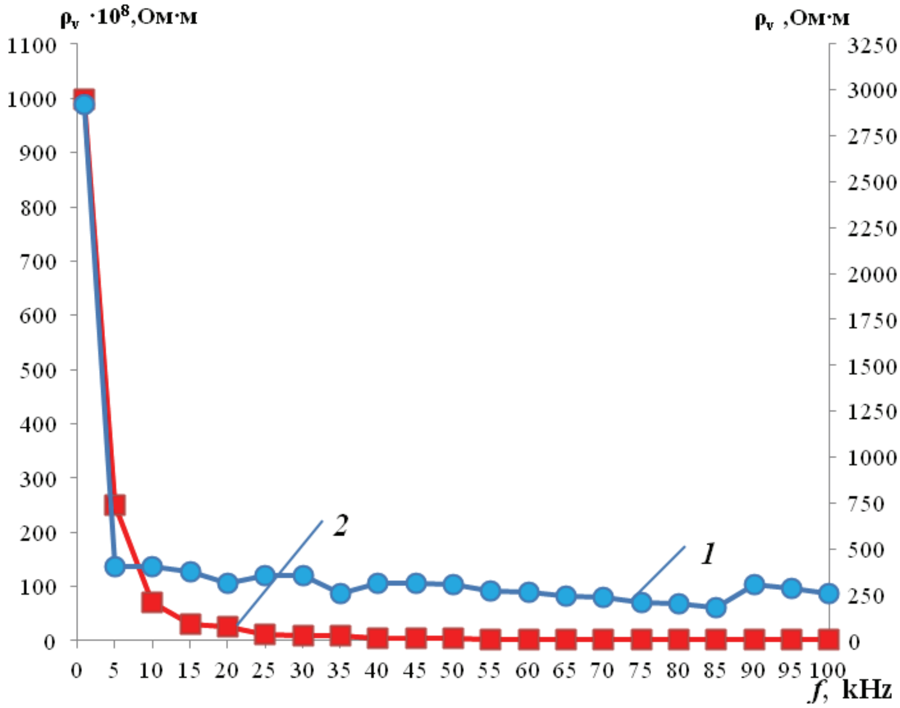

Figure 4. Dependence of resistivity from the frequency *f* of the original (1) and modified by propanetriol-1,2,3 (2) samples of polyethylene.

Graph of dependence of conductivity from frequency shown in fig. 5:

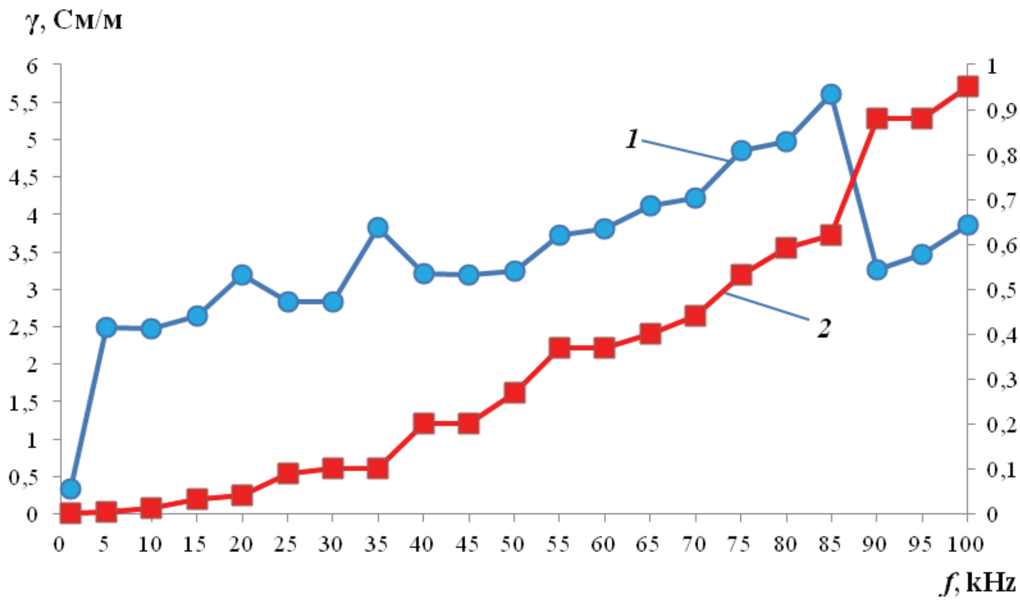

Figure 5. Dependence of conductivity from frequency *f* for the original (1) and modified by propanetriol-1,2,3 (2) samples of polyethylene

With the above-quoted graphs follows that the resistivity samples of polyethylene with increasing frequency is reduced, leading to an increase in conductivity, due to the presence of multiple bonds, which form conductive paths in macromolecules of the polymer. Also to be noted that in the modified sample quantity of conductivity less than in original sample, is explained by the fact that due to the formation of uneven distribution of electron density by means of double bonds, molecules of propanetriol-1,2,3 is located near them by blocking conductive paths that are in clear polyethylene.

Conclusions

–Found that the presence of double bonds in macromolecules of polyethylene caused by the presence of ketone, vinyl, trans-vinylene, vinylidene groups leads to uneven distribution of electron density in macromolecules of polyethylene, which creates conditions of physical interaction between propanetriol-1, 2,3 and macromolecules high-pressure polyethylene. Due to the occurrence of physical interactions, the molecule of propanepriol-1,2,3 placed in the intermolecular space of the polymer, some of them interact with groups that have double bonds, reducing the mutual influence of macromolecule polymer chains, some of these groups through chains sewn together, which strengthens the ties macromolecules and reduces the density of packing, creating increased mobility of segments in the polymer macromolecules. This enables you to predict what products based on a modified polymer with maintaining high strength properties, will have less brittleness and high strength at impact.

–The resistivity of the obtained polyethylene compositions with increasing frequency is reduced, leading to an increase in conductivity, due to the presence of multiple bonds, which form conductive paths in macromolecules of the polymer. In the modified sample quantity of conductivity less than in the original sample, is explained by the fact that due to the formation of uneven distribution of electron density by means of double bonds, molecules of propanetriol-1,2,3 is located near them by blocking conductive paths that were in pure polyethylene. That propanetriol-1,2,3 improves dielectric properties of high-pressure polyethylene, and polyethylene can be so widely used as insulator.

–The results of research are the basis for regulating the properties of polyethylene high-pressure by modification by propanetriol-1, 2.3, providing a higher level of technological and technical materials based on high-pressure polyethylene.

References

1. Полиэтилен высокого давления. Научно-теоретические основы промышленного синтеза / *А. В. Поляков. Ф. И. Дунтов, А. Э. Софиев и др.* – Л.: Химия, 1988. – 200 с.: ил.

2. *Д. С. Новак, Ю. О. Будаш, В. В Пахаренко, В.О. Пахаренко* // Поліетилегові композиції, що вміщують струмопровідний наповнювач. Структурно-морфологічні властивості. Хімічна промисловість України. 2011. №5. С. 35-43

3. *И. А. Чмутин, Н. Г. Рывкина, Е. А. Зубова, Л. И. Маневич* // Диффузия цепей в аморфно-кристаллическом полиэтилене: проявление в процесс ее диэлектрической релаксации. Высокомолекулярные соединения. 2008, том 50, № 2, с 295-305.

4. Физические и химические свойства глицерина / *Д. Л. Рахманкулов, Б. Х. Кимсанов, Р. Р. Чанышев.* – М.: Химия, 2003. – 200 с.; ил.

UDC 541.678.5

F.G. Fabulyak, D.Sc.; V.V. Palagnyuk, st.
(National Aviation University, Ukraine)

INFLUENCE OF ETHANEDIOL-1,2 ON DIELECTRIC PROPERTIES OF POLYETHYLENE OF HIGH PRESSURE

A study of the structure of polymeric materials based on polyethylene of high pressure. Constructed the dependencies that reflect the change in dielectric properties from frequency alternating electric field. The obtained data indicate the superiority of the modified polyethylene material in comparison with non-modified, which can be applied in various fields of electrical and other industries.

Production of synthetic polymers currently exceeds 100 million tons per year. The main of their volume take of large tonnage production of polyethylene, polystyrene and polyvinyl chloride. Polyethylene of high pressure has a valuable set of properties that make wide use of packaging food, for space technologies. In addition, he serves as a material for coating, which is able to various modifications [1-3].

Thus, the relevance of this work is that the polyethylene, which is the most common and accessible in the application of polymer, easily recyclable and is subject to modifications, you can use its to improve range of physical and mechanical properties such as dielectric, the introduction in the polymer small quantities of various substances before processing or in its process.

The main features of the molecular structure of LDPE is a highly developed branching and a large molecular weight distribution that determine the supramolecular structure and physical properties of polyethylene [4]. These features of molecular structure of LDPE and today different it from all known synthetic polymers derived by polymerization. The total number of branches in LDPE is 23.7 per 1000 C.

LDPE has high dielectric properties, which are caused by the structure of its macromolecules. Their combination with physico-mechanical and chemical properties makes LDPE high dielectric, which is widely used.

For dielectric properties LDPE similar to alcanes of normal structure. But unlike them he has a side branch of the CH_3-groups at the end of branches. About the content of CH_3 groups, unsaturated groups, and oxygen-containing group –C=O,–O–H and others. [4] (the remains of the initiators and groups formed by oxidation) can be seen from these data that are presented in Table 1.

Table 1

The content of CH_3 groups, unsaturated groups and oxygen groups in the LDPE

Groups	Content,%
CH_3/100 C	1,5 – 2,5
–C=C–/1000 C	0,3 – 0,5
Oxygen-containing group, %	10^{-3} – 10^{-4}

Dielectric loss of LDPE is very low. These losses are caused by the presence of a small number of polar groups and to a lesser extent $–CH_3$ groups and bonds –C=C–, which have small values of dipole moments. Each type of polar groups that are available in LDPE, contributes to the dielectric losses, what are cumulative.

Despite its chemical simplicity, plastic materials are usually have amorphous-crystalline and characterized developed morphology. Chemical inert LDPE, suggests that the presence ethanediol-1,2 does not prevent crystallization of LDPE in the preparation of samples of the polymer melt. Yes, most likely to localization ethanediol-1,2 will be in or amorphous areas LDPE, or even outside the plastic phase in intercrystalline or space between lamellae. It was necessary to find out which changes caused by the introduction ethanediol-1,2, influence at the dielectric behavior of samples.

Experimental part

For modification polyethylene material injected 2.5% ethanediol-1,2, such as the maximum number of CH_3 groups is contained in the branches of this brand of polyethylene (see Table 1).

Obtained examples of polymeric materials in the form of discs were placed and fixed between two electrodes an alternating current bridge. Further measurements were carried out: C_x, tgδ, ρ_v for each sample by changing the frequency of the electric field from 1 to 100 kHz, 5 kHz after starting the measurement in increments of 5 kHz.

Data dielectric permittivity, dielectric loss and conductivity of the pure sample LDPE and modified sample of LDPE by ethanediol-1,2 at different frequency electric field calculated by the formulas 1, 2 and 3, respectively, using Excel 2010.

$$\varepsilon' = \frac{C}{C_0} \tag{1}$$

$$\varepsilon'' = \varepsilon' \cdot tg\delta \tag{2}$$

$$\gamma = \frac{1}{P_v} \tag{3}$$

Based on experimental data obtained on an AC bridge, built tangent of the angle dependence of dielectric loss on frequency alternating electric field for LDPE sample (curve 1) and the sample of LDPE with the addition ethanediol-1,2 (curve 2), which is presented in Figure 1.

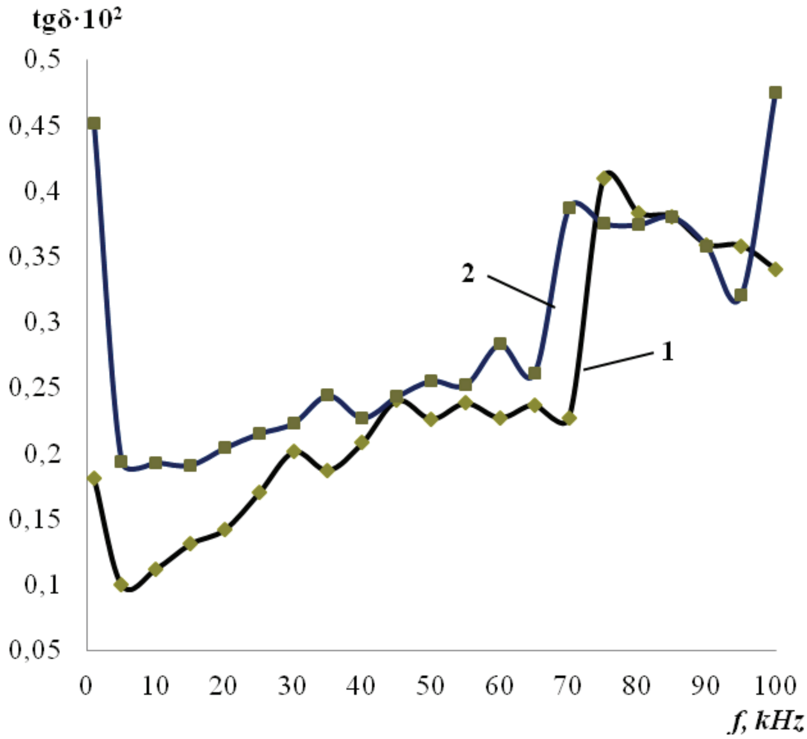

Figure 1. Dependence of dielectric loss tangent of the angle from the frequency of alternating electric field: 1 - LDPE 2 - LDPE with the addition of ethanediol-1,2.

Frequency dependence of factor of dielectric loss for structures LDPE with modified and non-modified polymer layer, recorded at room temperature. In general, these dependences have the form, which is typical for nonpolar polymers, i.e. low value tgδ in throughout the studied range with some increase in the advancement towards high frequencies.

Maximums (see Fig. 1) at frequencies from 10 to 50 kHz, corresponding to the process of defrosting segmental mobility in the studied films. The frequencies of the maximums at the dependences tgδ from f for modified LDPE shifted to the left, side of dipole-segmental losses on frequency scale, relative to the same dependence for unmodified sample. This fact is very significant, because it reinforces the increase in segmental mobility in the surface layers of LDPE modified by ethanediol-1, 2.

Dielectric permittivity LDPE depends on the presence therein polar groups (–C=O,–O–H et al.). With the advent and increasing in LDPE content the polar groups increasing dependence ε 'on frequency field. The nature of the changes of the dielectric constant with increasing frequency (Fig. 2) at 20 º C also shows the influence of ethanediol-1,2 on supramolecular structure of high pressure polyethylene.

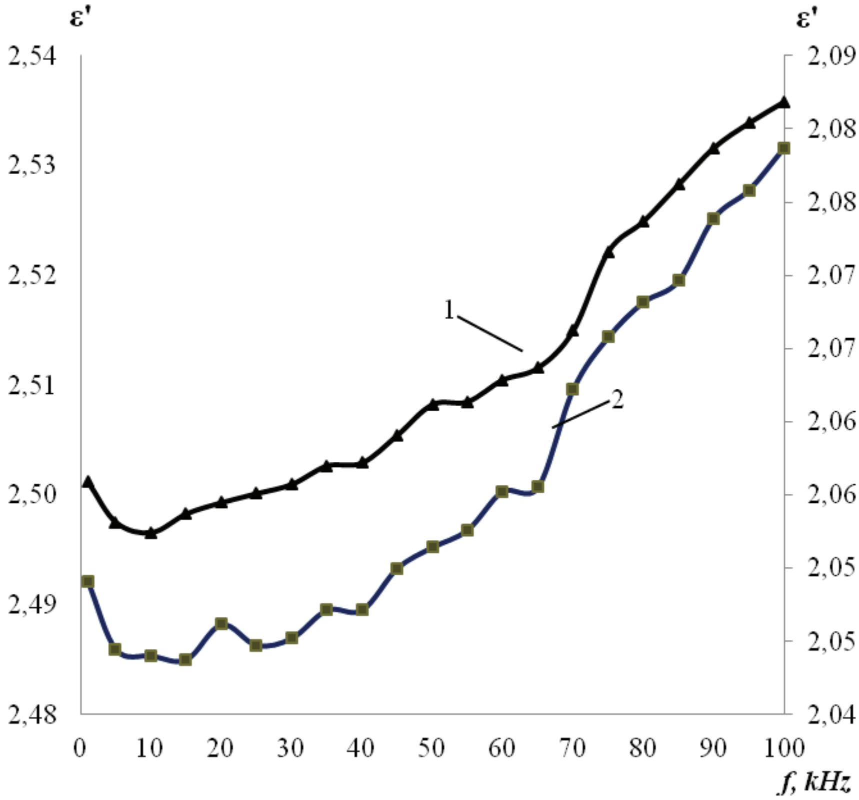

Figure 2. The dependence of the dielectric constant from frequency alternating electric field:
1 - LDPE 2 - LDPE with the addition of ethanediol-1,2.

The absolute value of ε 'for the modified sample is much lower than that observed for the whole dependence, with increasing frequency. The more polar asymmetric bonds in polymer are cause more shift the electron density, the higher its ε '.

In the obtained polymer samples observed several distinct relaxation processes, which are dielectric active and associated with the mobility of kinetic units. These relaxation processes are apparent in the frequency dependence of dielectric losses measured at constant temperature (Fig. 3). At the decrease of the frequency is gradually activated by different types of molecular motions and the associated dipoles.

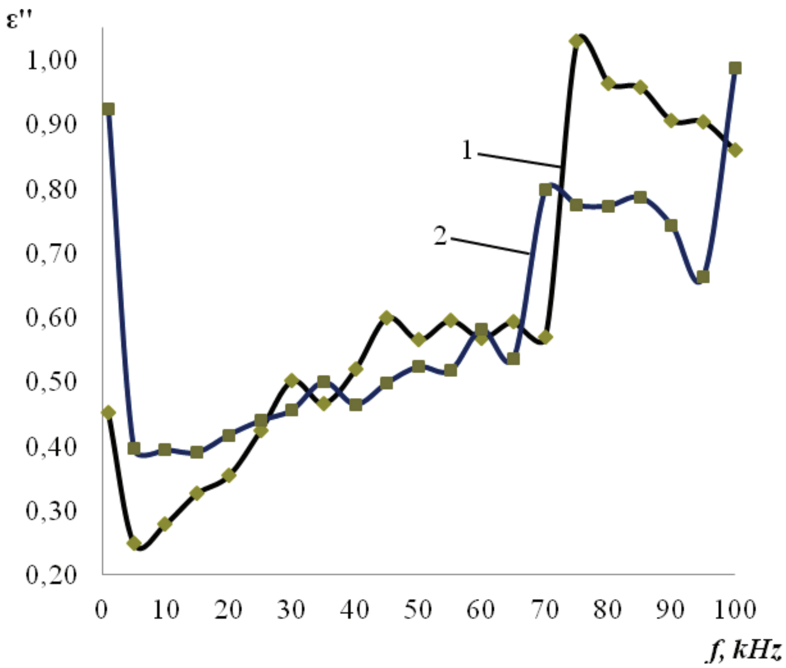

Figure 3. Dependence of dielectric loss from frequency alternating electric field:
1 - LDPE 2 - LDPE with the addition of ethandiol-1,2.

Complicated nature spectra of dielectric relaxation of polyethylene explained the presence of branching, which creating a pronounced relaxation processes associated with molecular motion at the point of branching, and presence crosslinks that significantly restrict some types of molecular motions.

Also decrease the value of dielectric losses, which contradicts the theory, which argues that the introduction of polar groups in nonpolar polymers - dielectric losses are increase, and try to reduce them by better cleaning of polymers from of polar impurities.

The dependence of resistivity and conductivity of composite materials based on HDPE frequency electric field is shown in Fig. 4.

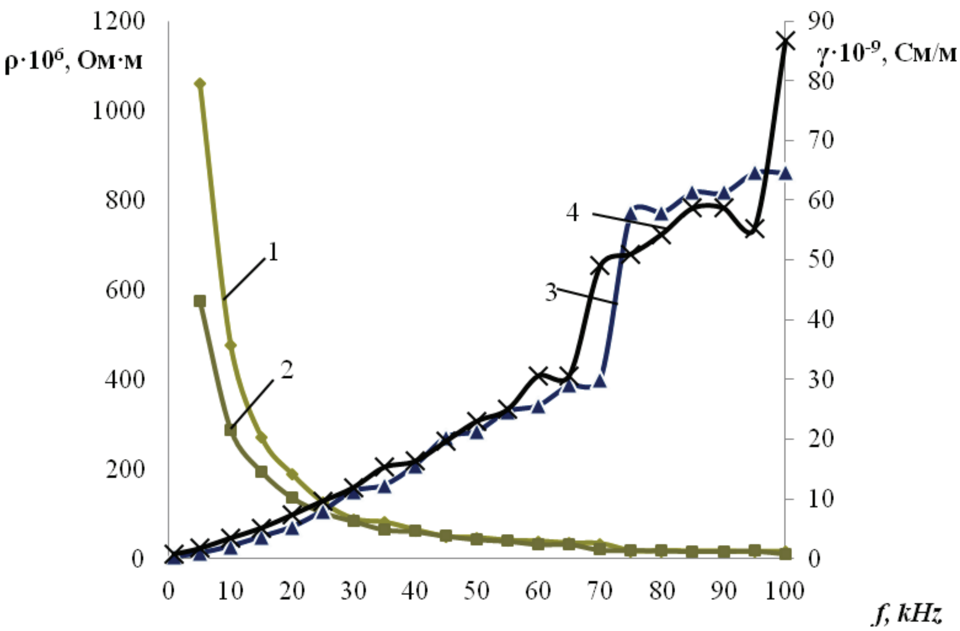

Figure 4. The dependence of resistivity (curve 1 - LDPE, curve 2 - LDPE with the addition of ethanediol-1,2) and conductivity (curve 3 - LDPE, curve 4 - LDPE with the addition of ethanediol-1,2) the frequency of the AC electric field.

From the analysis of induced dependence implies that in the investigated polymer samples based on LDPE and LDPE modified by ethanediol-1,2, with increasing frequency decreases resistivity and thus increasing conductivity. The presence in polyethylene of ethanediol-1,2 leads to a decrease in resistivity at lower frequency electric field. But with the frequency dependence of conductivity at frequencies from 74 kHz to 97 a decrease of conductivity of modified sample of LDPE compared to the unmodified.

Conclusions

Results of investigation of influence of ethanediol-1,2 in the polyethylene material at the change: the tangent of the angle of dielectric losses, permittivity, dielectric loss, resistivity and conductivity, showed that:

-ethanediol-1,2 reduces the mobility of side groups, shifting the maximum tgδ dipole-group losses towards lower frequencies, thus increasing the molecular mobility of the segments;

-the absolute value of the dielectric constant for the modified sample significantly below that observed in the whole dependence, with increasing frequency electric field;

-on the frequency dependence is observed decrease the value of dielectric loss for the modified sample of high pressure polyethylene;

-the presence in polyethylene of ethanediol-1,2 leads to a decrease in resistivity at low frequency electric field, but at high frequencies, a decrease of conductivity of modified sample of high pressure polyethylene compared to the unmodified.

Thus, all the results are as physical crosslinks polyethylene material, which is one way of modifying it, and leads to an increase in chemical, mechanical and thermal stability. Ethanediol-1,2, as a modifier, enters the physical interaction of macromolecules of polyethylene, crosslinking and supports a link between long chains due to electron clouds dissimilar charge on the macromolecules and crosslinking agent. Reduction in the dielectric constant, dielectric loss and conductivity (at high frequencies) is due to blocking and interaction of ethanediol-1, 2 with electronegative centers are generated branched structure of the polymer, due to oxidized groups, unsaturated bonds and methyl groups. Increase strength by adding ethanediol-1,2 due to increased mobility of supramolecular structures by passing an electric current oriented, which always promotes polymer.

References

1. *Ананьев В.В., Губанова М.И., Кирш И.А., Семенов Г.В., Казьмин Д.В.* Модификация полиэтилена, инициированная ультразвуком // Пластические массы – 2008. – №6. – С. 6-8.
2. *Гинзбург Б.М., Туйчиев Ш., Рашидов Д., Табаров С.Х., Суханова Т.Е.* Вылегжанина М.Э., Кутин А.А., Уголков В.Л. Влияние фуллерена C_{60} на структуру и механические свойства полиэтилена: технологический аспект // Высокомолекулярные соединения – 2011. – Т. 53. – № 6. – С. 883-896.
3. *Кулиев М.М.* Модификация свойств полиэтилена высокого давления добавками органической природы // Пластические массы – 2009. – №7. – С. 20-25.
4. *Поляков А.В., Дунтов Ф.И., Софиев А.Э.* Полиэтилен высокого давления. Научно-технические основы промышленного производства. – Л.: Химия, 1988. – 200 с.

UDC 621.352.6

I.I. Voytko, Kand.of Chem.Scien.; V.V. Babanov, student;
O.O. Zubriy, student; O.M. Kozlova, student
(National Aviation University, Ukraine)

SOME ASPECTS OF FUEL CELLS

This work provides literature data to improve solid oxide fuel cells by a direct methane fuel cell and electrode settings of uninterrupted space. The possibility of electrochemical generators SOFC as synthesis gas from natural gas. We describe progress in the creation of new nanomaterials for components SOFC and modern technologies for their manufacture. Briefly described features of the operation and use molten carbonate fuel cells and their accessories and SOFC in cogeneration system (three generation) energy and hybrid circuits.

Earlier, we had made an analytical review work on the fuel elements (FE), made to 2001 [1], the material is briefly described in the publication [2]. The purpose of this paper is to examine some of the later period of work relating mainly of solid oxide (SOFC) and molten carbonate (MCFC) fuel cells and electric power plants (EPP) at their base.

Considerable attention is presently paid to the development of direct methane SOFC [3]. From traditional, they differ in that they have fuel for methane directly, rather than synthesis gas obtained by selective oxidation, steam or gas autotermical conversion. Generation of electricity is a result of the deep oxidation of methane:

at the anode: $CH_4 + 4O^{2-} = CO_2 + 2H_2O + 8e^-$
at the cathode: $2O_2 + 8e^- = 4O^{2-}$

Due to the fact that direct methane SOFC off stage conversion of methane to higher efficiency than traditional SOFC, smaller size and simpler construction. The required anode resistant to cocking methane and which has a high electrochemical activity. This led to the replacement of nickel anode material for composite nanopowder involving zirconia and zirconium oxide (LSM).

Only a hundred years after the creation of traditional fuel cell with separated electrode spaces was proposed a simplified version - FC with uninterrupted electrode spaces. It's traditionally consists of two electrodes, but instead of resolving supply oxidant and reducing agent here in the anodic and cathodic spaces is identical in composition to the mixture. Of course it simplifies the design of FC, but makes new demands on the anode and cathode. They should have high catalytic activity towards deep oxidation reaction of fuel, as this will not remain on the electrodes of reagents, and IE stops working. At the same time the anode and cathode must exhibit activity for electrochemical oxidation of fuel and oxidant in the presence of electrochemical reduction of oxidant in the presence of fuel. Otherwise, the electromotive force of the fuel element is missing. This feature is provided by anodes based on Pt i Ni, in which a mixture of methane and air at first converted into synthesis gas, then N_2 and CO electrochemically oxidized to CO_2 and H_2O by ions O^{2-}. These ions are formed on the cathode material for them may be Ag, Au i LSM.

It seems development on the application of FC as electrochemical generators conversion of methane to synthesis gas, the cost of a traditional chemical methods of steam conversion of methane is very high. Greater interest is the high catalytic partial oxidation of methane by the reaction that is exothermic:

$CH_4 + 0{,}5\ O_2 = CO + 2H_2$.

Particularly noteworthy study of this process by means of electrochemical reactors in type SOFC:

CH_4, electrode-catalyst | YSZ | air electrode.

In these reactors, unlike conventional reactors for catalytic oxidation, the electrode-catalyst stream is methane, which contains no oxygen. Oxygen entering the reaction zone, generated directly by passing electric current through SOFC. In this case, the air electrode formed ions O^{2-} by the reaction:

$0{,}5O_2 + 2e^- = O^{2-}$,

are transferred through the solid electrolyte (YSZ) to the electrode-catalyst, where they oxidize methane:

$CH_4 + O^{2-} = CO + H_2 + 2e^-$.

This method of oxidation of methane to synthesis gas opens up new possibilities that can not be realized in the implementation of conventional catalytic reaction path.Thus, the electrochemical oxidation of methane can be obtained not only synthesis gas but also electricity, that the reactor can be operated using the FC. Reduces the likelihood of formation of explosive mixtures of methane and oxygen as the air divided solid electrolyte. Falls off the problem of branch products of the reaction of atmospheric nitrogen.

For the electrochemical oxidation of methane to synthesis gas can be used by water vapor and carbon dioxide, that is to carry out this reaction in reactors such as:

CH_4, electrode-catalyst | YSZ | electrode, H_2O or

CH_4, electrode-catalyst | YSZ | electrode, CO_2.

The success of the implementation of SOFC in many branches of engineering is impossible without improvement of production technologies and related materials.Today all technologies SOFC reduced to multiphasic (layer) structure forming element and followed by heat treatment multiple molded functional layers. This negatively affects the electrochemical characteristics of the element requires large energy consumption and stepwise control of the manufacturing process.

The solution to the problem can be used for the manufacture of SOFC nanodispersed powders, such as electrolyte-dioxide circus stabilized by yttrium oxide (YSZ), lanthanum manganite cathode-strontium (LSM), the anode-nickel cermets (Ni-YSZ) [3].

This opens up a number of significant opportunities. Firstly, the processes of sintering CDs nanopowders, unlike micron, occurring much more intense. It provides a dense ceramic materials in unconventional low temperature range, for example, YSZ - at 1100-1250 º C. Second, the solid electrolyte, resulting in lower temperature sintering is characterized by submicron structure and has a cleaner grain boundaries, which positively affects both its electrical and mechanical properties. Thirdly, the reduced firing temperature opens the possibility of co sintering multilayer structure without SOFC of products at the interface electrode / electrolyte, which adversely affect the properties of FC. Thus, in the laboratory developed technology manufacturing base tube SOFC-based electrolyte YSZ at once forming electrochemical structure "electrode-electrolyte-electrode" and subsequent sintering. On the basis of Nano components SOFC cast polymer-ceramic film thickness of 10-40 micrometers. Multi-piece for magnetic pulse compression rods formed in successive winding patterns of film components SOFC.

Seemed breakthrough invention Madrid University scientists FC, who works at room temperature. They went through the modification of known electrolyte YSZ, nanisshy on the surface layer of strontium titanate ($SrTiO_3$) 10 nanometers thick and upgrading the design of electrodes. Rozplavkarbonatni FC operating at temperatures of 600 - 750 ˚ C using an electrolyte Li_2CO_3 - Na_2CO_3. Melt can be in the free state, as a paste or in a matrix of porous ceramics, such as $LiAlO_2$. Anode material serves as nickel, chromium alloy, the cathode material - litiyovanyy oxide nickel. Advantages of MCFC are that the high operating temperature improves the kinetics of the reaction, which eliminates the need for noble metal catalyst. High temperature makes the cell less prone to carbon monoxide poisoning, which gives the opportunity to work on different fuels including solid after its internal cycle gasification. MCFC developed for electric power from a few kilowatts to several megawatts, operating on natural gas and coal. In Santa - Claire (USA) has working power plant capacity of 2 MW of electrical efficiency of 50%. However, if building in an MCFC in energy cogeneration system overall efficiency can be raised to 80 - 90% [8].

Currently pomyslovo developed countries undergo economic research service, quiet and environmentally clean electric power units (EPU) based SOFC and MCFC. The most successful development companies recognized joint Westinghouse (USA) and Siemens (Germany). On the basis of these producers created SOFC typical EEU for common generating heat and power capacity from 20 to 250 kW, operating on natural gas resource of over 20,000 hours, electrical efficiency of over 45% and overall efficiency of 80%. Coming experimental capacities of several megawatts. This cogeneration - the production of two forms of useful energy - electricity and heat - resulting in unprecedented for thermal power generation (35%) efficiency values. Particularly attractive is the so-called hybrid scheme in which vykorystovu.t electricity not only FC but also mikroturbin that utilize waste gas vysokotemperaturneteplo with FC. Low temperature heat can be used for heating, water, etc.. Cogeneration installations of this type of SOFC production company "Siemens Westinghouse" is set in Germany and Italy with 300 kW with overall thermal efficiency of 95%.

However, FC promising not only in the power and home and public services, but also in all kinds of transport, space and military technology, household appliances and more.An indication of the great future of FC was adoption by the European Union a new program of fuel cell technology. The program is designed for 7 years (from 2009 to 2015), its budget is 1 billion.

References

1. *Войтко І. І.* Пріоритетні напрямки використання паливних елементів в енергетиці. К. – 2002. 53с.

2. *Войтко І.І.* Вісник НАУ. – 2004. – №3 с. 107.

3. *Собянин В.А.* Высокотемпературные твердооксидные топливные элементы и конверсия метана: Ж. Рос.хим. инст. им Д.И.Менделеева, 2003, т.XLVII, №6.

UDC 54.678.5

A.U. Ostrogrud, Graduate student
(National Aviation University, Ukraine)

DIELECTRIC RESEARCH OF POLYISOPRENE MODIFIED BY CARBAMIDE

Conducted dielectric research of polyisoprene modification by polyacrylamide in the frequency range 1-100 kHz have shown the existence of increase or decrease in molecular mobility groups of atoms and cross-site segments of the mesh polyisoprene through the displacement of existing relaxation processes in the direction of high or low frequencies at various contents of polyacrylamide.

Introduction

Polyisoprene materials are widely used in various industries and in way of life.

Herewith in the science of polymers in recent years on one of the first place comes out the problem of creation of new polymer composites. It is materials based on polymers and fillers, organic and inorganic origin - the glass and synthetic fibers, aeros, silica, etc.

Development of scientific basis for obtaining such materials is fundamental important: it allows significantly expand the circle of polymer materials and the diversity of their features is based on the established and issued by industrial polymers. Of course, every time there is a need for a material with a new set of properties that can not be a new way to synthesize new polymers and to develop their production - it is a very complicated way, a long, expensive and not always crowned with success. Physical modification of existing polymers, their combination with substances of different origin, and the other structures - is one of the most promising ways to solve the problem. The other way - getting alloys of polymers similar how obtain alloys of metal. This is a new trend in polymer chemistry. On receipt of polymer alloys is closely tied with the problem - ligation polymers small additions of other polymers (also similar to how it is done in metallurgy). But in all these cases, the processes are very different from the processes that occur in metals.

The range of plastics and synthetic resins will expand through the development of new grades of polymerization oligomers, monomers, copolymers, and other types of compounds.

Maximum usage of polymeric materials will ensure solving of new challenges, improve product quality, increase labor productivity, and significantly increase the economic effect. In the future, the most important task of technological progress is the development of new high-yield technological process, obtaining large-tonnage polymers and on their basis - the creation of new materials by copolymerization, radiation, chemical, structuring modification, ligation, obtaining mixtures and composites. It is necessary to use new types of fibrous inorganic substances - the second major component of the component polymer composites.

In the future, will be widely applied not only to polymer composites, which today we might call traditional, but new ones - such as metal-based (sheeted and profiled metal products covered by polymers, polymer products with a metal frame, metal filled thermoplastics, etc.) Due to the fact that polymeric materials can give a different, often incompatible with the basic materials properties, the proportion of new polymeric materials will be more and more every year.

Up-to-date, the most common were leaf blades (PCB) based on the fabric, impregnated with synthetic resins, and glass - plastics, reinforced or filled with glass fiber. Among all types of plastics are the most massive fiberglass construction materials. They are mainly used in shipbuilding, transportation, construction, electrical, corrosion equipment.

Abroad and in our country has created a huge production, producing different types of materials based on both thermosets and thermoplastic binders. The basis of these productions is the fundamental studies of structure and properties of polymer compositions and processes taking place during the solidification of binder in the formation of polymeric materials. When designing and creating structures of these materials is very significant that virtually no stage of obtaining a composite material as such: it is always associated with the stage of formation of the finished product.

Advantages in using of modified polymers occur due to the significant increase in physical and mechanical characteristics of the material due to a combination of these properties of heterogeneous materials, decrease of polymers; reduce the cost of the material due to the introduction of non-deficient in its low-cost modifiers, in many cases, the possibility to use the essential technology and as a result this - the lack of significant capital expenditure, the possibility of using recycled polymer raw materials and polymer waste.

According to the information above, it was necessary to determine the effect of different contents of 8% polyacrylamide on to replace of dielectric relaxation. Therefore, the purpose of work is to investigate the high-frequency and low frequency relaxation processes of modified by polyacrylamide polyisoprene elastomers to evaluate the interactions of amino groups of polyacrylamide with negative charges, π- bonds and excess charges of polyisoprene and modifier.

Materials and methods

To investigate the influence of polyacrylamide on the properties of cross-linked polyisoprene materials here used natural rubber latex Revulteks and 8% polyacrylamide of factory production. Samples were prepared by thorough homogenization of polyacrylamide in the latex. The content of polyacrylamide was 1,3,4,6%. Polymerization was carried out with mixed compositions 85 ºC.

The investigation were conducted on the bridge AC R-5083 at frequencies of 1-100 kHz. Were conducted investigations of dielectric losses and permittivity modified by polyisoprene materials.

The results of experimental studies

Earlier studies were carried out temperature dependence of tgδ on the effect of low molecular weight additives on the reactionary behavior of the 8% polyacrylamide. The presence of the displacement of the relaxation of segments of macromolecules in the direction of higher temperatures, the dipole-group process - in the direction of lower temperatures - at the same time limiting the mobility of the segments due to the change in the total cross-site chain packing of the macromolecules, which facilitates the mobility of the groups. Of interest are the results to identify the dielectric losses of various concentrations of polyacrylamide in water. If the 9%-th aqueous solution of polyacrylamide in the temperature scale shows the main relaxation process at low temperatures, for a 19% polyacrylamide On this process even more mixed in the direction of low temperatures and a maximum of tgδ is much greater in magnitude, then the process of dry polyacrylamide relaxation appears at high temperature is very low intensity [1]. This shows that there is a dense packing of polyacrylamide between the macromolecular chains due to the interactions of groups – $CONH_2$ neighboring macromolecules, ie, there are no degrees of freedom of the kinetic relaxation oscillators, whereas in solutions of polyacrylamide create a free mobility of the macromolecular chains and their orientation when an electric field. In solutions of polyacrylamide water disrupts the interaction-creates the conditions of the relaxation behavior.

The peculiarity of the investigated mixed systems polyisoprene - polyacrylamide is that polyisoprene has negative p-bonds, which retard the electron density (electron cloud) and create super-charges (δ^-) with the simultaneous formation of excess charges (δ^+) groups of atoms monomer link, and amide groups polyacrylamide carbonyl pulls electron clouds are also forms heavy duty and excess charges. It should be noted that even in the presence of vulcanized polyisoprene π- bonds is reduced by 3-5%.

Since physical interactions are formed, -NH2(δ^+) with π -bond of one macromolecule polyisoprene, and the other macromolecule interacts polyisoprene π -bond with a positive molecular link polyacrylamide (δ^+), this leads to the fact that the macromolecule polyacrylamide whole or in part is located between the polyisoprene macromolecules, so the fact that the macromolecules of polyacrylamide are in the intermolecular space of polyisoprene with placing them on chain length of the macromolecules, the conditions for increasing the flexibility of macromolecules polyisoprene, which leads to an increase in the mobility of groups and segments of the polymer network.

The nature of physical interactions can be represented as follows:

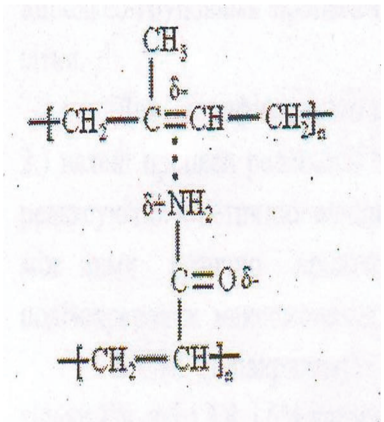

I. The interaction of the excess charge of nitrogen of the amide group with ties polyisoprene.

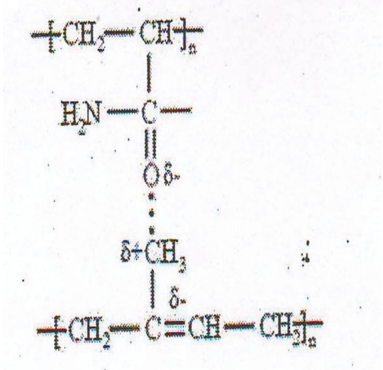

II. The interaction of the excess charge carbonyl amide group of polyacrylamide with excess charge of the CH_3 groups of polyisoprene.

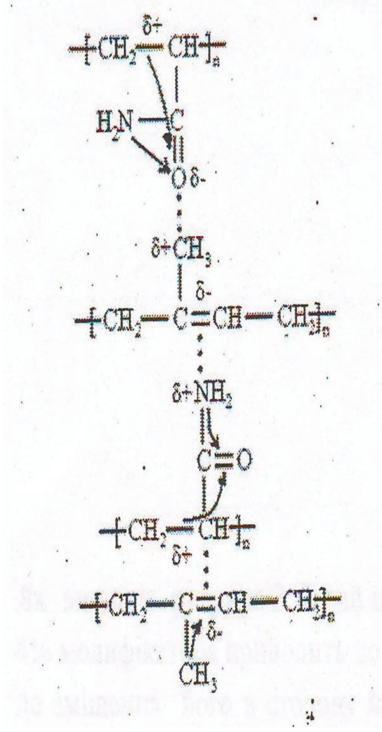

III. Interaction with macromolecules of polyacrylamide polyisoprene. Two of the macromolecule polyacrylamide takes a physical interaction with two molecules of polyisoprene.

Picture 1 shows the frequency dependence of dielectric loss for the output elastomer.

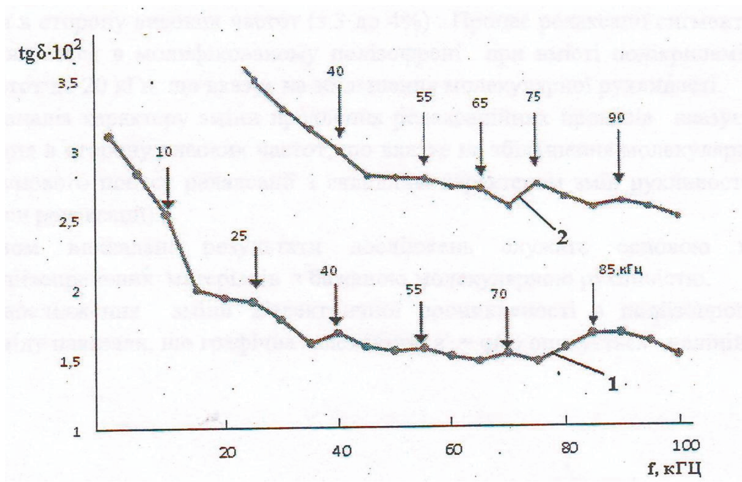

Picture 1. Frequency dependence of dielectric loss:
1 - polyisoprene, 2 - polyisoprene containing 1% polyacrylamide

As can be seen manifested six relaxation processes - with 85 kHz dipole-group, small quantities at 70 kHz groups of atoms larger in size compared to the first process. The relaxation process which manifests itself in the field of 55 kHz is the mean between the segments of the relaxation oscillator circuit and cross-site dipole-group relaxation processes. In areas 40, 27 and 10 kHz - manifesting segments of the polymer network.

For the modified polyisoprene material containing 1,0% polyacrylamide (Picture 1 - Curve 2, Picture 2). Relaxation processes are shifted to higher frequencies, i.e., increased molecular mobility of relaxing kinetic units due to increased free volume between molecules of polyisoprene and availability between physically interacting macromolecules of polyacrylamide, which formed a more flexible polyisoprene macromolecules.

Effect of polyacrylamide on the manifestations of change in the reclamation process is not only the content of polyacrylamide 1%, and 3.4%, and 6 illustrate in Picture 2.

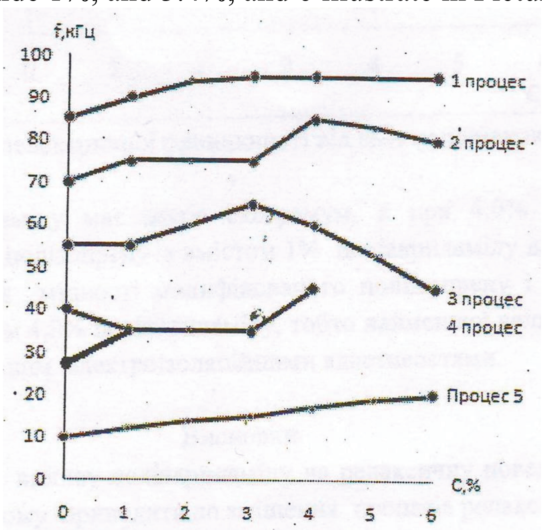

Picture 2. Depending on changes in frequency of occurrence of relaxation processes with different polyisoprene content of polyacrylamide

As seen in Picture 2, the second relaxation process with the content of 3% of the modifier almost is not mixed, but 4% of the modifier leads to a significant shift toward higher frequencies, 6% polyacrylamide shifts it toward lower frequencies. Segmental mobility of macromolecular chains of polyisoprene cross-site (27 kHz at 0%) shifted to higher frequencies (0-1%), and then remains constant (2 to 3%) and shifted to higher frequencies (from 3 to 4%). The process of relaxation of the segments of the net at 10 kHz (0% modifier) is shown in the modified polyisoprene when the content of 6% polyacrylamide with a shift to higher frequencies to 20 kHz, which indicates an increase in molecular mobility.

A general analysis of the change in manifestation of relaxation processes indicates that most of their shift is toward higher frequencies, which indicates an increase in molecular mobility of network segments and dipole-group relaxation process of the complex nature of changes in mobility relaxators mean values (2 and 3 of the relaxation process.)

Thus, the presented results of research are the basis for selection of modified polyacrylamide polyisoprene materials with the desired molecular mobility.

Conducted research of changes in the dielectric permeability of polyisoprene material containing polyacrylamide showed that the graphical dependence of ε'= φ (c) describes the nonlinear dependence.

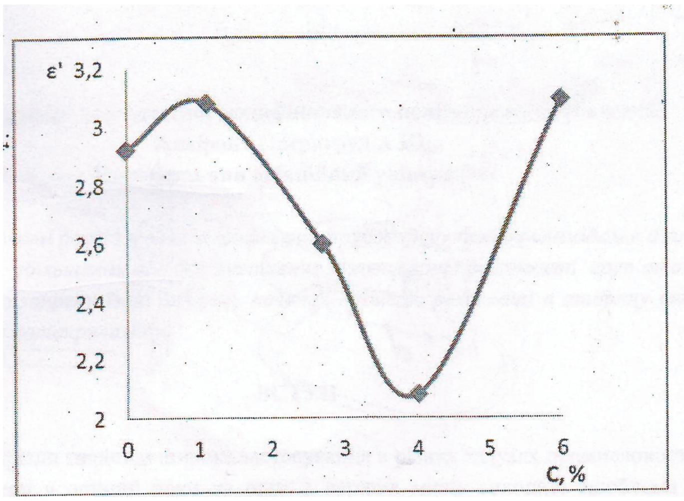

Picture 3. Dependence of the permittivity of the content of polyacrylamide in the polyisoprene

When the content of 1.0% polyacrylamide there is a extreme, and when the content of 4,0% -a deep minimum. High energy condition of the modified polyisoprene containing 1,0% polyacrilamide suggest the existence of a simultaneous increase in the strength of the modified polyisoprene and its linear elongation. Modified elastomer containing 4.0% polyacrylamide, i.e. the smallest value of e, has the lowest polarization and, therefore, high electrical insulating properties.

Conclusions

1. Investigated the effect of polyacrylamide on the relaxation of polyisoprene.

Established that polyacrylamide mostly leads to a shift of the relaxation to higher frequencies.

2. Found that polyacrylamide implemented in the intermolecular space of polyisoprene and the same way to create space between the macromolecules, and this leads to an increase in their flexibility and the conditions of the relationship of there groups with π-bonds of polyisoprene, with the possible partial increase in stiffness.

3. Conducted research of the dielectric constant is established that when the content of 4,0% polyacrylamide in the polyisoprene have the deep minimum ε'. This indicates that such a modified polyisoprene has the best insulating properties.

References

Fabulyak F.G. Molecular thermal motion in the surface layers of polymers. – Kiev: Naukova dumka, 1991, – 304 pages.

UDC 678,028 +66.085.3

T.G. Samarska, Assistant Professor, M.V. Lukomska, st., O.M. Melnyk st.
(National Aviation University, Ukraine)

STUDY OF SOME ADDITIVES ON PROCESS AROMATIC ACIDS CURING COMPOSITIONS BASED ON EPOXY RESIN ED-20

A study of the influence of supplements of some aromatic acids, the nature of solvent and temperature on the process of hardening of compositions based on epoxy resin ED - 20. The result is high quality polymer coating with a lower content of unbound epoxy groups and higher contents of gel fractions. Constructed according to the content of epoxy groups of unrelated temperature and gel fractions content in coatings on temperature. Experimental data indicate that the use of p-aminobenzoic acid as a catalyst for the hardening, acetonitrile as solvent, and raising the temperature to 80 ° C promotes the formation of crosslinked good spatial grid.

Due to the high chemical resistance of coatings and the ability to combine with many famous film forming substances epoxy oligomers today have a wide application in various industries [1].

The general lack diane epoxy resins in applying them as a basis for binding materials is their high viscosity, which strongly affects the manufacturability of epoxy binders. Also important drawback is their slow polymerization, which inhibits the production process. Therefore an important task is to develop compositions which are used as solvents in active compounds taking part in the formation of the spatial mesh and investigation of new catalytic additives that accelerate the processes of hardening [2,3].

Dominant position in the industry are epoxy resin based on 4,4 '-dyhidroksydyfenilpropan (Diana epoxy resin), which form after hardening polymers spatial structure [4]:

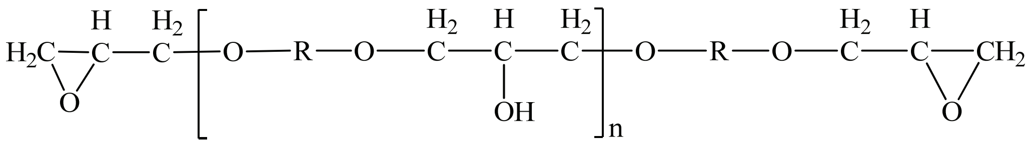

,

where R:

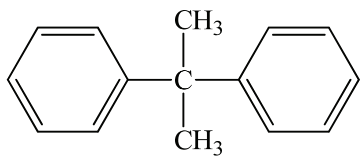

,

n – depending on the conditions of the process varies from 0 to 200.

Epoxy oligomers – reactive compounds that go into infusible and insoluble state only under retouching chalks. In some cases, during hardening involved than epoxy, and other functional groups such as hydroxyl [4].

The process of hardening epoxy compositions control the quantitative determination of unbound epoxy groups and the content of the gel – sol – fraction in the obtained coatings.

Experimental

The number of unbound epoxy groups in the original epoxy resins are:

$$X = 0{,}0043 \cdot (14{,}3 - 0{,}4) \cdot 100 \cdot \frac{0{,}1}{0{,}2220 \cdot 0{,}143} = 18{,}8\,\%$$

Defining the content of epoxy groups in epoxy resins investigated, we can conclude that this corresponds to GOST 10587-84 resin and is suitable for making polymer compositions.
For experiments were prepared composition of the next.

Table 1

The composition of paint compositions based on epoxy resins

№ composition	Components	Quantity, g	% component
1	pitch ED-20	10,050	71,3
	o-phenylenediamine	0,760	5,4
	aeros A-300	0,153	1,1
	acetonitrile	4 мл (3,131 г)	22,2
2	pitch ED-20	10,050	70,6
	o-phenylenediamine	0,760	5,3
	aeros A-300	0,153	1,1
	salicylic acid	0,149	1,0
	acetonitrile	4 мл (3,131 г)	22
3	pitch ED-20	5,0	62,3
	o-phenylenediamine	0,383	4,8
	aeros A-300	0,150	1,9
	salicylic acid	0,120	1,5
	ethanol	3 мл (2,37 г)	29,5
4	pitch ED-20	100	74,6
	o-phenylenediamine	7,6	5,7
	aeros A-300	1,5	1,2
	p-aminobenzoic acid	1,4	1,0
	acetonitrile	30 мл (23,484 г)	17,5

Continuation of the table 1

The study tracks the degree of hardening of the contents of unbound epoxy groups

After hardening of compositions analyzed the obtained coatings quantitative determination of unbound epoxy groups.

Based on studies of the compositions 1, 2 built graph of content unrelated groups X on the temperature T:

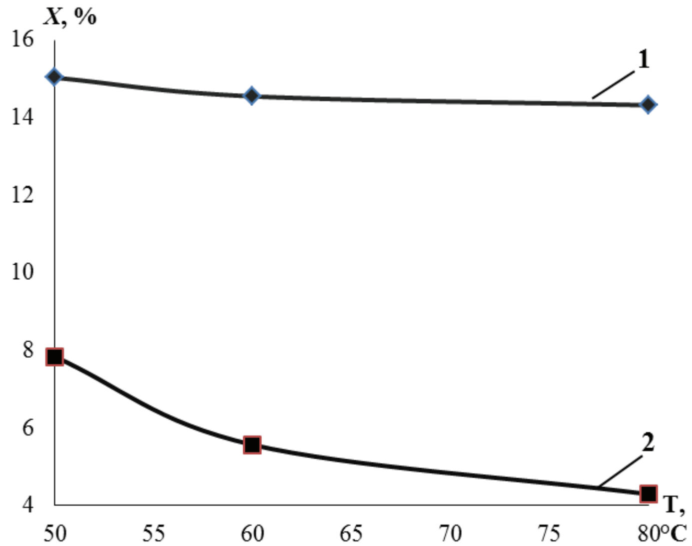

Fig. 1. Kinetic curve of the process of curing polymeric compositions based on epoxy pitch ED – 20. Solvent acetonitrile: 1 – a composition without the addition of salicylic acid; 2 – track 2 with the addition of salicylic acid (1.0%)

Based on the results of the experiment can be argued that salicylic acid is an effective catalyst for hardening compositions, since its use greatly reduces the number of unbound epoxy groups (curve 2).

With increasing temperature the process is more efficient. But without the addition of the catalyst process is inefficient because there are still many unrelated groups.

Based on studies of composition 3 constructed a graph of content unrelated groups X on the temperature T (Fig. 2).

Based on the experimental results show that ethanol affects the process of hardening compositions decreases as the number of unbound epoxy groups.

With increasing temperature the content of epoxy groups decreases from 19% to 18% (curve 1) and from 14% to 6% (curve 2), indicating a positive influence and its catalytic effect of salicylic acid.

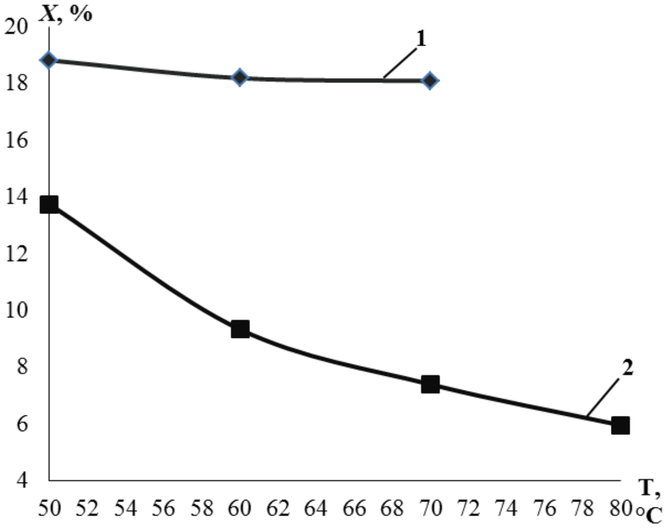

Fig. 2. Kinetic curve of the process of curing polymer composition 3, based on epoxy resin ED – 20.
Solvent ethanol: 1 – composition without the addition of salicylic acid;
2 – composition with the addition of salicylic acid

Based on studies of the compositions 1, 2 and 3 constructed a graph of groups of unrelated content X of temperature T for compositions with different solvents:

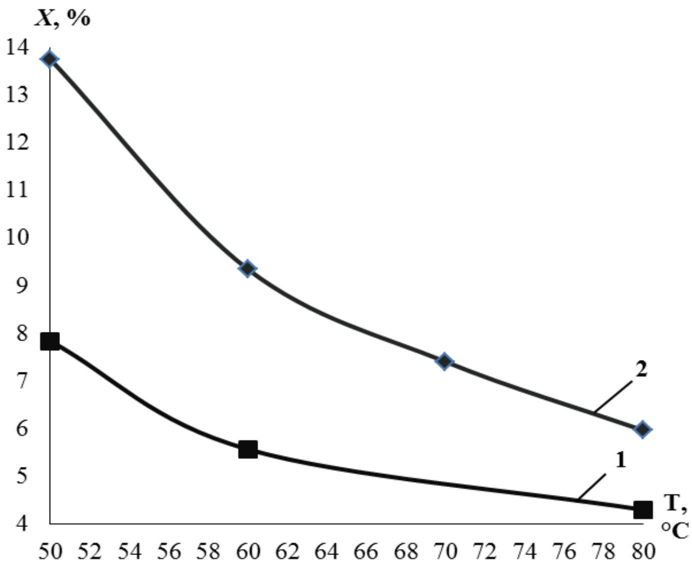

Fig. 3. The kinetic curve comparison process hardening of polymer composition:
1 – track 2. Solvent acetonitrile; 2 – Composition 3. Solvent ethanol

In tracing a number of epoxy groups varies from 8% to 4%, and curve 2 - varies from 14% to 6%. Hence we can conclude that the use of solvent composition in acetonitrile is smaller than the number of unbound epoxy groups, ie, its environment is better than curing in ethanol.

After hardening of composition 4 in the composition of which was added as catalytic additives sulfanilic acid remained adhesiveness of the surface layer, so it can be concluded that this acid can not be used as a catalyst for hardening epoxy compositions. In this case, further calculations were not carried out.

Based on studies of composition 5 constructed a graph of content unrelated groups X on the temperature T (fig. 4).

Based on the results, you can talk about the influence of para-aminobenzoic acid on hardening of the composition. With increasing temperature from 40 ° C to 80 ° C the number of unbound epoxy groups decreased from 13.6% to 5.4%, indicating the catalytic effect of para-aminobenzoic acid and the positive effect of temperature.

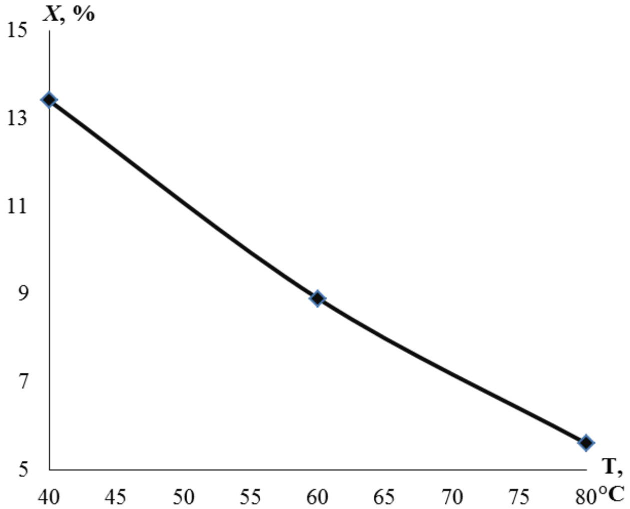

Fig. 4. Kinetic curve of the process of hardening of the polymer composition 4 with the addition of *p*-aminobenzoic acid. solvent acetonitrile

Investigation of sol-gel content in the compositions of fractions 1, 2, 3, 5.

Based on studies of coatings can be concluded that with increasing temperature decreases the percentage of sol-fractions and increased the percentage of gel fractions, indicating the significant effect of temperature on the efficiency of hardening of the composition.

Based on the data for the study of compositions constructed graph of the content of gel fraction on the temperature:

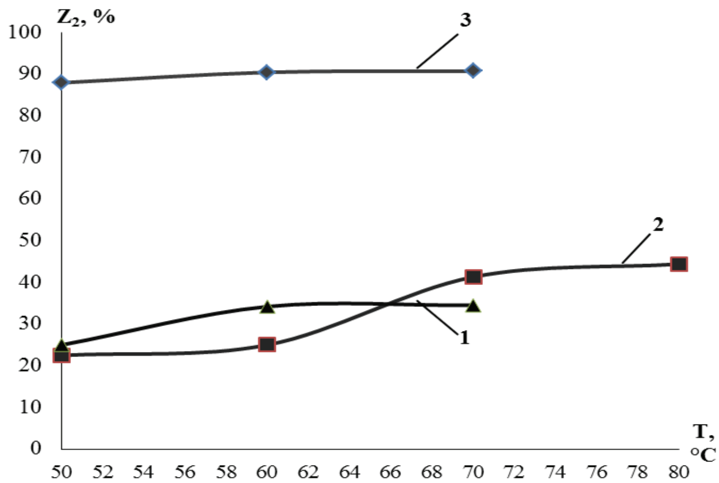

Fig. 5. Dependence of gel content in fractions of coatings obtained by hardening epoxy compositions on temperature:
1 – catalyst composition of salicylic acid, solvent acetonitrile;
2 – catalyst composition of salicylic acid, solvent ethanol; 3 – composition of the catalyst *p*-aminobenzoic acid, solvent acetonitrile

As seen from the data *p*-aminobenzoic acid promotes the formation of a high quality mesh structure of the polymer because of its surfaces formed using the highest content of gel fraction.

When comparing the coatings obtained from compositions based on solvent acetonitrile (curve 1) of the coatings obtained from compositions, comprising a solvent ethanol (curve 2), among the last produced more gel fractions. This is possible because in ethanol gel structure is formed with the participation of not only the epoxy group and hydroxyl group and carbon chain.

Conclusions

This work was the influence on the process of hardening epoxy resin compositions based on ED - 20 of some aromatic acids, the nature of solvent and temperature.

Hardening process studied by the content of residual epoxy groups by titration and determination of sol-gel fractions in the studied samples.

The process of hardening of compositions based on epoxy dian resin ED - 20 were carried out at temperatures of 40 ° C to 80 ° C in the presence of catalytic additives, salicylic acid and *p*-aminobenzoic acid, and among such solvents as ethanol and atsetonitril.

It was found that the least amount of unbound epoxy groups in the epoxy composition containing hardening at 80 ° C.

The process is most effective hardening occurs in the presence of *p*-aminobenzoic acid, the least efficient in the presence of sulfanilic acid. Intermediate place is salicylic acid.

In the environment of ethanol produced more gel fractions than in acetonitrile medium. It is believed that the use of ethanol produced different spatial structure involving not only epoxy groups, and hydroxyl groups. However, the use of acetonitrile as solvent, affects more effectively reduce the number of unbound epoxy groups in the composition based on epoxy resin as compared to ethanol.

So based on what was said above we can conclude that the use of *p*-aminobenzoic acid as a catalyst for the hardening, acetonitrile as solvent and increasing the temperature to 80 ° C promotes the formation of crosslinked good spatial grid.

References

1. *Бобелев В.А., Еселев А. Д.* Специальные эпоксидные смолы для клеев и герметиков // Композитный мир. – 2006. – №7. – С. 8-11.

2. *Туисов А.Г., Белоусов А.М.* Модификация эпоксидного связующего для стеклопластиков активным разбавителем Э181 // Ползуновский вестник. – 2007. – № 4. – С. 183-185.

3. *Гулиев К.Г. , Ищенко Н.Я., Нагиева А.А., Агаева С.А.* Модификация ЭД–20 эпокси- и циклопропансодержащими соединениями // Пластические массы. – 2007. – №7. – С. 22-27.

4. *Сорокин М.Ф.*, *Кочнова З.А.*, *Шоде Л.Г.* Химия и технология плёнкообразующих.

5. Лакофарбові матеріали цільового призначення: лабораторний практикум. / уклад.: *Іванов С.В., Самарська Т.Г.* – К.: НАУ-друк, 2009. – 52 с.

UDK 66 2.765 (043.2)

Evgeny F. Novoselov, candidate of chemistry;
Yaroslav Utchenko, student (National Aviation University, Ukraine)

BIOFUEL-PETROLEUM FUEL BLENDS RESEARCH

A research of performance properties of the fuel mixture of methyl estere of rape oil (MERO) with mineral diesel fuel in different percentages have been conducted and presented. It was determined that the optimal performance characteristic of the fuel mixture is near 30%. On the basis of the experimental data can be offered a state standard mixture consisting of 30% vol. MERO and 70% vol. off petroleum diesel fuel

We have studied the blends properties of petroleum derived diesel fuel and most popular kind of introduced into practice biofuel – “biodiesel”. Biodiesel is an environmentally friendly type of biofuels; it is produced from vegetable oil or animal fat and used to replace petroleum diesel fuel. From a chemical point of view it is a mixture of methyl and / or ethyl esters of long chained fatty acids (saturated and unsaturated).

Biodiesel appears as yellow, moderately viscous liquid, it almost does not mix with water, has a high boiling point and low pressure of saturated vapors. Made of uncontaminated raw materials biodiesel is nontoxic. It has relatively high flash temperature of 150 °C, which makes this fuel relatively fire safe.

Biodiesel is characterized by such parameters as viscosity, density, cetane number, cloud point and pour point, flash point, ash content, sulfur content, acid number.

Our studies have been conducted in order to determine some performance properties of the fuel mixture of biofuel (methyl esters of rape oil , MERO) with mineral diesel fuel in different percentages. It was determined that the optimal performance characteristic has the fuel mixture B30. So, on the basis of the experimental data it can be offered a state standard mixture consisting of 30% vol. MERO and 70% vol. of petroleum diesel fuel.

Preparation of fuel mixture of diesel mineral fuel with a biodiesel was conducted in the laboratory by gradual addition of petroleum diesel fuel to a definite volume of biodiesel (methyl esters of rape oil MERO) and subsequent shaking during 1 – 2 min. The volumes of fuel were measured with a burette. As a result of mixing there were prepared fuel mixtures B0, B10, B30, B50, B70, B90, B100 . Results are presented in table 1.

Table 1

Preparation of fuel mixtures of biodiesel MERO with an petroleum diesel fuel (DF)

Biodiesel, % / DF, %	0	10	30	50	70	90	100
100	B0	-	-	-	-	-	-
90	-	B10	-	-	-	-	-
70	-	-	B30	-	-	-	-
50	-	-	-	B50	-	-	-
30	-	-	-	-	B70	-	-
10	-	-	-	-	-	B90	-
0	-	-	-	-	-	-	B100

Viscosity study of fuel mixtures B0 -B100

Measuring of viscosity of the prepared fuel mixtures was executed on viscosimeter Ostwald with the diameter of capillary tube 0,62 mm. The recalculation of the time of effluence of fuel through a capillary on viscosity was carried out on a formula, according to the passport of viscosimeter:

$$\nu = \frac{g}{980.7} \cdot \tau.$$

ν – Kinematics viscosity, sSt;
τ – time of effluence, s;
g – acceleration, м/s^2.

Experimental data of recalculation the τ onto viscosity are given in tabl.2.

Table 2

Viscosity of MERO mixtures with a mineral diesel fuel in different ratios for temperature 20 ^oC

Content of methyl ester in blend with mineral DF , %	Viscosity m,sSt	Time of effluence of fuel τ, min.
0	3,7	6,19
10	3,8	6,3
30	4,5	7,43
50	5,4	9,04
70	6,8	11,37
90	8,5	14,1
100	9,3	15,56

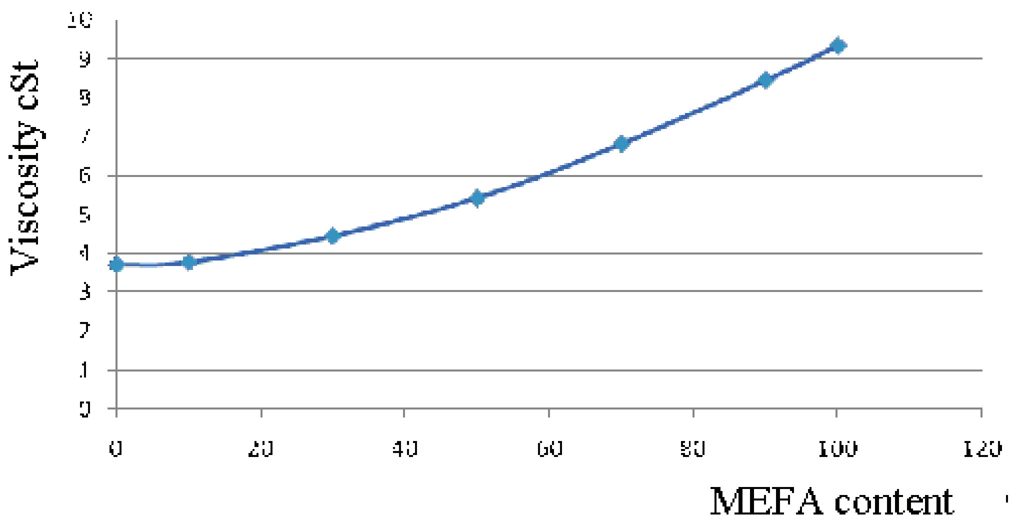

Fig. 1 Dependence of viscosity of MERO mixtures with DF at different content of methyl ester (0, 10, 30, 50, 70, 90, 100 % at.)

The curve of dependence of viscosity of MERO content is shown on fig.1. Linearity was observed starting from B30. Viscosity obviously grows with the increase of content of biodizel fuel. Untill addition of biodizelya up to 10 %, a substantial influence on the change of viscosity was not observed.

Study of density of mixtures B0, B0, B30, B50, B70, B90, B100

Measuring of density was carried out by an areometric method (oil densimetr). The results of experiment are presented in tabl.3.

Table 3

Dependence of density of mixture of mineral DF with MERO from content of methyl ester for temperatures 20,5 °C

Content of methyl esters in mineral DF	Density ρ, g/cm^3
0	0,825
10	0,830
30	0,842
50	0,855
70	0,867
90	0,878
100	0,886

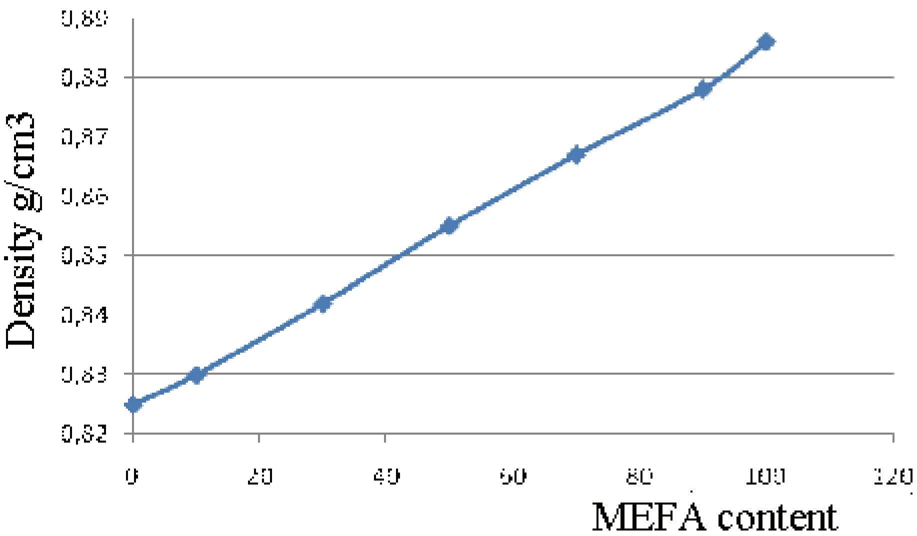

Fig. 2 Dependence of density of mixture of mineral DF with MERO from content of methyl ester for temperatures 20,5eS

On Fig. 2 is shown dependence of density on content MERO in a mineral diesel fuel. It is linear dependence. Density is an important index in fuel application. According density measurement (in relation to fuel mixtures) it is possible to define the percentage of biodizel fuel in a mineral diesel fuel as by an express-method.

Determination and study of cetane number for fuel mixtures BV0-B100

In the given work the cetane number of fuel was determined by an empiric method. There is dependence between density and viscosity of petroleum product and cetane number. This dependence is presented by equation:

$$ЦЧ = \frac{(\nu_{20} + 17,8) \cdot 1,5879}{\rho_4^{20}}$$

де ρ_4^{20} - relative density of fuel at 20eS, that is determined experimentally;
ν - kinematics viscosity of diesel fuel at 20eS, definite experimentally by means viscosimeter.

The calculated values of cetane number are presented in tabl. 4. It is seen that by addition of biodizel fuel MERO it is possible substantially promote the cetane number of a blend.

Table 4

Cetane number of fuel mixtures, calculated in relation to ρ and μ

Content of methyl esters in mineral DF	Density ρ, g/cm^3	Viscosity μ, cSt	CN
0	0,825	3,7	41,38
10	0,830	3,8	41,32
30	0,842	4,5	42,05
50	0,855	5,4	43,08
70	0,867	6,8	45,05
90	0,878	8,5	47,56
100	0,886	9,3	48,56

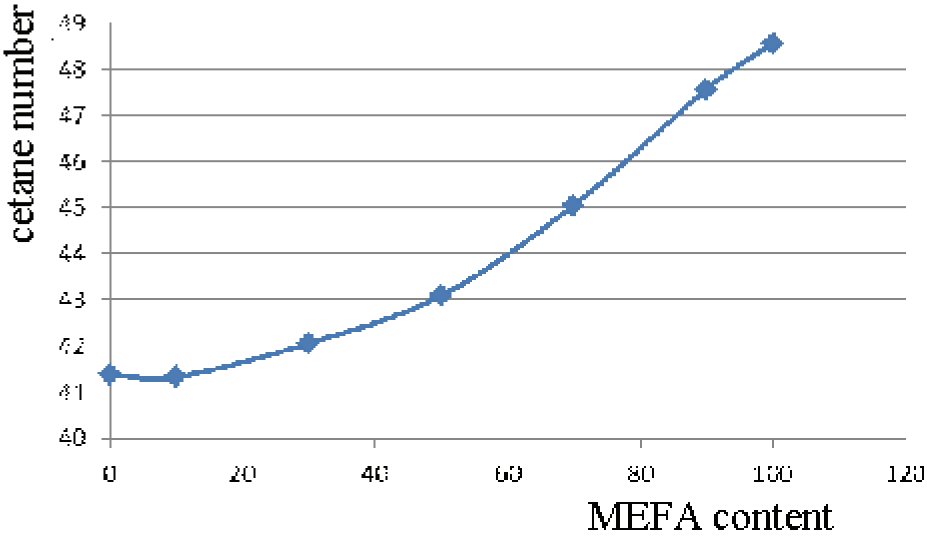

Fig. 3 Growths of cetane number depending on the increase of content of biodizelya in a fuel mixture

From the curves position it is seen, that biodiesel addition in a quantity 10 % does not affect cetane number. The rise of cetane number is observed in mixtures with greater content of biodiesel.

Research of temperature of freezing (pour point) of fuel mixtures

Table 5

Temperature of freezing of MERO mixtures with a mineral diesel fuel in different ratios

Content of methyl ester in mineral DF %	Temperature of freezing (pour point) oC
0	-15
10	-13
30	-15
50	-15
70	-10
90	-8
100	-8

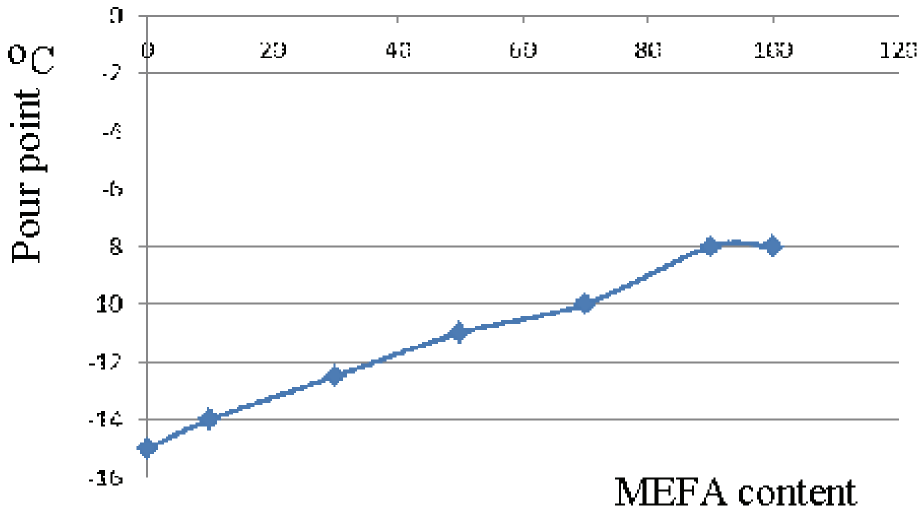

Fig. 4. Temperature of freezing of MERO mixtures with DF at different content of methyl ester (0, 10, 30, 50, 70, 90, 100 %)

Study of irelationship between viscosity and density for the mixtures of DF with MERO at different ratios

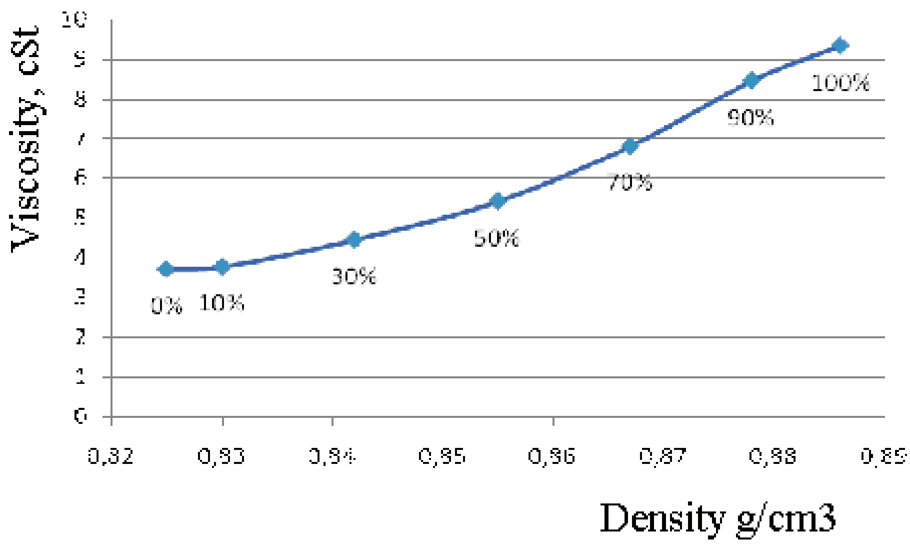

Fig. 5. Relationshiop between viscosity and density for the mixtures of DF with MERO at different ratios

Conclusions

As a result of our studies, were determined characteristic changes in parameters such as viscosity, density, cetane number and the freezing point of fuel mixtures B0, B10, B30, B50, B70, B90, B100.

Addition of MERO increases viscosity characteristics of diesel fuels; but up to 10% does not affect the viscosity . Linearity of this parameter is observed starting from 30%.

Dependence of density of the fuel mixture on the MERO content in diesel fuels blends is described by linear equations. The density is growing in the range B0 - B100 biodiesel additive - With increasing of MERO content cetane number of fuel blends also grows.

Biodiesel additive up to 10% MERO does not effect the cetane number – its increase observed for mixtures B12 - B100. Pour point increases with MERO content grows in blends while the pour point B90-B100 remains in the same range.

UDC 661.723.63:544.344 (045)

T.A. Haievska, assistant; I.V. Olshevsky, post graduate;
Yu.V. Bilokopitov, Dr.Sci. (National Aviation University, Ukraine)

INVESTIGATION OF THE MECHANISM OF HETEROGENEOUS-CATALYTIC OXIDATION OF 1,1,1- AND 1,1,2-TRICHLOROETHANE BY MASS-SPECTROMETRY

Formation of intermediate products of interaction of 1,1,1 - and 1,1,2-trichloroethane with the surface of chromium (III)oxide in the process of oxidation was investigated. Found, that on the surface of chromium oxide proceeds a sequential destruction of molecules with the break of C-C bond and formation of two dissimilar parts that form later at raising temperature formiates and carboxylate compounds attached to the surface with different force.

Industry of organochlorine compounds was continuously developed over the past 40 years. Increasing capacity of organochlorines production, expanding the scale of their use, resistance of these compounds to biodecomposition have become the factors of its accumulation in the environment [1-2]. Enterprises of organochlorines synthesis produce annually about 1.5 million tons of high toxicity waste [2]. Today these productions waste are incinerated. This leads not only to the loss of raw materials, but also to compounds containing chlorine pollutions, dangerous to human health. Thus, there is an urgent requirement for an economically justified utilization and disposal of hazardous organochlorine wastes. Now to solve these problems, one of the best way can become a research of catalytic processes of such waste disposal.

Today, the only obstacle to the introduction of catalytic methods for disposal of containing chlorine waste is the lack of sustainable active catalysts. Catalysts based on noble metals [3] show higher activity in reactions of chlorine containing compounds deep oxidation as compared with oxide catalysts. However, their disadvantages are high cost and short time of active work because of rapid deactivation. The advantage of oxide catalysts compared to catalysts based on noble metals is their higher stability and lower cost.

One of wastes at organochlorine production is trichloroethane. Therefore, we have investigated the formation of intermediate products of interaction of 1,1,1 - and 1,1,2-trichloroethane on one of the oxide catalysts for oxidation of these compounds – on chromium (III) oxide.

The study of interaction of 1,1,1 - and 1,1,2-trichloroethane with the surface of chromium oxide was carried out by programmed thermodesorption with the mass spectrometric analysis of products.

Experiments were performed on the experimental setup, the schematic diagram of which is shown in Figure 1. Installation consists of three main blocks:

1) absorption unit, at which is preparing the sample for adsorption of chloroalkane and its following adsorption.

This unit includes a vacuum system and diffusion pumps

1 – forvacuum pump, 2 – sensor of vacuum, 13 – trap with liquid nitrogen, 2, 6 – vacuum sensors, 3,4 – electric valve, 5 – forbaloon, 7, 8 , 9, 12, 16, 17, 18, 19, 23, 24 – valves, 10 – analyzer; 11 – funnel for supplying of liquid nitrogen, 14 – diffusion pump, 15 – oven of diffusion pump, 20, 21 – cuvette, 25 – three-way valve, 26 – mercury manometer;

2) block for programmed heating of the catalyst sample, which includes the oven 22 and the device for linear temperature elevation speed programming;

3) analyzer unit, which includes analyzer mass spectrometer 10 and the computer unit which records the data.

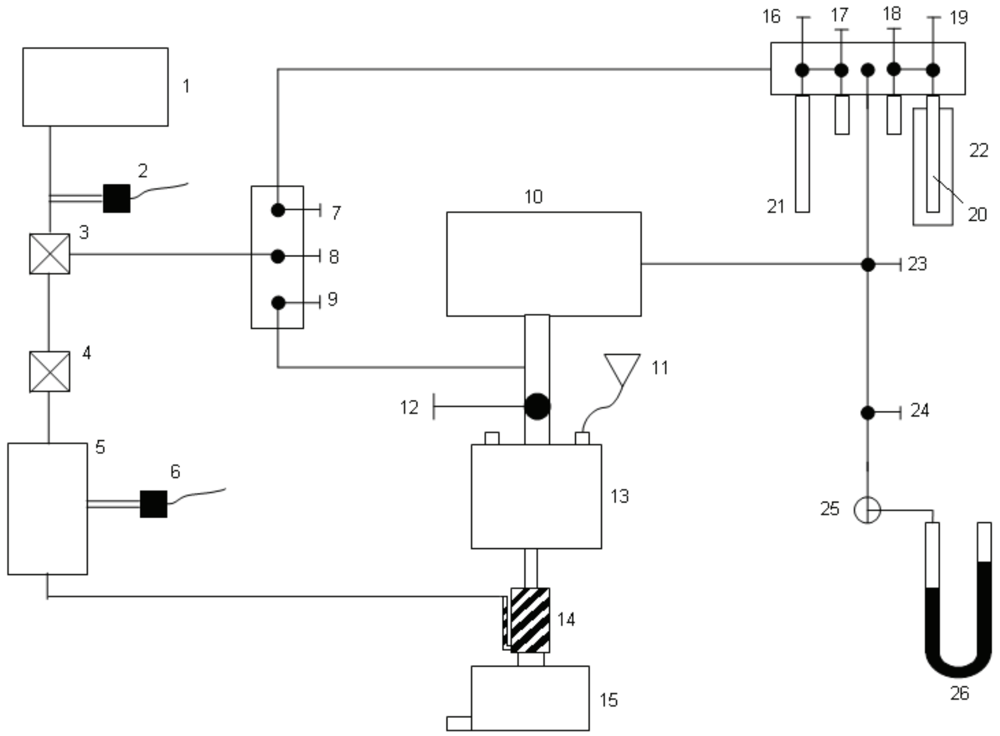

Figure 1. Schematic diagram of the setup for chloroalkanes investigation by programmed thermodesorption method with mass spectrometric analysis of products:
1 – vacuum pump, 2 – vacuum sensor, 3,4 – electric valve, 5 – forbaloon 6 – vacuum sensor, 7, 9, 12, 16, 17, 18, 19, 23, 24 - valves, 10 – mass analyzer , 11 – funnel for supplying of liquid nitrogen, 13 – trap, 14 – diffusion pump, 15 – oven of diffusion pump, 20 – experimental cuvette, 21 – cuvette for the adsorption of adsorbate; 22 – oven with programmable heating, 25 – three-way valve, 26 – mercury manometer

Sample of catalyst Cr_2O_3 was placed in the cuvette 20, from which with a vacuum pump was pumped out the air through the open solenoid valve 3 and via the open valves, 8, 7 and 18. To achieve the high vacuum (10^{-5} mm Hg) in the cuvette 20 were used diffusion pump 13 at a closed valve 8 and opened valves 12, 9, 7 and 18.

Before the adsorption of chloroalkane, the Cr_2O_3 catalyst sample was specially prepared by cleaning of its surface from substances sorbed from the atmosphere . For this purpose the model catalyst vere heated in pure oxygen at 600 ºC, followed by evacuation at pressure of 10^{-5} mm Hg.

The sample surface was considered clean, when from it were not desorbed any substance and therefore in the mass spectrum were absent any signals corresponding to the masses of the substances (except oxygen). Then the temperature of the sample was reduced to the temperature of adsorption and were made 1,1,1-trichloroethane or 1,1,2-trichloroethane injection into cuvette 20 , following the keeping of the sample in theirs atmosphere for 30 minutes.

At this time there occurred interaction between 1,1,1-trichloroethane or 1,1,2-trichloroethane with the surface of Cr_2O_3 with a formation of intermediate compounds which at a temperature of adsorbtion are not desorbed from the surface.

In the cuvette 21 was placed 1,1,2-trichloroethane adsorbate (or 1,1,1-trichloroethane) for ith further adsorption on the catalyst. To remove air from the adsorbate it was frozen with liquid nitrogen and from the mercury manometer 26 it air was evacuated through the opened valves 24, 7, 8, 3 (while valves 9 and 23 were closed). After chloroalkane thawing in cuvette 21, the vapors of adsorbate via the dosing valve 16 were injected into the cuvette 20, where the catalyst was held. The quantity of chloroalkane was controlled by the mercury manometer 26 (with the valves 7, 8, 9, 23 closed) and valve 24 - open. A vapor of adsorbate in contact with Cr_2O_3 was kept for 30 min at a given temperature of adsorption, and then at the same temperature the cuvette was evacuated to remove gas phase of the adsorbate. After some time, when were reached vacuum 10^{-5} mm Hg in the cuvette 20 , there was recorded the mass spectra of the products that were eliminated from the cuvette 20 and in case of their absence a rise in temperature of the sample was began by means of the oven 22 at a linear speed of 5 ºC /min. (control was carried out by recording the temperature vis. time with the the potentiometer.) from 30 ºC to 500 ºC. The products of thermodesorption via the open valves 18, 23 were injected into the analyzer of mass spectrometer while the valves 24, 17, 16, 9, 8, 7 were closed. Mass spectrum in the mass range from 4 to 150 was recorded in one second time and numerical values obtained were memorized in the computer. After reaching temperature of 600 ºC the experiment was complet and termodesorbtion spectra for the same sample weights in dependance on temperature were built. Results are shown in Figure 2, 3.

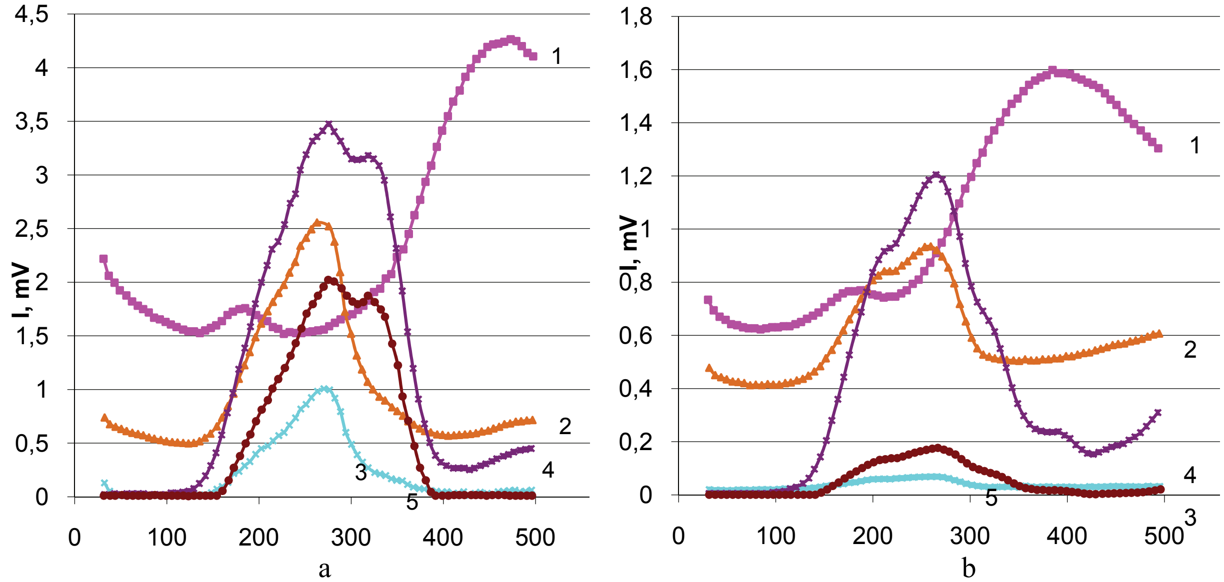

Figure 2. Thermal desorbtion spectra of 1,1,1-trichloroethane (a) and 1,1,2-trichloroethane (b) from the surface of chromium oxide at a temperature 120 ºC: *1* – water (m / z = 17 and 18), 2 – CO (m / z = 28), 3 – formiate compound (m / z = 29, intermediate), 4 – CO_2 (m / z = 44), 5 – carboxylate structure (m / z = 45, intermediate)

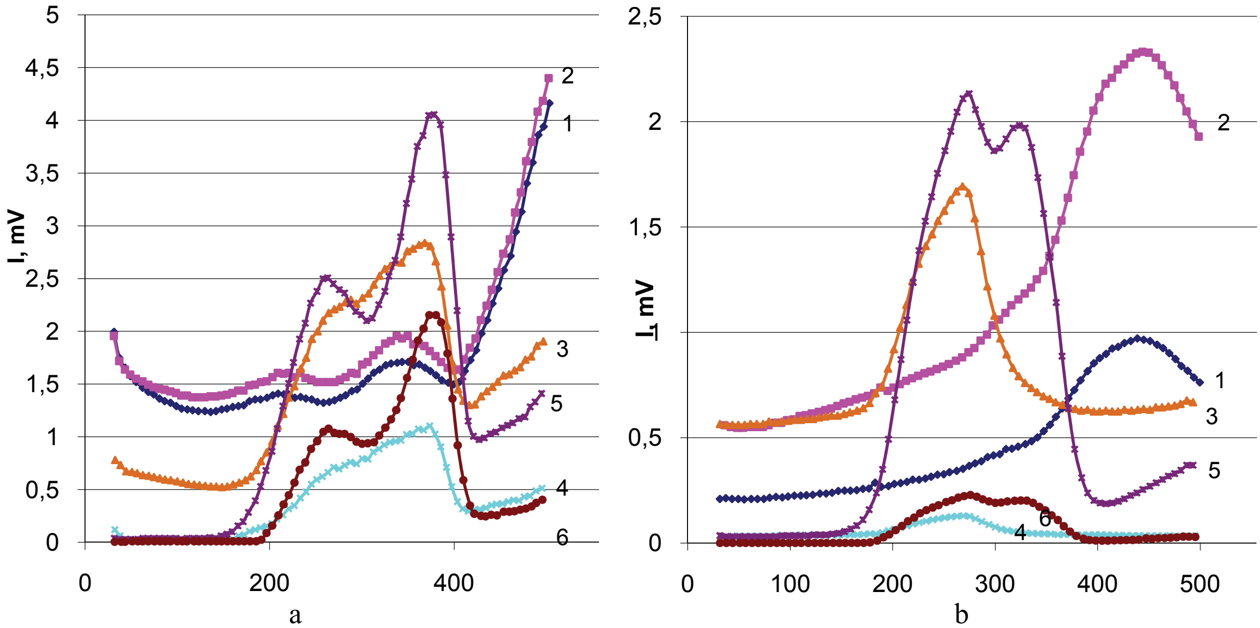

Figure 3. Thermal desorbtion spectra of 1,1,1-trichloroethane (a) and 1,1,2-trichloroethane (b) from the surface of chromium oxide at temperature of 150 ºC: 1 – water (m / z = 17 and 18), 2 – CO (m / z = 28), 3 – formiate compound (m / z = 29, intermediate), 4 – CO_2 (m / z = 44), 5 – carboxylate structure (m / z = 45, intermediate)

It is seen that from the catalyst surface are desorbed intermediate compounds with masses 17, 18, 28, 29, 44 and 45. These masses can be attributed to the following products: 1 – water (17, 18), 2 – CO (28), 3 – formiate compound (29), 4 – CO_2 (44), 5 – carboxylate structure (45). These masses peaks have several shoulders in the spectrum of thermodesorption. It can be explained by the fact that, probably on the surface of chromium oxide occures asequential destruction of molecules with the break of C-C bond and of two dissimilar parts (Figure 4) formation, which later form in the process of raising of temperature formiate 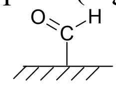 and carboxylate 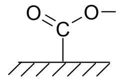 compounds with different strength of attachment to the surface.

a b

Fig.4. Possible intermediate compounds on the oxidation catalyst Cr_2O_3 surface , at destruction of 1,1,1-trichloroethane (a) and 1,1,2-trichloroethane (b)

It is seen that those spectra are slightly displaced according the temperature due to the destruction of some surface compounds and theirs transition into anothers.

Conclusions

The studies have indicated on phasic nature of the oxidation of 1,1,1-trichloroethane and 1,1,2-trichloroethane on the catalyst surface including a rupture of the C-C bond and subsequent transformation through formiate, carboxylate compounds .

References

1. *Занавескин Л.Н.* Окислительные методы переработки и детоксикации хлорорганических отходов. Курс на ресурсосбережение и экологическую безопасность // Химическая промышленность / Л. Н. Занавескин, О. А. Конорев, В. А. Аверьянов. — 2002, —№2, —С. 1—17.
2. *Курта С.А.* Вивчення дегідрохлорування хлорорганічних відходів на границі розділу фаз // Фізика і хімія твердого тіла / С. А. Курта, О.Ю. Закржевський, О. С. Курта. — 2006. — Т. 7. — № 3. — С. 523—526.
3. *Pinard L.* Oxidation of chlorinated hydrocarbons over Pt zeolite catalysts 1-mechanism of dichloromethane transformation over PtNaY catalysts // Journal of Catalysis / L. Pinard, J. Mijoin, P. Magnoux, M. Guisnet. — 2003. — V. 215. — P. 234—244.

UDC 66.091 (043.2)

N. Manchuk, cand.; E. Bagley, postgraduate student
(National Aviation University, Ukraine)

ADSORPTIONAL REMOVAL OF VANADIUM FROM HYDROCARBON SYSTEMS IN NATURAL MINERALS – LOESS

In this paperis studied the use of clay mineral - loess, as a sorbent in adsorption process of demetallization of oil and petroleum products. Sorption of vanadium was carried out on model hydrocarbon systems with a clay mineral - loess. In experimental studies were found that the loess has a high adsorption efficiency for the removal of vanadium from hydrocarbon systems. The experimental data can be used in further studies, using it as a contact material for removing metals from crude oil and heavy oil residues in the process of adsorptional demetallization.

In the global trend of increasing consumption of petroleum and petroleum refining industry further development is aimed at increasing of the depth of oil refining [1].

It should be noted that at least 60 % of the initial amount of oil remains in the subsoil, sealed in the pore space. Especially thick oil, which is heavy oil (bitumen, tar) can be extracted only by mine.

Were discovered sufficiently large reserves of tar sands (Canada, USA, CIS, Hungary). It is believed that the potential reserves of heavy oil and tar sands are approximately equal to the potential of crude oil with natural gas. Tar sands and heavy oil are considered a promising source of high-quality petroleum products. However there is a need for a new, less energy-intensive refining technology [2].

To solve such a problem is possible only through the widespread introduction of new cost-effective technologies of deep processing of heavy hydrocarbons containing asphaltenes in their composition and also heavy metals (vanadium and nickel), such as heavy oil, tar, heavy oil, etc.

Today in the oil found more than 60 trace elements, of which the most important and studied is vanadium, although its content in the raw material is low (10^{-6} – 10^{-2} %), it has a negative influence on many catalytic processes of oil refining. Considering the low content of vanadium in the ores (< 1500 g/t), its extraction from petroleum and petroleum products is very promising. The problem of studying the composition of trace elements of petroleum and petroleum products and to develop methods of extraction was studied for a long time. In connection with the depletion of light crude oils there apeears a serious problem associated with the production, transportation and processing of heavy oils with a high viscosity, density, high content of metals such as vanadium, nickel, etc., as well as the need for a deeper processing of oil, heavy oil residues containing the major metals and hetero-organic compounds and significant improvement of the technical and economic indices of production, processing and use of petroleum and petroleum products.

It is known that metals, including vanadium compounds are concentrated mainly in the fuel oil. The existing fuel oil combustion technology allows to trap at least 10 % of the total vanadium content in fuel oil.

The procedure for calculation of reserves of vanadium in crude oils is very different from the calculation of reserves of any useful by-products. In order to obtain reliable data, it is necessary to solve a number of issues that determine the specificity of methods of counting stocks of vanadium in such a complex and original materials such as oil. This is primarily the use of such methods for the determination of vanadium in petroleum, which would ensure the completeness of its assessments, known as volatile organic compounds of vanadium. And most importantly – the application of such technologies for the extraction and refining, which would not only realize the full raw oil potential, but to ensure the storage of the contained vanadium. It is obvious that the choice of this technology and those dependent on the concentration of vanadium in oils can be taken as conditioned.

So, the extraction of vanadium and other metals directly from crude oils and petroleum products is an important economic objective.

With the gradual depletion of traditional light oil reserves are becoming increasingly important the reserves of raw materials which has recently attracted little attention, which include high-viscosity oil, natural bitumen and oil shale. In addition, these minerals hydrocarbons contain a number of non-ferrous metals components, among which is also vanadium.

During the processing of oil-containing organometallic compounds, most of the heavy metals remain in stock. The concentration of vanadium in petroleum and petroleum products can reach a few percent, which could serve as a source of industrial extraction of this metal, together with vanadium ores. Removal and disposal of vanadium compounds from oils are important for improving the quality of petroleum products, and to protect the environment from the adverse effects of toxic oxides [1].

The use of fuel oil, which usually concentrates the bulk of trace elements, as of boiler fuels leads to pollution of the environment by significant quantities of active oxides. For example, an amount of V_2O_5, thrown every day with the smoke of modern power can be measured in hundreds or even thousands of pounds. On the other hand, fuel oil ash can serves as a rich source of valuable metals. Thus, in the ash obtained at burning of sulfur fuel oil, vanadium is much richer than in most of the industrial ores. Already the working to extract V_2O_5 from the ashes and the scale of this production is greatly expanded [3, 4].

The choice of a rational technology of petroleum and petroleum residues is a difficult task. The decision depends on the composition of raw materials, required range of petroleum products, the degree of development of the proposed technologies, the availability of equipment, the efficiency of industrial catalysts, the use of recycled materials. Currently available demetallization development of oil and oil products are at the level of research, which can be divided as follows:

1. Direct extraction of vanadium directly from crude oil by: stripping of vanadium and other metals with solutions of mineral acids, inorganic salts, inorganic reagents handling, microbiological activity, and sorption on inorganic and organic sorbents.
2. Disposal of waste of thermal power plants.
3. Coking: thermocontact way, the method of pre-gasification.
4. Hydrocracking of petroleum and petroleum residues on catalysts and their subsequent processing.

Analysis of these methods shows that the most effective is a combination of several of them, namely, sorption to inorganic sorbents and hydrocracking. There are known works on the adsorption removal of metals from crude oil, which are used as sorbents in smelter, petroleum coke, air gel.

The most common and cheapest method of removing metals from the hydrocarbon systems is adsorption on solid natural sorbents [5].

Experimental

When the first phase of laboratory studies were have synthesized organometallic components (vanadium-containing additives) for model hydrocarbon systems.

After analyzing the basic form of existence of vanadium compounds in crude oils and petroleum products, we have synthesized model chelate compounds - oxivanadyl acetylacetonate (IV), which is a component of the studied model hydrocarbon systems. For oxivanadyl acetylacetonate (IV) was used acetylacetone and oxivanadyl sulfate (IV). Scheme of laboratory setup for oxivanadyl acetylacetonate (IV) synthesis was given earlier. Synthesized organometallic complex was analyzed by chemical and physico-chemical methods (photocolorimetric, derivatographic analysis and infrared spectroscopy) [6].

When choosing a sorbent we were guided by its cheapness and prevalence in the territory of Ukraine. We used as a sorbent a clay mineral – loess, this is widespread in Ukraine. Loessial rocks are one of the most common types of continental deposits. Loess are wide spread in Europe, Asia, North and South America. It is estimated the average power Keylgaka loess at depth 10 m total area occupied by loess rocks on earth, amounts to 19 million km^2. In the territory of the CIS area covered by loess rocks is about 34 % of the continental part of the CIS. Loess is a solid cover a large part of Ukraine (80 %) and the southern European part of Russia.

The main feature of loess is its high dispersion. Dominated by the particle size of 0,02 – 0,01 mm (50 – 80 % of the total mass), clay particles smaller than 0.005 mm are present in an amount of 10 – 40, a number of particles of size 0,01 – 0,02 mm is represented by aggregates formed during coagulation of colloidal species. The porosity of loess 40 – 55 %, it is permeated by thin tubules (macrospores, traces of residue) [7].

As a model hydrocarbon solution were used hexane (TU 2631-003-05807999-98). As organometallic impurities in model hydrocarbon systems used oxyvanadyl acetylacetonate (IV).

Adsorption of vanadium from the model hydrocarbon systems on the contact material (loess) was performed in the reactor mixing. The process was carried out under static conditions. These conditions provide an apparatus for shaking off type brand АВУ – 6с. The adsorption process was carried out at room temperature and atmospheric pressure. Adsorption time was 10 hours. To carry out the process of sorption of vanadium from the model solutions on loess were prepared model hydrocarbon mixtures with concentrations of vanadium, respectively, 0,01 – 0,2 % (mass fraction). The size fractions of the sorbent was 0,02 – 0,01 mm.

Analysis of hydrocarbon systems in the vanadium content after the adsorption process for natural sorbent was carried out by the method of standard conditions. Based on experimental data obtained under equilibrium conditions at constant temperature, were built of the adsorption isotherm.

Figure 1 shows the sorption isotherm of vanadium model hydrocarbon systems on the clay minerals - loess.

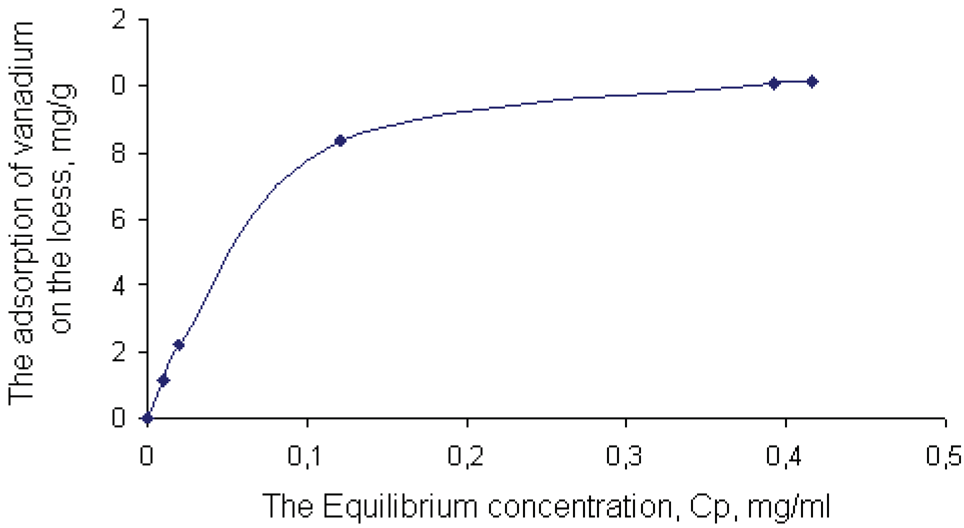

Figure 1. Adsorption isotherm of vanadium on loess

Isotherm, which is shown in Figure 1 corresponds to the Langmuir equation: $A = A_\infty \cdot \left[\frac{K_L \cdot C}{(K_L \cdot C + 1)} \right]$, where A∞ - limit adsorption, K_L - Langmuir adsorption constant, which has dimensions of reciprocal concentration.

The equation of the Langmuir adsorption for this type of relationship $\frac{1}{A_V} = f\left(\frac{1}{C}\right)$. Linear dependence $\frac{1}{A_V} = f\left(\frac{1}{C}\right)$ is expressed by the equation: $\frac{1}{A_V} = \frac{1}{A_\infty} + \left(\frac{1}{A_\infty \cdot K_L}\right) \cdot \frac{1}{C}$

This allows define graphically the Langmuir equation constants ($A\infty$ and K_L):

A ∞ = 10 mg/g or 0,196 mol/kg.

$-K_L = \frac{1}{tg\alpha \cdot A_\infty}$ = 1/0,196 = 5,102 ×10^3 m^3/mol.

Finding the value of the Langmuir adsorption constants (K_L), it becomes possible to determine Henry's law constant for the equation:

$K_G = K_L \times A\,\infty = 0{,}999 \times 10^3\ m^3$ / kg [9].

The limit for the adsorption on loess equals to 0,196 mol/kg, and adsorption of vanadium on loess – 90 – 95 %.

Analysis of the experimental results confirms a high efficiency of the natural clay mineral - loess to remove vanadium from the model hydrocarbon systems. The use of contact materials in the processes of demetallization is quite effective method to tackle the high levels of metals in the oil feedstock.

Thus it is possible to increase the depth of oil processing at the part of heavy oil residue and improve the quality of trade oil products, thus reducing the amount of harmful emissions of heavy metals into the environment from combustion plants and metal-processing oil residues.

Therefore, at present, during a high shortage of crude oil, it is necessary to develop processes that allows completely process reserves of crude oil. Such processes are the removal of metals from crude oil.

In subsequent studies we shall discuss some heavier model hydrocarbon systems containing complex compounds of vanadium and nickel.

References

1. *Ахмеджанов Т.К., Нуранбаева Б.М., Молдабаева Г.Ж.* Инновационные способы извлечения ванадия из нефти и нефтепродуктов. – Алматы: КНТУ им. К.И.Сатпаева,

2. *Товажнянський Л.Л., Левченко Б.О.* Паливно-енергетичний комплекс. Стратегія розвитку. – Харків: НТУ «ХПІ», 2009. – 400 с.

3. *Белов П.С. и др.* Экология производства химических продуктов из углеводородов нефти и газ. М.: Химия, 1991. – 252 с.

4. *Абрасимов А.А.* Экологические аспекты производства и применения нефтепродуктов. – М.: ВАС, 1999. – 731 с.

5. *Мералиев С.А., Теляшев Э.Г., Ахметов М.М., Хайрудинов И.Р.* Металлы в нефтяном сырье // Мир нефтепродуктов. – 2007. – № 1. – С. 1–5.

6. *Манчук Н.М., Баглєй Є.В.* Синтез металоорганічного комплексу – ацетилацетонату оксиванадію (IV). – Сб. тез XV-й Всеукраинской научно-практической конференции «Инновационный потенциал украинской науки – XXI век», Запорожье, 1-7 марта 2012.

7. *Кригер Н.И.* Лесс, его свойства и свазь с географической средой. – М.: Наука, 1986. – 243 с.

8. *ГОСТ 10364 – 90*. Нефть и нефтепродукты. Метод определения ванадия. – М.: ИПК издательство стандартов, 1990. – 14 с. – Действует с 11.12.90.

9. *Кельцев Н.В.* Основы адсорбционной техники. – М.: Химия, 1984. – 352 с.

UDC 541.135.2

G. Sokolsky, associate professor; M. Demchenko, postgraduate student; S. Kalenuk BS (National Aviation University, Ukraine)

ETHANOL OXIDATION ON MANGANESE DIOXIDE ELECTRODE. EFFECT OF MEDIUM AND CONDUCTIVE ADDITIVE

Manganese (IV) oxide electrodes prepared by electrodeposition from fluoride electrolytes are considered as a prospective alternative to Pt in binary Ru–Pt anodes of direct alcohol fuel cells. Anode oxidation of ethanol on MnO_2 electrode has been examined by the method of voltammetry. The behaviour of the electrode at various ratio active material: conductive additive as well as effect of acidic and alkaline medium were analysed.

The developments of direct methanol fuel cells (DMFC) and direct ethanol fuel cells (DMFC) demonstrate a significant progress over the past decade. Manganese dioxide polymorphs are octahedral molecular sieves (OMS) of manganese with n×m edge-shared MnO_6 octahedral chains that form one-dimensional tunnels. These oxide materials is shown to be relatively cheap and promising alternatives to noble metals electrode materials in DMFC [1] as well as an active catalysts of oxidation of organic compounds [2].

Electrodeposition from fluoride containing electrolytes is a prospective method of nanomaterials preparation at high rates [3]. Dopant-ions can be the templates of the OMS's tunnel size stabilisation during electrosynthesis [4].

To prepare the electrode material based on manganese dioxide various chemical and electrochemical methods can be applied. To stabilize a particular phase composition and defect structure of manganese dioxide the electrochemical deposition from sulfate, nitrate and chloride electrolytes is a well-known and promising alternative to chemical methods. In accordance with our data published earlier [5], in turn, the important advantage of fluorinecontaining electrolytes is their ability to realize manganese dioxide electrodeposition at higher rates. In addition, using bifunctional electrochemical system model it is possible to regulate the phase and chemical composition, as well as physical and chemical properties of electrodeposition products.

Therefore, the method of electrosynthesis from fluoride electrolytes was applied in our research [6]. The series of undoped and doped OMS samples was electrodeposited on a Pt anode in 0.2 M HF and 0.7 M $MnSO_4$ containing 0.001–0.17 mole·L^{-1} MOH (Li^+, Na^+, K^+, NH_4^+) or MSO_4 (Fe^{2+}, Co^{2+}) at a current density i = 0.1–10 A·dm^{-2}.

The aim of a research was to analyse manganese dioxide electrode preparation process for electrocatalytic oxidation of alcohols in alkaline and acid mediums. The powdered samples were filtered, rinsed with distilled water and dried 2h at 120 ^oC to remove physically sorbed water. Electrocatalitycally active oxide material was mixed with graphite conductive additive, fluoroplast emulsion (PTFE), thoroughly mixed in agate mortar, and pressed on stainless steel grid. Experimental steps of electrode preparation were the following ones: homogenization of powdered manganese dioxide and graphite by their grinding for 10 minutes, then PTFE emulsion addition (5% of the total weight of electrode mixture). The resulting mixture was pressed onto the steel grid pretreated substrate.

Experimental. Chemical analysis, XRD, TGA, FTIR, SEM data were the methods of samples characterisation. The main instrument of MnO_2 electrocatalytic properties investigation during anodic oxidation of organic compounds was cyclic voltammetry method on a potentiostat-galvanostat IRC-PRO.

Polarization studies were carried out in a standard 3-electrode electrochemical cell. The electrode potential was measured against a standard Ag/AgCl electrode. The auxiliary electrode was a plate of glassy carbon with 25 cm^2 area, which exceeds the anode surface by 10 times. The potential scan rate in this study was 10, 50, 100, 150 mV / s.

Electrocatalytic properties of electrodes obtained were studied in acidic (2.5M H_2SO_4) and alkaline (1M KOH) electrolytes.

The optimisation of electrocatalyst : conductive additive ratio. The several samples of electrodes with the following MnO_2: C ratio: 100:0; 30:100; 50:50; 70:30; 100:0 were chosen to select the optimal electrocatalytic MnO_2 component and conductive additive – C ratio.

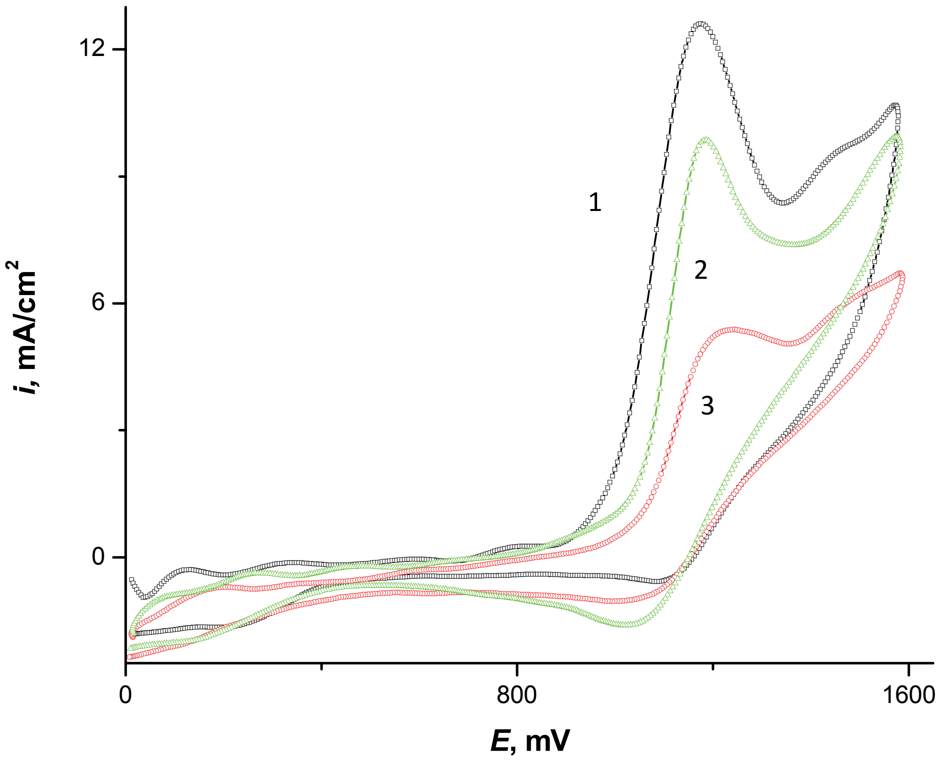

Fig. 1. Oxidation of ethanol in acid solution 2.5 M H_2SO_4 for MnO_2:C components ratio: 1 — 70:30, 2 — 50:50, 3 — 30:70

The C: MnO_2 = 70:30 ratio is the best in Fig. 1 that is evidenced by a shift of the alcohol oxidation process electrode potential (peak at 1200 mV) and higher values of the current density.

Oxidation of ethanol in acidic and alkaline solution. The next stage of our research was to check stability of the obtained electrodes in acid (Fig. 2) and alkaline (Fig. 3) environments.

Experimental studies of ethanol oxidation in both acidic and in alkaline medium is characterized by the stability of the electrode material. It has high adhesion to the surface of grid substrate and insoluble during the research. The ethanol oxidation peak with 1200 mV potential is observed in both solutions.

Comparison of industrial CMD and OMS-2 (doped by NH_4^+ in a laboratory) samples of manganese dioxide. To compare these samples of different origin two electrodes with the optimum ratio of C: MnO_2 = 70:30 were prepared. Figure 4 represents cyclic voltammogramms of ethanol oxidation on two samples.

At identical experimental conditions the most active electrocatalyst is the doped OMS-2 sample obtained by anodic deposition from fluoride electrolytes because of lower potential of oxidation and larger current density peak values.

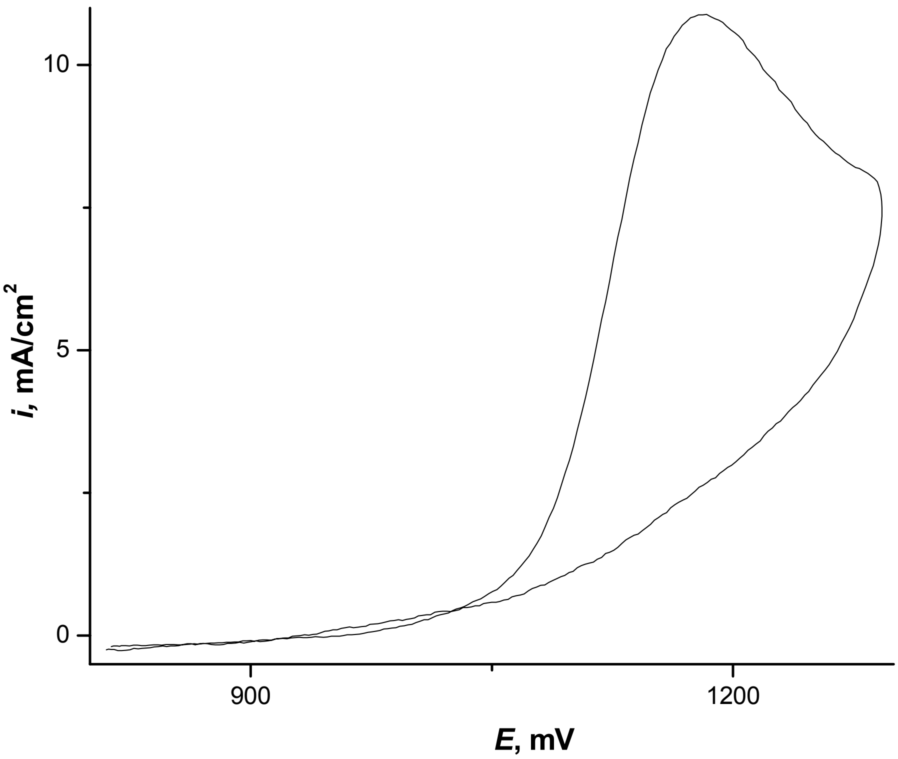

Fig. 2. Cyclic voltammograms of acid electrolyte of ethanol oxidation on electrode that has the ratio of the active components C: Mn = 70:30

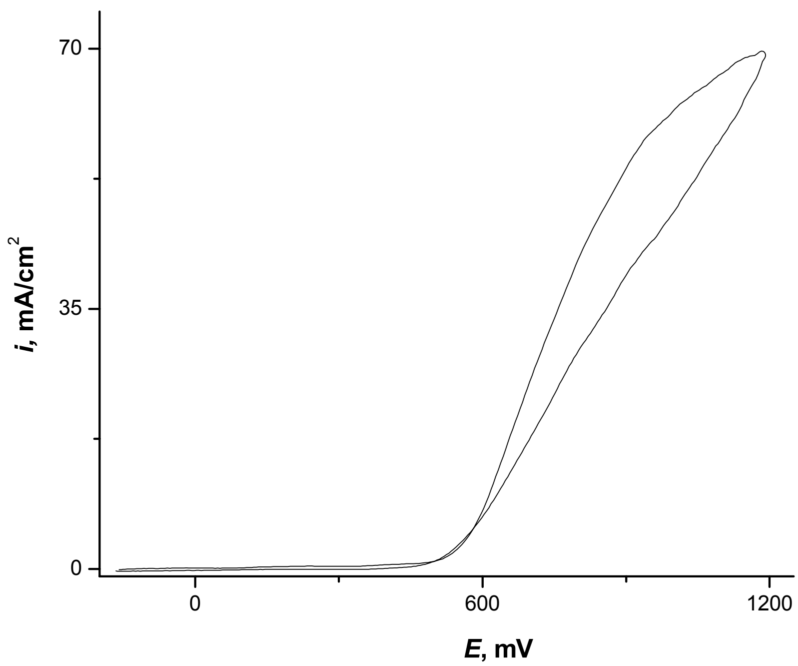

Fig. 3. Cyclic voltammograms of alkaline electrolyte of ethanol oxidation on electrode that has the ratio of the active components C: Mn = 70:30

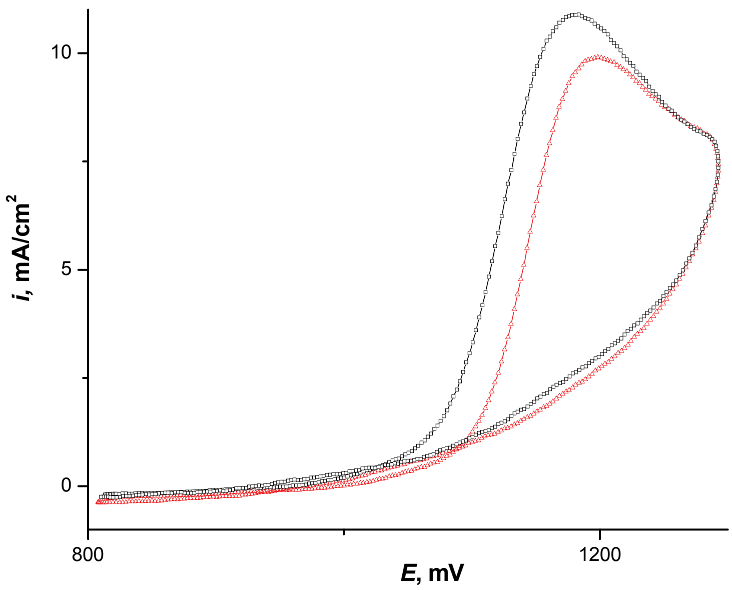

Fig 4. Cyclic voltammograms of acid electrolyte of ethanol oxidation on: 1 - CMD MnO_2, 2 - OMS-2 MnO_2.

Conclusions

Analysis of electrode preparation process for electrocatalytic oxidation of alcohols in alkaline and acid mediums was implemented in this research. The optimisation of electrocatalyst : conductive additive ratio was studied. It is demonstrated that the C: MnO_2 = 70:30 ratio is the best one due to the alcohol oxidation process electrode potential shift (peak at 1200 mV) and higher values of the current density.

Comparison of electrode activity in oxidation of ethanol in acidic and alkaline solutions was made. Experimental study of ethanol oxidation in both acidic and in alkaline medium confirmed electrode material stability. It had high adhesion to the surface of grid substrate and was insoluble during the research. Industrial CMD and OMS-2 (doped by NH_4^+ in a laboratory) samples of manganese dioxide were used in this work. At identical experimental conditions the more active electrocatalsyt is a doped OMS-2 sample obtained by anodic deposition from fluoride electrolytes because of lower potential of oxidation and larger current density peak values.

References

1. *Г.В. Сокольський, М.В. Демченко, С.В. Іванов, Д.О. Меленевський, А.Г. Держипольський.* Вольтамперометрія діоксидманганового електрода в кислотному розчині етанолу // Укр. Хім. Журн. — 2010, №11-12. — С. 51-57.

2. *Suib, S.L.* Chem. Innovation, 2000, 30, 27.

3. *Ivanova, N.D., Ivanov, S.V.* Russian Chem. Rev. 1993, 62, 907.

4. *Сокольський Г.В., Іванова Н.Д., Іванов С.В., Болдирєв Є.І.* Електрохімічне допування як метод направленого синтезу електродних матеріалів для хімічних джерел струму // Вісник ХНУ. — 2005. — №648, сер. Хімія.— вип. 12(35). — С. 58-61.

5. *Н.Д. Иванова, Е.И. Болдырев, Г.В. Сокольский.* Реализация бифункциональной электрохимической системы // Укр. хим. журн. — 2000. — 66, N 5-6. — С. 17-23.

6. *Иванова Н.Д., Болдырев Е.И., Макеева И.С., Сокольский Г.В.* Получение диоксида марганца из фторсодержащих электролитов // Журн. прикл. химии. — 1998. — 71, №7. — С. 1209-1211.

UDC 665.7.038

O.A. Spaska, assistant; S.V. Ivanov, Dr.Sci.
(National Aviation University, Ukraine)

EVAPORATION OF LIQUID HYDROCARBONS UNDER THE INFLUENCE OF GLASS MICROSPHERES

Influence of glass hollow spherical microspheres on natural evaporation from the surface of mirror of individual hydrocarbon liquids and their mixtures was explored. During conducting of system research were obtained unexpected results and a row of interesting phenomena: it is found, that a microspheres not only protect, but also promote evaporation of individual hydrocarbons C_6-C_{10}

During storage, handling and transportation of hydrocarbon fluids its considerable part is lost due to evaporation. This phenomena is one of the most important and most controversial properties of fuels. Evaporation is accompanied by loss of the most valuable fuel light fractions, mainly saturated hydrocarbons. On the way from the wells to the gas station and due only to storage, the annual loss is 0,6-2,8 wt. %.

Evaporation is crucial factor in fuel stability during storage, transportation and usage. It it assesses both qualitatively (the saturated vapor pressure, fractional composition., density, viscosity, heat capacity, diffusion coefficient) and quantitatively - by Budarov method at purging of fuel with a tenfold volume of air at 20 °C.

The process of evaporation of liquid hydrocarbons during storage is static and endothermic process, it belongs to the phase transitions of the first type, because this transition is characterized by isobaric-isothermal equality potentials of the two coexisting phases in equilibrium by hopping-like entropy (S) change and also volume (V) at transition of substance from one phase to another.

In Figure 1 are given the most typical examples of individual hydrocarbons evaporation, confirming the known laws: mass loss increases with time, proportionally to the increasing of the boiling point.

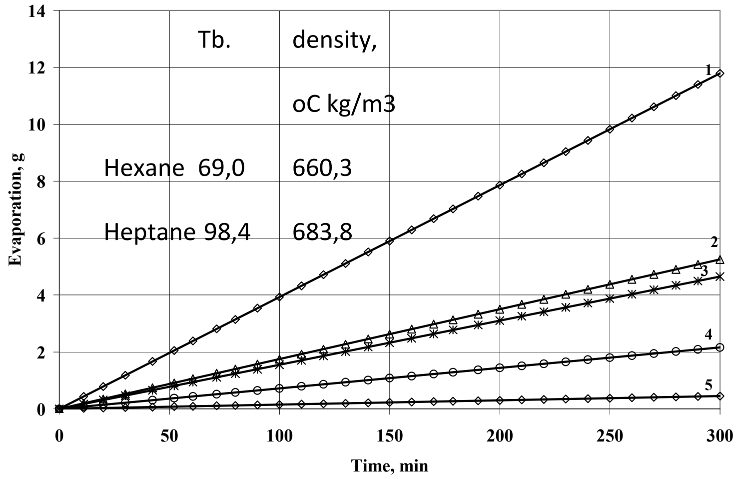

Figure 1. Dependence of evaporation of hydrocarbons from the time at 25 °C: 1 - hexane, 2 - heptane, 3 - octane, 4 - nonane 5 – decane

At evaporation into unmoved medium over the surface there forms convection currents caused by the diffusion of vapors, which intensify the process of evaporation. At evaporation of substances with molecular weight much smaller than the molecular weight of air (eg, H_2O), convective flows are directed upward. For liquid hydrocarbon fuels with molecular weight greater than air directed down. These flows intensify the detached from the surface of the liquid molecules loss , which accelerates the process of evaporation.

Most of the petroleum is a polycomponent mixture of hydrocarbons and heterocompounds that have different boiling points. The lightest oil are of cars (start of boiling - 35-40 °C) and aviation gasoline (boiling start above 40 °C). Therefore the quality of gasoline deteriorates mostly due to evaporation of most light hydrocarbons C_5-C_7, the temperature dependence of evaporation are shown in Figure 2.

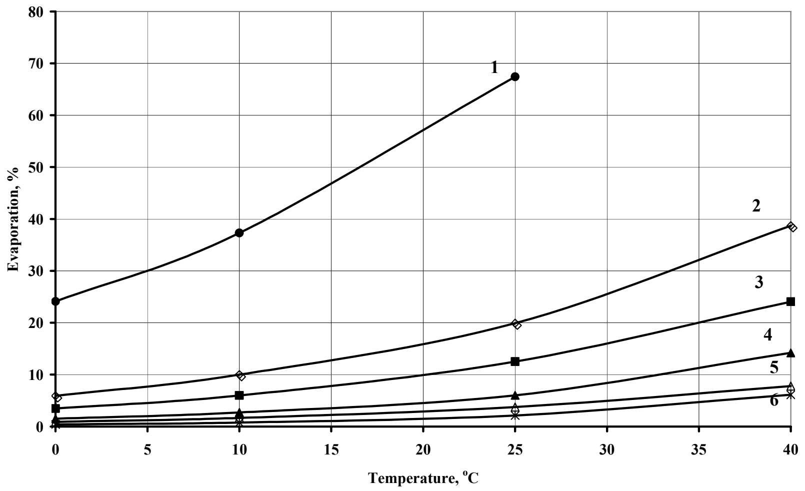

Figure. 2. Temperature dependence of evaporation of hydrocarbons: 1 - pentane, 2 - hexane, 3 - benzene, 4 - heptane, 5 - octane, 6 – toluene

The less volatile are oils obtained from the middle distillates - kerosene and gasoil. But also in jet and diesel fuels a change in quality due to improper storage can be substantial. The lowest evaporation have lubricating oils. As for tendency for evaporation, and hence to a change of quality all petroleum products can be placed in this series: gasoline> jet fuel> diesel fuel> gas turbine >boiler fuels> oils for jet engines> carbureted oil> diesel oil> oil for piston aircraft engines.

Since the saturated paraffin and aromatic hydrocarbons are the major components of petroleum hydrocarbon fuels, its light hydrocarbon liquids fractions evaporation decreases octane number, decreases the saturated vapor pressure and therefore increases the initial boiling point, evaporating primarily as the lightest fraction with the smallest b.p., and in some cases the temperature of the end of the boiling, increased density through weight increase of fraction. All these changes lead to negative consequences in the operation at transport and technology. Among the most effective for the availability, efficiency, simplicity, ease of use are high active, allocated on the interface aerated fluorocontaining surfactants system (SAS). However, they gradually break down by hydrocarbons, and therefore do not provide adequate fire proof, reliable and lasting protection of the environment from the vapour of hydrocarbon liquids.

Solving this problem by directional forming of SAS with a predefined protective properties are important in terms of general scientific and technological aspects of creating applications for the protection of the environment from vapors of hydrocarbon liquids and is a matter of great economic value. The purpose of the work are surface-active systems - effective protective coatings to reduce evaporation of hydrocarbon liquids, improving their safe storage and environment protection.

To create an ultra light technological systems we have used gas-filled glass microspheres MC-A9 and their analogues appretted by mixture of β- and γ-aminopropyltriethoxysilane (AGM-9, TU 5951-028-00204990-2006) which are fine granular powder of correct spherical form, diameter of 40-180 microns and density 200 kg/m^3.

However, there were found that the hollow spherical glass microspheres do not only protect but also increase the evaporation of individual hydrocarbons C_6-C_{10}.

Experimentally there were found the optimal composition of SAS which is able to form stable threephase foams, were set their concentration and the conditions under which such coating is provided with its buoyancy,stability and vapor impermeability. At carrying out systematic studies were examined a number of interesting phenomena. Using high buoyancy we primarily assessed the protective ability of microspheres. To do this, on the surface hydrocarbons or mixtures thereof we imposed various number layers of microspheres. Where obtained unexpected results, shown in Figure 4.

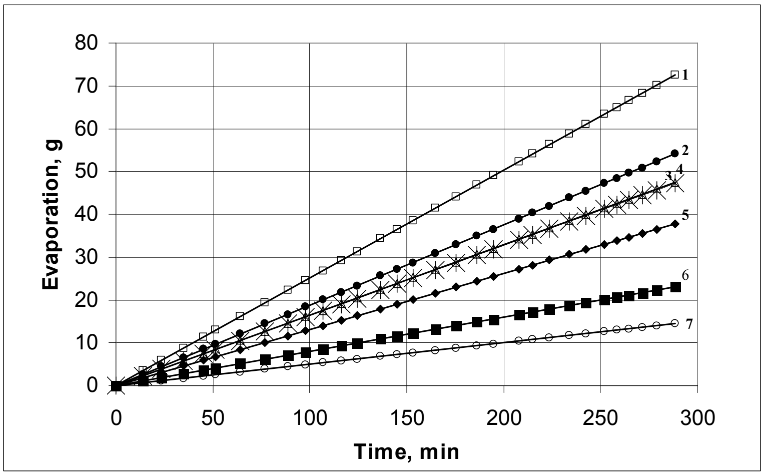

Figure. 3. Kinetics of evaporation of hexane without coating (1) and with layers of non appreted microspheres in % of the area evaporation surface: 15 - 2, 60 - 3, 140 - 4, 200 - 5, 300 – 6

Application of microspheres on hexane surface does not diminish, but increases evaporation (direct line 2).In addition, with increasing concentration of bubbles, the rate of evaporation increases (direct line 2-3). We believe this is due to thermal motion of microspheres, their rotation and increase both the surface area and also kinetic energy of hexane molecules separation. Another surprise was the increase of evaporation after formation of solid monodisperse layer at 2x or 3x microspheres concentration excess, relative to the evaporation surface mirror (direct line 5.6 in Figure 4).

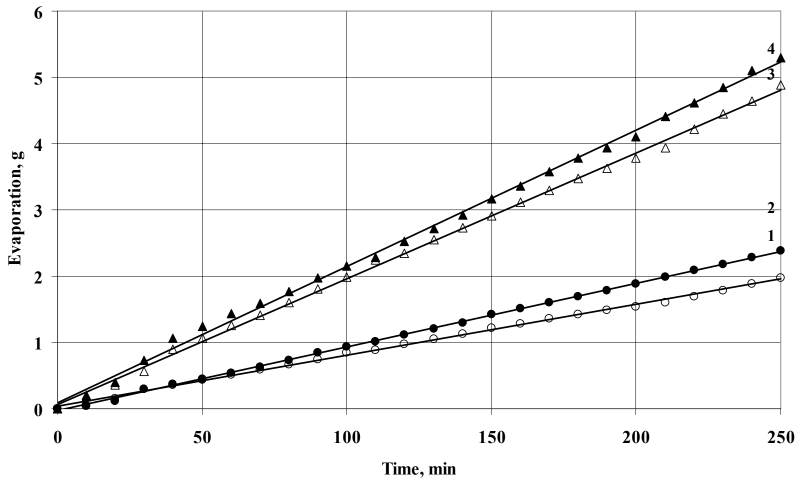

Figure. 4. Kinetics of evaporation of hexane (1) and heptane (3) without coating and with microspheres coated three layered integer evaporation surface , 2 and 4 respectively

Detailed long-term studies have allowed to explain this unusual fact. If we look at the vessel, used at experiments it is seen that in the process of evaporation of hexane balls hang up on the walls of the container.

As a result of adhesion on the side surfaces around the perimeter there formed a continuous layer, which certainly increases the surface area, and then through capillary forces increases also evaporation. Fair assessment of nominated assumptions is confirmed by the results obtained with using of appreted microspheres.

Similar patterns are observed for other homologues of saturated hydrocarbons – from heptane to decane (Figure 5).

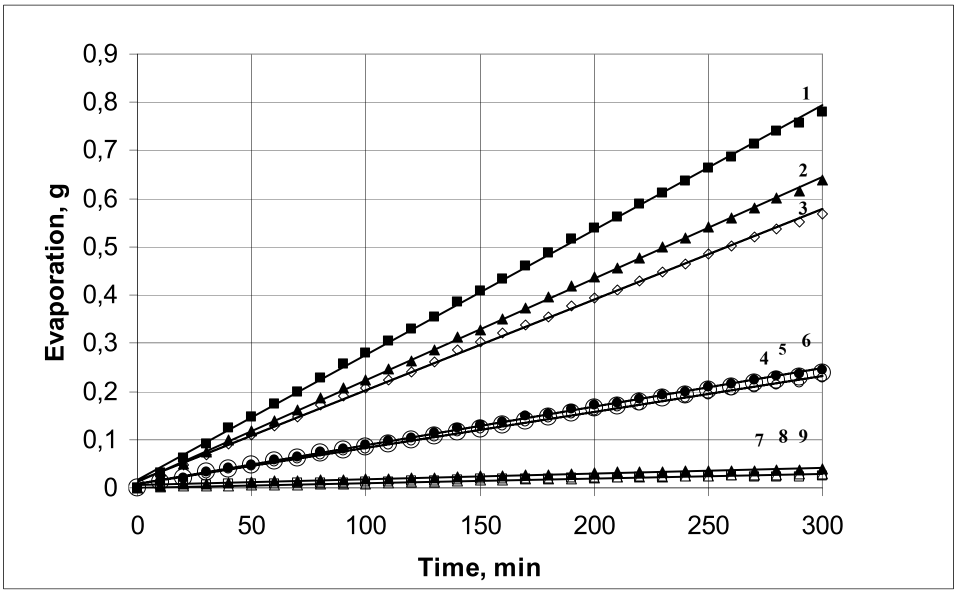

Figure. 5. Time dependence of the evaporation of octane (3), nonane (6), decane (9) and also over layers of non appreted microspheres in % of evaporation surface : 1,4,7 - 30 2,5,8 – 200

Unexpected results are that unlike pure hydrocarbons, in case of gasoline the evaporation is also reduced after an microspheres application of the surface , i.e. sorption of more hydrophilic compounds existing in fuels compared with paraffin hydrocarbons, such as oxygenates, results in their adsorption on the surface of glass microspheres and thus inhibition of their rotation. Conclusive proof of this are the results obtained at using microspheres appreted with hydrophobic mixture of aminopropyltriethoxysilanes. Organic appret removes the balls interaction with hydrocarbon solvent thus eliminates repulsion between the spheres and decelerates rotation and reduces evaporation.However, at applying several layers microspheres (curve 3) is registered accelerated evaporation as a result of microspheres adhering to the sides of the vessels walls, thereby increasing the evaporation surface.

Similar to evaporation rate of gasoline results are obtained regarding diesel fuel without coating and after microspheres deposition on the surface.

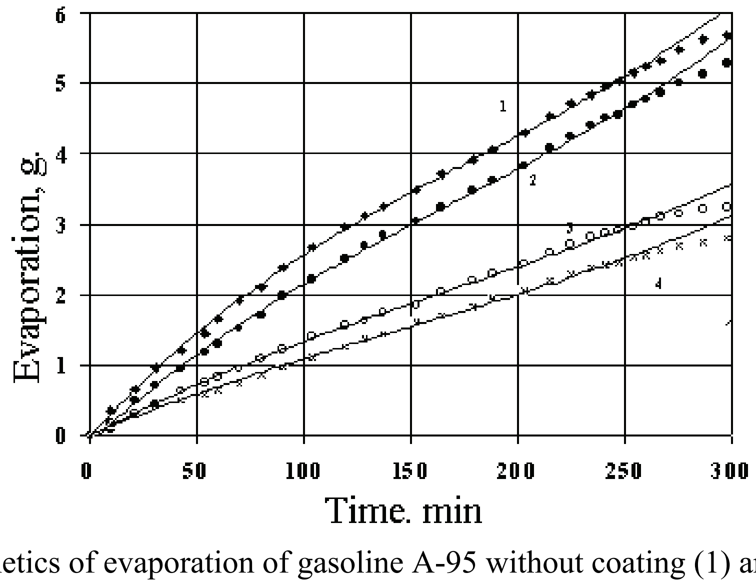

Figure. 6. Kinetics of evaporation of gasoline A-95 without coating (1) and with glass microspheres (% of the evaporation surface): 60 - 2, 200 - 3, 140 – 4

However, at applying several layers microspheres (curve 3) is registered accelerated evaporation as a result of microspheres adhering to the sides of the vessels walls, thereby increasing the evaporation surface.

Similar to evaporation rate of gasoline results are obtained regarding diesel fuel without coating and after microspheres deposition on the surface.

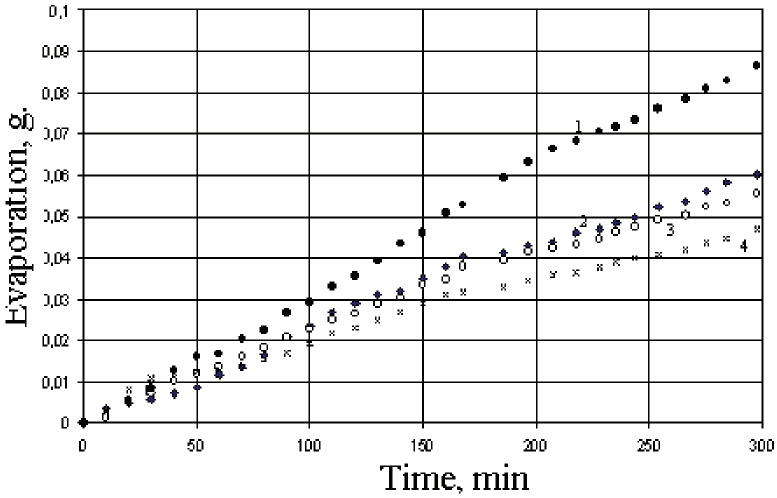

Fig.7. Dependence of evaporation of diesel fuel with no coating (1) and with glass microspheres layers, in % of evaporation surface: 2 - 30 3 - 200, 4-140

In comparison with gasoline A-95 evaporation chart, from which it is clearly seen that without coating evaporation most volatile fractions makes about 12% for 5 hours. But after the coating of thickness of 10 mm was held a major change. First, evaporation decreased by 2 orders of magnitude. In present scale, the most intense evaporation occurs for high volatile compounds, in particular for pentane 0.094 g, which on the previous chart because of low concentrations even not marked, for 2,3-dimethylpentane (0.83 g) and cyclopentane (0.038), methylcyclohexane (0.048) and trimethylcyclohexane (0.047), hexane, heptane and nonane (0.031), that total is 0.001% for 5 h. As a result of research of influence of temperature were nominated assumption that it is due to the microspheres rotation in the adsorption layer under the influence of thermal motion. With increasing of hydrocarbon radical length evaporation rate decreases and anomalous microspheres effect is leveled . For technical mixtures of hydrocarbons (gasoline, diesel), evaporation is reduced proportionally to the concentration of microspheres that is attributed to the sorption and to increase of interaction of fuel with hydrophilic surface of microspheres.

Conclusion

During conducting of system research of influence of glass hollow spherical microspheres on of individual hydrocarbon liquids and their mixtures were obtained unexpected results and a row of interesting phenomena: it is found, that a microspheres not only protect, but also promote evaporation of individual hydrocarbons C_6-C_{10} Unlike pure hydrocarbons, in case of gasoline the evaporation is also reduced after an microspheres application of the surface, i.e. sorption of more hydrophilic compounds existing in fuels compared with paraffin hydrocarbons, such as oxygenates, results in their adsorption on the surface of glass microspheres and thus inhibition of their rotation. Conclusive proof of this are the results obtained at using microspheres appreted with hydrophobic mixture of aminopropyltriethoxysilanes. Organic appret removes the balls interaction with hydrocarbon solvent thus eliminates repulsion between the spheres and decelerates rotation and reduces evaporation.

UDC 528.811:656.71(043.2)

V. A. Gliva (National aviation university, Ukraine),
L.O. Levchenko (National technical university of Ukraine, Ukraine)

DETERMINATION AND FORECAST OF ELECTROMAGNETIC ENVIRONMENT IN THE AIRPORT AREA USING MODELLING METHOD

Mathematical functions of spatial changes of different electromagnetic fields levels have been determined on the basis of theoretical studies. It enables to develop program for automatic distribution modelling and forecast of electromagnetic fields levels in the airport area with subsequent visualization.

Today aviation enterprises have many sources of electromagnetic fields (EMF) with broad spectrum of frequencies and amplitudes.

The decresase of this physical factor impact due to reduction of EMF sources quantity and their power lowering is impossible as they are necessary for the provision of flights safety and other needs of aviation enterprises.

Therefore, the main way of decreasing EMF negative impact on human is development of engineering, technical and sanitary-hygienic measures for protection of citizens and workers from EMF impact.

The research and applied developments aimed at solution of mentioned problem are carried out in Ukraine as well as in foreign countries [1-3]. But the problem of preliminary assessment of possibility of decreasing indoor and outdoor EMF levels to standard levels with current and necessary technical means is still actual. Meanwhile it is advisable to decrease EMF to technologically feasible levels according to [4], and it requires additional research.

Effecient tool of electromagnetic environment (EME) determination is mathematic modelling of EMF depending on quantity of installations. It makes possible forecasting EMF levels and their dynamics depending on installations power, electric load, etc.

Recent research are about modeling of spatial distribution of high voltage EMF sources [5], indoor EMF with fixed quantity of installations in one plane [6], which is area of personnel location and it doesn’t take into account the influence of EMF on adjoining rooms.

Usage of modern software tools for modelling of EMF powerline frequency allows getting models, which correlate well with in-situ measurements, but they also cover high voltage sources. Calculations for open space with finite element method require artificial limitation of investigated area and additional boundary conditions. Fundamental study [7] deals mainly with high frequency sources, which are radio transmitting equipment, locator equipment, etc.

Forecast of EME requires three-dimensional models, which take into account principles of formation and propagation of different EMF sources. It requires preliminary analysis and development of methodology for implementation of this modelling.

The aim of study is formation of methodological approach to modeling and forecast of EME in rooms with EMF sources of different nature and with different mechanisms of propagation, as well as visualization of received models.

Usually integral EMF forms of EMF different by nature. It is caused by constructional peculiarities of installations, located indoor and outdoor, which make EMF with hygienic significant levels. In these cases the formal usage of field superposition principle is sometimes not possible and rational because of different values of permissible levels of different EMF frequencies and different measurement units.

EMF generated by low frequency sources has different attenuation regularities.

For EMF linear sources, which are overhead and ground power lines

$$E = \frac{\tau}{2\pi\varepsilon\varepsilon_0 r} \text{ (V/m)}, \qquad B = \frac{\mu\mu_0 I_{e\phi}}{2\pi r} \text{ (T)},$$

where E – electric field,
B – magnetic field,
τ – linear charge density in line,

$I_{eф}$ – effective value of alternating current ($I_{eф} = \dfrac{I}{\sqrt{2}}$),

r – distance from phase conductor,
ε_0 , μ_0 – electric and magnetic constant,
ε, μ – permittivity and permeability (for air ε=μ=1).

It is necessary to take into account field attenuation in building structures for outdoor sources (according to present methods of attenuation calculation).

Taking into account electric field blocking by metal (cable armature, metal hoses, etc) and interconnection between electric and magnetic fields, it is necessary to consider magnetic field component. Electric field component can be defined from fundamental relation

$$\varepsilon\varepsilon_0 E^2 = \mu\mu_0 H^2, \quad B = \mu\mu_0 H, \qquad B = E\sqrt{\varepsilon\varepsilon_0\mu\mu_0}.$$

Parameters of field of linear conductor with finite size, that is typical for rooms, are determined as

$$B = \frac{\mu\mu_0}{4\pi}\cdot\frac{I_{eф}}{r}(\cos\varphi_1 - \cos\varphi_2),$$

where φ_1 , φ_2 – angles between conductor and directions from segment ends to determination point of magnetic field level.

If the conductor rounds the perimeter of room

$$B = \frac{2\mu\mu_0}{\pi}\cdot\frac{I_{eф}\sqrt{a^2+b^2}}{ab},$$

where a, b – length and width of room.

Calculations show, that unbalanced current 3 A, that is caused by pulse power units of computer, makes magnetic field with 600 nT induction (permissible level – 250 nT) in the 5×6 m room.

Magnetic fields of most technical facilities are fields of dipole type, it means that their levels decreasing at distance is described by inverse cubic relation.

Initial data for modeling EMF spatial distribution are calculated according to the value of vector-potential of magnetic dipole field A:

$$\mathbf{B} = \mathrm{rot}\mathbf{A} \qquad (1).$$

If the magnetic moment vector **m** coincides with positive direction of Z axis of orthogonal coordinate system, then to determine vector-potential in any point (X, Y, Z) it is necessary to take into account that $r^2 = x^2 + z^2$.

where r – distance from determination point of magnetic field, and

$$\sin\theta = \frac{\sqrt{x^2+y^2}}{r},$$

where Θ – angle between Z axis and direction **r .**

Absolute value of A in this point is equal to

$$A = \frac{m\sin\theta}{r^2} = \frac{m\sqrt{x^2+y^2}}{r^2}.$$

In XZ plane according to (1)

$$B_x = (\nabla\times A)_x,$$

$$B_y = (\nabla \times A)_y \; ,$$

$$B_z = (\nabla \times A)_z \; ,$$

where ∇ – Hamilton operator $\left(\nabla = \frac{\partial}{\partial x}\mathrm{i} + \frac{\partial}{\partial y}\mathbf{j} + \frac{\partial}{\partial z}\mathrm{k} \right)$, hence it appears

$$B_x = \frac{3m \sin\theta \cdot \cos\theta}{r^3} \; ,$$

$$B_z = \frac{m\left(3\cos^2\theta - 1\right)}{r^3} \; .$$

To get model of spatial distribution of magnetic fields from many sources the special program has been developed in Turbo Delfi. Database management has been provided with Microsoft SQLServer5. It has made possible to get map of distribution of magnetic fields levels from many sources. Its horizontal view is presented on pic.1.

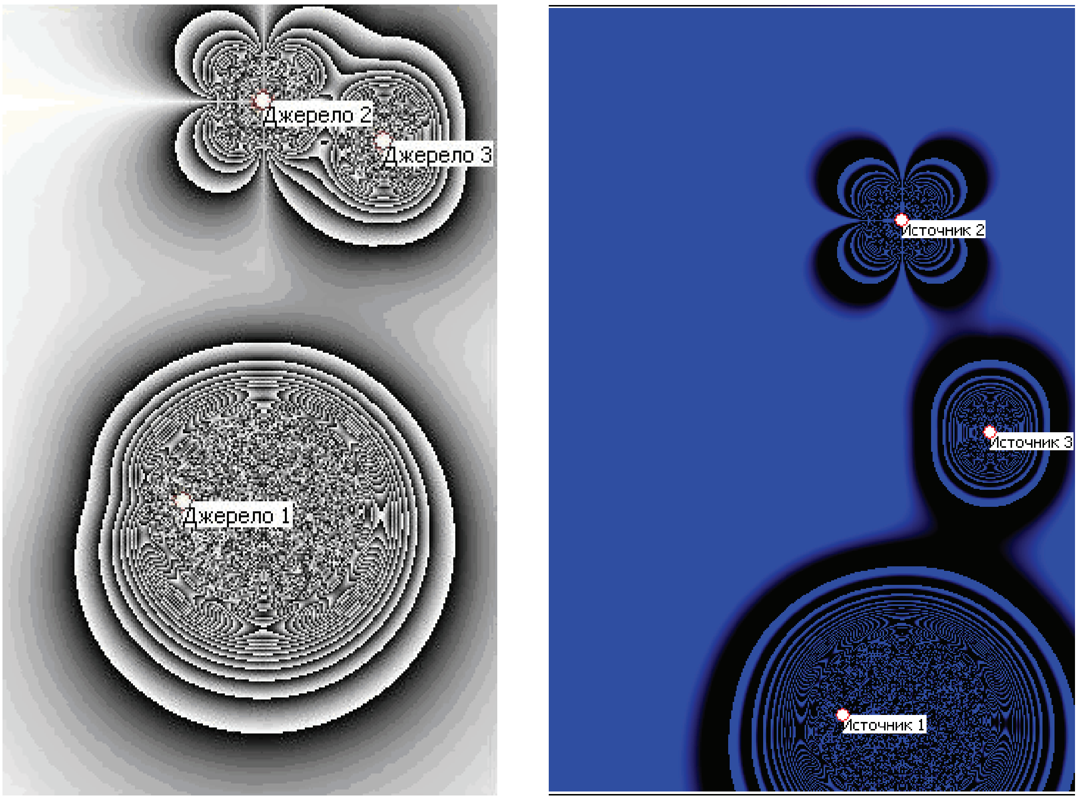

Pic.1. Examples of modelling of spatial distributions of magnetic fields levels

Quantitative data concerning field levels are marked on the screen with corresponding scale. Developed package makes possible to take into account room and field sources dimensions automatically.

Received results allow preliminarily determination of magnetic fields levels in every point of room depending on quantity and power of installations and electricity network load, and forecast their values with increasing equipment power supply, that affects values of **m** in initial functions.

Measures for decreasing electromagnetic load are defined according to predicted results. One of the most efficient is usage of fundamental effect of reflection and earlier developed dipole model of magnetic field source [8].

Research has showed that visualization of values of low frequency and high frequency fields on one model is unpractical because of bad perception of model visual image.

Development of two separate models with their following integration according to real levels of EMF of different frequency range by optimization method is the most reasonable. Solution of optimization problem is quite complex, because of presence of at least two different classes of EMF sources, and it requires further theoretical studies and experimental verification of received results.

Conclusions

Carried out theoretical studies and comparison of received results with experimental data have proved the possibility of correct modelling of EMF spatial distribution. This modeling could be used on the stages planning radio equipment location, industrial buildings, and modernization of technological equipment.

Preliminary determination of EMF levels in every specific case allows defining list and content of technical-organizational and hygienic measures for minimization of impact beforehand.

EMF distribution modeling is made for each frequency range with following optimization of technical equipment location. Priority in solution of optimization problem is determined on the basis of real and forecast levels of EMF in every range.

References

1 *Думанский Ю.Д.* Электромагнитное загрязнение окружающей среды – гигиеническая проблема, результаты и пути её решения в Украине / Ю.Д. Думанский, Н.Г.Никитина, С.В.Биткин, С.С.Галак // Итоги и перспективы научных исследований по проблеме экологии человека окружающей среды. – М., 2006. – С.248 – 253.

2 *Запорожец О.І.* Система електроживлення та електромагнітна безпека в енегронасичених будівлях і спорудах / О.І.Запорожець, В.А. Глива, В.І. Клапченко, Г.Д. Потапенко, А.В. Лук'янчиков // Вісник Національного авіаційного університету. - 2008. - №1. - С.113-116.

3 *Матоушек З.* Измерение паразитного излучения электрических приборов и оборудования / З.Матоушек , Й.Якуб, А.Гикел /// Вестник НТУ «ХПИ». – 2008. – Вип.27. – С.50 – 55.

4 Establishing a dialogue on risks from electromagnetic fields.-Geneva: World Health Organization, 2004. – 67 p.

5 *Krajewski W.* Numerical modeling of the electric field in HV substation / W. Krajewski // IEE Proc. Sci. Means. Technol. – 2004.- Vol. 151. - № 4. – P. 267 – 272.

6 *Шевченко С.Ю.* Исследование электрических полей промышленной частоты типовых подстанций ВН в городской черте / С.Ю. Шевченко, А.А. Окунь // Гігієна населених місць. – 2011. – Вип. 58. – С. 199 – 206.

7 Методологические подходы к определению и моделированию электромагнитных излучений при гигиенических исследованиях / С.В. Биткин, В.Ю. Думанский, Е.А. Сердюк и др. // Гігієна населених місць. – 2011. – Вип. 57. – С. 220 – 231

8 *Глива В.А.* Моделювання просторових розподілів електромагнітних полів множинних джерел // В.А.Глива, Л.О.Левченко, С.А.Теренчук // Новітні комп'ютерні технології: VII міжнародна наук.-техн.конф., 14-17 вересня 2010 р.: матеріали. Севастополь, 2010. – С.34-35.

UDC: 628.517.2:656.71 (045)

E. Konovalova, Candidate of technical sciences, Associate professor
(National Aviation University, Ukraine)

ANALYSIS OF THE NOISE MONITORING AND MITIGATION STRATEGIES AT MAJOR WORLD AIRPORTS

The paper gives an overview of international, national and local legislations and policies supporting noise management approaches at airports around the world. Analysis of noise monitoring and mitigation strategies that have been identified as "best practice" is presented.

Introduction

Airports, especially those, which were constructed close to conurbations, face several environmental constraints including noise, local air and water quality, climate change, waste management, and community relations. Traditionally, noise has been the key environmental constraint to airport development.

A significant number of the world's major airports and many small airports have adopted processes and systems to manage the impact of noise from the airport operations onto surrounding communities.

Usually the first step of solving the problem, after establishing appropriate regulations, is focusing on measuring environmental impact, specifically noise, through temporary or permanent noise monitoring terminals. Around 85% of the world's busiest airports have installed systems to monitor noise and to manage noise by the mitigation procedures [1]. Using the results of monitoring, airports manage their growth by ensuring regulatory compliance and minimizing their environmental footprint. Airports' authorities also use the results of monitoring for investigation and responding to noise complaints and defend the airport's position against an increasingly resistant community.

International regulations for noise management

There are a number of key legislations and policies supporting noise management approaches at airports around the world. International noise regulations have been maintained by the International Civil Aviation Organization (ICAO), the European Union and other international regulatory agencies.

ICAO, as the lead United Nations (UN) Agency in matters involving international civil aviation, continues to address the adverse environmental impacts that may be related to civil aviation activity. In carrying out its responsibilities, ICAO developed a range of standards, policies and guidance material for the application of integrated measures to address aircraft noise. One of the three major environmental goals, being adopted by ICAO in 2004, was limiting or reducing the number of people affected by significant aircraft noise via implementation of the concept of a "balanced approach" for the reduction of aircraft noise. ICAO Resolution A37-18 [2] outlines achieving maximum compatibility between safety, economic efficiency and demand for the development of civil aviation and the quality of the environment. The general approach concludes that solutions to noise problems need to be tailored to the specific characteristics of the airport concerned, which calls for an airport-by-airport approach, and that similar solutions could be applied if similar noise problems are identified at airports.

The Policy and Recommended Practices of Airport Council International (ACI) [3] encourages global consistency in the implementation of effective airport noise management programs. It outlines that the environmental monitoring of the site should provide the basis for the adaptation or introduction of long term ecological measures. The key relevant ACI policies relating to noise include noise monitoring at airports as an important process in understanding and dealing with aircraft noise impact. ACI also supports an ICAO integrated approach for addressing aircraft noise at airports.

A Directive of the European Parliament and of the Council 2002/30/EC [4] describes the framework for airport noise management procedures including production of noise maps and noise action plans for airports with more than 50,000 movements per year. It aims at monitoring the environmental problem caused by noise in major agglomerations and in the vicinity of main transport infrastructures, including airports. The Directive stipulates at making information on environmental noise and its effects available to the public. It, as well, prescribes requesting competent authorities to draw up action plans with a problem-solving approach to preventing and reducing environmental noise where necessary and preserving environmental noise quality where it is good.

A Directive of the European Parliament and of the Council 2002/49/EC [5] provides a basis for developing and completing the existing set of measures concerning noise emitted by the major sources, in particular aircraft, and for developing additional measures, in the short, medium and long term. For achieving a common understanding of the noise problem, data about environmental noise levels should therefore be collected and reported in accordance with comparable criteria. This implies the use of harmonized indicators and evaluation methods, as well as, criteria for the alignment of noise-mapping.

National regulations related to noise management at airports

Noise regulations including statutes or guidelines relating to aircraft noise have been established by national, state or provincial levels of government in many countries.

One of the best practices, if to consider national policies related to noise management strategies at airports, is the Airport Noise and Capacity Act [6] of 1990 in the USA. It established a national aviation noise policy (Sections 9308 and 9309). Subpart I — Operating Noise Limits — of FAR Part 91 [7] prescribes operating noise limits and related requirements that apply to the operation of civil aircraft in the United States. FAR Part 150 [8] directs to that noise monitoring may be utilized by airport operators for data acquisition and data refinement, but is not required for the development of noise exposure maps or airport noise compatibility programs.

The UK government has an important role in setting and developing the policy for aircraft noise control at UK airports. In December 2003 The Future of Air Transport White Paper outlined several new policies for airports which control, mitigate and compensate for aircraft noise with the aim of reducing and limiting the number of people significantly affected by aircraft noise. A range of noise controls relating directly to aircraft operations are set out in statutory notices and are published in the UK Aeronautical Information Package. These controls cover aspects such as Continuous Descent Approaches, noise abatement procedures and night flight restrictions. Government policy for aircraft noise includes land use and planning policies. These are set out in Planning policy guidance (PPG) note 24 [9], which guides local authorities on the use of their planning powers to minimize the adverse impact of noise. It outlines the considerations to be taken into account in determining planning applications both for noise-sensitive developments and for those activities which generate noise. PPG note 24 establishes that whilst monitoring may be costly and time-consuming this should not be regarded as sufficient reason for not using noise conditions where they are appropriate. The Civil Aviation Acts 1982 and 2006 – these Acts of Parliament grant the government powers to introduce noise control measures to limit or mitigate the effect of noise and vibration connected with taking off or landing aircraft at designated airports.

Section X "Protection of Environment" of the Air Code of Ukraine [10] contains two Chapters dedicated to protection of environment and residents from noise generated during aircraft operations. Regulations of aerodrome certification of Ukraine [11] that have been revised by 07.10.2011 established an obligatory determination of noise exposure maps and establishing of noise zones as limited areas, inside which special rules are defined for the new construction or reconstruction of any objects subject to noise sensitive activities.

Within these legislative and standardized essential principles, majority of airports have adopted a range of measures to meet normative requirements and to secure a harmonious relationship with their communities.

Local noise-related controls

Additional noise-related controls are introduced by local authorities as part of the planning system. This is often done by way of planning obligatory agreements made between the airport operator and the local authority.

Most operational noise regulations originate from individual airport authorities. This includes noise abatement procedures and operating limits, such as curfews and prohibitions of operation of individual types of aircraft at a particular airport. Operating limitations are incorporated into standard approach and departure procedures, which are recognized and used by Air traffic control. Some airports publish additional information for pilots describing airport-specific noise abatement procedures.

For example:

London Heathrow, one of the world's busiest airports and surrounded by dense population, has a night curfew and a complex night quota system. It uses analysis from their noise and operations management system to monitor compliance and to pursue violations.

London City Airport has adopted an extensive Noise Management Scheme for several years; the Scheme was formally approved for use in May 1993 by the local planning authority. The Noise Management Scheme includes provision and use of specialised equipment to measure noise of aircraft and to determine the flight tracks used by aircraft. The Scheme includes the systems of analysis of the measured information and its reporting. The Airport also has an approved Engine ground running scheme for aircraft test and maintenance.

Amsterdam Schiphol airport has a strictly monitored requirement to adhere to specific "noise load" limits at points around the airport, to the extent that they need to carefully plan their operational modes on a day to day basis to ensure that they do not run out of "load" for specific modes prior to the end of the year.

Frankfurt Airport (Fraport AG) formulated key fields of action for sustainable development fixing fields of action for environmental protection and published Environmental Statement 2011. Fraport AG operates 28 stationary measuring stations, three mobile measurement containers and a mobile measurement bus in the neighbourhood of the airport. The measuring stations provide continuous monitoring of aircraft noise development and documentation of unusual noise events.

Denver International Airport committed not to exceed specific noise loads at 100 points around its new Greenfield airport in 1985.

Airservices Australia has established a Noise and Flight Path Monitoring System at Australia's major airports. Operated from a single control centre, the system monitors aircraft operations and their environmental effects at airports across the Australian continent.

Noise monitoring strategies

Noise monitoring at airports is an important process in understanding and dealing with aircraft noise impacts. Noise monitoring involves the use of specialized equipment including microphones and computerized/automated logging/recording devices to measure the noise levels from aircraft. The reasons for monitoring vary and can include the following:

- Determining and tracking aircraft noise levels in residential areas;
- Compliance monitoring if individual aircraft or overall airport noise is subject to limits;
- Measuring individual aircraft noise events for the purpose of charging.

When locating a permanent or temporary monitoring site, consideration should be given to background or ambient noise sources such as roads, trains, weather, animals, and to security issues and access for regular calibration and maintenance.

If a monitor is located too far from the airport, aircraft noise levels may not be sufficiently high above ambient noise conditions to register as clear, separate noise events. The system must be able to distinguish between aircraft events and other noise events.

Automated systems should to be linked to radar or other aircraft identification systems to ensure that recorded noise events are aircraft movements and that a sufficient and representative proportion of all movements are captured.

Conclusions

Noise management at airports is standard practice in much of the world.

The following noise monitoring and mitigation strategy including a complex of monitoring and tracking systems has been identified as “best practice”. The complex of monitoring and tracking systems contains of:

- *Complaint Management System* maintaining a noise complaint system that provides a substantive and timely response to all noise complaints;
- *Flight Tracking System* that provides an accurate history of aircraft flight tracks;
- *Noise Monitoring System* providing accurate history of noise environment around the airport.

The efficiency of such complex approach depends not only from airport operator, but, to a greater extent, from aircraft operator compliance with noise abatement procedures. To make progress in efficiency airport should establish incentive-based techniques to encourage all operators to comply with all noise abatement measures.

The advanced research will embrace case study approach analysis of the efficiency of noise monitoring systems with regard to their key features and noise management strategies at airports.

References

1. *Legislation*, Regulation and Best Practise in Airport Noise Management. // White paper. Brüel & Kjær EMS.— May 2010. — 10 pages.
2. *ICAO Resolution* A37-18. Consolidated statement of continuing ICAO policies and practices related to environmental protection – General provisions, noise and local air quality. // ICAO 37th Assembly. — 28 September - 8 October 2010. Montreal, Canada. — 15 pages.
3. *Airport Council International* (ACI)’s Policy and Recommended Practices Handbook. // Airport Council International. Sicth Edition. — December 2008. — 135 pages.
4. *Directive* 2002/30/EC of the European Parliament and of the Council on the establishment of rules and procedures with regard to the introduction of noise-related operating restrictions at Community airports // Official Journal of the European Communities. — 26 March 2002. — 7 pages.
5. *Directive* 2002/49/EC of the European Parliament and of the Council related to assessment and management of environmental noise // Official Journal of the European Communities. — 25 June 2002. — 7 pages.
6. *Airport* Noise and Capacity Act // "Federal and State Coordination: Aviation Noise Policy and Regulation," 46 Administrative Law Review 413-427. — 1994.
7. *FAR Part* 91. General operating and flight rules. // Federal Aviation Administration, Department of Transportation. Doc. No. 18334, 54 FR 34292, Aug. 18, 1989, as amended by Amdt. 91–257, 64 FR 1079, Jan. 7, 1999; Amdt. 91–282, 69 FR 44880, July 27, 2004; Amdt. 91–297, 72 FR 63410, Nov. 8, 2007; Admt. 91–314, 75 FR 30193, May 28, 2010.
8. *FAR* Part 150. Airport noise compatibility planning. // Federal Aviation Administration, Department of Transportation. Doc. No. FAA–2004–19158, 69 FR 57625, Sept. 24, 2004
9. *Planning Policy Guidance* 24: Planning and Noise. // Department for Communities and Local Government, UK. — September 1994.
10. *Air code* of Ukraine dated 19.05.2011 № 3393-VI. // Parliament of Ukraine. — 17.09.2011.
11. *Regulations* of aerodrome certification of Ukraine. // The State Aviation Administration of Ukraine. — 25.10.2005 N 796.

UDC 001.8:57.022:502

A.V. Lukyanchykov, T.M. Lukyanchykova
(National Aviation University, Ukraine)

SAFETY OF LIFE ACTIVITY AND ENVIRONMENT SAFETY OF SURROUNDING AREA

Approaches to the perception of environment and life activity within the environment are examined.

Nowadays Safety of Life Activity (SLA) according to the typical curriculum [1] is based on the study of the Unified State System of prevention and reaction to natural and technogenic emergencies (USS) and State Control System of civil protection, which consider the following issues:

1) Emergencies forming factors that are determined by three characteristic periods (phases) of development and reaction (tab. 1):

Table 1.

Periods, their description and reaction.

Name of period	Description of period	System of reaction to an emergency involves:
initial period (early phase)	appearance of areas of potential risk on the territory, where the threat of possible exposure factors detection is increased	preventive measures
primary impacts period (phase of implementation)	appearance of exposure areas	rescue measures of reaction and localization of consequences
Postcrisis period (end or late phase)	postaction, secondary display of exposure factors (in the areas of postaction)	liquidation of consequences and restoration

2) Components of emergency counteraction process, which are determined in a functional aspect by the subsystems of the first and the second levels and are depicted on the chart (fig. 1).

Figure 1. State control system of civil protection

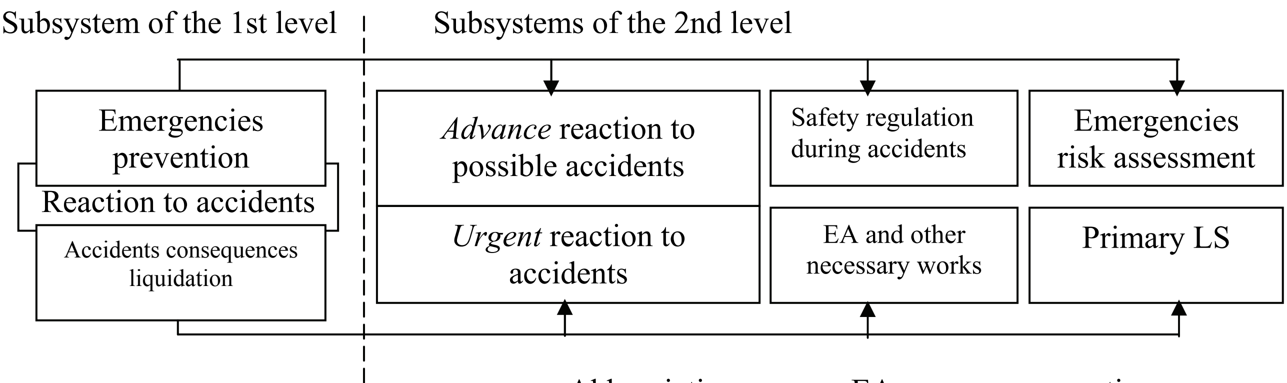

Abbreviation: EA - emergency actions

LS - life-support

The assessment of risk levels is defined by the State standard of Ukraine as identification of hazards and its possible sources and investigation of their origin mechanism, evaluation of probability of the identified hazards implementation and their consequences.

The most developed issue in this document is the process of identification, which belongs to the 2nd level subsystem "Emergencies risk assessment" and the 1st level subsystem "Emergencies prevention". Identification of hazards and their possible sources for economic objects is carried out by the approved procedure of the passportization (certification) system for enterprises and territories in relation to the risks of emergencies. The identification process results in the choice of codes and analysis of parameters of possible emergencies, description of sources of their origin, parameters of exposure factors, scenarios of emergencies development, which can be initiated by each of the defined hazard sources, to establish maximal possible emergency levels.

Approaches to the environment perception based on the idea of the USS is determined not only by perception - knowledge of the USS as social, natural, technosphere, as well as by perception of a person in the system as a process of life activity, which is the process of existence or presence of a person in the USS. Therefore, the identification is not only the process of **recognition** of hazard and its possible sources in the environment, but also **judgment** and **deduction** as an algorithmic process of description, and also the identification of a person, that is recognition of certain level of person's involvement in this world from the maximal presence in personal life activity to maximal absence or spending life time. A man is not only a thinking man, but also an active man.

In accordance with the philosophy of life activity safety the results of identification determine all next stages of the USS functioning and proper process of emergency counteraction.

Who teaches today this ability to identify, this ability of integral understanding, which is necessary for construction of scenarios of hazards development and adequate reaction to them in the field of life activity safety?

This is not only the question of private sciences and question of applied practical techniques, but also general issue of SLA and it is the question of world outlook, which is explored in religion, philosophy, methodologies, sciences and applied practice.

SLA is determined by the spiritual culture of personality, but it also depends on activity, communication, as well as thinking.

As J. Habermas marked, the classic world outlook supposed, that there was no mediator between subject being and cognitive intellect. This led to original idea of parallelism of being and consciousness. And the endless disputes of idealists and materialists flowed within the framework of this paradigm. But non-classical approach discovers that there is a mediator between intellect and being, and it is activity and language. It is possible to specify the Habermas's term and say these are types of activity and languages of culture. This mediator connects being and intellect, including the components of both poles. Thus, what reasonable world outlook sees in being is defined by the character of its rooting in this being. It is not unsubstantiated by intellect, but it is conditioned by social and cultural aspects [3].

Using language a man describes space. By activity a man lives in time. P. Florensky adds: «Space is determined mainly by amount, and time - quality» [4].

In modern education and science the scientific language of description as thinking process is studied in science methodology (thinking), and any activity as thinking process is studied in methodology of activity.

In non-classical perception of the world thought sees things dual and additional, as a result, SLA tries to form the integrative knowledge.

Accenting attention on the necessity of dual and additional character of the world perception can be seen in the report of UNESCO in 1996 on to the problems in the field of education, which states, that seven main types of contradictions exist in the world and affect education: between global and local, general and individual, traditional and modern, material and spiritual, long-term and short-term reasons, competition and equality of possibilities, unbelievable spread of knowledge and ability of man to master them. The list of contradictions pairs can be continued. New pairs can be close to the term field or content of the offered main types of contradiction pairs.

For the contradiction pair «single and plural», the following example can be given: «single» thinking is typical for technicians, when there is only one task solution on how to get from one point to another. The «plural» thinking is typical for humanist, when there is the great number of solutions for the same task. The pair «external and internal» can be presented by the example: a man thinks in things: external, for example, a military commander develops strategy or tactics using miniature figures on a map, that is actively cognizes possible movements from figures, or by internal things, for example, the listener of readings looks inside himself, contemplating his internal reactions to the read events.

Duality and complementarity are opened by physics of the XX century after refutation of the rationalism of the XVIII-XIX centuries, which tried to input everything in the intellect. New highly rational physics came instead of rational classic physics. The same happened in mathematics. Now it is clear that intellect cannot cognize the ideas of Non-Euclidean geometry, theory of relativity and quantum physics. Light - it is simultaneous wave and particle. He can not be only a wave or only particle and light is something one. The wave of light is a particle (by a photon) and the particle of light is a wave.

Shown to the apostles and professed by the fathers of the Chalcedon Cathedral about Christ, True Light, anticipated the discovery of quantum theory about creaturely light. The study about two natures of Christ, True Light, is ontological basis of corpuscular-wave dualism (two natures) of creaturely light. The said about light can be attributed to any particles and waves (electrons, sound and etc.).

The Definition of Chalcedon (451), which united 630 representatives of all Local Christian Churches, states, that thinking is primarily integral and dwells with initial integrity of all things that results in antinomianic differentiation. Integral thought of Christian sees plural as single and single as infinite set [2].

Consequently, the contradictions pairs offered by UNESCO are seen foremost as single, and then <u>dual</u> and <u>additionally</u> (according to the Chalcedon Cathedral: <u>unconfusedly</u> and <u>indivisibly</u>), and are named antinomies.

Today, for example, the practical use of antinomies could be seen in the principles of Orthodox pedagogic and ontological psychology (terms usual for scientific pedagogic are given in brackets): freedom and obedient, world (pan-cultural) and local (national), traditional and progressive (innovative), openness and autonomy, power and anarchy, silence (non-action) and instructions (activity), victory and defeat, romantic and real, mystic and rational, Dionysus and Apollo [5].

The study about an antinomy is deeply developed in the works of Father P. Florensky "Pillar and claim of truth". An antinomy is synthesis of thesis and antithesis. An antinomy is confession of both thesis and antithesis in their <u>unconfusedly</u> and <u>indivisibly</u> unity, or synthesis. Truth is antinomy and it is obtained by faith and experience.

Great antinomy: God and world. Non-antinomy (that is contradictory) consideration of them is such: a) a world will become God - this is Satanism; b) God is not present - this is atheism; c) God is world, and a world is God - this is pantheism (strongly developed in Buddhism), major representatives: Spinoza, Hegel, Schleiermacher. d) God and world are independent - this is deism, major representatives: Herbert Cherber, Tolland, Tyndall, Shaftesbury - in England; Voltaire, Russo and others - in France; Reymarus, Lessing - in Germany; Jefferson, Franklin, Alley - in America; Pnin, Lubkin, Ertov - in Russia.

Antinomic consideration is as follows. God is a Creator, Sustainer, Beginning, foundation and world purpose. God is not a creature, and a creature is not God. God is out of creature and in a creature, and creature is in God, that means Creator is transcendent and immanent in attitude to a creature. This is theism. As a rule, Judaism, Christianity and Islam are attributed to the theism.

Deism, pantheism, theism are attributed to the religious-philosophical systems of thought.

Theism in the synthesis of rationality and overrationality remains only the study, in a theory, that is a certain description of life activity, because the life activity of mind and heart, connected with attention, exploit and life experiencing. If theism is such, then per se it is also contradictory and not able to bring the substantial benefit of safe life activity.

Describing the above-mentioned points of non-antinomy consideration and ways to solve with the help of philosophic-methodological principles of the non-classical outlook and The Definition of Chalcedon the following table is received (tab. 2).

Table 2.

Methods of world perception of contiguity or communication in the pair of thing.

Points of pairs	**Description of a pair (character is an axiom)**	**Philosophical-methodological principles (character is a thesis by cataphatic theory)**	**According to the Chalcedon cathedral (character is a dogma by apophaticism)**
a)	replacement	constantly	unchanging (untransformability of one into another and vice versa)
b)	denial	collectively	inseparably (means a permanent alliance)
c)	confluence	dual (or plural)	unconfusedly (non-mixing, remain apart, not forming a new)
d)	indifference	additionally	indivisibly (do not exist separately)

Such great writers, as Skovoroda, Dostoevsky and others are the examples of antinomic thinking. Their works are not simply difficult, but alogic. And exactly this circumstance surprisingly makes the text clear and deep. And this opinion corresponds to the position of the known thinker G. Pomeranetz asserting, that a «depth can be expressed by either a poetic metaphor or by paradox. Value of paradox is that it can not be untwisted in a logical line. Logic operates only with the fragments of whole. Whole can only be observed, therefore metaphor and paradox are the language of depth».

Nichiporov B.P. writes about antinomies as about unity or about one, instead of two. They are agreed contradictions and oppositions. Antinomies are reunited and reconcilable poles of the same nature. Correct life activity or safe life activity «is sobriety, will to retention and self-retention in non-solid unity of these two ideas: about yourself and about a man». The action of including in antinomic nature is opened up to a man through that. «Sobriety is will and ability to retain simultaneously two poles in the acts of understanding. These poles are energetic and moral at the same time»[5].

If one compare contradictions and antinomies, it is impossible to reconcile contradictions, link them mechanically [5]. The contradictions are realized in the form of one of the items (tab. 1 – a, b, c, d) or combinations of them, or even all together. In its decision, the pairs are presented in the form of alliance or peace by fairness (for example, legally, economic, technically and their combinations). The main sign of union and peace is the agreement, contract relationships of the pair. Such union or peace can not reach its complete integrity, as that typical for antinomy. Antinomies are initially always integrity of all types of intercommunication by mercy (for example, as a sister-mercy care after patient). The main sign of intercommunication of antinomy is synergy in integrity.

Ability to retain principle-antinomy is the condition of safe life activity.

Husband and wife are initially integral unity, and then their difference. Besides, for a religious person this whole unity spreads out of time and space, that is in eternity and endlessness. Remember biblical story of Adam creation, and then division in two people by God. Ability to retain principle-antinomy explains the phenomenon of family solidity, widowhood in case of spouse loss, friendship. Friendship is unanimity of two people. Friend is alter ego, accepted in you (Psalm 54, line 14).

Scientific pedagogic and psychology teaches leadership, development of psycho-physiologic possibilities of man, educates gods of professions, sport gods, men and women gods. As a result there is the necessity of connection of these people and idea «All people must be equal».

Orthodox pedagogic and psychology proclaims fundamental unity, as primordial unity of non-solid and inseparable in between people, and as a result appears the idea «All people must not be equal» - idea of hierarchical society.

Considering the above presented orthodox and scientific pedagogic and psychology can be perceived either as contradiction or as an antinomy.

Philosophy and logic has, except for mentioned above, pair categories-contradictions-antimonies: assertion - denial; thesis - antithesis; form - content; single - general; individual - social; concrete - abstract; theory - practice; logic - intuition; rationalism - mysticism; induction - deduction; - analysis - synthesis (differential - integral); symmetry. The laws of symmetry operate in mathematics, physics, chemistry, biology. There is homotypic human body, his organs, skeleton, muscular system, vascular systems, nervous systems, symmetry (polarity) in illnesses and therapeutics. Left and right. Two eyes, two ears, two cheeks, nostrils, two hands, two feet. In Christianity, for example: Old testament and New testament, Adam and Christ. Law and Grace. Two tablets of testament, etc. In Orthodox Christianity the example is sacred Church Slavonic language for prayer and sacred liturgy. This is the example of unification in the antinomies of word and action, mind and heart, soul and body, man and man, God and man. Ability to gather all forces in one point opens a secret, why there are so many great people in our history. The presence of natural and sacred language in the orthodox countries explains the phenomenon of antinomic thinking and acts, which are often externally alogical, and, as a result, western fear of unpredictable, for example, Ukrainians, Russian, Byelorussian.

Contradict and antinomic thoughts always live in any man. Believers-Christians who follow the Definition of Chalcedon, have the perspective possibility to save the integrity and unity of life activity of mind and heart, soul and body, word and action, and consequently integrity and unity of life activity give result out of time and space, that is, in eternity and infinity. Imperishable relics, chronicles, life of Christians testify in favor of that. Having perishability in the sense of *separation* (tab 2., line - b) from the mortal body, the body of Christians are not subject to perishability. These treasures are accessible in churches, monasteries and large monasteries.

Conclusion: the life activity of man and society depends on man's perception of the world either as pairs of non-antimonic contradictions offered by UNESCO or as principles-antinomies of the Chalcedon cathedral.

References

1. Типова навчальна програма нормативної дисципліни «Безпека життєдіяльності» для ВНЗ для всіх спеціальностей // Типові навчальні програми нормативних дисциплін «Безпека життєдіяльності», «Основи охорони праці», «Охорона праці в галузі», «Цивільний захист» / *Запорожець О.І., Садковий В.П., Михайлюк В.О., Осипенко С.І. та ін.* – К.: МОНМС України, 2011. – С. 7 – 22.

2. *Прот. Геннадий Фаст* ТОЛКОВАНИЕ на АПОКАЛИПСИС. – М.: Никея, – 2009. – 496 с.

3. *В.С. Стёпин* Конструктивные и прогностические функции философии. // Вопросы философии, – 2009. – №1. – С. 5 – 10.

4. *Лазарев С.С.* Онтология точности и прогностичности. // Вопросы философии, – 2004. – №1. – С. 113 – 127.

5. *Остапенко А.А.* Педагогические антиномии протоиерея Бориса Ничипорова / Уч. записки ОГУ. - Т.IV. Религиоведение. – Вып. 4. – Орёл: ОГУ, ООО ПФ "Картуш". – 2006. 178 с., – С. 148-152.

UDC 504.054 (45)

N. Duchene, Aviation Environmental Consultant Partner (ENVISA, France)
K. Synylo, assistant (National Aviation University, Ukraine)

SENSITIVITY ANALYSES OF THE EMISSIONS OF NOX FROM A TURBOFAN ENGINE BASED ON ENGINE MODEL

Validation studies of emission model on the ground of measurement campaign results of engine testing for real operation conditions. Sensitivity analysis of developed Turbogas model which taking into account impact of operational and meteorological conditions on emission indexes

Introduction

Air pollution resulting from airport emission is a growing concern because of the expansion of air traffic over the years. On the ground of ICAO data, future air traffic movements are forecast to grow at a mean annual rate of 5 to 7 percents. A lot of studies are focusing on the aeronautic impact to the upper troposphere and lower stratosphere [1], during last decade a lot of investigation are also focusing on evaluation on aircraft engine impact on local and regional air quality in the vicinity of the airport [2,3,4,5]. Currently the basis objects of attention are NOx and fine particle emissions from aircraft engine emissions as initiators of photochemical smog and regional haze, which further direct impact on human health.

Emissions of aircraft at airports are usually calculated on the basis of certificated emission indexes, which is provided by the engine manufacturer and collecting in the database of International Civil Aviation organisation (ICAO) [6]. The emission indices rely on well-defined measurement procedures and conditions during engine certification. Under real circumstances, however, these conditions may vary and deviation from the certificated emission indices may occur. So, development model including the influence of the operational and meteorological conditions on emission indexes is actual task.

Experimental investigation of aircraft engine emission

Experimental investigation is providing a more accurate representation aircraft emissions contribution to total air pollution in the vicinity of the airport and allow precisely calculate the emission inventory of airports.

Some measurement campaigns were performed at major European airports using non-intrusive spectroscopic methods like Fourier transform infrared spectrometry and differential optical absorption spectroscopy [7,8]. Therefore, basic aim of these experimental investigations was estimation emission indexes for CO, NOx and comparison to the values given in the ICAO database. One of such projects is collaboration between FZK/IMK-IFU in Garmisch-Partenkirchen and Lufthansa Technik AG in Munich [9]. This project was aimed to obtain accurate emission characteristics of aircraft engines, reveal its dependences on operations' conditions (period of engine mode, fuel flow, rpm) and ambient temperature [9]. Measurement campaigns (number = 490) in fulfilled gases jet from CFM 56-5C2/F, which powers the aircraft A340-300 (D-AIGD, D-AIGF), were performed at the Munich airport during period of three years. Measured concentrations of NO, NOx, CO, CO_2 and H_2O were conducted at the nozzle exit of engine (or in plane parallel to engine nozzle at distance approximately 10 cm) by using Fourier transform infrared spectrometry method (FTIR) [9]. An absolute accuracy of this method is 20 to 30% to determine real in-use corresponding emission indices of NO, NOx, CO, CO_2, H_2O for Idle (N1 =20 - 22%, the beginning and the end of engine testing phase) and Cruise (N1 = 79 - 81%, climb-out and approach phase) engine operation modes [7, 9].

Measurement results were officially provided by Lufthansa Technik AG for validation studies of emission model of turbofan engine, which was developed in scope of Turbogas project of Clean Sky JTI company[10].

Validation results

Measured and calculated Emission Index data for NO_x in dependence with measured (for conditions of measurement campaign) Fuel Flow are shown in

Figure 1.

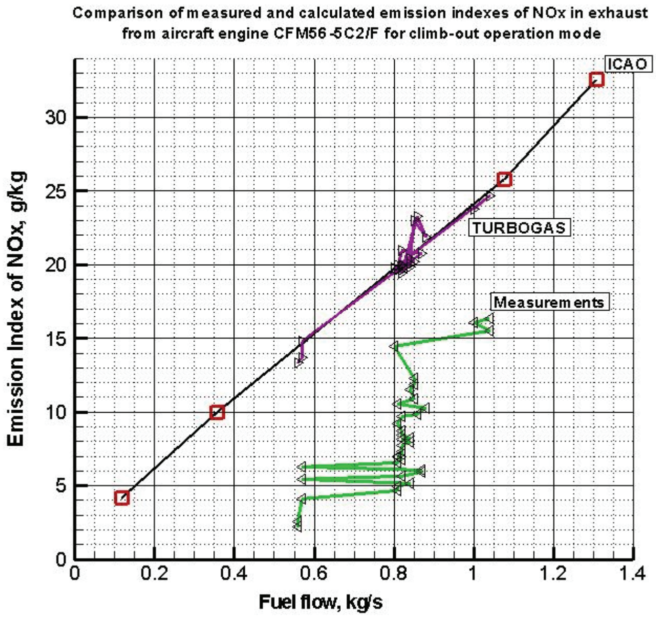

Figure 1: Graph for measured and calculated Emission Index data for NO_x in dependence with Fuel Flow and comparing with ICAO values for CFM-56-5C2/F

Calculation results of Turbogas model is lying above the curve for certification data for CFM-56-5C2/F, calculated EI NO_x are higher than measured analogues (for the same conditions as in measurement campaigns). The variance of the measured data is too wide (Figure 2). The variance of calculated data (for the same conditions as in measurements) is much less, which may show that not only conditions of measurements influenced on results – some value of accuracy in measurement method must be taken in mind, Fig.3 [7]. Calculated values of EI NOx via measured ones are shown in Figure 4, most part of the data are lying inside 0.95 Prediction Interval.

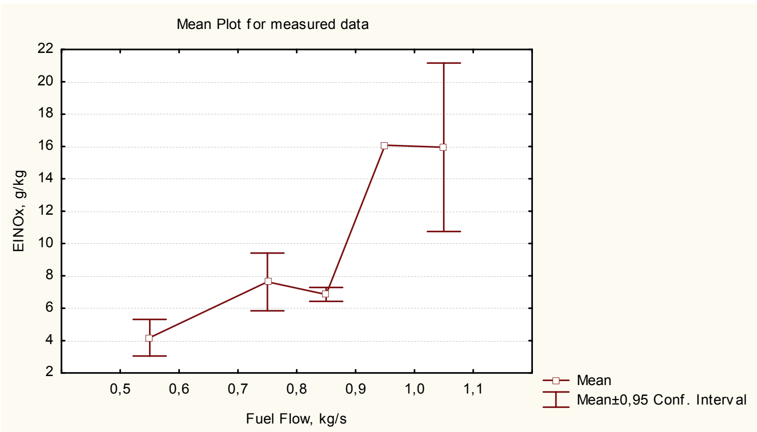

Figure 2: Graph for measured data of EI NOx in dependence with measured Fuel Flow

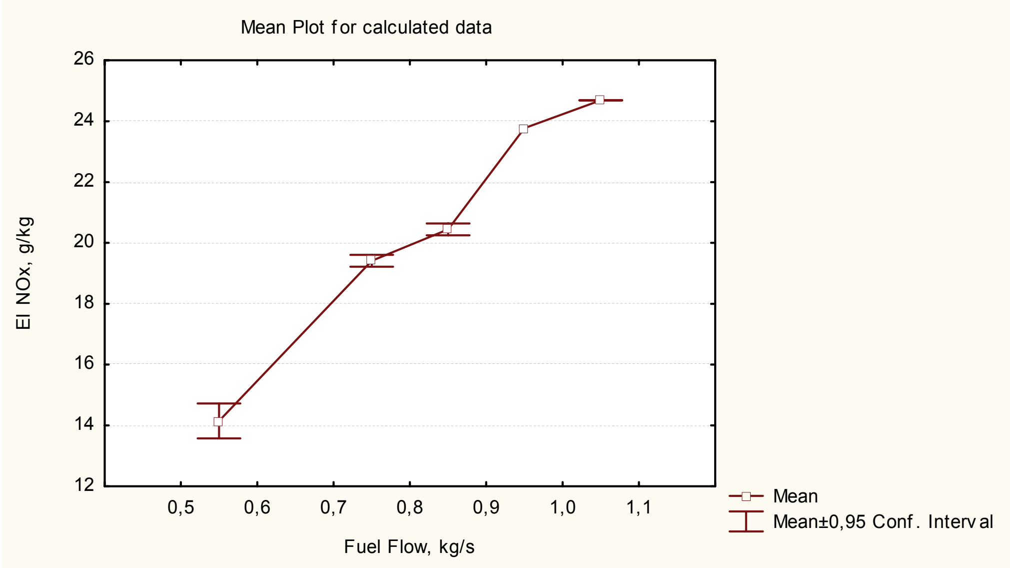

Figure 3: Graph for calculated data of EI NOx data in dependence with measured Fuel Flow

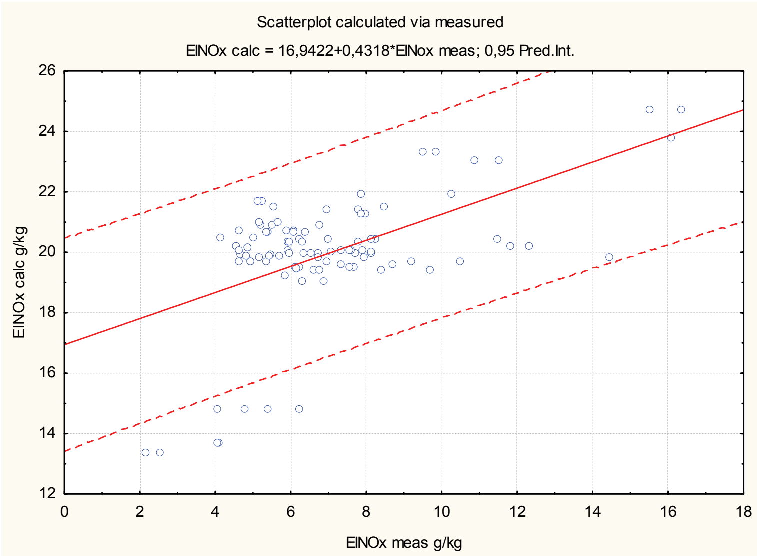

Figure 4: Calculated EI NOx via measured EI NOx with 0.95-prediction interval

Fine-tuning of Turbogas parameters

Regression analysis was done for EINOx data: for measurements (Figure 5) and for calculations (Figure 6). Regression lines are fitted in 0.95 prediction intervals via Fuel Flow (FF) with following prediction expressions:

- For measurements: EI NOx = -6.0944+16.02*FF;
- For calculations: EI NOx = 0.9408+23.2864*FF.

Regression analysis was done for EI NOx calculation data (Figure 7). Regression lines are fitted in 0.95 prediction intervals via Fuel Flow (FF) with following prediction expressions: EI NOx = 0.7559+29.3372*FF

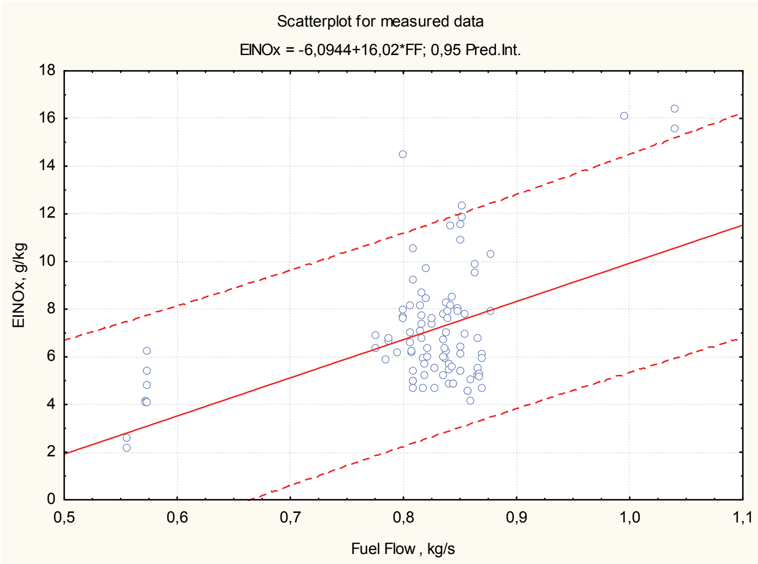

Figure 5: Line regression for calculated data of EI NOx via measured Fuel Flow

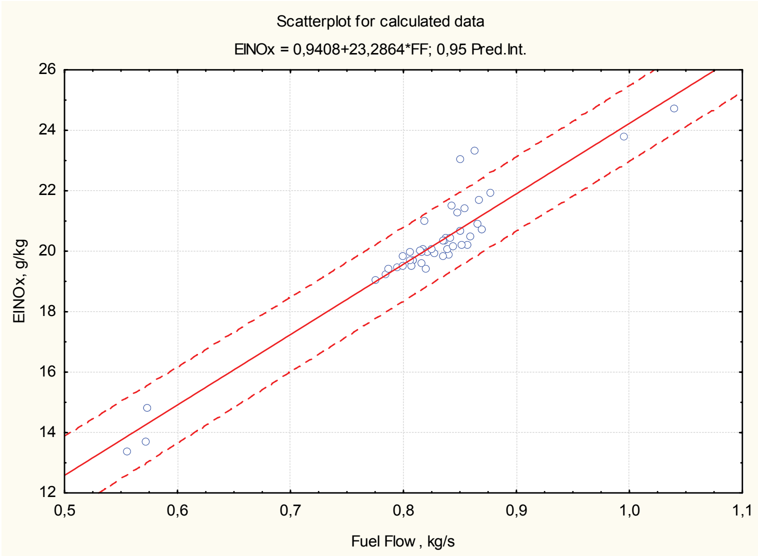

Figure 6: Line regression for calculated data of EI NOx via measured Fuel Flow

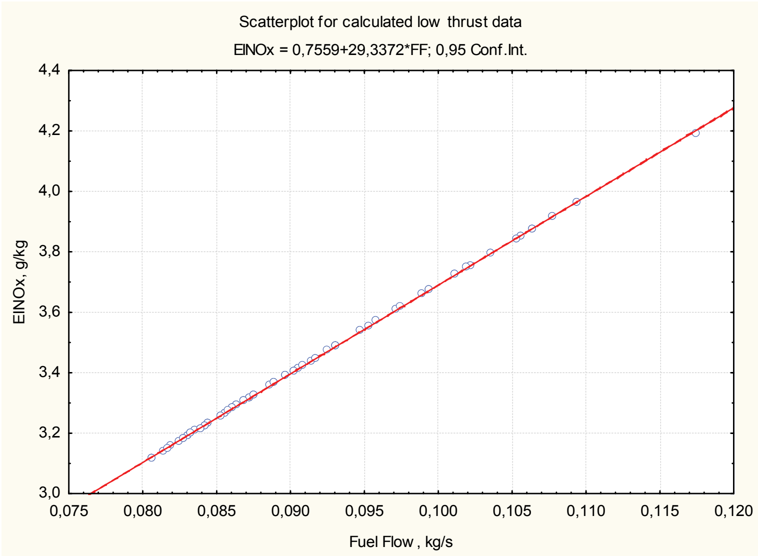

Figure 7: Line regression for calculated data of EI NOx via measured Fuel Flow for low thrust modes

For Low thrust modes the measurement data for EI NOx were equal to zero in total and the same tendency has been found for calculation with Turbogas model [10].

Sensitivity analysis of Turbogas model

Sensitivity analyses were performed for Turbogas emission model for aircraft A340-300 with engine CFM 56-5C2/F, using the input data for the cruising modes derived from the measurements performed by DLH [9]. The averaged values used for sensitivity tasks are shown below :

- FF_{mean} = 0.816761 g/s (Min = 0.555556, Max = 1.040000, Std Dev = 0.083559).
- FF = 2938.0 kg/h = 0.8161 kg/s (FF_{ref} = 2814.48 kg/h = 0.7818 kg/s)
- For temperature Ta = 11.5° C/284.65K
- For humidity H = 65.8%,
- For pressure Pa = 1009.7 mbar.

The objective of sensitivity studies is to investigate the changes in output (esp. EI NO_X) caused by variations of input data. The following parameters are studied, with step-wise variations on 2, 5 and 10%: fuel flow, temperature, pressure, humidity.

The results of the sensitivity analysis of the Turbogas model for engine CFM56-5C2 and the appropriate dependence of EI NO_X on fuel flow and ambient atmosphere conditions are represented on the following table and plot, Figure .

Table 1

Results from sensitivity studies for the CFM56-5C2

Parameter	**Range of parameter**	**Range of NOx (+/- %mean)**
Fuel flow	0.8161/0.8977	10.85
Ambient temperature	285 K to 313 K	27.7%
Ambient pressure	1010 mbar to 1011 mbar	5.0 %
Ambient relative humidity	66% to 72%	1%

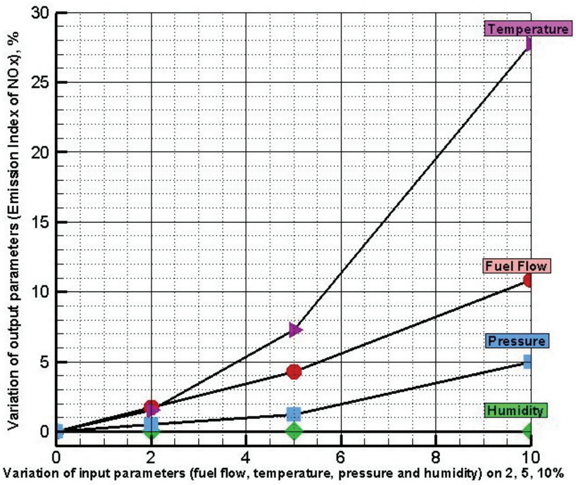

Figure 8: EI NO_X variability Vs input parameters for CFM 56-5C2/F

On the ground of the results obtained and of the comparison of the resulting differences, it can be concluded that the Turbogas model is not sensitive to air pressure and humidity. That is because the changes of these parameters input by 2% lead to variations of calculated EI NO_X lower than 2%. Likewise the changes of input parameters by 5% implied variations lower than 5%. The analysis of the modeled data showed that the Turbogas model was sensitive to ambient temperature. A change of temperature of 5% implied an increase of EI NO_X of 7.28%. At last the change of 10% lead to an increase in EI NO_X of 27.72%. Based on this last tendency it can be concluded that the Turbogas model is highly sensitive to the ambient temperature.

Also the analysis of obtained results confirm sensitivity of Turbogas model to fuel flow rate. The variation of this parameter on 2% lead to the change of EI NOx, however, the variation of input value on 10% implied and increase of EI NOx on 10.85%.

Conclusions

Calculated EINOx Turbogas tool for CFM-56 engine are higher than measured analogues (for the same conditions as in measurements). The variance of the measured data is very wide (Figure 22). The variance of calculated data (for the same conditions as in measurements) is much less (Figure 3), which may show that not only conditions of measurements influenced on results – some value of accuracy in measurements must be taken in mind. The method used for determination of EI NO_X on the basis of measured concentrations also had an impact on accuracy: in particular, NO_2 was not measured but rather estimated only which cause uncertainties to increase significantly in some cases. Results from validation tasks and sensitivity analysis concluded that developed emission model of turbofan engine taking into account the influence of the real operational (fuel flow rate) and meteorological conditions on emission indexes. According to calculation results by Turbogas model, the fuel flow rate and ambient atmosphere conditions (air temperature, pressure and humidity) have a large impact on the EI NO_X. In particular the sensitivity analysis showed that the model is highly sensitive to the fuel flow rate (increase EI NOx on 10.85% in case of change it on 10%) and ambient temperature (27.72% increase in EI NO_X in case of change it on 10%).

The research leading to these results has received funding from the European Union Seventh Framework Program (FP7/2007-2013) for the Clean Sky Joint Technology Initiative under grant agreement #CS-GA-2009-255674-TURBOGAS

Acknowledgements

First of all, the authors would like to thank Clean Sky JTI company for budget of research in scope of Turbogas project. The authors are very grateful to Prof. Klaus Schäfer from IMK-IFU, Garmish-Partenkirchen and Dr. Gerd Saueressig, Dr. Karlheinz Haag from Deutsche Lufthansa AG (DLH) for providing data of experimental investigation for validation tasks of Turbogas model/

References

1. *Rogers, H.L., Lee, D.S., Raper, D.W., Foster, P.M.d.F., Wilson, C.W., Newton, P.J.*, 2002. The impact of aviation on the atmosphere. Aeronautical Jounal 106, 521–546.

2. *Brasseur, G.P., Cox, R.A., Hauglustaine, D., Isaksen, I., Lelieveld, J., Lister, D.H., Sausen, R., Schumann, U., Wahner, A., Wiesen, P.,* 1998. European scientific assessment of the atmospheric effects of aircraft emission. Atmospheric Environment 32, 2329–2418.

3. *Klaus Schäfer, Carsten Jahn, Peter Sturm, Bernhard Lecher, Michael Bacher.* Aircraft emission measurements by remote sensing methodologies at airports. Atmospheric Environment, 37, 2003. – 5261-5271

4. *Gregor Schürmann, Klaus Schäfer, Carsten Jahn, Emanuel Fleuti*. The impact of NOx, CO and VOC emissions on the air quality of Zurich airport. Atmospheric Environment, 41, 2007. – 103 -118

5. *Asimakopoulos, Christoforos Halios, Ralf Kurtenbach, Anita Niedojadlo, Peter Wiesen, Evi Anamaterou, Michael O'Connor.* Airport air quality studies in Athens. First results of measurement campaign. – ECATS working paper, 2007

6. ICAO data bank of aircraft engine emissions. – Montreal: ICAO. Doc. 9646 - AN/943, 1995. – 152 pg.

7. *Heland, J., Schafer, K.:* Analysis of aircraft exhausts using FTIR-emissionspectroscopy. Applied Optics 36, (1997), Nr. 21, 4922-4931.

8. Opsis, DOAS User Guide. Opsis AB. – Furulund, Sweden, 1997.

9. Abschlussbericht zum Kooperationsvertrag zwischen Forschungszentrum Karlsruhe GmbH - IMK-IFU und Deutscher Lufthansa AG – Umweltkonzepte Konzern "Messung von Triebwerksemissionen zur Untersuchung von Alterungsprozessen mit Hilfe optischer Messverfahren", 2007

10. *N. Duchêne, K.Synylo and S. Carlier-Haouzi,* Deliverable D1 – Validation Test Report, CS-GA-2009-255674-TURBOGAS – TURBOGAS, 2011.

UDC 711.553.9:534.83

V.M. Zbrozhek, student (National Aviation University, Ukraine)

MOTIVATION OF THE BUILDING ZONE RESTRICTION AIRPORT "KIEV" (ZHULIANY) WITH PROVISION CONDITIONS OF AN AIRCRAFT NOISE AND FOR AIRCRAFT PARK DEVELOPMENTS.

Fleet article is devoted to the analysis of acoustic pollution in the vicinity of the airport "Kyiv", studies of aircraft fleet in the present conditions and in the future. Conducting this analysis allowed the area to justify limiting development around the airport in terms of aircraft noise.

Aircraft noise is still the most important problem of environmental protection in the operation of civil aviation. Aircraft noise makes a negative impact on a wide range of people, including not only the flight and technical personnel directly related to the operation of aircraft, other workers, passengers and airport visitors, but also and most numerous category of people - the population living in the area airport. The need for reducing the adverse effects of noise are particularly acute due to the increased fleet more noisy aircraft, increasing the intensity of their operation, expansion of airports and close to the boundaries of their neighborhoods with high population density [1].

The urgency of the work is necessary, research and development scenarios of formation and distribution of aircraft noise within the residential development around the airport Kyiv/Zhulyany from the perspective of fleet and exit the airport to the international arena to address environmental and acoustic problems associated with them.

The task of research were to:

- research aircraft noise pollution on the basis of calculation scripts flights of current and prospective;
- study zone limits development area near the airport "Kyiv" (Zhuliany).

Research methods - calculation of noise contours using the INM 6.1, analysis of the results of calculation and measurement (from other sources), the synthesis of recommendations for areas of building restrictions.

Airport "Kyiv" (Zhuliany) is virtually surrounded by residential buildings on all sides, that this city airport - it always requires more attention from research aircraft noise. During the last certification airport airport "Kyiv" (Zhuliany) in 2008 identified areas of aviation noise in force until today, the scenarios according to flight schedule aircraft current year and forecast scenarios 10 years ahead.

Today the problem of coexistence and the airport, taking into account perspectives of fleet (aircraft) airport and daily approach to residential development of the territory of the airport, are particularly acute Although not primarily an economic point of view, and to protect the environment and population first.

Therefore, using calculation software (INM 6.1), is a very important study propagation of noise in the area of residential development adjacent to the airport "Kyiv", predicting further development of airport infrastructure and in it [2].

Recent large-scale study on the airport zoning was conducted in 2008, but it involved primarily the use of aircraft like the Yak-40, Yak-42 and AN-24, and now, as already noted above, the basic aircraft is the A-320. Research in 2008 found that the standard takeoff aircrafts: Yak-42, AN-24 and Yak-40 had rates within zoning LÀ max 85 and 75 dB respectively, below gives practical and graphics on the areas of aircraft noise propagation (Figure 1, 2, 3) [3].

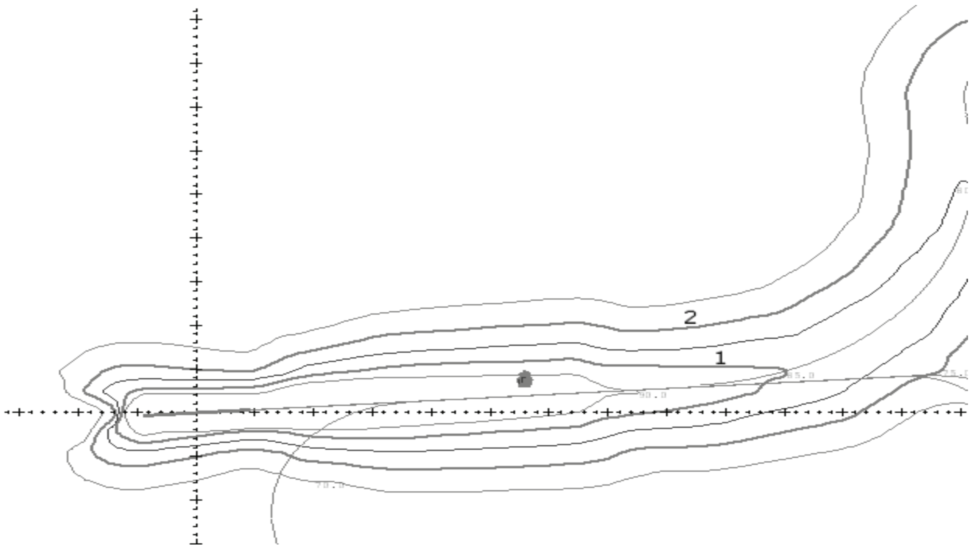

Fig. 1. YAk 42, $L_{A\ max}$, standard takeoff: 1 – 85; 2 – 75 dBA

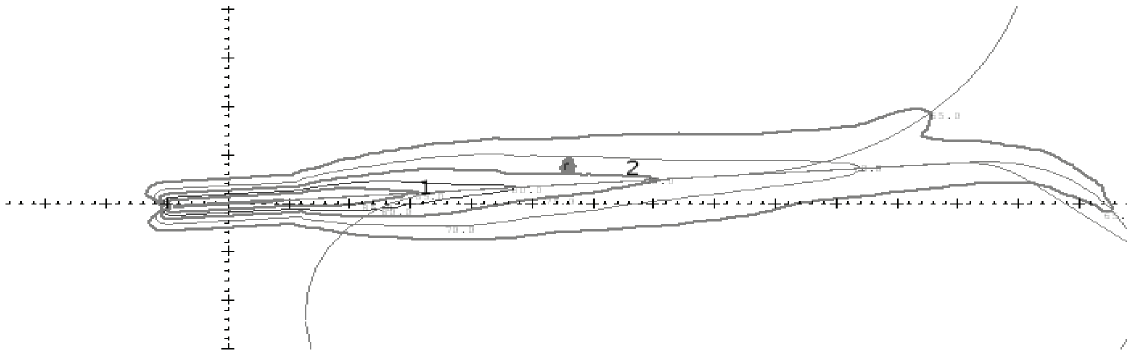

Fig.2. An-24, $L_{A\ max}$, standard takeoff: 1– 85; 2 – 75 dBA

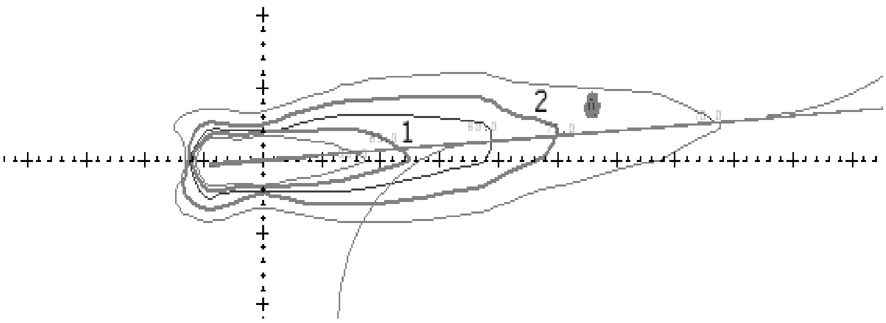

Fig.3. YAk -40, $L_{A\ msx}$, standard takeoff: 1 – 85; 2 – 75 dBA

But today with the arrival at the airport «Wizz Air» airline fleet filled with more modern aircraft, which replaced the old, noisy aircraft type Yak-42, came Airbus A-320. Airbus A-320 type is practically perfect in terms of acoustic characteristics ($L_{A\ max}$ shall not exceed the established norms) for airports located in the modern metropolis. It outlines the noise received in 2008, including aircraft type Yak-42 exceeded the noise contours projected in 2018, but by the time the flight with his participation occurred only once a day, and to a noise factor was influential, according to the current legislation of Ukraine such flights must be at least 5 takeoffs\landings during the day period. Other studied aircraft Yak-40 and An-24 do not exceed the established areas and criteria for airport noise. Currently in the fleet are available primarily A-320 aircraft and from aviation plant An-24.

The study is conducted for the script in 2011 showed that the area $L_{A\ eq}$ paths are less than forecast in 2018. It should be noted that the standard method of flight paths of noise in 2008 and 2011 almost coincide. Therefore, additional studies that with increasing intensity of flights at the airport “Kyiv” (Zhuliany) it would be to use methods of takeoff/climb ICAO And in both directions, the calculation of which is also represented in the work. This allows you to gain an advantage of about one kilometer along the route of flight zones prohibit housing. After increasing the intensity of flight A-320 by standard methods this should also take-off zones violation of noise pollution, and this development is actually desirable because of the existing administrative and residential buildings, the high cost of land because the airport would be advantageous to operate the aircraft that fit into these area [4].

At today in the course of research work has investigated the spread of noise contours ($L_{\grave{A}\ max}$) Aircraft type A-320 for the script as of 2011. Studies have shown that propagation paths of noise ($L_{\grave{A}\ max}$) near the airport “Kyiv” (Zhuliany) are in the same range of 85-65 dB, due to a higher intensity for flights of more powerful aircraft like A-320. Below is a calculation of the data confirmed graphics for standard take-off (Fig. 4) and the methodology ICAO (Fig. 5) and ICAO A (Fig. 6), where each path has its own respective area of distribution in three dimensions (km^2 , m^2 and acre), which allows to determine the exact location of residential areas under the influence of different levels of aircraft noise. Estimated data calculation zone propagation of noise from $L_{A\ eq}$ for 2018 will look, shown in Fig. 7 [5].

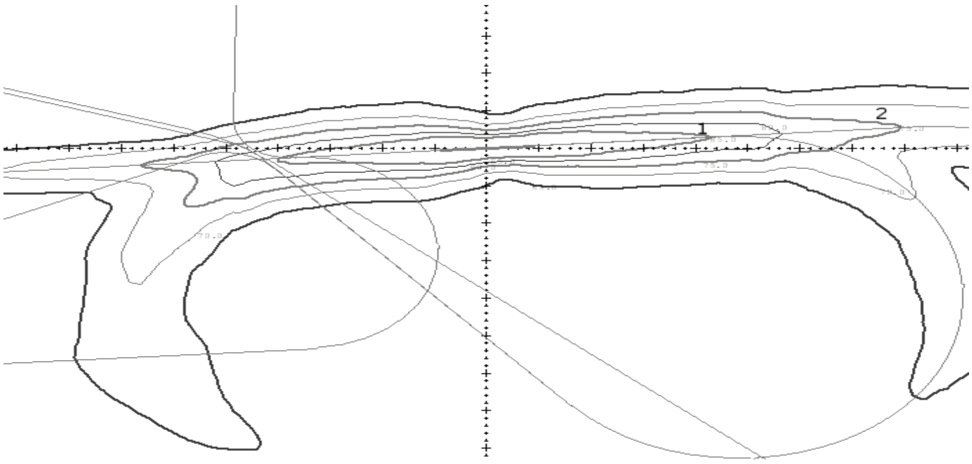

Fig. 4. A-320 $L_{A\ макс}$, standard takeoff: 1 – 85; 2 – 75 dBA

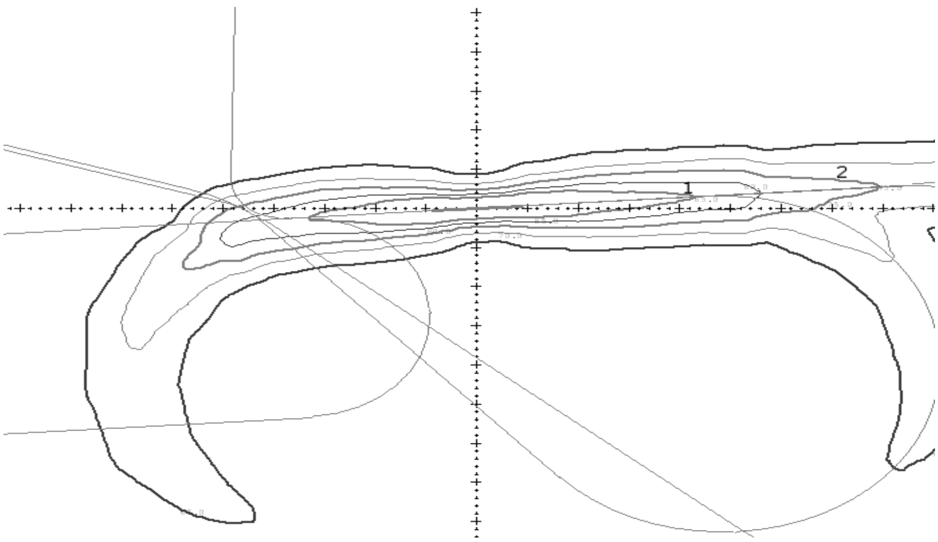

Fig. 5. A-320, ICAO B methodic: 1 – 85; 2 – 75 dBA

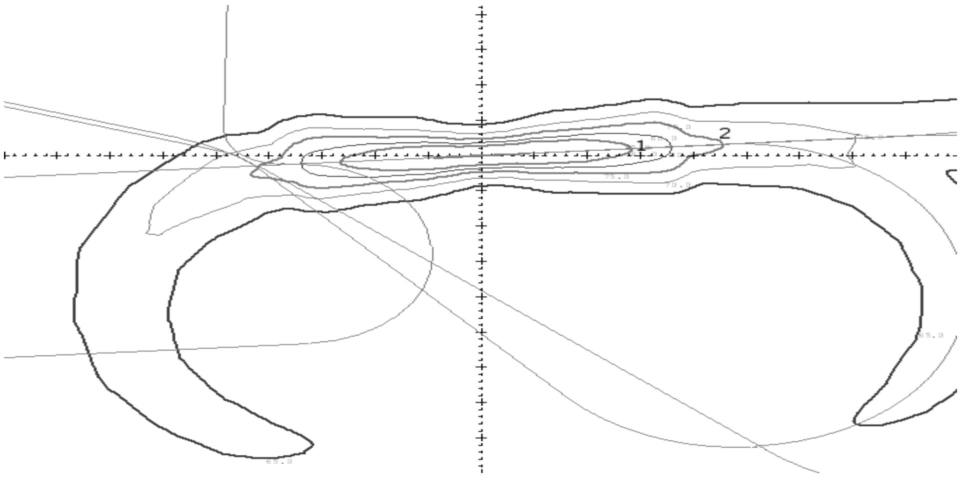

Fig. 6. A-320, ICAO A methodic: 1 – 85; 2 – 75 dBA

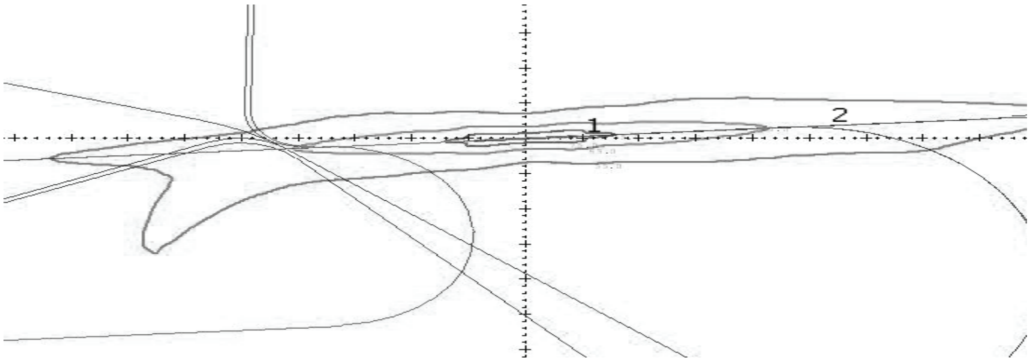

Fig. 7. Estimated data calculation zone propagation of noise from $L_{A\ eq}$ for 2018 airport "Kyiv": 1 – 75: 2 – 65.
Standard procedure

Conclusions

Thus, the results show that the introduction of the airport "Kyiv" (Zhuliany) manual transmission medium aircraft possible, but their noise characteristics must meet the requirements of Chapter 3 and Chapter 4 is better, Annex 16 and ICAO Convention. Modern A-320 specifications for noise standards meet Chapter 4 [6].

The basic measures to reduce aircraft noise in residential development within the airport "Kyiv" (Zhuliany):

1. Operations on how ICAO And during the night operation of aircraft;
2. gradual replacement of most noisy aircraft less noisy modern aircraft, establishing optimum noise on arrival and departure routes;
3. exclude the use of reverse thrust at landing the most noisy aircraft;
4. towing aircraft from parking areas to launch;
5. implementation of building and planning measures to reduce noise pollution around the airport "Kyiv" (Zhuliany).

In addition to:

1. provide limits residential development in the critical, the impact of noise zones;
2. recommend implementation of the airport "Kyiv" (Zhuliany) automated control aircraft noise system;
3. use the results of these studies and recommendations for implementation of measures to reduce aircraft noise near the airport "Kyiv" (Zhuliany).

Necessary to develop a new master plan for the airport and build a new forecast scenarios that will continue to justify the zone limits development in terms of noise. Forecast scenarios three years ago no longer meet the modern concept of the airport.

The airport should have a means of objective control environmental noise that will monitor compliance with regulations and the impact of noise around the airport, and thus - the requirements established zones.

References

1. ICAO technical guidance on environment using methodics for certification of aircrafts on noise. - Montreal: ICAO, Doc. 9501-AN/929, .2, 1995. – 112p.

2. INM Pre-approved List of Aircraft Substitutions. March 10, 1998. P.P. 1 – 6.

3. Directive 2002/49/EC of the European Parliament and of the Council of 25 June 2002 Relating to the Assessment and Management of Environmental Noise - 2002.

4. The recommended method of calculation of noise contours around airports. - Montreal: ICAO, Circular 205 AN/1/25, 1988. – 25p.

5. Guidance on implementation of flights. OPS. T.1: Procedure of implementation of flights. - Montreal: ICAO, Doc.8168-1, 4, 1993. - 116 p.

6. Summary statement about a permanent policy and practical worker ICAO in area of environment guard. Resolution of A31-11 of Assembly of ICAO, 1995. – 8p.

UDC 004.942:621.38 (045)

A.V. Vishnevsky, PhD (National Aviation University, Ukraine)

2D-MODELING OF AIRPORT TERMINAL MULTI-FREQUENCY ELECTROMAGNETIC POLLUTION

The two-dimention modeling of ecological monitoring system of airport's terminal two-frequency electromagnetic pollution has been considered

Introduction. A modern airport is a complex multiphysical system, that can be treated from ecological point of view in three main different ways: noise, chemical pollution and electromagnetic pollution (EMP) of environment [1-3]. The last is the object of investigation presented in these proceedings.

Mesh modeling. It is well known, that certain requirements exist, establishing maximum allowable levels (MAL) of electric tensity of the field, radiated by airport and aircraft radioequipment, for any used ranges of electromagnetic field. For example, these MAL for airport radioequipment, for frequency range 100-300 MHz, have been taken as 12 V/m [4]. In these range of frequencies work many aircraft's radiating antennas.

Aircraft *Antonov-148* uses antennas with working frequencies 118-136 MHz [5]. So, with help of *Comsol Multiphysics* ® modeling software [6], we will predict for such a range behavior of electromagnetic field radiated by three aircrafts situated in arbitrary positions near some abstract airport's terminal of square shape, which walls are made of thin glass. Mesh contains 45648 triangular elements. Shown only 9374 elements for good visibility (fig. 1).

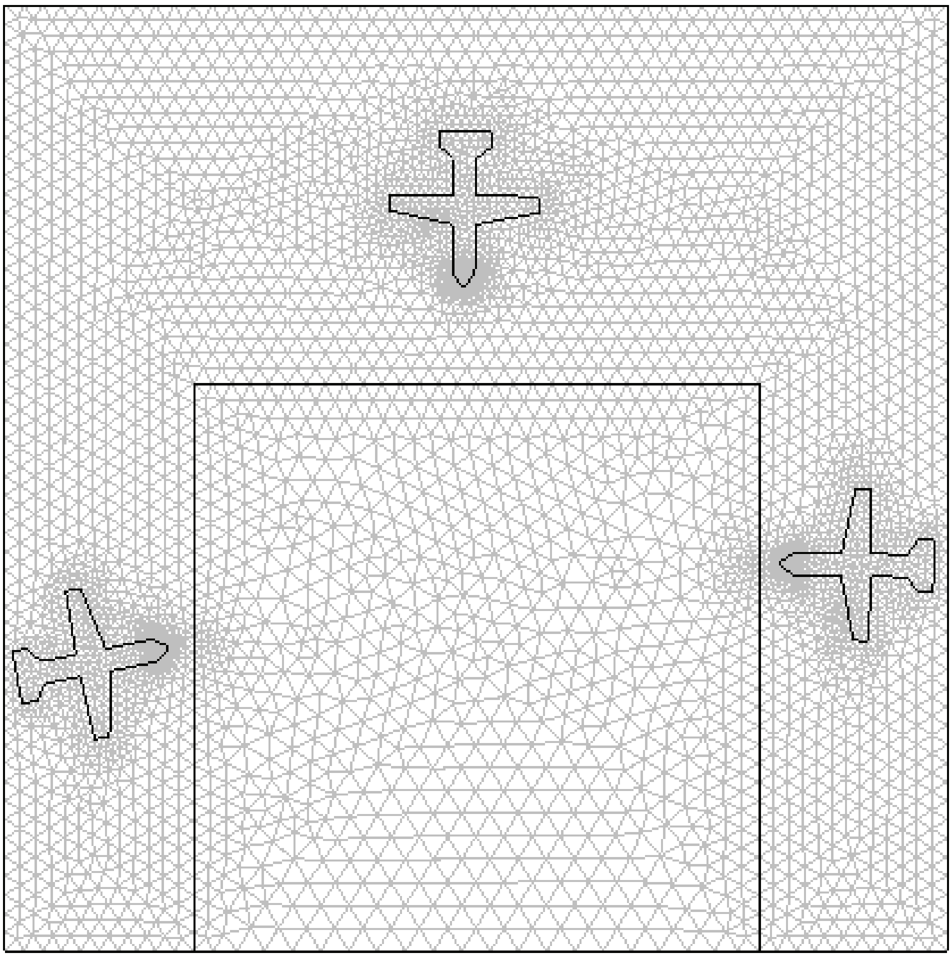

Fig. 1 Proxy mesh

Physics. The mathematical equation for description the physical processes for this model is the following one [7]:

$$\nabla \times (\mu_r^{-1} \nabla \times E) - (\varepsilon_r - j\sigma / \omega \varepsilon_0) k_0^2 E = 0,$$

where $м_r$ - relative magnetic permeability of substance; E - intensity of electric field at the monitoring point, (*V/m*); $е_r$ - relative dielectric permittivity of environment; у - conductivity of proxy element, (*Sm/m*); щ - circular frequency of oscillations, (Rad/s); $е_0 = \frac{10^{-9}}{36\pi}$ - electric constant, (*F/m*); $k_0 = \frac{2р}{л}$ - wave number; л - wavelength of oscillations.

Radiation modeling. Let us take a three finite elements models (FEM) of aicrafts 1, 2, and 3 placed at 10m distance from three adjoining walls of the terminal (fig. 2). Aircrafts 1 and 2 have same isotropic antenna at the front edge of left wing, in the middle, radiating at 120 MHz (power 15 W). Aircraft 3 has an isotropic antenna at the front edge of right wing, in the middle, radiating at 135 MHz (power 15 W).

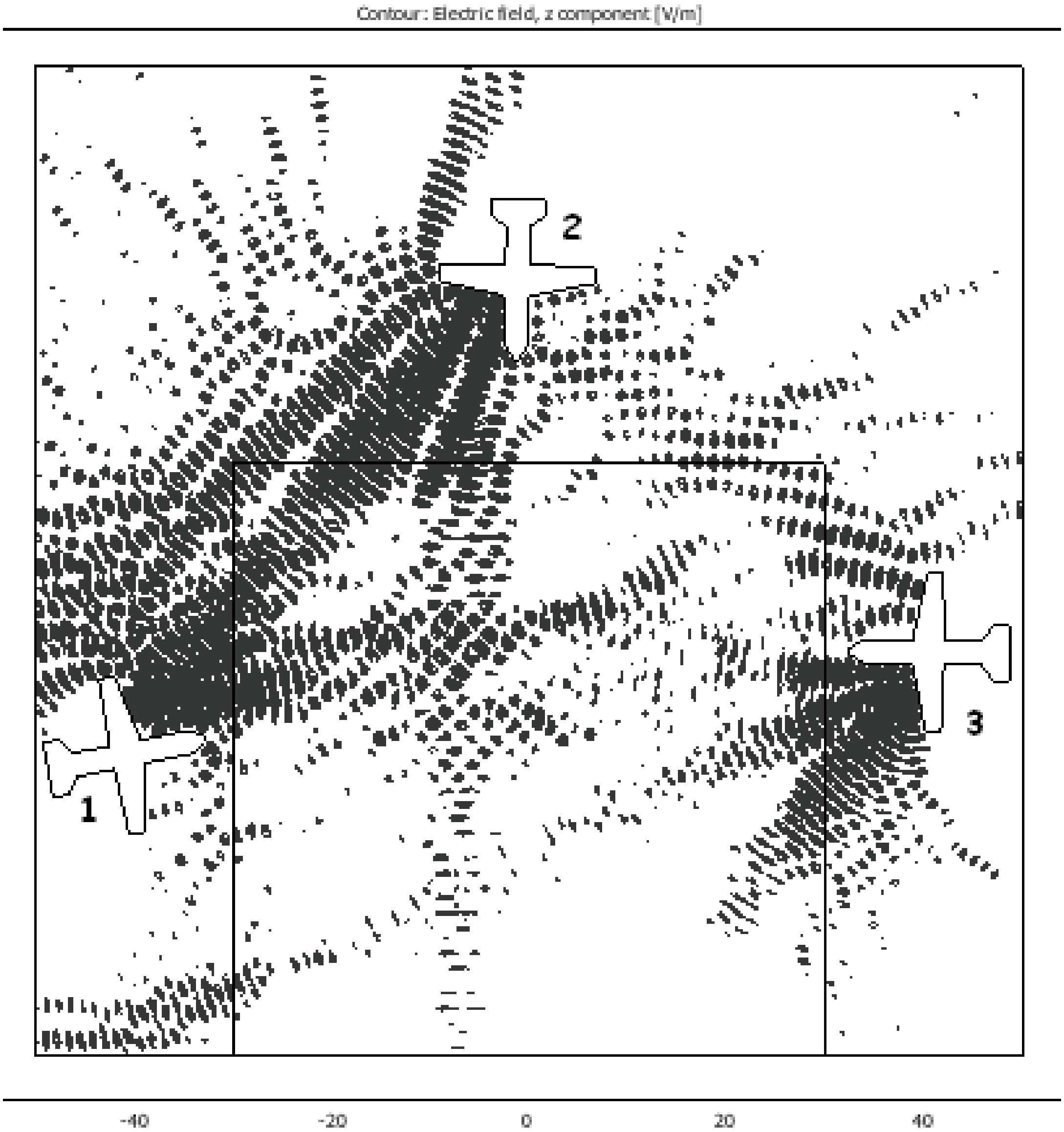

Fig. 2 Radiation pattern (contour plot)

All black regions on fig. 2 represent excess of MAL. Therefore, no passengers allowed in this area for possible health threat reasons.

Conclusions

Distribution of electric field is investigated for territories near airport's terminal for three radiating isotropic antennas, installed at the front edge of the aircraft wings (120 MHz and 135 MHz). Places in which corresponding EMP MALs are exceeded have been found out. Further researches are necessary, with the purpose of EMP modeling of the real airport terminal (three-dimensional design).

References

1. *Федорович Г.В.* «Экологический мониторинг электромагнитных полей». М., 2004. – 71 с.
2. *Грачев Н.Н.* Средства и методы защиты от электромагнитных и ионизирующих излучений.М., изд-во МИЭМ, 2005.– 215 с.
3. *Антипов В.В, Давыдов Б.И., Тихончук В.С.* Биологическое действие, нормирование и защита от электромагнитных излучений. М.: Энергоатомиздат, 2002. - 177 с.
4. Санитарные нормы предельно допустимых уровней напряженности электромагнитного поля НЧ, СЧ, ВЧ и ОВЧ диапазонов, излучаемого радиосвязными средствами аэропортов гражданской авиации (№ 4946-89), 1989 г.
5. *Vishnevsky A.V.* Computation Method of Mutual Impact Coefficient of the Quarter-wave Wire Antennas Placed on Airplane Wire-grid Model : Proceedings of the third world congress [«Aviation in the XXI-st century». «Safety in aviation and space technologies». IEEE «Microwaves, radar and remote sensing symposium (MRRS–2008)»], (Kyiv (Ukraine), September 22-24, 2008) / М-во освіти і науки України, Національний авіаційний університет. – К. : НАУ, 2008. – С.279-282.
6. http://www.comsol.com
7. *Vishnevsky A. V.* Radiation Of a Current-Conductive 2D Object of a Complex Shape : Proceedings of IEEE Microwaves, radar and remote sensing symposium 'MRRS–2011'. – Kiev: NAU, 2011, p.135-138.

UDC 534.6:629.7

A. Jagniatinskis, Dr. (VGTU Scientific Institute of Thermal Insulation, Vilnius, Lithuania)
O. Zaporozhets, Dr. Prof. (National Aviation University, Kyiv, Ukraine)
B Fiks, Dr. (VGTU Scientific Institute of Thermal Insulation, Vilnius, Lithuania)

FORECASTING THE AIRPORT NOISE CAPACITY FROM MEASUREMENT RESULTS

Summary
Relatively to estimation time interval the short-term noise monitoring in vicinity of airports with low flight intensity is suggested to be applied for the environmental noise assessment with mobile station in few sensitive points instead of the calculation of aircraft noise maps only. Statistical processing of all collected sound exposure levels for appropriate aircraft fly-bys allows to develop prediction of noise impact in the selected point based just on flight intensity.

1. Introduction

Environmental noise management Directive 2002/49/EC [1] establishes obligation to express noise limit values (noise impact) at least in terms of two long-term indicators: L_{DEN} and L_{night}. The value of such annual indicators highly depends from the variations of the equivalents levels $L_{\mathrm{Aeq},T}$ in appropriate reference time interval T (day, evening, night) during the year. Usually the needed values of $L_{\mathrm{Aeq},T}$ are obtained from calculations and presented as a noise counters on the map, while measurements are used just for results validation [2]. Common provision for aircraft noise in situ measurements are described in the standard ISO 1996-2 [3], which become as a guideline referred to general test method development. As stated in the standard the sound levels shall, if possible, be determined from sound exposure level (*SEL*) measurements of individual aircraft fly-bys. Looking to predict noise impact dependencies taking into account the aircrafts fleet and flies intensity, the set of measurement results of the *SEL* in long-enough continuous time interval (e.g. month) for selected point in the vicinity of airport include *SEL*'s of at least each aircraft performed fly-bys event.

From these statistical data obtained a single number noise indicator can be used to describe the aircraft noise pollution in selected measurement point. If the period of monitoring is sufficiently long to collect the set of data contain acoustical information related to all types of aircraft as well practical aircraft flight trajectories in vicinity of airport. In such case these set of the data may be considered as representative. Following the standard ISO 1996-2 provisions in a such way obtained characteristics (in our case – histogram of *SEL* distribution and energy average *SEL*) may be used to extrapolate measurement results on the other time intervals, e. g. one year [4, 5]. In this study obtained from representative set of *SEL* data energy average sound exposure level was investigated as a indicator for prediction noise impact by calculations of appropriates L_{Aeq} level at the chosen environment point.

2. Theoretical relations between statistical and energy sound indicators

The histograms for L_{AE} (*SEL*) obtained by dividing the full range (from min to max value) of the acquired sound exposure levels into J intervals (e. g. a width of 1 dB) and calculating the corresponding densities of the histogram (sampling probabilities) h_k: $h_k = n_k/N$, where N is a sum of all n_k (k = 1,...,J) and n_k is the amount of $L_{\mathrm{AE},k}$ or $L_{\mathrm{Amax,S},k}$ levels falling into k-th interval. In such a way everyone of k intervals in histogram is presented by two parameters - its middle value $L_{\mathrm{AE},k}$ (or $L_{\mathrm{Amax,S},k}$) as well its weight h_k. Commonly the equivalent sound level $L_{\mathrm{Aeq},T}$ for time interval T, during which the histogram data were collected, can be calculated as:

$$L_{\mathrm{Aeq},T} = 10\lg\left[\frac{\tau_{\mathrm{ref}}}{T}\sum_{i=1}^{N}\left(10^{L_{\mathrm{AE},i}/10}\right)\right], \qquad (1)$$

where $L_{\mathrm{AE},i}$ (i = 1,...,N, N – number of fly-bys in interval T) – sound exposure level of each fly-by.

As was shown in [6] that if N is sufficient large the sum in last formula can be presented on the base of corresponding J–th intervals of histogram data in the second view:

$$L_{\text{Aeq},T} = 10\lg\left[\frac{\tau_{\text{ref}}}{T} N \sum_{k=1}^{J}\left(h_k \times 10^{L_{\text{AE},k}/10}\right)\right], \tag{2}$$

where h_k (k = 1,...,J, J – number of histogram intervals) is a weight (component) of histogram for k–th interval (sum of h_k is equal to 1 (100%)); $L_{\text{AE},k}$ - middle value of exposure level for k–th interval.

Formula (1) for practical use can be presented in other view separating energy mean sound exposure level and number of flights N in estimated time interval T:

$$L_{\text{Aeq},T} = 10\lg\left[\frac{1}{N}\sum_{i=1}^{N}\left(10^{L_{\text{AE},i}/10}\right)\right] + 10\lg\left(\frac{\tau_{\text{ref}}}{T} N\right) == \overline{L}_{\text{AE}} + 10\lg\left(\frac{\tau_{\text{ref}}}{T} N\right), \tag{3}$$

where $\overline{L}_{\text{AE}}$ is the energy average of all N fly-bys in time interval T.

Similar transformations can be applied to the formula (2):

$$L_{\text{Aeq},T} = 10\lg\left[\sum_{k=1}^{J} h_k 10^{\frac{L_{\text{AE},k}}{10}}\right] + 10\lg\left(\frac{N\tau_{\text{ref}}}{T}\right). \tag{4}$$

It is necessary to emphasize that energy mean value $\overline{L}_{\text{AE}}$ at the same time represent a descriptor for statistical distribution of all obtained $L_{\text{AE},i}$:

$$\overline{L}_{\text{AE}} = 10\lg\left[\sum_{k=1}^{J}\left(h_k \times 10^{L_{\text{AE},k}/10}\right)\right], \tag{5}$$

Obtained dependences (3-5) shows useful way for estimation in long term interval in case of statistically enough number of sound exposure levels collected during the shorter measurement time. Selected sampling must at least cover full fleet of operated aircrafts and their de-facto trajectories near the point of estimation.

3. Experimental investigations by in-situ aircraft noise measurements

For the method under development a case study in the vicinity of Vilnius International Airport was carried out. By particular reasons the investigated point was selected just within the borders of L_{DEN} =55 dBA zone for aircraft noise. This point is placed 50 m from city arterial road, where traffic noise value have a similar value. As a result the total noise level L_{DEN} at the point of study is about 60 dBA. Aircraft noise footprints (green line) as well location of measurement point (designated as **M**) presented in Fig. 1. The distance of point M from the airport runway is equal to 3.9 km. The measurements were accomplished during January of 2012 and used to check possibility to estimate 2011 year average value from the number of flights as well to compare with the calculation results. The sound pressure level was calculated by formula (3) and (4) from one month duration measurement results and it is presented as a histogram of sound exposure levels and shown in Fig. 2. The energy average *SEL* values are presented in Tab. 1. Important to emphasize that *SEL* values were calculated for different time intervals of estimations during the one month measurements: day (12 h, 06:00-18:00); evening (4 h, 18:00-22:00) and night (8 h, 22:00-06:00), remain similar. It looks logical because statistically representative sampling during different time intervals of day covers all variances in aircraft acoustical and performance characteristics.

Table 1

Energy mean values of L_{AE} (dBA) for aircraft fly-bys at the point **M** during one month

Day	Evening	Night	Total
84.7	84.7	84.9	84.8

For better understanding influence the changes in the fly intensity on different parameters the number of everyday fly-bys (N) during the month of experiment is presented on Fig 3. Number of fly-bys during long time intervals is used to calculate long-term noise metric in accordance with formulas (3)-(4).

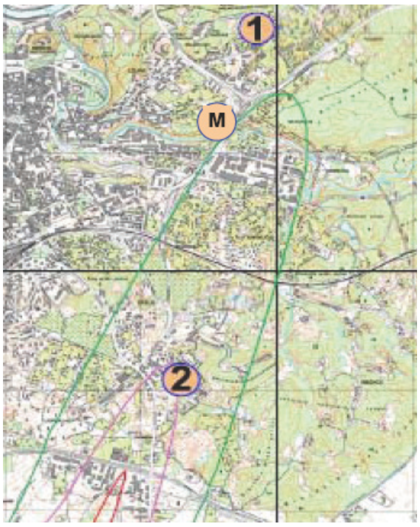

Fig. 1. Location of point **M** selected for investigations and permanent monitoring points 1, 2 in vicinity of Vilnius international airport: point **2** (magenta line) – L_{DEN} =60 dBA; point **M** (green line) - L_{DEN} =55 dBA

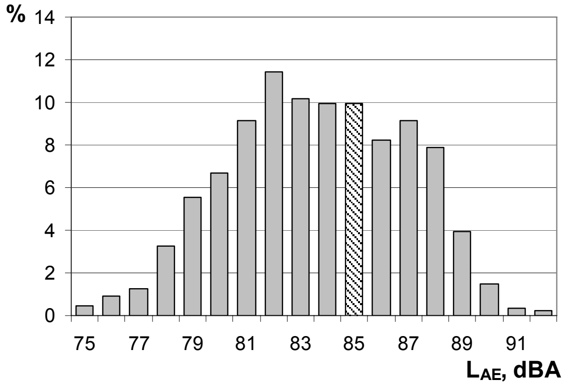

Fig. 2. Histogram of sound exposure levels (grey columns) collected during one month and its energy mean value (dashed column

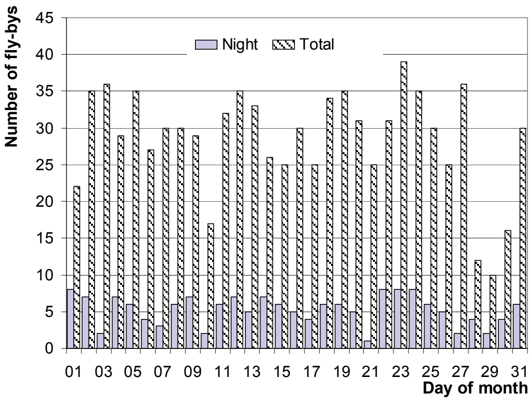

Fig. 3. Number of the full day (24h) and night time (8h) fly-bys during one month of investigation

Changes in the number of flights above the point M related not only to schedule, but also to weather conditions, especially a wind direction. Totally during time of experiment in airport was implemented 2243 flight operations in all directions, while in the point M was fixed only 885 fly-bys.

Fig. 4 shows L_{DEN} and L_{night} everyday values of aircraft noise assessed by two approaches. First apply full histogram data off all fly-bys [formula (4)] and next apply energy mean value [formula (3)]. Obtained results compared with directly every day from sound exposure levels measured L_{DEN} and L_{night} values [formula (1)]. The differences in results by the days in Fig. 4 show, that if the number of flights become smaller, statistical approach not applicable and we watch dissipation in results obtained in different ways. But, if measured set of data become statistically representative, like in case for full month measurements, we obtain similar results as that is showed in Tab. 2.

To check possibility of suggested approach to foresee annual value from one month measurements the 2011 annual aircraft noise levels at point M was assessed using in 2012 Year January measured data histogram (Fig. 2). Total energy average *SEL* is presented in Tab. 1 and Tab.3 due to flight intensity applying formula (3). The results are presented in Tab. 4 for comparing with 2011 results measured with permanent noise monitoring stations at points 1 and 2 (Fig. 1). Results in Tab. 4 are in a good conformity with calculated annual specific aircraft sound pressure values in the point M, -n Fig. 1 the point M is placed on aircraft noise contour 55 dBA.

Developing this approach assuming that representative value of *SEL* energy average in selected point is 84.8 dBA (Tab. 1) from formula (3) predicted noise pollution in selected vicinity of airport point may be calculated just from aircraft fly-bys. Fig. 5 and Fig. 6 show L_{Aeq} dependence from various reference time periods as a function of aircraft fly-bys number N and more practical fly-bys hourly intensity value (N/T).

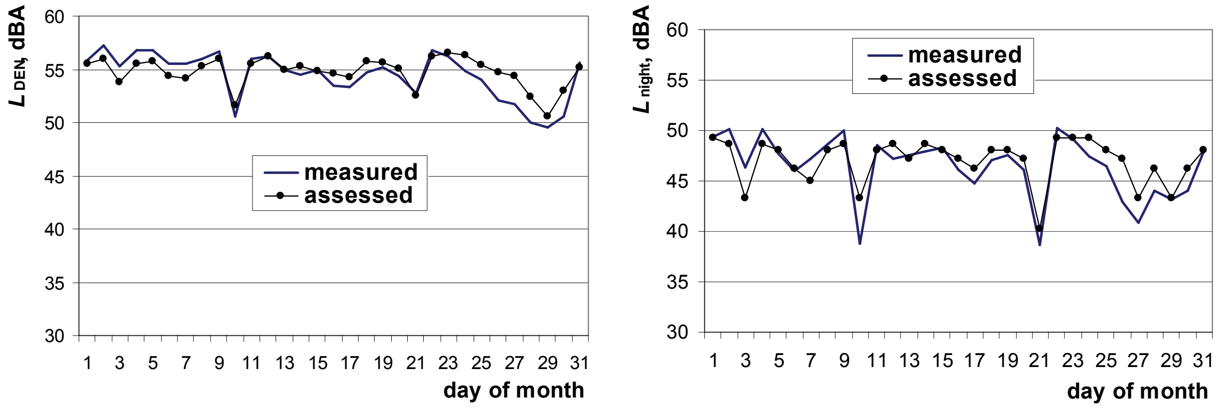

(a) (b)

Fig. 4. Measured and assessed by formula (4) L_{DEN} (a) and L_{night} (b) values of aircraft noise in point **M**

Table 2

Monthly aircraft noise sound pressure levels (in dBA) at the point **M** during day (06-18, 12h), evening (18-22, 4h) and night (22-06, 8h) periods, directly measured and estimated from mean *SEL* values

Descriptor	L_{day}	$L_{evening}$	L_{night}	L_{DEN}
Assessed	50.7	51.2	47.3	54.9
Measured	50.8	51.1	47.4	55.0

Table 3

Aircraft fly-bys number at point M in 2011

Day	Evening	Night	Total
6850	2056	1641	10547

Table 4

Measured (at points 1 and 2) and estimated (point M) 2011 annual aircraft noise sound pressure levels (dBA)

Point	L_{day}	$L_{evening}$	L_{night}	L_{DEN}
1	46.9	48.3	43.2	51.1
2	56.9	58.7	51.6	60.5
M	51.2	50.7	46.7	54.5

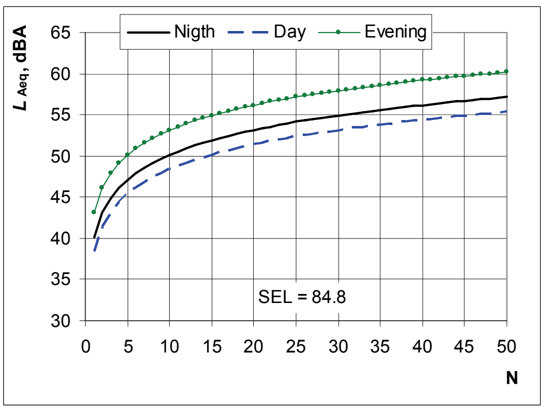

Fig. 5. Dependencies to predict equivalent noise level from number of fly-bys

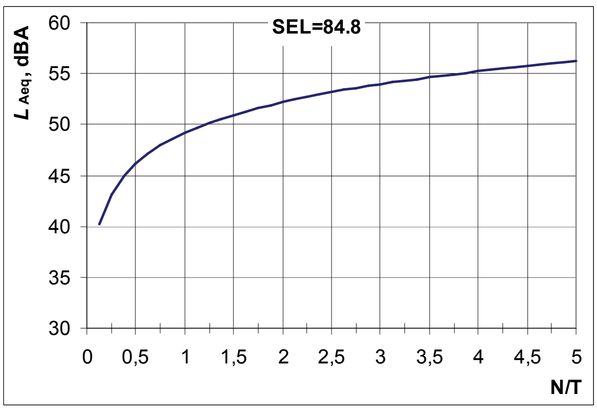

Fig. 6. Dependencies to predict equivalent noise level from fly-bys intensity

For example fig. 6 forecasts that in case of flight intensity not more than 1 flight per hour (in our case that happens at night, Fig. 3, and also in evening periods) the L_{Aeq} values will not exceed

50 dBA. In day periods when intensity grows till 3 – 4 flights per hour the L_{Aeq} values will not exceeds 55 dBA in point M.

In the moments of fly-bys near observation point the immediate noise impact duration can be evaluated from Fig. 7 and Fig. 8. Obtained noise estimated during different reference time give a big variety in values. For example the aircraft event noise is hearing on the ground on average 40 s and appropriate average outdoor sound equivalent level is about 68 dBA.

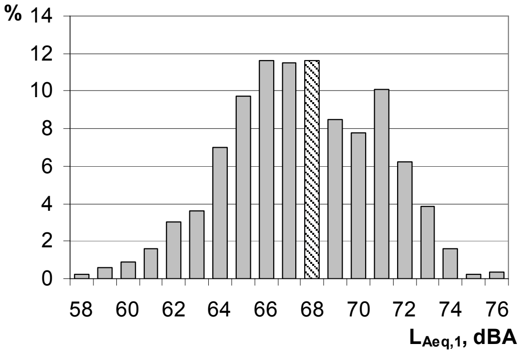

Fig. 7. Histogram of during one month collected sound equivalent levels of all aircraft fly-bys (grey columns) and its arithmetic mean (dashed column)

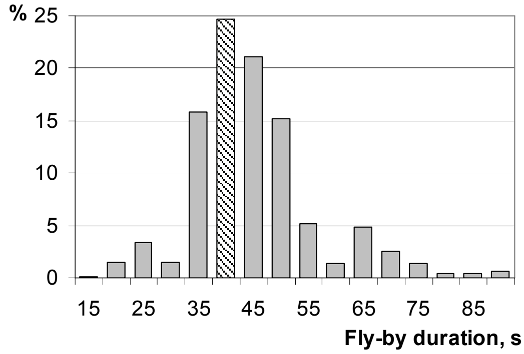

Fig. 8. Histogram of during one month collected fly-bys durations of all aircraft fly-bys (grey columns) and its arithmetic mean (dashed column)

Conclusions

It is shown theoretically and by results of experimental study that noise indicators, represented by as logarithmical function, such as a sound exposure level value, and collected by measurements as a statistically representative set of data, contain important information applicable to specify noise pollution. An obtained relation presented graphically and allows using the histogram of sound exposure levels calculate long-term sound pressure levels in the vicinity of airports, while energy average can be used as a sound exposure rating value.

Additionally shown that energy mean sound exposure value obtained during measurements carried out comparative shortly to estimation time interval may be used for forecasting (prediction) long term noise indicator values just on the base of flights number (or hourly flight intensity).

References

1. DIRECTIVE 2002/49/EC OF THE EUROPEAN PARLIAMENT AND OF THE COUNCIL of 25 June 2002 relating to the assessment and management of environmental noise. Official Journal of the European Communities, L 189, 18.07.2002.

2. Consultation on proposals for transposition and implementation of Directive 2002/49/EC of the European Parliament and of the Council of 25 June 2002 relating to the assessment and management of environmental noise. DEFRA Publications, London, February 2005, 126.

3. Standard ISO 1996-2:2007 Acoustics — Description, measurement and assessment of environmental noise —Part 2:Determination of environmental noise level

4. *Jagniatinskis A. Fiks B. Zaporozhets O.* Estimation of low intensity airport noise impact using different descriptors. Proc. EURONOISE 2012 Prague, Czech Republic, June 10-13, p. 1495-1500.

5. *Jagniatinskis A. Zaporozhets O. Kartyshev O. Fiks B.* Aircraft noise assessment in the vicinity of airports with different descriptors. Proc. Inter-Noise 2011 „Sound Environment as a Global Issue" Osaka, Japan, September 4-7, p. 4324-4331.

6. *Jagniatinskis A. Fiks B. Mickaitis M.* Statistical assessment of environmental noise generated by road traffic. Transport, 26: 1, 96-105 (2011) (To link to this Article: URL: http://dx.doi.org/10.3846/16484142.2011.568084).

Hansjochen Ehmer, MBA, PhD, Prof.
(International University of Applied Sciences Bad Honnef – Bonn, Germany, and German Aerospace Center, Institute of Air Transport, Cologne, Germany)

THE INCLUSION OF AVIATION IN THE EUROPEAN EMISSION TRADING SCHEME AND THE REACTIONS OF AIRLINES AND STATES – AN ETHICAL EVALUATION

The European Union has widened the Emission Trading Scheme (ETS) on the airlines. Flights starting or landing at the EU's airports have to attest certificates for their CO_2 emissions. Lots of airlines and states complain against ETS being unsupportable, anticompetitive or unfair. An ethical evaluation of these arguments is tried.

1. Introduction

Climate change is a more and more challenging development for the nations of the world. Though aviation plays only a minor role in the anthropogenic part of global warming, it is however seen as one of the most harming industries, especially the most harming transport mode. The reason is the high growth rate this industry was able to show over the last decades and the high dependency on fossil fuel.

Nearly all players of the aviation industry show on their different press releases, web pages and other public information all what they do to reduce their climate footprint. Therein is no difference if it is a public institution or a private one, if it is a lobby group or the corporations themselves. So it would be expected that any initiative which doesn't harm too much the daily business would be highly welcomed. But it has to be realized that the initiative of the EU which started in 2008 and is now implemented since January 2012 is more and more contested. It is still open if the EU will be able to pursue ETS for aviation as foreseen.

In the next chapter ETS will be introduced with its implications for aviation. Especially the competitive situation of airlines of different parts of the world will briefly be analyzed. On this base the reactions of the different institutions, public institutions as well as lobby groups and airlines will be described, before they are ethically analyzed finally.

2. Inclusion of Aviation under the European Emission Trading Scheme

2.1. Background

The idea of any Emission Trading Scheme (ETS) is to internalize the external cost of the harming effect of CO_2 emission. It is a question of fairness that those harming the society because they attribute with their emission to climate change have to bear the cost the society so far has to cover. Since these emissions have a global effect it would be best to find a global solution because each regional solution might have some anticompetitive effects.

The EU ETS – implemented for several industries in 2005 (European Commission, 2010) – is a supranational policy instrument aiming to reduce greenhouse gas emissions. The primary objective is to achieve the climate protection target that was defined in the Kyoto Protocol 1997 (Heymann, Härtel, 2011). In October 2008, the European Council adopted a resolution to integrate air traffic into the European ETS in order to counteract the rapidly increasing greenhouse gas emissions of the aviation sector. Contemporarily, air traffic accounts for approximately 3 % of the global CO_2 emissions, however this proportion is expected to double until 2020 (Faber & Brinke, 2011). Accordingly, any airline departing from or arriving at an airport located in the European Union as well as Iceland, Liechtenstein and Norway is required to attest certificates for the CO_2 emitted during the entire flight (Directive 2008/101/EC Annex). Flights flying through the European airspace without stopovers are not affected.

2.2. Methodological Implementation

ETS works on the basis of "cap and trade" indicating that there is a limit of total CO_2 which the industry is allowed to emit. For 2012, the limit for aviation "(the cap) is set at 97 % of the average total emissions in the years 2004-2006", resulting in approximately 213 million tons that are added to the total amount of CO_2 emissions traded through the EU ETS so far (Directive 2008/101/EC). The system in itself is half-open and works one way: allowances can only be sold within the aviation sector, however also be bought from participants of other industries. There is a fine for every ton CO_2 that is not covered by allowances (Directive 2008/101/EC).

The allocation of certificates will be executed as follows: the CO_2 emission of 2004 – 2006 of the aviation industry are taken as the baseline and related to the transport capacity of 2010. Thereby, 82 % of allowances are given to airlines for free. Furthermore, 15 % are sold by auction within the aviation sector and the remaining 3 % are kept for new or rapidly growing airline operators. Revenues generated through these auctions will be allocated to the respective airline's country of origin – in case of non-EU-airlines to the country where they auctioned their emission rights – and are supposed to be reinvested for climate protection measurements.

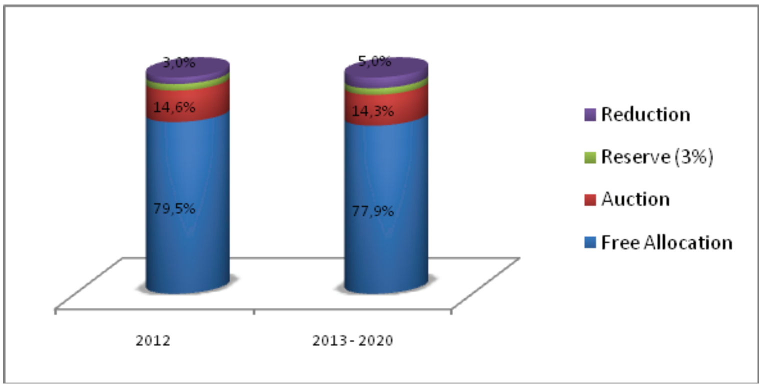

Figure 1: Allocation of Emission Allowances 2012 / 2013-2020

Adapted from Lufthansa Policy Brief, 2011

From 2013 to 2020, the amount of emission allowances is reduced by 5 % in reference to the baseline values from 2004-2006 (Heymann, Härtel, 2011). However, due to the fact that emission allowances can also be bought from other industries, the system will still allow airlines to grow because other industries have high reduction potential by the usage of alternative energies.

2.3. Competitive Impacts

The idea of the EU is that all airlines on the same route have to participate in the same way in the trading scheme – so far it is competitively fair, paying per ton of emission. The open question is if the definition of the relevant market being a single route as chosen by the EU Commission's competition authority is the correct one or if the network should be the relevant market.

The EU has set a benchmark for the allocation of free emission rights to encourage more efficient carriers. This leads to an advantage of **long haul flights** compared to short haul flights and of higher **seat load factors** and denser seating. In contrast to this airlines with an **above average growth rate** will see a disadvantage insofar that they have to auction more rights. So the 10 biggest non-European network carriers get 75.6 % of their needed rights for free, whereas the 10 biggest European ones get only 65.4 % for free because of their European feeder network. The 10 biggest European low cost carriers will get 67.5 % for free, according a calculation of the German Aerospace Center (Schäfer et al. 2010).

The European network carriers face further competition by non-European carriers, using **6th freedom rights**. On routes to south-east Asia the European carriers mostly fly non-stop whereas e.g. Turkish Airlines competes flying from the European airports via their hub Istanbul and then on to the end destination. Whereas the nonstop flying carriers have to cover for the whole distance the ETS cost, Turkish Airlines does it only up to their hub, an increasing cost advantage. But the passengers still have the advantage of a nonstop flight. Another example can be seen in the competition between European and non-European carriers competing for passengers flying between the North Atlantic and the Middle East. If the intermediate hub is outside the EU, the airline doesn't pay anything about ETS, whereas the European carriers have to cover it for the whole journey.

3. Reactions of Airlines, Airline Associations and states

The integration of air traffic under the EU ETS has caused widespread criticism under European and international airlines, airline associations and the respective states. The key arguments against the scheme are the competitive distortions resulting from the implementation, the consequential financial detriment, the EU ETS as a local approach to a global issue as well as legal concerns regarding the EU charging for routes over extraterritorial areas. In this context, the following paragraphs present different standpoints from airlines, airline associations and prospective states as well as the contemporary stance of the involved EU institutions.

3.1. European Reactions

The **Association of European Airlines** (AEA) "has consistently embraced the concept of ETS as a useful tool in the drive to manage the industry's greenhouse gas emissions" and considers it as essential from a business and ethical point of view to address this issue (AEA, 2007). Similarly, the **European Low Fares Airline Association** (ELFAA) stands behind the scheme and stated that "ETS is the most environmentally effective mechanism for tackling aviation's impact on climate change" (Reals, 2011). The majority of European airlines, however, do not share this opinion, as well as these lobby groups have changed opinion. So AEA spoke 2011 of institutional incompetence (AEA, 2011).

Lufthansa is afraid of the EU ETS "becoming a fiasco" (Karp, 2011) and particularly points out the cost side as the costs arising from the implementation may have negative effects on demand and hence on overall financial results. The company expects the shares of the emission allowances that have to be purchased between 30 and 40 % (Lufthansa Policy Brief, October 2011). Despite the belief of the EU Commission that airlines will be able to pass costs to the ticket price, the low expected worldwide airline margins will make it hard to raise prices. Furthermore, competitive distortions are a further major argument. Whereas EU-carriers have to surrender emission allowances for almost their entire network, non-EU carriers are only proportionally affected (Emirates 20 %, Air China 16 %, American Airlines 12 %, (Lufthansa Policy Brief, 2011).

Air France KLM stresses the competitive distortions. The former Air France president, Pierre-Henri Gourgeon, summarized it: „A carrier whose hub is located outside the European Union yet flies passengers from one side of the planet to the other while circumnavigating Europe, would have an unfair advantage over airlines with a hub in Europe. Some traffic flows would be diverted from European to non-European hubs and the efforts asked of European airlines in the fight against climate change would be wiped out" (Buyck, 2011). The company thus calls for a global solution and encourages the dialogue between national authorities, the European Union and the ICAO.

Willie Walsh, CEO of International Airline Group, owning **British Airways** and Spanish **Iberia**, urged the EU to delay plans to charge non-European airlines because of fear of retaliation measures by several countries protecting their own industries (Guardian 2011). The other countries might block flights by EU carriers or impose taxes.

In contrast **Easyjet** has been supporting the integration of air traffic under the EU ETS since 2003 under the conditions of the inclusion of non-EU carriers, the penalisation of environmental inefficiency and the support of environmentally efficient growth.

Ryanair however again heavily criticizes the consequences of the EU ETS, which according to Peter Sherrard, Ryanair Head of Communication, are particularly of negative nature and "do nothing whatsoever for the environment" (Ryanair Ltd., 2006).

The common denominator most EU-carriers share lies in the expectation of distorted competition and significant subsequent impacts on the economic performance as well as in the fear of the consequences of international reactions.

3.2. International Reactions

The decision of the EU to integrate international airlines into ETS have caused sharp international criticism and formed powerful oppositions. Though the strategy of the EU is known at least since 2003 when the first Directive about the inclusion of aviation was published, most of the reactions happened during 2011, the year before the introduction. Near the end of 2011 the reactions became even sharper, especially that not only airlines reacted but also a number of states the airlines are based in.

The **China Air Transport Association** and the **Arab Air Carriers Organization** have called the EU to reconsider their stance on the EU ETS. The **Air Transport Association of America** as well as the biggest U.S. airlines have brought the case to the European Court of Justice to examine the conformity with international law (NBAA, 2011; OJ 25.9.2010). They see an infringement of the Chicago Convention, the EU-US open skies agreement and the Kyoto Protocol.

The International Air Transport Association **IATA** also clearly takes positions against the EU ETS. CEO Tony Tyler described it as a “hornet’s nest” that needs to be resolved (Karp, 2011). The EU should first consider a global approach to aviation emissions and aims to achieve cooperation between the EU and ICAO.

In the last months the situation has changed so far that now not only airlines complain but also states start to react. 25 countries including Russia, India, China, Brazil and the U.S. have threatened EU-carriers to withdraw landing permits and rights to fly over their territory. Already in march 2011 the Directors General of **Civil Aviation Middle East Region** challenged the European scheme, but did not yet claim for counter measures (DGCA-MID/1-WP/27).

China has first argued that “the EU needs to take into account the different development status of countries” as the head of the CAA of China argues (Jing 2011). Then they have even threatened to cancel profitable purchase orders at Airbus. On top of this they intend to impose a tax for European airlines which would cover the cost of Chinese airlines they have to pay for ETS (Guardian 2011) and, together with **India**, forbid their airlines to participate. 10 airlines of the 2 States were the only ones not handing in the required data in May 2012.

Meanwhile, the **U.S. House of Representatives** has emitted the “European Emission Trading Scheme Prohibition Act of 2011”, which forbids US airlines to participate in the EU ETS (NBAA, 2011; atwonline 2011). The resolution was accepted by the majority and sent to the Senate. The main reason is the opinion that the EU cannot be allowed to install unilaterally a regulation which affects the sovereignty rights of non-EU countries by regulating emissions outside of EU airspace.

Recently, the **Indian government** has taken the opposition’s lead. The Ministry of Civil Aviation has gathered 25 other members of the **ICAO** council to elaborate a consolidated opposition against the inclusion of non-EU aircraft operators into the EU ETS (euractiv.com 04-10-2011). With the New Delhi joint declaration as the baseline, the ICAO Council adopted a non-binding working paper on 31. October 2011, initiated through the Indian representative. This paper basically reaffirms the role of the ICAO concerning environmental protection measures in the aviation sector and calls for coordinating a climate protection agreement between all stakeholders. At least all non-European carriers should be exempt from the regulation (airliners.de 3.11.2011).

Against growing international resistance, the **European Union** did not show any willingness to compromise. The European Court of Justice came to the conclusion that the integration of non-EU carriers into the EU ETS conforms to international law (Prolog, 2011). In addition, it threatened Asia and the United States with landing prohibitions in case they would not take part in the system. The EU reaffirmed that if extra-European countries present similar approaches to reduce aviation CO_2, they might be excluded from the scheme or that only flights out of Europe might be affected (Directive 2008/101/EC).

4. Ethical Evaluation

When we try to evaluate ethically the argumentations of the different airlines the main question has to be how far such a system can be fair, and how far it is fair in the current stage. Internalization of external cost is currently the most accepted way to deal with global problems like climate change, at least from a more theoretical viewpoint. Also from an ethical viewpoint this doesn't change since it is mostly accepted to pay for what you get.

It is understandable that an industry with an extreme low profit margin is more against an extra cost burden than other industries. But the costs of ETS are often overestimated and vary a lot. According to some recent calculations the cost of ETS will vary between 0.77 % and 1.51 % of the overall fuel cost in 2012 and between 1.44 % and 6.85 % in 2020 (Bloomberg 2011), according a low or high carbon price and a trend forecast for the energy prices. So we can conclude that the effect will be by far below the impact of energy price variations the airlines have overcome already with limited demand reactions.

An argument of higher ethical relevance is the one put forward especially by China: developing countries shouldn't underlie the same regulations as the developed countries. Since CO_2 emissions remain for years in the air the current problem of climate change is more caused by the last generations of the western world than by the current generation of the developing world. So the western world should give the developing world a chance to develop by setting different reduction limits. This would be applicable especially for domestic or regional air services – but these services are not affected by ETS. The intercontinental services especially between the developing countries and Europe compete with the European carriers for the same passengers. So if we abandon ETS for carriers out of these countries would give them a further cost advantage having already lower overall cost. Would this be fairer?

More interesting is the situation that the developing countries will suffer more of climate change compared to the western world. This should make them more aware of the situation, and this even more that the competitive disadvantage is more on the side of the European airlines.

More critical out of an ethical viewpoint is the self-presentation of a lot of airlines and especially of their lobby groups and the contradicting argumentation against ETS. They all try to show – more or less intensely – what they do for the environment, how far they have improved, and what the goals are they intend to achieve in the future. They all follow the NIMBY strategy (not in my backyard) – something good has to be done, but not by me. They follow mainly a very opportunistic behaviour based on limited rationality. According ethical theories they follow the Adam Smith based theory of egoism what in case of imperfect markets – and markets with external costs are imperfect – cannot lead to optimal solutions. This behaviour though these carriers have already a competitive advantage with the current regulation.

The often issued argument that only a global approach will be acceptable can be estimated as following the utilitarianism theory concentrating on the collective welfare. The EU tried to be as global as possible, but this is just one of the points often criticised, arguing the EU has to concentrate on European territory. So it has to be questioned if they really wait for such a solution well knowing that it will take years to achieve such a goal if at all it might be achievable. ICAO deals with ETS already since 2007 though no conclusion is foreseeable. A wait and see approach at least risks to increase cost in the future tremendously.

5. References

1. AEA. Q & A: Aviation and the EU emission trading scheme. AEA 2007. http://files.aea.be/News/Q_AvEmissions.pdf [Accessed 12 Nov. 2011]
2. AEA U. Schulte-Strathaus. Challenges Facing the European Airline Sector, 05 Oct. 2011, http://files.aea.be/News/sg_LOT_1011.pdf [Accessed 22 July 2012]
3. airliners.de 3.11.2011. EU bleibt im Streit um Emissionshandel hart ICAO lehnt Vorhaben ab. http://www.airliners.de/ddrucken/-eu-bleibt-im-streit-um-emissionhandel-hart/25614 [Accessed 11 Nov. 2011]
4. Atwonline 2011. US House of Representatives votes to keep airlines out of EU. http://atwonline.com/prin/216021 [Accessed 01 Dec. 2011]
5. Bloomberg 2011. Bloomberg New Energy Finance: EU ETS research note – Including aviation in the EU ETS – the burning question. 25.10.2011
6. Buyck, K. Air France president: Latest EU ETS proposal treats airlines as 'idiots'. Air

Transport World 2011. http://atwonline.com/international-aviation-regulation/news/air-france-president-latest-eu-ets-proposal-treats-airlines-i [Accessed 16 Nov. 2011]

7. DGCA-MID/1-WP/27 Directors General of Civil Aviation – Middle East Region First Meeting (DGCA-MID/1), Abu Dhabi, 22-24 March 2011

8. Directive 2008/101/EC of the European Parliament and of the Council of 19 Nov. 2008, Official Journal of the European Union, L 8 of 13.1.2009, p. 3-21

9. Easyjet. easyJet response to the European Parliament's vote on Emission Trading. Easyjet 2001. http://www.easyjet.com/en/news/european_parliament_vote_on_emission_trading.html [Accessed 15 Nov. 2011]

10. euractiv.com 04-10-2011: India, 25 others oppose EU airline carbon charge plan. http://www.euractiv.com/transport/india-25-oppose-eu-airline-carbon-charge-plan-news-508109 [Accessed 04 Oct. 2011]

11. European Commission. Emission Trading System (EU ETS). http://ec.europa.eu/clima/policies/ets/index_en.htm [Accessed 18 Nov. 2011]

12. Faber, J., L. Brinke. The inclusion of aviation in the EU emission trading system. *ICTSD Programme on Trade and Environment.* Switzerland: ICTS, 2011

13. Guardian 2011. China threatens trade war over EU emissions trading scheme, The Guardian 6 June 2011. http://www.guardian.co.uk/environment/2011/jun/06/china-trade-war-emissions-trading-scheme.htm [Accessed 04 Oct. 2011]

14. Heymann, E., J. Härtel. Emissions Trading in Aviation – Moderate burdens for the time being, perceptible competition effects. Deutsche Bank Research Briefing, Frankfurt, 9th Nov. 2011

15. Jing, L. Carbon rule may clip wings of China's aviation sector, in: *China Daily* of 18-05-2011, http://www.chinadaily.com.cn/china/2011-05/18/content_12529130.htm [Accessed 04 Oct. 2011]

16. Karp, A. IATA CEO: EU ETS is a 'hornet's nest' that needs to be resolved. Air Transport World 2011. http://atwonline.com/international-aviation-regulation/news/iata-ceo-eu-ets-hornets-nest-needs-be-resolved-1102 [Accessed 12 Nov. 2011]

17. Karp, A. Lufthansa: Airlines' inclusion in EU ETS in danger of becoming 'fiasco'. Air Transport World 2011. http://atwonline.com/eco-aviation/news/lufthansa-airlines-inclusion-eu-ets-danger-becoming-fiasco-0411 [Accessed 12 Nov. 2011]

18. Lufthansa Policy Brief. Emission trading: harsh criticism across the entire globe. http://presse.lufthansa.com/fileadmin/downloads/en/policy-brief/10_2011/LH-PolicyBrief-Oct.-2011-ETS.pdf [Accessed 12 Nov. 2011]

19. NBAA (National Business Aviation Association). European Union Emission Trading Scheme (EU ETS). http://www.nbaa.org/ops/environment/eu-ets/20111031-opposition-rising-to-eu-ets.php [Accessed 12 Nov. 2011]

20. OJ 25.9.2010. Case C-366/10, Official Journal of the European Union, C 260, p. 9-10

21. Prolog 2011. Press Release Distribution. The European Court of Justice Rules the EU ETS to be legal. http://www.prlog.org/11685861-the-european-court-of-justice-rules-the-eu-ets-to-be-legal.html [Accessed 15 Nov. 2011]

22. Reals, K. ROUTES: ELFAA gives rare note of support to EU emissions trading. http://www.flightglobal.com/news/articles/routes-elfaa-gives-rare-note-of-support-to-eu-emissions-trading-362875/ [Accessed 12 Nov. 2011]

23. Reuters 2011. EU court to rule on airline CO2 cap on December 21, Dec 6, 2011. http://www.reuters.com/assets/print?aid=USTRE7B51K720111206 [Accessed 08 Dec. 2011]

24. Ryanair Ltd. EU ETS proposals are just another tax for passengers that do nothing for the environment. 2006. http://www.ryanair.com/en/news/pro-en-201206 [Accessed 17 Nov. 2011]

25. Schäfer, M., J. Scheelhaase, W. Grimme, S. Maertens. The economic impact of the upcoming EU emissions trading system on airlines and EU Member States – an empirical estimation. *Eur. Transp. Res. Rev.* (2010) 2:189-200

Hansjochen Ehmer, MBA, Prof. PhD;
(International University of Applied Sciences Bad Honnef – Bonn, Germany)
A. Leipold, MBA, M. Murphy, MBA
(German Aerospace Center, Institute of Air Transport, Cologne, Germany)

ICAO'S BALANCED APPROACH TO NOISE MANAGEMENT AND ITS INFLUENCE ON THE ECONOMIC IMPACT OF AIR TRANSPORTATION

Caused by rising noise awareness more and more airports introduce operating restrictions harming their positive economic impact. To find a fairer solution, ICAO established the Balanced Approach in 2001. It consists of four pillars: reduction of noise at source, land-use planning and management, noise abatement operational procedures and operating restrictions.

1 Introduction

With rising living standards noise is more and more seen as a harming factor of the quality of life. The increasing noise awareness of the population especially in the Western world is the main driver for more and more intense regulations especially of airports. The aviation industry itself was able to reduce the noise per movement by new technologies especially up to the year 2000 about. But this reduction was paralleled by a high increase of movements which influenced more the perception of the population. However, in lots of cases people moved nearer to the airports – a sign of inappropriate land-use-planning around the airports.

The impact of these regulations on airlines is quite different according to different business models. Scheduled intercont services need often the late evening or very early morning arrival or departure time to optimize the different time windows they have to use on their flights. Holiday and some low cost carriers offer night flights to get a higher utilization rate of their aircraft. Evenmore affected are the cargo and especially the integrator carriers; to guarantee overnight deliveries they have to use night flights. These carriers feel often unfairly treated as the other business models get more capacity at day time whereas their capacity is more and more restricted over time.

2 ICAO's Balanced Approach

2.1Background

Noise problems are increasing because air traffic is growing and the sensitivity against noise becomes stronger. The number of people exposed to aircraft noise has increased considerably in the last half of the 20th century, and it still shows a positive trend for the future. This affects a growing number of airports worldwide. Increased public awareness of people affected in areas adjacent to airports has aroused community opposition to aircraft noise leading to opposition towards any kind of airport decision relative to capacities. In absence of a coordinated global approach, airports and airport authorities imposed own individual measures, including especially operating restrictions limiting airport capacity and the free flow of air traffic. Local, national and regional noise restrictions escalated worldwide, in order to address the concerns of the people affected. Since the 1970th several noise mitigation measures were introduced primarily in form of operating restrictions at individual airports to counteract this development (see figure below). [1]

However, the proliferation of uncoordinated noise mitigation programs at airports worldwide provoked the risk of disturbing the aviation system. On the one hand, airports suffer under limited opportunities to expand the infrastructure according to demand. On the other hand, aircraft operators face a high economic burden due to the arbitrariness of the implementation of noise mitigation programs at airports throughout the world.

Figure 1: Growth in airport noise restrictions

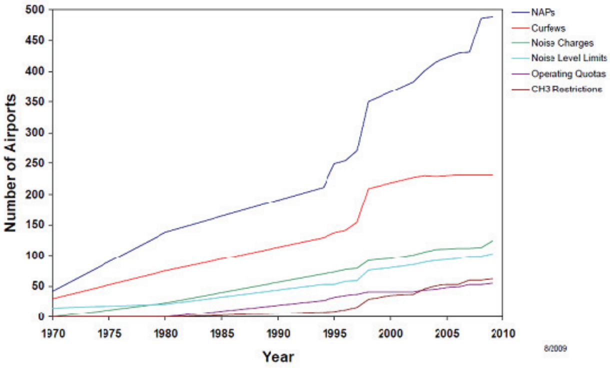

The uncoordinated approach of individual airports led to cumulative disputes between the different stakeholders and nations. Consequently, the necessity of a more common framework on a global level gained more and more weight. Thus, ICAO elaborate**d** a consistent and coordinated way to face this issue in an environmentally responsive and in the most cost-effective manner. Furthermore, it should promote consistency, harmonization and transparency in international civil aviation.

2.2The concept

In the 33rd Assembly in 2001, ICAO published the concept of the “Balanced Approach” in 2001 to noise management [2] which is based on the four principal elements:

(1) reduction of noise at source,

(2) land-use planning and management,

(3) noise abatement operational procedures and

(4) operating restrictions.

Since there are significant regional differences the Balanced Approach was formulated to be applied on an airport-by-airport basis to ensure the flexibility needed in order to be able to adjust and apply it according to specific circumstances. All principal elements should be considered equally. However, operating restrictions should only be implemented as a last resort and, if implemented, an appropriate phase-in time should be granted so that airlinescan adjust their business plans according to the new circumstances. The four elements do not represent a fixed catalogue of potential measures, but rather four main pillars which can be extended by various measures.

Figure 2: The four pillars of the ICAO Balanced Approach

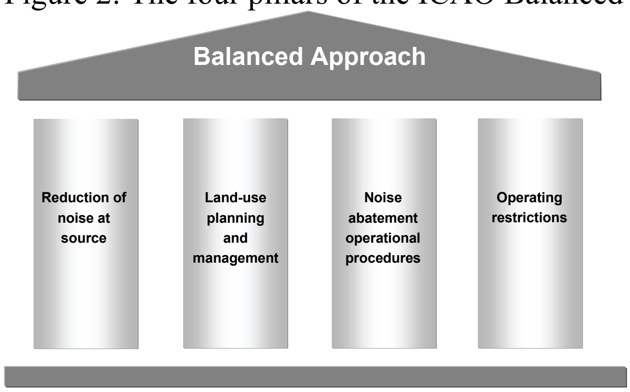

Source: DLR

In order to select the optimal measures for the particular airport and to ensure transparency, a comprehensive noise assessment and evaluation process should be performed consisting of the following steps [3]:

(1) assessment of the current and future noise impact at the airport concerned, compared to the noise objective to be achieved;

(2) evaluation of the likely costs and benefits of the various measures available;

(3) selection of measures with the goal to achieve maximum environmental benefits most cost-effectively;

(4) provision for dissemination of the evaluation results;

(5) provision for consultation with stakeholders at different stages from assessment to implementation;

(6) provision for dispute resolution.

The Contracting States committed themselves to adopt it on national level. The Balanced Approach has been amended continuously in the following ICAO Assemblies. For instance, public involvement was incorporated into the assessment and anevaluation process to underline the vital importance of the participation of the people affected in this process [4].

2.3The instruments

The four pillars of the ICAO Balanced Approach to noise management incorporate several measures that can be used to mitigate the noise level at airports. In order to get an overview of the available measures, we will briefly introduce the different elements of the four principal categories [5].

The **reduction of noise at source** has proven to be one of the most effective means to limit aircraft noise. Instruments in this category are typically the result of extensive research and development in the fields of aircraft and engine design, and thus are not initiated by or within the control of individual airports. Instead, they are induced by the adoption and implementation of noise certification standards in Annex 16, Volume I, to the Chicago Convention. Measures involve the introduction of newer, quieter aircraft types, as well as the reduction of acoustic output of existing aircraft types by modification.

Land-use planning and management measures aim at achieving compatibility of the land-use surrounding an airport with its activities. In order to reduce the number of people affected, airports have the choice among several options which can be further grouped into:

(1) *planning instruments*: comprehensive planning, noise zoning, subdivision regulations, transfer of development rights and easement acquisition;

(2) *mitigation instruments*: building codes, noise insulation, reallocation measures of buildings;

(3) *financial instruments*: capital improvements planning, economic incentives, noise-related airport charges for covering the expenses of alleviation or prevention of noise impacts.

Land-use planning and management means, particularly those of the categories (1) and (2), are appropriate during the design stage of new airports, since a proper planning process can mitigate ex ante the negative impact of aircraft noise on surrounding communities. Also existing airports can achieve positive impacts by applying land-use measures such as funding of soundproofing and construction of noise barriers and, in the long-term, the acquisition of property. Land-use planning and management measures can significantly reduce the adverse effects of aircraft noise in the vicinity of airports and should be taken into account by airports and authorities in order to minimize the number of noise affected people.

Noise abatement operational procedures reduce aircraft noise by changing the way how an aircraft approaches to or departs from a particular airport. There are several operational measures which can significantly reduce the aircraft noise exposure: Noise preferential runways and routes concentrate flights over the least noise-sensitive areas, or at least to evenly distribute the noise disturbance among the surrounding areas. Furthermore, the use of low noise flight procedures for the take-off and landing can achieve lower noise levels at comparatively low cost. The appropriateness of any of these measures is subject to the physical lay-out of the individual airport in its surrounding. In all cases, though, the procedure must give priority to safety considerations. Furthermore, several operating procedures constrain aircraft ground operations. Limiting engine-run up and using the aircraft’s auxiliary power unit in noise-sensitive areas or during a certain period of time, further reduces the level of noise exposure to the surrounding community can be further reduced.

Operating restrictions refer to noise-related bans or limitations in the operations of all or certain aircraft types at a particular airport. In order to limit the impact of aircraft noise especially during the most sensitive time periods, they are often of a temporary nature. Operating restrictions can be classified into global, aircraft-specific, partial and progressive restrictions. Potential measures of this group are cap rules and noise quotas. Cap rules define a maximum number of operations permitted for a particular period of time, whereas noise quotas allow for a limited, cumulative level of noise that determines the actual number of aircraft movements. However, while all elements should be considered equally, operating restrictions should be considered as a last resort.

2.4Noise management at European airports

In Europe, airports have already implemented several noise mitigation measures according to existing national legislation and complementary Union legislation.

Concerning noise reduction at the source, Directive 2006/93/EC regulates the operation of chapter-3-certificated civil subsonic jet aeroplanes. Furthermore, issues of land-use planning and managementas well asnoise abatement operational procedures fall into the exclusive legal competence of the respective Member States. Therefore, no harmonized approach can be found on European level.

In March 2002, the EC adopted the Directive 2002/30/EC [6] concerning the rules and procedures for noise-related operating restrictions at Community airports. The main objective of the Directive is to provide a common framework for the Member States to facilitate the introduction of operating restrictions of marginally compliant aircraft in a consistent manner at an individual airport level. The Balanced Approach as of 2001 was explicitly adopted into EU law and is defined in detail and in full consensus with the ICAO approach in Article 2(g).

In 2007, a first review on the application of Directive 2002/30/EC [7] has been carried out in order to evaluate its effectiveness. The study's strategy was based on a three-fold approach. Firstly, it contains an extensive analysis of aircraft movements in the base year 2002 and 2006 at 70 EU airports currently or potentially soon to be covered by the Directive's traffic limit of 50,000 aircraft movements per annum. Secondly, the same airports and other stakeholders have been interviewed and were asked to provide facts and figures on operating restrictions and other measures related to noise management. Thirdly, noise contours were modeled for five case study airports to estimate the effect of banning marginally compliant aircraft.

The surveyed airports indicated heterogeneous experiences with the legislation. The study results have been summarized by the EC[8]. As pointed out by the report, the present Directive is not sufficient to reduce noise around airports, particularly with regard to a growing traffic demand. Furthermore, measures of the Directive have been implemented by only a limited number of Community airports. Before a formal decision on further steps is made, the Commission expressed its willingness to receive comments from the stakeholders.

Furthermore, it should be taken into account that the implementation of the Balanced Approach by Directive 2002/30/EC is only one instrument which has to interact with several other measures on national level to solve noise problems within the European Union. This shows that the elements and the various measures within the Balanced Approach are existent in the Member States, however, have not yet been implemented in an integrated approach as intended by ICAO.The proposal of the airport package of December 2011 intends to give more importance to the introduction of the Balanced Approach [9].

2.5The US approach

The US aviation noise policy differs in its application compared with the approach applied in the EU. In response to the proliferation of individual operating restrictions, the US Congress enacted in 1990 the Airport Noise and Capacity Act (ANCA) to guarantee a coordinated and consistent approach for all airports in the United States. This regulation, implemented by the FAA (Federal

Aviation Administration) in 14 CFR (Code of Federal Regulations) Part 161 [10], establishes a program for reviewing noise and access restrictions concerning Chapter 2 and Chapter 3 aircraft.

Hence, the competence of the airports' authority to implement operating restrictions was reduced significantly. After the entry into force 1990, all restrictions affecting operations of Chapter 3 aircraft have to be approved by the FAA while existing restrictions were granted as grandfather rights. Airport proprietors have to apply for the implementation of an operating restriction which will then be evaluated by the agency.

A central element of the US approach for the selection of potential capacity-related airport projects, such as noise mitigation projects, is the **cost benefit analysis (**CBA**)** [11]. This guidance provides a consistent approach for comparable analyses. So the concerned airport has to prove the cost-effectiveness of the proposed measures. The systematic US approach with regard to operating restrictions considers a broader point of view on a federal level with the aim to ensure the functioning of the aviation system considering a great variety of aspects which might cause adverse effects (e.g. safety and economic issues).

Established prior to ANCA, 14 CFR Part 150 was issued under the authority of ASNA (Aviation Safety and Noise Abatement Act) of 1979 and is another central element in the Federal Aviation Regulation (FAR) of the United States. The aim was to standardize the process of identifying noise and land use incompatibilities and to develop effective abatement strategies. The regulations in Part 150 are voluntary, however, the rate of participation is quite high since Federal grants for noise abatement projects can be achieved. With these regulations as described above the United States already integrated all elements of the Balanced Approach into its national aviation noise policy.The Balanced Approach ha**s** also been subject to the second stage negotiations concerning a more liberal Open Skies Agreement between Europe and the US.

As in the U.S. the ICAO requires for every airport to combine and assess possible measures planned in the context of the Balanced Approach with a preceding economic analysis [12]. This analysis, may it be done in form of a benefit-cost analysis (CBA), a cost-effectiveness analysis (CEA) or a sensitivity analysisto fulfill the different needs of all involved stakeholders. So all measures are weighed carefully against each other and operating restrictions are not chosen prematurely. However, for Europe it was assumed that economic impact studies are not done in any case to assess the effects of noise abatement measures. However an analysis of economic impact studies showed that in general all air transport activities contribute to a large extent to the prosperity of a special region.Cargo and express operators with their night movements fulfill a special role in this framework. In the case of the implementation of operating restrictions, often even in the short-term and only politically determined, without an investigation of other alternatives a negative impact on the prosperity of a region in terms of job and income losses is foreseeable.

3 Conclusion

The overall analysis in the previous chapters has shown that it is very important, that successfully established transportation networks can operate for several years without deeper regulative intervention changes like in the form of operating restrictions as there is not much flexibility to change existing networks and adapt to new market conditions. Lacking planning security might lead to abandon operations completely or to switch to another location to the price of **sunk costs.** A prominent example is DHL and the relocation of its European hub from Brussels to Leipzig/Halle in 2008.Nevertheless, the population around airports' vicinities has to be protected from increasing aircraft noise. In order to solve this conflict the ICAO has developed the Balanced Approach with its four pillars to reconcile the different interests in order to find the most suitable solution on an **airport-to-airport basis.**

This process includes that a **CBA** is done for every planned measure in the light of the Balanced Approach, what shall guarantee to find the most cost-effective and most efficient option to handle noise problems correctly. We identified some potential improvement points resulting in the following recommendations:

- If measures are planned at an airport, **all** of the four **pillars** of the Balanced Approach should be regarded, especially by taking into account a preference of the first three ones against the operating restrictions. The first three pillars can already have a positive impact at lower cost as the fourth pillar can result in high economic disadvantages especially when an airport has a special traffic mix.
- For every intended measure linked to the four pillars a CBA should be undertaken in order to develop a set of alternatives to define the best one or a combination.
- The CBA should take the situation of all concerned stakeholders into account.
- Furthermore, the CBA should include monetized environmental benefits/disbenefits (with regard to noise) and monetized economic benefits/disbenefits (with regard to traffic figures/performance figures) which have to be compared to each other.
- With regard to the economic benefits/disbenefits it is very important that established and proven scientific metrics (e.g. employment, value added, and contribution to GDP) are used in order to facilitate comparisons between airports. The FAA can serve as a good reference case here as it already provides detailed information on CBA conduction and common standards [13].

All in all, these are first considerations how the current handling of the Balanced Approach framework especially with regard to CBAs could be improved.

References

[1] Boeing. *Growth in Airport Noise Restrictions*, 2011. http://www.boeing.com/commercial/noise/restrictions.pdf

[2] ICAO. *Resolution A33-7. Consolidated statement of continuing ICAO policies and practices related to environmental protection*,2001.

[3] ICAO. *Doc 9829. Guidance on the Balanced Approach to Aircraft Noise Management*, First Edition, p. 2-1, 2004.

[4] ICAO.*A36-WP/355, Assembly – 36th Session, Report of the Executive Committee on Agenda Item 17*, p. 17-1, 2007. http://www.icao.int/icao/en/assembl/a36/wp/wp355_en.pdf

[5] ICAO.*Doc 9829. Guidance on the Balanced Approach to Aircraft Noise Management,* 2004.

[6] EC. *Directive 2002/30/EC of the European Parliament and of the Council of 26 March 2002 on the establishment of rules and procedures with regard to the introduction of noise-related operating restrictions at Community airports*, 2002. http://eur-lex.europa.eu/LexUriServ/LexUriServ.do?uri=OJ:L:2002:085:0040:0046:EN:PDF

[7] MPD. *Study of Aircraft Noise Exposure at and around Community Airports: Evaluation of the Effect of Measures to Reduce Noise*, 2007. http://ec.europa.eu/transport/air/studies/doc/environment/2007_10_aircraft_noise_exposure_en.pdf

[8] EC. *Report the Commission to the Council and the European Parliament, Noise Operation Restrictions at EU Airports (Report on the application of Directive 2002/30/EC)*, COM(2008) 66 final, 2008.

[9] Proposal for a Regulation of the European Parliament and of the Council on the establishment of rules and procedures with regard to the introduction of noise-related operating restrictions at Union airports within a Balanced Approach andrepealing Directive 2002/30/EC of the European Parliament and of the Council, COM(2011) 828 final

[10] FAA. *Part 161 – Notice and Approval of Airport Noise and Access Restrictions*, 2010.

[11] FAA.*FAA Airport Benefit-Cost Analysis Guidance*, 1999.

[12] ICAO. *The Balanced Approach to Aircraft Noise Management*, 2001.

[13] FAA, *Cost Benefit Analysis*, 2012. http://www.faa.gov/airports/central/aip/benefit_cost/

UDC 504.03:534.83

Andrey V.Vasilyev, Doctor of Technical Sc., Professor, Olga V. Bynina, postgraduate (Togliatti State University, Togliatti, Russia)

APPROACHES TO NOISE INFLUENCE ESTIMATION TO HUMAN HEALTH TAKING TO ACCOUNT SOME OTHER PHYSICAL FACTORS

Negative noise influence to the population health may be significantly amplified in combination with other physical factors (e.g. vibration, electromagnetic fields etc.). Principles of noise influence estimation in combination with other physical factors are discussed. Results of combined estimation of noise influence in combination with electromagnetic fields for the territory of Togliatti city of Russia are presented. Data of different illnesses ranging and of correlation-regression analysis are discussed.

I. INTRODUCTION

As a function of many variables, population health represents an integrated indicator of environmental quality. It has been found that the combined influence of environmental factors on human health may yield different effects. For example, the common children's sickness rate depends both on air pollution with carbon monoxide, and from the city noise. Incidence rate increases (synergistic effect) with the combined effect of both factors. The prevalence of allergic diseases significantly affects by the atmospheric pollutions and poor housing conditions. In combination of these factors disease incidence increases more rapidly.

The same situation is with physical factors joint influence. It is well known that noise influence to the human health may depend on the temperature rate. Some efforts of Russian scientists are devoted to research of noise influence and effects to human health in combination with electromagnetic fields, vibration, ionization and other physical factors. Some approaches and results of Russian experience are described in this paper.

2. BRIEF ANALYSIS AND EXHAMPLE OF APPROACHES TO NOISE INFLUENCE ESTIMATION TO THE HUMAN HEALTH

In Russia for estimation of noise influence to the health of population typically different approaches are used:

- analysis of inhabitants complaints to noise disturbance:
- analysis and comparison of population sick rate in database of Russian medical institutions (polyclinics, hospitals etc) with measured results of noise measurement for the certain territories;
- Inhabitants self-estimation of health state depending on the conditions of protection from noise disturbance etc.

The following criteria of determination of risk of noise damage of the population health are suggested by authors (table 1).

As an example of approaches to estimation of noise influence to the health of population used in Russia let us show some results of estimation of noise impact to the health of population of Komsomolsky district of Togliatti city of Russia. Investigation of noise impact to the health of population included statistical data analysis of illnesses related with biological impact of noise to the inhabitants. The group of such illnesses includes in total 14 units of illnesses: cardio-vascular system, nervous system, alimentary canal etc.

Materials of population of Komsomolsky district of Togliatti city primary coming to the medical institutions for advice for the certain time period were used as sources of information about population sick rate. Using of certain procedures (one of which is method of I.A. Liepa) together with collaborators of the Institute of ecology of Volga basin of Russian Academy of Science estimation of parameters of equation of the plural linear regression and checking of significance of influence of investigated factors to the sick rate have been carried out [8]. Taking into account the results of measurements of noise levels of living territory of Komsomolsky district of Togliatti city and the primary medical statistical data of coming of population of Komsomolsky district to the medical institutions for advice, it is podssible to make a conclusion that there is exist reliable, statistically significant dependence of all 14 units of illnesses growth from the impact of acoustical pollution (figure 1). Measured noise load in the most noizy points of Komsomolsky district of Togliatti city is shown in figure 2. The points with noise levels exceeding the sanitary norms requirements are marked by the red colour.

Table 1

Ceiling sound levels (dB) for the different kind of population life for different classes of conditions (degrees of risk)

The kinds of life activity during the 24 hours	**Optimal conditions (risk is absent)**	**Admissible conditions (negligible risk)**	**Harmful conditions (endurable with protective measures risk)**	**Damage conditions (unadmissible risk)**
Sleeping	15	30	45	60
Rest	35	50	65	80
Work	50	80	100	110

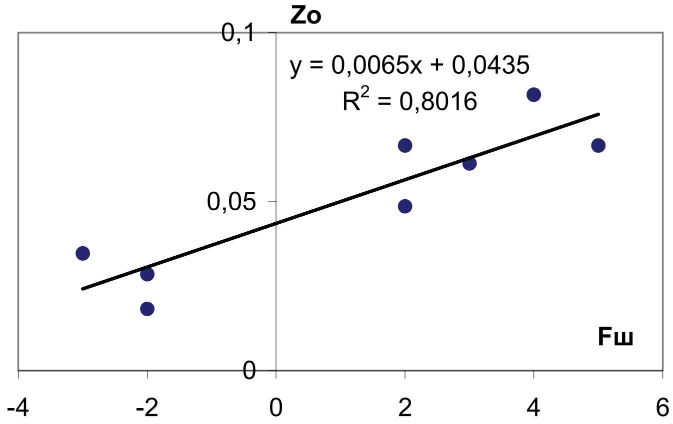

Figure 1. Dependence of population sick rate on all health units Z_0, taken into consideration, from noise impact $F_ш$

Surveying of population of Komsomolsky district of Togliatti city have been carried out in order to determine their subjective perception of real noise load. The main purpose of surveying was to reveal the dependence of receptivity to noise affection from the general state of health, age, duration of inhabitants residing etc. In total inhabitants of 4 houses were polled (about 100 people), here 2 houses were selected with noise levels exceeding normative values, and 2 houses with noise levels corresponding to sanitary norms. The quantity of polled inhabitants (respondents) have been selected proportionally to the quantity of flats in above mentioned houses for comparison of surveying results.

Analysis of collected questionnaire data allows to make the following conclusions:

- inhabitants of houses situated in zones with combined increased noise and electromagnetic fields levels the worse are appreciating their own living conditions the longer term of their living in the territory of investigations;

- the older age of inhabitants, the evidently their negative perception of presence of combined acoustical and electromagnetic fields pollution;
- the worse the respondents are appreciating the state of their own health, the worse (from the point of view of noise impact) they are appreciating the comfort of living conditions.
- 3 kinds of comfort of living conditions are selected: poor, satisfactory, good.

Noise level is corresponds to the sanitary norms requirements
Noise level is exceeding the sanitary norms requirements

Figure 2. Noise load in the most noizy points of Komsomolsky district of Togliatti city of Russia

3. CONCLUSIONS

The results of analysis of noise influence to the population health in combination with other physical factors are showing the amplification of negative impact and are proving the importance of the problem. The results of work are allowing to reduce negative impact of noise to the human health more efficiently.

4. REFERENCES

1. Directive 2002/49/EC of the European Parliament relating to the assessment and management of environmental noise. Official Journal of the European Communities L 189/12, 2002

2. H. Wolfert , Noise in cities: general approach and European network solutions, Proceedings of “European strategies for noise reduction and management”, 2009

3. Aloque V., Piwonski M., Schulte-Forthkamp B., Evaluation of a public space – Validation of the psychoacoustic infrastructure based on people’s perception and involvement in the conceptual design, EAA Euroregio Proceedings, Lubiana, 2010.

4. Vasilyev A.V. Monitoring of Physical Fields of Urban Territories: Modern Approaches, Problems, Prospects. The Special Issue "ELPIT-2005" of Scientific Edition "Proceedings of Samara Scientific Center of Russian Academy of Sciences", Samara, 2005, volume 1, pp. 111-118.

5. Vasilyev A.V., Rozenberg G.S. Monitoring of Noise Pollution in Living Area of Togliatti City and Estimation of It Influence to the Health of Inhabitants. Proc. of Scientific-Practical Journal "Safety in Technosphere", No 3, 2007, pp. 9-12.

UDC 54–414:[628.316.12:665.7]:629.7(045)

L.I. Pavliukh,
S.V. Boychenko, PhD, Professor
(National Aviation University, Ukraine)

APPLICATION OF NATURAL RAW PLANT MATERIALS BASED SORBENTS IN THE PURIFICATION SYSTEMS OF OIL CONTAMINATED WATERS OF AVIATION ENTERPRISES

The comparative analysis of different origin sorbents and the use of natural raw materials based sorbents have been demonstrated. The impact of temperature on the raising of purification level has been shown.

One of the main components of our environment is water. Large volumes of fresh water are being utilized very intensively. This is well known that water resources are highly exhaustible and the deficit of fresh water is closely connected with irrational usage of water at many enterprises in different brunches of national economy. There exist many reasons for water losses one of them being high level of equipment wear. The strategy of water resources saving is based on the effectiveness of waste waters purification at enterprises. It is necessary to note that Ukrainian enterprises do not effectively utilize and refine waste water.

All purification systems of contaminated flows contain means of primary purification from mechanical substances and final purification based on sorption materials.

Application of sorption methods are based on the contaminator physical state change. As a result nontoxic or less toxic compounds are received. The attempt has been made to draw attention to sorbents based on natural raw plant materials. The comparative analysis of sorbents based on natural raw plant materials is given in table 1.

Table 1

Comparative analysis of sorbents of different origin

Sorbent	Advantages	Disadvantages
Active carbon	1. Wide raw materials base; 2. High kinetics of sorption	1. Law degree of regeneration; 2. Improvement of sorption properties by means of sorbent surface modification by chemical reagents
Clay	1. Wide raw materials base; 2. Comparatively low cost	1. Insufficient activity in natural state, needs of additional treatment by chemical and thermal methods; 2. Can't be regenerated
Zeolite	1. Sufficiently wide raw materials base	1. Low sorption ability; 2.Needs of treatment by chemical compounds
Perlit	1. High oil sumption (oil capacity)	1. Flimsy shower proof properties; 2. Needs of treatment by chemical compounds
Peat	1. Sufficiently wide raw materials base	1. Temperature influence on oil sumption increase, magnetic and electric fields, organic, nonorganic and modificators influence is observed

Sapropel	1. Sufficiently wide raw materials base; 2. Comparatively low cost	1. Low oil sumption; 2. Needs of treatment by hydrophobic agents
Buckwheat	1. Wide raw materials base; 2. Low cost; 3. High level of oil sumption; 4. Possibility of utilization by burning	1. Thermal methods are applied for additional treatment
Sunflower husk	1. Wide raw materials base; 2. Low cost; 3. High level of oil sumption; 4. Possibility of utilization by burning	1. The increase of dispersion degree and carbonization is required
Walnut shuck	1. Wide raw materials base; 2. Low cost; 3. High level of oil sumption; 4. Possibility of utilization by burning	1. Fraction size reduction is applied
Lignine	1. Wide raw materials base; 2. Low cost; 3. High level of oil sumption	1. Additional treatment is necessary
Sawdust	1. Wide raw materials base; 2. Low cost; 3. High level of oil sumption; 4. Possibility of utilization by burning	1. Additional treatment by chemical compounds or by increased temperature is required
Cotton waste	1. Wide raw materials base; 2. High level of oil sumption	1. Low regeneration degree
Polivinihloride	1. Wide raw materials base; 2. High level of oil sumption	1. Additional treatment is required; 2. Hydrophilic properties; 3. Low regeneration degree

Table 1 shows the main advantages of sorbents based on natural raw materials. The raw materials base is wide enough, has high level of sumption, low cost characteristics compared with the utilization by burning.

Majority of natural raw materials are exposed to chemical and thermal treatment. The thermal treatment application procedures were studied by the authors. Positive impact of the high temperatures on sumption properties is established (fig. 1). This phenomenon can be explained by increasing of surface area of sorbents (fig. 2).

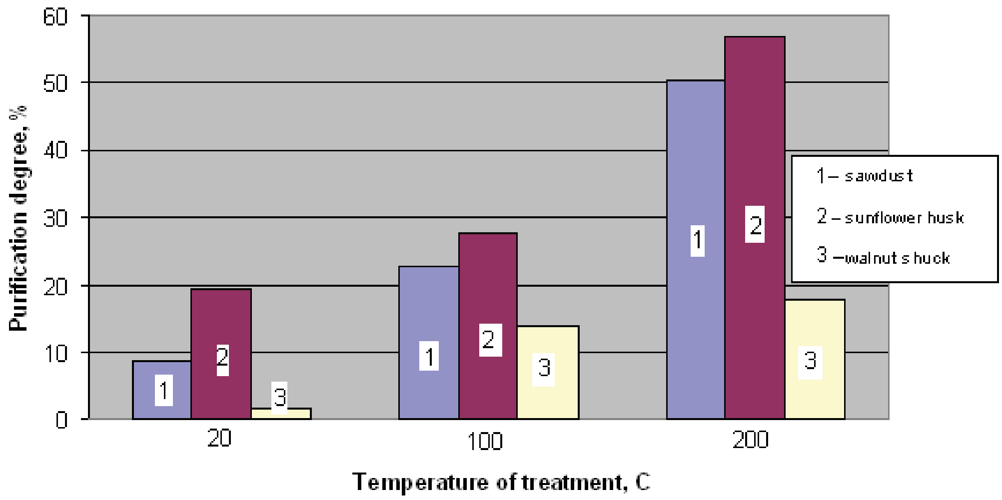

Fig. 1. Temperature impact on the purification degree of contaminated waters

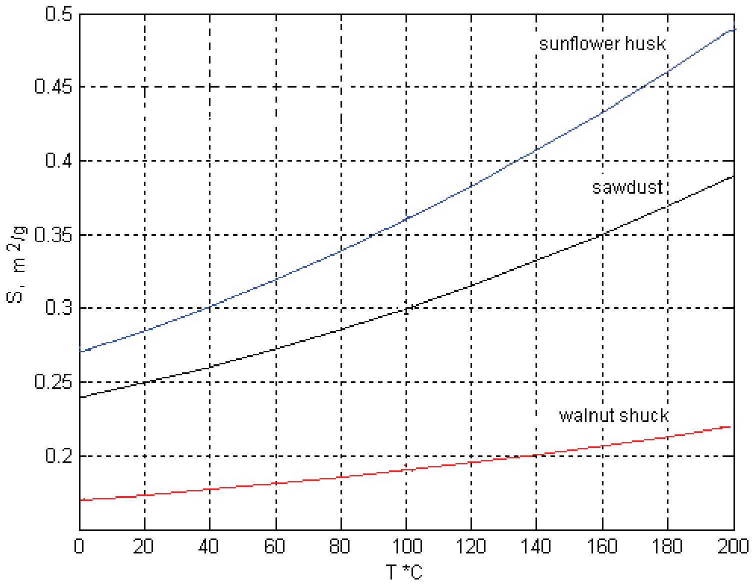

Fig. 2. Temperature impact on the sorbents surface area

Using of sorbents on natural raw materials for improving of waste waters purification quality on the enterprises of aviation fuel providing system is very perspective direction, that requires the new researches in this sphere.

References

1. Каменщиков Ф.А. Нефтяные сорбенты / Ф.А. Каменщиков, Е.И. Богомольный. – Москва-Ижевск : НИЦ “Регулярная и хаотическая динамика”, 2005. – 268 с.

2. Павлюх Л. І. Перспективи використання сорбентів на основі рослинної сировини для очищення стічних вод від нафтопродуктів / Л. І. Павлюх, С. В. Бойченко // Нафтова та газова промисловість України. – № 3. – 2011. – С. 54–56.

3. Павлюх Л. І. Фактори впливу на нафтопоглинальні властивості органічних сорбентів рослинного походження / Л. І. Павлюх, С. В. Бойченко // Вопросы химии и химической технологи. – № 6. – 2011. – С. 126–129.

4. Швец Д.И. Углеродные сорбенты растительного происхождения для очистки воды от нефти / Д.И. Швец, О.В. Кравченко, Н.М. Опенько, Г.Т. Ситкарев // Экотехнологии и ресурсосбережение. – 2003. – №4. – С. 29–32.

UDC 65.011.3:656.71:528.9 (043.2)

I. Gosudarska, assistant
(National Aviation University, Ukraine)

INDIVIDUAL RISK CALCULATION METHOD – LIGHT AIRCRAFT

This paper presents an individual risk calculation method at the point in the vicinity of airports. The crash distribution model adopted for aircraft less than 4 tonnes maximum take-off weight authorised. Evaluation of individual risk at y = 0 was related probability crashes of light aircraft in the vicinity of airports.

In order to investigate third party risk around airports, objective measures of risk are required. Individual risk is defined as the probability (per year) that a person permanently residing at a particular location in the area around the airport is killed as a direct consequence of an aircraft accident. Individual risk is location specific; it is present regardless of whether or not someone is actually residing at that location. This is used as a means to determine which areas should be considered too dangerous to build houses or vulnerable infrastructure.

Impact probability is calculated at a specified point using the Probability Density Functions (PDFs) and light aircraft crash rates. The distributions are PDFs in the form:

$$f(x, y) = f(x) \cdot f(x, y)$$

where $f(x)$ is function representing the longitudinal location along the direction of the extended runway centerline; $f(x, y)$ is lateral distribution perpendicular to the runway centerline.

The function $f(x)$ is derived from x coordinate data. The function $f(x, y)$ is derived from y coordinate data, for which the corresponding x coordinate is known.

The PDFs are based on the Gamma and Weibull distributions. The Gamma distribution for parameters c, α and β is:

$$f(x,\text{б},\text{в}) = \frac{1}{\text{в}^{\text{б}}\,\Gamma(\text{б})} x^{\text{б}-1} \exp\left[-\left(\frac{x}{\text{в}}\right)\right]$$

The Weibull distribution for parameters c, α and β is:

$$f(x,\text{б},\text{в}) = \frac{\text{б}}{\text{в}^{\text{б}}} x^{\text{б}-1} \exp\left[-\left(\frac{x}{\text{в}}\right)^{\text{б}}\right]$$

The level of individual risk at any given point near an airport varies in an approximately proportional fashion to the number of movements, the average crash rate, and the average destroyed area (resulting from a crash), for that airport. The model was produced for the distribution of airport related crashes for aircraft less than 4 tonnes maximum take-off weight authorised.

The following method can be used to calculate individual risk at a point (x_o, y_o) which is a distance:

- ‘x_o’ from the end of tarmac, along the runway extended centreline;
- ‘y_o’ perpendicular to the runway extended centreline.

The crash area is represented by a square, the length of whose sides are ‘b’. If a crash of light aircraft occurs centred at any point within the shaded square area, the point indicated in Figure 1, would be impacted.

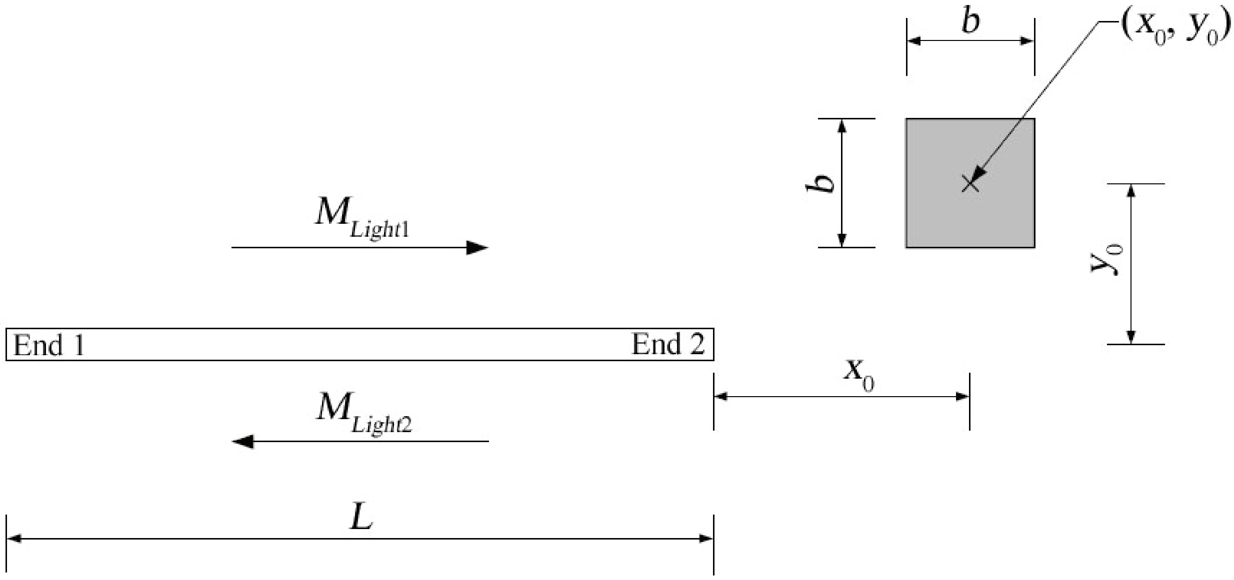

Figure 1. Individual Risk Calculation Schematic – Light Aircraft

Therefore, the individual risk at the point indicated in Figure 1 is the frequency with which a crash of light aircraft would occur within the shaded square. This is evaluated by the following integral, over two dimensions as shown in Equation 1:

$$IR_{Light} = \int_{x_0-\frac{b}{2}}^{x_0+\frac{b}{2}} \int_{y_0-\frac{b}{2}}^{y_0+\frac{b}{2}} \begin{bmatrix} 2R_{Light} M_{Light1} f_{TO}(x,y) + 2R_{Light} M_{Light1} f_{LO}(x+L,y) + \\ +2R_{Light} M_{Light1} f_{TC}(x,y) + 2R_{Light} M_{Light2} f_{TC}(-x-L,y) + \\ +2R_{Light} M_{Light1} f_{LC}(x+L,y) + 2R_{Light} M_{Light2} f_{LC}(-x,y) \end{bmatrix} dx\,dy \quad (1)$$

which can be expanded to:

$$IR_{Light} = 2R_{Light} M_{Light1} \int_{x_0-\frac{b}{2}}^{x_0+\frac{b}{2}} \int_{y_0-\frac{b}{2}}^{y_0+\frac{b}{2}} f_{TO}(x,y)\,dx\,dy + 2R_{Light} M_{Light1} \int_{x_0-\frac{b}{2}}^{x_0+\frac{b}{2}} \int_{y_0-\frac{b}{2}}^{y_0+\frac{b}{2}} f_{LO}(x+L,y)\,dx\,dy +$$

$$+2R_{Light} M_{Light1} \int_{x_0-\frac{b}{2}}^{x_0+\frac{b}{2}} \int_{y_0-\frac{b}{2}}^{y_0+\frac{b}{2}} f_{TC}(x,y)\,dx\,dy + 2R_{Light} M_{Light2} \int_{x_0-\frac{b}{2}}^{x_0+\frac{b}{2}} \int_{y_0-\frac{b}{2}}^{y_0+\frac{b}{2}} f_{TC}(-x-L,y)\,dx\,dy +$$

$$+2R_{Light} M_{Light1} \int_{x_0-\frac{b}{2}}^{x_0+\frac{b}{2}} \int_{y_0-\frac{b}{2}}^{y_0+\frac{b}{2}} f_{LC}(x+L,y)\,dx\,dy + 2R_{Light} M_{Light2} \int_{x_0-\frac{b}{2}}^{x_0+\frac{b}{2}} \int_{y_0-\frac{b}{2}}^{y_0+\frac{b}{2}} f_{LC}(-x,y)\,dx\,dy$$

where M_{Light1} is number movements light aircraft per year in Direction 1; M_{Light2} - is number movements light aircraft per year in Direction 2; R_{light} is crash probability rate per year of light aircraft; $f_{TO}(x, y)$ is probability density function for take-off overruns crashes of light aircrafts; $f_{LO}(x, y)$ is probability density function for landing overruns crashes of light aircrafts; $f_{TC}(x, y)$ is probability density function for take-off crashes (non overruns) crashes of light aircrafts; $f_{LC}(x, y)$ is probability density function for landing crashes (non overruns) crashes of light aircrafts; b is length of side for square crash area; y is distance perpendicular to the extended runway centreline; x is distance along the extended runway centerline.

The maximum extent of the contour occurs on the extended runway centerline (i.e. $y = 0$). Therefore, to calculate the maximum extent of the individual risk contours it is important to calculate the individual risk at $y = 0$. However, the PDFs exhibit singularities (i.e. are undefined or infinite) for $y = 0$. These singularities can be eliminated by mathematically transforming the PDFs according to the following scheme:

$$q(x,y,б,в,с) = \frac{1}{2} б \left(\frac{x^{с}}{в}\right)^{б} (|y|)^{б-1} \exp\left[-\left(|y|\frac{x^{с}}{в}\right)^{б}\right]$$

The function, q has a singularity at $y = 0$ for $\alpha < 1$, so it is split into a non-singular part (q_1) and a singular part (q_2) such that ($q = q_1 + q_2$) as shown in Equation 2 and Equation 3:

$$q_1(x,y,\text{б},\text{в},\text{с}) = \frac{1}{2}\text{б}\left(\frac{x^{\text{с}}}{\text{в}}\right)^{\text{б}} \left(|y|\right)^{\text{б}-1}\left\{\exp\left[-\left(|y|\frac{x^{\text{с}}}{\text{в}}\right)^{\text{б}}\right]-1\right\} \tag{2}$$

$$q_2(x,y,\text{б},\text{в},\text{с}) = \frac{1}{2}\text{б}\left(\frac{x^{\text{с}}}{\text{в}}\right)^{\text{б}} \left(|y|\right)^{\text{б}-1} \tag{3}$$

The singular part, q_2 can be integrated analytically. Providing y_0 is positive and is greater than $b/2$, the integral of q_2 from $y = y_0 - b/2$ to $y = y_0 + b/2$ is:

$$q_2(x,y_0,\text{б},\text{в},\text{с}) = \frac{1}{2}\left(\frac{x^{\text{с}}}{\text{в}}\right)^{\text{б}} \left\{\left(y_0+\frac{b}{2}\right)^{\text{б}} - \left(y_0-\frac{b}{2}\right)^{\text{б}}\right\} \quad \text{for } y_0 > b/2 > 0 \tag{4}$$

For calculation on, or close to the runway extended centerline, the integration must be treated differently, since q_2 is a function of the modulus of y expressed as $|y|$. However, if y_0 is positive (or zero) and is less than $b/2$, part of the crash area occupies the region where y is less than zero ($y < 0$), as illustrated in Figure 2.

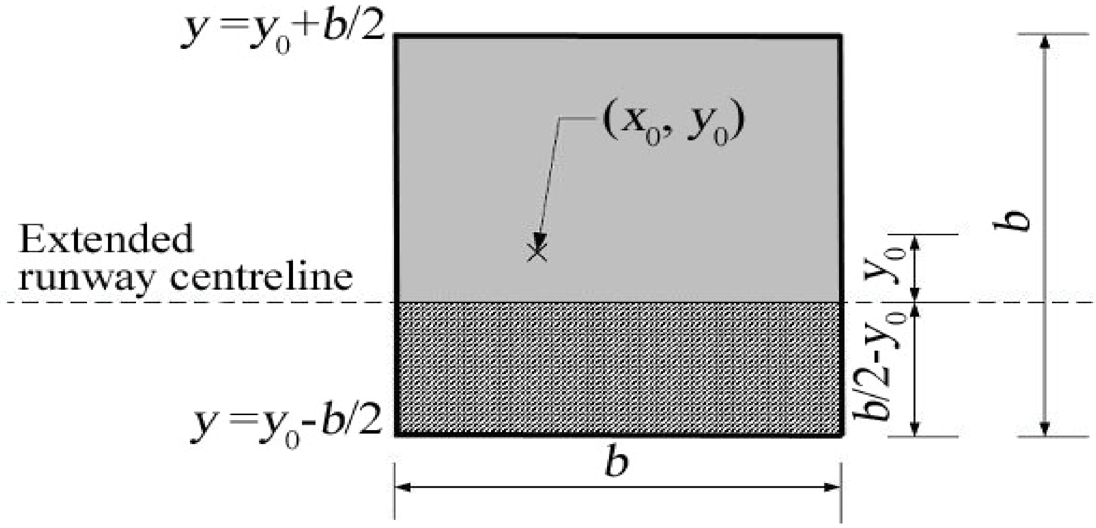

Figure 2. Illustration of the Case of Individual Risk Calculation
Close to the Runway Extended Centreline

The integral of q_2 from $y = y_0 - b/2$ to $y = y_0 + b/2$ is considered as follows:

$$\int_{y_0-\frac{b}{2}}^{y_0+\frac{b}{2}} q_2(x,y,\text{б},\text{в},\text{с})\,dx = \int_{y_0-\frac{b}{2}}^{0} q_2(x,y,\text{б},\text{в},\text{с})\,dx + \int_{0}^{y_0+\frac{b}{2}} q_2(x,y,\text{б},\text{в},\text{с})\,dx \tag{5}$$

Since q_2 is a function of the modulus of y, the following is true, by definition:

$$q_2(-x, y, \alpha, \beta, c) = q_2(x, y, \alpha, \beta, c)$$

Therefore, since $y_0 - b/2$ is negative,

$$\int_{y_0-\frac{b}{2}}^{0} q_2(x,y,\text{б},\text{в},\text{с})\,dx = \int_{0}^{\frac{b}{2}-y_0} q_2(x,y,\text{б},\text{в},\text{с})\,dx$$

This can then be substituted in Equation 5 to give,

$$\int_{y_0-\frac{b}{2}}^{y_0+\frac{b}{2}} q_2(x,y,\text{б},\text{в},\text{с})\,dx = \int_{0}^{\frac{b}{2}-y_0} q_2(x,y,\text{б},\text{в},\text{с})\,dx + \int_{0}^{y_0+\frac{b}{2}} q_2(x,y,\text{б},\text{в},\text{с})\,dx$$

Therefore, providing y_0 is positive (or zero) and is less than $b/2$, the integral of q_2 from $y = y_0 - b/2$ to $y = y_0 + b/2$ is:

$$q_2(x, y_0, б, в, c) = \frac{1}{2}\left(\frac{x^c}{в}\right)^б \left\{\left(\frac{b}{2} - y_0\right)^б + \left(y_0 + \frac{b}{2}\right)^б\right\} \text{ for } b/2 > y_0 \geq 0 \qquad (6)$$

Note that for $y_0 = b/2$ and 0, Equation 4 and Equation 6 are equivalent. For take-off overruns, the wreckage location PDFs ($x > 0$) is:

$$f_{TO}(x, y) = p \cdot f_W(x; 1{,}181; 283{,}3)\begin{bmatrix} q_1(x, y; 0{,}817; 39{,}65; 0{,}355) + \\ + q_2(x, y; 0{,}817; 39{,}65; 0{,}355) \end{bmatrix}$$

Therefore,

$$\int_{x_0-\frac{b}{2}}^{x_0+\frac{b}{2}}\int_{y_0-\frac{b}{2}}^{y_0+\frac{b}{2}} f_{TO}(x, y)\, dx\, dy =$$

$$= \int_{x_0-\frac{b}{2}}^{x_0+\frac{b}{2}}\int_{y_0-\frac{b}{2}}^{y_0+\frac{b}{2}} p \cdot f_W(x; 1{,}181; 283{,}3)\begin{bmatrix} q_1(x, y; 0{,}817; 39{,}65; 0{,}355) + \\ + q_2(x, y; 0{,}817; 39{,}65; 0{,}355) \end{bmatrix} dx\, dy$$

and

$$\int_{x_0-\frac{b}{2}}^{x_0+\frac{b}{2}}\int_{y_0-\frac{b}{2}}^{y_0+\frac{b}{2}} f_{TO}(x, y)\, dx\, dy =$$

$$= \int_{x_0-\frac{b}{2}}^{x_0+\frac{b}{2}}\int_{y_0-\frac{b}{2}}^{y_0+\frac{b}{2}} p \cdot f_W(x; 1{,}181; 283{,}3)\, q_1(x, y; 0{,}817; 39{,}65; 0{,}355)\, dx\, dy +$$

$$+ \int_{x_0-\frac{b}{2}}^{x_0+\frac{b}{2}}\int_{y_0-\frac{b}{2}}^{y_0+\frac{b}{2}} p \cdot f_W(x; 1{,}181; 283{,}3)\; q_2(x, y; 0{,}817; 39{,}65; 0{,}355)\, dx\, dy$$

So,

$$\int_{x_0-\frac{b}{2}}^{x_0+\frac{b}{2}}\int_{y_0-\frac{b}{2}}^{y_0+\frac{b}{2}} f_{TO}(x, y)\, dx\, dy =$$

$$= \int_{x_0-\frac{b}{2}}^{x_0+\frac{b}{2}}\int_{y_0-\frac{b}{2}}^{y_0+\frac{b}{2}} p \cdot f_W(x; 1{,}181; 283{,}3)\, q_1(x, y; 0{,}817; 39{,}65; 0{,}355)\, dx\, dy +$$

$$+ \int_{x_0-\frac{b}{2}}^{x_0+\frac{b}{2}} p \cdot f_W(x; 1{,}181; 283{,}3)\left[\int_{y_0-\frac{b}{2}}^{y_0+\frac{b}{2}} q_2(x, y; 0{,}817; 39{,}65; 0{,}355)\, dx\right] dy$$

and

$$\int_{x_0-\frac{b}{2}}^{x_0+\frac{b}{2}}\int_{y_0-\frac{b}{2}}^{y_0+\frac{b}{2}} f_{TO}(x, y)\, dx\, dy =$$

$$= \int_{x_0-\frac{b}{2}}^{x_0+\frac{b}{2}}\int_{y_0-\frac{b}{2}}^{y_0+\frac{b}{2}} p \cdot f_W(x; 1{,}181; 283{,}3)\, q_1(x, y; 0{,}817; 39{,}65; 0{,}355)\, dx\, dy + \qquad (7)$$

$$+ \int_{x_0-\frac{b}{2}}^{x_0+\frac{b}{2}} p \cdot f_W(x; 1{,}181; 283{,}3)\left[q_2(x, y_0; 0{,}817; 39{,}65; 0{,}355)\right] dy$$

To evaluate this integral on the extended runway centerline, $y_0 = 0$. Since the function q_2 involves the modulus of x, the function is symmetrical about the line representing $y = 0$. Therefore:

$$\int_{-\frac{b}{2}}^{\frac{b}{2}} q_2(x, y; 0{,}817; 39{,}65; 0{,}355)\, dx = 2\int_0^{\frac{b}{2}} q_2(x, y; 0{,}817; 39{,}65; 0{,}355)\, dx$$

Both terms of the integral defined in Equation 7 can be integrated numerically. Note that for y=0:

$$q_1(0,x;0{,}817;39{,}65;0{,}355)=0\ .$$

The principle for the other crash distributions is similar to that described for landing overruns. Therefore, a similar approach is employed for the other crash distribution functions. For landing overruns, the wreckage location PDFs ($x > 0$, $y = 0$) is:

$$f_{LO}(x,y)=f_G(x;1{,}109;203{,}4)\begin{bmatrix}q_1(x,y;0{,}815;32{,}1;0{,}345)+\\+q_2(x,y;0{,}815;32{,}1;0{,}345)\end{bmatrix}.$$

For take-off crashes, the impact location PDFs are:

$$f_{TC}(x,y)=p\cdot f_W(x;1{,}058;701{,}6)\begin{bmatrix}q_1(x,y;0{,}575;186{,}6;0{,}057)+\\+q_2(x,y;0{,}575;186{,}6;0{,}057)\end{bmatrix}\ \text{for } x>0,\ y=0$$

and

$$f_{TC}(x,y)=(1-p)\cdot f_G(|x|;0{,}929;775{,}8)\begin{bmatrix}q_1(|x|,y;0{,}85;352{,}7;0{,}04)+\\+q_2(|x|,y;0{,}85;352{,}7;0{,}04)\end{bmatrix}\ \text{for } x\le 0,\ y=0$$

For landing crashes, the impact location PDFs are:

$$f_{LC}(x,y)=p\cdot f_G(x;0{,}726;1000{,}9)\begin{bmatrix}q_1(x,y;0{,}576;24{,}38;0{,}323)+\\+q_2(x,y;0{,}576;24{,}38;0{,}323)\end{bmatrix}\ \text{for } x>0,\ y=0$$

and

$$f_{TC}(x,y)=(1-p)\cdot f_W(|x|;0{,}584;251{,}9)\begin{bmatrix}q_1(|x|,y;0{,}64;179{,}4;0{,}185)+\\+q_2(|x|,y;0{,}64;179{,}4;0{,}185)\end{bmatrix}\ \text{for } x\le 0,\ y=0$$

Conclusion

The traffic at some airports has a higher proportion of lighter aircraft, such as piston-engine aircraft, which tend to be at a higher risk of crashing than large aircrafts over 4 tonnes maximum take-off weight authorised. Therefore, here was presented the calculation of individual risk at the point from light aircraft crashes in the vicinity of airports. The model was produced for the distribution of airport related crashes for aircraft less than 4 tonnes maximum take-off weight authorised.

UDC: 504.06:656.71(477) (043.2)

K. Kazhan (National Aviation University, Ukraine)

MANAGEMENT OF THE AIRCRAFT FLEET STRUCTURE FOR ENHANCEMENT OF THE ENVIRONMENTAL SAFETY AND THE AIRPORT CAPACITY

The article presents the entropy approach and model for substantiation of the optimal aircraft fleet structure taking into account environmental concerns. The most sensitive factors of the aviation impact on environment: aviation noise and emission were analyzed.

A growth of an airport can be controlled by setting up flight safety, operational, economic and environmental limits (Fig.1). In addition to the increasing traffic demand, new constraints on the flow of traffic have been imposed and limited the capacity and efficiency of air transportation. Apart from airport and airspace capacity issues that need to be resolved to accommodate further growth, the air transport industry is also facing increasing constraints with respect to environmental pollution. More and more airports within Europe, as well as world-wide, are faced with noise and emission restrictions imposed by government or local authorities. Thus, the use of means of reducing noise and emissions to enhance environmental safety and to increase airport capacity is very topical.

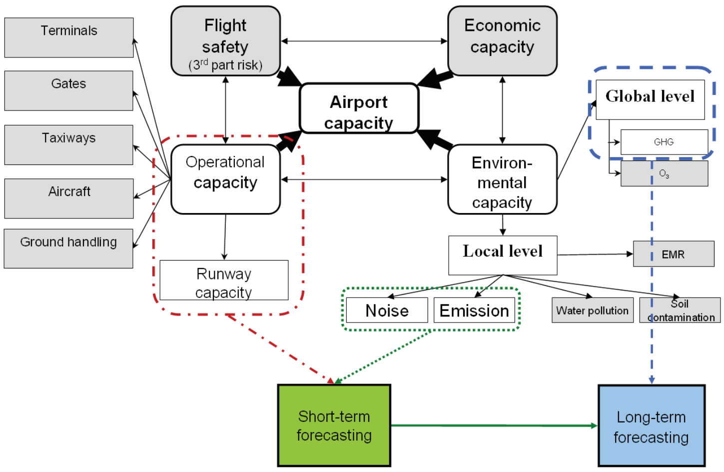

Fig.1. Scheme of the airport capacity

Environmental capacity (Fig.1) is one of the main constraints of the airport sustainable development now and can be increased with the introduction of effective transport management system. Operational procedures allow noise and emission reduction around airports with least expenses, without additional engineering or legal improvements [1]; and can improve environmental quality and thus perfect life quality of many thousands of people in the vicinity of airports.

The interrelationships between the environmental factors significantly intensify the problem of choosing of the operational procedures for aviation noise and emission impact reduction [2, 3].

The following problems of interrelationships of noise and emission are under discussion for last decades [2-7]: where interdependencies and trade-offs occur: research, design, technologies, operations, impacts and solutions; how the environmental trade-offs influence on aircraft/engine optimized design and operation; the expected achievements and future prospects of ongoing and future activities focused on addressing aviation environmental trade-offs and interdependencies.

In this vein **the aim of the investigation** is the development of the tool for substantiation of the optimal aircraft and airport operation modes taking into account noise and emission interdependencies, and increasing environmental airport capacity within the framework of sustainable development policies.

According to the environmental capacity concept [8] the “airport-environment” interaction is considered as the complex system with operational and environmental constrains (Fig.1).

Basic element of the system is an aircraft fleet with a number of possible flight procedures that can impact on environment in airport vicinity, causing permanent changes. Thus a maximum number of flights Q of aircraft type i =1,… Q_i (Q_i is a number of aircraft types in the fleet under consideration) distributed among routes j=1,… N_j (N_j is a number of the fixed flight routes in airport under consideration) and implementing the noise and emission control measures (noise and emission reduction procedures (N&ERPs)) of type k j=1,… N_k (N_k is a number of the N&ERPs under consideration) that can be accommodated in the airport during given period m and do not cause permanent effects on environment is called environmental airport capacity.

So the first task may be formulated as a global search of this maximum number of flights Q, which is considered as an “ideal value” of environmental airport capacity.

The usual for operation task is reduced to determine the number of aircraft T_{ij}^{km} of each type i on each route j that use the noise and emission reduction procedure k to reduce impact inside critical zone l (for example, residential areas, building and so on) at least till the normative level of the environmental factor under consideration (noise or emission). The task of capacity providing and reducing of the impact on environment is complicated by interrelationships of the most sensitive environmental factors in the airport vicinities – aircraft noise and emission.

Constraints of the operational capacity lie in given number of aircraft of specific type Q_i operated in the airport:

$$\sum_{j,k,m} T_{ij}^{km} = Q_i \tag{1}$$

Environmental constrains, taken into account, are the prescribed levels in critical zones.

$$\sum_{i,j,k,m} T_{ij}^{km} \cdot Z_{ij}^{km}(l) = 1, \tag{2}$$

where $Z_{ij}^{km}(l)$ depends on type of criteria for noise and/or emissions assessment from environmental rules in the critical zone l.

The criteria definition depends on type of forecasting (Table 1). In present model for short-term forecasting (for a day, or from month to year) it is proposed to use the maximum $L_{A\max}$, equivalent noise level L_{Aeq} and SEL (sound exposure level) for noise assessment. NEF (Noise Exposure Forecast) can be used in long-term forecasting – for period up to few decades. Masses of pollutants M or their concentrations C are offered for emission control.

Table 1

Criteria for the short-term and long-term forecasting models

Type of the forecasting		Short-term		Long-term
Period		Day	Month - Year	Few years - decade of years
Criteria	noise	L_{Amax}, L_{AeqD}, L_{AeqN}, SEL, ...		NEF, $EPNL$
	emission	Cn, Mn		Mn
v		$v_{ij}^{k} = C \cdot A_{V\,ij} \cdot B_{V}{}^{k}$	$v_{im} = ca_{im} b_m D_m S_m$	$v_{ijr} = V_{Vi} \cdot V_{ijr}$
		$\sum_{i,j,k} v_{ij}^{k} = 1$	$\sum_{i,m} v_{im} = 1$	$\sum_{i,j,r} v_{ijr} = 1$

There are different approaches exist for solving the task of combined effects (aircraft noise and emission) reducing within the framework of the environmental capacity concept: method of linear programming (Janec, 2003) [6]), geometrical probability’s method (Kazhan, 2008, 2010 [9-10], Tokarev 2009 [11]), numerical cost-effective methods (Ferrar, 1974 [7], Gaffal, 2005 [2], Fleming, 2007 [3], Hepting, 2009[4], Evans, 2010 [12]) et al. The necessity of using additional criteria of system state optimality is one the main disadvantages of listed approaches. The principle of maximum entropy states that the probability distribution which best represents the current state of information is the one with largest entropy.

The probable implementation of operational procedures and distribution of aircraft among the routes are defined by the relative extremum of the system entropy as shown in [13]:

$$S = \ln T! + \sum_{i,j,k,m} T_{ij}^{km} (\ln \frac{v_{ij}}{T_{ij}^{km}} + 1) \to \max, \quad (6)$$

where v_{ij} are the normalized frequencies of the usage of aircraft i along the route j.

Thus the probable distribution of aircraft T_{ij}^{km} is defined by the relative extreme of entropy (3) for the system with constraints (1-2) [8,9]:

$$T_{ij}^{km} = \frac{v_{ij} \cdot Q_i \cdot \exp\left(-\sum_l \beta_l \cdot Z_{ij}^{km}(l)\right)}{\sum_i v_{ij} \cdot \exp\left(-\sum_l \beta_l \cdot Z_{ij}^{km}(l)\right)}, \quad (7)$$

where β_l are the Lagrange coefficients.

Within the framework of the considered model the iterative equation (7) has a solution in the range $\beta_l^0 + 1 \geq \beta_l \geq \beta_l^0 + 10^6$ due to calculation time limit**.** If the constraints (1-2) are not fulfilled then the maximum environmental capacity is reached and the alternative noise and emission reduction method should be considered in the model.

Fig.2 shows an algorithm of the realization of the model under consideration. It should be noted that INM and EDMS (as the basic modeling system) are used during the two stages of the algorithm – data preparation and resulting check. The algorithm and application programs were designed using an informational data for local conditions.

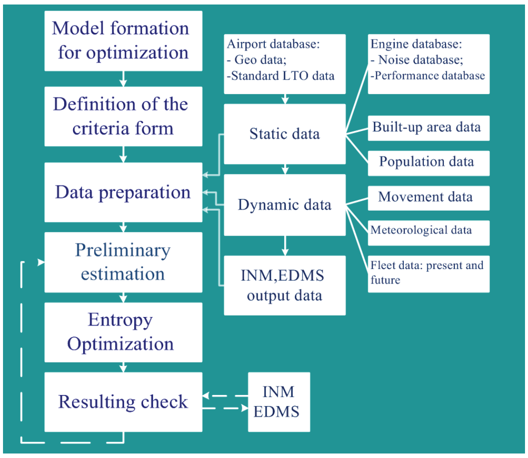

Fig. 2. Principal scheme of the algorithm of the Entropy Model

The main differences between long-term forecasting and the short-term ones lie in the definition of parameter v_{ir}, and noise and emission assessment criteria (Table 1). NEF and mass M of the polluted gases are used as the criteria for the long-term forecasting (prediction on few years or decades). The aim of the long-term forecasting lies in the equality of NEF and M value to the prescribed levels during forecasting period, for example, to the value of NEF_1 and M_1 in the first year of prediction ($r = 1$). For the description of noise constraints parameter Z (2) depends on quantity of aircraft T_{ir} of type i in year r, levels $EPNL_i$ and pollutant masses Mp_i that aircraft of type i creates during flying in the critical zone l and level NEF_r and total amount of pollutant M_r for each year r.

Number of tracks is neglected in this model because the criterion M (that assess during LTO cycle) does not significantly depend on the track trajectory.

Thus, following restrictions use in the long-term forecasting model:

$$\sum_i T_{ir} M_{ir} = 1,\ \sum_i T_{ir} P_i = 1,\ \sum_i T_{ir} = T_r \tag{8}$$

where $M_{ir} = \dfrac{Mp_i}{M_r}$, $P_i = 10^{-0,1 \cdot NEF_r - 8,8} \cdot 10^{0,1 \cdot EPNL_i}$, $NEF_r = NEF_1, M_r = M_1$.

In accordance to the maximum entropy method the aircraft type distribution is defined by the following equation:

$$T_{ijr} = \frac{T_r v_{ir} \exp(-\alpha_r M_{ir} - \beta_r P_i)}{\sum_i v_{ir} \exp(-\alpha_r M_{ir} - \beta_r P_i)}, \tag{9}$$

where the normalized frequency v_{ir} of the usage of aircraft i during the year r depends on the relative coefficients that take into account maximum and real average number of passenger on the broad of aircraft type V_{Vi}, and maximum and real average flight distance V_{ir} (Table 1).

To illustrate the model opportunities, the forecasting is performed for several scenarios and environmental factors that affect capacity: first, NO_x emission and aviation noise and, second, emission of greenhouse gases (GHGs): CO_2 and H_20 and noise, that is caused by the factor formation nature.

Input data for the operation situation in the airport are next: 22 aircraft types, one control zone, and the expected numbers of aircraft are T_r=100, 500, 1000 and 2000 accordingly for each of 4 studied years: 2009, 2013, 2017, 2019. Noise assessment $EPNL_i$ was held on the basis of Noise Certification Database [13] and pollutant masses Mp_i were determined with the help of emission indexes and fuel flows.

Entropy modelling shows us considerable excess of basic level NEF already for the second year; and masses of the NO_x, CO_2 and H_20 for the third year. It is possible to decrease either NEF in critical zone to level NEF$_1$, either mass to amount M_1, taking into account the results of entropy modeling on Fig. 8.

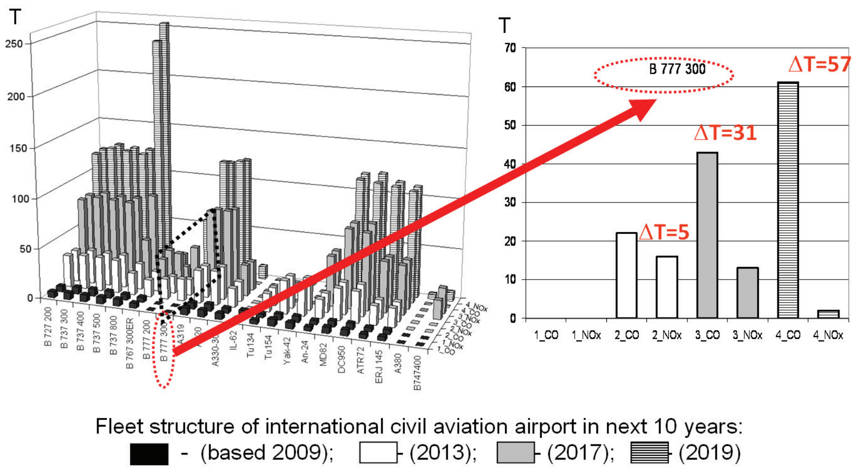

Fig.3. Comparison of the results of the long-term forecasting: noise and emission NO_x; noise and emission of GHGs.

In this case the increasing of the environmental capacity depends on phasing-out older aircraft types that do not meet ICAO requirements on noise and exhaust gases (in the given example such as Yak-40, Il-86, Il-76 and others aircraft), and putting into operation more effective types: 777300, A330, A340 and others aircraft. The overall prediction results obtained for two different scenarios are correlated with each other, but there are some differences in the results for NO_x and GHGs emission, that Fig. 3 shows. In particular for the second scenario (GHGs) the reduction of the share of some aircraft types (for example, B 777 300, B 767 300, B 777 200, A 330 301, A 380, B 747 400) in total fleet for year r=4 in comparison with the first scenario (NO_x) is noted.

This is explained by the design features of the aircraft types (for example, B 777 300, B 767 300, B 777 200, A 330 301, A 380, B 747 400) - relatively small emission index of NO_x and, at the same time, high fuel flow, which increases the total emission of GHGs.

Conclusions. To implement the concept of environmental airport capacity mathematical tools based on the maximum entropy method for short-term and long-term forecasting was proposed in the study. The approach corresponds to the basics of The ICAO Balanced approach [3] and has potential ability of use either for short-term measures, both long-term forecasting and planning of airport operations. The long-term forecasting can be used for development of the policy of airport management in the field of the land use planning and adjustment of aircraft fleet composition, introduction of fees for aircraft noise and emissions of pollutants, including greenhouse gases

Such aspects as perspective aircraft fleet and maximum environmental airport capacity were analysed during long-term forecasting. The results of the forecasting have shown strict constraints of the airport capacity in terms of 10-15 years in case of existing fleet mix operation. Phasing-out the aircraft that do not meet the ICAO's newest requirements will preserve the possibility of the airports' sustainable development.

References

1. *Review* of noise abatement procedure research & development and implementation results discussion of survey results. International Civil Aviation Organization. Preliminary Edition – 2007. – 29 p. Available on www.icao.int/env/reviewnadrd.pdf
2. *Gaffal R., Schwanke St., Kloiber Fl.* An approach for noise and emission trade off. – Proc. Aviation Noise & Air Quality Symposium. – Palm Springs. – 2005. – March.
3. *Fleming G. G.* Modeling Environmental Interdependencies. Environmental Measurement and Modeling Division. US Department of Transportation Research and Innovative Technology Administration. The Volpe centre. – Proc. ANERS 2007. La Baule. France. – 2007. – Jun. – 10 p.
4. *Hepting M*. European Toolset for Environmental Aviation Modelling. A Project Proposal in the 7th Framework Programme. Proceedings of the *3rd world congress "Aviation in XXI century"*. Safety in aviation and space technology. Sept. 22 – 24, 4 p., 2008.
5. *Zaporozhets, O.I. & Tokarev, V.I.* Aircraft noise modelling for environmental assessment around airports. // *Applied Acoustics*, vol. 55, No 2, p. 99-127, 1998
6. *Janic M.* Modeling operational, economic and environmental performance of an air transport network // Transportation Research. – Part 8. – 2003. – P. 415 – 432.
7. *Ferrar T.A.* The allocation of airport capacity with emphasis on environmental quality // Transportation research 8. – 1974. – p. 163-169.
8. *Callum Th.* The concept of airport environmental capacity. Manchester Metropolitan University. Department of Environmental & Geographical Sciences. Prepared for: Dr. Arthur Lieuwen, EUROCONTROL. – 2002. – Oct. – 85 p.
9. *Kazhan K.* Complex assessment of the environmental impact of noise and pollutant emissions in the airport vicinity // Proceedings of the 3rd world congress "Aviation in the XXI-st century". – Kiev, 2008. – V.2. – P. 4.16-4.18.
10. *Kazhan K.I.* Short-Term forecasting of noise abatement procedures implementation // Proceedings of the 4th world congress "Aviation in the XXI-st century". – Kiev, 2010. – V.2. – P. 101.4-101.7.
11. *Kazhan K., Tokarev V.* The optimal noise modelling in the airport vicinity // Proceedings of the 9th International Conference on Theoretical and Computational Acoustics. – Dresden, 2009. – P. 41-50.
12. *Evans A. D.* Simulating Airline Operational Responses to Environmental Constraints. – 2010. – 185 p. Available on http://www.arct.cam.ac.uk/aim/Documents/Thesis_ADEvans.pdf
13. http://noisedb.stac.aviation-civile.gouv.fr/

UDC 629.735.024:534.014.2(043.2)

UDC 504.064.2:656.71(043.2)

M.M. Radomska (National Aviation University, Ukraine)

EFFICIENT ENVIRONMENTAL IMPACT ASSESSMENT FOR AIRPORT PROJECTS

The article presents the analysis of the environmental impacts assessment procedure for the projects of airport construction, reconstruction and expansion. The most common shortcomings of available EIA Reports for airport related projects were analyzed. The list of possible impacts of these projects was developed for the needs of environmental assessment. The recommendations on information collection, working procedure organization, public involvement are given.

Aviation is known to be one of the fast growing sectors of global economy. It is associated with a number of social and economic benefits and a range of environmentally damaging consequences. Even the total economic recession cannot change the bright perspectives of aviation development. There is an unquestioning acceptance in governments that the rising demand for air travel will continue and that the land use planning implications (especially more terminals and runways) of this can be managed with minimal harm to the environment. The aviation industry has been very successful in its adoption of an environmental agenda (environmental reports, support of exotic, threatened environments, appointment of environmental managers, financial support of "sustainable aviation"), but has been less forthcoming on questions of growing all the following impacts and the need of these impacts total offsetting.

The case for expanding airports and growth of aviation is frequently supported by evidence on the economic gains (especially jobs) associated with this growth. However, traditional economic arguments fail to include a consideration of the economic impacts of environmental deterioration, health damage and climate change. If these considerations are factored in it may well be the case that a reduction in the demand for air travel will have positive economic benefits. Given the established harmful environmental effects of air travel, there is a case to restrict its growth. Thus, the efficient environmental management of construction and exploitation of airports comes to be among the most important priorities on the way to make airports truly environmentally friendly.

The first mean of negative impacts prevention is the fulfilled procedure of environmental impacts assessment and the subsequent environmental auditing of a site. EIA is a systematic process, which identifies, predicts and evaluates the environmental impacts a proposed project may have. An EIA should enable the decision makers to understand the actual likely environmental impacts that a project may have on the environment and, where applicable, identify mitigation measures that can be put in place to avoid, reduce, remedy or compensate for the identified adverse environmental impacts, or indeed to create or enhance environmental benefits. The EIA process functions as a “glue”, tying the planning of the different projects and the proponents together. The EIA draws attention to areas otherwise ignored, for example the project impacts on historical sites.

Therefore, the main purpose of the EIA in aviation is:

- to reveal positive and negative effects of the aviation infrastructure projects that could have a significant impact on the environment, natural resources and society;
- to ensure that these effects are given consideration in the planning and that the effects were known to the decision-makers;
- to clarify conditions for implementation of the project including mitigating measures and a monitoring programme.

The projects of airport construction, reconstruction and expansion must be filed with the EIA Report, which usually considers a range of the most common environmental impacts related to aviation. These impacts assessments often do not cover all the issues raised by airports and aviation expansion and are limited to noise and air pollution, effects of territory preparation, added pressure on local infrastructure and positive consequences for local communities. This list of impacts is obviously insufficient.

The analysis of the available EIA Reports in the industry shows that all of them lack some important element and the following disadvantages could be revealed from their investigation:

1. Inadequate consideration of the cumulative noise impacts from the project (noise created by planes together with cars, trains, etc. used to get to the airport).

2. The need for new land areas for the location of special installations is insufficiently discussed.

3. Long-term impacts on water resources are not properly addressed.

4. The social and economic impacts of projects on local communities are discussed from one positive point of view.

5. The EIA process often does not comprise a real evaluation of alternative locations of an airport.

6. Time framework implies that much of the input generated by the EIA process is only available after important decisions in the planning has been made.

7. Public opinion is not taken into account in full. The final EIA Reports often merely state that input from the public hearings has been incorporated in the process and consequently the final programme is almost identical to the preliminary programme. This leads to major conflicts in the project.

8. The EIAs fail to give a proper account of the environmental effects in conjunction with construction and operation of transport links of airports.

9. The EIA often ignore actual social effects for the population directly affected by the project, for example, people who were relocated because of the project.

Given the above, the efficiency of EIA procedure could be enhanced by thorough development and planning of all stages and elements of EIA.

First, considering the defined disadvantages of EIA scope the following impacts should be targeted for the analysis of:

- noise pollution;
- air pollution;
- greenhouse gases emissions and global climate change input;
- local climate changes;
- geology and soil impacts;
- forest resources impacts;
- water resources pollution, physical changes and degradation of waterbodies;
- recreational areas impacts;
- landscape deterioration and visual effects;
- flora and fauna/genetic resources impacts;
- wastes generation volumes and hazard levels;
- impacts on historical sites;
- social impacts: indirect regional impacts and direct local impacts;
- economic impacts for local municipalities.

Separately EIA should consider all aspects of the construction stages associated with the project. The following should be described:

- the construction programme;
- phasing and duration of the separate stages of the construction;
- main construction activities (including piling);
- numbers of vehicles used and their distribution over the construction period;
- infrastructure requirements such as access arrangements and construction compounds;
- production of construction waste, including the types of waste, estimates of the volumes to be produced and proposals for its management.

A good idea is to include a sustainability appraisal in the EIA process. The appraisal should assess the sustainability of the proposals as a whole scheme and not just detail the sustainable elements of the proposals. An assessment of the sustainability of the project should address issues such as:

- emission of greenhouse gases;
- contributions to and the maintenance of biodiversity;
- use of renewable and non-renewable resources;
- contribution to the economic well being of the community;
- contribution to the social well being of the community;
- effects on critical resources;
- waste generated by the project.

The approximate scope of possible impacts are presented in Table 1.

The sustainability appraisal should refer to the relevant national, regional and local policies; a link should to be made to traffic and local sustainable development priorities. Sustainable transport provisions such as green travel plans for staff could be considered.

Table 1

Possible impacts of airport related projects

Issue	Construction		Operation	
	Significant impact unlikely	Significant impact possible	Significant impact unlikely	Significant impact possible
Land Use and Material Assets		-		+/-
Traffic and Transport		-		+/-
Noise and Vibration		-		+/-
Air Quality and Climactic factors		-		+/-
Ground Quality, Contamination and Waste (including geology)		-	\/	
Water Resources (including water quality)		-	\/	
Landscape and Visual		-		-
Archaeology and Cultural Heritage		-		-
Ecology (including nature conservation)		-	\/	
Socio - economics (including health)		+/-		+/-
Cumulative Impacts		+/-		+/-

Note: “-” – negative impact, “+/–” – positive and negative impact, “\/” - impact unlikely to be significant

For the adequate and full assessment of possible impacts a list of verified information is necessary to be collected and assessed, such as:

- passenger forecasts;
- hours of operation;
- frequency of flights split by incoming and outgoing
- anticipated aircraft types (to include helicopters) and their numbers;
- anticipated flight types (passenger, cargo, training etc);
- noise levels produced from the engines related to the different aircraft types;
- details on other noise generating activities/equipment that may result in significant impacts, for example auxiliary power units; and
- flight paths for taking off and landing.

Where relevant this information should be provided for a range of scenarios including the busiest period in the year, with impacts predicted accordingly.

This should ensure that the worst case impacts are addressed. Thus, it should be highlighted that EIA should examine all feasible alternatives to the proposals. For example, alternative sites, site layouts, construction practices, technologies and equipment, and operating processes (where appropriate). In addition the EIA should consider the «do nothing» scenario.

In case of reconstruction or expansion of the existing airport, current operations at the airport should be described, i.e. the baseline. This should include:

- passenger numbers;
- hours of operation;
- flight types (passenger, cargo, training etc.);
- frequency of flights split to incoming and outgoing;
- flight paths;
- aircraft types (including helicopters);
- noise levels produced from the current operations at the airport;
- current environmental condition in the vicinity of the airport.

The layout of the airport and its infrastructure should be illustrated on an appropriate figure and placed into the context of surrounding land use. Any environmental issues associated with the current operation should be identified, along with the measures employed to control them. Specifically, any complaints received regarding environmental issues should be identified.

The EIA strategy to be developed in each case should give consideration to the methods by which information will be made available to interested parties, including the public, and feedbacks will be collected. This could include the following methods:

- public exhibitions and information posts;
- internet and traditional mass media (Electronic Newsletters, etc.);
- public meetings, presentations and hearings;
- appointment of a person or a working group responsible for public relations within the EIA team;
- initiation of Advisory Board with the representatives of EIA team, govermental and non-governmental organizations, public organizations and committees.

One of the most important elements of environmental safety provision is the system of impacts monitoring, which should be planned, implemented and carried out where appropriate. Criteria that could be used to determine the need to implement monitoring during the EIA procedure arethe need to demonstrate compliance with conditions or legislation (for example noise) anduncertainties relating to the prediction of impacts or the likely success of mitigation measures (for example species translocation).

The resulted Environmental statement should include the information about the real dimensions and footprint of the proposed project, anticipated objects and additional infrastructure changes (for example access arrangements, car parking facilities, and sewage and water supply arrangements).

The conduction of EIA on the principals described above all interested parties will be able to learn important project and surroundings details, results of alternatives comparison, evaluated impacts, proposed mitigation measures and residual environmental impacts. The last item, which is residual environmental impacts, is crucial for success of EIA as it is the mean of quality control for the whole assessment process: the longer the list of considered impacts and the shorter the list of residual impacts are, the better the work on EIA is.

References

1. *John Whitelegg.* AVIATION: the social, economic and environmental impact of flying. – London: Ashden Trust, 2000. – 30 p.
2. *Morten Stenstadvold*. EIA and its Role in Planning and Decision-making – the Case of the Gardermoen Airport Project // Proceedings from the 3rd Nordic EIA/SEA Conference, (Oslo, 22 - 23 November 1999) / Institute of transport economics. – Oslo: Institute of transport economics, 1999. – P. 199–209.
3. Scoping Opinion for an Environmental Impact Assessment of Proposals for London Ashford Airport, Lydd, Kent. – Lincoln: Institute of Environmental Management & Assessment, 2005. – 110 p.
4. The Environmental Effects of Air Transport: The Royal Commission on Environmental Pollution Study. – London: The Royal Commission on Environmental Pollution, 2002. – 264 p.

UDC: 504.055:629.9.3.015.6:004.942(043.2)

Y.S. Shevchenko, postgraduate student
(National Aviation University, Ukraine)

IMPROVED ALGORITHM OF TRAFFIC FLOWS NOISE MODELING

The method of traffic noise calculation was improved by incorporation of traffic flows modeling as function of traffic rate, density and vehicle speed. Results of macroscopic traffic flow modeling were used as input data for noise emission laws as a main tool for modeling of noise levels near traffic lights and congestions.

Nowadays traffic flow and congestion is one of the main societal and economical problems related to transportation in industrialized countries. This has direct link to one of the most urgent environmental problems of modern cities: air pollution with exhaust gases and noise.

The main purpose of traffic flow study, and in particular vehicular traffic flow, is carried out with the aim of understanding and assisting in the prevention and remedy of traffic congestion problems, which is directly connected with formation of sound fields along main street canyons and urban elements.

For today it is a real challenge for environmental modeling, in particular, analytical, to predict noise levels from traffic flows. Up-to-date European and American models are ready to determine noise levels from traffic flows on straight roads, away from traffic lights and especially traffic congestions. But road cross-sections and traffic jams are still problems for modeling.

The main idea of given work is to incorporate principles of traffic modeling into modeling noise levels from traffic flows as incoherent line source. Stages of noise levels calculation are shown on fig.1. In table 1 comparison of two approaches fro traffic modeling are presented: from the point of view of noise emission laws and traffic management.

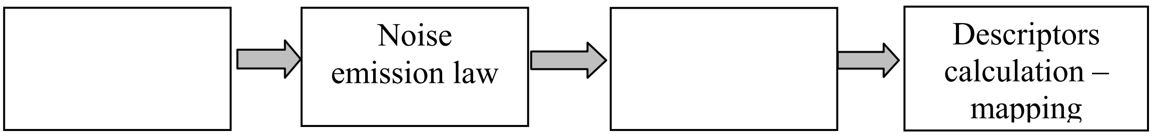

Fig.1. Global modeling chain for noise levels from traffic flows

Table 1

Comparison of traffic flow modeling in environmental acoustics and intelligent transport systems

Parameter of traffic flow modeling	Noise levels from traffic flow modeling	Traffic flow modeling in traffic management
Levels of modeling details	1. The *vehicle model*, describing the sound power of single moving vehicles; 2. The *traffic model*, combining the noise emission of numerous single vehicles into the sound power per metre length of the source line	1. *Microscopic simulation* models model describes both the space-time behaviour of the systems' entities (i.e. vehicles and drivers) as well as their interactions at a high level of detail (individually) 2. *Mesoscopic models* does not distinguish nor trace individual vehicles, but specifies the behaviour of individuals, for instance in probabilistic terms. 3. *Macroscopic models* describe traffic at a high level of aggregation as a flow without distinguishing

			its constituent parts.
Main variables	Density	-	$\Delta\rho = -\dfrac{\Delta N}{\Delta x}$, N - the number of cars per unit time t that pass observer
	Velocity	Deterministic input data	$v = f(\rho)$
	Traffic flow	Deterministic input data	$Q = \rho v$
	Additional input parameters	Vehicle category [4] v_{ref} = 70 - is the reference vehicle speed [km/h]	v_{free} - is the free flow speed ρ_{jam} is the jam density

Macroscopic flow model discard the real view of traffic in terms of individual vehicles or individual system components such as links or intersections and adopt instead a macroscopic fluid view of traffic in a network. The relationship between density, velocity, and flow is presented. The macroscopic models for traffic flow, whether they are one-equation or a system of equations, are based on the physical principle of conservation.

There is a close interrelationship between three traffic variables that is density, velocity and traffic flow. Supposing that cars are moving with constant velocity v, and constant density ρ such that the distance d between the cars is also constant and an observer measure the number of cars N per unit time t that pass-by (i.e. the traffic flow Q), this interrelationship can be represented by a following first-order partial differential equation [1], which can be solved by the method of characteristics:

$$\left(f(\rho) + \rho \frac{df}{d\rho} \right) \frac{\partial \rho}{\partial x} + \frac{\partial \rho}{\partial t} = 0 .$$

If the initial density and the velocity field are known, the above equation can be used to predict future traffic density. This leads us to choose the velocity function for the traffic flow model to be dependent on density and call it $V(\rho)$. The above equation assumes no generation or dissipation of vehicles. Sources and sinks may be added by including a function $g(x,t)$ on the right hand side of the equation.

Several velocity-density-flow models have been developed through the years. Some of the most well-known models include the Greenshields model, Greenberg model, the Underwood model and Eddie's model [1,2] and described in table 2 and depicted on fig. 2.

Table 2

Review of basic traffic flow models

Name of model	Functional dependency	Main peculiarities
The Greenshields Model	$v = v_f \left(1 - \dfrac{\rho}{\rho_{jam}} \right)$, where v_f is the free flow speed and ρ_{jam} is the jam density	The velocity is a linearly decreasing function of the traffic flow density. For zero density the model allows free flow speed v_f , while for maximum density ρ_{jam} we have 100% congestion where the speed is zero and no car is moving. Real traffic data shows that the speed-density relationship is indeed a rather linear negative slope function.
	$q = -\left(\dfrac{\rho_{jam}}{v_f} \right) v^2 + \rho v$	Parabolic equation for the flow-speed-density relationship. Real traffic data reflects somewhat the flow-density relationship for Greenshild's model, which follows a parabolic shape and shows that the flow increases to a maximum which occurs at some average density ρ and then it goes back to zero at high values of density.

The Greenberg's model	$v = v_f - \ln\left(\frac{\rho}{\rho_{jam}}\right)$	Speed-density logarithmic relationship
The Underwood model	$v = v_f e^{-\frac{\rho}{\rho_{jam}}}$	Speed-density exponential relationship
The Edie model	for densities $\rho \le 50$ $v = 54.9e^{-\frac{\rho}{163.9}}$ and for densities $\rho \geq 50$ $v = 28.6\ln\left(\frac{162.5}{\rho}\right)$	The model basically combines Greenberg's and Underwood's model

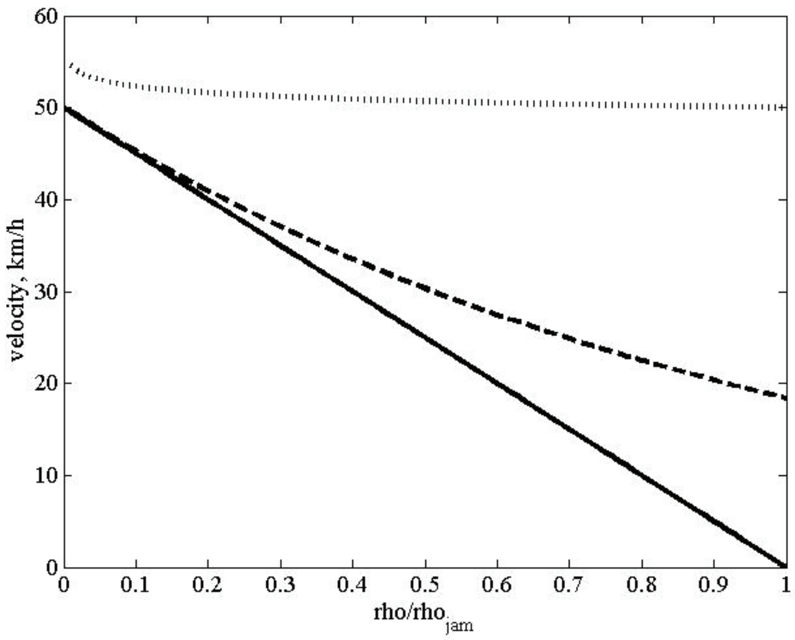

Fig.2. Comparison of three models for traffic velocity modeling: continuous line – Greenshields model, dashed line – Greenberg's model, dotted line – Underwood model

According to fig.1. noise estimation procedure follows the main four steps.

Step 1. Traffic modeling. The site is discretized into road segments whose length varies or stay constant. On the base of dynamic traffic modeling functional dependencies for vehicle flow rate, density and speed are obtained.

In macroscopic traffic flow models traffic is characterized by three variables: flow $Q(x, t)$, density $\rho(x, t)$, and flow speed $v(x, t)$ [5,6]. These three variables are linked by the following system:

- the conservation equation: $\frac{\partial Q(x,t)}{\partial x} + \frac{\partial \rho(x,t)}{\partial t} = 0$;
- the flow definition equation: $Q(x, t) = \rho(x, t)\, v(x, t)$;
- an equilibrium relationship Q_e, called fundamental diagram: $Q(x, t) = Q_e(\rho(x, t))$.

The fundamental diagram represents all the equilibrium situations that the traffic could encounter depending on the road configuration [5]. Two regimes can be distinguished on such a diagram: the free flow and the congested ones (see fig. 3). In free flow, a road can absorb more vehicles (density increase) without saturation (flow increase). In congestion, a road cannot absorb more vehicles and a density increase will increase the saturation (flow decrease). A triangular diagram has been shown to be an accurate representation of urban traffic while being computational. Such diagram is defined by three parameters: the maximal speed V_x reached when traffic is free, the wave speed w at which a starting wave downstream of a congestion climbs back the network, and the maximal density ρ_{max} reached when all vehicles are stopped in a queue (then flow speed is null).

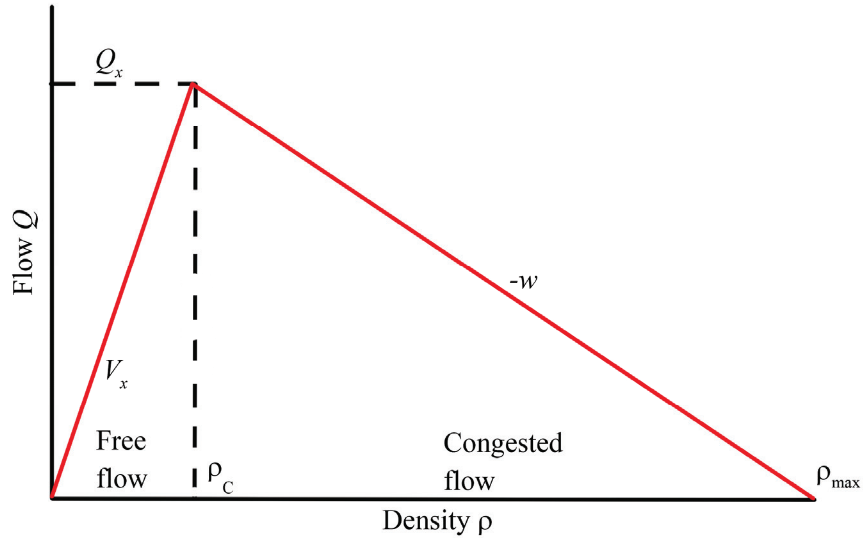

Fig.3. Fundamental diagram for a single lane: Q_x – maximal flow; ρ_{max} - maximal density; ρ_C - critical density; w - wave speed; V_x - maximal speed

Step 2. Noise emission laws. Data given by the traffic model feed noise emission laws to estimate the noise emission L_W of road segment. The laws used in this study distinguish three vehicle categories [4] and give L_W with respect to speed v, flow rate Q and driving conditions [3].

Outputs of the traffic model are used to assess noise emissions every time step by mean of noise emission laws. Such laws give global or spectrum emitted noise for each vehicle or for an aggregated number of vehicles.

Emission laws chosen for this study give power noise levels as a sum (eq. (1)) of a rolling noise L_{WRN} and a traction noise L_{WTN}. The rolling noise L_{WRN} depends on speed, road specificities and composition of regional vehicle park (eq. (2)). The traction noise L_{WTN} depends on speed and cruising mode: accelerating, cruising, or decelerating (eq. (3)).

The source power output by a separate moving vehicle integrated with results of dynamic traffic modeling is defined by the following formula [3]:

$$L_W = L_{WRN} \oplus L_{WTN}, \tag{1}$$

$$L_{WRN} = \alpha_{RN} + \beta_{RN} \lg\left(\frac{v(x,t)}{v_{ref}}\right) + 10\lg(0,8) + C_{dir} + C_{surf} + C_{region}, \tag{2}$$

$$L_{WTN} = \alpha_T + \beta_T\left(\frac{v(x,t) - v_{ref}}{v_{ref}}\right) + 10\lg(0,2) + C_{dir} + C_{dc}, \tag{3}$$

where L_{WRN} – rolling noise, L_{WTN} – traction noise, α_{RN} and β_{RN} – rolling noise coefficients, α_T та β_T – traction noise coefficients, v – vehicle speed (km/h), v_{ref} – reference vehicle speed (km/h), C_{dc} – coefficient for driving conditions (dB), C_{dir} – source directivity correction (dB), C_{surf} – correction for road surface relatively to reference road surface (dB), C_{region} – correction for deviation in sound pressure levels for local vehicle park (dB).

For integration of separate vehicles into traffic flow the following formula is used:

$$L'_W = L_W + 10\lg\left(\frac{Q(x,t)\, v_0}{1000\, Q_0\, v_{eq}}\right),$$

where v_0 - is the reference vehicle speed (1 km/h), v_{eq} - is the equivalent vehicle speed for vehicle category (km/h), Q_0 is the reference traffic flow (1 h^{-1}), Q - is the traffic flow for vehicle category (h^{-1}).

Step 3. Propagation calculation. Sound attenuation $\Delta L_{Att}(x)$ as a result of propagation from source to receiver point is defined by the following formula for each source position:

$$\Delta L_{Att}(x) = \Delta L_{scr} + \Delta L_{div} + \Delta L_{abs} - \Delta L_{ground} - \Delta L_{refl} \ ,$$

where ΔL_{div} - noise attenuation as a result of sound divergence, dB, ΔL_{abs} - absorption of sound waves in the air, ΔL_{scr} - sound diffraction on natural and artificial barriers, ΔL_{ground} - constructive/destructive interference of sound waves as a result of reflection from ground, ΔL_{refl} - constructive/destructive interference of sound waves as a result of reflection from vertical obstacles like building facades [7].

Step 4. Descriptors calculation – mapping. If a static traffic representation is involved, traffic variables and thus noise emissions are independent of time, and then only $L_{Aeq,T}$ can be calculated, where T is the observation period. If a dynamic traffic model is involved, traffic variables are estimated every 1 s, and then $L_{Aeq,1s}$ time evolution but also specific acoustic descriptors can be calculated. For calculated noise indexes horizontal or vertical maps are created [7].

Conclusions

Even though improved algorithm is am attempt of describing complicated traffic phenomena with considerable accuracy, their main limitations arise in their inability to accurately simulate severe traffic congestion situations, where the conservation equation does not represent the traffic flow so well. But the advantage of macroscopic models incorporation in noise levels modeling from traffic flows in modern cities is their flexibility since detailed interactions are overlooked, and the model's characteristics are shifted toward important parameters such as flow rate, concentration or traffic density, and average speed.

References

1. *Ahmed Abdel-Rahim.* Intelligent Transportation Systems // Ahmed Abdel-Rahim. – Rijeka: InTech, 2012. – 214 p.
2. *Serge P. Hoogendoorn*. State-of-the-art of Vehicular Traffic Flow Modelling // Journal of Systems and Control Engineering. – 46 p. - http://citeseerx.ist.psu.edu/viewdoc/download?doi=10.1.1.106.9913&rep=rep1&type=pdf
3. Engineering method for road traffic and railway noise after validation and fine-tuning, Harmonoise WP 3, Technical Report HAR32TR-040922-DGMR20, written by *Renez Nota, Robert Barelds, Dirk van Maercke*, agreed by *Hans van Leeuwen*, 2005.
4. ГОСТ 31330.1-2006 (ИСО 11819-1:1997). Шум. Оценка влияния дорожного покрытия на транспортный шум. Часть 1. Статистический метод. – Введ. 01.06.2007. – М.: Стандартинформ, 2007. – 43 с.
5. *Can A.* Dynamic estimation of urban traffic noise: Influence of traffic and noise source representations / *A. Can, L. Leclercq, J. Lelong* // Applied Acoustics. – Vol. 69 . – 2008. – p. 858–867.
6. *Can A.* Traffic noise spectrum analysis: Dynamic modeling vs. experimental observations/ *A. Can, L. Leclercq, J. Lelong, D. Botteldooren* // Applied Acoustics. – Vol. 71. – 2010. – p.764–770.
7. *Шевченко Ю.С.* Метод картографування шуму від транспортних потоків у сучасному місті / Ю.С. Шевченко // Вісник НАУ.– 2012.– № 4(53). – *в ред*.

UDC 629.735.024:534.014.2(043.2)

V.M. Makarenko (National Aviation University, Ukraine)

SOUND TRANSMISSION LOSS IMPROVEMENT OF AVIATION PANELS WITH CONCENTRATED MASSES

Mathematical model is developed for propagation of sound waves in diffuse field through cylindrical panel with typical reinforcement. The model allows to account the influence of attached to the panel concentrated masses. Optimization task for frequency averaged transmission loss of aviation panel is based on elaborated model. Optimization of concentrated mass parameters is done with genetic algorithm.

Let us consider curved aluminum rectangular cylindrical panel with size $a \times b \times h$ (fig. 1) as the obstacle for acoustic wave's propagation into airplane cabin.

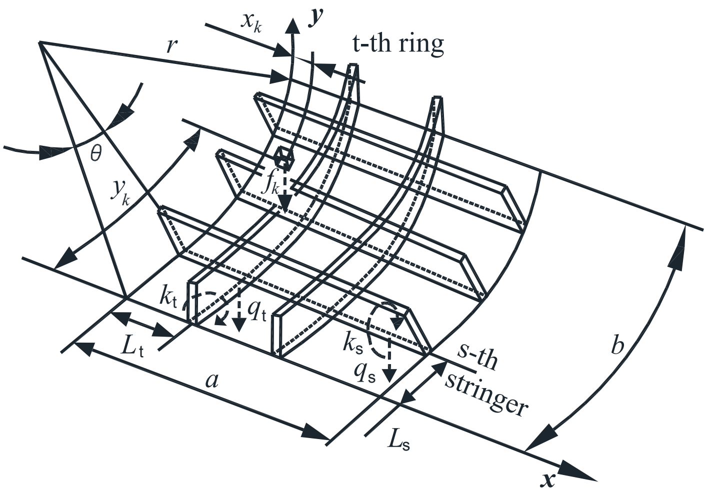

Fig. 1 Scheme of curved panel with reinforcement and mass.

Differential equations of curved panel vibration with attached stringers, rings and masses can be written in form of Donnel-Mushtari-Vlasov equations [1, 2]:

$$\begin{cases} D\left(\dfrac{\partial^4 w}{\partial x^4} + \dfrac{2}{r^2}\dfrac{\partial^4 w}{\partial x^2 \partial \theta^2} + \dfrac{1}{r^4}\dfrac{\partial^4 w}{\partial \theta^4}\right) + \dfrac{1}{r}\dfrac{\partial^2 \varphi}{\partial x^2} + \rho h \dfrac{\partial^2 w}{\partial t^2} = \\ = 2(p_i - p_r)_{z=0} - \sum\limits_{k=1}^{K} f_k \delta(x - x_k)\delta(y - y_k) - \\ -\sum\limits_{s=1}^{S} q_s \delta(y - L_s) - \sum\limits_{r=1}^{R} q_r \delta(x - L_r) - \sum\limits_{s=1}^{S} \kappa_s \delta'(y - L_s) - \sum\limits_{r=1}^{R} \kappa_r \delta'(x - L_r), \\ \dfrac{Eh}{r}\dfrac{\partial^2 w}{\partial x^2} - \left(\dfrac{\partial^4 \varphi}{\partial x^4} + \dfrac{2}{r^2}\dfrac{\partial^4 \varphi}{\partial x^2 \partial \theta^2} + \dfrac{1}{r^4}\dfrac{\partial^4 \varphi}{\partial \theta^4}\right) = 0, \end{cases} \quad (1)$$

where D – bending stiffness; φ – Airy's function; w – vibrational displacement; r – panel's curvature radius; ρ – panel material density; h – panel thickness; δ – Dirac delta function; p_i – pressure of incident wave acting on the panel surface; p_r denotes acoustic pressure, radiated by the panel, L_s arc length from the coordinate origin to s-th stringer, L_r – distance from coordinate origin to r-th ring, x_k, y_k – coordinate of k-th mass, R, S, K – quantity of rings, stringers and masses respectively.

Assume, that for clamped panel, transverse motion at panel harmonic oscillations can be written in form:

$$w(x,y)=\sum_m\sum_n w_{mn}X_m(x)Y_n(y), \quad (2)$$

where functions X_m and Y_n satisfy free and clamped boundary conditions respectively. Such beam functions have the following form [3]:

$$X_m(x)=\cos\frac{\lambda_m x}{a}+\operatorname{ch}\frac{\lambda_m x}{a}+\gamma_m\left(\sin\frac{\lambda_m x}{a}+\operatorname{sh}\frac{\lambda_m x}{a}\right)$$
$$Y_n(y)=\cos\frac{\lambda_n y}{b}-\operatorname{ch}\frac{\lambda_n y}{b}-\gamma_n\left(\sin\frac{\lambda_n y}{b}-\operatorname{sh}\frac{\lambda_n y}{b}\right), \quad (3)$$

where $\gamma_m=\dfrac{\sin\lambda_m+\operatorname{sh}\lambda_m}{\cos\lambda_m-\operatorname{ch}\lambda_m}$; $\gamma_n=\dfrac{\cos\lambda_n-\operatorname{ch}\lambda_n}{\sin\lambda_n-\operatorname{sh}\lambda_n}$, λ_n and λ_m can be found from characteristic equation $\cos\lambda_n\operatorname{ch}\lambda_n=1$.

Beam functions (3) are orthogonal, and have the following properties:

$$\int_0^a X_mX_p dx=\begin{cases}a & \text{if } m=p\\ 0 & \text{if } m\neq p\end{cases} \text{ та } \int_0^b Y_nY_q dx=\begin{cases}b & \text{if } n=q\\ 0 & \text{if } n\neq q\end{cases} \quad (4)$$

$$I_{mp}^{20}=\int_0^a\frac{d^2X_m}{dx^2}\frac{dX_p}{dx}dx=\frac{\bar{I}_{mp}^{20}}{a};\quad J_{nq}^{20}=\int_0^b\frac{d^2Y_n}{dy^2}\frac{dY_q}{dy}dy=\frac{\bar{J}_{nq}^{20}}{b};\ \frac{d^4X_m}{dx^4}=\left(\frac{\lambda_m}{a}\right)^4X_m;\ \frac{d^4Y_n}{dy^4}=\left(\frac{\lambda_n}{b}\right)^4Y_n;$$

By rewriting transverse motion in terms of eigenfunctions in equation (2) and application of their orthogonal properties, one can get the following system of equations:

$$\begin{cases}D\left[ab\left(\dfrac{\lambda_m}{a}\right)^4w_{mn}+2\sum\limits_{mn}w_{mn}I_{mp}^{20}J_{nq}^{20}+ab\left(\dfrac{\lambda_n}{b}\right)^4w_{mn}\right]+\dfrac{b}{r}\sum\limits_m\varphi_{mq}I_{mp}^{20}-\rho hab\omega^2w_{mn}=\\ =\int_0^a\int_0^b qX_pY_q dxdy\\ \dfrac{Ebh}{r}\sum\limits_m w_{mq}I_{mp}^{20}-ab\left[\left(\dfrac{\lambda_m}{a}\right)^4+\left(\dfrac{\lambda_n}{b}\right)^4\right]\varphi_{mn}-2\sum\limits_{mn}\varphi_{mn}I_{mp}^{20}J_{nq}^{20}=0\end{cases} \quad (5)$$

Applying the properties of Dirac's delta function to right hand side of first equation in (5) yields the following relation:

$$\int_0^a\int_0^b qX_pY_q dxdy=2\left(\int_0^a\int_0^b p_iX_pY_q dxdy-\mathrm{i}\,\omega\rho_0c_0\sum_{mn}w_{mn}Z_{pqmn}\right)-\sum_{k=1}^K f_kX_p(x_k)Y_q(y_k)-$$
$$-\sum_{s=1}^S Q_sY_q(L_s)-\sum_{r=1}^R Q_rX_p(L_r)+\sum_{s=1}^S M_sY_q'(L_s)+\sum_{r=1}^R M_rX_p'(L_r) \quad (6)$$

where $Q_s=\int_0^L q_s(x)X_p dx,\quad Q_r=\int_0^b q_r(y)Y_q dy,\quad M_s=\int_0^L\kappa_s(x)X_p dx,\quad M_r=\int_0^b\kappa_r(y)Y_q dy;$

f_k – force, created by k-th mass inertia, $\mathrm{i}=\sqrt{-1}$, ρ_0 and c_0 – density and velocity of sound in air, Z_{pqmn} specific radiation impedance.

Basic equation for bending and torsion displacements of stringers, rings and masses can be written in form [4]:

$$D_s\frac{d^4w_s}{dx^4}-m_s\omega^2w_s=q_s,\ T_s\frac{d^2\theta_s}{dx^2}-EI_w\frac{d^4\theta_s}{dx^4}+\rho_sI_p\omega^2\theta_s=\kappa_s$$
$$\left[D_r\left(\frac{d^4w_r}{dy^4}+\frac{2}{r^2}\frac{d^2w_r}{dy^2}+\frac{w_r}{r^4}\right)-m_r\omega^2\right]w_r=q_r,\ T_r\frac{d^2\theta_r}{dy^2}-E_r\frac{I_{ry}}{r^2}\theta_r+\rho_rI_{pr}\omega^2\theta_r=\kappa_r \quad (7)$$
$$-m_k\omega^2w_k=f_k$$

where D_s, D_r - stringer and ring bending stiffness respectively; m_s, m_r - mass per unit length of stringer, ring.

Input modal receptances of strings and rings to perpendicular force are determined from equations(7).

For s-th stringer bending:

$$\beta_m^{sQ} = \frac{1}{m_s a\left[\omega_{Qm}^2\left(1+\mathrm{i}\eta_s\right)-\omega^2\right]},\ \omega_{Qm}^2 = \frac{D_s}{m_s}\left(\frac{\lambda_m}{a}\right)^4 \tag{8}$$

For s-th stringer torsion:

$$\beta_m^{sM} = \frac{1}{\rho_s I_p a\left[\omega_{Mm}^2\left(1+\mathrm{i}\eta_s\right)-\omega^2\right]},\omega_{Mm}^2 = \frac{EI_w}{\rho_s I_p}\left(\frac{\lambda_m}{a}\right)^4 - \frac{T_s I_{mp}^{20}}{\rho_s I_p a} \tag{9}$$

For r-th ring bending:

$$\beta_n^{r} = \frac{1}{m_r\left[\omega_{Qn}^2\left(1+\mathrm{i}\eta_r\right)-\omega^2\right]},\ \omega_{Qn}^2 = \frac{D_r}{m_r}\left[\left(\frac{n\pi}{b}\right)^4 - \frac{2}{r^2}\left(\frac{n\pi}{b}\right)^2 + \frac{1}{r^4}\right], \tag{10}$$

For r-th ring torsion:

$$\beta_n^{rM} = \frac{1}{\rho_r I_{rp} b\left[\omega_{Mn}^2\left(1+\mathrm{i}\eta_r\right)-\omega^2\right]},\ \omega_{Mn}^2 = \frac{E_r I_{ry}}{\rho_r I_{rp} r^2} - \frac{T_r J_{nq}^{20}}{\rho_r I_{rp} b} \tag{11}$$

For k-th mass:

$$\beta_k = -\frac{1}{m_k\omega^2}.$$

Forces and moments, created by reinforcement and masses, are received from expressions for receptances:

$$Q_s = \frac{\sum_n w_{mn}\varphi_n\left(L_s\right)}{\beta_m^{sQ}},\quad Q_r = \frac{\sum_m w_{mn}X_m\left(L_r\right)}{\beta_n^{rQ}},$$

$$M_s = \frac{\sum_n w_{mn}Y_n\left(L_s\right)}{\beta_m^{sM}},\quad M_r = \frac{\sum_m w_{mn}X_m\left(L_r\right)}{\beta_n^{rM}},\ F_k = \frac{\sum_{mn} w_{mn}X_m\left(x_k\right)Y_n\left(y_k\right)}{\beta_k} \tag{12}$$

By substituting expressions (12) into (6), one can get:

$$\begin{aligned}
&\int_0^a\int_0^b qX_pY_q dxdy = 2\left(P_{pq}^i + P_{pq}^r\right) - L\sum_n w_{pn}\sum_{s=1}^{S}\left[D_s\left(\frac{\lambda_p}{a}\right)^4 - m_s\omega^2\right]Y_n\left(L_s\right)Y_q\left(L_s\right) - \\
&-b\sum_{r=1}^{R}\left\{\left[D_r\left(\left(\frac{\lambda_q}{b}\right)^4 + \frac{1}{r^4}\right) - m_r\omega^2\right]\sum_m w_{mq}X_m\left(L_r\right) + \frac{2D_r}{br^2}\sum_{mn} J_{nq}^{20}X_m\left(L_r\right)\right\}X_p\left(L_r\right) + \\
&+\omega^2\sum_{k=1}^{K}\sum_{mn} w_{mn}X_m\left(x_k\right)Y_n\left(y_k\right)X_p\left(x_k\right)Y_q\left(y_k\right) + \\
&+\sum_{s=1}^{S}\left\{T_s\sum_{mn} w_{mn}I_{mp}^{20}Y_n\left(L_s\right) + L\left[\rho_s I_p\omega^2 - EI_w\left(\frac{\lambda_m}{L}\right)^4\right]\sum_n w_{mn}Y_n\left(L_s\right)\right\}Y_q'\left(L_s\right) + \\
&+\sum_{r=1}^{R}\left\{T_r\sum_{mn} w_{mn}X_m\left(L_r\right)J_{nq}^{20} + b\sum_m w_{mn}X_m\left(L_r\right)\left(\rho_r I_{rp}\omega^2 - \frac{E_r I_{ry}}{r^2}\right)\right\}X_p'\left(L_r\right)
\end{aligned}$$

In order to simplify calculations, the influence of torsional stringer and ring vibrations is not included in equations (5), as soon as low frequency oscillations are considered. For considered aviation panel the influence of torsional vibrations of stringer becomes noticeable for oscillations at frequencies over 700 Hz. For frame it becomes important at frequencies more than 950 Hz, because at these frequencies there are the first resonances of these structural elements according to equations

(8-11). A similar situation takes place for other aircraft panels, because the frequency of torsional vibrations of the reinforcement elements is almost independent on the shape and size of their cross section.

Let us rewrite system of equations (5) for its further numerical solution in matrix form:

$$\left[\mathbf{A}-\omega^2\mathbf{B}+\omega\mathbf{A}_{pr}\right]\begin{bmatrix} w_{pq} \\ \varphi_{pq}\end{bmatrix}=\begin{bmatrix}\mathbf{C}^1 \\ 0\end{bmatrix}, \tag{13}$$

where $C_{pq}^1=2\int_0^L\int_0^b p_i X_p(x)Y_q(y)\mathrm{d}x\mathrm{d}y$, $\mathbf{A}_{pr}=\begin{bmatrix}\mathbf{A}_{pr}^{1w} & 0 \\ 0 & 0\end{bmatrix}$, $A_{pr,pqmn}^{1w}=2i\omega\rho_0 c_0 Z_{pqmn}$.

The value of natural frequencies ω for panel with reinforcement and mass, excluding the influence of sound radiation by panel, is determined by solving the generalized eigenvalue problem:

$$\mathbf{AV}=\mu\mathbf{BV},$$

where $\mathbf{V}$, μ are generalized eigenvector and eigenvalues of matrices **A** and **B**. Eigenfrequencies can be expressed through eigenvalues μ in the following way:

$$\omega=\sqrt{\mu}$$

In diffuse acoustic field transmission loss factor must be determined as an average for different sound waves' incidence angles. Hence factor value τ_d is equal to [5]:

$$\tau_d=2Q\left(\rho_0 c_0\right)^2 r\omega^2\sum_{m,n}\sigma_{mn}\int_0^{\phi_L} w_{mn}(\phi)\,w_{mn}^*(\phi)\sin\phi\,\mathrm{d}\phi. \tag{14}$$

where value Q depends upon angle ϕ_L: $Q=1$ - for diffuse sound propagation ($\phi_L=90^0$), $Q=1{,}022$ for angle value $\phi_L=78^0$. For harmonic oscillations in equation (14) w_{mn} and complex-conjugate modal amplitude of vibration displacement w_{mn}^* is determined from solution of system of equations (13).

Sound transmission loss is determined as:

$$TL=-10\lg\tau_d. \tag{15}$$

Objective function is the integral value of transmission loss in frequency range from $f_{\min}$ to $f_{\max}$:

$$\min\quad F_{obj}=10\lg\frac{1}{f_{\max}-f_{\min}}\int_{f_{\min}}^{f_{\max}}\tau_d\mathrm{d}f, \tag{16}$$

by mass parameters: $m_k, x_k, y_k,\ k=1,2,\ldots,K$,

with constraints $\sum_{k=1}^{K} m_k=\zeta M_{panel}$, $0+x_g<x_k<L-x_g, 0+y_g<y_k<b-y_g$;

where τ_d is determined from equation (15), $M_{panel}=\rho hLb$, assume ζ=0,1; x_g, y_g are gaps from the panel edges, which are related to complexity of ideal boundary condition implementation in practice.

Since the objective function (16) has many local minima, we apply the algorithm for global optimization. Modern computers have multiple cores, and it is possible to implement the parallel calculations on several computers that form a single cluster. Therefore, genetic algorithm has a significant advantage over other optimization algorithms.

Before staring of the optimization, it is necessary to prepare cubic polynomials, which provide interpolation of modal forces (2.15), and specific radiation impedance $Z_{pq,mn}$ (16) for all modes included in the investigated range of frequencies. This must be done, because these values do not depend on the parameters with which the optimization is performed and make up most of the calculation time of objective function. A number of other parameters, which include elements of matrix **B**, excluding the elements $\mathbf{B}_m^{1w}$, which include mass parameters, and matrix **A** is also calculated at the preparatory stage. Such approach reduces the calculation time of objective function (16) to 4,5-6,5 s for 8 modes. Due to the fact that the functions P^{i}_{mn} and $Z_{pq,mn}$ are continuous (fig. 2.1), their replacement by interpolation polynomials with steps of 5 Hz and 7,5 ° leads to the error in objective function (16), which does not exceed 0.01 dB. This is proved by interpolation with different steps of frequency f and angle of incidence ϕ of the plane acoustic wave.

Genetic algorithm sends relative coordinates $\overline{x_k}$, $\overline{y_k}$ to the program of objective function, that performs their scaling to absolute coordinates x_k, y_k on the real aircraft panels prior to calculation. Individual genes are the parameters of the masses $\overline{m_k}, \overline{x_k}, \overline{y_k}$.

Optimization of the objective function is done for 3 additional masses (15 parameters). The main modes in the range 100-200 Hz, in which the optimization is performed, are mode 1-1 and 2-1. At frequencies of these modes a significant reduction of sound transmission loss is observed (Fig. 2a). Also the optimization accounts for modes 1-2, 2-2, 3-1, 4-1, 3-2 1-3, which causes a reduction in sound transmission loss at frequencies that are close to a range of optimization. The result of optimization is the optimal location of the masses, which is shown in Fig. 2b. The main reduction of objective function (16) (increase of transmission loss) is observed on mode 2-1. There is a slight reduction in sound transmission loss on mode 1-1.

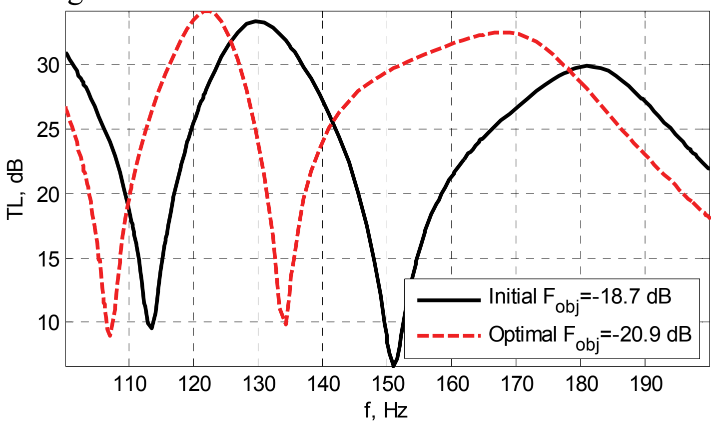

a

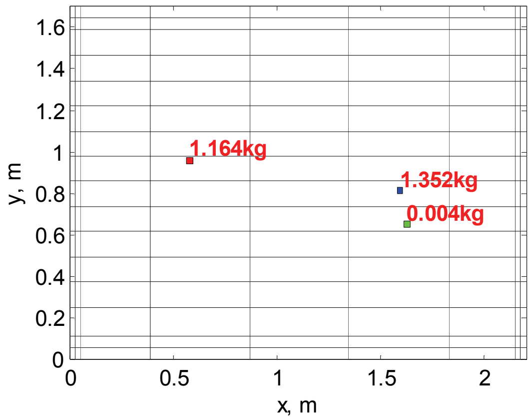

б

Fig. 2 (*a*) Sound transmission loss spectrum of aviation panel without and with optimally placed masses;
(*б*) Scheme of optimal location of mass on aviation panel

Conclusions

1. Conducted optimization proved the possibility of sound transmission loss improvement with concentrated masses.
2. Calculation of reinforcement elements' eigenfrequencies for different types of deformation has shown, that torsion of stringers and rings can be neglected.

References

1. *A.K. Mitchell, C.R. Hazell*, A simple frequency formula for clamped rectangular plates, *Journal of Sound and Vibration* **118**, 1987, 271–281.
2. *B. Liu, L. Feng, A. Nilsson*. Sound transmission through curved aircraft panels with stringer and ring frame attachment. *Journal of sound and vibration* **300**, 2007, 949-973.
3. *Berthelot J.-M.* Composite Matériels. Mechanical behavior and structural analysis, Springer,1999, 645p.
4. *Тимошенко С. П.* Колебания в инженерном деле. – М.: Наука, 1967, 444 с.
5. *Takahashi D.* Effect of panel boundedness on sound transmission problems. *J.Acoust. Soc. Am.* **98** (5), 1995, 2598 -2606.

CONGRESS SECRETARIAT
National Aviation University,
1, Kosmonavta Komarova ave.,
Kyiv, 03680, Ukraine
Tel: +38044 406-71-56
Fax: +38044 406-72-12
e-mail: aviacon@nau.edu.ua
Congress homepage: